

Univerzita Karlova, Praha
Matematicko-fyzikální fakulta

***Biofyzikální a farmakologické studie interakcí DNA s
protinádorovými komplexy platiny a ruthenia***

Olga Nováková

Habilitační práce

Brno, září 2015

Obsah

Úvodní komentář.....	3
Předmluva.....	4
I. Všeobecný úvod do problematiky, která je předmětem této habilitační práce	5
II. Shrnutí důležitých výsledků, které jsou obsahem publikací tvořících hlavní část habilitační práce.	21
III. Seznam publikovaných vědeckých prací, které jsou v plném znění součástí habilitační práce.....	24
IV. Metodický komentář.....	27
V. Kopie publikovaných vědeckých prací autorky v plném znění.....	46

Úvodní komentář

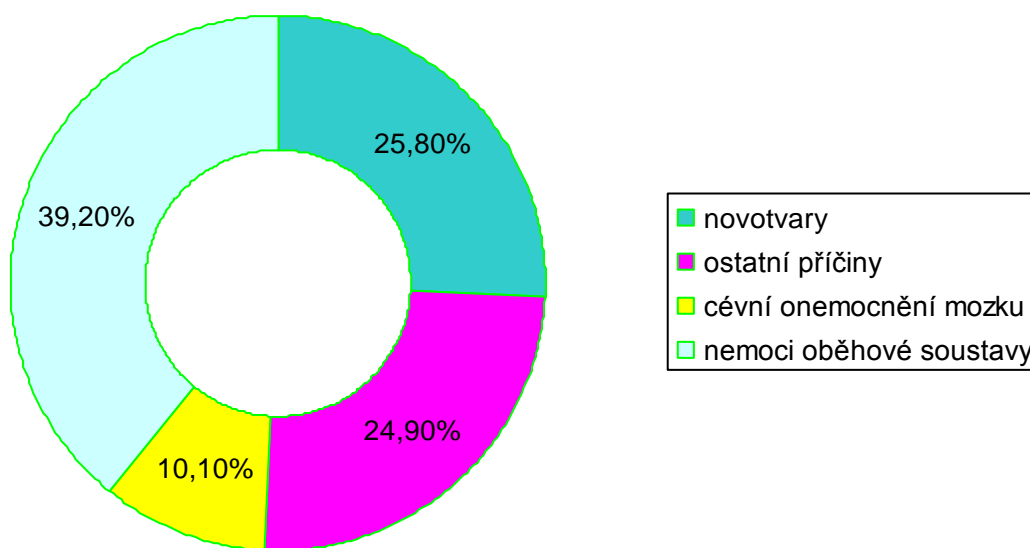
Předkládaná habilitační práce shrnuje výsledky studia interakcí deoxyribonukleové kyseliny (DNA) s komplexy těžkých kovů platinové skupiny, především protinádorově účinnými komplexy ruthenia a platiny, ve vztahu k možnému mechanismu jejich působení na buněčné úrovni. Tvoří ji komentovaný soubor 24 vybraných prací a jednoho přehledového článku, které byly v plném znění publikovány v mezinárodních recenzovaných odborných časopisech.

První část práce představuje stručný všeobecný úvod do autorkou řešené problematiky a zahrnuje i poznatky získané autorkou a jejími spoluautory, následuje shrnutí významných výsledků, které jsou obsahem publikací tvořících hlavní část habilitační práce autorky. Práci pak doplňuje metodický komentář, který by měl přispět k lepšímu porozumění a orientaci v autorkou řešené problematice.

Experimentální práce, která je popsána v přiloženém souboru publikací, byla autorkou a jejími českými spoluautory, vykonána na Biofyzikálním ústavu AV ČR v.v.i. v Brně.

V Brně, 1. září 2015

Problém nádorových onemocnění se posouvá do čela světových statistik z hlediska úmrtnosti v civilizovaném světě - z třetí příčky, kterou poslední desetiletí "rakovina" zaujímala, se dostává na příčku druhou. Pravděpodobnost, že se probojuje až na vedoucí pozici, se zvyšuje vzhledem k stále rostoucímu průměrnému věku a pokrokům v prevenci a účinnosti léčby kardiovaskulárních chorob. Vývoj nových a účinnějších protinádorových preparátů je důležitou součástí základního i klinického výzkumu. Významnou roli v protinádorové chemoterapii současnosti hrají platinová cytostatika.



Statistika příčin úmrtnosti v ČR v roce 2012 podle ČSÚ (upraveno)

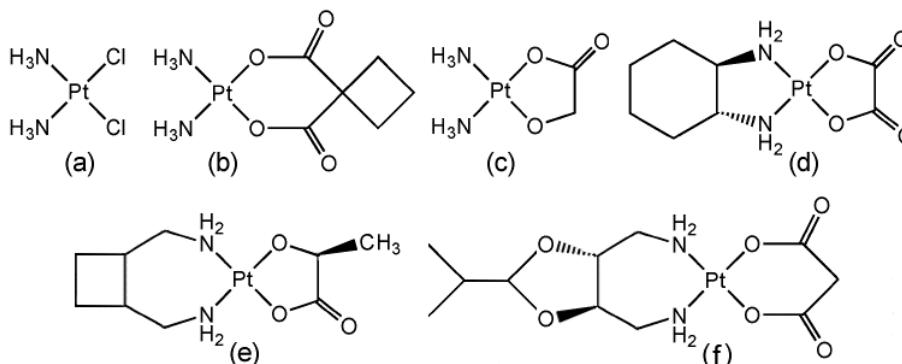
I. Všeobecný úvod do problematiky, která je předmětem této habilitační práce

Těžké kovy v protinádorové terapii

Koordinační komplexy těžkých kovů jsou předmětem výzkumu mnoha světových laboratoří již řadu desetiletí, důvodem tohoto velkého zájmu je jejich biologická aktivita. Jedná se především o koordinační sloučeniny s centrálními atomy platiny a ruthenia, dalšími kovy platinové skupiny (Os, Ir, Pd, Rh, Fe, Co), komplexy zlata, mědi, titanu, cínu, germánia a gália [1, 2].

Již v roce 1865 bylo popsáno využití sloučenin arzenu v protinádorové terapii [3]. Systematické studie vztahů mezi strukturou, aktivitou a toxicitou kovových komplexů se datují rokem 1931, kdy byla provedena první systematická studie inhibice růstu nádorů kovovými komplexy [4].

Moderní historie využití koordinačních komplexů těžkých kovů v protinádorové terapii se odvíjí od poloviny šedesátých let minulého století, kdy došlo, díky šťastné náhodě, při studiu vlivu elektromagnetického pole na růst bakterií *E. Coli*, k objevu cytostatických vlastností koordinačních sloučenin platiny, biofyzikem Barnettem Rosenbergem. Testování schopností skupiny platičitých a platnatých komplexů účinně inhibovat buněčné dělení, vedlo k výběru jednoduché, čtvercově planární anorganické sloučeniny- *cis*-diammindichloridoplatnatého komplexu - **cisplatin** [5, 6]. Komplexy cisplatin a jejích analogů dnes představují třídu chemoterapeutik, která jsou široce využívána v klinické medicíně především jako antineoplastické preparáty [7, 8, 9, 10].



Obr.1: Chemická struktura cisplatin (a) a jejích klinicky schválených derivátů - cytostatik I. a II. generace: karboplatiny (b), nedaplatiny (Japonsko) (c), oxaliplatin (d), lobaplatiny (Čína) (e) a heptaplatiny (J. Korea) (f).

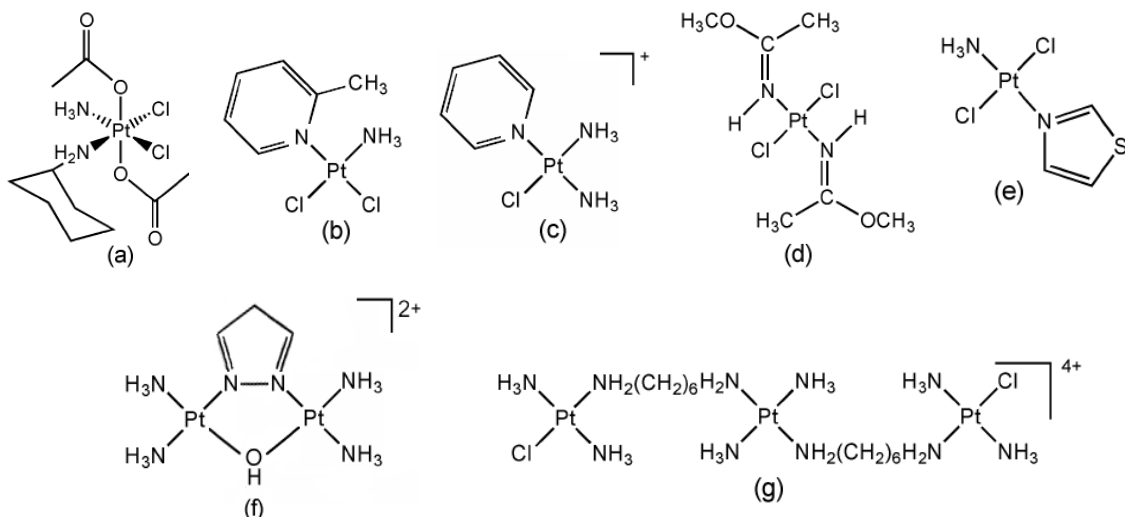
Vlastní struktura cisplatiny byla publikována již v roce 1844 [11], ale její standardní klinické využití v protinádorové terapii se datuje až od r. 1978 [12].

Cisplatina i její přímý analog karboplatina, (obr.1) je jedním z komerčně nejúspěšnějších cytostatik současnosti a je celosvětově aplikována pacientům s maligními novotvory. Představuje účinný preparát v boji s nádory urogenitálního traktu (vaječníku, varlat, močového měchýře), u nádorů varlat dochází k úplné remisi u více než 85% pacientů [12, 13]. Používá se také v kombinované terapii při léčbě karcinomů plic, nádorů žaludku a některých nádorů hlavy a krku. Její intravenózní podávání je ovšem spojeno s řadou komplikací. Jednou z nich jsou **vedlejší účinky** (nefrotoxicita, zvracení, ototoxicita, poruchy krve tvorby, myelotoxicita), dalším problémem je tzv. **získaná rezistence** při opakované nebo dlouhodobé terapii, která vede ke snížení účinků léčby. Cisplatina je bohužel **málo účinná nebo neúčinná** při léčbě často se vyskytujících nádorů, např. nádorů tlustého střeva nebo prsu. Také v případě metastáz je úspěšnost léčby cisplatinou malá [7, 14, 15]. Relativně úzké spektrum účinnosti a výše jmenované komplikace při podávání cisplatiny vedou ke snaze vyvinout nové protinádorové účinné látky na bázi koordinačních sloučenin kovů, které by se vyznačovaly nižší toxicitou, širším spektrem léčitelných nádorů a nevykazovaly křížovou rezistenci s cisplatinou [1, 12, 16].

Vývoj nových protinádorově účinných komplexů kovů se přizpůsobuje jak zdokonaleným teoretickým znalostem z oboru bioanorganické chemie, tak znalostem mechanismu biologického působení již podrobně prostudovaných platinových komplexů. Dala by se popsat následujícími 4 směry:

- 1) syntéza a testování analogů cisplatiny a jiných účinných platinových komplexů
- 2) syntéza a testování komplexů s jinými centrálními atomy
- 3) spojení protinádorově účinných komplexů s nosičovou nebo jinou biologicky aktivní molekulou/systémy, které povede k akumulaci v cílovém místě působení, k duálním nebo synergickým efektům
- 4) aktivace protinádorově účinných komplexů v cílovém místě působení (pomocí světla, tepla, ultrazvuku apod.)

ad1) Jako analogy cisplatiny jsou označována platinová cytostatika první, druhé a třetí generace, jsou zastoupeny řadou klinicky testovaných komplexů (obr. 2) nebo komplexů, které se klinicky již používají viz obr.1. Vyznačují se menší obecnou toxicitou a/nebo širším spektrem léčitelných nádorů a/nebo nevykazují křížovou rezistenci s cisplatinou.

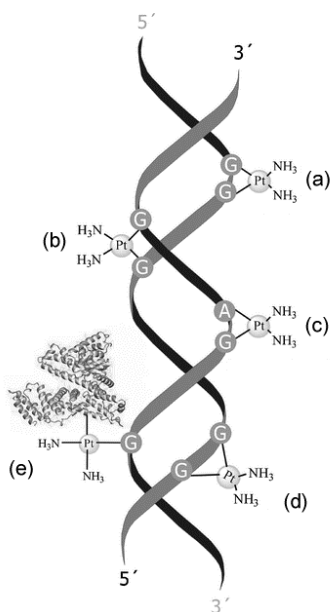


Obr. 2: Chemické struktury některých klinicky testovaných a nových "neklasických" analogů cisplatiny. Orálně podávaný čtyřmocný preparát JM216 - satraplatina (a), AMD473 - pikoplatina (b), monofunkční pyriplatina - cDPCP (c), *trans*-PtCl₂(iminoether)₂ (d), *trans*-[PtCl₂(NH₃)(thiazol)] (e) a zástupci vícejaderných Pt komplexů s protinádorovou aktivitou, dinukleární AMPZ (f) a trinukleární BBR3464 (g).

Cílovým místem farmakologického působení cisplatiny a jejích protinádorově účinných derivátů je DNA (deoxyribonukleová kyselina) [14, 17, 18]. Toto zjištění vede k potřebě detailního studia vlastností platinových i ostatních kovových komplexů a jejich interakcí s DNA, a to jak z hlediska strukturních, tak i kinetických a termodynamických parametrů.

Síla vazby centrálního atomu s ligandem vzrůstá s polarizovatelností elektronového obalu atomu, tedy s rostoucí atomovou hmotností v rámci jednotlivých skupin periodické tabulky. Afinity ligandů k dvojmocné platině klesá v pořadí: CN⁻ > NH₃ = guanin, adenin, OH⁻ > I⁻ > SCN⁻ > Br⁻ > Cl⁻ = PO₄³⁻, COO⁻ > H₂O > NO₃⁻, SO₄²⁻, ClO₄⁻. Z těchto výše uvedených vztahů vyplývá, že v případě cisplatiny budou odstupujícími ligandy chloridové ionty. Jejich výměna za vodu nebo ionty s nižší afinitou k Pt(II) vede k hydrolýze tohoto komplexu, která umožňuje jeho vazbu k DNA [19].

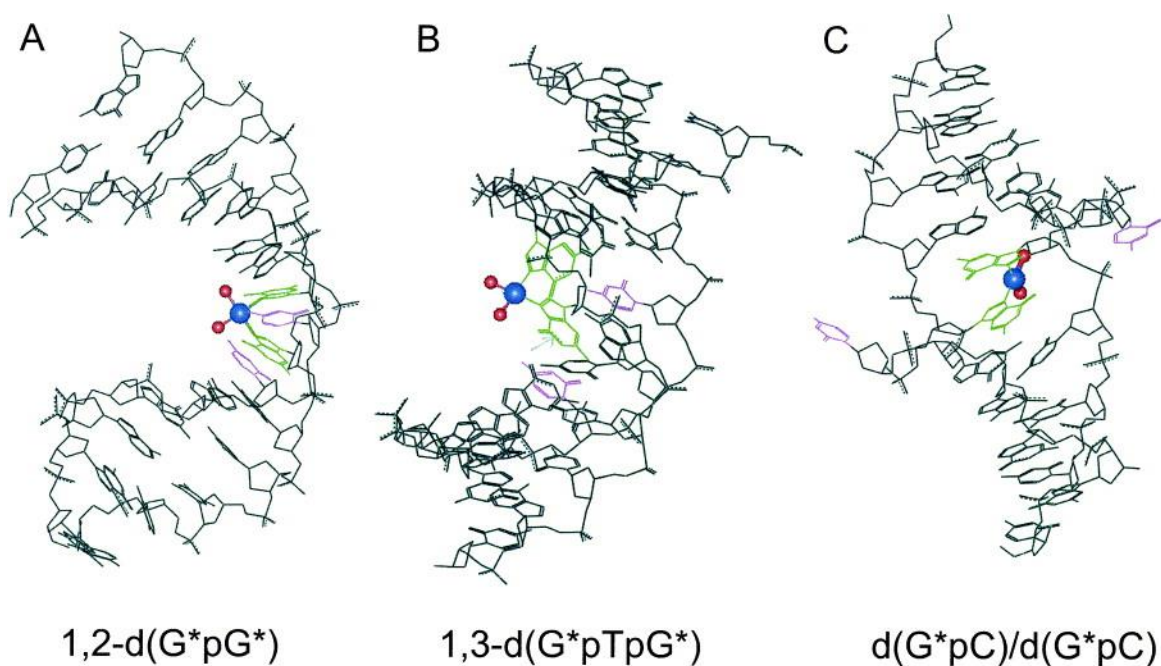
Cisplatina a její analogy se koordinují k purinovým bázím nukleových kyselin (především ke guaninům přes N7) a vytváří v molekulách DNA různé typy kovalentních můstků - aduktů (obr. 3, 4), které svojí přítomností mění lokální strukturu DNA, její fyzikální vlastnosti a inhibují buněčné procesy, jako jsou replikace a transkripce, což v důsledku vede k zastavení buněčného cyklu a smrti buňky (obr. 5, 6).



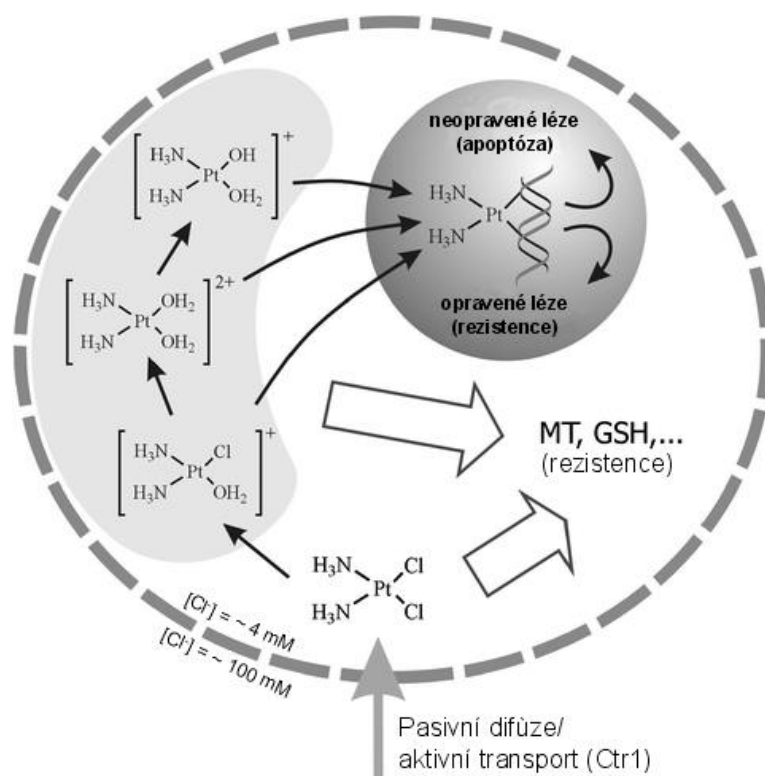
Obr. 3: Typy bifunkčních aduktů tvořených cisplatinou na DNA. 1,2-d(GpG) vnitrořetězcový můstek (a), 1,2-d(GG) meziřetězcový můstek (b), 1,2-d(ApG) vnitrořetězcový můstek (c), 1,3-d(GXG) nebo 1,4-d(GXXG) vnitrořetězcový můstek, kde X představuje libovolný nukleotid (d) a DNA-proteinový můstek (e). (adaptováno z [20], upraveno).

Nejfrekventovanějším typem aduktu je vnitrořetězcový můstek mezi dvěma sousedícími nukleotidy s purinovými zbytky. Mezi dvěma guaninovými zbytky (65%) a mezi jedním adeninovým a jedním guaninovým zbytkem ve směru 5'-3' (25%) [7, 21, 22, 23]. Tento typ poškození způsobuje rigidní ohyb DNA směrem do velkého žlábků (~35°) a rozvinutí dvoušroubovice o ~13 - 15°. Dochází také k narušení vodíkových vazeb mezi nukleotidy spojenými můstkem a jejich komplementárními nukleotidy v opačném řetězci a rozšíření malého žlábků [24, 25, 26]. Tato léze je navíc rozpoznávána celou řadou nukleárních proteinů včetně proteinů s **HMG** ("high mobility group") doménou, které hrají zřejmě jednu z klíčových rolí v mechanismu protinádorového efektu cisplatin [12, 27, 28, 29]. Tyto proteiny, konkrétně protein **HMGB1**, s vysokou afinitou k 1,2-d(GpG) vnitrořetězcovému můstku, jej "chrání" před rozpoznáním reparačními proteiny a odstraněním jadernými opravnými mechanismy. HMG proteiny jsou také důležitou součástí transkripčního mechanismu, kde hrají roli transkripčních faktorů [7, 30] a v případě vazby na adukt cisplatin mohou chybět v transkripčním procesu

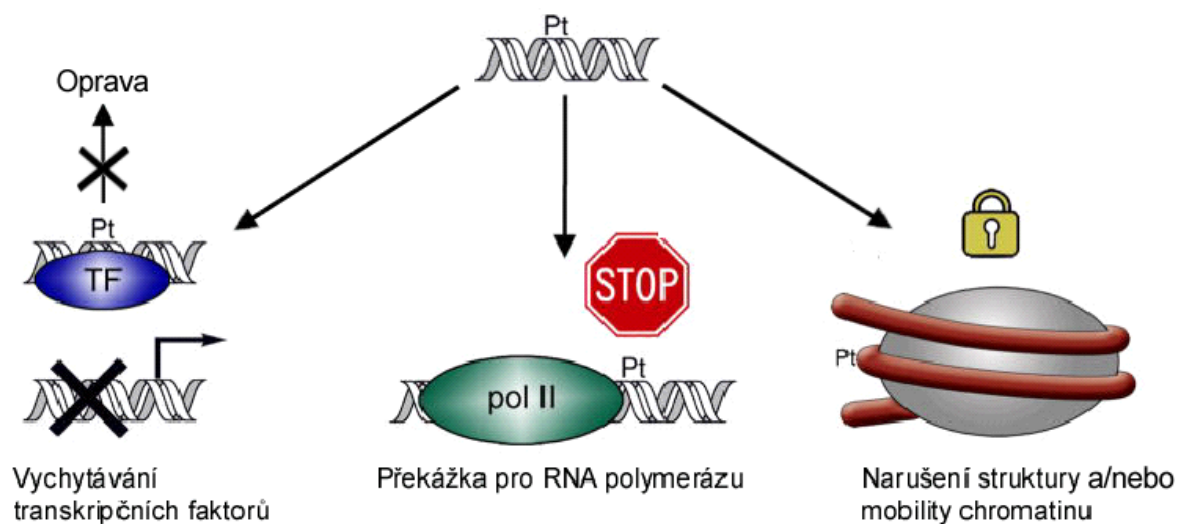
exprese genů, který tak mohou inhibovat (obr. 6). Uplatňují se i jako cytokiny - důležité regulátory buněčného cyklu [31]. Dalším významným typem poškození DNA je meziřetězcový můstek spojující dva guanidiny ve směru 5'-3' (6-8%) opačných řetězců molekuly DNA [32, 33]. Tento procentuálně minoritní typ aduktu způsobuje rozsáhlé poškození v místě modifikace: rozvinutí dvoušroubovice o $\sim 80^\circ$, ohyb do malého žlábků o $\sim 50^\circ$, zrušení vodíkových vazeb mezi modifikovanými guaniny a komplementárními cytosiny, které jsou navíc zcela vytlačeny z dvoušroubovice DNA. Ta v místě léze zaujímá konformaci podobnou levotočivé Z formě [34, 35]. Tento typ poškození je také rozpoznáván doménou B proteinu HMGB1 [36]. Meziřetězcový můstek nemůže být jednoduše odstraněn buněčným opravným systémem v podobě **NER** (nukleotidová excizní oprava), který se jinak přednostně uplatňuje při odstraňování vnítrořetězcových poškození DNA a hraje významnou roli v mechanismu rezistence nádorů k cisplatině a jejím analogům [7, 12, 28].



Obr. 4: Struktury nejvýznamnějších aduktů tvořených cisplatinou na DNA, získané pomocí NMR a rentgenové strukturní analýzy, hvězdičky označují modifikované báze (adaptováno z [37]).



Obr. 5: Celkové schéma aktivace a metabolizace cisplatiny v buňce (adaptováno z [20], upraveno); Ctr1(transportní protein pro Cu(II) kationty), MT (metallothionein), GSH (glutathion)



Obr. 6: Současná představa o protinádorovém působení cisplatiny a jejích derivátů. Role HMGB1 proteinu jako jednoho z transkripčních faktorů (TF) a mechanismus transkripční inhibice (převzato z [29] a upraveno).

O úspěšnosti komplexu rozhoduje jeho struktura - ligandové pole kolem centrálního atomu/atomů. Např. transplatina, strukturní izomer cisplatiny, kde se

nacházejí odstupující chloridové ligandy v poloze *trans*, nevykazuje protinádorovou aktivitu. Důvodem je především pomalé uzavírání bifunkčních můstků v jednom řetězci [38] a neschopnost vytvářet 1,2 vnitřetězcový můstek ze sterických důvodů. V případě záměny (modifikace) alespoň jednoho ligandu, které vede k vytvoření "stabilních" (z hlediska buněčného metabolismu) aduktů na DNA, dojde k dramatickému posunu v odezvě na takovéto poškození a vzniku cytotoxicity u nádorových buněčných linií. **Jen takový adukt, který výrazně ovlivňuje replikaci a transkripci a který nemůže být jednoduše opraven, vede k protinádorovému efektu.**

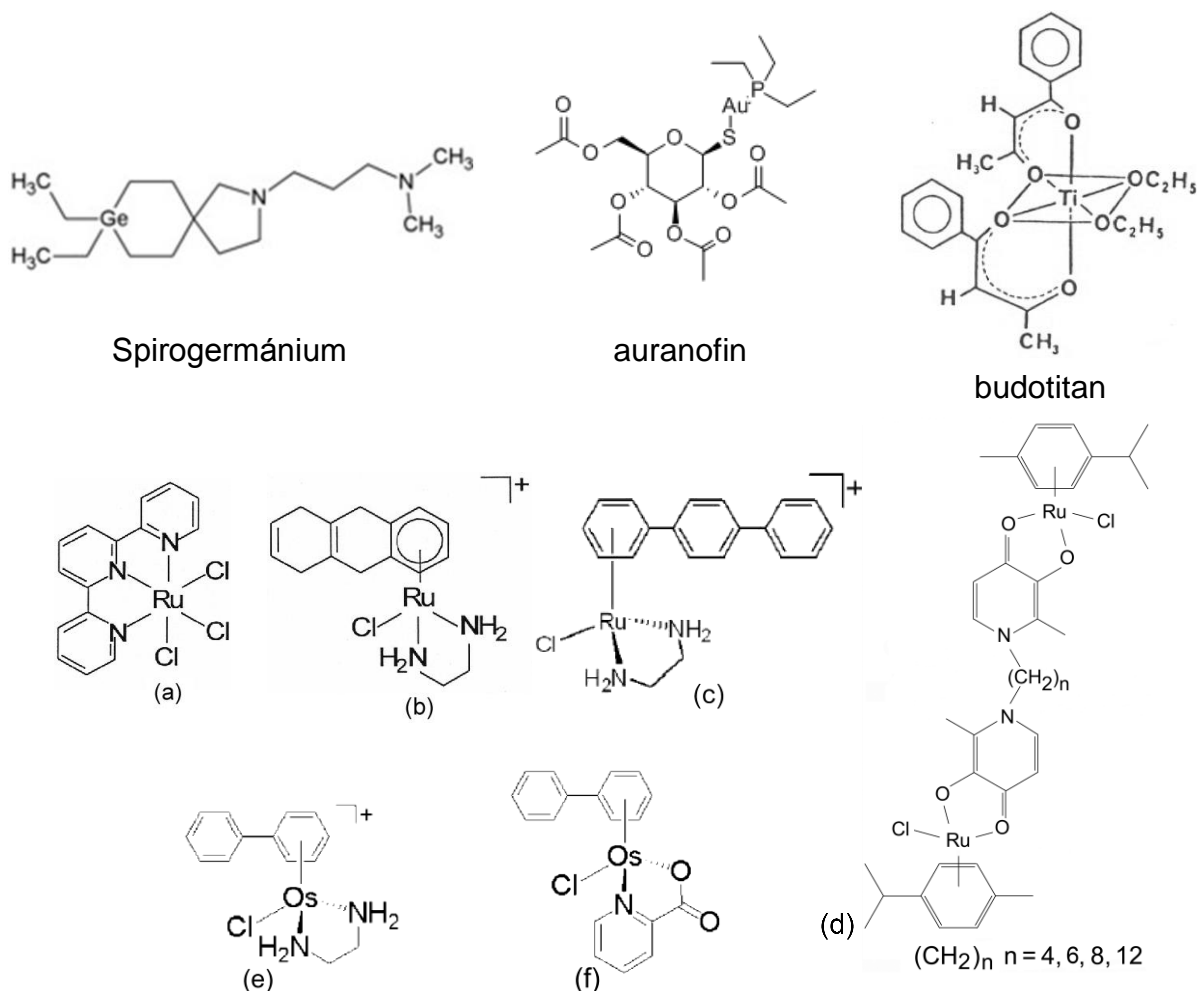
Na našem pracovišti dlouhodobě testovaná hypotéza, že strukturně odlišné komplexy, které vytvářejí na DNA jiný typ poškození než cisplatina a její přímé analogy způsobují také jiné biologické efekty, byla potvrzena molekulárně biofyzikálními a farmakologickými studiemi skupin nových "neklasických" platinových komplexů (obr. 2). U komplexů s *trans* geometrií odstupujících ligandů hovoříme o tzv. aktivaci *trans* geometrie [7, 9, 28, 39, 40, 41].

Vícejaderné platinové komplexy tvoří na DNA můstky dalekého dosahu, které jsou flexibilní nebo rigidní, ale rigidně neohýbají dvoušroubovici a nedoformují strukturu DNA a proto jsou špatně "viditelné" reparačními proteiny. Jejich kladný náboj jim pomáhá v transportu přes membránu pomocí transportérů organických kationtů. Monofunkční platinové komplexy se správnou geometrií a velikostí neodstupujících ligandů, mohou stericky bránit lidské RNA polymeráze II v transkripci a spouštět tak mechanismus transkripčně vázané opravy, který v důsledku vede ke smrti buňky [7, 29, 42].

Tetravalentní platinové komplexy umožňují orální podávání díky malé reaktivitě v čtyřmocném stavu (pomalá hydrolýza odstupujících ligandů), překonání získané rezistence v případě vazby oktaedrálního komplexu na DNA a redukce Pt(IV) komplexů na dvojmocné, čtvercově planární aktivní formy, dává také možnost jejich kombinace s dalšími biologicky aktivními molekulami, aby odstupujícími axiálními ligandy [2, 7, 43].

ad2) Příkladem takových komplexů mohou být sloučeniny řady přechodových kovů, jako germánia (spirogermánium), gália (dusičnan a chlorid galitý), titanu (budotitan), zlata (auranofin) a především dalších kovů platinové skupiny (obr.8) [1, 2, 7]. Čelní místo v této rozsáhlé skupině zaujímá ruthenium, jehož komplexy a

především interakce těchto komplexů s DNA, jsou významnou součástí habilitační práce autorky.

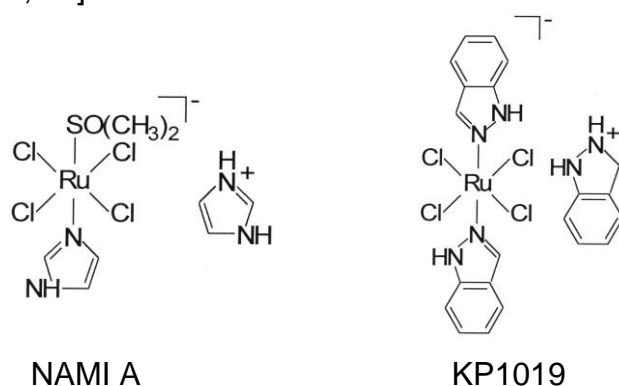


Obr. 8: Příklady chemických struktur neplatíkových kovových komplexů s biologickou aktivitou a struktur nových rutheniových a osmiových komplexů s protinádorovou účinností; *mer*-[Ru(II)Cl₃(terpy)] (a), [(η^6 -tetrahydroantracen) Ru(ethylenediamin)Cl]⁺(b), *para*-[(η^6 -terfenyl) Ru(ethylenediamin)Cl]⁺(c), dinukleární Ru arenové komplexy (d), [(η^6 -bifenyl) Os(ethylenediamin)Cl]⁺(e) a [(η^6 -bifenyl) Os(pikolinát)Cl] (f).

Výhody použití iontů přechodových kovů, jiných než platinových, obecně zahrnují:

- možnost dalších koordinačních míst v oktaedrálních komplexech a odlišný tvar komplexů
- odlišnou afinitu ligandů a substituční kinetiku
- změny oxidačního stupně
- možnost fotodynamické terapie

Využití ruthenia ve vývoji nové generace protinádorových preparátů je založeno především na vysoké afinitě rutheniových iontů k nádorové tkáni. Tato afinita je založena na chemické podobnosti atomů Ru a Fe a tedy podobnými vlastnostmi komplexů ruthenia(III) a železa(III), které je strategicky důležitým prvkem pro růst nádorové tkáně a váže se k řadě biologicky aktivních molekul. Je umocněna systémem netoxického transportu železa (pomocí transferinu, ferritinu) a citlivostí rutheniových komplexů k redukčnímu a oxidačnímu prostředí v buňkách nádorových a nenádorových [44, 45, 46]. Trojmocné rutheniové komplexy mohou působit jako "pre-agens", které se uvnitř hypoxických nádorových buněk aktivují na vysoce toxické dvojmocné analogy. Komplexy ruthenia interagují s DNA jak *in vitro*, tak *in vivo* a vytvářejí v ní adukty, které se od platinových liší díky jiné geometrii ligandů a velikosti komplexů [2, 47, 48]. Schopnost Ru komplexů vytvořit na DNA bifunkční a meziřetězcové adukty zvyšuje jejich cytotoxicitu [48, 49, 50]. Proti dvojmocným platinovým komplexům v klinickém použití nabízí komplexy ruthenia nízkou obecnou toxicitu, nový mechanismus účinku, překonání křížové rezistence a jiné spektrum citlivých nádorů [46, 48, 51, 52]. Z mnoha skupin studovaných Ru komplexů jsou vzhledem ke své protinádorové aktivitě zajímavé skupiny komplexů charakterizované dimethylsulfoxidovými (DMSO) a heterocyklickými dusíkatými ligandy (imidazol, indazol, pyridin, polypyridil aj.). Do těchto skupin také patří cytotoxický chloropolypyridilový komplex *mer*-[Ru(II)Cl₃(terpy)] (obr. 8) a oba zástupci klinicky testovaných komplexů, antimetastaticky působící NAMI A a KP1019, který je účinný v řadě nádorových linií a především v případě kolorektálního tumoru, rezistentního k cisplatině (obr. 9) [1, 8, 48, 53, 54].



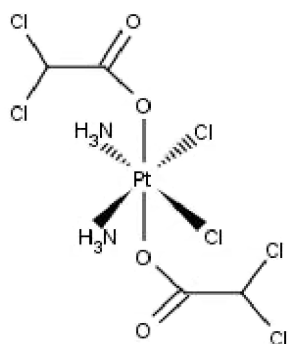
Obr. 9: Chemické struktury Ru(III) komplexů v pokročilých fázích klinického testování, NAMI A a KP1019.

Třetí skupinu představují rutheniové komplexy s arenovými ligandy, tzv. "piano-stool" strukturou $[(\eta^6\text{-aren})\text{Ru}(\text{N},\text{N}')(\text{L})]^+$ (obr. 8). Tyto organokovové Ru(II) komplexy reprezentují relativně novou skupinu rutheniových sloučenin s protinádorovou aktivitou a mechanismem účinku odlišným od Ru(III) komplexů NAMI A a KP1019, kde se uplatňují při potlačování nádorového bujení i interakce s transportními proteiny a oxidativní stres [2, 48]. Tyto mononukleární a dinukleární komplexy, po odstoupení chloridových ligandů během hydrolyzy, interagují preferenčně s N7 guaninu v dvoušroubovici DNA, která je také v tomto případě jejich farmakologickým cílovým místem působení [2, 48, 55]. Navíc interakce mezi DNA a komplexy s areny, jako bifenyl, terfenyl, dihydro- nebo tetrahydroantracen dovoluje jak koordinaci k N7 guaninu, tak nekovalentní hydrofobní interakci mezi arenovým ligandem a DNA, včetně interkalace a vazby do malého žlábků [48, 56, 57]. Duální vazebný mód se ukázal jako důležitý parametr umocňující protinádorovou účinnost mononukleárních arenových sloučenin [58, 59]. Polynukleární protinádorové rutheniové komplexy jsou skupinou mnohem méně probádanou ve srovnání s platinovými. Dinukleární arenové Ru komplexy, kde jsou spojeny dvě $\{(\eta^6\text{-p-isopropyltoluen})\text{RuCl}[\text{3-(oxo-}\kappa\text{O)-2-methyl-4-pyridinonato-}\kappa\text{O}_4]\}$ jednotky flexibilním uhlíkatým řetězcem různé délky $[(\text{CH}_2)_n \text{ (n = 4, 6, 8, 12)}]$ viz obr. 8, umožňují jak monofunkční vazbu, tak tvorbu vnitro i meziřetězcových můstků dalekého dosahu a ternární komplexy s proteiny, které se uplatňují při metabolizaci DNA. Unikátní vlastností je pak tvorba můstků mezi dvěma molekulami DNA. Rostoucí cytotoxicita na úrovni nádorových linií koreluje s délkou spojovacího alifatického řetězce a množstvím těchto vytvořených meziduplexových můstků [55]. Hydrofobní charakter, náboj, délka a flexibilita spojovacího linkeru, celkový náboj komplexu a geometrie odstupujících ligandů ovlivňují jak samotný transport do buněk, tak výsledný efekt na úrovni DNA a z něho vyplývajících následných biologických konsekvencí [55, 60].

ad3) V lidské krvi se nachází řada bílkovin, jejichž fyziologickou funkcí je transport kovových kationtů. Příkladem takových bílkovin je např. albumin, přenašeč pro ionty Cu(II), Zn(II) a Ca(II), makroglobulin, ceruloplasmin, transkobalamin a transferin, přenašeč trojmocného železa a manganu. V nádorových buňkách je díky jejich intenzivnímu metabolismu zapotřebí vysoká koncentrace železa a nesou na svém povrchu velké množství transferinových receptorů. Apotransferin

může do nádorové tkáně přenášet a uvolňovat kromě železa také protinádorové komplexy platiny(IV), již zmíněného Ru(III), titanu(IV) nebo Cu(II). Cytostatika se tak dostávají k nádorové tkáni navázána na aminokyselinové zbytky v kapse příslušného proteinu a dále endocytozou do nádorových buněk, kde dojde k jejich uvolnění. Tím se snižuje riziko toxických vedlejších účinků, způsobených nespecifickými interakcemi komplexů s biologicky aktivními molekulami v krvi a zvyšuje se koncentrace komplexů v aktivní formě v cílovém místě působení [61, 62, 63]. Selektivní transport aktivních platinových komplexů ve vysoké koncentraci do nádorové tkáně je filozofií nanočástic v podobě lipozomální enkapsulace komplexů - cisplatiny (Lipoplatin) a oxaliplatiny (Lipoxal). Aplikace nanočástic vede k dramatickému snížení vedlejších účinků a rozšířenému aktivnímu profilu včetně metastáz. Lipoplatin úspěšně absolvuje III. fázi klinického testování [64]. Selektivní transport Pt(IV) pre-agens, spojených nekovalentní vazbou s povrchem jedné rozpustné uhlíkové jednotěnné nanotrubičky (která pomocí klatrin-dependentní endocytózy dopraví v průměru 65 molekul komplexu léčiva do nádorové buňky) vede k výraznému zvýšení cytotoxicity konjugátu ve srovnání s cisplatinou nebo samotným Pt(IV) pre-agens [2, 65].

Spojení dvou látek s odlišnými biologickými vlastnostmi přímo do jedné molekuly, to je v současnosti myšlenka také rozvíjená ve skupině platinových cytostatik, kdy jsou syntetizovány platinové sloučeniny nesoucí jako ligandy např. inhibitory histonových deacetyláz (kyselina suberoylanilidhydroxamová - SAHA, kyselina valproová - VPA, aj.), regulátory buněčného cyklu (cytokininy), či látky ovlivňující metabolismus buňky (kyselina dichloroctová - DCA, estrogen, inhibitor GST-glutathion-S-transferázy) [43, 66, 67, 68]. Do této kategorie patří např. mitaplatina (obr.10), čtyřmocný Pt komplex, který vznikl spojením dvou molekul dichloroacetátu s molekulou cisplatiny. DCA je protinádorové činidlo, které může inhibovat glykolýzu. Metabolismus glykolýzy je propojený s rezistencí k apoptóze a



umožňuje přežití nádorových buněk. Negativní intracelulární redox potenciál nádorových buněk umožňuje redukci platinového komplexu na cisplatinu a dvě molekuly DCA. Mitaplatina ovlivňuje jadernou i mitochondriální DNA [69].

Obr. 10: Struktura mitaplatiny

ad4) Strategie např. fotochemické aktivace, umožňuje získat aktivní protinádorově účinné formy kovových sloučenin přímo v nádorové tkáni, po jejím ozáření. Vhodnými kandidáty takové fotochemické aktivace mohou být čtyřmocné platinové komplexy, které se jinak velmi pomalu spontánně redukují v buněčné cytoplazmě. Fotolabilní diammindiazidodihydroxyplatičitý komplex je ve tmě netoxický. Po jeho ozáření dochází k inhibici růstu nádorových buněk. Tyto komplexy nevykazují křížovou rezistenci s cisplatinou a liší se pravděpodobně způsobem, jakým dochází k jejich vazbě na DNA. Inkorporace pyridinového ligandu ještě zvyšuje jejich účinnost [2, 70]. Také klinicky neúčinná transplatina je po ozáření mnohem cytotoxičtější v buněčných nádorových liniích, v důsledku rychlého uzavírání bifunkčních můstků na DNA [38]. Byly nově syntetizovány také Ru(II) arenové komplexy z rodiny rutheniových komplexů s tzv. "piano-stool" strukturou $[(\eta^6\text{-aren})\text{Ru}(\text{N},\text{N}')(\text{L})][\text{PF}_6]_2$, kde monodentátní ligand (L) těchto komplexů může selektivně fotodisociovat po ozáření (excitaci) UVA nebo viditelným světlem. To umožňuje přesně řízený a kontrolovaný vznik reaktivních, hydrolyzovaných molekul komplexu, které ve tmě nevznikají. Vazebné studie s DNA ukázaly, že ozářené komplexy se na DNA váží a inhibují její transkripci, zatímco neozářené formy komplexů se na DNA váží jen zanedbatelně. *In vitro* studium interakcí mezi DNA a těmito Ru sloučeninami ukázalo jejich kombinovaný vazebný mód: slabou monofunkční koordinaci a interkalaci [71].

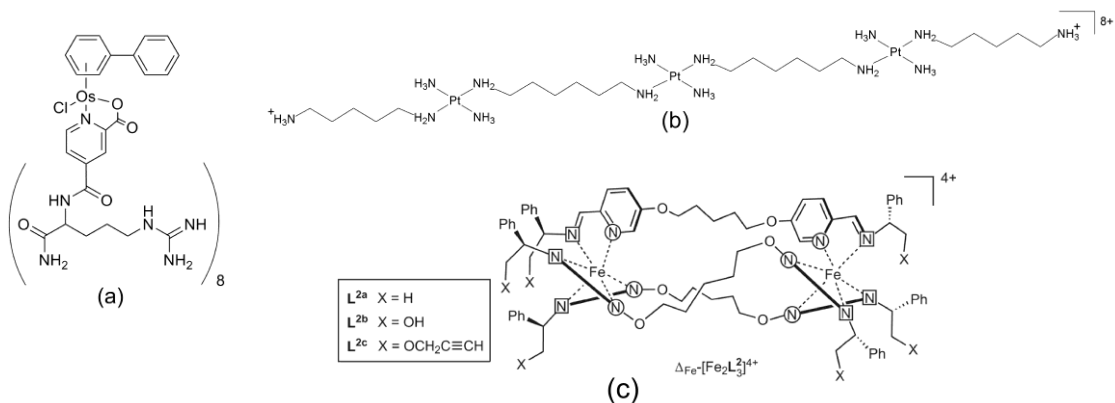
Nové strategie využití koordinačních sloučenin těžkých kovů v medicíně

Pohled na roli těžkých kovů, v syntéze nových účinných léčiv, se posouvá od představy kovu, jako reaktivního centra, k představě kovu v roli konstrukčního prvku-lešení při tvorbě třídimenzionálních struktur. Tento přístup supramolekulární chemie by měl vést k optimalizaci interakcí mezi léčivem a jeho pečlivě vybranou cílovou molekulou.

V případě DNA, jako cílové molekuly, se stále objevují nové zajímavé koordinační sloučeniny, např. arenové komplexy osmia a jejich peptidových konjugátů (obr. 8, 11). Přidáním peptidového řetězce došlo ke zlepšení biologické účinnosti tohoto komplexu a jeho schopnost kondenzovat DNA koreluje s jeho protinádorovým efektem na buněčné úrovni [72].

V centru pozornosti se objevují také nekovalentně se vážící komplexy, které interagují s DNA na základě hydrofobních interakcí, vodíkových vazeb,

elektrostatické interakce a tvaru. Mezi takové sloučeniny patří cytotoxická trinukleární Triplatina-NC (obr. 11), kterou její vysoký kladný náboj předurčuje jako efektivní kondenzační agens DNA [73] nebo dinukleární supramolekulární helikáty s Fe(II) nebo Ru(II) centrálními atomy. Tyto biologicky aktivní metalosupramolekulární komplexy se váží do velkého žlábků DNA a mohou se s vysokou afinitou vázat k neobvyklým strukturám DNA (tří- a čtyřcestné spojení, tetraplexy, vlásenky, výdutě apod.) [2, 74, 75, 76].



Obr. 11: Struktury peptidového konjugátu organokovového Os(II) protinádorového komplexu s polyargininovým řetězcem (a), TriplatinyNC (b) a metalo - supramolekulárního flexikátu (c).

Seznam použité literatury

- [1] Keppler, B. K. (ed.), *Metal Complexes in Cancer Chemotherapy*, VCH, Weinheim 1993.
- [2] Bruijninx, P. C. A., Sadler, P. J. (2008) *Curr. Op. Chem. Biol.* 12, 197.
- [3] Lissauer, (1865) *Berliner Klin. Woch.* 2, 403.
- [4] Collier, W. A., Krauss, F. (1931) *Zeitschrift fur Krebs.* 34, 527.
- [5] Rosenberg, B., VanCamp, L., Krigas, T. (1965) *Nature* 205, 698.
- [6] Rosenberg, B., VanCamp, L., Trosko, J. E., Mansour, V. H. (1969) *Nature* 222, 385.
- [7] Brabec, V. *Progress in Nucleic Acid Research and Molecular Biology*, Moldave, K. (ed.) San Diego/CA, Academic Press Inc. 2002, 71, 1.
- [8] Reedijk, J. (2003) *Proc. Natl. Acad. Sci. USA* 100, 3611.
- [9] Farrell, N. *Metal Ions in Biological Systems*, A. Sigel, A., Sigel, H. (eds.) New York, Basel, Marcel Dekker, Inc. 2004, 251.
- [10] Lovejoy, K. S., Serova, M., Bieche, I., Emami, S., D'Incalci, M., Broggin, M., Erba, E., Gespach, Ch., Cvitkovic, E., Faivre, S., Raymond, E., Lippard, S. J. (2011) *Mol. Cancer Ther.* 10, 1709.
- [11] Peyrone, M. (1844) *Ann. Chem. Pharm.* 51, 1.
- [12] Kelland, L. (2007) *Nature Reviews Cancer* 7, 573.
- [13] Brabec, V. (1990) *Biologické listy* 55, 42.

- [14] Johnson, N. P., Butour, J. L., Villani, G., Wimmer, F. L., Defais, M., Pierson, V., Brabec, V. (1989) *Progr. Clin. Biochem. Med.* 10, 1.
- [15] Pera, M. F., Zook, B. C., Harder, H. C. (1979) *Cancer Res.* 39, 1269.
- [16] Jung, Y., Lippard, S. J. (2007) *Chem. Rev.* 107, 1387.
- [17] Howle, J. A., Gale, G. R. (1970) *Biochem. Pharmacol.* 19, 2757.
- [18] Lepre, C. A., Chassot, L., Costello, C., Lippard, S. J. (1990) *Biochemistry* 29, 811.
- [19] Holler, E., *Metal Complexes in Cancer Chemotherapy*, Keppler, B. K. (ed.), VCH, Weinheim 1993, 40.
- [20] Esteban-Fernandez, D., Moreno-Gordaliza, E., Canas, B., Palacios, M. A., Gomez- Gomez, M. M. (2010) *Metallomics* 2,19.
- [21] Johnson, N. P., Mazard, J., Escalier, J., Macquet, J. P. (1985) *J. Am. Chem. Soc.* 107, 6376.
- [22] Eastman, A. (1987) *Pharmacol. Ther.* 34, 155.
- [23] Fichtinger-Schepman, A. M. J., van Oosterom, A. T., Lohman, P. H. M., Berends, F. (1987) *Cancer. Res.* 47, 3000.
- [24] Lippard, S. J. (1987) *Pure Appl. Chem.* 59, 731.
- [25] Sherman, S. Z., Lippard, S. J. (1987) *Chem. Rev.* 87, 1153.
- [26] Bellon, S. F., Coleman, J. H., Lippard, S. J. (1991) *Biochemistry* 30, 8026.
- [27] Pil, P. M., Lippard, S. J. (1992) *Science* 256, 234.
- [28] Brabec, V., Kasparkova, J. (2005) *Drug Resist. Updates* 8, 131.
- [29] Todd, R.C., Lippard, S.J. (2009) *Metallomics* 1, 280.
- [30] Lippard, S. J., *Bioinorganic chemistry*, Bertini, I., Gray, H. B., Lippard, S. J., Valentine, J. S. (eds.), Bioinorganic chemistry, U.S.A. 1994, 572.
- [31] Andersson, U., Erlandsson-Harris, H., Yang, H., Tracey, K. J. (2002) *J. Leukoc. Biol.* 72, 1084.
- [32] Jones, J. C., Zhen, W., Reed, E., Parker, R. J., Sancar, A., Bohr, V. A. (1991) *J. Biol. Chem.* 266, 7101.
- [33] Vrana, O., Boudny, V., Brabec, V. (1996) *Nucleic Acids Res.* 24, 3918.
- [34] Malinge, J. M., Giraud-Panis, M. J., Leng, M. (1999) *J. Inorg. Biochem.* 77, 23.
- [35] Coste, F., Malinge, J. M., Serre, L., Shepard, W., Roth, M., Leng, M., Zelwer, C. (1999) *Nucl. Acids Res.* 27, 1837.
- [36] Kasparkova, J., Delalande, O., Stros, M., Elizondo-Riojas, M. A., Vojtiskova, M., Kozelka, J., Brabec, V. (2003) *Biochemistry* 42, 1234.
- [37] Kartalou, M., Essigmann, J. M. (2001) *Mutation Res.* 478, 1.
- [38] Heringova, P., Woods, J., Mackay, F. S., Kasparkova, J., Sadler, P. J., Brabec, V. (2006) *J. Med. Chem.* 49, 7792.
- [39] Farrell, N. *Metal Ions in Biological Systems*, Sigel, A., Sigel, H. (eds.) Marcel Dekker, Inc., New York/Basel/Hong Kong 1996, 603.
- [40] Perez, J. M., Montero, E. I., Gonzalez, A. M., Solans, X., Font-Bardia, M., Fuertes, M. A., et al. (2000) *J. Med. Chem.* 43, 2411.
- [41] Natile, G., Coluccia, M. *Metal Ions in Biological Systems*, Sigel, A., Sigel, H. (eds.), Marcel Dekker, Inc., New York/Basel 2004, 209.
- [42] Park, G. Y., Wilson, J. J., Song, Y., Lippard, S. J. (2012) *Proc. Natl. Acad. Sci. USA* 109, 11987.
- [43] Barnes, K. R., Kutikov, A., Lippard, S. J. (2004) *Chem. Biol.* 11, 557.
- [44] Srivastava, S. C., Mausner, L. F., Clarke, M. J., *Progress in Clinical Biochemistry and Medicine - nonplatinum metal complexes in cancer chemotherapy*, Clarke, M. J. (ed.), Springer-Verlag, Berlin 1989, 111.
- [45] Clarke, M. J., *Progress in Clinical Biochemistry and Medicine-nonplatinum*

- metal complexes in cancer chemotherapy*, Clarke, M. J.(ed.), Springer-Verlag, Berlin 1989, 25.
- [46] Clarke, M. J. (2003) *Coord. Chem. Rev.* 236, 209.
 - [47] Yan, Y.K., Melchart, M., Habtemariam, A., Sadler, P.J. (2005) *Chem. Commun.*, 4764
 - [48] Brabec, V., Novakova, O. (2006) *Drug resist. updates* 9, 111.
 - [49] Novakova, O., Kasparkova, J., Vrana, O., van Vliet, P. M., Reedijk, J., Brabec, V. (1995) *Biochemistry* 34, 12369..
 - [50] Novakova, O., Hofr, C., Brabec, V. (2000) *Biochem Pharmacol* 60, 1761.
 - [51] Alessio, E., Mestroni, G., Bergamo, A., Sava, G. (2004) *Curr. Top. Med. Chem.* 4, 1525.
 - [52] Allardyce, C. S., Dyson, P. J. (2001). *Platinum Met. Rev.* 45, 62.
 - [53] Sava, G., and Bergamo, A. (2000) *Int J Oncol* 17, 353.
 - [54] Galanski, M., Arion, V. B., Jakupec, M. A., Keppler, B. K. (2003) *Curr. Pharm. Des.* 9, 2078.
 - [55] Novakova, O., Nazarov, A. A., Hartinger, Ch. G., Keppler, B. K., Brabec, V. (2009) *Biochem. Pharmacol.* 77, 364.
 - [56] Chen, H. M., Parkinson, J. A., Parsons, S., Coxall, R. A., Gould, R. O., Sadler, P. J. (2002) *J. Am. Chem. Soc.* 124, 3064.
 - [57] Novakova, O., Chen, H.M., Vrana, O., Rodger, A., Sadler, P.J., Brabec, V. (2003) *Biochemistry* 42, 11544.
 - [58] Novakova, O., Kasparkova, J., Bursova, V., Hofr, C., Vojtiskova, M., Chen, H.M., Sadler, P.J., Brabec, V. (2005) *Chemistry & Biology* 12, 121.
 - [59] Bugarcic, T., Novakova, O., Halamikova, A., Zerzankova, L., Vrana, O., Kasparkova, J., Habtemariam, A., Parsons, S., Sadler, P.J., Brabec, V. (2008) *J. Med. Chem.* 51, 5310.
 - [60] Mendoza-Ferri, M. G., Hartinger, Ch. G., Eichinger, R. E., Stolyarova, N., Severin, K., Jakupec, M. A., Nazarov, A. A., Keppler, B. K. (2008) *Organometallics* 27, 2405.
 - [61] Keppler, B. K., Lipponer, K. G., Stenzel, B., Kratz, F., *Metal Complexes in Cancer Chemotherapy*, Keppler, B. K. (ed), VCH Weinheim 1993, 189.
 - [62] Kratz, F., *Metal Complexes in Cancer Chemotherapy*, Keppler, B. K. (ed.), VCH, Weinheim 1993, 404.
 - [63] Bertini, I., Gray, H. B., Lippard, S. J., Valentine, J. S. (eds.), *Bioinorganic chemistry*, U.S.A. 1994
 - [64] Boulikas, T., Pantos, A., Bellis, E., Christofis, P. (2007) *Cancer Ther.* 5, 537.
 - [65] Feazell, R. P., Nakayama-Ratchford, N., Dai, H., Lippard, S. J. (2007) *J. Am. Chem. Soc.* 129, 8438.
 - [66] Ang, W.H., Khalaila, I., Allardyce, C. S., Juillerat-Jeanneret, L., Dyson, P. J. (2005) *J. Am. Chem. Soc.* 127, 1382.
 - [67] Travnicek, Z., Popa, I., Cajan, M., Zboril, R., Krystof, V., Mikulik, J. (2010) *J. Inorg. Biochem.* 104, 405.
 - [68] Griffith, D., Morgan, M. P., Marmion, C. J. (2009) *Chem. Commun.*, 6735.
 - [69] Dhar, S., Lippard, S.J. (2009) *Proc. Natl. Acad. Sci. USA* 106, 22199.
 - [70] Mackay, F. S. , Woods, J. A., Heringova, P., Kasparkova, J., Pizarro, A. M., Moggach, S. A., Parsons, S., Brabec, V., Sadler, P. J. (2007) *Proc. Natl. Acad. Sci. USA* 104, 20743.
 - [71] Betanzos-Lara, S., Novakova, O., Deeth, R. J., Pizarro, A. M., Clarkson, G. J., Liskova, B., Brabec, V., Sadler, P. J., Habtemariam, A. (2012) *J. Biol. Inorg. Chem.* 17, 1033.

- [72] Van Rijt, S.H., Kostrhunova, H., Brabec, V., Sadler, P.J. (2011) *Bioconjugate Chem.* 22, 218.
- [73] Komeda, S., Moulaei, T., Chikuma, M., Odani, A., Kipping, R., Farrell, N.P., Williams, L.D. (2011) *Nucl. Acids Res.* 39, 325.
- [74] Hannon, M.J. (2007) *Chem. Soc. Rev.* 36, 280.
- [75] Malina, J., Hannon, M.J., Brabec, V. (2008) *Nucl. Acids Res.* 36, 3630.
- [76] Howson, S.E., Bolhuis, A., Brabec, V., Clarkson, G.J., Malina, J., Rodger, A., Scott, P. (2012) *Nature Chemistry* 4, 31.

II. Shrnutí vybraných významných výsledků autorky, které jsou také obsahem publikací tvořících hlavní část habilitační práce

- Výměna NH_3 ligandů neúčinné transplatiny (*trans* - $[\text{PtCl}_2(\text{NH}_3)_2]$) za iminoether vede k významnému nárůstu cytotoxicity tohoto komplexu. *trans* - $[\text{PtCl}_2(E\text{-iminoether})_2]$ tvoří na DNA převážně monofunkční adukty vazbou na guaniny. Metodami molekulární biofyziky byla zjištěna lokální distorze DNA v místě aduktu a ohyb dvoušroubovice o 21° do malého žlábků. Léze není rozpoznávána proteinem HMGB1 a je snadno odstraněna NER (mechanismus nukleotidové excizní opravy). Monofunkční adukty *trans* - $[\text{PtCl}_2(E\text{-iminoether})_2]$ ovšem tvoří snadno ternární komplexy s nukleárními proteiny. Tyto ternární komplexy účinně zastavují polymerizaci DNA DNA polymerázami *in vitro* a inhibují odstranění tohoto aduktu z DNA pomocí NER. Komplex *trans* - $[\text{PtCl}_2(E\text{-iminoether})_2]$ je představitelem nové třídy platinových protinádorových komplexů, kde aktivace *trans* geometrie souvisí s možností vytvořit DNA-Pt-protein ternární můstek. (práce č. 19)

- Schopnost Ru komplexů *trans*- $[\text{Cl}_2(\text{Me}_2\text{SO})_4\text{Ru}]$, *mer*- $[\text{Ru(III)Cl}_3(\text{terpy})]$ a dinukleárních arenových komplexů vytvořit na DNA bifunkční adukty a zejména pak meziřetězcové můstky, zvyšuje jejich biologickou účinnost. V případě komplexu *mer*- $[\text{Ru(III)Cl}_3(\text{terpy})]$ koreluje schopnost tvořit meziřetězcové můstky přímo s jeho cytotoxicitou. (práce č. 13, 18, 24, 25)

- Mononukleární rutheniové arenové komplexy s obecnou strukturou $[(\eta^6\text{-aren})\text{Ru}(\text{ethyldiamin})\text{Cl}]^+$ interagují v dvoušroubovici DNA preferenčně s guaninem. DNA je pravděpodobným cílovým místem jejich farmakologického působení. Interakce mezi DNA a monofunkčními Ru komplexy s areny, jako *p*-terfenyl nebo tetrahydroantracen, dovoluje jak koordinaci k N7 guaninu, tak nekovalentní hydrofobní interakci mezi arenovým ligandem a DNA - interkalaci. Duální vazebný mód se ukázal jako důležitý parametr umocňující protinádorovou účinnost mononukleárních arenových sloučenin. Malá termodynamická destabilizace DNA v místě vazby komplexů koreluje s malou strukturní distorzí. Tyto léze účinně inhibují DNA dependentní DNA i RNA polymerázy, ale nejsou rozpoznány

opravnými proteiny NER a celková reparační syntéza je velmi malá. (práce č. 6, 9, 17, 21)

- Dinukleární arenové Ru komplexy, kde dvě jednotky $\{(\eta^6\text{-p-isopropyltoluen})\text{RuCl}[\text{3-(oxo-}\kappa\text{O)-2-methyl-4-pyridinonato-}\kappa\text{O}_4]\}$ spojuje flexibilní alifatický řetězec různé délky $[(\text{CH}_2)_n \text{ (n = 4, 6, 8, 12)}]$, umožňují jak monofunkční vazbu, tak tvorbu vnitro i meziřetězcových můstků dalekého dosahu a ternární komplexy s proteiny, které se uplatňují při metabolizaci DNA. Unikátní vlastností je pak tvorba můstků mezi dvěma molekulami DNA. Rostoucí cytotoxicita na úrovni nádorových linií koreluje s délkou spojovacího uhlíkového řetězce a s množstvím těchto vytvořených meziduplexových můstků. (práce č. 8)

- Fotoaktivace rutheniových arenových komplexů UV-A nebo viditelným světlem, umožňuje účinnější vazbu těchto látek na DNA a tvorbu lézí, které inhibují proces transkripce *in vitro*. Fotoaktivace dinukleárního Ru(II) arenového komplexu $[(\eta^6\text{-indan})\text{RuCl}]_2[\mu\text{-2,3-bis(2-pyridyl)pyrazine}](\text{PF}_6)_2$ vede k tvorbě vysoce reaktivních rutheniových sloučenin, které se účinně váží na DNA a fluorescentních značek v podobě volného arenu (indanu). Fotoreaktivní mechanismus není závislý na kyslíku, což umožňuje využít tento komplex jak k fotoindukci buněčné smrti, tak fluorescenční vizualizaci místa jeho působení a účinnosti fotoaktivačního procesu. (práce č. 3, 13)

- Vícenásobné methylace ligandu monofunkčního komplexu protinádorově neaktivní dienplatiny $[\text{PtCl}(\text{diethylentriamin})]^+$ významně ovlivňují rané fáze projevů biologické aktivity platinových cytostatik, tj. procesy spojené s vazbou na DNA. Biofyzikální vlastnosti DNA (termodynamické, termální a konformační) a biochemické procesy (polymerizace DNA, transkripce a oprava aduktů) jsou těmito analogy s objemnějšími methylovanými ligandy značně ovlivněny. S rostoucím počtem CH_3 skupin analogů dienplatiny roste jejich schopnost inhibovat DNA dependentní DNA i RNA polymerázy. Míra této inhibice je závislá na sekvenci nukleotidů v okolí modifikace a charakteru léze. S počtem CH_3 skupin platnatých komplexů se zvyšuje reaktivita chemických sond na modifikovaných duplexech ve všech studovaných sekvencích, ale termodynamická destabilizace

modifikovaného duplexu methylovanými komplexy je téměř totožná. Tyto experimentální výsledky jsou ve shodě s dalšími charakteristikami interakce methylovaných monofunkčních komplexů s DNA, jako je například reparační syntéza, kde jsou účinně opravovány pouze adukty methylovaných analogů dienplatiny, zatímco adukty dienplatiny nejsou rozpoznány a tedy ani opravovány. (práce č. 7)

- Derivát cisplatiny *cis*-[Pt(boh)₂Cl₂], kde jako neodstupující ligandy figurují dvě molekuly boheminu - [2-(3-hydroxypropylamino)-6-benzylamino-9-isopropylpurinu], syntetického inhibitoru cyklin-dependentních kináz (CDK), ukázal zajímavé protinádorové účinky zejména v buněčných liniích rezistentních k cisplatině. Přestože se nepotvrdila možnost duálního působení Pt(II) komplexu a CDK jím *in vitro* nebyly inhibovány, celkový profil protinádorového působení se od cisplatiny lišil na úrovni regulace buněčného cyklu, rychlosti a mechanismu buněčné smrti. Tento derivát je mnohem účinnější ve vyvolání apoptózy a/nebo nekrózy než cisplatina. Proniká účinněji do buněk a modifikuje účinněji také DNA, která je cílovou molekulou jejího protinádorového efektu. V cytosolu je pomaleji inaktivován vazbou na glutathion a jeho objemné adukty na DNA efektivně inhibují RNA polymerázy. (práce č. 4 a práce **Nováková, O.**, Lišková, B., Vystrčilová, J., Suchánková, T., Vrána, O., Štarha, P., Trávníček, Z., Brabec, V. (2014) Conformation and recognition of DNA damaged by antitumor cis-dichlorido platinum(II) complex of CDK inhibitor bohemine. *Eur. J. Med. Chem.*, 78, 54 - 64)

III. Seznam publikovaných vědeckých prací, které jsou v plném znění součástí této habilitační práce

1. Betanzos-Lara, S., **Novakova, O.**, Deeth, R. J., Pizarro, A. M., Clarkson, G. J., Liskova, B., Brabec, V., Sadler, P. J., Habtemariam, A. (2012) Bipyrimidine Ruthenium(II) Arene Complexes: Structure, Reactivity and Cytotoxicity. *J. Biol. Inorg. Chem.*, 17, 1033 - 1051.
2. Malina, J., **Novakova, O.**, Natile, G., Brabec, V. (2012) The Thermodynamics of Translesion DNA Synthesis Past Major Adducts of Enantiomeric Analogues of Antitumor Cisplatin. *Chem. Asian J.*, 7, 1026 - 1031.
3. Betanzos-Lara, S., Salassa, L., Habtemariam, A., **Novakova, O.**, Pizarro, A. M., Clarkson, G. J., Liskova, B., Brabec, V., Sadler, P. J. (2012) Photoactivatable Organometallic Pyridyl Ruthenium(II) Arene Complexes. *Organometallics*, 31, 3466 - 3479.
4. Liskova, B., Zerzankova, L., **Novakova, O.**, Kosthunova, H., Travnicek, Z., Brabec, V. (2012) Cellular Response to Antitumor cis Dichlorido Platinum(II) Complexes of CDK Inhibitor Bohemine and Its Analogues. *Chem. Res. Toxicol.*, 25, 500 - 509.
5. Triantafillidi, K., Karidi, K., **Novakova, O.**, Malina, J., Garoufis, A. (2011) DNA binding selectivity of oligopyridine-ruthenium(II)-lysine conjugate. *Dalton Trans.*, 40, 472 - 483.
6. **Novakova, O.**, Malina, J., Suchankova, T., Kasparkova, J., Bugarcic, T., Sadler, P.J., Brabec, V. (2010) Energetics, Conformation, and Recognition of DNA Duplexes Modified by Monodentate Ru^{II} Complexes Containing Terphenyl Arenes. *Chem. Eur. J.*, 16, 5744 - 5754.
7. **Novakova, O.**, Malina, J., Kasparkova, J., Halamikova, A., Bernard, V., Intini, F., Natile, G., Brabec, V. (2009) Energetics, Conformation, and Recognition of DNA Duplexes Modified by Methylated Analogues of [PtCl(dien)]⁺. *Chem. Eur. J.*, 15, 6211 – 6221.
8. **Novakova, O.**, Nazarov, A.A., Hartinger, Ch.G., Keppler, B.K., Brabec, V. (2009) DNA interactions of dinuclear Ru^{II} arene antitumor complexes in cell-free media. *Biochem. Pharmacol.*, 77, 364-374.
9. Bugarcic, T., **Novakova, O.**, Halamikova, A., Zerzankova, L., Vrana, O., Kasparkova, J., Habtemariam, A., Parsons, S., Sadler, P.J., Brabec, V. (2008) Cytotoxicity, cellular uptake, and DNA interactions of new monodentate ruthenium(II) complexes containing terphenyl arenes. *J. Med. Chem.*, 51, 5310-5319.
10. Kosthunova, H., Florian, J., **Novakova, O.**, Peacock, A.F.A., Sadler, P.J., Brabec, V. (2008) DNA interactions of monofunctional organometallic

- osmium(II) antitumor complexes in cell-free media. *J. Med. Chem.*, 51, 3635-3643.
11. Malina, J., **Novakova, O.**, Vojtiskova, M., Natile, G. and Brabec, V. (2007) Conformation of DNA GG intrastrand cross-link of antitumor oxaliplatin and its enantiomeric analog. *Biophys. J.*, 93, 3950-3962.
 12. Melchart, M., Habtemariam, A., **Novakova, O.**, Moggach, S.A., Fabbiani, F.P.A., Parsons, S., Brabec, V., Sadler, P.J. (2007) Bifunctional amine-tethered Ruthenium(II) arene complexes form monofunctional adducts on DNA. *Inorg. Chem.*, 46, 8950-8962.
 13. Magennis, S.W., Habtemariam, A., **Novakova, O.**, Henry, J.B., Meier, S., Parsons, S., Oswald, I.D. H., Brabec, V., Sadler, P.J. (2007) Dual triggering of DNA binding and fluorescence via photoactivation of a dinuclear ruthenium(II) arene complex. *Inorg. Chem.*, 46, 5059-5068.
 14. Moriarity, B., **Novakova, O.**, Farrell, N., Brabec, V. and Kasparkova, J. (2007) 1,2-GG intrastrand cross-link of antitumor dinuclear bifunctional platinum compound with spermidine linker inhibits DNA polymerization more effectively than the cross-link of conventional cisplatin. *Arch. Biochem. Biophys.*, 459, 264-272.
 15. Brabec, V. and **Novakova, O.** (2006) DNA binding mode of ruthenium complexes and relationship to tumor cell toxicity. *Drug Resist. Updates*, 9, 111-122.
 16. Marini, V., Christofis, P., **Novakova, O.**, Kasparkova, J., Farrell, N., Brabec, V. (2005) Conformation, protein recognition and repair of DNA interstrand and intrastrand cross-links of antitumor trans-[PtCl₂(NH₃)(thiazole)]. *Nucleic Acids Res.*, 33, 5819-5828.
 17. **Novakova, O.**, Kasparkova, J., Bursova, V., Hofr, C., Vojtiskova, M., Chen, H.M., Sadler, P.J., Brabec, V. (2005) Conformation of DNA modified by monofunctional Ru(II) arene complexes: Recognition by DNA binding proteins and repair. Relationship to cytotoxicity. *Chemistry & Biology*, 12, 121-129.
 18. Chen, H.M., Parkinson, J.A., **Novakova, O.**, Bella, J., Wang, F.Y., Dawson, A., Gould, R., Parsons S., Brabec, V., Sadler, P.J. (2003) Induced-fit recognition of DNA by organometallic complexes with dynamic stereogenic centers. *P. Natl. Acad. Sci. USA*, 100, 14623-14628.
 19. **Novakova, O.**, Kasparkova, J., Malina, J., Natile, G., Brabec, V. (2003) DNA-protein cross-linking by trans-[PtCl₂(E-iminoether)₂]. A concept for activation of the trans geometry in platinum antitumor complexes. *Nucleic Acids Res.*, 31, 6450-6460.
 20. Kasparkova, J., **Novakova, O.**, Marini, V., Najajreh, Y., Gibson, D., Perez, J.M., Brabec, V. (2003) Activation of trans geometry in bifunctional mononuclear platinum complexes by a piperidine ligand - Mechanistic studies on antitumor action. *J. Biol. Chem.*, 278, 47516-47525.

21. **Novakova, O.**, Chen, H.M., Vrana, O., Rodger, A., Sadler, P.J., Brabec, V. (2003) DNA interactions of monofunctional organometallic ruthenium(II) antitumor complexes in cell-free media. *Biochemistry*, 42, 11544-11554.
22. Kasparkova, J., **Novakova, O.**, Farrell, N., Brabec, V. (2003) DNA binding by antitumor *trans*-[PtCl₂(NH₃)(thiazole)]. Protein recognition and nucleotide excision repair of monofunctional adducts. *Biochemistry*, 42, 792-800.
23. Malina, J., **Novakova, O.**, Keppler, B.K., Alessio, E., Brabec, V. (2001) Biophysical analysis of natural, double-helical DNA modified by anticancer heterocyclic complexes of ruthenium(III) in cell-free media . *J. Biol. Inorg.Chem.*, 6, 435-445.
24. **Novakova, O.**, Hofr, C., Brabec, V. (2000) Modification of natural, double-helical DNA by antitumor *cis*- and *trans*-[Cl₂(Me₂SO)₄Ru] in cell-free media. *Biochem.Pharmacol.*, 60, 1761-1771.
25. **Novakova, O.**, Kasparkova, J., Vrana, van Vliet, P. M., Reedijk, J., Brabec, V. (1995) Correlation between Cytotoxicity and DNA Binding of Polypyridyl Ruthenium Complexes. *Biochemistry*, 34, 6781-6790.

IV. Metodický komentář

Vybrané metody biofyzikální analýzy, které byly využity autorkou této habilitační práce k charakterizaci interakcí DNA s koordinačními komplexy těžkých kovů (Pt, Ru a Os).

Při studiu mechanismu působení potenciálních cytostatik v podobě sloučenin těžkých kovů, hrají interakce těchto kovových komplexů s DNA velmi důležitou a u řady z nich přímo klíčovou roli (DNA je cílovým místem jejich farmakologického působení). Škála metod a technik, pomocí kterých je možno sledovat a vyhodnotit vazbu těchto komplexů na DNA, změny ve struktuře modifikované DNA a tím přispět k porozumění biologických souvislostí mezi vazbou a farmakologickou aktivitou, je velmi široká.

Mezi metody, využívané v naší laboratoři k charakterizaci **vlastní vazby** komplexů na DNA patří elektronová absorpční spektrofotometrie (EAS), bezplamenná atomová absorpční spektrometrie (FAAS či ET AAS), vysokoúčinná kapalinová chromatografie (HPLC, FPLC), polarografie (DPP - diferenční pulzní polarografie, dialýza, gelová filtrace a srážení DNA pomocí ethanolu (EtOH). **Důsledky této vazby**, které se projevují **změnami ve vlastnostech a struktuře** DNA byly studovány opět celou řadou metod, mezi které patří metody elektroforetické (ELFO) v nativním i denaturačním gelu, DPP, fluorometrie, měření cirkulárního a lineárního dichroismu (CD, LD), sledování teploty tání (T_m) DNA pomocí EAS, mikrokolorimetrie a biochemické a molekulárně biologické metody, jako transkripční mapování – inhibice transkripce, inhibice restrikčních endonukleáz, inhibice DNA dependentních DNA polymeráz. K případným „**biologickým souvislostem**“ pak přispívá také studium opravných procesů v buněčných (jaderných) extraktech i interakce jednotlivých proteinů, které se podílejí jak na opravě DNA, tak vystupují v roli transkripčních faktorů.

Vazba (rychlost, stechiometrie a charakter) studovaných koordinačních komplexů kovů na DNA v bezbuněčném prostředí probíhala v závislosti na možném typu vazby (kovalentní (koordinační) – monofunkční, bifunkční, polyfunkční,

elektrostatická, interkalační a kombinovaná), stupni hydrolýzy komplexu (počtu odstupujících skupin) a reakčním médiu. Proto bylo třeba znát základní vlastnosti studovaných kovových komplexů, tj. chemickou strukturu, stabilitu komplexů, rozpustnost a stabilitu ve vodném prostředí a pH (případně lipofilicitu), rychlost hydrolýzy či výměny ligandů. Tyto parametry byly pro nové komplexy většinou naměřeny v laboratořích kolegů autorky habilitační práce. Pokud tomu tak nebylo, bylo třeba se charakterizací samotných komplexů zabývat ještě před zahájením vlastních experimentů na úrovni DNA, protože neznalost těchto parametrů by mohla vést k zavádějícím výsledkům. Např. v případě komplexů s omezenou rozpustností ve vodném prostředí může docházet k jejich „vypadávání“ z roztoku v průběhu času a/nebo teploty, což mění jejich vstupní koncentraci a tím i množství navázaného komplexu na DNA, či množství v buňkách (např. práce č. 4). Některé komplexy, především nabitě organokovové komplexy ruthenia nebo komplexy platiny s aromatickými organickými neodstupujícími ligandy, měly tendenci se adsorbovat na povrch plastových nádobek (jako důsledek hydrofobních a elektrostatických interakcí) nebo „vnikaly“ do mikropórů ve skle, což opět vedlo ke komplikacím při kvantifikaci vazby a měření koncentrací volného komplexu metodou FAAS a DPP. **Atomová absorpční spektroskopie** je analytická metoda, která je široce rozšířena v biologicky orientovaném výzkumu i technických oborech a umožňuje kvantitativní stanovení většiny chemických prvků periodické tabulky, především kovů. Princip metody spočívá v absorpci záření v podobě světla určité vlnové délky, charakteristické pro měřený prvek, volnými atomy příslušného prvku v plynném stavu (atomizovaném). V případě elektrotermální, bezplamenné AAS byl kapalný vzorek obsahující studovaný komplex atomizován v grafitové kyvetě, kde dochází v teplotnímu gradientu postupně k jeho vysušení, pyrolýze a atomizaci. Kyveta je vyhřívána a chlazena elektricky. V případě FAAS většiny studovaných komplexů této habilitační práce se osvědčil přídavek malého množství „dlouhovláknové“ DNA z telecího brzlíku (1-10 $\mu\text{g/ml}$) ke vzorku měřeného komplexu kovu. DNA zde funguje jako polyaniont a zároveň organický polymer. Další možností byla změna polárnosti prostředí přídavkem polárního organického rozpouštědla (EtOH) na výslednou koncentraci alkoholu 50 - 60% v/v. Vyšší koncentrace EtOH vede k odpařování vzorku a změnám viskozity (jako v případě přídavků DNA), které ovlivňují koncentraci a

dávkování vzorků do grafitové cely. Přítomnost vyšších koncentrací DNA pak také přímo ovlivňovala atomizační proces a projevila se jako vliv matrice.

Měření **elektronových absorpčních spekter** patří mezi základní výzkumné metody přírodovědných disciplín. Poskytuje informace o elektronové struktuře molekul, jejich vzájemných interakcích a konformačních vlastnostech a změnách. V přiložených publikacích habilitační práce byla EAS rutinně využívána při sledování roztoků samotných kovových komplexů (stabilita, hydrolýza, změna oxidačního stupně (práce č. 25)) a měření jejich koncentrace, měření koncentrace DNA, „dlouhovláknové“, plasmidové a oligonukleotidů se specifickými sekvencemi. Její hlavní experimentální přínos tkvěl ve sledování vazby komplexů na DNA jak z hlediska vazebné kinetiky a úrovně modifikace, tak z hlediska strukturního. Touto metodou byly sledovány změny teploty tání sekundární struktury DNA po modifikaci studovanými komplexy (práce č. 3, 5, 9, 10, 12, 21, 23). Závislost absorbance při 260 nm na teplotě má tvar sigmoidní křivky. Tání dvouřetězcové (ds) DNA vlivem rostoucí teploty je kooperativní proces a **hodnota T_m** představuje teplotu, kdy přejde polovina molekul DNA z ds formy na jednořetězcovou (denaturovanou) (ss) formu v důsledku zrušení vodíkových vazeb mezi komplementárními bázemi. Tento přechod je doprovázen nárůstem absorbance (optické hustoty-OD) v důsledku zrušení hypochromního efektu paralelního uspořádání skupin chromoforů (bází DNA). Tento proces je závislý na kvalitativním stavu ds DNA, pH, složení DNA co do obsahu G-C párů a především na iontové síle (koncentraci Na^+ iontů) v roztoku DNA. Dvouřetězcová struktura DNA se záporně nabitými fosfátovými skupinami je stabilizována kladnými náboji jak média, tak navázaného tj. kladně nabitého studovaného komplexu. Vazba komplexu však zároveň vyvolávala ve struktuře DNA změny – poškození, distorze, které dvoušroubovici DNA destabilizovaly. Výsledný efekt v podobě změny T_m odrážel převažující charakter vazby daného komplexu. Měření T_m při vysoké iontové síle sice zvyšovalo tuto hodnotu pro nemodifikovanou DNA, ale zároveň nám umožnilo „odstínit“ stabilizační příspěvek navázaného komplexu a tak zjistit velikost destabilizace, kterou komplex svojí vazbou způsobil [1]. Specifickým případem je vytvoření kovalentního meziřetězcového můstku mezi studovaným komplexem a DNA, kdy v jeho důsledku nemohou řetězce plně denaturovat a T_m zůstává vysoké i přes značné konformační (denaturační) změny ve struktuře DNA.

Zda se jedná o meziřetězcovou vazbu, interkalaci nebo neodstíněný vliv stabilizujícího kladného náboje komplexu se dá experimentálně potvrdit měřením renaturační křivky nebo jinými metodami (ELFO za denaturačních podmínek).

Na rozdíl od metody FAAS, kterou bylo možno použít pouze ke kvantifikaci volných nebo vázaných studovaných komplexů, metoda **diferenční pulzní polarografie** umožňuje navíc studie strukturních změn v molekule DNA. Polarografie je elektrochemickou analytickou metodou, při které je sledována závislost proudu na napětí vkládaném na článek, sestavený z jedné polarizovatelné (rtuťové kapkové) a jedné nepolarizovatelné elektrody, ponořené do analyzovaného roztoku. V případě diferenční pulzní polarografie se na rovnoměrně rostoucí stejnosměrné polarizační napětí superponují pravoúhlé napěťové pulzy. Proud je měřen před vložením pulzu a ke konci doby pulzu, registrován je rozdíl těchto proudů. Záznam má tvar maxima (peaku), jedná se přibližně o derivaci klasické polarografické vlny. Intaktní ds DNA je polarograficky neaktivní, protože redukční místa v podobě bází adeninu nebo cytosinu jsou „ukryta“ uvnitř duplexu a „řádně“ spárována vodíkovými vazbami. K redukčnímu ději na povrchu pracovní rtuťové kapkové elektrody proto nedochází. Destabilizace ds DNA, „rozvolnění“ vodíkových vazeb - tzv. nedenaturační změny, se projeví vznikem malého signálu v záporné oblasti potenciálů (~ -1.36 V vs. SCE - standardní kalomelové elektrodě), označeného jako peak II. Denaturační změny spojené se zrušením vodíkových vazeb vedou ke vzniku dalšího polarografického signálu, který se objevuje při zápornější hodnotě potenciálu než peak II (~ -1.43 V vs. SCE) a který nese označení peak III. Tento signál odráží již jednotky procent denaturovaných oblastí v molekule DNA. Jeho citlivost a posun potenciálu je způsoben rozdílem adsorpčních vlastností jednořetězcových a dvouřetězcových molekul DNA na povrchu rtuťové kapkové elektrody [2]. V práci č. 24 byla tato metoda využita k charakterizaci strukturních změn způsobených v molekule DNA vazbou *cis*- a *trans*- isomerů dvojmocných rutheniových komplexů s dimethylsulfoxidovými ligandy. V obou případech docházelo pouze ke vzniku peaku II, stejně jako v případě modifikace DNA cisplatinou, ale *trans*-isomer byl při stejném stupni modifikace účinnější než *cis*-isomer a rozsah nedenaturačních změn ve struktuře DNA se blížil hodnotám pro cisplatinu. V práci č. 21 byl u rutheniového monofunkčního komplexu s *p*-cymenovým ligandem prokázán, při

vyšších úrovních modifikace DNA, vznik distorzí denaturačního charakteru, což potvrdilo stérický destabilizační příspěvek *p*-cymenového ligandu.

Pro měření koncentrací platinových komplexů metodou DPP je charakteristická vysoká citlivost měření (v případě cisplatiny se mez citlivosti pohybuje v subnanomolární škále (1×10^{-10} M)). To je dáno tvorbou katalytického proudu vodíku, který vzniká adsorpcí polarograficky aktivních formazonových komplexů dvojmocné platiny na povrchu rtuťové elektrody. Formazon vzniká reakcí formaldehydu s hydrazinem, obsažených spolu s kyselinou sírovou, v elektrolytu. Tato voltametrická metoda umožňuje rychlé stanovení množství volného Pt komplexu i v přítomnosti DNA. Je proto velmi vhodnou metodou na měření vazebných kinetik (měření úbytku volného komplexu v čase) [3]. U rutheniových komplexů z práce č. 25 byla situace komplikovanější a díky ligandovému poli Ru komplexů nedocházelo v prostředí „platinového elektrolytu“ k tvorbě analyticky využitelného signálu. Byla proto vyvinuta nová polarografická metoda, která také umožňovala stanovení velmi nízkých koncentrací nenavázaných Ru komplexů (1×10^{-9} M), díky tvorbě katalytického proudu vodíku v prostředí elektrolytu tvořeném 0.9 M octanem amonným a 0.15 M NaH_2PO_4 , pH = 5,4. Maximum měřeného signálu (proudu) se pohybovalo okolo -1.35 V vs. SCE. U všech polarografických analýz byl použit tříelektrodový systém, ve kterém tvořil pomocnou elektrodu platinový drát [4].

Elektroforetické metody v gelu jsou v přiložené habilitační práci autorky velmi široce zastoupené. Elektroforéza obecně má široké uplatnění při dělení látek biologického původu. Je to dáno především fyzikální podstatou této separační metody, která využívá pohybu nabitých částic v stejnosměrném elektrickém poli. Směs látek se při ní dělí podle různé pohyblivosti iontů na oddělené zóny jednotlivých složek směsi. Pohyblivost iontů závisí na velikosti náboje, velikosti, molekulové hmotnosti a tvaru molekuly, na povaze nosiče (gelu), elektrolytu, tzn. také na pH, viskozitě a teplotě. Rychlost částice je přímo úměrná síle pole a nepřímo úměrná viskozitě, která je silně závislá právě na teplotě. V případě gelové elektroforézy můžeme dosáhnout velmi účinného dělení studovaných látek na základě výběru vhodného gelu (stupeň zesíťování gelu udává velikost pórů, uplatňují se zde principy gelové chromatografie) a elektrolytu (alkalické pH nebo přítomnost močoviny udržují DNA po denaturaci v ss formě). Nukleové kyseliny a

jejich fragmenty nesou na svém povrchu dosti vysoký záporný náboj díky fosfátovým skupinám, hodnota náboje je téměř nezávislá na pH elektrolytu a elektroforetická separace je závislá hlavně na jejich tvaru a molekulové hmotnosti. „Velké“ molekuly DNA (~ 100 – 30 000 párů bází) lze účinně separovat na agarózových gelech (nativních i denaturačních), kratší fragmenty a oligonukleotidy (~ 1 – 1 000 párů bází) na gelech polyakrylamidových - PAA (nativních i denaturačních). Volba vloženého napětí (proudu) závisí na odvodu Jouleova tepla. Při separaci dlouhovláknových molekul DNA a plasmidových DNA většinou nepřekračuje hodnota napětí na agarózových gelech 5 - 6 V/cm, mohlo by dojít k nežádoucím nesespecifickým deformacím molekul DNA v důsledku jejich „protlačování“ gelem. PAA gely, které se připravují polymerací toxických monomerů akrylamidu s N, N'-methylenbisakrylamidem mají řadu předností. Změnou poměru vstupních složek se dosáhne různé úrovně zesíťování, což umožňuje analýzu vzorků v širokém rozsahu velikostí. Tepelná stabilita, pružnost a pevnost PAA gelů je předurčuje pro vertikální vysokonapěťové elektroforézy. Gely jsou transparentní, mají nízkou afinitu k barvivům (nízké hodnoty pozadí) a elektroosmotický efekt je zanedbatelný. Pohyblivost DNA v nativním (za mírných podmínek) gelu je výrazně ovlivněna její sekundární a terciární strukturou. Metody gelové elektroforézy se využívalo v habilitační práci autorky jak ke kvalitativní a kvantitativní analýze plasmidové DNA, fragmentů DNA a oligonukleotidů po jejich modifikaci studovanými komplexy, tak i k preparativním účelům.

Plasmidová DNA se může nacházet ve třech strukturních formách: nadšroubovicové (superhelikální, sc), relaxované (oc) a lineární. Tyto tři formy se liší rychlostí migrace v agarózovém gelu. Nejrychleji migruje gelem sc forma (je relativně kompaktní, v závislosti na počtu nadšroubovicových otáček), nejpomaleji migruje oc forma, která má kruhový tvar molekuly. Linearizovaná DNA migruje mezi těmito dvěma formami blíže sc nebo oc formě podle konkrétních podmínek analýzy. Po modifikaci plasmidové DNA studovanými komplexy, došlo k lokálním změnám (distorzím) v její sekundární struktuře, čímž byla ovlivněna i její terciární struktura (nadšroubovicové vinutí). Změna elektroforetické mobility negativně nadšroubovicově vinuté plasmidové DNA po její celkové modifikaci studovanými látkami umožňuje stanovit **úhel odvinutí (rozvíjení)** dvoušroubovice poškozené DNA [5, 6]. Při takto vedeném experimentu lze stanovit jen výsledný úhel Φ , který

se v případě tvorby více typů aduktů (monofunkční, bifunkční-vnitrořetězcové, meziřetězcové, apod.) může lišit od úhlu rozvinutí způsobeném jednotlivými adukty, v závislosti na jejich procentuálním zastoupení v molekule DNA. Například v případě cisplatiny je úhel rozvinutí $\Phi = 13^\circ$, což téměř odpovídá majoritnímu zastoupení 1,2-d(GpG) (65%, $\Phi = 15^\circ$) a 1,2-d(ApG) (23%, $\Phi = 13^\circ$) bifunkčních aduktů.

Pomocí této metody byla sledována změna nadšroubovicového vinutí v závislosti na stupni modifikace sc formy plasmidové DNA (pSP73, pUC19) v řadě publikací, které jsou součástí habil. práce autorky (práce č. 1, 3, 5, 8, 9, 10, 12, 13, 18, 21, 23, 24, 25). Komplexy, které rozvíjely dvoušroubovici DNA, snižovaly (v závislosti na vzrůstajícím stupni modifikace) počet sc otáček, takže superhelikální hustota uzavřené, kruhové DNA klesala (např. obr. 6 v práci 24). Tento pokles se projevil postupným zpomalováním migrace sc formy modifikované DNA v gelu, až došlo ke komigraci (úplnému odvinutí nadšroubovicového vinutí) s relaxovanou formou modifikované DNA. r_b - stupeň modifikace, který je dán poměrem počtu molekul komplexu připadajících na jeden nukleotid DNA, kdy dochází ke komigraci obou forem plasmidové DNA, se nazývá $r_b(c)$ - komigrační. Z jeho hodnoty a výchozí superhelikální hustoty σ plasmidové DNA byl vypočítán úhel rozvinutí Φ : $\Phi = 18\sigma/r_b(c)$

Naměřené hodnoty úhlu rozvinutí globálně modifikované DNA přispěly k objasnění vazebného módu studovaných komplexů. Komplexy, které vytvářely pouze monofunkční adukty a které nepřispívaly k destabilizaci duplexu DNA vytvořením rozsáhlé distorze v místě vazby, také obvykle málo rozvíjely dvoušroubovici DNA, $\Phi \sim 0 - 7^\circ$. To může souviset s jejich neúčinností blokovat DNA a/nebo RNA polymerázy a tak nepůsobit v nádorových buňkách na úrovni metabolizace DNA „problémy“, které by vedly k cytotoxicitě komplexu. Takovým příkladem by mohla být neúčinná dienplatina $[\text{PtCl}(\text{dien})]^+$, kde dien = diethylentriamin (např. práce č. 7). Komplexy, které vytvářejí v DNA rozsáhlejší poškození, ohýbají DNA, vytvářejí bifunkční adukty, které strukturu DNA distortují nebo se interkalují do dvoušroubovice DNA, mají úhel rozvinutí obvykle větší. Příkladem mohou být monofunkční komplexy dvojmocného ruthenia s arenovými ligandy (práce č. 9, 21), kdy byly studovány vazebné vlastnosti těchto cytotoxických komplexů. V práci č. 21 byly studovány čtyři rutheniové komplexy, kde tři z nich obsahovaly jako

neodstupující arenový ligand molekuly schopné interkalace do dvoušroubovice DNA (bifenyl, dihydroantracen a tetrahydroantracen). Čtvrtý komplex (s nejnižší cytotoxicitou na nádorových buněčných liniích) obsahoval *p*-cymen, který se ze sterických důvodů interkalovat nemohl. Experimentem sledujícím rozvíjení negativně nadšroubovicově vinuté modifikované plasmidové DNA těmito komplexy bylo zjištěno, že tři komplexy s potenciálním duálním charakterem vazby, kombinací kovalentní (koordinační) vazby a interkalací arenových ligandů, skutečně rozvíjely dvoušroubovici DNA účinněji ($\Phi = 13 - 15^\circ$), čtvrtý komplex s cymenovým ligandem rozvíjel ds DNA s poloviční účinností a úhel rozvíjení činil pouhých 7° . Podobné rozdíly byly naměřeny pro rutheniové komplexy z práce č. 9, kde monofunkční koordinaci rutheniového arenového komplexu s *p*-terfenylovým ligandem doplnila interkalace *p*-terfenylového zbytku mezi páry bází modifikované DNA.

Elektroforéza v alkalickém agarózovém gelu (denaturační) byla další hojně využívanou metodou k charakterizaci typu a zastoupení bifunkčních můstků. Studované koordinační komplexy kovů, které se díky počtu odstupujících ligandů mohly vázat na DNA bifunkčně, tedy vytvářet vnitro- nebo meziřetězcový můstek v molekule ds DNA, byly podrobeny experimentu, ve kterém byla sledována migrace modifikované lineární plasmidové DNA po její denaturaci za alkalických podmínek [7]. Pokud po inkubaci studovaného komplexu s DNA došlo k vytvoření meziřetězcového můstku i po alkalické denaturaci, migrovaly oba řetězce spojené touto vazbou mnohem pomaleji (díky dvojnásobné molekulové hmotnosti spojených řetězců), než molekuly jednotlivých řetězců denaturované DNA. V závislosti na stupni modifikace a procentuálnímu zastoupení pomaleji migrující frakce, bylo možné pomocí vztahu pro Poissonovo rozdělení vypočítat **frekvenci meziřetězcových vazeb** (XCL) na adukt. Tedy jejich procentuální zastoupení v celkovém počtu aduktů vzniklých na DNA: $\%XCL = 100 \times (-\ln ss \text{ frakce DNA}) / (\text{celkový počet nukleotidů DNA} \times r_b)$ [8]. Přítomnost meziřetězcových vazeb může korelovat s cytotoxicitou kovových komplexů, tento typ aduktů vyžaduje mnohem komplikovanější systém opravy (homologní rekombinantní oprava), než bifunkční adukty v jednom řetězci (NER - nukleotidová excizní oprava) a primárně také působí jako obtížnější překážka pro DNA dependentní DNA i RNA polymerázy (téměř neprobíhá translázová syntéza). I pro rutheniové komplexy

studované v této práci (práce č. 24, 25, nepublikovaná data pro dinukleární Ru komplex z práce č. 8) se ukázalo, stejně jako dříve pro cisplatinu, že nadšroubovicové vinutí plasmidové DNA umožnilo (díky energii pnutí způsobeném superhelikálním vinutím) zvýšenou tvorbu meziřetězcových vazeb. V plasmidové DNA, která byla modifikována v sc formě, zastoupení těchto vazeb několikanásobně vzrostlo, což by mohlo mít pro pochopení protinádorového účinku studovaných komplexů velký význam (práce č. 24, 25) [9]. Vertikální PAA elektroforéza v nativním i denaturačním gelu (v prostředí 7 - 8 M močoviny) sloužila v pracích autorky především k analýze produktů enzymatických reakcí, jako je polymerizace (především studie translázové syntézy) nebo transkripce (inhibice transkripce modifikované templátové DNA v důsledku vytvořených aduktů), izolaci specifických aduktů na oligonukleotidech, jejich charakterizace a stanovení velikosti distorze v duplexu DNA pomocí chemických sond, stanovení rozvíjení a ohybů způsobených jednotlivými specifickými adukty studovaných komplexů (práce č. 6, 10, 11, 14, 16, 17, 19, 20, 22).

Pomocí **chemických sond DNA konformace** bylo možno si udělat obrázek o rozsahu léze v místě aduktu. Chemické sondy jako diethylpyrokarbonát (DEPC), KMnO_4 nebo Br_2 reagují selektivně pouze s bázemi denaturované nebo silně distortované DNA. DEPC s adeniny a méně s guaniny, KMnO_4 s thyminy a Br_2 s cytosiny. Charakter a velikost destabilizace duplexu DNA v místě a okolí aduktu hraje významnou úlohu při rozpoznání poškozeného místa proteiny zapojenými do opravných mechanismů jako je NER [10, 11]. To se potvrdilo např. v práci č. 6, kdy protinádorově účinný monofunkční rutheniový komplex s terfenylovým ligandem byl i přes svou pouze monofunkční vazbu na N7 guaninu silným blokem pro polymerázy, díky velikosti arenového ligandu, ale díky charakteru tohoto ligandu, který se vmezeřil mezi páry bází, téměř nede stabilizoval dvoušroubovici DNA. V důsledku malé termodynamické destabilizace byl jeho adukt málo rozpoznáván opravnými systémy buňky a nebyl rozpoznáván ani proteiny NER, RPA a XPA, které se jinak váží v místě léze [12]. Také **rigidní ohyb** „správné“ velikosti a orientace, způsobený v ds DNA vytvořením aduktu, může vést k rozpoznání těmito proteiny a podpořit vazbu transkripčních faktorů, jako je tomu u cisplatinu. Její bifunkční vnitřetězcový můstek je rozpoznáván HMGB1 proteiny a tak je zároveň chráněn před opravou a odčerpává tyto transkripční faktory z jejich

vazebných míst, čímž brzdí transkripční procesy v buňce. Příkladem takových aduktů zmíněných v této habil. práci by mohly být vnitrořetězcové můstky 1,2 d(GpG) v TGGT sekvenci, studovaných *R,R* a *S,S* enantiomerů oxaliplatiny; komplexů [PtCl₂(DAB)] (DAB = 2,3-diaminobutan a [PtCl₂(DACH)] (DACH = 1,2-diaminohexan) (práce č. 2 a 11) nebo monofunkční adukt platnatého komplexu *trans*-[PtCl₂(NH₃)thiazol] (práce č. 16). Naopak velká flexibilita v místě bifunkčního aduktu dinukleárního platnatého komplexu se spermidinovým spojovacím řetězcem (práce č. 14) bránila polymerizačním procesům. Úhel ohybu byl studován pomocí vertikální nativní PAA elektroforézy ligačních produktů série oligonukleotidů obsahujících specifický adukt studovaného komplexu (práce č. 14, 16, 19). Z rozdílu elektroforetické mobility modifikovaných a nemodifikovaných ligačních fragmentů stejné délky byla získána zdánlivá délka oligomeru a vypočítán faktor K, který je definován jako poměr mezi zdánlivou a skutečnou délkou oligomeru. Dosazením jeho hodnoty do empirického vztahu $K - 1 = (9.6 \times 10^{-5} L^2 - 0.47)(RC)^2$, kde L představuje délku oligomeru o relativní mobilitě K, byl vypočítán relativní ohyb RC (relativní vzhledem k ohybu, který v DNA vyvolává sekvence šesti nukleotidů s adeninovými zbytky, tzv. A₆ trakt a který ohýbá dvoušroubovici DNA o 20°). Průměrný úhel ohybu připadající na jeden závit DNA byl vypočítán vynásobením relativního ohybu absolutní hodnotou ohybu A₆ traktu. Ze závislosti relativní mobility K na vzdálenosti mezi adukty na fragmentu stejné délky série oligonukleotidů různé délky monomeru bylo také možné stanovit úhel odvinutí dvoušroubovice DNA způsobený daným specifickým aduktem (práce č. 14, 16, 19) [13, 14].

Transkripční mapování „stop“ míst, tj. analýza délky fragmentů předčasně ukončené syntézy RNA, způsobené adukty komplexů na templátové DNA, bylo velmi užitečnou metodou ke stanovení vazebných preferencí studovaných komplexů (práce č. 1, 3, 4, 5, 7, 8, 9, 10, 12, 13, 18, 21, 23, 24) [15]. Většina z nich se přednostně vázala na guaniny, u bifunkčních aduktů byla pozorována i vazba na adeniny, minoritně byla identifikována „stop“ místa na cytosinu. U některých komplexů bylo také možné usuzovat z frekvence a sekvenční preference „stop míst“ na charakter vazby (mono-, bifunkční můstky, bifunkční můstky dalekého dosahu, meziřetězcové můstky). K přerušení transkripce bakteriální SP6 nebo T7 RNA polymerázy nedocházelo často přesně na

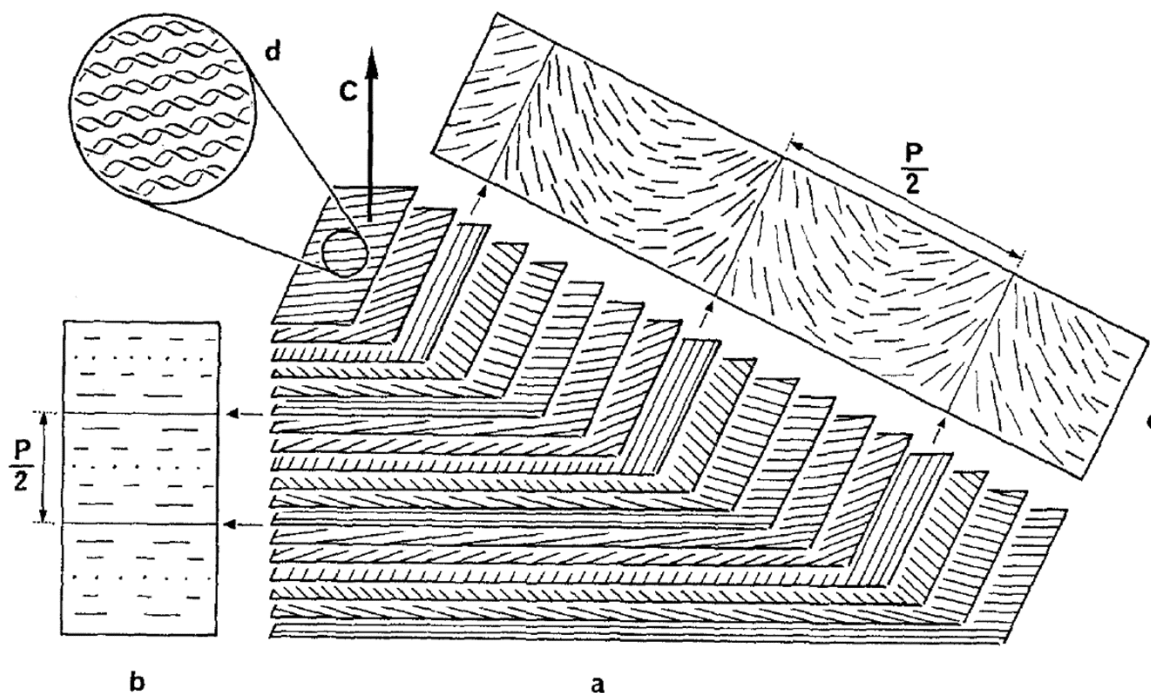
modifikovaném nukleotidu přepisovaného řetězce DNA, ale v jeho těsné blízkosti, podle velikosti sterické zábrany v podobě specifického aduktu studovaného komplexu. Pokud byl adukt „malý“, RNA polymeráza jeho přítomností nebyla vůbec inhibována nebo jen velmi málo, při vysokém stupni modifikace a tím velkému nakumulování takových aduktů v těsném sousedství. Jako příklad může posloužit porovnání inhibice transkripce modifikované dienplatiny, kdy zvětšením a změnou charakteru ligandů (methyloací) monofunkční neúčinné dienplatiny došlo k výrazné inhibici polymerizačních procesů (práce č. 7). Schopnost jednotlivých specifických aduktů, vytvořených modifikací oligonukleotidů, inhibovat DNA dependentní polymerázy byla studována s využitím jak prokaryotické DNA polymerázy (Klenowův fragment DNA polymerázy I s exonukleázovou i bez exonukleázové aktivity), tak lidské reverzní transkriptázy HIV-1. Oba tyto enzymy se vyznačují poměrně velkou tolerancí ke strukturním změnám v templátovém řetězci DNA. Při poškozeních, vzniklých na DNA adukty studovaných komplexů a při jejich opravě, hraje případná **translézová syntéza** (schopnost polymerázy „traverzovat“ přes vzniklou lézi) velkou roli a může přispívat k rezistenci k daným sloučeninám. Autorkou byla studována řada specifických aduktů komplexů platiny a ruthenia a jejich schopnost zastavovat polymerázy. Ukázalo se, že adukty, které vykazovaly schopnost polymerázy účinně zastavit a zároveň nebyly z různých důvodů (např. vazba s proteiny, malá termodynamická a prostorová destabilizace DNA) opravovány, vykazovaly vysokou cytotoxicitu na nádorových buněčných liniích (práce č. 6, 11, 14, 16, 17, 19, 20, 22) [16, 17].

Kapalinová chromatografie (LC), konkrétně HPLC (vysokoúčinná LC) nebo FPLC („fast protein nebo polynucleotide“ LC) byla další rutinně využívanou metodou přiložené práce. Právem patří spolu s elektroforézou k nejčastěji zastoupeným metodám v analýze biopolymerů. Tato fyzikálně chemická separační metoda má velmi široké spektrum využití opět vzhledem k jejímu fyzikálnímu principu, separaci molekul založené na fázových rovnováhách kapalina-pevná fáze. Separace probíhá na koloně s chromatografickým materiálem obsahujícím malé částice (stacionární fáze). Roztok nebo-li eluent (mobilní fáze) je tlačен (pomocí pumpy) touto kolonou se stacionární fází. Při takovémto uspořádání, složky vzorku, rozpuštěné v mobilní fázi, reverzibilně interagují se stacionární fází v opakovaném režimu. (Opakované ustavování adsorpčně-desorpčních rovnováh-

mnohonásobné vytváření rovnovážných stavů separovaných látek mezi stacionární a mobilní fází). Tento složitý děj se řídí adsorpční izotermou a Einsteinovou rovnicí pro difuzní koeficient. Van Deemterova dynamická difuzní teorie popisuje situaci na koloně pomocí difuzních dějů: $A + B/u + C u = H$, kde H je molekulární difuze a představuje tzv. výšku teoretického patra kolony, tedy vzdálenost, na které dojde k adsorpci a desorpci separované látky. A , B a C jsou faktory, které přispívají k této výšce, způsobené difuzními jevy - turbulentní („Eddy“) difuzí (A), molekulovou difuzí (B) a difuzí do stacionární fáze (C), tzv. odporu proti přestupu hmoty. Dráha, kterou mobilní fáze urazí za čas t se nazývá lineární rychlost toku (u). Role těchto faktorů je rovnocenná. Optimální podmínky separace nastanou, pokud je: u maximální a H minimální. Částice stacionární fáze v koloně tvoří sorbent s charakteristickými vlastnostmi odpovídajícími zvolené chromatografické metodě. Ty jsou v zásadě čtyři – gelová permeační, iontovýměnná, afinitní a na reverzní fázi, ale jejich principy se doplňují a kombinují. Každý biopolymer nebo jejich směs má vlastnosti, kterých lze při separaci pomocí HPLC přednostně využít (velikost, náboj, afinita k jiným molekulám, rozpustnost). Pro separaci oligonukleotidů, fragmentů a jednotlivých stavebních jednotek nukleových kyselin lze využít více technik kapalinové chromatografie. Iontovýměnná (konkrétně aniontovýměnná chromatografie byla zvolena jako jednoduchá a účinná metoda na analýzu a čištění specifických aduktů vytvořených na oligonukleotidech s definovanou sekvencí. Po modifikaci oligonukleotidu studovaným komplexem došlo, podle typu vazby, k odstínění jednoho nebo více záporných nábojů fosfátových skupin, což se projevilo zkrácením retenčního času (objemu) takto modifikovaného oligonukleotidu v gradientu vzrůstající iontové síly (NaCl) mobilní fáze. Pro tyto účely je možné využít i chromatografii na reverzní fázi, ale charakter ligandů studovaných kovových komplexů komplikoval analýzu jednotlivých aduktů. Při analýze nukleotidů, nukleosidů a bází je naopak chromatografie na reverzní fázi první volbou. Byla používána k analýze aduktů na nukleosidech po enzymatické hydrolýze modifikované dlouhovláknové DNA a oligonukleotidů nebo k analýze bází po kyselé hydrolýze kys. mravenčí (apurinace) nebo kys. chlorovodíkovou (všechny báze). Eluce byla dosažena snižováním polarity mobilní fáze v gradientu acetonitrilu nebo methanolu, pro analýzu nukleosidů bylo zvoleno kyselé prostředí 0.1 M octanu sodného, pH ~ 5,5 [18].

Chiroptické metody se v experimentální biofyzice velmi účinně využívají při studiu struktur chirálních biomakromolekul a jejich interakcí. Významnými metodami, které umožnily sledovat ovlivnění struktury globálně modifikované DNA studovanými komplexy, byly **metody cirkulárního a lineárního dichroismu** - CD, LD. Báze obsažené v polynukleotidech jsou opticky neaktivní. Po jejich spojení s opticky aktivními cukry (obsahují asymetrický uhlík) se u nich objeví v oblasti absorpčních maxim po průchodu cirkulárně polarizovaného světla Cottonovy efekty. Křivka cirkulárního dichroismu je rozdílem mezi absorpčním spektrem pro vlevo a vpravo kruhově polarizované světlo ($CD = \Delta A = A_L - A_R$, z Beer-Lambertova zákona pak $\Delta \varepsilon = (\varepsilon_L - \varepsilon_R) = \Delta A / cl$). Vzorek je pro danou vlnovou délku zkoumán monochromatickým světelným paprskem, jehož polarizace se periodicky mění z vlevo kruhové na vpravo kruhovou. Tato periodická změna polarizačního stavu paprsku se po průchodu opticky aktivním vzorkem, kde se ε_L liší od ε_R , projeví pravidelnými změnami intenzity prošlého světla. Tvar CD spektra DNA je závislý na konfiguraci cukr-báze, na orientaci těchto spojení a na jeho interakcích. Strukturní formy DNA jako B, A a Z mají rozdílná CD spektra, stejně jako jednotlivé nukleotidy nebo polynukleotidy se specifickými sekvencemi poly(dA-dT), poly(dG-dC) a pod. Metodou cirkulárního dichroismu byly sledovány změny v sekundární struktuře DNA, změny „stacking“ interakcí paralelních párů bází nebo odvinutí dvoušroubovice (práce č. 1, 3, 5, 8, 9, 18, 21, 23, 24). U komplexů s aromatickými ligandy bylo možno v oblasti jejich absorpčních maxim pozorovat také indukované Cottonovy jevy (indukované CD), které svědčí o orientaci ligandů koordinovaných komplexů a spolupráci jejich aromatických chromoforů s chromofory bází. U některých studovaných rutheniových komplexů se jednalo o interkalaci planárních aromatických ligandů mezi páry bází (práce č. 9, 18, 21). V případě optických izomerů, jako tomu bylo v práci č. 25, byla použita pravotočivá DNA v B formě k separaci λ a Δ enantiomerů rutheniových komplexů z racemické směsi. Metodou CD byla sledována kinetika vazby rutheniového racemátu na DNA a bylo zjištěno, že dochází k přednostní vazbě λ isomeru a teprve po delším časovém intervalu (cca 1 hod.) se začal vázat také druhý optický isomer. Po 24 hodinové inkubaci byly kvantitativně navázány oba enantiomery. V raných fázích vazebné kinetiky tak bylo filtrací přes membránový filtr možno získat směs nenavázaných isomerů obohacenou o Δ isomer. V práci č. 24 byla také pomocí

CD sledována stabilita tekutých krystalů modifikované sonikované DNA. Anizotropní cholesterické tekuté krystaly DNA byly tvořeny v roztoku PEG (polyethylenglykol) za přítomnosti jednomocných kationtů (Na^+) (obr. MK1). Komplexy kovů, které distortovaly a destabilizovaly ds DNA, rušily tvorbu tekutých krystalů uspořádaných molekul sonikované DNA přibližně stejné délky (~500 pb). Orientace molekul DNA v tekuté cholesterické krystalické disperzi je levotočivá a projevuje se výrazným záporným pásem v okolí 275 nm [19, 20].



Obr. MK1: Schematické znázornění organizace DNA v cholesterické fázi (také chirální nematická fáze) (a) s detaily uspořádání molekul DNA v jednotlivých pomyslných vrstvách (b) - (d). Molekuly dvoušroubovicová DNA jsou uspořádány paralelně (d) a jejich orientace se mění plynule podél cholesterické osy **C**. V obrázku jsou patrné jednotlivé vrstvy orientovaných molekul DNA pro lepší znázornění. $P/2$ představuje polovinu stoupání závitů orientovaných molekul DNA (adaptováno z [20]).

Samotná B forma DNA vykazuje pozitivní maximum okolo 280 nm a negativní pás okolo 245 nm přibližně stejné velikosti. A forma DNA má díky dehydrataci a tak změně vrstvení paralelně uspořádaných bází, strmější a vyšší pozitivní pás okolo 270 nm a negativní pás téměř vymizí. Levotočivá Z forma DNA má naopak negativní pás srovnatelný s B formou, ale pozitivní maximum chybí.

Koordinční komplexy kovů a zvláště platinová cytostatika mohou výrazně ovlivňovat přechod B formy DNA do Z formy, vyvolaný přítomností vysokých

koncentrací solí. Například cisplatina podporovala B – Z přechod za těchto podmínek, ale výsledné CD Z formy bylo deformované v důsledku distortované dvoušroubovice levotočivé DNA a kooperativita přechodu byla snížena [21]. Trojmocné koordinační komplexy ruthenia, jejichž vazba na DNA byla charakterizována v práci č. 23, nepodporovaly, na rozdíl od cisplatiny, přechod mezi B formou modifikované poly(dG-me⁵dC) DNA a její Z formou v prostředí vysoké iontové síly, ale vzájemně se od sebe v míře stabilizace B formy lišily, a silně narušovaly kooperativitu samotného přechodu.

Lineární dichroismus nám může poskytnout informace o relativní orientaci bází vzhledem k ose dvoušroubovice. Dlouhé molekuly (řádově tisíce párů bází) viskózního roztoku DNA se orientovaly vlivem stříhového napětí, vytvořeného ve speciální rotační kyvetě (obr. MK2).



Obr. MK2: Fotografie a popis speciální rotační kyvety na měření spekter lineárního dichroismu na pracovišti autorky.

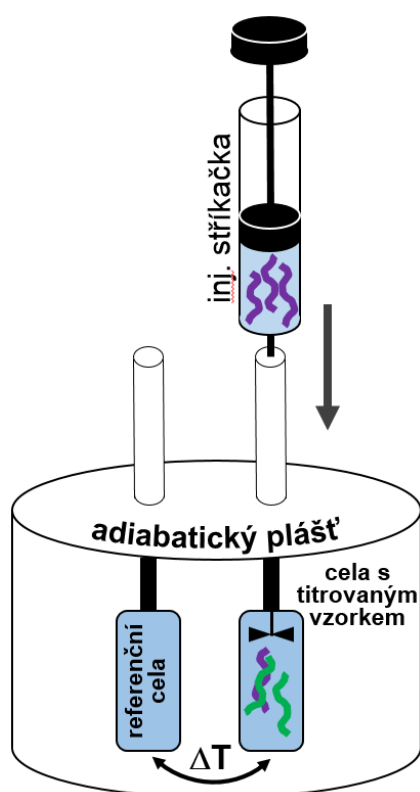
Uspořádané molekuly DNA z telecího thymu poskytovaly negativní absorpční pás v okolí 260 nm, což znamená, že většina bází je orientována kolmo ke směru toku (proudění). Pokud byla DNA modifikována komplexy, které narušily svou vazbou na DNA orientaci bází, došlo k poklesu velikosti negativního pásu LD. Naopak u komplexů, které se do dvoušroubovice DNA interkalovaly a orientaci párů bází nenarušily, se velikost negativního pásu nesnížila a mohlo dojít i k jeho prohloubení, v důsledku zvýšené rigidity molekul DNA (práce č. 1, 3, 5, 9, 10).

Pokud chromofory komplexu absorbovaly navíc i v části spektra odpovídající delším vlnovým délkám, objevil se indukovaný LD tohoto komplexu zorientovaného molekulou DNA. Tak tomu bylo u monofunkčního rutheniového komplexu s *p*-terfenylovým ligandem (práce č. 9), kde vznikl negativní indukovaný LD pás mezi ~300 – 350 nm. Jeho negativní orientace znamená, že úhel podélné osy molekuly komplexu s osou DNA je větší než 54°, jak je předpokládáno u většiny interkalátorů. Tento komplex se tedy, kromě monofunkční kovalentně-koordinační vazby, vázal na DNA jako planární interkalátor.

Metoda zhášení fluorescence ethidium bromidu (EtBr) byla další poměrně široce používanou metodou k charakterizaci vazby studovaných komplexů kovů na DNA (práce č. 3, 8, 9, 10, 21, 24). EtBr, který patří mezi dobře prostudované interkalátory, slouží jako fluorescenční sonda k rozpoznání interkalujících a neinterkalujících ligandů studovaných komplexů a charakteru kovalentně-koordinačních vazeb [22]. Interkalace EtBr do dvoušroubovice DNA je přímo úměrně snižována vznikem širokého spektra aduktů, včetně interkalátorů. To je provázeno snižováním intenzity fluorescence komplexu DNA-EtBr. Volný EtBr má fluorescenci v měřené oblasti emisního spektra jen zanedbatelnou, stejně jako DNA. Adukt, který „nezavazejí“ (stericky nebrání) EtBr v jeho interkalaci a který nedistortují DNA tak, že se EtBr nemůže vmezeřit mezi páry bází, zhášejí fluorescenci komplexu DNA-EtBr jen velmi málo. Takovým příkladem může být monofunkční adukt dienplatiny. Naopak meziřetězcové můstky, interkalátory a bifunkční adukty silně měnící uspořádání párů bází, snižují intenzitu fluorescence, v závislosti na rostoucím stupni modifikace, velmi účinně.

K termodynamické charakterizaci specifických aduktů studovaných komplexů platiny a ruthenia, vytvořených na oligonukleotidech s definovanou sekvencí (práce č. 2, 6, 7, 11, 17) byla v habilitační práci autorky využita **mikrokalorimetrie**. Mikrokalorimetrie je velmi užitečná biofyzikální metoda, protože tak jako v neživých systémech, tepelné změny se i v biologických systémech řídí zákony termodynamiky. Termodynamické studie biologicky důležitých procesů zahrnují specifické a nespecifické molekulární rozlišení (afinitu) i stabilitu makromolekul, jakou představuje i DNA. Výchozím bodem většiny termodynamických (TD) studií je experimentální stanovení vazebné konstanty K_b . Gibbsova volná energie ΔG studovaného procesu za dané teploty může být

určena ze standardního vztahu $\Delta G = -RT \ln K_b$, kde R je plynová konstanta, T je absolutní teplota v Kelvinech a K_b lze vyjádřit jako převrácenou hodnotu disociační konstanty K_d ($K_b = 1/K_d$). Pro detailnější TD studium je třeba znát teplotní závislost změny volné energie, která se odráží ve změně entalpie (ΔH) reakce. Stanovením entalpie je možné kvantifikovat skutečné příspěvky entalpie a entropie (ΔS) k celkové změně volné energie: $\Delta G = \Delta H - T\Delta S$. Kontinuálním měřením tepelné kapacity systému (C_p) v závislosti na teplotě pomocí **diferenční skenovací kalorimetrie** (DSC) lze přímo získat z naměřené křivky hodnoty T_m (z maxima křivky), ΔH (integrací plochy pod křivkou) a ΔS (konverzí hodnot změny tepelné kapacity): $\Delta H = \int C_p dT$ a $\Delta S = \int C_p/T dT$. Tato metoda obecně umožňuje sledovat tepelné změny indukované nárůstem nebo poklesem teploty – konformační změny, fázové přechody a tání duplexu molekuly DNA. **Izotermální titrační kalorimetrie** (ITC) měří přímo změnu entalpie vazebné interakce molekul (reakční teplo) za konstantní zvolené teploty (obr. MK3). Z takového měření lze získat všechny základní TD parametry spojené s vazbou „ligandu“, včetně K_b a stechiometrického (vazebného) poměru n .



Obr. MK3: Schematický nákres typické instrumentace v izotermální titrační kalorimetrii.

Diferenční skenovací a izotermální titrační mikrokolorimetrie bylo využito k získání termodynamických parametrů lézí ve struktuře DNA, vzniklých vytvořením aduktů s vybranými komplexy. Přítomnost aduktů v molekule DNA vyvolával její destabilizaci, která byla způsobena tím, že destabilizační příspěvek pocházející z poklesu entalpie (způsobené změnami v sekundární struktuře DNA - „stacking“ interakcí, vodíkových vazeb) nebyla plně kompenzována stabilizačním příspěvkem entropického členu (způsobeným zvýšenou flexibilitou DNA v místě léze, změnami v hydratačním obalu DNA). Výjimkou byl monofunkční adukt dienplatiny v GGT sekvenci, jehož vytvoření duplex stabilizovalo (práce č. 7). K jen velmi malému

poklesu záporné hodnoty ΔG také došlo po modifikaci duplexu monofunkčními adukty rutheniových komplexů s planárními arenovými ligandy, které se mohly interkalovat (práce č. 6, 17) (interkalátory stabilizují dvoušroubovici DNA, protože se zapojují do „stacking“ interakcí paralelních bází a svým vmezežením zvětšují vzdálenost mezi fosfátovými skupinami, čímž snižují repulzní síly záporných nábojů). Metoda DSC byla zvolena pro teplotně stabilní adukty platinových komplexů, které dlouhodobě „přežívaly“ v opakovaném denaturačně-renaturačním režimu DSC (práce č. 2, 7, 11). Metoda ITC (práce č. 6, 17) byla použita ke studiu aduktů rutheniových komplexů, které nabyly dostatečně stabilní za vyšších teplot. Hodnoty naměřených TD parametrů byly konfrontovány s dalšími výsledky, získanými pomocí chemických sond DNA konformace, polymerizačních experimentů a opravy poškozené DNA. Pomohly přispět k navržení nebo objasnění možného mechanismu protinádorové účinnosti některých studovaných komplexů nebo pomohly vysvětlit možné příčiny tolerance a/nebo rezistence nádorových buněk k těmto sloučeninám.

Odborná literatura, použitá autorkou k doplnění formulací základních principů a vztahů metodického komentáře:

Sinden, R. R. (ed.) *DNA Structure and Function*, Academic Press, Inc. San Diego 1994

Neidle, S. (ed.) *Principles of Nucleic Acid Structure*, Elsevier Inc. 2008

Kalous, V., Pavlíček, Z. (ed.) *Biofyzikální chemie*, SNTL, Praha 1980

Prosser, V. a kol. (ed.) *Experimentální metody biofyziky*, Academia, ČSAV Praha 1989

Tuszynski, J.A., Kurzynski, M. (ed.) *Introduction to Molecular Biophysics*, CRC Press LLC 2003

Rodger, A., Nordén, B. (ed.) *Circular Dichroism and Linear Dichroism*, Oxford University Press 1997

Ladbury, J. E., Doyle, M. L. (ed.) *Biocalorimetry 2*, John Wiley and Sons, Ltd 2004

Piljac, G., Piljac, V. (ed.) *Genetic Engineering-Liquid Chromatography*, TIZ, Čakovec 1986

Sambrook, J., Fritsch, E.F., Maniatis, T. (ed.) *Molecular cloning a Laboratory Manual*, Cold Spring Harbor Laboratory Press 1989

Odkazy v textu metodického komentáře:

[1] Zaludova, R., Kleinwachter, V., Brabec, V. (1996) *Biophys. Chem.* 60, 135.

- [2] Paleček, E., *Topics in Bioelectrochemistry and Bioenergetics*, Milazzo, G. (ed.), J Wiley, New York 1983, 5, 65.
- [3] Kim, S. D., Vrána, O., Kleinwächter, V., Niki, K., Brabec, V. (1990) *Anal. Lett.* 23, 1505.
- [4] Novakova, O., Kasparkova, J., Vrana, van Vliet, P. M., Reedijk, J., Brabec, V. (1995) *Biochemistry* 34, 6781.
- [5] Bauer, W.R. (1978) *Annu. Rev. Biophys. Bioeng.* 7, 287.
- [6] Keck, M.V., Lippard, S.J. (1992) *J. Am. Chem. Soc.* 114, 3386.
- [7] Lemaire, M. A., Schwartz, A., Rahmouni, A. R., Leng, M. (1991) *Proc. Natl. Acad. Sci. USA.* 88, 1982.
- [8] Farrell, N., Qu, Z., Van Houten, B. (1990) *Biochemistry* 29, 9522.
- [9] Vrána, O., Boudný, V., Brabec, V (1996) *Nucl. Acids Res.* 24, 3918.
- [10] Nielsen, P. E. (1990) *J. Mol. Recogn.* 3, 1.
- [11] Brabec, V., Sip, M., and Leng, M. (1993) *Biochemistry* 32, 11676.
- [12] Reardon, J. T., Vaisman, A., Chaney, S. G., Sancar, A. (1999) *Cancer Res.* 59, 3968.
- [13] Koo, H.S., Wu, H.M., Crothers, D.M. (1986) *Nature* 320, 501.
- [14] Bellon, S.F., Lippard, S.J. (1990) *Biophys. Chem.* 35, 179.
- [15] Lemaire, M.A., Schwartz, A., Rahmouni, A.R., Leng, M.(1991) *Proc. Natl. Acad. Sci. USA.* 88, 1982.
- [16] Comess, K. M., Burstyn, J. N., Essigmann, J. M., Lippard, S.J. (1992) *Biochemistry* 31, 3975.
- [17] Suo, Z., Lippard, S., Johnson, K. (1999) *Biochemistry* 38, 715.
- [18] Balcarova, Z., Kasparkova, J., Zakovska, A., Novakova, O., Sivo, M. F., Natile, G., Brabec, V. (1998) *Mol. Pharmacol.* 53, 846.
- [19] Livolant, F., Maestre, M. (1988) *Biochemistry* 27, 3056.
- [20] Livolant, F., Leforestier, A. (1996) *Prog. Polym. Sci.* 21, 1115.
- [21] Ushay, H.M., Santella, R.M., Caradonna, j.p.,Grunberger, D., Lippard, S.J. (1982) *Nucl. Acids Res.* 10, 3573.
- [22] Butour, J.L., Macquet, J.P. (1977) *Eur. J. Biochem.* 78, 455.

Další literární odkazy k příslušným experimentálním metodám a získaným výsledkům jsou součástí publikací tvořících tuto habilitační práci.

V. Kopie publikovaných vědeckých prací autorky v plném znění

1.

Bipyrimidine ruthenium(II) arene complexes: structure, reactivity and cytotoxicity

Soledad Betanzos-Lara · Olga Novakova · Robert J. Deeth · Ana M. Pizarro ·
Guy J. Clarkson · Barbora Liskova · Viktor Brabec · Peter J. Sadler ·
Abraha Habtemariam

Received: 29 March 2012 / Accepted: 15 June 2012
© SBIC 2012

Abstract The synthesis and characterization of complexes $[(\eta^6\text{-arene})\text{Ru}(\text{N},\text{N}')\text{X}][\text{PF}_6]$, where arene is *para*-cymene (*p*-cym), biphenyl (bip), ethyl benzoate (etb), hexamethylbenzene (hmb), indane (ind) or 1,2,3,4-tetrahydronaphthalene (thn), N,N' is 2,2'-bipyrimidine (bpm) and X is Cl, Br or I, are reported, including the X-ray crystal structures of $[(\eta^6\text{-p-cym})\text{Ru}(\text{bpm})\text{I}][\text{PF}_6]$, $[(\eta^6\text{-bip})\text{Ru}(\text{bpm})\text{Cl}][\text{PF}_6]$, $[(\eta^6\text{-bip})\text{Ru}(\text{bpm})\text{I}][\text{PF}_6]$ and $[(\eta^6\text{-etb})\text{Ru}(\text{bpm})\text{Cl}][\text{PF}_6]$. Complexes in which N,N' is 1,10-phenanthroline (phen), 1,10-phenanthroline-5,6-dione or 4,7-diphenyl-1,10-phenanthroline (bathophen) were studied for comparison. The Ru^{II} arene complexes undergo ligand-exchange reactions in aqueous solution at 310 K; their half-lives for hydrolysis range from 14 to 715 min. Density functional theory calculations on $[(\eta^6\text{-p-cym})\text{Ru}$

$(\text{bpm})\text{Cl}][\text{PF}_6]$, $[(\eta^6\text{-p-cym})\text{Ru}(\text{bpm})\text{Br}][\text{PF}_6]$, $[(\eta^6\text{-p-cym})\text{Ru}(\text{bpm})\text{I}][\text{PF}_6]$, $[(\eta^6\text{-bip})\text{Ru}(\text{bpm})\text{Cl}][\text{PF}_6]$, $[(\eta^6\text{-bip})\text{Ru}(\text{bpm})\text{Br}][\text{PF}_6]$ and $[(\eta^6\text{-bip})\text{Ru}(\text{bpm})\text{I}][\text{PF}_6]$ suggest that aquation occurs via an associative pathway and that the reaction is thermodynamically favourable when the leaving ligand is $\text{I} > \text{Br} \approx \text{Cl}$. $\text{p}K_{\text{a}}^*$ values for the aqua adducts of the complexes range from 6.9 to 7.32. A binding preference for 9-ethylguanine (9-EtG) compared with 9-ethyladenine (9-EtA) was observed for $[(\eta^6\text{-p-cym})\text{Ru}(\text{bpm})\text{Cl}][\text{PF}_6]$, $[(\eta^6\text{-hmb})\text{Ru}(\text{bpm})\text{Cl}]^+$, $[(\eta^6\text{-ind})\text{Ru}(\text{bpm})\text{Cl}]^+$, $[(\eta^6\text{-thn})\text{Ru}(\text{bpm})\text{Cl}]^+$, $[(\eta^6\text{-p-cym})\text{Ru}(\text{phen})\text{Cl}]^+$ and $[(\eta^6\text{-p-cym})\text{Ru}(\text{bathophen})\text{Cl}]^+$ in aqueous solution at 310 K. The X-ray crystal structure of the guanine complex $[(\eta^6\text{-p-cym})\text{Ru}(\text{bpm})(9\text{-EtG-N7})][\text{PF}_6]_2$ shows multiple hydrogen bonding. Density functional theory calculations show that the 9-EtG adducts of all complexes are thermodynamically preferred compared with those of 9-EtA. However, the bpm complexes are inactive towards A2780 human ovarian cancer cells. Calf thymus DNA interactions for $[(\eta^6\text{-p-cym})\text{Ru}(\text{bpm})\text{Cl}][\text{PF}_6]$ and $[(\eta^6\text{-p-cym})\text{Ru}(\text{phen})\text{Cl}][\text{PF}_6]$ consist of weak coordinative, intercalative and monofunctional coordination. Binding to biomolecules such as glutathione may play a role in deactivating the bpm complexes.

Electronic supplementary material The online version of this article (doi:10.1007/s00775-012-0917-9) contains supplementary material, which is available to authorized users.

S. Betanzos-Lara · R. J. Deeth · A. M. Pizarro ·
G. J. Clarkson · P. J. Sadler · A. Habtemariam (✉)
Department of Chemistry,
University of Warwick,
Coventry CV4 7AL, UK
e-mail: a.habtemariam@warwick.ac.uk

Present Address:

S. Betanzos-Lara
Departamento de Química Inorgánica,
Facultad de Química,
Universidad Nacional Autónoma de México (UNAM),
Ciudad Universitaria,
Coyoacán, Mexico, D.F. 04510, Mexico

O. Novakova · B. Liskova · V. Brabec
Institute of Biophysics,
Academy of Sciences of the Czech Republic,
v.v.i., Kralovopolska 135, 61265 Brno, Czech Republic

Keywords Ruthenium · Arene · Bipyrimidine ·
Hydrolysis · Nucleobase

Introduction

The well-established mechanism of action of the cytotoxic drug cisplatin is the alteration of the secondary structure of DNA via coordination to the N7 atom of a guanine or an adenine base, which requires its prior aquation in the cell to generate the more reactive aqua complexes

$[\text{Pt}(\text{NH}_3)_2(\text{OH}_2)\text{Cl}]^+$ and $[\text{Pt}(\text{NH}_3)_2(\text{OH}_2)_2]^{2+}$ [1, 2]. In general, aquation can be an important activation step for transition metal complexes prior to their coordination to biomolecules [3]. Certain organometallic Ru^{II} complexes of the type $[(\eta^6\text{-arene})\text{Ru}(\text{XY})\text{Z}]^{n+}$, where XY is a bidentate chelating ligand and Z is a leaving group, exhibit promising cytotoxic activity against a variety of cancer cell lines, including cisplatin-resistant cells [4, 5]. The nature of the arene, the chelating ligand and the leaving group can have a major influence on the rates of activation (towards hydrolysis and/or binding to biomolecules) as well as on the cytotoxic activity [6, 7]. It appears that the presence of a more hydrophobic arene ligand along with a single ligand-exchange site is often associated with significant anticancer activity. Blocking ligand-exchange reactions in the remaining two coordination sites can usually be achieved by coordination of a stable bidentate ligand; in this regard, particularly effective are those ligands containing N,N' heterocyclic groups [8–10].

In this work, we have studied and contrasted the chemical reactivity of a series of organometallic Ru^{II} complexes of the type $[(\eta^6\text{-arene})\text{Ru}(\text{N,N'})\text{X}][\text{PF}_6]$ containing an N,N' chelating ligand, as well as various arenes, and different halides (X). Their aqueous solution chemistry and the nucleobase binding to 9-ethylguanine (9-EtG) and

9-ethyladenine (9-EtA) were investigated. Their potential as cytotoxic agents was explored not only by determining IC_{50} values with regard to A2780 (human ovarian), A2780cis (human ovarian cisplatin resistant), A549 (human lung) or HCT116 (human colon) cancer cell lines but also by studying DNA interactions in cell-free media. γ -Glutamyl-cysteinyl-glycine (glutathione, GSH) coordination to Pt^{II} is known to inhibit DNA binding, contributing to cisplatin resistance in tumour cells [11–13], and depending on its relative concentration [14, 15], it can both facilitate and inhibit ruthenium interactions with DNA [16]. Reactions of GSH with a representative inactive Ru^{II} arene complex (**1**; Fig. 1) in aqueous solution at 310 K were therefore investigated to establish whether GSH may play a role in the activity of this family of complexes.

Materials and methods

Materials

$\text{RuCl}_3 \cdot 3\text{H}_2\text{O}$ was acquired from Precious Metals Online and used as received. 2,2'-Bipyrimidine (bpm), 1,10-phenanthroline (phen), 1,10-phenanthroline-5,6-dione (phendio),

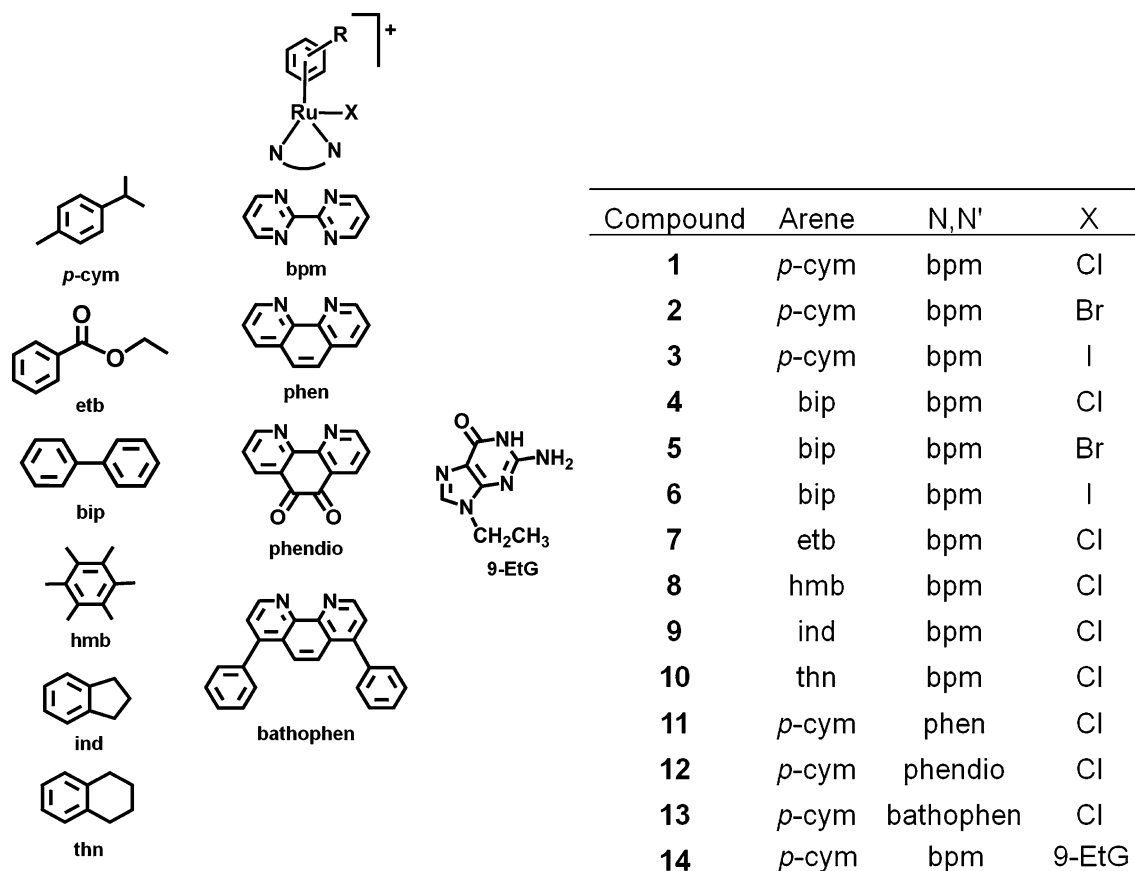


Fig. 1 General structures of the complexes studied in this work, synthesized as PF_6 salts

4,7-diphenyl-1,10-phenanthroline (bathophen), 9-EtG, 9-EtA and KPF₆ were obtained from Sigma-Aldrich. KBr and KI (reagent grade) were obtained from Fisher. The Ru^{II} arene precursor dimers [(η^6 -arene)RuX₂]₂, where arene is *para*-cymene (*p*-cym), biphenyl (bip), hexamethylbenzene (hmb), indane (ind) or tetrahydronaphthalene (thn) and X is Cl, Br or I, were synthesized according to a previously reported method [17–20]. The dimer [(η^6 -etb)RuCl₂]₂, where etb is ethyl benzoate, was synthesized following a literature procedure [21]. The solvents used for UV–vis absorption spectroscopy were dry MeOH (reagent grade) and deionized water. For NMR spectroscopy, the solvents used were acetone-*d*₆, dimethyl-*d*₆ sulfoxide, MeOH-*d*₄ and D₂O obtained from Aldrich. All chemicals were used without further purification. Cisplatin was obtained from Sigma-Aldrich (Prague, Czech Republic). Chloridodiethylenetriamineplatinum(II) chloride was a generous gift from Giovanni Natile (University of Bari). Restriction endonucleases *Nde*I and *Hpa*I were purchased from New England Biolabs. Acrylamide, bisacrylamide and ethidium bromide were obtained from Merck (Darmstadt, Germany). Agarose was purchased from FMC BioProducts (Rockland, ME, USA). Radioactive reagents were obtained from Amersham (Arlington Heights, IL, USA). Stock aqueous solutions of metal complexes (5×10^{-4} M) for the biophysical and biochemical studies were filtered and stored at room temperature in the dark. The concentrations of ruthenium or platinum in the stock solutions were determined by flameless atomic absorption spectrometry (FAAS). Calf thymus DNA (CT-DNA; 42 % G + C, mean molecular mass approximately 2×10^7) was also prepared and characterized as described previously [22, 23]. pSP73KB (2,455-bp) plasmid was isolated according to standard procedures [32, 33].

Synthesis of ruthenium complexes

Complexes [(η^6 -arene)Ru(N,N')X][PF₆], where arene is *p*-cym, bip, etb, ind, hmb or thn, N,N' is bpm, phen, phendio or bathophen and X is Cl, Br or I were synthesized as previously described [6, 7]. Typically, 2 mol equiv of the N,N' chelating ligand and 2 mol equiv of KPF₆ were added to a solution of 1 mol equiv of the appropriate Ru^{II} arene dimer in dry MeOH (20 mL) with constant stirring over 48 h, after which the precipitate formed was collected by filtration. The remaining solution was concentrated and portions of Et₂O were added to further precipitate the product, which was again collected by filtration. Both solids were combined and washed with portions of Et₂O and MeOH and dried overnight under a vacuum, resulting in microcrystalline products. Details of the amounts of reactants, volumes of solvents, colour changes and nature of the products are given in the electronic supplementary material for the individual reactions, as well as any

variations in the synthetic procedure. Some complexes were also characterized by ¹³C NMR spectroscopy.

X-ray crystallography

Diffraction data were collected either with an Oxford Diffraction Gemini four-circle system with a Ruby CCD area detector or with a Siemens SMART three-circle system with a CCD area detector equipped with an Oxford Cryosystems cooler. All structures were refined by full-matrix least squares against *F*² using SHELXL 97 [24]. The structures of complexes **3**, **4**, **6**, **7** and **14** were solved by direct methods using SHELXS [25, 26] (TREF), with additional light atoms found by Fourier methods. Hydrogen atoms were added at calculated positions and refined using a riding model with freely rotating methyl groups. Anisotropic displacement parameters were used for all non-hydrogen atoms; hydrogen atoms were given isotropic displacement parameters equal to 1.2 (or 1.5 for methyl hydrogen atoms) times the equivalent isotropic displacement parameter of the atom to which the hydrogen atom is attached.

NMR spectroscopy

¹H and ¹³C NMR spectra were acquired in 5-mm NMR tubes at 298 K (unless otherwise stated) using Bruker AV-400, DRX-500, AV III 600 or AV II 700 NMR spectrometers. All data processing was done using XWIN-NMR version 3.6 (Bruker UK). ¹H NMR chemical shifts were internally referenced to tetramethylsilane via 1,4-dioxane ($\delta = 3.71$) or residual MeOH ($\delta = 3.31$). One-dimensional spectra were recorded using standard pulse sequences. Typically, data were acquired with 128 transients into 16,384 data points over a spectral width of 14 ppm. Two-dimensional correlation spectroscopy or total correlation spectroscopy and nuclear Overhauser enhancement spectroscopy (NOESY) spectra were recorded using standard pulse–pulse sequences. Typically, data were acquired with 72 transients into 1,048,576 data points over a spectral width of 14 ppm using a relaxation delay of 1.5 s and a mixing time of 0.06 s.

Elemental analysis

Elemental analyses were performed by Exeter Analytical (UK) using an CE-440 elemental analyser.

High-resolution electrospray mass spectrometry

High-resolution mass spectrometry (HR-MS) data were obtained with a Bruker MaXis UHR-TOF instrument. All the samples were analysed by positive-ion electrospray ionization mass spectra. Samples were prepared in either 100 % H₂O or 95 % MeOH/5 % H₂O mixture and were

typically injected at $2 \mu\text{L min}^{-1}$. The settings were as follows: nebulizer gas (N_2) 0.4 bar, drying gas (N_2) 4 L min^{-1} and drying temperature 453 K, funnel RF 200V, multiple RF 200, quadrupole ion energy 4 eV, collision cell 5 eV, ion cooler RF settings, ramp from 50 to 250 V, unless otherwise stated.

UV–vis absorption spectroscopy

UV–vis absorption spectra were recorded with a Cary 50 Bio spectrophotometer with a PTP1 Peltier temperature controller or with a Beckman DU 7400 UV–vis spectrophotometer equipped with a thermoelectrically controlled cell holder, in 1 cm path length quartz cells (600 μL). Spectra were recorded at 310 K in deionized water from 220 to 800 nm and were processed using UV WinLab for Windows 95.

pH* measurement

pH values were measured at ambient temperature using a Corning 240 pH meter equipped with a micro combination KNO_3 (chloride-free) electrode calibrated with Aldrich buffer solutions of pH 4, 7 and 10. The pH* values (pH meter reading without correction for effects of deuterium on the glass electrode) of NMR samples in D_2O were measured at about 298 K directly in the NMR tube, before and after recording NMR spectra, using the same method. The pH* values were adjusted with dilute NaOH or HNO_3 solutions in D_2O .

pK_a^* values

For determinations of pK_a^* values (for solutions in D_2O), the pH* values of solutions of the aqua complexes in D_2O were varied from approximately pH* 1 to 12 by the addition of dilute NaOH or HNO_3 solutions in D_2O , and ^1H NMR spectra were recorded. The chemical shifts of the arene ring protons were plotted against pH* values. The pH* titration curves were fitted to the Henderson–Hasselbalch equation using Origin version 8.0 (OriginLab), with the assumption that the observed chemical shifts are weighted averages according to the populations of the protonated and deprotonated species. These pK_a^* values can be converted to pK_a values by use of the equation $\text{pK}_a = 0.929\text{pK}_a^* + 0.42$ suggested by Krezel and Bal [27] for comparison with related values in the literature.

Aqueous solution chemistry

Hydrolysis of the Ru^{II} arene halido complexes was monitored by UV–vis spectroscopy. The nature of the hydrolysis products and the extent of the reactions were verified by ^1H

NMR spectroscopy or HR-MS. For UV–vis spectroscopy, the complexes were dissolved in MeOH and diluted with H_2O to give 100 μM solutions (5 % MeOH/95 % H_2O). The absorbance was recorded at several time intervals at the selected wavelength (at which the maximum changes in absorbance were registered) over approximately 8–16 h at 310 K. Plots of the change in absorbance with time were computer-fitted to the pseudo-first-order rate equation, $A = C_0 + C_1 e^{-kt}$ (where C_0 and C_1 are computer-fitted constants and A is the absorbance corresponding to time) using Origin version 8.0 to give the half-lives ($t_{1/2}$, min) and rate constants (k , min^{-1}). For ^1H NMR spectroscopy, the complexes were dissolved in $\text{MeOD-}d_4$ and diluted with D_2O to give 100 μM solutions (5 % $\text{MeOD-}d_4$ /95 % D_2O). The spectra were acquired at various time intervals with a Bruker DMX 700 spectrometer (^1H frequency 700 MHz) using 5-mm-diameter tubes. All data processing was done using XWIN NMR version 2.0 (Bruker UK). The relative amounts of Ru^{II} arene halido species or aqua adducts (determined by integration of peaks in ^1H NMR spectra) were quantified.

Rate of arene loss

The complexes were dissolved in $\text{MeOD-}d_4$ and diluted with D_2O to give 100 μM solutions (5 % $\text{MeOD-}d_4$ /95 % D_2O). Arene loss over time was followed by ^1H NMR spectroscopy at 310 K for 24 h.

Computational studies

Density functional theory (DFT) calculations were performed using the 2009 version of the Amsterdam Density Functional (ADF) program [28, 29]. Uncontracted Slater-type orbital basis sets comprised a triple- ζ plus 5p orbital set on ruthenium with double- ζ plus polarization on all other atoms. Default convergence criteria were applied for self-consistent field and Cartesian geometry optimizations. For optimizations in internal coordinates, in particular transition state searches, the angle threshold was set to 1.5° (default of 0.5°). This criterion was relaxed because of the long bond lengths at the transition states, which make it harder to define torsional terms accurately. The same problem occurs for reactant and product species because the respective entering and leaving groups are included in the calculation, and their relatively weak interaction with the rest of the complex again leads to less well defined torsional terms. However, the energetic consequences of relaxing the angle constraints are negligible. The ADF program reported a single negative eigenvalue in the Hessian matrix for all transition state optimizations. A representative transition state was confirmed as a first-order

saddle point with frequency calculations as described earlier [30, 31]. The conductor-like screening model (COSMO) as implemented in ADF was used to simulate the aqueous environment with $\epsilon = 78.4$, probe radius 1.9 Å and the ND parameter, which controls integration accuracy, set to 4 (default 3). The atomic radii used were 1.950 Å for ruthenium, 1.517 Å for oxygen, 1.700 Å for carbon, 1.608 Å for nitrogen, 1.350 Å for hydrogen, 1.725 Å for chlorine, 1.850 Å for bromine and 1.967 Å or iodine.

DFT-geometry optimization of DNA model nucleobase adducts

Geometry optimizations were performed for the 9-EtG and 9-EtA adducts of $[(\eta^6\text{-}p\text{-cym})\text{Ru}(\text{bpm})(9\text{-EtG-N7})]^{2+}$ (**1**–9-EtG), $[(\eta^6\text{-}p\text{-cym})\text{Ru}(\text{bpm})(9\text{-EtA-N7})]^{2+}$ (**1**–9-EtA), $[(\eta^6\text{-hmb})\text{Ru}(\text{bpm})(9\text{-EtG-N7})]^{2+}$ (**8**–9-EtG), $[(\eta^6\text{-hmb})\text{Ru}(\text{bpm})(9\text{-EtA-N7})]^{2+}$ (**8**–9-EtA), $[(\eta^6\text{-ind})\text{Ru}(\text{bpm})(9\text{-EtG-N7})]^{2+}$ (**9**–9-EtG), $[(\eta^6\text{-ind})\text{Ru}(\text{bpm})(9\text{-EtA-N7})]^{2+}$ (**9**–9-EtA), $[(\eta^6\text{-thn})\text{Ru}(\text{bpm})(9\text{-EtG-N7})]^{2+}$ (**10**–9-EtG-N7), $[(\eta^6\text{-thn})\text{Ru}(\text{bpm})(9\text{-EtA-N7})]^{2+}$ (**10**–9-EtA), $[(\eta^6\text{-}p\text{-cym})\text{Ru}(\text{phen})(9\text{-EtG-N7})]^{2+}$ (**11**–9-EtG), $[(\eta^6\text{-}p\text{-cym})\text{Ru}(\text{phen})(9\text{-EtA-N7})]^{2+}$ (**11**–9-EtA), $[(\eta^6\text{-}p\text{-cym})\text{Ru}(\text{bathophen})(9\text{-EtG-N7})]^{2+}$ (**13**–9-EtG) and $[(\eta^6\text{-}p\text{-cym})\text{Ru}(\text{bathophen})(9\text{-EtA-N7})]^{2+}$ (**13**–9-EtA) for the free 9-EtG and 9-EtA molecules and for the Ru^{II} arene cations without the bound 9-EtG or 9-EtA. The energies of the separate optimized fragments were subtracted from the energy of the whole Ru^{II} arene nucleobase adducts to obtain the total binding energy of 9-EtG and 9-EtA in each complex.

DNA binding kinetics

CT–DNA and plasmid DNAs were incubated with the Ru^{II} arene complexes or platinum complexes in 10 mM NaClO_4 (pH \approx 6) at 310 K for 24 h. For each individual assay, the values of r_b (r_b values are defined as the number of atoms of the metal bound per nucleotide residue) were determined by FAAS.

DNA transcription by RNA polymerase in vitro

Transcription of the (*NdeI/HpaI*) restriction fragment of pSP73KB DNA with T7 RNA polymerase and electrophoretic analysis of the transcripts were performed as previously described [32, 33]. The DNA concentration used was 3.9×10^{-5} M (0.0125 $\mu\text{g}/\mu\text{L}$) (0.25 μg per sample) (related to the monomeric nucleotide content) and the concentration of complexes was approximately 1.17×10^{-6} M.

Unwinding of negatively supercoiled DNA

Unwinding of closed circular supercoiled pUC19 plasmid DNA was assayed by an agarose gel mobility shift assay [34]. The mean unwinding angle can be calculated from the equation $\Phi = -18\sigma/r_b(c)$, where σ is the superhelical density (representing the number of turns added or removed relative to the total number of turns in the relaxed plasmid, indicating the level of supercoiling), and $r_b(c)$ is the r_b value at which the supercoiled and nicked forms co-migrate [34]. Samples of plasmid DNA at a concentration of 1.0×10^{-4} M (0.5 μg per sample) (related to the monomeric nucleotide content) were incubated with the Ru^{II} arene complexes at 310 K for 24 h. All samples were precipitated by ethanol and redissolved in the tris(hydroxymethyl)aminomethane–acetate/EDTA, pH 8.0 buffer to remove free, unbound Ru^{II} arene complexes. One aliquot of the precipitated sample was subjected to electrophoresis on 1 % agarose gels running at 298 K with tris(hydroxymethyl)aminomethane–acetate/EDTA, pH 8.0 buffer, and the voltage was set at 25 V. The gels were then stained with ethidium bromide, followed by photography with a transilluminator. Electron absorption spectrometry and FAAS were used for the determination of r_b values.

Circular dichroism

Isothermal circular dichroism (CD) spectra of CT–DNA modified by the Ru^{II} arene complexes at a concentration of 3.3×10^{-4} M were recorded at 298 K in 10 mM NaClO_4 using a JASCO J-720 spectropolarimeter equipped with a thermoelectrically controlled cell holder. The cell path length was 1 cm. CD spectra were recorded in the range from 230 to 600 nm in 0.5-nm increments with an averaging time of 0.5 s.

Flow linear dichroism

Flow linear dichroism (LD) spectra were collected by using a flow Couette cell in a JASCO J-720 spectropolarimeter adapted for LD measurements. The flow cell consists of a fixed outer cylinder and a rotating solid quartz inner cylinder, separated by a gap of 0.5 mm, giving a total path length of 1 mm. LD spectra of DNA at a concentration of 3.3×10^{-4} M modified by the Ru^{II} arene complexes were recorded at 298 K in 10 mM NaClO_4 .

Other physical methods

The FAAS measurements were performed with a Varian AA240Z Zeeman atomic absorption spectrometer equipped with a GTA 120 graphite tube atomizer. The polyacrylamide gels were visualized by using a BAS 2500

FUJIFILM bioimaging analyser, with the AIDA image analyser program (raytest, Germany).

Cancer cell growth inhibition

After they had been plated, human ovarian A2780 and cisplatin-resistant A2780cis cancer cells were treated with Ru^{II} arene complexes on day 3, and human lung A549 and human colon HCT116 cancer cells were treated on day 2, at concentrations ranging from 0.1 to 100 μ M. Solutions of the Ru^{II} complexes were made up in 0.125 % dimethyl sulfoxide to assist dissolution (0.03 % final concentration of dimethyl sulfoxide per well in the 96-well plate). Cells were exposed to the complexes for 24 h, washed, supplied with fresh medium, allowed to grow for three doubling times (72 h) and then the protein content was measured (proportional to cell survival) using the sulforhodamine B assay [35].

Reactions with GSH

A solution containing $[(\eta^6\text{-}p\text{-cym})\text{Ru}(\text{bpm})\text{Cl}][\text{PF}_6]$ (**1**) (100 μ M) and GSH (10 mM) was incubated at 310 K in D₂O and the changes were monitored by ¹H NMR and UV–vis spectroscopy for 24 h.

Results and discussion

Synthesis and characterization

The $[(\eta^6\text{-arene})\text{Ru}(\text{N},\text{N}')\text{X}]^{n+}$ complexes studied in this work are shown in Fig. 1. The monocationic Ru^{II} arene

halido complexes **1–13** and the 9-EtG-N7 complex **14** were synthesized as PF₆ salts in good yields (more than 50 % in almost all cases). All the complexes were fully characterized by 1D and 2D ¹H NMR methods as well as 1D ¹³C NMR. The molecular structures of complexes **3**, **4**, **6**, **7** and **14** were determined by single-crystal X-ray diffraction. The molecular structure of complex **1** has been published previously [18]. Selected bond lengths and angles are given in Table 1, the structures with numbering schemes are shown in Fig. 2 and the crystallographic data are listed in Table S1. In all cases, the complexes adopt the familiar pseudo-octahedral three-legged piano stool geometry common to all other Ru^{II} arene structures [36, 37] with the Ru^{II} atom π -bonded to the corresponding arene ligand (*p*-cym in **3** and **14**; bip in **4** and **6**; or etb in **7**), coordinated to a chloride (**4** and **7**), to an iodide (**3** and **6**) or to N7 of 9-EtG (**14**) and to two nitrogen atoms of the chelating ligand bpm, which constitute the three legs of the piano stool.

The values for Ru–arene_(centroid) bond lengths are comparable to those for analogous Ru^{II} arene complexes containing N,N'-chelated ligands [38, 39, 76]. The nature of the corresponding N,N' chelating ligand, the nature of the arene and the nature of the halogen do not greatly influence the corresponding Ru–arene_(centroid) distances (approximately 1.70 Å). The corresponding Ru–I bond lengths in **3** and **6** are also within the same range (approximately 2.7 Å) and are slightly shorter compared with those of other Ru^{II} arene complexes containing iodide as a leaving group [40–42]. Similarly, the Ru–Cl bond lengths are almost the same (approximately 2.4 Å). The Ru(1)–N(1)_(bpm) and Ru(1)–N(8)_(bpm) bond lengths in these arene complexes are approximately 2.09 Å. For the four halido complexes, the

Table 1 Selected bond lengths (Å) and angles (°) for $[(\eta^6\text{-}p\text{-cym})\text{Ru}(\text{bpm})\text{I}][\text{PF}_6]$ (**3**), $[(\eta^6\text{-bip})\text{Ru}(\text{bpm})\text{Cl}][\text{PF}_6]$ (**4**), $[(\eta^6\text{-bip})\text{Ru}(\text{bpm})\text{I}][\text{PF}_6]$ (**6**), $[(\eta^6\text{-etb})\text{Ru}(\text{bpm})\text{Cl}][\text{PF}_6]$ (**7**) and $[(\eta^6\text{-}p\text{-cym})\text{Ru}(\text{bpm})(9\text{-EtG-N7})][\text{PF}_6]_2$ (**14**), where *p*-cym is *para*-cymene, bpm is 2,2'-bipyrimidine, bip is biphenyl, etb is ethyl benzoate and 9-EtG is 9-ethylguanine

	3	4	6	7	14
Ru–arene _(centroid)	1.704	1.691	1.693	1.684	1.693
Ru(1)–I(1)	2.706(3)	–	2.70476(16)	–	–
Ru(1)–Cl(1)	–	2.402(8)	–	2.3743(9)	–
Ru(1)–N(13)	2.091(2)	–	–	–	2.1125(19)
Ru(1)–N(1)	–	2.092(2)	2.0901(12)	2.073(3)	2.0972(18)
Ru(1)–N(8)	2.0833(19)	2.093(2)	2.0833(12)	2.081(3)	2.0941(18)
C(6)–C(7)	1.472(4)	1.476(4)	1.477(2)	1.472(5)	1.477(3)
N(8)–Ru(1)–N(1)	76.78(8)	76.72(9)	76.90(5)	77.06(12)	77.05(7)
I(1)–Ru(1)–N(8)	86.38(6)	–	82.60(3)	–	–
Cl(1)–Ru(1)–N(8)	–	83.64(6)	–	83.36(8)	–
I(1)–Ru(1)–N(1)	85.79(6)	–	88.00(3)	–	–
Cl(1)–Ru(1)–N(1)	–	83.00(7)	–	84.67(8)	–
N(13)–Ru(1)–N(8)	–	–	–	–	86.59(7)
N(13)–Ru(1)–N(1)	–	–	–	–	88.64(7)

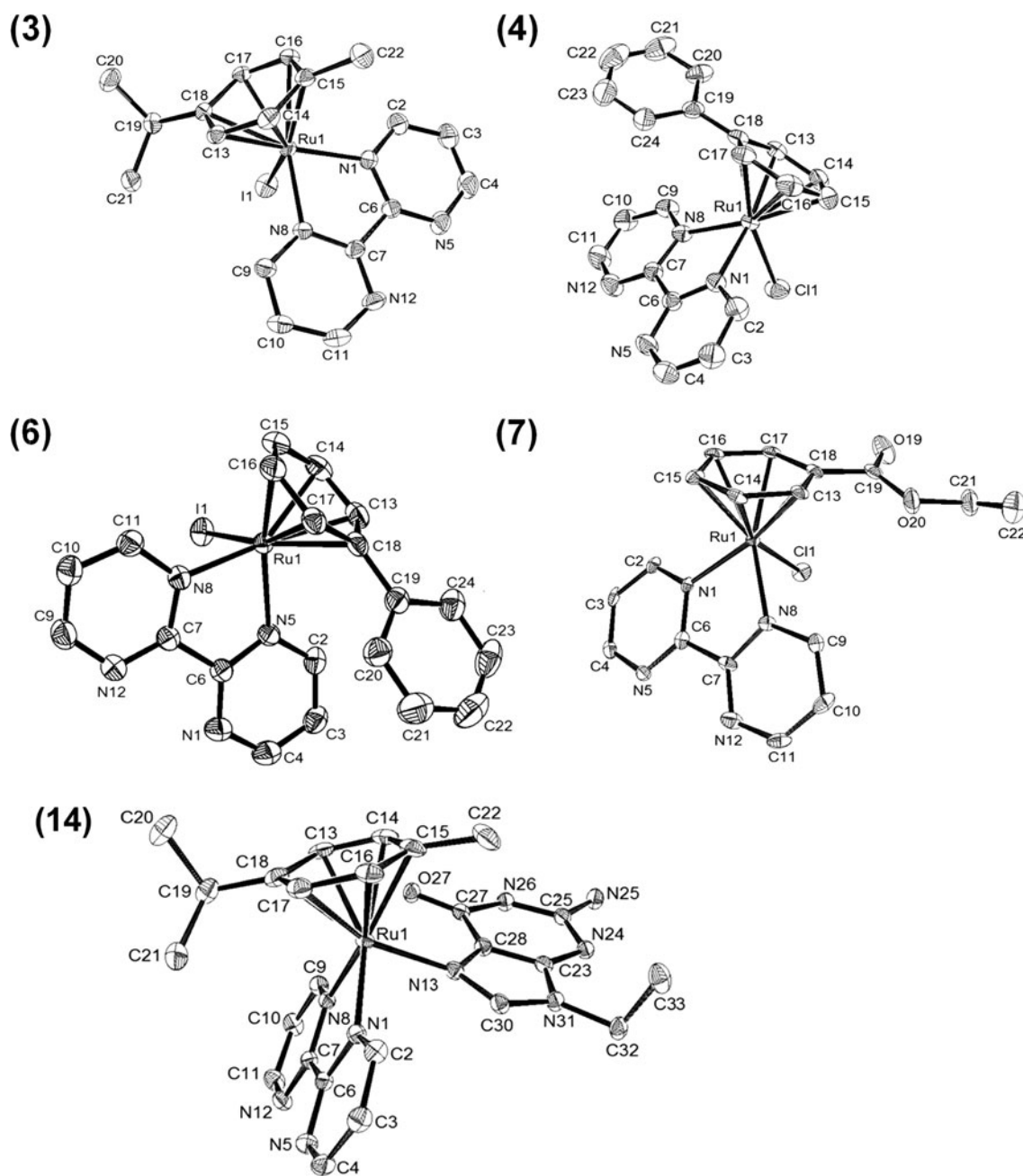


Fig. 2 X-ray structure of the cations in $[(\eta^6\text{-}p\text{-cym})\text{Ru}(\text{bpm})\text{I}][\text{PF}_6]$ (**3**), $[(\eta^6\text{-bip})\text{Ru}(\text{bpm})\text{Cl}][\text{PF}_6]$ (**4**), $[(\eta^6\text{-bip})\text{Ru}(\text{bpm})\text{I}][\text{PF}_6]_2$ (**6**), $[(\eta^6\text{-erb})\text{Ru}(\text{bpm})\text{Cl}][\text{PF}_6]$ (**7**) and $[(\eta^6\text{-}p\text{-cym})\text{Ru}(9\text{-EtG-N}7)][\text{PF}_6]_2$ (**14**).

Thermal ellipsoids show 50 % probability. The hydrogen atoms and counter ions have been omitted for clarity

Ru–N,N' bond lengths are significantly longer than those found in the crystal structures of similar arene Ru^{II} arene 2,2'-bipyridine (bpy) complexes [43]. The N(1)–Ru(1)–N(8) bond angles in complexes **3**, **4**, **6**, **7** and **14** do not differ significantly from each other. In the case of complex $[(\eta^6\text{-bip})\text{Ru}(\text{bpm})\text{Cl}][\text{PF}_6]$ (**4**), the Ru^{II} molecules lie back-to-back with an adjacent complex in an intermolecular π – π stacking interaction (Fig. S1). The X-ray crystal structures of compounds **3**, **4**, **6** and **7** show an increased number of

intramolecular and/or intermolecular π – π stacking interactions, particularly for complexes **4** and **6** (Fig. S2), which contain bip as the arene. Their crystal packing also displays strong hydrogen bonding throughout the unit cell, which is a common feature observed in similar Ru^{II} arene complexes containing extended aromatic rings [44, 45]. For complex **7**, CH– π interactions between the C–H protons of one of the pyrazine rings in the bpm chelating ligand and the centroid of one of the pyrazine rings in the bpm

belonging to a neighbouring molecule were observed (Fig. S3). The occurrence of CH $\cdots\pi$ interactions is now well established [46], and the interaction ranges from weak (CH $\cdots\pi$ centre 2.6–3.0 Å) to strong (CH $\cdots\pi$ centre less than 2.6 Å) [47]. Such interactions can play an important role in protein stability and in recognition processes. The CH $\cdots\pi$ interactions observed for complex **7** (2.9 Å) are within the weak-interaction range. The Ru–N7_(9-EtG) bond distance in guanine adduct **14** [2.1125(19) Å] is similar to the bond distances in related organometallic Ru^{II} guanine adducts [36, 37]. There are multiple hydrogen-bonding interactions throughout the crystal. The main fragments involved are bpm, 9-EtG and solvent molecules (water; Fig. S4). Such aggregations have been observed in a number of Ru^{II} and Pt^{II} crystal structures containing purine derivatives [48–50]. Water can play an important role in intercalation modes; specific binding of water to DNA complexes can make a significant contribution to the free energy of drug binding [51]. The 9-EtG adduct (**14**) was also characterized by ¹H NMR spectroscopy (Fig. S5 shows its 2D ¹H–¹H NOESY spectrum). A nuclear Overhauser enhancement cross-peak between H8 of bound 9-EtG and the 2,2'-H in bpm was observed, suggesting that these two atoms are in close proximity (as previously observed in analogous Ru^{II} arene complexes) [5, 52].

Aqueous solution chemistry

Dissolution of compounds **1–13** in 5 % MeOH/95 % H₂O at 310 K gave rise to ligand-exchange reactions as indicated by the concomitant changes in UV–vis absorption bands. The time-evolution spectra for all the Ru^{II} arene complexes at 310 K are shown in Fig. S6. The time dependence of the absorbance of all the complexes at selected wavelengths followed pseudo-first-order kinetics in each case. The corresponding rate constants and half-lives are listed in Table 2. The dependence of the absorbance at 332 nm over approximately 16 h during aquation of [(η^6 -*p*-cym)Ru(bpm)Cl][PF₆] (**1**) at 310 K is shown in Fig. S7.

To characterize the products of hydrolysis and to determine the extent of the reactions, freshly made 100 μ M (5 % MeOD-*d*₄/95 % D₂O) solutions of complexes **1–13** were allowed to equilibrate for 24–48 h at 310 K and were then studied at 310 K using ¹H NMR spectroscopy. The ¹H NMR spectra of complexes **1–11** and **13** initially contained one major set of peaks (halido species), and then a second set of peaks increased in intensity with time. The new set of peaks had the same chemical shifts as those of the aqua adducts (prepared independently) under the same conditions [approximately 100 μ M solutions (5 % MeOD-*d*₄/95 % D₂O) at 310 K]. The mass-to-charge ratios and isotopic models obtained from HR-MS spectra were

consistent with the formation of the aqua adducts (Table S2). Table 3 summarizes the equilibrium constants (calculated by integration of ¹H NMR signals) after 24 h of reaction for complexes **1–11** and **13**. For complexes **4**, **5**, **7** and **12** an additional set of peaks was also observed

Table 2 Hydrolysis data for complexes **1–13** determined by UV–vis spectroscopy as 100 μ M solutions (5 % MeOH/95 % H₂O) at 310 K

Complex	<i>t</i> _{1/2} (min)	<i>k</i> × 10 ^{−3} (min ^{−1}) ^a
[(η^6 - <i>p</i> -cym)Ru(bpm)Cl][PF ₆] (1)	92.3	7.51 ± 0.07
[(η^6 - <i>p</i> -cym)Ru(bpm)Br][PF ₆] (2)	22.4	31.0 ± 0.91
[(η^6 - <i>p</i> -cym)Ru(bpm)I][PF ₆] (3)	234.8	2.95 ± 0.08
[(η^6 -bip)Ru(bpm)Cl][PF ₆] (4) ^b	175.9	3.94 ± 0.04
[(η^6 -bip)Ru(bpm)Br][PF ₆] (5) ^b	39.7	17.0 ± 0.31
[(η^6 -bip)Ru(bpm)I][PF ₆] (6) ^b	714.6	0.97 ± 0.04
[(η^6 -etb)Ru(bpm)Cl][PF ₆] (7) ^b	14.5	50.0 ± 0.05
[(η^6 -hmb)Ru(bpm)Cl][PF ₆] (8)	40.2	17.2 ± 1.32
[(η^6 -ind)Ru(bpm)Cl][PF ₆] (9)	43.3	16.0 ± 0.15
[(η^6 -thn)Ru(bpm)Cl][PF ₆] (10)	89.9	7.71 ± 0.44
[(η^6 - <i>p</i> -cym)Ru(phen)Cl][PF ₆] (11)	22.8	30.5 ± 0.43
[(η^6 - <i>p</i> -cym)Ru(phendio)Cl][PF ₆] (12) ^b	59.6	11.6 ± 0.10
[(η^6 - <i>p</i> -cym)Ru(bathophen)Cl][PF ₆] (13)	16.9	40.8 ± 0.86

hmb hexamethylbenzene, *ind* indane, *thn* 1,2,3,4-tetrahydronaphthalene, *phen* 1,10-phenanthroline, *phendio* 1,10-phenanthroline-5,6-dione, *bathophen* 4,7-diphenyl-1,10-phenanthroline

^a The errors are fitting errors.

^b The rate constants for complexes that underwent arene loss detected by ¹H NMR spectroscopy (**4**, **5**, **7** and **12**) were determined over the period of time before the onset of arene loss.

Table 3 Equilibrium constants (*K*) and percentage of arene loss for Ru^{II} arene complexes at equilibrium after 24 h of the hydrolysis reaction in a 100 μ M (5 % MeOD-*d*₄/95 % D₂O) solution at 310 K of complexes **1–11** and **13** followed by ¹H NMR spectroscopy

Complex	<i>K</i> (μ M)	Arene loss (%)
[(η^6 - <i>p</i> -cym)Ru(bpm)Cl][PF ₆] (1)	280.5	0.0
[(η^6 - <i>p</i> -cym)Ru(bpm)Br][PF ₆] (2)	790.6	0.0
[(η^6 - <i>p</i> -cym)Ru(bpm)I][PF ₆] (3)	14.0	0.0
[(η^6 -bip)Ru(bpm)Cl][PF ₆] (4)	9.0	48.1
[(η^6 -bip)Ru(bpm)Br][PF ₆] (5)	10.4	68.3
[(η^6 -bip)Ru(bpm)I][PF ₆] (6)	0.2	0.0
[(η^6 -etb)Ru(bpm)Cl][PF ₆] (7)	4.5	2.9
[(η^6 -hmb)Ru(bpm)Cl][PF ₆] (8)	34.1	0.0
[(η^6 -ind)Ru(bpm)Cl][PF ₆] (9)	79.6	0.0
[(η^6 -thn)Ru(bpm)Cl][PF ₆] (10)	231.1	0.0
[(η^6 - <i>p</i> -cym)Ru(phen)Cl][PF ₆] (11)	61.6	0.0
[(η^6 - <i>p</i> -cym)Ru(bathophen)Cl][PF ₆] (13)	52.1	0.0

corresponding to the products which had undergone arene loss during the aquation. Complex **12** displayed a complicated ^1H NMR spectrum upon dissolution which could not be explained by hydrolysis alone.

Within the series of complexes having *p*-cym as the arene and bpm as the chelating ligand, the hydrolysis reactions of the chlorido (**1**) and bromido (**2**) complexes are more thermodynamically favoured (K of 790.6 and 280.5 μM , respectively) compared with the hydrolysis reaction of the iodido complex (**3**) ($K = 14.0 \mu\text{M}$). Similarly, in the bip/bpm series, the chlorido (**4**) and bromido (**5**) complexes were hydrolyzed to a larger extent (K of 9.0 and 10.4 μM , respectively) than the analogous iodido (**6**) complex ($K = 0.2 \mu\text{M}$). For complexes **1**, **11** and **13**, where *p*-cym (arene) and chloride (leaving group) are kept constant but the chelating ligand is varied, the amount of aqua adduct (and equilibrium constant) determined by ^1H NMR spectroscopy increases in the order bathophen (**13**) < phen (**11**) < bpm (**1**). When the chelating ligand is bpm and the leaving group is chloride, the extent of hydrolysis decreases with the arene in the order *p*-cym (**1**) > thn (**10**) > ind (**9**) > hmb (**8**) > etb (**7**) > bip (**4**).

Complexes **2**, **5**, **7–9** and **11–13** undergo relatively fast hydrolysis, with half-lives of less than 60 min at 310 K. The reported half-lives of aquation of the previously reported chlorido ethylenediamine Ru^{II} arene complexes $[(\eta^6\text{-dha})\text{Ru}(\text{en})\text{Cl}][\text{PF}_6]$, $[(\eta^6\text{-tha})\text{Ru}(\text{en})\text{Cl}][\text{PF}_6]$ and $[(\eta^6\text{-bip})\text{Ru}(\text{en})\text{Cl}][\text{PF}_6]$ [53], where dha is 9,10-dihydroanthracene and en is ethylenediamine, are 10–80 times smaller than those of these complexes under comparable conditions. Within the *p*-cym/chloride series containing various chelating ligands, the presence of a stronger π -acceptor chelating ligand reduces the electron density on the Ru^{II} centre, making it less favourable for the chlorido ligand to leave, thus slowing down the hydrolysis reaction. Thus, the rates increase in the order **1** (bpm) < **12** (phen-dio) < **11** (phen) < **13** (bathophen). The substituent heteroatoms on the chelating ligands (such as the extra pair of nitrogens in bpm or two oxygens in phen-dio), which are electron donors [54], may contribute to stabilization of the Ru–Cl bonds by π back-donation. Previous work [55] has shown that an N,N' chelating group such as bpy slows down substitution of the aqua ligand in $[(\eta^6\text{-C}_6\text{H}_6)\text{Ru}(\text{bpy})(\text{OH}_2)]^{2+}$ just as the replacement of ethylenediamine by acetylacetonate (acac) to form $[(\eta^6\text{-arene})\text{Ru}(\text{acac})]^+$ complexes accelerates hydrolysis. Within the Ru^{II} arene bpm/chloride series, the incorporation of arenes with either an increased aromatic character or electron-withdrawing substituents in the coordinated ring significantly decreases the rate of the hydrolysis reaction in the order **7** (etb) > **8** (hmb) > **9** (ind) > **10** (thn) > **1** (*p*-cym) > **4** (bip). Bip has a high aromaticity and competes as a π -acceptor [56] with the chelating ligand (bpm) for electron density. This leads

to a weakening of the corresponding Ru–arene bonds and consequently to the complete loss of the bip in the case of complex **4**. No arene loss is observed in the case of the complexes bearing other arenes, all of which have electron-donating aliphatic substituents on the ring. A similar arene loss was previously observed for other Ru^{II} bip complexes containing phenylazopyridines as π -acceptor ligands [57]. Within this same series of complexes **1–6**, the combination of a large leaving group (such as iodide) and a large arene (such as bip) in complexes **3** and **6** makes the Ru^{II} centre less accessible to an incoming ligand. This effect corresponds to the experimental observation of a very slow hydrolysis rate. The inclusion of a more electro-negative halide (such as chloride or bromide in **1** and **2** or **4** and **5**) leads to an increase in the hydrolysis rate when compared with the iodido derivatives, which is enhanced when the arene is replaced by a less sterically demanding ligand such as *p*-cym in complexes **1–3**. Arene ligands such as benzene are reported to exhibit a strong *trans*-labilizing effect for the aqua ligand in $[(\eta^6\text{-bz})\text{Ru}(\text{OH}_2)_3]^{2+}$, where bz is benzene [58]. This class of strong π -acid ligands is able to accept electron density from the central Ru^{II} atom, giving rise to a higher charge on the metal. Acidic hydrolysis of Ru^{III} complexes such as $[\text{Ru}(\text{NH}_3)_4(\text{X})_2]^+$ and $[\text{Ru}(\text{NH}_3)_5\text{X}]^{2+}$ (X is Cl, Br or I) occurs via an associative pathway in which bond-making is more important than bond-breaking [59].

Additionally, the changes in the ^1H NMR chemical shifts of the aromatic protons in either the corresponding arene rings or the corresponding N,N' chelating ligands of the aqua adducts of complexes **1**, **8–11** and **13** present in an equilibrated 100 μM (D_2O) solution at 310 K were followed with change in pH^* over the range approximately 1–12. Figure S8 shows how the peaks shift to higher field owing to deprotonation of the bound water molecule in the aqua adduct of complex **1**, $[(\eta^6\text{-p-cym})\text{Ru}(\text{bpm})(\text{OH}_2)]^{2+}$, but do not change in intensity, an indication that no other species are being formed. The pK_a^* values for complexes **1**, **8**, **9** and **11** are listed in Table 4. For complexes **1** (*p*-cym/bpm), **8** (hmb/bpm), **9** (ind/bpm) and **11** (*p*-cym/phen), the pK_a^* values are in the range from 6.91 to 7.32 and are all significantly lower (approximately 1.5 units)

Table 4 pK_a^* values for the aqua adducts of complexes **1**, **8**, **9** and **11** at 298 K

Complex	pK_a
$[(\eta^6\text{-p-cym})\text{Ru}(\text{bpm})\text{OH}_2]^{2+}$ (1)	6.96
$[(\eta^6\text{-hmb})\text{Ru}(\text{bpm})\text{OH}_2]^{2+}$ (8)	7.04
$[(\eta^6\text{-ind})\text{Ru}(\text{bpm})\text{OH}_2]^{2+}$ (9)	6.91
$[(\eta^6\text{-p-cym})\text{Ru}(\text{phen})\text{OH}_2]^{2+}$ (11)	7.32

than those reported for analogous $[(\eta^6\text{-arene})\text{Ru}(\text{N,N}')(\text{OH}_2)]^{2+}$ complexes [7, 60]. Such a decrease in acidity has been attributed before to an increased electron density on the metal centre favoured by a combination of electron-donating/ π -acceptor-arene/chelating ligands. Complexes **1**, **8**, **9** and **11** will therefore be present as a mixture of aqua and (less reactive) hydroxido adducts at pH 7.4.

Hydrolysis mechanism

DFT computational methods were employed to obtain information about the influence of the leaving group on the mechanism of hydrolysis for the *p*-cym/bpm series of Ru^{II} arene complexes **1–6**. A test of the structural accuracy of the functional PW91 with COSMO solvation was performed by comparing the fully optimized structures of the cations in complexes **1–6** with the corresponding X-ray crystal structures of **1** [18], **3**, **4** and **6**. The functional PW91 was found to overestimate the Ru^{II} bond lengths by approximately 0.01–0.04 Å, particularly for the computed Ru–X distances (approximately 2.44 Å), which were approximately 0.05 Å longer than those found in the solid state. However, the overall agreement with the experimental data was satisfactory. A scheme for the reaction modeled is shown in Fig. 3. For each of the resting states ($[\text{RS}] = \{[(\eta^6\text{-arene})\text{Ru}(\text{bpm})\text{X}]^+ \cdot \text{H}_2\text{O}\}$) and the corresponding products ($[\text{P}] = \{[(\eta^6\text{-arene})\text{Ru}(\text{bpm})(\text{OH}_2)]^{2+} \cdot \text{X}^-\}$), the entering (H_2O) and the leaving (X^-) groups are retained within the second coordination sphere of the Ru^{II} centre. Complex **1** was chosen as a model system on the basis of previously reported work [7] on analogous Ru^{II} arene complexes. A full geometry optimization of its transition state was performed, starting from Ru–Cl and Ru–OH_2 bond distances of 3.200 and 2.899 Å, respectively, in the initial geometry. The optimized structure for the transition state for the Ru^{II} arene cation $[(\eta^6\text{-p-cym})\text{Ru}(\text{bpm})\text{Cl}]^+$ is shown in Fig. 4. The geometry-optimized structure in the transition state of the Ru^{II} arene

cation in complex **1** gave Ru–Cl and Ru–OH_2 bond distances of 3.11 and 2.68 Å, respectively. The corresponding energy value determined for the transition state ($-6,657.51 \text{ kcal mol}^{-1}$) was $20.1 \text{ kcal mol}^{-1}$ larger than that for the chlorido compound in the resting state. Given that the hydrolysis reaction could be assumed to be an associative, a dissociative, or an interchange (I_a or I_d) process, a frequency calculation was performed for the transition state of the Ru^{II} arene cation in complex **1**. Two imaginary frequencies were retrieved from the computation, -152 and -20 cm^{-1} . The latter is small and arises from the numerical noise inherent in the finite difference method required when a COSMO field is enabled. The former (and more significant) frequency value (-152 cm^{-1}) gave a vibrational mode where the entering water molecule and leaving halido ligand (Cl^-) are moving in a concerted process consistent with an associatively activated reaction. The corresponding scaled displacement vectors are shown in Fig. S9. Under the assumption that the same associative hydrolysis mechanism applies for other related systems, the effects of varying X and the arene were explored. The results are listed in Table 5, from where it can be seen that the corresponding barrier heights do not vary significantly when the arene *p*-cym (in complexes **1–3**) is replaced by bip (in complexes **4–6**). The forward reaction barriers and overall reaction energies for the aquation of the corresponding halido ligand (Cl^- , Br^- , or I^-) follow the increasing order $\text{Cl}^- \approx \text{Br}^- < \text{I}^-$, and *p*-cym < bip.

The transition state obtained from DFT calculations suggested that aquation of the $[(\eta^6\text{-arene})\text{Ru}(\text{bpm})\text{X}]^+$ complexes, where arene is *p*-cym (**1–3**) or bip (**4–6**) and X is Cl, Br or I, proceeds via a concerted interchange (associative) mechanism rather than a stepwise dissociation/coordination process (dissociative). For the *p*-cym/bpm series of complexes (**1–3**), the reaction does not appear to be strongly associatively or dissociatively activated, because the corresponding Ru–X bonds at the transition state extend by approximately 0.66, 0.71 and 0.81 Å for Cl, Br, and I, respectively, relative to the reactant species. In

Fig. 3 Hydrolysis reaction modeled for the Ru^{II} arene cations $[(\eta^6\text{-arene})\text{Ru}(\text{bpm})\text{X}]^+$ of complexes **1–6**. $[\text{TS}]$ is the transition state

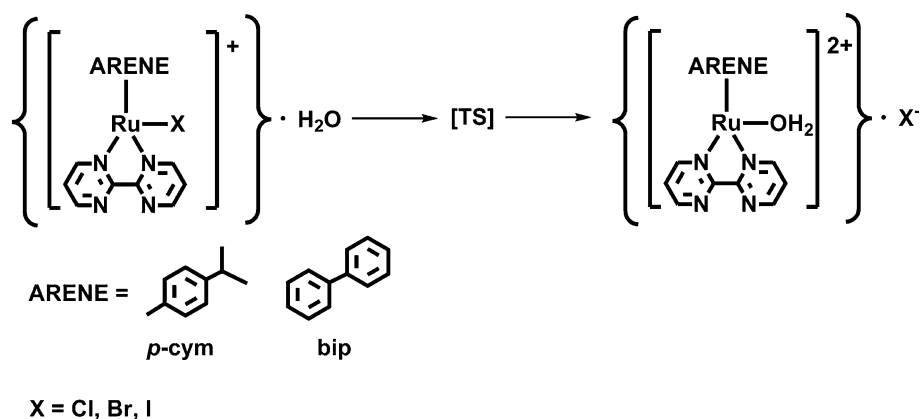


Fig. 4 Density-functional-theory-optimized geometry of the transition state during the hydrolysis reaction of the Ru^{II} arene cation $[(\eta^6\text{-}p\text{-cym})\text{Ru}(\text{bpm})\text{Cl}]^+$ (**1**)

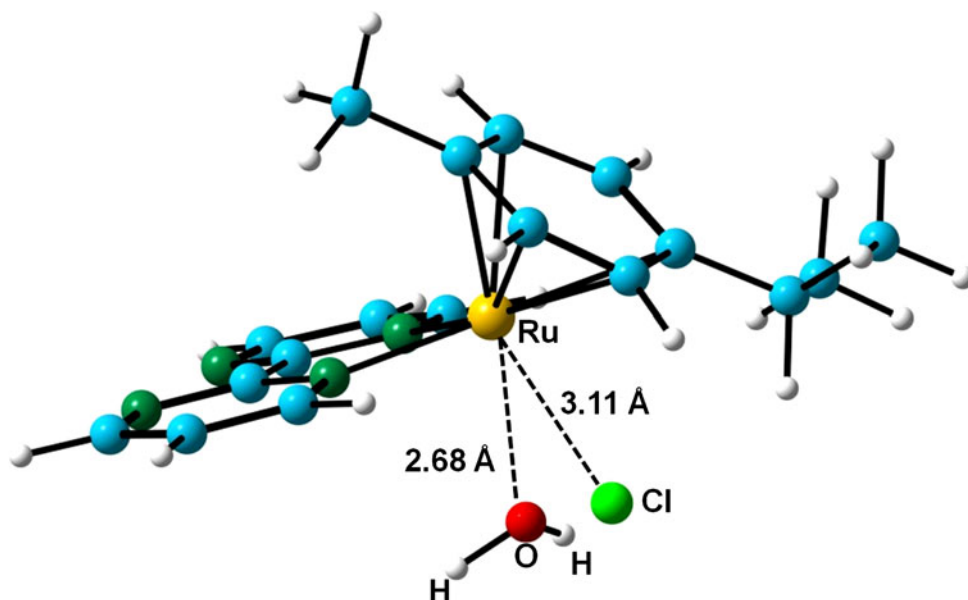


Table 5 Selected bond lengths, forward reaction barriers and overall reaction energies from density functional theory calculations for the modeled reaction $\{[(\eta^6\text{-}p\text{-cym})\text{Ru}(\text{bpm})\text{X}]^+\cdot\text{H}_2\text{O}\} \rightarrow \text{transition state} \rightarrow \{[(\eta^6\text{-}p\text{-cym})\text{Ru}(\text{bpm})\text{OH}_2]^{2+}\cdot\text{Cl}^-\}$

	Bond length (Å)			ΔE^\ddagger (kcal mol ⁻¹)	ΔE_{reac} (kcal mol ⁻¹)
	Ru-X/Ru-OH ₂ (RS)	Ru-X/Ru-OH ₂ (TS)	Ru-X/Ru-OH ₂ (P)		
<i>p</i> -cym/bpm					
1 Cl	2.44736/3.87080	3.1069/2.67606	4.00637/2.17416	20.09	5.5
2 Br	2.58087/3.93448	3.29409/2.67608	4.13680/2.17987	21.01	7.28
3 I	2.76784/4.08973	3.58007/2.68230	4.42902/2.19029	22.79	9.61
<i>bip</i> /bpm					
4 Cl	2.43726/3.82308	3.01943/2.71710	4.01419/2.16185	19.96	6.16
5 Br	2.57062/3.88138	3.18568/2.73201	4.15467/2.16741	20.94	7.51
6 I	2.76183/4.01231	3.45171/2.74296	4.41027/2.17431	22.28	10.28

ΔE_{reac} values relative to reactant species at zero energy.

RS resting state, TS transition state, P product

the case of the corresponding Ru–O bonds in the transition state, it was found that they are approximately 0.50 Å longer than in the aqua products in the three cases. The results for the *bip*/bpm series of complexes (**4–6**) showed that the hydrolysis might not be strongly associatively nor dissociatively activated either. The corresponding Ru–X bonds at the transition state extend by approximately 0.58, 0.61 and 0.69 Å for Cl, Br and I, respectively, relative to the reactant species, whereas the Ru–O bonds in the transition state were found to be approximately 0.55 Å longer than in the aqua products. Given that Ru–X bond-breaking alone is not the rate-controlling step in the associative pathway, a heavier (and larger) halide will impede the access of the H₂O molecule to the central Ru^{II} atom in associative states. This hypothesis is in good agreement with the experimental observation that complexes **3** and **6** (bearing iodide as the leaving group) display the slowest

rates of hydrolysis within the corresponding series. This assumption has also been suggested for ruthenium complexes displaying higher coordination numbers (i.e. seven) [61, 62]. The calculated reaction barriers and overall reaction energies for the aquation of the halido complexes **1–6** follow the increasing order Cl \approx Br < I. However, the effect of different halides on the experimental hydrolysis rates of these Ru^{II} arene complexes differs from the calculation and follows the increasing order Br < Cl < I. This trend has been experimentally observed before for platinum compounds of the type $[\text{PtX}_n(\text{OH}_2)_{4-n}]^{(2-n)+}$, for which Br analogues of Cl complexes hydrolyze faster in all three hydrolysis steps [38, 39]. The calculated higher activation energies might be responsible for the observed slower hydrolysis of the iodido complexes during the associative ligand interchange in each series. Furthermore, the electron-accepting effect of strong π -acid arene ligands

might be responsible for the shift towards a more associative pathway in the $I_d \leftrightarrow I_a$ mechanistic continuum for the $[(\eta^6\text{-}p\text{-cym})\text{Ru}(\text{N},\text{N}')\text{Cl}]^+$ complexes studied herein. The accuracy of the calculation was not sufficient to account for the differences found experimentally in the hydrolysis rates between the chlorido and bromido complexes.

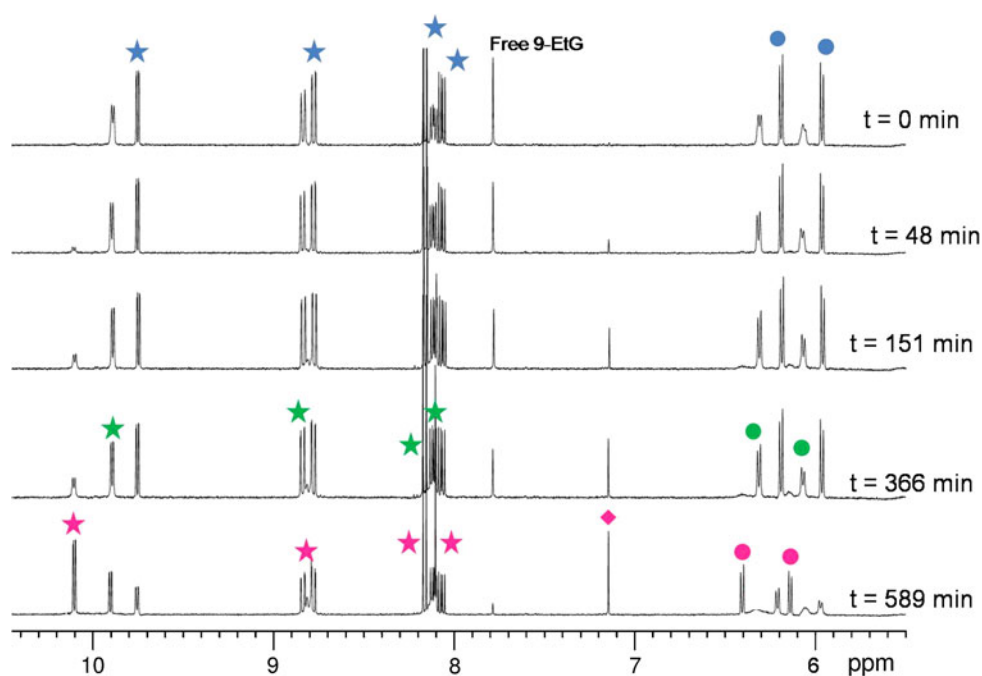
Interactions with nucleobases

Interactions of several complexes with 9-EtG and 9-EtA were studied by multidimensional ^1H NMR spectroscopy and the nature of the products was verified by HR-MS. All the reactions were performed in NMR tubes in D_2O and followed over 48 h at 310 K. Figure 5 shows the reaction of complex **11** with 9-EtG as an example. The ^1H NMR peaks corresponding to H8 in all the 9-EtG-*N7* adducts are shifted to high field (approximately 0.5 ppm) relative to free 9-EtG under the same conditions. Often, metallation at the *N7* site of purine bases (Fig. 6) produces a low-field shift of the H8 resonance by about 0.3–1 ppm [63, 64]. This effect has also been observed before for analogous Ru^{II} arene complexes containing bpy or acac [6] as the chelating ligand. The compounds studied in this work showed significant and rapid binding to 9-EtG-*N7* (detectable after approximately 10 min and to an extent of approximately 34–94 %). The reactions of complexes $[(\eta^6\text{-}p\text{-cym})\text{Ru}(\text{bpm})\text{Cl}]^+$ (**1**), $[(\eta^6\text{-}thn)\text{Ru}(\text{bpm})\text{Cl}]^+$ (**10**) and $[(\eta^6\text{-}p\text{-cym})\text{Ru}(\text{bathophen})\text{Cl}]^+$ (**13**) required approximately 8 h to reach equilibrium in each case. However, a different behaviour was observed for complexes $[(\eta^6\text{-}$

$\text{hmb})\text{Ru}(\text{bpm})\text{Cl}]^+$ (**8**) and $[(\eta^6\text{-ind})\text{Ru}(\text{bpm})\text{Cl}]^+$ (**9**), which reacted with 9-EtG much faster, reaching equilibrium after 56 and 52 min, respectively. Table S6 lists the percentage of species present in solution for the reactions of complexes **1**, **8–11** and **13** with 9-EtG after selected times. The reactions of complexes **8**, **9** and **10** with 9-EtG produced higher yields. Interestingly, for complex **10**, approximately 12 % of a second guanine-bound species (possibly $[(\eta^6\text{-}thn)\text{Ru}(\text{bpm})(9\text{-EtG-}N3)]^{2+}$) was also detected at equilibrium (approximately 510 min; Fig. S10). The mass-to-charge ratios and isotopic models obtained from HR-MS spectra were consistent with the formation of the guanine adducts as the corresponding products of the individual reactions (Table S3). The addition of an equimolar amount of 9-EtA (100 μM) to freshly prepared D_2O solutions of the complexes at 310 K resulted in no new species even after 48 h.

Since nucleobase binding is likely to require initial hydrolysis, the slow aquation rates and reduced extent of hydrolysis of these complexes at equilibrium may account for the observed extent of nucleobase binding. The calculated binding energies for 9-EtG in the corresponding nucleobase adducts appear to be related to the trend determined for the extent of nucleobase binding (vide infra). None of the Ru^{II} arene complexes **1**, **8–11** and **13** showed evidence of binding to 9-EtA. These complexes display a more discriminating behaviour towards binding to purine bases when compared with cisplatin, for which binding to adenine is also observed [65]. It has been found that hydrogen bonding from C6O in guanine to N–H protons in the bidentate chelating ligand ethylenediamine

Fig. 5 Time dependence of the ^1H NMR spectra of a 100 μM solution of $[(\eta^6\text{-}p\text{-cym})\text{Ru}(\text{phen})\text{Cl}][\text{PF}_6]$ (**11**) in D_2O at 310 K in the presence of an equimolar amount of 9-EtG. Blue symbols $[(\eta^6\text{-}p\text{-cym})\text{Ru}(\text{phen})\text{Cl}]^+$, green symbols $[(\eta^6\text{-}p\text{-cym})\text{Ru}(\text{phen})(\text{OH}_2)]^{2+}$, magenta symbols $[(\eta^6\text{-}p\text{-cym})\text{Ru}(\text{phen})(9\text{-EtG-}N7)]^{2+}$, stars phen, circles *p*-cym, diamond bound 9-EtG-*N7*



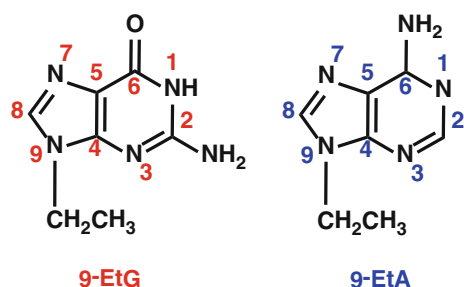


Fig. 6 Numbering scheme for the nucleobases 9-ethylguanine (9-EtG) and 9-ethyladenine (9-EtA)

contributes to the high preference for binding of $\{(\eta^6\text{-arene})\text{Ru}(\text{en})\}^{2+}$ to guanine versus adenine. However, replacement of ethylenediamine (NH as a hydrogen-bond donor) by bpm (no NH) in these series of complexes did not change the selectivity for guanine bases.

To gain further insight into the nature and relative stabilities of the guanine and adenine adducts of Ru^{II} arene complexes **1**, **8–11** and **13**, their optimized geometries were obtained using DFT calculations. Their minimum-energy structures are shown in Figs. S11 and S12 (for the 9-EtG-*N*7 and 9-EtA-*N*7 adducts, respectively). The total binding energies for both nucleobases are shown in Table 6. The binding energies include a COSMO contribution which simulates an aqueous environment. Under these conditions, the binding of 9-EtG was more favourable than that of 9-EtA by approximately $10.0 \text{ kcal mol}^{-1}$. Furthermore, the nucleobase 9-EtG shows significant binding energies for all compounds ($38.5 \text{ kcal mol}^{-1}$ or greater), the largest value being for the adduct $[(\eta^6\text{-thn})\text{Ru}(\text{bpm})(9\text{-EtG-}N7)]^{2+}$ (**10**–9-EtG), with a value of $41.0 \text{ kcal mol}^{-1}$. In the case of 9-EtA, a smaller binding energy for all compounds ($34.4 \text{ kcal mol}^{-1}$ or less) was found; the largest energy was calculated for the adduct $[(\eta^6\text{-thn})\text{Ru}(\text{bpm})(9\text{-EtA-}N7)]^{2+}$ (**10**–9-EtA). The binding of 9-EtG to the *N*3 position in complex **10** was also investigated. The minimum-energy structures are shown in Fig. S13 for the 9-EtG-*N*7 and 9-EtG-*N*3 adducts. The calculated total binding energies

Table 6 Solution (conductor-like screening model) 9-ethylguanine (9-EtG) and 9-ethyladenine (9-EtA) binding energies for adducts of Ru^{II} arene complexes **1**, **8–11** and **13**

Complex	Binding energy (kcal mol^{-1})	
	9-EtG	9-EtA
1	38.5	30.8
8	39.3	30.3
9	39.3	32.4
10	41.0	34.4
11	39.8	33.7
13	38.7	32.3

are 41.0 and $18.5 \text{ kcal mol}^{-1}$ for the 9-EtG-*N*7 and the 9-EtG-*N*3 adduct, respectively.

Despite the lack of cytotoxic activity, compounds **1** and **8–10** showed a significant calculated binding energy for 9-EtG-*N*7 (approximately $38.8 \text{ kcal mol}^{-1}$). As would be expected, the binding of 9-EtG to complex **10** through *N*7 is approximately 20 kcal mol^{-1} more stable than the binding through *N*3. The calculations were also able to reproduce the hydrogen-bond distance ($\text{CH}_{(\text{N},\text{N}'\text{-chelating})}\cdots\text{O}_{(9\text{-EtG})}$) found in the X-ray crystal structure of the 9-EtG adduct, complex **14**, within sufficient accuracy. Therefore, it is assumed that the analogous values from the DFT-optimized geometries for the rest of the 9-EtG adducts of complexes **1**, **8–11** and **13** will also be within the expected ranges. The calculations predict $\text{CH}_{(\text{N},\text{N}'\text{-chelating})}\cdots\text{O}_{(9\text{-EtG})}$ distances within the range from 2.20 to 3.11 Å and $\text{C-H}_{(\text{N},\text{N}'\text{-chelating})}\cdots\text{O}_{(9\text{-EtG})}$ angles within the range from 114.93° to 134.97° . The shortest hydrogen-bond distance was found for the 9-EtG adduct of complex **10**, which might explain the high binding energy calculated for this adduct.

DNA binding reactions in cell-free media

To explore the possibility of DNA as a potential target, two complexes $[(\eta^6\text{-}p\text{-cym})\text{Ru}(\text{bpm})\text{Cl}][\text{PF}_6]$ (**1**) and $[(\eta^6\text{-}p\text{-cym})\text{Ru}(\text{phen})\text{Cl}][\text{PF}_6]$ (**11**) were selected for further studies of CT–DNA interactions in cell-free media. The results of the DNA binding experiments are summarized in Table 7. Both complexes reacted with CT–DNA to a moderate extent and the reactions were complete after approximately 20 h. Complex **11** bound much faster and to a larger extent than complex **1**, with equilibrium for complex **11** being reached within the first 1.5 h. After 24 h of reaction, both complexes had reacted to a similar extent, approximately 60 % (Fig. S14). Dialysis against two different sodium salts indicated that the coordination of the Ru^{II} arene complexes to CT–DNA is reversible and dependent on the nature of the salt. In the case of complex **11**, dialysis against either 10 mM NaClO_4 or 0.1 M NaCl resulted in a decrease in the percentage of complex bound to DNA to approximately 20 %. For complex **1**,

Table 7 Percentage binding of complexes **1** and **11** to calf thymus DNA ($1.0 \times 10^{-4} \text{ M}$) in 10 mM NaClO_4 at 310 K as determined by flameless atomic absorption spectrometry after 24 h

Method	Ru^{II} bound (%)	
	1	11
DNA precipitation by EtOH	61.0	62.0
Dialysis against 10 mM NaClO_4	77.0	19.6
Dialysis against 0.1 M NaCl	21.6	17.3

Data are the average of two independent experiments.

dialysis against 10 mM NaClO₄ did not change the percentage of complex bound to DNA, whereas dialysis against 0.1 M of NaCl reduced the percentage to the same level as for complex **11** (approximately 20 %).

Further investigations were aimed at identifying the ruthenium binding sites in natural DNA for the reactions

of [(η^6 -*p*-cym)Ru(bpm)Cl][PF₆] (**1**) and [(η^6 -*p*-cym)Ru(phen)Cl][PF₆] (**11**). The autoradiogram for the inhibition of RNA synthesis by T7 RNA polymerase on pSP73KB DNA containing adducts of the Ru^{II} arene complexes or cisplatin is shown in Fig. 7. The bands corresponding to the transcription of DNA modified by complexes **1** and **11** yielded fragments of newly synthesized RNA of defined sizes, which indicates that RNA synthesis on these templates was prematurely terminated. The major stop sites occurred at similar positions in the gel and were solely at guanine residues, for both Ru^{II} arene complexes (Fig. 8).

The intensities of the bands corresponding to the transcription of DNA modified by complex **11** are considerably weaker than those of the bands corresponding to the transcription of DNA modified by complex **1** (Fig. 7). This may indicate that the efficiency of DNA adducts of **11** to prematurely terminate RNA synthesis by T7 RNA polymerase is lower than that of DNA adducts of **1**. We can speculate that this reduced efficiency is associated with lesser distortion of the DNA conformation exerted by DNA adducts of **11** (compared with DNA adducts of **1**) as deduced from the results of CD spectroscopy of DNA modified by these complexes (Fig. 10). Another possibility might be through the labilization of DNA–metal adducts by the phen chelating ligand in **11** being greater than that exerted by the bpm chelating ligand in **1** owing to the introduction of electron-withdrawing substituents in the 4,4' positions of bpm in complex **11** (which contains phen as a chelating ligand). As a consequence, some molecules of **11** originally bound to DNA might be displaced by T7 RNA polymerase during transcription of the template strand containing them and consequently would be unable to prematurely terminate RNA synthesis by this enzyme. The labilization of other metal-biologically relevant molecules by spectator ligands (in metal complexes) has already been demonstrated for Pt^{II} complexes [66].

The rate of binding to DNA for complex **1** is slower than that determined for the anticancer drug cisplatin (*t*_{1/2}

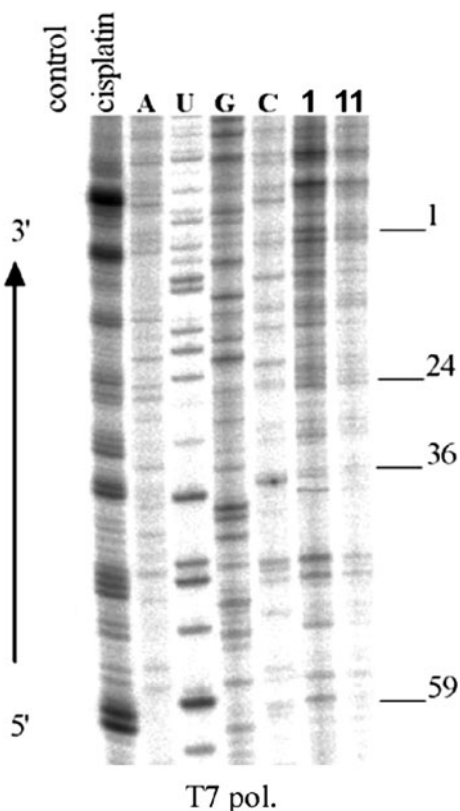
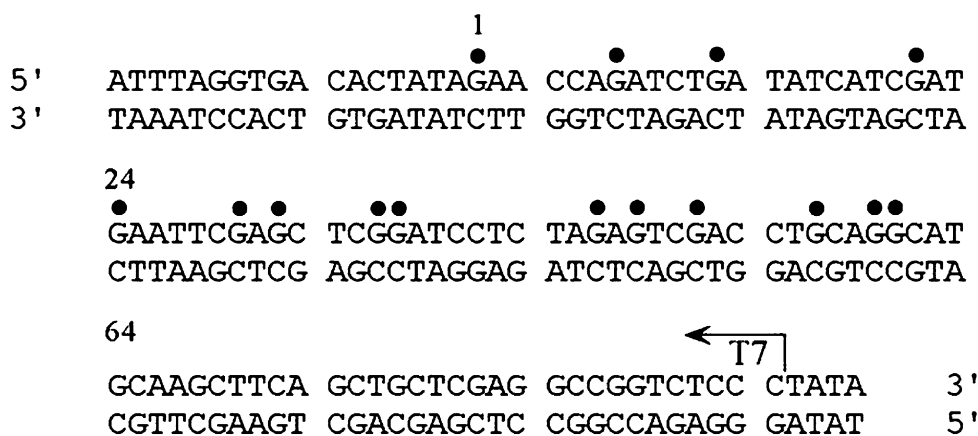


Fig. 7 Autoradiogram of 6 % polyacrylamide/8 M urea sequencing gel showing inhibition of RNA synthesis by T7 RNA polymerase on the *NdeI/HpaI* fragment containing adducts of Ru^{II} arene complexes and cisplatin. Control unmodified template; A, U, G and C chain-terminated marker RNAs; *cisplatin*, **1** and **11** the template modified by cisplatin at *r*_b = 0.02, Ru^{II} arene complex **1** at *r*_b = 0.02 or Ru^{II} arene complex **11** at *r*_b = 0.015, respectively

Fig. 8 The portion of the sequence used to monitor inhibition of RNA synthesis by Ru^{II} arene complexes. The arrow indicates the start of the T7 RNA polymerase, which used as a template the bottom strand of the *NdeI/HpaI* fragment of pSP73KB. The filled circles represent major stop sites for DNA modified by complex **1** or complex **11**, respectively. The numbers correspond to the nucleotide numbering in the sequence map of the pSP73KB plasmid



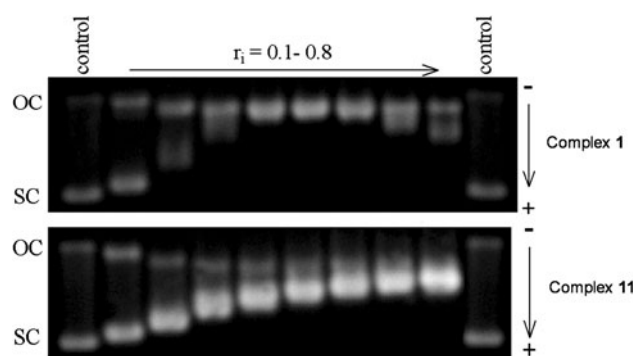


Fig. 9 The unwinding of supercoiled pUC19 plasmid DNA by complexes **1** (top) and **11** (bottom). The plasmid was incubated with Ru^{II} arene complexes in 10 mM NaClO₄, at pH 6 for 24 h at 310 K. Top: first lane (left) and tenth lane (right) control, unmodified DNA, second lane $r_b = 0.06$, third lane $r_b = 0.08$, fourth lane $r_b = 0.09$, fifth lane $r_b = 0.12$, sixth lane $r_b = 0.14$, seventh lane $r_b = 0.16$, eighth lane $r_b = 0.18$, ninth lane $r_b = 0.20$. Bottom: first lane and tenth lane control, unmodified DNA, second lane $r_b = 0.05$, third lane $r_b = 0.06$, fourth lane $r_b = 0.07$, fifth lane $r_b = 0.08$, sixth lane $r_b = 0.09$, seventh lane $r_b = 0.11$, eighth lane $r_b = 0.13$, ninth lane $r_b = 0.15$. OC nicked plasmid, SC closed, negatively supercoiled plasmid

Table 8 Unwinding of supercoiled pUC19 DNA by Ru^{II} arene complexes **1** and **11**

Complex	$r_b(c)$	Unwinding angle (°)
$[(\eta^6-p\text{-cym})\text{Ru}(\text{bpm})\text{Cl}][\text{PF}_6]$ (1)	0.13	7.7 ± 1.7
$[(\eta^6-p\text{-cym})\text{Ru}(\text{phen})\text{Cl}][\text{PF}_6]$ (11)	0.15	6.6 ± 1.7
Cisplatin	0.08	13.0 ± 0.4

approximately 2 h under similar conditions) [67], for which DNA binding is thought to be responsible for its cytotoxic properties. Interestingly, the corresponding binding rate for complex **11** was found to be in the same range as that of cisplatin. In contrast, other Ru^{II} arene analogues, e.g. $[(\eta^6\text{-bip})\text{Ru}(\text{en})\text{Cl}]^+$, which has also been shown to be toxic to cancer cells [38, 39, 68, 69], react much more rapidly with DNA under similar conditions ($t_{1/2}$ approximately 10 min).

The native agarose gels resulting from DNA modified by complexes $[(\eta^6-p\text{-cym})\text{Ru}(\text{bpm})\text{Cl}][\text{PF}_6]$ (**1**) and $[(\eta^6-p\text{-cym})\text{Ru}(\text{phen})\text{Cl}][\text{PF}_6]$ (**11**) are shown in Fig. 9. The DNA unwinding angles produced by the adducts of **1** and **11** were determined to be 7.7° and 6.6°, respectively, which is consistent with only a small reduction of the intensity of the negative CD band at approximately 245 nm of DNA modified by **1** or **11** (vide infra) [70, 71]. This DNA unwinding angle is smaller than that observed for other Ru^{II} arene complexes $[(\eta^6\text{-arene})\text{Ru}(\text{en})\text{Cl}]^+$ (range from 7° to 14°) [42] and resembles more DNA unwinding angles produced by monofunctional cisplatin adducts (6°) [34].

The co-migration point of the modified supercoiled and nicked DNA $r_b(c)$ was reached at r_b values of 0.13 and 0.15 (for **1** and **11**, respectively) as shown in Table 8.

CD spectra of CT-DNA modified by complexes **1** and **11** (at 298 K in 10 mM NaClO₄) were also recorded at r_b values in the range from 0.013 to 0.047. As can be seen from Fig. 10, small changes in the CD spectrum at wavelengths below 300 nm are observed upon interaction of complex **1** (and to a much lesser extent of complex **11**) with CT-DNA. As a consequence of the ruthenation of CT-DNA, the intensity of the positive CD band at around 280 nm increases for complex **1**, whereas the CD spectrum recorded for CT-DNA modified by **11** remains unchanged. The signature of complexes **1** and **11** bound to CT-DNA includes no isothermal CD. The changes in the CD spectra of CT-DNA (monitored at 246 and 278 nm) modified by Ru^{II} arene complexes **1** and **11** (at different r_b values) are shown in Table S4.

The CD spectra showed that the binding of **1** (and to a lesser extent of **11**) to DNA results in subtle conformational alterations in DNA that could be related to a denaturational character, similar to those induced in DNA by clinically ineffective transplatin. It is possible that these changes could also be associated with the bound Ru^{II} arene fragment given that these Ru^{II} arene complexes show maxima in the proximity of a DNA maximum.

Overall, these combined results might suggest the presence of combined covalent (coordinative), noncovalent intercalative, and monofunctional coordination binding modes of DNA binding for complexes **1** and **11** upon hydrolysis.

Binding of the Ru^{II} arene complexes to CT-DNA was also monitored by LD spectroscopy. It is well established that the magnitude of the LD signal measured within the DNA absorption band (i.e. at the 258-nm maximum) is a function of its persistence length [72–75]. The magnitudes of the LD signals at 258 nm decrease as a function of r_b for Ru^{II} arene complexes **1** and **11** (Fig. 11). The changes in the LD spectra of CT-DNA modified by the Ru^{II} complexes at different r_b values were monitored at 258.5 nm (Table S5). It can be seen that both complexes behave similarly and their changes are within the same range. These results might suggest that the formation of DNA adducts could be eventually accompanied by the appearance of flexible hinge joints at the site of the lesion.

Cancer cell growth inhibition

Halido complexes **1–6** (Fig. 1) were tested against the A2780 human ovarian, A2780 cisplatin-resistant human ovarian, A459 human lung, and HCT116 human colon cancer cell lines, whereas the remaining halido complexes, **8–11** and **13**, were tested against the A2780 human ovarian

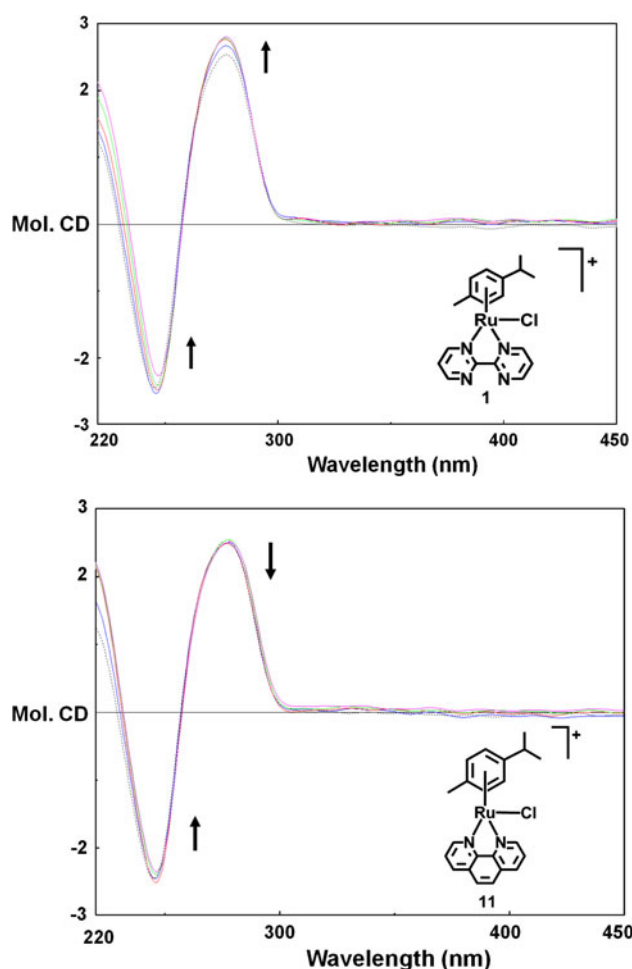


Fig. 10 Circular dichroism (CD) spectra of calf thymus DNA (CT-DNA) modified by Ru^{II} arene complexes **1** and **11**. CD spectra were recorded for DNA in 10 mM NaClO₄. The concentration of DNA was 3.3×10^{-4} M. The values of r_b were in the range from 0.013 to 0.047

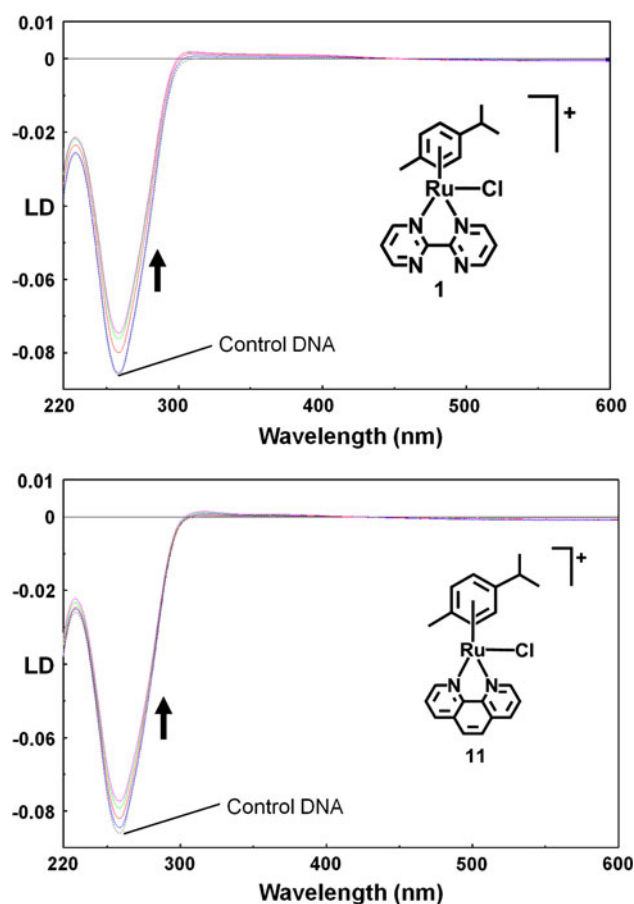


Fig. 11 Linear dichroism (LD) spectra of CT-DNA modified by Ru^{II} arene complexes **1** (top) and **11** (bottom). The LD spectra were recorded for DNA in 10 mM NaClO₄. The concentration of DNA was 3.3×10^{-4} M. The values of r_b were in the range from 0.013 to 0.047

cancer cell line. Strikingly, all the bpm-containing complexes (**1–6** and **8–10**) displayed IC₅₀ values larger than 100 μ M with regard to the corresponding cell lines tested (the IC₅₀ value for cisplatin was 1.0 μ M under the same conditions). Complexes **11** and **13**, bearing phen and bathophen as the chelating ligand, respectively, were cytotoxic to A2780 human ovarian cancer cells (Table 9). The most active complex is $[(\eta^6\text{-}p\text{-cym})\text{Ru}(\text{bathophen})\text{Cl}][\text{PF}_6]$ (**13**), with an IC₅₀ value of 0.5 μ M, comparable to that of cisplatin (IC₅₀ for cisplatin is 1.1 μ M under the same conditions). The IC₅₀ value for $[(\eta^6\text{-}p\text{-cym})\text{Ru}(\text{phen})\text{Cl}][\text{PF}_6]$ (**11**) with regard to this cancer cell line was 23 μ M.

A loss of cytotoxicity towards cancer cells has been previously observed for complexes of the type $[(\eta^6\text{-arene})\text{Ru}(\text{en})\text{Cl}]^+$ when ethylenediamine, a σ -donor, is replaced by bpy [76], a strong π -acceptor. Changing the electronic features of the chelating ligands by incorporating

Table 9 IC₅₀ values for Ru^{II} arene complexes **11** and **13** with regard to the A2780 human ovarian cancer cell line

Complex	IC ₅₀ (μ M) ^a
$[(\eta^6\text{-}p\text{-cym})\text{Ru}(\text{phen})\text{Cl}][\text{PF}_6]$ (11)	22.9
$[(\eta^6\text{-}p\text{-cym})\text{Ru}(\text{bathophen})\text{Cl}][\text{PF}_6]$ (13)	0.5
Cisplatin	1.1

^a Complexes **1–6** and **8–10** had IC₅₀ values larger than 100 μ M with regard to the cell line tested (cisplatin had a value of 1.1 μ M under the same conditions)

electron-donating heteroatoms in the 4,4' positions of bpm (such as in the phendio complex **12**) did not restore the cytotoxic activity. From a structural point of view, loss of activity in these derivatives could arise from the absence of N(*sp*³)H groups, which are known to stabilize nucleobase adducts through strong hydrogen bonding between an NH of ethylenediamine and C6O from the guanine nucleobase

[77]. The electronic properties of the complexes might also account for the observed loss of activity; metal–DNA bonds have been shown to be labilized by heteroarene ligands. After replacement of two water molecules by thiourea for instance, labilization of the Pt–N bond in the *trans* position forms a ring-opened trisubstituted $[\text{Pt}(\text{tu})_3(\text{N}-\text{N}_{\text{open}})]^{2+}$ species (where tu is thiourea) [67]. Similar reactions are also known in the biotransformation pathway of cisplatin, where the resulting products are inert to further substitution reactions and therefore limit the active concentration of the drug [78].

Interactions with GSH

^1H NMR and UV–vis absorption spectra of solutions containing the inactive complex $[(\eta^6\text{-}p\text{-cym})\text{Ru}(\text{bpm})\text{Cl}][\text{PF}_6]$ (**1**) (100 μM) and a 100-fold molar excess of GSH (10 mM, to mimic intracellular conditions) were acquired over 24 h at 310 K. The time-evolution spectra for Ru^{II} arene complex **1** are shown in Fig. S15. The ^1H NMR spectra of complex **1** initially contained one major set of peaks (chlorido species) and then a second set of peaks assignable to the aqua adduct $[(\eta^6\text{-}p\text{-cym})\text{Ru}(\text{bpm})\text{OH}_2]^{2+}$, which increased in intensity with time. A third set of peaks attributable to the GS-bound ruthenium adduct $[(\eta^6\text{-}p\text{-cym})\text{Ru}(\text{bpm})\text{GS}]^+$ (**1-GS**; Fig. 12) was also detected. The mass-to-charge ratio and isotopic model obtained from HR-MS spectra were consistent with the formation of the tripeptide-substituted Ru^{II} product, and the calculated m/z value for $\text{C}_{28}\text{H}_{36}\text{N}_7\text{O}_6\text{RuS}$ (700.1508); found m/z (700.1493). Some sulfur-bound thiolate adducts with platinum anticancer drugs are formed irreversibly and are also largely unreactive (e.g. towards DNA binding) [79].

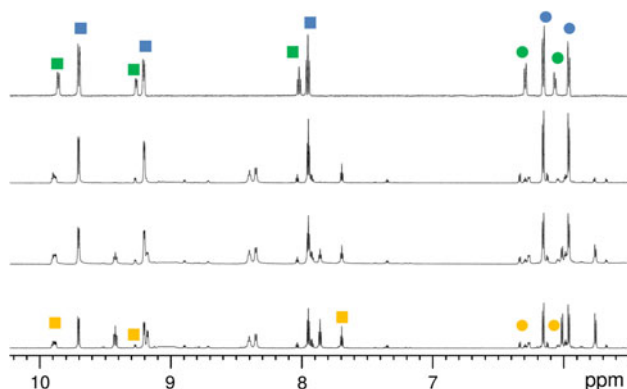


Fig. 12 ^1H NMR spectra of the reaction of a 100 μM solution of $[(\eta^6\text{-}p\text{-cym})\text{Ru}(\text{bpm})\text{Cl}][\text{PF}_6]$ (**2**) with 100-fold excess of glutathione (GSH) in D_2O at 310 K after 24 h. Blue symbols $[(\eta^6\text{-}p\text{-cym})\text{Ru}(\text{bpm})\text{Cl}]^+$, green symbols $[(\eta^6\text{-}p\text{-cym})\text{Ru}(\text{bpm})\text{OH}_2]^{2+}$, yellow symbols $[(\eta^6\text{-}p\text{-cym})\text{Ru}(\text{bpm})(\text{GS})]^+$, squares bpm, circles *p*-cym

Conclusions

We have shown that several bpm complexes $[(\eta^6\text{-arene})\text{Ru}(\text{bpm})\text{Cl}][\text{PF}_6]$ are inactive as anticancer agents towards human ovarian cancer cells. However, a change in the chelating ligand from bpm to phen or bathophen leads to activity. Significant changes in the chemical reactivity of the compounds towards hydrolysis are also observed; the hydrolysis rates of $[(\eta^6\text{-arene})\text{Ru}(\text{N},\text{N}')\text{X}]^+$ complexes differ over a wide range, from half-lives of minutes [14.5 min for $[(\eta^6\text{-etb})\text{Ru}(\text{bpm})\text{Cl}]^+$ (**7**)] to hours [12 h for $[(\eta^6\text{-bip})\text{Ru}(\text{bpm})\text{I}]^+$ (**6**)] at 310 K. DFT calculations on bpm complexes **1–6** suggest that aquation occurs via a more associative pathway in an $\text{I}_a \leftrightarrow \text{I}_d$ mechanistic continuum for which bond-making is of greater importance than bond-breaking. For both *p*-cym and bip bpm-containing complexes **1–6**, the calculated reaction barriers and overall reaction energies follow the order $\text{I} > \text{Br} \approx \text{Cl}$, which may explain the slow hydrolysis rate determined by UV–vis spectroscopy for iodo complexes **3** and **6**.

In general, we were not able to establish a correlation between hydrolysis rates and anticancer activity, which implies that the mechanism of action for these series of complexes does not depend solely on this process. The half-sandwich Ru^{II} arene complexes containing phen (**11**) or bathophen (**13**) as N,N' chelating ligands are more cytotoxic towards A2780 human ovarian cancer cells, in contrast to the analogous complexes containing bpm (**1–6**). X-ray crystal structures show that bip complexes (**4** and **6**) can form strong interligand and intraligand π – π interactions, which enforces planarity on the bpm ligand, particularly in the case of complex **4**. An interesting feature of the structure of complex **7** is the presence of aromatic CH– π (bpm) interactions. Strong binding to 9-EtG, but not to 9-EtA, was observed for complexes containing N,N' chelating ligands such as bpm, phen and bathophen, as well as different arenes such as *p*-cym, hmb, ind and thn. By the use of DFT calculations, the binding energies for model DNA nucleobases were assessed. DFT calculations show that the 9-EtG nucleobase adducts of all complexes are thermodynamically preferred compared with their 9-EtA adducts by approximately 10 kcal mol^{-1} , explaining the guanine-specific binding observed experimentally for complexes **1**, **8–11** and **13**. DNA binding studies show that complexes **1** and **11** bind to DNA, suggesting that it could be a target for these complexes, although the induced conformational changes are not significant. The reduced cytotoxic potency of the bpm-containing complexes might be due to the weakness of lesions on DNA or side reactions with other biomolecules such as GSH. The formation of a presumably largely unreactive Ru^{II} –GS adduct might contribute to the lack of cytotoxicity [79].

Acknowledgments S.B.-L. thanks WPRS/ORSAS (UK) and CONACyT (Mexico) for funding a research studentship. B.L., O.N. and V.B. were supported by the Czech Science Foundation (grants P301/10/0598 and 301/09/H004). We also thank EDRF and AWM (Science City) and ERC (grant no. 247450) for funding, and Ivan Prokes and Lijiang Song and Philip Aston of the University of Warwick for their help with NMR and HR-MS instruments, respectively.

References

- Jung Y, Lippard SJ (2007) *Chem Rev* 107:1387–1407
- van Zutphen S, Reedijk J (2005) *Coord Chem Rev* 249:2845–2853
- Pizarro AM, Habtemariam A, Sadler PJ (2010) *Top Organomet Chem* 32:21–56
- Aird RE, Cummings J, Ritchie AA, Muir M, Morris RE, Chen H, Sadler PJ, Jodrell DI (2001) *Br J Cancer* 86:1652–1657
- Yan YK, Melchart M, Habtemariam A, Sadler PJ (2005) *Chem Commun* 4764–4776
- Fernández R, Melchart M, Habtemariam A, Parsons S, Sadler PJ (2004) *Chem Eur J* 10:5173–5179
- Wang F, Habtemariam A, van der Geer EPL, Fernández R, Melchart M, Deeth RJ, Aird R, Guichard S, Fabbiani FPA, Lozano-Casal P, Oswald IDH, Jodrell DI, Parsons S, Sadler PJ (2005) *Proc Natl Acad Sci USA* 102:18269–18274
- Bloemink MJ, Engelking H, Karentzopoulos S, Krebs B, Reedijk J (1996) *Inorg Chem* 35:619–627
- Nováková O, Kasparkova J, Vrana O, van Vliet PM, Reedijk J, Brabec V (1995) *Biochemistry* 34:12369–12378
- Velders AH, Kooijman H, Spek AL, Haasnoot JG, De Vos D, Reedijk J (2000) *Inorg Chem* 39:2966–2967
- Ishikawa T, Ali-Osman F (1993) *J Biol Chem* 268:20116–20125
- Chen Y, Guo Z, Parkinson JA, Sadler PJ (1998) *J Chem Soc Dalton Trans* 3577–3585
- Teuben J-M, Reedijk J (2000) *J Biol Inorg Chem* 5:463–468
- Corazza A, Harvey I, Sadler PJ (1996) *Eur J Biochem* 236:697–705
- Buttke TM, Sandstrom PA (1994) *Immunol Today* 15:7–10
- Clarke MJ (2002) *Coord Chem Rev* 232:69–93
- Bennet MA, Smith AK (1974) *J Chem Soc Dalton Trans* 233–241
- Govindaswamy P, Canivet J, Therrien B, Süß-Fink G, Štěpnička P, Ludvík J (2007) *J Organomet Chem* 692:3664–3675
- Zelonka RA, Baird MC (1972) *J Organomet Chem* 35:C43–C46
- Melchart M, Habtemariam A, Nováková O, Moggach SA, Fabbiani FPA, Parsons S, Brabec V, Sadler PJ (2007) *Inorg Chem* 46:8950–8962
- Habtemariam A, Betanzos-Lara S, Sadler PJ (2010) *Inorg Synth* 35:160–163
- Brabec V, Palecek E (1970) *Biophysik* 6:290–300
- Brabec V, Palecek E (1976) *Biophys Chem* 4:79–92
- Sheldrick GM (1997) SHELXL97. University of Göttingen, Germany
- Sheldrick GM (1990) *Acta Crystallogr A* 46:467–473
- Sheldrick GM (2008) *Acta Crystallogr* 64:12–122
- Krezel A, Bal W (2004) *J Inorg Biochem* 98:161–166
- Te Velde G, Bickelhaupt FM, Baerends EJ, Fonseca Guerra C, Van Gisbergen SJA, Snijders JG, Ziegler T (2001) *J Comput Chem* 22:931–967
- Baerends EJ, Berces A, Bo C, Boerrigter PM, Cavallo L, Deng L, Dickson RM, Ellis DE, Fan L, Fischer TH et al (2000) *ADF* 2009. Free University, Amsterdam
- Wert C, Zener C (1949) *Phys Rev* 76:1169–1175
- Vineyard GH (1957) *J Phys Chem Solids* 3:121–127
- Brabec V, Leng M (1993) *Proc Natl Acad Sci USA* 90:5345–5349
- Lemaire MA, Schwartz A, Rahmouni AR, Leng M (1991) *Proc Natl Acad Sci USA* 88:1982–1985
- Keck MV, Lippard SJ (1992) *J Am Chem Soc* 114:3386–3390
- Skehan P, Storeng R, Scudiero D, Monks A, McMahon J, Vistica D, Warren JT, Bokesch H, Kenney S, Boyd MR (1990) *J Nat Cancer Inst* 82:1107–1112
- Morris RE, Aird RE, del Socorro Murdoch P, Chen H, Cummings J, Hughes ND, Parsons S, Parkin A, Boyd G, Jodrell DI, Sadler PJ (2001) *J Med Chem* 44:3616–3621
- Chen H, Parkinson JA, Parsons S, Coxall RA, Gould RO, Sadler PJ (2002) *J Am Chem Soc* 124:3064–3082
- Süss-Fink G (2010) *Dalton Trans* 39:1673–1688
- Singh A, Chandra M, Sahay AN, Pandey DS, Pandey KK, Mobin SM, Puerta MC, Valera P (2004) *J Organomet Chem* 689:1821–1834
- Flower KR, Pritchard RG (2001) *J Organomet Chem* 620:60–68
- Gül N, Nelson JH (1999) *Organometallics* 18:709–725
- Gül N, Nelson JH (1999) *Polyhedron* 18:1835–1843
- Bugarcic T, Habtemariam A, Stepankova J, Heringova P, Kašpárková J, Deeth RJ, Johnstone RDL, Prescimone A, Parkin A, Parsons S, Brabec V, Sadler PJ (2008) *Inorg Chem* 47:11470–11486
- van Rijt SH, Hebden AJ, Amaresekera T, Deeth RJ, Clarkson GJ, Parsons S, McGowan P, Sadler PJ (2009) *J Med Chem* 52:7753–7764
- Bugarcic T, Nováková O, Halámková A, Zerkánková L, Vrána O, Kašpárková J, Habtemariam A, Parsons S, Sadler PJ, Brabec V (2008) *J Med Chem* 51:5310–5319
- Brandl M, Weiss MS, Jabs A, Suhnel J, Hilgenfeld R (2001) *J Mol Biol* 307:357–377
- Bogdanovic GA, Spasojevic-de Bire A, Zaric SD (2002) *Eur J Inorg Chem* 1599–1602
- Dieter-Wurm I, Sabat M, Lippert B (1992) *J Am Chem Soc* 114:357–359
- Witkowschi H, Freisinger E, Lippert B (1997) *J Chem Soc Chem Commun* 1315–1316
- Sigel RKO, Freisinger E, Metzger S, Lippert B (1998) *J Am Chem Soc* 120:12000–12007
- Qu X, Chaires JB (2001) *J Am Chem Soc* 123:1–7
- Betanzos-Lara S, Salassa L, Habtemariam A, Sadler PJ (2009) *Chem Commun* 6622–6624
- Wang F, Chen H, Parsons S, Oswald IDH, Davidson JE, Sadler PJ (2003) *Chem Eur J* 9:5810–5820
- Kunkely H, Vogler A (2003) *Inorg Chim Acta* 343:357–360
- Dadci L, Elias H, Frey U, Hornig A, Koelle U, Merbach AE, Paulus H, Schneider JS (1995) *Inorg Chem* 34:306–315
- Koefod RS, Mann KR (1990) *J Am Chem Soc* 112:7287–7293
- Dougan SJ, Melchart M, Habtemariam A, Parsons S, Sadler PJ (2007) *Inorg Chem* 46:10882–10894
- Rapaport I, Helm L, Merbach AE, Bernhard P, Ludi A (1988) *Inorg Chem* 27:873–879
- Broomhead JA, Basolo F, Pearson RG (1964) *Inorg Chem* 3:826–832
- Takeuchi KJ, Thompson MS, Pipes DW, Meyer TJ (1984) *Inorg Chem* 23:1845–1851
- Basolo F, Pearson RG (1967) *Mechanisms of inorganic reactions: a study of metal complexes in solution*, 2nd edn. Wiley, New York, p 124
- Broomhead JA, Kane-Maguire LAP (1968) *Inorg Chem* 7:2519–2523
- Scheller KH, Scheller-Krattiger V, Martin RB (1981) *J Am Chem Soc* 103:6833–6839
- Peacock AFA, Habtemariam A, Fernández R, Walland V, Fabbiani Francesca PA, Parsons S, Aird RE, Duncan IJ, Sadler PJ (2006) *J Am Chem Soc* 128:1739–1748

65. Baik M-H, Friesner RA, Lippard SJ (2003) *J Am Chem Soc* 125:14082–14092
66. Summa N, Schiessl W, Puchta R, van Eikema Hommes N, van Eldik R (2006) *Inorg Chem* 45:2948–2959
67. Bancroft DP, Lepre CA, Lippard SJ (1990) *J Am Chem Soc* 112:6860–6871
68. Aird R, Cummings J, Ritchie A, Muir M, Morris R, Chen H, Sadler PJ, Jodrell D (2002) *Br J Cancer* 86:1652–1657
69. Nováková O, Kasparkova J, Bursova V, Hofr C, Vojtiskova M, Chen H, Sadler PJ, Brabec V (2005) *Chem Biol* 12:121–129
70. Ivanov VI, Minchenkova LE, Minyat EE, Frank-Kamenetskii MD, Schyolkina AK (1974) *J Mol Biol* 87:817–833
71. Vorlickova M (1995) *Biophys J* 69:2033–2043
72. Richards AD, Rodger A (2007) *Chem Soc Rev* 36:471–483
73. Coggan DZM, Haworth IS, Bates PJ, Robinson A, Rodger A (1999) *Inorg Chem* 38:4486–4497
74. Nováková O, Chen H, Vrana O, Rodger A, Sadler PJ, Brabec V (2003) *Biochemistry* 42:11544–11554
75. Lincoln P, Broo A, Norden B (1996) *J Am Chem Soc* 118:2644–2653
76. Habtemariam A, Melchart M, Fernández R, Parsons S, Oswald IDH, Parkin A, Fabbiani FPA, Davidson JE, Dawson A, Aird RE, Jodrell DI, Sadler PJ (2006) *J Med Chem* 49:6858–6868
77. Liu HK, Berners-Price SJ, Wang FY, Parkinson JA, Xu JJ, Bella J, Sadler PJ (2006) *Angew Chem Int Ed* 45:8153–8156
78. Wang D, Lippard JS (2005) *Nat Rev Drug Discovery* 4:307–320
79. Reedijk J (2003) *Proc Natl Acad Sci USA* 100:3611–3616

2.

The Thermodynamics of Translesion DNA Synthesis Past Major Adducts of Enantiomeric Analogues of Antitumor Cisplatin

Jaroslav Malina,^[a] Olga Novakova,^[a] Giovanni Natile,^[b] and Viktor Brabec^{*[a]}

Abstract: The Pt^{II}-coordination complex [PtCl₂(DAB)] (DAB=2,3-diaminobutane) belongs to a class of cytotoxic cisplatin analogues that contain chiral diamine ligands. Enantiomeric pairs of these compounds have attracted particular interest because they have different effects on different DNA conformations, which, in turn, influences the binding of damaged-DNA-processing enzymes that control downstream effects of the adducts, and thus exhibit different biological activities of the enantiomers. Herein, we studied the translesion synthesis across the major 1,2-d(GG) intrastrand cross-link formed by the *R,R* and *S,S* enantiomers

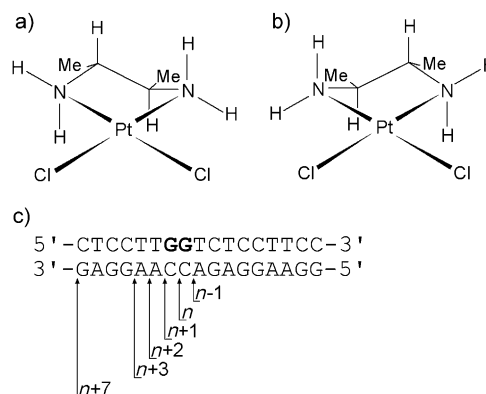
of [Pt(DAB)]²⁺ in the TGGT sequence by using the enzyme that catalyzes the polymerization of deoxyribonucleotides into a DNA strand. We also employed differential scanning calorimetry (DSC) to measure the thermodynamic changes associated with replication-bypass past 1,2-d(GG) adducts of the [Pt(DAB)]²⁺ enantiomers. In the sequence TGGT, the 1,2-d(GG) intrastrand cross-links that were formed by the enantiomeric pairs of [Pt(DAB)]²⁺

Keywords: calorimetry • chirality • DNA • thermodynamics • translesion

inhibited DNA polymerization in a chirality-dependent manner. The thermodynamic data helped to understand the effect of the alterations in thermodynamic stability of DNA caused by the Pt-d(GG) adducts upon DNA polymerization across these lesions. Moreover, these data can possibly explain the influence of these alterations on the ability of many DNA polymerases to bypass adducts of antitumor platinum drugs. These results also highlighted the usefulness of DSC in evaluating the impact of DNA adducts of platinum-coordinated compounds on the processing of these lesions by damaged-DNA processing-enzymes.

Introduction

[PtCl₂(DAB)] (DAB=2,3-diaminobutane; Scheme 1 a, b) and [PtCl₂(DACH)] (DACH=*trans*-1,2-diaminocyclohexane) belong to a class of cytotoxic cisplatin analogues that contain chiral diamine ligands. Enantiomeric pairs of these compounds have attracted particular interest because they exhibit different biological activities. For example, the *R,R* enantiomer of [PtCl₂(DACH)] exhibits higher antitumor activity than the *S,S* enantiomer,^[1,2] and the *S,S* enantiomers of both [PtCl₂(DACH)] and [PtCl₂(DAB)] are considerably more-mutagenic than the *R,R* enantiomers.^[3] Oxaliplatin, the *R,R* enantiomer of [Pt(oxalate)(DACH)], is currently in clinical use to treat metastatic colorectal cancer, against which cisplatin is inactive although it forms the same spectrum of DNA adducts.^[4] The major DNA adduct of cisplatin and its analogues is the 1,2-d(GG) intrastrand cross-link (CL), which is believed to play an important role in the



Scheme 1. Structures of a) *cis*-[PtCl₂(*R,R*-DAB)] and b) *cis*-[PtCl₂(*S,S*-DAB)]. c) Sequences of the template (top strand), primer (*n*–1 in the bottom strand), primer extensions (*n*, *n*+1, *n*+2, and *n*+3 in the bottom strand), and the full-length product (*n*+7 in the bottom strand). The bold letters in the top strand indicate the platinated residues.

[a] Dr. J. Malina, Dr. O. Novakova, Prof. Dr. V. Brabec
Institute of Biophysics
Academy of Sciences of the Czech Republic, v.v.i.
Kralovopolska 135, CZ-61265 Brno (Czech Republic)
Fax: (+420)541240499
E-mail: brabec@ibp.cz

[b] Prof. Dr. G. Natile
Department of Pharmaceutical Chemistry
University of Bari
I-70125 Bari (Italy)

mechanism of antitumor activity.^[5] We studied conformational alterations induced in DNA by 1,2-d(GG) intrastrand CLs that were formed by enantiomeric pairs of [Pt(DAB)]²⁺ and [Pt(DACH)]²⁺ and their recognition by high-mobility-group (HMG) domain proteins in various nucleotide sequences.^[6–9] We found that the structural alterations induced in DNA by 1,2-d(GG) intrastrand CLs that were formed in certain nucleotide sequences, such as TGGT, by [Pt(DAB)]²⁺ or [Pt(DACH)]²⁺, were chirality-dependent. It has

been shown^[8] that the structural and chiral differentiation of 1,2-d(GG) intrastrand CLs of $[\text{Pt}(\text{DAB})]^{2+}$ originates from clashes between the 5'-methyl group of the DAB ligand and the methyl group of the 5'-dT of the TGGT sequence. We also investigated the inhibitory effect of 1,2-d(GG) intrastrand CLs that were formed by $[\text{Pt}(\text{R,R-DACH})]^{2+}$ and $[\text{Pt}(\text{S,S-DACH})]^{2+}$ in the TGGT sequence on in vitro DNA polymerization; we observed chirality-dependent translesion DNA synthesis (TLS) across the adduct.^[9]

Herein, we studied the TLS across 1,2-d(GG) intrastrand CLs formed by the *R,R* and *S,S* enantiomers of $[\text{Pt}(\text{DAB})]^{2+}$ in the TGGT sequence by the Klenow fragment of DNA polymerase I. We also employed DSC to measure the thermodynamic changes that were associated with replication-bypass past the 1,2-d(GG) adducts of $[\text{Pt}(\text{DAB})]^{2+}$ enantiomers in the TGGT sequence.

Results and Discussion

DNA Polymerization by the Klenow Fragment of DNA Polymerase I

We examined DNA polymerization past the 1,2-d(GG) intrastrand CLs that were formed by the *R,R* and *S,S* enantiomers of $[\text{Pt}(\text{DAB})]^{2+}$ (Scheme 1 a,b) in the TGGT sequence by the Klenow fragment from DNA polymerase I (exonuclease minus, mutated to remove the 3'→5' proofreading domain). This DNA polymerase was selected because TLS-proficient DNA polymerases of the X and Y families shared some common properties, including the lack of associated 3'-5'-exonuclease-proofreading activity and because the proofreading mechanism itself may introduce effects that were more dependent on the adduct type.^[10]

The 8-mer primer was 5'-³²P-labeled and annealed to an unmodified 23-mer template or templates containing the 1,2-d(GG) intrastrand CLs of $[\text{Pt}(\text{R,R-DAB})]^{2+}$ or $[\text{Pt}(\text{S,S-DAB})]^{2+}$ that were formed in the TGGT sequence (Figure 1 a). The first eight nucleotides on the 3'-terminus of the 23-mer template strand were complementary with the nucleotides of the 8-mer primer, so that the 3' dG involved in the 1,2-d(GG) intrastrand CL on the template strand was located at the 13th position from the 3'-terminus (the 3'-end of the primer was five bases before the first platinated base in the template strand; Figure 1 a). The polymerization reaction was stopped after various time intervals and the products of the DNA synthesis were analyzed by denaturing polyacrylamide (PAA) electrophoresis and visualized by radiography (Figure 1 b). DNA polymerization by KF^- of the 8-mer/23-mer primer templates that contained the adduct of $[\text{Pt}(\text{R,R-DAB})]^{2+}$ or $[\text{Pt}(\text{S,S-DAB})]^{2+}$, which were formed in the TGGT sequence in the presence of all four deoxyribonucleotide triphosphates (dNTPs), proceeded rapidly up to the nucleotide that was opposite that preceding the 1,2-d(GG) intrastrand CL, such that 12-, 13-, and 14-mers accumulated to a significant extent. KF^- efficiently replicated the untreated template; only full-length products—and no intermediates—were seen with the 23-mer control templates

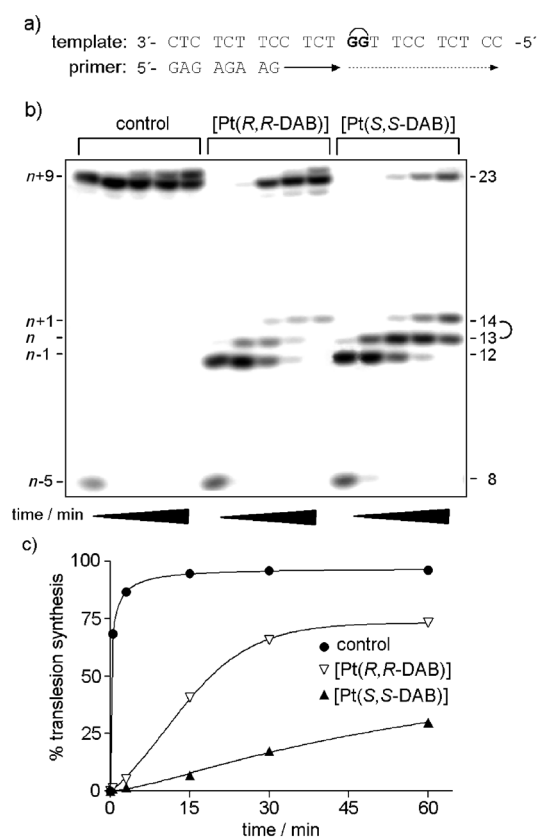


Figure 1. Primer-extension activity of KF^- on the 8mer:23mer primer/template duplex. a) The nucleotide sequences of the template and primer. b) The experiments were conducted by using undamaged templates or templates that contained single, site-specific 1,2-d(GG) intrastrand CLs of $[\text{Pt}(\text{R,R-DAB})]^{2+}$ and $[\text{Pt}(\text{S,S-DAB})]^{2+}$ in the TGGT sequence. The pause sites opposite the platinated guanine bases and a flanking residue on the 3' site are marked as 14, 13, and 12, respectively. c) Time-dependence of the inhibition of the DNA synthesis on undamaged (control) templates (●) and on DNA that contained 1,2-d(GG) intrastrand CLs of $[\text{Pt}(\text{R,R-DAB})]^{2+}$ (▽) and $[\text{Pt}(\text{S,S-DAB})]^{2+}$ (▲) in the TGGT sequence. The data are mean-averaged values from three experiments with two independent template preparations.

(Figure 1 b). There was also significant accumulation of the full-length products from the 23-mer templates that contained the CLs of $[\text{Pt}(\text{R,R-DAB})]^{2+}$ or $[\text{Pt}(\text{S,S-DAB})]^{2+}$, which were formed in the TGGT sequence at longer incubation times (60 min), although in a significantly smaller amount than with the unmodified template. Importantly, the amount of the full-length products that accumulated with the template that contained the 1,2-d(GG) intrastrand CL of $[\text{Pt}(\text{R,R-DAB})]^{2+}$ in the TGGT sequence was significantly larger than that with the same template modified by $[\text{Pt}(\text{S,S-DAB})]^{2+}$ (Figure 1 c).

On the whole, these results were very similar to those obtained previously with 1,2-d(GG) intrastrand CLs of $[\text{Pt}(\text{R,R-DACH})]^{2+}$ and $[\text{Pt}(\text{S,S-DACH})]^{2+}$, and showed that the inhibitory effect of 1,2-d(GG) intrastrand CLs formed by the enantiomeric pairs of $[\text{Pt}(\text{DAB})]^{2+}$ as well as $[\text{Pt}(\text{DACH})]^{2+}$ complexes on DNA polymerization in the sequence TGGT was chirality-dependent.

Differential Scanning Calorimetry

DSC was used to explore the thermodynamic aspects of the TLS across the 1,2-d(GG) intrastrand CLs of [Pt(*R,R*-DAB)]²⁺ and [Pt(*S,S*-DAB)]²⁺ that were formed in the TGGT sequence. The sequence of the model template probe (17 nucleotides long) was designed to contain a d(GG) sequence at which 1,2-d(GG) intrastrand CL of [PtCl₂(DAB)] enantiomers was formed (Scheme 1c). The template was paired with a primer (*n*–1–*n*+7) series (Scheme 1c) to simulate TLS past [Pt(DAB)]²⁺ adducts. The DSC thermograms for the unmodified template and the template/primer series that contained 1,2-d(GG) intrastrand CLs of [Pt(*R,R*-DAB)]²⁺ and [Pt(*S,S*-DAB)]²⁺ are shown in Figure 2.

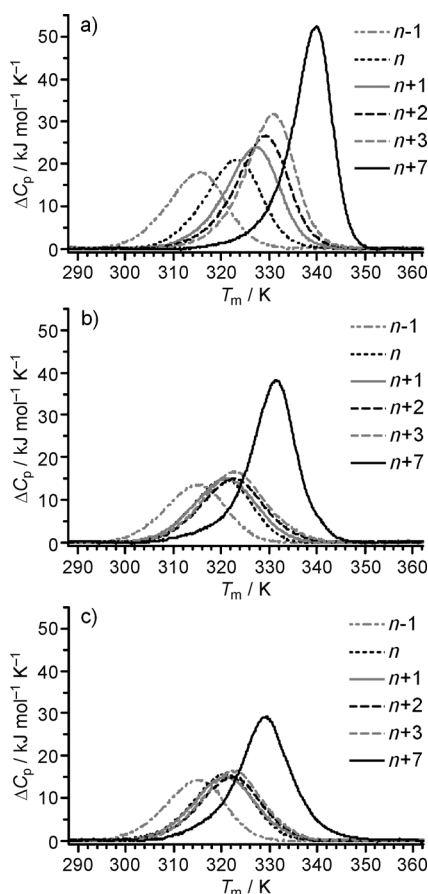


Figure 2. DSC thermograms of the template/primer series (*n*–1–*n*+7) for a) unmodified template, and b) template containing single, site-specific 1,2-GG intrastrand CLs of [Pt(*R,R*-DAB)]²⁺ or c) [Pt(*S,S*-DAB)]²⁺. The concentrations of the duplexes were 30 μM, and the buffer conditions were sodium phosphate (10 mM, pH 7.0) and NaCl (150 mM).

The DSC curves were analyzed to obtain the thermodynamic data (Table 1). The plots (Figure 3) showed the dependence of the melting temperature (*T*_m), and of the thermodynamic parameters, enthalpy (ΔH), entropy (ΔS), and Gibbs free energy (ΔG^0_{298}), on the length of the primer. As expected, the values of the melting temperature (*T*_m), en-

thalpy (ΔH), and Gibbs free energy (ΔG^0_{298}) for the unmodified template/primer series increased incrementally with primer length (Figure 3). Elongation of the primer from *n*–1 to *n* resulted in a significant increase of ΔH (by 42 kJ mol^{–1}), ΔG^0_{298} (by 9.0 kJ mol^{–1}), and *T*_m (by 7.7 K); this trend continued up to *n*+7 (Table 1). In contrast, the variations in thermodynamic parameters for templates that contained 1,2-d(GG) intrastrand CLs of [Pt(*R,R*-DAB)]²⁺ or [Pt(*S,S*-DAB)]²⁺ with increase in primer length were considerably different, and, furthermore, they differed from each other (Figure 3). Inspection of the thermodynamic parameters (Table 1) revealed that the template/*n*–1 duplexes that contained the CL of [Pt(*R,R*-DAB)]²⁺ or [Pt(*S,S*-DAB)]²⁺ in the template strand were enthalpically destabilized in comparison with the unmodified control template ($\Delta\Delta H$ = 65 and 49 kJ mol^{–1}, respectively; $\Delta\Delta G^0_{298}$ = 3.3 and 2.7 kJ mol^{–1}, respectively). Surprisingly, in contrast to the effects of the CLs of the two enantiomers on the overall thermodynamic stability of the full-length duplex, the duplex template/*n*–1 strand that contained the CL of [Pt(*S,S*-DAB)]²⁺ was more stable (ΔH = 246 kJ mol^{–1}, ΔG^0_{298} = 16.5 kJ mol^{–1}) than that containing the CL of [Pt(*R,R*-DAB)]²⁺ (ΔH = 228 kJ mol^{–1}, ΔG^0_{298} = 15.5 kJ mol^{–1}). This observation was consistent with the results obtained by using chemical probes of the DNA conformation,^[6] which indicated that the distortion induced by the 1,2-d(GG) intrastrand CLs of [Pt(DAB)]²⁺ complexes was not only localized at the platinated base-pairs, but extended over at least 5 base pairs around the CL. Even more interestingly, the pattern and degree of reactivity toward the chemical probes in the TGGT sequence demonstrated^[6] 1) a chirality-dependent character of the conformational distortions induced by the 1,2-d(GG) intrastrand CLs of [Pt(DAB)]²⁺ complexes in the TGGT sequence; and 2) that the CL formed by [Pt(*R,R*-DAB)]²⁺ distorted the double helix on the 3' side of the CL more than the CL of [Pt(*S,S*-DAB)]²⁺.

The incorporation of dC opposite the first (3') dG of the 1,2-d(GG) intrastrand CL of [Pt(*R,R*-DAB)]²⁺ and [Pt(*S,S*-DAB)]²⁺ resulted in gains in ΔH of only 18 and 20 kJ mol^{–1}, respectively, and in ΔG^0_{298} of only 4.7 and 5.1 kJ mol^{–1}, respectively, which was approximately 2-fold less than the gains in ΔH (42 kJ mol^{–1}) and ΔG^0_{298} (9.0 kJ mol^{–1}) that were observed for the unmodified control reaction. Further extension of the primer from *n* to *n*+1 (incorporation of the second dC opposite 5' dG of the 1,2-d(GG) intrastrand CL of [Pt(*R,R*-DAB)]²⁺ and [Pt(*S,S*-DAB)]²⁺) showed little change in the melting thermodynamics, and the impact persisted up to *n*+2. This long-range effect was also in accord with our previous results,^[6] which demonstrated that conformational distortion induced in DNA by 1,2-d(GG) intrastrand CLs of [Pt(*R,R*-DAB)]²⁺ and [Pt(*S,S*-DAB)]²⁺ extended over several base pairs around the lesion and at least two 5'-downstream base pairs.

Formation of the 1,2-d(GG) intrastrand CL of [Pt(*S,S*-DAB)]²⁺ resulted in a decrease in melting enthalpy (–7 kJ mol^{–1}) when the primer was extended from *n* to *n*+1. When the primer was further extended from *n*+1 to *n*+2,

Table 1. Thermodynamic parameters for the dissociation of duplexes derived from DSC experiments that simulated translesion DNA synthesis across 1,2-d(GG) intra-strand cross-links of [Pt(R,R-DAB)]²⁺ and [Pt(S,S-DAB)]²⁺.^[a]

Sequence	ΔH [kJ mol ⁻¹] ^[b]	ΔS [kJ K ⁻¹ mol ⁻¹] ^[b]	ΔG_{298}^0 [kJ mol ⁻¹] ^[b]	T_m [K]
Control				
<i>n</i> -1	275	0.875	14.1	315.7
<i>n</i>	317	0.984	23.1	323.4
<i>n</i> +1	345	1.058	29.2	327.3
<i>n</i> +2	376	1.147	33.8	329.4
<i>n</i> +3	419	1.272	39.6	331.1
<i>n</i> +7	557	1.648	65.3	339.9
[Pt(R,R-DAB)] ²⁺				
<i>n</i> -1	210 (-65)	0.669 (-0.206)	10.8 (-3.3)	315.3 (-0.4)
<i>n</i>	228 (-89)	0.714 (-0.270)	15.5 (-7.6)	321.0 (-2.4)
<i>n</i> +1	242 (-103)	0.753 (-0.305)	17.0 (-12.2)	321.3 (-3.0)
<i>n</i> +2	243 (-133)	0.754 (-0.393)	18.0 (-15.8)	322.9 (-6.5)
<i>n</i> +3	274 (-145)	0.849 (-0.423)	20.6 (-19.0)	323.1 (-8.0)
<i>n</i> +7	465 (-92)	1.412 (-0.236)	44.4 (-20.9)	331.6 (-8.3)
[Pt(S,S-DAB)] ²⁺				
<i>n</i> -1	226 (-49)	0.719 (-0.156)	11.4 (-2.7)	315.5 (-0.2)
<i>n</i>	246 (-71)	0.768 (-0.216)	16.5 (-6.6)	321.1 (-2.3)
<i>n</i> +1	239 (-106)	0.746 (-0.312)	16.6 (-12.6)	321.2 (-6.1)
<i>n</i> +2	239 (-137)	0.743 (-0.404)	17.3 (-16.5)	322.4 (-7.0)
<i>n</i> +3	259 (-160)	0.803 (-0.469)	19.1 (-20.5)	322.8 (-8.3)
<i>n</i> +7	405 (-152)	1.233 (-0.415)	37.4 (-27.9)	329.3 (-10.6)

[a] The ΔH and ΔS values are average values that were derived from three independent experiments. The experimental uncertainties of the parameters are as follow: T_m (± 0.5) K, ΔH ($\pm 2\%$), ΔS ($\pm 3\%$), ΔG_{298}^0 ($\pm 3\%$). The " $\Delta\Delta$ " parameters are given in parentheses (these parameters were computed by subtracting the appropriate value measured for the control reaction (unmodified duplex) from the value measured for the duplex containing the single, site-specific platinum adduct).

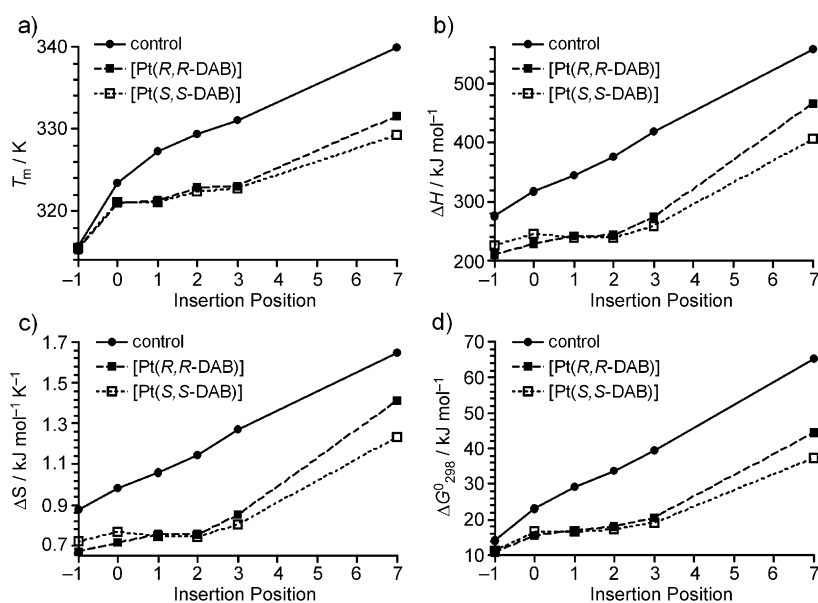


Figure 3. Plots of a) T_m , b) ΔH , c) ΔS , and d) ΔG_{298}^0 versus the insertion position (*n*-1-*n*+7) for unmodified templates (control, ●) and templates that contained 1,2-GG intrastrand CLs of [Pt(R,R-DAB)]²⁺ (■) and [Pt(S,S-DAB)]²⁺ (□).

the melting enthalpy remained unchanged; similarly, the formation of the 1,2-d(GG) intrastrand CL of [Pt(S,S-DAB)]²⁺ resulted in only a very small increase in the free energy of duplex dissociation at 298 K ΔG_{298}^0 (by 0.1 kJ mol⁻¹) when

the primer was extended from *n* to *n*+1, and when the primer was further extended from *n*+1 to *n*+2, ΔG_{298}^0 increased negligibly (by 0.7 kJ mol⁻¹; Table 1). These results implied that the incorporation of dC and dA opposite the platinated 5'-dG and adjacent dT on the 5'-side of the CL was enthalpically unfavored. This result was consistent with the strong stop-sites at positions 13 and 14, which corresponded to the positions *n* and *n*+1, that were observed for DNA polymerization across 1,2-d(GG) intrastrand CLs formed by [Pt(S,S-DAB)]²⁺ in the TGGT sequence by the DNA polymerase (KF⁻; Figure 1b). On the other hand, the 1,2-d(GG) intrastrand CL of [Pt(R,R-DAB)]²⁺ induced a small increase in both ΔH (14 and 1 kJ mol⁻¹, respectively) and ΔG_{298}^0 (1.5 and 1.0 kJ mol⁻¹, respectively). In particular the increase in ΔH seemed to be important because it had been proposed that the effect of enthalpy-entropy compensation was suppressed in the enzyme catalytic pocket so that the insertion was primarily modulated by the enthalpy.^[11] Indeed, the stop sites at positions 13 and 14, which corresponded to positions *n* and *n*+1, that were observed for DNA polymerization across the 1,2-d(GG) intrastrand CL formed by [Pt(R,R-DAB)]²⁺ in the TGGT sequence by the DNA polymerase (Figure 1b) were considerably weaker than across the CL of [Pt(S,S-DAB)]²⁺; consequently, the inhibition of TLS across the 1,2-d(GG) intrastrand CL of [Pt(R,R-DAB)]²⁺ was markedly lower (Figure 1c).

When the primers were extended to *n*+3, which was two nucleotides behind the platinum adduct on its 5'-side, the stability of the duplex that was modified by [Pt(R,R-DAB)]²⁺ was greater ($\Delta G_{298}^0 = 20.6$ kJ mol⁻¹, $\Delta H = 274$ kJ mol⁻¹, $T_m = 323.1$ K) than that of the duplex modified by [Pt(S,S-DAB)]²⁺ ($\Delta G_{298}^0 = 19.1$ kJ mol⁻¹, $\Delta H = 259$ kJ mol⁻¹, $T_m = 322.8$ K). Again, this result correlated very well with the analysis of conformational alterations induced in DNA by 1,2-d(GG) intrastrand CLs of [Pt(DAB)]²⁺ complexes by chemical probes of DNA conformations.^[6] This analysis clearly showed a greater distortion of the double helix on the 5'-side of the cross-linked bases by [Pt(S,S-DAB)]²⁺ in the TGGT sequence. The lesion at *n*-*n*+3 may have interfered with the ability of the distorted residues in-

volved in the CL or in the 5'-downstream base pairs to adopt regular undisturbed B-DNA conformations, thereby reducing the overall efficiency of DNA polymerase for incorporating deoxyribonucleoside triphosphates. Whilst there was considerable entropy compensation (Table 1), the data showed that the enthalpy terms were primarily responsible for the adduct-induced thermal and thermodynamic destabilization.

Conclusion

Translesion DNA synthesis by DNA polymerases past 1,2-d(GG) intrastrand CLs of [Pt(R,R-DAB)]²⁺ and [Pt(S,S-DAB)]²⁺ in the sequence TGGT was chirality-dependent. The thermodynamic data obtained by DSC described the energetic parameters that were associated with replication-bypass across 1,2-d(GG) intrastrand CLs of [Pt(DAB)]²⁺ enantiomers. These results highlighted the usefulness of DSC for evaluating how DNA adducts of platinum-coordination compounds affect processing of these lesions by DNA polymerases.

Experimental Section

Chemicals

[PtCl₂(R,R-DAB)] and [PtCl₂(S,S-DAB)] (Scheme 1a,b) were prepared and characterized according to literature procedures.^[3] Stock solutions of the platinum compounds were prepared at a concentration of 5 × 10^{−4} M in NaClO₄ (10 mM) and were stored at 277 K in the dark. The synthetic oligodeoxyribonucleotides were synthesized and purified according to literature procedures.^[12] KF[−] and T4 polynucleotide kinase were purchased from New England Biolabs (Beverly, MA). Deoxyribonucleoside 5'-triphosphates were purchased from Roche Diagnostics, GmbH (Mannheim, Germany). Acrylamide, bis(acrylamide), and urea were purchased from Merck KgaA (Darmstadt, Germany). Dimethyl sulfate (DMS) was purchased from Sigma (Prague, Czech Republic). Nonidet P-30 was purchased from Fluka (Prague, Czech Republic). Radioactive products were purchased from Amersham (Arlington Heights, IL, USA). ATP was purchased from Boehringer (Mannheim, Germany).

Platinations of Oligonucleotides

Oligonucleotides that contained single, central 1,2-GG intrastrand CLs of [Pt(R,R-DAB)]²⁺ or [Pt(S,S-DAB)]²⁺ were prepared according to literature procedures.^[12] The platinated oligonucleotides were purified by ion-exchange fast protein liquid chromatography (FPLC). It was verified by platinum flameless atomic absorption spectrophotometry (FAAS) and by the measurements of the optical density that the modified oligonucleotides contained one platinum atom. It was also verified using DMS footprinting of platinum on DNA^[13] that one Pt-DAB molecule was coordinated to the N7 atoms of both neighboring guanines. FPLC purification and FAAS measurements were carried out on a Pharmacia Biotech FPLC System with MonoQ 5/50 GL column and a Varian AA240Z Zeeman atomic absorption spectrometer equipped with a GTA 120 graphite tube atomizer, respectively.

Inhibition of DNA Polymerization

We investigated DNA polymerization by using templates that were site-specifically modified with [Pt(R,R-DAB)]²⁺ or [Pt(S,S-DAB)]²⁺ by KF[−]. The DNA polymerase I class of enzymes has been used as the prototype class for studying the structural and biochemical mechanisms of DNA replication.^[14,15] In addition, because the most-extensive genetic, bio-

chemical, and structural studies have been carried out on the Klenow fragment of DNA polymerase I (including its exonuclease-deficient analogue) this enzyme appeared to be an ideal model system for investigating the molecular mechanisms associated with template-directed DNA synthesis.^[14,15]

The 23-mer templates (Figure 1a) that contained a single 1,2-GG intra-strand adduct of [Pt(R,R-DAB)]²⁺ or [Pt(S,S-DAB)]²⁺ were prepared as described above. An 8-mer DNA primer (Figure 1a) was complementary to the 3' termini of the 23-mer templates. The DNA substrates were formed by annealing the template and the 5'-end labeled primer (5 × 10^{−8} M) in a molar ratio of 3:1. All experiments were performed at 298 K in a buffer containing Tris-HCl (50 μL, 50 mM, pH 7.4), MgCl₂ (10 mM), dithiothreitol (0.1 mM), bovine serum albumin (50 μg mL^{−1}), dATP (100 μM), dCTP (100 μM), dGTP (100 μM), TTP (100 μM), and 0.5 units of KF[−]. The reactions were terminated by the addition of ethylenediamine-tetraacetic acid so that its resulting concentration was 20 mM and by heating at 373 K for 30 s. Products were resolved by denaturing 20% PAA/8M urea gel and then visualized and quantified by using the FUJIFILM bio-imaging analyzer and AIDA image-analyzer software.

Differential Scanning Calorimetry (DSC)

Excess heat capacity (ΔC_p) versus temperature profiles for the thermally induced transitions of duplexes, which were obtained by pairing the unmodified templates or templates that contained unique 1,2-d(GG) intra-strand CLs of [Pt(R,R-DAB)]²⁺ or [Pt(S,S-DAB)]²⁺ with primers of different lengths (Scheme 1c), were measured by using a VP-DSC Calorimeter (Microcal, Northampton, MA). In the DSC experiments, the concentrations of the duplexes were 30 μM, the heating rate was 60 K h^{−1}, and the maximum temperature was 368 K. After reaching the maximum temperature, the samples were cooled at the same rate to the starting temperature (288 K). ΔC_p is defined as excess heat capacity, which was baseline-subtracted and concentration-normalized.^[16] The reference scans were subtracted from the sample scans to obtain profiles of ΔC_p versus temperature. Enthalpies (ΔH) and entropies of duplex melting (ΔS) were calculated from the areas under the experimental ΔC_p versus T and the derived $\Delta C_p/T$ versus T curves, respectively, by using ORIGIN v.5.0 software (Microcal). The free energy of duplex dissociation at 298 K (ΔG_{298}^0) was calculated by using the standard thermodynamic relationship given in [Eq. (1)] and the corresponding ΔH and ΔS values:

$$\Delta G_{298}^0 = \Delta H - (298.15) \Delta S \quad (1)$$

The duplexes were dissolved in a buffer that contained sodium phosphate (NaH₂PO₄/Na₂HPO₄, 10 mM, pH 7.0) and NaCl (150 mM). The melting transitions of both the platinated and unmodified duplexes were confirmed to be fully reversible by using literature procedures.^[17,18]

Acknowledgements

This work was supported by the Czech Science Foundation (Grant Nos P205/11/0856 and P301/10/0598).

- [1] Y. Kidani, K. Inagaki, M. Iigo, A. Hoshi, K. Kureitani, *J. Med. Chem.* **1978**, *21*, 1315–1318.
- [2] M. Noji, K. Okamoto, Y. Kidani, T. Tashiro, *J. Med. Chem.* **1981**, *24*, 508–514.
- [3] F. P. Fanizzi, F. P. Intini, L. Maresca, G. Natile, R. Quaranta, M. Coluccia, L. Di Bari, D. Giordano, M. A. Mariggio, *Inorg. Chim. Acta* **1987**, *137*, 45–51.
- [4] E. Raymond, S. Faivre, S. Chaney, J. Woynarowski, E. Cvitkovic, *Mol. Cancer Therap.* **2002**, *1*, 227–235.
- [5] E. R. Jamieson, S. J. Lippard, *Chem. Rev.* **1999**, *99*, 2467–2498.
- [6] J. Malina, C. Hofr, L. Maresca, G. Natile, V. Brabec, *Biophys. J.* **2000**, *78*, 2008–2021.
- [7] J. Malina, J. Kasparkova, G. Natile, V. Brabec, *Chem. Biol.* **2002**, *9*, 629–638.

- [8] O. Delalande, J. Malina, V. Brabec, J. Kozelka, *Biophys. J.* **2005**, *88*, 4159–4169.
- [9] J. Malina, O. Novakova, M. Vojtiskova, G. Natile, V. Brabec, *Biophys. J.* **2007**, *93*, 3950–3962.
- [10] G. Villani, N. T. Le Gac, L. Wasungu, D. Burnouf, R. P. Fuchs, P. E. Boehmer, *Nucleic Acids Res.* **2002**, *30*, 3323–3332.
- [11] J. Petruska, M. F. Goodman, M. S. Boosalis, L. C. Sowers, C. Cheong, I. Tinoco Jr., *Proc. Natl. Acad. Sci. USA* **1988**, *85*, 6252–6256.
- [12] V. Brabec, J. Reedijk, M. Leng, *Biochemistry* **1992**, *31*, 12397–12402.
- [13] J. Kašpárková, K. J. Mellish, Y. Qu, V. Brabec, N. Farrell, *Biochemistry* **1996**, *35*, 16705–16713.
- [14] W. C. Lam, E. J. C. Van der Schans, L. C. Sowers, D. P. Millar, *Biochemistry* **1999**, *38*, 2661–2668.
- [15] P. H. Patel, M. Suzuki, E. Adman, A. Shinkai, L. A. Loeb, *J. Mol. Biol.* **2001**, *308*, 823–837.
- [16] S. A. Leharne, B. Z. Chowdhry in *Biocalorimetry: Applications of Calorimetry in the Biological Sciences* (Eds.: J. E. Ladbury, B. Z. Chowdhry), Wiley, Chichester, UK, **1998**, pp. 157–182.
- [17] C. Hofr, N. Farrell, V. Brabec, *Nucleic Acids Res.* **2001**, *29*, 2034–2040.
- [18] C. Hofr, V. Brabec, *J. Biol. Chem.* **2001**, *276*, 9655–9661.

Received: October 27, 2011
Published online: February 28, 2012

3.

Photoactivatable Organometallic Pyridyl Ruthenium(II) Arene Complexes

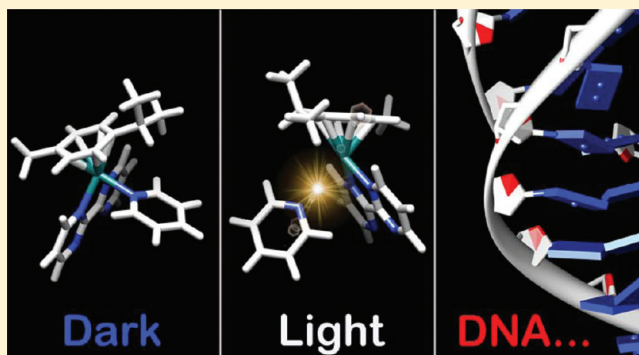
Soledad Betanzos-Lara,^{†,§} Luca Salassa,[†] Abraha Habtemariam,[†] Olga Novakova,[‡] Ana M. Pizarro,[†] Guy J. Clarkson,[†] Barbora Liskova,[‡] Viktor Brabec,[‡] and Peter J. Sadler^{*,†}

[†]Department of Chemistry, University of Warwick, Coventry, UK CV4 7AL

[‡]Institute of Biophysics, Academy of Sciences of the Czech Republic, v.v.i., Kralovopolska 135, CZ61265 Brno, Czech Republic

S Supporting Information

ABSTRACT: The synthesis and characterization of a family of piano-stool Ru^{II} arene complexes of the type $[(\eta^6\text{-arene})\text{Ru}(\text{N,N}')(\text{L})][\text{PF}_6]_2$, where arene is *p*-cymene (*p*-cym), hexamethylbenzene (hmb), or indane (ind), N,N' is 2,2'-bipyrimidine (bpm), 1,10-phenanthroline (phen), 1,10-phenanthroline-5,6-dione (phendio), or 4,7-diphenyl-1,10-phenanthroline (bathophen), and L is pyridine (Py), 4-methylpyridine (4-MePy), 4-methoxypyridine (4-MeOPy), 4,4'-bipyridine (4,4'-bpy), 4-phenylpyridine (4-PhPy), 4-benzylpyridine (4-BzPy), 1,2,4-triazole (trz), 3-acetylpyridine (3-AcPy), nicotinamide (NA), or methyl nicotinate (MN), are reported, including the X-ray crystal structures of $[(\eta^6\text{-p-cym})\text{Ru}(\text{bpm})(4\text{-MePy})]^{2+}$ (2), $[(\eta^6\text{-p-cym})\text{Ru}(\text{bpm})(4\text{-BzPy})]^{2+}$ (6), $[(\eta^6\text{-p-cym})\text{Ru}(\text{bpm})(\text{trz})]^{2+}$ (7), $[(\eta^6\text{-p-cym})\text{Ru}(\text{phen})(\text{Py})]^{2+}$ (10), and $[(\eta^6\text{-ind})\text{Ru}(\text{bpy})(\text{Py})]^{2+}$ (13). These complexes can selectively photodissociate the monodentate ligand (L) when excited with UVA or white light, allowing strict control of the formation of the reactive aqua species $[(\eta^6\text{-arene})\text{Ru}(\text{N,N}')(\text{OH}_2)]^{2+}$ that otherwise would not form in the dark. The photoproducts were characterized by UV-vis absorption and ¹H NMR spectroscopy. DFT and TD-DFT calculations were employed to characterize the excited states and to obtain information on the photochemistry of the complexes. All the Ru^{II} pyridine complexes follow a relatively similar photochemical L-ligand dissociation mechanism, likely to occur from a series of ³MC triplet states with dissociative character. The photochemical process proved to be much more efficient when UVA-range irradiation was used. More strikingly, light activation was used to phototrigger binding of these potential anticancer agents with discriminating preference toward 9-ethylguanine (9-EtG) over 9-ethyladenine (9-EtA). Calf thymus (CT)-DNA binding studies showed that the irradiated complexes bind to CT-DNA, whereas the nonirradiated forms bind negligibly. Studies of CT-DNA interactions in cell-free media suggest combined weak monofunctional coordinative and intercalative binding modes. The Ru^{II} arene complexes $[(\eta^6\text{-p-cym})\text{Ru}(\text{bpm})(\text{Py})]^{2+}$ (1), $[(\eta^6\text{-p-cym})\text{Ru}(\text{bpm})(4\text{-MeOPy})]^{2+}$ (3), $[(\eta^6\text{-p-cym})\text{Ru}(4,4'\text{-bpy})]^{2+}$ (4), $[(\eta^6\text{-hmb})\text{Ru}(\text{bpm})(\text{Py})]^{2+}$ (8), $[(\eta^6\text{-ind})\text{Ru}(\text{bpm})(\text{Py})]^{2+}$ (9), $[(\eta^6\text{-p-cym})\text{Ru}(\text{phen})(\text{Py})]^{2+}$ (10), $[(\eta^6\text{-p-cym})\text{Ru}(\text{bathophen})(\text{Py})]^{2+}$ (12), $[(\eta^6\text{-p-cym})\text{Ru}(\text{bpm})(\text{NA})]^{2+}$ (15), and $[(\eta^6\text{-p-cym})\text{Ru}(\text{bpm})(\text{MN})]^{2+}$ (16) were cytotoxic toward A2780 human ovarian cancer cell line in the absence of photoirradiation (IC₅₀ values in the range of 9.0–60 μM).



INTRODUCTION

Photochemical activation is an attractive approach for achieving precise spatial and temporal control of the biological action of transition-metal complexes that behave as inactive drugs in the dark.¹ Such a strategy has been applied to (poly)pyridyl complexes as diagnostic and therapeutic agents.^{2–4} The basic rationale involves the modification of the Ru^{II} molecules by introducing a group that can be selectively cleaved by the absorption of light, promoting its release and offering the possibility of controlling the location, timing, and dosage of the therapeutic metal complex. This requires breaking of a coordination bond by the use of high-energy UV-visible light photons. The photochemistry of half-sandwich species such as $[(\eta^6\text{-C}_6\text{H}_6)\text{Ru}(\eta^5\text{-C}_5\text{H}_5)]^+$ has been investigated.⁵ Photosubstitution of the arene is the dominant reaction

pathway, and benzene is released. Irradiation in aqueous solution of Ru^{II} complexes of the type $[(\eta^6\text{-arene})\text{Ru}(\text{L})_3]^{2+}$, where arene = benzene, toluene, isopropyltoluene and L = NH₃, H₂O, was found to lead in each case to the substitution of the arene by water molecules as the only observable photoreaction to produce $[\text{Ru}(\text{OH}_2)_3\text{L}_3]^{2+}$ plus the corresponding free arene.⁶ Other investigations have reported that $[(\eta^6\text{-arene})\text{Ru}(\text{P}(n\text{-Bu})_3)_2\text{Cl}_2]$ dissolved in aromatic solvents undergoes exchange of coordinated and solvent arenes on irradiation with UVA.⁷ A few dinuclear complexes based on the typical half-sandwich motif have been also studied. Among them, the complex $[(\eta^6\text{-ind})\text{Ru}(\text{Cl})_2(\mu\text{-2,3-dpp})_2]^{2+}$, where

Received: November 24, 2011

Published: February 23, 2012

dpp is 2,3-bis(2-pyridyl)pyrazine,⁸ releases the arene upon irradiation, generating vacant coordination sites that make it more reactive toward DNA binding.

Related complexes of general formula $[(\eta^6\text{-arene})\text{Ru}(\text{XY})\text{Z}]^{m+}$, where XY is a bidentate chelating ligand and Z is a leaving group (typically an halogen), have been extensively investigated for their promising cytotoxic properties toward various cancer cell lines.⁹ A crucial step in one mode of activation of these anticancer agents is generally the initial aquation of the Ru–Z bond to form a more reactive aqua species,^{10,11} which subsequently can bind to biological targets. It has been shown previously that fast hydrolysis can lead to cytotoxic complexes, whereas very slow hydrolysis often leads to low in vitro cytotoxicity:¹² for example, the complex $[(\eta^6\text{-hmb})\text{Ru}(\text{en})\text{Py}]^{2+}$ does not hydrolyze in aqueous solution at 310 K and is not cytotoxic (IC₅₀ value >100 μM).¹¹

We have recently shown that one key strategy to increase the potential of this class of complexes is to activate the release of the monodentate ligand Z by photoirradiation to promote the formation of the aqua adduct, which would otherwise not form in the dark.¹³ The work reported here is concerned with the synthesis and characterization of an extended series of organometallic Ru^{II} complexes of the type $[(\eta^6\text{-arene})\text{Ru}(\text{N,N'})\text{L}][\text{PF}_6]_2$, where N,N' is a bidentate chelating ligand and L is a pyridine or pyridine derivative that can be selectively dissociated upon photoirradiation (Figure 1). Their behavior in the dark and under photoirradiation in aqueous solution, as well as in the presence of nucleobases such as 9-ethylguanine (9-EtG) and 9-ethyladenine (9-EtA), has been investigated. A description of the excited states for all the Ru^{II} arene complexes was obtained with the aid of density functional theory (DFT) and time-dependent DFT (TD-DFT) calculations.¹⁴ Finally, their potential as cytotoxic agents was also investigated as a preliminary approach toward full photocytotoxicity investigations by performing cell growth inhibition assays (determination of IC₅₀ values) in various human cancer cell lines in the absence of irradiation and also by studying their interactions with DNA in cell-free media, both in the dark and upon photoirradiation.

EXPERIMENTAL SECTION

Materials. RuCl₃·3H₂O was purchased from Precious Metals Online (PMO Pty Ltd.) and used as received. 2,2'-Bipyrimidine (bpm), 1,10-phenanthroline (phen), 1,10-phenanthroline-5,6-dione (phendio), 4,7-diphenyl-1,10-phenanthroline (bathophen), pyridine (Py), 4-methylpyridine (4-MePy), 4-methoxypyridine (4-MeOPy), 4,4'-bipyridine (4,4'-bpy), 4-phenylpyridine (4-PhPy), 4-benzylpyridine (4-BzPy), 1,2,4-triazole (trz), 3-acetylpyridine (3-AcPy), nicotinamide (NA), methyl nicotinate (MN), 9-ethylguanine (9-EtG), 9-ethyladenine (9-EtA), and KPF₆ were obtained from Sigma-Aldrich. The Ru^{II} halido mononuclear precursors $[(\eta^6\text{-arene})\text{Ru}(\text{N,N'})\text{Cl}][\text{PF}_6]$, where arene is *p*-cymene (*p*-cym), hexamethylbenzene (hmb), or indane (ind) and N,N' is bpm, phen, phendio, bathophen, or bpy were synthesized according to a previously reported method.¹⁵ The solvents used for photochemistry and UV–vis absorption spectroscopy were dry methanol (reagent grade) and deionized water. For NMR spectroscopy the solvents used were acetone-*d*₆, DMSO-*d*₆, methanol-*d*₄, and D₂O obtained from Aldrich. All chemicals were used without further purification.

Synthesis of Ruthenium Complexes. Complexes of the form $[(\eta^6\text{-arene})\text{Ru}(\text{N,N'})\text{L}][\text{PF}_6]_2$, where arene is *p*-cym, hmb, or ind, N,N' is bpm, phen, phendio, bathophen, or bpy, and L is Py, 4-MePy, 4-MeOPy, 4,4'-bpy, 4-PhPy, 4-BzPy, trz, 3-AcPy, NA, or MN, were synthesized using a previously described procedure;⁹ the details and characterization are given in the Supporting Information. Complex 1

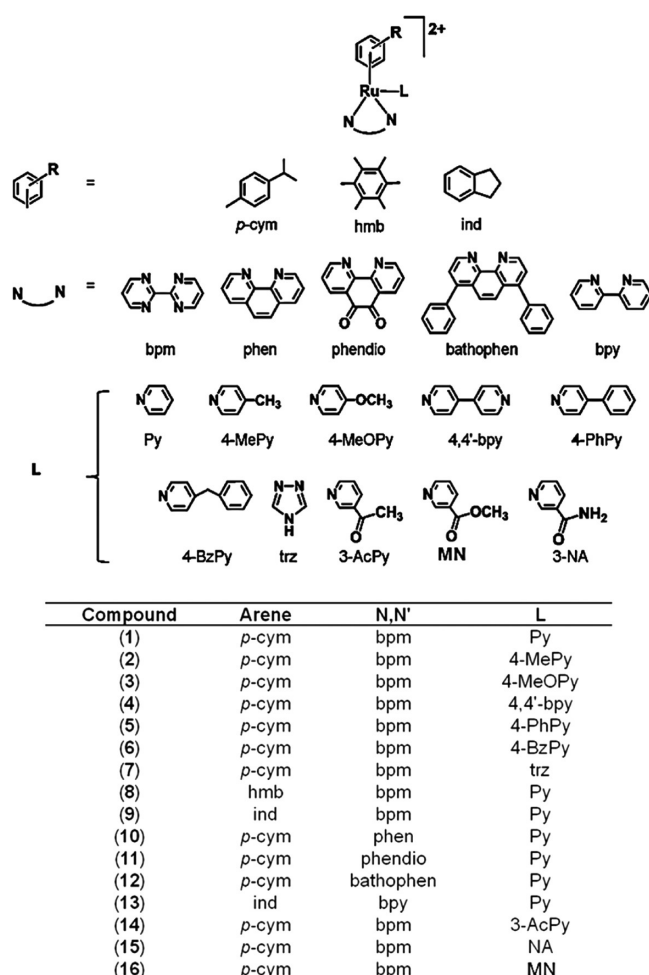


Figure 1. Structures of the dicationic complexes studied in this work, synthesized as PF₆ salts.

(L = Py) has been previously reported by us.¹³ Suitable crystals for X-ray crystallography were obtained from a saturated acetone solution at 278 K for the complexes $[(\eta^6\text{-p-cym})\text{Ru}(\text{bpm})(4\text{-MePy})]^{2+}$ (2) and $[(\eta^6\text{-p-cym})\text{Ru}(\text{bpm})(4\text{-BzPy})]^{2+}$ (6), from a saturated acetone-*d*₆ solution at 298 K for the complex $[(\eta^6\text{-p-cym})\text{Ru}(\text{bpm})(\text{trz})]^{2+}$ (7), and by slow diffusion of Et₂O at 298 K for $[(\eta^6\text{-ind})\text{Ru}(\text{bpy})(\text{Py})]^{2+}$ (13).

X-ray Crystallography. Diffraction data were collected either on an Oxford Diffraction Gemini four-circle system with a Ruby CCD area detector or on a Siemens SMART three-circle system with CCD area detector equipped with an Oxford Cryosystem Cryostream Cooler. All structures were refined by full-matrix least squares against *F*² using SHELXL 97.¹⁶ The structures of complexes 2, 6, 7, 10, and 13 were solved by direct methods using SHELXS¹⁷ (TREF) with additional light atoms found by Fourier methods. Hydrogen atoms were added at calculated positions and refined using a riding model with freely rotating methyl groups. Anisotropic displacement parameters were used for all non-H atoms; H atoms were given isotropic displacement parameters equal to 1.2 (or 1.5 for methyl hydrogen atoms) times the equivalent isotropic displacement parameter of the atom to which the H atom is attached.

X-ray crystallographic data for complexes 2[PF₆]₂, 6[PF₆]₂, 7[PF₆]₂, 10[PF₆]₂ and 13[PF₆]₂ are available as Supporting Information and have been deposited in the Cambridge Crystallographic Data Centre under the accession numbers CCDC 855333, 855330, 855331, 855334, and 855332, respectively. X-ray crystallographic data in CIF format are available from the Cambridge Crystallographic Data Centre (<http://www.ccdc.cam.ac.uk/>).

NMR Spectroscopy. ^1H and ^{13}C NMR spectra were acquired in 5 mm NMR tubes at 298 K (unless otherwise stated) on a Bruker DRX-500, Bruker AV III 600, or Bruker AV II 700 NMR spectrometer. All data processing was carried out using XWIN-NMR version 3.6 (Bruker U.K. Ltd.). ^1H chemical shifts were internally referenced to TMS via 1,4-dioxane (δ 3.71) or residual CHCl_3 (δ 7.27), MeOH (δ 3.31), or DMSO (δ 2.50). 1D spectra were recorded using standard pulse sequences. Typically, data were acquired with 128 transients into 16k data points over a spectral width of 14 ppm. 2D COSY or TOCSY and NOESY spectra were recorded using standard pulse–pulse sequences. Typically, the data were acquired with 72 transients into 2048k data points over a spectral width of 14 ppm using a relaxation delay of 1.5 s and a mixing time of 0.4–0.6 s.

Elemental Analysis. Elemental analyses were performed by the Warwick Analytical Service, which is the analytical division of Exeter Analytical (U.K. Ltd.), using an Exeter Analytical Elemental Analyzer (CE440).

High-Resolution Electrospray Mass Spectrometry (HR-MS). HR-MS data were obtained on a Bruker MaXis UHR-TOF instrument. All the samples were analyzed by positive-ion ESI(+) mass spectrometry. Samples were prepared either in 100% H_2O or a 95% MeOH/5% H_2O mixture and typically injected at $2\ \mu\text{L}\ \text{min}^{-1}$, nebulizer gas (N_2) 0.4 bar, dry gas (N_2) $4\ \text{L}\ \text{min}^{-1}$ and dry temperature 453 K, Funnel RF 200 V, Multiple RF 200, quadrupole ion energy 4 eV, collision cell 5 eV, ion cooler RF settings, ramp from 50 to 250 V.

UV–Vis Absorption Spectroscopy. UV–vis absorption spectra were recorded on a Cary 300 spectrophotometer using 1 cm path length quartz cuvettes (600 μL) and a PTP1 Peltier temperature controller. Spectra were recorded at 310 K in deionized water from 200 to 800 nm and were processed using Cary WinUV software for Windows XP. Absorption spectra of CT-DNA/ruthenium(II) complex solutions were obtained with a Beckman DU 7 4000 UV–vis spectrophotometer equipped with a thermoelectrically controlled cell holder and 1 cm path length quartz cells.

pH* Measurements. pH values were measured at ambient temperature using a Corning 240 pH meter equipped with a micro combination KNO_3 (chloride free) electrode calibrated with Aldrich buffer solutions of pH 4, 7, and 10. The pH* values (pH meter reading without correction for effects of deuterium on the glass electrode)¹⁸ of NMR samples in D_2O were measured at about 298 K directly in the NMR tube, before and after recording NMR spectra, using the same method. The pH* values were adjusted with dilute NaOH or HNO_3 solutions in D_2O .

Photoirradiation of Ru^{II} Arene Complexes. Aqueous solutions of the Ru^{II} arene complexes were photoirradiated at 310 K using the photoreactor LZC 4 V illuminator (Luzchem, Canada) with temperature controller and UVA ($\lambda_{\text{irr}} = 320\text{--}400\ \text{nm}$ with a maximum intensity at $\sim 360\ \text{nm}$, $1\ \text{J}\ \text{cm}^{-2}\ \text{h}^{-1}$) or white light lamps ($\lambda_{\text{irr}} = 400\text{--}660\ \text{nm}$ providing an average light power of $1\ \text{J}\ \text{cm}^{-2}\ \text{h}^{-1}$). These amount to relatively low doses of light (about 15 min in the midday sun). UV–vis absorption spectra of 100 μM solutions in deionized water or ^1H NMR spectra of 3 mM solutions in D_2O of the Ru^{II} arene complexes were recorded as previously stated (vide supra) at different stages of photoirradiation. Solutions were stored in the dark to minimize unwanted photoreactions between measurements.

Computational Details. The Gaussian 03 (G03) program¹⁹ employing the DFT method, Becke three-parameter hybrid functional, and Lee–Yang–Parr’s gradient corrected correlation functional (B3LYP)²⁰ were used. The LanL2DZ basis set²¹ and effective core potential were used for the Ru atom, and the 6-31G** basis set²² was used for all other atoms. Geometry optimizations in the ground state (S0) and lowest-lying triplet state (T0) were performed in the gas phase, and the nature of all stationary points was confirmed by normal-mode analysis. The conductor-like polarizable continuum model method (CPCM)²³ with water as solvent was used to calculate the electronic structure and the excited states in solution. Fifty singlet excited states and the corresponding oscillator strengths were determined with a time-dependent density functional theory (TD-DFT)²⁴ calculation. Eight triplet excited states were calculated by TD-

DFT using the lowest-lying triplet state geometry. The electronic distribution and the localization of the singlet and triplet excited states were visualized using electron density difference maps (EDDMs).²⁵ GaussSum1.05²⁶ was used for EDMs calculations and for the electronic spectrum simulation. A full summary of the computational results is reported in the Supporting Information.

DNA Binding Kinetics. Reaction mixtures of DNA and complexes $[(\eta^6\text{-}p\text{-cym})\text{Ru}(\text{bpm})(\text{Py})]^{2+}$ (**1**), $[(\eta^6\text{-}p\text{-cym})\text{Ru}(\text{bpm})(4,4'\text{-bpy})]^{2+}$ (**4**), and $[(\eta^6\text{-}p\text{-cym})\text{Ru}(\text{phen})(\text{Py})]^{2+}$ (**10**) were prepared in three ways: (A) in the dark (henceforth referred to as “nonirradiated”), (B) following the addition to DNA of previously irradiated **1**, **4**, and **10** (“preirradiated”), and (C) by addition of **1**, **4**, and **10** to DNA followed by photoirradiation of the resulting mixture (“irradiated”). The samples were photoirradiated with white light (λ_{irr} 400–660 nm) at selected photoirradiation times. The binding kinetics experiments with calf thymus DNA (CT-DNA) were then performed as described. CT-DNA and plasmid DNAs were incubated with **1**, **4**, and **10** or platinum complexes (cisplatin, transplatin, and (diethylenetriamine)-platinum) in 10 mM NaClO_4 (pH ~ 6) at 310 K for 24 h. For each individual assay, the values of r_b (r_b is the number of atoms of the metal bound per nucleotide residue) were determined by flameless atomic absorption spectrometry (FAAS). CT-DNA (42% G + C, mean molecular mass ca. 20 000 kD) was prepared and characterized as described previously.²⁷ Plasmids pUC19 (2686 base pairs (bp)) and pSP73KB (2455 bp) were isolated according to standard procedures.

DNA Transcription by RNA Polymerase in Vitro. Transcription of the (*NdeI/HpaI*) restriction fragment of pSP73KB DNA with T7 RNA polymerase and electrophoretic analysis of the transcripts were performed with complexes **1**, **4**, and **10** according to the protocols recommended by Promega (Promega Protocols and Applications, 43-46 (1989–1990)).²⁸ The DNA concentration used was $7.8 \times 10^{-5}\ \text{M}$ (0.5 $\mu\text{g}/20\ \mu\text{L}$) (related to the monomeric nucleotide content).

Unwinding of Negatively Supercoiled DNA. Unwinding of closed circular supercoiled pUC19 plasmid DNA was assayed by an agarose gel mobility shift assay.²⁹ The mean unwinding angle can be calculated from the equation $\Phi = -18\sigma/r_b(c)$, where σ is the superhelical density (representing the number of turns added or removed relative to the total number of turns in the relaxed plasmid, indicating the level of supercoiling) and $r_b(c)$ is the r_b value at which the supercoiled and nicked forms comigrate.³⁰ Samples of plasmid DNA at a concentration of $1.0 \times 10^{-4}\ \text{M}$ (0.5 $\mu\text{g}/15\ \mu\text{L}$) (related to the monomeric nucleotide content) were incubated with the Ru^{II} complexes at 310 K for 24 h. The preirradiated forms of **1**, **4**, and **10** (irradiation for 24 h) of the Ru^{II} arene pyridine complexes were used. All samples were precipitated by ethanol and redissolved in the TAE (Tris-acetate/EDTA, pH ~ 8.0) buffer to remove free, unbound Ru^{II} arene complexes. One aliquot of the precipitated sample was subjected to electrophoresis on 1% agarose gels running at 298 K with TAE buffer, and the voltage was set at 25 V. The gels were then stained with ethidium bromide (EtBr), followed by photography with a trans-illuminator. Electron absorption spectrometry (EAS) and/or flameless atomic absorption spectrometry (FAAS) was used for the determination of r_b values.

DNA Melting Temperature. CT-DNA at a concentration of 32 $\mu\text{g}/\text{mL}$ was modified by Ru^{II} arene complexes at various r_b values in 10 mM NaClO_4 with 1 mM Tris-HCl/0.1 mM EDTA and pH 7.4 at 310 K for 24 h. The samples were then dialyzed and the r_b values were determined by EAS and FAAS. The salt concentration was then further adjusted by the addition of NaClO_4 to values in the range of 0.01–0.22 M. The melting curves of CT-DNA were recorded by measuring the absorbance at 260 nm. The value of the melting temperature (t_m) was determined as the temperature corresponding to a maximum on the first-derivative profile of the melting curves. The t_m values could be thus determined with an accuracy of $\pm 0.5\ ^\circ\text{C}$.

Circular Dichroism (CD). Isothermal CD spectra of CT-DNA modified by **1**, **4**, and **10** at a concentration of $3.3 \times 10^{-4}\ \text{M}$ were recorded at 298 K in 10 mM NaClO_4 by using a Jasco J-720 spectropolarimeter equipped with a thermoelectrically controlled cell holder. The cell path length was 1 cm. CD spectra were recorded in

Table 1. Selected Bond Lengths (Å) and Angles (deg) for $[(\eta^6\text{-}p\text{-cym})\text{Ru}(\text{bpm})(4\text{-MePy})][\text{PF}_6]_2$ (**2**), $[(\eta^6\text{-}p\text{-cym})\text{Ru}(\text{bpm})(4\text{-BzPy})][\text{PF}_6]_2$ (**6**), $[(\eta^6\text{-}p\text{-cym})\text{Ru}(\text{bpm})(\text{trz})][\text{PF}_6]_2$ (**7**), $[(\eta^6\text{-}p\text{-cym})\text{Ru}(\text{phen})(\text{Py})][\text{PF}_6]_2$ (**10**), and $[(\eta^6\text{-ind})\text{Ru}(\text{bpy})(\text{Py})][\text{PF}_6]_2$ (**13**)

bond length/angle	2	6	7	10	13
Ru–arene(centroid)	1.691	1.703	1.699	1.698	1.703
Ru(1)–N(13)	2.110(2)	2.121(2)	2.1041(19)	2.1169(14)	2.1250(14)
Ru(1)–N(1)	2.099(2)	2.090(2)	2.0866(18)	2.0853(13)	2.0877(13)
Ru(1)–N(8)	2.094(2)	2.094(2)	2.0808(18)	2.0970(14)	2.0727(13)
C(6)–C(7)	1.478(4)	1.479(3)	1.493(3)	1.421(2)	1.466(2)
N(8)–Ru(1)–N(1)	76.86(9)	76.93(8)	77.09(7)	78.07(5)	77.23(5)
N(13)–Ru(1)–N(8)	87.40(9)	87.96(8)	85.94(7)	85.36(5)	86.22(5)
N(13)–Ru(1)–N(1)	86.40(9)	87.43(8)	83.94(7)	87.03(5)	87.05(5)

the range of 230–600 nm in 0.5 nm increments with an averaging time of 0.5 s.

Flow Linear Dichroism (LD). Flow LD spectra were collected by using a flow Couette cell in a Jasco J-720 spectropolarimeter adapted for LD measurements. The flow cell consists of a fixed outer cylinder and a rotating solid quartz inner cylinder, separated by a gap of 0.2 mm, giving a total path length of 1 mm. LD spectra of DNA at the concentration 3.3×10^{-4} M modified by **1**, **4**, and **10** were recorded at 298 K in 10 mM NaClO₄.

Ethidium Bromide (EtBr) Fluorescence. Measurements were performed on a Varian Cary Eclipse spectrofluorimeter using a 1 cm path length quartz cell. Fluorescence measurements of CT-DNA modified by **1**, **4**, and **10** in the presence of EtBr were performed at an excitation wavelength of 546 nm, and the emitted fluorescence was analyzed at 590 nm. The fluorescence intensity was measured at 298 K in 0.4 M NaCl to avoid secondary binding of EtBr to DNA.³¹ The concentrations were 0.01 mg/mL for DNA and 0.04 mg/mL for EtBr, which corresponded to the saturation of all intercalation sites for EtBr in DNA.³²

Other Physical Methods. The FAAS measurements were carried out on a Varian AA240Z Zeeman atomic absorption spectrometer equipped with a GTA 120 graphite tube atomizer. The PAA gels were visualized by using a BAS 2500 FUJIFILM bioimaging analyzer, with the AIDA image analyzer software (Raytest, Germany).

Cancer Cell Growth Inhibition. The A2780 human ovarian cancer cell line was obtained from the ECACC (European Collection of Animal Cell Cultures, Salisbury, U.K.). The cells were maintained in RPMI 1640 media (supplemented with 10% fetal calf serum, 1% L-glutamine, and 1% penicillin/streptomycin). All cells were grown at 310 K in a humidified atmosphere containing 5% CO₂. After plating, human ovarian A2780 was treated with the Ru^{II} arene complexes **1**, **3**, **4**, **8–10**, **12**, **15**, and **16** on day 3 at concentrations ranging from 0.1 to 100 μM. Solutions of the Ru^{II} complexes were made up under ambient light conditions in 0.125% DMSO to assist dissolution (0.03% final concentration of DMSO per well in the 96-well plate). Cells were exposed to the complexes for 24 h, washed, supplied with fresh medium, and allowed to grow for three doubling times (72 h), and then the protein content was measured (proportional to cell survival) using the sulforhodamine B (SRB) assay.³³

RESULTS

Synthesis and X-ray Crystal Structures. The complexes $[(\eta^6\text{-arene})\text{Ru}(\text{N},\text{N}')(\text{L})]^{2+}$ studied in this work are shown in Figure 1. The dicationic Ru^{II} arene complexes **1–16** were synthesized as PF₆ salts in good yields (>50% in almost all cases). The synthetic route involved the reaction of the corresponding $[(\eta^6\text{-arene})\text{Ru}(\text{N},\text{N}')\text{Cl}][\text{PF}_6]$ complex with AgNO₃ in a 1:1 mixture of MeOH and H₂O to afford the corresponding aqua species $[(\eta^6\text{-arene})\text{Ru}(\text{N},\text{N}')(\text{OH}_2)]^{2+}$, to which an excess of the appropriate ligand L and KPF₆ were added. All the synthesized complexes were fully characterized by spectroscopic and analytical methods.

The molecular structures of complexes **2**, **6**, **7**, **10**, and **13** were determined by single-crystal X-ray diffraction. Selected bond lengths and angles are given in Table 1, the structures with numbering schemes are shown in Figure 2, and the crystallographic data are given in Table S1 (Supporting Information). These complexes have very similar structural features between them and are found to adopt the familiar pseudo-octahedral three-legged piano-stool geometry common to other Ru^{II} arene structures,¹⁰ with the Ru atom π -bonded to the arene ligand (*p*-cym in **2**, **6**, **7**, and **10**; ind in **13**) and coordinated to a pyridine nitrogen (**2**, **6**, **7**, **10**, and **13**) and to two nitrogen atoms of the chelating ligand (bpm for **2**, **6**, and **7**; phen for **10**; bpy for **13**). Details of the crystal packing, hydrogen bonding, and π – π stacking interactions for complexes **2**, **6**, **7**, **10**, and **13** are reported in Figures S1–S6 (Supporting Information).

DFT Optimized Geometry Structures and Molecular Orbitals of Ru^{II} Arene Complexes. Geometry optimization of complexes **1–6** and **8–16**, shown in Figure 1, was performed for both the ground state (S0) and the lowest-lying triplet state (T0), employing the DFT method with the B3LYP functional. Complex **7** was not obtained in sufficient yields and therefore was not considered for further experimental or theoretical studies. Details of the computational results are summarized in Tables S2 and S3 (Supporting Information).

Ground State (S0) Geometry. All the DFT geometry optimized Ru^{II} arene complexes have a pseudo-octahedral structure in the ground state (S0). The overall agreement with the experimental data was satisfactory; however, in a few cases (particularly for complexes **2** and **6**) the functional used was found to underestimate the Ru–N(L) bond distances by ca. 0.01–0.04 Å in comparison to the X-ray crystal structures. Slight variations in the calculated Ru–*p*-cym(centroid) distances were also found in comparison to those determined by X-ray crystallography, especially for complexes **10** and **13**, where the value predicted is ca. 0.04 Å larger in the first case. A good agreement between calculated and experimental Ru–N(N,N') bond distances was found for all complexes.

Lowest-Lying Triplet State (T0) Geometry. The lowest-lying triplet state geometries were also optimized for complexes **1–6** and **8–16**, due to the key role that this state can play in their photochemistry. It was found that all complexes have similar Ru–N(L) distances of 2.14 ± 0.06 Å, which resemble those observed in the ground state (S0), except for complexes **1** and **5**, whose distances are slightly shorter. In contrast, complexes **10** and **12** have considerably elongated Ru–N(Py) distances (~2.5 Å). For complexes **1–6**, **8**, **9**, **13**, and **16** one of the Ru–N,N' bond distances in the T0 state is considerably longer than

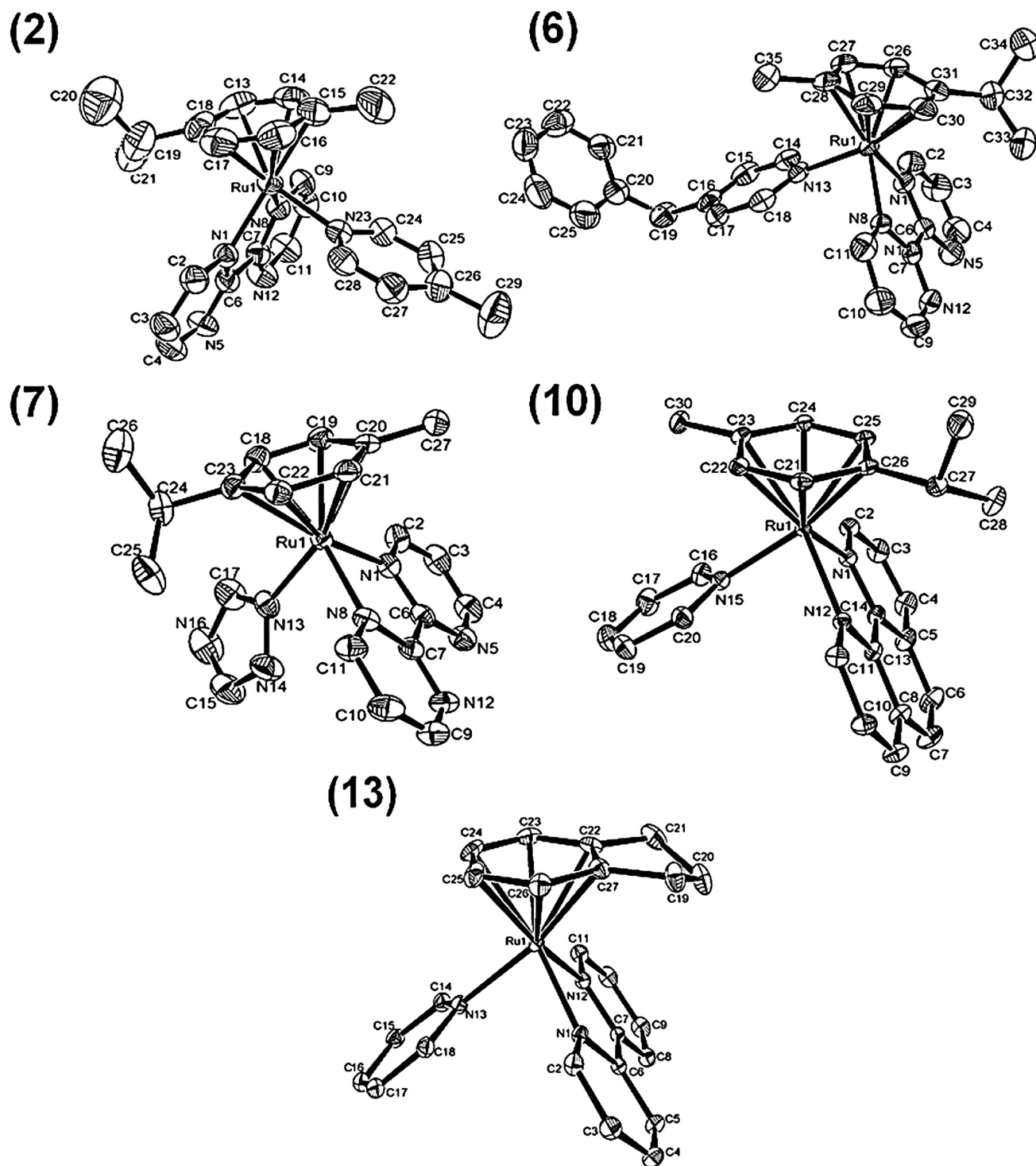


Figure 2. X-ray structures of the cations in $[(\eta^6\text{-}p\text{-cym})\text{Ru}(\text{bpm})(4\text{-MePy})][\text{PF}_6]_2$ (**2**), $[(\eta^6\text{-}p\text{-cym})\text{Ru}(\text{bpm})(4\text{-BzPy})][\text{PF}_6]_2$ (**6**), $[(\eta^6\text{-}p\text{-cym})\text{Ru}(\text{bpm})(\text{trz})][\text{PF}_6]_2$ (**7**), $[(\eta^6\text{-}p\text{-cym})\text{Ru}(\text{phen})(\text{Py})][\text{PF}_6]_2$ (**10**), and $[(\eta^6\text{-ind})\text{Ru}(\text{bpy})(\text{Py})][\text{PF}_6]_2$ (**13**). Thermal ellipsoids are at the 50% probability level. The PF_6^- anions and hydrogens have been omitted for clarity.

the other, typically 2.18 and 2.40 Å, whereas in the remaining complexes, the distance resembles more that obtained for the ground state. In almost all cases, each of the computed Ru–arene(centroid) distances are longer than those calculated for the ground state (~2.06 Å), complex **4** having the largest value (ca. 2.26 Å). Complex **11** was found to keep nearly the same geometry as in S_0 .

Orbital Analysis. The shape of selected frontier orbitals for the Ru^{II} arene complexes **1–6** and **8–16** in the ground state S_0

(Figure S7) and lowest-lying triplet state T_0 (Figure S8) in the T_0 geometry were calculated and analyzed.

Molecular Orbitals in the Ground State. Complexes **1–6** and **8–16** have HOMO orbitals that are generally localized on the Ru^{II} center and on the arene ligand. A few exceptions, however, are present. Complexes with extended monodentate pyridine ligands (namely **3** (4-MeOPy), **4** (4,4'-bpy), **5** (4-PhPy), and **6** (4-BzPy)) show increasing contributions from the pyridine ligand to the HOMOs. In the case of **6**, the HOMO is

actually fully centered on the 4-BzPy. Similarly, complex **12** shows a HOMO that is bathophen-centered. For all complexes **1–6** and **8–16**, the LUMO orbital is centered on the N,N' chelating ligand and at least one orbital among LUMO+1, LUMO+2, and LUMO+3 displays σ^* -antibonding character toward the Ru–L and one Ru–N,N' bond. Figure 3 shows LUMO+2 for complex **10** as an example.

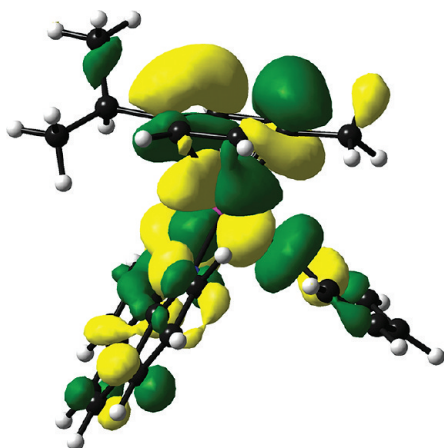


Figure 3. Calculated LUMO+2 orbital for the complex $[(\eta^6\text{-}p\text{-cym})\text{Ru}(\text{phen})(\text{Py})][\text{PF}_6]_2$ (**10**).

Molecular Orbitals in the Triplet State. Complexes **1–3** and **8–10** display a lowest-SOMO (*l*-SOMO) delocalized over the whole molecule, while the highest-SOMO (*h*-SOMO) has a prevalent Ru–arene character and resembles the σ^* -antibonding orbitals of the S0 geometry. For the other derivatives, the N,N'- or L-ligand character of the SOMOs is higher.

Electronic Absorption Spectra and Singlet Excited States. The experimental UV–vis absorption spectra with the corresponding maxima (λ , nm) and extinction coefficients (ϵ , $\text{M}^{-1} \text{cm}^{-1}$) are reported in Figure S9 and Table S4 (Supporting Information). A complete set of TD-DFT calculations was performed on complexes **1–6** and **8–16**, shown in Figure 1, at the B3LYP/LanL2Dz/6-31G** level to characterize their singlet excited states and electronic properties. Data for complex **3** are shown in Figure 4.

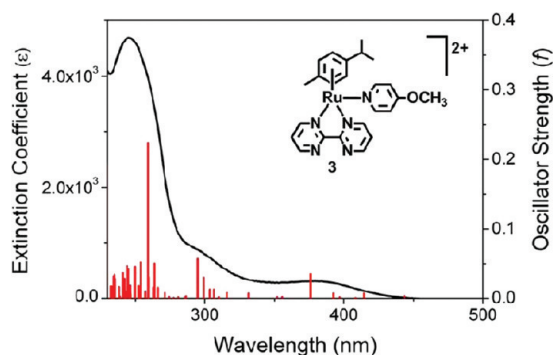


Figure 4. Experimental UV–vis spectrum (black) for $[(\eta^6\text{-}p\text{-cym})\text{Ru}(\text{bpm})(4\text{-MeOPy})][\text{PF}_6]_2$ (**3**) in aqueous solution at 310 K. Calculated singlet electronic transitions are shown as red vertical bars with heights equal to their oscillator strength.

For all complexes the absorbance tail in the 380–420 nm region is dominated by metal-centered (^1MC) and metal-to-

ligand charge transfer ($^1\text{MLCT}$) transitions. Some of these transitions are partially dissociative, since they have significant contributions from the Ru–N,N' and Ru–N(L) σ^* -antibonding orbitals. Not surprisingly, a poorer agreement between the experimental spectrum and the computed singlet transitions is observed in the case of complex **12** (TD-DFT overestimates the oscillator strengths of the transitions at around 370 nm). At higher energy (ca. 330–250 nm), almost pure $^1\text{MLCT}$ (Ru \rightarrow N,N') states are found for all complexes. However, in several cases (i.e. **10–12**) a more pronounced interligand (^1IL) or ligand-centered (^1LC) character is also found; complex **3** displays a maximum at 384 nm with $^1\text{MC}/^1\text{MLCT}$ character (the latter being predominant), a $^1\text{MLCT}$ shoulder at 300 nm, and an intense peak at 247 nm of mixed $^1\text{MLCT}/^1\text{LC}$ nature. Selected electron density difference maps (EDDMs) for complexes **1–6** and **8–16** are shown in Figures S10–S24 (Supporting Information). The orbital compositions of computed singlet transitions for all complexes are reported in Tables S5–S19 (Supporting Information).

Photoirradiation of Ru^{II} Arene Complexes with White Light or UVA Irradiation. The behavior under white light irradiation in aqueous solution of complexes **1–6**, **8–10**, and **12–16** was explored. Due to its instability in aqueous solution, photoirradiation of complex **11** was performed in an acetone solution.

In the dark, aqueous solutions of all the complexes were remarkably stable over a large range of pH* values (pH* 2–12) and no hydrolysis reaction was observed at ambient temperature over a period of ca. 2 months. As shown by UV–vis data, when aqueous solutions of **1–6**, **8–10**, and **12–16** are photoirradiated with white light (λ_{irr} 400–660 nm) the electronic absorption bands shift and change in intensity, the largest changes being observed around the 200–300 nm region (Figure S25). The presence of an isosbestic point at ca. 310 nm indicates the formation of a single photoproduct in all cases. The pH* values of the solutions were determined at the beginning and at the end of each photoirradiation experiment. In most cases a slight decrease in the values was registered, from an average of ~ 7.14 at the starting point down to ~ 6.52 at the final stage. ^1H NMR spectra recorded at different stages of photolysis with white light or UVA irradiation confirm that all the complexes selectively released their pyridine or pyridine-derivative ligand (L) with the subsequent in situ formation of the corresponding aqua adduct as the only metal-containing photoproduct. A similar behavior was previously reported by us for complex **1**.¹³ Both UV–vis and ^1H NMR spectra for complex **10** are shown in Figure 5 as a generic example for white light irradiation; for the remaining derivatives the observed changes were similar. Assignment of ^1H NMR resonances was achieved using standard 2D techniques. The mass-to-charge ratios and isotopic models obtained from HR-MS spectra are consistent with the formation of the aqua complexes as the corresponding photoproducts (Table S20).

Selected Ru^{II} arene complexes (**1**, **8–10**, and **13–16**) were also photoirradiated by UVA (λ_{irr} 320–400 nm) at 310 K and followed by UV–vis and ^1H NMR spectroscopy. Their UV–vis spectra are shown in Figure S26. Spectral changes similar to those produced with white light irradiation are observed, but half the time was needed. Additionally, a larger extent of photoconversion of all the selected complexes to their corresponding aqua adducts was also achieved. Table S21 gives the percentage of adducts detected by ^1H NMR after ca. 4–6 h of continuous UVA irradiation at 310 K for complexes **1**,

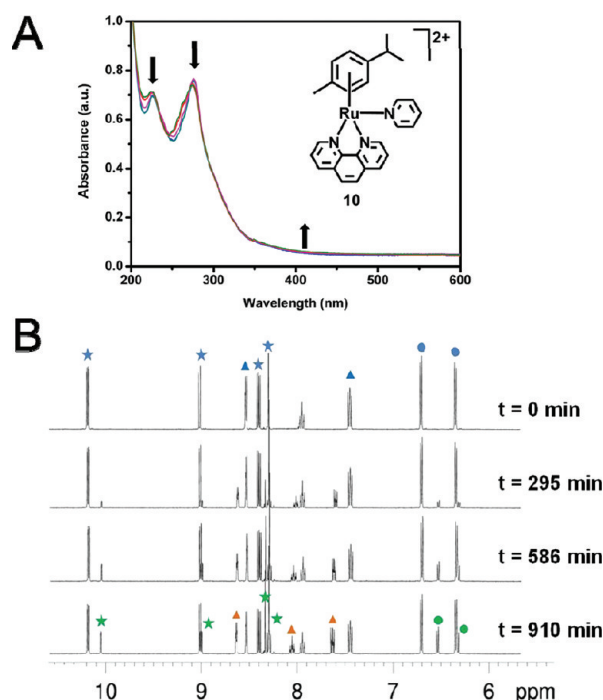


Figure 5. Selected (A) UV-vis and (B) ^1H NMR spectra of complex **10** during its aqueous photolysis ($\lambda_{\text{irr}} = 400\text{--}660\text{ nm}$): (blue) Py complex; (green) aqua adduct; (★) phen; (▲) Py; (●) *p*-cym. Free Py is indicated with an orange ▲.

8–10, and **13–16**. HR-MS spectra are consistent with the formation of the corresponding aqua complexes as the photoproducts, independent of the wavelength employed (Table S20).

In general, a dependence of the photoradiation extent on the nature of the ligands around the metal center was observed. Figures S27–S31 show and Tables S22–S26 give the percentage of species detected by ^1H NMR after ca. 10–12 h of continuous white light irradiation ($\lambda_{\text{irr}} 400\text{--}660\text{ nm}$) at 310 K (A) for complexes **1–6**, (B) for complexes **8–9**, (C) for complexes **10–12**, (D) for complex **13**, and (E) for complexes **14–16**; complex **1** is included for comparison. Within the first group (A), $[(\eta^6\text{-}p\text{-cym})\text{Ru}(\text{bpm})(4,4'\text{-bpy})]^{2+}$ (**4**) photoconverts at the slowest rate and to the least extent. Complexes **1** and **3**, where $\text{L} = \text{Py}$, 4-MeOPy, respectively, were found to convert to a higher extent. When L is 3-AcPy (**14**), NA (**15**), or MN (**16**), the amount of aqua adduct generated is greater after a shorter irradiation time in comparison to complex **1** (group B). Within group C, complex **11** appeared to be unstable in aqueous media and thus was irradiated in acetone. It can be seen that, after 628 and 610 min of irradiation, 75% and 60% of complexes **10** and **12**, respectively, are still present intact in solution. In group D, for complexes **8** and **9** 100% photocoverage to the aqua adduct was achieved after 305 and 425 min, respectively, but for complex **13** only 28% of photocoverage was achieved after 643 min.

Triplet Excited States. Due to the relevance of triplet states in the photophysics and photochemistry of transition-metal complexes, triplet excited states were calculated by DFT and TD-DFT. Analysis of the T0 geometry (obtained by unrestricted DFT) of complexes **1–6**, **8–10**, **12**, **13**, and **16** (shown in Figure 1) reveals that they have a distorted geometry, highlighting both an elongated Ru–N,N'(bpm) bond with respect to the ground state, which is typically ca.

0.3 Å longer, as well as an elongated Ru–N(L) bond in the case of complexes **2**, **3**, **5**, and **6**. The observed increase in the Ru–N distances can be ascribed to the population of a σ^* -antibonding h -SOMO that involves only one bound N within bpm; hence, dissociation of the chelating ligand is prevented by the strong coordination of the other pyrazine ring of the ligand. In the case of complexes **1**, **4**, and **14–15**, no Ru–N(L) bond elongation is observed. Spin density surfaces (Figure S32) show that the nature of the T0 for complexes **1–6**, **8–10**, **12**, **13**, and **16** is ^3MC . In the case of complex **11** the lowest-lying triplet is phen-dio-based, while for **14** and **15** it is L-centered (3-AcPy and NA, respectively).

The ^3MC nature of the lowest-lying triplet state for complexes **1–6**, **8–10**, **12**, **13**, and **16** was confirmed by the TD-DFT calculations on triplet transitions. ^3MC states and distorted triplet geometries are usually found to be in favor of nonemissive deactivation pathways and photochemical activity.³⁴ TD-DFT highlights that the three lowest triplet states have all ^3MC character, but none of them as a significant contribution from σ^* -antibonding orbitals. Dissociative ^3MC states have higher energy (Tables S27–S41 and Figures S33–S47), consistent with an inefficient photochemical conversion.

In the case of **11**, no distortions are observed on comparing ground state and triplet excited state geometries. The TD-DFT calculations show that there is a greater $^3\text{MLCT}$ character, with no significant involvement of the σ^* -antibonding orbitals and the ^3MC states. According to TD-DFT calculations, the lowest-lying triplet state for complex **14** is ^3MC and has a marked dissociative nature toward the Ru–N(L) bond (contribution from LUMO+1 and LUMO+3), while for **15** it is nicotamide (NA)-centered.

Photocontrolled Nucleobase Binding. Following our previous studies¹³ and in order to investigate the ability of the $[(\eta^6\text{-arene})\text{Ru}(\text{N,N}')(\text{L})][\text{PF}_6]_2$ complexes to bind to DNA bases, an irradiation experiment with white light ($\lambda_{\text{irr}} 400\text{--}660\text{ nm}$) at 310 K in the presence of 9-ethylguanine (9-EtG) and 9-ethyladenine (9-EtA) was performed for complexes **1–6**, **8–10**, and **12–16**. As shown in Figure 6 (selected example of $[(\eta^6\text{-}p\text{-cym})\text{Ru}(\text{bpm})(4\text{-MePy})]^{2+}$, complex **2**), irradiation of the complexes at 310 K in D_2O in the presence of 1 mol equiv of 9-EtG resulted in the initial formation of the corresponding aqua adduct $[(\eta^6\text{-arene})\text{Ru}(\text{N,N}')(\text{OH}_2)]^{2+}$ followed by coordina-

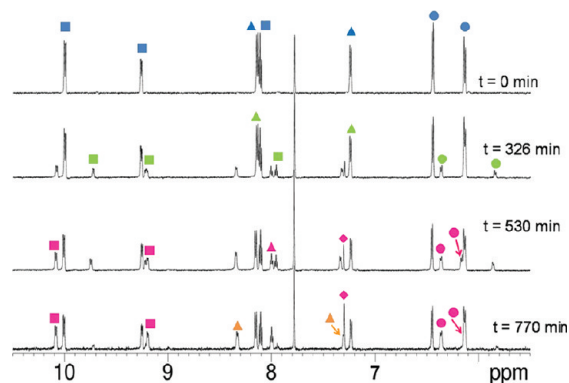


Figure 6. ^1H NMR spectra recorded during the photolysis ($\lambda_{\text{irr}} 400\text{--}660\text{ nm}$) of aqueous solutions of **2** in the presence of 9-EtG: (blue) $[(\eta^6\text{-}p\text{-cym})\text{Ru}(\text{bpm})(4\text{-MePy})]^{2+}$; (green) $[(\eta^6\text{-}p\text{-cym})\text{Ru}(\text{bpm})\text{-(OH}_2)]^{2+}$; (magenta) $[(\eta^6\text{-}p\text{-cym})\text{Ru}(\text{bpm})(9\text{-EtG-N7})]^{2+}$; (■) bpm; (▲) 4-MePy, (●) *p*-cym. Free 4-MePy is indicated with orange and coordinated 9-EtG with magenta ▲.

cym)Ru(bpm)(4-MePy)]²⁺, complex **2**), irradiation of the complexes at 310 K in D_2O in the presence of 1 mol equiv of 9-EtG resulted in the initial formation of the corresponding aqua adduct $[(\eta^6\text{-arene})\text{Ru}(\text{N,N}')(\text{OH}_2)]^{2+}$ followed by coordina-

tion of the nucleobase to the Ru center to form $[(\eta^6\text{-arene})\text{Ru}(\text{N},\text{N}')(\text{9-EtG-N7})]^{2+}$. The binding to 9-EtG is not reversible upon the termination of irradiation. Figure S48 shows the 2D ^1H – ^1H NOESY spectrum, which was used to assign the proton resonances and confirm the structure of $[(\eta^6\text{-}p\text{-cym})\text{Ru}(\text{bpm})(\text{9-EtG-N7})]^{2+}$ (from complex **15**).¹³ An NOE cross-peak between H(8) of 9-EtG and the 2,2'-CH of bpm was observed, suggesting coordination of 9-EtG through N7 as previously noted.³⁵ For the rest of the Ru^{II} arene complexes a similar behavior was observed when the irradiation was carried out in the presence of 9-EtG. The mass-to-charge ratios and isotopic models obtained from HR-MS spectra are consistent with the formation of the corresponding guanine adducts (Table S42). A similar irradiation experiment in the presence of 9-EtA resulted in no 9-EtA binding to the Ru^{II} center for any of the complexes.

Photocontrolled CT-DNA Interactions in Cell-Free Media. In order to explore the possibility and nature of the interactions with DNA, the complexes $[(\eta^6\text{-}p\text{-cym})\text{Ru}(\text{bpm})(\text{Py})]^{2+}$ (**1**), $[(\eta^6\text{-}p\text{-cym})\text{Ru}(\text{bpm})(4,4'\text{-bpy})]^{2+}$ (**4**), and $[(\eta^6\text{-}p\text{-cym})\text{Ru}(\text{phen})(\text{Py})]^{2+}$ (**10**) were selected for further studies.

DNA Binding Kinetics. The binding kinetics experiments with CT-DNA were performed as described in the Experimental Section. The results, summarized in Table S43, indicate that the nonirradiated forms of **1**, **4**, and **10** are not bound to DNA significantly in 10 mM NaClO_4 (less than 5% for **1** and **10** and ca. 20% of **4** after 48 h). Preirradiated and irradiated forms of complexes **1**, **4**, and **10** reacted with DNA to a similar extent, ca. 40%, 54%, and 56%, respectively, after 24 h. It can be seen that preirradiated Ru^{II} arene complexes bind more quickly but to the same extent as the irradiated DNA mixtures (Figure S49).

DNA Transcription by RNA Polymerase in Vitro. The autoradiogram of the inhibition of RNA synthesis by T7 RNA polymerase on pSP73KB DNA containing adducts of the Ru^{II} arene complexes or cisplatin is shown in Figure 7 (top). The bands corresponding to the transcription of DNA modified by the nonirradiated forms of complexes **1**, **4**, and **10** are rather faint in intensity, except for complex $[(\eta^6\text{-}p\text{-cym})\text{Ru}(\text{bpm})(4,4'\text{-bpy})][\text{PF}_6]_2$ (**4**), which was found to bind to DNA without irradiation (ca. 20%). The preirradiated and irradiated forms of **1**, **4**, and **10** yielded fragments of newly synthesized RNA of defined sizes. The major stop sites produced occurred at similar positions in the gel and were exclusively at guanine residues (Figure 7, bottom) and are identical for the three Ru^{II} arene complexes. The total intensity of the bands on the autoradiogram corresponding to transcripts of single-ruthenated DNA fragments (modified to the same level, same r_b value) differed. The intensities of those corresponding to the transcription of DNA modified by the preirradiated forms of complexes **1**, **4** and **10** are slightly stronger than those corresponding to the irradiated forms.

Unwinding of Supercoiled pUC19 Plasmid DNA. The native agarose gels resulting from DNA modified by the Ru^{II} arene complexes **1**, **4**, and **10** in their preirradiated and the corresponding irradiated forms are shown in Figure 8 (top and bottom, respectively). The DNA unwinding angles produced by the adducts formed by preirradiated and irradiated forms of the Ru^{II} arene complexes **1** and **4**, and **10** was determined to be 6.6 ± 1.7 , 5.2 ± 2.2 , and $6.1 \pm 2.2^\circ$, respectively. The comigration point of the modified supercoiled and nicked DNA ($r_b(c)$ value) was reached at $r_b = 0.16$, 0.19 , and 0.17 for complexes **1**, **4**, and **10**, respectively (Table S44). From the autoradiogram it

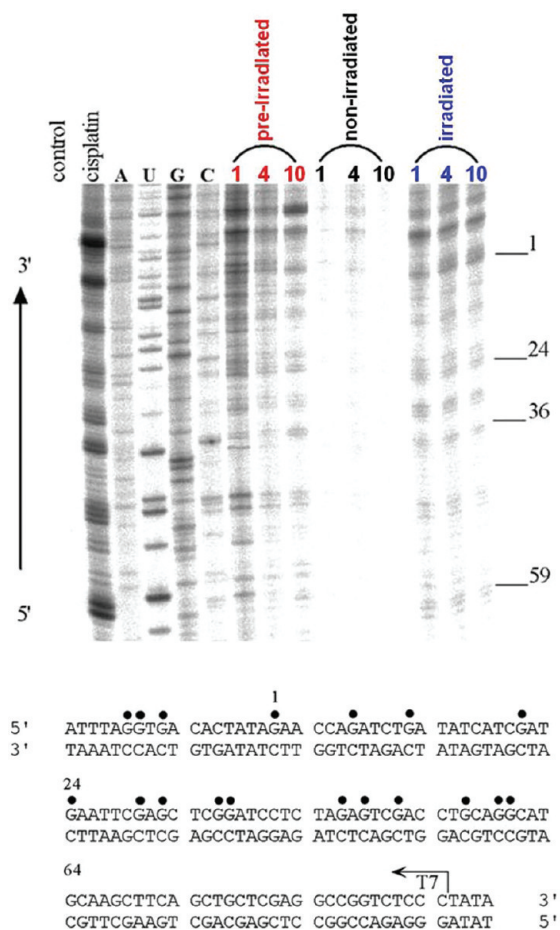


Figure 7. (top) Autoradiogram of 6% polyacrylamide/8 M urea sequencing gel showing inhibition of RNA synthesis by T7 RNA polymerase on pSP73KB DNA containing adducts of Ru^{II} arene complexes or cisplatin. Lanes: chain terminated marker RNAs, cisplatin, at $r_b = 0.02$; A, U, G and C, the template modified by Ru^{II} arene compounds. (bottom) Schematic diagram showing the portion of the sequence used to monitor inhibition of RNA synthesis by Ru^{II} arene complexes. The arrows indicate the start of the T7 RNA polymerase, which used as template the upper strand of pSP73KB DNA, respectively. The numbers correspond to the nucleotide numbering in the sequence map of pSP73KB plasmid. ● indicates major stop sites for DNA modified by ruthenation.

can also be noticed that an increasing amount of nicked (OC) form occurred during photoirradiation of the Ru^{II} arene complexes in the presence of DNA (irradiated form); $r_b(c)$ for **1** and **10** is not changed, whereas DNA is significantly more nicked with increasing ruthenation in the case of **4**.

DNA Melting Temperature. The observed trend for the three complexes **1**, **4**, and **10** is a constant oscillation of the t_m values (Table S45). The t_m changes are relatively small, and a slight stabilization effect is observed at low ionic strengths. At the highest ionic strength, a tendency for slight destabilization was observed.

Circular Dichroism (CD). CD spectra of DNA modified by complexes **1**, **4**, and **10** (at 298 K in 10 mM NaClO_4) were also recorded at r_b values in the range 0.010–0.125. As can be seen from Figure 9, the conservative CD spectrum transforms at wavelengths below 300 nm upon interaction of the three complexes with CT-DNA. There is an increase for complexes **1** and **4** and a decrease for complex **10** in the intensity of the positive band around 280 nm. The signature of complex **4**

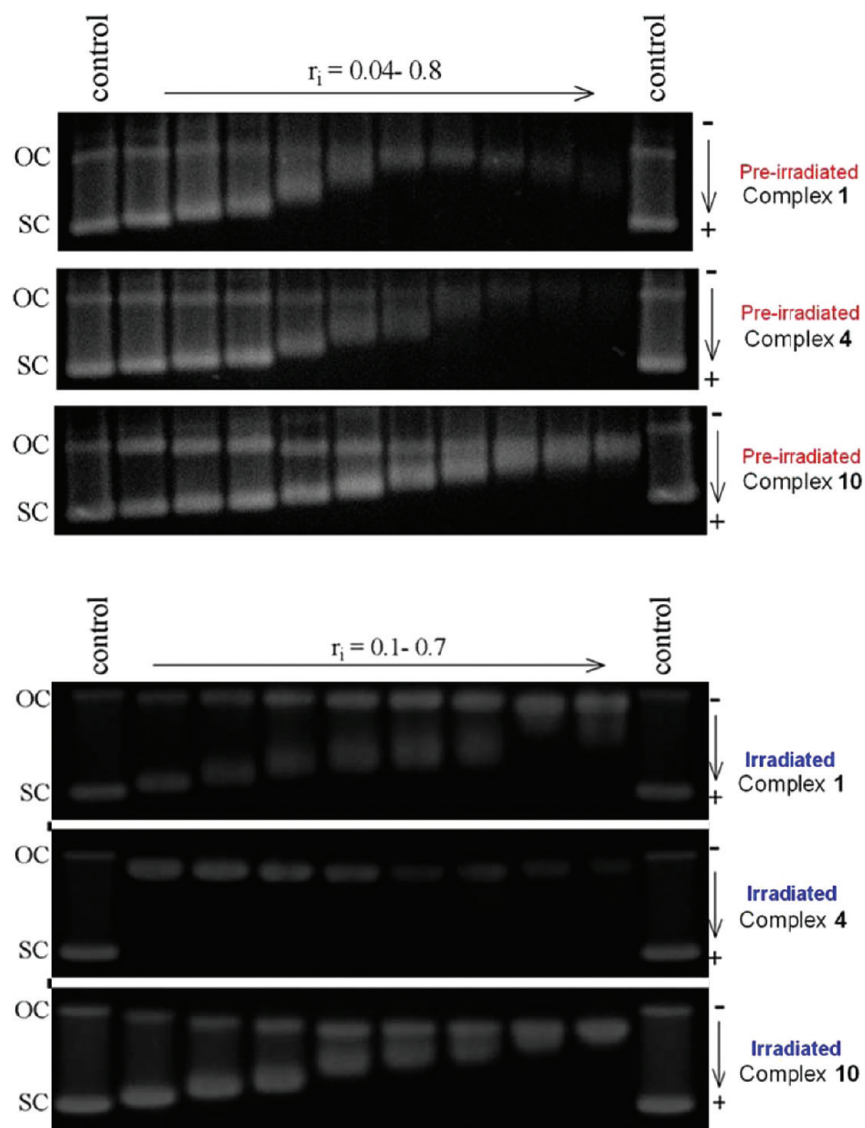


Figure 8. Unwinding of supercoiled pUC19 plasmid DNA (1.0×10^{-4} M, $0.5 \mu\text{g}/15 \mu\text{L}$) by complexes **1**, **4**, and **10** in their *preirradiated* forms (top) or by complexes **1**, **4**, and **11** in their *irradiated* forms (bottom). The left and right lanes are controls (unmodified DNA); r_i values increase on going from left to right lanes; top bands correspond to the form of nicked plasmid (OC) and the bottom bands to the closed, negatively supercoiled plasmid (SC).

coordinated to CT-DNA is a positive ICD centered at around 400 nm. The signature of complexes **1** and **10** bound to CT-DNA includes no such ICD. The changes in CD spectra of CT-DNA modified by Ru^{II} arene complexes **1** and **10** (at different r_b values) were monitored at 246 and 278 nm; the changes exerted by complex **4** were also monitored at 400 nm (Figure S50).

Flow Linear Dichroism (LD). Binding of all three Ru^{II} arene complexes to CT-DNA was also monitored by linear dichroism spectroscopy (Figure 10). The magnitudes of the LD signals at 258 nm decrease as a function of r_b for the irradiated forms of Ru^{II} arene complexes **1**, **4**, and **10**. The changes in the LD spectrum of CT-DNA modified by complexes **1**, **4**, and **10** (at different r_b values) were monitored at 258.5 nm (Figure S51). The largest changes are induced by complex **4**. Complexes **1** and **10** behave similarly within the same range.

Ethidium Bromide (EtBr) Fluorescence. The ability of complexes to displace the DNA intercalator EtBr from CT-DNA was probed by monitoring the relative fluorescence of the

EtBr–DNA adduct after treating the DNA with varying concentrations of the Ru^{II} arene complexes **1**, **4**, and **10** in their irradiated forms. Figure 11 shows a plot of relative fluorescence versus r_b for the three Ru^{II} arene complexes along with cisplatin (cisPt), transplatin (transPt), and monofunctional chlorodiethylenetriamineplatinum(II) chloride (dienPt). All three adducts of the Ru^{II} arene complexes decreased the EtBr fluorescence.

Cancer Cell Growth Inhibition (IC_{50} Values). The IC_{50} values with no irradiation provided for the Ru^{II} arene complexes (**1–6** and **8–16**) against the A2780 human ovarian cancer cell line are given in Table 2. In general, the complexes were moderately active and their potencies vary in several orders of magnitude. The most potent complex, $[(\eta^6\text{-}p\text{-cym})\text{Ru}(\text{bathophen})(\text{Py})][\text{PF}_6]_2$ (**12**), had an IC_{50} value of $7.4 \mu\text{M}$, comparable to that of cisplatin ($2.2 \mu\text{M}$) under the same conditions. As a general trend, the most active complexes contain *p*-cym as the arene and bpm as the N,N' chelating ligand. A change in the arene and chelating ligand to ind or

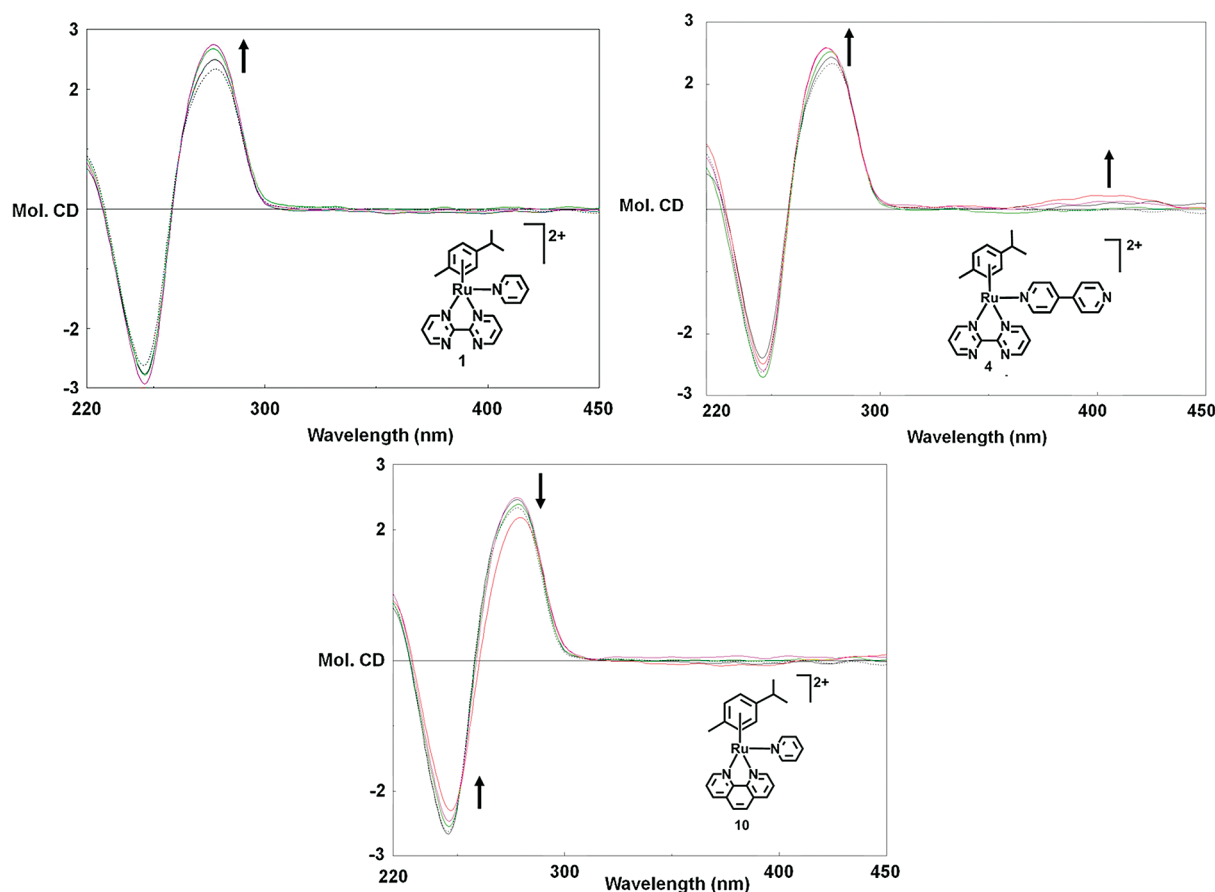


Figure 9. Circular dichroism (CD) spectra of CT-DNA (1×10^{-4} M) modified by Ru^{II} arene complexes **1**, **4**, and **10** in their irradiated forms; the medium was 10 mM NaClO_4 , pH 6.

hmb and phen in complexes **8–10**, respectively, was found to decrease the activity. Within the cytotoxic series of compounds, complexes that displayed activity have either Py or 3-substituted Py as the L group, the Py-bearing complexes being the most active.

DISCUSSION

X-ray Crystal Structures. The X-ray crystal structures of **2**, **6**, **7**, **10**, and **13** are the first reported examples of half-sandwich complexes of the type $[(\eta^6\text{-arene})\text{Ru}(\text{N},\text{N}')(\text{L})]^{2+}$, where L is 4-MePy (**2**), 4-BzPy (**6**), trz (**7**), or Py (**10**, **13**). The overall structures of the complexes do not differ greatly from each other. The corresponding bond lengths and angles are comparable to those of analogous Ru^{II} arene complexes containing N,N' chelated ligands.³⁵ Neither the nature of the corresponding N,N' chelating ligand nor that of the N σ -donor has an influence on the corresponding Ru–arene(centroid) distances (~ 1.70 Å). Interestingly, for all the complexes, one of the Ru–N,N' bonds is always longer than the other. A close inspection of the Ru–N(L) bond lengths for complexes **2** and **6** reveals no significant difference between them. A greater distortion from planarity on the bpm ligand is found for **2** compared to **6** (7.09 and 6.80° , respectively). The nature of the arene does not influence significantly the Ru–N,N'(bpm) bond lengths.

Photochemistry. The photochemistry in aqueous solution at 310 K of the Ru^{II} arene complexes **1–6**, **8–10**, and **12–16** was investigated under white light (λ_{irr} 400–660 nm) or UVA (λ_{irr} 320–400 nm) irradiation using both experimental (UV–

vis and ^1H NMR spectroscopy) as well as theoretical methods (DFT and TD-DFT calculations). The experimental results showed that this family of Ru^{II} arene complexes can selectively and exclusively dissociate the monodentate ligand (L) when excited with white light or UVA irradiation, while the corresponding bound arenes and chelating ligands remain intact. It was observed that, with the use of UVA irradiation, the formation of the corresponding aqua adduct can be achieved in a shorter period of time and the process is much more efficient than when white light is employed. This evidence is in good agreement with the more intense absorption bands in the UV region of the absorption spectrum displayed by all the Ru^{II} arene complexes studied. The presence of isosbestic points in their UV–vis absorption spectra and resonances corresponding to the Ru–OH₂ adduct and free L in the ^1H NMR spectra are consistent with the formation of a single photoproduct in all cases. It is clear that since the Ru–OH₂ species does not form in the dark, the photoactivation of the complexes allows strict control over the Ru–N(L) bond hydrolysis reaction. Their remarkable behavior is in contrast to that observed for the complexes of the form $[(\eta^6\text{-arene})\text{Ru}(\text{L})_3]^{2+}$, where arene = benzene, toluene, isopropyltoluene and L = NH_3 , H_2O , for which white light irradiation in solution leads in each case to substitution of the arene as the only observable photo-reaction.³⁶

As shown by the TD-DFT calculations, the selective photochemical dissociation of the L ligand is consistent with the presence of σ^* -antibonding orbitals (typically the LUMO +3), which participate in several singlet and triplet transitions.

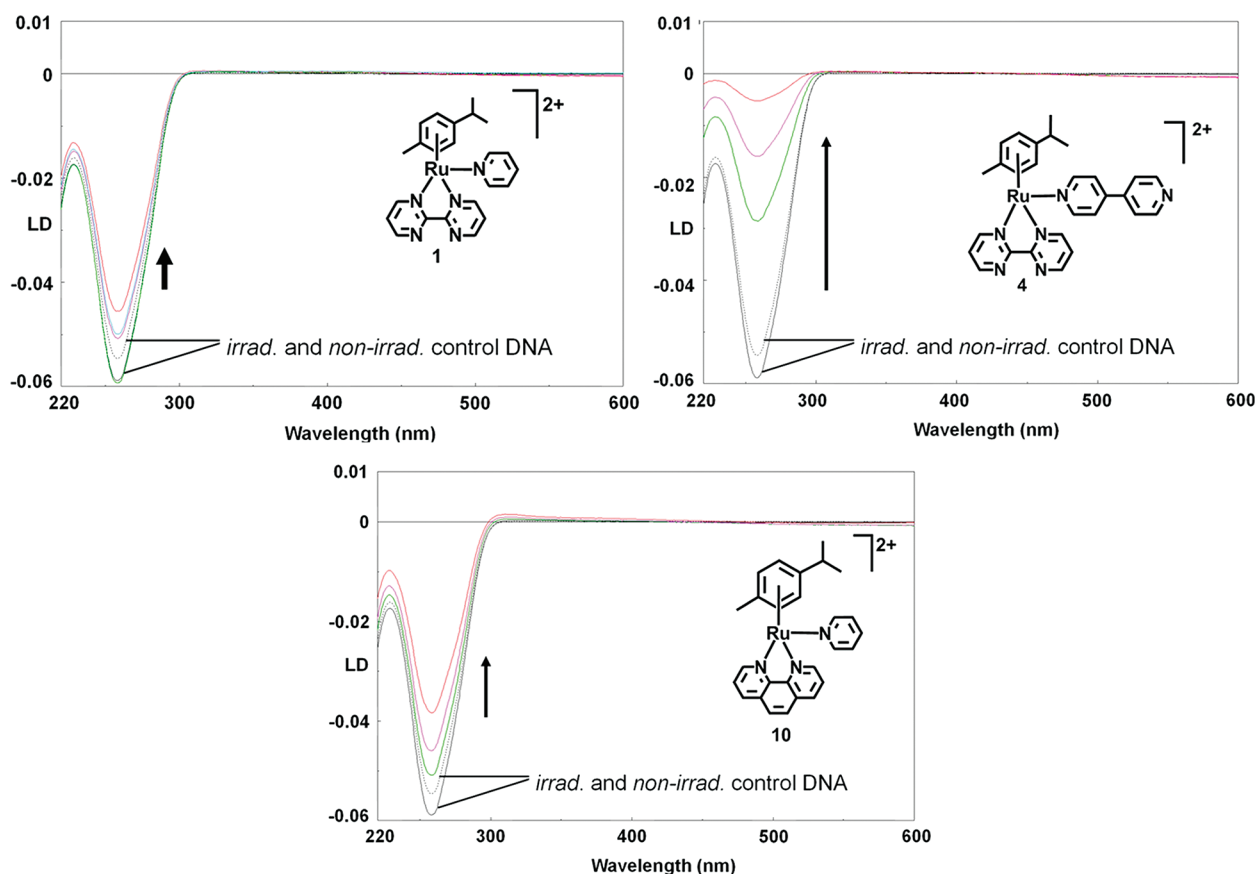


Figure 10. Linear dichroism spectra of CT-DNA modified by Ru^{II} arene complexes **1**, **4**, and **10**. LD spectra were recorded for DNA in 10 mM NaClO₄. The concentration of DNA was 2.3×10^{-4} M.

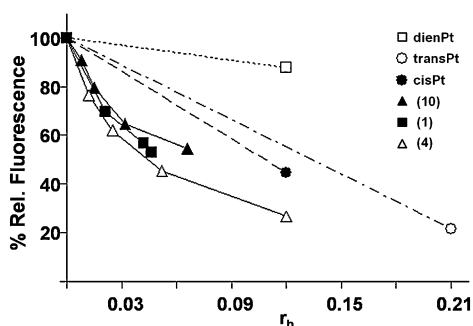


Figure 11. EtBr fluorescence versus r_b for DNA modified by cisplatin (●), dienPt (□), transPt (○), and Ru^{II} arene complexes **1** (■), **4** (Δ), and **10** (▲) in their irradiated forms in 10 mM NaClO₄ at 310 K (24 h photoirradiation followed by 24 h incubation).

On the basis of the DFT results, as well as photochemistry rates, triplet states are believed to play a key role in the ligand photodissociation mechanism of these Ru^{II} arene complexes. In fact, despite the presence of some dissociative singlet excited states, the slow formation of the Ru–OH₂ species (more than 10 h of photoirradiation with white light in some cases) confirms this hypothesis. As in the case of other Ru^{II} (poly)pyridyl complexes, a distorted lowest-lying triplet geometry^{37,38} and accessible dissociative triplet excited states yield free ligand molecules and a Ru^{II} (poly)pyridyl residue, generally an aqua or solvento complex.

From the computational point of view, it is believed that all the Ru^{II} pyridine complexes studied in this work follow a

Table 2. IC₅₀ Values for Ru^{II} Arene Complexes against the A2780 Human Ovarian Cancer Cell Line under Ambient Light Conditions

compd	IC ₅₀ , μ M
$[(\eta^6\text{-}p\text{-cym})\text{Ru}(\text{bpm})(\text{Py})][\text{PF}_6]_2$ (1)	9.0
$[(\eta^6\text{-}p\text{-cym})\text{Ru}(\text{bpm})(4\text{-MeOPy})][\text{PF}_6]_2$ (3)	70.0
$[(\eta^6\text{-}p\text{-cym})\text{Ru}(\text{bpm})(4,4'\text{-bpy})][\text{PF}_6]_2$ (4)	61.1
$[(\eta^6\text{-hmb})\text{Ru}(\text{bpm})(\text{Py})][\text{PF}_6]_2$ (8)	23.2
$[(\eta^6\text{-ind})\text{Ru}(\text{bpm})(\text{Py})][\text{PF}_6]_2$ (9)	92.0
$[(\eta^6\text{-}p\text{-cym})\text{Ru}(\text{phen})(\text{Py})][\text{PF}_6]_2$ (10)	25.9
$[(\eta^6\text{-}p\text{-cym})\text{Ru}(\text{bathophen})(\text{Py})][\text{PF}_6]_2$ (12)	7.4
$[(\eta^6\text{-}p\text{-cym})\text{Ru}(\text{bpm})(\text{NA})][\text{PF}_6]_2$ (15)	19.0
$[(\eta^6\text{-}p\text{-cym})\text{Ru}(\text{bpm})(\text{MN})][\text{PF}_6]_2$ (16)	9.2
cisplatin	1.5

^aComplexes **2**, **5**, **6**, **13**, and **14** had IC₅₀ values larger than 100 μ M against the cell line tested (vide supra).

relatively similar photoinduced ligand dissociation mechanism. It is likely that this dissociation occurs from a series of ³MC triplet states with dissociative character and higher energy than the lowest-lying triplet excited state (which conversely does not have a dissociative nature). The nature of these low-lying triplet states is also consistent with the absence of fluorescence of the complexes in solution. There is evidence that competitive radiationless decay processes are much faster than these potential photochemical processes for some d⁶ metal complexes.³⁹ After intersystem crossing promoted by the strong spin–orbital coupling, both ³MC nondissociative and dissociative triplet states can be populated. The nondissociative

³MC states are responsible for the return of the excited molecules to the ground state, while the dissociative ³MC states cause the selective dissociation of the L ligand.

An attempt to understand the relationship between the photoactivity and structure of the Ru^{II} arene pyridine and pyridine-derivative complexes was also made on the basis of the experimental data. The experimental observations can be summarized as follows.

- (a) Change of the Py ring for a 4-substituted Py ring. More electron-donating substituents on the Py ring in the 4-position moderately increase the extent of the photo-induced hydrolysis, whereas no effect on the rate is observed.
- (b) Change of the Py ring for a 3-substituted Py ring. Both the extent and the rate of photoinduced hydrolysis decrease on changing the 3-substituent on the Py ring, following the order ketone > amide ≈ ester.
- (c) Change of the arene. More electron-donating substituents on the arene ring increase both the extent and the rate of photoinduced hydrolysis.
- (d) Change of the N,N'-chelating ligand. The more aromatic character, the lesser the extent of photoinduced hydrolysis. However, no effect on the rate is observed.

This might be an indication that the corresponding rates and extents of the photolysis reactions could also be related to the formation of the more thermodynamically favored aqua adducts. Such a hypothesis is further supported by the experimental observations showing that the photoactivatable Ru^{II} arene complexes **8** and **9** displayed the highest rates and extent of the photoinduced hydrolysis (i.e., they generate ~100% of their corresponding aqua adduct in the shortest time of photoirradiation, with either white light or UVA irradiation). Also the chlorido derivatives of complexes **8** and **9** hydrolyze faster and to a larger extent when dissolved in aqueous media in comparison to other arene-bearing complexes.⁴⁰

Photocontrolled DNA Interactions in Cell-Free Media.

Three complexes were selected for further studies with CT-DNA in cell-free media: **1**, **4**, and **10** (Figure 1). As shown in the Results (vide supra), upon photoactivation the three complexes undergo a clean and selective photorelease of the pyridine (**1**, **10**) or the pyridine-derivative ligand 4,4'-bpy (**4**) to form the monofunctional reactive aqua species $[(\eta^6\text{-p-cym})\text{Ru}(\text{N},\text{N}')(\text{OH}_2)]^{2+}$. Although the mechanisms of photoactivation of these three Ru–L complexes are very similar, their effects on DNA differ from each other (both with and without photoirradiation), particularly in the case of complex **4**, suggesting that the nature of the pyridine-derivative ligand (both when bound and when photoreleased from the metal center) and the N,N' chelating ligand play a key role in the mode of interaction of these complexes. Incorporating an extended pyridine such as 4,4'-bpy (as in complex **4**) provides a low percentage, ca. 20% of interaction of Ru^{II} compound with DNA after 48 h in the dark (nonirradiated form), presumably of intercalative nature (see EtBr fluorescence). In comparison, less than 5% of interaction with DNA was determined for **1** and **10** after 48 h in the nonirradiated forms. Upon photoirradiation, all the aqua adducts were found to bind to DNA at varying rates. The preirradiated forms of these Ru^{II} complexes bind more quickly but to the same extent as the irradiated forms. The relatively long photoirradiation times needed to start generating the corresponding aqua adducts limits the initial binding of the Ru^{II} complexes to DNA, and in the cases

of complexes **1** and **4**, as soon as the full photoconversion is achieved, the overall extent does not vary significantly. The rate of binding to DNA, however, is slower than that determined for the anticancer drug cisplatin ($t_{1/2}$ ca. 2 h under similar conditions),⁴¹ for which DNA binding is thought to be responsible for its cytotoxic properties. In contrast, another Ru^{II} analogue $[(\eta^6\text{-bip})\text{Ru}(\text{en})\text{Cl}]^+$, which has also been shown to be cytotoxic to cancer cells,⁹ reacts much more rapidly with DNA under similar conditions ($t_{1/2}$ ca. 10 min). The relatively small extent of binding of the nonirradiated forms of the Ru complexes along with the slower kinetics of binding to DNA upon photoirradiation is an advantageous characteristic that may allow more drug to reach its target in vivo without being deactivated by reacting with other biological molecules.

The results of the transcription mapping experiments suggest that complexes **1**, **4**, and **10** bind to DNA upon photoirradiation, thus inhibiting RNA synthesis. For the preirradiated and irradiated forms of complexes **1**, **4**, and **10** the stop sites were only guanine residues. This phenomenon occurs in a similar fashion and with stop sites similar to those of cisplatin and to those of the Ru^{II} complex $[(\eta^6\text{-bip})\text{Ru}(\text{en})\text{Cl}]^+$, highlighting its good agreement with the photocontrolled nucleobase binding studies which show that these complexes bind significantly to 9-EtG but do not bind to 9-EtA. DNA binding upon irradiation of Ru^{II} complexes **1**, **4**, and **10** results in a low degree of unwinding (6–7°) which is very similar for the three complexes but smaller than that observed for the Ru^{II} complexes $[(\eta^6\text{-arene})\text{Ru}(\text{en})\text{Cl}]^+$ (in the range 7–14°).³⁰ The unwinding angles produced by the adducts of Ru^{II} arene compounds **1**, **4**, and **10** resemble more those produced by monofunctional cisplatin adducts (6 and 13° for mono- or bifunctional adducts, respectively).⁴² The binding of the Ru^{II} arene compounds **1**, **4**, and **10** to DNA upon photoirradiation affects to some extent its melting behavior. It is likely that some conformational distortions due to the formation of mono-adducts will destabilize the helix, as has been consistently observed in earlier studies with various other Ru^{II} and platinum compounds. The t_m changes induced by the Ru^{II} arene compounds **1**, **4**, and **10** in the irradiated forms are, however, small. It is possible that the fluctuations in the t_m values are a consequence of the DNA adducts being unstable at higher ionic strengths and temperatures, which in turn could be associated with a stabilizing effect arising from noncovalent interactions of the aromatic ligands with the duplex (arene or N,N' chelating). This hypothesis could be further supported by both the exhibited DNA unwinding angles (7° is a typical unwinding angle for monofunctional binders), the quenching of EtBr fluorescence, and the overall positive charge on these Ru^{II} arene compounds. The magnitudes of the LD signals at 258 nm decrease as a function of r_b for all Ru^{II} arene complexes in the irradiated forms. These results suggest that the formation of DNA adducts might be accompanied by the appearance of conformational changes at the site of the lesion. CD spectra showed that the binding of complexes **1** and **4** to DNA (together with the concomitant release of pyridine or 4,4'-bpy upon photoirradiation) results in conformational alterations in double-helical DNA of a nondenaturational character, similar to those induced in DNA by the antitumor drug cisplatin. In contrast, upon photoirradiation, the binding of **10** to DNA (accompanied by the photorelease of Py) results in conformational alterations in DNA of a denaturational character, similar to those induced in DNA by clinically ineffective transplatin. The signature of complex **4** coordinated to CT-DNA is a

positive ICD centered at around 400 nm. This could imply that the molecules become oriented as a consequence of their noncovalent interactions with DNA favored most probably with the phen ligand over bpm.

Cancer Cell Growth Inhibition (IC_{50} Values). Complexes **2**, **5**, **6**, **13**, and **14** (Figure 1) were noncytotoxic toward the A2780 human ovarian cancer cell line under ambient light conditions up to the maximum concentration tested (100 μ M). A loss of cytotoxicity toward cancer cells has been previously observed under ambient light conditions for complexes of the type $[(\eta^6\text{-hmb})\text{Ru}(\text{en})(\text{X})]^+$ when X is replaced by Py.¹¹ The loss of activity in this complex is assumed to arise from its negligible aquation, believed to be the first step toward anticancer activity. The discovery of complexes that do not hydrolyze over a large period of time but retain significant cytotoxicity implies a different mechanism of action for complexes **1**, **3**, **4**, **8–10**, **12**, **15**, and **16**. The cytotoxicity of several isomers of $[\text{Ru}(\text{azpy})_2(\text{bipy})]^{2+}$ which are incapable of hydrolysis has been reported,⁴³ as has significant anticancer activity for the complex $[(\eta^6\text{-hmb})\text{Ru}(\text{en})(\text{SPh})]^{2+}$, which does not undergo hydrolysis.¹¹

CONCLUSIONS

This work provides the first example of a family of piano-stool Ru^{II} arene complexes of the type $[(\eta^6\text{-arene})\text{Ru}(\text{N},\text{N}')(\text{L})]^{2+}$ (where N,N' is a chelating ligand and L is a pyridine or a pyridine derivative) that can selectively photodissociate the monodentate ligand (L) when excited with UVA or white light. Such a unique feature allows control of the hydrolysis reaction of the complexes and, therefore, the formation of a reactive aqua species that otherwise would not form in the dark. Insights into the photophysical and photochemical behavior of this series of compounds were obtained by combining experimental and theoretical techniques. The process proved to be much more efficient when UVA-range irradiation was used, and an initial structure–photoactivity relationship was established. The presence of a stronger electron-donating arene (such as hmb in **8** or ind in **9**) can promote formation of the aqua adduct. As demonstrated from the experiments of interactions with 9-EtG and 9-EtA, light activation can be used to phototrigger binding of these potential anticancer agents with discriminating preference toward 9-EtG. In order to investigate also the possibility of phototriggering the binding to DNA of the Ru^{II} arene pyridine or pyridine-derivative complexes, studies on CT-DNA interactions in cell-free media were carried out. The CT-DNA binding studies show that complexes **1**, **4**, and **10** (Figure 1) in the preirradiated forms bind more quickly but to the same extent as the irradiated forms. The nonirradiated forms, as expected, bind negligibly. Further results on DNA interactions in cell-free media strengthen the case for combined monofunctional coordination and intercalation binding modes of complexes **1**, **4**, and **10** upon photoirradiation. Under the premise that hydrolysis is known to be one mechanism which provides a pathway for cytotoxicity, we were not able to establish an obvious mechanism of action which would account for the cytotoxicity of these Ru^{II} arene pyridine or pyridine-derivative complexes in the absence of photoirradiation. Therefore, there is the possibility that the intact cations might exert a cytotoxic effect by other mechanisms, which are currently being investigated. These encouraging results indicate that the photochemistry of these Ru^{II} arene complexes can be exploited to integrate them with the promising biological

properties inherent in half-sandwich Ru^{II} complexes, thus increasing their potential as anticancer agents.

ASSOCIATED CONTENT

Supporting Information

Text giving details of the preparation of complexes, crystallographic data (Table S1), selected calculated bond distances in the ground state (S0) and lowest-lying triplet state (T0) (Tables S2 and S3), wavelength of absorption maxima (λ , nm) and extinction coefficients (ϵ , $\text{M}^{-1} \text{cm}^{-1}$) (Table S4), selected TDDFT singlet transitions for the Ru^{II} complexes (Tables S5–S19), mass-to-charge ratios obtained from HR-MS spectra for the photolysis products of Ru^{II} arene complexes (Table S20), percentage of species present after selected times of photoirradiation (Tables S21–S26), selected TDDFT triplet transitions for Ru^{II} complexes in the lowest-lying triplet-state optimized geometry (Tables S27–S41), mass-to-charge ratios obtained from HR-MS spectra for the photolysis products of Ru^{II} arene complexes in the presence of 9-EtG (Table S42), details of the cell-free media DNA interactions (Tables S43–S45), selected views of the X-ray crystal structures of Ru^{II} arene complexes (Figures S1–S6), calculated lowest and highest singly occupied molecular orbitals (Figures S7 and S8), experimental UV–vis spectrum of the Ru^{II} complexes (Figure S9), selected electron difference density maps (EDDMs) of singlet excited state transitions of Ru^{II} complexes (Figures S10–S24), UV–vis absorption spectra of the photolysis reaction of Ru^{II} arene complexes (Figures S25 and S26), a comparison chart showing the percentage of species formed after the photoirradiation of Ru^{II} arene complexes (Figures S27–S31), selected electron difference density maps (EDDMs) of triplet excited state transitions of Ru^{II} arene complexes (Figures S32–S47), ^1H – ^1H NOESY NMR spectrum of $[(\eta^6\text{-p-cym})\text{Ru}(\text{bpm})(9\text{-EtG-N7})]^{2+}$ (Figure S48), cell-free media DNA studies (Figures S49–S51), and CIF files giving crystallographic data. This material is available free of charge via the Internet at <http://pubs.acs.org>.

AUTHOR INFORMATION

Corresponding Author

*E-mail: P.J.Sadler@warwick.ac.uk.

Present Address

[§]Departamento de Química Inorgánica, Facultad de Química, Universidad Nacional Autónoma de México (UNAM), Ciudad Universitaria, Coyoacán, México, D.F. 04510 México.

Notes

The authors declare no competing financial interest.

ACKNOWLEDGMENTS

S.B.-L. thanks the WPRS/ORSAS (UK) and CONACyT (Mexico) for funding. L.S. was supported by the Marie Curie Intra European Fellowship 220281 PHOTORUACD within the 7th European Community Framework Programme and ERC BIOINCMED (Grant No. 247450 to P.J.S.). We also thank the ERDF and AWM for Science City funding and Dr. Ivan Prokes of the University of Warwick for his help with NMR as well as Dr. Lijiang Song and Mr. Philip Aston of the University of Warwick for their help with MS instruments. The research of B.L., O.N. and V.B. was supported by the Czech Science Foundation (Grant 301/09/H004) and the Academy of Sciences of the CR (Grant M200040901).

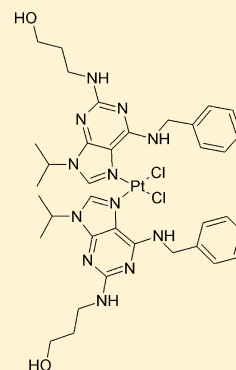
REFERENCES

- (1) Farrer, N. J.; Salassa, L.; Sadler, P. J. *Dalton Trans.* **2009**, 10690–10701.
- (2) (a) Sutin, N.; Creutz, C. *Pure Appl. Chem.* **1980**, *52*, 2717–2738. (b) Balzani, V.; Moggi, L.; Manfrin, M. F.; Bolletta, F.; Laurence, G. S. *Coord. Chem. Rev.* **1975**, *15*, 321–433. (c) Hager, G. D.; Crosby, G. A. *J. Am. Chem. Soc.* **1975**, *97*, 7031–7037.
- (3) (a) Fernández-Moreira, V.; Thorp-Greenwood, F.; Coogan, M. P. *Chem. Commun.* **2010**, 46, 186–202. (b) Puckett, C. A.; Barton, J. K. *Biochemistry* **2008**, *47*, 11711–11716. (c) Zhang, C. X.; Lippard, S. J. *Curr. Opin. Chem. Biol.* **2003**, *7*, 481–489.
- (4) Cosgrave, L.; Devocelle, M.; Forster, R. J.; Keyes, T. E. *Chem. Commun.* **2010**, 46, 103–105.
- (5) (a) Gill, T. P.; Mann, K. R. *Organometallics* **1982**, *1*, 485–488. (b) Schrenk, J. L.; Palazzotto, M. C.; Mann, K. R. *Inorg. Chem.* **1983**, *22*, 4047–4049. (c) McNair, A. M.; Schrenk, J. L.; Mann, K. R. *Inorg. Chem.* **1984**, *23*, 2633–2640.
- (6) Weber, W.; Ford, P. C. *Inorg. Chem.* **1986**, *25*, 1088–1092.
- (7) Bennett, M. A.; Smith, A. K. *J. Chem. Soc., Dalton Trans.* **1974**, 233–241.
- (8) Magennis, S. W.; Habtemariam, A.; Nováková, O.; Henry, J. B.; Meier, S.; Parsons, S.; Oswald, I. D. H.; Brabec, V.; Sadler, P. J. *Inorg. Chem.* **2007**, *46*, 5059–5068.
- (9) (a) Aird, R.; Cummings, J.; Ritchie, A.; Muir, M.; Morris, R.; Chen, H.; Sadler, P.; Jodrell, D. *Br. J. Cancer* **2002**, *86*, 1652–1657. (b) Morris, R. E.; Aird, R. E.; Murdoch, P. D.; Chen, H. M.; Cummings, J.; Hughes, N. D.; Parsons, S.; Parkin, A.; Boyd, G.; Jodrell, D. I.; Sadler, P. J. *J. Med. Chem.* **2001**, *44*, 3616–3621. (c) Nováková, O.; Kašpárková, J.; Bursova, V.; Hofr, C.; Vojtiskova, M.; Chen, H.; Sadler, P. J.; Brabec, V. *Chem. Biol.* **2005**, *12*, 121–129.
- (10) Pizarro, A. M.; Habtemariam, A.; Sadler, P. J. In *Topics in Organometallic Chemistry*; Jaouen, G., Metzler-Nolte, N., Eds.; Springer-Verlag: Berlin, 2010; Vol. 32, pp 21–56.
- (11) Wang, F.; Habtemariam, A.; van der Geer, E. P. L.; Fernández, R.; Melchart, M.; Deeth, R. J.; Aird, R.; Guichard, S.; Fabbiani, F. P. A.; Lozano-Casal, P.; Oswald, I. D. H.; Jodrell, D. I.; Parsons, S.; Sadler, P. J. *Proc. Natl. Acad. Sci. U.S.A.* **2005**, *102*, 18269–18274.
- (12) Peacock, A. F. A.; Habtemariam, A.; Moggach, S. A.; Prescimone, A.; Parsons, S.; Sadler, P. J. *Inorg. Chem.* **2007**, *46*, 4049–4059.
- (13) Betanzos-Lara, S.; Salassa, L.; Habtemariam, A.; Sadler, P. J. *Chem. Commun.* **2009**, 6622–6624.
- (14) (a) Salassa, L.; Phillips, H. I. A.; Sadler, P. J. *Phys. Chem. Chem. Phys.* **2009**, *11*, 10311–10316. (b) Salassa, L.; Garino, C.; Salassa, G.; Nervi, C.; Gobetto, R.; Lamberti, C.; Gianolio, D.; Bizzarri, R.; Sadler, P. J. *Inorg. Chem.* **2009**, *48*, 1469–1481. (c) Salassa, L.; Garino, C.; Salassa, G.; Gobetto, R.; Nervi, C. *J. Am. Chem. Soc.* **2008**, *130*, 9590–9597. (d) Cubo, L.; Pizarro, A. M.; Gómez Quiroga, A.; Salassa, L.; Navarro-Ranninger, C.; Sadler, P. J. *J. Inorg. Biochem.* **2010**, *104*, 909–918.
- (15) Govindaswamy, P.; Canivet, J.; Therrien, B.; Süß-Fink, G.; Štěpnička, P.; Ludvík, J. *J. Organomet. Chem.* **2007**, *692*, 3664–3675.
- (16) Sheldrick, G. M. *SHELXL97*; University of Göttingen, Göttingen, Germany, 1997.
- (17) (a) Sheldrick, G. M. *Acta Crystallogr.* **1990**, *A46*, 467–473. (b) Sheldrick, G. M. *Acta Crystallogr.* **2008**, *64*, 12–122.
- (18) Krezel, A.; Bal, W. *J. Inorg. Biochem.* **2004**, *98*, 161–166.
- (19) Frisch, M. J., et al. *Gaussian 03, revision D0.1*; Gaussian Inc., Wallingford, CT, 2004.
- (20) (a) Becke, A. D. *J. Chem. Phys.* **1993**, *98*, S648–S652. (b) Lee, C.; Yang, W.; Parr, R. G. *Phys. Rev. B* **1988**, *37*, 785–789.
- (21) Hay, P. J.; Wadt, W. R. *J. Chem. Phys.* **1985**, *82*, 270–283.
- (22) McLean, A. D.; Chandler, G. S. *J. Chem. Phys.* **1980**, *72*, S639–S648.
- (23) Cossi, M.; Rega, N.; Scalmani, G.; Barone, V. *J. Comput. Chem.* **2003**, *24*, 669–681.
- (24) (a) Casida, M. E.; Jamorski, C.; Casida, K. C.; Salahub, D. R. *J. Chem. Phys.* **1998**, *108*, 4439–4449. (b) Stratmann, R. E.; Scuseria, G. E.; Frisch, M. J. *J. Chem. Phys.* **1998**, *109*, 8218–8224.
- (25) Browne, W. R.; O’Boyle, N. M.; McGarvey, J. J.; Vos, J. G. *Chem. Soc. Rev.* **2005**, *34*, 641–663.
- (26) O’Boyle, N. M.; Vos, J. G., GaussSum; Dublin City University, available at <http://gausssum.sourceforge.net>, 2005.
- (27) (a) Brabec, V.; Palecek, E. *Biophysik* **1970**, *6*, 290–300. (b) Brabec, V.; Palecek, E. *Biophys. Chem.* **1976**, *4*, 79–92.
- (28) (a) Brabec, V.; Leng, M. *Proc. Natl. Acad. Sci. U.S.A.* **1993**, *90*, 5345–5349. (b) Lemaire, M. A.; Schwartz, A.; Rahmouni, A. R.; Leng, M. *Proc. Natl. Acad. Sci. U.S.A.* **1991**, *88*, 1982–1985.
- (29) Keck, M. V.; Lippard, S. J. *J. Am. Chem. Soc.* **1992**, *114*, 3386–3390.
- (30) Loskotova, H.; Brabec, V. *Eur. J. Biochem.* **1999**, *266*, 392–402.
- (31) (a) Butour, J. L.; Macquet, J. P. *Eur. J. Biochem.* **1977**, *78*, 455–463. (b) Butour, J. L.; Alvinerie, P.; Souchart, J. P.; Colson, P.; Houssier, C.; Johnson, N. P. *Eur. J. Biochem.* **1991**, *202*, 975–980.
- (32) Butour, J. L.; Macquet, J. P. *Eur. J. Biochem.* **1977**, *78*, 455–463.
- (33) Skehan, P.; Storeng, R.; Scudiero, D.; Monks, A.; McMahon, J.; Vistica, D.; Warren, J. T.; Bokesch, H.; Kenney, S.; Boyd, M. R. *J. Nat. Cancer Inst.* **1990**, *82*, 1107–1112.
- (34) (a) Mann, K. R.; Blough, A. M.; Schrenk, J. L.; Koefod, R. S.; Freedman, D. A.; Matachek, J. R. *Pure Appl. Chem.* **1995**, *67*, 95–101. (b) Wagenknecht, P. S.; Ford, P. C. *Coord. Chem. Rev.* **2011**, 591–616.
- (35) Yan, Y. K.; Melchart, M.; Habtemariam, A.; Sadler, P. J. *Chem. Commun.* **2005**, 4764–4776.
- (36) Laval, R. J.; Kutal, C. *J. Organomet. Chem.* **1998**, *562*, 97–104.
- (37) (a) Pinnick, D. V.; Durham, B. *Inorg. Chem.* **1984**, *23*, 1440–1445. (b) Durham, B.; Wilson, S. R.; Hodgson, D. J.; Meyer, T. J. *J. Am. Chem. Soc.* **1980**, *102*, 600–607. (c) Collin, J. P.; Jouvenot, D.; Koizumi, M.; Sauvage, J. P. *Inorg. Chem.* **2005**, *44*, 4693–4698.
- (38) Moucheron, C.; Kirsch-De Mesmaeker, A.; Kelly, J. M. *J. Photochem. Photobiol. B* **1997**, *40*, 91–106.
- (39) (a) Pinnick, D. V.; Durham, B. *Inorg. Chem.* **1984**, *23*, 1440–1445. (b) Durham, B.; Wilson, S. R.; Hodgson, D. J.; Meyer, T. J. *J. Am. Chem. Soc.* **1980**, *102*, 600–607. (c) Collin, J. P.; Jouvenot, D.; Koizumi, M.; Sauvage, J. P. *Inorg. Chem.* **2005**, *44*, 4693–4698. (d) Watts, R. J. *J. Chem. Educ.* **1983**, *60*, 834–842. (e) Baerends, E. J.; Rosa, A. *Coord. Chem. Rev.* **1998**, *177*, 97–125. (f) Vos, J. G.; Kelly, J. M. *Dalton Trans.* **2006**, 4869–4883.
- (40) Betanzos-Lara, S. Ph.D. Thesis, University of Warwick, Warwick, U.K., 2010.
- (41) Bancroft, D. P.; Lepre, C. A.; Lippard, S. J. *J. Am. Chem. Soc.* **1990**, *112*, 6860–6871.
- (42) Chen, H. M.; Parkinson, J. A.; Nováková, O.; Bella, J.; Wang, F. Y.; Dawson, A.; Gould, R.; Parsons, S.; Brabec, V.; Sadler, P. J. *Proc. Natl. Acad. Sci. U.S.A.* **2003**, *100*, 14623–14628.
- (43) Kemp, S.; Wheate, N. J.; Wang, S.; Collins, J. G.; Ralph, S. F.; Day, A. I.; Higgins, V. J.; Aldrich-Wright, J. R. *J. Biol. Inorg. Chem.* **2007**, *12*, 969–979.

4.

Cellular Response to Antitumor *cis*-Dichlorido Platinum(II) Complexes of CDK Inhibitor Bohemine and Its AnaloguesBarbora Liskova,^{†,‡} Lenka Zerzankova,^{†,‡} Olga Novakova,[†] Hana Kostrhunova,[†] Zdenek Travnicek,[‡] and Viktor Brabec^{*,†}[†]Institute of Biophysics, Academy of Sciences of the Czech Republic, v.v.i., Kralovopolska 135, CZ-61265 Brno, Czech Republic[‡]Regional Centre of Advanced Technologies and Materials, Department of Inorganic Chemistry, Faculty of Science, Palacky University, 17. listopadu 12, CZ-77146 Olomouc, Czech Republic

ABSTRACT: The cellular and molecular pharmacology of the new class of anticancer drugs, in which the CDK inhibitor bohemine and its analogues are coordinated to Pt(II) to form cisplatin derivatives, was investigated. The results revealed the unique anticancer profile of a cisplatin-derived platinum(II) dichlorido complex involving N(7)-coordinated bohemine (**C1**). Although the IC₅₀ values were ~6-fold higher for **C1** than for cisplatin in cisplatin-sensitive tumor cells, the tumor cells in which **C1** was also active are those which acquired resistance to cisplatin. In addition, among the novel conjugates of bohemine and its analogues with cisplatin, marked selectivity of **C1** for tumor cells relative to the nontumorigenic, normal cells was observed. However, coordination of bohemine to platinum in **C1** considerably reduced one of the dual functionalities anticipated to be effective after **C1** reaches the nucleus. Further studies performed in the cells with wt p53 status show differences between cisplatin and **C1** at the level of cell cycle regulation. Impedance-based real-time monitoring of the effects of **C1** and cisplatin on cell growth supported the thesis that critical differences exist in the rate and mechanisms of cell kill caused by the two agents and that **C1** was a more potent inducer of apoptosis and/or necrosis than cisplatin. The results also showed that the distinct differences in cell killing observed for **C1** and cisplatin might be associated with processes at the DNA level. The DNA binding experiments carried out in a cell-free medium demonstrated that modification reactions resulting in the irreversible coordination of **C1** to DNA were slower than that of cisplatin. Transcription mapping experiments and determination of interstrand cross-linking efficiency of **C1** suggested that several aspects of DNA binding mode of **C1** and cisplatin were similar. It was concluded that **C1** remains a promising prototype of compounds for the generation of novel drug candidates with cytotoxicity profiles different from those of the platinum drugs currently in use.



■ INTRODUCTION

Cytokinines (CK), such as 6-benzylaminopurine (BAP) and its benzyl-substituted derivatives, are a class of plant growth substances (phytohormones) that promote cell division in plant roots and shoots. Some artificial BAP derivatives (for instance, roscovitine, 2-(*R*)-(1-ethyl-2-hydroxyethylamino)-6-benzylamino-9-isopropylpurine) besides their potency to inhibit cyclin-dependent kinases (CDKs) also exhibit toxicity in several human cancer cell lines and have entered clinical trials alone or in combination therapy as candidates of anticancer drugs.^{1–4} Another artificial BAP derivative of this class of inhibitors of CDKs is 2-(3-hydroxypropylamino)-6-benzylamino-9-isopropylpurine (bohemine, **L1**, Figure 1), which is cytotoxic in several human cancer cell lines as well.^{5,6}

One of the strategies used to improve the chemotherapy of existing drugs is to synthesize novel drugs with improved therapeutic effect derived from their ability to target, aside from the original target, another molecular target. Such therapy has the potential to increase the total cytotoxicity due to the additive or synergetic effects, thereby decreasing the amount of original (existing) drug required and consequently reducing side effects on healthy, noncancerous tissues to broaden the spectrum of sensitive human tumors and/or to overcome

resistance to existing drugs. Hence, an interesting finding was that the coordination of bohemine to the Pt^{II} atom within the structure of the platinum(II) dichlorido complex considerably enhanced the toxicity of this CDK inhibitor in several human tumor cell lines.⁵

Here, we have studied a new class of anticancer drugs, in which the CDK inhibitor bohemine and its two analogues 2-chloro-6-(benzylamino)-9-isopropylpurine (**L2**) and 2-chloro-6-[(4-methoxybenzyl)amino]-9-isopropylpurine (**L3**) represent N-donor carrier ligands of the platinum(II) complexes derived from an anticancer compound, conventional cisplatin (*cis*-diamminedichloridoplatinum(II)) (Figure 1). Anticancer platinum agents, such as cisplatin and its analogues used in the clinic exert their therapeutic effect by their interaction with nuclear DNA.⁷ Hence, it could be anticipated that the novel conjugates of bohemine and its analogues with cisplatin with dual CDK inhibitory and DNA binding activity could bind DNA in much the same way as conventional cisplatin or its analogues used in the clinic, and because of its additional CDK inhibitory functionality, it might be active (i) at markedly lower

Received: December 3, 2011

Published: January 17, 2012



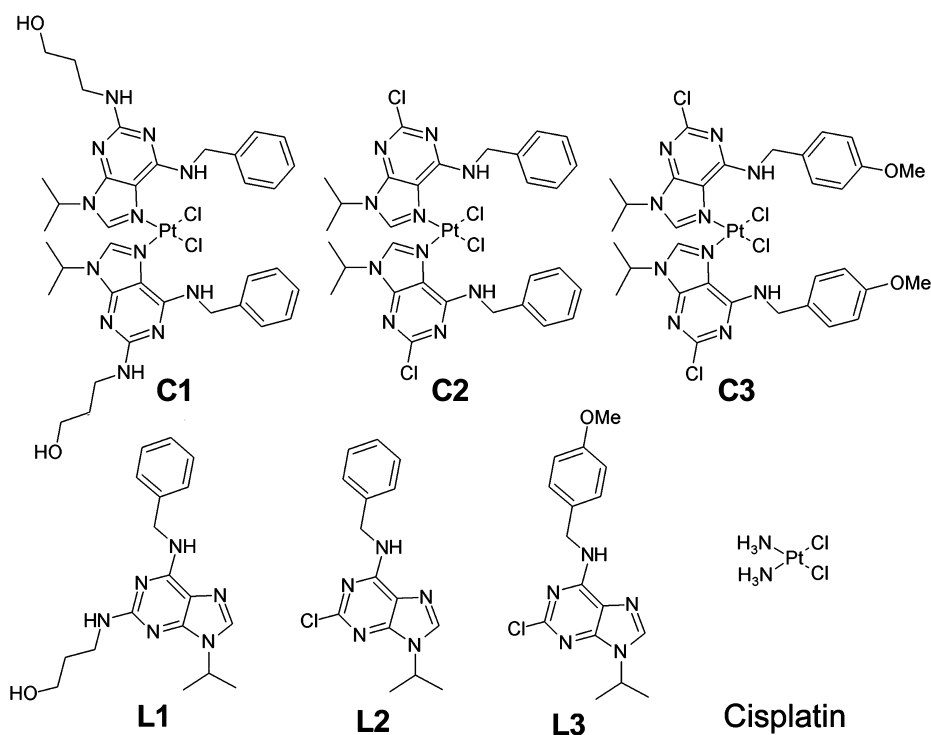


Figure 1. Schematic representations of the compounds tested in the present work.

doses than parental drugs, thereby reducing undesired side effects; and (ii) against a broader spectrum of human cancer cells. Thus, in our quest to understand more deeply the effects that may play an important role in the biological (pharmacological) properties of the cisplatin derivatives with boheminine (and its analogues), namely, *cis*-[Pt(2-(3-hydroxypropylamino)-6-benzylamino-9-isopropylpurine)₂Cl₂], *cis*-[Pt(L1)₂Cl₂] (C1), *cis*-[Pt(2-chloro-6-benzylamino-9-isopropylpurine)₂Cl₂], *cis*-[Pt(L2)₂Cl₂] (C2), and *cis*-[Pt(2-chloro-6-[(4-methoxybenzyl)amino]-9-isopropylpurine)₂Cl₂], *cis*-[Pt(L3)₂Cl₂] (C3) (Figure 1), the experiments described in the present study were carried out.

EXPERIMENTAL PROCEDURES

Material and Reagents. Cisplatin, *N,N'*-dimethylformamide (DMF), dimethylsulfoxide (DMSO), and propidium iodide were obtained from Sigma-Aldrich sro (Prague, Czech Republic). Compounds L1, L2, L3, C1, C2, and C3 were synthesized and characterized as described previously.^{5,8,9} Stock solutions of cisplatin for the biophysical and biochemical studies were prepared at a concentration of 5×10^{-4} M in water, filtered, and stored at room temperature in the dark. Stock solutions of boheminine, its analogues, cisplatin derivatives with boheminine, and its analogues for the biophysical and biochemical studies were prepared at a concentration of 5×10^{-2} M in DMF, stored at 4 °C in the dark, and diluted by water to the appropriate concentration just before use. The final concentration of DMF was less than 0.5%. Stock solutions of platinum complexes, boheminine, and its analogues for the cytotoxicity and cellular uptake studies were also prepared in DMF and used immediately after dissolution. The concentrations of platinum in the stock solutions and after dilution by water were determined by flameless atomic absorption spectrometry (FAAS). Calf thymus (CT) DNA (42% G + C, mean molecular mass ca. 2×10^7) was also prepared and characterized as described previously.^{10,11} Plasmids pSP73 [2464 base pairs (bp)] and pSP73KB (2455 bp) were isolated according to standard procedures. Restriction endonucleases were purchased from New England Biolabs. Acrylamide and bis(acrylamide) were obtained from Merck KgaA (Darmstadt, Germany). Proteinase K

and ATP were from Boehringer (Mannheim, Germany). MTT [3-(4,5-dimethylthiazol-2-yl)-2,5-diphenyltetrazolium bromide] was from Calbiochem (Darmstadt, Germany). Radioactive products were obtained from MP Biomedicals, LLC (Irvine, CA). RPMI 1640 medium, fetal bovine serum (FBS), trypsin/EDTA, and DMEM medium were from PAA (Pasching, Austria). Gentamycin was from Serva (Heidelberg, Germany).

In Vitro Growth Inhibition Assay. The human ovarian carcinoma cisplatin sensitive A2780 cells, cisplatin resistant A2780cisR (cisplatin resistant variant of A2780 cells), and noncarcinoma cell lines of human origin IMR-90 were kindly supplied by Professor B. Keppler, University of Vienna (Austria). The CHO-K1 cell line (wild type) and its mutant cell line MMC-2 were kindly supplied by Dr. M. Pírsel, Cancer Research Institute, Slovak Academy of Sciences, Bratislava (Slovakia). The A2780cisR cell lines were grown in RPMI 1640 medium supplemented with gentamycin ($50 \mu\text{g mL}^{-1}$) and heat inactivated FBS (10%). The acquired resistance of A2780cisR cells was maintained by supplementing the medium with cisplatin ($1 \mu\text{M}$) every second passage. The noncarcinoma cell lines of human origin IMR-90 and animal origin CHO-K1 and MMC-2 were grown in DMEM medium (high glucose, 4.5 g L^{-1}) supplemented with gentamycin ($50 \mu\text{g mL}^{-1}$) and 10% heat inactivated FBS. The cells were cultured in a humidified incubator at 37 °C in a 5% CO₂ atmosphere and subcultured 2–3 times a week with an appropriate plating density.

Stock solutions of drugs were prepared in DMF. Stock solutions were freshly prepared immediately prior to testing and serially diluted in DMF, giving the series of nine dilutions. The dilution series of substances were diluted 500-fold into culture medium to give concentrations 2-fold of the test concentration. Medium ($100 \mu\text{L}$) containing the test substance was added to each well. The final DMF concentration in all wells was 0.1%, which was shown not to affect cell growth.

The cell lines were incubated for 72 h with the platinum compounds (or the ligands), and cell death was evaluated by using a system based on the tetrazolium compound MTT in the same way as described previously.^{12,13}

The cells were seeded in 96-well tissue culture plates at a density of 10^4 cells/well in $100 \mu\text{L}$ of medium. After overnight incubation (16 h), the cells were treated with the compounds at the final concentrations

in the range of 0 to 100 μM in a final volume of 200 μL /well. After additional 72 h, 10 μL of a freshly diluted MTT solution (2.5 mg mL^{-1}) was added to each well, and the plate was incubated at 37 °C in a humidified 5% CO_2 atmosphere for 4 h. At the end of the incubation period, the medium was removed, and the formazan product was dissolved in 100 μL of DMSO. Cell viability was evaluated by measurement of the absorbance at 570 nm, using an Absorbance Reader Sunrise Tecan Schoeller. IC_{50} values (compound concentrations that produce 50% of cell growth inhibition) were calculated from curves constructed by plotting cell survival (%) versus drug concentration (μM). All experiments were done in triplicate. The reading values were converted to the percentage of control (% cell survival). Cytotoxic effects were expressed as IC_{50} .

Interaction of Platinum Compounds with Cells Monitored by Real-Time Cell Electronic Sensing. Background of the E-plates was determined in 100 μL of medium (RPMI), and subsequently, 50 μL of the A2780 cell suspension was added (10^4 cells/well). E-plates were immediately placed into the Real-time Cell Analyzer (RTCA) station (xCELLigence RTCA SP Instrument, ROCHE). Cells were grown for 24 h (in a humidified incubator at 37 °C in a 5% CO_2). Subsequently, the cells were treated with 50 μL of media alone (control) or with 50 μL of media containing varying inhibitory concentrations of C1 or cisplatin, and impedance was monitored for the first 6 h every 15 min and for the rest of the test period every 30 min. The electronic readout, cell-sensor impedance, is displayed as an arbitrary unit called cell index (CI). CI at each time point is defined as $(\text{Rt} - \text{Rb})/15$ where Rt is defined as the cell-electrode impedance of the well with the cells at different time points, and Rb is defined as the background impedance of the well with the media alone. Normalized CI is calculated by dividing the cell index at particular time points by the CI at the time of interest. Each treatment was performed in triplicate.

Cell Cycle Analysis. At each time point, floating cells (A2780) were collected, and attached cells were harvested by trypsinization (trypsin/EDTA in PBS). Total cells (floating + attached) were washed twice in PBS (4 °C), fixed in 70% ethanol, and stored at 4 °C. Cell pellets were subsequently rinsed with 0.5 mL of PBS and 0.5 mL of phosphate-citrate buffer [Na_2HPO_4 (0.2 M) and citric acid (0.1 M), pH 7.8]. After 5 min of incubation, the cells were sedimented and stained with Vindel's solution [Tris-Cl (10 mM, pH 8.0), NaCl (10 mM), Triton X100 (0.1%), RNase A (10 $\mu\text{g mL}^{-1}$, QIAGEN), and propidium iodide (50 $\mu\text{g mL}^{-1}$)] for 1 h at 37 °C in the dark. DNA content was measured using flow cytometry (BD FACSaria II Sorter). The percentages of cells in the individual cell cycle phases were analyzed using ModFit 2.0 software (Verity Software House).

Inhibition of Cyclin-Dependent Kinase (cdc2) Activity. Measurement of cdc2 kinase activity *in vitro* was carried out with the SignaTECT cdc2 Protein Kinase Assay System (Promega) according to the manufacturer's protocols. In these experiments, the extract from HeLa cells (mitotic cell extract) also prepared according to the protocol recommended by the manufacturer (Promega) was used. *In vitro* kinase assays were carried out in the presence of increasing concentrations of platinum complexes, boheminine, and its analogues. Measurement of the amount of [γ - ^{32}P]ATP remaining at the end of the reaction, carried out with a SignaTECT cdc2 Protein Kinase Assay System, was used to determine inhibition of kinase activity by compounds.

DNA Platination in Cells Exposed to Platinum Complexes. A2780 or A2780cisR cells grown to near confluence were exposed to 30 μM concentration of C1 or cisplatin for 5 h. After the incubation period, the cells were trypsinized and washed twice in ice-cold PBS. Cells were then lysed in DNAzol (DNAzol genomic DNA isolation reagent, MRC) supplemented with RNase A (100 $\mu\text{g mL}^{-1}$). The genomic DNA was precipitated from the lysate with ethanol, dried, and resuspended in water. The DNA content in each sample was determined by UV spectrophotometry. To avoid the effect of high DNA concentration on FAAS detection of platinum in the samples, the DNA samples were digested in the presence of hydrochloric acid (11 M) using a high pressure microwave mineralization system

(MARSS, CEM). Experiments were performed in triplicate, and the values are the means \pm SD.

Cellular Platinum Complex Uptake. Cellular uptake of C1 and cisplatin was measured in A2780 and A2780cisR cells. The cells were seeded in 100 mm tissue culture dishes (30 000/ cm^2). After overnight incubation, the cells were treated with the Pt^{II} complex (30 μM) for 5 h (these concentrations were still verified by the measurement of platinum in the growing medium by FAAS). The attached cells were washed twice with PBS (4 °C) and the pellet stored at -80 °C. The pellets were digested by a high pressure microwave digestion system (MARSS, CEM) with HCl to give a fully homogenized solution, and final platinum content was determined by FAAS. The results of cellular platinum uptake were corrected for adsorption effects.¹⁴ For other details, see the Results section. All experiments were performed in triplicate.

Platination Reactions in Cell-Free Media. If not stated otherwise, CT or plasmid DNAs were incubated with the platinum complex in NaClO_4 (10 mM) at 37 °C in the dark. After 24 h, the samples were exhaustively dialyzed against the medium required for subsequent biochemical or biophysical analysis. An aliquot of these samples was used to determine r_b values (the number of molecules of the platinum complex bound per nucleotide residue) by FAAS.

Sequence Preference of DNA Adducts. The transcription mapping assay¹⁵ was used to evaluate the sequence selectivity of DNA modification by platinum complexes. The (*NdeI/HpaI*) restriction fragment of pSP73KB DNA was incubated with Pt^{II} complexes to obtain $r_b = 0.01$ (cisplatin) or 0.012 (C1). The drug not bound to DNA was removed by ethanol precipitation. Transcription of the restriction fragment performed with T7 RNA polymerase and electrophoretic analysis of transcripts were performed according to the protocols recommended by Promega (Promega Protocols and Applications, 43–46 (1989/90)) and previously described in detail.¹⁵ The concentration of DNA used in this assay was 3.9×10^{-5} M (relative to the monomeric nucleotide content).

Interstrand (Intramolecular) Cross-Linking. C1 at varying concentrations was incubated for 24 h with 0.5 μg of a linear 2464-bp fragment of pSP73 plasmid linearized by *NdeI*. The linear fragment was first 3'-end labeled by means of the Klenow fragment of DNA polymerase I in the presence of [α - ^{32}P]dATP. The platinated samples were analyzed for DNA interstrand cross-links by previously published procedures.^{15,16} The number of interstrand cross-links was analyzed by electrophoresis under denaturing conditions on alkaline agarose gel (1%). After the electrophoresis had been completed, the intensities of the bands corresponding to single strands of DNA and interstrand cross-linked duplex were quantified. The frequency of interstrand cross-links was calculated as % ICL/ $\text{Pt} = \text{XL}/4928r_b$ (the DNA fragment contained 4928 nucleotide residues), where % ICL/ Pt is the number of interstrand cross-links per adduct multiplied by 100, and XL is the number of interstrand cross-links per molecule of the linearized DNA duplex and was calculated assuming a Poisson distribution of the interstrand cross-links as $\text{XL} = -\ln A$, where A is the fraction of molecules running as a band corresponding to the noncross-linked DNA.

Other Physical Methods. Absorption spectra were measured with a Beckman 7400 DU spectrophotometer equipped with a thermoelectrically controlled cell holder. The FAAS measurements were carried out on a Varian AA240Z Zeeman atomic absorption spectrometer equipped with a GTA 120 graphite tube atomizer. The gels were visualized on a BAS 2500 FUJIFILM bioimaging analyzer, and the radioactivity associated with bands was quantified with the AIDA image analyzer software (Raytest, Germany). Statistical evaluation of the untreated control cells and drug treated cells was carried out using Student's *t* test. If not stated otherwise, a probability of 0.05 or less was deemed statistically significant.

RESULTS

Cytotoxicity. The cytotoxic activity of compounds L1, L2, L3, C1, C2, and C3 and cisplatin was determined against cisplatin-sensitive and cisplatin-resistant ovarian cancer cell

lines A2780, and A2780cisR, respectively, and the non-tumorigenic, normal human fibroblast cells from embryonal lung tissue IMR-90 and Chinese hamster ovary cells CHO-K1 (Table 1). The cell lines were incubated for 72 h with L1, L2,

Table 1. Cytotoxicity [IC_{50} Mean Values (μM)] Obtained for Compounds C1, C2, C3, L1, L2, and L3 and Cisplatin^a

compd	A2780	A2780cisR	IMR-90	CHO-K1
C1	9.3 \pm 1.2	8.7 \pm 1.2	$\gg 100$	49.3 \pm 4.8
C2	1.0 \pm 0.1	0.6 \pm 0.1	2.4 \pm 0.9	1.7 \pm 0.2
C3	2.1 \pm 0.3	1.7 \pm 0.6	5.8 \pm 0.3	4.0 \pm 0.9
L1	21.7 \pm 4.5	38.3 \pm 10.0	ND ^b	44.8 \pm 3.6
L2	$\gg 100$	$\gg 100$	ND ^b	$\gg 100$
L3	60.0 \pm 5.1	51.3 \pm 4.2	ND ^b	67.6 \pm 7.7
cisplatin	1.6 \pm 0.3	24.7 \pm 3.3	13.9 \pm 1.4	35.3 \pm 1.2

^aThe experiments were performed in triplicate. The drug-treatment period was 72 h. The results are expressed as mean values \pm SD for three independent samples. ^bNot determined.

L3, C1, C2, C3, or cisplatin, and the cell survival in the culture treated with the compounds was evaluated as described in the Experimental Procedures section. All of the tested compounds, except for L2, showed activity in the tested concentration range(s), and their corresponding IC_{50} values are reported in Table 1. In general, the activity of boheminine (L1) and its analogues (L2 and L3) was considerably lower than that of cisplatin in both A2780 and A2780cisR cells. In contrast, the activity of the complexes C1, C2, and C3 was markedly better than that of parental boheminine (L1) and its analogues L2 and L3 involved in the structure of these complexes. The activity of C2 and C3 in cisplatin-sensitive A2780 cells was comparable to that of cisplatin, whereas the activity of C1 was somewhat lower than that of cisplatin (the IC_{50} was ca. 6-fold higher). Importantly, the activity of all three complexes C1, C2, and C3 was markedly better than that of cisplatin in cisplatin-resistant tumor cells A2780cisR, although the activity of C1 was lower than that of C2 and C3. Even more importantly, while we observed the markedly improved cytotoxicity of C1 in tumor A2780cisR cells and somewhat less toxicity in sensitive A2780 tumor cells as compared to cisplatin, C1 differs greatly from C2 or C3 in that it is markedly less toxic to the nontumorigenic, normal IMR-90, and CHO-K1 cells (Table 1). In other words, we observed a marked selectivity of C1 and not of C2 or C3 for tumor cells relative to the nontumorigenic, normal cells. Thus, it was mainly for this reason why C1 was selected as a representative of the cisplatin derivatives with boheminine and its analogues tested in the present work for most of the subsequent experiments.

Impedance-Based Monitoring in Real-Time the Effects on Cell Growth. We have used impedance-based time-dependent cell response profiling (TCRP) to measure and characterize cellular responses to C1 and cisplatin. It has been demonstrated that impedance-based monitoring of cellular responses to biologically active small molecule compounds produces time-dependent cellular response profiles (TCRPs), which can be predictive of the mechanism of action of small molecule compounds.¹⁷ Figure 2 shows the TCRPs of A2780 cells that have been treated with C1 or cisplatin. The TCRPs of both compounds is characterized by an initial negligible change in cell index in comparison with the control followed by a decrease in cell index below control levels, reflecting the ultimate cytotoxic response. Thus, the TCRP of C1 and

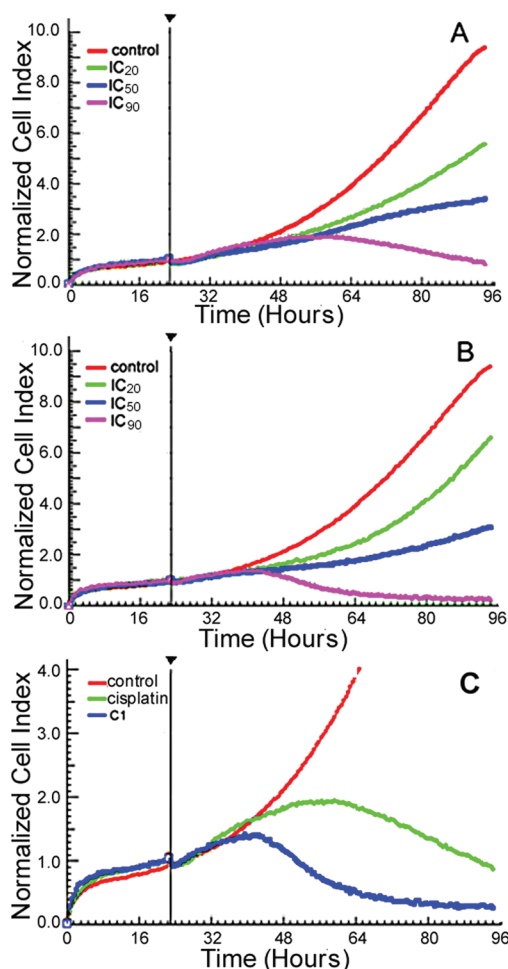


Figure 2. Interactions of cisplatin (A) and C1 (B) with A2780 cells monitored by a real-time cell analyzer (RTCA). For cisplatin, IC_{20} = 0.5 μM , IC_{50} = 1.6 μM , and IC_{90} = 15 μM ; for C1, IC_{20} = 5 μM , IC_{50} = 9.3 μM , and IC_{90} = 20 μM . The vertical lines indicate the start of treatment after allowing the cells to grow and adhere to the microelectrodes for 24 h. Cell indices were normalized to account for differences in cell counts that exist across the wells prior to treatment. Incubations were performed in triplicate with 10^4 cells/well using inhibitory drug concentrations determined for 72 h of incubation in a colorimetric cell viability assay. (C) Time-dependent cell response profiles (TCRPs) for A2780 cells: untreated (control) and treated with cisplatin or C1 at IC_{90} doses (IC_{90} were determined for 72 h of incubation in a MTT assay).

cisplatin coclustered with the TCRPs of compounds interfering with DNA synthesis and replication, transcription, and translation,¹⁷ which are also known to induce cell-cycle arrest followed by the induction of cell death. Nevertheless, C1 and cisplatin produced different TCRP. Most strikingly, while C1 at the highest concentration (IC_{90}) causes complete killing of adherent cells at the longest times of cell growth, cisplatin at the concentration corresponding to IC_{90} fails to kill adherent cells completely even at the longest times of their growth.

Cell Cycle Analysis. The status of the cell cycle for cells treated with C1 and L1 and for comparative purposes also with cisplatin was analyzed. The analysis of cell cycle perturbation was performed using A2780 cells exposed to C1, L1, or cisplatin for 24 h, 48 h, and 72 h (the concentrations of the drugs corresponded to their IC_{50} values determined by MTT for the cells treated with the drugs for 72 h; Table 1).

An evaluation of the effects of C1 and L1 compared to that of untreated control A2780 cells showed several significant differences in cell cycle modulation already after 24 h of the treatment and became more pronounced with increased treatment time (Figure 3). Exposure of A2780 cells to C1,

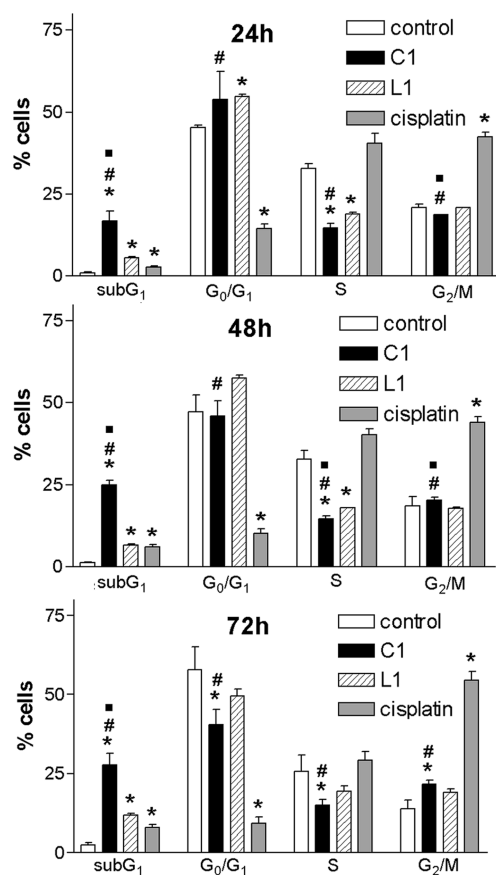


Figure 3. Effects of C1, L1, and cisplatin on cell cycle distribution. Untreated (control) A2780 cells or A2780 cells treated with 9.3 μ M C1, 21.7 μ M L1, or 1.6 μ M cisplatin for 24, 48, or 72 h were harvested, fixed, stained with propidium iodide, and assessed for cell cycle distribution by FACS analysis. The estimated percentages of A2780 cells in different phases of the cell cycle are indicated. The results are expressed as the mean \pm SEM of three independent experiments. The symbol (*) denotes significant difference ($p < 0.05$) from the untreated control; (#) denotes the significant difference ($p < 0.05$) between C1 and cisplatin; (■) denotes significant difference ($p < 0.05$) between C1 and L1.

L1, or cisplatin caused the appearance of a population in the sub-G₁ region of the profile, where apoptotic and necrotic cells are found. Appearance of a sub-G₁ peak is consistent with the onset of internucleosomal DNA cleavage in late apoptosis.¹⁸ Importantly, the efficiency of the compounds tested to cause the appearance of a population in the sub-G₁ region of the profile was different, and the trend was C1 \gg L1 > cisplatin. Also, importantly, the treatment with C1 and L1 affected the G₀/G₁ populations much less than the treatment with cisplatin,

which markedly decreased the G₀/G₁ populations. Similarly, the treatment with C1 and L1 somewhat decreased the peaks corresponding to the S phase in contrast to the peaks corresponding to this phase in case of the treatment with cisplatin, which were only affected slightly (Figure 3). In addition, both C1 and cisplatin caused an accumulation of cells in the G₂ phase (see Figure 3). Whereas this marked block was apparent already after a 24-h exposure to cisplatin, C1 induced a smaller, but significant G₂ block in A2780 cells only after a 72-h exposure to this conjugated compound. Thus, different effects were observed for C1 and L1 on the one hand and cisplatin on the other hand. The fact that C1 and cisplatin had different effects on cell cycle progression suggests that conjugation of cisplatin with bohemine (L1) in C1 changed the mechanism of action of the parent platinum drug.

Inhibition of Cyclin-Dependent Kinase (cdc2) Activity.

The ability of bohemine (L1) and C1 as well as known inhibitor CDKs olomoucine (6-(benzylamino)-2-[(2-(hydroxyethyl)amino]-9-methylpurine)¹⁹ to inhibit cdc2 was investigated in triplicate using Promega kit SignaTECTProtein Kinase Assay System (Table 2). This is a cell-free assay which utilizes a biotinylated peptide substrate derived from histone H1 to measure cdc2 kinase activity directly in cell lysates. The IC₅₀ value (compound concentration that produces 50% of CDK inhibition) for bohemine compares favorably with that found for olomoucine, whereas its cdc2 inhibitory activity was lost as a consequence of its coordination to cisplatin through the N(7) atom of purine ring in C1. This suggests that the presence of the Pt^{II} substituent in C1 adversely affects its CDK inhibitory activity.

Is DNA the Target? We determined the cytotoxic effect of complex C1 in the Chinese hamster ovary CHO-K1 cell line (wild type) and its mutant cell line MMC-2 carrying ERCC3/XPB mutation (ERCC3 is an ATP-dependent DNA helicase that plays an essential role in nucleotide excision repair).²⁰ The tumor cell lines were incubated for 72 h with complex C1, and the cell survival in the culture treated with the Pt^{II} complex was evaluated by MTT assay as described in the Experimental Procedures section. The corresponding IC₅₀ values determined for complex C1 were 49 ± 5 μ M and 18 ± 4 μ M in CHO-K1 and MMC-2 cells, respectively. It was also verified that the uptake of the drug in these cells was identical. Thus, the cells which are deficient in DNA repair were more sensitive to killing by complex C1 than wild type cells.

DNA-Bound Platinum in Cells Exposed to C1. To further corroborate our conclusion that DNA is a potential target for C1, platinum levels on nuclear DNA were determined after the exposure of A2780 or A2780cisR cells to 30 μ M C1 or cisplatin for 5 h. The levels of platinum on DNA were determined by FAAS (Table 3). The platinum content of DNA from the A2780 and A2780cisR cells treated with C1 was approximately 11- and 24-fold greater, respectively, than that from the cells treated with cisplatin.

Cellular Uptake. The factor that is usually thought to contribute to drug cytotoxicity is cellular uptake. To examine the accumulation of C1, the cellular levels of this compound

Table 2. Inhibition of Cyclin-Dependent Protein Kinase Activity by Compounds C1, C2, C3, L1, L2, and L3 and Olomoucine^a

	C1	C2	C3	L1	L2	L3	olomoucine
IC ₅₀ (μ M)	>100	>100	>100	5.1 \pm 0.2	92 \pm 8	6.1 \pm 0.3	19 \pm 1

^aShown are the mean values derived from at least three replicates, together with the standard deviations (SD) from the means.

Table 3. Platinum Content of DNA Isolated from A2780 or A2780cisR Cells Exposed to C1 or Cisplatin^a

	cisplatin	C1
A2780	0.7 ± 0.2	7.5 ± 0.8
A2780cisR	0.17 ± 0.07	4.0 ± 0.3

^aCells were exposed to C1 or cisplatin (30 μM) for 5 h. Each value shown in the table is in pmol of Pt/μg of DNA. Results are expressed as the mean ± SD for three independent samples.

were measured after a 5 h exposure of the A2780 and A2780cisR cells to the drugs. The accumulation of C1 in the A2780 and A2780cisR cells was approximately 70- and 290-fold greater, respectively, than that of cisplatin (Table 4).

Table 4. Uptake of C1 and Cisplatin into A2780 or A2780cisR Cells^a

	cisplatin	C1
A2780	0.090 ± 0.003	6.3 ± 1.6
A2780cisR	0.027 ± 0.002	7.8 ± 1.7

^aThe table shows the uptake of C1 and cisplatin (30 μM) into A2780 or A2780cisR cells after 5 h. Each value shown in the table is in nmol of Pt/10⁶ cells. Results are expressed as the mean ± SD for three independent samples.

DNA Binding in Cell-Free Media. We also tested the ability of C1 to bind DNA in cell-free media and compared it with that of parental compounds cisplatin. The efficiency of binding to CT DNA was determined at an r_i (molar ratio of free platinum complex to nucleotide phosphate) of 0.08 in 10 mM NaClO₄ at 37 °C in the dark. The platinum complex was incubated with the CT DNA, aliquots withdrawn at various time intervals were quickly cooled on an ice bath, and then the free (unbound) platinum compound was removed by gel filtration chromatography using Sephadex G50 columns. The content of platinum and the concentration of DNA in these DNA samples was determined by FAAS and absorption spectrophotometry. Cisplatin bound quantitatively, whereas only ca. 53% of C1 was bound after 24 h. The DNA binding experiments carried out in the present work indicated that modification reactions resulting in the irreversible coordination of C1 was slower than that of cisplatin, so that only a part of C1 present in the bulk of solution was bound to DNA even after a relatively long time of incubation (24 h).

The binding experiments carried out in this work indicated that modification reactions resulted in the irreversible coordination of C1 to CT DNA, which thus facilitated sample analysis. Hence, it was possible to prepare samples of DNA modified by C1 at a preselected value of r_b . Thus, except where stated, samples of DNA modified by C1 and analyzed further by biophysical or biochemical methods were prepared in NaClO₄ (10 mM) at 37 °C. After 24 h of the reaction of DNA with the complex, the samples were precipitated in ethanol and dissolved in the medium necessary for a particular analysis, and the r_b value in an aliquot of this sample was checked by FAAS. In this way, if not stated otherwise all analyses described in the present article were performed in the absence of unbound (free) Pt complex.

Transcription Mapping. Cutting of pSP73KB DNA by *NdeI* and *HpaI* restriction endonucleases yielded a 212-base pairs (bp) fragment (a substantial part of its nucleotide sequence is shown in Figure 4B). This fragment contained a T7

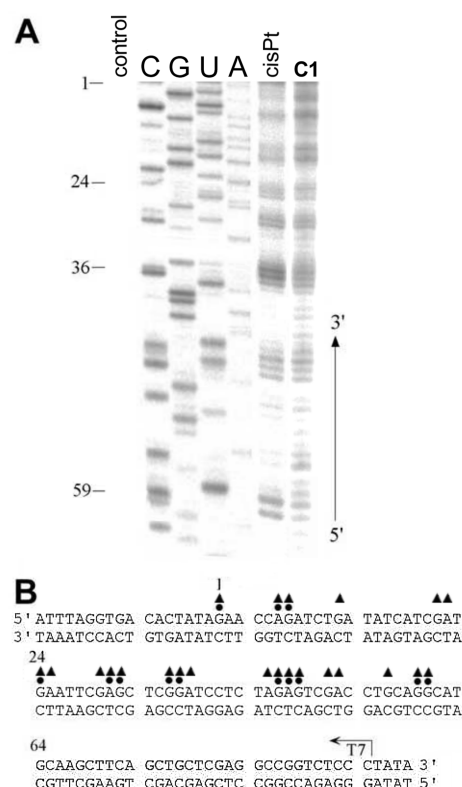


Figure 4. Inhibition of RNA synthesis by T7 RNA polymerase on the *NdeI/HpaI* fragment of pSP73KB plasmid modified by C1 or cisplatin. (A) Autoradiogram of 6% polyacrylamide/8 M urea sequencing gel. Lanes: control, unmodified template; C, G, U, and A, chain terminated marker RNAs; cisPt, the template modified by cisplatin at $r_b = 0.01$; C1, the template modified by C1 at $r_b = 0.012$. (B) Schematic diagram showing the portion of the nucleotide sequence of the template of the *NdeI/HpaI* fragment used to monitor inhibition of RNA synthesis by C1 and cisplatin. The arrow indicates the start of the T7 RNA polymerase. The circles and triangles represent major stop signals for DNA modified by cisplatin or C1, respectively. The numbers correspond to the nucleotide numbering in the sequence map of pSP73KB plasmid.

RNA polymerase promoter. *In vitro* RNA synthesis by RNA polymerases on this DNA template modified by C1 at $r_b = 0.012$ can be prematurely terminated at the level or in the proximity of adducts (Figure 4A). Interestingly, monofunctional DNA adducts of several platinum complexes are unable to terminate RNA synthesis. The major stop sites observed for C1 correspond to sites for cisplatin, indicating similar DNA binding modes for both cis compounds.

Interstrand DNA Cross-Linking. Bifunctional platinum compounds, which coordinate base residues in DNA, form various types of interstrand and intrastrand cross-links. Considerable evidence suggests that the antitumor efficacy of bifunctional platinum compounds is the result of the formation of these lesions, but their relative efficacy remains unknown. Therefore, we have decided to quantitate the interstrand cross-linking efficiency of C1 in linearized pSP73 plasmid. This plasmid DNA was linearized by *NdeI* (*NdeI* cuts only once within pSP73 plasmid) and globally modified by C1 or cisplatin. The samples were analyzed for the interstrand cross-links by agarose gel electrophoresis under denaturing conditions.¹⁵ Upon electrophoresis, 3'-end labeled strands of linearized pSP73 plasmid containing no interstrand cross-links

migrate as a 2464-base single strand, whereas the interstrand cross-linked strands migrate more slowly as a higher molecular mass species (Figure 5). The experiments were carried out with

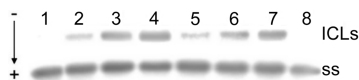


Figure 5. DNA interstrand cross-linking. The formation of interstrand cross-links by **C1** in linearized pSP73 plasmid DNA. Autoradiogram of a denaturing 1% agarose gel of linearized DNA which was 3'-end labeled; the interstrand cross-linked DNA appears as the top bands migrating on the gel more slowly than the single-stranded DNA (contained in the bottom bands). Lanes: 1,8, control, nonmodified DNA; 2–4, DNA modified by cisplatin at $r_b = 0.00025$, 0.0005, 0.001, respectively; 5–7, DNA modified by **C1** at $r_b = 0.00025$, 0.0005, 0.001, respectively.

DNA samples that were modified by the platinum complex at various r_b values. The intensity of the more slowly migrating band increased with the growing level of the platination. The radioactivity associated with the individual bands in each lane was measured to obtain estimates of the fraction of noncross-linked or cross-linked DNA under each condition. The DNA interstrand cross-linking efficiency of **C1** was 4–6%. It implies that interstrand cross-links represent only a minor portion of the adducts formed in DNA by **C1**, i.e., also in this respect it behaves like parent cisplatin whose interstrand cross-linking efficiency is under identical conditions (6%; Figure 5 and ref 15).

DISCUSSION

The success of cisplatin and its analogues as anticancer drugs has inspired the synthesis and investigation of numerous platinum compounds as drug candidates.^{7,21,22} Of these compounds, the most promising antitumor platinum complexes for clinical use exhibit improved toxicity in tumor cells, toxicity in tumor cells resistant to platinum drugs already used in the clinic (due to different mechanisms of action), or reduced side effects. The cellular and molecular pharmacology of the new class of anticancer drugs, in which CDK inhibitors bohemine and its two analogues (Figure 1) were combined with another anticancer compound, conventional cisplatin, were investigated and directly compared with parental cisplatin. Because many variables such as passage number or culture conditions can affect the characteristics of a particular cell line, we ran parallel experiments with these new conjugated complexes and parental compounds including cisplatin on cells plated at the same time from a single flask. This experimental design produced data (Table 1) showing the unique anticancer profile of the cisplatin-derived platinum(II) dichlorido complex involving N(7)-coordinated bohemine, *cis*-[Pt(**L1**)₂Cl₂] (**C1**). Although the IC_{50} values are ~6 times higher for **C1** than for cisplatin in cisplatin-sensitive tumor cells A2780, it is clear that the tumor cell lines in which **C1** is also active are those which acquired resistance to cisplatin (activity of **C1** was identical in A2780 and A2780cisR and was considerably better in cisplatin-resistant A2780cisR cells than that of cisplatin, Table 1). Thus, the cytotoxicity profile of **C1** is distinct from that of cisplatin. In addition, we observed marked selectivity of **C1** (not **C2** and **C3**, i.e., complexes which contain analogues of bohemine **L2** or **L3**) for tumor cells relative to the nontumorigenic, normal cells.

N6-substituted adenine derivatives, such as bohemine (**L1**), olomoucine, or roscovitine behave as potent inhibitors of subset CDKs including *cdc2*, *cdk2*, and *cdk5*.¹⁹ Our results reveal that the *cdc2* inhibitory activity of bohemine was lost as a consequence of its coordination to the Pt(II) atom in **C1** (Table 2). This suggests that the presence of the Pt^{II} substituent in **C1** adversely affects its CDK inhibitory activity. In other words, the coordination of bohemine through the N7 atom to Pt(II) in **C1** considerably reduces one of the dual functionalities anticipated to be effective after the novel **C1** conjugate reaches the nucleus. However, **C1** offers a distinct advantage over treatments involving cisplatin alone or **C2** and **C3** as the nontoxic **C1** may act in cisplatin-resistant tumor cells and exhibit low toxicity in nontumorigenic, normal cells thereby reducing nonspecific effects.

Activation of cell cycle checkpoints is a general cellular response after exposure to cytotoxic agents. Previous studies have indicated that cisplatin and other platinum agents predominantly inhibit cell cycle progression at the S- and/or G₂/M phase.^{23–25} Our studies performed in the cell line with wt p53 status show differences between cisplatin and **C1** at the level of cell cycle regulation (Figure 3). We found differences in type and dynamics of cell cycle perturbations induced by these two compounds. Nuclear debris from apoptotic or necrotic cells is observed as a sub-G₁ population for cells treated with **C1**, which is markedly lower for cisplatin-treated cells (Figure 3). While cisplatin markedly blocks A2780 cells in the G₂-phase already after 24-h exposure, **C1** induced a much smaller G₂ block in A2780 cells only after 72-h exposure to this conjugated compound.

The conclusion that there are differences in type and dynamics of cell cycle perturbations induced by **C1** and cisplatin is also supported by the results of impedance-based real-time monitoring of the effects of these metallodrugs on cell growth. In contrast to standard methods for cell viability or proliferation [e.g., MTT, WST assays (WTS = water-soluble tetrazolium salt), etc.] representing end-point analysis of whole cell population, this method makes it possible to register very small and rapid changes in cell count, cell adhesion, and cell morphology due to drug toxicity. The results of these experiments indicate (Figure 2) that both **C1** and cisplatin produce a concentration-dependent decrease in impedance, suggesting that the reduced cell viability determined in the colorimetric assay translates into cell death. By contrast, an increase in cisplatin dose does not kill cells to an extent that would be expected from the IC_{90} values determined by MTT assay. More interestingly, **C1** kills A2780 cells significantly more efficiently than cisplatin at equitoxic concentrations (IC_{90}) determined by the MTT assay. These findings suggest that critical differences exist in the rate and mechanisms of cell kill caused by the two agents. Previous studies have shown that platinum drugs, while generally believed to induce apoptotic cell death, may require concentrations significantly higher than IC_{50} values to produce the morphological features of apoptosis.²⁶ However, the preapoptotic signaling in various cancer cell lines has been demonstrated to be defective causing inefficient cell kill by cisplatin.²⁷ Thus, it appears that **C1** is a more potent inducer of apoptosis than cisplatin consistent with markedly higher nuclear debris from apoptotic or necrotic cells observed as a sub-G₁ population for cells treated with **C1** (Figure 3).

The target may be defined as a site within the cell which is altered by the drug and whose modification leads to cell death.

There are several criteria used to suggest that a certain type of lesions is the critical lesion which kills the tumor cells. One of the criteria used to suggest that DNA is the target is based on the observation that the drug exhibits a higher toxicity in cells which are deficient in DNA repair.²⁸ This is so because the persistence of DNA lesions depends on the capacity of cells to repair the damage. We used in the present work the assay based on introducing a point mutation in a gene coding one of the proteins necessary for the repair of DNA. Our results (vide supra) indicate that the cells which are deficient in DNA repair were more sensitive to killing by complex C1 than wild type cells. Hence, these results show that the cell must remove or bypass the DNA lesion to survive treatment with C1 and imply that unrepaired DNA damage contributes to its cytotoxicity.

To further corroborate the conclusion that DNA is a potential target for C1, platinum levels on nuclear DNA were determined after exposure of A2780 or A2780cisR cells to C1 or cisplatin (Table 3). The amount of platinum found on the DNA of A2780 and A2780cisR cells incubated with C1 was markedly greater than that from the cells treated with cisplatin suggesting that penetrating the nucleus and binding to nuclear DNA may provide an important contribution to the mechanism of cytotoxicity of C1. DNA may therefore be a potential target for this cytotoxic complex in which CDK inhibitor bohemine was combined with cisplatin, although we cannot rule out the possibility that nuclear DNA may not be the only target.

Thus, the distinct differences in cell killing observed for C1 and cisplatin may be associated with processes at the DNA level. DNA adducts of cisplatin inhibit DNA replication to an extent that slows cell cycle progression through the S phase but allows cells to accumulate in the G₂ phase.²⁹ Efficient repair of the cross-links and replicative bypass across the adducts by translesion DNA polymerases contribute to the survival of cisplatin-treated cells.³⁰ However, the fact that a small accumulation of cells in the G₂ phase and a still significant cell killing observed in A2780 cells treated with C1 suggests that inhibition of DNA synthesis by adducts of this agent is more lethal to the cells than DNA adducts of cisplatin. In summary, the fact that cisplatin and C1 had different effects on cell cycle progression suggests that the two drugs do not have the same cellular mechanism of action.

It is notable that the increase of the amount of platinum found on the DNA of A2780 and A2780cisR cells incubated with C1 or cisplatin parallels the increase in cell accumulation (Table 4) or cytotoxicity (Table 1) of these complexes. It seems reasonable to suggest that these data also show that using ligands such as bohemine gives rise to increased hydrophobicity, leading to higher cellular uptake and higher cytotoxicity in cisplatin-resistant cells A2780cisR (Table 1). Thus, C1 appears hydrophobic enough to partition efficiently into cells and yet hydrophilic enough to exhibit reasonable aqueous solubility.

The finding that the C1 conjugate is capable of delivering platinum to DNA in the cell nucleus prompted us to examine the binding of C1 conjugate to DNA in a cell-free medium. The resulting DNA damage triggers downstream effects including the inhibition of replication and transcription, and cell cycle arrest.^{7,31} The DNA binding experiments carried out in the present work in a cell-free medium indicated that modification reactions resulting in the irreversible coordination of C1 was slower than that of cisplatin and that only a part of C1 present in the bulk of solution was bound to DNA even after a relatively long time of incubation (24 h). In addition,

transcription mapping experiments (Figure 4) and determination of interstrand cross-linking efficiency of C1 (Figure 5) suggest that several aspects of the DNA binding mode of C1 are similar to those of parental cisplatin. However, it cannot be excluded that identical types of DNA adducts of C1 and cisplatin can distort DNA conformation differently and can be processed by cellular components differently. We made a rough estimate of the percentage of the amount of platinum in the DNA fraction of the total platinum in the cells treated with C1 and cisplatin considering data in Tables 3 and 4. Of the total Pt taken up by the cells, a considerably lower fraction of C1 was bound to DNA in comparison with the treatment with cisplatin (Table 5). A plausible explanation of these estimations is that

Table 5. Platinum Content of DNA Fraction Isolated from A2780 or A2780cisR Cells Exposed to C1 or Cisplatin Expressed as a Percentage of the Total Platinum in the Cell^a

	cisplatin	C1
A2780	2.7%	0.4%
A2780cisR	2.2%	0.2%

^aCells were exposed to C1 or cisplatin (30 μ M) for 5 h.

sterically hindered C1 binds to DNA at a much slower rate than cisplatin (see DNA Binding in Cell-Free Media). The introduction of steric bulk at the platinum center of C1 (using two bohemine nonleaving ligands) predicts a dissociative mechanism of substitution rather than the associative mechanism that predominates with cisplatin.³²

The bifunctional Pt-CDK inhibitory conjugate C1 was designed with the intention to synthesize the platinum complex which would exhibit besides its DNA binding properties a CDK inhibitory activity so that the resulting combined Pt complex could bind DNA in much the same way as conventional platinum drugs. Although C1 apparently does not fulfill the original expectations that it might exhibit CDK inhibitory and/or DNA binding activity, antiproliferative activity of C1 is clearly different from cisplatin, and even more importantly, it exhibits marked selectivity for tumor cells relative to the nontumorigenic, normal cells (Table 1). Hence, C1 remains a promising prototype of compounds for the generation of novel drug candidates with different cytotoxicity profiles from those of platinum drugs currently in use.

AUTHOR INFORMATION

Corresponding Author

*Tel: +420-541517148. Fax: +420-541240499. E-mail: brabec@ibp.cz.

Author Contributions

[†]These authors contributed equally to this work.

Funding

This research of B.L., L.Z., O.N., H.K., and V.B. was supported by the Czech Science Foundation (Grants 301/09/H004 and P301/10/0598). The research of Z.T. was supported by the Operational Program Research and Development for Innovations—European Regional Development Fund (Grant CZ.1.05/2.1.00/03.0058).

ACKNOWLEDGMENTS

We thank Dr. Pavel Starha for help with the preparation of the studied compounds.

■ ABBREVIATIONS

BAP, benzylaminopurine; bohemeine, 2-(3-hydroxypropylamino)-6-benzylamino-9-isopropylpurine; bp, base pair; CDK, cyclin-dependent kinase; CI, cell index; cisplatin, *cis*-diamminedichloridoplatinum(II); CK, cytokinin; CT, calf thymus; DMF, *N,N'*-dimethylformamide; DMSO, dimethylsulfoxide; FAAS, flameless atomic absorption spectrometry; FBS, fetal bovine serum; IC₅₀, compound concentrations that produce 50% of cell growth inhibition; MTT, [3-(4,5-dimethylthiazol-2-yl)-2,5-diphenyltetrazolium bromide]; olomoucine, 6-(benzylamino)-2-[(2-(hydroxyethyl)amino]-9-methylpurine; r_b , the number of molecules of the platinum complex bound per nucleotide residue; r_i , molar ratio of free platinum complex to nucleotide phosphate; TCRP, time-dependent cellular response profile; WTS, water-soluble tetrazolium salt.

■ REFERENCES

- (1) Diaz-Padilla, I., Siu, L., and Duran, I. (2009) Cyclin-dependent kinase inhibitors as potential targeted anticancer agents. *Invest. New Drugs* 27, 586–594.
- (2) Lapenna, S., and Giordano, A. (2009) Cell cycle kinases as therapeutic targets for cancer. *Nat. Rev. Drug Discovery* 8, 547–566.
- (3) Krystof, V., and Uldrijan, S. (2010) Cyclin-dependent kinase inhibitors as anticancer drugs. *Curr. Drug Targets* 11, 291–302.
- (4) Cienas, J., and Valius, M. (2011) The CDK inhibitors in cancer research and therapy. *J. Cancer Res. Clin. Oncol.* 137, 1409–1418.
- (5) Travnicek, Z., Malon, M., Zatloukal, M., Dolezal, K., Strnad, M., and Marek, J. (2003) Mixed ligand complexes of platinum(II) and palladium(II) with cytokinin-derived compounds Bohemeine and Olomoucine: X-ray structure of [Pt(BohH⁺-N7)Cl₃].9/5H₂O {Boh=6-(Benzylamino)-2-[(3-(Hydroxypropyl)-amino]-9-isopropylpurine, Bohemeine}. *J. Inorg. Biochem.* 94, 307–316.
- (6) Raynaud, F. I., Whittaker, S. R., Fischer, P. M., McClue, S., Walton, M. I., Barrie, S. E., Garrett, M. D., Rogers, P., Clarke, S. J., Kelland, L. R., Valenti, M., Brunton, L., Eccles, S., Lane, D. P., and Workman, P. (2005) In vitro and in vivo pharmacokinetic-pharmacodynamic relationships for the trisubstituted aminopurine cyclin-dependent kinase inhibitors olomoucine, bohemeine and CYC202. *Clin. Cancer Res.* 11, 4875–4888.
- (7) Kelland, L. (2007) The resurgence of platinum-based cancer chemotherapy. *Nature Rev. Cancer* 7, 573–584.
- (8) Havlicek, L., Hanus, J., Vesely, J., Leclerc, S., Meijer, L., Show, G., and Strnad, M. (1997) Cytokinin-derived cyclin-dependent kinase inhibitors: Synthesis and cdc2 inhibitory activity of olomoucine and related compounds. *J. Med. Chem.* 40, 408–412.
- (9) Szücs, L., Travnicek, Z., Popa, I., and Marek, J. (2008) Preparation and cis-to-trans transformation study of square-planar [Pt(L_n)₂Cl₂] complexes bearing cytokinins derived from 6-benzylaminopurine (L_n) by view of NMR spectroscopy and X-ray crystallography. *Polyhedron* 27, 2710–2720.
- (10) Brabec, V., and Palecek, E. (1970) The influence of salts and pH on polarographic currents produced by denatured DNA. *Biophysik* 6, 290–300.
- (11) Brabec, V., and Palecek, E. (1976) Interaction of nucleic acids with electrically charged surfaces. II. Conformational changes in double-helical polynucleotides. *Biophys. Chem.* 4, 76–92.
- (12) Bugarcic, T., Novakova, O., Halamikova, A., Zerkankova, L., Vrana, O., Kasparkova, J., Habtemariam, A., Parsons, S., Sadler, P. J., and Brabec, V. (2008) Cytotoxicity, cellular uptake, and DNA interactions of new monodentate ruthenium(II) complexes containing terphenyl arenes. *J. Med. Chem.* 51, 5310–5319.
- (13) Novakova, O., Malina, J., Suchankova, T., Kasparkova, J., Bugarcic, T., Sadler, P. J., and Brabec, V. (2010) Energetics, conformation, and recognition of DNA duplexes modified by monodentate Ru^{II} complexes containing terphenyl arenes. *Chem.—Eur. J.* 16, 5744–5754.
- (14) Egger, A. E., Rappel, C., Jakupec, M. A., Hartinger, C. G., Heffeter, P., and Keppler, B. K. (2009) Development of an experimental protocol for uptake studies of metal compounds in adherent tumor cells. *J. Anal. Atom. Spectrom.* 24, 51–61.
- (15) Brabec, V., and Leng, M. (1993) DNA interstrand cross-links of trans-diamminedichloroplatinum(II) are preferentially formed between guanine and complementary cytosine residues. *Proc. Natl. Acad. Sci. U.S.A.* 90, 5345–5349.
- (16) Farrell, N., Qu, Y., Feng, L., and Van Houten, B. (1990) Comparison of chemical reactivity, cytotoxicity, interstrand cross-linking and DNA sequence specificity of bis(platinum) complexes containing monodentate or bidentate coordination spheres with their monomeric analogues. *Biochemistry* 29, 9522–9531.
- (17) Abassi, Y. A., Xi, B., Zhang, W. F., Ye, P. F., Kirstein, S. L., Gaylord, M. R., Feinstein, S. C., Wang, X. B., and Xu, X. (2009) Kinetic cell-based morphological screening: Prediction of mechanism of compound action and off-target effects. *Chem. Biol.* 16, 712–723.
- (18) Clodi, K., Kliche, K. O., Zhao, S. R., Weidner, D., Schenk, T., Consoli, U., Jiang, S. W., Snell, V., and Andreeff, M. (2000) Cell-surface exposure of phosphatidylserine correlates with the stage of fludarabine-induced apoptosis in chronic lymphocytic leukemia and expression of apoptosis-regulating genes. *Cytometry* 40, 19–25.
- (19) Vesely, J., Havlicek, L., Strnad, M., Blow, J. J., Donelladeana, A., Pinna, L., Letham, D. S., Kato, J., Detivaud, L., Leclerc, S., and Meijer, L. (1994) Inhibition of cyclin-dependent kinases by purine analogs. *Eur. J. Biochem.* 224, 771–786.
- (20) Hall, H., Gursky, J., Nicodemou, A., Rybanska, I., Kimlickova, E., and Pirsell, M. (2006) Characterization of ERCC3 mutations in the Chinese hamster ovary 27–1, UV24 and MMC-2 cell lines. *Mutat. Res.* 593, 177–186.
- (21) Brabec, V., and Kasparkova, J. (2005) Platinum-Based Drugs, in *Metallotherapeutic Drugs and Metal-Based Diagnostic Agents: The Use of Metals in Medicine* (Gielen, M., and Tiekink, E. R. T., Eds.) pp 489–506, John Wiley & Sons, Ltd, Chichester, England.
- (22) Lovejoy, K. S., and Lippard, S. J. (2009) Non-traditional platinum compounds for improved accumulation, oral bioavailability, and tumor targeting. *Dalton Trans.*, 10651–10659.
- (23) Ormerod, M., O'Neill, C., Robertson, D., Kelland, L., and Harrap, K. (1996) *cis*-Diamminedichloroplatinum(II)-induced cell death through apoptosis in sensitive and resistant human ovarian carcinoma cell lines. *Cancer Chemother. Pharmacol.* 37, 463–471.
- (24) Siddik, Z. H. (2003) Cisplatin: mode of cytotoxic action and molecular basis of resistance. *Oncogene* 22, 7265–7279.
- (25) Kisova, A., Zerkankova, L., Habtemariam, A., Sadler, P. J., Brabec, V., and Kasparkova, J. (2011) Differences in the cellular response and signaling pathways between cisplatin and monodentate organometallic Ru(II) antitumor complexes containing a terphenyl ligand. *Mol. Pharmaceutics* 8, 949–957.
- (26) O'Neill, C. F., Ormerod, M. G., Robertson, D., Titley, J. C., Cumber-Walswee, Y., and Kelland, L. R. (1996) Apoptotic and non-apoptotic cell death induced by cis and trans analogues of a novel ammine(cyclohexylamine)dihydroxodichloroplatinum(IV) complex. *Br. J. Cancer* 74, 1037–1045.
- (27) Gonzalez, V. M., Fuentes, M. A., Alonso, C., and Perez, J. M. (2001) Is cisplatin-induced cell death always produced by apoptosis? *Mol. Pharmacol.* 59, 657–663.
- (28) Johnson, N. P., Butour, J.-L., Villani, G., Wimmer, F. L., Defais, M., Pierson, V., and Brabec, V. (1989) Metal antitumor compounds: The mechanism of action of platinum complexes. *Prog. Clin. Biochem. Med.* 10, 1–24.
- (29) Sorenson, C. M., and Eastman, A. (1988) Mechanism of *cis*-diamminedichloroplatinum(II)-induced cytotoxicity - Role of G2 arrest and DNA double-strand breaks. *Cancer Res.* 48, 4484–4488.
- (30) Kartalou, M., and Essigmann, J. M. (2001) Mechanisms of resistance to cisplatin. *Mutat. Res.* 478, 23–43.
- (31) Wang, D., and Lippard, S. J. (2005) Cellular processing of platinum anticancer drugs. *Nature Rev. Drug Discovery* 4, 307–320.
- (32) Holford, J., Sharp, S. Y., Murrer, B. A., Abrams, M., and Kelland, L. R. (1998) In vitro circumvention of cisplatin resistance by the novel

sterically hindered platinum complex AMD473. *Br. J. Cancer* 77, 366–373.

5.

DNA binding selectivity of oligopyridine-ruthenium(II)-lysine conjugate†

Katelitsa Triantafillidi,^a Konstantina Karidi,^a Olga Novakova,^b Jaroslav Malina^b and Achilleas Garoufis^{*a}

Received 26th May 2010, Accepted 10th October 2010

DOI: 10.1039/c0dt00554a

The synthesis, characterization and DNA binding properties of the complex [Ru(terpy)(4,4'-(COLysCONH₂)₂bpy)Cl]³⁺ (**1**) have been studied. Complex (**1**) hydrolyzes to (**2**) with a calculated rate constant $K_h = 2.35 \pm 0.08 \times 10^{-4} \text{ s}^{-1}$ and binds coordinatively to ct-DNA, with a saturation *r*-value at about 0.1. Stabilization of the ct-DNA helix at low electrolyte (NaClO₄) concentration (10 mM) and destabilization at higher electrolyte concentrations (50–200 mM) was observed. Circular dichroism studies indicate that the hydrolyzed complex binds to DNA, increasing the unwinding of the DNA helix with an unwinding angle calculated as $\Phi = 12 \pm 2^\circ$. The positive LD signal observed at 350 nm indicates some kind of specificity in complex orientation towards the global DNA axis. Complex (**2**) binds specifically to G4 on the central part of the oligonucleotide duplexes d(CGCGCG)₂ and d(GTCGAC)₂, as evidenced by NMR spectroscopy. Both lysine moieties were found to interact most likely electrostatically with the DNA phosphates, assisting the coordinative binding and increasing the DNA affinity of the complex. Photoinduced DNA cleavage by (**2**), upon UVA irradiation was observed, but despite its relative high DNA affinity, it was incomplete (~12%).

1. Introduction

The several side effects of cisplatin in cancer chemotherapy have led in the development of metal-based antitumor agents with metal ions other than platinum.^{1–5} Among them, ruthenium compounds NAMI-A and KP1019 have shown the most promising results in preclinical and clinical trials.^{6,7} Organometallic Ru(II)-arene compounds have stimulated an enormous research interest in the last few years, due to the significant anticancer activity they exhibit.^{8–13} In these complexes, the arene ring occupies three coordination sites, a diamine or other bidentate ligand occupies two more sites, while a chloride occupies the remaining site in a pseudo-octahedral “piano-stool” geometry. Hydrolysis of the above complexes produces aquated species, which are more active with biological targets.¹⁴ These complexes have been reported to form strong adducts with DNA, acting both coordinatively through the ruthenium center and non-covalently through hydrophobic interactions of the arene moiety with DNA bases.⁹ In contrast, similar octahedral ruthenium oligopyridine complexes, involving only one available coordination site (e.g. [Ru(trpy)(bpy)(H₂O)]²⁺),¹⁵ have been reported to have relatively low DNA affinity. However, this affinity is increased with modifications of their ligands, which contribute the binding with additional interactions.^{15–17}

Attempts to improve the DNA affinity of the oligo and polypyridine ruthenium complexes by tethering peptides^{18–25} or amino acids^{26,27} to ruthenium ligands have been reported. However, only the complex [Ru(terpy)(4-CO-(GHK)4'-Mebpy)Cl]⁺ (GHK = Gly-His-Lys) has the ability to bind coordinatively to DNA.²⁵ In this case the binding is assisted by further interactions of the tethered peptide with the DNA molecule (only for the positional isomer *I* of the complex), as evidenced from ³¹P NMR spectroscopy.

Herein, we aim to design and synthesise a complex similar to [Ru(terpy)(4-CO-(GHK)4'-Mebpy)Cl]⁺, with the ligand 4,4'-(COLysCONH₂)₂bpy, which involves two symmetrically conjugated lysine moieties in both pyridine rings of bpy. The complex is designed to be able to bind coordinatively to the DNA bases, while the conjugated lysines could offer additional interactions with the helix. The geometry of the complex allows amino-acid DNA interactions, since one of the two pyridine rings of ligand 4,4'-(COLysCONH₂)₂bpy, is close to the binding site. Also, the prepared complex [Ru(terpy)(4,4'-(COLysCONH₂)₂bpy)Cl]³⁺ (**1**) is an alternative proposal to study synergistic interactions, other than intercalation, between ligands and DNA, in cases where complexes are bound coordinatively to DNA. Electrostatic or other interactions with DNA, originated from ligands of complex (**1**), were studied in detail, in the basis of understanding the role of the conjugated amino acids.

2. Experimental

2.1. Materials

2,2':6',2''-Terpyridine was purchased from Aldrich Chemical Company and used without further purification. Hydrated

^aLaboratory of Inorganic Chemistry, Department of Chemistry, University of Ioannina, Ioannina, 45210, Greece. E-mail: agaroufi@cc.uoi.gr; Fax: +30 26510 98786; Tel: +30 26510 98409

^bInstitute of Biophysics, Academy of Sciences of the Czech Republic, v.v.i., Kralovopolska 135, CZ-61265, Brno, Czech Republic

† Electronic supplementary information (ESI) available: Experimental details. See DOI: 10.1039/c0dt00554a

ruthenium trichloride, $\text{RuCl}_3 \cdot 3\text{H}_2\text{O}$, was purchased from Pressure Chemical Company (Pittsburgh, USA). Calf thymus DNA (ct-DNA 42% G + C, mean molecular mass 2×10^7 D), agarose, ethidium bromide and PIPES (piperazine $\text{N,N}'$ -bis(2-ethanesulfonic acid)) were purchased from Sigma Chemical Company. Plasmids pUC19 (2686 bp) and pSP73KB (2455 bp) were isolated according to standard procedures. The deoxynucleotides $\text{d}(5'-\text{CGCGCG}-3')_2$ and $\text{d}(5'-\text{GTCGAC}-3')_2$ were purchased from Oswel DNA (University of Southampton U.K.) and purified by chromatography on a 120×2.5 cm Sephadex G-25 superfine column.²³ Oligonucleotide concentrations were quantified by measuring the absorbance at 260 nm as previously reported.²⁸ The Fmoc-protected Rink Amide resin (TentaGel S RAM) for the amino acid immobilization and the protected amino acid Fmoc-Lys-(Boc)-OH were purchased from Rapp Polymere Ltd and CBL Patras Ltd respectively. All solvents were of analytical grade and were used without further purification. The complex $\text{Ru}(\text{terpy})\text{Cl}_3$ ²⁹ and the ligand $\text{bpy}' = 4,4'-(\text{CO LysCONH}_2)_2\text{bpy}$,²⁶ were prepared according to the literature methods.

2.2. Synthesis

2.2.1. Synthesis of the $[\text{Ru}(\text{terpy})(4,4'-(\text{COLysCONH}_2)_2\text{bpy})\text{Cl}]\text{Cl}_3$, (1). 300 mg (0.08 mmol) of the resin bound ligand $4,4'-(\text{COLysCONH}_2)_2\text{bpy}$ (substitution 0.26 mmol g^{-1}), was refluxed with 175 mg (0.40 mmol) $\text{Ru}(\text{terpy})\text{Cl}_3$ in 8 mL of DMF/EtOH (3:1) for 8 h, under argon. After filtering, the resin with the immobilized complex was carefully washed with DMF (5×3 mL) and CH_2Cl_2 (3×3 mL). The cleavage of the complex and the protecting groups from the resin was achieved using 5 mL of TFA/ H_2O (95/5, v/v). The crude product was precipitated by the addition of 50 mL diethyl ether and cooling at 7 °C overnight. The red-brown precipitate was filtered, dissolved in 1 mL of methanol and added to a saturated aqueous solution of NH_4PF_6 and the complex was precipitated as $[\text{PF}_6]^-$ salt. Transformation to its $[\text{Cl}]^-$ salt was obtained by dissolving the complex in a minimum amount of acetone and precipitated from a saturated acetic solution of LiCl. Finally, the complex was purified by reverse-phase HPLC on a Dionex chromatograph, with a Waters C18 column. Yield: ~40%. *Anal.* Calcd. for $\text{C}_{39}\text{H}_{47}\text{N}_{11}\text{O}_4\text{Cl}_4\text{Ru}$; C, 47.9; H, 4.8; N, 15.8%, Found: C, 47.6; H, 4.9; N, 15.6%. ESI-MS: $m/z = 290$ $[\text{Ru}(\text{terpy})(4,4'-(\text{COLysCONH}_2)_2\text{bpy})\text{Cl}]^{3+}$; 453, $[\{\text{Ru}(\text{terpy})(4,4'-(\text{COLysCONH}_2)_2\text{bpy})\text{Cl}\}]^{2+}$. ¹H NMR (400.14 MHz, CD_3OD , 310 K, δ in ppm); $\delta = 10.33$ (d, 1H, bpyH6), 9.30 (s, 1H, bpyH3), 9.03 (s, 1H, bpyH3'), 8.68 (d, 2H, terpyH3''H5''), 8.53 (d, 2H, terpyH6H6'), 8.40 (d, 1H, bpyH5), 8.23 (t, 1H, terpyH4''), 7.95 (t, 2H, terpyH5H5'), 7.63 (d, 2H, terpyH3H3'), 7.62 (d, 1H, bpyH6'), 7.43 (d, 1H, bpyH5'), 7.32 (t, 2H, terpyH4H4'), 4.74 (d, 1H, LysH $_{\alpha}$), 4.54 (d, 1H, Lys'H $_{\alpha}$), 3.00 (d, 2H, LysH $_{\epsilon}$), 2.96 (d, 2H, Lys'H $_{\epsilon}$), 2.08 (m, 2H, LysH $_{\beta}$), 1.92 (m, 2H, Lys'H $_{\beta}$), 1.81 (m, 2H, LysH $_{\delta}$), 1.71 (m, 2H, Lys'H $_{\delta}$), 1.49 (m, 2H, LysH $_{\gamma}$), 1.49 (m, 2H, Lys'H $_{\gamma}$). UV-Vis (in MeOH); 278 nm ($\epsilon = 25 \times 10^3$ $\text{M}^{-1} \text{cm}^{-1}$), 319 nm ($\epsilon = 28 \times 10^3$ $\text{M}^{-1} \text{cm}^{-1}$), 492 nm ($\epsilon = 5 \times 10^2$ $\text{M}^{-1} \text{cm}^{-1}$), $\Lambda_M = 240$ $\text{ohm}^{-1} \text{cm}^2 \text{mol}^{-1}$.

2.2.2. $[\text{Ru}(\text{terpy})(4,4'-(\text{COLysCONH}_2)_2\text{bpy})(\text{H}_2\text{O})]\text{Cl}_4$, (2). The complex (2) was achieved from hydrolysis of (1) in buffer phosphates solutions. ESI-MS: $m/z = 462$, $[\{\text{Ru}(\text{terpy})(4,4'-(\text{COLysCONH}_2)_2\text{bpy})(\text{H}_2\text{O})\text{Cl}_2\}]^{2+}$. ¹H NMR (400.14 MHz, D_2O buffer phosphates 50 mM, pH = 7.0, 298 K, δ in ppm); $\delta = 9.73$

(d, 1H, bpyH6), 9.12 (s, 1H, bpyH3), 8.77 (s, 1H, bpyH3'), 8.60 (d, 2H, terpyH3''H5''), 8.46 (d, 2H, terpyH6H6'), 8.37 (d, 1H, bpyH6'), 8.29 (t, 1H, terpyH4''), 7.98 (t, 2H, terpyH5H5'), 7.58 (d, 1H, bpyH5), 6.97 (d, 1H, bpyH5'), 7.72 (d, 2H, terpyH3H3'), 7.32 (t, 2H, terpyH4H4'), 4.63 (d, 1H, LysH $_{\alpha}$), 4.42 (d, 1H, Lys'H $_{\alpha}$), 3.17 (d, 2H, LysH $_{\epsilon}$), 3.04 (d, 2H, Lys'H $_{\epsilon}$), 2.06 (m, 2H, LysH $_{\beta}$), 1.85 (m, 2H, Lys'H $_{\beta}$), 1.73 (m, 2H, Lys'H $_{\delta}$), 1.59 (m, 2H, LysH $_{\delta}$), 1.43 (m, 2H, LysH $_{\gamma}$), 1.43 (m, 2H, Lys'H $_{\gamma}$). UV-Vis (aqueous buffer phosphates 50 mM, pH = 7.0); 274 nm ($\epsilon = 23 \times 10^3$ $\text{M}^{-1} \text{cm}^{-1}$), 314 nm ($\epsilon = 27 \times 10^3$ $\text{M}^{-1} \text{cm}^{-1}$), 480 nm ($\epsilon = 4 \times 10^2$ $\text{M}^{-1} \text{cm}^{-1}$).

2.3. Physical measurements

2.3.1. General methods. C, H and N determinations were performed on a Perkin-Elmer 2400 Series II analyser. The conductivity measurements were performed in an E365B Conductoscope, Metrohm Ltd., Herisau, Switzerland. The infrared spectra were recorded on a Perkin-Elmer GX-FT IR spectrophotometer using the diffuse reflectance technique. High performance liquid chromatography was used for the purification of the complexes using a DIONEX chromatographic system and a Waters C18 column. Electrospray ionisation mass spectra (ESI-MS) were obtained on an Agilent Technology LC/MSD trap SL instrument. Absorption spectra were measured in a Beckmann DU-7400 spectrophotometer. FAAS measurements were carried out on a Varian AA240Z Zeeman spectrometer equipped with a GTA 120 graphite tube. CD and LD spectra were recorded on a Jasco J-720 in a 1-cm path length cuvette for the region 600–220 nm. The irradiation of the solutions was carried out in a photoreactor LZC-ICH2 with a UVA lamp (4.3 mW cm^{-2} ; $\lambda_{\text{max}} = 350$ nm). For the electrophoretic mobility assay, the samples were analysed by gel electrophoresis on 1% (w/v) agarose gel. The gels were stained with EtBr and photographed with a transilluminator. The PAA gels were visualized by using a BAS 2500. The DNA concentration ($[\text{DNA}]$), expressed as moles of nucleotides per litre, was determined from the absorbance at 260 nm ($\epsilon_{260} = 6600$ $\text{M}^{-1} \text{cm}^{-1}$, $T = 298$ K).

2.3.2. NMR analysis. NMR spectra were recorded on Bruker Avance spectrometers operating at proton frequencies of 400 and 500 MHz and were processed using Topspin 1.3 (Bruker Analytik GmbH). The spectra of the complex were recorded in CD_3OD or in D_2O (50 mM phosphate buffer, pH = 7.0, 298 or 310 K). The spectra of complex added to the oligonucleotide at increasing ratios were recorded at $\text{H}_2\text{O}/\text{D}_2\text{O}$ (9:1) or D_2O (99.96%) (50 mM phosphate buffer, pH 7.0, 298 K). Chemical shifts are referenced to the HOD signal at 4.75 ppm. One-dimensional spectra were recorded for samples with oligonucleotide concentration of approximately 50 OD_{260} units, while 2D NMR experiments were performed with more concentrated samples (*ca.* 200 OD_{260}).

2.3.3. DNA melting. Thermal denaturation experiments were performed in quartz cuvettes. Samples were continuously being heated, with a 0.5 °C min^{-1} rate of temperature increase while monitoring the absorbance changes at 260 nm, in a Varian Cary 4000 instrument. The investigated interval of temperature ranged from 25 to 98 °C. Values for melting temperatures (T_m) and for the melting interval (ΔT_m) were determined according to the reported procedures.³⁰

2.3.4. DNA transcription by RNA polymerase *in vitro*. Transcription of the (*NdeI/HpaI*) restriction fragment of pSP73KB DNA with T7 RNA polymerase and electrophoretic analysis of transcripts were performed according to the protocols recommended by Promega³¹ and previously described in detail.^{32,33} Before the aliquots containing the transcripts were loaded on the PAA gel, the radioactivity associated with these samples was adjusted so that equal amounts of the radioactivity were loaded into each well.

2.3.5. Unwinding of negatively supercoiled DNA. Unwinding of closed circular supercoiled pUC19 plasmid DNA was assayed by an agarose gel mobility shift assay.³⁴ The unwinding angle Φ induced per ruthenium-DNA adduct was calculated upon determination of the r value in which complete transformation of the supercoiled to the relaxed form of the plasmid was attained. A sample of pUC 19 plasmid DNA was incubated with the ruthenium complex for 48 h, precipitated by ethanol and dissolved in TAE buffer. An aliquot of the precipitated sample was subjected to electrophoresis on 1% native agarose gel running at 25 °C in the dark. The other aliquot was used for the determination of the r -values by FAAS.

2.3.6. Hydrolysis of the complex (1). The hydrolysis of complex (1) to (2) was monitored by ¹H NMR spectroscopy at 310 K in buffer phosphate solution (50 mM, pH = 7.0) and was processed using TOPSPIN 1.3 (Bruker Analytik GmbH). The initial concentration of (1) was 2 mM and the spectrum was recorded at cycles of 10 min. Integrating selected proton signals of (1) and the hydrolyzed product (2), relative to (TMS) as an internal standard, gave their time depended concentrations. The equilibrium concentration C_{eq} of complex (1) was calculated (0.18 mM) from the plot of concentration of (1) vs. time, at t_{∞} . The graph of $\ln((C_0 - C_{eq})/(C_t - C_{eq}))$ vs. t , where C_0 is the initial concentration of (1) and C_t is the concentration of (1) at a given time, provide a linear plot for at least the first hours of the reaction. The rate constant k_h was determined by linear fitting of the graph traces according to equation:

$$\ln((C_0 - C_{eq})/(C_t - C_{eq})) = (C_0/C_{eq})k_h t.$$

2.3.7. ct-DNA binding kinetics. A solution of complex (1) (0.032 mM) in buffer phosphates (50 mM, pH = 7.0) was added to a solution of ct-DNA (0.32 mM) (buffer phosphate 50 mM, pH = 7.0) at ratio 1/10. During the reaction time, aliquots of the reaction mixture were withdrawn and the reaction was stopped by cooling at -30 °C. The DNA was then precipitated by the addition of ethanol and centrifugation. Determination of the free ruthenium complex and DNA in the supernatant was obtained by atomic absorption spectroscopy (FAAS) and by UV-spectroscopy (A_{260}), respectively.³⁵

3. Results and discussion

3.1. Synthesis and characterization of $[\text{Ru}(\text{terpy})(4,4'-(\text{COLysCONH}_2)_2\text{bpy})\text{Cl}]\text{Cl}_3$

The resin bound ligand $4,4'-(\text{COLysCONH}_2)_2\text{bpy}$ reacted with the complex $\text{Ru}(\text{terpy})\text{Cl}_3$ through solid phase method to produce the immobilized complex (1). This method has advantages over the liquid synthesis method eliminating the most of byproducts. The

use of DMF as component of the reaction solvent was proposed for the resin unwrapping.²⁵ The elemental analyses and mass spectra (ESI-MS) of the prepared compounds were found to be consistent with the identified formula. Moreover, the molar conductivity value of (1) ($\Lambda_m = 240 \text{ ohm}^{-1} \text{ cm}^2 \text{ mol}^{-1}$) corresponds to 1:3 electrolyte, indicating that the terminal amino groups of the lysine moieties are most likely protonated. The solid phase synthetic method is presented in Fig. 1.

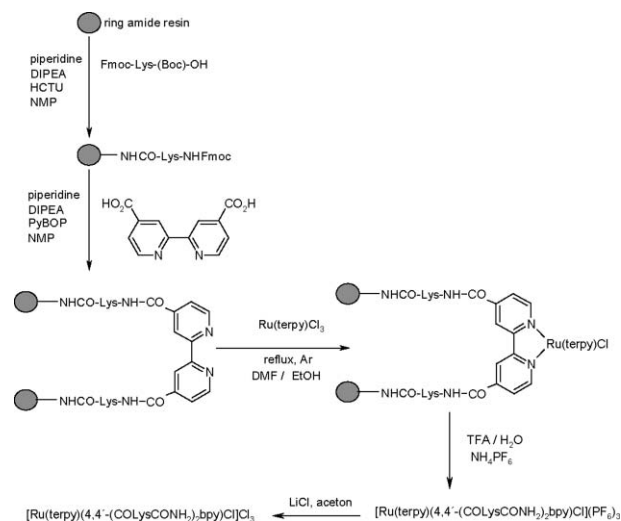


Fig. 1 Procedure of solid phase synthesis of the complex $[\text{Ru}(\text{terpy})(4,4'-(\text{CO LysCONH}_2)_2\text{bpy})\text{Cl}]\text{Cl}_3$.

The electronic spectrum of (1) in methanol exhibits two intense bands at 278 nm ($\epsilon = 25 \times 10^3 \text{ M}^{-1} \text{ cm}^{-1}$) and 319 nm ($\epsilon = 28 \times 10^3 \text{ M}^{-1} \text{ cm}^{-1}$), as well as a band of lower energy at 492 nm ($\epsilon = 5 \times 10^2 \text{ M}^{-1} \text{ cm}^{-1}$). The high-energy bands at 278 and 319 nm are assigned to intraligand $\pi \rightarrow \pi^*$ transitions (e.g. $\pi(\text{terpy}) \rightarrow \pi^*(\text{terpy})$, $\pi(4,4'-(\text{COLysCONH}_2)_2\text{bpy}) \rightarrow \pi^*(4,4'-(\text{COLysCONH}_2)_2\text{bpy})$). The low-energy band at 492 nm is attributed to $\text{d}\pi(\text{Ru}) \rightarrow \pi^*(\text{COLysCONH}_2)_2\text{bpy}$ and $\text{d}\pi(\text{Ru}) \rightarrow \pi^*(\text{terpy})$ MLCT transitions.³⁶ ¹H NMR spectra of (1) were recorded at 298 K in MeOH-d_4 . Assignments of the resonances were assisted by homonuclear ¹H-¹H COSY and ¹H-¹H TOCSY experiments. In the spectra of the complex (1) in MeOH-d_4 only one set of terpy proton signals were observed, while separated proton resonances of each of the two pyridine moieties of the ligand $4,4'-(\text{COLysCONH}_2)_2\text{bpy}$ appeared. Since both pyridine rings are chemically equivalent in the free ligand, the differences in the electron density environment of their protons probably arises from the placement of one pyridine ring over the terpy aromatic system and the other close to the coordinated chlorine. The higher downfield signal at 10.33 ppm is assigned to the H6 neighboring to chlorine.³⁷ Using the scalar couplings from the ¹H-¹H TOCSY protons H3 and H5 were also assigned. The H6' resonance was observed at 7.62 ppm due to a strong shielding effect from the terpy aromatic ring system (Fig. 2).

3.2. Hydrolysis of complex (1)

Since the DNA binding of metal-based drugs containing chloro-ligands presupposes the hydrolysis of the M-Cl bonds, the kinetic of chloro-ligand replacement with a water molecule in complex (1)

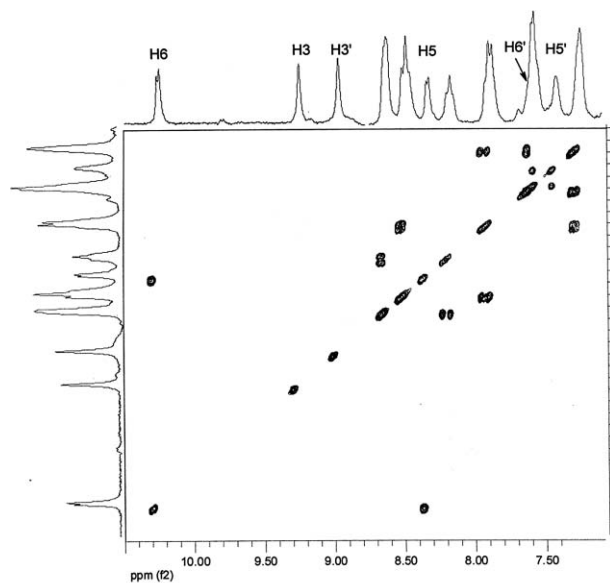


Fig. 2 Aromatic region (10.50–6.00 ppm) of 400 MHz $^1\text{H}/^1\text{H}$ COSY spectrum of complex $[\text{Ru}(\text{terpy})(4,4'-(\text{COLysCONH}_2)_2\text{bpy})\text{Cl}]\text{Cl}_3$ in $\text{MeOH}-d_4$ at 310 K, with schematic illustrating of the complex structure.

was studied in aqueous buffer phosphate solution (50 mM, pH = 7.0) by ^1H NMR spectroscopy at 310 K. In the spectrum of a freshly prepared solution of (1), double resonances were observed for protons H6 and H5 of the one-pyridine ring of the ligand $(\text{COLysCONH}_2)_2\text{bpy}$, while the other signals of the spectrum were slightly broadened. Over a time period of 15 h the hydrolysis reaction was completed, producing an almost clear spectrum of the complex $[\text{Ru}(\text{terpy})(4,4'-(\text{COLysCONH}_2)_2\text{bpy})(\text{H}_2\text{O})]^{4+}$ (2). Significant upfield shifts were observed for protons H6 ($\delta = 9.73$ ppm) and H5 ($\delta = 7.60$ ppm), confirming the strong deshielding effect of the chlorine to the neighboring pyridine ring in comparison with the H_2O (Fig.S1, ESI†).

The hydrolytic process follows pseudo-first-order kinetics (Fig. 3) during the first hours of incubation, with a calculated rate constant $k_h = 2.35 \pm 0.08 \times 10^{-4} \text{ s}^{-1}$, ($R^2 = 0.997$) and $t_{1/2} = 49$ min. (see 2.3.6). This value is one order of magnitude lower than that of the bifunctional antitumor compound $[\text{Ru}(\eta^6\text{-}p\text{-cymene})(\text{pta})\text{Cl}_2]$ ($\text{pta} = 1,3,5\text{-triazia-7-phosphatricyclo}[3.3.1.1]\text{decane}$)³⁸ ($3.33 \pm 0.02 \times 10^{-3} \text{ s}^{-1}$ at 150 mM NaClO_4 , 298 K),³⁹ indicating that complex (1) hydrolyzes significantly slower than $[\text{Ru}(\eta^6\text{-}p\text{-cymene})(\text{pta})\text{Cl}_2]$. Also, the monofunctional anticancer arene $\text{Ru}(\text{II})$ complexes of the general formula $[\text{Ru}(\eta^6\text{-arene})(\text{en})\text{Cl}]^+$ ($\text{en} = \text{ethylenediamine}$) hydrolyze at least three times faster than complex (1), with values ranging from $3.95\text{--}6.84 \times 10^{-3} \text{ s}^{-1}$ (100 mM NaClO_4 , 310 K).¹⁴ It is notable that for $\text{cis-}[\text{Pt}(\text{NH}_3)_2\text{Cl}_2]$ the hydrolysis rate constants were calculated to be $1.9 \pm 0.2 \times 10^{-4} \text{ s}^{-1}$ for

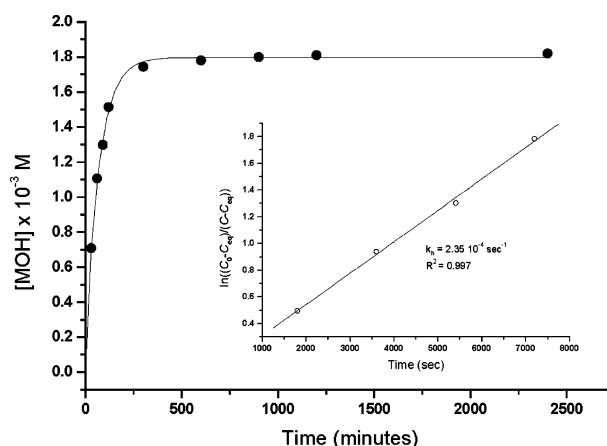


Fig. 3 Hydrolysis kinetics plot of $[\text{Ru}(\text{terpy})(4,4'-(\text{COLysCONH}_2)_2\text{bpy})\text{Cl}]\text{Cl}_3$. Inset the graph of $\ln((C_0 - C_{\text{eq}})/(C_t - C_{\text{eq}}))$ vs. t , with linear fitting of the traces.

the first aquation process (k_1) and $2.3 \pm 0.2 \times 10^{-4} \text{ s}^{-1}$ for the second aquation process (k_2) (100 mM NaClO_4 , 318.2 K),⁴⁰ while $\text{Pt}(\text{II})$ amine monofunctional complexes were hydrolyzed much slower, with rate constants in the range of 10^{-5} s^{-1} (unbuffered aqueous solutions, $4.2 < \text{pH} < 5.4$, 293 K).⁴¹

3.3. DNA binding studies of complex (2)

3.3.1. DNA binding kinetics. A solution of ct-DNA (0.0032 mM) and a solution of complex (2) at ratio $r = 0.1$, were incubated at 37°C in 50 mM buffer phosphates (pH = 7.0). The percentage of the complex (2) bound to ct-DNA was calculated as described in 2.3.7, increasing with time and bound almost completely ($\sim 85\%$) after 2 h. Fig. 4, curve a presents the percentage of ruthenated DNA as a function of the reaction time, in 50 mM buffer phosphates and in the additional presence of 150 mM NaCl (Fig. 4, curve b). The plot traces were fitted by a non-linear optimization method using the software Microcal Origin v. 5.0 and second-order rate kinetic equations. The half-life time ($t_{1/2}$) value was calculated from the plot and found to be about 50 min. for curve (a). The observed $t_{1/2}$ value is similar to that observed for the complex $\text{Na}[trans\text{-Cl}_4\text{Im}(\text{DMSO})\text{Ru}^{\text{III}}]$

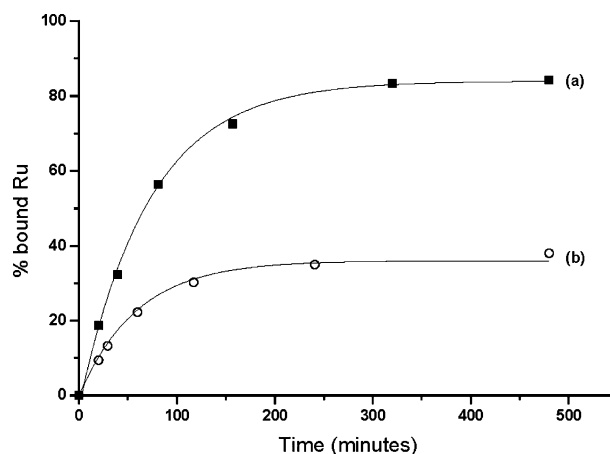


Fig. 4 Binding kinetics of $[\text{Ru}(\text{terpy})(4,4'-(\text{COLysCONH}_2)_2\text{bpy})(\text{H}_2\text{O})]\text{Cl}_4$ to ct-DNA at (■) 37°C , 50 mM buffer phosphates (pH = 7.0), $r = 0.1$ and (○) in the additional presence of 150 mM NaCl .

(~ 1 h, 37 °C, 10 mM NaClO₄),³⁵ in which the hydrolysis of only one chloro-ligand is enough to bind to DNA.

In an attempt to confirm the above conclusion, the DNA binding kinetic of complex (1) was studied in the presence of 150 mM NaCl to inhibit the complex hydrolysis (Fig. 4, curve b). Clearly, the equilibrium between the M–Cl and M–OH₂ moved to the side of M–Cl, giving a total percent of ruthenated DNA at about 35% (as calculated from the plot). This percentage most probably corresponds to the same percentage of the hydrolyzed complex, indicating that the M–Cl form is unable to bind to DNA. In addition, the $t_{1/2}$ value was calculated again at about 50 min., since it represents the half-life time for the same reaction.

3.3.2. DNA thermal denaturation (T_m) studies. The effect on ct-DNA T_m of complex (2) at various ratios ($r = 0.025$ to $r = 0.125$), as a function of the electrolyte (NaClO₄) concentration (10 mM to 200 mM) was studied. Increasing the salt ionic strength, without addition of complex (2), causes an increase in the DNA melting temperature, as a consequence of stabilization of the helix. At high salt concentration, the repulsion of the negatively charged DNA phosphates is reduced due to a “shield” effect of the electrolyte counter ions. Thus, the necessary energy to separate the DNA strands is higher than needed in the case where the phosphates are less “shielded” from the electrolyte positively charged counter ions and consequently, the DNA helix is stabilized.⁴² Stabilization effects due to the positive charge of a metal complex, located on the metal center or/and the ligand moiety, upon binding to DNA strands have also been reported.⁴³ Furthermore, formation of interstrand cross links caused by bifunctional metal complexes (e.g. *cis*-[Pt(NH₃)₂Cl₂]) stabilize the DNA helix while conformational distortions due to the complex binding destabilize the helix.⁴³

Fig. 5 presents the ct-DNA ΔT_m at various NaClO₄ concentrations upon addition of (2) at different ratios (r). At low concentration of NaClO₄ (10 mM) the binding of the complex resulted in an increase of T_m (+ 2.5 °C for $r = 0.1$), indicating that the energy to separate the two strands is higher when the complex is bound to DNA. An explanation for this result is that the positive charge of the bound complex additionally “shields” the negatively charged DNA strands, stabilizing the DNA helix.

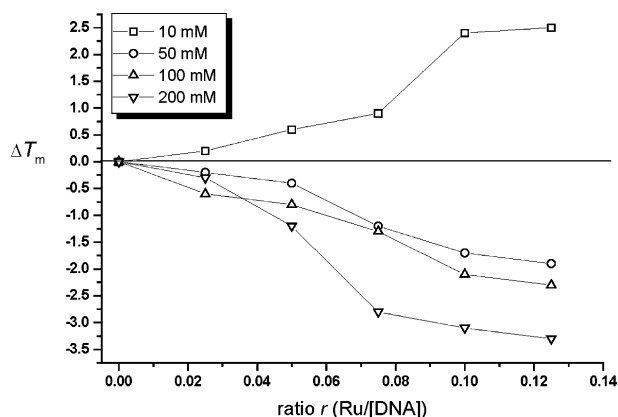


Fig. 5 ΔT_m of ct-DNA modified by [Ru(terpy)(4,4'-(COLysCONH₂)₂-bpy) (H₂O)]Cl₄ versus r , measured at different concentrations of NaClO₄.

At higher concentrations of NaClO₄ (50–200 mM) where the “shield” effect of Na⁺ counterions on DNA phosphates is

significant, the energy to separate the strands is expected to be higher. However, the measured values of ΔT_m indicate that less energy is needed to separate the helix, as a consequence of complex (2) binding. In other words complex (2) destabilizes the DNA helix at concentrations of NaClO₄ between 50 and 200 mM. This means that there should be a significant destabilization factor, over the positive charge of the bound complex and the electrolyte concentration. This factor should be considered among destabilization factors such as, (i) intrastrand conformational distortions, or/and (ii) difficulty to form C–W hydrogen bonds due to the bulky shape of bound (2), or/and (iii) a positive charge, which is introduced by (2) in DNA strands. The latter, in conjunction with the high electrolyte concentration, saturate the strands with positive charges, which are repulsed. Thus, the well-known effect of DNA helix stabilization, due to high electrolyte concentration, changes to a helix destabilization in cases where positive charges are introduced into DNA strands. This behavior is in contrast with that observed for *cis*-[Pt(NH₃)₂Cl₂] in the same conditions. *cis*-[Pt(NH₃)₂Cl₂] modification of ct-DNA results in a decrease of T_m in a wide range of NaClO₄ concentrations (10–200 mM),⁴³ reflecting the destabilization of the helix due to local denaturational changes in the DNA. No comparison can be made with the complex [Ru(terpy)(bpy)(H₂O)]²⁺¹⁵ which stabilizes the helix of ct-DNA but in different conditions.

3.3.3. Circular dichroism (CD) spectroscopy studies. The interaction of complex (2) with ct-DNA was studied by circular dichroism spectroscopy in aqueous buffer solutions (pH = 7.0), at various ratios ($r = [\text{Ru}]/[\text{DNA}]$) $r = 0.025, 0.050, 0.075, 0.100$ and 0.125). A solution of complex (2), incubated for 24 h, was added to a ct-DNA solution (1×10^{-4} M) in such a way so as to produce the final ratios (r). The increasing amounts of (2), added to ct-DNA, clearly affect the CD spectrum of ct-DNA (Fig. 6).

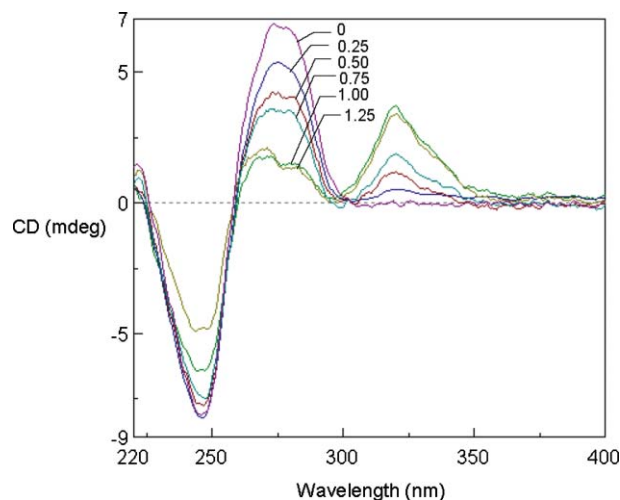


Fig. 6 CD spectra of ct-DNA upon addition of [Ru(terpy)(4,4'-(COLysCONH₂)₂-bpy)(H₂O)]Cl₄ at ratios $r = 0, 0.025, 0.050, 0.075, 0.100$ and 0.125 .

The intensities of the characteristic bands of ct-DNA at 245 nm and 277 nm changed and additionally a new positive CD band at 320 nm appeared. The intensity of the positive band (277 nm), which reflects the stacking interactions between the DNA bases,⁴⁴ decreases progressively at low ratios ($r = 0.025$ – 0.100), but remains

almost unaffected when the ratio increases from $r = 0.100$ to $r = 0.125$. These results suggest that the DNA helix is untwisted, disrupting locally the base stacking, due to the binding of complex (2). However, this effect seems to be completed until $r = 0.1$, indicating that the saturation r -value of DNA modification by complex (2) is close to this value. This result is in agreement with the results of DNA melting profiles (Fig. 6), where insignificant ΔT_m changes were observed over $r = 0.1$. Moreover, the intensity of the DNA negative band (245 nm), which is related to the DNA helicity,⁴⁴ remains almost unaffected indicating that the ruthenated DNA adopts a B-type conformation. On the other hand, at $r = 0.100$ and 0.125 , where no more complexes bind to DNA, the intensity of negative CD band decreases drastically as a consequence of excess of (2) in the solution, suggesting an unwinding of the helix.⁴⁵ Once again, the high positive charge of complex $[\text{Ru}(\text{terpy})(4,4'-(\text{COLysCONH}_2)_2\text{bpy})(\text{H}_2\text{O})]^{4+}$ seems to neutralize the polyanion phosphates by two ways: (i) non reversibly, introducing positive charge to strands due to the binding and (ii) electrostatically, distorting locally the B-type structure of ct-DNA.⁴⁶

Moreover, a new positive CD signal appears at 320 nm from $r = 0.025$, increasing progressively with the ratio until $r = 0.1$. Over this ratio the intensity of this band remains constant, confirming the suggestion of a saturation r -value close to 0.1. The CD spectrum of the free complex shows a weak and broad signal at about 250 nm originated from the chiral carbon center in lysine moieties. Thus, the new signal at 320 nm should be induced from the complex binding to the DNA helix. In addition, the appearance of such positive CD bands is related in the literature by non-intercalating DNA binders (e.g. Netropsin (320 nm $r = 0.1$),⁴⁷ Distamycin-A (330 nm, $r = 0.1$)⁴⁸ and bis-quaternary ammonium heterocycle SN-16814 (310 nm, $r = 0.1$)⁴⁹) which all bind to the DNA minor groove. Recently, it has been reported that a similar positive CD band beyond 310 nm was observed for dinuclear Ru(II) complexes selectively binding to guanine residues of ct-DNA. It is worth mentioning that these dinuclear complexes bind monofunctionally to ct-DNA, through each Ru(II) center that they involve.⁵⁰

3.3.4 Linear dichroism (LD) spectroscopy studies. Flow oriented LD was used to give information about the relative orientation of DNA bases along the DNA helix axis. Ct-DNA exhibits a negative absorption band, with a minimum at 258 nm, suggesting that the average orientation of the ct-DNA bases was near perpendicular relative to the flow direction. The addition, at increasing amounts, of a solution of complex (2) which had been incubated for 24 h, to a ct-DNA solution with constant concentration (1×10^{-4} M), produces the final ratios ($r = [\text{Ru}]/[\text{DNA}]$) $r = 0.025, 0.050, 0.075, 0.100$ and 0.125 . In the spectra of the above samples the LD signal at 258 nm decreases in magnitude of the initial signal at about 55% at $r = 0.1$ (Fig. S2†), indicating a significant deviation of perpendicularity of the orientation of the DNA relative to the flow direction.

At least three major reasons could be responsible for the orientation loss of the DNA bases: (i) bending of the DNA axis, where the bases are locally oriented perpendicularly along an intrinsic axis, but globally oriented randomly along the DNA length, (ii) coiling into a more compact structure, where the bases lose their orientation and (iii) alterations of the DNA

flexibility, where some of the nucleotides were unpaired, “melting” the helix locally, due to introduction of local positive charges. The introduction of local positive charges can also increase the flexibility of the DNA helix without disruption of the hydrogen bonds between the bases. However, the disruption of hydrogen bonds should be rather excluded as a consequence of complex (2) binding, since if this occurs, the energy to melt the DNA helix would be significantly less than that observed in 3.3.2.

DNA bending/coiling has been reported to be mediated by highly positively charged metallo-supramolecular cylinders of ruthenium(II)^{51,52} and iron(II)^{53–55} noticeably affecting the magnitude of the ct-DNA LD negative band. For iron(II) helicates, enantiomeric discrimination on the percentage of LD signal decrease has been reported, ranging between 43–95% at low $r = 0.025$.⁵⁵ On the other hand, dinuclear ruthenium(II) complexes of the type $[\text{Ru}_2(\text{L-L})\text{L}^1]^{4+}$ ($\text{L} = \text{bpy}$ or phe and $\text{L}^1 = \text{bis}(\text{pyridylimine})$) bind to ct-DNA strongly ($K_b = 3.6\text{--}5.1 \times 10^6 \text{ M}^{-1}$) affecting modestly the ct-DNA LD negative band (2–20% at low $r = 0.33$), which indicates they cause bending/coiling of the DNA less than iron(II) helicates.⁵⁶ In the case of complex (2) the decrease in the magnitude of the ct-DNA LD negative signal is about 25% at ratio $r = 0.33$, somewhat higher than the most of $[\text{Ru}_2(\text{L-L})\text{L}^1]^{4+}$, indicating a higher degree of DNA coiling.

At about 350 nm, where DNA is silent, a new positive low in the intensity signal appears, increasing with ratio, probably originating from $\pi \rightarrow \pi^*$ intraligand transitions of complex (2). In principle, LD signals from small molecules bound to DNA are obtained only if they are orientated specifically due to interaction with the DNA.⁵⁷ The positive LD signal observed in the case of (2) indicates an orientation more parallel than perpendicular of the transition moment towards the alignment axis. However, which ligand plane of (2) (terpy or $4,4'-(\text{CO LysCONH}_2)_2\text{bpy}$) is oriented parallel to the DNA axis can not be concluded, since their aromatic planes are perpendicular to each other and thus, no LD signal will occur.

3.3.5 Unwinding of DNA. In order to determine the induced unwinding of DNA due to complex (2) binding, electrophoretic mobility studies in plasmide pUC19 at various ratios r were carried out (Fig. 7).

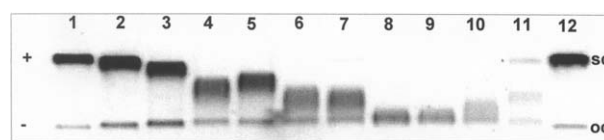


Fig. 7 Unwinding of negatively supercoiled pUC19 plasmide DNA by $[\text{Ru}(\text{terpy})(4,4'-(\text{COLysCONH}_2)_2\text{bpy})(\text{H}_2\text{O})]\text{Cl}_4$, incubated for 48 h. Lanes (2–11); $r = 0.02, 0.04, 0.06, 0.08, 0.09, 0.10, 0.11, 0.12, 0.13, 0.15$, respectively. Lanes (1 and 12) unmodified pUC19 plasmide DNA. Top bands (sc) correspond to the form of closed negatively supercoiled and bottom bands (oc) correspond to open circular form.

The pUC19 in the absence of any unwinding compound exists mainly in supercoiled form (sc). The number of supercoils in pUC19 supercoiled form (sc) decreases upon superhelical unwinding and consequently the rate of the migration through the agarose gel decreases. Fig. 7 shows the electrophoresis gel of pUC19 upon gradual addition of (2). The ratio of bound complex $r_b(c)$ corresponding to the removal of all supercoils from DNA is calculated at $r = 0.11$, where both the supercoiled and relaxed

forms are comigrated.³⁴ Beyond this point $r > 0.11$ and until $r = 0.15$ the bands are diffused, probably due to a partial separation of the plasmide strands. The DNA unwinding can be quantified from the value of torsion angle Φ , calculated per bound molecule of complex (2) to pUC19.

The unwinding angle can be calculated according to the equation $\Phi = -18\sigma/r_b(c)$, where σ is the superhelical density estimated to -0.063 for these experimental conditions⁵⁸ and $r_b(c)$ is the ratio of the bound complex to DNA. According to the DNA binding kinetic studies of complex (2) (3.3.1) and the plot of Fig. 4, it can be suggested that the percentage of bound (2) is about 85% after 24 h of incubation. This gives a value of the $r_b(c) = 0.11 \times 0.85 = 0.093$ and therefore the value for the average unwinding angle is $\Phi = 12 \pm 2^\circ$. Metal complexes, bound monofunctionally to DNA, induce small unwinding angles ($[\text{Pt}(\text{NH}_3)_3]^{2+} = 6 \pm 1^\circ$,⁵⁸ $[\text{Pt}(\text{dien})]^{2+} = 6 \pm 1^\circ$)⁵⁸ unless additional DNA-ligand interactions take place. In cases where a ligand is specifically oriented between the DNA bases, large unwinding angles were observed (*cis*- $[\text{Pt}(\text{NH}_3)_2(\text{N}3\text{-Etd})]^{2+} = 15 \pm 1^\circ$,⁵⁸ *cis*- $[\text{Pt}(\text{NH}_3)_2(\text{N}8\text{-Etd})]^{2+} = 19 \pm 3^\circ$,⁵⁸ $[\text{Ru}(\eta^6\text{-}p\text{-terp})(\text{en})]^{2+} = 14 \pm 1^\circ$)⁹ Also, complexes that monofunctionally bind to DNA, involving ligands able to intercalate but located away from the DNA helix, induced a small unwinding of DNA, such as *trans*- $[\text{Pt}(\text{NH}_3)_2(\text{N}8\text{-Etd})]^{2+}$ with $\Phi = 8^\circ$.⁵⁸ Based on the above-mentioned literature results it can be suggested that complex (2) is bound to DNA in such a way, so as to interact with its ligands with the DNA helix. Taking into account that the complex $[\text{Ru}(\text{trpy})(\text{bpy})\text{Cl}]^+$ unwinds insignificantly the DNA ($\Phi \ll 7^\circ$),⁵⁹ it can be suggested that the conjugated lysine moieties of ligand 4,4'-(COLysCONH₂)₂bpy interacting with the DNA helix cause significant unwinding of the helix. Alternatively, it can also be suggested that the highly positive charge of complex (2) introduced to DNA strands upon (2) binding, unwind the helix. These results are in accordance with the observations of circular dichroism studies (3.3.3), where unwinding of the DNA helix has been suggested. Moreover, it seems to be clear that the significant decrease in the intensity of the LD band observed in (3.3.4), reflects a bending of the DNA axis rather than a coiling to a more compact structure.

3.4. NMR studies on the interactions of complex (2) with the hexanucleotides d(5'-CGCGCG-3')₂ and d(5'-GTCGAC-3')₂

In an attempt to further investigate the interactions of complex (2) with the DNA, NMR experiments with two different sequences of hexanucleotide duplexes were performed.

3.4.1. ¹H NMR assignments of d(5'-CGCGCG-3')₂ and d(5'-GTCGAC-3')₂. Both duplexes are self-complementary, and the bases are numbered as d(5'-C₁G₂C₃G₄C₅G₆-3')₂ and d(5'-G₁T₂C₃G₄A₅C₆-3')₂. Assignments of exchangeable and non-exchangeable protons of the hexanucleotide duplexes were performed according to the approaches described previously^{24,26,60} in H₂O/D₂O (9:1) at 298 K in 50 mM phosphate buffer, using the sequential connectivity of NOESY maps assisted by 2D ¹H, ¹H TOCSY experiments. The spectra of the imino region exhibit the expected W-C (Watson-Creek) imino signals for both sequences. For the sequence d(5'-CGCGCG-3')₂ two signals, at 12.98 ppm and 13.01 ppm, were observed, indicating that the terminal C-G base pairs of the duplex do not form W-C hydrogen bonding or these protons were exchange rapidly with the solvent.

The observed signals were assigned to G2-C5 and G4-C3 imino hydrogen bonding protons correspondingly. Furthermore, in the region of 8–9 ppm two broad but clear signals at 8.32 ppm (G2) and 8.23 ppm (G4), corresponding to the hydrogen-bonded exocyclic amino group protons of guanine moieties were observed. The non-hydrogen-bonded protons of the same amino groups were observed at a higher field (6–7.5 ppm). Similarly, in the spectrum of the sequence d(5'-GTCGAC-3')₂ two signals, at 13.80 ppm and 12.76 ppm, were observed. These signals were assigned to T2-A5 and G4-C3 imino hydrogen bonding protons correspondingly. Furthermore, in the region of 8–9 ppm one broad signal at 8.49 ppm (G4) corresponding to the hydrogen-bonded exocyclic amino group protons of cytosine and guanine moieties was observed, while the non-hydrogen-bonded protons of the same amino group was observed at 6.83 ppm. However, the proton signal corresponding to A5 amino group was not observed at the region 8–9 ppm, indicating that the second W-C of the AT base pair is either not formed or exchanged more rapidly with the solvent. The characteristic assignments of the exchangeable and non-exchangeable protons for both oligonucleotide sequences are presented in Table S1 (ESI†).

3.4.2. Titration of the d(CGCGCG)₂ with complex (2). 1D ¹H NMR spectra of samples containing the d(5'-CGCGCG-3')₂ and complex (2), at ratios [Ru]/[nucleotide], 1:0.25, 1:0.5, 1:0.75 and 1:1, were recorded in the same conditions with those of the free oligonucleotide (303 K, H₂O/D₂O (9:1), 50 mM phosphate buffer pH = 7.0). Upon addition of complex (2), at the imino region of the spectra, the signal corresponding to the W-C hydrogen-bonded proton between G4N1 and C3N3, gradually reduced in intensity. Simultaneously, a build-up in signal appears at 12.96 ppm, which increased in intensity until the ratio became 1:1, while the resonance of the other imino proton (G2N1-C5N3) remained intact (Fig. 8C). In addition, the signal of the hydrogen-bonded amino proton of G4N2 at 8.42 ppm decreased in intensity and two new signals at 8.37 and 8.31 ppm appeared (Fig. 8B). Furthermore four NOESY cross-peaks originated from the imino (G2N1 and G4N1) to amino (G4N2/C3N4 and G2N2/C5N4) protons were observed. These cross-peaks were assigned to (i) the G2N1 imino proton with the amino protons of G2N2 and C5N4, (ii) the remaining residue of G4N1 with the amino protons G4N2, (iii) the ruthenated Ru-G4N1 with the Ru-G4N2, and (iv) the Ru-G4N1 with C3N4 (Fig. 8D). Consequently, the binding of (2) to the oligonucleotide, does not widely interrupt the hydrogen bonds between the bases, confirming the results of ΔT_m studies (3.3.2). Thus, it seems that the base G4 is the most affected base of the sequence, probably due to the higher electronegativity of the G4N7.

Due to this slow reaction kinetic, two sets of (2) proton resonances, (bound and free) were observed. The co-existence in the solution of at least three different species (free complex (2), free oligonucleotide and ruthenated oligonucleotide) and several minor species resulted to a spectrum with many overlapping signals.

In the aromatic region of the spectra the signal corresponding to the G4H8 (Fig. 8E) gradually reduced in intensity until the ratio became 1:1, while the two other signals of G2H8 and G6H8 remained almost intact. The new signal arose at 8.66 ppm could most probably be assigned to the ruthenated G4, since no

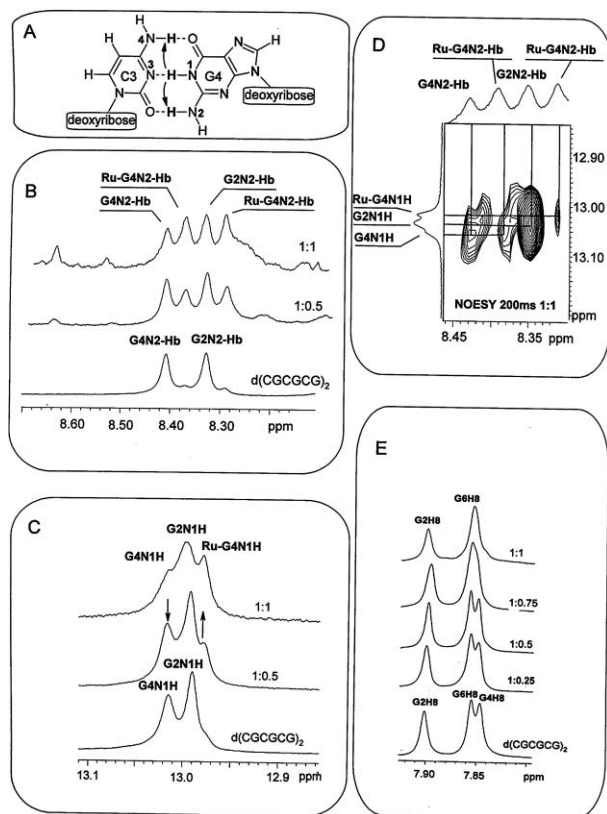


Fig. 8 (A) C–W hydrogen bonds with numbered atoms between G4 and C3 of the duplex $d(CGCGCG)_2$. The arrows indicate the dipolar (through space) coupling between protons G4N1H with C3N4H and G4N1H with G4N2H. (B) Aromatic region (8.40–8.70 ppm) of 1D 1H NMR spectra (500 MHz, H_2O/D_2O 9 : 1, 50 mM phosphate buffer, pH = 7.0, 298 K) of the duplex $d(CGCGCG)_2$ treated with complex (2) at ratios $r = 0.5$ and 1. The signals to the hydrogen bonded protons G4N2-Hb and G2N2-Hb, were shifted to new signals corresponding to the ruthenated oligonucleotide. (C) Imino region (12.80–13.10) of 1D 1H NMR spectra (500 MHz, H_2O/D_2O 9 : 1, 50 mM phosphate buffer, pH = 7.0, 298 K) of the free duplex $d(CGCGCG)_2$ and treated with complex (2) at ratios $r = 0.5$ and 1. The signal of the G4 hydrogen bonded imino proton (G4N1H) was shifted upfield, while the signal corresponding to G2 imino proton, remains intact. (D) Part of 1H - 1H NOESY spectrum (500 MHz, H_2O/D_2O 9 : 1, 50 mM phosphate buffer, pH = 7.0, 298 K, 200 ms, $r = 1 : 1$) showing the cross peaks between the imino and amino protons of the free and the ruthenated oligonucleotide duplex. (E) 1D 1H NMR spectra (500 MHz, H_2O/D_2O 9 : 1, 50 mM phosphate buffer, pH = 7.0, 298 K) of the guanine (G2, G6 and G4) H8 proton signals of duplex $d(CGCGCG)_2$, treated with complex (2) at increasing ratios. The signal of G4H8 was shifted, while the signals of the G2H8 and G6H8 remain intact.

correlation with other protons in spin system of COSY spectra were observed. Moreover, it is known that N7 ruthenation of the guanine moiety of oligonucleotides causes downfield shifts of H8 in the range of 0.5–0.8 ppm.^{61,62}

In the region 0–3 ppm only the signals of lysine aliphatic protons appeared. Using the scalar connectivities from the 1H - 1H COSY spectra of a sample containing the oligonucleotide and the complex at ratio 1 : 1 (Figures S3A & S3B, ESI[†]), it is possible to assign most of the protons of the bound complex. The chemical shifts are presented in Table S2 (ESI[†]). Separated proton resonances for both pyridine rings of the ligand, 4,4'-(CO

LysCONH₂)₂bpy were observed, while the terpy proton signals appeared as one set of signals, as in the case of free complex (2). The pyridine ring located over the terpy aromatic system was less affected from the binding of (2) to oligonucleotide, than the other ring that is close to the coordinated site. Mixed upfield and downfield shifts were observed for all protons of the complex (2), which are more pronounced for both lysine moieties of the ligand, 4,4'-(CO LysCONH₂)₂bpy. It is remarkable that the observed upfield shifts of –0.05 and –0.06 ppm for LysH ϵ and Lys'H ϵ correspondingly, were followed by upfield shifts of their neighboring H δ protons (–0.07 ppm LysH δ and –0.34 ppm Lys'H δ). In general, the observed upfield shifts for the lysine H ϵ protons could be interpreted as an electron density increase, most possibly due to the involvement of the positively charged lysine terminal amino group (–NH₃⁺) to electrostatic interactions with the oligonucleotide phosphates. In an attempt to further investigate the oligonucleotide-complex interaction, NOESY spectra were recorded in D₂O, where the aromatic region is better resolved without signals from the non-exchangeable protons. However a few cross-peaks between the aromatic protons of terpy (terpyH3H3' → G4H1', terpyH4H4' → G4H1') and the ligand, 4,4'-(CO LysCONH₂)₂bpy (bpyH5 → G4H1', bpyH5 → C5H6, bpyH6 → G4H1') were unambiguously assigned. No cross-peak between the lysine side chain and the oligonucleotide protons was observed, indicating that only the terminal amino group (–NH₃⁺) interacts with the oligonucleotide phosphates.

To further investigate the binding of (2) to the central GC base pair of the oligonucleotide $d(CGCGCG)_2$, a different sequence, which includes the same central part but different sequence ends, was chosen.

3.4.3. Titration of the $d(GTCGAC)_2$ with complex (2). A similar titration, as in the case of $d(CGCGCG)_2$ at ratios [Ru]/[nucleotide], 1 : 0.25, 1 : 0.5, 1 : 0.75 and 1 : 1, was performed. Upon addition of complex (2) the signal at the imino region of the spectra corresponding to the W–C hydrogen-bonded proton between G4N1 and C3N3, was split. The new signal that appeared at 12.73 ppm increased in intensity until the ratio became 1 : 1, while the resonance of the W–C hydrogen-bonded T2N3–A5N1 imino proton remained rather intact (Fig. 9A). In addition, the signal corresponding to the hydrogen bonding G4N2–Hb decreased in intensity and a new signal built-up at 8.42 ppm, assigned to the ruthenated G4 (Fig. 9B). Once again, it seems that the W–C hydrogen bonds formed between the bases of the sequence remain unbroken and the W–C hydrogen bonds formed between the G4 and C3 are the most affected.

The aromatic region of the spectra exhibits signals corresponding to the H8 of G4 and G1 as well the A5H8 and A5H2. Upon complex (2) addition, the signal corresponding to the G4H8 gradually reduced in intensity until the ratio became 1 : 1, while the other signals of G1H8, A5H8 and A5H2 remained almost intact (Fig. 10A). A new signal that arose at 8.70 ppm could probably be assigned to the ruthenated G4, since no correlation for this signal with other protons can be observed in the COSY spectra. In addition, the T2CH₃/T2H5 and T2CH₃/G1H8 cross-peaks in the NOESY spectra were split due to the co-existence of the ruthenated and the free oligonucleotide in the solution, indicating that the ruthenation of G4 also affects the signals of T2CH₃ and T2H5, both shifted downfield at about +0.05 ppm,

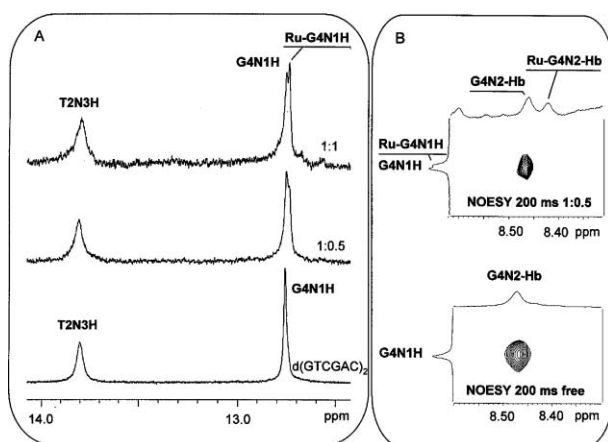


Fig. 9 (A) Imino region (12.50–14.10) of 1D ^1H NMR spectra (500 MHz, $\text{H}_2\text{O}/\text{D}_2\text{O}$ 9:1, 50 mM phosphate buffer, pH = 7.0, 298 K) of the free duplex $\text{d}(\text{GTCGAC})_2$ and treated with complex (2) at ratios $r = 0.5$ and 1. The signal of the G4 hydrogen bonded imino proton (G4N1H) was slightly shifted upfield, while the signal corresponding to T2N3H imino proton remains intact. (B) The same part of ^1H - ^1H NOESY spectra (500 MHz, $\text{H}_2\text{O}/\text{D}_2\text{O}$ 9:1, 50 mM phosphate buffer, pH = 7.0, 298 K, 200 ms) for free and ruthenated oligonucleotide ($r = 1:0.5$), showing the cross peaks between the free and ruthenated G4 imino and amino protons.

correspondingly. It is notable that the signal corresponding to G1H8 remained intact, eliminating the possibility of a general perturbation of the oligonucleotide helix. On the other hand, the downfield shift observed for T2H5 and T2CH₃ is not enough to conclude that complex (2) binds to T2.⁶¹ A possible explanation might be that an interaction occurs between the bound complex (2) or/and the ruthenated G4 of one strand, with the T2 in the parallel strand (Figs. 10B & 10C).

Despite the difficulty to assign all the proton resonances of the nucleotide and complex (2) (Table S2†), only the lysine aliphatic protons appeared in the spectral region of 0 to 2.5 ppm. Upfield shifts were observed, as in the case of the sequence 5'-CGCGCG-3', at the lysine terminal aliphatic protons (−0.08 and −0.06 ppm for LysHε and Lys'Hε, correspondingly, and −0.09 ppm LysHδ and 0.30 ppm Lys'Hδ). Since the lysine moieties of complex (2) interact non-specifically with the oligonucleotide sequence, it was concluded that they interact rather electrostatically. The slow reaction kinetics between complex (2) and the oligonucleotide on the NMR time scale, observed for both sequences, clearly lead to the conclusion that (2) binds coordinatively to the oligonucleotide, since groove interaction and simple electrostatic interactions are usually in fast exchange.⁶³ Moreover, intercalation binding of aromatic ligands between the DNA bases is, in the most cases, of intermediate exchange kinetics on the NMR time scale and at ambient temperature.⁶⁴

3.5. Transcription mapping of DNA adducts

Cleavage of pSP73KB DNA by *NdeI* and *HpaI* restriction endonucleases yielded a 212-bp fragment (a substantial part of its nucleotide sequence is shown in Fig. 11B) containing a T7 RNA polymerase promoter. The experiments were carried out using this linear DNA fragment, treated with *cis*- and *trans*-[Pt(NH₃)₂Cl₂] and complex (2), noted in Fig. 11A as *cis*Pt, *trans*Pt and [Ru(terpy)(bpy)(Lys)₂Cl]Cl, at $r = 0.01$.

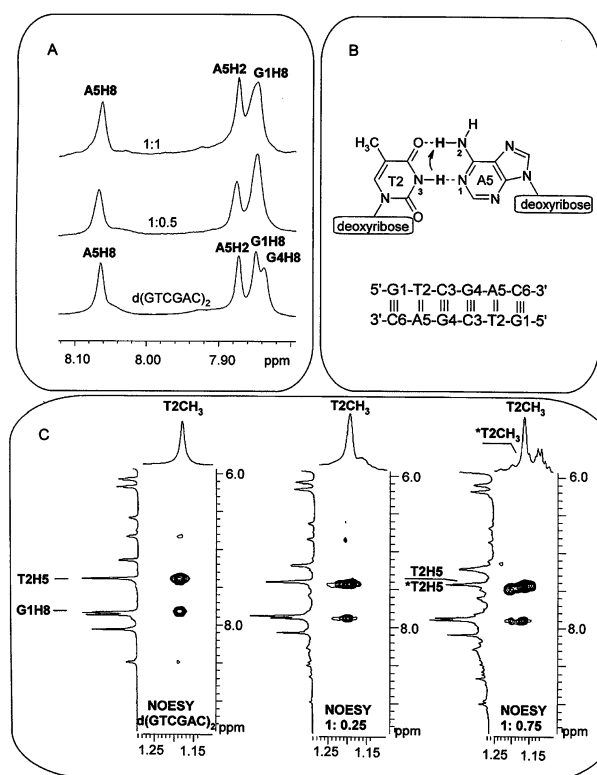


Fig. 10 (A) 1D ^1H NMR spectra (500 MHz, $\text{H}_2\text{O}/\text{D}_2\text{O}$ 9:1, 50 mM phosphate buffer, pH = 7.0, 298 K) of the guanine (G1, G4) H8 proton signals and adenine (A5) H8, H2, of duplex $\text{d}(\text{GTCGAC})_2$, treated with complex (2) at increasing ratios. The signal of G4H8 was shifted, while the other signals remain intact. (B) C–W hydrogen bonds with numbered atoms between T2 and A5 of the duplex $\text{d}(\text{GTCGAC})_2$. The arrow indicates the dipolar (through space) coupling between the T2N3H with A5N2H. (C) Part of the ^1H - ^1H NOESY spectrum (500 MHz, $\text{H}_2\text{O}/\text{D}_2\text{O}$ 9:1, 50 mM phosphate buffer, pH = 7.0, 298 K, 200 ms) showing the cross peaks between the T2CH₃ and T2H5, as well as T2CH₃ and G1H8, of the free duplex $\text{d}(\text{GTCGAC})_2$ and upon addition of (2) to the ratios $r = 0.25$ and 0.75.

It is known that *in vitro* RNA synthesis by RNA polymerases on DNA templates containing several types of bifunctional adducts of platinum complexes can be prematurely terminated at the level or in the proximity of adducts.^{32,33,65} However, monofunctional DNA adducts of platinum complexes, such as [PtCl(dien)]Cl or [PtCl(NH₃)₃]Cl, are unable to terminate the RNA synthesis.³³ In contrast, the production of monofunctional DNA adducts by Ru(II) complexes, such as arene compound^{9,12} [Ru(terpy)(bpy)Cl]Cl⁵⁹ terminates the RNA synthesis. RNA synthesis on the template modified by complex (2) yielded fragments of almost clear sizes, indicating that the RNA synthesis was terminated. The major stop sites that appeared were almost at all the guanine bases of the sequence, indicating that complex (2) binds almost exclusively to this base. In comparison with *cis*Pt, the termination sites seems to be the same with complex (2), but the bands in the case of the Ru(II) complex are more (for everything G at the sequence) and slightly diffused in intensity. Diffusion in the band intensities can be interpreted on the basis that complexes that bind monofunctionally, stop the RNA polymerases due to steric reasons if they contain bulky ligands. Thus, stop sites

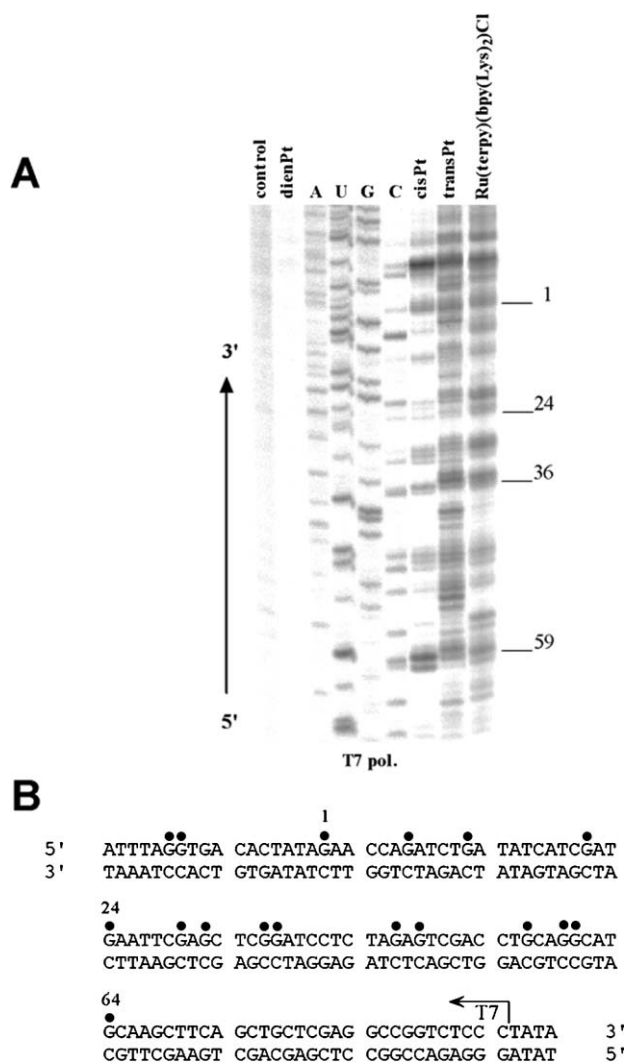


Fig. 11 Inhibition of RNA synthesis by T7 RNA polymerases on the *NdeI/HpaI* fragment of pSP73KB plasmid modified by [Ru(terpy)(bpy(Lys)₂)Cl]Cl. (A) Autoradiograms of 6% PAA/8 M urea sequencing gels showing inhibition of RNA synthesis by T7 RNA polymerase on the *NdeI/HpaI* fragment containing adducts of complex (2) and selected platinum complexes. Lanes: control, unmodified template; dienPt, cisPt, transPt and [Ru(terpy)(bpy(Lys)₂)Cl]Cl, the template modified by dienplatin, cisplatin, transplatin or (2) at $r = 0.01$, respectively; A, U, G and C, chain terminated marker RNAs. (B) Schematic diagram showing the portion of the sequence used to monitor inhibition of RNA synthesis by platinum complexes. The arrow indicates the start of the T7 RNA polymerase, which used as template the upper strand of *NdeI/HpaI* fragment of pSP73KB DNA. (●), major stop signals (from A) for DNA modified by complex (2). The numbers correspond to the nucleotide numbering in the sequence map of pSP73KB plasmid.

can be even 1 or 2 bases before the binding base, depending on the bulk of the ligands. The termination sites corresponding to transPt are different from those of complex (2). TransPt forms different adducts than complex (2) and, in particular, relatively large amount of interstrand cross-links between guanine and cytosine. This difference is more pronounced between bases 38 and 58 of the sequence, where complex (2) most likely binds to guanines only.

3.6. DNA photocleavage

Agarose gel electrophoresis was applied to determine the cleavage of the plasmide DNA pUC19 upon addition of complex (2) at $r = 0.04$. The sample was incubated in the dark for 24 h at 37 °C and irradiated with UVA for 15, 30, 60, 90 min. Then, it was analyzed by gel electrophoresis together with a sample of pUC19 in the absence of complex (2) kept in the dark (k lane) and a sample pUC19 irradiated with UVA for 90 min (*k lane). Fig. 12A presents the gel electrophoresis of pUC19 treated by complex (2) and Fig. 12B shows the % oc form of pUC19, which was measured for each experiment as function of the time. The results indicate that complex (2) cleaves the plasmide DNA pUC19 with a yield at about 12% after irradiation for 90 min.

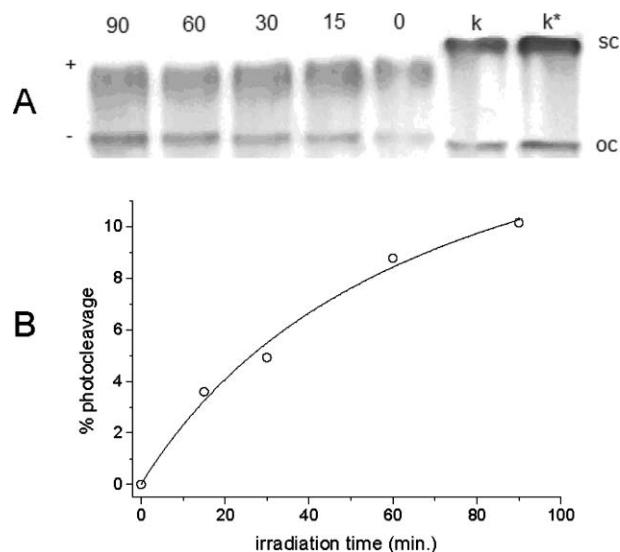


Fig. 12 (A) Agarose gel electrophoresis of the plasmide DNA pUC19 upon addition of complex (2) at $r = 0.04$ irradiated with UVA for 0, 15, 30, 60 and 90 min. Also, pUC19 in the absence of complex (2) (k lane) and pUC19 irradiated with UVA for 90 min (*k lane). (B) % (oc) form of the pUC19, normalized after subtraction of the % (oc) form containing in the free plasmide, as a function of the irradiation time.

This type of incomplete DNA photocleavage has been reported for the similar complex [Ru(terpy)(dpp)Cl]⁺ (dpp = 2,3-bis(2-pyridyl)pyrazine), associated with the low value of its DNA binding constant ($K_b = 8.8 \times 10^2 \text{ M}^{-1}$). Moreover, the complex [Ru(MePhterpy)(dpp)Cl]⁺ (MePhterpy = 4'-(4-methylphenyl)-2,2':6',2''-terpyridine) with a higher $K_b = 6.2 \times 10^3 \text{ M}^{-1}$, cleaves the DNA almost completely at the same irradiation conditions.¹⁶ Efficient DNA cleavage, through Ru(IV) species generated electrochemically from Ru(II) complexes [Ru(bzimpy)(bpy)(OH₂)²⁺ and [Ru(bzimpy)(phen)(OH₂)²⁺ (bzimpy = 2,6-bis(benzimidazolyl)pyridine) has been reported¹⁷ and their DNA affinities ($K_b = 3.58 \pm 0.25 \times 10^4 \text{ M}^{-1}$ and $K_b = 2.87 \pm 0.2 \times 10^4 \text{ M}^{-1}$, respectively) were found to be significantly higher than those of similar complexes. Despite the fact that the photometrically determined (DS1, ESI⁺) K_b value of complex (2) is relatively high ($K_b = 55 \pm 1.5 \times 10^4 \text{ M}^{-1}$), complex (2) cleaves the DNA incompletely. Comparing this K_b value with that observed for the complex [Ru(terpy)(bpy)(OH₂)²⁺ ($K_b = 7.7 \times 10^2 \text{ M}^{-1}$) it seems that the contribution from the conjugated lysine

moieties of (2) affects its DNA affinity. However, a correlation between the binding affinity and the DNA cleavage is not observed, suggesting that the mechanism of the photoinduced DNA cleavage is governed more by factors related to the photoexcitation of the Ru(II), and therefore by the structure of the ligands.⁶⁶

4. Conclusions

The spectroscopic and analytical data presented herein show clearly that complex (2) is bound to DNA coordinatively (NMR data), towards the global DNA axis (LD data), preferentially to the N7 of guanine bases (NMR and transcription mapping of DNA). The observation that the lysine moieties of complex (2) interact in the same manner (NOESY) with two different oligonucleotide sequences, leads to the conclusion that their interaction is not specific and most likely electrostatic, increasing the DNA affinity of the complex. The conjugated lysines offer a +4 positive charge to the whole complex, significantly affecting its binding to DNA. Thus, slightly destabilizing the DNA helix (T_m data) and increasing its unwinding (CD data) with an unwinding angle calculated as $\Phi = 12 \pm 2^\circ$. Finally, by comparing the DNA affinity of complex (2) with that of $[\text{Ru}(\text{terpy})(\text{bpy})(\text{OH}_2)]^{2+}$, it is suggested that it binds stronger, assisted by an additional interaction between the positive charged terminal amino group of the lysines and the DNA phosphate backbone. Photoinduced DNA cleavage by (2) with UVA irradiation was observed, but despite its relatively high DNA affinity, it was incomplete (~12%).

Acknowledgements

The Greek General Secretariat of Research and Technology is thanked for financial support through the bilateral Greek–Czech Research Program (2005–2008, no. 216).

References

- 1 M. J. Clarke, F. C. Zhu and D. R. Frasca, *Chem. Rev.*, 1999, **99**, 2511.
- 2 W. H. Ang and P. J. Dyson, *Eur. J. Inorg. Chem.*, 2006, 4003.
- 3 P. J. Dyson and G. Sava, *Dalton Trans.*, 2006, 1929.
- 4 K. Strohsfeldt and M. Tacke, *Chem. Soc. Rev.*, 2008, **37**, 1174.
- 5 C. G. Hartinger and P. J. Dyson, *Chem. Soc. Rev.*, 2009, **38**, 391.
- 6 J. M. Rademaker-Lakhai, D. van den Bongard, D. Pluim, J. H. Beijnen and J. H. M. Schellens, *Clin. Cancer Res.*, 2004, **10**, 3717.
- 7 C. G. Hartinger, M. A. Jakupc, S. Zorbas-Seifried, M. Groessl, A. Egger, W. Berger, H. Zorbas, P. J. Dyson and B. K. Keppler, *Chem. Biodiversity*, 2008, **5**, 2140.
- 8 W. Kandioller, C. G. Hartinger, A. A. Nazarov, C. Bartel, M. Skocic, M. A. Jakupc, V. B. Arion and B. K. Keppler, *Chem.–Eur. J.*, 2009, **15**, 12283.
- 9 T. Bugarcic, O. Novakova, A. Halamikova, L. Zerzankova, O. Vrana, J. Kasparkova, A. Habtemariam, S. Parsons, P. J. Sadler and V. Brabec, *J. Med. Chem.*, 2008, **51**, 5310.
- 10 M. Melchart, A. Habtemariam, O. Novakova, S. A. Moggach, F. P. A. Fabbiani, S. Parsons, V. Brabec and P. J. Sadler, *Inorg. Chem.*, 2007, **46**, 8950.
- 11 O. Novakova, J. Kasparkova, V. Bursova, C. Hofr, M. Vojtkova, H. M. Chen, P. J. Sadler and V. Brabec, *Chem. Biol.*, 2005, **12**, 121.
- 12 O. Novakova, H. M. Chen, O. Vrana, A. Rodger, P. J. Sadler and V. Brabec, *Biochemistry*, 2003, **42**, 11544.
- 13 A. Bergamo, A. Masi, A. F. A. Peacock, A. Habtemariam, P. J. Sadler and G. Sava, *J. Inorg. Biochem.*, 2010, **104**, 79.
- 14 F. Wang, H. M. Chen, S. Parsons, L. D. H. Oswald, J. E. Davidson and P. J. Sadler, *Chem.–Eur. J.*, 2003, **9**, 5810.
- 15 G. A. Neyhart, N. Grover, S. R. Smith, W. A. Kalsbeck, T. A. Fairley, M. Cory and H. H. Thorp, *J. Am. Chem. Soc.*, 1993, **115**, 4423.
- 16 A. Jain, C. Slebodnick, B. S. J. Winkel and K. J. Brewer, *J. Inorg. Biochem.*, 2008, **102**, 1854.
- 17 V. G. Vaidyanathan and B. U. Nair, *Dalton Trans.*, 2005, 2842.
- 18 K. D. Copeland, A. M. K. Lueras, E. D. A. Stemp and J. K. Barton, *Biochemistry*, 2002, **41**, 12785.
- 19 K. D. Copeland, M. P. Fitzsimons, R. P. Houser and J. K. Barton, *Biochemistry*, 2002, **41**, 343.
- 20 H. A. Wagenknecht, E. D. A. Stemp and J. K. Barton, *J. Am. Chem. Soc.*, 2000, **122**, 1.
- 21 A. Myari, N. Hadjiliadis, A. Garoufis, J. Malina and V. Brabec, *JBIC, J. Biol. Inorg. Chem.*, 2007, **12**, 279.
- 22 A. Myari, N. Hadjiliadis and A. Garoufis, *Bioinorg. Chem. Appl.*, 2005, **3**, 109.
- 23 A. Myari, N. Hadjiliadis and A. Garoufis, *J. Inorg. Biochem.*, 2005, **99**, 616.
- 24 A. Myari, N. Hadjiliadis and A. Garoufis, *Eur. J. Inorg. Chem.*, 2004, 1427.
- 25 K. Karidi, A. Garoufis, N. Hadjiliadis and J. Reedijk, *Dalton Trans.*, 2005, 728.
- 26 K. Triantafillidi, K. Karidi, J. Malina and A. Garoufis, *Dalton Trans.*, 2009, 6403.
- 27 K. Karidi, J. Reedijk, N. Hadjiliadis and A. Garoufis, *J. Inorg. Biochem.*, 2007, **101**, 1483.
- 28 A. Garoufis, J. G. Liu, L. N. Ji and N. Hadjiliadis, *J. Inorg. Biochem.*, 2003, **93**, 221.
- 29 B. P. Sullivan, J. M. Calvert and T. J. Meyer, *Inorg. Chem.*, 1980, **19**, 1404.
- 30 W. D. Wilson, F. A. Tanios, M. Fernandez-Saiz, C. T. Rigl, in: *Methods in Molecular Biology*, ed. K. R. Fox, Humana Press, Clifton, NJ, USA, 1997, vol. 90.
- 31 Promega, Protocols and Applications.
- 32 M. A. Lemaire, A. Schwartz, A. R. Rahmouni and M. Leng, *Proc. Natl. Acad. Sci. U. S. A.*, 1991, **88**, 1982.
- 33 V. Brabec and M. Leng, *Proc. Natl. Acad. Sci. U. S. A.*, 1993, **90**, 5345.
- 34 M. V. Keck and S. J. Lippard, *J. Am. Chem. Soc.*, 1992, **114**, 3386.
- 35 J. Malina, O. Novakova, B. K. Keppler, E. Alessio and V. Brabec, *JBIC, J. Biol. Inorg. Chem.*, 2001, **6**, 435.
- 36 G. M. Bryant, J. E. Fergusson and H. K. J. Powell, *Aust. J. Chem.*, 1971, **24**, 257.
- 37 C. M. Hartshorn, K. A. Maxwell, P. S. White, J. M. DeSimone and T. J. Meyer, *Inorg. Chem.*, 2001, **40**, 601.
- 38 C. S. Allardyce, P. J. Dyson, D. J. Ellis and S. L. Heath, *Chem. Commun.*, 2001, 1396.
- 39 C. Sclaro, C. G. Hartinger, C. S. Allardyce, B. K. Keppler and P. J. Dyson, *J. Inorg. Biochem.*, 2008, **102**, 1743.
- 40 M. Mikola and J. Arpalahti, *Inorg. Chem.*, 1994, **33**, 4439.
- 41 N. Marti, G. H. B. Hoa and J. Kozelka, *Inorg. Chem. Commun.*, 1998, **1**, 439.
- 42 C. Schildkraut and S. Lifson, *Biopolymers*, 1965, **3**, 195.
- 43 R. Zaludova, V. Kleinwachter and V. Brabec, *Biophys. Chem.*, 1996, **60**, 135.
- 44 Y. F. Long, Q. G. Liao, C. Z. Huang, J. Ling and Y. F. Li, *J. Phys. Chem. B*, 2008, **112**, 1783.
- 45 Y. M. Zhao, W. J. He, P. F. Shi, J. H. Zhu, L. Qiu, L. P. Lin and Z. J. Guo, *Dalton Trans.*, 2006, 2617.
- 46 A. M. Liquori, L. Costantino, V. Crescenzi, V. Elia, E. Giglio, R. Puliti, M. De, Santis Savino and V. Vitagliano, *J. Mol. Biol.*, 1967, **24**, 113.
- 47 C. Zimmer and U. Wahnert, *Prog. Biophys. Mol. Biol.*, 1986, **47**, 31.
- 48 G. Luck, C. Zimmer, K. E. Reinert and F. Arcamone, *Nucleic Acids Res.*, 1977, **4**, 2655.
- 49 G. Burckhardt, C. Zimmer and B. Baguley, *J. Biomol. Struct. Dyn.*, 1987, **4**, 813.
- 50 Y. Nakabayashi, H. Inada, Y. Minoura, N. Iwamoto and O. Yamauchi, *Inorg. Chim. Acta*, 2009, **362**, 869.
- 51 E. Corral, A. C. G. Hotze, H. den Dulk, A. Leczkowska, A. Rodger, M. J. Hannon and J. Reedijk, *JBIC, J. Biol. Inorg. Chem.*, 2009, **14**, 439.
- 52 J. Malina, M. J. Hannon and V. Brabec, *Chem.–Eur. J.*, 2008, **14**, 10408.
- 53 E. Moldrheim, M. J. Hannon, I. Meistermann, A. Rodger and E. Sletten, *JBIC, J. Biol. Inorg. Chem.*, 2002, **7**, 770.

- 54 I. Meistermann, V. Moreno, M. J. Prieto, E. Moldrheim, E. Sletten, S. Khalid, P. M. Rodger, J. C. Peberdy, C. J. Isaac, A. Rodger and M. J. Hannon, *Proc. Natl. Acad. Sci. U. S. A.*, 2002, **99**, 5069.
- 55 M. J. Hannon, V. Moreno, M. J. Prieto, E. Moldrheim, E. Sletten, I. Meistermann, C. J. Isaac, K. J. Sanders and A. Rodger, *Angew. Chem. Int. Ed.*, 2001, **40**, 880.
- 56 Y. Parajo, J. Malina, I. Meistermann, G. J. Clarkson, M. Pascu, A. Rodger, M. J. Hannon and P. Lincoln, *Dalton Trans.*, 2009, 4868.
- 57 A. Rodger and B. Norden, *Circular and Linear Dichroism*, 1997, Oxford: Oxford University Press.
- 58 W. Keller, *Proc. Natl. Acad. Sci. U. S. A.*, 1975, **72**, 2550.
- 59 O. Novakova, J. Kasparkova, O. Vrana, P. M. Vanvliet, J. Reedijk and V. Brabec, *Biochemistry*, 1995, **34**, 12369.
- 60 S. Steinkopf, A. Garoufis, W. Nerdal and E. Sletten, *Acta Chem. Scand.*, 1995, **49**, 495.
- 61 A. Anagnostopoulou, E. Moldrheim, N. Katsaros and E. Sletten, *JBIC, J. Biol. Inorg. Chem.*, 1999, **4**, 199.
- 62 F. Zobi, M. Hohl, W. Zimmermann and R. Alberto, *Inorg. Chem.*, 2004, **43**, 2771.
- 63 A. Garoufis, G. Malandirinos and N. Hadjiliadis, *Eur. J. Inorg. Chem.*, 2004, 3326.
- 64 C. M. Dupureur and J. K. Barton, *Inorg. Chem.*, 1997, **36**, 33.
- 65 J. Kasparkova, O. Novakova, O. Vrana, N. Farrell and V. Brabec, *Biochemistry*, 1999, **38**, 10997.
- 66 A. Juris, V. Balzani, F. Barigelletti, S. Campagna, P. Belser and A. Vonzelewsky, *Coord. Chem. Rev.*, 1988, **84**, 85.

6.

Energetics, Conformation, and Recognition of DNA Duplexes Modified by Monodentate Ru^{II} Complexes Containing Terphenyl Arenes

Olga Novakova,^[a] Jaroslav Malina,^[a] Tereza Suchankova,^[b] Jana Kasparkova,^[a]
Tijana Bugarcic,^[c] Peter J. Sadler,^[c] and Viktor Brabec^{*,[a]}

Abstract: We studied the thermodynamic properties, conformation, and recognition of DNA duplexes site-specifically modified by monofunctional adducts of Ru^{II} complexes of the type [Ru^{II}(η^6 -arene)(Cl)(en)]⁺, in which arene = *para*-, *meta*-, or *ortho*-terphenyl (complexes **1**, **2**, and **3**, respectively) and en = 1,2-diaminoethane. It has been shown (*J. Med. Chem.* **2008**, *51*, 5310) that **1** exhibits promising cytotoxic effects in human tumor cells, whereas **2** and **3** are much less cytotoxic; concomitantly with the high cytotoxicity of **1**, its DNA binding mode involves combined intercalative and monofunctional (coordination) binding modes, whereas less cytotoxic compounds **2** and **3** bind to DNA only through a monofunctional coordination to DNA bases. An

analysis of conformational distortions induced in DNA by adducts of **1** and **2** revealed more extensive and stronger distortion and concomitantly greater thermodynamic destabilization of DNA by the adducts of nonintercalating **2**. Moreover, affinity of replication protein A to the DNA duplex containing adduct of **1** was pronouncedly lower than to the adduct of **2**. On the other hand, another damaged-DNA-binding protein, xeroderma pigmentosum protein A, did not recognize the DNA adduct of **1** or **2**. Importantly, the adducts of **1** induced a considerably

lower level of repair synthesis than the adducts of **2**, which suggests enhanced persistence of the adducts of the more potent and intercalating **1** in comparison with the adducts of the less potent and nonintercalating **2**. Also interestingly, the adducts of **1** inhibited DNA polymerization more efficiently than the adducts of **2**, and they could also be bypassed by DNA polymerases with greater difficulty. Results of the present work along with those previously published support the view that monodentate Ru^{II} arene complexes belong to a class of anticancer agents for which structure–pharmacological relationships might be correlated with their DNA-binding modes.

Keywords: arenes • calorimetry • DNA • DNA recognition • ruthenium

Introduction

Ruthenium complexes have attracted much interest as alternative drugs to cisplatin (*cis*-diamminedichloridoplatinum(II)) and its analogues in cancer chemotherapy. Organometallic Ru^{II}–arene complexes of the type [Ru^{II}(η^6 -arene)(Cl)(en)]⁺[PF₆[−]] (en = 1,2-diaminoethane) constitute a relatively new group of anticancer compounds.^[1–4] These monodentate complexes appear to be novel anticancer agents with a mechanism of action different from those of platinum and other ruthenium complexes that have been tested for antitumor activity. Although the pharmacological target for antitumor ruthenium compounds has not been unequivocally identified, there is a large body of evidence indicating that the cytotoxicity of several ruthenium complexes correlates with their ability to bind DNA,^[5] although several exceptions have been reported.^[6,7] Because the Ru^{II}–arene complexes bind strongly to DNA,^[8–15] DNA modifications

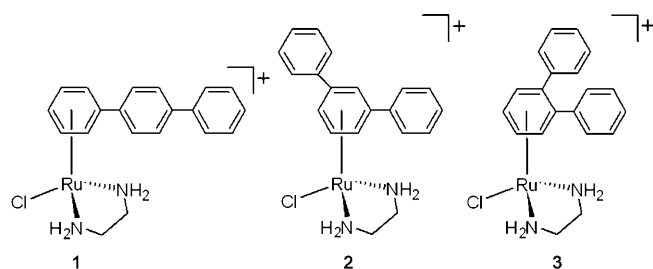
[a] Dr. O. Novakova, Dr. J. Malina, Dr. J. Kasparkova,
Prof. Dr. V. Brabec
Institute of Biophysics
Academy of Sciences of the Czech Republic, v.v.i., Kralovopolska 135
61265 Brno (Czech Republic)
Fax: (+420) 541240499
E-mail: brabec@ibp.cz

[b] T. Suchankova
Laboratory of Biophysics
Department of Experimental Physics, Faculty of Sciences
Palacky University
771 46 Olomouc (Czech Republic)

[c] Dr. T. Bugarcic, Prof. Dr. P. J. Sadler
Department of Chemistry
University of Warwick
Coventry CV4 7AL (UK)

Supporting information for this article is available on the WWW
under <http://dx.doi.org/10.1002/chem.200903078>.

and the downstream effects of these modifications are of great interest. It has been shown that Ru^{II} -arene complexes of the type $[\text{Ru}^{\text{II}}(\eta^6\text{-arene})(\text{Cl})(\text{en})][\text{PF}_6]$ can form monofunctional adducts with DNA at guanine residues. Some of these Ru^{II} complexes, in particular those containing multi-ring arenes, bind to DNA not only through coordination to the N7 atoms of guanine (G), but also noncovalently through hydrophobic interactions between the arene and DNA.^[9,10,13] These hydrophobic interactions might include intercalation of the noncoordinated arenes between DNA bases and minor-groove binding.



Recently, new complexes of the type $[\text{Ru}^{\text{II}}(\eta^6\text{-arene})(\text{Cl})(\text{en})]^+$ (arene = *ortho*-, *meta*-, or *para*-terphenyl) have been synthesized to investigate the effect on cytotoxicity and DNA binding of structural isomerization of the multi-ring terphenyl arene ligand.^[13] Importantly, the complex containing *para*-terphenyl as the arene ligand (complex **1**) exhibits promising cytotoxic effects in several human tumor cell lines, including those resistant to conventional cisplatin. In contrast, complexes containing *meta*- or *ortho*-terphenyl arene ligands (complexes **2** and **3**, respectively) are much less cytotoxic. Complexes **1** and **2** were selected for an initial study focused on global modification of natural, high-molecular-mass DNA.^[13] The results of this study have revealed that, concomitant with the relatively high cytotoxicity of **1** in tumor cells, its DNA-binding mode involves combined intercalative and monofunctional (coordination) binding modes. In contrast, complex **2**, which is much less cytotoxic, binds to DNA through only a monofunctional coordination to DNA bases. Therefore, the results of our initial work^[13] have further supported the view that the presence of the arene ligand in $[\text{Ru}^{\text{II}}(\eta^6\text{-arene})(\text{Cl})(\text{en})]^+$ complexes capable of noncovalent, hydrophobic interaction with DNA considerably enhances cytotoxicity in tumor cell lines.

Herein, we have studied the thermodynamic properties, conformation, and recognition of DNA duplexes uniquely and site-specifically modified by the two monodentate Ru^{II} -arene complexes $[\text{Ru}^{\text{II}}(\text{Cl})(\text{en})(\eta^6\text{-}p\text{-terphenyl})]^+$ (**1**) and $[\text{Ru}^{\text{II}}(\text{Cl})(\text{en})(\eta^6\text{-}m\text{-terphenyl})]^+$ (**2**) to elucidate in detail the DNA-binding mode of these Ru^{II} arene complexes. We compare previously obtained cytotoxicity data^[13] with new data obtained in the present work on conformational distortions induced by single, site-specific monofunctional adducts of the Ru^{II} in short oligodeoxyribonucleotide duplexes, associated alterations in the thermodynamic stability of these du-

plexes, recognition and repair of these adducts by two specific proteins, that is, the important factors that modulate the antitumor effects of antitumor metallodrugs already used in clinic.

Results

Differential scanning calorimetry (DSC) and thermal stability of ruthenated DNA duplexes: Previous studies have demonstrated that DSC is a very useful tool to characterize the thermodynamic stability of DNA duplexes containing adducts of various antitumor metallodrugs.^[10,16–25] Therefore, our initial studies characterizing the effect of the monofunctional adducts of complexes **1** and **2** on the thermal stability and energetics of DNA duplexes were performed by using DSC. As in our previous studies, we analyzed the 15 bp DNA duplex CAL (its nucleotide sequence is shown in Figure 1D) site-specifically modified by complexes **1** or **2**. DSC makes it possible to measure excess heat capacity versus temperature profiles for the thermally induced transitions of nonmodified DNA duplexes and those containing a unique adduct of the metal-based drug. Thermograms were recorded with the heating rate of 60 K h^{-1} , and after reaching the maximum temperature of 368 K, the samples were cooled at the same rate to the starting temperature of 288 K. Inspection of the thermograms of the ruthenated duplexes revealed that the first scans differed markedly from the following scans, which were superimposable with the melting profile of the nonmodified duplex. The duplexes containing unique Ru^{II} adducts were exposed to higher temperatures during the first scan for a relatively long period of time (for instance, for 90 min to temperatures $\geq 323 \text{ K}$). A plausible explanation of the DSC results might be that the adducts of complexes **1** and **2** were unstable at higher temperatures (Ru^{II} complexes dissociated from their DNA-binding sites during the first scan so that the following melting profiles coincided with that of the nonmodified duplex). Therefore, we first verified the stability of the adducts of complexes **1** and **2** at various temperatures. Consistent with previous findings,^[26] we found that these adducts formed in the duplex CAL were stable for more than 12 h only at temperatures lower than 333 K. Therefore, it is apparent that DSC cannot be used to analyze duplexes containing the adducts of these two Ru^{II} arene complexes.

Isothermal titration calorimetry (ITC): ITC represents a suitable alternative that makes it possible to study the thermodynamic parameters of the duplex formation from its two complementary single strands over a range of temperatures, including relatively low temperatures at which the DNA adducts of Ru^{II} arene compounds are stable for long enough to complete the ITC experiment. Representative examples of ITC profiles of duplex CAL formation from its nonmodified bottom strand titrated into the complementary nonmodified top strand or into the same strand containing a single monofunctional adduct of **1** or **2** at 293 K are depicted

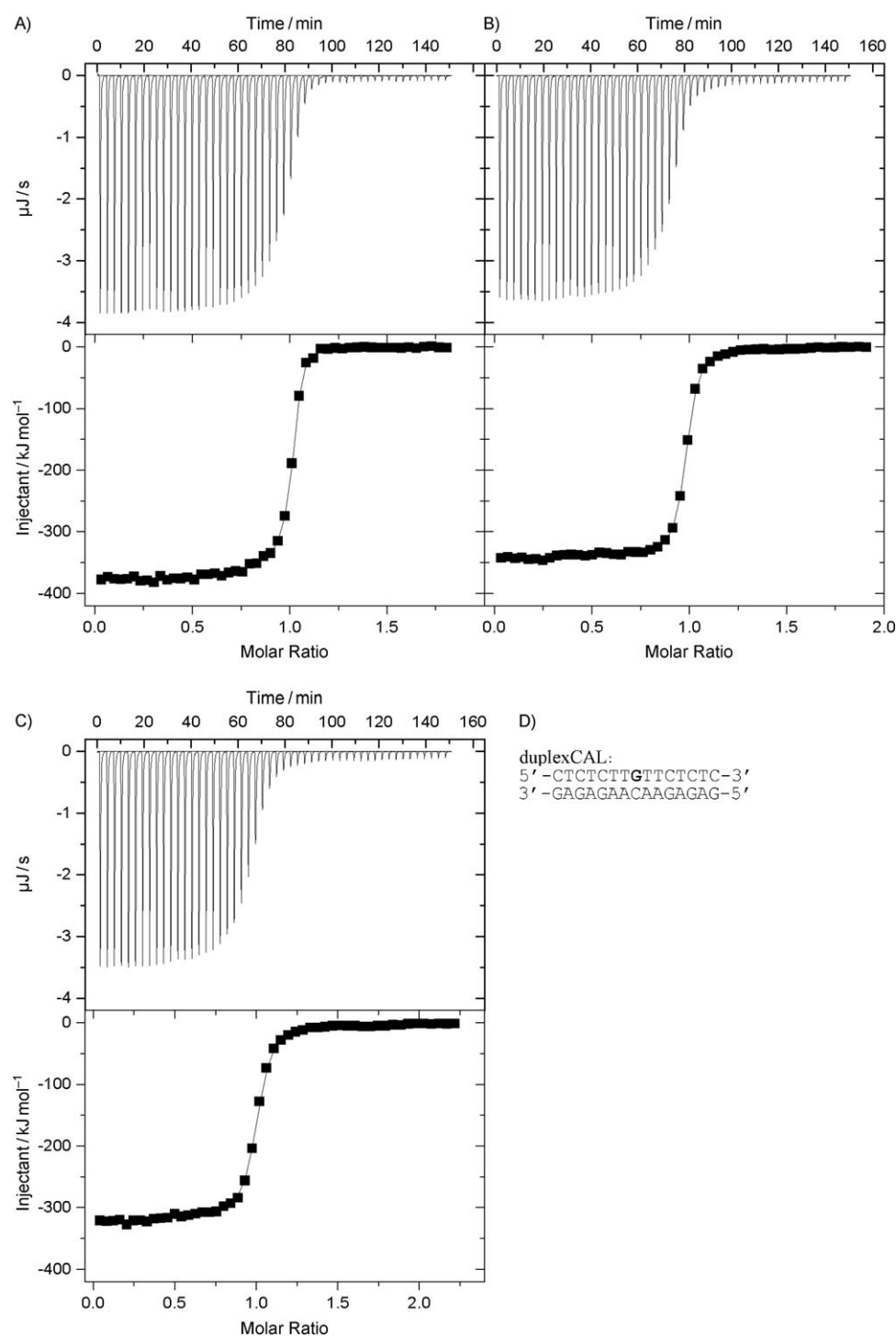


Figure 1. ITC binding isotherms for the association of the top strand of the 15 bp duplexCAL (nucleotide sequence shown in D) for A) nonmodified duplex and B,C) a duplex containing a single, monofunctional adduct of **1** or **2**, respectively, with the complementary (nonmodified) strand (bottom strand at 293 K) in phosphate buffer (10 mM, pH 7.0) containing NaCl (50 mM). The upper panels in A)–C) show the total heat released upon injecting 5 μ L aliquots of the bottom strand (50 μ M) into a 1.4 mL reaction cell containing the top strand (5 μ M). The lower panels show the resultant binding isotherms (■) obtained by integrating the peak areas of each injection; — represents the nonlinear least squares fit of the enthalpy change (ΔH), entropy change (ΔS), stoichiometry (n), and equilibrium constant (K) for strand association to a single-site binding model. For other details, see the text. D) Sequence of the 15 bp duplexCAL used in the calorimetric experiments; the central G residue in the top strand indicates the location of the monofunctional adduct of the Ru^{II} arene complex.

in Figure 1A, B, and C, respectively. The same measurements were performed also at 298, 303, and 310 K. The ITC profiles were analyzed to obtain the thermodynamic parameters listed in Table 1. Thermodynamic data for the association of strands modified by **2** at 310 K could not be obtained because the presence of the monofunctional adduct of this Ru^{II}–arene complex lowered the melting temperature of the duplexCAL so that the duplex partially melted at 310 K. Figure 2 shows the dependence of the thermodynamic parameters K , ΔH , $T\Delta S$, and ΔG on the temperature.

The values of ΔH (Figure 2B) and $T\Delta S$ (Figure 2C) obtained for association of complementary non-modified strands of duplexCAL were almost independent of the temperature. Consequently ΔG (Figure 2D), calculated by using the standard thermodynamic relationship $\Delta G = \Delta H - T\Delta S$, increased only slightly with increasing temperature from $-46.9 \text{ kJ mol}^{-1}$ at 293 K to $-43.1 \text{ kJ mol}^{-1}$ at 310 K. The equilibrium constant for the strand association (K) depended strongly on the temperature and decreased steeply with increasing temperature from $2.26 \times 10^8 \text{ M}^{-1}$ at 293 K to $1.74 \times 10^7 \text{ M}^{-1}$ at 310 K, which is more than an order of magnitude over a 17 K temperature range.

Inspection of the thermodynamic parameters revealed that the exothermic formation of the single monofunctional adduct in the duplexCAL by complexes **1** and **2** enthalpically destabilized the duplexCAL relative to its nonmodified counterpart at 293 K ($\Delta\Delta H = 38.0$ and 58.2 kJ mol^{-1} , respectively). In addition, the formation of monofunctional adducts by **1** and **2** resulted in a substantial increase in the entropy

Table 1. Calorimetrically derived thermodynamic parameters for the formation of the 15 bp duplexCAL unmodified or containing a single site-specific monofunctional adduct of **1** or **2** at 293, 298, 303, and 310 K.^[a]

	ΔH [kJ mol ⁻¹]	$T\Delta S$ [kJ mol ⁻¹]	ΔG [kJ mol ⁻¹]	K [M ⁻¹]	n	$\Delta\Delta H$ [kJ mol ⁻¹]	$T\Delta\Delta S$ [kJ mol ⁻¹]	$\Delta\Delta G$ [kJ mol ⁻¹]
293 K								
control	-379.2	-332.3	-46.9	2.26×10^8	0.98			
1	-341.2	-294.6	-46.6	1.96×10^8	0.98	38.0	37.7	0.3
2	-321.0	-276.0	-45.0	9.77×10^7	0.99	58.2	56.3	1.9
298 K								
control	-378.0	-331.6	-46.5	1.36×10^8	1.00			
1	-343.9	-298.0	-46.0	1.11×10^8	0.99	34.1	33.6	0.5
2	-322.9	-279.6	-43.3	3.70×10^7	1.00	55.1	52.0	3.2
303 K								
control	-376.9	-331.8	-45.2	5.76×10^7	1.00			
1	-346.9	-302.4	-44.5	4.45×10^7	1.00	30.0	29.4	0.7
2	-324.9	-283.7	-41.2	1.24×10^7	0.98	52.0	48.1	4.0
310 K								
control	-379.1	-336.0	-43.1	1.74×10^7	0.99			
1	-351.9	-308.0	-43.9	2.42×10^7	0.98	27.2	28.0	-0.8

[a] ΔH , ΔS , and ΔG denote the enthalpy, entropy, and free energy (at corresponding temperature), respectively, of duplex formation. K and n denote the association constant and binding stoichiometry, respectively, for strand association. $\Delta\Delta$ parameters are computed by subtracting the appropriate value measured for the control, unmodified duplex from the value measured for the duplex containing the single, site-specific ruthenium adduct.

of the duplexCAL ($T\Delta\Delta S = 37.7$ and 56.3 kJ mol⁻¹, respectively). In other words, the monofunctional adducts of **1** and **2** increased the entropy of the ruthenated duplexes and, in this way, entropically stabilized the duplex. Thus, the enthalpic destabilization of the duplexCAL due to the monofunctional adduct of **1** and **2** is partially, but not completely, compensated by the entropic stabilization of the duplex induced by these adducts. The net result of these enthalpic and entropic effects is that the formation of the monofunc-

tionally adducts of **1** and **2** with the duplexCAL induced a decrease of duplex thermodynamic stability at 293 K ($\Delta\Delta G$) of 0.3 and 1.9 kJ mol⁻¹, respectively, with this destabilization being enthalpic in origin. However, the effect of monofunctional adducts of **1** and **2** on the thermodynamic stability of the duplex changed with increasing temperature.

The enthalpic destabilization ($\Delta\Delta H$) of duplexCAL induced by adduct formation with **1** decreased with increasing temperature from 38.0 kJ mol⁻¹ at 293 K to 27.2 kJ mol⁻¹ at 310 K. The entropic stabilization ($T\Delta\Delta S$) compensating the enthalpic destabilization also decreased from 37.7 to 28.0 kJ mol⁻¹ over this temperature range. The net result of these enthalpic and entropic effects was that the presence of the monofunctional adduct of **1** had little effect on the thermodynamic stability (ΔG) of duplexCAL. The values of $\Delta\Delta G$ were 0.3, 0.5, 0.7, and -0.8 kJ mol⁻¹ at 293, 298, 303, and 310 K, respectively. The slope of the linear least-squares fit to the dependence of the binding enthalpy (ΔH) on the temperature in Figure 2B gave a negative heat capacity change for duplexCAL formation, ΔC_p , of (-632 ± 29) J K⁻¹ mol⁻¹. The values of the association constant (K) were very close to the association constants of the nonmodified strands at all temperatures. Interestingly, at 310 K the association constant K reached a value of 2.42×10^7 M⁻¹, which was only slightly higher than that of nonmodified strands (1.74×10^7 M⁻¹). The entropic stabilization at 310 K ($T\Delta\Delta S = 28.0$ kJ mol⁻¹) was higher than the enthalpic destabilization ($\Delta\Delta H = 27.2$ kJ mol⁻¹), which implies that the adduct of **1** induced a slight increase in the thermodynamic stability of duplexCAL ($\Delta\Delta G = -0.8$ kJ mol⁻¹), with this stabilization being entropic in origin.

The adduct of duplexCAL with **2** behaved similarly to the duplex modified by **1**. The enthalpic destabilization ($\Delta\Delta H$) of duplexCAL induced by for-

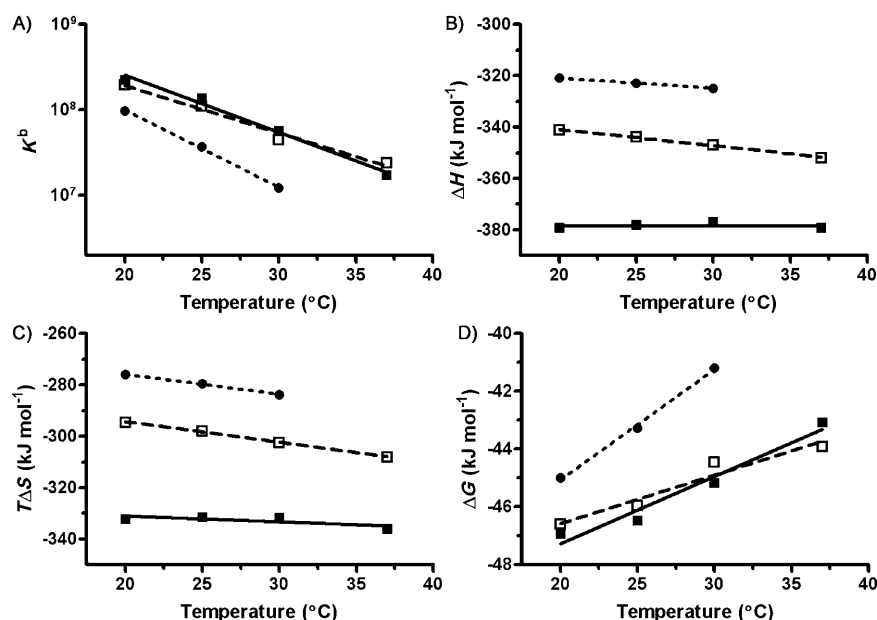


Figure 2. The variations in A) K , B) ΔH , C) $T\Delta S$, and D) ΔG with temperature. ■: control, nonmodified duplexCAL; □: duplexCAL containing monofunctional adduct of **1**; ●: duplexCAL containing monofunctional adduct of **2**. For other details, see Figure 1 and the text.

mation of an adduct with **2** decreased with increasing temperature. The entropic stabilization ($T\Delta\Delta S$) also decreased with temperature, but the reduction was more pronounced and resulted in a decrease in the thermodynamic stability ($\Delta\Delta G$) of the duplex with increasing temperature from 1.9 kJ mol^{-1} at 293 K to 4.0 kJ mol^{-1} at 303 K. The binding enthalpy (Figure 2B) exhibited a decrease with increase in temperature, giving a negative heat capacity change (ΔC_p) of $(-394 \pm 8) \text{ kJ K}^{-1} \text{ mol}^{-1}$. The association constants (K) range from $9.77 \times 10^7 \text{ M}^{-1}$ at 293 K to $1.24 \times 10^7 \text{ M}^{-1}$ at 303 K, which is approximately 2–4 times lower than the association constants of the non-modified strands.

Chemical probes for DNA conformation: We previously demonstrated that complexes **1** and **2** bind preferentially to G residues in natural double-helical DNA to form monofunctional adducts.^[13] To obtain information on how these adducts affect DNA conformation, oligonucleotide duplexes containing a site-specific monofunctional adduct of **1** or **2** at the G residue were further analyzed by chemical probes of DNA conformation. The ruthenated 15 bp duplex (duplex-CAL) was treated with two chemical agents, KMnO_4 and diethylpyrocarbonate (DEPC), which are used as tools for monitoring the existence of conformations other than canonical B DNA. They react preferentially with single-stranded DNA and distorted double-stranded DNA.^[27,28] For this analysis, we used exactly the same methodology as in our recent studies dealing with DNA adducts of various antitumor platinum drugs (for example, see refs. [28,29] for the details of this experiment), and representative gels showing piperidine-induced specific strand cleavage at KMnO_4 -modified and DEPC-modified bases in the unruthenated 15 bp duplex or the duplex-containing the single monofunctional adduct of **1** or **2** are illustrated in Figure S1 in the Supporting Information. The results are schematically summarized in Figure 3. The pattern and degree of reactivity toward the chemical probes found for the adducts of **1** and **2** indicate that the distortion induced by the adduct of complex **1** was markedly less extensive than that induced by the adduct of **2**.

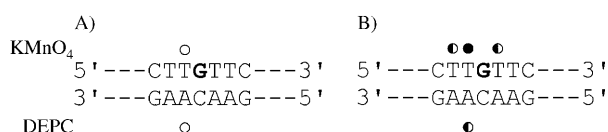


Figure 3. Summary of the reactivity of chemical probes with 15 bp duplex-CAL containing a monofunctional adduct of **1** (A) or **2** (B). Filled, half-filled, and empty circles designate strong, medium, and weak reactivity, respectively.

Recognition of the duplexes containing adducts of Ru^{II} -arene complexes by RPA and XPA proteins: Having characterized the effects of the monofunctional adducts of complexes **1** and **2** on thermodynamics of the DNA duplex-CAL, we have employed an electrophoretic mobility shift assay (EMSA) to determine how replication protein A (RPA) and

xeroderma pigmentosum group A protein (XPA) interact with DNA that has been damaged by these monofunctional adducts. Substrates (30 bp) were designed to contain a single, site-specific monofunctional adduct of **1** or **2** in the 15 bp central sequence, identical to that of the 15 bp duplex-CAL used for calorimetric measurements. The sequences in these longer 30 bp duplexes (duplexes-EMSA) on both sides of the central TGT sequences were chosen to contain only thymines and cytosines in the top strands and adenines and guanines in the bottom strands.

Under the conditions determined to minimize RPA binding to undamaged DNA,^[30] increasing concentrations of RPA were employed in an EMSA to examine duplexes-EMSA in the presence or absence of single, site-specific monofunctional adduct of **1** or **2** (Figure 4). Quantification

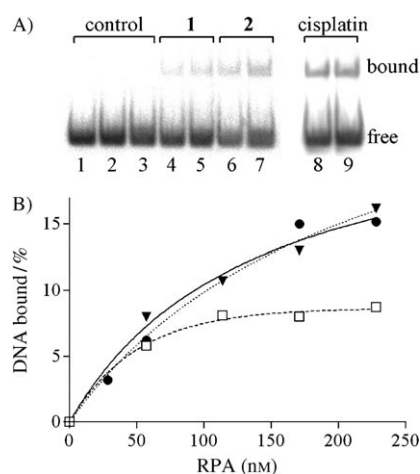


Figure 4. A) RPA binding of undamaged 30 bp duplexes-EMSA (lanes 1–3) or the duplexes-EMSA containing a monofunctional adduct of **1** (lanes 4, 5), **2** (lanes 6, 7), or 1,2-GG intrastrand crosslink of cisplatin (lanes 8, 9). EMSAs were performed by using no added RPA (lane 1), 171 nM RPA (lanes 2, 4, 6, and 8), or 228 nM RPA (lanes 3, 5, 7, and 9). The products were separated on 6% native polyacrylamide (PAA) and visualized by using autoradiography. B) Quantification of increasing concentrations of RPA binding to a duplex containing a 1,2-GG intrastrand crosslink of cisplatin (○) or a monofunctional adduct of **1** (□) or **2** (▼). The results are the average of two individual experiments.

of the gels (some representative reactions are shown Figure 4A) shows that RPA bound to the duplex-EMSA that contained the adduct of **1** with approximately half the affinity of that containing the adduct of **2** (Figure 4B). It was also verified (not shown) that RPA did not bind to the unmodified duplex-EMSA even at the highest concentration of the protein (228 nM) used in these experiments.

Results showing XPA protein binding to a duplex-EMSA identical to those used in the experiments demonstrating RPA binding are presented in Figure 5. Lanes 1–3 in Figure 5A represent the control undamaged duplex-EMSA and revealed only a very low level of XPA protein binding compared with the duplex containing a 1,2-GG intrastrand adduct of cisplatin in lanes 4–6. Quantification of the gels shows a 4.2-fold increase in XPA protein binding to the

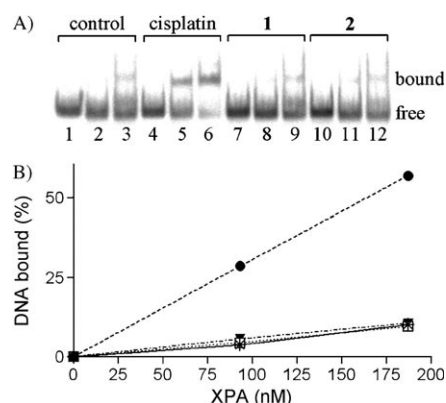


Figure 5. A) XPA binding of undamaged 30 bp duplexes EMSA (lanes 1–3), or the duplexes EMSA containing a 1,2-GG intrastrand crosslink of cisplatin (lanes 4–6) or a monofunctional adduct of **1** (lanes 7–9) or **2** (lanes 10–12). EMSAs were performed by using no added XPA (lanes 1, 4, 7, and 10), 93 nM XPA (lanes 2, 5, 8, and 11), or 187 nM XPA (lanes 3, 6, 9, and 12). The products were separated on 6% native PAA and visualized by autoradiography. B) Quantification of increasing concentrations of XPA binding to the undamaged duplex (*), the duplex containing a 1,2-GG intrastrand crosslink of cisplatin (●), a monofunctional adduct of **1** (□) or **2** (▼). The results are the average of two individual experiments.

duplex containing 1,2-intrastrand adduct of cisplatin compared with the undamaged control (Figure 5B). Interestingly, a very low binding of XPA protein was evident for the duplex EMSA containing a monofunctional adduct of **1** or **2** comparable to the unmodified duplex.

DNA repair synthesis by human cell extract: DNA repair efficiency in a pUC19 plasmid (2686 bp) globally modified by **1** or **2** at $r_b=0.03$ was tested by using cell-free extract (CFE) of repair-proficient HeLa cells (r_b is defined as the number of molecules of the Ru^{II}–arene complex bound per nucleotide residue). Repair activity was monitored by measuring the amount of incorporated radiolabeled nucleotide. The incorporation of radioactive material was corrected for the relative DNA content in each band. As illustrated in Figure 6, damage-induced DNA repair synthesis detected in the plasmid modified by **1** was only approximately 30% of that found for the plasmid modified by **2** at the same level of modification.

Inhibition of DNA polymerization: It has been demonstrated that DNA modifications by various transition-metal-based complexes have significant effects on the activity of a number of prokaryotic, eukaryotic, and viral DNA polymerases.^[31–37] Interestingly, for DNA templates containing site-specifically placed adducts of various platinum compounds, a number of prokaryotic and eukaryotic DNA polymerases are blocked, but others can traverse through platinum adducts depending on their character and conformational alterations induced in the DNA. It is, therefore, of great interest to examine whether DNA polymerases that process DNA substrates containing monofunctional adducts of **1** or **2** can reveal potential differences in alterations im-

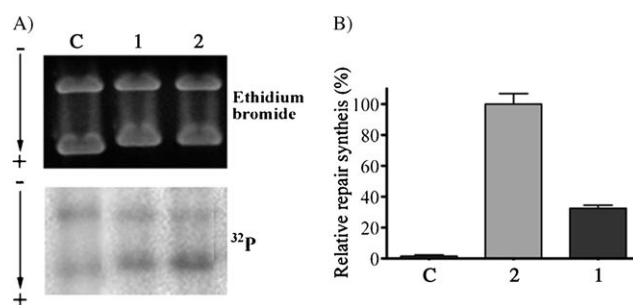


Figure 6. In vitro DNA repair synthesis assay of an extract prepared from the repair-proficient HeLa cell line. Repair synthesis used pBR322 plasmids (nonmodified) plus pUC19 plasmids (nonmodified (lane C) or modified at $r_b=0.03$ by **1** (lane 1) or **2** (lane 2)) as substrates. A) Results of a typical experiment. Top: a photograph of the EtBr-stained gel; bottom: an autoradiogram of the gel showing incorporation of [α -³²P]dCMP. B) Incorporation of dCMP into a nonmodified or ruthenated pUC19 plasmid. For all quantifications representing mean values of three separate experiments, incorporation of radioactive material is corrected for the relative DNA content in each band. The radioactivity associated with the incorporation of [α -³²P]dCMP into DNA modified by **1** was taken as 100%. Bars indicate the standard error of the mean (SEM).

posed on DNA by adducts of these two Ru^{II} arene complexes with different nonleaving arene ligands.

Herein, we investigate DNA polymerization by using templates site-specifically modified by the monofunctional adduct of **1** or **2** by using Klenow fragments from DNA polymerase I (exonuclease minus, mutated to remove the 3'→5' proofreading domain; KF[−]) as a model, which is a well-characterized enzyme frequently used in studies aimed at understanding the processes in which nucleic acid polymerases take part.

We constructed the 8-mer/23-mer primer–template duplexes (Figure 7) unruthenated or containing a single monofunctional adduct of the Ru^{II}–arene complex. The first eight nucleotides on the 3'-terminus of the 23-mer template strand were complementary to the nucleotides of the 8-mer primer so that the 3' guanine involved in the adduct on the template strand was located at the 14th position from the 3'-terminus (Figure 7A). After annealing the 8-nucleotide primer to the 3'-terminus of the unruthenated or ruthenated template strand (positioning the 3'-end of the primer five bases before the adduct in the template strand), we examined DNA polymerization through the adduct of **1** or **2** by using KF[−] in the presence of all four deoxyribonucleoside triphosphates (dNTPs). The reaction was stopped at various time intervals, and the products were analyzed by using a sequencing gel (Figure 7A). Polymerization by KF[−] of the 8-mer/23-mer primer templates containing the adduct of **1** or **2** in the presence of all four dNTPs proceeded rapidly up to the nucleotide opposite the ruthenated base, such that the 14-nucleotide intermediate products accumulated to a significant extent (shown in Figure 7A). In particular, there was an extensive accumulation of full-length (23-nucleotide) products from the templates containing the adduct of **2** (Figure 7A, lanes 11–15, and Figure 7B), whereas considerably lower accumulation of full-length products was seen with

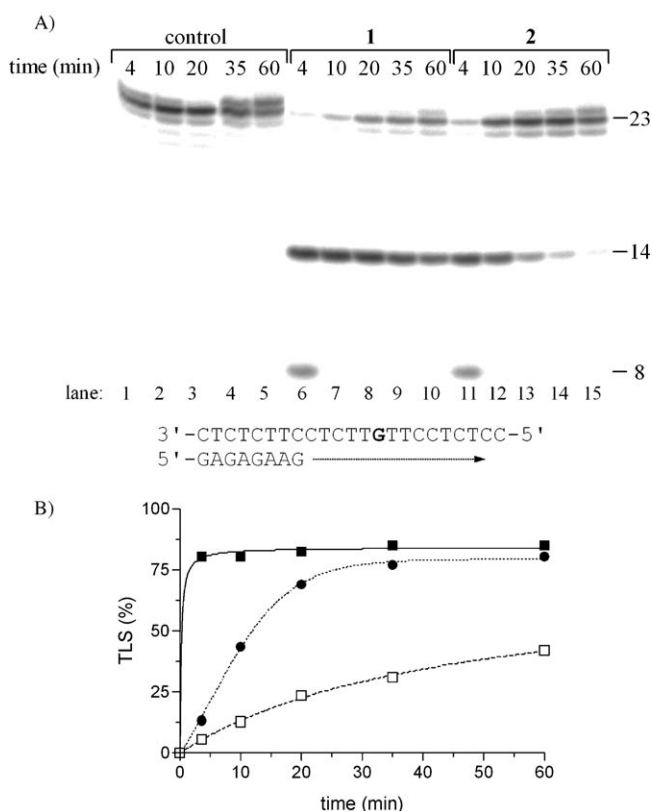


Figure 7. Primer extension activity of KF^- . The experiments were conducted by using the 8-mer/23-mer (“running start” experiment) primer-template duplex for the times indicated. This duplex was unruthenated or contained a single, monofunctional adduct formed by **1** or **2** at the G residue in the TGT sequence. The nucleotide sequences of the templates and the primers are shown below the gels; see the text for details. A) The strong band marked 8 corresponds to the 8-mer primer, the strong pause site opposite the ruthenated guanine is marked 14, and the bands marked 23 correspond to the full-length products. B) The time dependence of the inhibition of DNA synthesis on undamaged (control) template (■), DNA containing the adduct of **1** (□) or **2** (●). Data are means (\pm SEM) from three different experiments with two independent template preparations.

the template containing the adduct of **1** (Figure 7A, lanes 6–10, and Figure 7B). Only full-length products and no intermediates were seen with the 23-mer unruthenated control template (shown in Figure 7A, lanes 1–5).

Discussion

We have demonstrated in our recent work^[13] that the DNA-binding mode of organometallic complex **1**, which is cytotoxic towards tumor cell lines and contains *para*-terphenyl as an arene ligand, involves combined intercalative and monofunctional (coordination) binding, whereas the markedly less cytotoxic complex **2**, which contains a *meta*-terphenyl arene ligand, binds to DNA through mainly a monofunctional coordination to DNA bases. The pharmacological activity of several metallodrugs is modulated by the “downstream” effects of damaged DNA, such as recognition of damaged DNA by specific proteins and/or repair of this

damage.^[38,39] In addition, distortion of DNA conformation induced by metallodrugs and changes in the thermodynamic stability of DNA induced by the damage represent important factors that affect these “downstream” cellular events.^[17,23,40,41] Thus, to assess how these factors might assert themselves in the cellular processing of DNA damage induced by **1** and **2**, we characterized further DNA adducts of these two Ru^{II}-arene complexes by using chemical probes of DNA conformation and ITC. An analysis of conformational distortions induced in DNA by **1** and **2** revealed substantial differences in the character of these distortions. Their analysis by chemical probes of DNA conformation demonstrated (Figure 3) that the distortion induced by the nonintercalating **2** extended over at least 4 bp, whereas the distortion induced by **1** was markedly less extensive and weaker (Figure 3). Thus, these data suggest that the adducts of both **1** and **2** should thermodynamically destabilize DNA and if ruthenium is bound to the central phenyl ring as in **2**, the DNA should be destabilized significantly more than in the case when ruthenium is bound to a terminal phenyl ring as in **1**.

The results of the ITC analysis (Table 1) are consistent with these suggestions. The association constant K for the formation of duplexCAL was reduced markedly less by the adduct of intercalating complex **1** than by the adduct of nonintercalating complex **2** at all temperatures tested. A plausible explanation of this observation is that the intercalators thermodynamically stabilize DNA because they lengthen and unwind DNA, increasing the phosphate spacing along the helix axis.^[42,43] Also consistent with the intercalation of **1** and associated smaller thermodynamic destabilization of duplexCAL by the adduct of this complex is the observation that a heat capacity change for formation of the duplexCAL (ΔC_p) that contained an adduct of **1** was markedly more negative than that for formation of the duplexCAL that contained an adduct of **2** (-632 ± 29 vs. -394 ± 8) $\text{JK}^{-1} \text{mol}^{-1}$). The analysis in this study cannot address the origins of the observed changes in the ΔC_p values, but the main categories of potential sources can be discussed. One of the major factors responsible for a negative ΔC_p in macromolecular interactions is the burial of nonpolar surfaces upon folding (hydrophobic effect).^[44–46] Thus, in the case of formation of an adduct of duplexCAL with **1** or **2**, the burial of hydrophobic base residues and/or aromatic terphenyl ligands might be major forces that determine the extent of the negative heat capacity change for formation of this duplex. Thus, the less-negative value of ΔC_p found for the formation of the adduct of duplexCAL with **2** (compared with that of the adduct with **1**) might be due to the higher accessibility to water of: 1) base residues in the duplexCAL–**2** adduct as revealed by chemical probes of DNA conformation (Figure 3) and consistent with a lower thermodynamic stability of this duplex (Table 1); and/or 2) the nonintercalating aromatic *meta*-terphenyl arene ligand in the adduct with **2**.

Our results demonstrate that there is a distinct difference between the DNA binding modes of **1** and **2**, including the capability of their adducts to affect the conformation and

thermodynamic stability of DNA, and that this difference correlates with the difference in cytotoxicity between the two Ru^{II}–arene complexes.^[13] Damage to DNA in cells activates various “downstream” processes that determine biological effects of DNA-damaging agents. Recognition of DNA damage by specific proteins represents the initial step of these processes. The energetics and character of DNA damage can play an important role in defining protein–DNA affinity.^[16,47–49] Distortion of DNA has been shown to increase the binding affinity of some proteins,^[50,51] presumably by removing the thermodynamic penalty associated with deformation of the DNA double helix. Therefore, we were interested to know whether differences in the properties of DNA modified by **1** and **2** are also reflected by the affinity of DNA adducts of **1** and **2** for two proteins that exhibit distinctly different preferences for high-affinity interactions with damaged double-helical DNA.^[52] We examined the affinity of DNA duplexes containing single, site-specific adducts of **1** or **2** for XPA protein and RPA, which have been implicated in the recognition of damaged DNA in mammalian cells.^[53]

The results of the present work (Figure 4) demonstrate that the affinity of RPA for a DNA duplex adduct with **1** was markedly lower than for that containing the adduct with **2**. Concomitantly, the adducts of **1** were shown to distort and thermodynamically destabilize DNA much less than the adducts of **2** (Figure 3 and Table 1). Thus, these results are consistent with the known property of RPA, which preferentially binds to heavily distorted DNA, including DNA that contains single-stranded regions, when such a distortion is accompanied by an increased thermodynamic destabilization of DNA, but does not recognize backbone bending.^[23,52] On the other hand, XPA protein binds most efficiently to rigidly bent duplexes but not to single-stranded DNA.^[52,54] Thus, our observation (Figure 5) that XPA protein does not recognize the DNA adducts of **1** or **2**, but exhibits a high affinity for DNA containing a 1,2-GG intrastrand crosslink of cisplatin (which is known to rigidly bend DNA^[55]) apparently has a connection to the inability of monodentate **1** and **2** to rigidly bend DNA.

RPA protein, which discriminates between DNA modified by **1** and **2**, is an indispensable player in almost all DNA metabolic pathways, such as DNA replication, recombination, cell cycle, and DNA repair.^[56,57] Moreover, an important feature of the mechanism underlying the antitumor effects of DNA-binding metallodrugs is repair of their DNA adducts.^[38,39] A persistence of these DNA adducts might potentiate their antitumor effects in cells that are sensitive to these compounds.^[38,39,58,59] DNA repair synthesis was investigated in the present work by using the CFE from human tumor cells and DNA substrates randomly modified by **1** or **2** (Figure 6). Importantly, the adducts of **1** induced a considerably lower level of repair synthesis than the adducts of **2**; this suggests a less efficient removal from DNA and enhanced persistence of the adducts of the more potent and intercalating **1** in comparison with the adducts of less potent and nonintercalating **2**.

Also interestingly, the adducts of **1** inhibit DNA polymerization more efficiently than the adducts of **2** (Figure 7), and they are more difficult for DNA polymerases to bypass. Numerous studies have indicated that the level of DNA adduct tolerance, which has been correlated with the increased ability of DNA polymerases to replicate DNA past metal adducts, inversely correlates with sensitivity to other antitumor metallodrugs, such as platinum drugs.^[60,61] In other words, the sensitivity of tumor cells to metallodrugs can be enhanced as a consequence of a lowered adduct tolerance mediated by reduced ability of DNA polymerases to replicate past metal adducts. Herein, we find that DNA adducts of **1** impede elongation of DNA by a model prokaryotic DNA polymerase K⁺ to a markedly greater extent than those of **2** (Figure 7). Because there is a high degree of structural and sequence conservation of the domains among DNA polymerases,^[62] the results of the studies performed with the K⁺ should be also applicable to other (eukaryotic) DNA polymerases.^[63–65] Thus, the stronger inhibition of DNA polymerization by the adducts of **1** in comparison with the adduct of **2** might help identify additional factors that explain why the intercalation ability of the arene ligand in monodentate Ru^{II} arene complexes affects processes underlying biological effects of this class of metallodrugs. In addition, the stronger inhibition of DNA polymerization by the adducts of **1** might explain its enhanced cytotoxicity in comparison with **2**.^[13] This suggests that chemotherapy based on monodentate Ru^{II} complexes containing arenes that bind to DNA not only through coordination to G N7, but also noncovalently (through hydrophobic interactions between the arene and DNA), might be also less likely (compared with Ru^{II} complexes containing arene ligands incapable of the noncovalent binding) to induce secondary tumors.

Transition-metal-based compounds constitute a discrete class of chemotherapeutics that are widely used in the clinic as antitumor and antiviral agents.^[7,66,67] However, drug resistance and side effects have limited their clinical utility. These limitations have prompted a search for more effective and less toxic antitumor metallodrugs. As a part of this search, we and others have been systematically testing a hypothesis that new transition-metal-based drugs that bind to DNA in a fundamentally different manner from that of conventional metallodrugs already used in the clinic might have altered pharmacological properties. This hypothesis was formulated on the basis of the generally accepted fact that DNA is one of the major pharmacological targets of platinum antitumor drugs.^[68,69] Some of the efforts motivated by this hypothesis have been also directed toward the design of antitumor ruthenium complexes.^[4,70] Although the pharmacological target for antitumor ruthenium compounds has not been unequivocally identified, there is a large body of evidence indicating that the cytotoxicity of several ruthenium complexes in tumor cell lines correlates with the ability of these complexes to bind DNA and affect its properties and cellular processing in a specific way.^[5] Results of the present work along with those previously published^[8,10–15] further

support the view that monodentate Ru^{II}–arene complexes belong among antitumor ruthenium compounds for which the structure–pharmacological activity relationship may be formulated on the basis of their DNA binding mode. On the other hand, we cannot rule out possibility that the mechanism underlying the cytotoxic activity of monofunctional Ru^{II}–arene complexes involves factors not acting at the DNA level, although experimental data that might support this alternative are as yet lacking.

Experimental Section

Starting materials: Complexes **1** and **2** were prepared by methods described in detail previously.^[13] Cisplatin, glycogen, and dimethyl sulfate (DMS) were obtained from Sigma. The stock solutions of ruthenium and platinum complexes in H₂O (5×10^{-4} M) were prepared in the dark at 298 K. Plasmids pUC19 (2686 bp) and pBR322 (4363 bp) were isolated according to standard procedures. The synthetic oligodeoxyribonucleotides were purchased from VBC-Genomics (Vienna, Austria) and were purified as described previously.^[71] Restriction endonucleases, T4 polynucleotide kinase, KF[−], and bovine serum albumin were purchased from New England Biolabs GmbH (Frankfurt am Main, Germany). The N-terminal His6-tagged XPA protein was obtained by expressing the plasmid DNA pET15b/XPA template^[72] in RTS 500 *E. coli* HY (Roche) and purified on Ni²⁺–NTA agarose and by hydroxyapatite chromatography.^[52] Human recombinant RPA purified from *E. coli*^[73] was a kind gift from John J. Turchi. A CFE was prepared from the HeLa S3 cell line as described elsewhere.^[74,75] Acrylamide, agarose, bis(acrylamide), ethidium bromide (EtBr), urea, and NaCN were purchased from Merck. Creatine phosphokinase and creatine phosphate were purchased from MP Biochemicals (Irvine, USA). The radioactive products from Amersham were purchased from AP Czech, s.r.o. (Praha, Czech Republic).

Metalation of oligonucleotides: The single-stranded oligonucleotides (the top, pyrimidine-rich strands containing a single central G of the duplexCAL and duplexEMSA, or the template strand used in the studies of DNA polymerization) were reacted in stoichiometric amounts with either **1**, **2**, or cisplatin. The ruthenated or platinated oligonucleotides were purified by using ion-exchange HPLC. We verified that the modified oligonucleotides contained one ruthenium or platinum atom by using ruthenium or platinum flameless atomic absorption spectrophotometry (FAAS) and optical density measurements. We also verified that one molecule of ruthenium or platinum complex was coordinated to the N7 atom of the single G in the pyrimidine-rich strand by using DMS footprinting of ruthenium or platinum on DNA.^[76] The strands containing a single, central 1,2-GG intrastrand crosslink of cisplatin were prepared as described elsewhere.^[18] The nonmodified, ruthenated, or platinated duplexes used in the studies of recognition by XPA and RPA proteins were purified by electrophoresis on native 15% PAA gels (mono/bis[acrylamide] ratio = 29:1).

Microcalorimetry

Differential scanning calorimetry (DSC): Excess heat capacity (ΔC_p) vs. temperature profiles for the thermally induced transitions of DNA duplexes were measured by using a VP-DSC calorimeter (Microcal, Northampton, MA). In the DSC experiments, the concentrations of the duplexes were 30 μ M, the heating rate was 60 K h^{−1}, the maximum temperature was 368 K and the standard buffer for these studies contained NaCl (50 mM) with phosphate buffer (10 mM, Na₂HPO₄/NaH₂PO₄, pH 7.0). After reaching the maximum temperature, the samples were cooled at the same rate to the starting temperature of 288 K.

Isothermal titration calorimetry (ITC): Heat flow during isothermal titration was measured by using a VP-ITC microcalorimeter (MicroCal, Northampton, MA). The standard titration buffer for these studies contained NaCl (50 mM) with phosphate buffer (10 mM, Na₂HPO₄/NaH₂PO₄, pH 7.0). Stock solutions of the strands for ITC studies were prepared in

the standard titration buffer and were exhaustively dialyzed against this buffer. For each titration, a solution of the top strand of nonmodified duplexCAL (for the sequence, see Figure 1D) or that containing the single, site-specific monofunctional adduct of **1** or **2** (5×10^{-6} M) in the titration buffer was loaded into the 1.4 mL sample cell and maintained at the selected temperature. A solution of the bottom strand of duplexCAL (5×10^{-5} M) in the titration buffer was loaded into a 300 μ L injection syringe. The stirring rate of the injection syringe was 490 rpm and samples were thermally equilibrated until the baseline has leveled off prior to titration. A titration consisted of 50 injections of 5 μ L volume and 10 s duration, with 180 s between injections. It was verified that the enthalpies of ITC injections of each individual oligomer into buffer, of buffer into buffer, and of excess oligomer into a solution of duplex were all the same as water into water injections, within the error range. Data from individual titrations were analyzed by using the Origin 5.0 software package (Origin, Northampton, MA) and fitted to a single set of identical sites model to extract the relevant thermodynamic parameters (the enthalpy change (ΔH), entropy change (ΔS), stoichiometry (n), and equilibrium constant (K) for strand association).

Chemical probing of the DNA conformation: The modification of the ruthenated oligonucleotide 15 bp duplexCAL by KMnO₄ and DEPC was performed as described previously.^[28] The top or bottom strands of the oligonucleotide duplexes were 5′-end labeled with [γ -³²P]ATP and T4 polynucleotide kinase. In the case of the ruthenated oligonucleotides, the ruthenium complex was removed after reaction of the duplex with the probe by incubation with NaCN (0.2 M, pH 11) at 318 K for 10 h in the dark.

Reactions with XPA and RPA: ³²P-labeled DNA substrates (2.0 nM) and the indicated amounts of XPA or RPA were incubated at 293 K in 15 or 20 μ L reactions containing Hepes–KOH (25 mM, pH 8.3), KCl (30 mM), MgCl₂ (4 mM), EDTA (1 mM), dithiothreitol (0.9 mM), bovine serum albumin (45 μ g mL^{−1}), and glycerol (10%). To assess the binding at equilibrium, reactions were stopped after 30 min by cooling the samples to 273 K. Following addition of gel loading buffer (4 μ L) containing Tris–HCl (0.1 M, pH 8.3), glycerol (10%), and orange G (0.05%), the extent of binding was determined on native 6% PAA gels. Electrophoresis was performed for 50 min at 277 K.

DNA repair synthesis by human cell extract: Repair DNA synthesis of CFEs was assayed by using the pUC19 plasmid. Each reaction of 50 μ L contained nonmodified pBR322 (600 ng) and nonmodified or ruthenated pUC19 (r_0 = 0.03; 600 ng); ATP (2 mM); KCl (30 mM); creatine phosphokinase (rabbit muscle; 0.05 mg mL^{−1}); dGTP, dATP, and TTP (20 mM each); dCTP (8 mM); [α -³²P]dCTP (74 kBq) in the buffer composed of HEPES–KOH (40 mM, pH 7.5); MgCl₂ (5 mM); dithiothreitol (0.5 mM); creatine phosphate (22 mM); bovine serum albumin (1.4 mg mL^{−1}); and CFE from the HeLa S3 cells (20 mg). Reactions were incubated for 3 h at 303 K and terminated by adding EDTA (to a final concentration of 20 mM), SDS (0.6%), and proteinase K (250 μ g mL^{−1}), and then incubating for 20 min. The products were extracted with one volume of 1:1 phenol/chloroform. The DNA was precipitated from the aqueous layer by addition of 3 M NaOAc (0.1 volume) and EtOH (2.5 volumes). After 30 min of incubation at 253 K and centrifugation at 12000 g for 30 min at 277 K, the pellet was washed with 80% EtOH (0.2 mL) and dried in a vacuum centrifuge. The DNA was finally linearized prior to electrophoresis on a 1% agarose gel. The resulting gel was stained with EtBr. The experiments were made in quadruplicate.

Inhibition of DNA polymerization: The primer extension assays with all four dNTPs were performed with the 23-mer templates containing a single monofunctional adduct of **1** or **2**. DNA substrates were generated by annealing the 23-mer template containing site-specific adducts of **1** or **2** to the 8-mer 5′-³²P-labeled oligomer primer. In the control undamaged DNA substrates, unruthenated 23-mer template was used. The nucleotide sequence of DNA substrate containing 23-mer template oligonucleotides annealed to the primers is shown in Figure 7A. Standard DNA polymerase (KF[−]) reactions (50 μ L, 298 K) contained Tris–HCl (50 mM, pH 7.4), MgCl₂ (10 mM), dithiothreitol (0.1 mM), bovine serum albumin (50 μ g mL^{−1}), dNTPs (100 μ M), 5′-³²P-labeled oligonucleotide primer (40 nM) annealed to an oligonucleotide template, and KF[−] (0.5 unit,

6 nm). At various intervals, aliquots (10 μ L) were withdrawn, and the reactions in these aliquots were terminated by the addition of loading buffer (5 μ L) containing EDTA (20 mM), formamide (80%), bromophenol blue (0.1%), and xylene cyanol blue (0.1%) and by heating at 363 K for 1 min. The reaction products were resolved on 20% PAA gels containing urea (8M), then visualized and quantified. Other details were published previously.^[35,77]

Other physical methods: Absorption spectra were measured by using a Beckman 7400 DU spectrophotometer by using quartz cells with a path length of 1 cm and a thermoelectrically controlled cell holder. The oligonucleotides were purified by HPLC on a Waters HPLC system consisting of a Waters 262 pump, a Waters 2487 UV detector, and a Waters 600S controller with a MonoQ 5/50 GL column. The FAAS measurements were carried out by using a Varian AA240Z Zeeman atomic absorption spectrometer equipped with a GTA 120 graphite tube atomizer. For FAAS analyses, DNA was precipitated with EtOH and dissolved in 0.1 M HCl. The gels were visualized by using a BAS 2500 FUJIFILM bioimaging analyzer and the radioactivity associated with the bands was quantified by using the AIDA image analyzer software (Raytest, Germany).

Acknowledgements

This research was supported by the Ministry of Education of the Czech Republic (MSMT LC06030, 6198959216, ME08017, ME10066, OC08003, and OC09018), the Academy of Sciences of the Czech Republic (grants KAN200200651, M200040901, AV0Z50040507, and AV0Z50040702), the Grant Agency of the Academy of Sciences of the Czech Republic (IAA400040803), and the Grant Agency of the Czech Republic (301/09/H004 and P301/10/0598). J.K. is an international research scholar of the Howard Hughes Medical Institute. The authors also acknowledge that their participation in the EU COST Action D39 has enabled them to regularly exchange their most recent ideas in the field of anticancer metallo-drugs with several European colleagues.

- [1] R. E. Morris, R. E. Aird, P. D. Murdoch, H. M. Chen, J. Cummings, N. D. Hughes, S. Parsons, A. Parkin, G. Boyd, D. I. Jodrell, P. J. Sadler, *J. Med. Chem.* **2001**, *44*, 3616–3621.
- [2] R. Aird, J. Cummings, A. Ritchie, M. Muir, R. Morris, H. Chen, P. Sadler, D. Jodrell, *British J. Cancer* **2002**, *86*, 1652–1657.
- [3] Y. K. Yan, M. Melchart, A. Habtemariam, P. J. Sadler, *Chem. Commun. (Cambridge)* **2005**, 4764–4776.
- [4] S. J. Dougan, P. J. Sadler, *Chimia* **2007**, *61*, 704–715.
- [5] V. Brabec, O. Novakova, *Drug Resist. Updates* **2006**, *9*, 111–122.
- [6] M. A. Jakupec, E. Reisner, A. Eichinger, M. Pongratz, V. B. Arion, M. Galanski, C. G. Hartinger, B. K. Keppler, *J. Med. Chem.* **2005**, *48*, 2831–2837.
- [7] P. J. Dyson, G. Sava, *Dalton Trans.* **2006**, 1929–1933.
- [8] H. Chen, J. A. Parkinson, O. Novakova, J. Bella, F. Wang, A. Dawson, R. Gould, S. Parsons, V. Brabec, P. J. Sadler, *Proc. Natl. Acad. Sci. USA* **2003**, *100*, 14623–14628.
- [9] O. Novakova, H. Chen, O. Vrana, A. Rodger, P. J. Sadler, V. Brabec, *Biochemistry* **2003**, *42*, 11544–11554.
- [10] O. Novakova, J. Kasparkova, V. Bursova, C. Hofr, M. Vojtiskova, H. Chen, P. J. Sadler, V. Brabec, *Chem. Biol.* **2005**, *12*, 121–129.
- [11] M. Melchart, A. Habtemariam, O. Novakova, S. A. Moggach, F. P. A. Fabbiani, S. Parsons, V. Brabec, P. J. Sadler, *Inorg. Chem.* **2007**, *46*, 8950–8962.
- [12] S. W. Magennis, A. Habtemariam, O. Novakova, J. B. Henry, S. Meier, S. Parsons, I. D. H. Oswald, V. Brabec, P. J. Sadler, *Inorg. Chem.* **2007**, *46*, 5059–5068.
- [13] T. Bugarcic, O. Novakova, A. Halamkova, L. Zerzankova, O. Vrana, J. Kasparkova, A. Habtemariam, S. Parsons, P. J. Sadler, V. Brabec, *J. Med. Chem.* **2008**, *51*, 5310–5319.
- [14] T. Bugarcic, A. Habtemariam, J. Stepankova, P. Heringova, J. Kasparkova, R. J. Deeth, R. D. L. Johnstone, A. Prescimone, A. Parkin, S. Parsons, V. Brabec, P. J. Sadler, *Inorg. Chem.* **2008**, *47*, 11470–11486.
- [15] O. Nováková, A. A. Nazarov, C. G. Hartinger, B. K. Keppler, V. Brabec, *Biochem. Pharmacol.* **2009**, *77*, 364–374.
- [16] N. Poklar, D. S. Pilch, S. J. Lippard, E. A. Redding, S. U. Dunham, K. J. Breslauer, *Proc. Natl. Acad. Sci. USA* **1996**, *93*, 7606–7611.
- [17] D. S. Pilch, S. U. Dunham, E. R. Jamieson, S. J. Lippard, K. J. Breslauer, *J. Mol. Biol.* **2000**, *296*, 803–812.
- [18] C. Hofr, N. Farrell, V. Brabec, *Nucleic Acids Res.* **2001**, *29*, 2034–2040.
- [19] C. Hofr, V. Brabec, *J. Biol. Chem.* **2001**, *276*, 9655–9661.
- [20] J. Malina, O. Novakova, B. K. Keppler, E. Alessio, V. Brabec, *J. Biol. Inorg. Chem.* **2001**, *6*, 435–445.
- [21] C. Hofr, V. Brabec, *Biopolymers* **2005**, *77*, 222–229.
- [22] V. Bursova, J. Kasparkova, C. Hofr, V. Brabec, *Biophys. J.* **2005**, *88*, 1207–1214.
- [23] V. Brabec, K. Stehlikova, J. Malina, M. Vojtiskova, J. Kasparkova, *Arch. Biochem. Biophys.* **2006**, *446*, 1–10.
- [24] J. Malina, O. Novakova, M. Vojtiskova, G. Natile, V. Brabec, *Biophys. J.* **2007**, *93*, 3950–3962.
- [25] O. Nováková, J. Malina, J. Kašpárková, A. Halámiková, V. Bernard, F. Intini, G. Natile, V. Brabec, *Chem. Eur. J.* **2009**, *15*, 6211–6221.
- [26] H. K. Liu, S. J. Berners-Price, F. Y. Wang, J. A. Parkinson, J. J. Xu, J. Bella, P. J. Sadler, *Angew. Chem.* **2006**, *118*, 8333–8336; *Angew. Chem. Int. Ed.* **2006**, *45*, 8153–8156.
- [27] P. E. Nielsen, *J. Mol. Recognit.* **1990**, *3*, 1–24.
- [28] V. Brabec, M. Sip, M. Leng, *Biochemistry* **1993**, *32*, 11676–11681.
- [29] H. Kostrhunova, V. Brabec, *Biochemistry* **2000**, *39*, 12639–12649.
- [30] S. M. Patrick, J. J. Turchi, *Biochemistry* **1998**, *37*, 8808–8815.
- [31] K. M. Comess, J. N. Burstyn, J. M. Essigmann, S. J. Lippard, *Biochemistry* **1992**, *31*, 3975–3990.
- [32] Z. Suo, K. Johnson, *J. Biol. Chem.* **1998**, *273*, 27259–27267.
- [33] A. Vaisman, M. W. Warren, S. G. Chaney, *J. Biol. Chem.* **2001**, *276*, 18999–19005.
- [34] E. Bassett, A. Vaisman, J. M. Havener, C. Masutani, F. Hanaoka, S. G. Chaney, *Biochemistry* **2003**, *42*, 14197–14206.
- [35] J. Kasparkova, O. Novakova, V. Marini, Y. Najajreh, D. Gibson, J.-M. Perez, V. Brabec, *J. Biol. Chem.* **2003**, *278*, 47516–47525.
- [36] B. Moriarity, O. Novakova, N. Farrell, V. Brabec, J. Kasparkova, *Arch. Biochem. Biophys.* **2007**, *459*, 264–272.
- [37] A. Alt, K. Lammens, C. Chiochini, A. Lammens, J. C. Pieck, D. Kuch, K. P. Hopfner, T. Carell, *Science* **2007**, *318*, 967–970.
- [38] Y. Jung, S. J. Lippard, *Chem. Rev.* **2007**, *107*, 1387–1407.
- [39] V. Brabec, J. Kasparkova in *Role of DNA Repair in Antitumor Effects of Platinum Drugs* (Eds.: N. Hadjilias, E. Sletten), Wiley, New York, **2009**, pp. 175–208.
- [40] G. E. Plum, C. A. Gelfand, K. J. Breslauer in *Physicochemical Approaches to Structural Elucidation: Effects of 3,N4-Ethenodeoxycytidine on Duplex Stability and Energetics* (Eds.: B. Singer, H. Bartsch), International Agency for Research on Cancer, Lyon, **1999**, pp. 169–177.
- [41] N. E. Geacintov, S. Broyde, T. Buterin, H. Naegeli, M. Wu, S. X. Yan, D. J. Patel, *Biopolymers* **2002**, *65*, 202–210.
- [42] Y. Maeda, K. Nunomura, E. Ohtsubo, *J. Mol. Biol.* **1990**, *215*, 321–329.
- [43] M. T. Bjorndal, D. K. Fygenon, *Biopolymers* **2002**, *65*, 40–44.
- [44] J. M. Sturtevant, *Proc. Natl. Acad. Sci. USA* **1977**, *74*, 2236–2240.
- [45] R. S. Spolar, M. T. Record, Jr., *Science* **1994**, *263*, 777–784.
- [46] P. J. Mikulecky, A. L. Feig, *Nucleic Acids Res.* **2004**, *32*, 3967–3976.
- [47] W. B. Peters, S. P. Edmondson, J. W. Shriver, *Biochemistry* **2005**, *44*, 4794–4804.
- [48] Y. Zhang, Z. Xi, R. S. Hegde, Z. Shakked, D. M. Crothers, *Proc. Natl. Acad. Sci. USA* **2004**, *101*, 8337–8341.
- [49] J. Malina, J. Kasparkova, G. Natile, V. Brabec, *Chem. Biol.* **2002**, *9*, 629–638.
- [50] R. E. Dickerson, T. K. Chiu, *Biopolymers* **1997**, *44*, 361–403.
- [51] S. M. Cohen, E. R. Jamieson, S. J. Lippard, *Biochemistry* **2000**, *39*, 8259–8265.

- [52] M. Missura, T. Buterin, R. Hindges, U. Hubscher, J. Kasparkova, V. Brabec, H. Naegeli, *EMBO J.* **2001**, *20*, 3554–3564.
- [53] R. Dip, U. Camenisch, H. Naegeli, *DNA Repair* **2004**, *3*, 1409–1423.
- [54] Y. Liu, Y. Liu, Z. Yang, C. Utzat, G. Wang, A. K. Basu, Y. Zou, *Biochemistry* **2005**, *44*, 7361–7368.
- [55] S. F. Bellon, S. J. Lippard, *Biophys. Chem.* **1990**, *35*, 179–188.
- [56] C. Iftode, Y. Daniely, J. A. Borowiec, *Crit. Rev. Biochem. Mol. Biol.* **1999**, *34*, 141–180.
- [57] Y. Zou, Y. Liu, X. Wu, S. M. Shell, *J. Cell. Physiol.* **2006**, *208*, 267–273.
- [58] J. Kasparkova, J. Zehnulova, N. Farrell, V. Brabec, *J. Biol. Chem.* **2002**, *277*, 48076–48086.
- [59] V. Brabec, *Prog. Nucleic Acid Res. Mol. Biol.* **2002**, *71*, 1–68.
- [60] E. L. Mamenta, E. E. Poma, W. K. Kaufmann, D. A. Delmastro, H. L. Grady, S. G. Chaney, *Cancer Res.* **1994**, *54*, 3500–3505.
- [61] S. W. Johnson, P. B. Laub, J. S. Beesley, R. F. Ozols, T. C. Hamilton, *Cancer Res.* **1997**, *57*, 850–856.
- [62] U. Hübscher, H. P. Nasheuer, J. E. Syvaoja, *Trends Biochem. Sci.* **2000**, *25*, 143–147.
- [63] W. C. Lam, E. J. C. Van der Schans, L. C. Sowers, D. P. Millar, *Biochemistry* **1999**, *38*, 2661–2668.
- [64] T. A. Steitz, *J. Biol. Chem.* **1999**, *274*, 17395–17398.
- [65] S. Lone, L. J. Romano, *Biochemistry* **2003**, *42*, 3826–3834.
- [66] L. Ronconi, P. J. Sadler, *Coord. Chem. Rev.* **2007**, *251*, 1633–1648.
- [67] P. C. Bruijninx, P. J. Sadler, *Curr. Opin. Chem. Biol.* **2008**, *12*, 197–206.
- [68] N. P. Johnson, J.-L. Butour, G. Villani, F. L. Wimmer, M. Defais, V. Pierson, V. Brabec, *Prog. Clin. Biochem. Med.* **1989**, *6*, 1–24.
- [69] E. R. Jamieson, S. J. Lippard, *Chem. Rev.* **1999**, *99*, 2467–2498.
- [70] E. Alessio, G. Mestroni, A. Bergamo, G. Sava, *Curr. Top. Med. Chem.* **2004**, *4*, 1525–1535.
- [71] V. Brabec, J. Reedijk, M. Leng, *Biochemistry* **1992**, *31*, 12397–12402.
- [72] C. J. Jones, R. D. Wood, *Biochemistry* **1993**, *32*, 12096–12104.
- [73] I. L. Hermanson-Miller, J. J. Turchi, *Biochemistry* **2002**, *41*, 2402–2408.
- [74] J. L. Manley, A. Fire, A. Cano, P. A. Sharp, M. L. Gefter, *Proc. Natl. Acad. Sci. USA* **1980**, *77*, 3855–3859.
- [75] J. T. Reardon, A. Vaisman, S. G. Chaney, A. Sancar, *Cancer Res.* **1999**, *59*, 3968–3971.
- [76] V. Brabec, M. Leng, *Proc. Natl. Acad. Sci. USA* **1993**, *90*, 5345–5349.
- [77] O. Novakova, J. Kasparkova, J. Malina, G. Natile, V. Brabec, *Nucleic Acids Res.* **2003**, *31*, 6450–6460.

Received: November 9, 2009

Published online: April 6, 2010

7.

Energetics, Conformation, and Recognition of DNA Duplexes Modified by Methylated Analogues of $[\text{PtCl}(\text{dien})]^+{}^{**}$

Olga Nováková,^[a] Jaroslav Malina,^[a] Jana Kašpárková,^[a, b] Anna Halámiková,^[a] Vladan Bernard,^[a] Francesco Intini,^[c] Giovanni Natile,^[c] and Viktor Brabec^{*[a]}

Abstract: In early studies of empirical structure–activity relationships, monodentate Pt^{II} complexes were considered to be biologically inactive. Examples of such inactive monodentate Pt^{II} compounds are $[\text{PtCl}(\text{dien})]^+$ (dien = diethylenetriamine) and $[\text{PtCl}(\text{NH}_3)_3]^+$. DNA is considered the major biological target of platinum compounds. Thus, monodentate DNA binding of Pt^{II} compounds was previously expected to display insignificant biological effects because it was assumed to affect DNA conformation and downstream cellular processes markedly less than the cross-links of bifunctional Pt^{II} complexes. More recently it was shown that some monodentate Pt^{II} complexes do exhibit biological effects; the active monodentate Pt^{II} complexes commonly

feature bulkier amine ligands than the hitherto used dien or NH_3 groups. We were therefore interested in determining whether a simple but marked enhancement of the bulkiness of the dien ligand in monodentate $[\text{Pt}(\text{NO}_3)(\text{dien})]^+$ by multiple methylation of this ligand affects the early phases in which platinum compounds exert their biological activity. More specifically, the goals of this study, performed in cell-free media, were to determine how the modification of DNA duplexes by methylated analogues of $[\text{Pt}(\text{NO}_3)(\text{dien})]^+$ affects their energetics and

how the alterations of this biophysical parameter are reflected by the recognition of these duplexes by DNA polymerases and the DNA repair system. We have found that the impact of the methylation of $[\text{Pt}(\text{NO}_3)(\text{dien})]^+$ on the biophysical properties of DNA (thermodynamic, thermal, and conformational properties) and its biochemical processes (DNA polymerization and the repair of DNA adducts) is remarkable. Hence, we conclude that monodentate DNA binding of Pt^{II} compounds may considerably affect the biophysical properties of DNA and consequently downstream cellular processes as a result of a large increase in the bulkiness of the nonleaving ligands in this class of metal complex.

Keywords: DNA • DNA recognition • DNA structures • platinum • polymerization

Introduction

Monofunctional Pt^{II} compounds, such as $[\text{PtCl}(\text{dien})]\text{Cl}$ (dien = diethylenetriamine = 1,4,7-triazaheptane; Figure 1A)

[a] Dr. O. Nováková, Dr. J. Malina, Dr. J. Kašpárková, Dr. A. Halámiková, V. Bernard, Prof. Dr. V. Brabec
Institute of Biophysics
Academy of Sciences of the Czech Republic, v.v.i.
Kralovopolska 135, CZ-61265 Brno (Czech Republic)
Fax: (+420) 541240499
E-mail: brabec@ibp.cz

[b] Dr. J. Kašpárková
Laboratory of Biophysics
Department of Experimental Physics Faculty of Sciences
Palacky University, 771 46 Olomouc (Czech Republic)

[c] Dr. F. Intini, Prof. Dr. G. Natile
Department of Pharmaceutical Chemistry
University of Bari, 70125 Bari (Italy)

[**] dien = diethylenetriamine

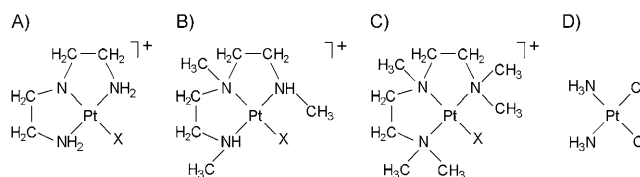


Figure 1. Structures of the platinum compounds used in this work: A) $[\text{PtCl}(\text{dien})]^+$, B) $[\text{Pt}(\text{NO}_3)(\text{dien-Me}_3)]^+$, C) $[\text{Pt}(\text{NO}_3)(\text{dien-Me}_3)]^+$, and D) cisplatin.

or $[\text{PtCl}(\text{NH}_3)_3]\text{Cl}$, have been frequently used in the studies of mechanisms underlying the biological effects of bifunctional antitumor Pt^{II} drugs such as cisplatin (Figure 1D), carboplatin, and oxaliplatin as model compounds.^[1–4] These monofunctional compounds have made it possible to simulate and examine the first step of binding of bifunctional Pt^{II} compounds to DNA, which is considered the major pharma-

cological target of platinum drugs.^[4–6] In addition, monodentate DNA binding of Pt^{II} compounds was previously expected not to display significant biological effects because it was assumed to affect DNA conformation and downstream cellular processes markedly less than the cross-links of bifunctional Pt^{II} complexes.^[1–3]

However, several groups have shown that some monofunctional Pt^{II} complexes do exhibit biological effects.^[7–14] Interestingly, the new active Pt^{II} complexes that exhibit monodentate DNA binding are noted for one or two considerably bulkier amine ligands. In addition, in contrast to DNA adducts of inefficient [PtCl(dien)]⁺ or [PtCl(NH₃)₃]⁺, the monofunctional adducts of several cytotoxic Pt^{II} compounds markedly distort the conformation of DNA with a reduction in DNA repair and terminate DNA and/or RNA polymerization. Also, interestingly, monodentate *cis*-diammine(pyridine)chloridoplatinum(II) (*cis*-[PtCl(NH₃)₂(py)]⁺), in addition to the already mentioned effects of other monodentate cytotoxic Pt^{II} complexes, preferentially accumulates in cells that express organic cationic transporters in comparison to those that lack them.^[14]

The active monofunctional Pt^{II} complexes (fundamentally different to that of [PtCl(dien)]⁺ or [PtCl(NH₃)₃]⁺) commonly feature more bulky amine ligands than the hitherto used dien or NH₃ groups. We were therefore interested in determining whether a simple but marked enhancement of the bulkiness of the dien ligand in monodentate [Pt(NO₃)(dien)]⁺ by multiple methylation (Figure 1B,C) affects the early phases in which platinum compounds exert their biological activity. In addition, we have also noted the need for further studies to establish correlations between the thermodynamic characteristics of well-defined DNA damage and the susceptibility of this damage to removal by DNA repair enzymes and its efficiency to block DNA polymerization catalyzed by DNA polymerases. Thus, the goals of this study, performed in cell-free media, were to determine how modification of DNA duplexes by methylated analogues of [Pt(NO₃)(dien)]⁺ (Figure 1B,C) affects their energetics and how the alterations of this biophysical parameter are reflected by the recognition of these duplexes by DNA polymerases and the DNA repair system. These two processes are crucial initial cellular responses to DNA damage by Pt^{II} agents.^[6,15,16]

Results

DNA binding in a cell-free medium: The rate of binding of [PtCl(dien)]⁺ and its methylated analogues to double-helical calf thymus (CT) DNA was determined at an *r_i* of 0.04 and 0.1 (*r_i* is defined as the molar ratio of the free platinum complex to nucleotides at the onset of incubation with DNA) in 10 mM NaClO₄ at 37°C in the dark. After 24 h, an aliquot of the reaction mixture was withdrawn and assayed by differential pulse polarography (DPP) for platinum not bound to DNA. After 24 h of reaction, the binding of [PtCl(dien)]⁺ and [Pt(NO₃)(dien-Me₃)]⁺ was complete. A consequence of

more extensive methylation, such as that in the pentamethylated analogue [Pt(NO₃)(dien-Me₅)]⁺, was that the binding of this analogue was not quantitative; 83 % of the pentamethylated complex was bound after 24 h.

The binding experiments carried out in this work indicated that modification reactions resulted in the irreversible coordination of the Pt^{II}–dien compounds, which thus facilitated sample analysis. Hence, it was possible to prepare samples of DNA modified by Pt^{II}–dien compounds at a preselected value of *r_b* (*r_b* values are defined as the number of atoms of metal bound per nucleotide residue). Thus, unless stated otherwise, samples of DNA modified by Pt^{II}–dien compounds and analyzed by biophysical or biochemical methods were prepared in NaClO₄ (10 mM) at 37°C. After the reactions of DNA with the complexes for 24 h, the samples were precipitated in ethanol, dissolved in the medium necessary for a particular analysis, and the *r_b* values of aliquots of the samples were determined by flameless atomic absorption spectrophotometry (FAAS). In this way, all analyses described in this paper were performed in the absence of unbound (free) Pt^{II}–dien complex.

The preferential DNA binding sites of the monofunctional complexes [Pt(NO₃)(dien-Me₃)]⁺ and [Pt(NO₃)(dien-Me₅)]⁺ were determined by transcription mapping.^[17,18] pSP73KB DNA contained T7 RNA polymerase promoter (part of the nucleotide sequence of this plasmid used for mapping is shown in Figure 2B). In vitro RNA synthesis by the action of RNA polymerases on this DNA template containing cross-links of several bifunctional Pt^{II} compounds can be prematurely terminated at the level or in the proximity of the cross-links.^[17–20] Interestingly, monofunctional DNA adducts of some platinum complexes, such as [PtCl(dien)]⁺ or [PtCl(NH₃)₃]⁺, are unable to terminate RNA synthesis.^[17,18,21] Importantly, in contrast to [PtCl(dien)]⁺, its methylated analogues, such as [Pt(NO₃)(dien-Me₃)]⁺ and [Pt(NO₃)(dien-Me₅)]⁺, formed DNA adducts that efficiently terminate RNA synthesis (Figure 2A). The major stop sites were roughly identical for both methylated Pt^{II}–dien complexes and their profiles are similar to that obtained for DNA treated with the anticancer drug cisplatin (lane cisPt in Figure 2A). The major stop sites for DNA modified by [Pt(NO₃)(dien-Me₃)]⁺, [Pt(NO₃)(dien-Me₅)]⁺, and cisplatin are shown in Figure 2B. Thus, these results suggest that the major sites in DNA at which the monofunctional complexes [Pt(NO₃)(dien-Me₃)]⁺ and [Pt(NO₃)(dien-Me₅)]⁺ preferentially bind are guanine residues.

Differential scanning calorimetry (DSC): A calorimetric technique was used to characterize the influence of the monofunctional adduct formed by Pt^{II}–dienPt complexes on the thermal stability and energetics of the site-specific platinated 15-base-pair (bp) DNA duplexes (their nucleotide sequences are shown in Figure 3D). Such thermodynamic data can reveal how the platinum adduct influences duplex stability, a property that has been shown to play a significant role in the mechanism of biological activity of platinum antitumor drugs.^[22–27] In this work we studied oligodeoxyribonu-

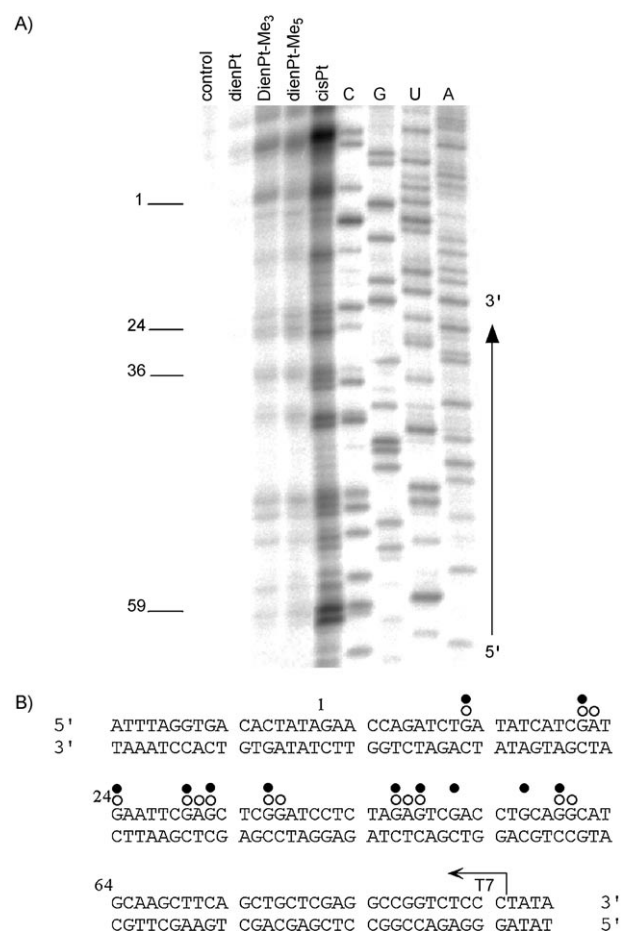


Figure 2. Inhibition of RNA synthesis by T7 RNA polymerase on the pSP73KB plasmid modified by Pt^{II}-dien complexes and cisplatin. A) Autoradiogram of a polyacrylamide (6%) / urea (8M) sequencing gel showing the inhibition of RNA synthesis by T7 RNA polymerase on the pSP73KB plasmid containing adducts of Pt^{II}-dien complexes and cisplatin. Lanes: control, unmodified template; dienPt, dienPt-Me₃, dienPt-Me₃, and cisPt, the template modified by [PtCl(dien)]⁺, [Pt(NO₃)(dien-Me₃)]⁺, [Pt(NO₃)(dien-Me₃)]⁺, and cisplatin at $r_b = 0.01$, respectively; C, G, U, and A, chain-terminated marker DNAs. B) Schematic diagram showing the portion of the sequence used to monitor the inhibition of RNA synthesis by cisplatin and Pt^{II}-dien complexes. The arrow indicates the start of the T7 RNA polymerase, which used as template the upper strand of the pSP73KB plasmid. The open and closed circles represent major stop signals for DNA modified by cisplatin or [Pt(dien-Me₃)(NO₃)]⁺, respectively. The numbers correspond to the nucleotide numbering in the sequence map of the pSP73KB plasmid.

cleotide duplexes containing unique monofunctional adducts formed by [PtCl(dien)]⁺, [Pt(NO₃)(dien-Me₃)]⁺, and [Pt(NO₃)(dien-Me₃)]⁺ complexes at guanine residues in three different sequence contexts, TGT, 5'-AGT, and 5'-(7-deazaG)GT. In pyrimidine-rich strands containing the central sequence 5'-GGT, 5'-G was replaced by 7-deazaguanine (7-deazaG). The 7-deazaG is an isosteric analogue of native guanine in which the aromatic N7 atom is replaced by C-H, which accurately mimics the properties of the natural base. As the guanine N7 is the site at which platinum complexes preferentially react in DNA, 7-deazaG is incapable of forming platinum adducts.^[28] Thus, 7-deazaG makes it possible to

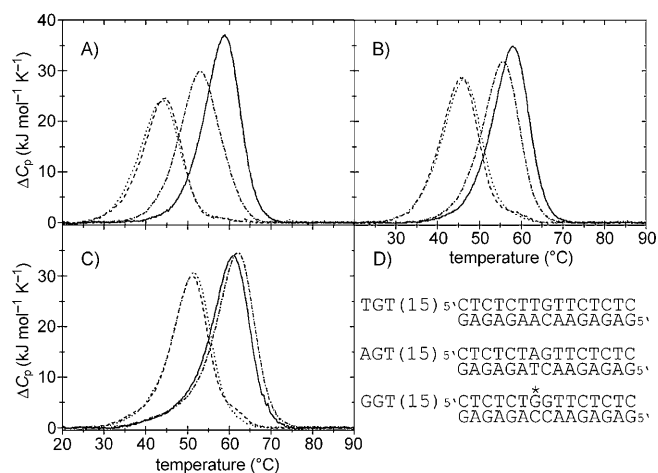


Figure 3. DSC thermograms of A) TGT(15), B) AGT(15), and C) GGT(15) duplexes unmodified (solid lines) and containing in the top strand the monofunctional adduct of [PtCl(dien)]⁺ (dotted and dashed line), [Pt(NO₃)(dien-Me₃)]⁺ (dashed line), and [Pt(NO₃)(dien-Me₃)]⁺ (dotted line). The concentrations of the duplexes were 30 μ M and the buffer conditions were sodium phosphate (10 mM, pH 7.0) and NaCl (150 mM). D) Sequences of the synthetic oligodeoxyribonucleotides with their abbreviations. The top strand of the duplex GGT(15) contained 7-deazaG in the central sequence 5'-GGT instead of the native 5'-G.

prepare a single monofunctional adduct of Pt^{II}-dienPt complexes at the central G in a 5'-GGT sequence context of pyrimidine-rich oligodeoxyribonucleotides, that is, 5'-G is 7-deaza-G. Figure 3A–C shows DSC melting profiles (ΔC_p versus T) for the parent unmodified 15 bp duplexes TGT(15), AGT(15), and GGT(15) (solid curves) and the same duplexes containing a single monofunctional adduct of [PtCl(dien)]⁺ (dotted and dashed curves), [Pt(NO₃)(dien-Me₃)]⁺ (dashed curves), and [Pt(NO₃)(dien-Me₃)]⁺ (dotted curves). Each transition showed negligible changes in the heat capacities between the initial and final states, and denaturation (heating) and renaturation (cooling) curves for the unmodified and platinated duplexes were superimposable (not shown), which is consistent with the reversibility of the melting equilibrium. Our calorimetric data, described below, were interpreted on the assumption that the thermodynamic parameters for the melting of the unmodified and platinated duplexes can be ascribed to differences in the initial duplex states. This implies that the final single-stranded states should be thermodynamically equivalent at the elevated temperatures at which they are formed. This assumption was verified (not shown) similarly to earlier reports by recording identical circular dichroic spectra for samples of unplatinated and platinated duplexes heated at high temperatures (90 °C).^[23–25,29,30] Overall, meaningful thermodynamic data from the calorimetric measurements described below could be obtained.

DSC melting profiles were analyzed as described in the Experimental Section and the results are listed in Table 1. All thermodynamic parameters discussed in this work refer to the duplex dissociation process. Differences in the dissociation thermodynamics due to the presence of an adduct are

Table 1. Calorimetrically derived thermodynamic parameters for the dissociation (melting) of the 15-bp duplexes that are unmodified or contain a single, site-specific monofunctional adduct of [PtCl(dien)]⁺, [Pt(NO₃)(dien-Me₃)]⁺, or [Pt(NO₃)(dien-Me₅)]⁺.

TGT(15)	T_m [°C] ^[a]	ΔH_{cal} [kJ mol ⁻¹] ^[a]	ΔS [kJ mol ⁻¹] ^[a]	ΔG_{25}° [kJ mol ⁻¹] ^[a]	K_D [μ M] ^[b]
no Pt (control)	58.9	417	1.261	41	0.066
[PtCl(dien)] ⁺	53.0	386 (-31)	1.187 (-0.074)	32 (-9)	2.48
[Pt(NO ₃)(dien-Me ₃)] ⁺	44.5	307 (-110)	0.968 (-0.293)	18 (-23)	702.4
[Pt(NO ₃)(dien-Me ₅)] ⁺	43.9	304 (-113)	0.959 (-0.302)	18 (-23)	702.4
AGT(15)	T_m [°C] ^[a]	ΔH_{cal} [kJ mol ⁻¹] ^[a]	ΔS [kJ mol ⁻¹] ^[a]	ΔG_{25}° [kJ mol ⁻¹] ^[a]	K_D [μ M] ^[b]
no Pt (control)	58.0	401	1.216	38	0.22
[PtCl(dien)] ⁺	55.4	371 (-30)	1.133 (-0.083)	33 (-5)	1.65
[Pt(NO ₃)(dien-Me ₃)] ⁺	45.7	348 (-53)	1.092 (-0.124)	22 (-16)	139.84
[Pt(NO ₃)(dien-Me ₅)] ⁺	46.4	354 (-47)	1.110 (-0.106)	23 (-15)	93.46
GGT(15)	T_m [°C] ^[a]	ΔH_{cal} [kJ mol ⁻¹] ^[a]	ΔS [kJ mol ⁻¹] ^[a]	ΔG_{25}° [kJ mol ⁻¹] ^[a]	K_D [μ M] ^[b]
no Pt (control)	61.1	426	1.284	43	0.029
[PtCl(dien)] ⁺	62.3	444 (18)	1.335 (0.051)	46 (3)	0.0087
[Pt(NO ₃)(dien-Me ₃)] ⁺	51.1	367 (-59)	1.136 (-0.148)	28 (-15)	12.43
[Pt(NO ₃)(dien-Me ₅)] ⁺	51.7	378 (-48)	1.170 (-0.114)	29 (-14)	8.31

[a] The ΔH and ΔS values are averages derived from three independent experiments. The experimental uncertainties of the parameters are as follows: T_m ($\pm 0.5^\circ\text{C}$), ΔH ($\pm 2\%$), ΔS ($\pm 3\%$), ΔG_{25}° ($\pm 3\%$). The “ $\Delta\Delta$ ” parameters are given in parentheses (these parameters are computed by subtracting the appropriate value measured for the control, the unmodified duplex, from the value measured for the duplex containing the single, site-specific platinum adduct). [b] K_D denotes the dissociation constant for strand dissociation ($\Delta G_{25}^\circ = -RT \ln K_D$; T is the temperature in Kelvin, and R is the universal gas constant ($8.314472 \text{ J K}^{-1} \text{ mol}^{-1}$)).

presented as “ $\Delta\Delta$ ” parameters. These parameters are computed by subtracting the appropriate value measured for the control, the unmodified duplex, from the value measured for the duplex containing the single, site-specific platinum adduct and are reported in Table 1 in parentheses. Inspection of these thermodynamic parameters reveals a number of interesting features. First, the formation of monofunctional adducts by [PtCl(dien)]⁺, [Pt(NO₃)(dien-Me₃)]⁺, and [Pt(NO₃)(dien-Me₅)]⁺ reduced the duplex thermal stability (except for the adduct formed by [PtCl(dien)]⁺ in the sequence GGT, which increased the melting temperature of the duplex by 1.2°C). The efficiency of the adducts to reduce the DNA melting temperature increased as a consequence of the methylation of the Pt^{II}-dien complexes in all three sequence contexts, although the efficiency of the adducts of [Pt(NO₃)(dien-Me₃)]⁺ and [Pt(NO₃)(dien-Me₅)]⁺ was in this respect almost identical. However, the efficiency of the adducts to reduce the DNA melting temperature differed depending on the sequence context; the trend was TGT \gg AGT $>$ GGT.

Interestingly, the formation of monofunctional adducts by Pt^{II}-dien complexes resulted in a large decrease in the enthalpy of duplex dissociation (Table 1 and Figure 4). In other words, the monofunctional adducts of these platinum complexes enthalpically destabilized the duplex relative to their unmodified counterpart. On the other hand, the formation of monofunctional adducts by Pt^{II}-dien complexes resulted in a substantial decrease in the duplex dissociation entropy (Table 1 and Figure 4). Thus, the net result of these enthalpic and entropic effects was that the formation of monofunctional adducts by [PtCl(dien)]⁺, [Pt(NO₃)(dien-Me₃)]⁺, and [Pt(NO₃)(dien-Me₅)]⁺ induced a decrease in the free energy of duplex dissociation at 25°C (ΔG_{25}° ;

Table 1 and Figure 4), this duplex destabilization being enthalpic in origin. In this respect, the monofunctional adducts of the methylated analogues of [PtCl(dien)]⁺ were almost equally effective, and markedly more effective than the nonmethylated complex. Moreover, the efficiency of the adducts to enthalpically destabilize the duplex depended on the sequence context; the trend was similar to that observed for the efficiency of the adducts to reduce the DNA melting temperature (see above), that is, TGT(15) \gg AGT(15) \geq GGT(15).

Shape analysis of the experimental DSC curves allows model-dependent ΔH_{vH} enthalpies to be calculated.^[31] We found that ΔH_{vH} values were

similar to ΔH_{cal} ratios for all duplexes and platinum compounds tested in this work; the ratios of $\Delta H_{\text{vH}}/\Delta H_{\text{cal}}$ were in the range of 1.06–1.11.

DNA polymerization: It has been demonstrated that DNA modifications by various platinum complexes have signifi-

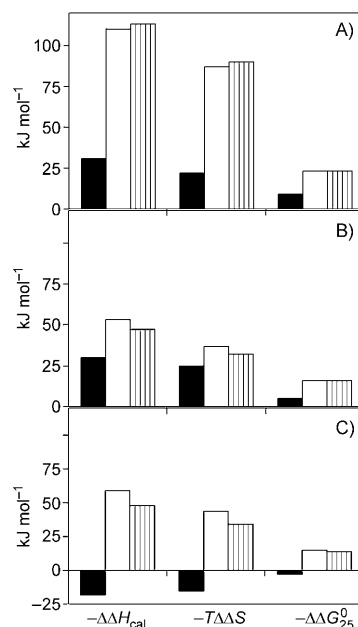


Figure 4. The contributions of enthalpic and entropic effects to the stability (free energy change) of the 15-bp duplexes TGT(15) (A), AGT(15) (B), and GGT(15) (C) containing the monofunctional adduct of [PtCl(dien)]⁺ (solid bars), [Pt(NO₃)(dien-Me₃)]⁺ (open bars), or [Pt(NO₃)(dien-Me₅)]⁺ (vertical striped bars). The units of each parameter ($\Delta\Delta H_{\text{cal}}$, $T\Delta\Delta S$, and $\Delta\Delta G_{25}^\circ$) are kJ mol^{-1} and $T = 25^\circ\text{C}$.

cant effects on the processivity of a number of prokaryotic, eukaryotic, and viral DNA polymerases.^[32–38] Interestingly, with DNA templates containing site-specifically placed adducts of various platinum compounds, a number of prokaryotic and eukaryotic DNA polymerases were blocked, but they could also traverse through platinum adducts, depending on their character and the conformational alterations induced in DNA. It is therefore of great interest to examine whether DNA polymerases, which process DNA substrates containing monofunctional adducts of Pt^{II}–dien complexes, could reveal potential differences in the alterations imposed on DNA by the adducts of the three Pt^{II}–dien complexes, which differ in the level of methylation of the dien moiety.

In this work we investigated DNA polymerization using templates site-specifically modified by [PtCl(dien)]⁺, [Pt(NO₃)(dien-Me₃)]⁺, or [Pt(NO₃)(dien-Me₅)]⁺ by two DNA polymerases, which differ in their processivity and fidelity. In the first series of experiments, we used the Klenow fragment of *E. coli* DNA polymerase I deficient in 3'-to-5' proofreading exonuclease activity (KF⁻) as a model enzyme frequently used in studies aimed at understanding the processes in which nucleic acid polymerases take part.

We constructed 17-mer/30-mer (Figure 5A) primer template duplexes unplatinated or containing a monofunctional adduct of the Pt^{II}–dien complex formed at the guanine residue in the central TGT, 5'-AGT, or 5'-(7-deazaG)GT sequence. The first 17 nucleotides on the 3' terminus of the 30-mer template strand were complementary to the nucleotides of the 17-mer primer, and the guanine involved in the

monofunctional adduct on the template strand was located 20 bases from the 3' terminus (Figure 5A). After annealing the 17-nucleotide primer to the 3' terminus of the unplatinated or platinated template strand (positioning the 3'-end of the primer three bases before the adduct in the template strand), we examined DNA polymerization by using the single monofunctional adduct of [PtCl(dien)]⁺, [Pt(NO₃)(dien-Me₃)]⁺, or [Pt(NO₃)(dien-Me₅)]⁺ on the template by KF⁻ in the presence of all four deoxyribonucleoside 5'-triphosphates (dNTP). The reaction was stopped after various intervals of time and the products were analyzed by using a sequencing gel (Figure 5A).

Polymerization by KF⁻ using the 17-mer/30-mer primer templates containing the monofunctional adducts of the methylated Pt^{II}–dien complexes ([Pt(NO₃)(dien-Me₃)]⁺ or [Pt(NO₃)(dien-Me₅)]⁺) in the presence of all four dNTP proceeded rapidly up to the nucleotide opposite the adduct, such that the 20-nucleotide intermediate product accumulated to a significant extent (shown in Figure 5A). There was only a slight accumulation of larger DNA intermediates and full length products in particular using the templates containing the adduct of [Pt(NO₃)(dien-Me₃)]⁺, whereas no intermediate products were seen with the 30-mer control template or the template containing the adduct of nonmethylated [PtCl(dien)]⁺ as the full-length product only was being formed (shown in Figure 5A). This result indicates that the character of the monofunctional adducts of the methylated Pt^{II}–dien complexes, such as [Pt(NO₃)(dien-Me₃)]⁺ or [Pt(NO₃)(dien-Me₅)]⁺, and alterations induced in DNA by

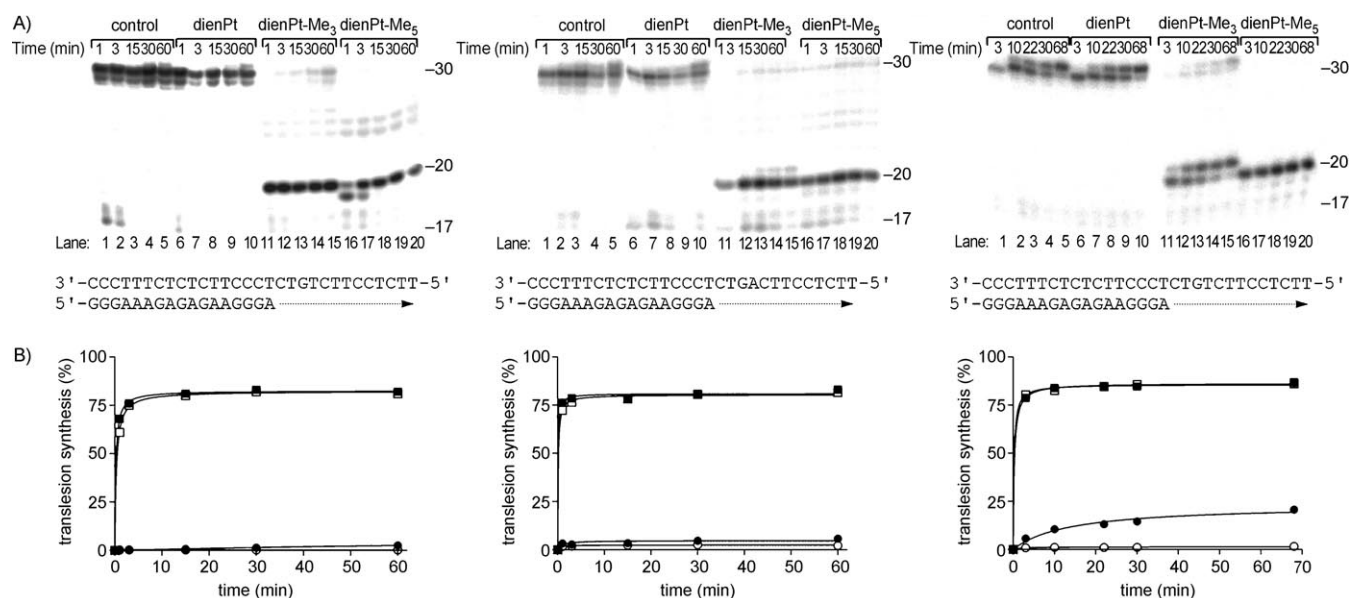


Figure 5. A) Primer extension activity of the exonuclease-deficient Klenow fragment of DNA polymerase I. The experiments were conducted by using the 17-mer/30-mer primer-template duplexes for the times indicated. These duplexes were unplatinated or contained the monofunctional adduct of the Pt^{II}–dien complex formed at the guanine residue in the central TGT (left panel), 5'-AGT (middle panel), or 5'-(7-deazaG)GT sequence (right panel). The nucleotide sequences of the templates and the primers are shown beneath the gels. See the text for details. Lanes 1–5, undamaged template; lanes 6–10, the template containing monofunctional adducts of [PtCl(dien)]⁺; lanes 11–15, the template containing monofunctional adducts of [Pt(NO₃)(dien-Me₃)]⁺; lanes 16–20, the template containing monofunctional adducts of [Pt(NO₃)(dien-Me₅)]⁺. The strong pause site opposite the platinated guanines is marked 20. B) The time dependence of the inhibition of DNA synthesis on the undamaged (control) template (■), DNA containing the adduct of [PtCl(dien)]⁺ (□), [Pt(NO₃)(dien-Me₃)]⁺ (●), or [Pt(NO₃)(dien-Me₅)]⁺ (○). The data points are the means (±SE) of three different experiments with two independent template preparations.

their adducts were distinctly different to those induced by the adduct of plain (nonmethylated) $[\text{PtCl}(\text{dien})]^+$ such that the increase in the bulkiness of the monofunctional Pt^{II} -dien complexes due to their methylation led to DNA adducts that could potentially impede the elongation of DNA.

We have also examined the effects of the monofunctional adducts of Pt^{II} -dien complexes on the polymerization by reverse transcriptase of human immunodeficiency virus type 1 (RT HIV-1) in the presence of all four dNTPs. This enzyme also possesses DNA template-dependent DNA polymerase activity, but relatively low processivity and fidelity.^[39] In these studies, the elongation of the 17-mer/30-mer primer template duplexes (identical to those used in the experiments with KF^- (see above)) was studied. As is shown in Figure 6, we also confirmed by using this DNA polymerase, which operates by a different mechanism to KF^- , that in contrast to the monofunctional adducts of plain (nonmethylated) $[\text{PtCl}(\text{dien})]^+$, the adducts of its methylated analogues are also a fairly strong block to DNA synthesis catalyzed by RT HIV-1. The only substantial difference between the polymerization by KF^- and RT HIV-1 was that the adducts of $[\text{Pt}(\text{NO}_3)(\text{dien-Me}_3)]^+$ represented a somewhat weaker block to DNA catalyzed by RT HIV-1 (cf. Figures 5b and 6b). In other words, the adducts of $[\text{Pt}(\text{NO}_3)(\text{dien-Me}_3)]^+$ could potentially impede the elongation of DNA by KF^- to a greater extent than the elongation by RT HIV-1.

DNA repair: Figure 7 illustrates an experiment in which DNA repair synthesis by repair-proficient HeLa cell-free extract (CFE) in pSP73KB plasmid modified by cisplatin, $[\text{PtCl}(\text{dien})]^+$, $[\text{Pt}(\text{NO}_3)(\text{dien-Me}_3)]^+$, and $[\text{Pt}(\text{NO}_3)(\text{dien-Me}_3)]^+$ at $r_b=0.035$ was examined. The repair activity was monitored by measuring the amount of incorporated radio-labeled nucleotide. The incorporation of radioactive material was corrected for the relative DNA content in each band. Approximately the same levels of damage-induced DNA repair synthesis were detected in the plasmid modified by cisplatin and methylated Pt^{II} -dien complexes (Figure 7A, lanes cisPt, dienPt-Me₃, and dienPt-Me₅, and Figure 7B). In contrast, the adducts of nonmethylated $[\text{PtCl}(\text{dien})]^+$ only induced a very low level of repair synthesis (approximately only 10 % of that observed for repair synthesis in the plasmid modified by cisplatin; Figure 7A, lane dienPt, and Figure 7B).

Discussion

The results of the transcription mapping experiments (Figure 2) are consistent with the view that multiple methylation of the dien ligand does not affect preferential DNA binding sites of this class of monofunctional Pt^{II} complexes, that is, guanine residues. Similarly three methyl groups on the dien ligand affect DNA binding only slightly. On the other hand, the pentamethylated complex binds to DNA slightly less quantitatively after 24 h, likely due to the steric hindrance associated with the bulkiness of its nonleaving group.

DSC can provide quantitative, model-independent characterization of the effects of the lesion on duplex thermodynamics. The duplex melting temperatures (thermal stability parameter), T_m , and thermodynamic stability data, the

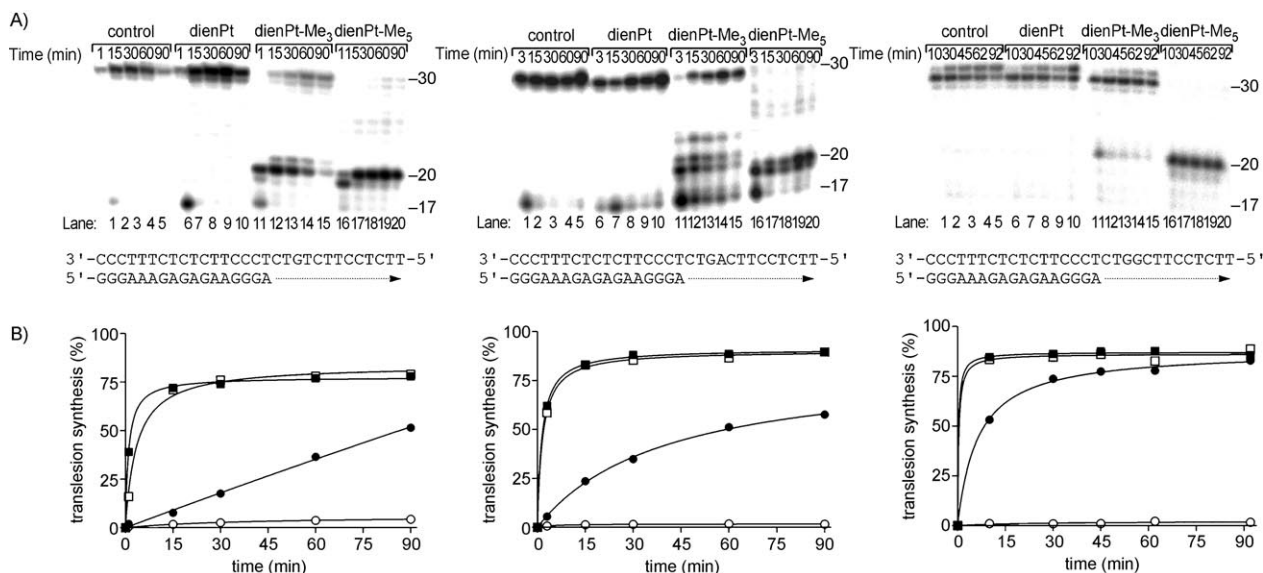


Figure 6. Primer extension activity of RT HIV-1. The experiments were conducted using the 17-mer/30-mer primer-template duplexes for the times indicated. These duplexes were unplatinated or contained monofunctional adduct of the Pt^{II} -dien complex formed at the guanine residue in the central TGT (left panel), 5'-AGT (middle panel) or 5'-(7deazaG)GT sequence (right panel). The nucleotide sequences of the templates and the primers are shown beneath the gels. See the text for details. Lanes 1–5, undamaged template; lanes 6–10, the template containing monofunctional adducts of $[\text{PtCl}(\text{dien})]^+$; lanes 11–15, the template containing monofunctional adducts of $[\text{Pt}(\text{NO}_3)(\text{dien-Me}_3)]^+$; lanes 16–20, the template containing monofunctional adducts of $[\text{Pt}(\text{NO}_3)(\text{dien-Me}_5)]^+$. The strong pause site opposite the platinated guanines is marked 20. (B) The time dependence of the inhibition of DNA synthesis on undamaged (control) template (■), DNA containing adduct of $[\text{PtCl}(\text{dien})]^+$ (□), $[\text{Pt}(\text{NO}_3)(\text{dien-Me}_3)]^+$ (●), or $[\text{Pt}(\text{NO}_3)(\text{dien-Me}_5)]^+$ (○). Data are means (\pm SE) from three different experiments with two independent template preparations.

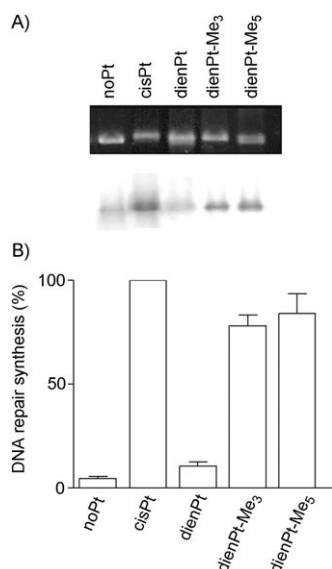


Figure 7. In vitro repair synthesis assay of the extract prepared from the repair-proficient HeLa cell line. Repair synthesis used as substrates pSP73KB plasmid unmodified (lane noPt) or modified at $r_b=0.035$ by cisplatin, $[\text{PtCl}(\text{dien})]^+$, $[\text{Pt}(\text{NO}_3)(\text{dien-Me}_3)]^+$, and $[\text{Pt}(\text{NO}_3)(\text{dien-Me}_5)]^+$ (lanes cisPt, dienPt, dienPt-Me₃, and dienPt-Me₅, respectively). A) Results of a typical experiment. The top panel is a photograph of the EtBr stained gel and the bottom panel is the autoradiogram of the gel and shows the incorporation of $[\alpha\text{-}^{32}\text{P}]\text{dATP}$. B) Incorporation of dATP into unmodified or platinated plasmids. For all quantifications representing mean values of two independent experiments, incorporation of radioactive material is corrected for the relative DNA content in each band. The bars indicate the standard error of the mean (SEM).

duplex dissociation enthalpies, ΔH_{cal} , and entropies, ΔS , derived from analyses of the calorimetrically measured excess heat capacity, ΔC_p , versus temperature profiles are listed in Table 1 along with the corresponding ΔG_{25}° values calculated at 25°C. Analysis of the T_m values reveals that methylation of $[\text{PtCl}(\text{dien})]^+$ markedly enhances the efficiency of the monofunctional adducts of these Pt^{II} compounds to reduce the thermal stability of DNA. However, the melting temperature is not a thermodynamic parameter. Therefore, we also examined how the introduction of the monofunctional adduct of methylated analogues of $[\text{PtCl}(\text{dien})]^+$ affects the thermodynamic stability (ΔG_{25}°) of DNA duplexes.

The thermodynamic parameters derived from DSC data reveal that the two methylated complexes destabilize the double helices tested in this work significantly more than the nonmethylated $[\text{PtCl}(\text{dien})]^+$, as indicated by a 14–23 kJ mol^{-1} increase in the Gibbs free energy for duplex formation at 25°C (Table 1). Interestingly, the $\Delta\Delta G_{25}^\circ$ values observed for the melting of each duplex containing the adduct of $[\text{Pt}(\text{NO}_3)(\text{dien-Me}_3)]^+$ or $[\text{Pt}(\text{NO}_3)(\text{dien-Me}_5)]^+$ are identical or very similar (–23 kJ mol^{-1} for the duplex TGT(15), –16 or –15 kJ mol^{-1} for the duplex AGT(15) and –15 or –14 kJ mol^{-1} for the duplex GGT(15), see Table 1), which suggests that the monofunctional adducts of the two methylated Pt^{II} analogues, the bulkiness of which is in-

creased by three or five methyl groups, induce in DNA similar conformational alterations. Interestingly, these $\Delta\Delta G_{25}^\circ$ values represent an equilibrium preference for the unmodified duplexes over those modified by the nonmethylated $[\text{PtCl}(\text{dien})]^+$ or the methylated $[\text{Pt}(\text{NO}_3)(\text{dien-Me}_3)]^+$ or $[\text{Pt}(\text{NO}_3)(\text{dien-Me}_5)]^+$ of, respectively, 38, 10642, or 10642 to 1 for the TGT(15) duplex, 8, 635, or 424 to 1 for the AGT(15) duplex, and ~0.3, 429, or 287 to 1 for the GGT(15) duplex. Thus, these results support the view that multiple methylation of the dien moiety in the adducts of these monofunctional complexes markedly enhances the thermodynamic destabilization of DNA, which is most pronounced if the adduct is formed in the TGT sequence. This enhanced destabilization is likely to be associated with a markedly more extensive distortion of the DNA conformation.

Inspection of Table 1 also shows that the melting of each duplex accompanied by unfavorable free-energy terms results from characteristic compensation of unfavorable enthalpy and favorable entropy terms. In general, the unfavorable enthalpy terms correspond mainly to the disruption of the base-pair stacks, whereas the favorable entropy terms arise from contributions of the favorable dissociation of two strands and the release of counterions and water molecules. In short, relative to the unmodified parent duplexes TGT(15), AGT(15), or GGT(15), their transition enthalpies can be perturbed by as much as 110–113, 47–53, or 48–59 kJ mol^{-1} , respectively, by the monofunctional adduct of methylated analogues compared with only 18–31 kJ mol^{-1} by the monofunctional adduct of the nonmethylated complex. The magnitude of this effect of the adducts of the methylated complexes, particularly of those formed in the TGT sequence, is remarkable because it represents a loss of ~26% of the total enthalpy of dissociation of the parent duplexes although only 1 of the 15 base pairs is chemically altered. On the basis of nearest-neighbor predictions,^[40] complete loss of stacking on both sides of the platinated guanine residue of the duplexes TGT(15), AGT(15), or GGT(15) is expected to reduce the value of ΔH_{cal} considerably less.

The observed endothermic enthalpies result primarily from the endothermic heats for the disruption of base pairs and base–base stacks in the duplex. Hence, the formation of the monofunctional adducts of the methylated complexes in the TGT, 5'-AGT, or 5'-(7-deazaG)GT sequence of the duplex is more deleterious energetically than the complete loss of stacking on both sides of the unmodified base pair at that site. On the other hand, relative to duplexes containing the adduct of the nonmethylated complex $[\text{PtCl}(\text{dien})]^+$, their transition enthalpies are perturbed by the adduct formed in the sequence TGT or 5'-AGT by only ~30 kJ mol^{-1} , and, quite surprisingly, if the adduct is formed by $[\text{PtCl}(\text{dien})]^+$ at the 5'-(7-deazaG)GT sequence, the transition enthalpy of the duplex is even slightly increased. These observations can be explained in terms of a considerably more extensive decrease in stacking interactions caused by the adducts of the methylated analogues compared with the adducts of the nonmethylated $[\text{PtCl}(\text{dien})]^+$, which re-

sults from conformational alterations induced by these monofunctional adducts.

The changes in the thermodynamic stability of the duplexes examined in this work, $\Delta\Delta G_{25}^\circ$, caused by the formation of a single site-specific monofunctional adduct of the methylated analogues $[\text{Pt}(\text{NO}_3)(\text{dien-Me}_3)]^+$ or $[\text{Pt}(\text{NO}_3)(\text{dien-Me}_5)]^+$ reflect a combination of enthalpic ($\Delta\Delta H_{\text{cal}}$) and entropic ($\Delta\Delta S$) effects. The magnitudes of these effects vary with the sequence context. The relative contributions of the adduct-induced changes in the enthalpy and entropy terms for the disturbance of the duplexes TGT(15), AGT(15), and GGT(15) can be seen in Figure 4. Interestingly, the differences in the transition free-energy change, $\Delta\Delta G_{25}^\circ$, observed upon formation of the monofunctional adducts of $[\text{Pt}(\text{NO}_3)(\text{dien-Me}_3)]^+$ or $[\text{Pt}(\text{NO}_3)(\text{dien-Me}_5)]^+$ are significantly smaller than the observed differences in the transition enthalpy change ($\Delta\Delta H_{\text{cal}}$; Figure 4). The values of $\Delta\Delta H_{\text{cal}}$ range from -47 to -113 kJ mol^{-1} , whereas the values of $\Delta\Delta G_{25}^\circ$ range from only -14 to -23 kJ mol^{-1} . Regardless of the magnitude of $\Delta\Delta H_{\text{cal}}$, there is a considerable, but not complete, compensating change in the entropy term. Interestingly, the higher transition enthalpy change due to the adducts formed in the TGT sequence (compared with in the AGT or GGT sequence) is accompanied by a higher entropic compensation. The impact of the monofunctional adducts of methylated Pt^{II} complexes tested in this work on the enthalpy is always destabilizing, whereas the entropy term is always stabilizing. The compensation does not result in invariant stability with respect to sequence context and the type of monofunctional Pt^{II} complex. In addition, we have tried to answer the question whether sequence has any effect on the magnitude of the enthalpy-driven destabilization. Measured enthalpy differences of 16 , -9 , and -25 kJ mol^{-1} for the unmodified duplexes ($\Delta H_{\text{cal}}[\text{TGT}(15)] - \Delta H_{\text{cal}}[\text{AGT}(15)]$, $\Delta H_{\text{cal}}[\text{TGT}(15)] - \Delta H_{\text{cal}}[\text{GGT}(15)]$, and $\Delta H_{\text{cal}}[\text{AGT}(15)] - \Delta H_{\text{cal}}[\text{GGT}(15)]$, respectively) have been found (Table 1). On the other hand, the enthalpy differences between the three duplexes (TGT(15)–AGT(15), TGT(15)–GGT(15), or AGT(15)–GGT(15)) modified by $[\text{Pt}(\text{NO}_3)(\text{dien-Me}_3)]^+$ (the values obtained for $[\text{Pt}(\text{NO}_3)(\text{dien-Me}_5)]^+$ are given in parentheses) are equal to -41 (-50), -60 (-74), and -19 (-24) kJ mol^{-1} , respectively (Table 1), which indicates that the monofunctional adducts formed by methylated $[\text{Pt}(\text{NO}_3)(\text{dien-Me}_3)]^+$ or $[\text{Pt}(\text{NO}_3)(\text{dien-Me}_5)]^+$ in the TGT sequence induces more extensive unstacking interactions than in the 5'-AGT or 5'-(7-deazaG)GT sequence, which leads to a greater exposure of the nonpolar surface to the solvent. This allows us to predict that inclusion of the monofunctional adduct of the methylated analogue $[\text{Pt}(\text{NO}_3)(\text{dien-Me}_3)]^+$ or $[\text{Pt}(\text{NO}_3)(\text{dien-Me}_5)]^+$ into the TGT sequence yields more pronounced conformational alterations at the site of the adduct than in the 5'-AGT or 5'-(7-deazaG)GT sequence.

The $\Delta H_{\text{vH}}/\Delta H_{\text{cal}}$ ratio makes it possible to determine whether duplex-unfolding takes place in two-state transitions or through the formation of intermediates.^[31] If the $\Delta H_{\text{vH}}/\Delta H_{\text{cal}}$ ratio is equal to 1 then the transition takes place

in an all-or-none fashion.^[31] We obtained $\Delta H_{\text{vH}}/\Delta H_{\text{cal}}$ ratios in the range of 1.06–1.11, which confirms that each duplex examined in this work unfolds in a two-state transition. Hence, despite affecting the thermal and thermodynamic parameters of the unfolding of the host duplexes, methylation of $[\text{PtCl}(\text{dien})]^+$ does not affect the properties of the monofunctional adducts to the extent that they would markedly change the cooperativity of the melting transition of the host duplex. This demonstrates that neither the monofunctional adduct nor the identity of the base flanking the adduct on its 5' site alters the ability of the duplex to propagate those interactions required for cooperative melting.

In mammalian cells, various DNA repair pathways are important mechanisms for the removal of DNA adducts, including those generated by various chemotherapeutics. For instance, efficient repair by several repair systems of various cross-links produced by bifunctional platinum drugs has been reported.^[41–46] It has been suggested^[47–49] that the initial recognition event of the DNA lesion repair process is dependent on the lesion-induced alterations of duplex energetics. Only a very low level of repair synthesis is noticed if DNA containing monofunctional adducts of nonmethylated $[\text{PtCl}(\text{dien})]^+$ is used as a substrate for the DNA repair system (shown in Figure 7, lane dienPt). This observation is consistent with the view that monofunctional lesions induced in DNA by monofunctional adducts of Pt^{II} compounds, such as those of $[\text{PtCl}(\text{dien})]^+$, are not recognized by the components of DNA repair systems. Therefore we have also examined whether the enhancement of the bulkiness of monofunctional adducts of Pt^{II} –dien compounds by multiple methylation affects their DNA adducts to the extent that they become a substrate for DNA repair system(s). Markedly higher levels of damage-induced DNA repair synthesis are detected if DNA containing monofunctional adducts of methylated analogues are used as a substrate for the DNA repair system (Figure 7A, lanes dienPt-Me₃ and dienPt-Me₅, and Figure 7B). Thus, this markedly enhanced level of repair of the bulkier DNA adducts of methylated analogues correlates with the considerably higher thermodynamic destabilization of DNA induced by these complexes.

Similarly, monofunctional adducts of the plain and relatively small (nonmethylated) Pt^{II} complexes, such as $[\text{PtCl}(\text{dien})]^+$, are bypassed by DNA and RNA polymerases (see refs.^[18,46,50,51] and Figures 5 and 6). The results of this work (Figures 5 and 6) demonstrate that in contrast to the monofunctional adducts of the small $[\text{PtCl}(\text{dien})]^+$, the adducts of its considerably bulkier methylated analogues are a fairly strong block to DNA synthesis catalyzed by DNA polymerases. Thus, similarly to the case of DNA repair, the markedly enhanced efficiency of DNA adducts of the bulkier methylated analogues to block DNA polymerization correlates with a considerably higher thermodynamic destabilization of DNA induced by these complexes. Interestingly, there is no distinct difference between the efficiency of the adducts of $[\text{Pt}(\text{NO}_3)(\text{dien-Me}_3)]^+$ and $[\text{Pt}(\text{NO}_3)(\text{dien-Me}_5)]^+$ to reduce the thermodynamic stability of DNA and conse-

quently the DNA adducts of these different methylated complexes block DNA polymerization by KF[−] approximately equally (Figure 5). In contrast, the efficiency of the DNA adducts of the bulkiest pentamethylated complex to block DNA polymerization is distinctly higher than that of the less bulky [Pt(NO₃)(dien-Me₃)]⁺ if DNA polymerization is catalyzed by RT HIV-1 (Figure 6). The different processing of the DNA adducts of the methylated complexes by KF[−] and RT HIV-1 may be associated with the fact that RT HIV-1 is markedly more flexible than other nucleic acid synthesizing enzymes^[52] so that it can polymerize DNA across and beyond bulkier adducts more easily than other DNA polymerases. Thus, RT HIV-1, which has a sterically more flexible active site, may recognize not only the reduced thermodynamic stability of DNA and the enhanced bulkiness of DNA adducts, but, to a greater extent than other DNA polymerases, also their structure or shape.

The current models of recognition of DNA damage propose that the presence of a chemically modified nucleotide and the resulting destabilization of the duplex structure, either by the direct disruption of base-pair alignments or by more subtle perturbations, such as the unwinding or bending of the helix, are both required for DNA repair activity.^[49,53] The minimally perturbed structures of the duplexes modified by a relatively small molecule of [PtCl(dien)]⁺ and their only slightly affected thermodynamic stability are consistent with the view and the observations of this work (Figures 5–7) that the [PtCl(dien)]⁺ adduct is a very poor substrate for DNA repair systems and that it does not represent a strong block to DNA polymerization. On the other hand, the structures of the duplexes perturbed considerably more by the adducts of bulkier, multiply methylated [Pt(NO₃)(dien-Me₃)]⁺ and [Pt(NO₃)(dien-Me₅)]⁺ and the markedly reduced thermodynamic stability of these duplexes are in an excellent agreement with our results (Figures 5–7), which demonstrates that the adducts of [Pt(NO₃)(dien-Me₃)]⁺ and [Pt(NO₃)(dien-Me₅)]⁺ are very good substrates for DNA repair systems and represent a strong block to DNA polymerization. A common feature of various DNA lesions induced by Pt^{II} complexes, including those examined in this work, is the enthalpically driven thermodynamic destabilization of the helix.^[23–27,29,30,54,55] A reduction in the stability of double helices should make them susceptible to recognition of the damage. For example, less stable DNA should be more flexible and therefore should have a greater propensity to adopt the altered structure required in its productive complexes with components of DNA repair systems. So far as the catalytic efficiency of DNA polymerases is concerned, an enhanced flexibility of DNA may impede the formation of a gently tuned catalytically active structure of the ternary DNA polymerase primer/template DNA incoming dNTP complex.

The impact of methylation of [PtCl(dien)]⁺, which results in a considerable increase in the bulkiness of the nonleaving ligand, on the biophysical properties of DNA (such as thermodynamic, thermal, and conformational properties) and its biochemical processes (DNA polymerization and repair of

DNA adducts) is remarkable (see above). Hence, it is reasonable to suggest that the bulkiness of the DNA adducts of the Pt^{II} compounds is an important parameter that controls processes associated with the biological effects of these compounds. In other words, the results of this work demonstrate that monodentate DNA binding of Pt^{II} compounds, previously expected not to play a significant role in the biological effects of these complexes,^[1–3] may considerably affect the biophysical properties of DNA and consequently downstream cellular processes as a result of the large increase in the bulkiness of the nonleaving ligand in this class of metal complexes. For instance, if the adducts escape repair and survive to the next round of DNA replication, error-prone translesion bypass can occur, giving rise to mutations and ultimately to cancer. In addition, the results of this work confirm that changes in the thermodynamic properties of DNA induced by its modification by Pt^{II} complexes can be used as predictors of recognition by DNA polymerases and cellular repair proteins, including the efficiency of repair mechanisms to remove the lesion from DNA and the ability of the Pt^{II} compound to block DNA polymerization catalyzed by DNA polymerases across and beyond its adduct.

It is generally accepted that DNA repair and polymerization catalyzed by DNA polymerases play an important role in downstream cellular processes following DNA damage, such as mutagenesis, carcinogenesis, and cytotoxicity. It is important to understand each of these processes individually on a molecular level to assess the potency of DNA-damaging agents to exert biological effects. The results of this work also expand the database correlating the thermodynamic characteristics of well-defined DNA damage and the susceptibility of this damage to removal by DNA repair enzymes and its efficiency to block DNA polymerization catalyzed by DNA polymerases.

Experimental Section

Starting materials: Cisplatin and dimethyl sulfate (DMS) were obtained from Sigma–Aldrich s.r.o. (Prague, Czech Republic). [PtCl(dien)]Cl, [Pt(NO₃)(dien-Me₃)](NO₃), and [Pt(NO₃)(dien-Me₅)](NO₃) (Figure 1) were prepared and characterized as described below. Stock solutions of platinum compounds for the biophysical and biochemical studies were prepared in water and stored at room temperature in the dark. The concentrations of platinum in the stock solutions were determined by FAAS. CT DNA (42% G + C, mean molecular mass ca. 2 × 10⁷ Da) was prepared and characterized as described previously.^[56,57] pSP73KB (2455 bp) plasmid was isolated according to standard procedures. The synthetic oligodeoxyribonucleotides were purchased from VBC-Genomics (Vienna, Austria) and purified as described previously.^[58,59] Restriction endonuclease *Eco*RI, T4 polynucleotide kinase, and KF[−] were purchased from New England Biolabs. RT HIV-1 was from Amersham Pharmacia Biotech (Newport, UK). Acrylamide, bis(acrylamide), dithiothreitol, NaCN, ethidium bromide (EtBr), and urea were from Merck KGaA (Darmstadt, Germany). Nonidet P-30 was from Fluka (Prague, Czech Republic). Agarose was from FMC BioProducts (Rockland, ME). Radioactive products were from MP Biomedicals, LLC (Irvine, CA). Riboprobe Gemini System II for transcription mapping containing T7 RNA polymerase was purchased from Promega (Madison, WI). A cell-free extract (CFE) was prepared from the repair-proficient HeLa S3 cell line as described previously.^[43,60]

Synthesis and characterization of Pt^{II}-dien complexes: *N,N,N',N',N'*-Pentamethyldiethylenetriamine (Me₅dien) and *N,N',N''*-trimethyldiethylenetriamine (Me₃dien) from Aldrich were used as received. The complex [Pt(NO₃)(Me₅dien)](NO₃) was prepared as described previously.^[61] The complex [Pt(NO₃)(Me₃dien)](NO₃) was prepared from [PtI(Me₅dien)]₂·[Pt₂I₆].^[62] In a typical experiment [PtI(Me₅dien)]₂·[Pt₂I₆] (0.394 g, 0.184 mmol) was suspended in water (50 mL) and treated with silver nitrate (0.125 g, 0.736 mmol). The reaction mixture was stirred for about 1 h at 50 °C in the dark. The solution was filtered through Celite and then evaporated to dryness. The residue was treated with methanol and, after filtration, the solution was evaporated to give an oil that was mixed with ethanol (2 mL) to afford the pure product as white crystalline powder. Yield: 0.072 g, 79.5%; elemental analysis calcd (%) for C₉H₂₃N₅O₄Pt (493.11): C 21.95, H 4.71, N 14.22; found: C 22.29, H 4.77, N 13.82; ¹H NMR data in D₂O are as reported in the paper of Carloni^[61] for [Pt(H₂O)(Me₅dien)]²⁺ and [Pt(H₂O)(Me₃dien)]²⁺; ¹⁹⁵Pt NMR: δ = −2474 and −2392 ppm for [Pt(H₂O)(Me₅dien)]²⁺ and [Pt(H₂O)(Me₃dien)]²⁺, respectively; the value reported for [Pt(H₂O)(dien)]²⁺ was −2547 ppm.^[63]

Platination reactions: CT or plasmid DNA was incubated with the platinum complex in 10 mM NaClO₄ at 37 °C for 24 h in the dark unless stated otherwise. The number of molecules of the platinum compound bound (coordinated) per nucleotide residue (*r_b* values) was determined by FAAS or by DPP.^[64] For example, CT DNA (0.096 mg mL^{−1}) was incubated with the platinum complex at an initial *r_i* of 0.1 in NaClO₄ (10 mM) at 37 °C. After various intervals of time an aliquot of the reaction mixture was withdrawn and assayed by DPP for platinum not bound to DNA. The amount of platinum bound to DNA (*r_b*) was calculated by subtracting the amount of free (unbound) platinum from the total amount of platinum present in the reaction. The single-stranded oligonucleotide (the pyrimidine-rich strand) containing a single central G (5 × 10^{−5} M) was treated with stoichiometric amounts of the Pt^{II}-dien complexes. The platinated oligonucleotides were purified by ion-exchange HPLC. It was verified by FAAS and by absorbance measurements that one molecule of the modified oligonucleotides contained one platinum atom. It was also verified by DMS footprinting^[18] that one molecule of the Pt^{II}-dien complex was coordinated to the N7 atom of the single G in the top strand of each duplex.

DNA transcription by RNA polymerase in vitro: Transcription of the pSP73KB DNA with T7 RNA polymerase and electrophoretic analysis of the transcripts were performed as previously described.^[17,18] The concentration of DNA used in this assay was 3.9 × 10^{−5} M (relative to the monomeric nucleotide content).

Differential scanning calorimetry: Excess heat capacity (Δ*C_p*) versus temperature profiles for the thermally induced transitions of TGT(15), AGT(15), and GGT(15) duplexes (see Figure 3D for their sequences) unmodified or containing a unique monofunctional adduct of [PtCl(dien)]⁺, [Pt(dien-Me₃)(NO₃)]⁺, or [Pt(dien-Me₅)(NO₃)]⁺ were measured by using a VP-DSC calorimeter (Microcal, Northampton, MA). In the DSC experiments, the concentrations of the duplexes were 30 μM, the heating rate was 60 °C h^{−1}, and the maximum temperature was 95 °C. After reaching the maximum temperature the samples were cooled at the same rate to the starting temperature of 25 °C. In this study Δ*C_p* is defined as the excess heat capacity, which is baseline-subtracted and concentration-normalized.^[65] The reference scans were subtracted from the sample scans to obtain Δ*C_p* versus temperature profiles. The enthalpies (Δ*H_{cal}*) and entropies (Δ*S*) of duplex melting were calculated from the areas under the experimental Δ*C_p* versus *T* and the derived Δ*C_p*/*T* versus *T* curves, respectively, by using ORIGIN v.5.0 software (Microcal, Studio City, CA). The free energy of duplex dissociation at 25 °C (Δ*G₂₅*[°]) was calculated by using the standard thermodynamic relationship given by Equation (1) and the corresponding Δ*H_{cal}* and Δ*S* values.

$$\Delta G_{25}^{\circ} = \Delta H_{\text{cal}} - 298.15 \Delta S \quad (1)$$

The duplexes were dissolved in buffer at pH 7.0 containing sodium phosphate (NaH₂PO₄/Na₂HPO₄, 10 mM) and NaCl (150 mM). It was also verified, as described previously,^[24,25] that the melting transitions of both the platinated and unmodified duplexes were fully reversible.

Inhibition of DNA polymerization: The primer extension assays with all four dNTPs were performed with the 30-mer templates (see Figures 5A and 6A) containing a single monofunctional adduct of a Pt^{II}-dien complex prepared as described above in the section on platination reactions. The 17-mer DNA primer (its nucleotide sequence is shown in Figures 5A and 6A) was complementary to the 3' termini of the 30-mer templates. The DNA substrates (5 × 10^{−8} M) were formed by annealing the templates and 5'-end-labeled primers in a molar ratio of 3:1. All experiments using RT HIV-1 were performed at 37 °C in a volume of 50 μL in a buffer containing Tris-HCl (50 mM, pH 8.0), MgCl₂ (10 mM), KCl (50 mM), dithiothreitol (3 mM), Nonidet P-30 (0.1 %), dATP (100 μM), dCTP (100 μM), dGTP (100 μM), and TTP (100 μM), and RT HIV-1 (1.0 unit). The experiments with KF[−] were performed with the same 30-mer templates and 17-mer DNA primers and the same volume, but at 25 °C in a buffer consisting of Tris-HCl (50 mM, pH 7.4), MgCl₂ (10 mM), dithiothreitol (0.1 mM), and bovine serum albumin (50 μg mL^{−1}) the nucleoside triphosphates were at a concentration of 100 μM and 0.5 unit of KF[−] was used. Reactions were terminated after various intervals of time by the addition of EDTA (to give a resulting concentration of 20 mM) and heating at 100 °C for 30 s. Products were resolved by denaturing 15 % polyacrylamide/8 M urea gel and quantified by phosphor-imaging analysis. Other details have been published previously.^[36,46]

DNA repair synthesis by human cell extracts: Repair DNA synthesis of CFEs was assayed by using pSP73KB plasmid. Each reaction mixture of 50 μL contained unmodified or platinated pSP73KB (500 ng), ATP (2 mM), KCl (30 mM), creatine phosphokinase (rabbit muscle; 0.05 mg mL^{−1}), dGTP (20 mM), dCTP (20 mM), TTP (20 mM), dATP (8 mM), 74 kBq of [α-³²P]dATP in a buffer composed of HEPES-KOH (40 mM, pH 7.5), MgCl₂ (5 mM), dithiothreitol (0.5 mM), creatine phosphate (22 mM), bovine serum albumin (1.4 mg mL^{−1}), and CFE (150 μg). Reactions were incubated for 3 h at 25 °C and terminated by adding Na₂H₂EDTA to give a final concentration of 20 mM, sodium dodecyl sulfate to 0.6 %, and proteinase K to 250 μg mL^{−1} followed by incubation for 30 min. The products were extracted with one volume of 1:1 phenol/chloroform. The DNA was precipitated from the aqueous layer by the addition of 1/50 volume NaCl (5 M), glycogen (5 mg) and 2.5 volumes ethanol. After 20 min of incubation on dry ice and centrifugation at 12000 g for 30 min at 4 °C, the pellet was washed with 0.5 mL 70 % ethanol and dried in a vacuum centrifuge. DNA was finally linearized before electrophoresis on a 1 % agarose gel containing EtBr (0.3 mg mL^{−1}).

Other physical methods: Absorption spectra were measured with a Beckman 7400 DU spectrophotometer using quartz cells with a path length of 1 cm and a thermoelectrically controlled cell holder. The oligonucleotides were purified by HPLC on a Waters HPLC system consisting of a Waters 262 pump, a Waters 2487 UV detector, and a Waters 600S controller with a MonoQ HR 5/50 GL column. The FAAS measurements were carried out on a Varian AA240Z Zeeman atomic absorption spectrometer equipped with a GTA 120 graphite tube atomizer. For FAAS analyses, DNA was precipitated with ethanol and dissolved in HCl (0.1 M). DPP was performed with an EG&G Princeton Applied Research Corporation Model 384B Polarographic Analyzer. The gels were visualized by using a BAS 2500 FUJIFILM bioimaging analyzer and the radioactivity associated with the bands was quantified by using the AIDA image analyzer software (Raytest, Germany).

Acknowledgements

This research was supported by the Ministry of Education of the CR (MSMT LC06030, 6198959216, ME08017, OC08003, and OC09018), the Academy of Sciences of the Czech Republic (Grants 1QS500040581, KAN200200651, AV0Z50040507, and AV0Z50040702), the Grant Agency of the Academy of Sciences of the CR (IAA400040803), the Grant Agency of the CR (203/06/1239), the University of Bari, and MIUR (Italy). J.K. is an international research scholar of the Howard Hughes Medical Institute. The authors also acknowledge that their participation in the EU COST Action D39 has enabled them to exchange regularly

their most recent ideas in the field of anticancer metallodrugs with several European colleagues.

- [1] M. J. Cleare, J. D. Hoeschele, *Bioinorg. Chem.* **1973**, 2, 187–210.
- [2] S. E. Sherman, S. J. Lippard, *Chem. Rev.* **1987**, 87, 1153–1181.
- [3] J. Reedijk, *Chem. Commun.* **1996**, 801–806.
- [4] V. Brabec, V. Kleinwächter, J. L. Butour, N. P. Johnson, *Biophys. Chem.* **1990**, 35, 129–141.
- [5] E. R. Jamieson, S. J. Lippard, *Chem. Rev.* **1999**, 99, 2467–2498.
- [6] V. Brabec, *Prog. Nucleic Acid Res. Mol. Biol.* **2002**, 71, 1–68.
- [7] L. S. Hollis, A. R. Amundsen, E. W. Stern, *J. Med. Chem.* **1989**, 32, 128–136.
- [8] L. S. Hollis, W. I. Sundquist, J. N. Burstyn, W. J. Heiger-Bernays, S. F. Bellon, K. J. Ahmed, A. R. Amundsen, E. W. Stern, S. J. Lippard, *Cancer Res.* **1991**, 51, 1866–1875.
- [9] J. Y. Zhang, X. Y. Wang, C. Tu, J. Lin, J. Ding, L. P. Lin, Z. M. Wang, C. He, C. H. Yan, X. Z. You, Z. J. Guo, *J. Med. Chem.* **2003**, 46, 3502–3507.
- [10] R. C. Taylor, S. G. Ward in *The Antiviral Activity of Some Selected Inorganic and Organometallic Complexes. Possible New Chemotherapeutic Strategies* (Eds.: M. Nicolini, L. Sindellari), Raven Press, New York, **1991**, pp. 63–90.
- [11] M. Coluccia, A. Boccarelli, C. Cermelli, M. Portolani, G. Natile, *Met.-Based Drugs* **1995**, 2, 249–256.
- [12] Z. Balcarova, J. Kašpárková, A. Zakovska, O. Nováková, M. F. Sivo, G. Natile, V. Brabec, *Mol. Pharmacol.* **1998**, 53, 846–855.
- [13] N. Margiotta, G. Natile, F. Capitelli, F. P. Fanizzi, A. Boccarelli, P. De Rinaldis, D. Giordano, M. Coluccia, *J. Inorg. Biochem.* **2006**, 100, 1849–1857.
- [14] K. S. Lovejoy, R. C. Todd, S. Z. Zhang, M. S. McCormick, J. A. D'Aquino, J. T. Reardon, A. Sancar, K. M. Giacomini, S. J. Lippard, *Proc. Natl. Acad. Sci. USA* **2008**, 105, 8902–8907.
- [15] D. Wang, S. J. Lippard, *Nat. Rev. Drug Discovery* **2005**, 4, 307–320.
- [16] L. Kelland, *Nat. Rev. Cancer* **2007**, 7, 573–584.
- [17] M. A. Lemaire, A. Schwartz, A. R. Rahmouni, M. Leng, *Proc. Natl. Acad. Sci. USA* **1991**, 88, 1982–1985.
- [18] V. Brabec, M. Leng, *Proc. Natl. Acad. Sci. USA* **1993**, 90, 5345–5349.
- [19] H. Loskotova, V. Brabec, *Eur. J. Biochem.* **1999**, 266, 392–402.
- [20] R. Prokop, J. Kašpárková, O. Nováková, V. Marini, A. M. Pizarro, C. Navarro-Ranninger, V. Brabec, *Biochem. Pharmacol.* **2004**, 67, 1097–1109.
- [21] V. Brabec, V. Boudny, Z. Balcarova, *Biochemistry* **1994**, 33, 1316–1322.
- [22] J. Malina, C. Hofr, L. Maresca, G. Natile, V. Brabec, *Biophys. J.* **2000**, 78, 2008–2021.
- [23] D. S. Pilch, S. U. Dunham, E. R. Jamieson, S. J. Lippard, K. J. Breslauer, *J. Mol. Biol.* **2000**, 296, 803–812.
- [24] C. Hofr, V. Brabec, *J. Biol. Chem.* **2001**, 276, 9655–9661.
- [25] C. Hofr, N. Farrell, V. Brabec, *Nucleic Acids Res.* **2001**, 29, 2034–2040.
- [26] V. Brabec, K. Stehlikova, J. Malina, M. Vojtiskova, J. Kašpárková, *Arch. Biochem. Biophys.* **2006**, 446, 1–10.
- [27] J. Malina, O. Nováková, M. Vojtiskova, G. Natile, V. Brabec, *Biophys. J.* **2007**, 93, 3950–3962.
- [28] S. M. Cohen, Y. Mikata, Q. He, S. J. Lippard, *Biochemistry* **2000**, 39, 11771–11776.
- [29] N. Poklar, D. S. Pilch, S. J. Lippard, E. A. Redding, S. U. Dunham, K. J. Breslauer, *Proc. Natl. Acad. Sci. USA* **1996**, 93, 7606–7611.
- [30] C. Hofr, V. Brabec, *Biopolymers* **2005**, 77, 222–229.
- [31] L. A. Marky, K. J. Breslauer, *Biopolymers* **1987**, 26, 1601–1620.
- [32] K. M. Comess, J. N. Burstyn, J. M. Essigmann, S. J. Lippard, *Biochemistry* **1992**, 31, 3975–3990.
- [33] Z. Suo, K. Johnson, *J. Biol. Chem.* **1998**, 273, 27259–27267.
- [34] A. Vaisman, M. W. Warren, S. G. Chaney, *J. Biol. Chem.* **2001**, 276, 18999–19005.
- [35] E. Bassett, A. Vaisman, J. M. Havener, C. Masutani, F. Hanaoka, S. G. Chaney, *Biochemistry* **2003**, 42, 14197–14206.
- [36] J. Kasparkova, O. Nováková, V. Marini, Y. Najajreh, D. Gibson, J.-M. Perez, V. Brabec, *J. Biol. Chem.* **2003**, 278, 47516–47525.
- [37] B. Moriarity, O. Nováková, N. Farrell, V. Brabec, J. Kašpárková, *Arch. Biochem. Biophys.* **2007**, 459, 264–272.
- [38] A. Alt, K. Lammens, C. Chiochini, A. Lammens, J. C. Pieck, D. Kuch, K. P. Hopfner, T. Carell, *Science* **2007**, 318, 967–970.
- [39] K. A. Johnson, *Annu. Rev. Biochem.* **1993**, 62, 685–713.
- [40] J. SantaLucia, Jr., *Proc. Natl. Acad. Sci. USA* **1998**, 95, 1460–1465.
- [41] D. B. Zamble, D. Mu, J. T. Reardon, A. Sancar, S. J. Lippard, *Biochemistry* **1996**, 35, 10004–10013.
- [42] B. Koberle, K. A. Grimaldi, A. Sunter, J. A. Hartley, L. R. Kelland, J. R. W. Masters, *Int. J. Cancer* **1997**, 70, 551–555.
- [43] J. T. Reardon, A. Vaisman, S. G. Chaney, A. Sancar, *Cancer Res.* **1999**, 59, 3968–3971.
- [44] J. Malina, J. Kašpárková, G. Natile, V. Brabec, *Chem. Biol.* **2002**, 9, 629–638.
- [45] J. Kasparkova, O. Nováková, N. Farrell, V. Brabec, *Biochemistry* **2003**, 42, 792–800.
- [46] O. Novakova, J. Kašpárková, J. Malina, G. Natile, V. Brabec, *Nucleic Acids Res.* **2003**, 31, 6450–6460.
- [47] G. E. Plum, K. J. Breslauer, *Ann. N.Y. Acad. Sci.* **1994**, 726, 45–56.
- [48] G. E. Plum, C. A. Gelfand, K. J. Breslauer in *Physicochemical Approaches to Structural Elucidation. Effects of 3,N4-Ethenodeoxycytidine on Duplex Stability and Energetics Publication No. 150* (Eds.: B. Singer, H. Bartsch), International Agency for Research on Cancer, Lyon, **1999**, pp. 169–177.
- [49] N. E. Geacintov, S. Broyde, T. Buterin, H. Naegeli, M. Wu, S. X. Yan, D. J. Patel, *Biopolymers* **2002**, 65, 202–210.
- [50] Y. Corda, C. Job, M.-F. Anin, M. Leng, D. Job, *Biochemistry* **1993**, 32, 8582–8588.
- [51] R. Zaludova, A. Zakovska, J. Kašpárková, Z. Balcarova, O. Vrana, M. Coluccia, G. Natile, V. Brabec, *Mol. Pharmacol.* **1997**, 52, 354–361.
- [52] A. P. Silverman, E. T. Kool, *J. Am. Chem. Soc.* **2007**, 129, 10626–10627.
- [53] M. Missura, T. Buterin, R. Hindges, U. Hubscher, J. Kašpárková, V. Brabec, H. Naegeli, *EMBO J.* **2001**, 20, 3554–3564.
- [54] J. Malina, O. Nováková, B. K. Keppler, E. Alessio, V. Brabec, *J. Biol. Inorg. Chem.* **2001**, 6, 435–445.
- [55] V. Bursova, J. Kašpárková, C. Hofr, V. Brabec, *Biophys. J.* **2005**, 88, 1207–1214.
- [56] V. Brabec, E. Palecek, *Biophys. Chem.* **1976**, 4, 79–92.
- [57] V. Brabec, E. Palecek, *Biophysik* **1970**, 6, 290–300.
- [58] V. Brabec, J. Reedijk, M. Leng, *Biochemistry* **1992**, 31, 12397–12402.
- [59] J. Kasparkova, N. Farrell, V. Brabec, *J. Biol. Chem.* **2000**, 275, 15789–15798.
- [60] J. L. Manley, A. Fire, A. Cano, P. A. Sharp, M. L. Gefter, *Proc. Natl. Acad. Sci. USA* **1980**, 77, 3855–3859.
- [61] M. Carlone, F. P. Fanizzi, F. P. Intini, N. Margiotta, L. G. Marzilli, G. Natile, *Inorg. Chem.* **2000**, 39, 634–641.
- [62] R. Cini, F. P. Intini, L. Maresca, C. Pacifico, G. Natile, *Eur. J. Inorg. Chem.* **1998**, 1305–1312.
- [63] P. S. Pregosin, *Annu. Rep. NMR Spectrosc.* **1986**, 24, 285–349.
- [64] S. D. Kim, O. Vrana, V. Kleinwächter, K. Niki, V. Brabec, *Anal. Lett.* **1990**, 23, 1505–1518.
- [65] S. A. Leharne, B. Z. Chowdhry in *Thermodynamic Background to Differential Scanning Calorimetry* (Eds.: J. E. Ladbury, B. Z. Chowdhry), Wiley, New York, **1998**, pp. 157–182.

Received: February 11, 2009
Published online: May 15, 2009

8.

available at www.sciencedirect.comjournal homepage: www.elsevier.com/locate/biochempharm

DNA interactions of dinuclear Ru^{II} arene antitumor complexes in cell-free media

Olga Nováková^a, Alexey A. Nazarov^b, Christian G. Hartinger^b,
Bernhard K. Keppler^b, Viktor Brabec^{a,*}

^a Institute of Biophysics, Academy of Sciences of the Czech Republic, v.v.i., CZ-61265 Brno, Czech Republic

^b Institute of Inorganic Chemistry, University of Vienna, A-1090 Vienna, Austria

ARTICLE INFO

Article history:

Received 4 September 2008

Accepted 21 October 2008

Keywords:

Dinuclear ruthenium complex

Arene

Antitumor

DNA

Cross-links

Cytotoxicity

ABSTRACT

We recently synthesized and characterized water-soluble dinuclear Ru^{II} arene complexes, in which two $\{(\eta^6\text{-p-isopropyltoluene})\text{RuCl}[3\text{-(oxo-}\kappa\text{O)-2-methyl-4-pyridinonato-}\kappa\text{O}_4]\}$ units were linked by flexible chains of different length $[(\text{CH}_2)_n \text{ (} n = 4, 6, 8, 12)]$. These new dinuclear ruthenium drugs were found to exert promising cytotoxic effects in human cancer cells. In the present work DNA modifications by these new dinuclear Ru^{II} arene compounds, which differed in the length of the linker between the two Ru^{II} centers, were examined by biochemical and biophysical methods. The complexes bind DNA forming intrastrand and interstrand cross-links in one DNA molecule in the absence of proteins. An intriguing aspect of the DNA-binding mode of these dinuclear Ru^{II} compounds is that they can cross-link two DNA duplexes and also proteins to DNA—a feature not observed for other anti-tumor ruthenium complexes. Thus, the concept for the design of interhelical and DNA–protein cross-linking agents based on dinuclear Ru^{II} arene complexes with sufficiently long linkers between two Ru centers may result in new compounds which exhibit a variety of biological effects and can be also useful in nucleic acids research.

© 2008 Elsevier Inc. All rights reserved.

1. Introduction

Ruthenium(II) organometallic complexes have been gaining popular interest as potential anticancer agents [1–6]. One group of these compounds that exhibit anticancer activity, including activity against cisplatin (cis-diamminedichlorido-

platinum(II)) resistant cancer cells, comprises organoruthenium complexes of the type $[(\eta^6\text{-arene})\text{Ru}^{\text{II}}(\text{en})\text{Cl}]^+$, where arene = benzene or a benzene derivative, and en = 1,2-diaminoethane [7,8]. This class of complexes readily interact with DNA, which is considered an important pharmacological target of a number of metal-based antitumor drugs [5,9,10],

* Corresponding author. Tel.: +420 541517148; fax: +420 541240499.

E-mail address: brabec@ibp.cz (V. Brabec).

Abbreviations: bp, base pair; CD, circular dichroism; cisplatin, cis-diamminedichloridoplatinum(II); CL, cross-link; CT, calf thymus; DMS, dimethyl sulphate; EtBr, ethidium bromide; FAAS, flameless atomic absorption spectrometry; IC₅₀, the concentration of the compound that afforded 50% cell killing; ICD, induced circular dichroism; KF[−], Klenow fragment from DNA polymerase I, exonuclease minus mutated to remove the 3′ → 5′ proofreading activity; [PtCl(dien)]Cl, chloridodiethylenetriamineplatinum(II) chloride; r_b , the number of molecules of the metal-based compound bound per nucleotide residue; r_i , the molar ratio of free metal complex to nucleotides at the onset of incubation with DNA; Ru(4), 1,4-bis[chlorido[3-(oxo- κ O)-2-methyl-4-pyridinonato- κ O₄](η^6 -p-isopropyltoluene)ruthenium]butane; Ru(6), 1,6-bis[chlorido[3-(oxo- κ O)-2-methyl-4-pyridinonato- κ O₄](η^6 -p-isopropyltoluene)ruthenium]hexane; Ru(8), 1,8-bis[chlorido[3-(oxo- κ O)-2-methyl-4-pyridinonato- κ O₄](η^6 -p-isopropyltoluene)ruthenium]octane; Ru(12), 1,12-bis[chlorido[3-(oxo- κ O)-2-methyl-4-pyridinonato- κ O₄](η^6 -p-isopropyltoluene)ruthenium]dodecane; SDS, sodium dodecyl sulphate.

0006-2952/\$ – see front matter © 2008 Elsevier Inc. All rights reserved.

doi:10.1016/j.bcp.2008.10.021

and they can form stable monofunctional adducts with DNA. These adducts affect the DNA conformation and are recognized by downstream cellular systems in a unique way [11–13]. Therefore, much attention is being paid at present to the design of new ruthenium complexes that would exhibit new DNA-binding properties that differ from those already described [5,14].

An interesting class of metallodrugs that bind to DNA in a unique way, and consequently exhibit new biological properties is represented by polynuclear platinum or ruthenium complexes with flexible or sterically rigid linking groups [15–23]. Recently, water-soluble dinuclear Ru^{II} arene complexes, in which two $\{(\eta^6\text{-p-isopropyltoluene})\text{RuCl}[\text{3-(oxo-}\kappa\text{O)-2-methyl-4-pyridinonato-}\kappa\text{O}_4]\}$ units were linked by chains of different length $[(\text{CH}_2)_n \text{ (} n = 4, 6, 8, 12)]$ (Fig. 1), were reported [24]. These new dinuclear ruthenium drugs were found to exert promising cytotoxic effects in human cancer cells being markedly more active than the mononuclear analogues [24] and even more interestingly, their potency increased with growing length of the linker between the ruthenium centers. In addition, several studies on chemical behavior of these dinuclear Ru(II) arene complexes have been conducted [25] and manuscript in preparation. The hydrolysis appears to be very fast and complete. These studies also demonstrate that both chloro groups in the dinuclear ruthenium complexes are replaced by water ligands. No evidence for cleavage of the dinuclear species was observed in these studies, and the hydrolysis was the only alteration of the original molecules. If the dinuclear ruthenium complexes reacted with monomeric nucleotides, a very fast reaction with guanosine- and adenosine-monophosphates was observed, but no reaction with cytidine, uridine, or thymidine monophosphates.

We analyzed in the present work the DNA-binding mode of these new dinuclear ruthenium arene complexes by various methods of molecular biology and biophysics and found that they bound to DNA in a unique way forming also interhelical

and DNA–protein cross-links—a feature not observed for other ruthenium complexes hitherto tested for biological activity.

2. Materials and methods

2.1. Starting materials

The dinuclear Ru^{II} arene complexes (Fig. 1) were prepared and characterized as described previously [24,25]. Cisplatin was obtained from Sigma–Aldrich s.r.o. (Prague, Czech Republic). Chloridodiethylenetriamineplatinum(II) chloride ($[\text{PtCl}(\text{dien})]\text{Cl}$) was a generous gift of Prof. G. Natile from the University of Bari. Stock solutions of metal complexes for the biophysical and biochemical studies were prepared at a concentration of 4×10^{-4} M in double distilled water and stored at -20°C in the dark. The concentrations of ruthenium or platinum in the stock solutions were determined by flameless atomic absorption spectrometry (FAAS) or electron absorption spectrophotometry. Calf-thymus (CT) DNA (42% G + C, mean molecular mass ca. 2×10^7) was also prepared and characterized as described previously [26,27]. pSP73 [2464 base pairs (bp)] and pSP73KB (2455 bp) plasmids were isolated according to standard procedures. 107-bp, 221-bp, and 801-bp DNA fragments were isolated and purified in the same way as described recently [28]. Restriction endonucleases EcoRI, HpaI, NdeI, and PvuI, T4 polynucleotide kinase, and Klenow fragment from DNA polymerase I (exonuclease minus-KF[−], mutated to remove the 3' → 5' proofreading activity) were purchased from New England Biolabs (Frankfurt am Main, Germany). O'GeneRuler™ 1 kb Plus DNA Ladder Plus, ready-to-use was from Fermentas UAB (Vilnius, Lithuania) and histone H1 from Roche Diagnostics, GmbH (Mannheim, Germany). Dithiothreitol and ethidium bromide (EtBr) were from Merck KGaA (Darmstadt, Germany), sodium dodecyl sulphate (SDS) from Serva (Heidelberg, Germany), and proteinase K from Boehringer (Mannheim, Germany). Agarose and Metaphor® agarose were from FMC BioProducts (Rockland, ME). Wizard® SV and PCR Clean-Up System used to extract and purify 107-bp, 221-bp, and 801-bp DNA fragments (*vide infra*) were purchased from Promega (Mannheim, Germany). Nonidet P-30 was from Fluka (Prague, Czech Republic), and radioactive products were from MP Biomedicals, LLC (Irvine, CA).

2.2. Metalation reactions

CT DNA and plasmid DNAs were incubated with ruthenium or platinum complex in 10 mM NaClO₄ (pH ~ 6) at 37 °C for 24 h in the dark, if not stated otherwise. The number of atoms of the metal-based compound bound per nucleotide residue (r_b values) were determined by FAAS and/or absorption spectrophotometry.

2.3. Preparation of proteins

The final composition of the storage buffers were: KF[−]: 10 mM Tris pH 8, 0.5 mM EDTA, 100 µg bovine serum albumin/mL, 50% glycerol and 2 mM MgSO₄; histone H1: 10 mM Tris pH 7.9, 20 mM NaCl for histone H1. The commercially available sample of KF[−] was in the manufacturer's storage buffer

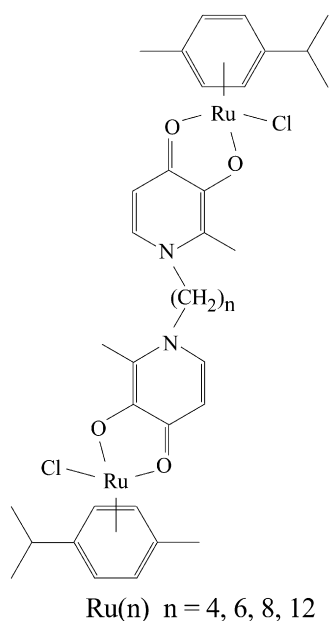


Fig. 1 – Structures of the dinuclear Ru^{II} arene complexes used in the present work and their abbreviations.

containing dithiothreitol and was exchanged for that specified above using microcon concentrators.

2.4. DNA transcription by RNA polymerase *in vitro*

Transcription of the (NdeI/HpaI) restriction fragment of pSP73KB DNA with T7 RNA polymerase and electrophoretic analysis of the transcripts were performed according to the protocols recommended by Promega [Promega Protocols and Applications, 43–46 (1989/90)] [29,30]. The DNA concentration used in this assay was 2.2×10^{-4} M (related to the monomeric nucleotide content).

2.5. Fluorescence measurements

The measurements were performed on a Varian Cary Eclipse spectrofluorophotometer using a 1 cm quartz cell. Fluorescence measurements of DNA modified by ruthenium and platinum complexes at a concentration of 32 $\mu\text{g/mL}$ in the presence of EtBr were performed at an excitation wavelength of 546 nm, and the emitted fluorescence was analyzed at 590 nm. The fluorescence intensity was measured at 25 °C in 0.4 M NaCl to avoid secondary binding of EtBr to DNA [31,32]. The concentrations were 0.01 mg/mL for DNA and 0.04 mg/mL for EtBr, which corresponds to the saturation of all intercalation sites of EtBr in DNA [31].

2.6. Unwinding of negatively supercoiled DNA

Unwinding of closed circular supercoiled pSP73KB plasmid DNA was assayed by an agarose gel mobility shift assay [33]. The unwinding angle Φ , induced per DNA adduct of dinuclear Ru^{II} arene complex, was calculated upon the determination of the r_b value at which the complete transformation of the supercoiled plasmid to the relaxed form was attained. Samples of plasmid DNA at a concentration of 1.6×10^{-4} M (related to the monomeric nucleotide content) were incubated with complexes Ru(4), Ru(6), Ru(8), or Ru(12) at 37 °C in the dark for 24 h. All samples were precipitated by ethanol and redissolved in the TAE (Tris-acetate/EDTA) buffer. One aliquot of the precipitated sample was subjected to electrophoresis on 1% agarose gels running at 25 °C in the dark with TAE buffer and the voltage set at 25 V. The gels were then stained with EtBr, followed by photography with a transilluminator. The other aliquot was used for the determination of r_b values by FAAS.

2.7. Circular dichroism (CD)

Isothermal CD spectra of CT DNA modified by dinuclear Ru^{II} arene complexes were recorded at 25 °C in 10 mM NaClO_4 by using a Jasco J-720 spectropolarimeter equipped with a thermoelectrically controlled cell holder with a cell pathlength of 1 cm. The spectra were recorded in the range of 230–500 nm in 0.5 nm increments with an averaging time of 0.25 s, speed 200 nm/min and 3 accumulations.

2.8. DNA interstrand cross-linking

The dinuclear Ru^{II} arene complexes were incubated with 1 μg of a 221-bp NdeI/HpaI fragment of pSP73 DNA. The DNA

fragment was first 3'-end labeled by means of KF^- in the presence of $[\alpha\text{-}^{32}\text{P}]\text{dATP}$. The ruthenated samples were precipitated by ethanol and analyzed for DNA interstrand CLs by previously published procedures [29,34]. After the ruthenation, the samples were precipitated by ethanol and the pellet was dissolved in 18 μL of a solution containing 30 mM NaOH, 1 mM EDTA, 6.6% sucrose and 0.04% bromophenol blue. The amount of interstrand cross-links was analyzed by electrophoresis under denaturing conditions on alkaline agarose gel (1%). After the electrophoresis was completed, the intensities of the bands corresponding to single strands of DNA and interstrand cross-linked duplex were quantified by means of a bio-imaging analyzer.

2.9. Interhelical cross-linking

An equimolar mixture of pSP73 plasmid linearized by NdeI (2464 bp) and short 801-bp PvuI/NdeI restriction fragment of pSP73 uniquely 5'-end labeled at the NdeI restriction site was ruthenated in 0.08 M NaClO_4 at $r_b = 0.025\text{--}0.1$ in a reaction volume of 13 μL . The total amount of DNA in these mixtures was 1.0 pmol. Aliquots were subjected to electrophoresis in a 1% agarose gel in TAE buffer [35]. The location of the linearized pSP73 plasmid in the gel was visualized by fluorescence under UV irradiation after staining the gel with EtBr; subsequently, the gel was dried and subjected to autoradiography, revealing the location of the radioactively labeled fragment.

2.10. DNA-protein cross-linking

The ruthenated DNA (107-bp NdeI/EcoRI fragment of pSP73 plasmid at a concentration of 20 nM or 221-bp NdeI/HpaI fragment of pSP73 plasmid at a concentration of 10 nM) was incubated with proteins (KF^- or histone H1) at a concentration of 0.2 μM overnight in the dark at room temperature in the appropriate buffer: 10 mM Tris pH 8, 10 mM EDTA, 0.1 μM bovine serum albumin, 0.8% glycerol and 2 mM MgSO_4 (KF^-); 10 mM Tris pH 7.9 and 20 mM NaCl (histone H1). The ability to form cross-links between DNA fragments and proteins was assessed by 1.3% agarose (agarose and Metaphor[®] agarose 1:1) gel electrophoresis after mixing the samples with the loading buffer (50 mM Tris-HCl, pH 6.8, 2% SDS, 0.1% bromophenol blue, 10% glycerol) and denaturing by heat at 60 °C for 5 min. Gels were electrophoresed for 3 h at 40 V, dried and visualized with a bio-imaging analyzer.

2.11. Other physical methods

Absorption spectra were measured with a Beckmann DU-7400 spectrophotometer. FAAS measurements were carried out with a Varian AA240Z Zeeman atomic absorption spectrometer equipped with a GTA 120 graphite tube atomizer. For FAAS analysis DNA was precipitated with ethanol and dissolved in double distilled water. The gels were visualized by using a BAS 2500 FUJIFILM bio-imaging analyzer, and the radioactivities associated with bands were quantitated with the AIDA image analyzer software (Raytest, Germany).

3. Results

3.1. DNA binding in cell-free media

Solutions of double-helical CT DNA at a concentration of 0.1 mg/mL were incubated at 37 °C with the complexes Ru(4), Ru(6), Ru(8), or Ru(12) in 10 mM NaClO₄ at an r_i value of 0.05 (r_i is defined as the molar ratio of free ruthenium complex to nucleotide-phosphates at the onset of incubation with DNA).

At various time intervals, aliquots of the reaction mixtures were withdrawn, the reactions were stopped by adding 1.5 M NaCl (1/10 of the total volume), quickly cooled on an ice bath, DNA was precipitated by ethanol, and the content of ruthenium in the supernatant of these samples was determined by FAAS. The amount of DNA bound dinuclear Ru^{II} arene compounds (r_b) increased with time. All complexes bind rapidly (the times at which the binding reached 30% was ca. 10 s and the maximum binding was reached in less than ca.

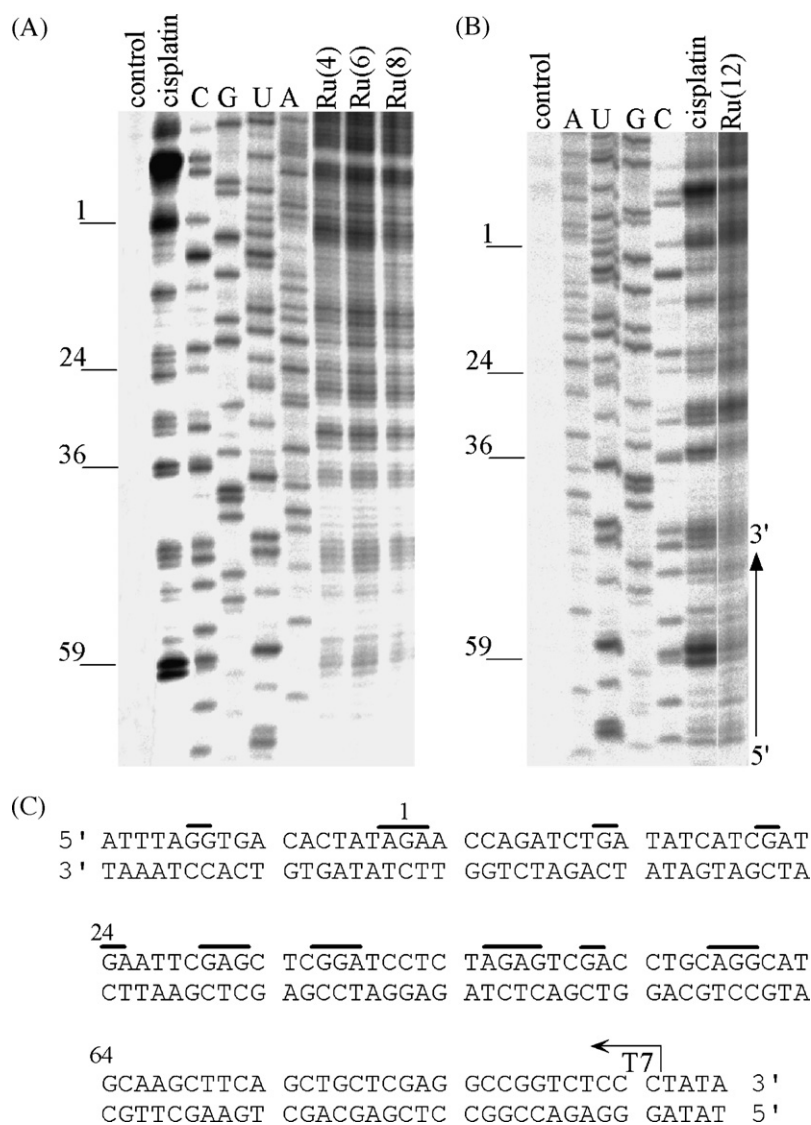


Fig. 2 – Inhibition of RNA synthesis by T7 RNA polymerase on the NdeI/HpaI fragment of pSP73KB plasmid modified by the dinuclear Ru^{II} arene complexes and cisplatin. (A and B) Autoradiograms of a 6% polyacrylamide/8 M urea sequencing gel showing the inhibition of RNA synthesis by T7 RNA polymerase on the NdeI/HpaI fragment containing adducts of Ru^{II} arene complexes and cisplatin. Lanes in left panel: control, unmodified template; A, U, G and C, chain terminated marker DNAs; cisplatin, Ru(4), Ru(6), Ru(8), the template modified by cisplatin, dinuclear Ru^{II} arene complexes Ru(4), Ru(6), Ru(8) at $r_b = 0.01$, respectively. Lanes in right panel: control, unmodified template; A, U, G and C, chain terminated marker DNAs; cisplatin, Ru(12), the template modified by cisplatin and dinuclear Ru^{II} arene complex Ru(12) at $r_b = 0.01$, respectively. (C) Schematic diagram showing the portion of the nucleotide sequence used to monitor the inhibition of the RNA synthesis by cisplatin and the dinuclear Ru^{II} arene complexes. The arrow indicates the start of the T7 RNA polymerase, which used the upper strand of the NdeI/HpaI fragment of pSP73KB as template. The short lines above the sequence represent major stop signals for DNA modified by cisplatin or dinuclear Ru^{II} arene complexes, respectively. The numbers correspond to the nucleotide numbering in the sequence map of the pSP73KB plasmid.

10 min), but not quantitatively, ca. 60% of the complexes Ru(4), Ru(6), and Ru(8) and ca. 75% of complex Ru(12) were bound after 40 h. Similar results were obtained if solutions of DNA were incubated with the complexes at an r_i value of 0.08.

The binding experiments indicate that modification reactions resulted in the irreversible binding of the dinuclear Ru^{II} arene complexes to CT DNA, which thus facilitated further sample analysis, and it was possible to prepare samples of DNA modified by the complexes Ru(4), Ru(6), Ru(8), or Ru(12) at a preselected value of r_b . Thus, except where stated, samples of DNA modified by the dinuclear Ru^{II} arene compounds Ru(4), Ru(6), Ru(8), or Ru(12) were prepared in 10 mM NaClO₄ at 37 °C for further analysis by biophysical or biochemical methods. After 24 h of the reaction of DNA with the complex, the samples were precipitated in ethanol and dissolved in the medium necessary for a particular analysis, and the r_b value in an aliquot of this sample was checked by FAAS. Accordingly, all analyses were performed in the absence of unbound (free) dinuclear Ru^{II} arene complex.

3.2. Transcription mapping of DNA adducts

In vitro RNA synthesis by RNA polymerases on DNA templates containing several types of adducts of platinum or ruthenium complexes can be prematurely terminated at the level or in the proximity of adducts [11,29]. Cutting of pSP73KB DNA [29] by NdeI and HpaI restriction endonucleases yielded a 212-bp fragment (a substantial part of its nucleotide sequence is shown in Fig. 2C). This fragment contained T7 RNA polymerase promoter [in the upper strand close to its 3'-end (Fig. 2C)]. The experiments were carried out using this linear DNA fragment, modified at $r_b = 0.01$ by Ru(4), Ru(6), Ru(8), or Ru(12) and for comparative purposes also by cisplatin, for RNA synthesis by T7 RNA polymerase (Fig. 2A, lanes Ru(4), Ru(6), Ru(8), and cisplatin and Fig. 2B, lanes Ru(12) and cisplatin). RNA synthesis on the template modified by all ruthenium complexes and cisplatin yielded fragments of defined sizes, which indicates that RNA synthesis on these templates was prematurely terminated (Fig. 2A and B). The major stop sites, primarily guanine residues, were roughly identical for all dinuclear Ru^{II} arene complexes (Fig. 2A and B). The profiles are similar to that obtained for DNA treated with the anticancer drug cisplatin (lane cisplatin in Fig. 2A and B) and also to those reported previously for other type of mononuclear Ru^{II} arene complexes, such as $[(\eta^6\text{-arene})\text{Ru}(\text{en})\text{Cl}]^+$ where en = 1,2-diaminoethane and arene = biphenyl, dihydroanthracene, tetrahydroanthracene, *p*-cymene, or benzene [11], but somewhat different from that obtained for DNA treated with the clinically inefficient transplatin [29]. The major stop sites for DNA modified by complex Ru(8) and cisplatin are demonstrated in Fig. 2C. These results suggest that the preferred binding sites for Ru(4), Ru(6), Ru(8), and Ru(12) on DNA are guanine residues.

3.3. Ethidium bromide (EtBr) fluorescence

The ability of the complexes to displace the DNA intercalator EtBr from CT DNA was probed by monitoring the relative fluorescence of the EtBr-DNA adduct after treating the DNA with varying concentrations of ruthenium or platinum

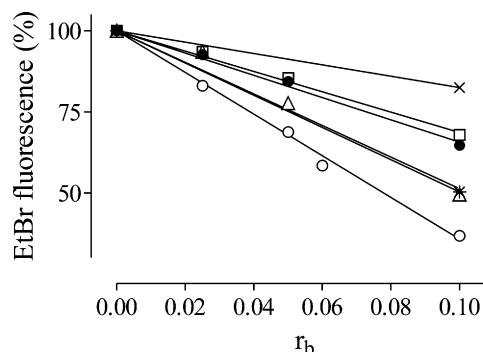


Fig. 3 – Plots of the EtBr fluorescence versus r_b values for calf-thymus DNA modified by cisplatin, [PtCl(dien)]Cl and the dinuclear Ru^{II} arene complexes in 10 mM NaClO₄ at 37 °C for 24 h: (x), [PtCl(dien)]Cl; (*), cisplatin; (Δ), Ru(4); (□), Ru(6); (●), Ru(8); (○) Ru(12). Data points were measured in triplicate and varied on average $\pm 3\%$ from their mean.

complexes. Fig. 3 shows a plot of relative fluorescence versus r_b for the complexes Ru(4), Ru(6), Ru(8), and Ru(12), cisplatin and [PtCl(dien)]Cl. DNA intercalated EtBr was markedly more effectively replaced by adduct formation with the dinuclear Ru^{II} arene compounds than with monofunctional [PtCl(dien)]Cl. Complex Ru(12) was the most effective compound in replacing EtBr and it was even considerably more effective than the adducts of bifunctional cisplatin.

3.4. DNA unwinding

The unwinding of supercoiled plasmid DNA induced by the four dinuclear Ru^{II} arene complexes Ru(4), Ru(6), Ru(8), and Ru(12) was determined by incubating the plasmid pSP73KB with the ruthenium complexes at various r_b values (Fig. 4). The resulting electrophoresis in native agarose gels of DNA modified by Ru(4) and Ru(12) are shown in Fig. 4 (top and bottom panels, respectively) as examples. A decrease in the rate of migration is the result of unwinding the DNA as this reduces the number of supercoils. The mean unwinding angle is calculated from the equation $\Phi = -18\sigma/r_b(c)$, where σ is the superhelical density and $r_b(c)$ is the r_b value at which the supercoiled and nicked forms comigrate [33]. Under the present experimental conditions, σ was calculated to be -0.04 on the basis of the data of cisplatin for which the $r_b(c)$ was determined in this study and $\Phi = 13^\circ$ was assumed [33]. It can be seen in Fig. 4 (bottom) that the complex Ru(12) causes an unwinding of the DNA (Φ) by $7 \pm 1^\circ$, the comigration point of the modified supercoiled and nicked DNA, $r_b(c)$, was reached at $r_b = 0.1$. In contrast, complexes Ru(4), Ru(6) and Ru(8) do not unwind the DNA significantly, and the comigration point of the modified supercoiled and nicked DNA was not reached at an r_b value as high as 0.14 (shown for complex Ru(4) in Fig. 4, top).

3.5. Circular dichroism (CD)

To gain further information on the structural changes induced by the dinuclear complexes in DNA, CD spectra of DNA

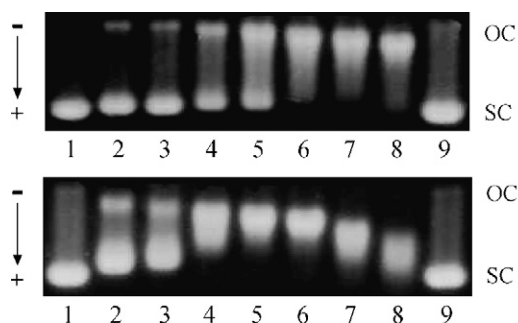


Fig. 4 – The unwinding of supercoiled pSP73KB plasmid DNA by Ru(4) (top) and Ru(12) (bottom). The plasmid was incubated with the dinuclear Ru^{II} arene complexes in 10 mM NaClO₄ at pH 6 for 24 h at 37 °C. Lanes in the top panel: (1 and 9) control, unmodified DNA; (2) $r_b = 0.036$; (3) $r_b = 0.048$; (4) $r_b = 0.060$; (5) $r_b = 0.072$; (6) $r_b = 0.096$; (7) $r_b = 0.120$; (8) $r_b = 0.144$. Lanes in the bottom panel: (1 and 9) control, unmodified DNA; (2) $r_b = 0.043$; (3) $r_b = 0.058$; (4) $r_b = 0.072$; (5) $r_b = 0.086$; (6) $r_b = 0.115$; (7) $r_b = 0.144$; (8) $r_b = 0.173$. The top bands in each panel correspond to the form of nicked plasmid, and the bottom bands, to the closed, negatively supercoiled plasmid.

modified by the complexes Ru(4), Ru(6), Ru(8), and Ru(12) were recorded (Fig. 5). These ruthenium complexes have no intrinsic CD signals so that any CD signal above 300 nm can be attributed to the interaction of complexes with DNA. Below 300 nm any change from the DNA spectrum is either due to the DNA induced CD (ICD) of the metal complex or due to the

metal complex induced perturbation of the DNA spectrum. The signatures of complexes Ru(4), Ru(6), and Ru(8) bound to CT DNA are positive ICDs centered at around 325–335 nm (Fig. 5A–C). Complex Ru(12) bound to CT DNA yields a negative ICD at around 308 nm and a positive ICD centered at around 335 nm (Fig. 5D). Unfortunately these complexes also absorb in the DNA region (below 300 nm) so that the ICD signals in the DNA region are due to changes in both the intrinsic DNA CD and the ligand-induced CD, which impedes unambiguous interpretation of the CD spectra in Fig. 5 in the DNA region (<300 nm) in terms of alterations of DNA conformation or the DNA-binding mode of complexes Ru(4), Ru(6), Ru(8), and Ru(12).

3.6. Interstrand cross-linking

Bifunctional compounds that covalently bind to DNA may form various types of interstrand and intrastrand cross-links. Therefore, we have decided to quantitate the interstrand cross-linking efficiency of Ru(4), Ru(6), Ru(8), and Ru(12) in the 221-bp NdeI/HpaI fragment of the pSP73 plasmid. This fragment was 3'-end labeled by [α -³²P] ATP and modified at $r_b = 0.01$ by Ru(4), Ru(6), Ru(8), or Ru(12) and for comparative purposes also by cisplatin, which is known to form ca. 6% interstrand cross-links [29]. The samples were analyzed for the interstrand cross-links by agarose gel electrophoresis under denaturing conditions. Upon electrophoresis, the 3'-end-labeled strands of the DNA fragment containing no interstrand cross-links migrate as a 221-base single strand, whereas the interstrand cross-linked strands migrate more slowly as a higher molecular mass species (Fig. 6). The radioactivity associated with the individual bands in each lane

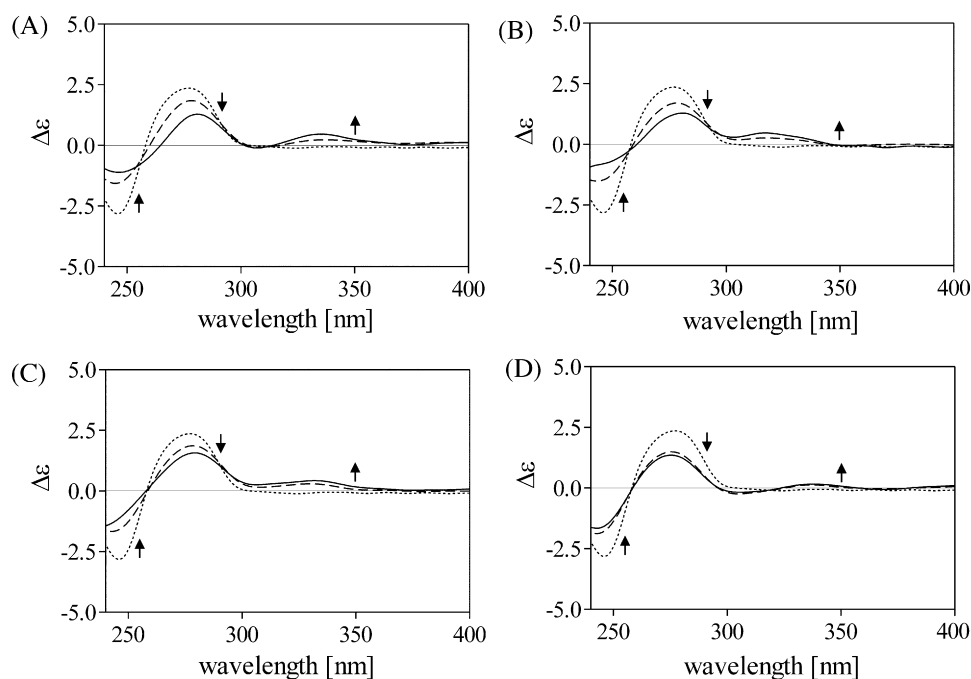


Fig. 5 – Circular dichroism (CD) spectra of calf-thymus DNA (1×10^{-4} M) modified by the dinuclear Ru^{II} arene complexes in 10 mM NaClO₄, pH 6. DNA was modified by Ru(4) (A), Ru(6) (B), Ru(8) (C) at $r_b = 0$ (dotted line), 0.05 (dashed line), 0.1 (solid line) and by complex Ru(12) (D) at $r_b = 0$ (dotted line), 0.05 (dashed line), 0.06 (solid line). The arrows in (A–D) show a change of CD with increasing r_b value.

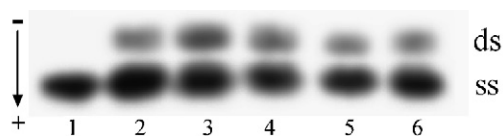


Fig. 6 – The formation of interstrand cross-links by dinuclear Ru^{II} arene complexes and cisplatin in the 221-bp NdeI/HpaI fragment of the pSP73 plasmid. Autoradiogram of a denaturing 1% agarose gel of the DNA fragment which was 3'-end labeled and modified at $r_b = 0.01$; the interstrand cross-linked DNA appears as the top bands migrating on the gels more slowly than the single-stranded DNA (contained in the bottom bands); lanes: (1–6) control, cisplatin, Ru(4), Ru(6), Ru(8), and Ru(12), respectively.

was measured to obtain estimates of the fraction of non-cross-linked or cross-linked DNA under each condition. The frequency of interstrand cross-links (% ICL/Pt) was calculated using the Poisson distribution from the fraction of non-cross-linked DNA in combination with the r_b values and the fragment size. The DNA interstrand cross-linking efficiency of Ru(4), Ru(6), Ru(8), or Ru(12) was ca. 5% and therefore similar to that of cisplatin.

3.7. Interhelical cross-linking

A large number of DNA cross-linking agents are known, but the reactive moieties of such compounds usually bind to the same DNA duplex because binding of one moiety inevitably leaves the other in close proximity to other binding sites in the same duplex, leading to intramolecular cross-linking. However, if the reactive sites of the cross-linking agents are connected by a linker that forces those sites to point in opposite directions and if the stereochemistry of the reactive sites of such cross-linking agents proves appropriate, such agents could bind to adjacent duplexes [36–38].

To assess whether the dinuclear Ru^{II} arene complexes are able to form interhelical cross-links, i.e., cross-links between two DNA duplexes, gel electrophoresis was used. The radioactively labeled NdeI/PvuI fragment of pSP73 (810 bp) (short fragment) and linearized pSP73 plasmid (2464 bp) (long fragment) were mixed at 1:1 molar ratio, the mixture was ruthenated by Ru(4), Ru(6), Ru(8), or Ru(12) at $r_b = 0.025, 0.05$, and 0.1 and the reaction products were analyzed by native agarose gel electrophoresis. In order to minimize the electrostatic repulsion between the sugar-phosphate backbones of two different duplexes, the mixture of the two DNA fragments was ruthenated in a medium containing a high concentration of counter cations (0.08 M Na⁺). Migration of the linearized

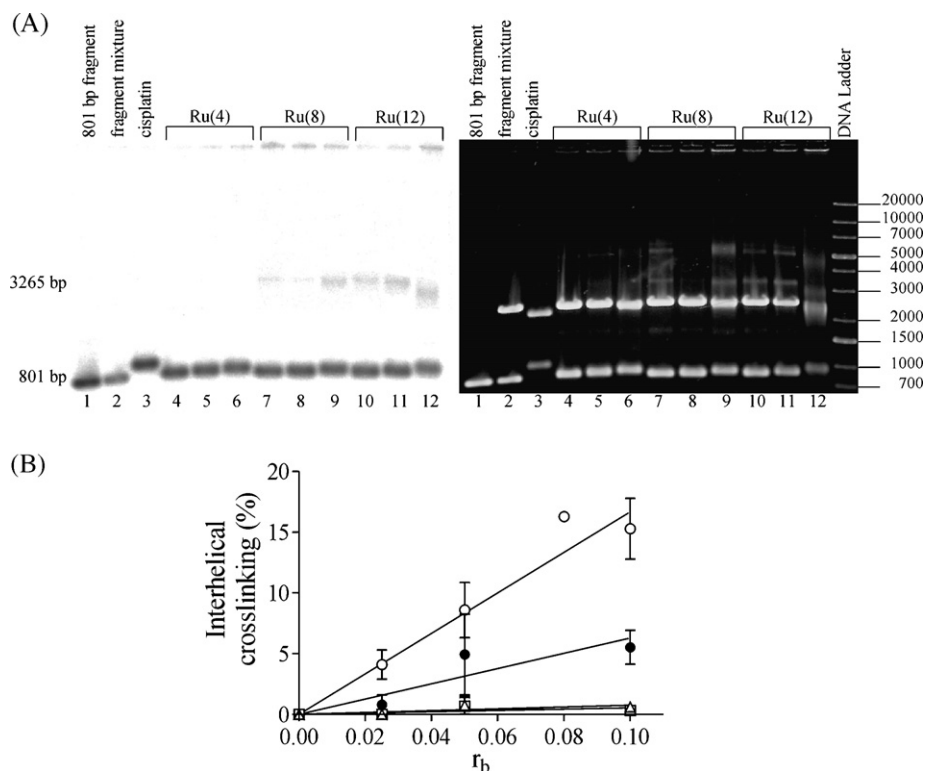


Fig. 7 – Formation of interhelical cross-links. The radioactively labeled NdeI/PvuI fragment of pSP73 (810 bp) and linearized pSP73 plasmid (2464 bp) (not labeled) were mixed at 1:1 molar ratio, the mixture was ruthenated by Ru(4), Ru(8), or Ru(12) at $r_b = 0.025, 0.05$, and 0.1 and the reaction products were analyzed by native 1% agarose gel electrophoresis. The mixture of the two DNA fragments was ruthenated in 0.08 M NaClO₄. (A) The migration of the labeled fragment was detected by autoradiography of the gel (left). The linearized pSP73 as well as the molecular size markers, derived from a lambda phage digest of HindIII, were detected by fluorescence under UV irradiation after staining with EtBr (right). (B) Plots of interhelical crosslinking (%) of 810-bp and 2464-bp fragments by dinuclear Ru^{II} complexes versus the r_b values: (Δ), Ru(4); (□), Ru(6); (●), Ru(8); (○) Ru(12).

pSP73 DNA (long fragment) through the gel was detected by fluorescence under UV light after staining the gel with EtBr (right part of Fig. 7A). Subsequently, autoradiography of the same, but dried gel was performed to localize the labeled short fragment (left part of Fig. 7A). Discernible bands corresponding to fraction of the labeled short fragment were found to migrate along with the linearized plasmid. The intensity of these bands increased with a growing level of the modification by each dinuclear ruthenium complex and the maximum efficiency of these complexes to cross-link short and long fragments was observed for Ru(12) (Fig. 7B). It should be pointed out that at higher levels of the ruthenation not all of the labeled DNA enters the gel. It is assumed that this may be due to interhelical cross-linking of a mixture of DNA fragments which results in a DNA matrix of high molecular weight. Such structures have been hypothesized for cisplatin [39] and observed for this antitumor mononuclear platinum complex under conditions of mild hyperthermia [40].

3.8. DNA–protein cross-linking

The dinuclear Ru^{II} arene complexes were investigated for their ability to form ternary DNA–protein complexes. For these studies proteins were chosen that bind to DNA with a relatively high affinity. Kf[−] and the linker histone H1 were selected as representatives of non-sequence specific DNA-binding proteins with enzymatic or structural function. One strand 3′-end-labeled 221-bp duplex (NdeI/HpaI fragment of pSP73 plasmid) was globally modified by Ru(4), Ru(6), Ru(8), or Ru(12) at $r_b = 0.03$. The fragment modified by either Ru complex (10 nM) was mixed with Kf[−] or histone H1 (the molar ratio protein/duplex was 10) and incubated overnight. Ternary DNA–(Ru–Ru)–protein cross-linking efficiency was assessed by a 1.3% agarose (agarose and Metaphor[®] agarose 1:1) gel shift assay. Fractions were detected with significantly retarded mobility (shown for Kf[−] in Fig. 8, lanes 9–12) and compared with that of the free probe (Fig. 8, lane 7). These more slowly migrating fractions were also eliminated after treatment with proteinase K (not shown) converting them to those of the unmodified probes. Importantly, the amount of radioactivity associated with the bands corresponding to ternary DNA–protein complexes formed by cisplatin was markedly lower (Fig. 8, lane 8). The same experiments were performed with the shorter 107-bp duplex (NdeI/EcoRI fragment of pSP73 plasmid) globally modified with the dinuclear Ru^{II} arene complexes. The yields of the DNA–protein cross-linking reactions were considerably lower (not shown).

4. Discussion

Recently, dinuclear Ru^{II} arene complexes based on pyridinone ligands, such as those shown in Fig. 1, were found to exert promising cytotoxic effects in human tumor cell lines and an intriguing feature of biological effects of these compounds is that their two Ru centers act synergistically [24]. Also interestingly, their activity against human tumor cells increases with the length of the linker. Previous studies with platinum compounds have shown that bifunctional dinuclear

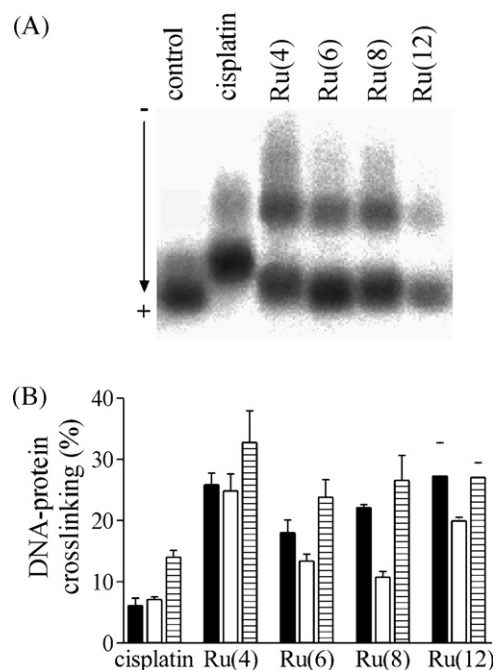


Fig. 8 – Formation of DNA–protein cross-links of unmodified and ruthenated DNA fragment globally modified by cisplatin, Ru(4), Ru(6), Ru(8), or Ru(12) with Kf[−] assessed by agarose gel electrophoresis; the fragment was incubated with the protein for 20 h. (A) Electrophoretogram. Lanes: control, the non-modified 221-bp fragment incubated with Kf[−]. cisPt, Ru(4), Ru(6), Ru(8), Ru(12), the 221-bp fragment modified at $r_b = 0.03$ by cisplatin, Ru(4), Ru(6), Ru(8), Ru(12), respectively, incubated with Kf[−]. (B) Percentual evaluation of formation of DNA cross-linked to proteins. The 107-bp DNA fragment globally modified by cisplatin, Ru(4), Ru(6), Ru(8), or Ru(12) ($r_b = 0.05$) with Kf[−] (solid bars) and histone H1 (open bars); the 221-bp DNA fragment globally modified by cisplatin, Ru(4), Ru(6), Ru(8), or Ru(12) ($r_b = 0.03$) with Kf[−] (striped bars). See the text for other details.

complexes can lead to novel DNA lesions, which can be important in the avoidance of cellular cross-resistance [22,41–48]. We report in the present work the detailed DNA-binding study of the bifunctional dinuclear Ru^{II} arene complexes Ru(4), Ru(6), Ru(8), and Ru(12) (Fig. 1). In addition, we investigated the effects and extent of changes induced in the DNA upon binding of the dinuclear Ru^{II} arene complexes, and these observations are compared with other metal-based anticancer agents.

It is notable that all these complexes bind polymeric DNA. Binding to DNA has often been associated with the cytotoxic action of metal-based anticancer agents [1,5,10] and therefore DNA may be a possible biological target for this class of dinuclear Ru^{II} arene complexes.

Our studies of the binding of the dinuclear Ru^{II} arene complexes Ru(4), Ru(6), Ru(8), and Ru(12) to natural double-helical CT DNA show that the reactions are markedly faster than that for cisplatin. The DNA adducts of complexes Ru(4), Ru(6), Ru(8), and Ru(12) are relatively stable, with little loss of bound Ru after extensive dialysis (against 1.0 M NaCl).

Transcription mapping experiments (Fig. 2) have shown that guanine residues are the preferential binding sites when polymeric DNA is modified with dinuclear Ru^{II} arene complexes in a random fashion. The selectivity for G bases was also found previously in our studies of the monofunctional and mononuclear Ru^{II} arene ethylenediamine complexes [11].

It is reasonable to expect that DNA-binding mode of monomeric Ru units constituting the dinuclear complexes tested in the present work is identical. However, the binding of the dinuclear complex Ru(12) to DNA results in some degree of unwinding (7°; Fig. 4) whereas the binding of the other compounds does not. The DNA unwinding efficiency of Ru(12) can be explained by the contribution to unwinding associated with the interaction of the arene ligands in complex Ru(12) with the duplex upon binding of Ru central atom(s). In other words, the arene moiety(ies) in DNA adducts of the dinuclear Ru^{II} arene compound Ru(12) could be geometrically positioned favorably to interact with the double helix. In contrast, the complexes Ru(4), Ru(6), and Ru(8) do not unwind the DNA significantly (Fig. 4). The explanation behind this phenomenon is unclear, nevertheless it may be hypothesized that the length of the linkers is not favorable for the interaction of the arene rings in the Ru(4), Ru(6), and Ru(8) complexes with the double helix. In summary, it seems reasonable to suggest that the ligands in Ru(4), Ru(6), and Ru(8) do not interact with the double helix in a way similar to Ru(12), thus also supporting a different DNA-binding mode for this compound in comparison with the other three complexes.

EtBr as a fluorescent probe can be used to characterize DNA binding of small molecules such as platinum and ruthenium antitumor drugs [11,33,49]. Binding of EtBr to DNA by intercalation is blocked in a stoichiometric manner by a wide spectrum of DNA-binding ligands. On the other hand, the modification of DNA by monofunctional ligands, such as [PtCl(dien)]Cl, results in only a slight decrease of EtBr fluorescence intensity as compared with that for the complex of non-metalated DNA with EtBr. Competitive binding of other intercalators leads to the loss of fluorescence because of depletion of the DNA–EtBr complex (free EtBr is poorly fluorescent).

The formation of adducts of the dinuclear complexes with DNA is accompanied by a release of the EtBr intercalator (Fig. 3). The adducts of compounds Ru(4), Ru(6), and Ru(8) do not unwind DNA (Fig. 4). Thus, the results of the unwinding experiments are consistent with the view that the arene ligands or other groups in Ru(4), Ru(6), and Ru(8) do not interact substantially with the double helix upon coordination of the dinuclear Ru^{II} complexes.

In contrast, Ru(12) unwinds the DNA (by ca. 7°, Fig. 4), but replaces the EtBr intercalator more efficiently than the other three compounds and even markedly more than cisplatin (Fig. 3). It seems reasonable to suggest that the arene ligands or other groups in Ru(12) do interact with the double helix, although not very strongly. It cannot be excluded that some DNA-binding properties of Ru(12) observed in the present work may be also associated with a higher lipophilicity of this complex [24]. Thus, the solution behavior of the DNA adducts of dinuclear Ru^{II} arene complexes appears interesting and merits further study.

In addition, comparison with bifunctional platinum polynuclear complexes [41,45,46] suggests that the conformational

distortion induced in DNA by the adducts of Ru(12) is delocalized and spans more base pairs around the binding sites. Thus, the EtBr fluorescence results (Fig. 3) suggest formation of long-range cross-links or of other lesions that would extend over more than two base pairs.

The CD spectra of DNA modified by complexes Ru(4), Ru(6), Ru(8), and Ru(12) (Fig. 5A–D) indicate that the binding of these complexes results in conformational alterations in double-helical DNA. All complexes bound to CT DNA yield a positive ICD centered at around 335 nm (Fig. 5A–D). On the other hand, complex Ru(12) bound to CT DNA yields also a broad negative ICD centered at around 310 nm (Fig. 5D).

The results of our biophysical studies are consistent with intrastrand and interstrand cross-links formed by dinuclear Ru^{II} arene complexes within one DNA duplex. Intrastrand cross-linking was difficult to quantify, but interstrand cross-links were found to be formed in DNA by the dinuclear Ru^{II} arene complexes Ru(4), Ru(6), Ru(8), and Ru(12) in cell-free media and in absence of proteins with the same frequency (Fig. 6) as observed for the antitumor drug cisplatin [29]. Another interesting phenomenon specific for the DNA binding of these dinuclear Ru^{II} arene complexes is that they also form interduple cross-links that are tethered by ruthenium–DNA bonds (Fig. 7). A plausible explanation of this observation might be that DNA that has been modified by Ru(4), Ru(6), Ru(8), and Ru(12) aggregates to an extent that allows interduple contacts that are sufficient for the interduple cross-linking.

Interestingly, in accordance with the ability of dinuclear Ru^{II} arene complexes to cross-link two DNA duplexes, the results of the present work convincingly demonstrate that these dinuclear complexes also form specific DNA lesions which can efficiently cross-link proteins to DNA (Fig. 8). If such a ternary complex is formed, it is reasonable to expect that in the first step relatively flexible DNA-binding proteins (such as those tested in the present work, i.e., KF[−] and the linker histone H1) come into close contact with DNA at the site of ruthenation. Then one molecule of the dinuclear Ru^{II}-arene complex can be bound simultaneously to a base residue in DNA and a reactive group in the protein, but only if a non-covalent preassociation takes place first. The formation of DNA–protein ternary complexes mediated by dinuclear Ru^{II} arene complexes raises the possibility of “suicide” lesions, which may irreversibly sequester various DNA-binding proteins, such as transcription factors or repair proteins [15,50]. In addition, the cross-linking procedures involving these ruthenium agents may provide a tool for identification of proteins or protein domains closely positioned to DNA including mapping of protein-binding sites on DNA *in vivo* [51,52].

In conclusion, the concept for the design of interhelical and DNA–protein cross-linking agents based on dinuclear Ru^{II} arene complexes with sufficiently long linkers may result in new compounds which exhibit a variety of biological effects and can be also useful in nucleic acids research. The earlier observation [24] that complex Ru(12) is markedly more potent than cisplatin in human cancer cells, including colon adenocarcinoma cells with the IC₅₀ of Ru(12) being more than one order of magnitude lower than that of cisplatin, is consistent with this idea. Such results indicate promising compounds with which to tackle the common problem of

developed cisplatin resistance, frequently occurring during chemotherapy.

Acknowledgments

This research was supported by the Grant Agency of the CR (203/06/1239), Ministry of Education of the CR (LC06030, ME08017, OC08003), and the Academy of Sciences of the Czech Republic (1QS500040581, KAN200200651, AV0Z50040507 and AV0Z50040702). The authors also acknowledge that their participation in the EU COST Action D39 enabled them to exchange regularly the most recent ideas in the field of anticancer metallodrugs with several European colleagues. The authors also thank M.G. Mendoza-Ferri for assistance with synthesis and characterization of the dinuclear Ru^{II} arene complexes used in the present work.

Authors' contributions: ON and VB designed research; ON performed research; AAN synthesized compounds; CGH and BKK supervised AAN; ON and VB analyzed data; and VB wrote the paper.

REFERENCES

- [1] Zhang CX, Lippard SJ. New metal complexes as potential therapeutics. *Curr Opin Chem Biol* 2003;7:481–9.
- [2] Zhao G, Lin H. Metal complexes with aromatic N-containing ligands as potential agents in cancer treatment. *Curr Med Chem - Anti-Cancer Agents* 2005;5:137–47.
- [3] Yan YK, Melchart M, Habtemariam A, Sadler PJ. Organometallic chemistry, biology and medicine: ruthenium arene anticancer complexes. *Chem Commun* 2005;4764–76.
- [4] Dyson PJ, Sava G. Metal-based antitumour drugs in the post genomic era. *Dalton Trans* 2006;1929–33.
- [5] Brabec V, Novakova O. DNA binding mode of ruthenium complexes and relationship to tumor cell toxicity. *Drug Resist Updates* 2006;9:111–22.
- [6] Kostova I. Ruthenium complexes as anticancer agents. *Curr Med Chem* 2006;13:1085–107.
- [7] Aird R, Cummings J, Ritchie A, Muir M, Morris R, Chen H, et al. In vitro and in vivo activity and cross resistance profiles of novel ruthenium (II) organometallic arene complexes in human ovarian cancer. *Br J Cancer* 2002;86:1652–7.
- [8] Habtemariam A, Melchart M, Fernandez R, Parsons S, Oswald IDH, Parkin A, et al. Structure–activity relationships for cytotoxic ruthenium(II) arene complexes containing N,N-, N,O-, and O,O-chelating ligands. *J Med Chem* 2006;49:6858–68.
- [9] Jamieson ER, Lippard SJ. Structure, recognition, and processing of cisplatin–DNA adducts. *Chem Rev* 1999;99:2467–98.
- [10] Brabec V. DNA modifications by antitumor platinum and ruthenium compounds: their recognition and repair. *Prog Nucleic Acid Res Mol Biol* 2002;71:1–38.
- [11] Novakova O, Chen H, Vrana O, Rodger A, Sadler PJ, Brabec V. DNA interactions of monofunctional organometallic ruthenium(II) antitumor complexes in cell-free media. *Biochemistry* 2003;42:11544–5.
- [12] Novakova O, Kasparkova J, Bursova V, Hofr C, Vojtiskova M, Chen H, et al. Conformation of DNA modified by monofunctional Ru(II) arene complexes: recognition by DNA-binding proteins and repair. Relationship to cytotoxicity. *Chem Biol* 2005;12:121–9.
- [13] Bugarcic T, Novakova O, Halamikova A, Zerkankova L, Vrana O, Kasparkova J, et al. Cytotoxicity, cellular uptake, and DNA interactions of new monodentate ruthenium(II) complexes containing terphenyl arenes. *J Med Chem* 2008;51:5310–9.
- [14] Gallori E, Vettori C, Alessio E, Vilchez FG, Vilaplana R, Orioli P, et al. DNA as a possible target for antitumor ruthenium(III) complexes—a spectroscopic and molecular biology study of the interactions of two representative antineoplastic ruthenium(III) complexes with DNA. *Arch Biochem Biophys* 2000;376:156–62.
- [15] van Houten B, Illenye S, Qu Y, Farrell N. Homodinuclear (Pt,Pt) and heterodinuclear (Ru,Pt) metal compounds as DNA–protein cross-linking agents: potential suicide DNA lesions. *Biochemistry* 1993;32:11794–801.
- [16] Komeda S, Lutz M, Spek A, Chikuma M, Reedijk J. New antitumor-active azole-bridged dinuclear platinum(II) complexes: synthesis, characterization, crystal structures, and cytotoxic studies. *Inorg Chem* 2000;39:4230–6.
- [17] Chen H, Parkinson JA, Novakova O, Bella J, Wang F, Dawson A, et al. Induced-fit recognition of DNA by organometallic complexes with dynamic stereogenic centers. *Proc Natl Acad Sci USA* 2003;100:14623–8.
- [18] Wheate NJ, Collins JG. Multi-nuclear platinum complexes as anti-cancer drugs. *Coord Chem Rev* 2003;241:133–45.
- [19] Farrell N. Polynuclear platinum drugs. In: Sigel A, Sigel H, editors. *Metal ions in biological systems*. New York, Basel: Marcel Dekker, Inc.; 2004. p. 251–96.
- [20] Brabec V, Kasparkova J. DNA interactions of platinum anticancer drugs. Recent advances and mechanisms of action. In: Perez-Martin J-M, Fuertes MA, Alonso C, editors. *Metal compounds in cancer chemotherapy*. Trivandrum, Kerala (India): Research Signpost; 2005. p. 187–218.
- [21] Wheate NJ, Collins JG. Multi-nuclear platinum drugs: a new paradigm in chemotherapy. *Curr Med Chem - Anti-Cancer Agents* 2005;5:267–79.
- [22] Brabec V, Christofis P, Slamova M, Kostrhunova H, Novakova O, Najajreh Y, et al. DNA interactions of new cytotoxic tetrafunctional dinuclear platinum complex trans, trans-[[PtCl₂(NH₃)₂](piperazine)]. *Biochem Pharmacol* 2007;73:1887–900.
- [23] Magennis SW, Habtemariam A, Novakova O, Henry JB, Meier S, Parsons S, et al. Dual triggering of DNA binding and fluorescence via photoactivation of a dinuclear ruthenium(II) arene complex. *Inorg Chem* 2007;46:5059–68.
- [24] Mendoza-Ferri M-G, Hartinger CG, Eichinger RE, Stolyarova N, Severin K, Jakupec MA, et al. Influence of the spacer length on the in vitro anticancer activity of dinuclear ruthenium–arene compounds. *Organometallics* 2008;27:2405–7.
- [25] Mendoza-Ferri MG. Synthesis and investigations of multinuclear ruthenium(II)- and osmium(II)-arene complexes based on N-substituted pyridinone ligands as new anticancer agents. Vienna: University of Vienna; 2007.
- [26] Brabec V, Palecek E. Interaction of nucleic acids with electrically charged surfaces. II. Conformational changes in double-helical polynucleotides. *Biophys Chem* 1976;4:76–92.
- [27] Kim SD, Vrana O, Kleinwachter V, Niki K, Brabec V. Polarographic determination of subnanogram quantities of free platinum in reaction mixture with DNA. *Anal Lett* 1990;23:1505–18.
- [28] Chvalova K, Brabec V, Kasparkova J. Mechanism of the formation of DNA–protein cross-links by antitumor cisplatin. *Nucleic Acids Res* 2007;35:1812–21.
- [29] Brabec V, Leng M. DNA interstrand cross-links of trans-diamminedichloroplatinum(II) are preferentially formed

- between guanine and complementary cytosine residues. *Proc Natl Acad Sci USA* 1993;90:5345–9.
- [30] Lemaire MA, Schwartz A, Rahmouni AR, Leng M. Interstrand cross-links are preferentially formed at the d(GC) sites in the reaction between cis-diamminedichloroplatinum(II) and DNA. *Proc Natl Acad Sci USA* 1991;88:1982–5.
- [31] Butour JL, Macquet JP. Differentiation of DNA–platinum complexes by fluorescence. The use of an intercalating dye as a probe. *Eur J Biochem* 1977;78:455–63.
- [32] Butour JL, Alvinerie P, Souchard JP, Colson P, Houssier C, Johnson NP. Effect of the amine nonleaving group on the structure and stability of DNA complexes with cis-[Pt(R-NH₂)₂(NO₃)₂]. *Eur J Biochem* 1991;202:975–80.
- [33] Keck MV, Lippard SJ. Unwinding of supercoiled DNA by platinum ethidium and related complexes. *J Am Chem Soc* 1992;114:3386–90.
- [34] Farrell N, Qu Y, Feng L, Van Houten B. Comparison of chemical reactivity, cytotoxicity, interstrand cross-linking and DNA sequence specificity of bis(platinum) complexes containing monodentate or bidentate coordination spheres with their monomeric analogues. *Biochemistry* 1990;29:9522–31.
- [35] Roberts JD, Vanhouten B, Qu Y, Farrell NP. Interaction of novel bis(platinum) complexes with DNA. *Nucleic Acids Res* 1989;17:9719–33.
- [36] Mullins ST, Annan NK, Cook PR, Lowe G. Bisintercalators of DNA with a rigid linker in an extended configuration. *Biochemistry* 1992;31:842–9.
- [37] Carpenter ML, Lowe G, Cook PR. The structure of 4-way DNA junctions: specific binding of bis-intercalators with rigid linkers. *Nucleic Acids Res* 1996;24:1594–601.
- [38] Matsumoto L, Kurek K, Larocque K, Gustafson G, Pires R, Zhang J, et al. Biological effects of a bifunctional DNA crosslinker—I. Generation of triradial and quadriradial chromosomes. *Mutation Res* 1999;426:79–87.
- [39] Macquet JP, Butour JL. Modifications of the DNA secondary structure upon platinum binding: a proposed model. *Biochimie* 1978;60:901–14.
- [40] Halamikova A, Vrana O, Kasparkova J, Brabec V. Biochemical studies of the thermal effects on DNA modifications by the antitumor cisplatin and their repair. *ChemBioChem* 2007;8:2008–15.
- [41] Kasparkova J, Vrana O, Farrell N, Brabec V. Effect of the geometry of the central coordination sphere in antitumor trinuclear platinum complexes on DNA binding. *J Inorg Biochem* 2004;98:1560–9.
- [42] Kasparkova J, Zehnulova J, Farrell N, Brabec V. DNA interstrand cross-links of the novel antitumor trinuclear platinum complex BBR3464. Conformation, recognition by high mobility group domain proteins, and nucleotide excision repair. *J Biol Chem* 2002;277:48076–8.
- [43] Zehnulova J, Kasparkova J, Farrell N, Brabec V. Conformation, recognition by high mobility group domain proteins, and nucleotide excision repair of DNA intrastrand cross-links of novel antitumor trinuclear platinum complex BBR3464. *J Biol Chem* 2001;276:22191–9.
- [44] Kasparkova J, Farrell N, Brabec V. Sequence specificity, conformation, and recognition by HMG1 protein of major DNA interstrand cross-links of antitumor dinuclear platinum complexes. *J Biol Chem* 2000;275:15789–98.
- [45] Kasparkova J, Novakova O, Vrana O, Farrell N, Brabec V. Effect of geometric isomerism in dinuclear platinum antitumor complexes on DNA interstrand cross-linking. *Biochemistry* 1999;38:10997–1005.
- [46] Brabec V, Kasparkova J, Vrana O, Novakova O, Cox JW, Qu Y, et al. DNA modifications by a novel bifunctional trinuclear platinum Phase I anticancer agent. *Biochemistry* 1999;38:6781–90.
- [47] Zaludova R, Zakovska A, Kasparkova J, Balcarova Z, Kleinwachter V, Vrana O, et al. DNA interactions of bifunctional dinuclear platinum(II) antitumor agents. *Eur J Biochem* 1997;246:508–17.
- [48] Kasparkova J, Mellish KJ, Qu Y, Brabec V, Farrell N. Site-specific d(GpG) intrastrand cross-links formed by dinuclear platinum complexes. Bending and NMR studies. *Biochemistry* 1996;35:16705–13.
- [49] Kasparkova J, Marini V, Najajreh Y, Gibson D, Brabec V. DNA binding mode of the cis and trans geometries of new antitumor nonclassical platinum complexes containing piperidine, piperazine or 4-picoline ligand in cell-free media. Relations to their activity in cancer cell lines. *Biochemistry* 2003;42:6321–32.
- [50] He C, Verdine GL. Trapping distinct structural states of a protein/DNA interaction through disulfide crosslinking. *Chem Biol* 2002;9:1297–303.
- [51] Travers A. Mapping histone positions in chromatin by protein-directed DNA crosslinking and cleavage. In: Travers A, Buckle M, editors. *DNA–protein interactions*. Oxford University Press: Oxford, New York; 2000. p. 229–38.
- [52] Barker S, Weinfeld M, Murray D. DNA–protein crosslinks: their induction, repair, and biological consequences. *Mut Res* 2005;589:111–35.

9.

Cytotoxicity, Cellular Uptake, and DNA Interactions of New Monodentate Ruthenium(II) Complexes Containing Terphenyl Arenes

Tijana Bugarcic,^{†,‡,⊥} Olga Nováková,^{§,⊥} Anna Halámková,[§] Lenka Zerzánková,[§] Oldřich Vrána,[§] Jana Kašpárková,^{§,||} Abraha Habtemariam,[‡] Simon Parsons,[†] Peter J. Sadler,[‡] and Viktor Brabec^{*,§}

School of Chemistry, University of Edinburgh, West Mains Road, Edinburgh EH9 3JJ, United Kingdom, Department of Chemistry, University of Warwick, Gibbet Hill Road, CV4 7AL, United Kingdom, Institute of Biophysics, Academy of Sciences of the Czech Republic, v.v.i., Kralovopolska 135, CZ-61265 Brno, Czech Republic, Laboratory of Biophysics, Department of Experimental Physics, Faculty of Sciences, Palacky University, tr. Svobody 26, CZ-771 46 Olomouc, Czech Republic

Received March 19, 2008

We have compared the cancer cell cytotoxicity, cell uptake, and DNA binding properties of the isomeric terphenyl complexes $[(\eta^6\text{-arene})\text{Ru}(\text{en})\text{Cl}]^+$, where the arene is *ortho*- (**2**), *meta*- (**3**), or *para*-terphenyl (**1**) (*o*-, *m*-, or *p*-terp). Complex **1**, the X-ray crystal structure of which confirms that it has the classical “piano-stool” geometry, has a similar potency to cisplatin but is not cross-resistant and has a much higher activity than **2** or **3**. The extent of Ru uptake into A2780 or A2780cis cells does not correlate with potency. Complex **1** binds to DNA rapidly and quantitatively, preferentially to guanine residues, and causes significant DNA unwinding. Circular and linear dichroism, competitive binding experiments with ethidium bromide, DNA melting, and surface-enhanced Raman spectroscopic data are consistent with combined intercalative and monofunctional (coordination) binding mode of complex **1**. This unusual DNA binding mode may therefore make a major contribution to the high potency of complex **1**.

Introduction

Organoruthenium complexes of the type $[(\eta^6\text{-arene})\text{Ru}^{\text{II}}(\text{en})\text{Cl}]^+$, where arene = benzene or a benzene derivative and en = 1,2-diaminoethane, exhibit anticancer activity, including activity against cisplatin (*cis*-diamminedichloridoplatinum(II)) resistant cancer cells.^{1,2} This class of complexes can form strong monofunctional adducts with DNA.² Modifications of natural DNA by $[(\eta^6\text{-bip})\text{Ru}(\text{en})\text{Cl}]^+$, where bip = biphenyl,³ studied using several different techniques,³ have shown preferential binding to guanine (G) residues. $[(\eta^6\text{-bip})\text{Ru}(\text{en})\text{Cl}]^+$ binds to DNA through coordination to G N7 as well as noncovalently, through hydrophobic interactions between the arene and DNA. These hydrophobic interactions may include intercalation of the noncoordinated phenyl ring between DNA bases and minor groove binding. Intramolecular π – π arene–nucleobase stacking has been observed in the crystal structure of $[(\eta^6\text{-bip})\text{Ru}(\text{en})(9\text{-EtG-N7})][\text{PF}_6]_2$,⁴ and strong H-bonding between an NH of en and C6O from G contributes to the G specificity.⁵

We have synthesized new complexes of the type $[(\eta^6\text{-arene})\text{Ru}(\text{en})\text{Cl}]^+$, where the arene is *ortho*-, *meta*-, or *para*-

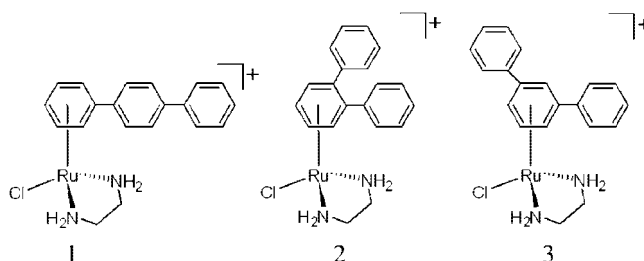


Figure 1. Structures of Ru^{II} arene complexes. **1**, $[(\eta^6\text{-}p\text{-terp})\text{Ru}(\text{en})\text{Cl}]^+$; **2**, $[(\eta^6\text{-}o\text{-terp})\text{Ru}(\text{en})\text{Cl}]^+$; **3**, $[(\eta^6\text{-}m\text{-terp})\text{Ru}(\text{en})\text{Cl}]^+$.

terphenyl (*o*-, *m*-, or *p*-terp; Figure 1) to investigate the effect on cytotoxicity of an additional phenyl ring compared to bip as arene. Such complexes are expected to show enhanced arene intercalation compared to the bip analogue. In the case of *p*-terp, Ru is bound to a terminal phenyl ring, whereas in the cases of *o*- and *m*-terp, Ru is bound to the central phenyl ring. Aromatic hydrocarbons consisting of a chain of three benzene rings, terphenyls (terps), have three isomers in which the terminal rings are *o*-, *m*-, or *p*-substituents of the central ring. Most of the natural terphenyls are *p*-terp derivatives. Very few *m*-terp derivatives occur naturally, and *o*-terps have not been found in nature.⁶ In recent years, it has been reported that some terphenyls exhibit significant biological activity such as neuroprotective, antithrombotic, anticoagulant, and cytotoxic activity. It has also been found that some popular edible mushrooms are rich in terphenyls, a sign that the toxicity of terphenyls is low.

We have investigated in the present work the relationship between cytotoxicity, cell uptake of ruthenium, and DNA binding for the group of complexes consisting of the *p*-, *o*-, and *m*-terp arenes (complexes **1**, **2**, and **3**, respectively). Their activity toward human ovarian tumor cell lines A2780 (parent, cisplatin-sensitive) and A2780cisR (with acquired cisplatin resistance), human ovarian carcinoma CH1 (cisplatin sensitive),

* To whom correspondence should be addressed. Phone: +420-541517148. Fax: +420-541240499. E-mail: brabec@ibp.cz.

[†] University of Edinburgh.

[‡] University of Warwick.

[§] Institute of Biophysics, Brno.

^{||} Palacky University, Olomouc.

[⊥] The first two authors are joint first authors.

^a Abbreviations: bip, biphenyl; bp, base pair; cisplatin, *cis*-diamminedichloridoplatinum(II); CD, circular dichroism; CT, calf thymus; dien, bis(2-aminoethyl)amine; DMEM, Dulbecco's modified Eagle's medium; DMSO, dimethylsulfoxide; EtBr, ethidium bromide; en, 1,2-diaminoethane; FAAS, flameless atomic absorption spectrophotometry; IC₅₀, concentration inhibiting cell growth by 50%; ICD, induced circular dichroism; LD, linear dichroism; MTT, 3-(4,5-dimethyl-2-thiazolyl)-2,5-diphenyl-2H-tetrazolium bromide; r_b , the number of atoms of the metal bound per nucleotide residue; r_i , the molar ratio of free metal complex to nucleotide-phosphates at the onset of incubation with DNA; SERS, surface-enhanced Raman spectrometry; $t_{50\%}$, the times at which the binding reached 50%; terp, terphenyl; t_m , DNA melting temperature; Δt_m , the difference between the t_m values of ruthenated and nonmodified DNAs.

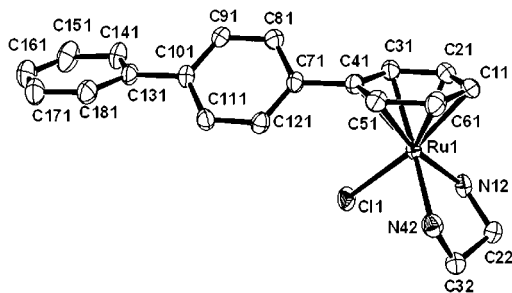


Figure 2. ORTEP diagram for cation of complex **1** $[(\eta^6\text{-}p\text{-terp})\text{Ru}(\text{en})\text{Cl}][\text{PF}_6]$, with 50% probability thermal ellipsoids. All hydrogen atoms have been omitted for clarity.

Table 1. X-ray Crystal Structure Data for Complex **1**

formula	$\text{C}_{20}\text{H}_{22}\text{ClF}_6\text{N}_2\text{PRu}$
molar mass	571.89
crystal system	monoclinic
crystal size/mm	$0.27 \times 0.21 \times 0.21$
space group	$P2_1/c$
crystal	yellow/block
$a/\text{\AA}$	19.0359(10)
$b/\text{\AA}$	10.1405(5)
$c/\text{\AA}$	11.2966(5)
α/deg	90
β/deg	105.218(3)
γ/deg	90
T/K	150(2)
Z	4
$R [F > 4\sigma(F)]^a$	0.0479
R_w^b	0.1256
GOF ^c	1.041
$\Delta\rho$ max and min/ $\text{e}\text{\AA}^{-3}$	1.557, -0.814

^a $R = \sum ||F_o| - |F_c|| / \sum |F_o|$. ^b $R_w = [\sum w(F_o^2 - F_c^2)^2 / \sum wF_o^2]^{1/2}$. ^c GOF = $[\sum w(F_o^2 - F_c^2)^2 / (n - p)]^{1/2}$, where n = number of reflections and p = number of parameters.

Table 2. Selected Bond Lengths (\AA) and Angles (deg) for Complex **1**

bond/angle	length/angle
Ru—Cl	2.3929 (11)
Ru—N12	2.125 (4)
Ru—N42	2.126 (4)
Ru—C11	2.174 (4)
Ru—C21	2.152 (5)
Ru—C31	2.190 (4)
Ru—C41	2.225 (4)
Ru—C51	2.191 (4)
Ru—C61	2.157 (5)
N12—Ru—N42	78.76 (14)
N12—Ru—Cl	83.65 (10)
N42—Ru—Cl	84.57 (11)

and human mammary carcinoma SKBR3 (intrinsically cisplatin resistant) cell lines was also investigated.

Results

Crystal Structure. The X-ray crystal structure of the cation of complex **1** $[(\eta^6\text{-}p\text{-terp})\text{Ru}(\text{en})\text{Cl}][\text{PF}_6]$ is shown in Figure 2. The crystallographic data are listed in Table 1, and selected bond lengths and angles in Table 2. In the complex, Ru^{II} adopts the familiar “three-legged piano-stool” geometry with an η^6 π -bonded arene, forming the seat of the stool. The legs of the stool are Cl and the N atoms of the en chelating ligand. The Ru—Cl bond length in complex **1** is 2.3929(11) \AA (Table 2). A twisting of the phenyl rings is present in the crystal structure of complex **1**. The twist angle between the bound and the central ring is 43.21°, and between the central and the terminal ring 38.47°. The planes of the terminal and bound rings are twisted

Table 3. IC₅₀ Mean Values (μM) Obtained for Ru^{II} Arene Complexes Tested in the Present Work^{a,b}

complex	CH1	SKBR3	A2780	A2780cisR ^c
cisplatin	0.9 ± 0.1	8 ± 2	2.8 ± 0.7	18.6 ± 0.4 (6.7)
1	2.2 ± 0.3	8 ± 1	4 ± 1	1.4 ± 0.6 (0.4)
2	23 ± 1	13 ± 3	30 ± 4	18.3 ± 0.8 (0.6)
3	51 ± 9	80 ± 5	42 ± 4	31 ± 4 (0.7)

^a Drug treatment period was 72 h. ^b The experiments were performed in quadruplicate. ^c Resistance factor, defined as IC₅₀ (resistant)/IC₅₀ (sensitive), is given in parentheses.

Table 4. Uptake of Ru^{II} Arene Complexes and Cisplatin into Cells^{a,b}

	cisplatin	complex 1	complex 2	complex 3
A2780	30 ± 2	350 ± 20	2130 ± 130	630 ± 50
A2780cisR	47 ± 3	150 ± 10	1010 ± 90	490 ± 80

^a Table shows the uptake of cisplatin and complexes **1–3** at their equitoxic concentrations (corresponding to the IC₅₀ values shown in Table 1) into A2780 or A2780cisR cells after 72 h. Each value shown in the Table 4 is in pmole of Ru or Pt/10⁶ cells. ^b The experiments were performed in triplicate.

by 5.62°. A CH— π interaction is present between the C61H proton of the bound ring of *p*-terp (Figure S1 of Supporting Information) from one molecule and the center of the π -system of the central ring of *p*-terp from another molecule (distance = 2.624 \AA). The distances between carbons of the bound arene ring and the metal center range from 2.152(5) to 2.225(4) \AA .

Cytotoxicity. The cytotoxic activity of the new Ru^{II} arene complexes **1–3** was determined against four different cisplatin sensitive and resistant cancer cell lines (Table 3). The human ovarian carcinoma cell lines A2780, CH1 (both cisplatin sensitive), A2780cisR (with acquired cisplatin resistance), and human mammary carcinoma cell line SKBR3 (intrinsically cisplatin resistant) were employed. A2780cisR cells are resistant to cisplatin through a combination of decreased uptake, enhanced DNA repair/tolerance, and elevated reduced-glutathione levels.^{7,8} The tumor cell lines were incubated for 72 h with Ru^{II} arene complexes or cisplatin, and the cell survival in the culture treated with Ru^{II} complexes was evaluated as described in the Experimental Section. All complexes show activity and their corresponding IC₅₀ values (IC₅₀ = concentration inhibiting cell growth by 50%) are reported in Table 3. In general, activity follows the order **1**, cisplatin \gg **2** $>$ **3**, with all Ru complexes lacking cross-resistance with cisplatin.

Cellular Ruthenium Complex Uptake. An important factor that usually contributes to transition metal-based drug cytotoxicity is cellular uptake. To examine accumulation of complexes **1–3**, the cellular levels of these Ru^{II} arene complexes were measured after a 72 h exposure of the A2780 and A2780cisR cells to the drugs at equitoxic concentrations (i.e., at the concentrations corresponding to the IC₅₀ values shown in Table 3). The amount of ruthenium in cells (in pmol/10⁶ cells, Table 4), **2** \gg **3** $>$ **1**, does not correlate with their cytotoxicity (IC₅₀ value). Because complexes **1–3** were tested at their equitoxic doses, the results shown in Table 4 imply that notably less molecules of complex **1** inside the cells in comparison with complexes **2** and **3** are necessary to induce the same cytotoxic effect.

DNA-Bound Ruthenium in Cells Exposed to Ru^{II} Arene Complexes. Distortions of DNA structure often correlate with anticancer activity.^{9,10} Hence, it is of great importance to understand in detail DNA binding properties of the new Ru^{II} arene complexes and their possible relationship to cytotoxicity in tumor cell lines. Complexes **1** and **3** exhibited the highest and lowest potency, respectively (Table 1), so these complexes were selected for a more detailed DNA binding study. We

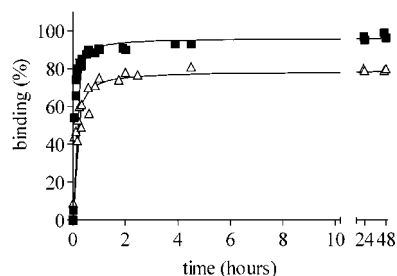


Figure 3. Kinetics of the binding of complexes **1** (■) and **3** (△) to calf thymus DNA in the medium of 10 mM NaClO₄, at 37 °C and pH 6. The concentration of DNA was 3×10^{-4} M (related to the monomeric nucleotide content), and r_1 was 0.08.

examined DNA-bound ruthenium in A2780 cells after exposure to complexes **1** and **3**. Measurements of DNA-bound ruthenium after 2 h of 50 μ M drug exposure revealed that the amount of ruthenation by complexes **1** and **3** was 5.0 ± 2.0 and 14.0 ± 4.0 pg Ru/ μ g DNA, respectively. Hence, complex **1** requires fewer DNA lesions than does complex **3** to achieve cell growth inhibition.

DNA Binding in Cell-Free Media. Kinetics of Binding to Calf Thymus (CT) DNA. The rate of binding of Ru^{II} arene complexes **1** and **3** to CT DNA was determined at an r_1 (molar ratio of free Ru^{II} arene complex to nucleotide phosphate) ratio of 0.08 in 10 mM NaClO₄ at 37 °C in the dark. Ru^{II} arene complexes were incubated with the CT DNA and aliquots removed at various time intervals, rapidly cooled, precipitated out by addition of ethanol, and the content of the supernatant determined by flameless atomic absorption spectrometry (FAAS) (Figure 3). Intriguingly, both complexes bind rapidly ($t_{50\%}$ ca. 5 and 9 min for complexes **1** and **3**, respectively). Complex **1** binds almost quantitatively, whereas only ca. 80% of the complex **3** is bound after 48 h.

The binding experiments carried out in this work indicated that modification reactions resulted in the irreversible coordination of the Ru^{II} arene complexes **1** and **3** to CT DNA, which thus facilitated sample analysis. Hence, it was possible to prepare samples of DNA modified by complexes **1** or **3** at a preselected value of r_b (r_b values are defined as the number of atoms of the metal bound per nucleotide residue). Thus, except where stated, samples of DNA modified by Ru^{II} arene compounds **1** and **3** and analyzed further by biophysical or biochemical methods were prepared in 10 mM NaClO₄ at 37 °C. After 24 h of the reaction of DNA with the complex, the samples were precipitated in ethanol and dissolved in the medium necessary for a particular analysis, and the r_b value in an aliquot of this sample was checked by FAAS. In this way, all analyses described in the present paper were performed in the absence of unbound (free) Ru^{II} arene complex.

Transcription Mapping. Cutting of pSP73KB DNA by *Nde*I and *Hpa*I restriction endonucleases yielded a 212-base pairs (bp) fragment (a substantial part of its nucleotide sequence is shown in Figure 4B). This fragment contained T7 RNA polymerase promoter. In vitro RNA synthesis by RNA polymerases on this DNA template modified by Ru^{II} arene complexes **1** and **3** at the same level of the ruthenation ($r_b = 0.01$) can be prematurely terminated at the level or in the proximity of adducts (Figure 4A). Interestingly, monofunctional DNA adducts of several platinum complexes are unable to terminate RNA synthesis.^{11–13} The major stop sites, primarily guanine residues, were roughly identical for both Ru^{II} arene complexes (Figure 4B). The profiles are similar to that obtained for DNA treated with the anticancer drug cisplatin (lane cisPt in Figure 4A) and also to those reported

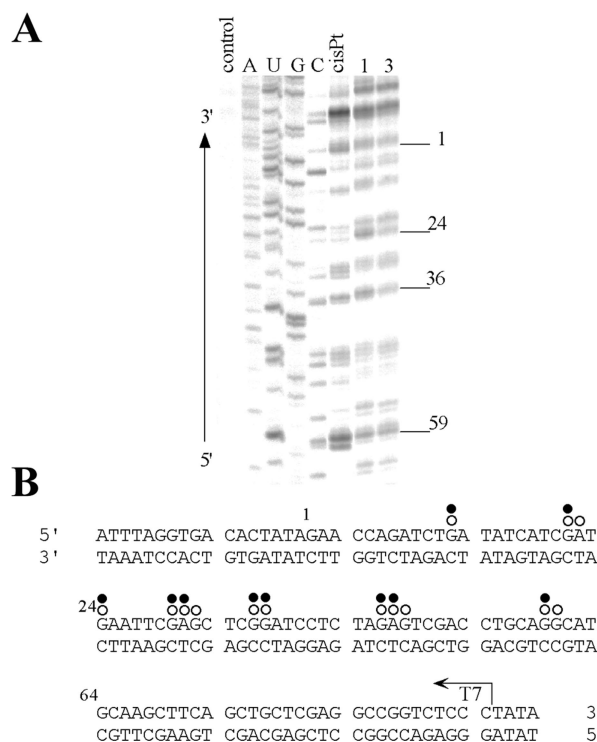


Figure 4. Inhibition of RNA synthesis by T7 RNA polymerase on the *Nde*I/*Hpa*I fragment of pSP73KB plasmid modified by Ru^{II} arene complexes and cisplatin. (A) Autoradiogram of 6% polyacrylamide/8 M urea sequencing gel showing inhibition of RNA synthesis by T7 RNA polymerase on the *Nde*I/*Hpa*I fragment containing adducts of Ru^{II} arene complexes and cisplatin. Lanes: control, unmodified template; A, U, G and C, chain terminated marker DNAs; cisPt, **1** and **3**, the template modified by cisPt, Ru^{II} arene complexes **1** or **3** at $r_b = 0.01$, respectively. (B) Schematic diagram showing the portion of the sequence used to monitor inhibition of RNA synthesis by cisplatin and Ru^{II} arene complexes. The arrow indicates the start of the T7 RNA polymerase, which used as template the upper strand of the *Nde*I/*Hpa*I fragment of pSP73KB. The open and closed bullets represent major stop signals for DNA modified by cisplatin or complex **1**, respectively. The numbers correspond to the nucleotide numbering in the sequence map of the pSP73KB plasmid.

previously for other type of Ru^{II} arene complexes such as $[(\eta^6\text{-arene})\text{Ru}(\text{en})\text{Cl}]^+$, where arene = biphenyl, dihydroanthracene, tetrahydroanthracene, *p*-cymene, or benzene.³ The major stop sites for DNA modified by complex **1** and cisplatin are demonstrated in Figure 4B. Thus, these results suggest that the major sites in DNA at which complexes **1** and **3** preferentially bind are guanine residues.

Circular Dichroism (CD). To gain further information, we also recorded CD spectra of DNA modified by complexes **1** and **3** (Figure 5). Complexes **1** and **3** have no intrinsic CD signals, as they are achiral so that any CD signal above 300 nm can be attributed to the interaction of complexes with DNA. Below 300 nm, any change from the DNA spectrum is due either to the DNA induced CD (ICD) of the metal complex or the metal complex induced perturbation of the DNA spectrum. The signature of complex **1** bound to CT DNA is a strong negative ICD at around 308 nm and a strong positive ICD centered at 376 nm, with the crossover at 351 nm (Figure 5A). On the other hand, the signature of complex **3** bound to CT DNA is only a very weak and broad positive ICD centered at 376 nm (Figure 5B). These results reflect different binding modes of complexes **1** and **3** to DNA. Unfortunately these complexes also absorb in the DNA region (Figure 5C) so that this ICD signal is due to changes in both the intrinsic DNA CD and the ligand-induced

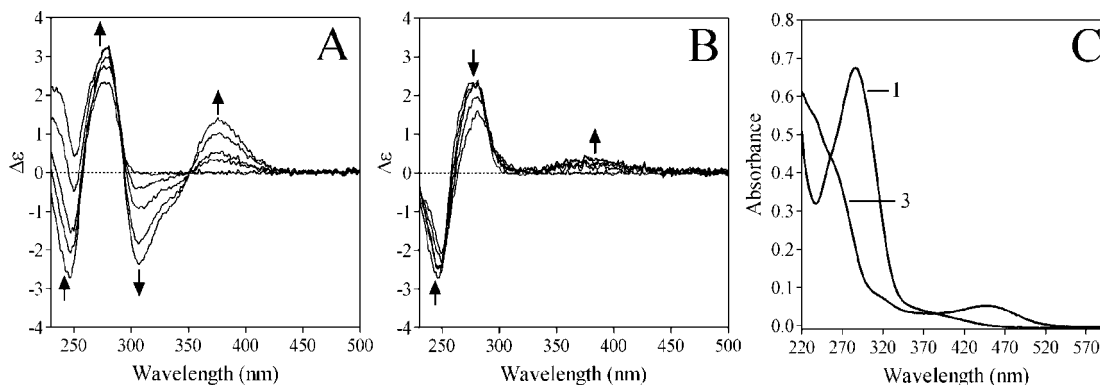


Figure 5. Circular dichroism (CD) spectra (A,B) of calf thymus DNA (1×10^{-4} M) modified by complexes **1** and **3** and UV-vis spectra of complexes **1** and **3** (C); the medium was 10 mM NaClO₄, pH 6. (A) DNA was modified by complex **1** at $r_b = 0, 0.013, 0.029, 0.087, 0.125$ (curves 1–5, respectively). (B) DNA was modified by complex **3** at $r_b = 0, 0.013, 0.033, 0.071, 0.118$ (curves 1–5, respectively). (C) Complexes **1** and **3** were at the concentration of 2.7×10^{-5} and 2.75×10^{-5} M, respectively. The arrows in (A,B) show a change of CD with increasing r_b value.

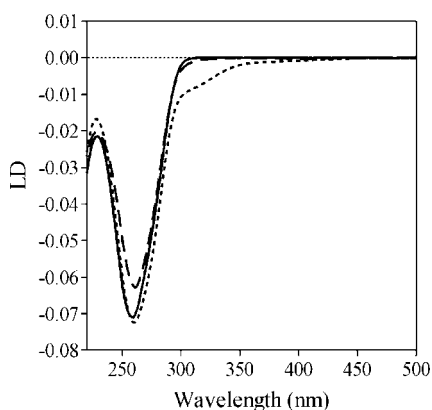


Figure 6. Linear dichroism (LD) spectra of calf thymus DNA modified by Ru^{II} arene complexes. LD spectra were recorded for DNA in 10 mM NaClO₄, at pH 6.0. The concentration of DNA was 3×10^{-4} M and r_b was 0.1. Thick solid line: control, nonmodified DNA. Dotted line: DNA modified by complex **1**. Dashed line: DNA modified by complex **3**.

CD, which impedes unambiguous interpretation of the CD spectra in Figure 5A,B in the DNA region (<300 nm) in terms of alterations of DNA conformation or the DNA binding mode of complexes **1** and **3**.

Linear Dichroism (LD). LD, which can be used to probe the orientation of molecules, was also exploited to characterize further DNA binding mode of complexes **1** and **3**. Long molecules such as DNA (minimum length of ~ 250 base pairs) can, in a flow Couette cell, be orientated through viscous drag.¹⁴ Small unbound molecules are not orientated in the experiment and show no signal. Similarly molecules bound randomly to CT DNA show no signal. However, molecules bound in a specific orientation with respect to the CT DNA show a LD signal.

Complexes **1** and **3** are too small to be orientated and thus show no intrinsic LD signal. Any LD signals that arise in the spectroscopic regions of complexes **1** and **3** in the presence of CT DNA, therefore, indicate binding of the complex to the CT DNA in a specific orientation(s). For the sample of CT DNA in the presence of complex **3**, we observed no bands in LD spectra in the region above 300 nm (Figure 6). In contrast, the LD signal yielded by the sample of CT DNA in the presence of complex **1** is slightly decreased in the region above 300 nm (in the range of 295–350 nm).

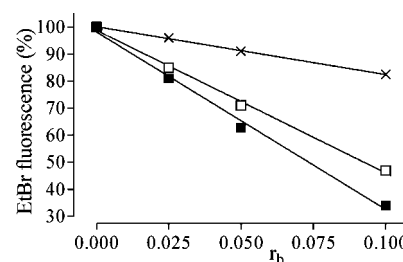


Figure 7. Plots of the EtBr fluorescence versus r_b for DNA modified by cisplatin, [PtCl(dien)]Cl, and Ru^{II} arene complexes in 10 mM NaClO₄ at 37 °C for 24 h: (x), [PtCl(dien)]Cl; (■), complex **1**; (□), complex **3**. Data points measured in triplicate varied on average $\pm 3\%$ from their mean.

The CT DNA LD bands (220–300 nm) confirm that the CT DNA modified by complexes **1** and **3** remains in the B-DNA conformation. While the intensity of the negative CT DNA LD band at 260 nm decreases due to the modification by complex **3**, an increase in the amplitude of the 260 nm LD band of DNA is observed due to the modification of CT DNA by complex **1** (Figure 6).

Ethidium Bromide (EtBr) Fluorescence. The ability of the complexes to displace the DNA intercalator EtBr from CT DNA was probed by monitoring the relative fluorescence of the EtBr-DNA adduct after treating the DNA with varying concentrations of **1** and **3**. Figure 7 shows a plot of relative fluorescence vs r_b for complexes **1** and **3**, and monofunctional chlorobis(2-aminoethyl)amineplatinum(II) chloride ([PtCl(dien)]Cl). The adducts of both monofunctional Ru^{II} arene complexes competitively replaced intercalated EtBr markedly more effectively than the adducts of monofunctional [PtCl(dien)]Cl. Notably, the ability of complex **1** to displace DNA intercalator EtBr from CT DNA was greater than that of complex **3**.

DNA Melting. CT DNA was modified by Ru^{II} arene complexes **1** or **3** at various r_b values (0–0.24) in 10 mM NaClO₄ at 37 °C for 24 h. The salt concentration was then further adjusted by addition of NaClO₄ to values in the range 0.01–0.2 M. The effect on DNA melting temperature (t_m) is dependent both on the amount of ruthenium bound and on the salt concentration. At low concentrations of NaClO₄ (0.01 M), an increase in t_m was observed for complex **1**, and this became more pronounced with increasing r_b values (Figure 8A). With increasing ionic strength, the enhancement of t_m (Δt_m , defined as the difference between the values of ruthenated and non-modified DNAs) due to the presence of the complex decreased.

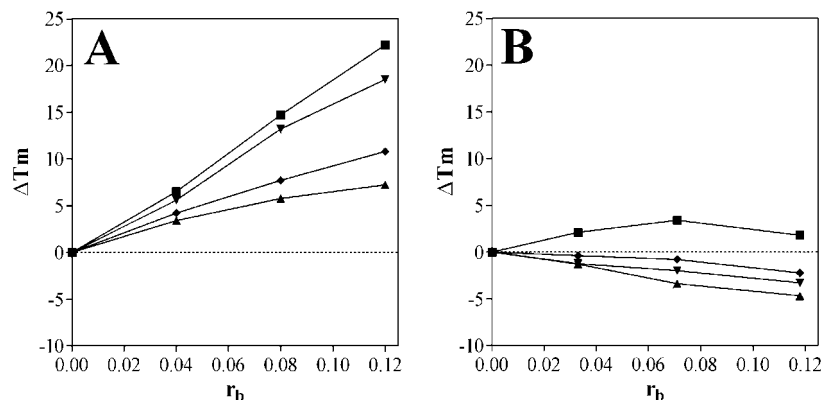


Figure 8. Plots showing the dependence of ΔT_m values on r_b for calf thymus DNA modified by Ru^{II} arene complexes **1** (A) and **3** (B). The melting curves were measured in the media of 1 mM Tris-HCl with 0.1 mM EDTA at pH 7.4 and varying concentrations of NaClO₄: (■), 0.01 M; (▼), 0.055 M; (◆), 0.105 M; (▲), 0.205 M. ΔT_m is defined as the difference between the T_m values of ruthenated and nonmodified DNAs. Data measured in triplicate varied on average $\pm 5\%$ from their mean.

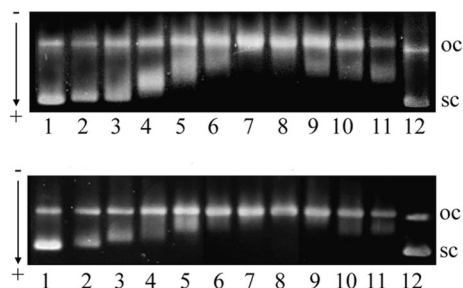


Figure 9. The unwinding of supercoiled pSP73KB plasmid DNA by complexes **1** (top) and **3** (bottom). The plasmid was incubated with Ru^{II} arene complexes in 10 mM NaClO₄, at pH 6 for 24 h at 37 °C. Lanes in the top panel: 1 and 12, control, unmodified DNA; 2, $r_b = 0.008$; 3, $r_b = 0.016$; 4, $r_b = 0.024$; 5, $r_b = 0.031$; 6, $r_b = 0.039$; 7, $r_b = 0.047$; 8, $r_b = 0.055$; 9, $r_b = 0.063$; 10, $r_b = 0.071$; 11, $r_b = 0.079$. Lanes in the bottom panel: 1 and 12, control, unmodified DNA; 2, $r_b = 0.017$; 3, $r_b = 0.033$; 4, $r_b = 0.050$; 5, $r_b = 0.058$; 6, $r_b = 0.066$; 7, $r_b = 0.074$; 8, $r_b = 0.083$; 9, $r_b = 0.091$; 10, $r_b = 0.099$; 11, $r_b = 0.108$. The top bands in each panel correspond to the form of nicked plasmid and the bottom bands to the closed, negatively supercoiled plasmid.

CT DNA modified by complex **3** exhibited a different melting behavior. At high concentrations of NaClO₄ (0.2 M), a decrease in T_m was observed for modification by complex **3**, and this became more pronounced with increasing r_b values (Figure 8B). With increasing ionic strength, the ΔT_m due to the modification by complex **3** decreased. At a concentration of NaClO₄ as low as 0.01 M for DNA modified by complex **3**, a slight increase in T_m was first observed with increasing r_b ($r_b \leq 0.07$), but at higher r_b values, ΔT_m decreased with increasing r_b .

Unwinding of Supercoiled DNA. The unwinding of supercoiled plasmid pSP73KB DNA induced on binding complexes **1** and **3** was determined by incubating the plasmid with **1** or **3** for 24 h at 37 °C at various r_b (different lanes in the gel). The native agarose gels resulting from DNA modified by **1** or **3** are shown in Figure 9 (top and bottom panels, respectively). A decrease in the rate of migration is the result of unwinding the DNA as this reduces the number of supercoils. The mean unwinding angle can be calculated from the equation $\Phi = -18\sigma/r_b(c)$, where σ is the superhelical density and $r_b(c)$ is the r_b at which the supercoiled and nicked forms comigrate.¹⁵ It can be seen in Figure 9 (top) that complex **1** causes a significant unwinding of the DNA ($\Phi = 14 \pm 1^\circ$, the comigration point of the modified supercoiled and nicked DNA, $r_b(c)$, was reached at $r_b = 0.0471$). In contrast, complex **3** unwinds the DNA

significantly less ($\Phi = 8 \pm 1^\circ$, the comigration point of the modified supercoiled and nicked DNA, $r_b(c)$, was reached at $r_b = 0.0827$). The high level of unwinding induced by complex **1** similar to that induced by cisplatin is notable.

Surface-Enhanced Raman Spectroscopy (SERS). SERS is a powerful tool for the study of the interactions of drugs, especially fluorescent molecules, with biomacromolecules at very low concentrations and quantities.^{16,17} This technique has been also exploited to investigate nucleic acids and their interactions.^{18–23} Metal colloids can be adapted for applications to the study of biological systems, because they do not disturb to a great extent the structures of biomolecules adsorbed on their surface.^{21,24,25} To further clarify the binding modes of complexes **1** and **3** to double helical DNA, SERS spectra were measured.

The SERS spectra of complexes **1** and **3** at a concentration of 10 μM recorded in the range of wavenumbers of 300–1520 cm^{-1} are shown in parts A and B of Figure 10 (curves a), respectively. In agreement with the previous reports,^{23,26} 100 μM linearized double helical pSP73 DNA gives no SERS signal (spectrum not shown). Curve b in Figure 10B shows the SERS spectrum of 100 μM plasmid DNA modified by complex **3** at $r_b = 0.1$ (all molecules of the complex were bound to plasmid DNA, i.e., no free ruthenium complex was present in this sample). Some bands of complex **3** completely disappear. However, several bands yielded by complex **3** bound to DNA still remain preserved in the SERS spectrum, but their relative intensity is reduced. In contrast, all SERS bands of complex **1** disappear as a consequence of its binding to double helical DNA (curve b in Figure 10A).

Discussion

New complexes of the type $[(\eta^6\text{-arene})\text{Ru}(\text{en})\text{Cl}]^+$, where the arene is *ortho*-, *meta*-, or *para*-terphenyl (*o*-, *m*-, or *p*-terp, complexes **2**, **3**, and **1**, respectively; Figure 1), were synthesized and characterized (Figure 2, Tables 1 and 2) and their effect on cytotoxicity, cellular Ru^{II} complex uptake, and DNA binding mode investigated.

The CH– π interaction observed between the C61H proton of the bound ring of *p*-terp (Figure S1 of Supporting Information) from one molecule and the center of the π -system of the central ring of *p*-terp to another molecule, can be classified as borderline between weak and strong (weak: CH $\cdots\pi$ center 2.6–3.0 Å, strong: CH $\cdots\pi$ center <2.6 Å).²⁷ The bond length between Ru and the substituted carbon of *p*-terp in the crystal

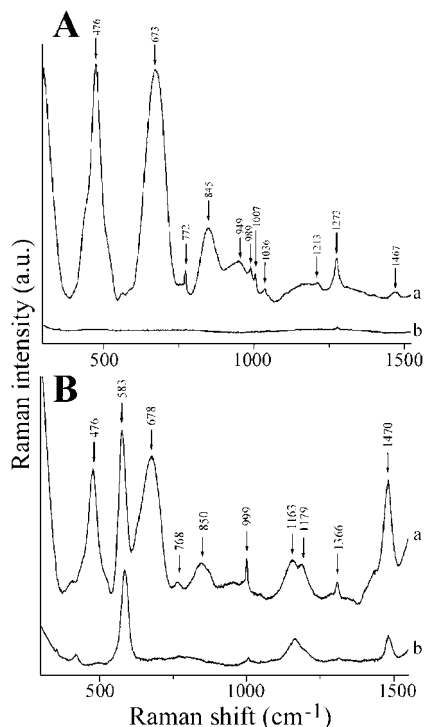


Figure 10. Surface-enhanced Raman scattering (SERS) spectra (300–1520 cm^{-1}). (A) 10 μM complex **1** (curve a); 100 μM linearized pSP73 DNA modified by complex **1** at $r_b = 0.1$ (curve b). (B) 10 μM complex **3** (curve a); 100 μM linearized pSP73 DNA modified by complex **3** at $r_b = 0.1$ (curve b).

structure of complex **1**, (2.225(4) Å) is 0.034 Å longer than any other Ru–C bond in the molecule.

The cytotoxic activity of Ru^{II} arene complexes **1–3** was determined against different cisplatin sensitive and resistant cancer cell lines (Table 3). The highest activity in all cell lines is exhibited by the *p*-terp complex **1**. Interestingly, in A2780, CH1, and SKBR3 cells, complex **1** shows potency comparable with that of conventional cisplatin. Importantly, the cytotoxicity of all Ru^{II} arene complexes tested in the present work in the cisplatin-resistant line A2780cisR is characterized by remarkably low resistance factors, less than 1 (Table 3); complex **1** shows the best circumvention of cisplatin resistance (lowest value of resistance factor) in comparison with its Ru^{II} arene congeners. On the other hand, complex **3** is the least potent in all cell lines with IC₅₀ values in the range of 31–75 μM . Notably all Ru^{II} arene complexes **1–3** show higher potency toward cisplatin resistant compared to cisplatin sensitive A2780 cells, indicating a mechanism of cytotoxicity of this class of Ru^{II} complexes different from that of cisplatin. Measurements of cellular Ru^{II} complex uptake indicate that intracellular damage induced by complex **1** and responsible for cytotoxic effects is more efficient than those induced by complexes **2** and **3**.

DNA is an important potential biological target for many metal-based anticancer agents. The results of the present work show that in general there is no direct correlation between cellular drug uptake or extent of DNA adduct formation in cells on one hand and tumor cell growth inhibition on the other hand. Thus, the type of adduct formed on DNA may be critical to activity.

The results of our studies of the binding of complexes **1** and **3** to natural double-helical CT DNA (in a cell-free medium) are summarized in Table 5. These results show that the reactions of these complexes with CT DNA are markedly faster than that for conventional cisplatin (Figure 3). The rate of binding is

Table 5. Summary of DNA Binding Studies for Complexes **1** and **3**

study	complex 1	complex 3
DNA binding	rapid ($t_{50\%} = 5$ min)/quantitative	rapid ($t_{50\%} = 9$ min)/80% (48 h)
circular dichroism	strong ICD negative (308 nm)/positive (376 nm)	weak and broad ICD positive (376 nm)
linear dichroism	binds to DNA in a specific orientation (planar intercalator)	binds to DNA in a nonspecific orientation (nonintercalative mode)
DNA unwinding/deg	14	8
DNA melting, °C, ΔT_m ($r_b = 0.12$; 0.205 M NaClO ₄)	+6	−4
EtBr displacement	greater replacement	less replacement
SERS	buried	partially buried

dependent on the type of the arene ligand: complex **3**, a complex with *m*-terp arene, binds to CT DNA more slowly than complex **1** (a complex with *p*-terp arene). The binding is quantitative in the case of complex **1** but not quantitative (~80% after 48 h) in the case of complex **3**. It can be deduced that hydrophobic interactions contribute to the driving force for the binding of chlorido Ru^{II} arene complexes to double-helical DNA. Hence, a faster reaction between CT DNA and complex **1** suggests that DNA binding mode of complex **1** involves not only its coordination to the base residues in DNA but also hydrophobic interactions such as intercalation of the *p*-terp arene. This interpretation also implies that the significance of these hydrophobic interactions in DNA binding mode of complex **3** is diminished.

Transcription mapping experiments (Figure 4) have shown that guanine residues are the preferential binding sites when polymeric DNA is modified with Ru^{II} arene complexes **1** and **3** in a random fashion.

The CD spectra of DNA modified by complex **1** or **3** (Figure 5) indicate that the binding of these complexes results in conformational alterations in double-helical DNA. Complex **1** bound to CT DNA yields a strong negative ICD at around 308 nm and a strong positive ICD centered at 376 nm (Figure 5A). On the other hand, complex **3** bound to CT DNA yields only a very weak and broad positive ICD centered at 376 nm (Figure 5B). These results are consistent with different binding modes of complexes **1** and **3** to DNA and support the hypothesis that the DNA binding mode, particularly of complex **1**, may involve its interaction in specific orientations.

No bands in LD spectra in the region above 300 nm were yielded by the sample of CT DNA modified by complex **3** (Figure 6). This result indicates that complex **3** is bound to CT DNA in nonspecific orientations consistent with only a very weak CD signal above 300 nm produced by the same sample (Figure 5B). In contrast, LD yielded by the sample of CT DNA modified by complex **1** was slightly decreased in the region above 300 nm (in the range of 295–350 nm), suggesting that this complex binds to CT DNA in a specific orientation. In addition, the negative sign of the LD signal above 300 nm indicates that the angle of the long axis of complex **1** to the axis of the DNA double helix is more than 54° as expected for an intercalator. These data suggest that complex **1** binds to the DNA also as a planar intercalator.^{14,28,29}

The CT DNA LD bands (220–300 nm) (Figure 6) confirm that the CT DNA modified by complexes **1** and **3** remains in the B-DNA conformation. However, some structural changes in CT DNA due to the modification by complex **3** are not excluded based on the decrease in the intensity of the negative CT DNA LD band at 260 nm (Figure 6). The LD signal at 260 nm of CT DNA modified by complex **3** is consistent with a

nonintercalative mode of interaction. Intercalation results in DNA stiffening, which is usually associated with an increase in the amplitude of the 260 nm LD band of DNA.^{14,29,30} It is well established that the magnitude of the LD signal measured within the DNA absorption band is a function of its persistence length. It is known that changes in flexibilities, or the formation of rigid bends or kinks induced by strongly bound compounds, can manifest themselves as decreases in the abilities of the modified DNA molecules to align themselves in the hydrodynamic flow gradient of the LD cell. Hence, the decrease of the magnitudes of the LD signals at 260 nm upon addition of complex **3** (Figure 6) suggests that the formation of strongly bound adducts derived from this Ru^{II} arene complex is accompanied by the appearance of flexible hinge joints at the site of the lesion and/or rigid bends or kinks. Further experiments are needed to distinguish between these two possibilities. In contrast, an increase in the amplitude of the 260 nm LD band of DNA is observed due to the modification of CT DNA by complex **1** (Figure 6). Hence, the dominant DNA binding mode for complex **1** can be concluded to involve also intercalation because intercalators usually stiffen the DNA, and that should lead to a larger DNA LD signal at 260 nm.^{14,29,30}

The CD changes observed for double-helical DNA modified by complexes **1** and **3** also correlate with the results of competitive EtBr displacement (Figure 7) and DNA unwinding (Figure 9) experiments. The monofunctional adducts of *p*-terp complex **1** are considerably more efficient in DNA-EtBr fluorescence quenching and in DNA unwinding than those of *m*-terp complex **3**. This observation may be explained by additional contributions to fluorescence quenching and unwinding from intercalation of the extended arene ligand of complex **1** into the duplex or from other types of noncovalent interaction of this complex with DNA upon its monofunctional binding. The large unwinding angle of 14° produced by complex **1** could be interpreted to mean that the arene moiety in the monofunctional adduct of complex **1** is geometrically well positioned to intercalate between the base pairs of the helix, so producing also the induced CD bands (Figure 5). Consistent with this conclusion is the observation that DNA adducts of complex **3**, which produce only very weak induced CD bands in the visible spectrum and quench DNA-EtBr fluorescence only slightly, unwind DNA only by 8° (Figure 9), a similar behavior to that of the monofunctional adducts of [Pt(dien)Cl]Cl (unwinding angle 6°).¹⁵ Thus, the results of unwinding experiments support the view that *p*-terp arene ligand in complex **1** interacts substantially with the double helix upon coordination of Ru^{II} complex. Hence, these results strengthen the case for combined intercalative and monofunctional binding mode of complex **1**. On the other hand, it seems reasonable to suggest that *m*-terp ligand in complex **3** does not interact with the double helix in a similar way, thus also supporting a different DNA binding mode for this complex in comparison with **1**.

Melting of DNA modified by complex **1** or **3** (Figure 8) also deserves discussion. The following factors can be invoked to account for the thermal stability of DNA modified by monofunctional Ru^{II} arene complexes:³ (i) Stabilizing effects of the positive charge on ruthenium, favorable stacking interactions between the base residues and the arene, and the separation of negative backbone charges inherent to intercalating arene residue (due to elongation and unwinding of DNA), that is, changes in solvent structure and the counterion distribution around the phosphate groups that may help to overcome electrostatics unfavorable for the hybridization of the strands of the duplex.^{31,32} (ii) A destabilizing effect of conformational distortions induced

in DNA by ruthenium coordination. The dependence of the *t_m* value of DNA modified by nonintercalating ruthenium drugs on ionic strength can be explained by competing electrostatic effects as the salt concentration is varied.³³ Thus, the observed change in *t_m* will reflect the relative proportion and contribution of all limiting binding modes.

At low ionic strength (0.01 M), it is reasonable to conclude that the increase in *t_m* due to the modification of DNA by complex **1** (Figure 8A) is caused by positive charges on ruthenium [(η⁶-arene)Ru(en)Cl]⁺ groups and by the intercalation. The smaller increase in *t_m* due to the modification by complex **1** observed at high ionic strength is a consequence of reduced stabilizing effects because the electrostatic stabilizing effects of this complex are apparently lowered with increasing concentration of Na⁺ counterions.

The melting behavior of DNA modified by complex **3** is different (Figure 8B). Modification by this complex already decreases *t_m* at concentrations of Na⁺ as low as 0.055 M, indicating that the effects of the factors responsible for the thermal stabilization of DNA (the positive charge on ruthenium and intercalation of the arene ligand into the duplex) are noticeably reduced so that the destabilization effect of conformational alterations induced by complex **3** predominates already at low salt concentrations. Thus, the results of DNA melting experiments are consistent with the formation of a monofunctional adduct of *m*-terp complex **3** with DNA (coordination to G N7) and the absence of intercalation.

The arene–DNA hydrophobic interactions may also affect SERS behavior. The effect of decreasing the SERS intensity as a consequence of the binding of various compounds to the DNA has been well documented^{16,23,25,34} and explained in terms of short-range character of Raman enhancement in colloid systems. Thus, the SERS spectrum of plasmid DNA modified by complex **3** indicates the decrease in the overall accessibility of complex **3** for its direct interaction with colloids due to its binding to DNA. The fact that various vibrations in complex **3** are affected by its binding to double helical DNA to a different extent indicates that various groups in complex **3** are buried in the double helix differently or that only a portion of the chromophore is involved in direct contacts with DNA.

In other words, when complex **3** binds to double helical DNA, it seems to be partially buried inside the double helix. Hence, a reasonable interpretation of the SERS from DNA modified by complex **3** is that its DNA binding mode also involves, besides coordination to DNA bases (presumably guanine residues), a mixed noncovalent binding mode such as the external binding (possibly also stacking) and/or partial intercalation.

In contrast, all SERS bands of complex **1** disappear as a consequence of its binding to double-helical DNA (curve b in Figure 10A). In terms of the short-range character of the SERS (vide supra), the SERS quenching can be interpreted in terms of a loss of accessibility for complex **1** bound to double helical DNA to the Ag colloids. Thus, complex **1** presents a typical intercalating mode because the molecule is intercalated between the base pairs in DNA and thus becomes undetectable by SERS.^{19,21,23,35}

In summary, complex **1** containing *p*-terp arene ligand exhibits promising cytotoxic effects in several human tumor cell lines including those resistant to conventional cisplatin and concomitantly its DNA binding mode involves combined intercalative and monofunctional (coordination) binding modes. In contrast, complex **3** containing *m*-terp arene ligand is much less cytotoxic and binds to DNA via only a monofunctional coordination to DNA bases. In the case of complex **1**, ruthenium

is bound to a terminal phenyl ring, whereas in the case of complexes **2** and **3**, ruthenium is bound to the central phenyl ring. It is therefore possible that the distance between marginal phenyl rings in complex **3** (or in complex **2**) and Ru coordinated to DNA bases is too short to allow these marginal phenyl rings to adopt configurations that allow intercalation into DNA. On the other hand, the distance between the distant marginal phenyl ring in complex **1** and Ru coordinated to DNA bases is greater, allowing this phenyl ring to adopt a configuration appropriate for intercalation. In any case, the results of the present work further support the view that the presence of the arene ligand in $[(\eta^6\text{-arene})\text{Ru}(\text{en})\text{Cl}]^+$ complexes capable of noncovalent, hydrophobic interaction with DNA considerably enhances cytotoxicity in tumor cell lines. Thus, the results of the present work represent a further improvement in the structure–pharmacological relationship needed for the design of new antitumor ruthenium drugs and chemotherapeutic strategies.

Experimental Section

Starting Materials. The starting dimers $[(\eta^6\text{-arene})\text{RuCl}_2]_2$, arene = *p*-terphenyl (*p*-terp, bound to the Ru through the terminal phenyl ring), *o*-terphenyl (*o*-terp, bound to the Ru through the central phenyl ring), and *m*-terphenyl (*m*-terp, bound to the Ru through the central phenyl ring) were prepared according to literature methods.³⁶ $\text{RuCl}_3 \cdot \text{XH}_2\text{O}$ was purchased from Precious Metals Online and was used as received. The arenes were purchased from Sigma-Aldrich, reduced and purified using the previously published procedures.³⁷ 1,2-Diaminoethane was purchased from Sigma-Aldrich. Ethanol and methanol were dried over Mg/I_2 .

Cisplatin and dimethylsulfoxide (DMSO) were obtained from Sigma-Aldrich s.r.o. (Prague, Czech Republic). $[\text{PtCl}(\text{dien})]\text{Cl}$ was a generous gift of Professor G. Natile from University of Bari. Stock solutions of metal complexes for the biophysical and biochemical studies were prepared at a concentration of 5×10^{-4} M in water, filtered, and stored at room temperature in the dark. Stock solutions of metal complexes for the cytotoxicity and cellular uptake studies were prepared in DMSO and used immediately after dissolution. The concentrations of ruthenium or platinum in the stock solutions were determined by FAAS. CT DNA (42% G + C, mean molecular mass ca. 2×10^7) was also prepared and characterized as described previously.^{38,39} pSP73 (2464 bp) and pSP73KB (2455 bp) plasmids (superhelical density $\sigma = -0.063$ and -0.036 , respectively) were isolated according to standard procedures. Restriction endonucleases *NdeI*, *HpaI*, and T4 polynucleotide kinase were purchased from New England Biolabs. Acrylamide, bis(acrylamide), and EtBr were obtained from Merck KgaA (Darmstadt, Germany). Agarose was purchased from FMC BioProducts (Rockland, ME). Radioactive products were obtained from MP Biomedicals, LLC (Irvine, CA).

Preparation of Complexes. All complexes were synthesized using a similar procedure. Typically the ligand (2 mol equiv) was added to a methanolic solution of the dimer $[(\eta^6\text{-arene})\text{RuCl}_2]_2$. Details for individual reactions are described below.

$[(\eta^6\text{-}p\text{-terp})\text{Ru}(\text{en})\text{Cl}][\text{PF}_6]$ (complex **1).** To a suspension of $[(\eta^6\text{-}p\text{-terp})\text{RuCl}_2]_2$ dimer (0.10 g, 0.125 mmol) in dry, freshly distilled methanol (50 mL) en (17 μL , 0.250 mmol) was added. The reaction mixture was stirred at ambient temperature under argon overnight, and the resulting clear yellow solution was filtered. NH_4PF_6 (0.061 g, 0.375 mmol) was added and the flask shaken. A precipitate started to appear almost immediately. The flask was kept at -20°C overnight, and the product was collected by filtration, washed with cold methanol and ether, and dried in air to give an orange solid.

Yield: 87%. Crystals suitable for X-ray analysis were obtained by slow evaporation of a methanolic solution at ambient temperature and the complex crystallized as $[(\eta^6\text{-}p\text{-terp})\text{Ru}(\text{en})\text{Cl}][\text{PF}_6]$. ESI-MS: calcd for $\text{C}_{20}\text{H}_{22}\text{ClRuN}_2^+ [\text{M}]^+ m/z$ 426.9, found 427.0. ^1H NMR in $\text{DMSO}-d_6$: δ 7.87 (d, 2H), 7.80 (d, 2H), 7.74 (d, 2H), 7.52 (t, 2H), 7.42 (t, 1H), 6.50 (d, 2H; NH), 6.22 (d, 2H), 5.90 (t, 1H), 5.82 (t, 2H), 4.20 (d, 2H; NH), 2.31 (m, 2H), 2.22 (m, 2H).

Anal. Calcd for $\text{C}_{20}\text{H}_{22}\text{ClRuN}_2\text{PF}_6$: C, 42.00; H, 3.88; N, 5.00. Found: C, 42.75; H, 3.97; N, 4.90.

$[(\eta^6\text{-}o\text{-terp})\text{Ru}(\text{en})\text{Cl}][\text{PF}_6]$ (complex **2).** To a suspension of $[(\eta^6\text{-}o\text{-terp})\text{RuCl}_2]_2$ dimer (0.05 g, 0.06 mmol) in dry, freshly distilled methanol (50 mL) en (8 μL , 0.12 mmol) was added. The rest of the procedure was the same as described for complex **1**. After addition of NH_4PF_6 (0.03 g, 0.18 mmol), the fine yellow solid was isolated as described for complex **1** and recrystallized from methanol/ether.

Yield: 65%. ESI-MS: calcd for $\text{C}_{20}\text{H}_{22}\text{ClRuN}_2^+ [\text{M}]^+ m/z$ 426.9, found 427.0. ^1H NMR in $\text{DMSO}-d_6$: δ 7.43 (m, 4H), 7.31 (m, 2H), 7.26 (m, 4H), 6.49 (d, 2H; NH), 5.95 (m, 4H), 4.31 (d, 2H; NH), 2.36 (m, 2H), 2.23 (m, 2H). Anal. Calcd for $\text{C}_{20}\text{H}_{22}\text{ClRuN}_2\text{PF}_6$: C, 42.00; H, 3.88; N, 5.00. Found: C, 42.06; H, 3.75; N, 4.17.

$[(\eta^6\text{-}m\text{-terp})\text{Ru}(\text{en})\text{Cl}][\text{PF}_6]$ (complex **3).** To a suspension of $[(\eta^6\text{-}m\text{-terp})\text{RuCl}_2]_2$ dimer (0.053 g, 0.065 mmol) in dry, freshly distilled methanol (50 mL), en (8.7 μL , 0.13 mmol) was added. The rest of the procedure was the same as described above. After addition of NH_4PF_6 (0.032 g, 0.19 mmol), brownish solid was isolated as described for complex **1** and recrystallized from methanol.

Yield: 63%. ESI-MS: calcd for $\text{C}_{20}\text{H}_{22}\text{ClRuN}_2^+ [\text{M}]^+ m/z$ 426.9, found 427.0. ^1H NMR in $\text{DMSO}-d_6$: δ 7.92 (d of d, 4H), 7.52 (m, 6H), 6.60 (s, 1H), 6.43 (d of d, 2H), 6.35 (d, 2H; NH), 5.85 (t, 1H), 4.17 (d, 2H; NH), 2.30 (m, 2H), 2.15 (m, 2H). Anal. ($\text{C}_{20}\text{H}_{22}\text{ClRuN}_2\text{PF}_6$) C, H, N.

X-ray Crystallography. Diffraction data for **1** were collected using Mo K α radiation on a Bruker Smart Apex CCD diffractometer equipped with an Oxford Cryosystems low-temperature device operating at 150 K. An absorption correction was applied using the multiscan procedure SADABS.⁴⁰ The structure was solved by Patterson methods (DIRDIF)⁴¹ and refined by full-matrix least-squares against $|F|^2$ using all data (SHELXL).⁴² Hydrogen atoms were placed in calculated positions, and all non-H atoms were modeled with anisotropic displacement parameters. The final conventional *R* factor (based on *F* and 3564 out of 4590 with $F > 4\sigma(F)$) was 0.0479. Other crystal and refinement data are collected in Table 1. The crystal structure of **1** has been deposited in the Cambridge Crystallographic Data Center under the accession number CCDC 681045.

NMR Spectroscopy. All the NMR spectra were recorded on either Bruker DMX (500 MHz) or AVA (600 MHz) spectrometers. ^1H NMR signals were referenced to the residual solvent peak, δ 2.52 (DMSO). All spectra were recorded at 25°C using 5 mm diameter tubes. The data were processed using XWIN-NMR (Version 3.6 Bruker UK Ltd.).

Electrospray Mass Spectrometry. ESI-MS were obtained on a Micromass Platform II mass spectrometer and solutions were infused directly. The capillary voltage was 3.5 V, and the cone voltage was 25 V. The source temperature was 80°C .

Elemental Analysis. Elemental analyses were carried out by the Warwick Analytical Service or by the University of Edinburgh, using an Exeter analytical analyzer CE 440.

Cytotoxicity. The tumor cell lines A2780, A2780cisR, CH1, and SKBR3 were cultured in RPMI 1640 medium (Gibco) (A2780 and A2780cisR) and Dulbecco's modified Eagle's medium (DMEM) (CH1 and SKBR3), supplemented with 10% FBS, 50 $\mu\text{g/mL}$ gentamycin at 37°C in an atmosphere of 95% of air and 5% CO_2 . Cell death was evaluated by using a system based on the tetrazolium compound MTT [3-(4,5-dimethyl-2-thiazolyl)-2,5-diphenyl-2H-tetrazolium bromide], which is reduced by living cells to yield a soluble formazan product that can be detected colorimetrically.⁴³ Cells were seeded in 96-well sterile plates at a density of 10^4 cells/well in 100 μL of medium and were incubated 16 h. The final concentration of DMSO in cell culture medium did not exceed 0.25%. Complexes were added to final concentrations from 0 to 256 μM in a volume of 100 μL /well. Then 72 h later, 10 μL of a freshly diluted MTT solution (2.5 mg/mL) was pipetted into each well and the plate was incubated at 37°C in a humidified 5% CO_2 atmosphere. After 5 h, the medium was removed and the formazan product was dissolved in 100 μL of DMSO. The cell viability was evaluated by measurement of the absorbance at 570 nm by using

an Absorbance Reader SUNRICE TECAN SCHOELLER. IC₅₀ values (compound concentration that produces 50% of cell growth inhibition) were calculated from curves constructed by plotting cell survival (%) versus drug concentration (μ M). All experiments were made in quadruplicate.

Cellular Ruthenium Complex Uptake. Cellular uptake of complexes **1–3** and cisplatin was measured in A2780 and A2780cisR cells (sensitive and resistant to cisplatin, respectively). The cells were seeded in 60 mm tissue culture dishes (30 000/cm²). After overnight incubation, the cells were treated with the ruthenium complex for 72 h at the concentrations corresponding to the IC₅₀ values (Table 3, these concentrations were still verified by the measurement of ruthenium in the growing medium by FAAS). The attached cells were washed twice with PBS (4 °C), the pellet stored at –80 °C, and ruthenium content determined by FAAS. For other details, see the Results section. All experiments were performed in quadruplicate.

DNA Ruthenation in Cells Exposed to Ru^{II} Arene Complexes. A2780 cells grown to near confluence were exposed to 50 μ M concentration of complexes **1** or **3** for 2 h. DNA was extracted according to standard procedures involving lysis in the presence of 1 mg proteinase K overnight at 37 °C. DNA content was determined spectrophotometrically, and ruthenium content was measured by inductively coupled plasma mass spectroscopy (ICP-MS).⁴⁴ Experiments were performed in duplicate, and the values are the means \pm SD of three independent experiments.

Metalation Reactions in Cell-Free Media. CT DNA and plasmid DNAs were incubated with ruthenium or platinum complex in 10 mM NaClO₄ (at pH 6) at 37 °C for 24 h in the dark, if not stated otherwise. The values of r_b were determined by FAAS.

DNA Transcription by RNA Polymerase In Vitro. Transcription of the (*NdeI/HpaI*) restriction fragment of pSP73KB DNA with T7 RNA polymerase and electrophoretic analysis of the transcripts were performed according to the protocols recommended by Promega (Promega Protocols and Applications, 43–46 (1989/90)) and previously described in detail.^{11,12}

Circular Dichroism (CD). Isothermal CD spectra of CT DNA modified by ruthenium complexes were recorded at 25 °C in 10 mM NaClO₄ by using a Jasco J-720 spectropolarimeter equipped with a thermoelectrically controlled cell holder. The cell path length was 1 cm. Spectra were recorded in the range of 230–500 nm in 0.5 nm increments with an averaging time of 1 s.

Flow Linear Dichroism (LD). Flow LD spectra were collected by using a flow Couette cell in a Jasco J-720 spectropolarimeter adapted for LD measurements. Long molecules, such as DNA (minimum length of \sim 250 bp), can be orientated in a flow Couette cell. The flow cell consists of a fixed outer cylinder and a rotating solid quartz inner cylinder, separated by a gap of 0.5 mm, giving a total path length of 1 mm.^{45,46} LD spectra of CT DNA modified by Ru^{II} arene complexes were recorded at 25 °C in 10 mM NaClO₄.

Fluorescence Measurements. These measurements were performed on a Shimadzu RF 40 spectrofluorophotometer using a 1 cm quartz cell. Fluorescence measurements of CT DNA modified by Ru^{II} arene complexes or [PtCl(dien)]Cl, in the presence of EtBr, were performed at an excitation wavelength of 546 nm, and the emitted fluorescence was analyzed at 590 nm. The fluorescence intensity was measured at 25 °C in 0.4 M NaCl to avoid secondary binding of EtBr to DNA.^{47,48} The concentrations were 0.01 mg/mL for DNA and 0.04 mg/mL for EtBr, which corresponded to the saturation of all intercalation sites of EtBr in DNA.⁴⁷

DNA Melting. The melting curves of CT DNAs were recorded by measuring the absorbance at 260 nm. The melting curves of unmodified or ruthenated DNA were recorded in a medium containing 10 mM NaClO₄ with 1 mM Tris-HCl/0.1 mM EDTA, pH 7.4. The value of t_m was determined as the temperature corresponding to a maximum on the first-derivative profile of the melting curves. The t_m values could be thus determined with an accuracy of \pm 0.3 °C.

Unwinding of Negatively Supercoiled DNA. Unwinding of closed circular supercoiled pSP73KB plasmid DNA was assayed by an agarose gel mobility shift assay.¹⁵ The unwinding angle Φ ,

induced per ruthenium–DNA adduct, was calculated upon the determination of the r_b value at which the complete transformation of the supercoiled to relaxed form of the plasmid was attained. Samples of plasmid DNA were incubated with complexes **1** or **3** at 37 °C in the dark for 24 h. All samples were precipitated by ethanol and redissolved in the TAE (Tris-acetate/EDTA) buffer. One aliquot of the precipitated sample was subjected to electrophoresis on 1% agarose gels running at 25 °C in the dark with TAE buffer and the voltage set at 25 V. The gels were then stained with EtBr, followed by photography with transilluminator. The other aliquot was used for the determination of r_b values by FAAS.

Surface-Enhanced Raman Spectrometry (SERS). Ag colloids were prepared by reducing AgNO₃ with hydroxylamine/sodium hydroxide according to the reported method,⁴⁹ i.e., 10 mL of hydroxylamine/sodium hydroxide (1.5×10^{-2} M/ 3×10^{-3} M) was added dropwise to 90 mL of silver nitrate (1.11×10^{-3} M). The Ag colloid/complex **1** or **3** (or Ag colloid/plasmid DNA) SERS active systems were prepared by mixing equal volumes of the solution of Ru^{II} complex or plasmid DNA with the Ag colloid to obtain the concentration of Ru^{II} arene complex or linearized pSP73 DNA (nonmodified or ruthenated) of 5×10^{-7} M or 5×10^{-6} M (related to the monomeric nucleotide content), respectively. The final concentration of the colloid was 9×10^{-4} M. In these SERS experiments, plasmid DNA pSP73 linearized by *NdeI* restriction endonuclease nonmodified or ruthenated at $r_b = 0.1$ was used (*NdeI* cuts only once within this plasmid). The spectra were measured immediately after mixing the complex or DNA with Ag colloid at 25 °C.

SERS spectra were recorded in conventional 90° geometry on Jobin Yvon R64000 Raman spectrometer. The samples (10 μ L) were sealed in glass capillary. Spectra were excited at 488 nm using an argon ion laser (Coherent Innova FreD90C). The radiation power at the sample was 100 mW. The measurement of whole spectrum was divided into two parts and each part consisted of several accumulations (16×2 s).

Other Physical Methods. Absorption spectra were measured with a Beckman DU 7 4000 spectrophotometer equipped with a thermoelectrically controlled cell holder and quartz cells with the path length of 1 cm. The FAAS measurements were carried out on a Varian AA240Z Zeeman atomic absorption spectrometer equipped with a GTA 120 graphite tube atomizer. For FAAS analysis, DNA was precipitated with ethanol and dissolved in 0.1 M HCl. The gels were visualized by using a BAS 2500 FUJIFILM bioimaging analyzer, and the radioactivity associated with bands was quantitated with the AIDA image analyzer software (Raytest, Germany).

Acknowledgment. This research was supported by the Ministry of Education of the CR (MSMT LC06030, 6198959216, ME08017, OC08003), the Academy of Sciences of the Czech Republic (grants 1QS500040581, KAN200200651, AV0Z50040507, and AV0Z50040702), the Grant Agency of the CR (203/06/1239), the Grant Agency of the Academy of Sciences of the CR (IAA400040803), and the Grant Agency of the Ministry of Health of the CR (NR8562-4/2005). J.K. is the international research scholar of the Howard Hughes Medical Institute. The authors also acknowledge that their participation in the EU COST Action D39 enabled them to exchange regularly the most recent ideas in the field of anticancer metallodrugs with several European colleagues. Ruthenium content was measured by ICP-MS at the Research Centre for Environmental Chemistry and Ecotoxicology, Masaryk University, Brno, Czech Republic.

Supporting Information Available: Elemental analysis of complex **3**; intermolecular interaction for complex **1**. This material is available free of charge via the Internet at <http://pubs.acs.org>.

References

- (1) Aird, R.; Cummings, J.; Ritchie, A.; Muir, M.; Morris, R.; Chen, H.; Sadler, P.; Jodrell, D. In vitro and in vivo activity and cross resistance profiles of novel ruthenium (II) organometallic arene complexes in human ovarian cancer. *Br. J. Cancer* **2002**, *86*, 1652–1657.
- (2) Morris, R. E.; Aird, R. E.; Murdoch, P. D.; Chen, H. M.; Cummings, J.; Hughes, N. D.; Parsons, S.; Parkin, A.; Boyd, G.; Jodrell, D. I.; Sadler, P. J. Inhibition of cancer cell growth by ruthenium(II) arene complexes. *J. Med. Chem.* **2001**, *44*, 3616–3621.
- (3) Novakova, O.; Chen, H.; Vrana, O.; Rodger, A.; Sadler, P. J.; Brabec, V. DNA interactions of monofunctional organometallic ruthenium(II) antitumor complexes in cell-free media. *Biochemistry* **2003**, *42*, 11544–11554.
- (4) Chen, H. M.; Parkinson, J. A.; Parsons, S.; Coxall, R. A.; Gould, R. O.; Sadler, P. J. Organometallic ruthenium(II) diamine anticancer complexes: Arene–nucleobase stacking and stereospecific hydrogen-bonding in guanine adducts. *J. Am. Chem. Soc.* **2002**, *124*, 3064–3082.
- (5) Liu, H. K.; Berners-Price, S. J.; Wang, F. Y.; Parkinson, J. A.; Xu, J. J.; Bella, J.; Sadler, P. J. Diversity in guanine-selective DNA binding modes for an organometallic ruthenium arene complex. *Angew. Chem., Int. Ed.* **2006**, *45*, 8153–8156.
- (6) Liu, J.-K. Natural terphenyls: Developments since 1877. *Chem. Rev.* **2006**, *106*, 2209–2223.
- (7) Behrens, B. C.; Hamilton, T. C.; Masuda, H.; Grotzinger, K. R.; Whang-Peng, J.; Louie, K. G.; Knutsen, T.; McKoy, W. M.; Young, R. C.; Ozols, R. F. Characterization of a *cis*-diamminedichloroplatinum(II)-resistant human ovarian cancer cell line and its use in evaluation of platinum analogues. *Cancer Res.* **1987**, *47*, 414–418.
- (8) Zhang, C. X.; Lippard, S. J. New metal complexes as potential therapeutics. *Curr. Opin. Chem. Biol.* **2003**, *7*, 481–489.
- (9) Brabec, V. DNA modifications by antitumor platinum and ruthenium compounds: their recognition and repair. *Prog. Nucleic Acid Res. Mol. Biol.* **2002**, *71*, 1–68.
- (10) Brabec, V.; Novakova, O. DNA binding mode of ruthenium complexes and relationship to tumor cell toxicity. *Drug Resist. Updates* **2006**, *9*, 111–122.
- (11) Brabec, V.; Leng, M. DNA interstrand cross-links of *trans*-diamminedichloroplatinum(II) are preferentially formed between guanine and complementary cytosine residues. *Proc. Natl. Acad. Sci. U.S.A.* **1993**, *90*, 5345–5349.
- (12) Lemaire, M. A.; Schwartz, A.; Rahmouni, A. R.; Leng, M. Interstrand cross-links are preferentially formed at the d(GC) sites in the reaction between *cis*-diamminedichloroplatinum(II) and DNA. *Proc. Natl. Acad. Sci. U.S.A.* **1991**, *88*, 1982–1985.
- (13) Brabec, V.; Boudny, V.; Balcarova, Z. Monofunctional adducts of platinum(II) produce in DNA a sequence-dependent local denaturation. *Biochemistry* **1994**, *33*, 1316–1322.
- (14) Rodger, A.; Marington, R.; Geeves, M. A.; Hicks, M.; de Alwis, L.; Halsall, D. J.; Dafforn, T. R. Looking at long molecules in solution: what happens when they are subjected to Couette flow? *Phys. Chem. Chem. Phys.* **2006**, *8*, 3161–3171.
- (15) Keck, M. V.; Lippard, S. J. Unwinding of supercoiled DNA by platinum ethidium and related complexes. *J. Am. Chem. Soc.* **1992**, *114*, 3386–3390.
- (16) Nabiev, I.; Chourpa, I.; Manfait, M. Applications of Raman and surface-enhanced Raman-scattering spectroscopy in medicine. *J. Raman Spectrosc.* **1994**, *25*, 13–23.
- (17) Kneipp, K.; Kneipp, H.; Kartha, V. B.; Manoharan, R.; Deinum, G.; Itzkan, I.; Dasari, R. R.; Feld, M. S. Detection and identification of a single DNA base molecule using surface-enhanced Raman scattering (SERS). *Phys. Rev. E* **1998**, *57*, R6281–R6284.
- (18) Brabec, V.; Niki, K. Raman scattering from nucleic acids adsorbed at a silver electrode. *Biophys. Chem.* **1985**, *23*, 63–70.
- (19) Lee, C. J.; Kang, J. S.; Kim, M. S.; Lee, K. P.; Lee, M. S. The study of doxorubicin and its complex with DNA by SERS and UV-resonance Raman spectroscopy. *Bull. Korean Chem. Soc.* **2004**, *25*, 1211–1216.
- (20) Murza, A.; AlvarezMendez, S.; SanchezCortes, S.; GarciaRamos, J. V. Interaction of antitumoral 9-aminoacridine drug with DNA and dextran sulfate studied by fluorescence and surface-enhanced Raman spectroscopy. *Biopolymers* **2003**, *72*, 174–184.
- (21) Gaudry, E.; Aubard, J.; Amouri, H.; Lévi, G.; Cordier, C. SERS study of the DNA binding by Ru(II) tris-(bipyridyl) complexes bearing one carboxylic group. *Biopolymers* **2006**, *82*, 399–404.
- (22) Aminzadeh, A. FT-SERS study of adriamycin–DNA interaction. *Iran J. Chem. Chem. Eng., Int. Engl. Ed.* **2003**, *22*, 9–11.
- (23) Wei, C.; Jia, G.; Yuan, J.; Feng, Z.; Li, C. A spectroscopic study on the interactions of porphyrin with G-quadruplex DNAs. *Biochemistry* **2006**, *45*, 6681–6691.
- (24) de Groot, J.; Hester, R. E. Surface-enhanced resonance Raman spectroscopy of oxyhemoglobin adsorbed onto colloidal silver. *J. Phys. Chem.* **1987**, *91*, 1693–1696.
- (25) Nabiev, I.; Baranov, A.; Chourpa, I.; Beljebbar, A.; Sockalingum, G. D.; Manfait, M. Does adsorption on the surface of a silver colloid perturb drug–DNA interactions: Comparative SERS, FT-SERS, and resonance Raman study of mitoxantrone and its derivatives. *J. Phys. Chem.* **1995**, *99*, 1608–1613.
- (26) Nabiev, I.; Chourpa, I.; Manfait, M. Comparative-studies of antitumor DNA intercalating agents, aclacinomycin and saintopin, by means of surface-enhanced Raman-scattering spectroscopy. *J. Phys. Chem.* **1994**, *98*, 1344–1350.
- (27) Bogdanovic, G. A.; Spasojevic-de Bire, A.; Zaric, S. D. Evidence based on crystal structures and calculations of a C-H $\cdots\pi$ interaction between an organic moiety and a chelate ring in transition metal complexes. *Eur. J. Inorg. Chem.* **2002**, *2002*, 1599–1602.
- (28) Boerner, L. J. K.; Zaleski, J. M. Metal complex–DNA interactions: from transcription inhibition to photoactivated cleavage. *Curr. Opin. Chem. Biol.* **2005**, *9*, 135–144.
- (29) Ihara, T.; Ikegami, T.; Fujii, T.; Kitamura, Y.; Sueda, S.; Takagi, M.; Jyo, A. Metal ion-directed cooperative DNA binding of small molecules. *J. Inorg. Biochem.* **2006**, *100*, 1744–1754.
- (30) Chou, P.-J.; Johnson, W. C. Base inclinations in natural and synthetic DNAs. *J. Am. Chem. Soc.* **1993**, *115*, 1205–1214.
- (31) Maeda, Y.; Nunomura, K.; Ohtsubo, E. Differential scanning calorimetric study of the effect of intercalators and other kinds of DNA-binding drugs on the stepwise melting of plasmid DNA. *J. Mol. Biol.* **1990**, *215*, 321–329.
- (32) Bjorndal, M. T.; Fygenson, D. K. DNA melting in the presence of fluorescent intercalating oxazole yellow dyes measured with a gel-based assay. *Biopolymers* **2002**, *65*, 40–44.
- (33) Zaludova, R.; Kleinwächter, V.; Brabec, V. The effect of ionic strength on melting of DNA modified by platinum(II) complexes. *Biophys. Chem.* **1996**, *60*, 135–142.
- (34) Breuzard, G.; Millot, J. M.; Riou, J. F.; Manfait, M. Selective interactions of ethidiums with G-quadruplex DNA revealed by surface-enhanced Raman scattering. *Anal. Chem.* **2003**, *75*, 4305–4311.
- (35) Hu, R. D.; Lin, Q. Y.; Huang, W.; Yu, Q. S. Spectroscopy study on crystal structure of Ce(NO₃)₃(phen)₂ and interactions of Ce(NO₃)₃(phen)₂ with DNA. *J. Rare Earths* **2005**, *23*, 372–376.
- (36) Zelonka, R. A.; Baird, M. C. Benzene complexes of ruthenium(II). *Can. J. Chem.* **1972**, *50*, 3063–3057.
- (37) Harvey, R. G.; Lindow, D. F.; Rabideau, P. W. Metal–ammonia reduction. XIII. Regiospecificity of reduction and reductive methylation in the terphenyl series. *J. Am. Chem. Soc.* **1972**, *94*, 5412–5420.
- (38) Brabec, V.; Palecek, E. The influence of salts and pH on polarographic currents produced by denatured DNA. *Biophysik* **1970**, *6*, 290–300.
- (39) Brabec, V.; Palecek, E. Interaction of nucleic acids with electrically charged surfaces. II. Conformational changes in double-helical polynucleotides. *Biophys. Chem.* **1976**, *4*, 76–92.
- (40) Sheldrick, G. M. *SADABS, 2006/1*; University of Gottingen: Gottingen, Germany, 2006.
- (41) Beurskens, P. T.; Beurskens, G.; Bosman, W. P.; Gelder, R. d.; Garcia-Granda, S.; Gould, R. O.; Smits, R. I. J. M. M.; *Crystallography Laboratory*; University of Nijmegen: Nijmegen, The Netherlands, 1999.
- (42) Sheldrick, G. M. *SHELXTL, 6.10*; University of Gottingen: Gottingen, Germany, 2001.
- (43) Alley, M. C.; Scudiero, D. A.; Monks, A.; Hursey, M. L.; Czerwinski, M. J.; Fine, D. L.; Abbott, B. J.; Mayo, J. G.; Shoemaker, R. H.; Boyd, M. R. Feasibility of drug screening with panels of human tumor cell lines using a microculture tetrazolium assay. *Cancer Res.* **1988**, *48*, 589–601.
- (44) Bonetti, A.; Apostoli, P.; Zaninelli, M.; Pavanel, F.; Colombatti, M.; Cetto, G. L.; Franceschi, T.; Sperotto, L.; Leone, R. Inductively coupled plasma mass spectroscopy quantitation of platinum–DNA adducts in peripheral blood leukocytes of patients receiving cisplatin- or carboplatin-based chemotherapy. *Clin. Cancer Res.* **1996**, *2*, 1829–1835.
- (45) Rodger, A. Linear Dichroism. In *Metallobiochemistry, Part C*; Academic Press Inc.: San Diego, 1993; Vol. 226, pp232–258.
- (46) Rodger, A.; Norden, B. *Circular Dichroism and Linear Dichroism*; Oxford University Press: Oxford, New York, Tokyo, 1997.
- (47) Butour, J. L.; Macquet, J. P. Differentiation of DNA–platinum complexes by fluorescence. The use of an intercalating dye as a probe. *Eur. J. Biochem.* **1977**, *78*, 455–463.
- (48) Butour, J. L.; Alvinerie, P.; Souchart, J. P.; Colson, P.; Houssier, C.; Johnson, N. P. Effect of the amine nonleaving group on the structure and stability of DNA complexes with *cis*-[Pt(R-NH₂)₂(NO₃)₂]. *Eur. J. Biochem.* **1991**, *202*, 975–980.
- (49) Leopold, N.; Lendl, B. A new method for fast preparation of highly surface-enhanced Raman scattering (SERS) active silver colloids at room temperature by reduction of silver nitrate with hydroxylamine hydrochloride. *J. Phys. Chem. B* **2003**, *107*, 5723–5727.

10.

DNA Interactions of Monofunctional Organometallic Osmium(II) Antitumor Complexes in Cell-Free Media

Hana Kostrhunova,[†] Jakub Florian,[†] Olga Novakova,[†] Anna F. A. Peacock,[‡] Peter J. Sadler,[§] and Viktor Brabec^{*†}

Institute of Biophysics, Academy of Sciences of the Czech Republic, v.v.i., Královopolská 135, CZ-61265 Brno, Czech Republic, School of Chemistry, University of Edinburgh, West Mains Road, Edinburgh EH9 3JJ, U.K., and Department of Chemistry, University of Warwick, Gibbet Hill Road, Warwick CV4 7AL, U.K.

Received December 10, 2007

This work is the first in-depth study of osmium binding to DNA and confirms the pharmacological activity of a new class of anticancer metallodrugs. We investigated the interactions between the potential biological target DNA and four osmium(II) arene complexes, of the type $[(\eta^6\text{-arene})\text{Os}(\text{LL})\text{Cl}]^{n+}$, where arene = biphenyl or *p*-cymene and LL = ethylenediamine, picolinate, or oxinate in an effort to understand their mechanism of action. Most notably we show that these complexes bind to DNA. DNA adducts of the Os^{II} complexes that exhibit promising cytotoxic effects in ovarian tumor cell lines largely distort its conformation. The data are consistent with DNA binding of the complexes containing biphenyl as the arene ligand that involves combined coordination to guanine residues and noncovalent interactions between the arene ligand and DNA. The results also indicate both a mechanism of action and a detoxification mechanism for Os^{II} arene compounds different from those of cisplatin.

Introduction

Platinum coordination compounds are widely used as anti-tumor drugs. The clinical efficacy of these anticancer drugs is diminished by intrinsic and acquired tumor resistance and side effects. Owing to these limitations, there is an intense effort to design new transition metal-based compounds containing transition-metal ions other than platinum that are capable of overcoming problems associated with platinum chemotherapy while delivering the therapeutic effect. Possible advantages in using transition-metal ions other than platinum include the availability of additional coordination sites in octahedral complexes, the altered shape of the complex, alterations in ligand affinity and substitution kinetics, and changes in oxidation state. In the design of these new drugs, ruthenium complexes^{1–3} and quite recently also osmium complexes^{4,5} have attracted much interest.

Certain Ru^{II} arene complexes of the type $[(\eta^6\text{-arene})\text{Ru}(\text{LL})\text{-(X)}][\text{Z}]$ (where LL is a chelating ligand such as ethylenediamine (en)⁶, X a leaving group such as Cl^- , and Z a counterion) exhibit both in vitro and in vivo activity, in some cases with activity comparable to that of cisplatin and carboplatin.^{6–8} Similar to conventional cisplatin, these Ru^{II} arene complexes preferentially bind to guanine residues of DNA forming monofunctional DNA adducts that are recognized and repaired in the cell in a manner different from the bifunctional DNA adducts of cisplatin.⁸

Nevertheless, in spite of the difference in chemical structure, DNA binding and downstream intracellular effects of cisplatin and organometallic Ru^{II} arene complexes, the formation and processing of their DNA adducts leads in both cases to cell death.

Recently, arene complexes of the heavier congener Os^{II} have been designed, and their chemical and cytotoxic activity has been described.^{4,5,9,10} Interestingly, some half-sandwich Os^{II} arene complexes of the type $[(\eta^6\text{-arene})\text{Os}(\text{XY})\text{Cl}]$ where arene = *p*-cymene (cym) or biphenyl (bip) and XY = N,O-chelating ligands such as picolinate (pico) showed promising activity toward human lung and ovarian cancer cells.⁵

DNA is an important potential biological target for many metal-based anticancer agents.¹¹ Distortions of DNA structure often correlate with anticancer activity.^{2,12} Hence, it is of great importance to understand in detail DNA binding properties of these new osmium complexes and their possible relationship to cytotoxicity in different tumor cell lines. This may provide grounds for establishing new structure-pharmacological activity relationships for this class of metal-based complexes as new antitumor drugs. No work has been reported so far on the reactivity of Os arene complexes toward polymeric DNA. To address some fundamental questions about DNA binding modes of Os^{II} arene antitumor compounds, the experiments described in the present paper were carried out. More specifically, the interactions of polymeric B-DNAs with $[(\eta^6\text{-arene})\text{Os}(\text{XY})\text{Cl}]$ where arene = *p*-cym or bip and XY = N,O-chelating ligands pico or 8-hydroxyquinolate (oxinate) and $[(\eta^6\text{-bip})\text{Os}(\text{en})\text{-Cl}][\text{BF}_4]$ (en = ethylenediamine; Figure 1) in cell-free media were investigated by various biochemical and biophysical methods with the goal of understanding their promising effects in cancer cell lines and to establish the foundations of structure-pharmacological relationships for this class of cytotoxic osmium compounds.

Results

Cytotoxicity. The cytotoxicity of complexes **1–4** toward both cisplatin-sensitive human ovarian A2780 and resistant (A2780cisR)

* Corresponding author. Tel.: +420-541517148. Fax: +420-541240499. E-mail: brabec@ibp.cz.

[†] Academy of Sciences of the Czech Republic.

[‡] University of Edinburgh.

[§] University of Warwick.

^a Abbreviations: bip, biphenyl; bp, base pair; cisplatin, *cis*-diamminedichloridoplatinum(II); CT, calf thymus; DEPC, diethyl pyrocarbonate; dienPt, chloridodiethylenetriamineplatinum(II) chloride; EtBr, ethidium bromide; en, ethylenediamine; FAAS, flameless atomic absorption spectrophotometry; HPLC, high pressure liquid chromatography; IC₅₀, concentration inhibiting cell growth by 50%; ICP OES, inductively coupled plasma optical emission spectroscopy; oxine, 8-hydroxyquinoline; PAGE, polyacrylamide gel electrophoresis; *p*-cym, *p*-cymene; pico, picolinate; r_b , the number of molecules of the metal complex bound per nucleotide residue; r_i , the molar ratio of free metal complex to nucleotide-phosphates at the onset of incubation with DNA; $t_{50\%}$, the times at which the binding reached 50%; t_m , DNA melting temperature.

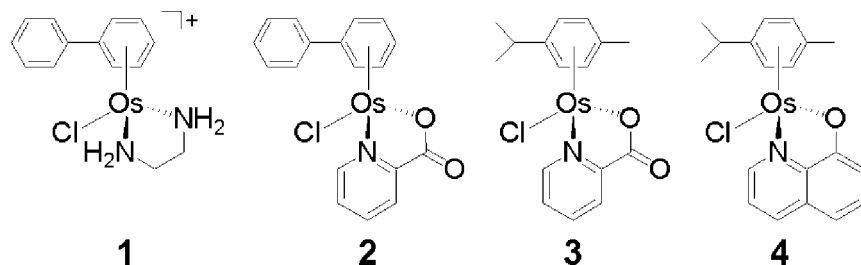


Figure 1. Structures of Os^{II} arene complexes. **1**, [(η^6 -biphenyl)Os(ethylenediamine)Cl]⁺; **2**, [(η^6 -biphenyl)Os(picolate)Cl]; **3**, [(η^6 -*p*-cymene)Os(picolate)Cl]; **4**, [(η^6 -*p*-cymene)Os(oxinate)Cl].

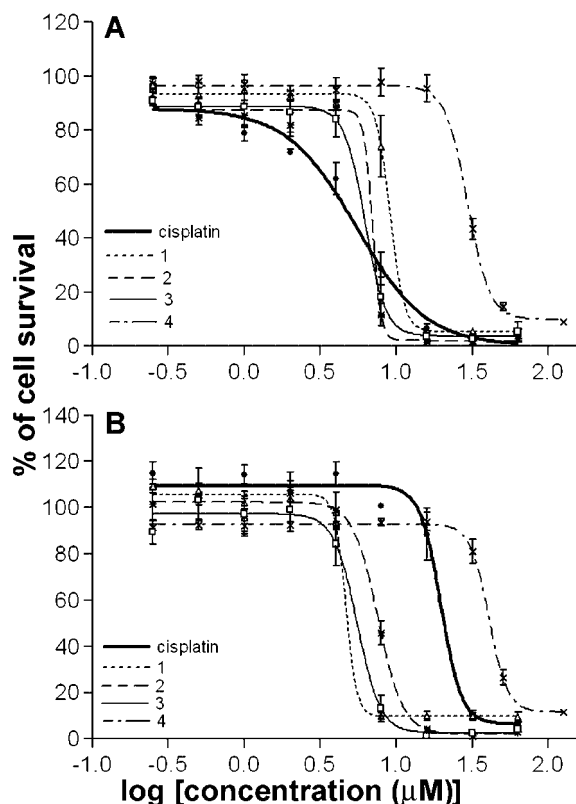


Figure 2. Dose response effects on the survival of A2780 (A) and A2780cisR (B) cancer cell lines. The cells were exposed to the Os^{II} arene complexes and cisplatin for 72 h in the concentration range of 0 to 128 μ M. Cell death was determined by MTT assay. The drug concentrations causing 50% inhibition (IC₅₀) were calculated. The results are expressed as mean \pm standard deviations of four independent experiments; all concentrations were tested in three replicates.

Table 1. In Vitro Growth Inhibition of Human Ovarian Cisplatin Sensitive and Resistant A2780 Cells, IC₅₀ (μ M)^a

complex	sensitive	resistant ^b
cisplatin	3.6 \pm 0.3	21.4 (5.9)
1	9.0 \pm 0.6	5.0 (0.55)
2	6.8 \pm 0.4	7.7 (1.13)
3	5.9 \pm 0.4	5.6 (0.95)
4	30.3 \pm 0.9	36.3 (1.2)

^a Drug-treatment period was 72 h. Each value represents the mean \pm SEM for three independent experiments. ^b Resistance factor, defined as IC₅₀ (resistant)/IC₅₀ (sensitive), is given in parentheses.

cancer cell lines was investigated. All complexes showed activity (Figure 2), and their corresponding IC₅₀ (concentration inhibiting cell growth by 50%) values are reported in Table 1. Similar activity was found for complexes **1–3** with IC₅₀ values ranging from 5.0 to 9.0 μ M, with [η^6 -*p*-cym)Os(pic)Cl] (**3**) showing

Table 2. Osmium and Cisplatin Uptake in A2780 Cells^a

complex	uptake ^b
cisplatin	11.4 \pm 0.2
1	13.3 \pm 1.0
2	14.0 \pm 1.2
3	34.9 \pm 2.3
4	31.6 \pm 1.8

^a Cellular osmium and cisplatin accumulation was measured by ICP OES after 6 h of treatment at equimolar concentrations of the indicated compound. Each point represents the mean \pm SEM for three independent experiments.

^b Each value shown in this table is in pmole Os(Pt)/10⁶ cells/ μ M.

the highest activity in cells sensitive to cisplatin and with [η^6 -bip)Os(en)Cl]⁺ (**1**) in cells resistant to cisplatin. In contrast the complex [η^6 -*p*-cym)Os(oxinate)Cl] (**4**) was the least potent with IC₅₀ values of 30 and 36 μ M in sensitive and resistant cells, respectively. Notably these complexes show similar potency in both the cisplatin-sensitive and resistant A2780 cell lines, indicating a different detoxification mechanism than cisplatin. Intriguingly, complexes **1** and **3** actually show higher activity in the cisplatin resistant A2780 cell line (5.0 and 5.6 μ M, respectively) compared to the cisplatin sensitive cells (9.0 and 5.9 μ M).

Cellular Uptake. A factor that is usually thought to contribute to metallodrug cytotoxicity is cellular uptake. To examine accumulation of complexes **1–4**, the cellular levels of these compounds were measured after a 6 h exposure of human ovarian A2780 cancer cells to equimolar concentrations of the drugs. The uptake of these compounds was comparable with that of cisplatin for complexes **1** and **2** and approximately 2–3 times higher for complexes **3** and **4** (Table 2).

Kinetics of Binding to Calf Thymus (CT) DNA. Reactions of the cytotoxic complexes **1–4** with polymeric DNA were investigated, as binding to DNA is often associated with the cytotoxic action of metal anticancer drugs.^{2,12} The rate of binding of the osmium complexes to CT DNA was determined at different ratios of *r*_i (molar ratio of free Os complex to nucleotide phosphate), 0.05 and 0.1, in 10 mM NaClO₄ at 37 °C in the dark. The Os^{II} complexes were incubated with the CT DNA and aliquots removed at various time intervals, rapidly cooled, and precipitated out by addition of ethanol and the Os content of the supernatant determined by inductively coupled plasma optical emission spectroscopy (ICP OES). The times at which the binding reached 50% (*t*_{50%}) in these binding reactions and total % bound after 48 h can be found in Table 3. Intriguingly, complexes **2** [(η^6 -bip)Os(pic)Cl] and **4** [(η^6 -*p*-cym)Os(oxinate)Cl] bind rapidly (*t*_{50%} ca. 2 h) and almost quantitatively, whereas the complex [(η^6 -*p*-cym)Os(pic)Cl] (**3**) binds most slowly (*t*_{50%} 4.9 and 8.3 h at *r*_i 0.05 and 0.1, respectively), and only ca. 75% is bound after 48 h.

Transcription Mapping. Cutting of pSP73KB DNA by *Nde*I and *Hpa*I restriction endonucleases yielded a 212-bp fragment

Table 3. Kinetics of Binding of Osmium(II) Arene Complexes to Calf Thymus DNA^a

	$t_{50\%}^b$ (h) at $r_i = 0.05$	48 h (%) at $r_i = 0.05$	$t_{50\%}^b$ (h) at $r_i = 0.1$	48 h (%) at $r_i = 0.1$
1	2.1 ± 0.2	76.0 ± 0.7	4.6 ± 0.2	72.1 ± 0.8
2	1.8 ± 0.2	98.5 ± 0.6	2.1 ± 0.2	94.8 ± 0.7
3	4.9 ± 0.2	76.8 ± 0.8	8.3 ± 0.2	71.8 ± 0.8
4	0.9 ± 0.1	87.2 ± 0.7	1.6 ± 0.1	84.9 ± 0.6

^a The concentration of DNA was 32 μg/mL. Each value represents the mean ± SEM for three independent experiments. ^b The times at which the binding reached 50%.

(a substantial part of its nucleotide sequence is shown in Figure 3B). This fragment contained the T7 RNA polymerase promoter. In vitro RNA synthesis by RNA polymerases on these DNA templates modified by osmium arene complexes **1–4** at the same level of metalation ($r_b = 0.005$) can be prematurely terminated at the level or in the proximity of adducts (Figure 3A). Interestingly, monofunctional DNA adducts of several platinum complexes are unable to terminate RNA synthesis.^{13–15} The major stop sites, primarily guanine residues, with some adenine bases, were roughly identical for all Os complexes. The profiles are similar to that obtained for DNA treated with the anticancer drug cisplatin (lane Cisplatin in Figure 3A) and also to those reported previously for the ruthenium arene compounds, such as $[(\eta^6\text{-arene})\text{Ru}(\text{en})\text{Cl}]^+$.¹⁶ The major stop sites for DNA modified by **3** are demonstrated in Figure 3B. Intriguingly the distribution of the stop sites produced by biphenyl ethylenediamine complex **1** is rather in favor of shorter fragments, which is consistent with the view that the adduct of this complex presents the most difficult obstacle for RNA polymerase.

Chemical Probes. A 21-base pair (bp) DNA duplex (for its sequence, see Figure 4B) was site-specifically modified with osmium arene complexes **1–3** so as to form a single monofunctional G-adduct in the middle of the top, pyrimidine-rich strand. The duplex containing the DNA adduct of the *p*-cymene oxinate osmium complex **4** was impossible to prepare, purify and isolate apparently because of the instability of this adduct during the high pressure liquid chromatography (HPLC) purification process. The metalated duplexes were subsequently treated with the chemical agents KMnO₄, diethyl pyrocarbonate (DEPC), and bromine that are used as tools for monitoring the existence of conformations other than canonical B-DNA. These agents react preferentially with base residues in single stranded and/or in distorted double stranded DNA but not with the base residues in intact, double-stranded DNA.^{17,18} The pattern and degree of reactivity toward the chemical probes were identical for the adducts formed by all three osmium arene complexes **1–3** (Figure 4A), indicating a similar character of the conformational distortion. The results shown in Figure 4 also suggest that the adducts formed with the DNA cause distortions which extend 4 base pairs around the adduct and that these distortions are more pronounced in the base pairs containing the metalated adduct and that containing the thymine residue flanking this adduct on its 5' side (Figure 4B). Also interestingly, the adduct of the complex $[(\eta^6\text{-}p\text{-cym})\text{Os}(\text{pico})\text{Cl}]$ (**3**) appears to distort DNA less than the adducts of the biphenyl complexes **1** and **2**.

Electrophoretic Mobility of Multimers of 21 bp Oligonucleotides. Intrinsic bending of DNA duplexes results in the abnormal electrophoretic mobility of DNA fragments. A gel migration anomaly has been found for DNA fragments containing bidentate adducts formed by cisplatin at the d(GG), d(AG), and d(GTG) sites.^{19,20} On the other hand, the monofunctional binding of *cis*-[Pt(NH₃)₂(Am)Cl]⁺ cations, in which Am is a derivative of pyridine, pyrimidine, purine, or aniline at the d(G)

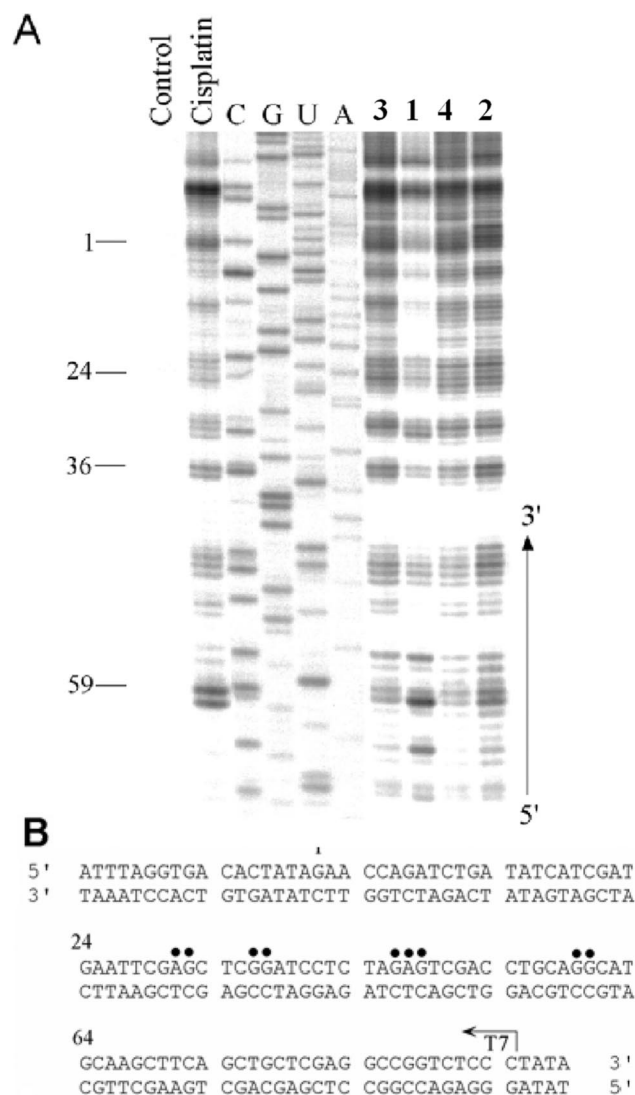


Figure 3. Inhibition of RNA synthesis by T7 RNA polymerase on the *NdeI/HpaI* fragment of pSP73KB plasmid modified by Os^{II} arene complexes and cisplatin. (A) Autoradiogram of 6% polyacrylamide/8 M urea sequencing gel showing inhibition of RNA synthesis by T7 RNA polymerase on the *NdeI/HpaI* fragment containing adducts of osmium complexes and cisplatin. Lanes: control, unmodified template; cisplatin, 1–4, the template modified by cisplatin and Os^{II} arene complexes **1–4** at $r_b = 0.005$, respectively; A, U, G, and C, chain terminated marker DNAs. (B) Schematic diagram showing the portion of the sequence used to monitor inhibition of RNA synthesis by cisplatin and osmium complexes. The arrow indicates the start of the T7 RNA polymerase, which was used as the template in the upper strand of the *NdeI/HpaI* fragment of pSP73KB. The bullets represent major stop signals for DNA modified by **3**. The numbers correspond to the nucleotide numbering in the sequence map of the pSP73KB plasmid.

site¹⁹ and dienPt at the d(G) site,²¹ keeps the helix rodlike. We have compared the electrophoretic mobility of the multimers of the ligated 21-mer duplex (for its sequence, see Figure 4B) with and without single monofunctional adducts of complexes **1–3** formed at the central G residue in the top strand. The corresponding multimers exhibit virtually no gel mobility shifts, migrating at almost exactly the same positions as the ladder of nonmodified multimers (results not shown). We can, therefore, conclude that no bending is induced in DNA containing monofunctional osmium adducts of **1–3**.

Unwinding of Supercoiled DNA. The unwinding of supercoiled plasmid DNA induced on binding the four osmium

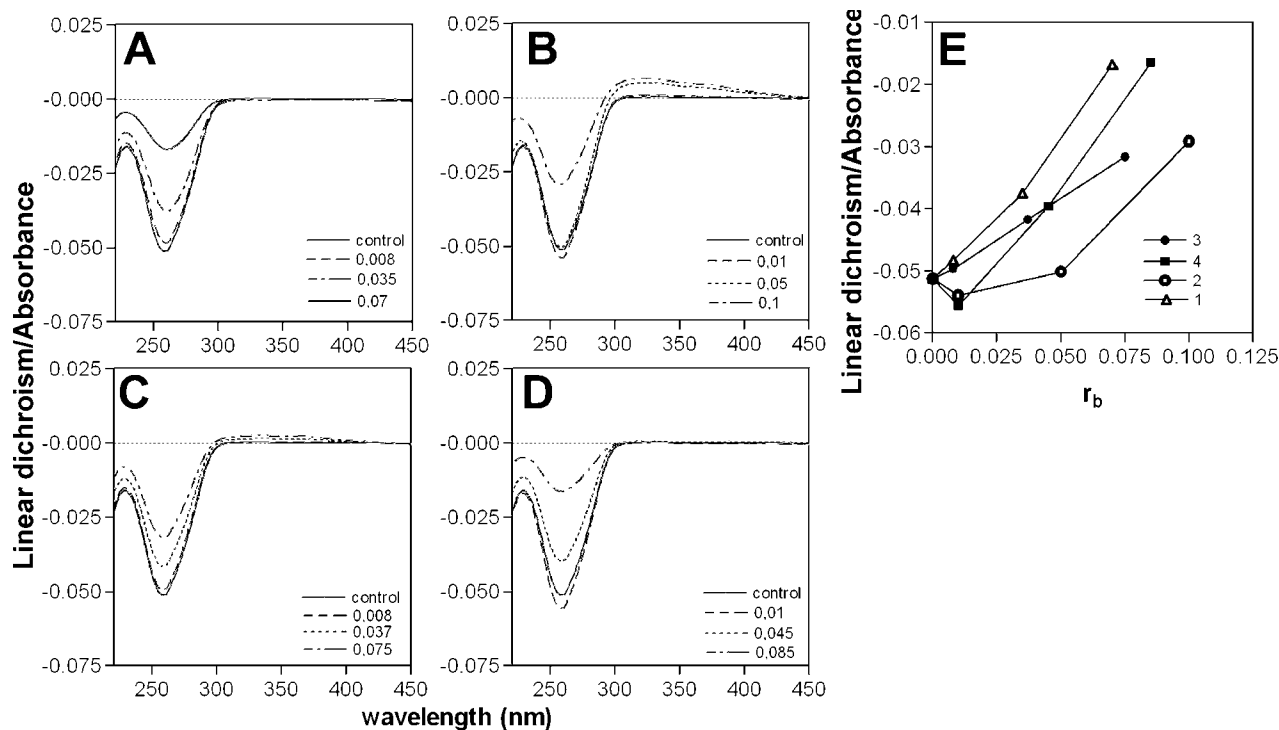


Figure 7. Linear dichroism spectra of CT DNA modified by Os^{II} arene complexes. LD spectra were recorded for DNA in 10 mM NaClO₄, 20 mM NaCl, and 10 mM sodium cacodylate, pH 7.0. The concentration of DNA was 0.1 mg/mL. (A–D) LD spectra of CT DNA modified by **1** (A) (thick solid line, control, nonmodified DNA; dashed line, $r_b = 0.008$; dash-dotted line, $r_b = 0.035$; solid line, $r_b = 0.07$); **2** (B) (thick solid line, control, nonmodified DNA; dashed line, $r_b = 0.01$; dotted line, $r_b = 0.05$; dash-dotted line, $r_b = 0.1$); **3** (C) (thick solid line, control, nonmodified DNA; dashed line, $r_b = 0.008$; dotted line, $r_b = 0.037$; dash-dotted line, $r_b = 0.075$); and **4** (D) (thick solid line, control, nonmodified DNA; dashed line, $r_b = 0.01$; dotted line, $r_b = 0.045$; dash-dotted line, $r_b = 0.085$). (E) Plots of the intensity of the band in LD spectra at 258 nm of DNA modified by complexes **1** (Δ), **2** (\circ), **3** (\bullet), and **4** (\blacksquare) versus r_b .

contrary, there is little difference between the complexes carrying the same axial ligand, either *p*-cymene or biphenyl.

Linear Dichroism. Binding of all three osmium complexes to CT DNA was also monitored by linear dichroism spectroscopy (Figure 7). It is well established that the magnitude of the LD signal measured within the DNA absorption band (e.g., at the 258 nm maximum) is a function of its persistence length. It is known that changes in flexibilities, or the formation of rigid bends or kinks induced by strongly bound compounds, can manifest themselves as decreases in the abilities of the modified DNA molecules to align themselves in the hydrodynamic flow gradient of the LD cell. The magnitudes of the LD signals at 258 nm decrease as a function of r_b for all Os^{II} arene complexes **1–4** (Figure 7E). These results suggest that the formation of strongly bound adducts derived from Os^{II} arene complexes is accompanied by the appearance of flexible hinge joints at the site of the lesion. Another eventuality, such as appearance of rigid bends or kinks, is unlikely based on the results of gel electrophoresis analysis of multimers of site-specifically modified oligonucleotides (vide supra). In addition, treatment of the DNA with complexes **2** and **3** produces a new and weak positive band at 330 nm, which increases more significantly for the biphenyl picolinate complex **2** compared to the *p*-cymene picolinate complex **3**.

Ethidium Bromide (EtBr) Fluorescence. The ability of a complex to displace the DNA intercalator EtBr from CT DNA was probed by monitoring the relative fluorescence of the EtBr–DNA complex after treating the DNA with varying concentrations of the Os^{II} arene complexes **1–4**. Figure 8 shows a plot of relative fluorescence versus r_b for complexes **1–4**, cisplatin, and monofunctional dienPt (chloridodiethylenetri-

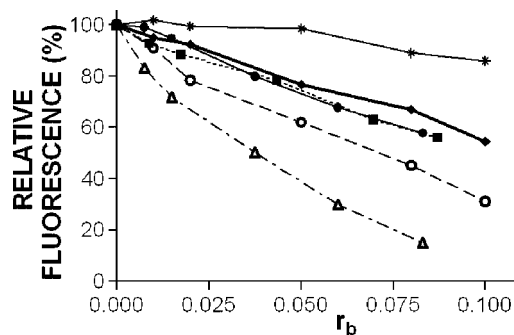


Figure 8. Plots of the EtBr fluorescence versus r_b for DNA modified by cisplatin, dienPt, and Os^{II} arene complexes in 10 mM NaClO₄ at 37 °C for 24 h: (\blacklozenge) cisplatin, ($*$) [PtCl(dien)]Cl, **1** (Δ), **2** (\circ), **3** (\bullet), and **4** (\blacksquare). Data points measured in triplicate varied on average $\pm 3\%$ from their mean.

amineplatinum(II) chloride). The adducts of all four monofunctional Os^{II} arene complexes competitively replaced intercalated EtBr markedly more effectively than the adducts of monofunctional dienPt. The adducts of biphenyl complexes **1** and **2** are most potent. The adducts of the other two Os^{II} *p*-cymene complexes reduced EtBr fluorescence less effectively but still slightly more than the adducts of bifunctional cisplatin.

Discussion

The four complexes investigated differ from each other in the following ways. First of all complex **1**, $[(\eta^6\text{-bip})\text{Os}(\text{en})\text{Cl}]^+$, is the only positively charged complex and after hydrolysis (believed to activate the complex) would possess an overall

positive charge of +2. Clearly its electrostatic interactions with negatively charged DNA will be different than for the remaining three complexes. Second the chelated NH_2 groups in complex **1** are capable of hydrogen bonding.²³ In contrast, in the remaining complexes the N-donor group is a pyridine, which is unable to take part in hydrogen bonding. Complexes **2** and **3** differ from one another in that the arene varies, extended biphenyl arene in **2** (capable of intercalation in the adducts of analogous Ru^{II} arene complexes containing a symmetrical *N,N*-chelating ligand¹⁶) and a single ring arene with bulky substituents (*p*-cymene) in **3**. Complex **4** differs from **3** primarily in the nature of the O-donor group, which in the latter case is an aryloxide donor as opposed to the carboxylate group in **3**. A major difference is the pK_a of this chelated oxygen (its acidity) and the higher partial negative charge donated to the osmium. Clearly the chemistry of these four complexes is different,^{5,9} and consequently we would anticipate that their effects on DNA would be different as well.

We report in the present work the first detailed DNA binding study of Os^{II} arene complexes, which have been shown^{5,24} to be a potential new class of anticancer agents (Table 1). In addition, we investigated the effects and extent of changes induced in the DNA on binding of osmium and compared these observations with other metal-based anticancer agents.

Though we have previously reported the binding of these complexes to nucleobases,^{4,5,9} it is notable that these complexes all bind polymeric DNA. Binding to DNA has often been associated with the cytotoxic action of metal-based anticancer agents,^{2,11,12} and therefore DNA may be a possible biological target for this class of Os^{II} arene complexes. The cell uptake studies (Table 2) also suggest that the type of DNA lesion is important for activity since, despite its low activity, the cellular levels of Os from **4** are higher than those of complexes **1** or **2**.

CT DNA was treated with osmium solutions, yet their subsequent rates of reaction with DNA (Table 3) do not correlate with their rates of hydrolysis. Rates of irreversible binding to DNA increase in the order **3** (binds most slowly) < **1** ~ **2** < **4** (rapid binding), whereas their rates of hydrolysis, previously determined at 25 °C and pH 2, are such that **1** hydrolyzes most slowly, followed by **2** and then **3**, with **4** hydrolyzing too rapidly to be measured by ^1H NMR.^{4,5,9} Therefore although hydrolysis may be rate-determining for some complexes (e.g., **4**) other factors such as electrostatic interactions may also play a role.

The rate of binding to DNA compares well with that determined for the anticancer drug cisplatin ($t_{1/2}$ ca. 2 h under similar conditions),²⁵ for which DNA binding is thought to be responsible for its cytotoxic properties. In contrast, the Ru^{II} analogue of **1**, $[(\eta^6\text{-bip})\text{Ru}(\text{en})\text{Cl}]^+$, which has also been shown to be cytotoxic to cancer cells,^{6–8} reacts much more rapidly with DNA under similar conditions (t_{50} ca. 10 min).¹⁶ The slower kinetics of osmium binding (28 times slower comparing **1** with its lighter Ru^{II} analogue) may allow more of it to reach its target in vivo than the ruthenium analogue, which is more reactive and likely to be deactivated by reacting with other biological molecules before reaching the target DNA within the cell nucleus. The Os^{II} biphenyl picolinate complex, $[(\eta^6\text{-bip})\text{Os}(\text{pic})\text{Cl}]$ (**2**), reacts almost quantitatively with the DNA and is the only complex to do so. In addition, replacing the extended biphenyl arene by the single ring arene, *p*-cymene, as in **3**, results in a marked decrease in DNA binding (to ca. 76%). For all the osmium complexes, >90% of the equilibrium had been reached within the first 24 h.

Osmium binding to DNA inhibits RNA synthesis in a similar fashion and with similar stopsites to cisplatin and the ruthenium

analogue of **1**, $[(\eta^6\text{-bip})\text{Ru}(\text{en})\text{Cl}]^+$, and in both cases is thought to be significant in their cytotoxic mechanism of action (Figure 3). The major stopsites were guanine residues, which agrees well with the small molecule binding studies performed previously which show that complex **1** binds selectively to monomeric guanine⁹ and complex **3** binds more strongly and selectively to monomeric guanine in competition experiments.⁵

The distortions induced on binding to DNA extend 4 base pairs around the adduct for the three Os^{II} arene complexes studied (**1–3**) (Figure 4B), which is similar compared to DNA binding of ruthenium arene analogues containing multiring arene ligands.¹⁶

The significant result obtained from the ligation experiment was that formation of the DNA adducts of Os^{II} arene compounds does not result in DNA bending. As this bending and subsequent binding of HMG (high mobility group) proteins to damaged/bent DNA is thought to be responsible for the cytotoxic action of cisplatin in tumor cells,^{12,26} we can conclude that the cytotoxic mechanism of action of Os^{II} arene complexes is different from that of cisplatin.

The binding of Os^{II} complexes **1–3** to DNA results in a significantly large degree of unwinding (21–27°; Table 4), much larger than that observed for the Ru^{II} complexes $[(\eta^6\text{-arene})\text{Ru}(\text{en})\text{Cl}]^+$ (7–14°)¹⁶ or cisplatin (6° and 13° for mono- or bifunctional adducts, respectively).²² Similar large unwinding angles in the range of 17–30° have been observed for the adducts of several antitumor platinum compounds containing heterocyclic planar or nonplanar ligands.^{27,28} Thus, the large unwinding angles produced by the adducts of Os^{II} arene compounds **1–3** can be explained by the additional contribution to unwinding associated with the interaction of the arene ligand with the duplex upon strong binding of osmium. Complex **4** consistently behaves differently to the other Os^{II} arene complexes, which is similar to the reports of its aqueous solution behavior (rapid hydrolysis and high acidity of coordinated water). Most notably it was reported that the chelated oxygen atom is readily protonated about physiological pH, and a dynamic pH-dependent ring-opening process at the osmium center was observed.⁵ This suggests that adducts of **4** on DNA would be less stable and the chelate ring opening would not allow the osmium to enforce any significant constraints on the DNA. In other words, the arene moiety in DNA adducts of Os^{II} arene compounds **1–3** could be geometrically well-positioned to interact with the double helix. In contrast, the oxinate complex, $[(\eta^6\text{-p-cym})\text{Os}(\text{oxinate})\text{Cl}]$ (**4**), does not unwind the DNA significantly (<2.5°). The explanation behind this phenomenon is unclear, nevertheless it may be hypothesized that the presence of the oxinate chelating ligand in Os^{II} arene complexes is not favorable for the interaction of the arene rings in these complexes with the double helix. In summary, it seems reasonable to suggest that the ligands in **4** do not interact with the double helix in a way similar to other Os^{II} complexes **1–3**, thus also supporting a different DNA binding mode for this compound in comparison with the other three Os^{II} arene complexes studied in the present work. In particular, complexes **1** and **2** containing the extended biphenyl arene capable of intercalating were potent at replacing the EtBr intercalator compared to complexes **3** and **4** containing the single arene ring, *p*-cymene.

EtBr as a fluorescent probe can be used to distinguish intercalating and nonintercalating ligands.^{16,22,28} Binding of EtBr to DNA by intercalation is blocked in a stoichiometric manner by formation of a wide spectrum of DNA-binding ligands including intercalators. On the other hand, modification of DNA

by monofunctional nonintercalative ligands, such as dienPt, results in only a slight decrease of EtBr fluorescence intensity as compared with that for the complex of nonmodified DNA with EtBr. Competitive binding of other intercalators leads to a loss of fluorescence because of depletion of the DNA–EtBr complex (free EtBr is poorly fluorescent).

The adducts of all Os^{II} complexes replace the EtBr intercalator slightly or markedly more efficiently than those of cisplatin (Figure 8). The adducts of compounds **1–3** unwind DNA by 21–27° (Table 4); that is, the values of the unwinding angles are considerably higher than those produced by the monofunctional adducts of dienPt (unwinding angle 6°^{16,22,28}). Thus, the results of unwinding experiments are consistent with the view that the arene ligands in **1–3** interact substantially with the double helix upon coordination of the osmium complex.^{16,22,28} Hence, these results strengthen the case for combined noncovalent, perhaps intercalative and monofunctional coordination binding modes of **1–3**.

In contrast, the oxinate complex, [(η^6 -*p*-cym)Os(oxinate)Cl] (**4**), does not unwind the DNA significantly (<2.5°, Table 4) but replaces the EtBr intercalator as efficiently as the Os^{II} complex **3**. In aggregate, it seems reasonable to suggest that the ligands in **4** do not interact with the double helix in a way similar to other Os^{II} complexes **1–3**, thus also supporting a different DNA binding mode for this compound in comparison with the other three Os arene complexes studied in the present work.

The noncovalent interactions of arenes, which may be involved in the binding of the Os^{II} arene compounds **1** and **2** to double-helical DNA (vide supra), may also affect its melting behavior (Figure 6). Previously,¹⁶ two important factors have been invoked to account for the thermal stability of DNA modified by monofunctional Ru^{II} complexes in media of relatively low ionic strength (0.01 M Na⁺): (i) a destabilizing effect of conformational distortions and (ii) a stabilizing effect of the positive charge on the ruthenium moieties and of noncovalent binding, such as changes in solvent structure and the counterion distribution around the phosphate groups of DNA which may help to overcome electrostatics unfavorable for the hybridization of the strands of the duplex.^{29,30} Under the conditions of our experiments, we expect all Os^{II} arene complexes to have produced monofunctional adducts. Inherently, we predict that conformational distortions due to the formation of the adducts will destabilize the helix, as has been consistently observed in earlier studies with various ruthenium and platinum compounds. Hence, it is possible that the less pronounced decrease in t_m due to the modification by the Os^{II} compounds **1** and **2** (Figure 6) is a consequence of compensation of destabilizing effects of conformational changes. This stabilizing compensation might be associated with noncovalent interaction of the arene ligand with the duplex inferred from DNA unwinding (Figure 5, Table 4) and quenching EtBr fluorescence (Figure 8) and with the overall positive charge on these Os^{II} compounds. In addition, the stabilizing effects of the positive charge on the osmium atom of the compounds **3** and **4** might be considerably reduced due to a substantially different location of the osmium atom in the adducts of these compounds relative to the DNA sugar–phosphate backbone. This location might be unfavorable from the viewpoint of the efficiency of the positive charge on the osmium atom to neutralize negative charges of DNA phosphate groups. Thus, the solution behavior of the DNA adducts of Os^{II} arene complexes appears interesting and merits further study.

The results of DNA unwinding experiments (Figure 5, Table 4) suggest that the arene ligand (*p*-cymene) in **3** also interacts with the double helix upon coordination of the osmium complex. However, the adducts of this Os^{II} complex thermally destabilize DNA similarly as those of **4** [whose arene ligand (*p*-cymene) apparently does not interact noncovalently with DNA to induce distinct unwinding of its double helical structure]. The explanation of this is unclear but may be associated with a different DNA noncovalent binding mode of the *p*-cymene ligand in Os^{II} arene complexes compared to that of the biphenyl ligand. This hypothesis is corroborated by the observation that the single-ring *p*-cymene arene ligand (in contrast to double-ring biphenyl arene ligand) in analogous monofunctional Ru^{II} arene ethylenediamine complexes does not intercalate in the DNA base-pair stack.^{16,31}

The results of the present work demonstrate cytotoxicity for these complexes in ovarian cell lines, and importantly, the activity in the cells sensitive and resistant to cisplatin was also determined (Figure 2 and Table 1). That the osmium(II) arene complexes show very similar activity in both cell lines is highly significant and indicates a different detoxification mechanism for this class of complexes. Intriguingly, complex **1**, [(η^6 -bip)Os(en)Cl]⁺, shows even greater activity in the cisplatin-resistant cell line (resistance factor of 0.55). Such results indicate promising compounds with which to tackle the common problem of developed cisplatin resistance which can occur during chemotherapy treatment. On the other hand, the markedly lower activity associated with complex **4**, [(η^6 -*p*-cym)Os(oxinate)Cl], correlates with its different binding to DNA and with its different aqueous solution chemistry compared with the picolinate complexes (**2** and **3**).

Experimental Section

Starting Materials. The osmium complexes were prepared and characterized as described previously.^{5,9} Cisplatin was obtained from Sigma-Aldrich sro (Prague, Czech Republic). dienPt was a generous gift of Professor G. Natile from University of Bari. Stock solutions of metal complexes for the biophysical and biochemical studies were prepared at the concentration of 2×10^{-4} M in 10 mM NaClO₄ and stored at 4 °C in the dark. Stock solutions of metal complexes for the cytotoxicity studies were prepared in DMSO and used immediately after dissolution. The concentrations of osmium or platinum in the stock solutions were determined by ICP OES. CT DNA (42% G + C, mean molecular mass ca. 2×10^7) was also prepared and characterized as described previously.^{32,33} pSP73KB (2455 bp) and pUC19 (2686 bp) plasmids (superhelical density $\sigma = -0.063$ and -0.055 , respectively) were isolated according to standard procedures. The synthetic oligodeoxyribonucleotides (21-mers) were purchased from VBC-Genomics (Vienna, Austria) and purified as described previously.^{21,34} Restriction endonucleases *Eco*RI and *Nde*I and T4 polynucleotide kinase were purchased from New England Biolabs. Dimethyl sulfate (DMS), DMSO, KMnO₄, DEPC, KBr, and KHSO₅ were from Sigma (Prague, Czech Republic). Acrylamide, bis(acrylamide), and EtBr were from Merck KgaA (Darmstadt, Germany). Agarose was from FMC BioProducts (Rockland, ME). Radioactive products were from MP Biomedicals, LLC (Irvine, CA).

Metalation Reactions. CT DNA and plasmid DNAs were incubated with osmium or platinum complex in 10 mM NaClO₄ (pH ~ 6) at 37 °C for 48 h in the dark, if not stated otherwise. The number of atoms of the metal bound per nucleotide residue (r_b values) was determined by ICP OES (osmium) or FAAS (platinum).

The single-stranded oligonucleotide (the top, pyrimidine rich, strand containing a single central G of the TGT(21) duplex, Figure 4B) (5×10^{-4} M) was reacted in stoichiometric amounts with **1**, **2**, and **3**. The metalated oligonucleotides were purified by ion-exchange HPLC. It was verified by ICP OES and by absorbance

measurements that the modified oligonucleotides contained one osmium atom per mole. It was also verified using DMS footprinting¹³ that one molecule of osmium complex was coordinated to the N7 atom of the single G in the top strand of each duplex.

DNA Transcription by RNA Polymerase in Vitro. Transcription of the (*NdeI/HpaI*) restriction fragment of pSP73KB DNA with T7 RNA polymerase and electrophoretic analysis of the transcripts was performed according to the protocols recommended by Promega (Promega Protocols and Applications, 43-46 (1989/90)) and previously described in detail.^{13,14} The DNA concentration used in this assay was 3.9×10^{-5} M (related to the monomeric nucleotide content).

Chemical Modifications. The modification of the metalated oligonucleotide duplexes by KMnO_4 , DEPC, and KBr/KHSO_5 was performed as described previously.^{18,35-37} The top or bottom strands of the oligonucleotide duplexes were 5'-end labeled with [γ -³²P]ATP and T4 polynucleotide kinase.

Ligation and Electrophoresis of Oligonucleotides. Unmodified 21-mer single strand (bottom strand of the duplex described in the Results section, DNA Unwinding and Bending paragraph) were 5'-end-labeled with [γ -³²P]ATP by using T4 polynucleotide kinase. Then they were annealed with their phosphorylated complementary strands (unmodified or containing the monofunctional osmium adduct). The duplexes were allowed to react with T4 DNA ligase. The resulting samples along with ligated unmetalated duplexes were subsequently examined on 8% native PAA [mono:bis(acrylamide) ratio = 29:1] electrophoresis gels. Other details of these experiments were as described in previous papers.^{19,34,38}

Unwinding of Negatively Supercoiled DNA. Unwinding of closed circular supercoiled pUC19 plasmid DNA was assayed by an agarose gel mobility shift assay.²² The unwinding angle Φ , induced per osmium–DNA adduct, was calculated upon the determination of the r_b value at which the complete transformation of the supercoiled to relaxed form of the plasmid was attained. Samples of plasmid DNA at the concentration of 1.6×10^{-4} M (related to the monomeric nucleotide content) were incubated with complexes 1–4 at 37 °C in the dark for 24 h. All samples were precipitated by ethanol and redissolved in the TAE (Tris-acetate/EDTA) buffer. One aliquot of the precipitated sample was subjected to electrophoresis on 1% agarose gels running at 25 °C in the dark with TAE buffer, and the voltage was set at 25 V. The gels were then stained with EtBr, followed by photography with transilluminator. The other aliquot was used for the determination of r_b values by ICP OES.

DNA Melting. The melting curves of CT DNAs at the concentration of 32 $\mu\text{g/mL}$ were recorded by measuring the absorbance at 260 nm. The melting curves of unmodified or metalated DNA were recorded in the medium containing 0.01 M NaClO_4 with 1 mM Tris-HCl/0.1 mM EDTA, pH 7.4. The value of t_m was determined as the temperature corresponding to a maximum on the first-derivative profile of the melting curves. The t_m values could be thus determined with an accuracy of ± 0.3 °C.

Flow Linear Dichroism (LD). Flow LD spectra were collected by using a flow Couette cell in a Jasco J-720 spectropolarimeter adapted for LD measurements. Long molecules, such as DNA (minimum length of ~ 250 bp), can be orientated in a flow Couette cell. The flow cell consists of a fixed outer cylinder and a rotating solid quartz inner cylinder, separated by a gap of 0.5 mm, giving a total path length of 1 mm. LD spectra of DNA at the concentration of 0.1 $\mu\text{g/mL}$ modified by the osmium complexes were recorded at 25 °C in 10 mM NaClO_4 plus 20 mM NaCl and 10 mM sodium cacodylate, pH 7.0.^{39,40}

Fluorescence Measurements. These measurements were performed on a Shimadzu RF 40 spectrofluorophotometer using a 1 cm quartz cell. Fluorescence measurements of DNA modified by osmium at the concentration of 32 $\mu\text{g/mL}$ in the presence of EtBr were performed at an excitation wavelength of 546 nm, and the emitted fluorescence was analyzed at 590 nm. The fluorescence intensity was measured at 25 °C in 0.4 M NaCl to avoid secondary binding of EtBr to DNA.^{41,42} The concentrations were 0.01 mg/

mL for DNA and 0.04 mg/mL for EtBr, which corresponded to the saturation of all intercalation sites of EtBr in DNA.⁴¹

Other Physical Methods. Absorption spectra were measured with a Varian Cary 4000 UV–vis spectrophotometer equipped with a thermoelectrically controlled cell holder and quartz cells with a path length of 1 cm. Purification of oligonucleotides with the aid of HPLC was carried out on a Waters HPLC system consisting of Waters 262 pump, Waters 2487 UV detector, and Waters 600S controller with MonoQ HR 5/5 column. The analysis with the aid of ICP OES was performed using Jobin Yvon, Ultracore 170 equipment. The FAAS measurements were carried out on a Varian AA240Z Zeeman atomic absorption spectrometer equipped with a GTA 120 graphite tube atomizer. For ICP OES and FAAS analyses, DNA was precipitated with ethanol and dissolved in 0.1 M HCl. The gels were visualized by using a BAS 2500 FUJIFILM bioimaging analyzer, and the radioactivity associated with bands was quantitated with the AIDA image analyzer software (Raytest, Germany).

Cytotoxicity. The human ovarian tumor cell lines A2780 (parent, cisplatin-sensitive) and A2780cisR (with acquired cisplatin resistance) were cultured in RPMI 1640 medium (Gibco), supplemented with 10% FBS, 2 mM glutamine, 50 $\mu\text{g/mL}$ gentamycin at 37 °C in an atmosphere of 95% air and 5% CO_2 . Cell death was evaluated by using a system based on the tetrazolium compound MTT [3-(4,5-dimethyl-2-thiazolyl)-2,5-diphenyl-2H-tetrazolium bromide] which is reduced by living cells to yield a soluble formazan product that can be detected colorimetrically.⁴³ Cells were seeded in 96-well sterile plates at a density of 10^4 cells/well in 100 μL of medium and were incubated for 16 h. Osmium complexes were dissolved in DMSO; the stock solutions were freshly prepared before use. The final concentration of DMSO in cell culture medium did not exceed 0.25%. The compounds were added to final concentrations from 0 to 128 μM in a volume of 100 μL /well. Seventy-two hours later 10 μL of a freshly diluted MTT solution (2.5 mg/mL) was pipetted into each well, and the plate was incubated at 37 °C in a humidified 5% CO_2 atmosphere. After 5 h the medium was removed and the formazan product was dissolved in 100 μL of DMSO. The cell viability was evaluated by measurement of the absorbance at 570 nm, using an Absorbance Reader SUNRICE TECAN SCHOELLER. All experiments were made in triplicate. IC_{50} values (compound concentration that produces 50% of cell growth inhibition) were calculated from curves constructed by plotting cell survival (%) versus drug concentration (μM). All experiments were made in triplicate.

Cellular Os^{II} Arene Complex Uptake. Cellular uptake of Os^{II} arene compounds and cisplatin was measured in A2780 cells. The cells were seeded in 60 mm tissue culture dishes ($30\,000/\text{cm}^2$). After overnight incubation, the cells were treated with the osmium compound or cisplatin for 6 h at equimolar concentration (10 μM); this concentration was verified by the measurement of osmium or platinum in the growing medium by ICP OES. The attached cells were washed twice with PBS (4 °C) and centrifuged at 2500 rpm, and the pellet was stored at -80 °C. Afterward, the pellets were digested with 12 M HNO_3 , 30% H_2O_2 , and 12.1 M HCl. Osmium and platinum content was determined by ICP OES.

Acknowledgment. This research was supported by the Ministry of Education of the CR (MSMT LC06030, ME08017, OC08003), the Academy of Sciences of the Czech Republic (Grants 1QS500040581, KAN200200651, IAA400040803, AV0Z50040507, and AV0Z50040702), the Grant Agency of the CR (203/06/1239) and the Grant Agency of the Ministry of Health of the CR (NR8562-4/2005), EPSRC (studentship for A.F.A.P.), and the Wellcome Trust (International Collaboration Award for P.J.S. and V.B.). The authors also acknowledge that their participation in the EU COST Action D39 enabled them to exchange regularly the most recent ideas in the field of anticancer metallodrugs with several European colleagues.

References

- Alessio, E.; Mestroni, G.; Bergamo, A.; Sava, G. Ruthenium anticancer drugs. *Metal Ions in Biological Systems: Metal Complexes in Tumor Diagnosis and as Anticancer Agents*; Marcel Dekker: New York, 2004; Vol. 42, pp 323–351.
- Brabec, V.; Novakova, O. DNA binding mode of ruthenium complexes and relationship to tumor cell toxicity. *Drug Resist. Updates* **2006**, *9*, 111122.
- Dyson, P. J.; Sava, G. Metal-based antitumor drugs in the post genomic era. *Dalton Trans.* **2006**, 1929–1933.
- Peacock, A. F. A.; Habtemariam, A.; Moggach, S. A.; Prescimone, A.; Parsons, S.; Sadler, P. J. Chloro half-sandwich osmium(II) complexes: Influence of chelated N,N-ligands on hydrolysis, guanine binding and cytotoxicity. *Inorg. Chem.* **2007**, *46*, 4049–4059.
- Peacock, A. F. A.; Parsons, S.; Sadler, P. J. Tuning the hydrolytic aqueous chemistry of osmium arene complexes with N,O-chelating ligands to achieve cancer cell cytotoxicity. *J. Am. Chem. Soc.* **2007**, *129*, 3348–3357.
- Aird, R.; Cummings, J.; Ritchie, A.; Muir, M.; Morris, R.; Chen, H.; Sadler, P.; Jodrell, D. In vitro and in vivo activity and cross resistance profiles of novel ruthenium(II) organometallic arene complexes in human ovarian cancer. *Br. J. Cancer* **2002**, *86*, 1652–1657.
- Morris, R. E.; Aird, R. E.; Murdoch, P. D.; Chen, H. M.; Cummings, J.; Hughes, N. D.; Parsons, S.; Parkin, A.; Boyd, G.; Jodrell, D. I.; Sadler, P. J. Inhibition of cancer cell growth by ruthenium(II) arene complexes. *J. Med. Chem.* **2001**, *44*, 3616–3621.
- Novakova, O.; Kasparkova, J.; Bursova, V.; Hofr, C.; Vojtiskova, M.; Chen, H.; Sadler, P. J.; Brabec, V. Conformation of DNA modified by monofunctional Ru(II) arene complexes: recognition by DNA-binding proteins and repair. Relationship to cytotoxicity. *Chem. Biol.* **2005**, *12*, 121–129.
- Peacock, A. F. A.; Habtemariam, A.; Fernandez, R.; Walland, V.; Fabbiani, F. P. A.; Parsons, S.; Aird, R. E.; Jodrell, D. I.; Sadler, P. J. Tuning the reactivity of osmium(II) and ruthenium(II) arene complexes under physiological conditions. *J. Am. Chem. Soc.* **2006**, *128*, 1739–1748.
- Peacock, A. F. A.; Melchart, M.; Deeth, R. J.; Habtemariam, A.; Parsons, S.; Sadler, P. J. Osmium(II) and ruthenium(II) arene maltolato complexes: rapid hydrolysis and nucleobase binding. *Chem. Eur. J.* **2007**, *13*, 2601–2613.
- Zhang, C. X.; Lippard, S. J. New metal complexes as potential therapeutics. *Curr. Opin. Chem. Biol.* **2003**, *7*, 481–489.
- Brabec, V. DNA modifications by antitumor platinum and ruthenium compounds: their recognition and repair. *Prog. Nucleic Acid Res. Mol. Biol.* **2002**, *71*, 1–68.
- Brabec, V.; Leng, M. DNA interstrand cross-links of trans-diamminedichloroplatinum(II) are preferentially formed between guanine and complementary cytosine residues. *Proc. Natl. Acad. Sci. U.S.A.* **1993**, *90*, 5345–5349.
- Lemaire, M. A.; Schwartz, A.; Rahmouni, A. R.; Leng, M. Interstrand cross-links are preferentially formed at the d(GC) sites in the reaction between cis-diamminedichloroplatinum(II) and DNA. *Proc. Natl. Acad. Sci. U.S.A.* **1991**, *88*, 1982–1985.
- Brabec, V.; Boudny, V.; Balcarova, Z. Monofunctional adducts of platinum(II) produce in DNA a sequence-dependent local denaturation. *Biochemistry* **1994**, *33*, 1316–1322.
- Novakova, O.; Chen, H.; Vrana, O.; Rodger, A.; Sadler, P. J.; Brabec, V. DNA interactions of monofunctional organometallic ruthenium(II) antitumor complexes in cell-free media. *Biochemistry* **2003**, *42*, 11544–11554.
- Nielsen, P. E. Chemical and photochemical probing of DNA complexes. *J. Mol. Recognit.* **1990**, *3*, 1–24.
- Brabec, V.; Sip, M.; Leng, M. DNA conformational distortion produced by site-specific interstrand cross-link of trans-diamminedichloroplatinum(II). *Biochemistry* **1993**, *32*, 11676–11681.
- Bellon, S. F.; Lippard, S. J. Bending studies of DNA site-specifically modified by cisplatin, trans-diamminedichloroplatinum(II) and cis-[Pt(NH₃)₂(N3-cytosine)Cl]⁺. *Biophys. Chem.* **1990**, *35*, 179–188.
- Bellon, S. F.; Coleman, J. H.; Lippard, S. J. DNA unwinding produced by site-specific intrastrand cross-links of the antitumor drug cis-diamminedichloroplatinum(II). *Biochemistry* **1991**, *30*, 8026–8035.
- Brabec, V.; Reedijk, J.; Leng, M. Sequence-dependent distortions induced in DNA by monofunctional platinum(II) binding. *Biochemistry* **1992**, *31*, 12397–12402.
- Keck, M. V.; Lippard, S. J. Unwinding of supercoiled DNA by platinum ethidium and related complexes. *J. Am. Chem. Soc.* **1992**, *114*, 3386–3390.
- Chen, H. M.; Parkinson, J. A.; Parsons, S.; Coxall, R. A.; Gould, R. O.; Sadler, P. J. Organometallic ruthenium(II) diamine anticancer complexes: Arene-nucleobase stacking and stereospecific hydrogen-bonding in guanine adducts. *J. Am. Chem. Soc.* **2002**, *124*, 3064–3082.
- Allardyce, C. S.; Dyson, P. J.; Ellis, D. J.; Heath, S. L. [Ru(η^6 -p-cymene)Cl₂(pta)] (pta = 1,3,5-triaza-7-phosphatricyclo-[3.3.1.1]decane): a water soluble compound that exhibits pH dependent DNA binding providing selectivity for diseased cells. *Chem. Commun.* **2001**, 1396–1397.
- Bancroft, D. P.; Lepre, C. A.; Lippard, S. J. Pt-195 NMR kinetic and mechanistic studies of cis-diamminedichloroplatinum and trans-diamminedichloroplatinum(II) binding to DNA. *J. Am. Chem. Soc.* **1990**, *112*, 6860–6871.
- Cohen, S. M.; Lippard, S. J. Cisplatin: From DNA damage to cancer chemotherapy. *Prog. Nucleic Acid Res. Mol. Biol.* **2001**, *67*, 93–130.
- Zakovska, A.; Novakova, O.; Balcarova, Z.; Bierbach, U.; Farrell, N.; Brabec, V. DNA interactions of antitumor trans-[PtCl₂(NH₃)(quinoline)]. *Eur. J. Biochem.* **1998**, *254*, 547–557.
- Kasparkova, J.; Marini, V.; Najajreh, Y.; Gibson, D.; Brabec, V. DNA binding mode of the cis and trans geometries of new antitumor nonclassical platinum complexes containing piperidine, piperazine or 4-picoline ligand in cell-free media. Relations to their activity in cancer cell lines. *Biochemistry* **2003**, *42*, 6321–6332.
- Maeda, Y.; Nunomura, K.; Ohtsubo, E. Differential scanning calorimetric study of the effect of Intercalators and other kinds of DNA-binding drugs on the stepwise melting of plasmid DNA. *J. Mol. Biol.* **1990**, *215*, 321–329.
- Bjorndal, M. T.; Fygenson, D. K. DNA melting in the presence of fluorescent intercalating oxazole yellow dyes measured with a gel-based assay. *Biopolymers* **2002**, *65*, 40–44.
- Liu, H. K.; Berners-Price, S. J.; Wang, F. Y.; Parkinson, J. A.; Xu, J. J.; Bella, J.; Sadler, P. J. Diversity in guanine-selective DNA binding modes for an organometallic ruthenium arene complex. *Angew. Chem., Int. Ed.* **2006**, *45*, 8153–8156.
- Brabec, V.; Palecek, E. Interaction of nucleic acids with electrically charged surfaces. II. Conformational changes in double-helical polynucleotides. *Biophys. Chem.* **1976**, *4*, 76–92.
- Kim, S. D.; Vrana, O.; Kleinwachter, V.; Niki, K.; Brabec, V. Polarographic determination of subnanogram quantities of free platinum in reaction mixture with DNA. *Anal. Lett.* **1990**, *23*, 1505–1518.
- Kasparkova, J.; Farrell, N.; Brabec, V. Sequence specificity, conformation, and recognition by HMG1 protein of major DNA interstrand cross-links of antitumor dinuclear platinum complexes. *J. Biol. Chem.* **2000**, *275*, 15789–15798.
- Bailly, C.; Gentle, D.; Hamy, F.; Purcell, M.; Waring, M. J. Localized chemical reactivity in DNA associated with the sequence-specific bisintercalation of echinomycin. *Biochem. J.* **1994**, *300*, 165–173.
- Ross, S. A.; Burrows, C. J. Cytosine-specific chemical probing of DNA using bromide and monoperoxysulfate. *Nucleic Acids Res.* **1996**, *24*, 5062–5063.
- Bailly, C.; Waring, M. J. Diethylpyrocarbonate and osmium tetroxide as probes for drug-induced changes in DNA conformation in vitro. In *Drug-DNA Interaction Protocols*; Fox, K. R., Ed.; Humana Press Inc: Totowa, NJ, 1997; pp 51–79.
- Koo, H. S.; Wu, H. M.; Crothers, D. M. DNA bending at adenine thymine tracts. *Nature* **1986**, *320*, 501–506.
- Rodger, A. Linear Dichroism. *Methods Enzymol.* **1993**, *226*, 232–258.
- Rodger, A.; Norden, B. *Circular Dichroism and Linear Dichroism*; Oxford University Press: Oxford, New York, 1997.
- Butour, J. L.; Macquet, J. P. Differentiation of DNA - platinum complexes by fluorescence. The use of an intercalating dye as a probe. *Eur. J. Biochem.* **1977**, *78*, 455–463.
- Butour, J. L.; Alvinerie, P.; Souhard, J. P.; Colson, P.; Houssier, C.; Johnson, N. P. Effect of the amine nonleaving group on the structure and stability of DNA complexes with cis-[Pt(R-NH₂)₂(NO₃)₂]. *Eur. J. Biochem.* **1991**, *202*, 975–980.
- Alley, M. C.; Scudiero, D. A.; Monks, A.; Hursey, M. L.; Czerwinski, M. J.; Fine, D. L.; Abbott, B. J.; Mayo, J. G.; Shoemaker, R. H.; Boyd, M. R. Feasibility of drug screening with panels of human tumor cell lines using a microculture tetrazolium assay. *Cancer Res.* **1988**, *48*, 589–601.

JM701538W

11.

Conformation of DNA GG Intrastrand Cross-Link of Antitumor Oxaliplatin and Its Enantiomeric Analog

Jaroslav Malina,* Olga Novakova,* Marie Vojtiskova,* Giovanni Natile,[†] and Viktor Brabec*

*Institute of Biophysics, Academy of Sciences of the Czech Republic, CZ-61265 Brno, Czech Republic; and

[†]Department of Pharmaceutical Chemistry, University of Bari, I-70125 Bari, Italy

ABSTRACT Downstream processes that discriminate between DNA adducts of a third generation platinum antitumor drug oxaliplatin and conventional cisplatin are believed to be responsible for the differences in their biological effects. These different biological effects are explained by the ability of oxaliplatin to form DNA adducts more efficient in their biological effects. In this work conformation, recognition by HMG domain protein and DNA polymerization across the major 1,2-GG intrastrand cross-link formed by cisplatin and oxaliplatin in three sequence contexts were compared with the aid of biophysical and biochemical methods. The following major differences in the properties of the cross-links of oxaliplatin and cisplatin were found: i), the formation of the cross-link by oxaliplatin is more deleterious energetically in all three sequence contexts; ii), the cross-link of oxaliplatin bends DNA slightly but systematically less in all sequence contexts tested; iii), the affinity of HMG domain protein to the cross-link of oxaliplatin is considerably lower independent of the sequence context; and iv), the Klenow fragment of DNA polymerase I pauses considerably more at the cross-link of oxaliplatin in all sequence contexts tested. We have also demonstrated that the chirality at the carrier ligand of oxaliplatin can affect its biological effects.

INTRODUCTION

Since the introduction of cisplatin [*cis*-diamminedichlorido-platinum(II)] (Fig. 1 A), only [*cis*-diamminecyclobutanedicarboxylatoplatinum(II)] (carboplatin) and [(1*R*,2*R*-diamminocyclohexane)oxalatoplatinum(II)] (oxaliplatin) (Fig. 1 A) have received worldwide approval and achieved routine clinical use (1). Carboplatin is less toxic than cisplatin and can be given at a much higher dose than cisplatin. Unfortunately, carboplatin is still only active in the same range of tumors as cisplatin (2). As of yet, oxaliplatin, administered as a single agent, has not demonstrated substantial advantages over cisplatin or carboplatin although it has shown potential for use in some cisplatin-resistant tumors if administered in combination with 5-fluorouracil or folinic acid (3).

DNA is considered the major pharmacological target of platinum compounds (4–6). Direct analogs of cisplatin, which have already achieved routine clinical use, such as carboplatin and oxaliplatin, produce on DNA adducts similar to those produced by the parent drug, though different in their relative rates of formation (6,7). Hence, from a mechanistic DNA-binding point of view, it is not too surprising that the introduction of the new platinum antitumor drugs in the clinic does not represent a fundamental breakthrough in the treatment of cancer with platinum agents. This conclusion is in accordance with the hypothesis systematically tested by us and others that platinum agents, which bind to DNA in a fundamentally different manner, may have altered pharmacological properties (8–10). Nevertheless, the studies on DNA interactions of cisplatin, carboplatin, and oxaliplatin and their closely related analogs or models afforded a

number of interesting results that broaden theoretical background needed for the design of new, more effective, platinum anticancer drugs.

For the reaction of oxaliplatin with DNA to occur, the parent compound must become aquated. The hydrolysis of oxaliplatin to form reactive diaqua species $[\text{Pt}(\text{R,R-DACH})(\text{H}_2\text{O})_2]^{2+}$ (DACH = 1,2-diaminocyclohexane, Fig. 1 A) is a slower process than the hydrolysis of cisplatin. Therefore, oxaliplatin is inherently less able than cisplatin to form DNA adducts (11), but the sites in DNA of oxaliplatin adducts and their spectrum are nearly identical to the situation when DNA is modified by cisplatin (12). On the other hand, oxaliplatin adducts are removed from DNA by a nucleotide excision repair system (13) or by recombination repair (14) with similar efficiency as cisplatin adducts. In contrast, DNA adducts of oxaliplatin and cisplatin are processed by a mismatch repair system (15) and translesion DNA polymerases (16–18) differently. Despite lower DNA reactivity, oxaliplatin exhibits similar or greater cytotoxicity in several human tumor cell lines. Thus, oxaliplatin requires fewer DNA lesions than does cisplatin to achieve cell growth inhibition (11).

The overall conformational alterations induced in DNA by the major 1,2-GG intrastrand cross-link (CL) of cisplatin and the same adduct of oxaliplatin in the TGGT sequence were studied by x-ray crystallography (19). The 1,2-GG intrastrand CLs of cisplatin and oxaliplatin have been shown to be similar although they differ in several details. The bulky DACH ring of the oxaliplatin adduct fills much of the DNA major groove, making it narrower and less polar at the site of the CL. Recently, the solution structures of the 1,2-GG intrastrand CL of oxaliplatin and cisplatin formed in the AGGC sequence were solved (20,21), and again several

Submitted July 8, 2007, and accepted for publication August 10, 2007.

Address reprint requests to Viktor Brabec, E-mail: brabec@ibp.cz.

Editor: Jonathan B. Chaires.

© 2007 by the Biophysical Society

0006-3495/07/12/3950/13 \$2.00

doi: 10.1529/biophysj.107.116996

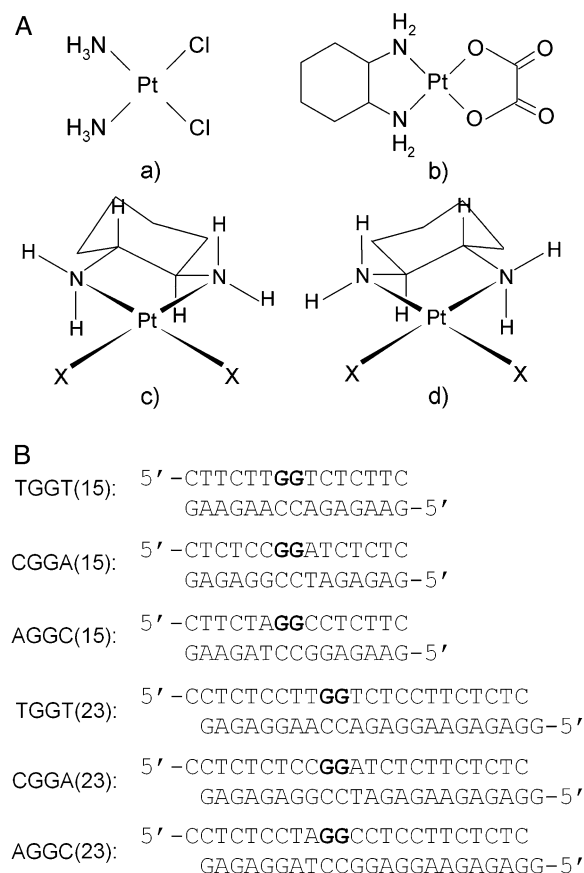


FIGURE 1 Structures of platinum compounds and sequences of the synthetic oligodeoxyribonucleotides with their abbreviations. (A) Structures: a, cisplatin; b, oxaliplatin; c, $[\text{Pt}(\text{R,R-DACH})]^{2+}$; d, $[\text{Pt}(\text{S,S-DACH})]^{2+}$. (B) Sequences: the top and bottom strands of each pair in the figure are designated "top" and "bottom", respectively, throughout. The boldface letters in the top strands of the duplexes indicate the platinated residues.

conformational differences were observed between the cisplatin-GG adduct and the oxaliplatin-GG adduct.

The structure of an oxaliplatin-GG adduct has been so far described only for two sequence contexts, such as TGGT and AGGC, although under different conditions. Besides $[\text{Pt}(\text{R,R-DACH})]^{2+}$ (oxaliplatin), another enantiomeric form of this complex exists so that the biological activity of platinum complexes with enantiomeric amine ligands such as $[\text{PtX}_2(\text{R,R-DACH})]^{2+}$ and $[\text{PtX}_2(\text{S,S-DACH})]^{2+}$ (Fig. 1 A) are also of great interest. For instance, the DACH carrier ligand has been shown to significantly affect the ability of platinum-DNA adducts to block essential processes such as replication and transcription (22). Also, importantly, the $[\text{PtCl}_2(\text{S,S-DACH})]^{2+}$ complex, having an *S* configuration at the asymmetric carbon atoms, is markedly more mutagenic toward several strains of *Salmonella typhimurium* than $[\text{PtCl}_2(\text{R,R-DACH})]^{2+}$ (23). Even more importantly, oxaliplatin (having λ -*gauche* conformation of the diamine chelate ring) exhibits higher activity toward various cancers than the *S,S*-enantiomer (having δ -*gauche* conformation) so that

oxaliplatin and not its *S,S*-enantiomer has been approved for clinical use (24). Hence, although the asymmetry in the amine ligand in these platinum complexes does not involve the coordinated nitrogen atom but rather an adjacent carbon atom, a dependence of the biological activity on the configuration of the amine is observed.

To allow drawing a more definite conclusion relating the structural differences between the 1,2-GG intrastrand CLs of oxaliplatin and cisplatin to the biological differences between these two platinum drugs, we performed a more complex study including the effect of the sequence context on the structure of 1,2-GG intrastrand adduct of oxaliplatin using gel electrophoretic retardation (phasing) assay, chemical probes of DNA conformation, and differential scanning calorimetry (DSC). We also performed studies aimed at recognition of this adduct by HMG domain protein and the inhibitory effect of this adduct on DNA polymerization *in vitro*. The latter factors play an important role in the mechanism underlying antitumor effects of cisplatin (6,25). In addition, we have also given several examples of how chirality at the carbon atom of the carrier DACH ligand affects some important factors that play a significant role in the mechanism of biological effects of cisplatin and its analogs.

MATERIALS AND METHODS

Chemicals

$[\text{Pt}(\text{R,R-DACH})(\text{H}_2\text{O})_2](\text{SO}_4)$ or $[\text{Pt}(\text{S,S-DACH})(\text{H}_2\text{O})_2](\text{SO}_4)$ (Fig. 1 A) were prepared from the corresponding dichloro species (23) by treatment with Ag_2SO_4 (26). Cisplatin was obtained from Sigma (Prague, Czech Republic). The stock solutions of platinum compounds were prepared at a concentration of 5×10^{-4} M in 10 mM NaClO_4 and stored at 4°C in the dark. The synthetic oligodeoxyribonucleotides were synthesized and purified as described previously (27). Expression and purification of domain A (residues 1–84) of the HMGB1 protein (HMGB1a) (HMG = high-mobility group) were carried out as described (28,29). T4 DNA ligase, the Klenow fragment from DNA polymerase I (exonuclease minus, mutated to remove the 3' → 5' proofreading domain) (KF[−]), restriction endonuclease *Eco*RI, and T4 polynucleotide kinase were purchased from New England Biolabs (Beverly, MA). Deoxyribonucleoside 5'-triphosphates were from Roche Diagnostics (Mannheim, Germany). Acrylamide, bis(acrylamide), urea, and NaCN were from Merck (Darmstadt, Germany). Dimethyl sulfate (DMS), KMnO_4 , diethyl pyrocarbonate (DEPC), KBr, and KHSO_5 were from Sigma. Nonidet P-30 was from Fluka (Prague, Czech Republic). Radioactive products were from Amersham (Arlington Heights, IL). Proteinase K and ATP were from Boehringer (Mannheim, Germany).

Platinations of oligonucleotides

The duplexes containing single, central 1,2-GG intrastrand CL of $[\text{Pt}(\text{R,R-DACH})]^{2+}$, $[\text{Pt}(\text{S,S-DACH})]^{2+}$, or cisplatin in the pyrimidine-rich top strands were prepared as described (27). The platinated oligonucleotides were purified by ion-exchange fast protein liquid chromatography (FPLC). It was verified by platinum flameless atomic absorption spectrophotometry (FAAS) and by the measurements of the optical density that the modified oligonucleotides contained one platinum atom. It was also verified using DMS footprinting of platinum on DNA (30) that one DACH or cisplatin molecule was coordinated to the N7 atom of the single G in the top strands of each duplex. FPLC purification and FAAS measurements were carried out

on a Pharmacia Biotech (Piscataway, NJ) FPLC System with MonoQ HR 5/5 column and a Varian (Palo Alto, CA) AA240Z Zeeman atomic absorption spectrometer equipped with a GTA 120 graphite tube atomizer, respectively. The unmodified or platinated duplexes used in the studies of recognition by HMGB1 domain proteins were still purified by electrophoresis on native 15% polyacrylamide (PAA) gel (mono/bis(acrylamide) ratio = 29:1). Other details have been described previously (27,31).

Ligation and electrophoresis of oligonucleotides

Unplatinated 20–23-mer single strands (bottom strands of the duplexes described in the section DNA unwinding and bending) were 5'-end-labeled with [γ - 32 P]ATP by using T4 polynucleotide kinase. Then they were annealed with their phosphorylated complementary strands (unplatinated or containing the platinum CL). The duplexes were allowed to react with T4 DNA ligase. The resulting samples along with ligated unplatinated duplexes were subsequently examined on 8% native PAA (mono/bis(acrylamide) ratio = 29:1) electrophoresis gels. Other details of these experiments were as described in previous articles (32–34).

Chemical modifications

The modification by KMnO₄, DEPC, and KBr/KHSO₅ were performed as described previously (31,35–37). The strands of the duplexes were 5'-end labeled with [γ - 32 P]ATP. In the case of the platinated oligonucleotides, the platinum complex was removed after reaction of the DNA with the probe by incubation with 0.2 M NaCN (pH 11) at 45°C for 10 h in the dark.

Gel mobility shift assay

The 5'-end-labeled 22-bp oligonucleotide duplexes with blunt ends (their sequences were identical to those of the duplexes TGGT (23), CGGA (23), and AGGC (23) shown in Fig. 1 B except that they did not contain terminal overhanging nucleotides) either unplatinated (controls) or containing the central platinum adduct in their top strands were used, and their reaction with HMGB1a protein was performed and analyzed as described previously (38).

Inhibition of DNA polymerization

We investigated in this work DNA polymerization using the templates site specifically modified by [Pt(R,R-DACH)]²⁺, [Pt(S,S-DACH)]²⁺, or cisplatin by KF[−]. The DNA polymerase I class of enzymes has served as the prototype for studies on structural and biochemical mechanisms of DNA replication (39,40). In addition, as the most extensive genetic, biochemical, and structural studies have been carried out on a Klenow fragment of DNA polymerase I (including its exonuclease-deficient analog), this enzyme appears to be an ideal model system for investigating the molecular mechanisms associated with template-directed DNA synthesis (39,40).

The 23-mer templates (see Fig. 5 B, *bottom*) containing a single 1,2-GG intrastrand adduct of [Pt(R,R-DACH)]²⁺, [Pt(S,S-DACH)]²⁺, or cisplatin were prepared in the same way as described in the section Platinations of oligonucleotides (*vide supra*); 8-mer DNA primer whose sequence is also shown in Fig. 5 B was complementary to the 3' termini of the 23-mer templates. The DNA substrates were formed by annealing templates and 5'-end-labeled primer (5×10^{-8} M) at a molar ratio of 3:1. All experiments were performed at 25°C in a volume of 50 μ l in a buffer containing 50 mM Tris-HCl (pH 7.4), 10 mM MgCl₂, 0.1 mM dithiothreitol, 50 μ g/ml bovine serum albumin, 100 μ M deoxyadenosine 5'-triphosphate, 100 μ M deoxycytidine 5'-triphosphate, 100 μ M deoxyguanosine 5'-triphosphate, and 100 μ M thymidine 5'-triphosphate and 0.5 unit of KF[−]. Reactions were terminated by the addition of EDTA so that its resulting concentration was 20 mM and by heating at 100°C for 30 s. Products were resolved by denaturing 20% PAA/8 M urea gel and then visualized and quantified by using the FUJIFILM bioimaging analyzer and AIDA image analyzer software.

Differential scanning calorimetry

Excess heat capacity (ΔC_p) versus temperature profiles for the thermally induced transitions of TGGT (15), CGGA (15), and AGGC (15) duplexes (see Fig. 1 B for their sequences) unmodified or containing a unique 1,2-GG intrastrand CL of cisplatin, [Pt(R,R-DACH)]²⁺, or [Pt(S,S-DACH)]²⁺ were measured using a VP-DSC calorimeter (Microcal, Northampton, MA). In the DSC experiments the concentrations of the duplexes were 30 μ M, the heating rate was 60°C/h, and the maximum temperature was 95°C. After reaching the maximum temperature the samples were cooled at the same rate to the starting temperature of 25°C. In this study ΔC_p is defined as excess heat capacity, which is baseline subtracted and concentration normalized (41). The reference scans were subtracted from the sample scans to obtain ΔC_p versus temperature profiles. Enthalpies (ΔH_{cal}) and entropies (ΔS) of duplex melting were calculated from the areas under the experimental ΔC_p versus T and derived $\Delta C_p/T$ versus T curves, respectively, using ORIGIN v.5.0 software (Microcal, Studio City, CA). The free energy of duplex dissociation at 25°C (ΔG_{25}) was calculated using the standard thermodynamic relationship given in Eq. 1 and the corresponding ΔH and ΔS values:

$$\Delta G_{25}^0 = \Delta H - (298.15)\Delta S. \quad (1)$$

The duplexes were dissolved in the buffer containing 10 mM sodium phosphate (NaH₂PO₄/Na₂HPO₄) pH 7.0 and 150 mM NaCl. It was also verified in the same way as described in previous articles (42,43) that the melting transitions of both the platinated and unmodified duplexes were fully reversible.

RESULTS

Conformational changes produced in double helical DNA by the site-specific 1,2-GG intrastrand cross-link

The goal of our work was to establish whether the steric structure of the nonleaving group of platinum DACH enantiomers could influence the distortions induced in DNA by the formation of the 1,2-GG intrastrand CL. We directed our studies on establishing distortions and other biophysical properties of oligodeoxyribonucleotide duplexes containing a single, site-specific 1,2-GG intrastrand CL of [Pt(R,R-DACH)]²⁺ or [Pt(S,S-DACH)]²⁺ in three central sequences, such as TGGT, AGGC, and CGGA.

Differential scanning calorimetry

A calorimetric technique was used to characterize the influence of the 1,2-GG intrastrand CL of [Pt(R,R-DACH)]²⁺ or [Pt(S,S-DACH)]²⁺ on the thermal stability and energetics of the site specifically platinated 15-mer DNA duplexes. Such thermodynamic data can reveal how the platinum adduct influences duplex stability, a property that has been shown to play a significant role in the mechanism of antitumor activity of platinum drugs (42,44,45). Recently, calorimetric and spectroscopic techniques were used to characterize the influence of the 1,2-GG intrastrand CL on the thermal stability and energetics of a 20-mer DNA duplex site specifically modified by cisplatin, antitumor dinuclear platinum complex, and [Pt(R,R-DAB)]²⁺ or [Pt(S,S-DAB)]²⁺ (DAB = 2,3-diaminobutane) (42,46,47). We expanded these studies

on the oligodeoxyribonucleotide duplex containing unique 1,2-GG site-specific intrastrand adducts of the $[\text{Pt}(\text{R,R-DACH})]^{2+}$ or $[\text{Pt}(\text{S,S-DACH})]^{2+}$ complexes.

Fig. 2 shows DSC melting profiles (ΔC_p versus T) for the parent, nonmodified 15-bp duplexes TGGT (15), AGGC (15), and CGGA (15) (*solid curves*) and the same duplexes containing single 1,2-GG intrastrand CL of cisplatin (*dot and dashed curves*), $[\text{Pt}(\text{R,R-DACH})]^{2+}$ (*dashed curves*), or $[\text{Pt}(\text{S,S-DACH})]^{2+}$ (*dotted curves*). Each transition shows negligible changes in the heat capacities between the initial and final states, and denaturation (heating) and renaturation (cooling) curves for the unmodified and platinated duplexes

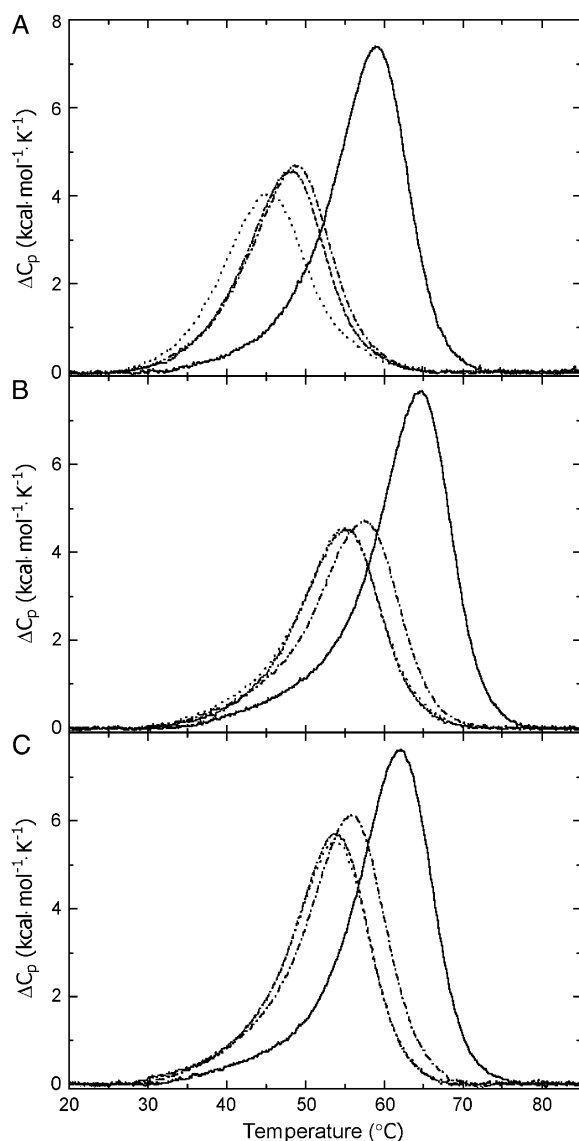


FIGURE 2 DSC thermograms for the (A) TGGT (15), (B) CGGA (15), and (C) AGGC duplexes unmodified (*solid lines*) and containing in the top strand 1,2-GG intrastrand adduct of cisplatin (*dot and dashed line*), $[\text{Pt}(\text{R,R-DACH})]^{2+}$ (*dashed line*), and $[\text{Pt}(\text{S,S-DACH})]^{2+}$ (*dotted line*). The concentrations of the duplexes were 30 μM , and the buffer conditions were 10 mM sodium phosphate pH 7.0 and 150 mM NaCl.

were superimposable (not shown), which is consistent with the reversibility of the melting equilibrium. The interpretation of our calorimetric data described below is also based on the assumption that all thermodynamic parameters for melting of the unmodified and platinated duplexes are ascribed to differences in the initial duplex states. This implies that the final single-stranded states should be thermodynamically equivalent at the elevated temperatures at which they are formed. This assumption has been verified similarly as in earlier reports by recording identical circular dichroic spectra for the samples of nonplatinated and platinated duplexes that were heated to high temperatures (42–44,46,48). In aggregate, meaningful thermodynamic data from our calorimetric measurements described below could be obtained.

DSC melting profiles were analyzed as described in Materials and Methods to obtain the results listed in Table 1. All thermodynamic parameters discussed in this work refer to the duplex dissociation process. Differences in the dissociation thermodynamics due to the presence of the adduct are presented as “ $\Delta\Delta$ ” parameters. These parameters are computed by subtracting the appropriate value measured for control, unmodified duplex from the value measured for the duplex containing the single, site-specific platinum adduct and are reported in Table 1 in parentheses.

Inspection of these thermodynamic parameters reveals a number of interesting features: First, CL formation of $[\text{Pt}(\text{R,R-DACH})]^{2+}$ or $[\text{Pt}(\text{S,S-DACH})]^{2+}$ reduced the duplex thermal stability. The CLs of both enantiomers reduced DNA melting temperature to the same extent that they would if they were formed in the sequences AGGC or CGGA; and this reduction was slightly greater than that induced by the CL of cisplatin formed in the same sequences. Interestingly, CL formation of cisplatin and DACH complexes reduced the duplex thermal stability more extensively if these CLs were formed in the TGGT sequence than in the other two sequences. In addition, whereas the CL of $[\text{Pt}(\text{R,R-DACH})]^{2+}$ reduced DNA melting temperature to the same extent as cisplatin, the CL of $[\text{Pt}(\text{S,S-DACH})]^{2+}$ was in this respect more efficient. Second, CL formation by cisplatin and DACH complexes resulted in a large decrease of the enthalpy of duplex dissociation (Table 1). In other words, the intrastrand CL of these platinum complexes enthalpically destabilizes the duplex relative to their nonmodified counterpart. Third, CL formation by $[\text{Pt}(\text{R,R-DACH})]^{2+}$, $[\text{Pt}(\text{S,S-DACH})]^{2+}$, or cisplatin resulted in a substantial decrease in duplex dissociation entropy (Table 1). In other words, the intrastrand CL of both DACH enantiomers and cisplatin increases the entropy of the duplex. Fourth, the net result of these enthalpic and entropic effects is that 1,2-GG intrastrand CL formation by $[\text{Pt}(\text{R,R-DACH})]^{2+}$, $[\text{Pt}(\text{S,S-DACH})]^{2+}$, or cisplatin in TGGT, CGGA, or AGGC sequences induces a decrease in the free energy for duplex dissociation at 25°C (ΔG_{25}) (Table 1), this duplex destabilization being enthalpic in origin. In this respect, the intrastrand CLs of DACH complexes were more effective than that of cisplatin if the

TABLE 1 Calorimetrically derived thermodynamic parameters for dissociation (melting) of the 15-bp duplexes unmodified or containing a single, site-specific 1,2-GG intrastrand CL of cisplatin, [Pt(*R,R*-DACH)]²⁺, or [Pt(*S,S*-DACH)]²⁺

TGGT(15)	<i>T_m</i> (°C)	ΔH (kcal/mol)	ΔS (cal/mol)	ΔG_{25}^0 (kcal/mol)
no Pt (control)	58.9	96.8	294.1	9.1
cisplatin	48.7	63.0 (−33.8)	196.7 (−97.4)	4.4 (−4.7)
[Pt(<i>R,R</i> -DACH)] ²⁺	48.1	59.9 (−36.9)	187.3 (−106.8)	4.1 (−5.0)
[Pt(<i>S,S</i> -DACH)] ²⁺	45.3	56.7 (−40.1)	178.4 (−115.7)	3.5 (−5.6)
CGGA(15)	<i>T_m</i> (°C)	ΔH (kcal/mol)	ΔS (cal/mol)	ΔG_{25}^0 (kcal/mol)
no Pt (control)	64.5	102.1	305.2	11.1
cisplatin	57.5	67.8 (−34.3)	206.8 (−98.4)	6.1 (−5.0)
[Pt(<i>R,R</i> -DACH)] ²⁺	55.0	61.4 (−40.7)	188.0 (−117.2)	5.3 (−5.8)
[Pt(<i>S,S</i> -DACH)] ²⁺	54.9	64.4 (−37.7)	197.8 (−107.4)	5.4 (−5.7)
AGGC(15)	<i>T_m</i> (°C)	ΔH (kcal/mol)	ΔS (cal/mol)	ΔG_{25}^0 (kcal/mol)
no Pt (control)	62.1	99.8	300.2	10.3
cisplatin	55.8	84.2 (−15.6)	257.7 (−42.5)	7.4 (−2.9)
[Pt(<i>R,R</i> -DACH)] ²⁺	53.9	72.2 (−27.6)	221.9 (−78.3)	6.0 (−4.3)
[Pt(<i>S,S</i> -DACH)] ²⁺	53.9	73.6 (−26.2)	226.6 (−73.6)	6.0 (−4.3)

The ΔH and ΔS values are averages derived from three independent experiments. The experimental uncertainties of the parameters are as follows: *T_m* ($\pm 0.5^\circ\text{C}$), ΔH_{cal} ($\pm 2\%$), ΔS ($\pm 3\%$), ΔG_{25}^0 ($\pm 3\%$). “ $\Delta\Delta$ ” parameters are in parentheses (these parameters are computed by subtracting the appropriate value measured for control, unmodified duplex from the value measured for the duplex containing the single, site-specific platinum adduct).

CLs were formed in the CGGA or AGGC sequences. On the other hand, if the CLs of [Pt(*R,R*-DACH)]²⁺ and cisplatin were formed in the TGGT sequence, the difference in the ability of these CLs to thermodynamically destabilize the duplex was notably small. Interestingly, the intrastrand CL of [Pt(*S,S*-DACH)]²⁺ formed in this latter sequence thermodynamically destabilized the duplex considerably more than its *R,R* counterpart.

DNA unwinding and bending

Among the alterations of secondary and tertiary structure of DNA to which it may be subjected, the role of intrinsic bending and unwinding of DNA is increasingly recognized as being potentially important in regulating replication and transcription functions through specific DNA-protein interactions. For cisplatin adducts, the structural details responsible for bending and subsequent protein recognition have recently been elucidated (49,50). Given the recent advances in our understanding of the structural basis for the bending of DNA caused by cisplatin, it is of considerable interest to examine how the character of a carrier amine in the 1,2-GG intrastrand adduct affects conformational properties of DNA, such as bending and unwinding. In this work we further performed studies on the bending and unwinding induced by single, site-specific intrastrand CLs of [Pt(DACH)]²⁺ enantiomers formed in oligodeoxyribonucleotide duplexes between neighboring guanine residues in three sequence contexts.

As in the previous study (47), we used electrophoretic retardation as a quantitative measure of the extent of planar curvature to analyze bending and unwinding induced by the single, site-specific 1,2-GG intrastrand CL formed by [Pt(*R,R*-DACH)]²⁺ or [Pt(*S,S*-DACH)]²⁺ in the sequences

TGGT, CGGA, and AGGC. The oligodeoxyribonucleotide duplexes TGGT (20–23), CGGA (20–23), and AGGC (20–23), used for DNA bending and unwinding studies, were 20–23-bp long and had sequences identical or similar to those of the duplexes TGGT (21), CGGA (21), or AGGC (21) (Fig. 1 *B*), respectively; the 20-bp duplexes had one terminal C·G pair deleted, whereas one additional T·A pair was added to the 3′ end in the 22-bp duplex and T·A and C·G pairs were added to the 3′ end in the 23-bp duplex). The ligation products of these unplatinated or [Pt(DACH)]-containing duplexes were analyzed on native PAA electrophoresis gel. Experimental details of these studies are given in our recent report (47). A representative gel and its analysis showing the mobility of the ligation products of 20–23-bp duplexes containing single, site-specific 1,2-GG intrastrand CL of [Pt(*R,R*-DACH)]²⁺ or [Pt(*S,S*-DACH)]²⁺ at the central sequence TGGT in a PAA gel is demonstrated in the Supplementary Material (Fig. S1). The results are summarized in Table 2. The DNA bending toward the major groove in the range of 29°–33° and unwinding in the range of 18°–22° due to the single, site-specific 1,2-GG intrastrand CL formed by [Pt(*R,R*-DACH)]²⁺ or [Pt(*S,S*-DACH)]²⁺ were similar for both enantiomers if the CLs were formed in the CGGA or AGGC sequences. The direction of the bend was determined using the 33-bp duplexes, which also contained, besides the single 1,2-GG intrastrand CL formed by either Pt-DACH enantiomer, the (A·T)₅ tract located “in phase” from the CL (the cross-linked basepair and the center of the A tract were separated by 11 bp), in the same way as in our recent articles (51–53). Somewhat different results were obtained for the CLs in the TGGT sequence. The bending toward the major groove due to the single, site-specific 1,2-GG intrastrand CL formed by [Pt(*R,R*-DACH)]²⁺ was markedly greater than

TABLE 2 DNA bending and unwinding induced by the 1,2-GG intrastrand CL of cisplatin, [Pt(*R,R*-DACH)]²⁺ or [Pt(*S,S*-DACH)]²⁺ within the TGGT, CGGA, and AGGC contexts, as determined by the gel electrophoresis retardation assay

	cisplatin*	[Pt(<i>R,R</i> -DACH)] ²⁺	[Pt(<i>S,S</i> -DACH)] ²⁺
TGGT			
bending [†]	34°	31°	23°
unwinding	20°	19°	16°
CGGA			
bending [†]	34°	30°	30°
unwinding	19°	18°	18°
AGGC			
bending [†]	33°	28°	34°
unwinding	20°	20°	22°

*Data from Stehlikova et al. (64).

[†]Toward major groove.

that induced by [Pt(*S,S*-DACH)]²⁺, and similarly the unwinding angle due to the CL of [Pt(*R,R*-DACH)]²⁺ was greater than that due to the CL of [Pt(*S,S*-DACH)]²⁺.

Chemical probing of conformational distortions

To further characterize the distortion induced in DNA by intrastrand CLs of [Pt(*R,R*-DACH)]²⁺ or [Pt(*S,S*-DACH)]²⁺, the 23-bp duplexes TGGT (23), CGGA (23), or AGGC (23) containing the 1,2-GG intrastrand CL of either enantiomer were treated with several chemical agents that are used as tools for monitoring the existence of conformations other than canonical B-DNA. These agents included KMnO₄, bromine, or DEPC as probes for thymine, cytosine, and adenine/guanine residues, respectively (31,35–37,54). These chemical probes react, under the conditions used, with base residues in single-stranded DNA and distorted double-stranded DNA, but not with the base residues in intact, double-stranded DNA (31,35–37,54).

For this analysis, we used exactly the same methodology as in our recent studies dealing with DNA adducts of various antitumor platinum drugs. Thus, the details of this experiment can be found in those articles (31,55), and a representative gel showing piperidine-induced specific strand cleavage at KMnO₄-modified, KBr/KHSO₅-modified, and DEPC-modified bases in the 23-bp TGGT duplex unplatinated or containing single 1,2-GG intrastrand CL of [Pt(*R,R*-DACH)]²⁺ or [Pt(*S,S*-DACH)]²⁺ is demonstrated in the Supplementary Material (Fig. S2). The results are schematically summarized in Fig. 3. The pattern and degree of reactivity toward the chemical probes were identical for the CLs formed by both enantiomers in the sequences CGGA or AGGC, indicating a similar character of the conformational distortion. This is in contrast to the results of the analogous experiments carried out with the duplex containing the CLs in the sequence TGGT, where the pattern and degree of reactivity toward the chemical probes was different for the CLs of the two enantiomers (Fig. 3), indicating a chirality-dependent character of the conformational distortion.

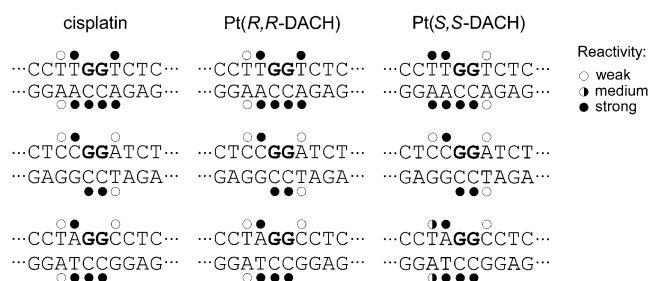


FIGURE 3 Summary of the reactivity of chemical probes with the duplexes TGGT, CGGA, and AGGC containing 1,2-GG intrastrand CL of cisplatin, [Pt(*R,R*-DACH)]²⁺, or [Pt(*S,S*-DACH)]²⁺. Solid, half-solid and open circles designate strong, medium, or weak reactivity, respectively.

Recognition by domain A of HMGB1 protein

An important feature of the mechanism of action of cisplatin is that the major adducts of this platinum drug, the 1,2-GG intrastrand CLs, are recognized by proteins containing HMG domains (6,25,56). Importantly, DNA modified by transplatin or monodentate platinum(II) compounds, such as [PtCl(dien)]⁺ (dien = *N*-(2-aminoethyl)ethane-1,2-diamine) or [PtCl(NH₃)₃]⁺, is not recognized by these cellular proteins (57). It has been shown (25,50) that the binding of these proteins to DNA treated with cisplatin may mediate the antitumor effects of this platinum drug. In addition, it has been shown (58,59) that the replacement of one or both ammine groups in cisplatin by various, mostly cyclic, non-leaving ligands altered the affinity of HMG box proteins for the 1,2-GG intrastrand CLs. Hence, it was of great interest to examine whether the replacement of the ammine ligands of cisplatin by the chiral DACH ligand could also affect the affinity of HMG box proteins for this adduct.

HMGB1 is an abundant chromosomal protein which binds preferentially without sequence specificity to bent or distorted DNA structures including CLs formed by cisplatin. HMGB1 consists of two tandem HMG box domains (A and B, HMGB1a and HMGB1b, respectively) which share a common HMG box structure. It has been shown that HMGB1a has a markedly higher binding affinity for distorted DNA including 1,2-GG intrastrand CLs. Thus, the full-length HMGB1 protein binds to the 1,2-GG intrastrand CL of cisplatin primarily through domain A (60). As it is mainly domain A that is essential for binding to the specific structure produced by the 1,2-GG intrastrand CL of cisplatin, the interactions of this domain (HMGB1a) with the 1,2-GG intrastrand CLs of [Pt(*R,R*-DACH)]²⁺ or [Pt(*S,S*-DACH)]²⁺ were investigated using gel mobility shift assay. In these experiments, the 22-bp duplexes containing the central sequence TGGT, CGGA, or AGGC (these 22-bp oligonucleotide duplexes had blunt ends and their sequences were identical to those of the duplexes TGGT (23), CGGA (23), and AGGC (23) shown in Fig. 1 *B* except that they did not contain terminal overhanging nucleotides) were modified so that they contained a single, site-specific 1,2-GG

intrastrand CL of cisplatin, $[\text{Pt}(\text{R,R-DACH})]^{2+}$, or $[\text{Pt}(\text{S,S-DACH})]^{2+}$.

The binding of the HMGB1a to these DNA probes was detected by retardation of the migration of the radiolabeled 22-bp probes through the gel (Fig. 4). HMGB1a exhibited negligible binding to the unmodified 22-bp duplexes. As indicated by the presence of a shifted band whose intensity increases with increasing protein concentration, HMGB1a recognizes the duplexes TGGT, CGGA, or AGGC containing the 1,2-GG intrastrand CL of $[\text{Pt}(\text{R,R-DACH})]^{2+}$, $[\text{Pt}(\text{S,S-DACH})]^{2+}$, or cisplatin (shown for HMGB1a and CLs formed by $[\text{Pt}(\text{R,R-DACH})]^{2+}$, $[\text{Pt}(\text{S,S-DACH})]^{2+}$, or cisplatin in the TGGT sequence in Fig. 4 A). Interestingly, HMGB1a binds the probes containing the 1,2-GG intrastrand CL in the CGGA and AGGC of either enantiomer with an affinity which is very similar for both sequences and for both enantiomers and approximately half as much as that of cisplatin (Fig. 4 B). In contrast to this observation was the affinity of HMGB1a protein to the 1,2-GG intrastrand CLs of $[\text{Pt}(\text{R,R-DACH})]^{2+}$ or $[\text{Pt}(\text{S,S-DACH})]^{2+}$ formed in the 22-bp duplex containing a central TGGT sequence in the top strand. Whereas the protein binds to the CL of $[\text{Pt}(\text{R,R-DACH})]^{2+}$ and cisplatin with comparable affinities and these are, on the average, greater than those observed for the CLs formed in the CGGA or AGGC sequences, a very weak binding is observed for the 1,2-GG intrastrand CL formed by $[\text{Pt}(\text{S,S-DACH})]^{2+}$, which is even lower than those observed for the CL formed by this complex in the CGGA and AGGC sequences (Fig. 4 B).

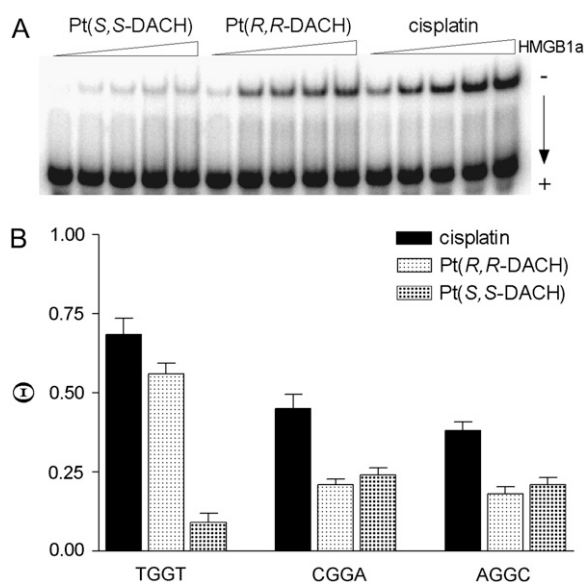


FIGURE 4 The differential binding of HMGB1a to the 22-bp duplexes with central TGGT, CGGA, or AGGC sequences (in the *top strand*) containing the single, site-specific 1,2-GG intrastrand CL of cisplatin, $[\text{Pt}(\text{R,R-DACH})]^{2+}$, or $[\text{Pt}(\text{S,S-DACH})]^{2+}$; the concentration of the duplex was 10 nM and the concentration of HMGB1a was in the range of 2–30 nM. (A) Representative gel showing binding of HMGB1a to the duplex with central TGGT sequence. (B) Bar graph illustrating Θ values (protein-bound duplex/total duplex ratio).

In aggregate, the affinity of HMGB1a protein to the 1,2-GG intrastrand CLs of either $[\text{Pt}(\text{DACH})]^{2+}$ enantiomer was considerably lower than that to the same CL of cisplatin (Fig. 4 B) except the CL formed in the TGGT sequence; the affinity of HMGB1a to the CL of cisplatin and $[\text{Pt}(\text{R,R-DACH})]^{2+}$ were very similar and relatively high, whereas that to the CL of $[\text{Pt}(\text{S,S-DACH})]^{2+}$ was particularly low.

DNA polymerization by Klenow fragment of DNA polymerase I

To learn more about the molecular basis of the replication of DNA modified by oxaliplatin, we investigated in this work DNA polymerization using the DNA templates site specifically modified with 1,2-GG intrastrand CLs of $[\text{Pt}(\text{R,R-DACH})]^{2+}$ or $[\text{Pt}(\text{S,S-DACH})]^{2+}$ in the TGGT, CGGA, or AGGC sequences.

The DNA polymerization was examined by the Klenow fragment of DNA polymerase I (61). The exonuclease-deficient Klenow fragment (KF^-) was selected here because translesion synthesis (TLS) proficient DNA polymerases of the X or Y families share some common properties including lack of associated 3'–5' exonuclease proofreading activity, and, not least, the proofreading mechanism itself may introduce effects more dependent on the adduct type (62).

To assess the translesion replication capacity of KF^- we investigated its capacity to elongate a 5' ^{32}P -labeled 8-mer primer annealed to untreated 23-mer templates or to 23-mer templates containing the 1,2-GG intrastrand CL of $[\text{Pt}(\text{R,R-DACH})]^{2+}$, $[\text{Pt}(\text{S,S-DACH})]^{2+}$, or cisplatin formed in the TGGT, CGGA, or AGGC sequences depicted in Fig. 5 B. The 3' guanine involved in the 1,2-GG intrastrand CL on the template strand was located at its 13th position from the 3' terminus (positioning the 3'-end of the primer five bases before the first platinated base in the template strand) (Fig. 5 B). The newly synthesized DNA products were resolved by denaturing PAA gel electrophoresis and visualized by radiography.

DNA polymerization through the single 1,2-GG intrastrand CL of $[\text{Pt}(\text{R,R-DACH})]^{2+}$, $[\text{Pt}(\text{S,S-DACH})]^{2+}$, or cisplatin formed in the TGGT, CGGA, or AGGC sequences of the templates by KF^- in the presence of all four deoxyribonucleoside 5'-triphosphates was stopped at various time intervals, and the products were resolved by a sequencing gel (shown in Fig. 5 A for the CLs formed by $[\text{Pt}(\text{R,R-DACH})]^{2+}$ or $[\text{Pt}(\text{S,S-DACH})]^{2+}$ in the TGGT sequence). Polymerization proceeded rapidly up to the nucleotide opposite that preceding the 1,2-intrastrand CLs, such that the 12-, 13-, and 14-mer products accumulated to a significant extent. KF^- efficiently replicated the untreated template; no intermediate products were seen with the 23-mer control templates as the full-length products were formed (Fig. 5 A). There was no accumulation of other shorter or larger DNA intermediates. Significant amounts of the full-length products were also noticed with the 23-mer templates containing the CLs of

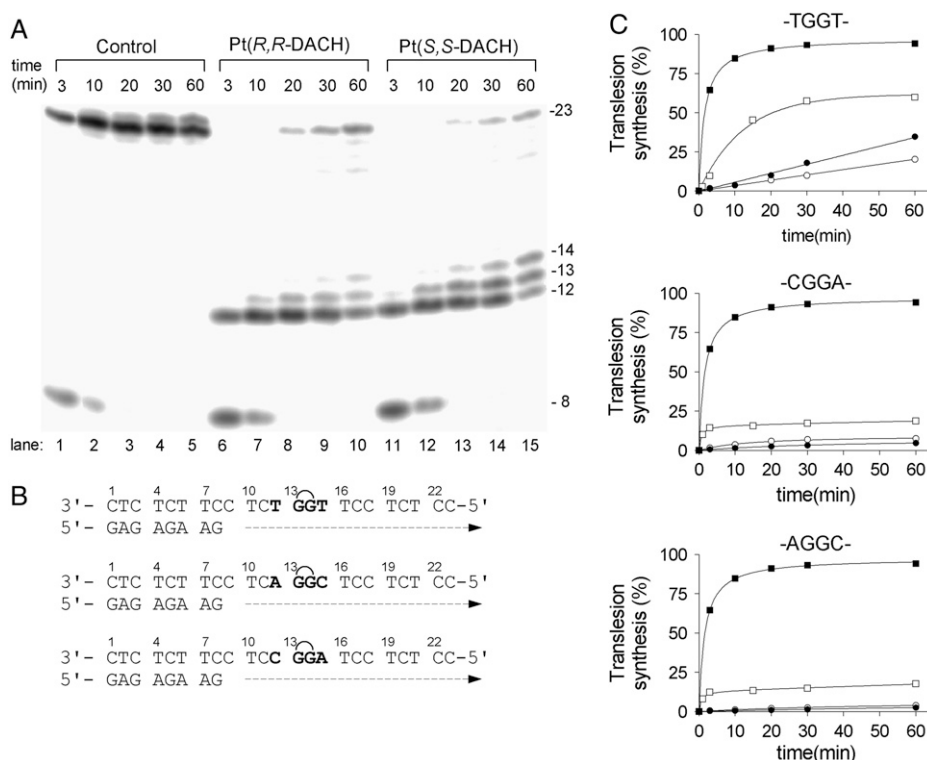


FIGURE 5 Primer extension activity of KF^- using the 8-mer/23-mer, primer/template duplex. (A) The experiments were conducted for the times indicated in the figure (3–60 min) using undamaged template (lanes 1–5), the template containing single, site-specific 1,2-GG intrastrand CL in the TGGT sequence of $[Pt(R,R-DACH)]^{2+}$ (lanes 6–10) or $[Pt(S,S-DACH)]^{2+}$ (lanes 11–15). The pause sites opposite the platinated guanines and a flanking residue on the 3' site are marked 14, 13, and 12, respectively. (B) The nucleotide sequences of the templates containing central TGGT, CGGA, or AGGC sequences and the primer. See the text for details. (C) The time dependence of the inhibition of DNA synthesis on undamaged (control) templates (solid squares), DNA-containing 1,2-GG intrastrand CL of $[Pt(R,R-DACH)]^{2+}$ (solid circles), $[Pt(S,S-DACH)]^{2+}$ (open circles), or cisplatin (squares) in the TGGT (top), AGGC (middle), or CGGA (bottom) sequence. Data are means from three different experiments with two independent template preparations.

$[Pt(R,R-DACH)]^{2+}$, $[Pt(S,S-DACH)]^{2+}$, or cisplatin formed in the TGGT, CGGA, and AGGC sequences at longer times of incubation of the templates with KF^- (60 min), although in a markedly smaller amount than with the nonmodified template; the amount of the full-length products accumulated with the template containing the CL of cisplatin was always greater than those accumulated with the templates containing the CL of $[Pt(R,R-DACH)]^{2+}$ or $[Pt(S,S-DACH)]^{2+}$ in all sequence contexts tested (Fig. 5 C). Importantly, the amount of the full-length products noticed with the 23-mer template containing the CLs of $[Pt(R,R-DACH)]^{2+}$, $[Pt(S,S-DACH)]^{2+}$, or cisplatin formed in the CGGA or AGGC sequences was pronouncedly smaller than that observed for the templates containing the CLs in the TGGT sequence (Fig. 5 C).

DISCUSSION

This complex study was performed to help clarify a more definite correlation between the structural differences of 1,2-GG intrastrand CLs of oxaliplatin and cisplatin and differences in biological effects of these two platinum drugs. We focused in this work on the effects of flanking sequences on DNA conformation at the site of the adduct and in its proximity. In addition, since DNA is a chiral molecule, it may interact in a different way with the platinum complexes containing enantiomeric amine ligands, such as $[Pt(R,R-DACH)]^{2+}$ (oxaliplatin) or $[Pt(S,S-DACH)]^{2+}$. Hence, we also paid attention to understanding how the chirality at the carbon atoms of the carrier ligand in $[Pt(R,R-DACH)]^{2+}$ or $[Pt(S,S-DACH)]^{2+}$

can affect properties of the 1,2-GG intrastrand CL, which is the major DNA lesion of conventional cisplatin and most likely relevant to its antitumor effects.

DNA is considered a major pharmacological target of platinum anticancer drugs (4,25). Hence, a possible explanation for the different biological activity of oxaliplatin ($[Pt(R,R-DACH)]^{2+}$) and cisplatin on one hand and $[Pt(R,R-DACH)]^{2+}$ and $[Pt(S,S-DACH)]^{2+}$ enantiomers on the other hand can be associated with the different conformational distortions induced in DNA by the adducts of these compounds and their different processing in the cell. To test this hypothesis the experiments described in this work were carried out.

The presence of the 1,2-GG intrastrand adduct of cisplatin, $[Pt(R,R-DACH)]^{2+}$ (oxaliplatin), and $[Pt(S,S-DACH)]^{2+}$ reduces the thermal stability of the duplexes TGGT (15), CGGA (15), or AGGC (15). However, the thermal melting is not a thermodynamic parameter. DSC can also provide quantitative, model-independent characterizations of effects of the lesion on duplex thermodynamics. Introduction of the 1,2-GG intrastrand adduct of cisplatin, $[Pt(R,R-DACH)]^{2+}$, and $[Pt(S,S-DACH)]^{2+}$ decreases the ΔG_{25} for dissociation of all duplexes. Interestingly, the ΔG_{25} values observed for melting of the CGGA (15) and AGGC (15) duplexes containing CL of $[Pt(R,R-DACH)]^{2+}$ or $[Pt(S,S-DACH)]^{2+}$ were identical (5.3/5.4 or 6.0 kcal/mol, respectively, Table 1), suggesting that the conformational alterations induced by the CLs formed by both enantiomers in either CGGA or AGGC sequences were similar. On the other hand, the above

mentioned ΔG_{25} values observed for melting of the duplexes CGGA (15) and AGGC (15) containing CL of $[\text{Pt}(\text{R,R-DACH})]^{2+}$ or $[\text{Pt}(\text{S,S-DACH})]^{2+}$ were considerably lower than those observed for the same duplexes containing the CL of cisplatin (6.1 or 7.4 kcal/mol, respectively). These differences in free energy represent an equilibrium preference for the CGGA (15) duplex modified by the CL of cisplatin over that modified by the CL of $[\text{Pt}(\text{R,R-DACH})]^{2+}$ or $[\text{Pt}(\text{S,S-DACH})]^{2+}$ of ~ 4 to 1 (~ 11 to 1 for the platinated AGGC (15) duplex).

Different results were, however, obtained for melting the duplexes containing the CL in the sequence TGGT. The ΔG_{25} values observed for melting the TGGT (15) duplex containing the CL of $[\text{Pt}(\text{R,R-DACH})]^{2+}$ or cisplatin were similar (4.1 or 4.4 kcal/mol, Table 1). This result implies similar conformational alterations induced by the 1,2-GG intrastrand CLs of cisplatin and oxaliplatin formed in the TGGT sequence in contrast to the case when the CLs of these drugs were formed in CGGA and AGGC sequences (vide supra). Another striking difference between the 1,2-GG intrastrand CLs formed in CGGA or AGGC sequences on one hand and a TGGT sequence on the other hand consists of the different effects of the CLs of $[\text{Pt}(\text{R,R-DACH})]^{2+}$ and $[\text{Pt}(\text{S,S-DACH})]^{2+}$ enantiomers, the latter being more effective in destabilizing double-helical DNA, but only if it was formed in the TGGT sequence (ΔG_{25} of 3.5 kcal/mol, Table 1).

Inspection of Table 1 shows that the melting of each duplex is accompanied by unfavorable free energy terms which result from characteristic compensation of unfavorable enthalpy and favorable entropy terms. In general, the unfavorable (endothermic) enthalpy results primarily from the endothermic heats for disrupting basepairs and base-base stacks of the duplex, whereas the favorable entropy terms arise from contributions of the favorable dissociation into two separate strands. Relative to the duplexes containing the 1,2-GG intrastrand CL of cisplatin, those containing the CL of oxaliplatin $\{[\text{Pt}(\text{R,R-DACH})]^{2+}\}$ are higher in enthalpy for all sequences tested, mostly if the CL was formed in the AGGC sequence, whereas the least perturbation was observed for the CL formed in the TGGT sequence. Hence, the formation of the 1,2-GG intrastrand adduct by oxaliplatin is more deleterious energetically than the formation of the same adduct by cisplatin. This observation may be explained in terms of a higher decrease in stacking interactions due to the CL of oxaliplatin than due to that of cisplatin although the extent of this decrease appears to be dependent on the sequence context.

The changes in free energy of the duplexes (TGGT, CGGA, and AGGC), ΔG_{25} , as a consequence of the formation of the single, site-specific intrastrand CL of cisplatin, $[\text{Pt}(\text{R,R-DACH})]^{2+}$, and $[\text{Pt}(\text{S,S-DACH})]^{2+}$ between guanine residues in the top strands ($\Delta\Delta G_{25}$), reflect a combination of enthalpic ($\Delta\Delta H$) and entropic ($\Delta\Delta S$) effects (see the values in parentheses in Table 1). The magnitudes of these effects vary with the platinum complex and sequence context. The observed $\Delta\Delta G_{25}$ values are significantly

smaller than the observed $\Delta\Delta H$ values (the values of $\Delta\Delta H$ range from -40.7 to -15.6 kcal/mol, whereas the values of $\Delta\Delta G_{25}$ range from only -5.8 to -2.9 kcal/mol). This result is the consequence of a considerable, but not complete, compensation of the change in $\Delta\Delta S$. Interestingly, the higher $\Delta\Delta H$ is accompanied by the higher $\Delta\Delta S$.

Structural features of DNA, such as local bending and unwinding at the site of the 1,2-GG intrastrand CLs of cisplatin, play a very important role in the mechanism of antitumor effects of this metallodrug (63). Interestingly, local bending and unwinding due to the 1,2-GG intrastrand CL of cisplatin are very little affected by the bases flanking the CL (64). On the other hand, the bending and unwinding angles due to the 1,2-GG intrastrand CLs of the chiral analogs $[\text{Pt}(\text{DACH})]^{2+}$ as well as the closely related $[\text{Pt}(\text{DAB})]^{2+}$ (DAB = 2,3-diaminobutane) are dependent on the sequence context (65). For instance, the character of distortions determined by chemical probes and phasing assay due to the single, site-specific 1,2-GG intrastrand CL formed by the chiral analog of cisplatin $[\text{Pt}(\text{DAB})]^{2+}$ in the CGGA sequence were identical for both enantiomers; in contrast, these properties of the 1,2-GG CLs formed in the sequence context of TGGT by $[\text{Pt}(\text{DAB})]^{2+}$ depend pronouncedly on the chirality of the diamine (47). It has been shown (65) that the latter structural and chiral differentiation of DNA adducts of $[\text{Pt}(\text{DAB})]^{2+}$ originates from clashes of the 5'-oriented methyl group of the DAB ligand with the methyl group of the 5'-thymine of the TGGT sequence. This explanation was fully consistent with the observation that this chiral differentiation disappeared if the 5' thymine was replaced by cytosine such as in the sequence CGGA (65). The strict analogy between DACH and DAB complexes suggests that the dependence of distortion, including DNA bending and unwinding angles due to the 1,2-GG intrastrand CLs of $[\text{Pt}(\text{DACH})]^{2+}$ on sequence context and on $[\text{Pt}(\text{DACH})]^{2+}$ chirality, can be explained in a similar way. Hence, the structural differentiation also observed for $[\text{Pt}(\text{DACH})]^{2+}$ enantiomers is likely to originate from clashes of the 5'-oriented methylene group of $[\text{Pt}(\text{S,S-DACH})]^{2+}$ with the methyl group of the 5'-thymine in the TGGT sequence. On the other hand, owing to the absence of such clashes in the CGGA sequence no effect of chirality of DACH compounds on the bending and unwinding angles is observed (Table 2).

We also examined conformational alterations induced in DNA by the 1,2-GG intrastrand CL of $[\text{Pt}(\text{R,R-DACH})]^{2+}$ or $[\text{Pt}(\text{S,S-DACH})]^{2+}$ formed in a third sequence, AGGC. The overall character of these structural distortions induced in DNA by the CL of $[\text{Pt}(\text{R,R-DACH})]^{2+}$ is very similar to that observed for this enantiomer or cisplatin in both TGGT and CGGA sequences. The only difference between the 1,2-GG intrastrand CLs of $[\text{Pt}(\text{R,R-DACH})]^{2+}$ and cisplatin consists of a smaller bending angle (by 3° – 4°) found for the CL of oxaliplatin in all sequence contexts tested in this work. It is possible that the bulky DACH group located in the major groove restricts to some degree the DNA bending toward

the major groove required for the formation of the 1,2-intrastrand CL. In aggregate, we have found no distinctly pronounced dependence of the structural properties of 1,2-GG intrastrand CLs of $[\text{Pt}(\text{R,R-DACH})]^{2+}$ (oxaliplatin), such as local DNA bending and unwinding on the sequence context, as it was also observed earlier in our laboratory for the same CLs of cisplatin (64).

On the other hand, these structural features of 1,2-GG intrastrand CLs of $[\text{Pt}(\text{DACH})]^{2+}$ formed at an AGGC sequence are chirality dependent, but apparently differently than in the TGGT sequence. Thus, DNA bending and unwinding due to the 1,2-GG intrastrand CL of $[\text{Pt}(\text{S,S-DACH})]^{2+}$ are considerably more dependent on sequence context than the same adducts of cisplatin or oxaliplatin. Further structural studies are needed to explain this observation.

An important feature of the mechanism of action of cisplatin is that the 1,2-intrastrand CLs formed by this drug are specifically recognized by various proteins, including those containing HMG domains (6,25,56). We have found (47) that the recognition by domains of HMGB1 protein of the 1,2-GG intrastrand CLs formed in the sequence context of TGGT by the chiral $[\text{Pt}(\text{DAB})]^{2+}$ (which is closely related to $[\text{Pt}(\text{DACH})]^{2+}$) depends on the chirality of the asymmetric centers (66). We have also found (65) that this structural differentiation originates from clashes of the 5'-oriented methyl group of the DAB ligand with the methyl group of the 5'-thymine and that this chiral differentiation disappears in sequences XGG, with X being different from T. On the other hand, the domains of HMGB1 proteins have been shown to bind to the GG CL of $[\text{Pt}(\text{R,R-DAB})]^{2+}$ and $[\text{Pt}(\text{S,S-DAB})]^{2+}$ within the CGGA sequence with the same affinity (65). We have demonstrated in this and earlier (65) work that the recognition by HMGB1a, which dominates the interaction between HMGB1 and platinum-damaged DNA (58), of the 1,2-GG intrastrand CLs formed in the sequence context of TGGT and CGGA by the chiral $[\text{Pt}(\text{DACH})]^{2+}$ depends on the chirality of the asymmetric centers in a way very similar to that of $[\text{Pt}(\text{DAB})]^{2+}$, i.e., only if the CL is formed in the TGGT sequence different binding of HMGB1a protein to the CLs of the two enantiomers is observed. In addition, no marked differences in the recognition by HMGB1a of the 1,2-GG intrastrand CLs formed in the sequence context of AGGC was observed (Fig. 4).

As shown for the 1,2-GG intrastrand CL of cisplatin (49), HMGB1a binds to DNA around the site of this adduct in the minor groove whereas the ammine ligands coordinated to platinum reside in the major groove. It is therefore unlikely that the affinity of HMGB1a to the 1,2-GG intrastrand CLs of $[\text{Pt}(\text{R,R-DACH})]^{2+}$ and $[\text{Pt}(\text{S,S-DACH})]^{2+}$ is affected in a dominant way by direct interactions of the enantiomeric nonleaving ligands with the protein. The very important structural elements that contribute to recognition of cisplatin adducts by cellular proteins are bending toward major groove and unwinding of the DNA helix (56). However, no apparent correlation exists between the binding affinity of

HMGB1a to the 1,2-GG intrastrand CL formed by $[\text{Pt}(\text{R,R-DACH})]^{2+}$ or $[\text{Pt}(\text{S,S-DACH})]^{2+}$ in various sequence contexts and the bend or unwinding angles induced by these adducts (Table 2). This result may be interpreted to mean that DNA prebending toward the major groove due to the 1,2-GG intrastrand CL of $[\text{Pt}(\text{R,R-DACH})]^{2+}$ or $[\text{Pt}(\text{S,S-DACH})]^{2+}$ plays an important role in its recognition by HMG domain proteins, but other factors contribute to the stability of the complex formed between platinated DNA and these proteins.

DNA adducts of antitumor platinum drugs, such as cisplatin, are believed to exert their cytotoxic effects by inhibiting both replication and/or transcription and inducing programmed cell death (apoptosis) or necrosis (67). On the other hand, in vitro bypass by replicative DNA polymerases of helix-distorting DNA lesions, including DNA adducts of some platinum compounds, has been observed as well (68–71). Several DNA polymerases have been shown to bypass 1,2-GG intrastrand CLs of oxaliplatin with different efficiency than cisplatin-CLs (17,72), which has been proposed to contribute to the different biological effects of these drugs.

We have demonstrated in this work that DNA polymerase KF^- paused at the site of the 1,2-GG intrastrand CL formed by $[\text{Pt}(\text{DACH})]^{2+}$ enantiomers in all sequence contexts tested in this work considerably more than at the CL of cisplatin (Fig. 5). This result is consistent with a higher TLS observed past cisplatin adducts compared to that past oxaliplatin adducts observed in several tumor cell lines (73,74). It is possible that bulkier DACH lesions can interfere with the conformational change of the polymerase to the closed catalytically active ternary complex (DNA-polymerase-dNTP) more than cisplatin lesions. Presumably, these bulky adducts may alter the structure and stability of the ternary complex, thus affecting an important step that is crucial in determining the rate of the nucleotide incorporation step.

The TLS past 1,2-GG intrastrand CL of $[\text{Pt}(\text{DACH})]^{2+}$, which was considerably smaller than that past the CL of cisplatin, was also chirality dependent (Fig. 5). More pronounced differences were observed mainly if the CL was formed in the TGGT sequence (Fig. 5 C) where TLS past the CL of $[\text{Pt}(\text{R,R-DACH})]^{2+}$ was markedly more extensive than that past the CL of $[\text{Pt}(\text{S,S-DACH})]^{2+}$. Much information is available regarding the TLS efficiencies of various lesions and polymerases, but a number of important details of the structural features of the DNA polymerase-DNA substrate interaction that are required to accomplish TLS have yet to be revealed. The inability of a polymerase to carry out DNA synthesis past DNA damage may reflect the polymerase's inability to position a lesion-containing basepair in a geometric conformation that allows active site assembly and catalysis. Thus, inhibition of synthesis may also be due to the inability of the polymerase to extend the 3' lesion-containing terminus. Interestingly, the pattern and degree of reactivity toward the chemical probes were different, but only for the CLs of the two enantiomers formed in the TGGT sequence (Fig. 3). This observation indicates a chirality-dependent character of the conformational distortion

in this sequence, which correlates with a chirality-dependent TLS past the $[\text{Pt}(\text{DACH})]^{2+}$ -CL (Fig. 5) only observed in this sequence context. The striking feature of the structure of the 1,2-GG intrastrand CL of $[\text{Pt}(\text{DACH})]^{2+}$ enantiomers revealed by chemical probes is that distortions induced by these CLs are different mainly on the 3' side of the lesion, the distortion being more extensive on this side of the CL for the $[\text{Pt}(\text{R,R-DACH})]^{2+}$ enantiomer. Thus, our data support the idea that an important factor facilitating TLS by KF^- past 1,2-GG intrastrand CL of cisplatin and its direct analogs is an extensive distortion on the 3' side of this lesion.

CONCLUSIONS

DNA is considered a major pharmacological target of antitumor effects of platinum drugs. Downstream processes that discriminate between DNA adducts of oxaliplatin and cisplatin are believed to be responsible for the differences in biological effects of these two metallodrugs used clinically, such as antitumor activity and mutagenicity. In addition, different biological effects of oxaliplatin in comparison with cisplatin are often explained by the ability of oxaliplatin to form fewer DNA adducts, but due to their different structural properties these adducts are more effective for biological effects. The major DNA adduct of cisplatin is an intrastrand CL formed between neighboring purine bases so that considerable attention has been paid to differences between properties of this adduct formed by cisplatin and oxaliplatin. Some structural differences have already been demonstrated (19,20), but a definite conclusion about factors involved in the mechanism underlying different cytotoxic and mutagenic response to these metallodrugs cannot yet be drawn. In this work we focused on comparison of conformation, recognition by HMG domain protein, and DNA polymerization across 1,2-GG intrastrand CL formed by cisplatin and oxaliplatin in three sequence contexts with the aid of biophysical and biochemical methods. We found the following:

1. The formation of the 1,2-GG intrastrand adduct by oxaliplatin is more deleterious energetically than the formation of the same adduct by cisplatin in all three sequence contexts. The calorimetric data suggest that oxaliplatin CLs exhibit a higher efficiency to reduce stacking interactions in DNA than the CLs of cisplatin, although the extent of this reduction appears to be dependent on the sequence context.
2. The 1,2-GG intrastrand CLs of oxaliplatin $\{[\text{Pt}(\text{R,R-DACH})]^{2+}$ enantiomer $\}$ bends DNA slightly, but systematically less than the CL of cisplatin (by 3° – 4°) in all sequence contexts tested in this work. It is suggested that the bulky DACH group located in the major groove restricts in some degree the DNA bending toward the major groove required for the formation of the 1,2-intrastrand CL. On the other hand, the structural properties of 1,2-GG intrastrand CLs of (oxaliplatin), such as

local DNA bending and unwinding, are almost independent of the sequence context as observed earlier in our laboratory for the same CLs of cisplatin (64).

3. The affinity of HMG domain protein (HMGB1a) to the 1,2-GG intrastrand CLs of oxaliplatin is considerably lower than that to the same CL of cisplatin independent of the sequence context. It is suggested that the bulky DACH group in the 1,2-GG intrastrand CL restricts to some extent the additional DNA bending required for the protein binding.
4. DNA polymerase KF^- , which serves as the prototype for studies on structural and biochemical mechanisms of DNA replication, pauses at the site of the 1,2-GG intrastrand CL of oxaliplatin in all sequence contexts tested in this work considerably more than at the CL of cisplatin. It is suggested that bulkier DACH lesions can interfere with the conformational change of the polymerase to the closed catalytically active ternary complex (DNA-polymerase-dNTP) more than cisplatin lesions.

We hypothesize that if not all, at least some of the differences between properties of the 1,2-GG intrastrand CL of cisplatin and oxaliplatin and its processing observed in this work could be involved in the different biological effects of these two metallodrugs. However, cisplatin and its antitumor analogs also form other types of adducts on DNA. The relative efficacy of DNA adducts in antitumor effects of these metallodrugs has not been univocally determined. Thus, it cannot be excluded that there are still distinct differences in the properties of other adducts of cisplatin and oxaliplatin and in their cellular processing. Revelation of these differences will complement theoretical background needed to explain differences in biological effects of these clinically used metallodrugs and could also help in the design of new platinum drugs.

In addition, we have also demonstrated examples of how the chirality at the carrier DACH ligand can affect some important factors that play a significant role in the mechanism of biological effects of cisplatin and its analogs. Interestingly, we notice specific properties of the 1,2-GG intrastrand CLs formed by $[\text{Pt}(\text{DACH})]^{2+}$ complexes in the TGGT sequence, which may give rise to specific, hitherto undisclosed biological effects of these lesions. The information contained in this work can be useful for better understanding how the stereochemistry of the carrier amine ligands of cisplatin analogs can modulate their anticancer and mutagenic properties.

SUPPLEMENTARY MATERIAL

To view all of the supplemental files associated with this article, visit <http://www.biophysj.org>.

The authors acknowledge that their participation in the European Cooperation in the field of Scientific and Technical Research Actions D39 enabled them to regularly exchange the most recent ideas in the field of platinum anticancer drugs with several European colleagues.

This research was supported by the Grant Agency of the Czech Republic (Grants 305/05/2030 and 203/06/1239), the Grant Agency of the Academy of Sciences of the Czech Republic (Grant B400040601), Ministry of Education of the Czech Republic (MSMT LC06030), and the Academy of Sciences of the Czech Republic (Grants 1QS500040581 and KAN200200651) and the University of Bari.

REFERENCES

- Lokich, J. 2001. What is the "best" platinum: cisplatin, carboplatin, or oxaliplatin? *Cancer Invest.* 19:756–760.
- Boulikas, T., and M. Vougiouka. 2003. Cisplatin and platinum drugs at the molecular level. *Oncol. Rep.* 10:1663–1682 [review].
- Di Francesco, A. M., A. Ruggiero, and R. Riccardi. 2002. Cellular and molecular aspects of drugs of the future: oxaliplatin. *Cell. Mol. Life Sci.* 59:1914–1927.
- Johnson, N. P., J.-L. Butour, G. Villani, F. L. Wimmer, M. Defais, V. Pierson, and V. Brabec. 1989. Metal antitumor compounds: the mechanism of action of platinum complexes. *Prog. Clin. Biochem. Med.* 10:1–24.
- Brabec, V., and J. Kasparkova. 2005. Modifications of DNA by platinum complexes: relation to resistance of tumors to platinum antitumor drugs. *Drug Resist. Updat.* 8:131–146.
- Brabec, V. 2002. DNA modifications by antitumor platinum and ruthenium compounds: their recognition and repair. *Prog. Nucleic Acid Res. Mol. Biol.* 71:1–68.
- Brabec, V., and J. Kasparkova. 2005. DNA interactions of platinum anticancer drugs. Recent advances and mechanisms of action. In *Metal Compounds in Cancer Chemotherapy*. J.-M. Perez-Martin, M. A. Fuertes, and C. Alonso, editors. Research Signpost, Trivandrum, Kerala, India. 187–218.
- Vrana, O., V. Brabec, and V. Kleinwächter. 1986. Polarographic studies on the conformation of some platinum complexes: relations to anti-tumour activity. *Anticancer Drug Des.* 1:95–109.
- Farrell, N., Y. Qu, and M. P. Hacker. 1990. Cytotoxicity and antitumor activity of bis(platinum) complexes: a novel class of platinum complexes active in cell lines resistant to both cisplatin and 1,2-diaminocyclohexane complexes. *J. Med. Chem.* 33:2179–2184.
- Farrell, N. 1993. Nonclassical platinum antitumor agents: perspectives for design and development of new drugs complementary to cisplatin. *Cancer Invest.* 11:578–589.
- Woynarowski, J. M., S. Faivre, M. C. S. Herzig, B. Arnett, W. G. Chapman, A. V. Trevino, E. Raymond, S. G. Chaney, A. Vaisman, M. Varchenko, and P. E. Juniewicz. 2000. Oxaliplatin-induced damage of cellular DNA. *Mol. Pharmacol.* 58:920–927.
- Woynarowski, J. M., W. G. Chapman, C. Napier, M. C. S. Herzig, and P. Juniewicz. 1998. Sequence- and region-specificity of oxaliplatin adducts in naked and cellular DNA. *Mol. Pharmacol.* 54:770–777.
- Reardon, J. T., A. Vaisman, S. G. Chaney, and A. Sancar. 1999. Efficient nucleotide excision repair of cisplatin, oxaliplatin, and bis-aceto-amine-dichloro-cyclohexylamine-platinum(IV) (JM216) platinum intrastrand DNA diadducts. *Cancer Res.* 59:3968–3971.
- Wu, H. I., J. A. Brown, M. J. Dorie, L. Lazzaroni, and J. M. Brown. 2004. Genome-wide identification of genes conferring resistance to the anticancer agents cisplatin, oxaliplatin, and mitomycin C. *Cancer Res.* 64:3940–3948.
- Vaisman, A., M. Varchenko, A. Umar, T. A. Kunkel, J. I. Risinger, J. C. Barrett, T. C. Hamilton, and S. G. Chaney. 1998. The role of hMLH1, hMSH3, and hMSH6 defects in cisplatin and oxaliplatin resistance: correlation with replicative bypass of platinum-DNA adducts. *Cancer Res.* 58:3579–3585.
- Vaisman, A., C. Masutani, F. Hanaoka, and S. G. Chaney. 2000. Efficient translesion replication past oxaliplatin and cisplatin GpG adducts by human DNA polymerase η . *Biochemistry*. 39:4575–4580.
- Vaisman, A., and S. G. Chaney. 2000. The efficiency and fidelity of translesion synthesis past cisplatin and oxaliplatin GpG adducts by human DNA polymerase β . *J. Biol. Chem.* 275:13017–13025.
- Bassett, E., A. Vaisman, J. M. Havener, C. Masutani, F. Hanaoka, and S. G. Chaney. 2003. Efficiency of extension of mismatched primer termini across from cisplatin and oxaliplatin adducts by human DNA polymerases beta and eta in vitro. *Biochemistry*. 42:14197–14206.
- Spingler, B., D. A. Whittington, and S. J. Lippard. 2001. 2.4 Å crystal structure of an oxaliplatin 1,2-d(GpG) intrastrand cross-link in a DNA dodecamer duplex. *Inorg. Chem.* 40:5596–5602.
- Wu, Y., P. Pradhan, J. Havener, G. Boysen, J. A. Swenberg, S. L. Campbell, and S. G. Chaney. 2004. NMR solution structure of an oxaliplatin 1,2-d(GG) intrastrand cross-link in a DNA dodecamer duplex. *J. Mol. Biol.* 341:1251–1269.
- Wu, Y., D. Bhattacharyya, C. L. King, I. Baskerville-Abraham, S.-H. Huh, G. Boysen, J. A. Swenberg, B. Temple, S. L. Campbell, and S. G. Chaney. 2007. Solution structures of a DNA dodecamer duplex with and without a cisplatin 1,2-d(GG) intrastrand cross-link: comparison with the same DNA duplex containing an oxaliplatin 1,2-d(GG) intrastrand cross-link. *Biochemistry*. 46:6477–6487.
- Page, J. D., I. Husain, A. Sancar, and S. G. Chaney. 1990. Effect of the diaminocyclohexane carrier ligand on platinum adduct formation, repair, and lethality. *Biochemistry*. 29:1016–1024.
- Fanizzi, F. P., F. P. Intini, L. Maresca, G. Natile, R. Quaranta, M. Coluccia, L. Di Bari, D. Giordano, and M. A. Mariggio. 1987. Biological activity of platinum complexes containing chiral centers on the nitrogen or carbon atoms of a chelate diamine ring. *Inorg. Chim. Acta*. 137:45–51.
- Misset, J. L. 1998. Oxaliplatin in practice. *Br. J. Cancer*. 77(S4):4–7.
- Jamieson, E. R., and S. J. Lippard. 1999. Structure, recognition, and processing of cisplatin-DNA adducts. *Chem. Rev.* 99:2467–2498.
- Benedetti, M., L. G. Marzilli, and G. Natile. 2005. Rotamer stability in *cis*-[Pt(diA)G₂] complexes (diA=diamine derivative and G=guanine derivative) mediated by carrier-ligand amine stereochemistry as revealed by circular dichroism spectroscopy. *Chem. Eur. J.* 11:5302–5310.
- Brabec, V., J. Reedijk, and M. Leng. 1992. Sequence-dependent distortions induced in DNA by monofunctional platinum(II) binding. *Biochemistry*. 31:12397–12402.
- Stros, M. 1998. DNA bending by the chromosomal protein HMG1 and its high mobility group box domains. Effect of flanking sequences. *J. Biol. Chem.* 273:10355–10361.
- Stros, M. 2001. Two mutations of basic residues within the N-terminus of HMG-1 B domain with different effects on DNA supercoiling and binding to bent DNA. *Biochemistry*. 40:4769–4779.
- Kasparkova, J., K. J. Mellish, Y. Qu, V. Brabec, and N. Farrell. 1996. Site-specific d(GpG) intrastrand cross-links formed by dinuclear platinum complexes. Bending and NMR studies. *Biochemistry*. 35:16705–16713.
- Brabec, V., M. Sip, and M. Leng. 1993. DNA conformational distortion produced by site-specific interstrand cross-link of trans-diamminedichloroplatinum(II). *Biochemistry*. 32:11676–11681.
- Koo, H. S., H. M. Wu, and D. M. Crothers. 1986. DNA bending at adenine · thymine tracts. *Nature*. 320:501–506.
- Bellon, S. F., and S. J. Lippard. 1990. Bending studies of DNA site-specifically modified by cisplatin, trans-diamminedichloroplatinum(II) and *cis*-Pt(NH₃)₂(N3-cytosine)Cl⁺. *Biophys. Chem.* 35:179–188.
- Kasparkova, J., N. Farrell, and V. Brabec. 2000. Sequence specificity, conformation, and recognition by HMG1 protein of major DNA interstrand cross-links of antitumor dinuclear platinum complexes. *J. Biol. Chem.* 275:15789–15798.
- Bailly, C., D. Gentle, F. Hamy, M. Purcell, and M. J. Waring. 1994. Localized chemical reactivity in DNA associated with the sequence-specific bisintercalation of echinomycin. *Biochem. J.* 300:165–173.
- Ross, S. A., and C. J. Burrows. 1996. Cytosine-specific chemical probing of DNA using bromide and monoperoxysulfate. *Nucleic Acids Res.* 24:5062–5063.

37. Bailly, C., and M. J. Waring. 1997. Diethylpyrocarbonate and osmium tetroxide as probes for drug-induced changes in DNA conformation in vitro. In *Drug-DNA Interaction Protocols*. K. R. Fox, editor. Humana Press, Totowa, NJ. 51–79.
38. He, Q., U.-A. Ohndorf, and S. J. Lippard. 2000. Intercalating residues determine the mode of HMG1 domains A and B binding to cisplatin-modified DNA. *Biochemistry*. 39:14426–14435.
39. Lam, W. C., E. J. C. Van der Schans, L. C. Sowers, and D. P. Millar. 1999. Interaction of DNA polymerase I (Klenow fragment) with DNA substrates containing extrahelical bases: implications for proofreading of frameshift errors during DNA synthesis. *Biochemistry*. 38:2661–2668.
40. Patel, P. H., M. Suzuki, E. Adman, A. Shinkai, and L. A. Loeb. 2001. Prokaryotic DNA polymerase I: evolution, structure, and “base flipping” mechanism for nucleotide selection. *J. Mol. Biol.* 308:823–837.
41. Lehar, S. A., and B. Z. Chowdhry. 1998. Thermodynamic background to differential scanning calorimetry. In *Biocalorimetry: Applications of Calorimetry in the Biological Sciences*. J. E. Ladbury and B. Z. Chowdhry, editors. J. Wiley & Sons, Chichester, UK. 157–182.
42. Hofr, C., N. Farrell, and V. Brabec. 2001. Thermodynamic properties of duplex DNA containing a site-specific d(GpG) intrastrand crosslink formed by an antitumor dinuclear platinum complex. *Nucleic Acids Res.* 29:2034–2040.
43. Hofr, C., and V. Brabec. 2001. Thermal and thermodynamic properties of duplex DNA containing site-specific interstrand cross-link of antitumor cisplatin or its clinically ineffective *trans* isomer. *J. Biol. Chem.* 276:9655–9661.
44. Pilch, D. S., S. U. Dunham, E. R. Jamieson, S. J. Lippard, and K. J. Breslauer. 2000. DNA sequence context modulates the impact of a cisplatin 1,2-d(GpG) intrastrand cross-link and the conformational and thermodynamic properties of duplex DNA. *J. Mol. Biol.* 296:803–812.
45. Brabec, V., K. Stehlikova, J. Malina, M. Vojtkova, and J. Kasparkova. 2006. Thermodynamic properties of damaged DNA and its recognition by xeroderma pigmentosum group A protein and replication protein A. *Arch. Biochem. Biophys.* 446:1–10.
46. Poklar, N., D. S. Pilch, S. J. Lippard, E. A. Redding, S. U. Dunham, and K. J. Breslauer. 1996. Influence of cisplatin intrastrand cross-linking on the conformation, thermal stability, and energetics of a 20-mer DNA duplex. *Proc. Natl. Acad. Sci. USA*. 93:7606–7611.
47. Malina, J., C. Hofr, L. Maresca, G. Natile, and V. Brabec. 2000. DNA interactions of antitumor cisplatin analogs containing enantiomeric amine ligands. *Biophys. J.* 78:2008–2021.
48. Hofr, C., and V. Brabec. 2005. Thermal stability and energetics of 15-mer DNA duplex interstrand cross-linked by trans-diamminedichloroplatinum(II). *Biopolymers*. 77:222–229.
49. Ohndorf, U. M., M. A. Rould, Q. He, C. O. Pabo, and S. J. Lippard. 1999. Basis for recognition of cisplatin-modified DNA by high-mobility-group proteins. *Nature*. 399:708–712.
50. Zamble, D. B., and S. J. Lippard. 1999. The response of cellular proteins to cisplatin-damaged DNA. In *Cisplatin. Chemistry and Biochemistry of a Leading Anticancer Drug*. B. Lippert, editor. VCH, Wiley-VCH, Zürich, Weinheim, Germany. 73–110.
51. Kasparkova, J., J. Zehnulova, N. Farrell, and V. Brabec. 2002. DNA interstrand cross-links of the novel antitumor trinuclear platinum complex BBR3464. Conformation, recognition by high mobility group domain proteins, and nucleotide excision repair. *J. Biol. Chem.* 277:48076–48086.
52. Kasparkova, J., O. Novakova, N. Farrell, and V. Brabec. 2003. DNA binding by antitumor trans-[PtCl₂(NH₃)(thiazole)]. Protein recognition and nucleotide excision repair of monofunctional adducts. *Biochemistry*. 42:792–800.
53. Loskotova, H., and V. Brabec. 1999. DNA interactions of cisplatin tethered to the DNA minor groove binder distamycin. *Eur. J. Biochem.* 266:392–402.
54. Nielsen, P. E. 1990. Chemical and photochemical probing of DNA complexes. *J. Mol. Recognit.* 3:1–24.
55. Zehnulova, J., J. Kasparkova, N. Farrell, and V. Brabec. 2001. Conformation, recognition by high mobility group domain proteins, and nucleotide excision repair of DNA intrastrand cross-links of novel antitumor trinuclear platinum complex BBR3464. *J. Biol. Chem.* 276:22191–22199.
56. Kartalou, M., and J. M. Essigmann. 2001. Recognition of cisplatin adducts by cellular proteins. *Mutat. Res.* 478:1–21.
57. Pil, P. M., and S. J. Lippard. 1992. Specific binding of chromosomal protein-HMG1 to DNA damaged by the anticancer drug cisplatin. *Science*. 256:234–237.
58. Wei, M., S. M. Cohen, A. P. Silverman, and S. J. Lippard. 2001. Effects of spectator ligands on the specific recognition of intrastrand platinum-DNA cross-links by high mobility group box and TATA-binding proteins. *J. Biol. Chem.* 276:38774–38780.
59. Kasparkova, J., O. Novakova, Y. Najajreh, D. Gibson, J.-M. Perez, and V. Brabec. 2003. Effects of a piperidine ligand on the mechanism of action of antitumor cisplatin. *Chem. Res. Toxicol.* 16:1424–1432.
60. Jung, Y. W., and S. J. Lippard. 2003. Nature of full-length HMG1 binding to cisplatin-modified DNA. *Biochemistry*. 42:2664–2671.
61. Turner, R. M., N. D. F. Grindley, and C. M. Joyce. 2003. Interaction of DNA polymerase I (Klenow fragment) with the single-stranded template beyond the site of synthesis. *Biochemistry*. 42:2373–2385.
62. Villani, G., N. T. Le Gac, L. Wasungu, D. Burnouf, R. P. Fuchs, and P. E. Boehmer. 2002. Effect of manganese on in vitro replication of damaged DNA catalyzed by the herpes simplex virus type-1 DNA polymerase. *Nucleic Acids Res.* 30:3323–3332.
63. Cohen, S. M., and S. J. Lippard. 2001. Cisplatin: from DNA damage to cancer chemotherapy. *Prog. Nucleic Acid Res. Mol. Biol.* 67:93–130.
64. Stehlikova, K., H. Kostrhunova, J. Kasparkova, and V. Brabec. 2002. DNA bending and unwinding due to the major 1,2-GG intrastrand cross-link formed by antitumor *cis*-diamminedichloroplatinum(II) are flanking-base independent. *Nucleic Acids Res.* 30:2894–2898.
65. Delalande, O., J. Malina, V. Brabec, and J. Kozelka. 2005. Chiral differentiation of DNA adducts formed by enantiomeric analogues of antitumor cisplatin is sequence-dependent. *Biophys. J.* 88:4159–4169.
66. Malina, J., J. Kasparkova, G. Natile, and V. Brabec. 2002. Recognition of major DNA adducts of enantiomeric cisplatin analogs by HMG box proteins and nucleotide excision repair of these adducts. *Chem. Biol.* 9:629–638.
67. Fuertes, M. A., J. Castilla, C. Alonso, and J. M. Perez. 2003. Cisplatin biochemical mechanism of action: from cytotoxicity to induction of cell death through interconnections between apoptotic and necrotic pathways. *Curr. Med. Chem.* 10:257–266.
68. Hoffmann, J.-S., M.-J. Pillaire, D. Garcia-Estefania, S. Lapalu, and G. Villani. 1996. In vitro bypass replication of the cisplatin-d(GpG) lesion by calf thymus DNA polymerase beta and human immunodeficiency virus type I reverse transcriptase is highly mutagenic. *J. Biol. Chem.* 271:15386–15392.
69. Suo, Z., S. Lippard, and K. Johnson. 1999. Single d(GpG)/*cis*-diammineplatinum(II) adduct-induced inhibition of DNA polymerization. *Biochemistry*. 38:715–726.
70. Novakova, O., J. Kasparkova, J. Malina, G. Natile, and V. Brabec. 2003. DNA-protein cross-linking by trans-[PtCl₂(E-iminoether)₂]. A concept for activation of the *trans* geometry in platinum antitumor complexes. *Nucleic Acids Res.* 31:6450–6460.
71. Marini, V., P. Christofis, O. Novakova, J. Kasparkova, N. Farrell, and V. Brabec. 2005. Conformation, protein recognition and repair of DNA interstrand and intrastrand cross-links of antitumor *trans*-[PtCl₂(NH₃)(thiazole)]. *Nucleic Acids Res.* 33:5819–5828.
72. Vaisman, A., S. E. Lim, S. M. Patrick, W. C. Copeland, D. C. Hinkle, J. J. Turchi, and S. G. Chaney. 1999. Effect of DNA polymerases and high mobility group protein 1 on the carrier ligand specificity for translesion synthesis past platinum-DNA adducts. *Biochemistry*. 38:11026–11039.
73. Gibbons, G. R., W. K. Kaufmann, and S. G. Chaney. 1991. Role of DNA replication in carrier-ligand-specific resistance to platinum compounds in L1210 cells. *Carcinogenesis*. 12:2253–2257.
74. Mamenta, E. L., E. E. Poma, W. K. Kaufmann, D. A. Delmastro, H. L. Grady, and S. G. Chaney. 1994. Enhanced replicative bypass of platinum-DNA adducts in cisplatin-resistant human ovarian carcinoma cell lines. *Cancer Res.* 54:3500–3505.

12.

Bifunctional Amine-Tethered Ruthenium(II) Arene Complexes Form Monofunctional Adducts on DNA

Michael Melchart,[†] Abraha Habtemariam,[§] Olga Novakova,[‡] Stephen A. Moggach,[†] Francesca P. A. Fabbiani,[†] Simon Parsons,[†] Viktor Brabec,[‡] and Peter J. Sadler^{*,§}*School of Chemistry, University of Edinburgh, West Mains Road, Edinburgh, EH9 3JJ, U.K.,**Department of Chemistry, University of Warwick, Coventry CV4 7AL, U.K., Institute of**Biophysics, Academy of Sciences of the Czech Republic, Kralovopolska 135,**61265 Brno, Czech Republic*

Received April 26, 2007

The tethered Ru^{II} half-sandwich complexes [$\eta^6\text{-}\eta^1\text{-C}_6\text{H}_5(\text{CH}_2)_n\text{NH}_2$]RuCl₂ **1** ($n = 3$) and **2** ($n = 2$) have been synthesized as potential bifunctional anticancer complexes, and their X-ray crystal structures have been determined. They hydrolyze rapidly in aqueous solution to give predominantly mono-aqua mono-chlorido species. Mono-9EtG adducts, where 9EtG = 9-ethylguanine, form rapidly, but the second 9EtG binds more slowly and more weakly. In the X-ray crystal structure of the di-9EtG adduct [$(\eta^6\text{-}\eta^1\text{-C}_6\text{H}_5(\text{CH}_2)_3\text{NH}_2)\text{Ru}(\text{9EtG})_2$](CF₃SO₃)₂·H₂O (**8**·H₂O), one of the Ru–N7 bonds is significantly longer than the other (2.1588(18) vs 2.101(2) Å). The bound guanine bases adopt a head-to-head configuration, stabilized by tether NH₂ hydrogen bonding to C6O of 9EtG. The X-ray crystal structure of the dinitrato complex [$(\eta^6\text{-}\eta^1\text{-C}_6\text{H}_5(\text{CH}_2)_3\text{NH}_2)\text{Ru}(\text{NO}_3)_2$] (**3**) showed both nitrates to be bound to ruthenium. This complex readily rutheniated calf thymus DNA but failed to produce stop sites on pSP73KB plasmid DNA during DNA transcription by an RNA polymerase. This suggested that only monofunctional DNA adducts formed, as did interstrand cross-linking assays. Also, the unwinding angle induced in negatively supercoiled DNA ($9 \pm 1^\circ$) was less than that induced by cisplatin (13°). These findings may explain why complexes such as **1** and **2** exhibited low cytotoxicities (IC₅₀ values >100 μM) toward A2780 human ovarian cancer cells.

Introduction

Metal complexes offer potential as anticancer agents.¹ We have shown that some organometallic Ru^{II} arene complexes of the type [$(\eta^6\text{-arene})\text{Ru}(\text{XY})\text{Z}]^+$, where XY is a bidentate chelating ligand and Z is a leaving group, can exhibit promising cytotoxicity against various cancer cell lines, including cisplatin-resistant cells.^{2,3} Complexes such as [$(\eta^6\text{-arene})\text{Ru}(\text{en})\text{Cl}]^+$ have one reactive site available and form monofunctional adducts with biomolecules.^{4,5} A particularly

attractive feature of Ru^{II} arene complexes is the possibility of altering their framework, which provides considerable scope for the optimization of their design, in terms of mechanisms of action, selection of target sites, and modulation of possible side-effects.⁶ It is clear from studies so far that the nature of the arene, of the chelating ligand, and of the leaving group can have a major influence on rates of activation (hydrolysis, binding to biomolecules such as DNA bases) as well as activity.^{3,7}

It was of interest to explore a different profile of reactivity for ruthenium arene complexes. Structural differences could lead to a different spectrum of activity and increase the scope of this type of complex. Whereas the exact mode of action of cytotoxic ruthenium arene compounds is not known, recent results suggest that DNA may be an important target site

* To whom correspondence should be addressed. E-mail: p.j.sadler@warwick.ac.uk.

[†] University of Edinburgh.

[‡] Institute of Biophysics, Brno.

[§] University of Warwick.

(1) Guo, Z.; Sadler, P. J. *Angew. Chem. Int. Ed.* **1999**, *38*, 1512–1531.

(2) Aird, R. E.; Cummings, J.; Ritchie, A. A.; Muir, M.; Morris, R. E.; Chen, H.; Sadler, P. J.; Jodrell, D. I. *Br. J. Cancer* **2002**, *86*, 1652–1657.

(3) Habtemariam, A.; Melchart, M.; Fernández, R.; Parsons, S.; Oswald, I. D. H.; Parkin, A.; Fabbiani, F. P. A.; Davidson, J. E.; Dawson, A.; Aird, R. E.; Jodrell, D. I.; Sadler, P. J. *J. Med. Chem.* **2006**, *49*, 6858–6868.

(4) Wang, F.; Bella, J.; Parkinson, J. A.; Sadler, P. J. *J. Biol. Inorg. Chem.* **2005**, *10*, 147–155.

(5) Chen, H.; Parkinson, J. A.; Morris, R. E.; Sadler, P. J. *J. Am. Chem. Soc.* **2003**, *125*, 173–186.

(6) Yan, Y. K.; Melchart, M.; Habtemariam, A.; Sadler, P. J. *Chem. Commun.* **2005**, 4764–4776.

for $\{(\eta^6\text{-arene})\text{Ru}(\text{en})\}^{2+}$ complexes.^{7b} Thus, we are attempting to design ruthenium arene compounds with a variety of potential DNA binding modes. Incorporation of two features into ruthenium arene complexes, which have been closely linked with the mode of action of the anticancer drug cisplatin, appeared particularly attractive. First, cisplatin has two reactive sites available and can bind to its target DNA in a bifunctional manner, forming intra- and interstrand cross-links on DNA.⁸ A similar profile of reactivity might be achievable for ruthenium arene complexes because coordination to two guanine bases has been demonstrated for the fragment $\{(\eta^6\text{-benzene})\text{Ru}\}^{2+}$.⁹ Second, the activity of platinum am(m)ine anticancer compounds appears to depend on the presence of hydrogen-bond-donating NH groups.¹⁰ Similarly, the critical role of coordinated ligands in Ru^{II} arene complexes in controlling and promoting interactions with DNA nucleobases has been demonstrated.^{5,7a,11} For example, in reactions with guanine, cytosine, adenine, and thymine nucleobase derivatives $\{(\eta^6\text{-arene})\text{Ru}(\text{en})\}^{2+}$ react exclusively with guanine derivatives.^{5,12} This site-selectivity appears to be controlled by the NH₂ groups of the en ligand, which can form strong hydrogen bonds with the C6O carbonyl group of guanine bases.¹³

Thus, the presence of an hydrogen-bond donor, for example, an amine group, may be an important feature in the design of bifunctional Ru^{II} arene complexes to observe, for example, interstrand cross-links on DNA. Reports in the literature suggest that coordinated monodentate NH₂R ligands in $[(\eta^6\text{-}p\text{-cymene})\text{Ru}(\text{NH}_2\text{CMe}_3)\text{Cl}_2]$ and $[(\eta^6\text{-arene})\text{Ru}(\text{L-alaMe})\text{Cl}_2]$ complexes, where L-alaMe = L-alanine methyl ester, can undergo substitution reactions,^{14,15} and complexes such as $[(\eta^6\text{-mesitylene})\text{Ru}(\text{NHR}_2)\text{Cl}_2]$, where R = Et or Bu, decompose in solution.¹⁶ For potential anticancer applications, the chemistry of such complexes might be difficult to predict or control. Stabilization of amine coordination to the ruthenium center can be achieved via chelation. Here, we consider the incorporation of a chelated amine group via a

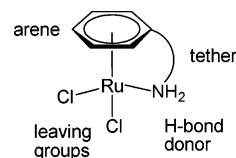


Figure 1. General features of amino-tethered di-chlorido Ru^{II} arene complexes, illustrating the features that might be important for biochemical reactivity.

tether to the arene to give a bifunctional Ru^{II} arene complex (Figure 1).

Research on tethered Ru^{II} arene complexes has received increasing attention over the past few years, mainly due to potential applications in catalysis.¹⁷ Most of the documented examples are bifunctional complexes containing monodentate phosphine ligands and two chloride ligands.¹⁸ Ru^{II} arene complexes containing sulfur¹⁹ and oxygen²⁰ tethers are also known. At the start of these studies, nitrogen tethers in Ru^{II} arenes had received very little attention. Reported examples include compounds with two²¹ or three²² tethering side-arms, complexes with amine tethers, where either one or both remaining coordination sites on ruthenium are occupied by phosphine ligands or 2,2'-bipyridine respectively,^{20,23} and complexes with nitrogen-containing tethered chelating ligands (e.g., $[(\eta^6\text{-C}_6\text{H}_5(\text{CH}_2)_3\text{NH}(1\text{S},2\text{S-CHC}_6\text{H}_5)_2\text{NSO}_2\text{C}_6\text{H}_4\text{CH}_3\text{-}N,N)\text{RuCl}]$) for use in catalysis.²⁴ Tethered complexes have mainly been studied in organic solvents.^{17a-c,25} In contrast, the emphasis in the present investigations into potential

- (7) (a) Fernández, R.; Melchart, M.; Habtemariam, A.; Parsons, S.; Sadler, P. J. *Chem.—Eur. J.* **2004**, *10*, 5173–5179. (b) Wang, F.; Habtemariam, A.; van der Geer, E. P. L.; Fernández, R.; Melchart, M.; Deeth, R. J.; Aird, R.; Guichard, S.; Fabbiani, F. P. A.; Lozano-Casal, P.; Oswald, I. D. H.; Jodrell, D. I.; Parsons, S.; Sadler, P. J. *Proc. Natl. Acad. Sci. U.S.A.* **2005**, *102*, 18269–18274. (c) Dougan, S. J.; Melchart, M.; Habtemariam, A.; Parsons, S.; Sadler, P. J. *Inorg. Chem.* **2006**, *45*, 10882–10894.
- (8) (a) Jamieson, E. R.; Lippard, S. J. *Chem. Rev.* **1999**, *99*, 2467–2498. (b) Brabec, V.; Kasparkova, J. *Metal Compounds in Cancer Chemotherapy* **2005**, 187–218. (c) Wang, D.; Lippard, S. J. *Nature Rev. Drug Discovery* **2005**, *4*, 307–320.
- (9) Korn, S.; Sheldrick, W. S. *J. Chem. Soc., Dalton Trans.* **1997**, 2191–2199.
- (10) Reedijk, J. *Chem. Rev.* **1999**, *99*, 2499–2510.
- (11) Melchart, M.; Habtemariam, A.; Parsons, S.; Moggach, S. A.; Sadler, P. J. *Inorg. Chim. Acta* **2006**, *359*, 3020–3028.
- (12) Morris, R. E.; Aird, R. E.; Murdoch, P. del S.; Chen, H.; Cummings, J.; Hughes, N. D.; Parsons, S.; Parkin, A.; Boyd, G.; Jodrell, D. I.; Sadler, P. J. *J. Med. Chem.* **2001**, *44*, 3616–3621.
- (13) Chen, H.; Parkin, J. A.; Parsons, S.; Coxall, R. A.; Gould, R. O.; Sadler, P. J. *J. Am. Chem. Soc.* **2002**, *124*, 3064–3082.
- (14) Sheldrick, W. S.; Heeb, S. *Inorg. Chim. Acta* **1990**, *168*, 93–100.
- (15) Bates, R. S.; Begley, M. J.; Wright, A. H.; *Polyhedron* **1990**, *9*, 1113–1118.
- (16) Carter, L.; Davies, D. L.; Fawcett, J.; Russell, D. R. *Polyhedron* **1993**, *12*, 1123–1128.

- (17) (a) Fürstner, A.; Liebl, M.; Lehmann, C. W.; Picquet, M.; Kunz, R.; Bruneau, C.; Touchard, D.; Dixneuf, P. H. *Chem.—Eur. J.* **2000**, *6*, 1847–1857. (b) Jan, D.; Delaude, L.; Simal, F.; Demonceau, A.; Noels, A. F. *J. Organomet. Chem.* **2000**, *606*, 55–64. (c) Çetinkaya, B.; Demir, S.; Özdemir, I.; Toupet, L.; Esmeril, D.; Bruneau, C.; Dixneuf, P. H. *Chem.—Eur. J.* **2003**, *9*, 2323–2330. (d) Simal, F.; Jan, D.; Demonceau, A.; Noels, A. F. *Tetrahedron Lett.* **1999**, *40*, 1653–1656. (e) Umezawa-Vizzini, K.; Lee, T. R. *Organometallics* **2003**, *22*, 3066–3076. (f) Miyaki, Y.; Onishi, T.; Ogoshi, S.; Kurosawa, H. *J. Organomet. Chem.* **2000**, *616*, 135–139.
- (18) (a) Therrien, B.; Ward, T. R.; Pilkington, M.; Hoffmann, C.; Gilardoni, F.; Weber, J. *Organometallics* **1998**, *17*, 330–337. (b) Smith, P. D.; Wright, A. H. *J. Organomet. Chem.* **1998**, *559*, 141–147. (c) Bennett, M. A.; Edwards, A. J.; Harper, J. R.; Khimyak, T.; Willis, A. C. *J. Organomet. Chem.* **2001**, *629*, 7–18. (d) Nelson, J. H.; Ghebreyessus, K. Y.; Cook, V. C. *Organometallics* **2002**, *21*, 1727–1733. (e) Jung, S.; Ilg, K.; Brandt, C. D.; Wolf, J.; Werner, H. *J. Chem. Soc., Dalton Trans.* **2002**, 318–327. (f) Umezawa-Vizzini, K.; Guzman-Jimenez, I. Y.; Whitmire, K. H.; Lee, T. R. *Organometallics* **2003**, *22*, 3059–3065.
- (19) Bennett, M. A.; Goh, L. Y.; Willis, A. C. *J. Am. Chem. Soc.* **1996**, *118*, 4984–4992.
- (20) (a) Miyaki, Y.; Onishi, T.; Kurosawa, H. *Inorg. Chim. Acta* **2000**, *300*–302, 369–377. (b) Soleimannejad, J.; Sisson, A.; White, C. *Inorg. Chim. Acta* **2003**, *352*, 121–128. (c) Kitaura, R.; Miyaki, Y.; Onishi, T.; Kurosawa, H. *Inorg. Chim. Acta* **2002**, *334*, 142–148. (d) Eubril, J.; Hartenbach, I.; Schleid, T.; Winter, R. F. *Z. Anorg. Allg. Chem.* **2006**, *632*, 400–408.
- (21) (a) Therrien, B.; Ward, T. R. *Angew. Chem. Int. Ed.* **1999**, *38*, 405–408. (b) Therrien, B.; König, A.; Ward, T. R. *Organometallics* **1999**, *18*, 1565–1568.
- (22) (a) Hartshorn, C. M.; Steel, P. J. *Aust. J. Chem.* **1995**, *48*, 1587–1599. (b) Hartshorn, C. M.; Steel, P. J. *Angew. Chem., Int. Ed. Engl.* **1996**, *35*, 2655–2657. (c) Sun, W. Y.; Xie, J.; Okamura, T.; Huang, C. K.; Ueyama, N. *Chem. Commun.* **2000**, 1429–1430.
- (23) Sclaro, C.; Geldbach, T. J.; Rochat, S.; Dorcier, A.; Gossens, C.; Bergamo, A.; Cocchiello, M.; Tavernelli, I.; Sava, G.; Rothlisberger, U.; Dyson, P. J. *Organometallics* **2006**, *25*, 756–765.
- (24) (a) Cheung, F. K.; Hayes, A. M.; Hannedouche, J.; Yim, A. S. Y.; Wills, M. J. *Org. Chem.* **2005**, *70*, 3188–3197. (b) Hayes, A. M.; Morris, D. J.; Clarkson, G. J.; Wills, M. J. *Am. Chem. Soc.* **2005**, *127*, 7318–7319.

bifunctional amine-tethered ruthenium arene complexes for anticancer applications is on studies in aqueous media.

In this article, we describe the synthesis and characterization, both in solution and in the solid state, of water-soluble bifunctional amine-tethered Ru^{II} arene complexes.²⁶ We have studied their hydrolysis behavior and have investigated their interactions with the DNA model base 9-ethylguanine (9EtG), both in solution and by X-ray crystallography. The studies are complemented by biophysical experiments using plasmid DNA, and the data are discussed in relation to the observed lack of biological activity.

Experimental Section

Materials. The ruthenium dimer precursor $[(\eta^6\text{-etb})\text{RuCl}_2]_2$, where etb = ethyl benzoate, was prepared according to a previously published route (also, see Supporting Information).^{18a} Most reagents were obtained from Aldrich, including D₂O (99.9%) and CDCl₃ (99.8%). Nucleobase derivatives were acquired from Sigma Aldrich. Most solvents, as well as silver nitrate and sodium chloride, were supplied by Fisher. Ethanol was dried over Mg/I₂. 1,4-Dioxane was supplied by Rathburn, 1,2-dichloroethane was obtained from both Prolabo and Aldrich, and RuCl₃·xH₂O from Alfa Aesar. *cis*-Diamminedichloridoplatinum(II) (cisplatin) and *trans*-diamminedichloridoplatinum(II) (transplatin) were purchased from Sigma (Prague). Chlorodiethylenetriamineplatinum(II) chloride, [Pt(dien)Cl]Cl, was a kind gift of Professor Giovanni Natile from the University of Bari.

Stock solutions (5×10^{-4} M) of **3** and platinum complexes for use in DNA studies were prepared in the dark at 298 K. Calf thymus (CT) DNA (42% guanine + cytosine, mean molecular mass ca. 2×10^7) was also prepared and characterized as described previously.^{27,28} Plasmids pSP73KB and pSP73 (2455 and 2464 bp, respectively)²⁹ were isolated according to standard procedures and banded twice in CsCl/EtBr equilibrium density gradients. Restriction endonucleases were purchased from New England Biolabs (Beverly, MA). Riboprobe Gemini System II for transcription mapping containing SP6 and T7 RNA polymerases was purchased from Promega (Madison, WI). Ethidium bromide (EtBr) and agarose were from Merck KgaA (Darmstadt, Germany). The radioactive products were obtained from Amersham (Arlington Heights, IL).

Preparations. $[(\eta^6\text{-}\eta^1\text{-C}_6\text{H}_5(\text{CH}_2)_3\text{NH}_2)\text{RuCl}_2]_2$ (**1**). $[(\eta^6\text{-etb})\text{RuCl}_2]_2$ (372.4 mg, 0.58 mmol) and 3-phenyl-1-propylamine (148.5 mg, 1.10 mmol) were dissolved in 1,2-dichloroethane (50 mL). A few drops of THF were added, the solution was stirred for 60 min, and then was heated to reflux for 90 h under argon. The solvent was removed on a rotary evaporator, and the product was extracted with methanol, which was concentrated on a rotary evaporator until precipitation of the product occurred. Diethyl ether was added, and the solution was stored at 253 K overnight. The yellow-orange microcrystalline solid (129.2 mg, 0.42 mmol, 42.1% yield) was collected by filtration, washed with diethyl ether, and dried in air. ¹H NMR (CDCl₃): δ 5.88 (t, 2H, *J* = 6 Hz), 5.73 (t, 1H, *J* = 6 Hz), 5.16 (d, 2H, *J* = 6 Hz), 3.22 (b, 2H), 2.95 (m, 2H, *J* = 5.5

Hz), 2.49 (t, 2H, *J* = 6 Hz), 2.20 (m, 2H). Elemental analysis: Calcd for C₉H₁₃NRuCl₂: C, 35.19; H, 4.27; N, 4.56. Found: C, 35.45; H, 3.85; N, 4.51. Crystals of **1**, suitable for X-ray diffraction, were obtained from a methanol solution at 253 K.

$[(\eta^6\text{-}\eta^1\text{-C}_6\text{H}_5(\text{CH}_2)_2\text{NH}_2)\text{RuCl}_2]_2$ (**2**). $[(\eta^6\text{-etb})\text{RuCl}_2]_2$ (420.5 mg, 0.65 mmol) and 2-phenethylamine (150.0 mg, 1.24 mmol) were dissolved in 1,2-dichloroethane (50 mL). A few drops of THF were added, the solution was stirred for 60 min, and then was heated to reflux for 41 h under argon. The solvent was removed on a rotary evaporator, and the product was extracted with methanol, which was concentrated on a rotary evaporator until precipitation occurred. Diethyl ether was added, and the solution was stored at 253 K for 2 d. The orange microcrystalline solid (182.8 mg, 0.62 mmol, 50.4% yield) was collected by filtration, washed with diethyl ether, and dried in air. ¹H NMR (CDCl₃): δ 5.94 (t, 2H, *J* = 5.5 Hz), 5.53 (t, 1H, *J* = 5.5 Hz), 5.22 (d, 2H, *J* = 5.5 Hz), 3.90 (m, 2H, *J* = 5.5 Hz), 3.60 (b, 2H), 2.84 (m, 2H, *J* = 6.5 Hz). Elemental analysis: Calcd for C₈H₁₁NRuCl₂: C, 32.78; H, 3.78; N, 4.78. Found: C, 33.08; H, 3.83; N, 4.76. Crystals of **2**, suitable for X-ray diffraction, were grown from water, after the addition of NaCl, at ambient temperature.

$[(\eta^6\text{-}\eta^1\text{-C}_6\text{H}_5(\text{CH}_2)_3\text{NH}_2)\text{Ru}(\text{NO}_3)_2]$ (**3**). Complex **1** (110.3 mg, 0.36 mmol) and silver nitrate (121.9 mg, 0.72 mmol) were dissolved in water (25 mL), and the solution was stirred for 150 min. After filtration, the solvent was removed on a rotary evaporator, and the product was extracted with water. Filtration and removal of the solvent on a rotary evaporator yielded an orange powder (121.5 mg, 0.34 mmol, 93.9% yield), which was collected by filtration, washed with diethyl ether, and dried in air. ¹H NMR (90% H₂O/10% D₂O, pH 4.10): δ 6.07 – 6.02 (m, 3H), 5.43 (d, 2H, *J* = 6 Hz), 3.96 (b, 2H), 2.97 (m, 2H), 2.57 (t, 2H, *J* = 6 Hz), 2.30 (m, 2H). X-ray diffraction quality crystals of **3** were obtained by slow diffusion of diethyl ether into an acetone solution of **3** at ambient temperature.

$[(\eta^6\text{-}\eta^1\text{-C}_6\text{H}_5(\text{CH}_2)_3\text{NH}_2)\text{Ru}(\text{9EtG})_2](\text{NO}_3)_{0.25}(\text{PF}_6)_{1.75}$ (**7**). **3** (43.8 mg, 122 μ mol) and 9EtG (47.2 mg, 264 μ mol) were dissolved in methanol (15 mL), and the mixture was stirred for 20 h. The solution was concentrated to ca. 5 mL on a rotary evaporator and heated to dissolve the greenish precipitate. Addition of NH₄PF₆ (177.5 mg, 1.09 mmol) was followed by addition of diethyl ether, which led to the formation of a greenish precipitate, and the solution was stored at ambient temperature overnight. The light-green powder (98.1 mg) was collected by filtration, washed with diethyl ether, and dried in air. ¹H NMR (D₂O, pH meter reading pH* 6.56): δ 8.25 (s, 1H), 5.88 (t, 2H, *J* = 6 Hz), 5.81 (t, 1H, *J* = 6 Hz), 5.79 (d, 2H, *J* = 6 Hz), 5.42 (m, 1H), 4.17–4.03 (m, 4H), 2.73 (m, 2H), 2.65 (m, 2H), 2.32 (m, 2H), 1.33 (t, 3H, *J* = 7 Hz). Crystals of $[(\eta^6\text{-}\eta^1\text{-C}_6\text{H}_5(\text{CH}_2)_3\text{NH}_2)\text{Ru}(\text{9EtG})_2](\text{NO}_3)_2$ (**6A**), which diffracted poorly, were grown by slow evaporation of an acetone solution containing **7** at ambient temperature. Elemental analysis: Calcd for C₂₃H₃₁N_{11.25}O_{2.75}RuP_{1.75}F_{10.5}: C, 31.98; H, 3.62; N, 18.24. Found: C, 31.94; H, 3.57; N, 18.55.

$[(\eta^6\text{-}\eta^1\text{-C}_6\text{H}_5(\text{CH}_2)_3\text{NH}_2)\text{Ru}(\text{9EtG})_2](\text{CF}_3\text{SO}_3)_2$ (**8**). **1** (37.9 mg, 123 μ mol) and 9EtG (51.4 mg, 287 μ mol) were dissolved in methanol (25 mL), and the mixture was stirred for 22 h. The solution was concentrated to ca. 10 mL on a rotary evaporator and NaCF₃SO₃ (176.3 mg, 1.02 mmol) was added. The solvent was removed on a rotary evaporator, and the product was extracted with acetone. The solution was filtered, the solvent was removed on a rotary evaporator, and a yellow-green powder (228.4 mg) was collected, washed with diethyl ether, and dried in air. The powder was washed with a minimal amount of ethanol to dissolve the excess NaCF₃SO₃. The solution was filtered, and the yellow powder was

- (25) (a) Faller, J. W.; D'Allesio, D. G. *Organometallics* **2003**, *22*, 2749–2757. (b) Faller, J. W.; Fontaine, P. P. *Organometallics* **2005**, *24*, 4132–4138.
 (26) Presented in part at the First European Conference on Chemistry for Life Sciences, Rimini, Italy, 4–8 October, 2005. Abstract p 148.
 (27) Brabec, V.; Palecek, E. *Biophysik* **1970**, *6*, 290–300.
 (28) Brabec, V.; Palecek, E. *Biophys. Chem.* **1976**, *4*, 76–92.
 (29) Lemaire, M. A.; Schwartz, A.; Rahmouni, A. R.; Leng, M. *Proc. Natl. Acad. Sci. U.S.A.* **1991**, *88*, 1982–1985.

then washed with diethyl ether. X-ray diffraction quality crystals were obtained as **8**·H₂O by diffusion of diethyl ether into an acetone solution of **8** at ambient temperature.

Methods and Instrumentation. (a) X-ray Crystallography. All of the diffraction data were collected using a Bruker Smart Apex CCD diffractometer equipped with an Oxford Cryosystems low-temperature device operating at 150 K. Absorption corrections for all of the data sets were performed with the multiscan procedure SADABS.³⁰ Structures were solved using direct methods (*SHELXS*³¹ or *SIR92*³²) or Patterson methods (*DIREDF*).³³ Complexes were refined against *F*² using *CRYSTALS*³⁴ (**1** and **4**) or *SHELXL* (**2** and **3**).³⁵ Hydrogen atoms were placed in idealized positions. The crystal of **1** was twinned via a 2-fold rotation about the [100] direct lattice direction; the twin scale factor was 0.477(5). The tether is also disordered over two conformations. The structure is very close to being in *Pnma*; however, reflections that would have been absent for the *n* and 2₁ symmetry elements were clearly stronger than the absences corresponding to the genuine glide. In **2**, one carbon atom of the tether is disordered about a crystallographic mirror plane. In **4**, one terminal methyl group of one of the 9EtG ligands is disordered over two positions. Disordered acetone of crystallization was treated with the van der Sluis–Spek procedure.³⁶ X-ray crystallographic data for complexes **1–4** are available in the Supporting Information and have been deposited in the CCDC under accession numbers 639637–639640, respectively.

(b) NMR Spectroscopy. ¹H NMR spectra were acquired for samples in 5 mm NMR tubes at 298 K (unless stated otherwise) on either a Bruker DMX 500 or a Bruker AVA 600 NMR spectrometer, using TBI [¹H, ¹³C, X] or TXI [¹H, ¹³C, X] probeheads equipped with *z*-field gradients. All of the data processing was carried out using *XWIN-NMR* version 3.6 (Bruker U.K. Ltd.). ¹H NMR chemical shifts were internally referenced to TSP or TMS via 1,4-dioxane (3.75 ppm) or CHCl₃ (7.27 ppm).

1D and 2D spectra were recorded using standard pulse sequences, which were modified by Dr. Dusan Uhrin and Mr. Juraj Bella, at the University of Edinburgh. Water signals were suppressed using Presaturation or Shaka methods.³⁷

In time-course ¹H NMR experiments, the time of dissolution of the reactants, or when solutions of all of the reactants were mixed, is taken as *t* = 0 min.

(c) pH Measurements. The pH values of NMR solutions were measured at ambient temperature directly in the NMR tube, before and after recording NMR spectra, using a Corning 145 pH meter equipped with an Aldrich micro combination electrode calibrated with Aldrich buffer solutions at pH 4, 7, and 10. The pH values

were adjusted with dilute HClO₄ and NaOH. No correction has been applied for the effect of deuterium on the glass electrode. For measurements in D₂O, pH* = pH meter reading of the solution.

(d) CHN Analysis. CHN elemental analysis was performed by the CHN service at the University of St Andrews.

(e) Chloride Titrations. Chloride was added to the NMR samples as aliquots of a 3 M solution of sodium chloride. [Cl[−]]_t refers to the concentration of total chloride in solution. The amount of bound chloride was calculated from the relative proportions of the signals for the di-chlorido, the mono-aqua and the di-aqua species by integration. Hydrolysis equilibrium constants were calculated using the following equations. *K*₁ = ([Ru(Cl)H₂O] * [Cl[−]]_f)/[RuCl₂] and *K*₂ = ([Ru(H₂O)₂] * [Cl[−]]_f)/[Ru(Cl)H₂O], where [Cl[−]]_f = the concentration of free chloride in solution.

(f) Time-Course of Reactions with 9EtG. All of the experiments were carried out in 90% H₂O/10% D₂O at 298 K, unless stated otherwise. Reactants were added to 5 mm NMR tubes, which contained 600 μL of a 2.2 mM solution of 9EtG and 5 μL of a 1% solution of 1,4-dioxane.

[(^η⁶:^η¹-C₆H₅(CH₂)₃NH₂)Ru(NO₃)₂] (**3**). A 58.4 μL aliquot of a 12.9 mM solution of **3** was added to the NMR tube, and the pH of the solution was measured (5.19). ¹H NMR spectra were recorded at *t* = 24 min, *t* = 46 min, and then every 20 min from *t* = 46 min for a period of 16.5 h. The pH of the solution after 16.5 h was 6.22.

[(^η⁶:^η¹-C₆H₅(CH₂)₃NH₂)RuCl₂] (**1**) in the presence of chloride ([Cl[−]]_t = 21.7 mM). A 4.4 μL aliquot of a 3 M solution of NaCl was added to the NMR tube, followed by 58.4 μL of a 11.3 mM solution of **1**, and the pH of the solution was measured (6.08). ¹H NMR spectra were recorded at *t* = 45 min, and five times between *t* = 45–134 min, and then every 30 min from *t* = 134 min for a period of 18 h. The pH of the solution after 18 h was 6.53.

[(^η⁶:^η¹-C₆H₅(CH₂)₂NH₂)RuCl₂] (**2**) in the presence of chloride ([Cl[−]]_t = 21.7 mM). A 4.4 μL aliquot of a 3 M solution of NaCl was added to the NMR tube, followed by 58.4 μL of a 11.3 mM solution of **2**, and the pH of the solution was measured (6.08). ¹H NMR spectra were recorded at *t* = 32 min, *t* = 53 min, and then every 30 min from *t* = 123 min for a period of 41 h. The pH of the solution after 41 h was 6.23.

Hydrolysis of [(^η⁶:^η¹-C₆H₅(CH₂)₃NH₂)Ru(9EtG)₂]²⁺. The ¹H NMR spectrum of a solution of [(^η⁶:^η¹-C₆H₅(CH₂)₃NH₂)Ru(9EtG)₂](NO₃)_{0.25}(PF₆)_{1.75} (**7**) (3.0 mM) in D₂O at pH* 6.67 was recorded at *t* = 10 min, *t* = 19 min, and then every 20 min from *t* = 42 min for a period of 20 h. The pH* of the solution after 20 h was 6.02.

(g) DNA Metalation Reactions. Solutions of double-helical CT DNA and plasmid DNA at a concentration of 0.1 mg/mL were incubated with **3** or platinum complex in 10 mM NaClO₄ (pH ~6) at 310 K for 24 h in the dark, at the *r*₁ value of 0.1 (*r*₁ is defined as the molar ratio of metal complex to nucleotide phosphates at the onset of incubation with DNA). At various time intervals, an aliquot of the reaction mixture was withdrawn, quickly cooled on an ice bath, precipitated by ethanol, and the content of ruthenium (or platinum) in the supernatant of these samples was determined by flameless atomic absorption spectrophotometry (FAAS), thus allowing determination of the number of atoms of the metal bound per nucleotide residue (*r*_b values).³⁸ The binding of the ruthenium compounds to CT DNA was also quantified in a different way. Aliquots of the reaction mixture withdrawn at various time intervals were quickly cooled on an ice bath and filtered using Sephadex G50 to remove free (unbound) ruthenium compound. The content

(30) Sheldrick, G. M. *SADABS Version 2006-1*; University of Göttingen, Göttingen, Germany, 2006.

(31) Sheldrick, G. M. *SHELXS-97*, University of Göttingen, Göttingen, Germany, 1997.

(32) Altomare, A.; Cascarano, G.; Giacovazzo, C.; Guagliardi, A.; Burla, M. C.; Polidori, G.; Camalli, M. *SIR92: A Program for Automatic Solution of Crystal Structures by Direct Methods*, *J. Appl. Cryst.* **1994**, *27*, 435–435.

(33) Beurskens, P. T.; Beurskens, G.; Bosman, W. P.; de Gelder, R.; Garcia-Granda, S.; Gould, R. O.; Israel, R.; Smits, J. M. M. *The DIREDF96 Program System*, University of Nijmegen: Nijmegen, The Netherlands, 1996.

(34) Betteridge, P. W.; Carruthers, J. R.; Cooper, R. I.; Prout, K.; Watkin, D. J. *CRYSTALS*, version 12: software for guided crystal structure analysis, *J. Appl. Cryst.* **2003**, *36*, 1487.

(35) Sheldrick, G. M. *SHELXL-97*, University of Göttingen: Göttingen, Germany, 1997.

(36) van der Sluis, P.; Spek, A. L. *BYPASS: An Effective Method for the Refinement of Crystal Structures Containing Disordered Solvent Regions*, *Acta Crystallographica, Section A* **1990**, *46*, 194–201.

(37) Hwang, T. L.; Shaka, A. J. *J. Magn. Reson. Series A* **1995**, *112*, 275–279.

(38) Malina, J.; Novakova, O.; Keppler, B. K.; Alessio, E.; Brabec, V. *J. Biol. Inorg. Chem.* **2001**, *6*, 435–445.

of ruthenium in these DNA samples was determined by FAAS. Results identical to those obtained using the assay based on DNA precipitation by ethanol were obtained.

(h) DNA Transcription by RNA Polymerase In Vitro. Transcription of the (*NdeI/HpaI*) restriction fragment of pSP73KB DNA with T7 RNA polymerase and electrophoretic analysis of transcripts were performed according to the protocols recommended by Promega (Promega Protocols and Applications, 43–46 (1989/90) and previously described in detail.^{29,39}

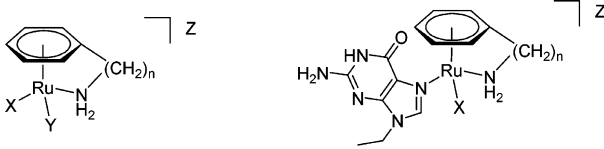
(i) DNA Interstrand Crosslinking Assay. Complex **3** or cisplatin were incubated with 1 μ g of pSP73 DNA linearized by *EcoRI* at various r_b values (0.001–0.01). The metalated samples were precipitated by ethanol and analyzed for DNA interstrand cross-links, in the same way as described recently.^{39,40} The linear duplexes were first 3'-end labeled using a Klenow fragment of DNA polymerase I in the presence of [α -³²P]dATP. The samples were deproteinized by phenol, precipitated by ethanol, and the pellet was dissolved in 18 μ L of a solution containing 30 mM NaOH, 1 mM EDTA, 6.6% sucrose, and 0.04% bromophenol blue. The amount of interstrand cross-links was analyzed by electrophoresis under denaturing conditions on an alkaline agarose gel (1%). After the electrophoresis was completed, the intensities of the bands corresponding to single strands of DNA and interstrand cross-linked duplex were quantified. The radioactivity associated with the individual bands in each lane was measured to obtain estimates of the fraction of noncross-linked or cross-linked DNA under each condition. The frequency of interstrand cross-links (%ICL per platinum) was calculated using the Poisson distribution from the fraction of noncross-linked DNA, in combination with the r_b values and the fragment size.

(j) Unwinding of Negatively Supercoiled DNA. Unwinding of closed circular supercoiled pSP73KB plasmid DNA was assayed by an agarose gel mobility shift assay.⁴¹ The unwinding angle μ induced per metal–DNA adduct was calculated upon the determination of the r_b value at which the complete transformation of the supercoiled to relaxed form of the plasmid was attained. Samples of pSP73KB plasmid were incubated with **3** or cisplatin in 10 mM NaClO₄ at 310 K in the dark for 24 h. All of the samples were precipitated by ethanol and redissolved in 10 mM NaClO₄. An aliquot of the precipitated sample was subjected to electrophoresis on 1% agarose gels, running at 298 K in the dark with TAE buffer (0.04 M tris-acetate + 1 mM EDTA, pH 7.0) with the voltage set at 30 V. The gels were then stained with EtBr, followed by photography on Polaroid 667 film with a transilluminator. The other aliquot was used for the determination of r_b values by FAAS.

(k) Other Methods. Absorption spectra were measured with a Beckmann DU-7400 spectrophotometer. FAAS measurements were carried out with a Varian AA240Z Zeeman atomic absorption spectrometer equipped with a GTA 120 graphite tube atomizer. The gels were visualized using a BAS 2500 FUJIFILM bioimaging analyzer, and the radioactivities associated with bands were quantitated with the AIDA image analyzer software (Raytest, Germany).

(l) Cytotoxicity. Complexes **1** and **2** were tested against the A2780 human ovarian cancer cell line, according to a previously published protocol.³

Chart 1. Tethered Ruthenium Arene Complexes Studied in This Work



	n	X	Y	Z		n	X	Z
1	3	Cl	Cl		4	3	Cl	Cl
1A	3	Cl	H ₂ O	Cl	4A	3	H ₂ O	2Cl
1B	3	H ₂ O	H ₂ O	2Cl	4B	3	9EtG	2Cl
2	2	Cl	Cl		5	2	Cl	Cl
2A	2	Cl	H ₂ O	Cl	5A	2	H ₂ O	2Cl
2B	2	H ₂ O	H ₂ O	2Cl	5B	2	9EtG	2Cl
3	3	NO ₃	NO ₃		6	3	H ₂ O	2NO ₃
3A	3	H ₂ O	H ₂ O	2NO ₃	6A	3	9EtG	2NO ₃
					7	3	9EtG	(NO ₃) _{0.25} (PF ₆) _{1.75}
					7A		H ₂ O	(NO ₃) _{0.25} (PF ₆) _{1.75}
					8	3	9EtG	2CF ₃ SO ₃

Results

Synthesis and Characterization. The precursor diene ethyl-1,4-cyclohexadiene-3-carboxylate for the synthesis of ruthenium dimer $[(\eta^6\text{-etb})\text{RuCl}_2]_2$ was synthesized via the Birch reduction of benzoic acid, followed by esterification, because the direct reduction of ethyl benzoate⁴² gave rise to mainly benzoic acid under the reported conditions (Chart S1).

The syntheses of $[(\eta^6:\eta^1\text{-C}_6\text{H}_5(\text{CH}_2)_3\text{NH}_2)\text{RuCl}_2]$ (**1**) and $[(\eta^6:\eta^1\text{-C}_6\text{H}_5(\text{CH}_2)_2\text{NH}_2)\text{RuCl}_2]$ (**2**) (Chart 1) were based on the route employed by Ward et al.^{18a} and involve the thermal displacement of ethyl benzoate (etb) from $[(\eta^6\text{-etb})\text{RuCl}_2]_2$ by the appropriate nitrogen-donor derivative (Chart S2). Reactions of $[(\eta^6\text{-etb})\text{RuCl}_2]_2$ with either 3-phenyl-1-propylamine or 2-phenethylamine in 1,2-dichloroethane heated under reflux and an argon atmosphere resulted in **1** and **2**, respectively, with satisfactory yields and purity.

The complexes were characterized by CHN elemental analysis and ¹H NMR spectroscopy. The arene ¹H NMR signals (triplet, triplet, doublet in a 2:1:2 ratio) for the amine-tethered complexes **1** and **2** are shifted to high field by ca. 1.4–2.0 ppm compared to those of the respective free ligands. The signals for the bound NH₂ groups are shifted to low field by 1.9–2.2 ppm compared to the free ligand. The chemical shifts of the CH₂ groups of the tether are also shifted by coordination to ruthenium by as much as 0.9 ppm to low field for the CH₂ group adjacent to the amine in **2**. For **1**, the shift changes for the tether CH₂ peaks range from 0.2 ppm to high field to 0.4 ppm to low field upon the coordination of the tether. Assignment of the CH₂ peaks was aided by the coupling of the CH₂ protons to the amine protons. This was not observed for the free ligands. The assignment of peaks was confirmed for complex **1** by a 2D NOESY spectrum (Figure S1).

The synthesis of di-aqua complex $[(\eta^6:\eta^1\text{-C}_6\text{H}_5(\text{CH}_2)_3\text{NH}_2)\text{Ru}(\text{H}_2\text{O})_2](\text{NO}_3)_2$ (**3A**) was attempted by abstraction of the chloride ligands from $[(\eta^6:\eta^1\text{-C}_6\text{H}_5(\text{CH}_2)_3\text{NH}_2)\text{RuCl}_2]$ (**1**) with silver nitrate in water. The complex, however, crystal-

(39) Brabec, V.; Leng, M. *Proc. Natl. Acad. Sci. U.S.A.* **1993**, *90*, 5345–5349.

(40) Farrell, N.; Qu, Y.; Feng, L.; Van Houten, B. *Biochemistry* **1990**, *29*, 9522–9531.

(41) Keck, M. V.; Lippard, S. J. *J. Am. Chem. Soc.* **1992**, *114*, 3386–3390.

(42) Rabideau, P. W.; Huser, D. L.; Nyikos, S. J. *Tetrahedron Lett.* **1980**, *21*, 1401–1404.

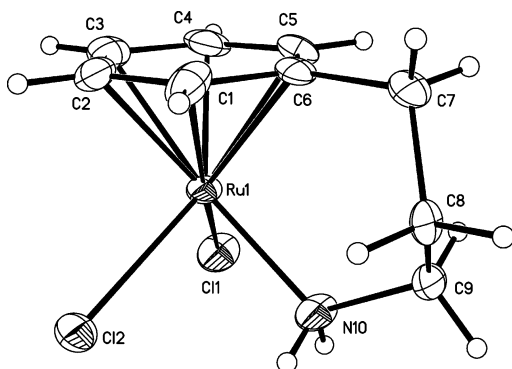


Figure 2. Ortep diagram (50% probability ellipsoids) and atom numbering scheme for the X-ray crystal structure of $[(\eta^6:\eta^1\text{-C}_6\text{H}_5(\text{CH}_2)_3\text{NH}_2)\text{RuCl}_2]$ (**1**). The tether is disordered, and the alternative conformation is shown in Figure S2.

lized as the dinitrato adduct $[(\eta^1:\eta^6\text{-C}_6\text{H}_5(\text{CH}_2)_3\text{NH}_2)\text{Ru}(\text{NO}_3)_2]$ (**3**) (vide infra) rather than as the nitrate salt of the di-aqua adduct.

The di-9EtG adduct $[(\eta^6:\eta^1\text{-C}_6\text{H}_5(\text{CH}_2)_3\text{NH}_2)\text{Ru}(\text{9EtG})_2](\text{NO}_3)_{0.25}(\text{PF}_6)_{1.75}$ (**7**) was synthesized by the reaction of complex **3** with 2.2 mol equiv of 9EtG. Addition of $\text{NH}_4\text{-PF}_6$ resulted in a complex with mixed counteranions according to CHN analysis. $[(\eta^6:\eta^1\text{-C}_6\text{H}_5(\text{CH}_2)_3\text{NH}_2)\text{Ru}(\text{9EtG})_2](\text{CF}_3\text{SO}_3)_2$ (**8**) was synthesized similarly to **7** starting from complex **1**.

X-ray Crystal Structures. In the structure of amine-tethered complex $[(\eta^6:\eta^1\text{-C}_6\text{H}_5(\text{CH}_2)_3\text{NH}_2)\text{RuCl}_2]$ (**1**), the three-carbon tether adopts two orientations due to disorder (Figures 2 and S2). The crystal data are shown in Table S1 and bond angles and lengths in Table S3. The Ru–Cl bond lengths are 2.425(3) and 2.437(3) Å, and the Ru–N distance is 2.129(5) Å. The Ru–C(arene) bond lengths in **1** are in the range of 2.161(9)–2.196(7) Å, and the Ru–centroid distance is 1.65 Å. The Ru–C6–C7 angle, where C6 is the arene carbon connected to the tether and C7 is the first carbon atom of the tether, is 127.17°. The angle between the plane defined by the arene carbons and that containing C6, Ru, and N is 88.77°.

Complex $[(\eta^6:\eta^1\text{-C}_6\text{H}_5(\text{CH}_2)_2\text{NH}_2)\text{RuCl}_2]$ (**2**), which contains two carbon atoms in the tether backbone, crystallized with the tether disordered over two positions, similar to **1**, and contains a mirror plane through atoms C4, C1, C5, Ru, and N1 (Figures 3 and S3). The crystal data are shown in Table S1 and bond angles and lengths in Table S4. The Ru–Cl bond lengths are 2.4133(7) Å, and the Ru–N distance is 2.117(3) Å. The Ru–C(arene) bond lengths are in the range of 2.095(3)–2.199(4) Å, and the Ru–centroid distance is 1.63 Å. The arene carbon C4 (to which the tether is connected) is displaced toward the ruthenium center by 0.0733 Å, with respect to the plane defined by carbon atoms C2 and C3, whereas the opposite carbon C1 is the furthest away from the metal (by 0.0066 Å, with respect to the plane defined by carbon atoms C2 and C3) resulting in buckling of the arene ring. The Ru–C4–C5 angle, where C5 is the first carbon atom of the tether, is 114.74°. The angle between the plane defined by the arene carbons and that containing C4, Ru, and N is 90.00°.

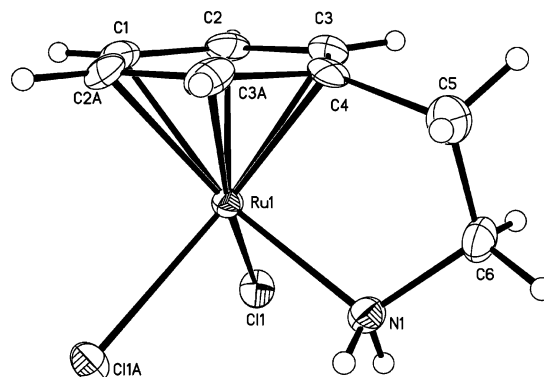


Figure 3. Ortep diagram (50% probability ellipsoids) and atom numbering scheme for the X-ray crystal structure of $[(\eta^6:\eta^1\text{-C}_6\text{H}_5(\text{CH}_2)_2\text{NH}_2)\text{RuCl}_2]$ (**2**). The tether is disordered, and the alternative conformation is shown in Figure S3.

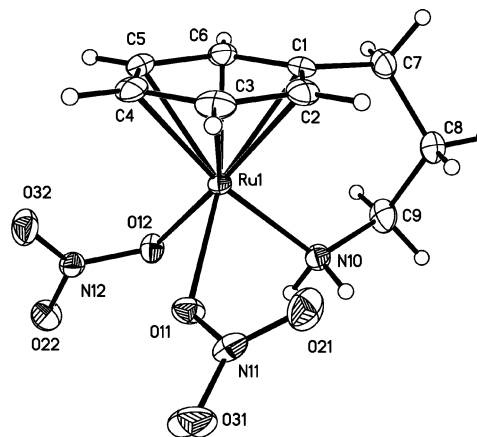


Figure 4. Ortep diagram (50% probability ellipsoids) and atom numbering scheme for the X-ray crystal structure of $[(\eta^6:\eta^1\text{-C}_6\text{H}_5(\text{CH}_2)_3\text{NH}_2)\text{Ru}(\text{NO}_3)_2]$ (**3**).

The X-ray crystal structure of $[(\eta^1:\eta^6\text{-C}_6\text{H}_5(\text{CH}_2)_3\text{NH}_2)\text{Ru}(\text{NO}_3)_2]$ (**3**) is shown in Figure 4, and the crystal data are listed in Table S2 and bond angles and lengths in Table S5. The Ru–O bond lengths are 2.1172(10) and 2.1250(10) Å, and the Ru–N distance is 2.1241(13) Å. The Ru–C(arene) bond lengths are in the range of 2.1697(15)–2.1986(17) Å, and the Ru–centroid distance is 1.66 Å. Strong hydrogen bonds between the amine protons and oxygen atoms of the nitrate ligands result in the formation of dimers (Figure S4). The angle between the plane defined by the arene carbons and that containing C1 (to which the tether is connected) Ru, and N(tether) is 83.96°.

The X-ray crystal structure of $[(\eta^6:\eta^1\text{-C}_6\text{H}_5(\text{CH}_2)_3\text{NH}_2)\text{Ru}(\text{9EtG})_2](\text{NO}_3)_2$ (**6A**), obtained from an acetone solution containing $[(\eta^6:\eta^1\text{-C}_6\text{H}_5(\text{CH}_2)_3\text{NH}_2)\text{Ru}(\text{9EtG})_2](\text{NO}_3)_{0.25}(\text{PF}_6)_{1.75}$ (**7**), was not fully refined because the crystals were of poor quality (Figure S5). However, good quality crystals of the triflate salt $[(\eta^6:\eta^1\text{-C}_6\text{H}_5(\text{CH}_2)_3\text{NH}_2)\text{Ru}(\text{9EtG})_2](\text{CF}_3\text{SO}_3)_2\cdot\text{H}_2\text{O}$ (**8**· H_2O) were obtained. The structure is shown in Figure 5, and the crystal data are listed in Table S2 and bond angles and lengths in Table 1. The Ru–N(tether) bond length is 2.121(2) Å, and the Ru–N(9EtG) distances are 2.101(2) and 2.1588(18) Å, respectively. The Ru–C(arene) bond lengths are between 2.165(2)–2.232(3) Å, and the Ru–centroid distance is 1.67 Å. The angle between the plane

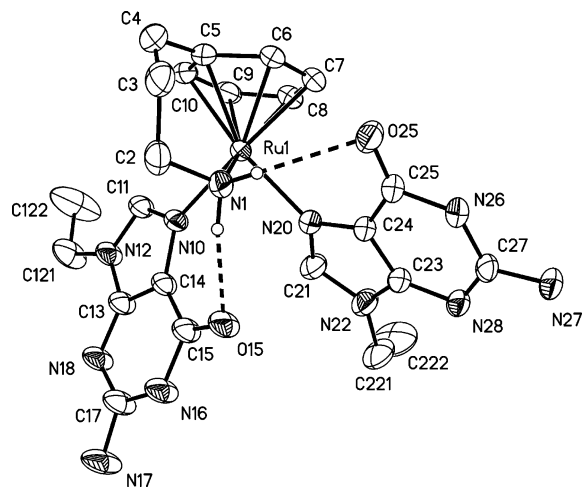


Figure 5. Ortep diagram (50% probability ellipsoids) and atom numbering scheme for the cation in the X-ray crystal structure of $[(\eta^7\text{-}1\text{-C}_6\text{H}_5(\text{CH}_2)_3\text{-NH}_2)\text{Ru}(\text{9EtG})_2](\text{CF}_3\text{SO}_3)_2\cdot\text{H}_2\text{O}$ (**8**·H₂O). The hydrogen atoms, with the exception of the tether NH₂ protons, have been omitted for clarity. Both of the tether amine protons show intramolecular hydrogen bonds with the carbonyl groups of the two 9EtG ligands, where H11...O15 = 1.98 Å (N1...O15 = 2.869(3) Å) and H12...O25 = 2.32 Å (N1...O25 = 3.085(3) Å).

Table 1. Selected Bond Lengths (Angstroms) and Angles (Degrees) for $[(\eta^6\text{-}\eta^1\text{-C}_6\text{H}_5(\text{CH}_2)_3\text{NH}_2)\text{Ru}(\text{9EtG})_2](\text{CF}_3\text{SO}_3)_2 \cdot \text{H}_2\text{O}$ (**8**·H₂O)

bond	length	bond	length/angle
Ru—N1	2.121(2)	Ru—C10	2.191(2)
Ru—N10	2.1588(18)	Ru—centroid	1.6718(11)
Ru—N20	2.101(2)	N1—Ru—N10	86.94(8)
Ru—C5	2.178(2)	N1—Ru—N20	82.96(8)
Ru—C6	2.172(2)	N10—Ru—N20	87.49(8)
Ru—C7	2.165(2)	Ru—N1—C2	117.26(17)
Ru—C8	2.210(3)	Ru—C5—C4	123.85(19)
Ru—C9	2.232(3)	N1—Ru—C5	89.94(10)

defined by all of the arene carbons and that of C5 (to which the tether is connected), Ru, and N(tether) is 72.77°. The coordinated 9EtG ligands show a number of hydrogen-bond interactions with the tether amine, residual solvent water, the CF₃SO₃ counteranion, and neighboring 9EtG ligands (Figure S6). Both the tether amine protons are involved in intramolecular hydrogen bonds of 1.98 and 2.32 Å, with the carbonyl groups of the two 9EtG ligands.

Aqueous Chemistry. Di-chlorido tethered complexes $[(\eta^6\text{-}\eta^1\text{-C}_6\text{H}_5(\text{CH}_2)_3\text{NH}_2)\text{RuCl}_2]$ (**1**) and $[(\eta^6\text{-}\eta^1\text{-C}_6\text{H}_5(\text{CH}_2)_2\text{NH}_2)\text{RuCl}_2]$ (**2**) have good aqueous solubility. Solutions of **1** (7.2 mM, pH* 5.66) and **2** (7.0 mM Ru, pH* 5.60) in D₂O at 298 K showed no evidence of decomposition over a period of 24 h, as judged by ¹H NMR spectroscopy.

Upon dissolution of **1** in D₂O, the ¹H NMR spectrum suggested the presence of a number of species in solution with some of the signals seemingly overlapped. A 2D TOCSY spectrum confirmed the presence of three independent spin systems (Figure S7). The ¹H NMR spectrum of **2** showed 11 separate peaks in the arene region of 5.1–6.2 ppm. Integration suggested that they corresponded to three species; two with three signals in a 2:1:2 ratio and one with five signals integrating for 1H each.

To characterize the three species present, chloride titrations for complexes **1** (6.5 mM Ru) and **2** (6.8 mM Ru) were followed by ^1H NMR spectroscopy in D_2O at 298 K. The

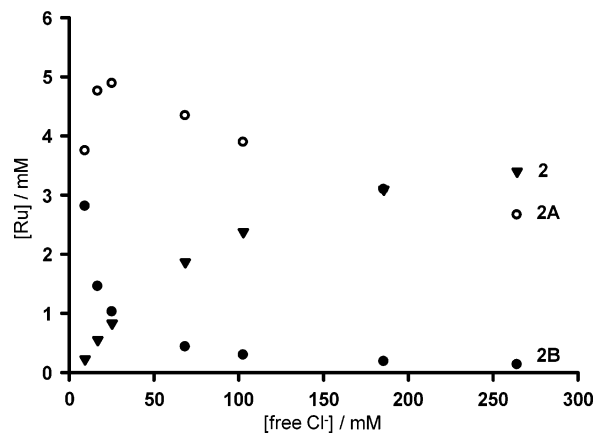


Figure 6. Plot of the concentration of ruthenium species versus the concentration of free chloride for $[\eta^6\text{-}\eta^1\text{-C}_6\text{H}_5(\text{CH}_2)_2\text{NH}_2]\text{RuCl}_2$ (**2**) on the basis of the integration of ^1H NMR peaks. The initial concentration of **2** was 6.8 mM. Symbols: (●) = $[\eta^6\text{-}\eta^1\text{-C}_6\text{H}_5(\text{CH}_2)_2\text{NH}_2]\text{Ru}(\text{H}_2\text{O})_2]^{2+}$ (**2B**), (○) = $[\eta^6\text{-}\eta^1\text{-C}_6\text{H}_5(\text{CH}_2)_2\text{NH}_2]\text{Ru}(\text{H}_2\text{O})\text{Cl}]^+$ (**2A**), and (▼) = $[\eta^6\text{-}\eta^1\text{-C}_6\text{H}_5(\text{CH}_2)_2\text{NH}_2]\text{RuCl}_2$ (**2**).

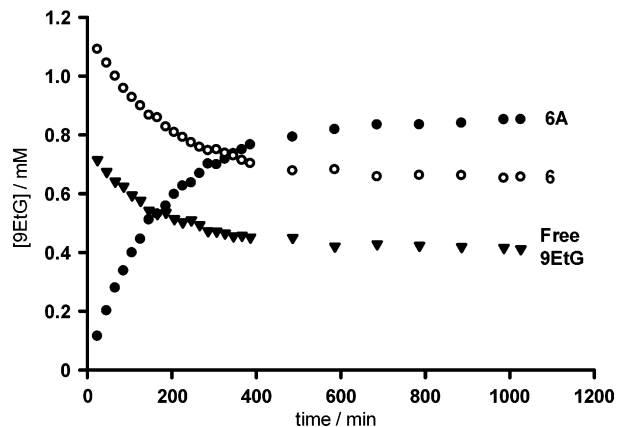
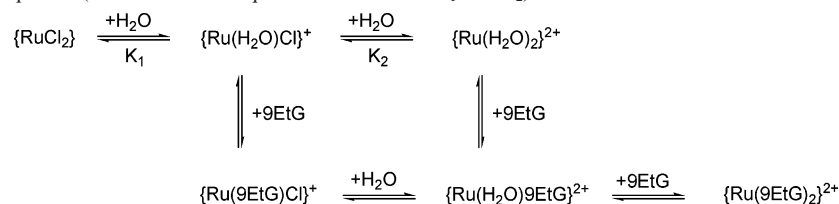


Figure 7. Plot of the concentration of 9EtG in the species versus time for the reaction of $[(\eta^6\text{-}\eta^1\text{-C}_6\text{H}_5(\text{CH}_2)_3\text{NH}_2)\text{Ru}(\text{NO}_3)_2]$ (**3**) (1.1 mM Ru) with 1.75 mol equiv of 9EtG at 298 K (pH 5.19 (start)–6.22 (finish)). Symbols: (○) = $[(\eta^6\text{-}\eta^1\text{-C}_6\text{H}_5(\text{CH}_2)_3\text{NH}_2)\text{Ru}(\text{EtG})_2\text{H}_2\text{O}]^{2+}$ (**6**), (●) = $[(\eta^6\text{-}\eta^1\text{-C}_6\text{H}_5(\text{CH}_2)_3\text{NH}_2)\text{Ru}(\text{EtG})_2]^{2+}$ (**6A**), and (▼) = free 9EtG.

relative intensities of the three species present in solution changed with increasing concentrations of added chloride (Figures S8–S10). Integration of the arene proton peaks gave the relative proportions of the three species present in solution at each chloride concentration, as shown for complex **2** in Figure 6. The concentration of one adduct (**2B**) approached zero with increasing chloride concentration. The concentration of species **2A** appeared to reach a maximum at ca. 40 mM free chloride and decreased in the presence of further added chloride. The concentration of species **2** increased as the concentration of chloride increased. The variation in the concentrations of the three related ruthenium species with the concentration of free chloride for **1** was very similar to that for **2** (Figure S11). Equilibria appeared to be reached quickly, because spectra recorded after 20 min showed no changes when re-recorded after 22 h for solutions of **1** with $[\text{Cl}^-]_{\text{t}} = 12.9$ or 273.1 mM and solutions of **2** with $[\text{Cl}^-]_{\text{t}} = 13.6$ or 273.6 mM, where $[\text{Cl}^-]_{\text{t}}$ = total chloride concentration. This allowed the equilibrium constants to be determined, on the basis of the dependence shown in Chart 2. The equilibrium constants for **1** of $K_1 = 145$ and $K_2 = 5.4$ mM

Chart 2. Scheme for the Aquation (with Associated Equilibrium Constants K_1 and K_2) and Reaction of 9EtG with Tethered Ru^{II} Arene Complexes^a

^a Tethered ligands ($(\eta^6\text{-}\eta^1\text{-C}_6\text{H}_5(\text{CH}_2)_n\text{NH}_2)$, where $n = 2$ or 3 , have been omitted in the formulas.

(Figure S12) are comparable with those of **2**, $K_1 = 154$ and $K_2 = 6.5$ mM, despite the poorer fit for the value of K_2 (Figure S13).

The ^1H NMR spectrum of a solution of $[(\eta^1\text{-}\eta^6\text{-C}_6\text{H}_5(\text{CH}_2)_3\text{NH}_2)\text{Ru}(\text{NO}_3)_2]$ (**3**) in 90% $\text{H}_2\text{O}/10\%$ D_2O (9.4 mM) showed the presence of only one species at the initial pH 4.1. The observed ^1H NMR peaks have the same chemical shifts as those of the di-aqua adduct **1B** observed in an aqueous solution of the di-chlorido complex $[(\eta^6\text{-}\eta^1\text{-C}_6\text{H}_5(\text{CH}_2)_3\text{NH}_2)\text{RuCl}_2]$ (**1**), and the species is assumed to be $[(\eta^1\text{-}\eta^6\text{-C}_6\text{H}_5(\text{CH}_2)_3\text{NH}_2)\text{Ru}(\text{H}_2\text{O})_2](\text{NO}_3)_2$ (**3A**). A pH titration was followed by ^1H NMR in an attempt to determine the $\text{p}K_a$ values associated with the coordinated aqua ligands. Raising the pH by the stepwise addition of NaOH led to precipitation at pH values as low as 4.8. At pH 7.7, the color of the solution was pale yellow. Peaks due to the initial di-aqua species began shifting to high field above pH 5.4. However, they had almost disappeared at pH 6.6, thus preventing the determination of the associated $\text{p}K_a$ value(s) (Figure S14). During each experiment, the pH values measured before recording the spectrum were higher on average 0.2 pH units than those measured after. Three new species were present in solution, and the position of their signals did not shift between pH 5.0 to 11.0. When the pH was raised from 8.9 to 11.0, a fourth species appeared. Formation of these species was reversible, because on lowering the pH to 1.0, only the di-aqua species was observed to be present in solution. In addition, the precipitate redissolved. Upon raising the pH of an acidic solution of **3** directly to pH 10.1, the presence of peaks assignable to the four similar species was detected but in different proportions and no precipitate formed.

Reactions with Nucleobases. In a reaction of $[(\eta^6\text{-}\eta^1\text{-C}_6\text{H}_5(\text{CH}_2)_3\text{NH}_2)\text{Ru}(\text{NO}_3)_2]$ (**3**) with 1.75 mol equiv of 9EtG in 90% $\text{H}_2\text{O}/10\%$ D_2O at pH 5.19, all of starting complex **3** appeared to have reacted by the time the first spectrum was recorded (24 min). H8 peaks for two new 9EtG adducts, a major one at 8.16 ppm (**6**) and a minor one at 8.25 ppm (**6A**), were observed in addition to the H8 peak for free 9EtG (7.82 ppm). Over time, the peaks corresponding to free 9EtG and **6** decreased in intensity, whereas those of **6A** increased in intensity. The product peaks can be assigned to $[(\eta^6\text{-}\eta^1\text{-C}_6\text{H}_5(\text{CH}_2)_3\text{NH}_2)\text{Ru}(\text{9EtG})\text{H}_2\text{O}]^{2+}$ (**6**) and $[(\eta^6\text{-}\eta^1\text{-C}_6\text{H}_5(\text{CH}_2)_3\text{NH}_2)\text{Ru}(\text{9EtG})_2]^{2+}$ (**6A**) by the integration of the signals in the ^1H NMR spectra and by comparison with the shifts of the synthesized di-9EtG adduct $[(\eta^6\text{-}\eta^1\text{-C}_6\text{H}_5(\text{CH}_2)_3\text{NH}_2)\text{Ru}(\text{9EtG})_2](\text{NO}_3)_{0.25}(\text{PF}_6)_{1.75}$ (**7**). Figure 7 shows a plot of the concentration of 9EtG in the adducts formed versus time. Formation of mono-9EtG adduct (**6**) is rapid and appears to have reached completion by the time the first spectrum was

recorded. In contrast, formation of the di-9EtG adduct (**6A**) appeared to reach equilibrium after ca. 700 min and did not go to completion. With increasing time, a further, minor set of arene proton signals was noted, which did not appear to be assignable to a 9EtG adduct.

In a reaction of $[(\eta^6\text{-}\eta^1\text{-C}_6\text{H}_5(\text{CH}_2)_3\text{NH}_2)\text{RuCl}_2]$ (**1**) with 2 mol equiv of 9EtG in the presence of chloride ($[\text{Cl}^-]_t = 21.7$ mM), three sets of H8 peaks for 9EtG adducts were observed (8.16 ppm, two overlapped signals, **4** and **4A**, and 8.26 ppm (**4B**), in addition to an H8 peak for free 9EtG (7.82 ppm)).

In a reaction of $[(\eta^6\text{-}\eta^1\text{-C}_6\text{H}_5(\text{CH}_2)_2\text{NH}_2)\text{RuCl}_2]$ (**2**) with 2 mol equiv of 9EtG in the presence of chloride ($[\text{Cl}^-]_t = 21.7$ mM), complex **2** appeared to have completely reacted within 53 min, and $[(\eta^6\text{-}\eta^1\text{-C}_6\text{H}_5(\text{CH}_2)_2\text{NH}_2)\text{Ru}(\text{H}_2\text{O})\text{Cl}]^+$ (**2A**) within 183 min. No di-aqua complex $[(\eta^6\text{-}\eta^1\text{-C}_6\text{H}_5(\text{CH}_2)_2\text{NH}_2)\text{Ru}(\text{H}_2\text{O})_2]^{2+}$ (**2B**) was detected by the time the first spectrum was recorded (32 min). Three new 9EtG H8 peaks (8.21, 8.26, and 8.28 ppm) were observed in addition to that for free 9EtG. Figure 8 shows a plot of the concentration of bound 9EtG in the adducts formed during the reaction versus time. Similar to the reaction with the dinitrato (di-aqua) complex (**3**), formation of the di-9EtG adduct (**5B**, H8 peak at 8.28 ppm) from dichloride complex **2** is time-dependent, and equilibrium was reached after ca. 22 h. The chemical shifts of the H8 peaks were compared to those observed in a separate experiment, in which the abstraction of chloride from **2** by silver nitrate in water was followed by the reaction with ca. 0.8 mol equiv of 9EtG. This suggested assignment of one of the two species as $[(\eta^6\text{-}\eta^1\text{-C}_6\text{H}_5(\text{CH}_2)_2\text{NH}_2)\text{Ru}(\text{9EtG})\text{H}_2\text{O}]^{2+}$ (**5A**, H8 peak at 8.26 ppm). Addition of NaCl and comparison of the chemical shifts of the new signals suggested the assignment of the other species as $[(\eta^6\text{-}\eta^1\text{-C}_6\text{H}_5(\text{CH}_2)_2\text{NH}_2)\text{Ru}(\text{9EtG})\text{Cl}]^+$ (**5**, H8 peak at 8.21 ppm).

The ^1H NMR spectrum of $[(\eta^6\text{-}\eta^1\text{-C}_6\text{H}_5(\text{CH}_2)_3\text{NH}_2)\text{Ru}(\text{9EtG})_2](\text{NO}_3)_{0.25}(\text{PF}_6)_{1.75}$ (**7**) in D_2O showed the 9EtG H8 peaks as a singlet at 8.25 ppm, a low-field shift of 0.43 ppm compared to free 9EtG. The broad tether-NH₂ signal, which was still detectable after 24 h, had shifted to low field from 3.92 for the di-aqua complex to 5.41 ppm (Figure 9A). Over the course of the experiment, the singlet at 8.25 ppm decreased in intensity, and two new H8 signals at 8.14 and 7.82 ppm, assignable to mono-9EtG adduct **7A** and free 9EtG respectively, increased in intensity. Equilibrium appeared to be reached after ca. 700 min. Part B of Figure 9 shows the plot of the concentration of **7**, **7A**, and free 9EtG versus time for the hydrolysis of **7**.

DNA Metalation Reactions. In reactions of $[(\eta^6\text{-}\eta^1\text{-C}_6\text{H}_5(\text{CH}_2)_3\text{NH}_2)\text{Ru}(\text{NO}_3)_2]$ (**3**) with double-helical CT DNA,

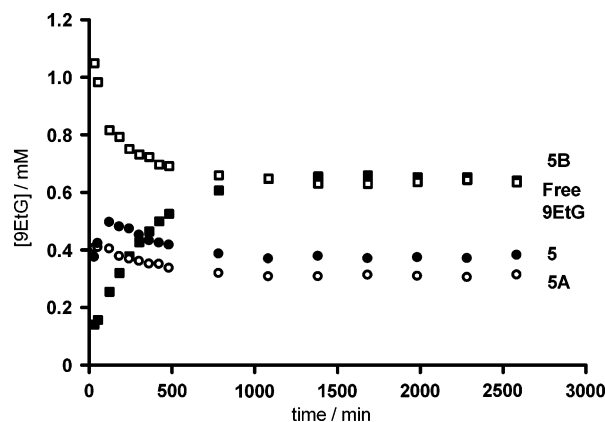


Figure 8. Plot of the concentration of 9EtG in the species formed during the reaction of $[(\eta^6:\eta^1\text{-C}_6\text{H}_5(\text{CH}_2)_3\text{NH}_2)\text{RuCl}_2]$ (**2**) (0.99 mM Ru) with 2.0 mol equiv of 9EtG at 298 K in the presence of chloride ($[\text{Cl}^-]_i = 21.7$ mM, pH 6.08 (start) – 6.23 (finish)) versus time. Symbols: (●) = $[(\eta^6:\eta^1\text{-C}_6\text{H}_5(\text{CH}_2)_3\text{NH}_2)\text{Ru}(\text{9EtG})\text{Cl}]^+$ (**5**), (○) = $[(\eta^6:\eta^1\text{-C}_6\text{H}_5(\text{CH}_2)_3\text{NH}_2)\text{Ru}(\text{9EtG})\text{H}_2\text{O}]^{2+}$ (**5A**), (■) = $[(\eta^6:\eta^1\text{-C}_6\text{H}_5(\text{CH}_2)_3\text{NH}_2)\text{Ru}(\text{9EtG})_2]^{2+}$ (**5B**), and (□) = free 9EtG.

the amount of ruthenium coordinated to DNA (r_b) increased with time. After ca. 20 min, all of the ruthenium from **3** present in the reaction mixture was bound to DNA. In this binding reaction, the time at which the binding reached 50% ($t_{50\%}$) was ca. 3 min. Importantly, the analytical methods that monitored the binding of ruthenium to DNA are not affected by any subsequent closure of monofunctional adducts to bifunctional lesions. The binding experiments indicated that such rutheniation reactions resulted in the coordination of all of the molecules of **3**, which made it possible to prepare easily and precisely samples of DNA modified by complex **3** at a preselected value of r_b .

DNA Transcription by RNA Polymerase In Vitro. In vitro RNA synthesis by RNA polymerases on DNA templates containing several types of bifunctional adducts of platinum complexes can be prematurely terminated at the level of or in the proximity of adducts.^{29,39} On the other hand, monofunctional DNA adducts of several platinum complexes (such as $[\text{Pt}(\text{dien})\text{Cl}]\text{Cl}$ or $[\text{PtCl}(\text{NH}_3)_3]\text{Cl}$) are unable to terminate RNA synthesis.^{29,39,43} Cutting of pSP73KB DNA³⁹ by *NdeI* and *HpaI* restriction endonucleases yielded a 212 bp fragment (a substantial part of its nucleotide sequence is shown in part B of Figure S15). This fragment contained a T7 RNA polymerase promoter (in the upper strand close to its 3' end (Figure S15)). The experiments were carried out using this linear DNA fragment, modified at $r_b = 0.008$ by **3** and for comparative purposes also by cisplatin, transplatin, or $[\text{Pt}(\text{dien})\text{Cl}]\text{Cl}$, for RNA synthesis by T7 RNA polymerase (Figure S15; lanes **3**, cisPt, transPt and dienPt, respectively). RNA synthesis on the template modified by bifunctional platinum complexes (cisplatin or transplatin) yielded fragments of defined sizes, which indicates that RNA synthesis on these templates was prematurely terminated (Figure S15). On the other hand, no stop sites were produced by the adducts of the monofunctional platinum complex $[\text{Pt}(\text{dien})\text{Cl}]\text{Cl}$ and by **3**. These results are consistent with the view that **3** forms mainly monofunctional adducts on DNA.

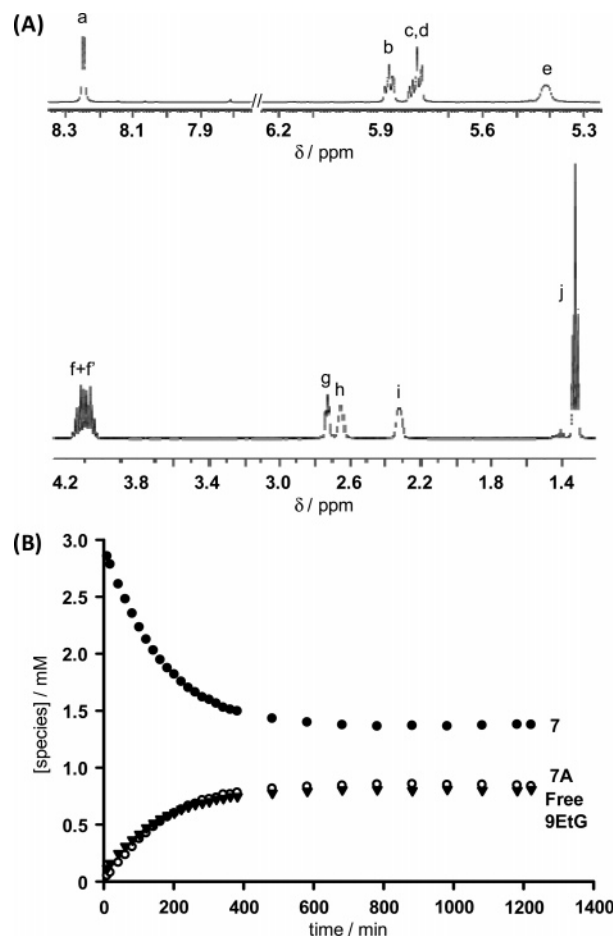


Figure 9. (A) ^1H NMR spectrum of $[(\eta^6:\eta^1\text{-C}_6\text{H}_5(\text{CH}_2)_3\text{NH}_2)\text{Ru}(\text{9EtG})_2]-(\text{NO}_3)_{0.25}(\text{PF}_6)_{1.75}$ (**7**) in D_2O at 298 K (4.3 mM Ru) after dissolution at $\text{pH}^* 6.47$. Assignments: a = H8; b, c, d = arene protons; e = NH_2 tether; f+f' = CH_2 (9EtG); g, h, i = $(\text{CH}_2)_3$ (tether); j = CH_3 (9EtG). (B) Plot of the concentration of species versus time for the hydrolysis of 9EtG from **7** (3.0 mM Ru) in D_2O at 298 K ($\text{pH}^* 6.67$ (start) – 6.02 (finish)). Symbols: (●) = $[(\eta^6:\eta^1\text{-C}_6\text{H}_5(\text{CH}_2)_3\text{NH}_2)\text{Ru}(\text{9EtG})_2]^{2+}$ (**7**), (○) = $[(\eta^6:\eta^1\text{-C}_6\text{H}_5(\text{CH}_2)_3\text{NH}_2)\text{Ru}(\text{9EtG})\text{H}_2\text{O}]^{2+}$ (**7A**), and (▼) = free 9EtG.

DNA Interstrand Crosslinking Assay. Bifunctional compounds that bind strongly to DNA may form various types of interstrand and intrastrand cross-links. Therefore, we quantitated the interstrand cross-linking efficiency of **3** in linearized pSP73 plasmid (2464 bp). This plasmid DNA was linearized by *EcoRI* (*EcoRI* cuts only once within the pSP73 plasmid), 3'-end-labeled by $[\alpha\text{-}^{32}\text{P}]$ ATP, and modified by **3**. Cisplatin, which is known to form ca. 6% interstrand cross-links, was used for comparative purposes.³⁹ Upon electrophoresis, the 3'-end-labeled strands of linearized plasmid DNA containing no interstrand cross-links migrate as a 2464 base single strand, whereas the interstrand cross-linked strands migrate more slowly as a higher molecular mass species (Figure 10). This more slowly migrating band was observed when the DNA fragment was modified by cisplatin at r_b values as low as 0.0005, and its intensity increased with increasing levels of modification. For **3**, the slowly migrating band was observed only when the DNA fragment was modified at a considerably higher r_b value. The DNA interstrand cross-linking efficiency of **3** was almost independent of r_b and was only 0.2%. Thus, the DNA interstrand cross-linking efficiency of **3** was markedly lower

(43) Brabec, V.; Boudny, V.; Balcarova, Z. *Biochemistry* **1994**, *33*, 1316–1322.

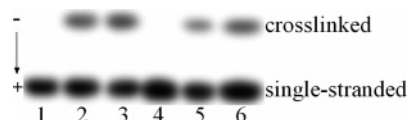


Figure 10. Formation of interstrand cross-links by $[(\eta^6\text{-}\eta^1\text{-C}_6\text{H}_5(\text{CH}_2)_3\text{NH}_2)\text{Ru}(\text{NO}_3)_2]$ (**3**) and cisplatin in pSP73 plasmid that was linearized by *EcoRI*. Autoradiogram of denaturing 1% agarose gels of linearized DNA that was 3'-end labeled. The interstrand cross-linked DNA appears as the top bands (marked as cross-linked), which migrated on the gel more slowly than the single-stranded DNA (contained in the bottom bands and marked as single-stranded). The fragment was nonplatinated (control) (lane 1) or modified by cisplatin at $r_b = 5 \times 10^{-4}$, 1×10^{-3} (lanes 2, 3, respectively) or by **3** at $r_b = 5 \times 10^{-4}$, 1×10^{-3} , 1×10^{-2} (lanes 4–6, respectively).



Figure 11. Unwinding of supercoiled pSP73KB plasmid DNA by complex $[(\eta^6\text{-}\eta^1\text{-C}_6\text{H}_5(\text{CH}_2)_3\text{NH}_2)\text{Ru}(\text{NO}_3)_2]$ (**3**). The plasmid was incubated with **3** for 24 h at 37 °C in 10 mM NaClO₄. Lanes: 1, 12 are controls consisting of nonmodified DNA ($r_b = 0$); 2 – $r_b = 0.01$; 3 – $r_b = 0.03$; 4 – $r_b = 0.05$; 5 – $r_b = 0.06$; 6 – $r_b = 0.07$; 7 – $r_b = 0.08$; 8 – $r_b = 0.09$; 9 – $r_b = 0.10$; 10 – $r_b = 0.15$; 11 – $r_b = 0.20$. The top bands correspond to nicked plasmid and the bottom bands to closed, negatively supercoiled plasmid.

than that of cisplatin (6%), consistent with the results of transcription mapping (Figure S15), indicating that this complex forms mainly monofunctional lesions on DNA.

Unwinding of Negatively Supercoiled DNA. A compound that unwinds the DNA duplex reduces the number of supercoils in closed, negatively supercoiled DNA so that the negative superhelical density of closed circular DNA decreases. This decrease upon the binding of unwinding agents causes a decrease in the rate of migration through agarose gel, which makes it possible to observe and quantify the unwinding. Figure 11 shows electrophoresis gels in which increasing amounts of **3** have been bound to a mixture of relaxed and negatively supercoiled pSP73KB DNA. The unwinding angle is given by $\mu = 18 \sigma / r_b(c)$, where σ is the superhelical density and $r_b(c)$ is the value of r_b at which the supercoiled and relaxed forms comigrate. Under the present experimental conditions, σ was calculated to be -0.04 on the basis of the data for cisplatin for which the $r_b(c)$ was determined in this study and $\mu = 13^\circ$ was assumed. Using this approach, a DNA unwinding angle for **3** of $9 \pm 1^\circ$ was determined.

Cytotoxicity. Complexes **1** and **2** were tested for cytotoxicity against the human ovarian cancer cell line A2780. The maximum test concentration employed was 100 μM , and at those concentrations, no significant inhibition of cell growth was observed. The complexes were thus deemed inactive.

Discussion

Synthesis and Characterization. The synthesis of tethered Ru^{II} arene complexes $[(\eta^6\text{-}\eta^1\text{-C}_6\text{H}_5(\text{CH}_2)_n\text{NH}_2)\text{RuCl}_2]$ **1** ($n = 3$) and **2** ($n = 2$) was carried out via the thermal displacement of ethyl benzoate by a pendent arene. Arene exchange reactions are believed to proceed via the progressive dissociation of the arene ligand via η^6 to η^4 and η^2 coordination.⁴⁴ THF was added to the reaction mixture because of observations made by Bennett et al., who found

that this shortened reaction times and gave higher yields for the synthesis of some phosphine-tethered complexes.^{18c}

For **1** and **2**, the dramatic changes in the ¹H NMR shifts of the arene upon coordination to ruthenium and the associated 2:1:2 signal intensity pattern (cf. multiplet for uncoordinated arene) due to the equivalence of the two ortho and two meta protons, respectively, are the most significant evidence of coordination.⁴⁵ The pronounced low-field shift of the NH₂ signals by 1.4–2.0 ppm compared to the respective free ligands is characteristic of coordination.

X-ray Crystal Structures. The X-ray crystal structures of complexes $[(\eta^6\text{-}\eta^1\text{-C}_6\text{H}_5(\text{CH}_2)_3\text{NH}_2)\text{RuCl}_2]$ (**1**) and $[(\eta^6\text{-}\eta^1\text{-C}_6\text{H}_5(\text{CH}_2)_2\text{NH}_2)\text{RuCl}_2]$ (**2**) appear to be the first examples of di-chlorido Ru^{II} arene complexes containing a nitrogen-bound tether. Reported examples of neutral bifunctional complexes have mainly contained phosphorus-coordinated tethers.¹⁸

For phosphine-containing tethered complexes, the Ru–C(arene) bond lengths of compounds with three carbon atoms in the backbone are in the range of 2.16–2.27 Å, whereas those in **1** lie within the more narrow range of 2.161(9)–2.196(7) Å, together with a ca. 0.04–0.05 Å shorter Ru–centroid distance.^{17,18b,c,46} This is similar to two-carbon tethers for which ranges of 2.15–2.28 Å have been reported. The Ru–centroid distance in **2** is ca. 0.06–0.08 Å shorter than in comparable analogues.^{18a,f,21,23}

The structure of **2** appears to be more strained than that of **1**. The observed buckling of the coordinated arene in **2** seemingly is a consequence of the arene accommodating the strain exerted by the chelating tether. The added flexibility offered by three-atom tethered molecule **1** results in the arene adopting a more planar conformation. Strain is also reflected by a change in the Ru–C(arene)–C(tether) angle, which is 114.74° for **2** in contrast to 127.17° for **1**. Even though the crystal structures show the strain imposed on the arene by the tether in complex **2** with its 2-carbon tether, complexes **1** and **2** appear to have similar stability and hydrolysis behavior in aqueous solution. However, in donor organic solvents such as DMSO, complex **2** appears to undergo decomposition via the loss of arene, probably as a direct consequence of the strain.

There appears to be no previous report of a Ru^{II} arene complex containing two monodentate nitrate ligands such as those that are present in $[(\eta^6\text{-}\eta^1\text{-C}_6\text{H}_5(\text{CH}_2)_3\text{NH}_2)\text{Ru}(\text{NO}_3)_2]$ (**3**). Nitrate generally is a weak ligand for ruthenium; however, there are other reported examples of dinitrato adducts including $\alpha\text{-}[\text{Ru}^{\text{II}}(\text{azpy})_2(\text{NO}_3)_2]$,⁴⁷ where azpy = 2-(phenylazo)pyridine, and *cis*- $[\text{Ru}^{\text{III}}\text{Cl}(\text{NO}_3)_2(\text{pdma})\text{NO}]$,⁴⁸ where pdma = 1,2-phenylenebis(dimethylarsine), which both have shorter Ru–O bond lengths than **3**. Mono-nitrato

(44) Howell, J. A. S.; Ashford, N. F.; Dixon, D. T.; Kola, J. C. *Organometallics* **1991**, 10, 1852–1864.

(45) Smith, P. D.; Gelbrich, T.; Hursthouse, M. B. *J. Organomet. Chem.* **2002**, 659, 1–9.

(46) (a) Ghebreyessus, K. Y.; Nelson, J. H. *Organometallics* **2000**, 19, 3387–3392. (b) Pinto, P.; Marconi, G.; Heinemann, F. W.; Zenneck, U. *Organometallics* **2004**, 23, 374–380.

(47) Hotze, A. C. G.; Velders, A. H.; Ugozzoli, F.; Biagini-Cingi, M.; Manotti-Lanfredi, A. M.; Haasnoot, J. G.; Reedijk, J. *Inorg. Chem.* **2000**, 39, 3838–3844.

Table 2. Ru–N7 Bond Lengths (Angstroms) of Ruthenium Complexes Containing Guanine Derivatives^m

complex	Ru–N7
[(η^6 -ben)Ru(9EtG)Cl ₂]	2.101(4) ^a
[Ru ₂ (O ₂ CMe) _{1.82} (O ₂ CCF ₃) _{0.18} (9EtG) ₂ (MeOH) ₂]–(O ₂ CCF ₃) ₂ ·2MeOH·0.5Et ₂ O	2.064(9), 2.078(9) ^b
[(η^6 -ben)Ru(9EtG) ₂ H ₂ O](CF ₃ SO ₃) ₂	2.124, 2.133 ^c
[(η^6 -ben)Ru(L-ala)9EtG]Cl	2.115(6), 2.112(7) ^a
[(η^6 -bip)Ru(en)9EtG](PF ₆) ₂ ·MeOH	2.128(5) ^d
[(η^6 -bip)Ru(en)Guo](PF ₆) ₂ ·3.75H ₂ O	2.120(5) ^d
[(η^6 -DHA)Ru(en)9EtG](PF ₆) ₂ ·2MeOH	2.1173(15) ^d
[(η^6 -THA)Ru(en)9EtG](PF ₆) ₂ ·MeOH	2.128(3) ^d
Δ -[Ru(bpy) ₂ (9MeG) ₂](CF ₃ SO ₃) ₂	2.122(5), 2.131(4) ^e
<i>cis</i> -[Ru(bpy) ₂ (9EtG)ClCl·1.5H ₂ O]	2.143(5) ^f
[RuCl ₃ (9EtG)H ₂ O(DMSO)]	2.148(3) ^g
[(η^6 -bip)Ru(Et-en)9EtG](PF ₆) ₂	2.123(5) ^h
[(η^6 - <i>p</i> -cym)Ru(glycine)9EtG]PF ₆	2.136(3) ⁱ
[(η^6 - <i>p</i> -cym)Ru(Ph ₂ acac)9EtG](CF ₃ SO ₃) ₂ ·2tol	2.126(3), 2.140(3) ^j
<i>mer</i> -[RuCl ₃ (acv)DMSO(CH ₃ OH)]·0.5CH ₃ OH	2.127(5) ^k
<i>mer</i> -[RuCl ₃ (acv)DMSO(H ₂ O)]·H ₂ O	2.132(2) ^k
<i>mer</i> -[RuCl ₃ (acv)DMSO(C ₂ H ₅ OH)]·C ₂ H ₅ OH	2.148(6) ^l

^a Ref 14. ^b Ref 51a. ^c Ref 9. ^d Ref 13. ^e Ref 51b. ^f Ref 52a. ^g Ref 52b. ^h Ref 52d. ⁱ Ref 3. ^j Ref 52f. ^k Ref 52c. ^l Ref 52e. ^m Abbreviations: 9MeG = 9-methylguanine, acv = acyclovir, ben = benzene, bip = biphenyl, bpy = 2,2'-bipyridine, DHA = dihydroanthracene, en = ethylenediamine, Et-en = Et(H)NCH₂CH₂NH₂, Guo = guanosine, L-ala = deprotonated L-alanine, THA = tetrahydroanthracene.

ruthenium complexes are also known, including [(η^5 -Cp)-Ru(CO)(AsPh₃)NO₃]₄₉ where Cp = cyclopentadienyl, and [(η^6 -*p*-cym)₂Ru₂(6,6'-Me₂dppz)(NO₃)₂]₄₉ where 6,6'-Me₂-dppzH = 2,2'-(1*H*-pyrazole-3,5-diyl)-bis(6-methylpyridine), which again have shorter Ru–O bond lengths than 3.

The unrefined structure of [(η^6 : η^1 -C₆H₅(CH₂)₃NH₂)Ru(9EtG)₂](NO₃)₂ (**6A**) confirmed the CHN elemental analysis that suggests that the attempted counterion metathesis from NO₃[–] to PF₆[–] in [(η^6 : η^1 -C₆H₅(CH₂)₃NH₂)Ru(9EtG)₂](NO₃)_{0.25}(PF₆)_{1.75} (**7**) was only partial, possibly due to the ability of nitrate to participate in hydrogen bond interactions with N1H and N2H (Figure S5).

Two features of the X-ray crystal structure of [(η^6 : η^1 -C₆H₅(CH₂)₃NH₂)Ru(9EtG)₂](CF₃SO₃)₂·H₂O (**8**·H₂O) are of particular interest. First, the significant difference between the two Ru–N7(9EtG) bond lengths of ca. 0.06 Å. Other Ru^{II} di-guanine derivative structures have more similar bond lengths (maximum difference of 0.015 Å) for the two coordinated guanines (Table 2).^{9,14,51} Compared to reported di- and mono-guanine adducts of ruthenium,^{3,13,14,52} the Ru–N7(9EtG) distance of 2.10 Å (Ru–N20, Table 1) found for one of the coordinated 9EtG molecules in the structure of **8**·H₂O appears to be one of the shortest. In contrast, the other Ru–N7(9EtG) bond length of 2.16 Å (Ru–N10, Table 1) in the structure of **8**·H₂O appears to be one of the longest reported. This difference in the Ru–N(9EtG) bond distances

in **8**·H₂O could result from an electronic effect, where good overlap of the binding orbitals is not possible for the second molecule of 9EtG, or it could arise from steric hindrance around the metal center. Steric hindrance in the complex *cis*-[Ru(bpy)₂(9MeG)₂]²⁺, where bpy = 2,2'-bipyridine and 9MeG = 9-methylguanine, resulting in hindered rotation of guanine, gives rise to two different H8 peaks for the coordinated 9MeG ligands.^{51b} The ¹H NMR studies of [(η^6 : η^1 -C₆H₅(CH₂)₃NH₂)Ru(9EtG)₂](NO₃)_{0.25}(PF₆)_{1.75} (**7**) in water show that the H8 signal for the two coordinated 9EtG ligands is a singlet integrating for 2H. This suggests that some degree of rotational freedom does exist for the two H8 protons. Interestingly, however, the CH₂ protons from the ethyl group of 9EtG in complex **7** give rise to two separate peaks (part A of Figure 9), which may be a consequence of rotational hindrance and slow exchange between conformations.

The formation of di-guanine adducts at metal centers have been particularly well studied for Pt^{II} complexes, mainly for cisplatin. For these systems, the relative orientation of the bases has received much attention.⁵³ They have been classified as head-to-head (HH) and head-to-tail (HT) orientations, with HH being energetically more favorable. In square-planar Pt^{II} systems, HH describes an orientation in which the two guanine bases are oriented in the same direction (i.e., the carbonyl groups are pointing in the same direction), and for HT, the bases are oriented in the opposite direction (i.e., the carbonyl groups point away from each other).

The second significant feature in the crystal structure of **8**·H₂O is the apparent directional influence of the tether amine group on the orientation of the coordinated 9EtG ligands via the formation of intramolecular hydrogen bonds. In the three reported ruthenium di-guanine derivative adducts, the orientation of the 9EtG and 9MeG ligands is HT.^{9,51} Interestingly, in the structure of [(η^6 : η^1 -C₆H₅(CH₂)₃NH₂)Ru(9EtG)₂](CF₃SO₃)₂·H₂O (**8**·H₂O), the two 9EtG ligands are oriented toward each other, that is, they adopt an HH orientation. The influence of the amine group on this conformation is indicated by the angle between the plane defined by all of the arene carbons and that of C5 (where the tether is connected), Ru, and N(tether). This angle can be viewed as a measure of the outward swing of the tether. For the structures of three-atom tethered complexes [(η^6 : η^1 -C₆H₅(CH₂)₃NH₂)RuCl₂] (**1**) and [(η^6 : η^1 -C₆H₅(CH₂)₃NH₂)Ru(NO₃)₂] (**3**), this angle is close to 90°, whereas for **8**·H₂O it is 72.77°. This is presumably a consequence of the flexibility of the three-carbon tether, which enables the amine group to position itself so as to increase the hydrogen-bond

(48) Coe, B. J.; McDonald, C. I.; Beddoes, R. L. *Polyhedron* **1998**, *17*, 1997–2007.

(49) Cao, M.; Do, L. V.; Hoffman, N. W.; Kwan, M. L.; Little, J. K.; McGilvray, J. M.; Morris, C. B.; Söderberg, B. C.; Wierzbicki, A.; Cundari, T. R.; Lake, C. H.; Valente, E. J. *Organometallics* **2001**, *20*, 2270–2279.

(50) Catalano, V. J.; Craig, T. J. *Polyhedron* **2000**, *19*, 475–485.

(51) (a) Crawford, C. A.; Day, E. F.; Saharan, V. P.; Folting, K.; Huffman, J. C.; Dunbar, K. R.; Christou, G. *Chem. Commun.* **1996**, 1113–1114. (b) Zobi, F.; Hohl, M.; Zimmermann, I.; Alberto, R. *Inorg. Chem.* **2004**, *43*, 2771–2772.

(52) (a) van Vliet, P. M.; Haasnoot, J. G.; Reedijk, J. *Inorg. Chem.* **1994**, *33*, 1934–1939. (b) Price, C.; Shipman, M. A.; Gummerson, S. L.; Houlton, A.; Clegg, W.; Elsegood, M. R. *J. Chem. Soc., Dalton Trans.* **2001**, 353–354. (c) Turel, I.; Peñanac, M.; Golobbiè, A.; Alessio, E.; Serli, B. *Eur. J. Inorg. Chem.* **2002**, 1928–1931. (d) Chen, H.; Parkinson, J. A.; Nováková, O.; Bella, J.; Wang, F.; Dawson, A.; Gould, R.; Parsons, S.; Brabec, V.; Sadler, P. J. *Proc. Natl. Acad. Sci. U.S.A.* **2003**, *100*, 14623–14628. (e) Turel, I.; Peñanac, M.; Golobbiè, A.; Alessio, E.; Serli, B.; Bergamo, A.; Sava, G. *J. Inorg. Biochem.* **2004**, *98*, 393–401. (f) Melchart, M.; Habtemariam, A.; Parsons, S.; Sadler, P. J. *J. Inorg. Biochem.*, in press.

(53) Ano, S. O.; Kuklenyik, Z.; Marzilli, L. G. In *Cisplatin*; Lippert, B., Ed.; Verlag Helvetica Chimica Acta: Zürich, Switzerland, 1999; pp 247–291.

Table 3. Hydrolysis Equilibrium Constants for Metal Di-Chlorido Complexes

complex	K_1	K_2	I (M)	T (K)
cisplatin ^a	3.3–3.9	0.2–0.4	0.3	298–308
cisplatin ^b	6.4	0.3	0.1	298
cisplatin ^c	2.52	0.03	0.01	310
$[(\eta^6\text{-}p\text{-cym})\text{Ru}(\text{pta})\text{Cl}_2]^d$	0.03	107		298
$[(\eta^6\text{-}\eta^1\text{-C}_6\text{H}_5(\text{CH}_2)_3\text{NH}_2)\text{RuCl}_2]$ (1)	145	5.4		298
$[(\eta^6\text{-}\eta^1\text{-C}_6\text{H}_5(\text{CH}_2)_2\text{NH}_2)\text{RuCl}_2]$ (2)	154	6.5		298

^a Ref 54a. ^b Ref 54b. ^c Ref 54c. ^d Ref 55; *p*-cym = para-cymene, pta = 1,3,5-triaza-7-phosphaadamantane.

interactions with both of the carbonyl groups. The carbonyl group with the strongest hydrogen bond to the tether amine protons belongs to the 9EtG ligand, which has the longest Ru–N7(9EtG) bond length. The observed low-field shift of ca. 1.5 ppm of the tether NH₂ protons in the ¹H NMR spectrum of **7** in D₂O is also characteristic of hydrogen-bonding interactions.

Aqueous Chemistry. Important features of the tethered complexes studied in this work are their aqueous solubility at millimolar concentrations and the stability of the tether chelate ring.

It is apparent that both coordinated chloride ligands in complexes **1** and **2** can undergo hydrolysis (Figures 6 and S8–S11). At extracellular chloride concentrations (ca. 0.1 M), the majority of the complexes could be expected to be present as the respective mono-aqua adducts, together with some di-chlorido complex, with negligible amounts of the di-aqua adduct. For the present tethered systems, aquation and loss of chloride are strongly favored, as is evident from the pronounced presence of monohydrolyzed species at chloride concentrations as high as 275 mM. Such a mono-aqua species would be expected to react readily with biomolecules.

With the exception of cisplatin,⁵⁴ there appear to be few reports of hydrolysis equilibrium constants for metal di-chlorido complexes. The equilibrium constants K_1 and K_2 determined for complexes **1** and **2** are considerably higher than those of cisplatin (Table 3); however, in all of the cases $K_2 < K_1$. Curiously, hydrolysis equilibrium constants reported for a phosphine-containing di-chlorido ruthenium arene complex⁵⁵ are very different from those reported here.⁵⁶ For both complexes **1** and **2**, the value for K_2 is comparable to

that reported for the aquation of some monofunctional Ru^{II} arene complexes of the type $[(\eta^6\text{-arene})\text{Ru}(\text{en})\text{Cl}]^+$.⁵⁷

Dissolution of $[(\eta^6\text{-}\eta^1\text{-C}_6\text{H}_5(\text{CH}_2)_3\text{NH}_2)\text{Ru}(\text{NO}_3)_2]$ (**3**) in water produces signals for one species only, assumed to be the fully aquated complex. Similar complete aquation of the di-nitrato complex $\alpha\text{-}[\text{Ru}(\text{azpy})_2(\text{NO}_3)_2]$ in water has been reported.⁴⁷ The formation of four species over the range pH 4.1–11.0, the ¹H NMR signals of which did not shift over that pH range, and the reversible formation of the di-aqua species upon acidification suggest the involvement of hydroxides (or oxides) as bridging ligands, comparable to complexes such as $[(\eta^6\text{-C}_6\text{H}_6)\text{Ru}(\mu\text{-OH})_4]^{4+}$ and $[(\eta^6\text{-C}_6\text{H}_6)\text{Ru}_2(\mu\text{-OH})_3]^+$, for which X-ray structures have been reported.^{58,59} The proposed formation of hydroxo-bridged species appears to reflect a general feature exhibited by multifunctional metal complexes in aqueous solution. The facile formation of a precipitate at comparatively low pH values has also been observed for metallocenes. Kuo et al. have shown the existence of monomer–dimer equilibria for molybdocenes in water at pD 3.5.⁶⁰ In addition, Marks and Toney showed that titanocene can form an insoluble poly oxo- and hydroxo-bridged species in water.⁶¹ Similarly, the formation of a poly oxo-bridged species by the Ru^{III} complex NAMI-A occurs in water at low pH values.⁶²

Adducts with Nucleobases. Reaction of $[(\eta^6\text{-}\eta^1\text{-C}_6\text{H}_5(\text{CH}_2)_3\text{NH}_2)\text{Ru}(\text{NO}_3)_2]$ (**3**) with 9EtG in water results in the rapid formation (<24 min at 298 K) of the mono-9EtG adduct $[(\eta^6\text{-}\eta^1\text{-C}_6\text{H}_5(\text{CH}_2)_3\text{NH}_2)\text{Ru}(9\text{EtG})\text{H}_2\text{O}]^{2+}$ (**6**) and the comparatively slow and incomplete formation of the di-9EtG adduct $[(\eta^6\text{-}\eta^1\text{-C}_6\text{H}_5(\text{CH}_2)_3\text{NH}_2)\text{Ru}(9\text{EtG})_2]^{2+}$ (**6A**). This, together with the results of the reverse reaction, the displacement of 9EtG from $[(\eta^6\text{-}\eta^1\text{-C}_6\text{H}_5(\text{CH}_2)_3\text{NH}_2)\text{Ru}(9\text{EtG})_2]^{2+}$ (**7**) by water, suggests weak binding of the second 9EtG molecule. Interestingly, the 9EtG–N7 bond lengths in the structure of **8**·H₂O appear to correlate with the relatively strong binding of one 9EtG and the relatively weak binding of the other 9EtG ligand, when compared to other reported structures (Table 2).

It was of interest to study the reactivity of both $[(\eta^6\text{-}\eta^1\text{-C}_6\text{H}_5(\text{CH}_2)_3\text{NH}_2)\text{RuCl}_2]$ (**1**) and $[(\eta^6\text{-}\eta^1\text{-C}_6\text{H}_5(\text{CH}_2)_2\text{NH}_2)\text{RuCl}_2]$ (**2**) with 9EtG in the presence of ca. 22 mM chloride, comparable to cytoplasmic $[\text{Cl}^-]$.⁶³ The equilibria were reached after ca. 22 h, significantly longer than in the chloride-free reaction of $[(\eta^6\text{-}\eta^1\text{-C}_6\text{H}_5(\text{CH}_2)_3\text{NH}_2)\text{Ru}(\text{NO}_3)_2]$ (**3**). Because in the chloride titration of complex **2**, the major species present at ca. 20 mM $[\text{Cl}^-]_{\text{f}}$ was the mono-aqua mono-chlorido adduct **2A**, the reaction of **2** with 9EtG presumably proceeds via the initial formation of $[(\eta^6\text{-}$

(54) (a) Reishus, J. W.; Martin, D. S. *J. Am. Chem. Soc.* **1961**, *83*, 2457–2462. (b) Hindmarsh, K.; House, D. A.; Turnbull, M. M. *Inorg. Chim. Acta* **1997**, *257*, 11–18. (c) Kankia, B.; Funck, T.; Marky, L. A. *J. Solution Chem.* **1999**, *28*, 1249–1261.

(55) Scolaro, C.; Bergamo, A.; Brescacin, L.; Delfino, R.; Cocchietto, M.; Laurenczy, G.; Geldbach, T. J.; Sava, G.; Dyson, P. J. *J. Med. Chem.* **2005**, *48*, 4161–4171.

(56) In the context of hydrolysis of bifunctional complexes, loss of a negatively-charged chloride ligand from a neutral complex (mono-aquation) would be expected to be more favorable than further loss of chloride from a positively-charged complex (i.e., second aquation step), reflected by $K_2 < K_1$. For the bifunctional ruthenium arene complex $[(\eta^6\text{-}p\text{-cymene})\text{Ru}(\text{pta})\text{Cl}_2]$, where pta = 1,3,5-triaza-7-phosphaadamantane, simultaneous hydrolysis of both chloride ligands was proposed.⁵⁵ However, in subsequent ¹H NMR solution studies the presence of only the mono-aqua species was detected (A. Dorcier et al., *Organometallics* **2006**, *25*, 4090–4096), that is, preferential mono-aquation, which appears not to conform to the proposed hydrolysis pathway and thus the reported equilibrium constants.

(57) Wang, F.; Chen, H.; Parsons, S.; Oswald, I. D. H.; Davidson, J. E.; Sadler, P. J. *Chem.—Eur. J.* **2003**, *9*, 5810–5820.

(58) Gould, R. O.; Jones, C. L.; Robertson, D. R.; Stephenson, T. A. *J. Chem. Soc., Chem. Comm.* **1977**, 222–223.

(59) Arthur, T.; Robertson, D. R.; Tocher, D. A.; Stephenson, T. A. *J. Organomet. Chem.* **1981**, *208*, 389–400.

(60) Balzarek, C.; Weakley, T. J. R.; Kuo, L. Y.; Tyler, D. R. *Organometallics* **2000**, *19*, 2927–2931.

(61) Toney, J. H.; Marks, T. J. *J. Am. Chem. Soc.* **1985**, *107*, 947–953.

(62) Bouma, M.; Nuijen, B.; Jansen, M. T.; Sava, G.; Flaibani, A.; Bult, A.; Beijnen, J. H. *Int. J. Pharm.* **2000**, *248*, 239–246.

(63) Jennerwein, M.; Andrews, P. A. *Drug Metab. Dispos.* **1995**, *23*, 178–184.

$\eta^1\text{-C}_6\text{H}_5(\text{CH}_2)_2\text{NH}_2\text{Ru}(\text{9EtG})\text{Cl}]^+$ (**5**) via the displacement of water from **2A**. Successive, possibly fast, hydrolysis of the chloride from **5** would result in an increase in the presence of $[(\eta^6:\eta^1\text{-C}_6\text{H}_5(\text{CH}_2)_2\text{NH}_2)\text{Ru}(\text{9EtG})\text{H}_2\text{O}]^{2+}$ (**5A**), which can then further react with another molecule of 9EtG.

On the basis of the results of the binding experiments, a scheme for the reaction of tethered Ru^{II} arene complexes with 9EtG in the presence of chloride can be proposed (Chart 2). Formation of the di-9EtG adduct is inhibited by competition from aquation. In addition, the presence of chloride not only inhibits the formation of the di-9EtG adduct further, but also slows down the formation of mono-9EtG adducts, compared to reactions of the di-aqua species.

DNA Binding. The values of DNA unwinding angles are affected by the nature of the ligands in the coordination sphere of the metal and the stereochemistry at the metal center. Previous systematic work^{41,64} has revealed that, for instance, Pt^{II} compounds fall into different classes, according to their DNA binding modes. It has been shown that Pt^{II} compounds with the smallest unwinding angles (6°) are those that can bind DNA only monofunctionally ($[\text{Pt}(\text{dien})\text{Cl}]\text{Cl}$ or $[\text{Pt}(\text{NH}_3)_3\text{Cl}]\text{Cl}$). In contrast, platinum compounds that bind in a bifunctional manner unwind DNA by $10\text{--}13^\circ$. Examples include cisplatin, its trans isomer, and bifunctional polynuclear complexes. The observation that $[(\eta^6:\eta^1\text{-C}_6\text{H}_5(\text{CH}_2)_3\text{NH}_2)\text{Ru}(\text{NO}_3)_2]$ (**3**), which unwound DNA by $\sim 9^\circ$, can be grouped together with monofunctional Pt^{II} compounds that unwind DNA only slightly is readily understood in terms of an adduct structure in which **3** is preferentially coordinated to DNA in a monodentate manner. This monofunctional adduct, however, is formed readily, because the reactivity of **3** with 9EtG and double-helical CT DNA, both in terms of the rate and the extent of binding, was found to be very similar.

Cytotoxicity. Complexes **1** and **2** were found to not exhibit cytotoxic activity against the human ovarian cell line A2780 at a significant concentration ($\text{IC}_{50} > 100\ \mu\text{M}$). This is in agreement with other tested ruthenium arene compounds with two potentially reactive sites, containing pyridine and phosphine ligands, which showed only negligible cytotoxicity against some cancer cell lines.^{12,55} The results of this work suggest that, under cell-testing conditions, complexes **1** and **2** would be expected to be present to a large extent as the mono-aquated complex in the extracellular medium ($[\text{Cl}^-]$ ca. $0.1\ \text{M}$). Thus, the complexes might react with components of the cell culture medium and become deactivated. In addition, the possible formation of hydroxo-bridged species at physiological pH would also contribute toward the deactivation of these complexes. Such factors could limit the comparatively strong, monofunctional binding of, for example, complex **3** to DNA and result in little cytotoxicity. Furthermore, the observed lack of interstrand cross-link formation on DNA by complex **3** could lead to deactivation

via the second vacant binding site on the ruthenium center, for example by protein binding, which could weaken the $\text{Ru}\text{--DNA}$ bond (cf. hydrolysis of 9EtG from **7**) and lead to the removal of ruthenium from DNA. This could explain why other ruthenium arene complexes of the type $[(\eta^6\text{-arene})\text{--Ru}(\text{en})\text{Cl}]^+$, which form stable monofunctional adducts with, for example DNA, are considerably cytotoxic³ whereas the tethered complexes are not.

Conclusions

The bifunctional di-chlorido, nitrogen-tethered Ru^{II} arene complexes $[(\eta^6:\eta^1\text{-C}_6\text{H}_5(\text{CH}_2)_3\text{NH}_2)\text{RuCl}_2]$ (**1**) and $[(\eta^6:\eta^1\text{-C}_6\text{H}_5(\text{CH}_2)_2\text{NH}_2)\text{RuCl}_2]$ (**2**) were synthesized. These complexes are water-soluble and undergo rapid aquation to form mono- and di-aqua adducts. Loss of one chloride is strongly favored, and anation was not complete even in the presence of a large excess of chloride (ca. $275\ \text{mM}$). Hydroxo-bridged species appear to be formed from the di-aqua adduct over a range of pH $5.4\text{--}11.0$. Thus, in aqueous biological media, these complexes may be deactivated by reactions with biomolecules or by the formation of unreactive bridged species.

The reactivity of these bifunctional tethered Ru^{II} arene complexes toward 9-ethylguanine was investigated. In the absence of chloride, rapid binding of one 9EtG was observed followed by the slow formation of a di-9EtG adduct, over a period of ca. $10\ \text{h}$. Formation of di-9EtG adducts appears to be suppressed by the presence of chloride. The X-ray crystal structure of the di-9EtG adduct $[(\eta^6:\eta^1\text{-C}_6\text{H}_5(\text{CH}_2)_3\text{NH}_2)\text{Ru}(\text{9EtG})_2](\text{CF}_3\text{SO}_3)_2\cdot\text{H}_2\text{O}$ (**8** $\cdot\text{H}_2\text{O}$) revealed an unusual HH orientation of the two bases, with the formation of intramolecular hydrogen bonds between the tether NH_2 group and $\text{C6O}(\text{9EtG})$. Furthermore, the X-ray structure is consistent with the strong binding of one 9EtG ligand and the weak binding of the other, as observed in aqueous solution. Biophysical measurements on plasmid DNA showed only monofunctional binding of $[(\eta^6:\eta^1\text{-C}_6\text{H}_5(\text{CH}_2)_2\text{NH}_2)\text{Ru}(\text{NO}_3)_2]$ (**3**), again consistent with the weak binding of a second nucleobase observed by ^1H NMR solution studies. Overall, the (bio)chemical reactivity of the bifunctional tethered complexes **1** and **2** appears not to be compatible with anticancer activity. However, the low toxicity of these complexes might be a useful feature, tuneable for other biological applications.

Acknowledgment. We thank Oncosense Ltd for support for P.J.S., the Grant Agency of the Czech Republic (Grants 305/05/2030 and 203/06/1239), and the Academy of Sciences of the Czech Republic (Grants 1QS500040581 and KAN200200651) for support for V.B., COST D20/D39 for stimulating discussions, Emily Jones and Daniel Cole (Oncosense Ltd) for carrying out the cytotoxicity tests, and Mr. Juraj Bella, at the University of Edinburgh, for NMR advice and assistance.

Supporting Information Available: Details of synthesis of ethylbenzoate dimer, synthetic routes as Charts S1 and S2, crystallographic data in Tables S1–S5, NMR spectra, X-ray structures, and a gel showing restriction mapping as Figures S1–S15.

IC700799W

(64) (a) Zaludova, R.; Zakovska, A.; Kasparkova, J.; Balcarova, Z.; Vrana, O.; Coluccia, M.; Natile, G.; Brabec, V. *Mol. Pharmacol.* **1997**, *52*, 354–361. (b) Balcarova, Z.; Kasparkova, J.; Zakovska, A.; Novakova, O.; Sivo, M. F.; Natile, G.; Brabec, V. *Mol. Pharmacol.* **1998**, *53*, 846–855. (c) Brabec, V.; Kasparkova, J.; Vrana, O.; Novakova, O.; Cox, J. W.; Qu, Y.; Farrell, N. *Biochemistry* **1999**, *38*, 6781–6790. (d) Kasparkova, J.; Marini, V.; Najajreh, Y.; Gibson, D.; Brabec, V. *Biochemistry* **2003**, *42*, 6321–6332.

13.

Dual Triggering of DNA Binding and Fluorescence via Photoactivation of a Dinuclear Ruthenium(II) Arene Complex

Steven W. Magennis,^{*,†} Abraha Habtemariam,[‡] Olga Novakova,[§] John B. Henry,[‡] Samuel Meier,[‡] Simon Parsons,[‡] Iain D. H. Oswald,[‡] Viktor Brabec,[§] and Peter J. Sadler^{*,‡}

School of Physics and the Collaborative Optical Spectroscopy, Micromanipulation and Imaging Centre (COSMIC), The University of Edinburgh, King's Buildings, Edinburgh EH9 3JZ, U.K., School of Chemistry, The University of Edinburgh, King's Buildings, Edinburgh EH9 3JJ, U.K., and Institute of Biophysics, Academy of Sciences of the Czech Republic, v.i.i. Kralovopolska 135, CZ-61265 Brno, Czech Republic

Received November 6, 2006

The dinuclear Ru^{II} arene complexes [$\{(\eta^6\text{-arene})\text{RuCl}\}_2(\mu\text{-2,3-dpp})\}(\text{PF}_6)_2$, arene = indan (**1**), benzene (**2**), *p*-cymene (**3**), or hexamethylbenzene (**4**) and 2,3-dpp = 2,3-bis(2-pyridyl)pyrazine, have been synthesized and characterized. Upon irradiation with UVA light, complexes **1** and **2** readily underwent arene loss, while complexes **3** and **4** did not. The photochemistry of **1** was studied in detail. In the X-ray structure of [$\{(\eta^6\text{-indan})\text{RuCl}\}_2(\mu\text{-2,3-dpp})\}(\text{PF}_6)_2$ (**1**), 2,3-dpp bridges two Ru^{II} centers 6.8529(6) Å apart. In water, aquation of **1** in the dark occurs with replacement of chloride with biexponential kinetics and decay constants of $100 \pm 1 \text{ min}^{-1}$ and $580 \pm 11 \text{ min}^{-1}$. This aquation was suppressed by 0.1 M NaCl. UV or visible irradiation of **1** in aqueous or methanolic solution led to arene loss. The fluorescence of the unbound arene is ~ 40 times greater than when it is complexed. Irradiation of **1** also had a significant effect on its interactions with DNA. The DNA binding of **1** is increased after irradiation. The non-irradiated form of **1** preferentially formed DNA adducts that only weakly blocked RNA polymerase, while irradiation of **1** transformed the adducts into stronger blocks for RNA polymerase. The efficiency of irradiated **1** to form DNA interstrand cross-links was slightly greater than that of cisplatin in both 10 mM NaClO₄ and 0.1 M NaCl. In contrast, the interstrand cross-linking efficiency of non-irradiated **1** in 10 mM NaClO₄ was relatively low. An intermediate amount of cross-linking was observed when the sample of DNA already modified by non-irradiated **1** was irradiated. DNA unwinding measurements supported the conclusion that both mono- and bifunctional adducts with DNA can form. These results show that photoactivation of dinuclear Ru^{II} arene complexes can simultaneously produce a highly reactive ruthenium species that can bind to DNA and a fluorescent marker (the free arene). Importantly, the mechanism of photoreactivity is also independent of oxygen. These complexes, therefore, have the potential to combine both photoinduced cell death and fluorescence imaging of the location and efficiency of the photoactivation process.

Introduction

Anticancer treatments that use site-selective photoinduced cytotoxicity have the potential to eliminate the unwanted side effects of conventional chemotherapy by avoiding damage to healthy cells. Photoactivation may also allow new and more toxic reaction pathways to be accessed. Photodynamic

therapy (PDT), which involves the use of drugs (usually porphyrins or related molecules) that absorb light and subsequently react with cellular components to produce cytotoxic species, has received the most attention to date.¹ The most widely used drug, Photofrin, is an ill-defined mixture of up to 60 different substances and remains in the body for six to eight weeks, resulting in prolonged skin sensitivity. Photofrin requires oxygen for its mechanism of toxicity in PDT, even though tumors often have poor oxygen

* To whom correspondence should be addressed. E-mail: s.magennis@ed.ac.uk (S.W.M.); p.j.sadler@ed.ac.uk (P.J.S.).

[†] School of Physics and Collaborative Optical Spectroscopy, Micromanipulation and Imaging Centre (COSMIC), The University of Edinburgh.

[‡] School of Chemistry, The University of Edinburgh.

[§] Institute of Biophysics, Academy of Sciences of the Czech Republic.

(1) Dolmans, D. E. J. G. J.; Fukumura, D.; Jain, R. K. *Nat. Rev. Cancer* 2003, 3, 380–387.

supply. Second-generation photosensitizers address some of these problems, but despite progress, PDT is not yet considered to be a front-line treatment for cancer. Therefore, there is a need for alternative photoactive drugs.

The unique reactivity of metal complexes makes them interesting candidates for chemotherapy.² A notable example is the platinum drug cisplatin, *cis*-[Pt^{II}(NH₃)₂Cl₂], one of the most widely used anticancer agents for chemotherapy, despite its severe side-effects and acquired drug resistance.² This drug and several other platinum anticancer complexes are believed to act through formation of adducts with cellular DNA. In principle, metal-based photoactivated anticancer drugs might offer significant advantages over porphyrin-based phototherapies. Much progress has been made in this area over the past decade.^{3,4} Metallointercalators can photocleave nucleic acids from DNA,⁵ photoreactions of Pt^{IV} azide complexes can induce Pt^{II}–DNA cross-links similar to those established for cisplatin,^{6,7} while the photochemistry of many other metal complexes has also been studied.^{8–15}

The present study concerns a ruthenium complex in the class [(η^6 -arene)Ru(XY)Z], where XY is a chelating diamine and Z is a leaving group such as Cl[−]. Such “piano-stool” complexes have been shown to be cytotoxic to cancer cell lines, including lines that have become resistant to cisplatin.¹⁶ Furthermore, previous studies with platinum compounds have shown that dinuclear complexes can lead to novel DNA lesions, which can be important in the avoidance of cellular cross-resistance.¹⁷ Here we report the synthesis, characterization, and photochemistry of organometallic dinuclear Ru^{II} complexes [(η^6 -arene)RuCl]₂(μ -2,3-dpp)](PF₆)₂ containing 2,3-dpp (2,3-bis(2-pyridyl)pyrazine) as a bridging ligand and

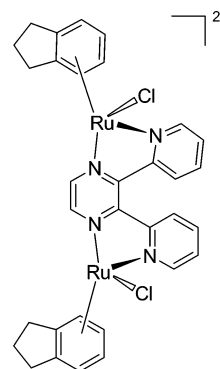
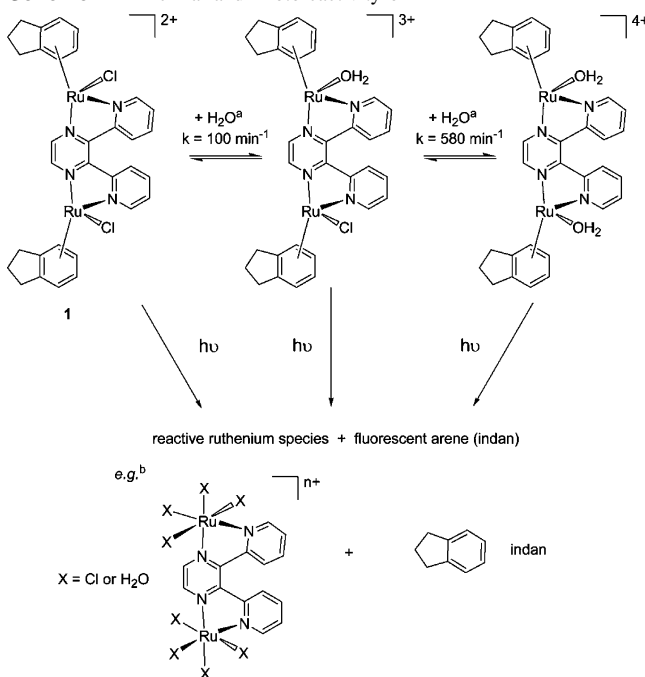


Figure 1. Structure of [(η^6 -indan)RuCl]₂(μ -2,3-dpp)](PF₆)₂ (**1**).

Scheme 1. Thermal and Photoreactivity of **1**



^a Note that additional hydroxo complexes may also exist because of the deprotonation of aqua ligands. ^b The ruthenium species indicated here are only possible photoproducts. The detailed photochemical reaction pathways will be the subject of further investigation.

indan (**1**), benzene (**2**), *p*-cymene (**3**), or hexamethylbenzene (**4**) as the arene. We show that [(η^6 -indan)RuCl]₂(μ -2,3-dpp)](PF₆)₂ (**1**), Figure 1, can be photoactivated to produce a highly reactive ruthenium species that can bind to DNA and a fluorescent marker (Scheme 1). Importantly, the mechanism of photoreactivity is also independent of oxygen. These complexes, therefore, have the potential to combine both photoinduced cell death and fluorescence imaging of the location and efficiency of the photoactivation process.

Experimental Section

Materials. [Ru(bpy)₃]₂Cl₂·6H₂O (bpy = 2,2′-bipyridine) (99.5%), 2,3-bis(2-pyridyl)-pyrazine (2,3-dpp), indan (95%), and NH₄PF₆ were obtained from Aldrich. Cisplatin was obtained from Sigma. [Ru(indan)Cl₂]₂ was prepared following literature methods.¹⁸ NaCl (reagent grade) was obtained from Fisher. The solvents used for photochemistry and fluorescence spectroscopy were methanol and

- (2) Guo, Z. J.; Sadler, P. J. *Angew. Chem., Int. Ed.* **1999**, *38*, 1513–1531.
- (3) Clarke, M. J. *Coord. Chem. Rev.* **2003**, *236*, 209–233.
- (4) Szaciłowski, K.; Macyk, W.; Drzewiecka-Matuszek, A.; Brindell, M.; Stochel, G. *Chem. Rev.* **2005**, *105*, 2647–2694.
- (5) Erkkila, K. E.; Odom, D. T.; Barton, J. K. *Chem. Rev.* **1999**, *99*, 2777–2795.
- (6) Müller, P.; Schröder, B.; Parkinson, J. A.; Kratochwil, N. A.; Coxall, R. A.; Parkin, A.; Parsons, S.; Sadler, P. J. *Angew. Chem., Int. Ed.* **2003**, *42*, 335–339.
- (7) Kratochwil, N. A.; Parkinson, J. A.; Bednarski, P. J.; Sadler, P. J. *Angew. Chem., Int. Ed.* **1999**, *38*, 1460–1463.
- (8) Brindell, M.; Kuliš, E.; Elmroth, S. K. C.; Urbanińska, K.; Stochel, G. *J. Med. Chem.* **2005**, *48*, 7298–7304.
- (9) Holder, A. A.; Swavey, S.; Brewer, K. J. *Inorg. Chem.* **2004**, *43*, 303–308.
- (10) Benites, P. J.; Holmberg, R. C.; Rawat, D. S.; Kraft, B. J.; Klein, L. J.; Peters, D. G.; Thorp, H. H.; Zaleski, J. M. *J. Am. Chem. Soc.* **2003**, *125*, 6434–6446.
- (11) Singh, T. N.; Turro, C. *Inorg. Chem.* **2004**, *43*, 7260–7262.
- (12) Lutterman, D. A.; Fu, P. K.-L.; Turro, C. *J. Am. Chem. Soc.* **2006**, *128*, 738–739.
- (13) Menon, E. L.; Perera, R.; Navarro, M.; Kuhn, R. J.; Morrison, H. *Inorg. Chem.* **2004**, *43*, 5373–5381.
- (14) Uji-i, H.; Foubert, P.; De Schryver, F. C.; De Feyter, S.; Gicquel, E.; Etoc, A.; Moucheron, C.; Kirsch-De Mesmaeker, A. *Chem. Eur. J.* **2006**, *12*, 758–762.
- (15) Gicquel, E.; Paillous, N.; Vicendo, P. *Photochem. Photobiol.* **2000**, *72*, 583–589.
- (16) Aird, R. E.; Cummings, J.; Ritchie, A. A.; Muir, M.; Morris, R. E.; Chen, H.; Sadler, P. J.; Jodrell, D. I. *Br. J. Cancer* **2002**, *86*, 1652–1657.
- (17) Zaludova, R.; Zakovska, A.; Kasparkova, J.; Balcarova, Z.; Kleinwächter, V.; Vrana, O.; Farrell, N.; Brabec, V. *Eur. J. Biochem.* **1997**, *246*, 508–517.
- (18) Bennett, M. A.; Smith, A. K. *J. Chem. Soc., Dalton Trans.* **1974**, 233–241.

water (HPLC, Fisher). NMR spectroscopy used methanol- d_4 (99.8%), acetonitrile- d_3 , and D_2O from Aldrich.

Preparation and Characterization of $[(\eta^6\text{-Indan})\text{RuCl}_2](\mu\text{-2,3-dpp})(\text{PF}_6)_2$ (1**).** The dimer $[\text{Ru}(\text{indan})\text{Cl}_2]_2$ (0.150 g, 0.26 mmol) was dissolved in MeOH (40 mL), and 2,3-dpp (0.077 g, 0.30 mmol) was added to this mixture. The solution turned deep red, and the reaction mixture was stirred at ambient temperature for 1.5 h. It was then filtered, and the volume of the filtrate was reduced on a rotary evaporator to ~ 25 mL. NH_4PF_6 (0.254 g, 1.56 mmol) was added to the mixture, and the flask was shaken. A precipitate started to appear almost immediately. The flask was kept at 253 K overnight. The precipitate was collected by filtration, washed with cold methanol and ether, and dried in air to give an orange-red solid (yield: 200 mg, 75%). Crystals suitable for X-ray diffraction studies were obtained by slow evaporation of a methanolic solution at ambient temperature. ^1H NMR ($\text{CD}_3\text{CN}-d_3$): δ 9.20 (d, 2H), 9.17 (m, 2H) 8.45 (d, 2H), 8.02 (t, 2H), 7.79 (t, 2H), 6.10–5.86 (m, 8H), 3.09–2.78 (m, 8H), 2.18 (m, 4H). Anal. Calcd for $\text{C}_{32}\text{H}_{30}\text{Cl}_2\text{F}_{12}\text{N}_4\text{P}_2\text{Ru}_2$: C, 37.19; H, 2.93; N, 5.42. Found: C, 36.9; H, 3.68; N, 5.58.

The three other dinuclear ruthenium(II) arene complexes in the series $[(\eta^6\text{-arene})\text{RuCl}_2](\mu\text{-2,3-dpp})(\text{PF}_6)_2$, where arene = benzene (**2**), *p*-cymene (**3**), or hexamethylbenzene (**4**), were synthesized and characterized as described in the Supporting Information.

NMR Spectroscopy. ^1H NMR spectra were acquired on a Bruker DMX 500 spectrometer (^1H = 500 MHz). All data processing was carried out using XWIN NMR, version 2.0 (Bruker U.K. Ltd.). ^1H NMR chemical shifts for aqueous solutions were internally referenced to 1,4-dioxane (3.77 ppm), to the methyl singlet of TSP (0 ppm), or to residual protiated solvent in acetonitrile- d_3 (1.94 ppm) and methanol- d_4 (3.31 ppm).

X-ray Crystallography. Diffraction data were collected using Mo $K\alpha$ radiation ($\lambda = 0.71073$ Å) on a Bruker Smart Apex CCD diffractometer equipped with an Oxford Cryosystems LT device operating at 150 K. Crystals suitable for X-ray diffraction were grown from a methanol solution at ambient temperature: orange block of dimensions $0.12 \times 0.12 \times 0.12$ mm³; formula $\text{C}_{33}\text{H}_{34}\text{Cl}_2\text{F}_{12}\text{N}_4\text{OP}_2\text{Ru}_2$, $M = 1065.62$; monoclinic, space group $P2_1/n$; $a = 12.1038(8)$ Å, $b = 16.8908(11)$ Å, $c = 18.8556(12)$ Å, $\beta = 101.1960(10)^\circ$, $V = 3781.5(4)$ Å³; $Z = 4$, $D_{\text{calcd}} = 1.872$ Mg m⁻³; $\mu = 1.120$ mm⁻¹; $F(000) = 2112$. The structure was solved using direct methods (SHELXS)¹⁹ and was refined against F^2 using SHELXL.²⁰ Hydrogen atoms were placed in calculated positions, and the non-H atoms were refined with anisotropic displacement parameters. The final conventional R factor [R_1 , based on $|F|$ and 6645 data points with $F > 4\sigma(F)$] was 0.0381, and the weighted wR_2 (based on F^2 and all 7741 unique data from $\theta = 1.6$ to 26.4°) was 0.0810. The final ΔF synthesis extremes were +0.77 and -0.51 e Å⁻³.

Photochemistry and Fluorescence Spectroscopy. UV–vis spectra were recorded on a Cary 50-Bio spectrophotometer. Typical concentrations of **1** were 0.05–0.2 mM. Solutions were stored in the dark to minimize unwanted photoreactions between measurements. For photochemical studies, methanolic or aqueous solutions of **1** were irradiated with a high-pressure mercury lamp (Nikon model LH-M100CB-1). The lamp output was passed through a bandpass filter (Nikon) in the range of 340–380 or 465–495 nm and was focused onto the sample cuvette, providing average light power of 100 and 42 mW, respectively. Solutions were handled in

air at room temperature (~ 294 K), unless stated otherwise. The effect of oxygen on the photochemistry was assessed by degassing methanolic solutions using three freeze–pump–thaw cycles to a final pressure of 6.4–7.4 mbar for 5 min. Care was taken to minimize the exposure of the degassing cell to light during the degassing procedure, with spectra recorded before and after degassing to ensure that no reaction had taken place during the process. The degassing procedure was verified by observation of the reversible increase in fluorescence of $[\text{Ru}(\text{bpy})_3]\text{Cl}_2$ in methanol upon degassing.²¹

Time-resolved fluorescence measurements were made by time-correlated single-photon counting (TCSPC). The output of a femtosecond laser system (10 W Verdi and Mira Ti-Sapphire laser, Coherent) was passed through a pulse picker (to reduce the repetition rate to 4.75 MHz) and frequency tripled to either 260 nm for **1** or to 300 nm for $[\text{Ru}(\text{bpy})_3]\text{Cl}_2$ and biphenyl. The fluorescence was measured at the magic angle in a spectrometer equipped with TCC900 photon-counting electronics (Edinburgh Instruments). The emission monochromator bandpass was 9 nm. The instrument response was ~ 50 ps full width at half-maximum. Decay curves were analyzed with tail fits using F900 software (Edinburgh Instruments). The quality of these fits was determined by the value of the χ^2 statistical parameter and visualization of residuals. Steady-state fluorescence spectra were either acquired using a SPEX Fluoromax ($\lambda_{\text{ex}} = 260$ nm; 5 nm excitation and emission slits) or with the same setup used for time-resolved measurements above. There was negligible solvent fluorescence.

The photochemical quantum yield of **1** in 0.1 M NaCl with excitation through the 340–380 nm filter was estimated by measurement of the lamp power at 360 nm with a calibrated power meter (Fieldmaster with LM10 head, Coherent) and the absorption of the complex at the excitation wavelength. It was assumed that the photochemical reaction had gone to completion when there was no further change in absorption or fluorescence. The photochemical quantum yield was measured by calculation of the amount of light required to convert 20% of the sample to product. No corrections were made for absorption by the photoproducts or reflection of the excitation light from the surfaces of the cuvette.

Kinetic parameters for aquation of **1** were obtained by fitting the curve of absorbance of **1** in water at 440 nm versus time to a biexponential decay (linear least-squares fitting in Origin 7 software).

DNA Binding. Reaction mixtures of DNA and **1** were prepared in three ways: in the dark (henceforth referred to as “non-irradiated”), by addition of pre-irradiated **1** to DNA (“pre-irradiated”), or by addition of **1** to DNA followed by irradiation of the resulting mixture (“irradiated”). A stock solution of **1** at a concentration of 5×10^{-4} M in 10 mM NaClO_4 was prepared in the dark at 298 K. A sample of **1** dissolved in 0.1 M NaCl was prepared by the addition of NaCl to a stock solution of **1** in 10 mM NaClO_4 . Pre-irradiated samples of **1** were prepared by irradiation of the stock solution of **1** in 10 mM NaClO_4 . Calf thymus (CT) DNA (42% G + C, mean molecular mass ~ 20 000 kD) was prepared and characterized as described previously.^{22,23} Plasmid pSP73KB [2455 base pairs (bp)] was isolated according to standard procedures. Restriction endonucleases and Klenow fragment of DNA polymerase I were purchased from New England Biolabs. Riboprobe Gemini System II for transcription mapping containing T7 RNA polymerase was purchased from Promega and ethidium

(19) Sheldrick, G. M. *SHELXS*; University of Göttingen: Göttingen, Germany, 1997.

(20) Sheldrick, G. M. *SHELXL*; University of Göttingen: Göttingen, Germany, 1997.

(21) Demas, J. N.; McBride, R. P.; Harris, E. W. *J. Phys. Chem.* **1976**, *80*, 2248–2253.

(22) Brabec, V.; Palecek, E. *Biophysik* **1970**, *6*, 290–300.

(23) Brabec, V.; Palecek, E. *Biophys. Chem.* **1976**, *4*, 79–92.

bromide and agarose from Merck KgaA (Darmstadt, Germany). Acrylamide, bis(acrylamide), and urea were purchased from Merck KgaA, and the radioactive products were obtained from MP Biomedicals, LLC (Irvine, CA).

Irradiation. Samples were irradiated at 310 K using the LZC-4V illuminator (photoreactor) (Luzchem, Canada) with temperature controller and with UVA lamps (300–400 nm with a maximum intensity at ~ 360 nm, 5 mW cm^{-2}) for 60 min.

Ruthenation Reactions. CT DNA and plasmid pSP73KB were incubated with **1** in 10 mM NaClO_4 or 0.1 M NaCl at 310 K. The number of atoms of ruthenium bound per nucleotide residue (r_b value) was determined by flameless atomic absorption spectrophotometry (FAAS).

DNA Transcription by RNA Polymerase In Vitro. Transcription of the (*NdeI/HpaI*) restriction fragment of pSP73KB DNA with DNA-dependent T7 RNA polymerase and electrophoretic analysis of transcripts were performed according to the protocols recommended by Promega [Promega Protocols and Applications, 43–46 (1989/90)] and were previously described in detail.^{24,25}

DNA Interstrand Cross-linking. The amount of interstrand cross-links formed by **1** in linear DNA was measured in pSP73KB plasmid (2455 bp), which was first linearized by *EcoRI* (*EcoRI* cuts only once within pSP73 plasmid), 3'-end labeled by means of Klenow fragment of DNA polymerase I in the presence of [α -³²P]-dATP, and subsequently modified by the ruthenium complex. Linearized DNA (1 μg) was incubated with the complex for 20 h so that an r_b value of 0.001 was reached, unless stated otherwise. The samples were precipitated by ethanol to remove unbound ruthenium, and the pellet was dissolved in 18 μL of a solution containing 30 mM NaOH, 1 mM EDTA, 6.6% sucrose, and 0.04% bromophenol blue. The samples were analyzed for interstrand CLs by agarose gel electrophoresis under denaturing conditions (on alkaline 1% agarose gel).^{25,26} After the electrophoresis was completed, the intensities of the bands corresponding to single strands of DNA and interstrand cross-linked duplex were quantified by means of a Phosphor Imager (Fuji BAS 2500 system with AIDA software). The frequency of the interstrand cross-links (the number of interstrand cross-links per molecule of the ruthenium complex bound to DNA) was calculated using the Poisson distribution from the fraction of non-cross-linked DNA in combination with the r_b values and the fragment size. Other details of this assay can be found in previously published papers.^{25–27}

Unwinding of Negatively Supercoiled DNA. The unwinding of closed circular supercoiled pSP73KB plasmid DNA was assayed by an agarose gel mobility shift assay.²⁸ The unwinding angle, Φ , induced per DNA adduct of **1** was calculated upon the determination of the r_b value at which the complete transformation of the supercoiled to relaxed form of the plasmid was attained. Samples of the pSP73KB plasmid were incubated with **1** for 20 h, precipitated by ethanol, and redissolved in TAE buffer (0.04 M Tris-acetate + 1 mM EDTA, pH 7.0). An aliquot of the precipitated sample was subjected to electrophoresis on 1% agarose gels running at 298 K in the dark with TAE buffer at 30 V. The gels were then stained with ethidium bromide, followed by photography on

Table 1. Selected Bond Lengths (Å) and Angles (deg) for **1**^a

Ru(1A)–Cl(1A)	2.3853(9)
Ru(1B)–Cl(1B)	2.3947(8)
Ru(1A)–N1	2.082(3)
Ru(1A)–N8	2.075(3)
Ru(1B)–N11	2.057(3)
Ru(1B)–N18	2.074(3)
Ru(1A)–C(1A)	2.184(4)
Ru(1A)–C(2A)	2.213(3)
Ru(1A)–C(6A)	2.222(3)
Ru(1A)–C(7A)	2.201(4)
Ru(1A)–C(8A)	2.149(4)
Ru(1A)–C(9A)	2.182(4)
Ru(1B)–C(1B)	2.194(3)
Ru(1B)–C(2B)	2.205(3)
Ru(1B)–C(6B)	2.221(9)
Ru(1B)–C(7B)	2.188(3)
Ru(1B)–C(8B)	2.182(3)
Ru(1B)–C(9B)	2.165(3)
N1–Ru(1A)–N8	76.75(10)
N11–Ru(1B)–N18	76.64(10)

^a For the numbering scheme, see Figure 2.

Polaroid 667 film with transilluminator. The other aliquot was used for the determination of the r_b values by FAAS.

Other Methods. FAAS measurements were made on a Varian AA240Z Zeeman atomic absorption spectrometer equipped with a GTA 120 graphite tube atomizer. The gels were dried and visualized by using the FUJIFILM bioimaging analyzer, and the radioactivities associated with bands were quantified with AIDA image analyzer software.

Results and Discussion

Synthesis and Characterization. The bimetallic complexes [$\{(\eta^6\text{-arene})\text{RuCl}\}_2(\mu\text{-2,3-dpp})](\text{PF}_6)_2$, arene = indan (**1**), benzene (**2**), *p*-cymene (**3**), or hexamethylbenzene (**4**), were prepared by the reaction of the appropriate dimer [$(\eta^6\text{-arene})\text{RuCl}_2$]₂ with an equimolar amount of 2,3-dpp. The products were isolated as hexafluorophosphate salts and were characterized by ¹H NMR spectroscopy, elemental analysis, and for **1**, X-ray crystallography. It is possible that two isomers can form because the coordinated chloride ligands take either cis or trans positions. However, ¹H NMR spectroscopy studies suggested that only one species is present in solution, and the solid-state structure of **1** shows that the compound crystallized with the chloride ligands in a cis position (vide infra).

X-ray Crystallography. Crystals of **1** suitable for X-ray diffraction studies were obtained from methanol at 273 K. Selected bond lengths and angles are shown in Table 1, and the structure with numbering scheme is shown in Figure 2. The 2,3-dpp bridge holds the two ruthenium centers at an intermolecular distance of 6.8529(6) Å, which is comparable to those found for other pyrazine-bridged ruthenium dimers (6.779–7.026 Å) (CSD). The Ru–Cl bonds are in a mutually cis configuration with a separation of 6.306(3) Å between chlorides. In contrast, the related bimetallic complex [$\{(\eta^6\text{-p-cymene})\text{RuCl}\}_2(\mu\text{-2,3-dpp})](\text{PF}_6)_2$ crystallized with Ru–Cl in a trans configuration.²⁹ As a consequence, there are major differences in the crystal packing of the two structures.

(24) Lemaire, M. A.; Schwartz, A.; Rahmouni, A. R.; Leng, M. *Proc. Natl. Acad. Sci. U.S.A.* **1991**, *88*, 1982–1985.

(25) Brabec, V.; Leng, M. *Proc. Natl. Acad. Sci. U.S.A.* **1993**, *90*, 5345–5349.

(26) Farrell, N.; Qu, Y.; Feng, L.; Van Houten, B. *Biochemistry* **1990**, *29*, 9522–9531.

(27) Brabec, V.; Kasparkova, J.; Vrana, O.; Novakova, O.; Cox, J. W.; Qu, Y.; Farrell, N. *Biochemistry* **1999**, *38*, 6781–6790.

(28) Keck, M. V.; Lippard, S. J. *J. Am. Chem. Soc.* **1992**, *114*, 3386–3390.

(29) Singh, A.; Singh, S. K.; Trivedi, M.; Pandey, D. S. *J. Organomet. Chem.* **2005**, *690*, 4243–4251.

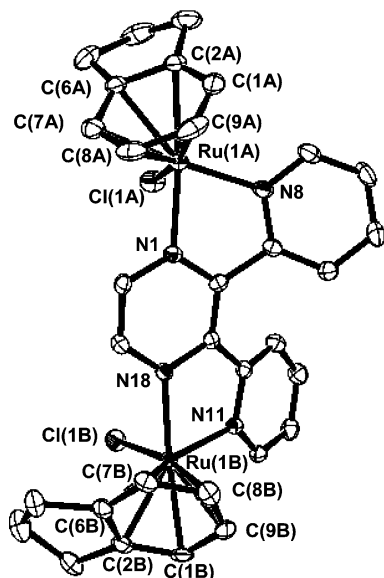


Figure 2. X-ray crystal structure of $[(\eta^6\text{-indan})\text{RuCl}]_2(\mu\text{-}2,3\text{-dpp})(\text{PF}_6)_2$ (**1**), showing numbering scheme. Ellipsoids enclose 30% probability surfaces. $\text{Ru(1A)}\text{--Ru(1B)} = 6.8529(6)$ Å.

Interactions (intra- and inter-) between C–H and X (X = Cl, F), as well as $\pi\text{--}\pi$ interactions, in $[(\eta^6\text{-}p\text{-cymene})\text{RuCl}]_2(\mu\text{-}2,3\text{-dpp})(\text{PF}_6)_2$ are believed to stabilize the crystal packing arrangement, which involves parallel helical chains.²⁹ This type of packing was not observed in the crystal structure of **1**, where only weak interactions were observed between C–H and F. The bimetallic complexes containing the fragment $\{\text{Ru}^{\text{II}}(\text{L})\text{Cl}\}$, L = 2-(C₅H₄N)–N=N–C₆H₄Me³⁰ and L = bipyridine (bpy),³¹ bridged by [2,3,5,6-tetrakis(2-pyridyl)pyrazine] (tppz) show both the cis and trans isomers with respect to coordinated chloride ligands in solution, with the former preferentially crystallizing as the trans isomer. Similarly, the bimetallic complex containing two $\{\text{Ru}^{\text{II}}(\text{[9]-aneS}_3)\text{Cl}\}$ units bridged by 2,2'-bipyrimidine (bpym)³² show both cis and trans forms with respect to coordinated chloride ligands in solution, with the trans isomer being preferentially crystallized. The Ru–Cl bond lengths for Ru(1A) and Ru(1B) are slightly different (2.3853 and 2.3947 Å), and the Ru–N distances are in the range of 2.057–2.082 Å. These values are within the range found for other structures of Ru^{II} arene complexes.³³ The 2,3-dpp ligand bridging the two Ru metal centers is substantially distorted from planarity, with the three rings twisting out of plane with respect to one another by 21.74°. The coordination geometry around each ruthenium center is distorted octahedral, which is reflected in the small bite angle of 2,3-dpp [N(1)–Ru(1A)–N(8) (76.75°) and N(11)–Ru(1B)–N(18) (76.64°)], and represents

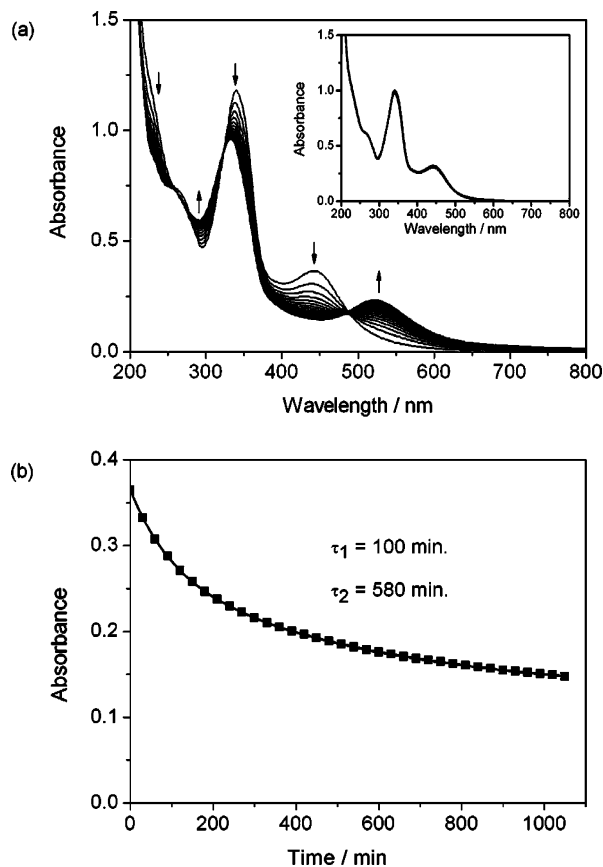


Figure 3. Thermal reactivity of **1** in aqueous solution. (a) Absorption spectra of **1** in water recorded hourly for 17 h. The inset shows the absorption spectra of **1** in 0.1 M NaCl recorded hourly for 18 h. In each case, the first spectrum was recorded ~10 min after dissolution. (b) Time-dependence of absorbance at 440 nm of **1** in water. The solid line is a fit of the data as a biexponential decay, with decay constants of 100 ± 1 and 580 ± 11 min^{−1} and amplitudes of 39 and 61%, respectively ($R = 0.9999$).

a major deviation from an ideal octahedral geometry; similar distortions were also observed for the bimetallic complexes cited above. The ruthenium-to-arene centroid ring distances [1.6822(15) and 1.6808(14) Å] are slightly longer than those of the Ru^{II} arene complexes containing ethylenediamine (en) but are shorter than those of the Ru^{II} arene complexes containing the π -acidic chelating ligand azopyridine (azpy). For example, the ruthenium-to-arene centroid ring distances for $[(\eta^6\text{-}p\text{-cymene})\text{RuCl}(\text{en})](\text{PF}_6)$ and $[(\eta^6\text{-}p\text{-cymene})\text{RuCl}(\text{azpy})](\text{PF}_6)$ are 1.6692(14)³⁴ and 1.7203(16) Å,³⁵ respectively. The lengthening of the centroid bond in the latter complex is attributed to an increased extent of back-bonding competition for Ru 4d⁶ electron density between the π -acceptor ligands, arene, and azopyridine and may explain the ease of arene loss in solution for this class of complexes.

Thermal Reactivity. Freshly dissolved **1** in water undergoes a chemical change in the absence of light. Figure 3a shows absorption spectra recorded every hour for 17 h for a solution of **1** in water. The spectrum immediately after dissolution contains two peaks at 340 ($\epsilon = 1 \times 10^4$ M^{−1}

(30) Chanda, N.; Laye, R. H.; Chakraborty, S.; Paul, R. L.; Jeffery, J. C.; Ward, M. D.; Lahiri, G. K. *J. Chem. Soc., Dalton Trans.* **2002**, 3496–3504.

(31) Hartshorn, C. M.; Daire, N.; Tondreau, V.; Loeb, B.; Meyer, T. J.; White, P. S. *Inorg. Chem.* **1999**, *38*, 3200–3206.

(32) Araújo, C. S.; Drew, M. G. B.; Félix, V.; Jack, L.; Madureira, J.; Newell, M.; Roche, S.; Santos, T. M.; Thomas, J. A.; Yellowlees, L. *Inorg. Chem.* **2002**, *41*, 2250–2259.

(33) Habtemariam, A.; Melchart, M.; Fernández, R.; Parsons, S.; Oswald, I. D. H.; Parkin, A.; Fabbiani, F. P. A.; Davidson, J.; Dawson, A.; Aird, R. E.; Jodrell, D. I.; Sadler, P. J. *J. Med. Chem.* **2006**, *49*, 6858–6868.

(34) Morris, R. E.; Aird, R. E.; Murdoch, P. S.; Chen, H.; Cummings, J.; Hughes, N. D.; Parsons, S.; Parkin, A.; Jodrell, D. I.; Sadler, P. J. *J. Med. Chem.* **2001**, *44*, 3616–3621.

(35) Dougan, S. J.; Melchart, M.; Habtemariam, A.; Parsons, S.; Sadler, P. J. *Inorg. Chem.* **2006**, *45*, 10882–10894.

cm^{-1}) and 440 nm ($\epsilon = 4 \times 10^3 \text{ M}^{-1} \text{ cm}^{-1}$). In accordance with the analysis given for related Ru^{II} complexes of bispyridylpyrazine and arenes, the peak at 340 nm is assigned to a LC transition on 2,3-dpp, while the peak at 440 nm is assigned to an MLCT transition from Ru to 2,3-dpp.^{36,37} The most apparent change is the decrease in the absorbance of the 440 nm peak and the appearance of a new peak at 520 nm.

The decrease in absorbance at 440 nm with time for **1** in water is shown in Figure 3b. It has a biexponential dependence, as shown by the fit to the data, with decay constants of 100 ± 1 and $580 \pm 11 \text{ min}^{-1}$ and amplitudes of 39 and 61%, respectively. Related mononuclear Ru^{II} arene complexes undergo a monoexponential decrease in absorbance because of loss of chloride and substitution by water.³⁸ In **1**, there are two chloride ligands (one on each Ru) that can be substituted by water. The loss of the first chloride would be expected to be faster than the substitution of the second chloride because of the increased positive charge on the molecule, hence the biexponential kinetics (Scheme 1). This also explains the absence of a clear isosbestic point at around 490 nm in Figure 3a. The new peak at 520 nm in Figure 3a is assigned to an MLCT transition, which is shifted to lower energy for the aqua complex. This is attributed to increased electron density from the water ligand, in comparison to the chloride ligand, which makes the Ru^{II} easier to oxidize.

Experiments were also performed in 0.1 M NaCl. The inset of Figure 3a shows absorption spectra for **1** in 0.1 M NaCl every hour for 18 h. The change in the spectrum with time is negligible, showing that high concentrations of chloride suppress the aquation of **1**.

Photochemistry and Fluorescence Spectroscopy. Ruthenium(II) arene complexes can undergo photoinduced reactions, and this has proven to be a useful synthetic method for the preparation of new ruthenium complexes.^{39–41} For example, Ford et al. showed that ruthenium(II) arene complexes of formula $[\text{Ru}(\eta^6\text{-arene})\text{L}_3]^{2+}$ ($\text{L} = \text{NH}_3$ or H_2O) undergo loss of the arene and aquation of the metal when irradiated in deaerated aqueous solution.⁴² Irradiation of **1** in aqueous or methanolic solutions also resulted in the formation of new species, as evidenced by absorption, NMR, and fluorescence spectroscopy. In general, the course of the photochemical reaction was the same in both water and methanol.

Figure 4 shows the changes in the absorption spectra during irradiation of a 0.1 M NaCl solution of **1**. The new peaks are different from those of the aquated form of **1**. Irradiation of aquated **1** also resulted in spectral changes: the absorption at long wavelength increased, and the peak

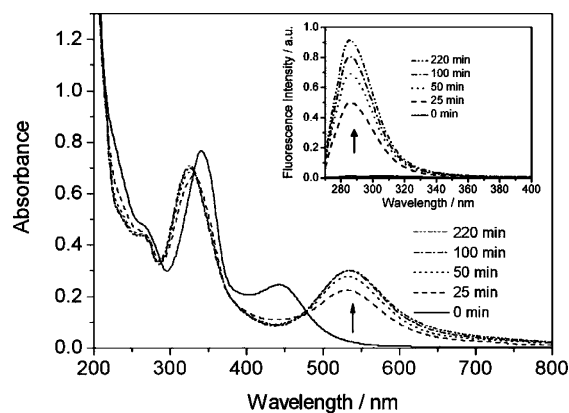


Figure 4. Absorption spectra of **1** in 0.1 M NaCl following irradiation at 340–380 nm (power of 160 mW at 360 nm). Absorption spectra were recorded after 0, 25, 50, 100, and 220 min of irradiation. The inset shows fluorescence spectra for the same solution after irradiation ($\lambda_{\text{ex}} = 260 \text{ nm}$).

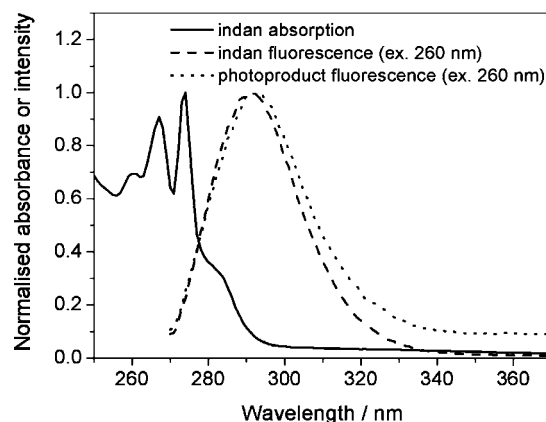


Figure 5. Absorption and fluorescence spectra of indan in methanol and fluorescence spectra of **1** in methanol after irradiation for 220 min ($\lambda_{\text{ex}} = 260 \text{ nm}$; see Figure S2 for absorption and fluorescence spectra of **1** upon irradiation in methanol).

position shifted from 522 to 530 nm. Furthermore, the photoproducts of **1** in water and 0.1 M NaCl are different (see Figure S1). Similar changes in the absorption spectra were also obtained after irradiation of methanolic solutions of **1** (see Figure S2).

In addition to the absorption changes, it was found that the solution of **1** became fluorescent as a result of irradiation. Prior to irradiation, **1** was nonemissive when excited in the UV–vis range in water or methanol, with the exception of a weak fluorescence around 285–315 nm when excited at 260–270 nm. After irradiation, this short-wavelength emission increased significantly in intensity (see inset to Figure 4). When excited at 260 nm, the fluorescence in 0.1 M NaCl is ~ 40 times greater after irradiation. Since arene loss was a possible explanation for the photochemistry of **1**, the fluorescence of the free arene, indan, was also examined. Figure 5 shows the emission spectrum of the photoproduct of **1** in methanol, together with the absorption and emission spectra for indan in methanol. Indan has a strong absorption in the UV region, with $\epsilon_{267} = 1950 \text{ M}^{-1} \text{ cm}^{-1}$ in methanol, and its emission spectrum is very similar to that of the photoproduct. It should be noted that the ligand 2,3-dpp is also emissive when free in solution, but the fluorescence is at a much longer wavelength (peak at 400 nm).

- (36) Campagna, S.; Denti, G.; De Rosa, G.; Sabatino, L.; Ciano, M.; Balzani, V. *Inorg. Chem.* **1989**, *28*, 2565–2570.
- (37) Di Marco, G.; Bartolotta, A.; Ricevuto, V.; Campagna, S.; Denti, G.; Sabatino, L.; De Rosa, G. *Inorg. Chem.* **1991**, *30*, 270–275.
- (38) Wang, F.; Chen, H.; Parsons, S.; Oswald, I. D. H.; Davidson, J. E.; Sadler, P. J. *Chem. Eur. J.* **2003**, *9*, 5810–5820.
- (39) Gill, T. P.; Mann, K. R. *Organometallics* **1982**, *1*, 485–488.
- (40) Lavalley, R. J.; Kutal, C. J. *Organomet. Chem.* **1998**, *562*, 97–104.
- (41) Hayashida, T.; Nagashima, H. *Organometallics* **2002**, *21*, 3884–3888.
- (42) Weber, W.; Ford, P. C. *Inorg. Chem.* **1986**, *25*, 1088–1092.

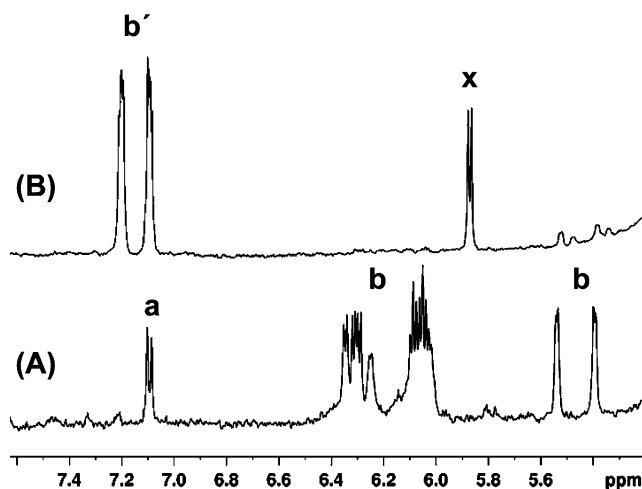


Figure 6. ^1H NMR spectra of **1** [$\{(\eta^6\text{-indan})\text{RuCl}\}_2(\mu\text{-2,3-dpp})(\text{PF}_6)_2$] in methanol- d_4 (A) before irradiation, in the dark. Peak assignments: (a) part of bound 2,3-dpp and (b) bound indan. (B) The same sample after irradiation. Peak assignments: (b') free indan and (x) unassigned. There is also a series of complicated multiplets between 7.5 and 9.8 ppm suggesting that 2,3-dpp is present in a variety of different environments in the products, possibly including polynuclear species.

We used time-resolved fluorescence measurements to help identify the photoproduct. While the fluorescence of indan in methanol fitted a single decay time of 7.96 ns, the photoproduct decay was best described by biexponential kinetics with a major component of 7.97 ns (pre-exponential factor of 92%) and a minor component of 2.06 ns (8%). Therefore, it is clear that irradiation of **1** leads to loss of arene into the solution. The photochemical quantum yield for the reaction of **1** in 0.1 M NaCl was estimated to be $\sim 2 \times 10^{-4}$. The precise nature of the photoproducts is unknown, although plausible species are indicated in Scheme 1. If there is a mixture of photoproducts, then the estimated photochemical quantum yield will represent an average for the different photochemical reactions.

For possible phototherapeutic applications, it is important to assess the importance of oxygen on the photochemistry of **1**. The photolysis of a degassed methanolic solution of **1** was performed under the same conditions that were used for the aerated solutions, and the changes in the absorption spectra were identical to those of the aerated solution. Therefore, oxygen is not involved in the photochemical reaction. It was also necessary to eliminate the possibility of thermal effects during irradiation contributing to the observed spectral changes. The temperature of a solution of **1** in 0.1 M NaCl after irradiation for 25 min (360 nm, 160 mW) was 310–313 K. When an identical solution of **1** was heated in the dark at 328 K for 25 min, this resulted in a small decrease in overall absorption but did not result in the formation of a new band at long wavelength. Therefore, the spectral changes are photoinduced, not thermal.

Confirmation that irradiation of **1** leads to arene loss was provided by ^1H NMR spectroscopy. Figure 6 shows ^1H NMR spectra of **1** in deuterated methanol before and after irradiation. It is clear that there is a large change in the aromatic region of the ^1H spectrum of **1**. In the dark, the peaks at 5.4–5.6 ppm (labeled b) correspond to the protons of indan

bound to Ru. After irradiation, new peaks appear at 7.0–7.2 ppm (labeled b'), which have the same chemical shifts as those of free indan. The peaks for 2,3-dpp appear as complicated multiplets after irradiation and were not further analyzed. It is reasonable to suppose that there is a variety of environments for 2,3-dpp in the photoproducts, some of which may be polymeric.

Although only complex **1** was studied in detail, it was apparent from initial photochemical investigations of complexes **2**, **3**, and **4** that the nature of the arene has a significant effect on the course of the reaction. As for complex **1**, complex **2** containing benzene as the arene underwent arene loss upon irradiation (Figures S3 and S4), but complexes **3** and **4** containing *p*-cymene and hexamethylbenzene, respectively, as arenes did not readily undergo arene loss (see Supporting Information). Hence it appears that complexes containing arenes which are the strongest donors (e.g., hexamethylbenzene) are the most stable to light.

DNA Binding. The samples of DNA and **1** were prepared in three ways: in the dark (henceforth referred to as non-irradiated), following the addition of pre-irradiated **1** to DNA (pre-irradiated), or by addition of **1** to DNA followed by irradiation of the resulting mixture (irradiated). The samples were irradiated by light with peak intensity at 360 nm for 60 min. Solutions of CT DNA at a concentration of $50 \mu\text{g mL}^{-1}$ were incubated with **1** at an r_i value of 0.1 in 10 mM NaClO_4 or 0.1 M NaCl at 310 K (r_i is defined as the molar ratio of free ruthenium complex to nucleotide-phosphates at the onset of incubation with DNA). At various time intervals, an aliquot of the reaction mixture was withdrawn, quickly cooled in an ice bath, and precipitated by ethanol and the content of ruthenium in the supernatant of these samples was determined by FAAS. The number of atoms of ruthenium bound per nucleotide residue, r_b , was calculated by subtraction of the amount of free (unbound) ruthenium from the total amount of ruthenium present in the reaction. The binding of the ruthenium compounds to CT DNA was also quantified in two other ways. The samples containing the reaction mixture were quickly cooled on an ice bath and then exhaustively dialyzed against 10 mM NaClO_4 at 277 K or filtered using Sephadex G50 to remove free (unbound) ruthenium. The content of ruthenium in these DNA samples was determined by FAAS. The values of r_b obtained using this assay were identical to those based on DNA precipitation by ethanol.

The binding experiments (summarized in Table 2) indicate that the non-irradiated, pre-irradiated, and irradiated forms of **1** reacted with DNA readily in 10 mM NaClO_4 (95, 100, and 100%, respectively, reacted after 20 h), while the presence of the 0.1 M NaCl reduced the amount bound to DNA, particularly in the case of the reactions of the non-irradiated **1**. The binding of non-irradiated, pre-irradiated, or irradiated **1** to DNA was almost complete after 20 h, although that of non-irradiated **1** was slower (Table 2). Importantly, the analytical method used monitors the relatively strong binding of the ruthenium complex to DNA (so that the results are not affected by eventual subsequent closure of monofunctional adducts to cross-links). No pH

Table 2. Binding of Non-Irradiated, Pre-irradiated, or Irradiated **1** to Calf Thymus DNA in 10 mM NaClO₄ or 0.1 M NaCl as Determined by FAAS

medium	non-irradiated 1 ^a		pre-irradiated 1 ^{a,b}		irradiated 1 ^{a,c}	
	<i>B</i> _{20h} (%) ^d	<i>t</i> _{50%} (h) ^e	<i>B</i> _{20h} (%) ^d	<i>t</i> _{50%} (h) ^e	<i>B</i> _{20h} (%) ^d	<i>t</i> _{50%} (h) ^e
10 mM NaClO ₄	95	5.4	100	1.1	100	2.6
0.1 M NaCl	<10	NA ^f	70	ND ^g	70	ND ^g

^a Incubations with DNA were at 310 K. The concentration of DNA was 50 μg mL⁻¹, and *r*₁ was 0.1. Data are the average of three independent experiments. ^b Irradiation of **1** was carried out in absence of DNA for 60 min, followed by a further incubation with DNA in the dark. ^c Irradiation of **1** was carried out in presence of DNA for 60 min, followed by a further incubation in the dark. ^d Amount of bound ruthenium after 20 h. ^e The incubation time needed to reach 50% binding. ^f Not applicable. ^g Not determined.

changes were observed for reaction mixtures containing DNA and non-irradiated, pre-irradiated, or irradiated **1** within 20 h after mixing DNA with the ruthenium complex. Because of the relatively very low binding rate for the non-irradiated form of **1** in 0.1 M NaCl, further experiments with DNA were performed

with non-irradiated or pre-irradiated forms of **1** in 10 mM NaClO₄ or **1** was irradiated in the presence of DNA in 10 mM NaClO₄ for 60 min and further incubated in the dark for additional 24 h; experiments in which DNA was modified in 0.1 M NaCl were performed only with pre-irradiated **1**.

In Vitro Transcription of DNA Containing Adducts of **1.** In vitro RNA synthesis by RNA polymerases on DNA templates containing several types of bifunctional adducts of platinum or ruthenium complexes can be prematurely terminated at the level or in the proximity of DNA adducts. Importantly, monofunctional DNA adducts of several platinum complexes are unable to terminate RNA synthesis.²⁵

Cutting of pSP73KB DNA by *Nde*I and *Hpa*I restriction endonucleases yielded a 212-bp fragment (a substantial part of its nucleotide sequence is shown in Figure 7b).²⁵ This fragment contained a T7 RNA polymerase promotor [close to the 3'-end of the top strand (Figure 7b)]. The experiments were carried out using this linear DNA fragment, modified at *r*_b = 0.005 by both non-irradiated (with and without subsequent irradiation at 360 nm) and pre-irradiated forms of **1** in 10 mM NaClO₄ or by pre-irradiated **1** in 0.1 M NaCl, for RNA synthesis by T7 RNA polymerase (Figure 7a, lanes 1–5). In addition, **1** was irradiated for 60 min in the presence of the unmodified fragment (in 10 mM NaClO₄) and subsequently incubated in the dark for an additional 20 h (Figure 7a, lane 6).

RNA synthesis on the fragment modified by non-irradiated, pre-irradiated, and irradiated forms of **1** yielded fragments of newly synthesized RNA of defined sizes, which indicates that RNA synthesis on these templates was prematurely terminated. The major stop sites produced by all samples of ruthenated DNA fragments occurred at similar positions in the gel and were mainly at guanine residues. Interestingly, the total intensity of the bands on the autoradiogram corresponding to transcripts of single-ruthenated DNA fragments [modified to the same level (*r*_b)] differed.

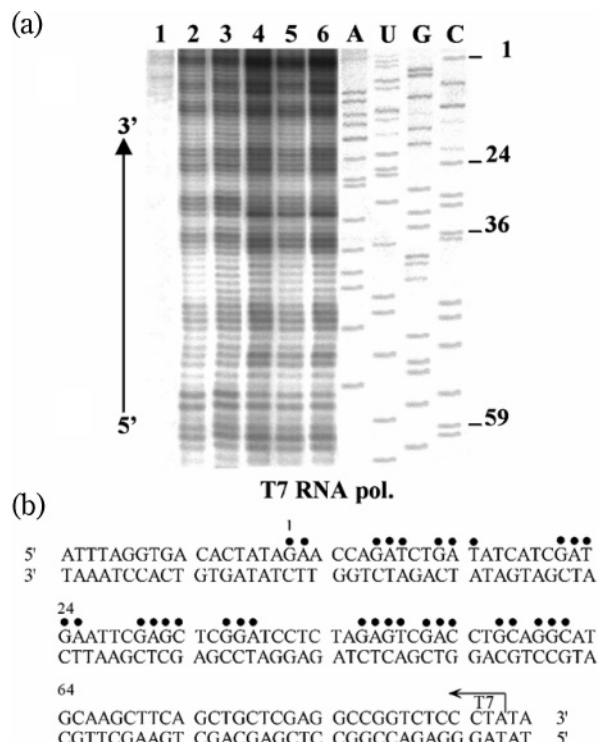


Figure 7. Inhibition of RNA synthesis by T7 RNA polymerase on the *Nde*I/*Hpa*I fragment of the pSP73KB plasmid modified by **1**. This linear DNA fragment was modified for 20 h by non-irradiated **1** (with or without subsequent irradiation for 60 min at 360 nm, lanes 2 and 3 in Figure 7a), pre-irradiated **1** in 10 mM NaClO₄ (lane 4), pre-irradiated **1** in 0.1 M NaCl (lane 5), or the unmodified fragment was mixed with non-irradiated **1** in 10 mM NaClO₄ and the mixture was irradiated for 60 min and subsequently incubated in the dark for additional 20 h (lane 6 in Figure 7a) so that the resulting *r*_b value was 0.005. (a) Autoradiogram of 6% polyacrylamide/8 M urea sequencing gel. Lanes: (1) control, nonmodified template; (2) the template modified by non-irradiated **1**; (3) the same as in lane 2, but the sample was subsequently irradiated; (4 and 5) the template modified by pre-irradiated **1** in 10 mM NaClO₄ or 0.1 M NaCl, respectively; (6) the template was mixed with non-irradiated **1** in 10 mM NaClO₄ and the mixture was irradiated for 60 min and subsequently incubated in the dark for additional 20 h; (A, U, G, C) chain-terminated marker RNAs. For the details, see the text. (b) Schematic diagram showing the portion of the nucleotide sequence of the template of the *Nde*I/*Hpa*I fragment used to monitor inhibition of RNA synthesis. The arrow indicates the start of the T7 RNA polymerase and ● indicates the major stop signals (from Figure 7a, lane 3). The numbers correspond to the nucleotide numbering in the sequence map of pSP73KB plasmid.

The bands corresponding to the transcription of DNA modified by the non-irradiated **1** were faint (Figure 7a, lane 2); the intensity of those corresponding to the transcription of DNA modified by the non-irradiated **1** that was subsequently irradiated was moderate (Figure 7a, lane 3), and the intensity of those corresponding to the transcription of DNA modified by pre-irradiated **1** or if the unmodified fragment was irradiated together with **1** (and subsequently incubated in the dark for additional 20 h) were strongest (Figure 7a, lanes 4 and 6, respectively). In addition, the bands produced by the transcripts of DNA fragments modified by pre-irradiated **1** in the presence of 0.1 M NaCl were weaker (Figure 7a, lane 5) in comparison with those modified in 10 mM NaClO₄. Taken together, the results of the transcription mapping experiments (Figure 7) suggest that the non-irradiated form of **1** preferentially forms DNA adducts that represent only a weak block for RNA polymerase, presumably monofunctional adducts. The subsequent irradiation of

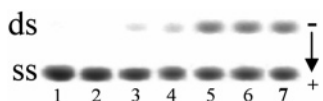


Figure 8. Formation of the interstrand cross-links by **1** in pSP73KB plasmid (2455bp) linearized by *EcoRI*. DNA was incubated with the complex for 20 h so that the r_b value was 0.001. Autoradiograms of denaturing 1% agarose gels of linearized DNA which was 3'-end labeled. The interstrand cross-linked DNA appears as the top bands migrating on the gel more slowly than the single-stranded DNA (contained in the bottom bands). Lanes: (1 and 2) control, nonmodified DNA in 10 mM NaClO₄ and 0.1 M NaCl, respectively; (3) DNA modified by non-irradiated **1** in 10 mM NaClO₄; (4) the same as in lane 3, but the sample was subsequently irradiated; (5 and 6) DNA modified by pre-irradiated **1** in 10 mM NaClO₄ and 0.1 M NaCl, respectively; (7) DNA was mixed with non-irradiated **1** in 10 mM NaClO₄ and the mixture was irradiated for 60 min and subsequently incubated in the dark for additional 20 h.

DNA already modified by the non-irradiated **1** transforms the adducts so that they become stronger blocks for RNA polymerase, presumably to some type of cross-links. The modification of DNA by the pre-irradiated form of **1** results in adducts which efficiently terminate RNA synthesis so that it is reasonable to suggest that pre-irradiated **1** preferentially forms cross-links. In addition, the results of transcription mapping indicate that the presence of chloride in the medium in which DNA was modified somewhat lowers the propensity of the pre-irradiated form of **1** to form bifunctional adducts, implying that the Ru–Cl bonds are less reactive than Ru–OH₂ bonds in **1**.

DNA Interstrand Cross-linking. Bifunctional platinum- or ruthenium-based drugs form both intrastrand and interstrand cross-links on DNA. Although some of these compounds (for instance cisplatin) form interstrand cross-links on DNA with only a low frequency, these lesions are also considered relevant to the antitumor effects of metal-based drugs.¹⁷ The amounts of interstrand CLs formed by both non-irradiated and pre-irradiated forms of **1** in the presence or absence of DNA in pSP73KB plasmid linearized by *EcoRI* (which cuts this plasmid only once) were determined. The experiments were carried out using this linear DNA fragment, modified at $r_b = 0.001$ by non-irradiated **1** in 10 mM NaClO₄ or by pre-irradiated **1** in 0.1 M NaCl. The fragment modified by non-irradiated **1** was divided into two parts, and one was subsequently irradiated for 60 min by light with peak intensity at 360 nm. The samples were analyzed for interstrand CLs by agarose gel electrophoresis under denaturing conditions.^{25–27} The very faint bands corresponding to more slowly migrating interstrand-cross-linked fragments were observed (Figure 8). The radioactivity associated with the individual bands in each lane was measured to obtain estimates of the fraction of non-cross-linked or cross-linked DNA under each condition. The frequencies of interstrand CLs produced by **1** under different conditions are shown in Table 3.

The efficiency of pre-irradiated **1** to form DNA interstrand cross-links in both 10 mM NaClO₄ and 0.1 M NaCl under the conditions described in the experimental section is slightly higher than that of cisplatin. In contrast, the interstrand crosslinking efficiency of non-irradiated **1** in 10 mM NaClO₄ is relatively low. Somewhat enhanced amounts of interstrand cross-links were observed if the sample of

Table 3. DNA Interstrand Cross-Linking of Linearized pSP73KB Plasmid by **1**^a

medium	non-irradiated 1 ^b	irradiated after incubation with DNA ^c	pre-irradiated 1 ^d	irradiated 1 ^e
10 mM NaClO ₄	2%	4%	7%	7%
0.1 M NaCl	ND ^f	ND ^f	7%	ND ^f

^a The r_b was 0.001. Data are the average of three independent experiments. ^b The linearized plasmid was incubated with non-irradiated **1** for 20 h. ^c The linearized plasmid was incubated with non-irradiated **1** in the dark for 20 h, and then it was irradiated for 60 min with light of maximum intensity at 360 nm [in the absence of free (unbound) ruthenium complex]. ^d An aqueous solution of **1** was pre-irradiated for 60 min (in the absence of DNA) and then added to the linearized plasmid and incubated for 20 h. ^e Irradiation of **1** was carried out in presence of DNA for 60 min, followed by a further incubation in the dark. ^f Not determined.

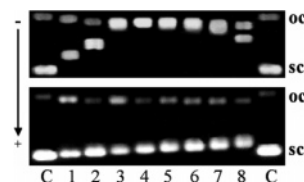


Figure 9. Unwinding of supercoiled pSP73KB plasmid DNA modified by pre-irradiated **1** in 10 mM NaClO₄ (top panel) or 0.1 M NaCl (bottom panel). Lanes: (C) control, unmodified DNA; (1–8) $r_b = 0.040, 0.060, 0.075, 0.085, 0.095, 0.11, 0.12$, and 0.14 , respectively. The top bands correspond to the form of nicked plasmid (oc) and the bottom bands to closed negatively supercoiled plasmid (sc).

DNA already modified by non-irradiated **1** [in absence of free (unbound) ruthenium complex] was then irradiated. This observation is consistent with the idea that the subsequent irradiation of DNA already modified by non-irradiated **1** transforms some adducts into interstrand cross-links. In addition, the results on interstrand cross-linking indicate that the presence of chloride in the medium in which DNA was modified does not lower the propensity of pre-irradiated **1** to form interstrand cross-links.

DNA Unwinding. Electrophoresis of native agarose gels can be used to determine the unwinding induced in negatively supercoiled pSP73 plasmid by monitoring the degree of supercoiling (Figure 9).²⁸ A compound that unwinds the DNA duplex reduces the number of supercoils in closed circular DNA. This decrease upon binding of unwinding agents causes a decrease in the rate of migration through agarose gel, which makes it possible to observe and quantify the mean value of unwinding per adduct.

Variable amounts of **1** (pre-irradiated, irradiated in the presence of DNA, or non-irradiated forms in 10 mM NaClO₄ and the pre-irradiated form in 0.1 M NaCl) were bound to a mixture of relaxed and negatively supercoiled pSP73 DNA. The resulting products were analyzed by gel electrophoresis (shown in Figure 9 for the modification by pre-irradiated **1** in 10 mM NaClO₄ in the top panel and in 0.1 M NaCl in the bottom panel). The mean unwinding angle is given by $\Phi = 18\sigma/r_b(c)$, where σ is the superhelical density and $r_b(c)$ is the value of r_b at which the supercoiled and nicked forms comigrate.²⁸ Under the present experimental conditions, σ was calculated to be -0.063 using the data for cisplatin, for which the $r_b(c)$ was determined in this study and $\Phi = 13^\circ$ was assumed. The DNA unwinding angle produced by the adducts formed by non-irradiated, pre-irradiated, and irradi-

ated forms of **1** in 10 mM NaClO₄ was determined to be $13 \pm 2^\circ$, using this approach. In contrast, no comigration of the supercoiled and nicked forms was reached from modification of DNA by pre-irradiated **1** in 0.1 M NaCl even at an r_h value as high as 0.14 (Figure 9, bottom panel) so that the adducts formed by pre-irradiated **1** unwound DNA only negligibly ($<3^\circ$). Thus, the adducts of **1** formed on DNA in 10 mM NaClO₄ share a common conformational feature responsible for a relatively high level of DNA unwinding. On the other hand, the conformation of DNA adducts formed by the pre-irradiated form of **1** in 0.1 M NaCl is apparently considerably different and does not induce DNA unwinding.

Conclusions

We have shown that the dinuclear Ru^{II} arene complex $\{(\eta^6\text{-indan})\text{RuCl}\}_2(\mu\text{-}2,3\text{-dpp})(\text{PF}_6)_2$ (**1**) can undergo hydrolysis in aqueous solution in the dark. Ru–OH₂ bonds are more reactive than Ru–Cl bonds, and the aqua adducts can bind to DNA and, to a small extent, can form interstrand cross-links on plasmid DNA. The transcription mapping experiments suggest that guanines might be preferential binding sites. Subsequent irradiation of the ruthenated DNA or irradiation of **1** in the presence of DNA led to an increased frequency of cross-linking. This was explained on the basis of the increased reactivity of ruthenium caused by arene loss upon irradiation. Photoinduced arene loss from the complex, in the absence of DNA, was readily monitored by its increased fluorescence intensity ($\sim 40\times$) when unbound compared to bound. Indan release was confirmed by time-resolved fluorescence and NMR spectroscopy. Mononuclear Ru^{II} arene complexes $[(\eta^6\text{-arene})\text{Ru}(\text{N,N})\text{Cl}]^+$, including indan derivatives, where (N,N) is a chelating diamine ligand,

can exhibit anticancer activity and are usually stable in the light. The dinuclear indan complex studied here is a member of a new family of potential anticancer complexes for which it might be possible to enhance activity by photoactivation. Although the benzene analog (**2**) can also undergo photoinduced arene loss, complexes with more strongly bound arenes (e.g., hexamethylbenzene) do not. Photoactivation of metal complexes may have the advantage of producing novel types of DNA cross-links that cannot be readily achieved by chemical reactions alone. These novel lesions may avoid repair mechanisms and lack cross-resistance with other classes of anticancer agents. The detection of fluorescence from the released arene offers the possibility of monitoring the course of such cytotoxic reactions inside tissues or, even, individual cells.

Acknowledgment. This research was supported by the Scottish Higher Education Funding Council (COSMIC), the Grant Agency of the Czech Republic (Grants 305/05/2030 and 203/06/1239), and the Academy of Sciences of the Czech Republic (Grants 1QS500040581 and KAN200200651). The authors also acknowledge that their participation in the EU COST Action D20 enabled them to exchange ideas with European colleagues.

Supporting Information Available: UV–vis spectra for photoproducts of **1** in water and 0.1 M NaCl and UV–vis and fluorescence spectra in methanol (Figures S1 and S2), syntheses and irradiation experiments for complexes **2**, **3**, and **4**, UV–vis and NMR spectra for irradiation of **2** (Figures S3 and S4), and X-ray crystallographic data for **1** in CIF format. This material is available free of charge via the Internet at <http://pubs.acs.org>.

IC062111Q

14.

1,2-GG intrastrand cross-link of antitumor dinuclear bifunctional platinum compound with spermidine linker inhibits DNA polymerization more effectively than the cross-link of conventional cisplatin

Branden Moriarity ^{a,1,2}, Olga Nováková ^{a,1}, Nicholas Farrell ^b, Viktor Brabec ^a,
Jana Kašpárková ^{a,*}

^a Institute of Biophysics, Academy of Sciences of the Czech Republic, Brno, Czech Republic

^b Department of Chemistry, Virginia Commonwealth University, Richmond, USA

Received 1 November 2006, and in revised form 26 November 2006

Available online 6 December 2006

Abstract

In order to learn more about the molecular basis for the inhibition of DNA replication produced by antitumor platinum drugs, we investigated DNA polymerization using DNA templates site-specifically modified with the 1,2-GG intrastrand cross-link of dinuclear bifunctional [*trans*-PtCl(NH₃)₂]₂[1-spermidine-N1, N8]³⁺ (BBR3571) or conventional mononuclear cisplatin. These cross-links which have the same nature, but differ in the size and character of the conformational alteration induced in double-helical DNA, were analyzed for bypass ability with reverse transcriptase of human immunodeficiency virus type 1 and Klenow fragment of DNA polymerase I deficient in exonuclease activity. We found that the 1,2-GG intrastrand CL of BBR3571 inhibited DNA translesion synthesis markedly more than the same adduct of cisplatin. This result was explained by a larger size of the cross-link of BBR3571 and by a flexibility induced in DNA by this cross-link which can make the productive binding of this adduct at the polymerase site more difficult.

© 2006 Elsevier Inc. All rights reserved.

Keywords: DNA replication; Translesion DNA synthesis; DNA conformation; Antitumor platinum drugs; Cisplatin; Gel electrophoresis; Chemical probes of DNA conformation

The interaction of DNA polymerases with a DNA adduct is an important determinant of the propensity of a given adduct to be cytotoxic, mutagenic, or ultimately of no long term consequence. The result of DNA polymerase encounter with an adduct is dependent on polymerase and adduct type and may entail blocking or stalling, or

bypass with nucleotide incorporation. The molecular mechanisms of these processes are not completely clear.

Inhibition of DNA replication also plays a very important role in the mechanism underlying antitumor effects of platinum coordination complexes. It is therefore of considerable interest to collect as much information as possible about the processes by which DNA polymerization is inhibited by these metallodrugs.

It has been demonstrated using DNA templates containing site-specifically placed adducts of several antitumor mononuclear platinum compounds that a number of prokaryotic and eukaryotic DNA polymerases are blocked but could also traverse through platinum adducts (this

* Corresponding author. Fax: +420 541240499.

E-mail address: jana@ibp.cz (J. Kašpárková).

¹ The authors wish it to be known that, in their opinion, the first two authors should be regarded as joint First Authors.

² On leave from the Saint Olaf College, Minnesota, USA.

process is called translesion synthesis, TLS³). The extent of the TLS depends on the type of lesion, the DNA sequence context, and the DNA polymerase. Such studies have been performed mainly with *cis*-diamminedichloroplatinum(II) (cisplatin) and its analogues [1–5], which form in DNA mainly intrastrand cross-link (CL) between neighboring purine residues (1,2-intrastrand CL) [6]. In a few cases these studies have also been performed with other mononuclear platinum compounds, which are not cisplatin analogues, but are considered potential antitumor drugs [7–9].

Polynuclear platinum compounds comprise a unique class of new anticancer platinum agents with distinct chemical and biological properties different from mononuclear platinum drugs [10]. In examining structure-activity relationships within this class of compounds, linear polyamine-linked dinuclear platinum complexes were designed which represent a further sub-class of dinuclear compounds with promising preclinical activity [10,11]. For instance, dinuclear bifunctional $\{[trans-PtCl(NH_3)_2]_2\{1-spermidine-N1, N8\}\}^{3+}$ compound (BBR3571) (Fig. 1A) was significantly more cytotoxic than cisplatin in all cell lines tested [10]. This dinuclear platinum complex with two monofunctional coordination spheres may be capable of intrastrand CL formation (in analogy with cisplatin, platination of two adjacent G bases on the same DNA strand) and interstrand CL formation (each Pt moiety binds to opposite strands of the DNA) [12]. The (Pt,Pt) intrastrand CL is thus the direct analog of the major cisplatin adduct.

The interactions of antitumor polynuclear platinum compounds with target DNA are distinctly different from the mononuclear-based cisplatin family and, indeed, unlike those of any DNA-damaging agent in clinical use [10,13]. It has also been demonstrated that polynuclear platinum complexes produce adducts on DNA whose character is different when compared with conventional mononuclear platinum compounds [14–18]. This suggests that these platinum compounds may escape, at least in part, the conventional mechanism of cisplatin resistance related to DNA damage recognition and repair. Despite the fact that these compounds are relatively new, some data on the structure of their DNA adducts, repair of these adducts, their recognition by specific proteins and on cytotoxicity of these new platinum compounds in tumor cell lines are already available. Nonetheless, much less details of molecular mechanisms underlying their biological effects are available in comparison with mononuclear platinum compounds. For instance, no data on how polynuclear platinum compounds inhibit DNA polymerization by DNA polymerases have been obtained so far in spite of the fact that the relative

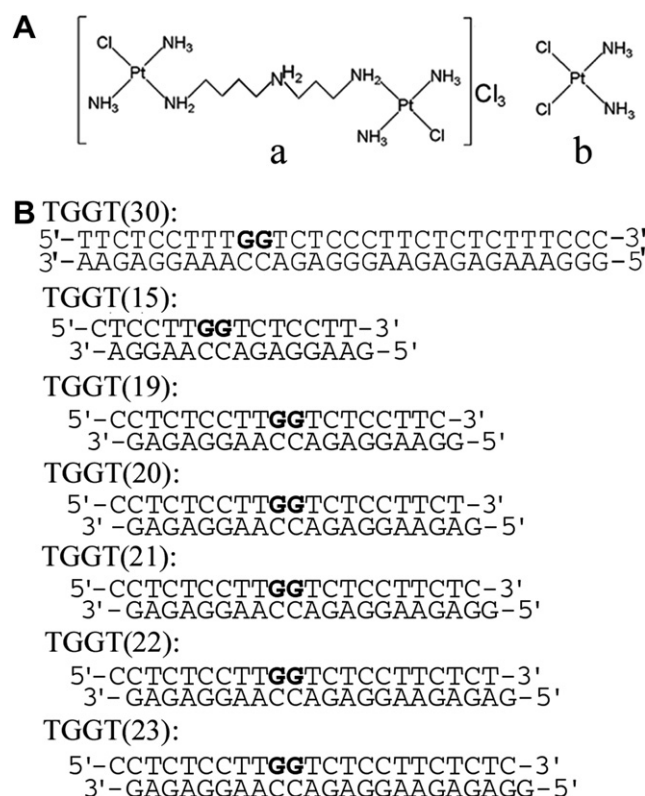


Fig. 1. Structures of platinum compounds and sequences of the synthetic oligodeoxyribonucleotides with their abbreviations. (A) Structures: a, BBR3571; b, cisplatin. (B) Sequences: the top and bottom strands of each pair in the figure are designated 'top' and 'bottom', respectively, throughout. The boldface letters in the top strands of the duplexes indicate the platinated residues.

efficiency of the biological action of platinum compounds (also including DNA replication and antitumor effects) is dependent on the specific structure of the Pt-DNA adduct formed; or even more specifically that the extent and specificity of resistance for platinum compounds have been shown to correlate with the ability of cells to elongate DNA chains that contain platinum adducts [19,20].

In order to learn more about the molecular basis for the inhibition of replication produced by platinum antitumor drugs, we investigated in the present work DNA polymerization using the DNA templates site-specifically modified with two types of the 1,2-GG intrastrand CL formed in the same TGGT sequence by either dinuclear bifunctional BBR3571 or conventional mononuclear (also bifunctional) cisplatin. The DNA polymerization was examined by two DNA polymerases, namely reverse transcriptase of human immunodeficiency virus type 1 (RT HIV-1), which also possesses DNA template-dependent DNA polymerase activity [21] and Klenow fragment of DNA polymerase I (KF) as a model enzyme frequently used in the studies aimed at understanding the processes in which nucleic acid polymerases take part. The DNA polymerase I class of enzymes has served as the prototype for studies on structural and biochemical mechanisms of DNA replication [22,23]. The Klenow fragment deficient in 3' to 5' proof-

³ Abbreviations used: BBR 3571, $\{[trans-PtCl(NH_3)_2]_2\{1-spermidine-N1, N8\}\}^{3+}$; bp, base pair; cisplatin, *cis*-diamminedichloroplatinum(II); CL, cross-link; DEPC, diethyl pyrocarbonate; DMS, dimethyl sulfate; FAAS, flameless atomic absorption spectrophotometry; KF, Klenow fragment of DNA polymerase I; KF⁻, KF deficient in 3'-5' proofreading exonuclease activity; RT HIV-1, reverse transcriptase of human immunodeficiency virus type 1; TLS, translesion synthesis.

reading exonuclease activity (KF^-) was selected here because the proofreading mechanism itself may introduce effects dependent on the adduct type. A thorough characterization of the effects of distinctly different DNA adducts on lesion bypass catalyzed by RT HIV-1 and KF^- should provide an interesting basis for making similar comparisons with other prokaryotic or eukaryotic polymerases.

Materials and methods

Chemicals

Cisplatin was obtained from Sigma. BBR3571 was prepared and characterized by published methods [24]. The stock solutions of platinum compounds were prepared at the concentration of 5×10^{-4} M in deionised water and stored at room temperature in the dark. The synthetic oligodeoxyribonucleotides (Figs. 1B and 2A) were purchased from VBC-Genomics (Vienna, Austria) and were purified as described previously [25]. KF^- , T4 DNA ligase, and T4 polynucleotide kinase were purchased from New England Biolabs (Beverly, MA). RT HIV-1 was from Amersham Pharm. Biotech. Nonidet P-30 was from Fluka (Prague, Czech Republic). Acrylamide, bis(acrylamide), urea, and NaCN were from Merck KgaA (Darmstadt, Germany). Dimethyl sulfate (DMS), $KMnO_4$, diethyl pyrocarbonate (DEPC), KBr and $KHSO_5$ were from Sigma (Prague, Czech

Republic). ATP was from Boehringer (Mannheim, Germany) and $[\gamma - ^{32}P]ATP$ from MP Biomedicals, LLC (Irvine, CA).

Platination of oligonucleotides

The duplexes containing single, 1,2-GG intrastrand CL of cisplatin or BBR3571 in the top strand (the duplexes are shown in Fig. 1B) were prepared and characterized as described [7,26,27].

Inhibition of DNA polymerization

The 30mer templates (see Fig. 2A) containing a single 1,2-GG intra-strand CL of cisplatin or BBR3571 were prepared in the same way as described in the previous papers [7,26,27]. 17mer DNA primer (its nucleotide sequence is shown in Fig. 2A) was complementary to the 3' termini of the 30mer templates. The DNA substrates (5×10^{-8} M) were formed by annealing templates and 5'-end-labeled primers at a molar ratio of 3:1. All experiments using RT HIV-1 were performed at 37 °C in a volume of 50 μ l in a buffer containing 50 mM Tris-HCl (pH 8.0), 10 mM $MgCl_2$, 50 mM KCl, 3 mM dithiothreitol, 0.1% Nonidet P-30, 100 μ M dATP, 100 μ M dCTP, 100 μ M dGTP, and 100 μ M TTP and 1.0 unit of RT HIV-1. The experiments with KF^- were performed with the same 30mer templates and 17mer DNA primers (see Fig. 2A) using the same volume, but at 25 °C in the buffer consisting of 50 mM Tris-HCl (pH 7.4), 10 mM $MgCl_2$, 0.1 mM dithiothreitol, 50 μ g bovine serum albumin/ml; the nucleoside triphosphates were at a concentration of 25 μ M and 1.0

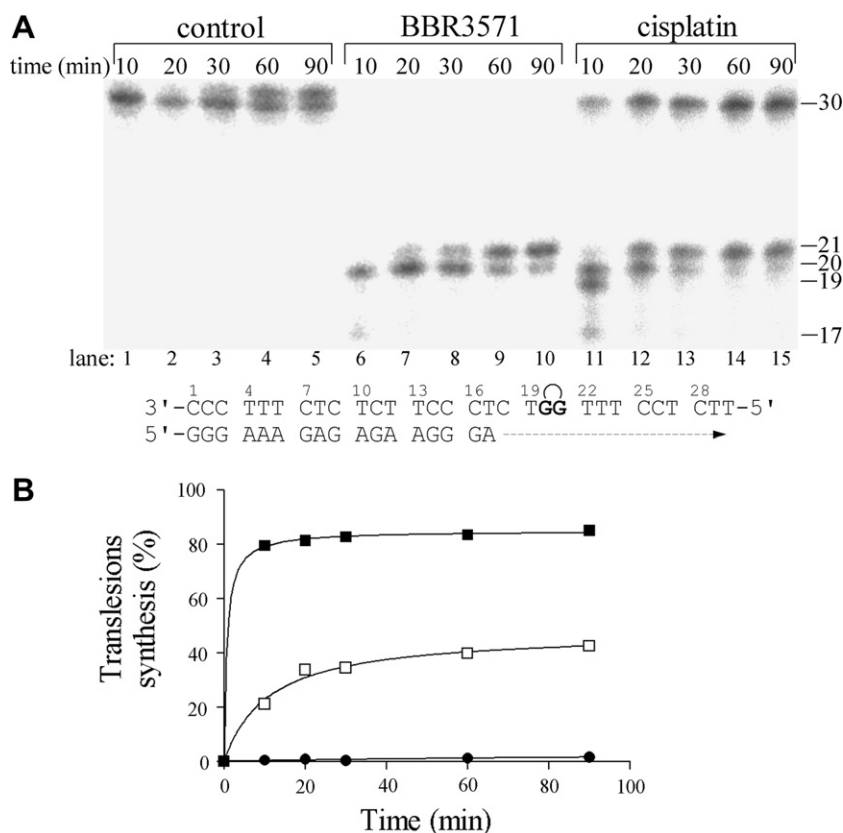


Fig. 2. Primer extension activity of RT HIV-1 using the 17mer/30mer, primer/template duplex. (A) The experiments were conducted for the times indicated in the figure (10–90 min) using undamaged templates (lanes 1–5), the template containing single, site specific 1,2-GG intrastrand CL of BBR3571 (lanes 6–10), and the template containing single, site specific 1,2-GG intrastrand CL of cisplatin (lanes 11–15). The pause sites opposite the platinated guanines and a flanking residue on the 3' site are marked 21, 20, 19, respectively. The nucleotide sequences of the templates and the primers are shown beneath the gels. See the text for details. (B) The time dependence of the inhibition of DNA synthesis on undamaged (control) template (full squares), DNA containing 1,2-GG intrastrand CL of BBR3571 (circles) or cisplatin (open squares). Data are means (\pm SE) from three different experiments with two independent template preparations.

unit of KF^- was used. Reactions were terminated by the addition of EDTA so that its resulting concentration was 20 mM, and heating at 100 °C for 30 s. Products were resolved by denaturing 15% PAA/8 M urea gel. Other details were published previously [8,9].

Chemical probes of DNA conformation

The platinated top strand of the duplex TGGT(30) was allowed to anneal with unplatinated complementary strand (the bottom strand of the duplex TGGT(30)) in 0.02 M NaClO_4 and used immediately in further experiments. The top or bottom strands of the duplex were 5'-end-labeled with $[\gamma\text{-}^{32}\text{P}]\text{ATP}$. This annealing procedure included a rapid heating of the mixture of the complementary oligonucleotides to 55 °C followed by the incubation at 25 °C for 2 h. The modifications of double-stranded oligonucleotides by KMnO_4 , DEPC, and KBr/KHSO_5 were performed as described previously [26]. In the case of the platinated oligonucleotides, the platinum complex was removed after reaction of the DNA with the probe by incubation with 0.2 M NaCN (pH 11) at 45 °C for 10 h in the dark.

Ligation and gel electrophoresis of oligonucleotides

Unplatinated 15mer and 19–23mer single strands (bottom strands of the duplexes TGGT(15,19–23) shown in Fig. 1B) were 5'-end-labeled with $[\gamma\text{-}^{32}\text{P}]\text{ATP}$ by using T4 polynucleotide kinase. Then they were annealed (see above) with their phosphorylated complementary strands (unplatinated or containing 1,2-GG intrastrand CL of BBR3571 or cisplatin). Unplatinated and intrastrand CL-containing duplexes were allowed to react with T4 DNA ligase. The resulting samples along with ligated unplatinated duplexes were subsequently examined on 8% native polyacrylamide (mono:bis(acrylamide) ratio 29:1) electrophoresis gels. Other details of these experiments were as described in previously published papers [15,28,29].

Other physical methods

Absorption spectra were measured with a Beckmann DU-7400 spectrophotometer. FAAS measurements were carried out with a Varian AA240Z Zeeman atomic absorption spectrometer equipped with a GTA 120 graphite tube atomizer. For FAAS analysis, modified oligonucleotides were dialysed against deionised water. Purification of oligonucleotides with the aid of HPLC was carried out with MonoQ HR 5/5 column on a Waters HPLC system consisting of Waters 262 Pump, Waters 2487 UV detector and Waters 600S Controller. Gels were visualized using the BAS 2500 FUJIFILM bioimaging analyzer, and the radioactivities associated with bands were quantitated with AIDA image analyzer software (Raytest, Germany).

Results

DNA synthesis by RT HIV-1 and KF^-

We investigated in the present work DNA polymerization using the templates site-specifically modified by 1,2-GG intrastrand CLs of BBR3571 or cisplatin by RT HIV-1 as a model enzyme frequently used in the studies aimed at understanding the processes in which nucleic acid polymerases take part. We constructed the 17mer/30mer primer-template duplexes (for its sequence, see Fig. 2A) unplatinated or containing 1,2-GG intrastrand CL of either BBR3571 or cisplatin in the central TGGT sequence. The first 17 nucleotides on the 3' terminus of the 30mer template strand were complementary to the nucleotides

of the 17mer primer, and the 3' guanine involved in the 1,2-GG CL on the template strand was located at its 20th position from the 3' terminus (Fig. 2A). After annealing the 17mer primer to the 3' terminus of the unplatinated or platinated template strand (positioning the 3'-end of the primer two bases before the adduct in the template strand), we examined DNA polymerization through the single 1,2-CL of BBR3571 or cisplatin on the template by RT HIV-1 in the presence of all four deoxyribonucleoside 5'-triphosphates. The reaction was stopped at various time intervals, and the products were analyzed using a sequencing gel (Fig. 2A).

Polymerization using the template containing the CL of cisplatin proceeded rapidly up to the nucleotide preceding and at the sites opposite the CL, such that the 20- and 21-nucleotide products accumulated to a significant extent (shown in Fig. 2A, lanes 11–15). No intermediate products were seen with the 30mer control template as the full-length product was being formed (shown in Fig. 2A, lanes 1–5). The full-length products were also noticed with the 30mer template containing the CL of cisplatin, although in a smaller amount. This result is in an agreement with previously published work [1,8,30]. In contrast, under the same experimental conditions, DNA polymerization by RT HIV-1 using the template containing the 1,2-GG intrastrand CL of BBR3571 proceeded up to the nucleotide at the site opposite the 3' G involved in the CL (Fig. 2A, lanes 6–10). There was no accumulation of shorter and larger DNA intermediates, and importantly, no full length products accumulated. This result indicates that the character of the 1,2-GG intrastrand CLs of BBR3571 and alterations induced in DNA by this adduct are distinctly different from the features of the same adduct of cisplatin so that the adducts of BBR3571 could potentially impede elongation of DNA to a markedly higher extent than the same adducts of cisplatin (Figs. 2A and B).

We have also examined the effects of the 1,2-GG intrastrand CLs of BBR3571 or cisplatin on polymerization by KF^- . This enzyme also possesses DNA template-dependent DNA polymerase activity but even higher processivity and fidelity [21]. In these studies, elongation of the 17mer/30mer primer-template duplexes was tested and the results analogous to those obtained with RT HIV-1 were obtained (not shown).

The extent of the TLS depends on the type of lesion. In order to shed light on the specific character of 1,2-GG intrastrand CLs of BBR3571, further studies of the present work were focused on analysis of the distortion induced by this adduct with the aid of chemical probes of DNA conformation and phasing assay. These methods allow determination of some important parameters of the conformational distortion, such as its extent and local DNA bending and unwinding, which may serve as important structural motifs recognized by the components of downstream cellular systems processing DNA adducts of platinum compounds including the inhibition of replication produced by platinum antitumor drugs [31,32].

Chemical probes of DNA conformation

We have designed a synthetic oligodeoxyribonucleotide duplex, TGGT(30) (its top strand was used as a template for DNA synthesis by RT HIV-1; the sequence of this duplex is shown in Fig. 1B). The duplex was modified (see Materials and methods) so that it contained a single 1,2-GG intrastrand adduct of BBR3571. This duplex was further analyzed by chemical probes of DNA conformation. The intrastrand cross-linked duplex was treated with several chemical agents that are used as tools for monitoring the existence of conformations other than canonical B-DNA. These agents include KMnO_4 , DEPC, and bromine. They react preferentially with single-stranded DNA and distorted double-stranded DNA [26,33–36].

KMnO_4 is hyperreactive with thymine (T) residues in single-stranded nucleic acids and in distorted DNA as

compared with B-DNA [33,34,37,38]. The intrastrand cross-linked duplexes showed strong reactivity of the two 5' T residues adjacent to the adduct (Fig. 3A (left panel, lane IAC)). A somewhat weaker reactivity was also observed for the third 5' T adjacent to the CL.

DEPC carbetoxyates purines at the N7 position [33,34,39,40]. Within the double-stranded oligonucleotides containing the CL, other A residues in the bottom strand became reactive (Fig. 3A (middle panel, lane IAC)). These are readily identified as the A residues complementary to the reactive T residues of the top strand. Importantly, A residues complementary to strongly reactive T residues also reacted with DEPC strongly whereas A residue complementary to more weakly reactive T residue also reacted with DEPC more weakly.

Bromination of cytosine (C) residues and formation of piperidine-labile sites are observed when two simple salts, KBr and KHSO_5 , are allowed to react with single-stranded or distorted double-stranded oligonucleotides [36]. The only two C residues in the bottom strand of the platinated TGGT(30) duplex (complementary to the platinated G residues in the top strand) were reactive (Fig. 3A, right panel, lane IAC). Within the double-stranded duplex containing the intrastrand CL, no C residue in the top strand was reactive (data not shown).

The results of the analysis by chemical probes are summarized in Fig. 4. The 1,2-GG intrastrand CL of BBR3571 creates a local conformational distortion revealed by the chemical probes which occurs only on the 5' side of the CL and extends mainly over five base pairs (bps). This is in distinct contrast to the distortion induced in DNA by the same adduct of cisplatin. The 1,2-GG intrastrand CL of cisplatin creates a local conformational distortion which also extends mainly over five bps, but occurs on both sides of the CL being stronger on the 5' side.

DNA unwinding and bending

Among the alterations of secondary and tertiary structure of DNA, the role of intrinsic bending of DNA is increasingly recognized as of potential importance in

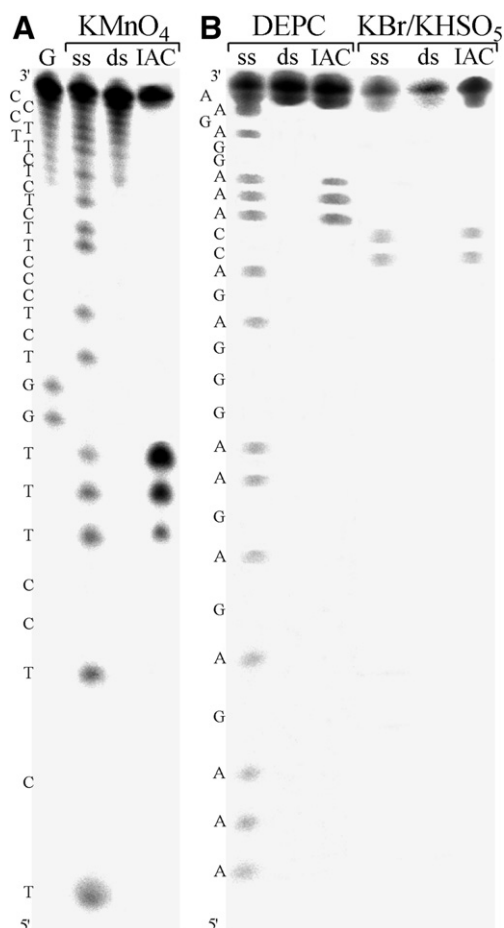


Fig. 3. Chemical probes of DNA conformation. Piperidine-induced specific strand cleavage at KMnO_4 -modified (left panel), DEPC-modified (middle panel), and KBr/ KHSO_5 -modified (right panel) bases in the 30-bp duplex TGGT(30) unplatinated or containing single, 1,2-GG intrastrand CL of BBR3571. Lanes: ss, the unplatinated strand; ds, the unplatinated duplex; IAC, the duplex containing a unique adduct of BBR3571; G, a Maxam–Gilbert specific reaction for the unplatinated duplex. The oligomers were 5'-end labeled at the top strand (left panel) or bottom (middle and right panel) strand.

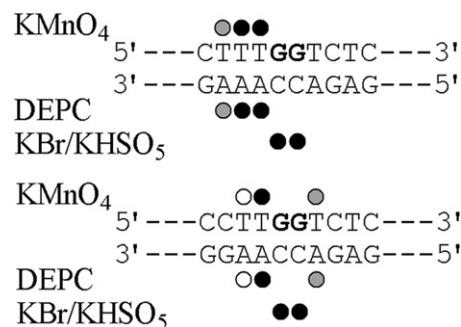


Fig. 4. Summary of the reactivity of chemical probes with the duplex containing single, 1,2-GG intrastrand CL of BBR3571 (top) and cisplatin (bottom). Black, gray and open circles designate strong, medium or weak reactivity, respectively.

regulating replication, transcription and repair functions through specific DNA-protein interactions. For DNA adducts of cisplatin, the structural details responsible for bending and subsequent protein recognition have recently been elucidated [41,42]. Given the recent advances in our understanding of the structural basis for the bending of DNA caused by 1,2-GG intrastrand CL of cisplatin, it is of considerable interest to examine how the same adduct of dinuclear BBR3571 affects conformational properties of DNA such as unwinding and bending. In this work we performed further studies on the bending induced by single, site-specific 1,2-GG intrastrand CL of BBR3571 (and for comparative purposes also of cisplatin) formed in the oligodeoxyribonucleotide duplexes using electrophoretic retardation as a quantitative measure of the extent of planar curvature [43].

The oligodeoxyribonucleotide duplexes TGGT(15,19–23) (for their sequences, see Fig. 1B) were used for the bending studies of the present work in the same way as in previously published work [26–28,44]. Autoradiograms

of electrophoresis gels revealing resolution of the ligation products of unplatinated TGGT(15,19–23) duplexes or containing a unique 1,2 GG intrastrand CL of BBR3571 or cisplatin were obtained (shown in Fig. 5A) for the duplexes TGGT(19–23) and analyzed (Figs. 5B–D).

A significant retardation was observed for the multimers of all platinated duplexes. Decreased gel electrophoretic mobility may result from a decrease in the DNA end-to-end distance [45]. Various platinum(II) complexes have been shown to form DNA adducts, which decrease gel mobility of DNA fragments due to either stable curvature of the helix axis or increased isotropic flexibility [7–9,26,28,30,46,47]. DNA multimers of identical length and number of stable bend units, but with differently phased bends, have different end-to-end distances. The DNA bends of a multimer must be, therefore, spaced evenly and phased with the DNA helical repeat in order to add constructively. Such constructively phased bends add in plane, yielding short end-to-end distances and the most retarded gel migration. In other words, gel electrophoresis

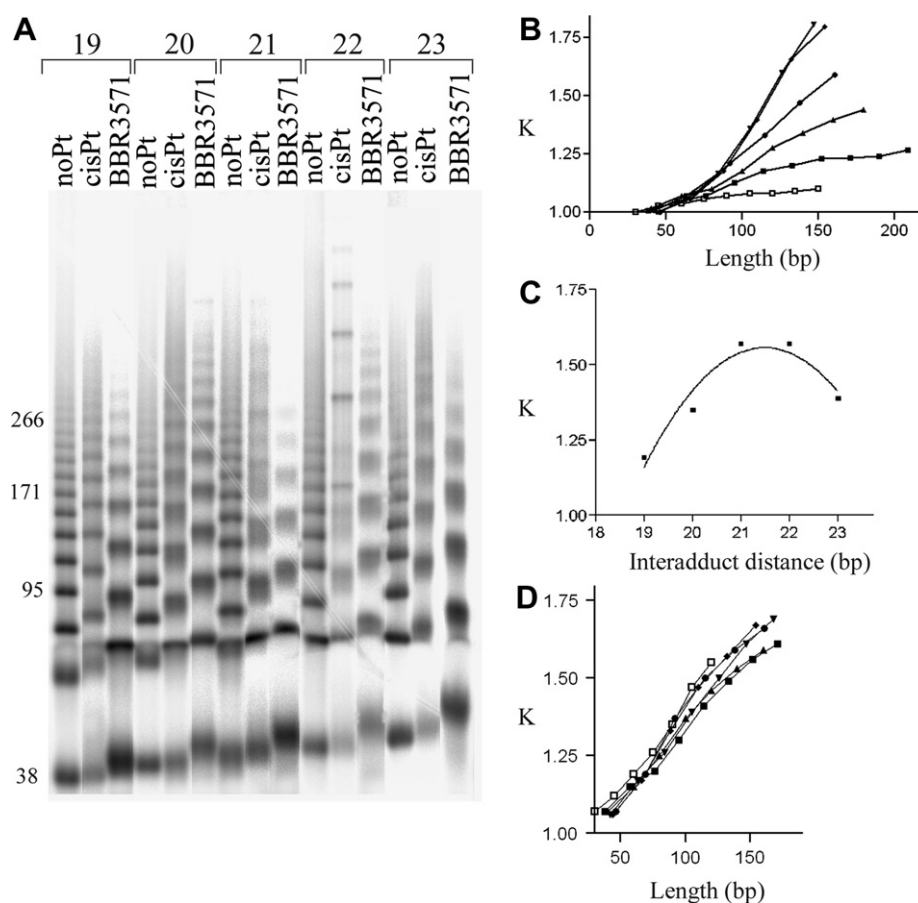


Fig. 5. (A) Autoradiograms of the ligation products of TGGT duplexes (19–22) containing a unique 1,2-GG intrastrand CL of BBR3571 or cisplatin separated on an 8% polyacrylamide gel. Unplatinated oligomers, lanes No Pt; oligomers modified by cisplatin, lanes cisPt; oligomers modified by BBR3571, lanes BBR3571. (B) Plot showing the relative mobility K versus sequence length curves for the oligomers TGGT (15,19–22) modified by cisplatin denoted, respectively, as 15mer, 19–22mer. (C) Plots showing the relative mobility K versus interadduct distance in bp for the duplexes TGGT(19–23) intrastrand cross-linked by cisplatin with a total length of 120 bp. The experimental points represent the average of three independent electrophoresis experiments. The curves represent the best fit of these experimental points to the equation $K = ad^2 + bd + c$ [28,44,49]. (D) Plot showing the relative mobility K versus sequence length curves for the oligomers TGGT (15,19–22) modified by BBR3571 denoted, respectively, as 15mer, 19–22mer.

of multimers of oligonucleotide duplexes that only differ in length and contain a stable curvature induced by the same platinum adduct should exhibit a phase effect, i.e., the maximum retardation should be observed for the multimers having the bends in phase with helix screw. In contrast, the normal electrophoretic mobility should be observed for the multimers having the bends separated by a half-integral number of DNA turns. Importantly, a gel mobility retardation of multimers due to the platinum adducts introducing isotropic flexibility rather than stable curvature is not expected to display a phase dependence [48]. The K factor is defined as the ratio of calculated to actual length. The calculated length is based on a multimer's mobility and is obtained from a calibration curve constructed from the mobilities of unplatinated multimers. Experimental details of these studies are given in our previous work [26].

The variations of K factor *versus* sequence length obtained for multimers of the TGGT 15,19–23 bp long and containing the unique 1,2-GG intrastrand CL of cisplatin and *versus* interadduct distance for the duplexes TGGT(19–23) intrastrand cross-linked by cisplatin with a total length of 120 bp are shown in Figs. 5B and C, respectively. The rigid, directional DNA bending of $32 \pm 2^\circ$ toward the major groove and unwinding of $18 \pm 2^\circ$ due to the single, site-specific 1,2-GG intrastrand CL formed by cisplatin were identical with the previously published results [28,44,49]. In contrast, no significant change in the slopes of the K factor *versus* sequence length plots obtained for multimers of the TGGT 15,19–23 bp long and containing the unique 1,2-GG intrastrand CL of BBR3571 was observed in a broad range of the lengths of the monomeric TGGT duplexes (15 and 19–23 bp) (Fig. 5D). This result suggests that conformational distortion induced in double-stranded DNA by 1,2-GG intrastrand CL by BBR3571 does not result in a stable curvature (rigid directional bending).

As it is mentioned in the Discussion section (*vide infra*), an important factor involved in the mechanism of the TLS through the platinum adducts by DNA polymerases is flexibility of the duplex at the site of the adduct. In order to further support this hypothesis, we also examined TLS through the 1,3-GTG intrastrand CL of cisplatin. This adduct has a similar size as the 1,2-GG intrastrand CL of cisplatin and distortion induced in DNA by this adduct has several features similar to those of the distortion induced by the 1,2-GG intrastrand CL [50,51]. However, DNA at the site of the 1,3-intrastrand CL of cisplatin is locally denatured and consequently flexible [50,51]. We have also examined the effects of the 1,3-GTG intrastrand CLs of cisplatin on polymerization by RT HIV-1. DNA polymerization proceeded up to the nucleotide at the site opposite the 3' G involved in the CL (Fig. 6A, lanes 6–10). There was no accumulation of shorter DNA intermediates. The full-length products were also noticed, although in a considerably smaller amount compared with DNA polymerization using the template containing the 1,2-GG intrastrand CL of cisplatin (cf. Figs. 2B and 6B).

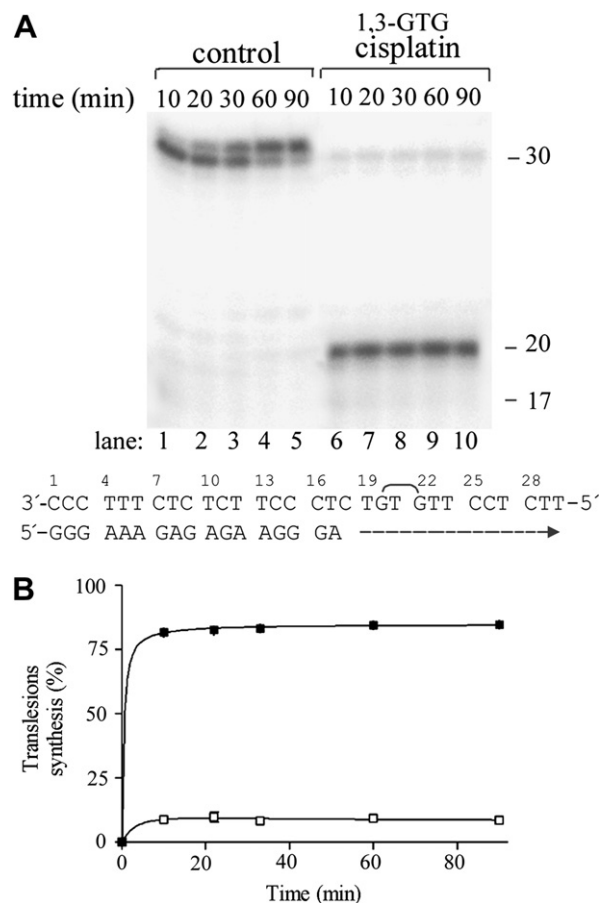


Fig. 6. Primer extension activity of RT HIV-1 using the 17mer/30mer, primer/template duplex. (A) The experiments were conducted for the times indicated in the figure (10–90 min) using undamaged templates (lanes 1–5) and the template containing single, site specific 1,3-GTG intrastrand CL of cisplatin (lanes 6–10). The pause site opposite the platinated 3' guanine is marked 20. The nucleotide sequences of the template and the primer are shown beneath the gel. See the text for details. (B) The time dependence of the inhibition of DNA synthesis on undamaged (control) template (full squares) and DNA containing 1,3-GTG intrastrand CL of cisplatin (open squares). Data are means (\pm SE) from three different experiments with two independent template preparations.

Discussion

DNA lesions that escape repair pathways can cause arrested DNA replication. This replication block can be processed by TLS, which is carried out by a number of specialized DNA polymerases. A number of results have been obtained to describe TLS efficiencies of various lesions and polymerases. However, the structural features of the DNA polymerase-DNA substrate interaction that are required to accomplish TLS have not been uniquely determined. The inability of a polymerase to incorporate a base opposite the lesion reflects the polymerase's inability to position a lesion-containing base pair in a geometric conformation that allows active site assembly and catalysis.

To expand the database of the structural features of the DNA polymerase-DNA substrate interaction that are required to accomplish TLS, we performed in the present

work studies of oligodeoxyribonucleotides containing 1,2-GG intrastrand CL of cisplatin and BBR3571. These CLs which have the same nature, but differ in the size and the character of the conformational alteration induced by these adducts in double-helical DNA, were analyzed for bypass ability with two DNA polymerases, namely RT HIV-1 and KF^- . The abundance of information available on these DNA polymerases, due to previous genetic and biochemical studies, make RT HIV-1 and KF^- ideal models for studies of the interactions involved with TLS. Moreover, these two DNA polymerases have been also chosen because they have been used in a great number of studies with a broad range of DNA adducts. We found that both polymerases partially bypassed 1,2-GG intrastrand CL of cisplatin, but were blocked at the same adduct formed by BBR3571.

The size or bulkiness of DNA adducts, along with distortions induced by these adducts in DNA are considered key factors in mechanism of the blockage of DNA polymerases. Small adducts are bypassed fairly readily whereas TLS through and beyond bulky adducts is dramatically decreased [52]. Thus, markedly higher efficiency of the 1,2-GG intrastrand CL of BBR3571 to inhibit TLS can be at least partially explained by its larger size in comparison with the same adduct of cisplatin.

The major 1,2-GG intrastrand CL of cisplatin distorts conformation of DNA [32,53]. It induces a roll between the platinated purine residues, displacement of the platinum atom from the planes of the purine rings, a directional and rigid bend of the helix axis toward the major groove and a local unwinding. In addition, severe perturbation of hydrogen-bonding within the 5'-coordinated G-C bp, widening and flattening of the minor groove opposite the cisplatin adduct, creation of a hydrophobic notch, global distortion extending over 4–5 bp and additional helical parameters characteristic of the A-form of DNA have been also reported. Hence, the conformational alteration induced in double-helical DNA by 1,2-GG intrastrand CL of cisplatin is similar to that induced in DNA complexed with RT HIV-1 [54]. The crystal structure of this complex revealed the duplex to have an unusual and unexpected bend at the active site [54]. The majority of the duplex region is in B-conformation, but in the vicinity of the polymerase active site there are several base pairs of DNA which adopt A-conformation, and at the B–A junction of the duplex there is a marked bend (40–45°). Hence, the similar and rigid, directional bending caused by the 1,2-GG intrastrand CL of cisplatin (32–35°, [28,49]) and the observation that several base pairs close to the CL have some features of A-conformation may facilitate the binding of DNA containing this CL at the polymerase site of RT HIV-1 in a productive mode (the productive mode of binding is defined as a state whereby the DNA is configured to rapidly accept an incoming nucleotide [1]). On the other hand, lack of phase dependence of the retardation of gel mobility of DNA containing the 1,2-GG intrastrand CL of BBR3571 is consistent with the view that formation of this CL results in a flexible nondirectional bend, which

may reflect the inherently more flexible dinuclear adduct. We suggest that a flexibility induced in DNA by the 1,2-GG intrastrand CL of BBR3571 can make the productive binding of this adduct at the polymerase site of RT HIV-1 more difficult.

The view that a flexibility induced in DNA at the site of the adduct may favor an adduct conformation that is associated with less efficient primer extension beyond the lesion is further corroborated by the results demonstrating the inhibition of TLS across the 1,3-GTG intrastrand CL of cisplatin (Fig. 6). In comparison with the 1,2-GG intrastrand CL, the 1,3-CL of cisplatin has almost the same size and also distortion induced in DNA by this adduct has several features similar [bends and locally unwinds DNA in a similar extent (by $\sim 30^\circ$ and $\sim 19^\circ$, respectively)] [50,51]. On the other hand, in contrast to the 1,2-intrastrand CL of cisplatin, DNA is locally denatured and consequently flexible at the site of the 1,3-intrastrand CL of this drug [50,51]. Thus, consistent with the view that the enhanced flexibility of the template backbone at the site of the adduct within the polymerase active site is an important parameter making the TLS across the adduct more difficult (*vide supra*), the TLS through the 1,3-intrastrand CL of cisplatin is inhibited considerably more than that through the 1,2-intrastrand CL (cf. Figs. 2B and 6B).

The results of the analysis by chemical probes (Fig. 3B) demonstrate that the 1,2-GG intrastrand CLs of cisplatin create local conformational distortions which occur on both sides of the CL, but those on 5' side of the CL are more intense. Interestingly, the local conformational distortion induced by the CL of BBR3571 only occurs on its 5' side. Hence, a factor contributing to the stronger inhibition of the TLS through the 1,2-intrastrand CL of BBR3571 (compared to the TLS through the same CL of cisplatin) appears a more intense conformational distortion induced by this CL on its 5' side.

We also found by using KF^- (showing a different mechanism underlying its catalytic activity than RT HIV-1) that the 1,2-GG intrastrand CL of BBR3571 represented a markedly stronger block to DNA synthesis than the same adduct of conventional cisplatin. Since there is a high degree of structural and sequence conservation of the domains among eukaryotic, prokaryotic, and viral polymerases [55], insights gleaned from studies of the RT HIV-1 and KF^- should be also applicable to other DNA polymerases [22,56,57]. Hence, the repercussion of stronger inhibition of DNA polymerization by the 1,2-GG intrastrand CL of BBR3571 in comparison with the same adduct of cisplatin adds a new dimension to the impact of DNA modifications by polynuclear platinum compounds on biological processes, possibly including replication or DNA repair.

Acknowledgments

This research was supported by the Grant Agency of the Ministry of Health of the Czech Republic (NR8562-4/

2005), the Grant Agency of the Czech Republic (Grants 305/05/2030 and 203/06/1239), Ministry of Education of the CR (MSMT LC06030) and the Academy of Sciences of the Czech Republic (Grants IQS500040581 and KAN200200651). J.K. is the international research scholar of the Howard Hughes Medical Institute. The research of B.M. was supported in part by a grant to Saint Olaf College, Minnesota, from the Howard Hughes Medical Institute through the Undergraduate Science Education Program. The authors also acknowledge that their participation in the EU COST Actions D20 and D21 (Grants MSMT CR 1P05OC070, 1P05OC071, 1P05OC072) enabled them to exchange regularly the most recent ideas in the field of platinum anticancer drugs with several European colleagues.

References

- [1] Z. Suo, S. Lippard, K. Johnson, *Biochemistry* 38 (1999) 715–726.
- [2] S.G. Chaney, A. Vaisman, in: L.R. Kelland, N.P. Farrell (Eds.), *Platinum-based Drugs in Cancer Therapy*, Humana Press Inc., Totowa/NJ, 2000, pp. 129–148.
- [3] A. Vaisman, M.W. Warren, S.G. Chaney, *J. Biol. Chem.* 276 (2001) 18999–19005.
- [4] S.G. Chaney, S.L. Campbell, E. Bassett, Y. Wu, *Crit. Rev. Oncol. Hematol.* 53 (2005) 3–11.
- [5] M.E. Arana, L. Song, N.T. Le Gac, D.S. Parris, G. Villani, P.E.B. Boehmer, *DNA Repair* 3 (2004) 659–669.
- [6] A.M.J. Fichtinger-Schepman, J.L. Van der Veer, J.H.J. Den Hartog, P.H.M. Lohman, J. Reedijk, *Biochemistry* 24 (1985) 707–713.
- [7] J. Kasparkova, O. Novakova, N. Farrell, V. Brabec, *Biochemistry* 42 (2003) 792–800.
- [8] J. Kasparkova, O. Novakova, V. Marini, Y. Najajreh, D. Gibson, J.-M. Perez, V. Brabec, *J. Biol. Chem.* 278 (2003) 47516–47525.
- [9] O. Novakova, J. Kasparkova, J. Malina, G. Natile, V. Brabec, *Nucleic Acids Res.* 31 (2003) 6450–6460.
- [10] N. Farrell, in: A. Sigel, H. Sigel (Eds.), *Metal Ions in Biological Systems*, Marcel Dekker Inc., New York, Basel, 2004, pp. 251–296.
- [11] N. Farrell, in: L.R. Kelland, N.P. Farrell (Eds.), *Platinum-based Drugs in Cancer Therapy*, Humana Press Inc., Totowa/NJ, 2000, pp. 321–338.
- [12] T.D. McGregor, A. Hegmans, J. Kasparkova, K. Nepelchova, O. Novakova, H. Penazova, O. Vrana, V. Brabec, N. Farrell, *J. Biol. Inorg. Chem.* 7 (2002) 397–404.
- [13] V. Brabec, J. Kasparkova, in: J.-M. Perez-Martin, M.A. Fuertes, C. Alonso (Eds.), *Metal Compounds in Cancer Chemotherapy*, Research Signpost, Trivandrum, Kerala (India), 2005, pp. 187–218.
- [14] V. Brabec, J. Kasparkova, O. Vrana, O. Novakova, J.W. Cox, Y. Qu, N. Farrell, *Biochemistry* 38 (1999) 6781–6790.
- [15] J. Kasparkova, O. Novakova, O. Vrana, N. Farrell, V. Brabec, *Biochemistry* 38 (1999) 10997–11005.
- [16] J. Kasparkova, N. Farrell, V. Brabec, *J. Biol. Chem.* 275 (2000) 15789–15798.
- [17] J. Zehnulova, J. Kasparkova, N. Farrell, V. Brabec, *J. Biol. Chem.* 276 (2001) 22191–22199.
- [18] J. Kasparkova, J. Zehnulova, N. Farrell, V. Brabec, *J. Biol. Chem.* 277 (2002) 48076–48086.
- [19] E.L. Mamenta, E.E. Poma, W.K. Kaufmann, D.A. Delmastro, H.L. Grady, S.G. Chaney, *Cancer Res.* 54 (1994) 3500–3505.
- [20] G.R. Gibbons, W.K. Kaufmann, S.G. Chaney, *Carcinogenesis* 12 (1991) 2253–2257.
- [21] K.A. Johnson, *Annu. Rev. Biochem.* 62 (1993) 685–713.
- [22] W.C. Lam, E.J.C. Van der Schans, L.C. Sowers, D.P. Millar, *Biochemistry* 38 (1999) 2661–2668.
- [23] P.H. Patel, M. Suzuki, E. Adman, A. Shinkai, L.A. Loeb, *J. Mol. Biol.* 308 (2001) 823–837.
- [24] H. Rauter, R. DiDomenico, E. Menta, A. Oliva, Y. Qu, N. Farrell, *Inorg. Chem.* 36 (1997) 3919–3927.
- [25] V. Brabec, J. Reedijk, M. Leng, *Biochemistry* 31 (1992) 12397–12402.
- [26] V. Brabec, M. Sip, M. Leng, *Biochemistry* 32 (1993) 11676–11681.
- [27] J. Kasparkova, K.J. Mellish, Y. Qu, V. Brabec, N. Farrell, *Biochemistry* 35 (1996) 16705–16713.
- [28] S.F. Bellon, S.J. Lippard, *Biophys. Chem.* 35 (1990) 179–188.
- [29] H.S. Koo, H.M. Wu, D.M. Crothers, *Nature* 320 (1986) 501–506.
- [30] V. Marini, P. Christofis, O. Novakova, J. Kasparkova, N. Farrell, V. Brabec, *Nucleic Acids Res.* 33 (2005) 5819–5828.
- [31] S.M. Cohen, S.J. Lippard, *Prog. Nucleic Acid Res. Mol. Biol.* 67 (2001) 93–130.
- [32] V. Brabec, *Prog. Nucleic Acid Res. Mol. Biol.* 71 (2002) 1–68.
- [33] C. Bailly, D. Gentle, F. Hamy, M. Purcell, M.J. Waring, *Biochem. J.* 300 (1994) 165–173.
- [34] C. Bailly, M.J. Waring, in: K.R. Fox (Ed.), *Drug-DNA Interaction Protocols*, Humana Press Inc., Totowa/NJ, 1997, pp. 51–79.
- [35] P.E. Nielsen, *J. Mol. Recognition* 3 (1990) 1–24.
- [36] S.A. Ross, C.J. Burrows, *Nucleic Acids Res.* 24 (1996) 5062–5063.
- [37] J.G. McCarthy, L.D. Williams, A. Rich, *Biochemistry* 29 (1990) 6071–6081.
- [38] J.G. McCarthy, A. Rich, *Nucleic Acids Res.* 19 (1991) 3421–3429.
- [39] W. Herr, *Proc. Natl. Acad. Sci. USA* 82 (1985) 8009–8013.
- [40] B.H. Johnston, A. Rich, *Cell* 42 (1985) 713–724.
- [41] U.M. Ohndorf, M.A. Rould, Q. He, C.O. Pabo, S.J. Lippard, *Nature* 399 (1999) 708–712.
- [42] D.B. Zamble, S.J. Lippard, in: B. Lippert (Ed.), *Cisplatin. Chemistry and Biochemistry of a Leading Anticancer Drug*, VCH, Zürich, Weinheim, 1999, pp. 73–110.
- [43] H.F. Huang, L.M. Zhu, B.R. Reid, G.P. Drobny, P.B. Hopkins, *Science* 270 (1995) 1842–1845.
- [44] S.F. Bellon, J.H. Coleman, S.J. Lippard, *Biochemistry* 30 (1991) 8026–8035.
- [45] H.S. Koo, D.M. Crothers, *Proc. Natl. Acad. Sci. USA* 85 (1988) 1763–1767.
- [46] J. Malina, C. Hofr, L. Maresca, G. Natile, V. Brabec, *Biophys. J.* 78 (2000) 2008–2021.
- [47] J. Malina, M. Vojtiskova, V. Brabec, C.I. Diakos, T.W. Hambley, *Biochem. Biophys. Res. Commun.* 332 (2005) 1034–1041.
- [48] M. Leng, *Biophys. Chem.* 35 (1990) 155–163.
- [49] K. Stehlikova, H. Kostrhunova, J. Kasparkova, V. Brabec, *Nucleic Acids Res.* 30 (2002) 2894–2898.
- [50] M.F. Anin, M. Leng, *Nucleic Acids Res.* 18 (1990) 4395–4400.
- [51] J.M. Teuben, C. Bauer, A.H.J. Wang, J. Reedijk, *Biochemistry* 38 (1999) 12305–12312.
- [52] A.M. Woodside, F.P. Guengerich, *Biochemistry* 41 (2002) 1027–1038.
- [53] E.R. Jamieson, S.J. Lippard, *Chem. Rev.* 99 (1999) 2467–2498.
- [54] A. Jacobo-Molina, J. Ding, R.G. Nanni, A.D. Clark Jr., X.-J. Lu, C. Tantillo, R.L. Williams, G. Kamer, A.L. Ferris, P. Clark, A. Hizi, S.H. Hughes, E. Arnold, *Proc. Natl. Acad. Sci. USA* 90 (1993) 6320–6324.
- [55] U. Hubscher, H.P. Nasheuer, J.E. Syvaaja, *Trends Biochem. Sci.* 25 (2000) 143–147.
- [56] T.A. Steitz, *J. Biol. Chem.* 274 (1999) 17395–17398.
- [57] S. Lone, L.J. Romano, *Biochemistry* 42 (2003) 3826–3834.

15.

DNA binding mode of ruthenium complexes and relationship to tumor cell toxicity

Viktor Brabec^{*}, Olga Nováková

Institute of Biophysics, Academy of Sciences of the Czech Republic, Královopolská 135, CZ-61265 Brno, Czech Republic

Received 12 March 2006; received in revised form 11 May 2006; accepted 15 May 2006

Abstract

Transition-metal-based compounds constitute a discrete class of chemotherapeutics, widely used in the clinic as antitumor and antiviral agents. Examples of established antitumor metallodrugs, routinely used in the clinic, are cisplatin [*cis*-diamminedichloroplatinum(II)] and its analogues carboplatin and oxaliplatin. However, drug resistance and side effects have limited their clinical utility. These limitations have prompted a search for more effective and less toxic metal-based antitumor agents. Some of the efforts have been directed in the design of non-platinum, transition-metal-based antitumor agents and ruthenium complexes have attracted much interest as alternative drugs to cisplatin in cancer chemotherapy. Ruthenium complexes demonstrate similar ligand exchange kinetics to those of platinum(II) antitumor drugs already used in the clinic while displaying only low toxicity. This is in part due to the ability of ruthenium complexes to mimic the binding of iron to molecules of biological significance, exploiting the mechanisms that the body has evolved for transport of iron. In addition, the redox potential between the different accessible oxidation states occupied by ruthenium complexes enables the body to catalyze oxidation and reduction reactions, depending on physiological environment. The biochemical changes that accompany cancer alter physiological environment, enabling ruthenium complexes to be selectively activated in cancer tissues. Due to differing ligand geometry between their complexes, ruthenium compounds bind to DNA affecting its conformation differently than cisplatin and its analogues. In addition, non-nuclear targets, such as the mitochondrion and the cell surface, have also been implicated in the antineoplastic activity of some ruthenium complexes. Thus, ruthenium compounds offer the potential over antitumor platinum(II) complexes currently used in the clinic of reduced toxicity, a novel mechanism of action, the prospect of non-cross-resistance and a different spectrum of activity. In other words, some chemical properties make ruthenium compounds well suited for medicinal applications and as an alternative to platinum antitumor drugs in the treatment of cancer cells resistant to cisplatin. Although the pharmacological target for antitumor ruthenium compounds has not been unequivocally identified, there is a large body of evidence indicating that the cytotoxicity of many ruthenium complexes correlates with their ability to bind DNA although few exceptions have been reported. This review summarizes results demonstrating that several ruthenium compounds that exhibit antitumor effects different from cisplatin or its analogues bind DNA and modify it differently than cisplatin or its analogues.

© 2006 Elsevier Ltd. All rights reserved.

Keywords: DNA; Transition metals; Ruthenium anticancer drugs; Polynuclear metal-based compounds; Intercalation; Topoisomerase II

1. Introduction

Transition-metal-based compounds constitute a class of chemotherapeutics, which are widely used in the clinic as antitumor and antiviral agents. The interest in this structural class has its origin in the 1960s, with the serendipitous discovery by Rosenberg of the inhibition of division of bacterial cells by platinum complexes (Rosenberg et al., 1965, 1969).

The first transition-metal anticancer drug introduced in the clinic was cisplatin [*cis*-diamminedichloroplatinum(II)]. This very simple inorganic molecule, which belongs to bifunctional reagents, is highly effective for the treatment of testicular and ovarian cancer and is used in combination regimens for a variety of other carcinomas, including bladder, small cell lung and head and neck cancers (Weiss and Christian, 1993; Wong and Giandomenico, 1999; Giaccone, 2000; Ho et al., 2003). However, its clinical utility is limited to a relatively narrow range of tumors, because of primary resistance to cisplatin and the development of resistance

^{*} Corresponding author. Tel.: +42 541517148; fax: +42 541240499.

E-mail address: brabec@ibp.cz (V. Brabec).

secondary to the initial treatment (Wernyj and Morin, 2004). In addition, cisplatin is administered intravenously due to its limited solubility in water and has severe side effects (Wong and Giandomenico, 1999).

These limitations have prompted a search for more effective and less toxic alternative metal-based antitumor agents. The result has been the synthesis of thousands of platinum complexes and their evaluation as antitumor agents. Of these, only few have reached clinical trials and have been approved for clinical administration. They are close analogues of cisplatin, namely carboplatin [*cis*-diamminecyclo-butanedicarboxylato-platinum(II)], oxaliplatin {[*(1R,2R)*-diamminocyclohexane]oxalato-platinum(II)} [*(1,2)*-diamminocyclo-hexane = DACH}] and nedaplatin [*cis*-diammineglycolato-platinum(II)]. Thus, the search for new metal-based antitumor drugs has continued beyond platinum, in the hope of improvements in cancer treatment.

There have been efforts to rationally design unconventional platinum complexes, such as polynuclear platinum compounds (Farrell, 2004) and analogues of clinically ineffective *trans*-diamminedichloroplatinum(II) (transplatin) (Farrell, 1996; Perez et al., 2000; Brabec, 2002; Natile and Coluccia, 2004; Brabec and Kasparkova, 2005a). Additional efforts have been directed in the design of other transition-metal antitumor agents (Clarke et al., 1999; Brabec, 2002; Alessio et al., 2004a). Theoretical advantages in using ions of transition metals other than platinum include:

- a. the availability of additional coordination sites in octahedral complexes and altered shape of the complex,
- b. alterations in ligand affinity and substitution kinetics,
- c. changes in oxidation state,
- d. photodynamic approaches to therapy.

2. Ruthenium complexes

Ruthenium complexes have attracted much attention as building blocks for new transition-metal-based antitumor agents. Ruthenium compounds offer the potential over antitumor platinum(II) complexes currently used in the clinic of reduced toxicity, a novel mechanism of action, the prospect of non-cross-resistance (Zeller et al., 1991; Coluccia et al., 1993) and a different spectrum of activity (Clarke, 2003; Alessio et al., 2004a). Non-cross-resistance in cisplatin-resistant cancer cells and reduced toxicity, which is in part due to the ability of ruthenium complexes to mimic the binding of iron to molecules of biological significance, exploiting the mechanisms that the body has evolved for non-toxic transport of iron (Allardyce and Dyson, 2001), is a particularly attractive feature of ruthenium complexes (Allardyce and Dyson, 2001). In addition, some chemical properties, such as rate of ligand exchange, range of accessible oxidation states, and ability of ruthenium to mimic iron in binding to certain biological molecules make these compounds well suited for medicinal applications as an alternative to platinum antitumor

drugs in the treatment of cancer cells resistant to cisplatin and its analogues justifying further development of this novel and interesting group of metal complexes.

It is generally accepted that the anticancer activity of platinum coordination complexes arises from their ability to damage DNA, with adducts forming various types of cross-links (Johnson et al., 1989; Cohen and Lippard, 2001; Brabec, 2002). Owing to the octahedral structure of ruthenium(II) and ruthenium(III) complexes, as opposed to the square-planar geometry of platinum(II) compounds, ruthenium antitumor complexes probably function in a manner different from that of cisplatin. Hence, the overall objective of this review is to ask a fundamental question: can the unique DNA binding mode of ruthenium compounds lead to a profile of anticancer activity genuinely different from that seen with the platinum antitumor agents already used in the clinic?

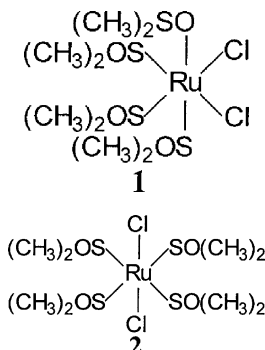
The pharmacological target of antitumor ruthenium complexes has not been unequivocally identified, but it is generally accepted that their cytotoxicity is related to their ability to bind DNA (Fruhauf and Zeller, 1991; Gallori et al., 2000), although some exceptions have been reported (Zhang and Lippard, 2003). Several ruthenium compounds have been shown to inhibit DNA replication, possess mutagenic activity, induce SOS repair, bind to nuclear DNA and reduce RNA synthesis, which are all consistent with DNA binding of these compounds *in vivo*. Thus, by analogy to platinum antitumor drugs, DNA interactions of antitumor ruthenium agents are of a great interest.

Several reviews have appeared recently that summarize anticancer effects of ruthenium complexes (Sava et al., 1990; Keppler et al., 1993; Sava and Bergamo, 2000; Allardyce and Dyson, 2001; Clarke, 2003; Galanski et al., 2003; Alessio et al., 2004a, 2004b), although only little attention has been paid to details of molecular mechanisms underlying these effects. The present review focuses on one of several important aspects of the molecular mechanism underlying anticancer effects of ruthenium compounds, which is DNA modifications brought about by these complexes in cell-free media. In particular, it deals with DNA interactions of ruthenium compounds for which anticancer activity has also been reported.

2.1. Dimethyl sulfoxide complexes

Dimethyl sulfoxide (DMSO) complexes of both ruthenium(II) and ruthenium(III) exhibit antitumor activity comparable to cisplatin at equitoxic dosage in animal models of metastasizing tumors, but with less severe side effects and prolonged host survival times (Sava et al., 1999). A small series of complexes whose parent compounds are *cis*- and *trans*-[Ru(II)(DMSO)₄Cl₂] (compounds 1 and 2) constitute one class of dimethyl sulfoxide ruthenium compounds (Clarke et al., 1999; Sava et al., 1999). Examination of their effects on primary tumor and on metastasis has revealed antimetastatic activities superior to effects on primary tumor growth. The initial studies were performed

with *cis*-[Ru(II)(DMSO)₄Cl₂] because of its similarity to cisplatin. However, comparison of the antitumor effects of *cis*- and *trans*-[Ru(II)(DMSO)₄Cl₂] have revealed superiority of the latter.



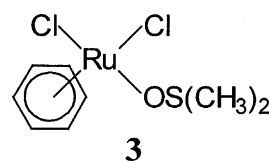
Cis- and *trans*-[Ru(II)(DMSO)₄Cl₂] contain two chlorides in the octahedral structure (Mestroni et al., 1989). In *cis*-[Ru(II)(DMSO)₄Cl₂] the three DMSO molecules are S-bound in a facial configuration and the fourth is O-bonded. In *trans*-[Ru(II)(DMSO)₄Cl₂] all the DMSOs are S-bound. When dissolved in water, the *cis* isomer immediately undergoes loss of the O-bonded DMSO ligand whereas the *trans* compound rapidly loses two S-bonded DMSO ligands yielding *cis*-diaqua species. Both hydrolyzed isomers then undergo slow reversible chloride dissociation forming cationic compounds. After this step, the *trans* compound contains three reactive groups while the *cis* isomer only two (Mestroni et al., 1989). In addition, the three remaining DMSO ligands in the *cis* isomer represent a considerable steric hindrance, which makes the *cis* aqua species inert relative to the *trans* isomer. This difference correlates with a higher potency of the *trans* isomer as an antitumor agent (Loseto et al., 1991).

Both *cis*- and *trans*-[Ru(II)(DMSO)₄Cl₂] bind to DNA in cell-free media (Loseto et al., 1991; Novakova et al., 2000). Some early studies based on analysis of circular dichroism (CD) spectra of DNA have suggested that coordination of the *cis* isomer to DNA does not significantly alter the conformation of B-DNA (Mestroni et al., 1989). The *trans* isomer binds to DNA more rapidly with some changes in the CD spectra indicating conformational alterations (Mestroni et al., 1989). Both isomers have a limited preference for bifunctional binding to neighboring guanine residues at their N7 atoms with the *trans* isomer being more effective (Novakova et al., 2000). The DNA binding mode of *trans*-[Ru(II)(DMSO)₄Cl₂] includes formation of bifunctional adducts such as intrastrand cross-links between neighboring purine residues and a small amount (~1%) of interstrand cross-links. *Cis*-[Ru(II)(DMSO)₄Cl₂] forms on natural DNA mainly monofunctional lesions. These findings are consistent with the results of the binding of *cis*- and *trans*-[Ru(II)(DMSO)₄Cl₂] to the dinucleotide d(GpG) demonstrating a considerably slower binding of the *cis* isomer (Anagnostopoulou et al., 1999). Both ruthenium isomers induce conformational alterations in DNA of non-denaturational character, the *trans* compound

being more effective. In addition, DNA adducts of *trans*-[Ru(II)(DMSO)₄Cl₂] are capable of inhibiting RNA synthesis by DNA-dependent RNA polymerases while the adducts of the *cis* isomer are not. Thus, several features of the DNA binding mode of *trans*-[Ru(II)(DMSO)₄Cl₂] are similar to those of antitumor cisplatin (Novakova et al., 2000), which may be relevant to the biological effects of this antitumor ruthenium drug. On the other hand, the different DNA binding mode of *cis*-[Ru(II)(DMSO)₄Cl₂] is consistent with its less pronounced biological effects.

The cytotoxicity and photocytotoxicity of *cis*- and *trans*-[Ru(II)(DMSO)₄Cl₂] complexes was tested in two melanoma cell lines, human (SK-MEL 188) and mouse (S91) (Brindell et al., 2005). The *trans* isomer was found to be more effective for cell growth inhibition than its *cis* analogue both in the presence and in the absence of light. However, the antiproliferative activity of both isomers was significantly enhanced after irradiation with UVA light in comparison with their activity in the dark.

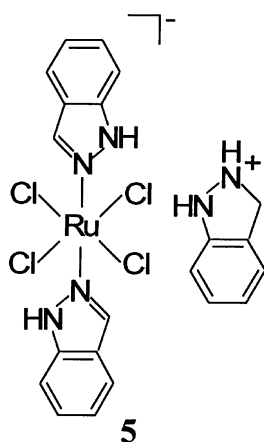
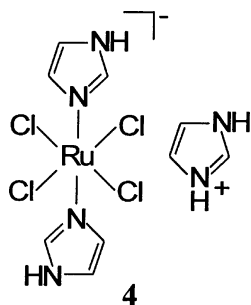
Interesting results have been also obtained in studies of the mechanism of antitumor activity of Ru(II)(C₆H₆)(DMSO)Cl₂ complex (compound 3) (Gopal et al., 1999). This compound exhibits a strong DNA-binding affinity, but binding does not affect substantially DNA conformation. On the other hand, it could completely inhibit DNA relaxation activity of topoisomerase II by trapping it into a ternary complex with DNA. A model has been proposed for this ternary complex, in which the ruthenium atom is coordinately bound to DNA and its ligands are cross-linked to topoisomerase II.



2.2. Heterocyclic complexes

Heterocyclic complexes of ruthenium(III) constitute a relatively new group of potential anticancer compounds (Keppler et al., 1993; Clarke et al., 1999). The general formula of this structural class is (HB)[Ru(III)B₂Cl₄], where B stands for a heterocyclic base, such as imidazole (Im) or indazole (compounds 4 and 5, respectively). These complexes exhibit activity in various tumor models and are particularly effective against cisplatin-resistant colorectal tumors (Keppler et al., 1993). The complex (HInd)[Ru(III)Cl₄(Ind)₂] (KP1019) (compound 5) is highly active against a colorectal tumor cells both *in vivo* and *in vitro* (Berger et al., 1989; Galeano et al., 1992; Seelig et al., 1992; Sava and Bergamo, 2000; Galanski et al., 2003), is completely devoid of side effects and drug induced lethality at therapeutically relevant doses (Keppler et al., 1993). Its therapeutic index is better than that of (HIm)[Ru(III)Cl₄(Im)₂] (compound 4). The complex (HInd)[Ru(III)Cl₄(Ind)₂] has been shown to be efficiently taken up into the cells probably

via interaction with transferrin (Kratz et al., 1994; Frasca et al., 2001; Pongratz et al., 2004). It induces apoptosis (Kapitza et al., 2005b), but the cellular mechanisms of the apoptosis induction are still largely unknown.

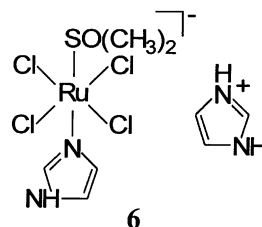


Ruthenium belongs to the same group of elements as iron (iron-triad), which is reflected by its strong affinity for transferrin and by the necessity of its reductive activation (Frasca et al., 1996; Clarke, 2003) in cells. It can be assumed that Ru(III) can substitute Fe(III) which induces Fenton type redox processes and intracellular radicals. This may well result in cellular damage that induces apoptosis. Hence, induction of oxidative stress seems to be an essential component of the cytotoxic effect of Ru(III) complexes. This cellular mechanism may not only provide an explanation of the rapid onset of Ru(III) induced apoptosis, but also allows for the protection of normal tissues by the combination with moderate amounts of antioxidants.

(HInd)[Ru(III)Cl₄(Ind)₂] interacts with DNA (*vide infra*) and forms cross-links or induces strand breaks. This complex induces formation of H₂O₂ and DNA-strand breaks in colorectal tumor cells in a dose-dependent way (Kapitza et al., 2005a). Both effects are inhibited by *N*-acetylcysteine and concomitantly cytotoxicity is reduced. Induction of apoptosis has been shown by loss of mitochondrial membrane potential and by caspase-dependent cleavage of poly-(ADP-ribose)-polymerase (PARP). Both effects were inhibited by *N*-acetylcysteine, which reduced the population with depolarized mitochondrial membranes and prevented cleavage by poly-(ADP-ribose)-polymerase indicating an

important role of oxidative stress in apoptosis induced by (HInd)[Ru(III)Cl₄(Ind)₂].

Later an analogue of these complexes was developed, namely Na[*trans*-Ru(III)((DMSO)Cl₄(Im))] (NAMI) and more recently, the corresponding imidazolium salt, (H₂Im)[*trans*-Ru(DMSO)Cl₄(Im)] (NAMI-A) (compound **6**) was synthesized with the aim of improving the solid state stability of the complex. Both NAMI and NAMI-A exhibit encouraging antitumor and antimetastatic properties, NAMI-A exhibits a high efficiency *in vivo* against lung metastasis and is currently on clinical trial as an antimetastatic drug (Sava et al., 1999; Sava and Bergamo, 2000; Rademaker-Lakhai et al., 2004). Thus, the spectrum of the antitumor effects of these ruthenium compounds differs significantly from that of cisplatin while showing lower systemic toxicity than platinum(II) compounds (Keppler, 1993).



(HIm)[Ru(III)Cl₄(Im)₂], (HInd)[Ru(III)Cl₄(Ind)₂], Na[*trans*-Ru(III)((CH₃)₂SO)Cl₄(Im)] and (H₂Im)[*trans*-Ru(III)((CH₃)₂SO)Cl₄(Im)] are pseudo-octahedral with four equatorial chloride ligands and the heterocyclic bases and DMSO as axial ligands. The complexes lose their chloride ligands and transform into the corresponding, more reactive, aquated species (Keppler et al., 1993; Clarke et al., 1999; Sava et al., 1999). The complexes (HIm)[Ru(III)Cl₄(Im)₂], (HInd)[Ru(III)Cl₄(Ind)₂] and NAMI bind irreversibly to DNA (Malina et al., 2001). Their DNA binding mode is, however, different from that of cisplatin. Interestingly, NAMI binds to DNA considerably faster than other two ruthenium compounds and cisplatin. In addition, when NAMI binds to DNA it exhibits an enhanced base sequence specificity in comparison with other two ruthenium complexes. NAMI also forms on double-helical DNA bifunctional intrastrand adducts capable of terminating RNA synthesis *in vitro* while capability of other two ruthenium compounds to form such adducts is markedly lower. This observation has been interpreted to mean that the bifunctional adducts of (HInd)[Ru(III)Cl₄(Ind)₂] and (HInd)[Ru(III)Cl₄(Ind)₂] formed on rigid double-helical DNA are sterically more crowded by their octahedral geometry than those of NAMI. In addition, the adducts of all three heterocyclic ruthenium compounds affect the conformation of DNA, NAMI being most effective. It has been suggested that similarly as in the case of dimethyl sulfoxide ruthenium complexes the altered DNA binding mode of these ruthenium compounds in comparison with cisplatin is an important factor responsible for altered cytostatic activity of this class of ruthenium compounds in tumor cells.

A recent study (Pluim et al., 2004) focused on potential factors associated with the mechanism underlying anticancer effects of NAMI-A. The cytotoxicity, intracellular accumulation and DNA adduct formation of the NAMI-A were compared *in vitro* with those of cisplatin in four human tumor cell lines: Igrov-1, 2008, MCF-7, and T47D. Interestingly, NAMI-A was on average 1053 times less cytotoxic than cisplatin. The cytotoxicity of cisplatin was linearly related to both intracellular platinum accumulation and DNA binding, while the cytotoxicity of NAMI-A was significantly related only to DNA binding and not to intracellular ruthenium accumulation. Intracellular accumulation of NAMI-A and its DNA binding were on average 4.8 and 42 times less, respectively, than those of cisplatin. In addition, the numbers of 1,2-GG and 1,2-AG intrastrand adducts induced by NAMI-A were 418 and 51 times lower, respectively. NAMI-A and cisplatin had the same binding capacity to calf thymus DNA in cell-free media. NAMI-A was 25–40% less bound to cellular proteins than cisplatin. This indicates that the low binding of NAMI-A to cellular DNA cannot simply be explained by a lower capacity to bind to DNA per se. It was suggested that the lower cytotoxicity of NAMI-A in comparison with that of cisplatin may at least partly be explained by its reduced reactivity to DNA in intact cells.

On the other hand, the results of other studies support the view that the mechanism underlying the antimetastatic activities of NAMI-A does not involve DNA binding as the most significant process. Instead, they interfere with type IV collagenolytic activity and reduce the metastatic potential of the tumors (Clarke, 2003).

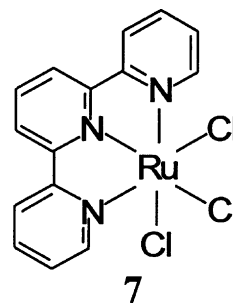
It was shown that (HIm)[Ru(III)Cl₄(Im)₂], (HInd)[Ru(III)Cl₄Ind₂], [Ru(C₆H₆)(DMSO)Cl₂] and its derivatives effectively poison the activity of topoisomerase II by forming a ternary cleavage complex of DNA-drug-topoisomerase II (Gopal and Kondapi, 2001; Gopal et al., 2002). Importantly, the inhibition of cancer cell proliferation correlated with topoisomerase II poisoning. Topoisomerase II is a major nuclear enzyme that maintains DNA topology in the complex chromosomal milieu and is an important target for many DNA binding anticancer drugs. Though these data do not give direct evidence for topoisomerase II antagonism as the cause of their activity, they suggest that topoisomerase II antagonism may at least partly account for the anticancer activity of this class of ruthenium drugs.

2.3. Polypyridyl compounds

A third group of antitumor ruthenium compounds discussed in this article are the ruthenium complexes of polypyridyl ligands. Some of these complexes exist as chiral molecules capable of enantioselective recognition of DNA. The DNA binding and cleavage properties of various polypyridyl ruthenium compounds have been intensively investigated, because they have been also proposed as useful probes of the DNA conformation (Barton, 1986)

or DNA cleavage agents (Grover et al., 1994; Neyhart et al., 1995). Analogues of these ruthenium complexes containing – besides polypyridyl ligands – also aqua or chloro groups, have been also synthesized and have been found to bind DNA covalently in cell-free media (Barton and Lolis, 1985; Grover et al., 1994). The aqua or chloro-ligands in these complexes represent leaving-ligands in contrast to the kinetically more stable pyridyl groups.

The cytotoxicity of chloropolypyridyl ruthenium complexes of structural formulas [Ru(II)Cl(bpy)(terpy)]Cl, *cis*-[Ru(II)(bpy)₂Cl₂] and *mer*-[Ru(II)Cl₃(terpy)] (compound 7) (bpy = 2,2'-bipyridyl, terpy = 2,2':6',2''-terpyridine) has been demonstrated in murine and human tumor cell lines (Novakova et al., 1995). *mer*-[Ru(II)Cl₃(terpy)] exhibits a remarkably higher cytotoxicity than the other complexes. Moreover, investigations of antitumor activity (studied on murine lymphosarcoma LS/BL ascitic tumor) have revealed the highest efficiency for *mer*-[Ru(II)Cl₃(terpy)]. In a cell-free medium, the ruthenium complexes coordinate to DNA preferentially at guanine residues (Novakova et al., 1995; van Vliet et al., 1995). The resulting adducts terminate DNA synthesis *in vitro*. The reactivity of the complexes to DNA, their efficiency to unwind closed, negatively supercoiled DNA and a sequence preference of their DNA adducts do not show a correlation with biological activity. On the other hand, the cytotoxic *mer*-[Ru(II)Cl₃(terpy)] exhibits a significant DNA interstrand cross-linking, in contrast to the less active complexes. Thus, this potential new class of metal-based antitumor compounds may act by a mechanism involving DNA interstrand cross-linking.



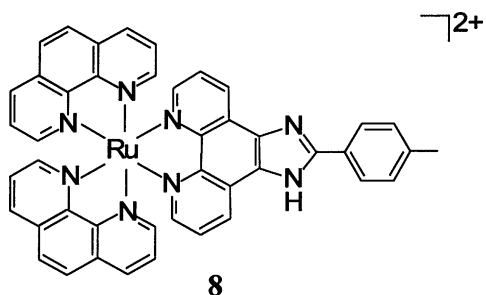
The three isomeric dichlororuthenium(II) complexes α -, β -, and γ -[Ru(II)(azpy)₂Cl₂] (azpy = 2-phenylazopyridine) have been investigated for their cytotoxic properties against a series of tumor cell lines (Hotze et al., 2005). The complex α -[Ru(II)(azpy)₂Cl₂] exhibits a very high cytotoxicity (markedly higher than cisplatin), which stands in contrast to the much lower cytotoxicity of the *trans*-dichloro complex γ -[Ru(II)(azpy)₂Cl₂] and the *cis*-dichloro isomer β -[Ru(II)(azpy)₂Cl₂]. The binding of the complex α -[Ru(II)(azpy)₂Cl₂] to monomeric 9-ethylguanine and guanosine has been studied and compared with previously obtained results for the binding of these monomers to the bis(bipyridyl)ruthenium(II) complex (Hotze et al., 2005). The ligands 9-ethylguanine and guanosine form monofunctional adducts. The guanine derivatives in the azpy com-

plexes can have more orientations than found for related *cis*-[Ru(II)(bpy)₂Cl₂] species. This versatility is considered to be important in the binding of the α -[Ru(II)(azpy)₂Cl₂] complex to DNA and very likely related to the cytotoxicity of this compound.

Tris(ligand) complexes [RuL₃](PF₆)₂ (L = 2-phenylazopyridine or *o*-tolylazopyridine) and mixed ligand [RuL₂L'']₂(PF₆)₂ (L' and L'' are 2-phenylazopyridine or bpy) have been synthesized, structurally characterized and investigated for cytotoxic activity (Hotze et al., 2005). These complexes were designed to test the hypothesis that the compound α -[Ru(II)(azpy)₂Cl₂] exhibits a high cytotoxicity due to its two *cis* chloride ligands, which might be exchanged for biological targets such as DNA as in the case of cisplatin. Remarkably, the cytotoxicity of *mer*-[Ru(II)(azpy)₃](PF₆)₂ and *mer*-[Ru(II)(tazpy)₃](PF₆)₂ (tazpy = *o*-tolylazopyridine) for tumor cell lines (A498, EVSA-T, H226, IGROV, M19, MCF-7 and WiDR) was moderate. So, even though no chloride ligands are present in these tris(ligand) complexes, cytotoxic activity is observed. This would imply that the 2-phenylazopyridine ruthenium(II) complexes act by a completely different mechanism than cisplatin.

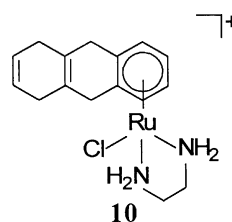
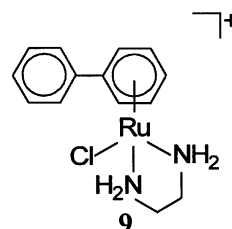
A series of monochloro-ruthenium complexes, [Ru(II)(terpy)(NN)Cl]⁺ (NN, bidentate nitrogen ligand), containing different electron-donating groups were also prepared (Cheng et al., 2000). DNA binding and formation of Ru–DNA adducts were confirmed by gel mobility shift assay. The preferential DNA binding sites of [Ru(II)(terpy)(tmphen)Cl]⁺ (tmphen = tetramethylphenanthroline) were purine residues. Surprisingly, [Ru(II)(terpy)(tmphen)Cl]⁺ inhibited bacterial cell growth (wild type *E. coli*) at lower concentrations than *cis*-[Ru(II)(bpy)₂Cl₂]. It was suggested on the basis of these results that these ruthenium complexes modified with electron-rich groups may represent a new class of anticancer ruthenium drugs.

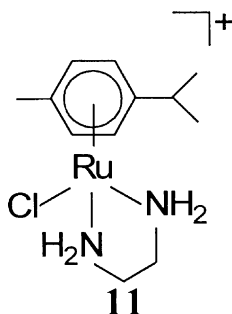
The interactions of a metal complex [Ru(II)(phen)₂PMIP]²⁺ {phen = 1,10-phenanthroline, PMIP = 2-(4-methylphenyl)imidazo[4,5-*f*]1,10-phenanthroline} (compound **8**) with yeast transfer RNA and calf thymus DNA have been investigated (Xu et al., 2005). Binding modes of these Ru(II) polypyridyl complex to both nucleic acids involve intercalation. The results also suggest that interactions with these nucleic acids are enantioselective, with the Δ -enantiomer of the complex binds more favorably than the Λ -enantiomer.



2.4. Ruthenium(II) arene complexes

Organometallic ruthenium(II) complexes with arene ligands represent a relatively new group of ruthenium compounds with antitumor activity. The monodentate ruthenium(II) arene complexes of the type [(η^6 -arene)Ru(II)(en)Cl][PF₆] (en = ethylenediamine) constitute a group of anticancer compounds (Morris et al., 2001; Aird et al., 2002; Novakova et al., 2005) with a mechanism of action different from those of the ruthenium(III) complexes NAMI-A and (HInd)[Ru(III)Cl₄(Ind)₂], which are currently on clinical trials (Alessio et al., 2004a, 2004b). The (η^6 -arene)Ru(II) π -bonds in the monofunctional [(η^6 -arene)Ru(II)(en)(Cl)]⁺ complexes are inert toward hydrolysis, but the chloride ligand is readily lost and the complex is transformed into the corresponding, more reactive, aquated species (Wang et al., 2003). It has also been shown that in cell-free media ethylenediamine Ru(II) arene compounds, in which arene = biphenyl (compound **9**), dihydroanthracene, tetrahydroanthracene (compound **10**), *p*-cymene (compound **11**), or benzene, bind preferentially to guanine residues in natural double-helical DNA. DNA may be a favored reaction site for these ruthenium anticancer complexes since a recent study (Wang et al., 2005) demonstrates that the presence of cytochrome *c* or L-histidine had little effect on the course of the reaction with the short DNA fragment. In addition, DNA binding of the complexes containing biphenyl, dihydroanthracene, or tetrahydroanthracene ligands can involve combined coordination to guanine N7 and non-covalent, hydrophobic interactions between the arene ligand and DNA, which may include arene intercalation and minor groove binding (Chen et al., 2002; Novakova et al., 2003). In contrast, the single hydrocarbon rings in the *p*-cymene and benzene ruthenium complexes cannot interact with double-helical DNA by intercalation (Novakova et al., 2003). Interestingly, adducts of the complex containing the *p*-cymene ligand, which has methyl and isopropyl substituents, distort the conformation and thermally destabilize double-helical DNA distinctly more than the adducts of the tricyclic-ring Ru(II) arene compounds.





The activity of two Ru(II) arene complexes containing the tetrahydroanthracene or *p*-cymene ligand was also examined in two tumor cell lines A2780 and HT29. These two complexes were chosen as representatives of two different classes of Ru(II) arene compounds for which initial studies of global modification of natural DNA revealed (Novakova et al., 2003) different binding modes: one that may involve DNA intercalation (tricyclic-ring Ru(II) complex containing the tetrahydroanthracene ligand) and the other (mono-ring Ru(II) complex containing the *p*-cymene ligand) that cannot interact with double-helical DNA by intercalation. The presence of the arene ligand in this class of ruthenium complexes capable of non-covalent, hydrophobic interaction with DNA considerably enhances the cytotoxicity in tumor cell lines (Novakova et al., 2005). An analysis of DNA duplexes modified by the mono-ring and tricyclic ring Ru(II) compounds revealed substantial differences in the impact of their monofunctional adducts on the conformation and thermodynamic stability of DNA and DNA polymerization *in vitro* (Novakova et al., 2005). In addition, the adducts of mono-ring Ru(II) compound are removed from DNA more efficiently than those of the tricyclic ring Ru(II) compound. Interestingly, the adducts of Ru(II) arene compounds are preferentially removed from DNA by mechanisms other than by nucleotide excision repair. This repair mechanism is believed to be the main process by which major cisplatin adducts are removed from DNA (Kartalou and Essigmann, 2001a) so that the latter observation provides additional support for a mechanism underlying antitumor activity of Ru(II) arene compounds different from that of cisplatin (Novakova et al., 2005). Thus, these results support the view that the different character of conformational alterations induced in DNA as a consequence of its global modification by Ru(II) arene compounds may affect differently further “downstream” effects of damaged DNA and consequently may result in different biological effects of this new class of metal-based antitumor compounds (Novakova et al., 2005).

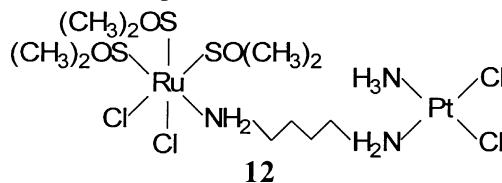
2.5. Dinuclear compounds

Polynuclear metal-based compounds represent a novel class of anticancer agents (Farrell, 2004; Brabec and Kasparkova, 2005a, 2005b). These compounds were designed to overcome limitations associated with both acquired and intrinsic resistance to the antitumor drug cisplatin, because they are capable of forming a completely

different range of DNA adducts compared to cisplatin and its analogues. Chain length and flexibility, hydrogen-bonding capacity and charge of the linker, and the geometry of the chloro-ligand to the linker chain emerge as the major factors in designing polynuclear platinum antitumor drugs (Farrell, 2004). A challenging extension of the polynuclear concept is to introduce a different metal in the coordination sites.

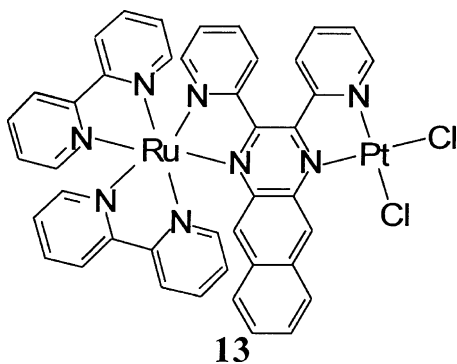
The field of anticancer polynuclear ruthenium compounds is much less explored in comparison with anticancer polynuclear platinum drugs. The biological and antitumor activity of a series of dinuclear ruthenium complexes, such as $\text{Na}_2[\{\text{Ru(III)Cl}_4(\text{DMSO-S})\}_2(\mu\text{-bipy})]$ and $\text{NH}_4[\{\text{Ru(III)Cl}_4(\text{DMSO-S})\}(\mu\text{-pyz})\{\text{Ru(III)Cl}_3(\text{DMSO-S})(\text{DMSO-O})\}]$ was examined (Bergamo et al., 2003). The two ruthenium(II) units in these dinuclear compounds are linked by heterocyclic ligands, 4,4'-bipyridine (bipy) and pyrazine (pyz), respectively. These compounds exhibit a mild cytotoxic activity against human and murine tumor cell lines and modify the cell cycle distribution of murine adenocarcinoma cells similarly as NAMI-A. The results were consistent with the view that this class of dinuclear ruthenium complexes may behave similarly as monomeric NAMI-A. In addition, *in vitro* tests demonstrated that these dinuclear ruthenium compounds are capable of forming interstrand cross-links with a considerably higher frequency than NAMI-A (Alessio et al., 2000).

In general ruthenium complexes are less reactive than platinum compounds and the combination of ruthenium and platinum units in one polynuclear molecule may be used to enhance selectivity of these polynuclear molecules to react with particular DNA sequences and to facilitate unique DNA modification. Therefore, another heteronuclear compound containing both platinum and ruthenium, $[\{\text{cis-Ru(II)((CH}_3)_2\text{SO)}_3\text{Cl}_2\}\text{NH}_2(\text{CH}_2)_4\text{NH}_2\{\text{cis-PtCl}_2(\text{NH}_3)\}]$ (compound 12) has been synthesized (van Houten et al., 1993). The ternary coordination complexes between DNA treated with the heterodinuclear compound and the *E. coli* UvrA and UvrB repair proteins have been identified. The DNA lesion responsible for efficient DNA–protein cross-linking is interstrand cross-link in which each metal atom is coordinated with one strand of the DNA double helix. The detailed structure of these ternary complexes awaits further study, but the formation of DNA repair protein associated DNA cross-links suggests a novel action mechanism for these anticancer compounds.



Complexes of the general form $[(\text{bpy})_2\text{M}(\text{dpb})\text{PtCl}_2]\text{Cl}_2$ [where M = Ru(II) (compound 13) or Os(II), (dpb = 2,3-bis(2-pyridyl) benzoquinoxaline)] have been designed (Milkevitch et al., 1997a, 1997b) to form the basis of a new type of structural motif for metal-based complexes which bind to DNA.

These systems are of interest because they couple a light-absorbing ruthenium or osmium site to a reactive platinum site. The platinum site contains the *cis*-dichloroplatinum(II) moiety thought to be responsible for the anticancer activity of cisplatin. The bridging ligand used, dpb, has an extended π system. Complexes of similar structures containing polyazine ligands with extended π systems have been shown to undergo binding to DNA, often in an intercalative fashion. The design of these complexes was to couple a light absorber to a *cis*-dichloroplatinum(II) moiety using a ligand, which is capable of intercalative binding to DNA. This provided a system with two potential modes of binding to DNA, intercalative and covalent. The results indicate that $[(bpy)_2M(dp b)PtCl_2]Cl_2$ complexes, like cisplatin, form primarily intrastrand cross-links. Interestingly, interstrand cross-links were also formed and even at a higher frequency compared to interstrand cross-linking efficiency of cisplatin. These studies showed that probing the detailed nature of the interaction of these mixed-metal complexes with DNA is of interest since they form the basis of a new class of metal-based systems that interact with DNA in a manner that is similar to but not the same as that of cisplatin. The higher water solubility of these complexes also makes them attractive as potential chemotherapeutic agents. These mixed-metal systems are modular in their design, which allows for synthetic modification of individual parts of the molecule to probe the change in DNA binding characteristics as a function of particular components.



Moreover, in order to continue in achieving selective specificity and reactivity at each metal center, the highly flexible heterodinuclear ruthenium(II)–platinum(II) complex $[(terpy)Ru(II)(dtdeg)PtCl]Cl_3$ (dtdeg = bis[terpy-terpyridyl]-diethyleneglycol ether) was designed and synthesized (van der Schilden et al., 2004). A long and flexible bridging terpyridine ligand (dtdeg) has been used to link the two metal moieties. The design and subsequent development of the dinuclear complex have been inspired by the cytotoxic mononuclear platinum complex $[Pt(terpy)Cl]Cl \cdot 2H_2O$, which can both intercalate and coordinate to DNA. Moreover, substitution-inert ruthenium polypyridyl complexes are known to be able to bind to DNA in a non-covalent mode, such as electrostatic or surface binding, or partial intercalation. It is thought that the ruthenium moiety of $[(terpy)Ru(II)(dtdeg)PtCl]Cl_3$ increases the DNA affin-

ity by its 2+ charge, thereby directing the complex to its target. Subsequently, both metal moieties can exert the DNA-binding features of their parental mononuclear complexes. The results suggest that the platinum moiety is able to both intercalate and coordinate to the DNA without being hindered by the ruthenium unit, which simultaneously allows for additional electrostatic binding to the DNA. Despite the relatively low cytotoxicity of the presented complex, it is a unique example of a new series of potentially antitumor-active complexes of which variation of the terminal terpy ligand of the ruthenium unit offers great possibilities to improve non-covalent DNA-binding modes as well as DNA coordination abilities. In view of the relatively long intramolecular ruthenium–platinum separation of 1.45 nm found for $[(terpy)Ru(II)(dtdeg)PtCl]Cl_3$, this approach can lead to compounds capable of forming delocalized long-range DNA adducts so that this new series of heterodinuclear ruthenium–platinum complexes could exhibit unique antitumor effects.

2.6. Miscellaneous compounds

A new potential antitumor soluble drug, $K[Ru(III)(eddp)Cl_2] \cdot 3H_2O$, (eddp = ethylenediamine-*N,N'*-di-3-propionate) has been synthesized and characterized (Grguric-Sipka et al., 2003). The analysis of the interaction of this complex with plasmid DNA by CD spectroscopy shows that the ruthenium complex initially induces alteration of both CD positive and negative features resembling those previously observed for monofunctional platinum complexes. In addition, the DNA binding data suggest that the plasmid is cleaved by $K[Ru(III)(eddp)Cl_2]$ in the presence of physiological concentrations of ascorbate. These results support the hypothesis that reactive Ru(II) species may be formed from Ru(III) upon incubation with a reductant agent such as ascorbate. This complex showed a remarkable and selective, antiproliferative effect against the cervix carcinoma HeLa and colon adenocarcinoma HT-29 cell lines whereas it showed no substantial antiproliferative effects in human breast carcinoma BT-20 and malign melanoma ADLD (Grguric-Sipka et al., 2003).

Two ruthenium(III) complexes bearing the thiazole ligand, namely, thiazolium (bisthiazole)tetrachlororuthenate and thiazolium (thiazole, DMSO) tetrachlororuthenate were prepared and characterized (Mura et al., 2004). The structures of both complexes were found to match closely those of the corresponding imidazole complexes. The replacement of imidazole with thiazole, a less basic ligand, produces a significant decrease of the ligand exchange rates in the case of the NAMI-like compound. Notably, both complexes exhibit higher reactivity toward serum albumin than toward calf thymus DNA. The cytotoxicity *in vitro* of both complexes was evaluated against the human tumor cell line A2780 (ovarian carcinoma). Both complexes at the concentration so high as 50 μM did not significantly inhibit tumor cell growth (Mura et al., 2004) (for instance the concentration of cisplatin that afforded 50% killing of A2780 cells is more than by one order

of magnitude lower; Kasparkova et al., 2003). Hence, the low rate of the reaction of these ruthenium complexes with DNA correlates with their low toxicity in tumor cell lines.

3. Conclusions and future directions

Several ruthenium compounds are transported into cells relatively easily and bind to cellular DNA. While the initial DNA binding site of several ruthenium complexes is the same as that of conventional cisplatin and its analogues, their DNA binding mode is different. The major adduct formed on DNA by cisplatin is the intrastrand cross-link formed between two neighboring purine residues. This cross-link, which is a likely candidate for the lesion responsible for antitumor effects of cisplatin, distorts conformation of DNA (Gelasco and Lippard, 1999; Jamieson and Lippard, 1999); it induces a roll between the platinated purine residues, displacement of the platinum atom from the planes of the purine rings, a directional and rigid bend of the helix axis toward the major groove and a local unwinding. Severe perturbation of hydrogen-bonding within the 5'-coordinated G·C base pair, widening and flattening of the minor groove opposite the adduct, creation of a hydrophobic notch, global distortion extending over 4–5 base pairs and additional helical parameters characteristic of the A-form of DNA have been also reported. In addition, antitumor activity of cisplatin is mediated by the recognition of its DNA adducts by cellular proteins, such as repair enzymes, transcription factors, histones and HMG-domain proteins (HMG=high mobility group) and mechanisms have been proposed to explain how they mediate antitumor effects of cisplatin (Zamble and Lippard, 1999; Kartalou and Essigmann, 2001b; Brabec, 2002; Torigoe et al., 2005). Referring to foregoing parts of this article a number of cytotoxic ruthenium complexes induce different conformational distortions in DNA from those induced by cisplatin and its analogues. In addition, several studies (*vide supra*) have demonstrated that the ruthenium compounds discussed in this article are cytotoxic in tumor cell lines exhibiting inherent or acquired resistance to cisplatin. Thus, the results resumed in this article suggest that the DNA binding mode of ruthenium compounds (which is different from that of cisplatin) may correlate with their anticancer effects different from those of cisplatin and that this correlation may explain at least in part the toxic effects of some ruthenium compounds in the cancer cells resistant to cisplatin.

This review has provided support for the concept (Vrana et al., 1986; Farrell et al., 1992) that transition-metal-based drugs which bind to DNA in a fundamentally different manner to that of “classical” platinum complexes like cisplatin may have altered pharmacological properties. The chemistry of ruthenium is well developed and provides a platform for many approaches to innovative new metallopharmaceuticals. Although we present in this article several examples of the correlation between DNA binding mode of ruthenium complexes and their cytotoxic effects in tumor cells, it is necessary

to bear in mind that the antitumor effects of metallodrugs, such as ruthenium complexes, represent very complex processes. These processes involve many events triggered by DNA modifications (such as for instance DNA damage recognition by specific proteins and enzymes, repair of DNA damage, various signaling processes, apoptosis, necrosis). All these “downstream” processes have to be still examined in detail to understand the mechanism of antitumor activity of ruthenium drugs to the extent that this knowledge becomes usable for design of new metallodrugs representing a breakthrough in anticancer drug design. In addition, the mechanism underlying antitumor activity of ruthenium compounds may involve factors not operating directly at the level of the DNA adducts, such as those affecting the amount of ruthenium complex that can reach DNA (by influencing either the cell accumulation of the complexes or the levels of intracellular rutheniophiles that act as detoxification agents) or affecting a target different from DNA (Bergamo et al., 2000). In any case, new concepts for the design of new antitumor ruthenium drugs (also emerging from the studies of the mechanism underlying their antitumor effects including those at the level of DNA damage) may only lead to new clinically useful compounds if their full clinical testing is carried out.

Acknowledgements

This work was supported by grants from the Grant Agency of the CR (305/05/2030 and 203/06/1239), the Academy of Sciences of the CR (1QS500040581), and Ministry of Education of the CR (MSMT LC06030). It is a pleasure to thank all our collaborators, especially Bernhard Keppler, Enzo Alessio, and Peter J. Sadler for their expertise and for providing us with the new ruthenium complexes discussed in this review. The authors also acknowledge that this work was also carried out within the Institutional Research Plan AVOZ50040507 “Biophysics of dynamic structures and functions of biological systems” and that their participation in the EC/NSF COST Chemistry Action D20 enabled them to exchange regularly the most recent ideas in the field of ruthenium anticancer drugs with several European colleagues. The reference list provided is not exhaustive; preference has been given to the most recent research papers and reviews in order to enable the reader to trace earlier contributions.

References

- Aird, R., Cummings, J., Ritchie, A., Muir, M., Morris, R., Chen, H., Sadler, P., Jodrell, D., 2002. In vitro and in vivo activity and cross resistance profiles of novel ruthenium (II) organometallic arene complexes in human ovarian cancer. *Br. J. Cancer* 86, 1652–1657.
- Alessio, E., Iengo, E., Zorzet, S., Bergamo, A., Coluccia, M., Boccarelli, A., et al., 2000. Antimetastatic properties and DNA interactions of the novel class of dimeric Ru(III) compounds $\text{Na}_2[\{\text{trans-RuCl}_4(\text{Me}_2\text{SO})\}_2(\mu\text{-L})]$ (L = ditopic, non-chelating aro-

- matic N-ligand). A preliminary investigation. *J. Inorg. Biochem.* 79, 173–177.
- Alessio, E., Mestroni, G., Bergamo, A., Sava, G., 2004a. Ruthenium anticancer drugs. In: Sigel, A., Sigel, H. (Eds.), *Metal Ions in Biological Systems. Metal Complexes in Tumor Diagnosis and as Anticancer Agents*, vol. 42. Marcel Dekker, New York, pp. 323–351.
- Alessio, E., Mestroni, G., Bergamo, A., Sava, G., 2004b. Ruthenium antimetastatic agents. *Curr. Top. Med. Chem.* 4, 1525–1535.
- Allardice, C.S., Dyson, P.J., 2001. Ruthenium in medicine: current clinical uses and future prospects. *Platinum Met. Rev.* 45, 62–69.
- Anagnostopoulou, A., Moldrheim, E., Katsaros, N., Sletten, E., 1999. Interaction of *cis*- and *trans*-RuCl₂(DMSO)₄ with the nucleotides GpA, d(GpA), ApG, d(ApG) and d(CCTGGTCC): high-field NMR characterization of the reaction products. *J. Biol. Inorg. Chem.* 4, 199–208.
- Barton, J.K., 1986. Metals and DNA: molecular left-handed complements. *Science* 233, 727–734.
- Barton, J.K., Lolis, E., 1985. Chiral discrimination in the covalent binding of bis(phenanthroline)dichlororuthenium(II) to B-DNA. *J. Am. Chem. Soc.* 107, 708–709.
- Bergamo, A., Stocco, G., Gava, B., Cocchietto, M., Alessio, E., Serli, B., et al., 2003. Distinct effects of dinuclear ruthenium(III) complexes on cell proliferation and on cell cycle regulation in human and murine tumor cell lines. *J. Pharmacol. Exp. Ther.* 305, 725–732.
- Bergamo, A., Zorzet, S., Gava, B., Sorc, A., Alessio, E., Iengo, E., Sava, G., 2000. Effects of NAMI-A and some related ruthenium complexes on cell viability after short exposure of tumor cells. *Anti-cancer Drugs* 11, 665–672.
- Berger, M.R., Garzon, F.T., Keppler, B.K., Schmahl, D., 1989. Efficacy of new ruthenium complexes against chemically-induced autochthonous colorectal-carcinoma in rats. *Anticancer Res.* 9, 761–765.
- Brabec, V., 2002. DNA modifications by antitumor platinum and ruthenium compounds: their recognition and repair. *Prog. Nucleic Acid Res. Mol. Biol.* 71, 1–68.
- Brabec, V., Kasparkova, J., 2005a. DNA interactions of platinum anticancer drugs. Recent advances and mechanisms of action. In: Perez-Martin, J.-M., Fuertes, M.A., Alonso, C. (Eds.), *Metal Compounds in Cancer Chemotherapy*. Research Signpost, Trivandrum, Kerala, India, pp. 187–218.
- Brabec, V., Kasparkova, J., 2005b. Modifications of DNA by platinum complexes: relation to resistance of tumors to platinum antitumor drugs. *Drug Resist. Update* 8, 131–146.
- Brindell, M., Kulis, E., Elmroth, S.K.C., Urbanska, K., Stochel, G., 2005. Light-induced anticancer activity of [RuCl₂(DMSO)₄] complexes. *J. Med. Chem.* 48, 7298–7304.
- Chen, H.M., Parkinson, J.A., Parsons, S., Coxall, R.A., Gould, R.O., Sadler, P.J., 2002. Organometallic ruthenium(II) diamine anticancer complexes: arene-nucleobase stacking and stereospecific hydrogen-bonding in guanine adducts. *J. Am. Chem. Soc.* 124, 3064–3082.
- Cheng, C.C., Lee, W.L., Su, J.G., Liu, C.L., 2000. Covalent interaction of Ru(terpy)(tphen)Cl⁺ with DNA: a potential ruthenium-based anticancer drug. *J. Chin. Chem. Soc.* 47, 213–220.
- Clarke, M.J., 2003. Ruthenium metallopharmaceuticals. *Coord. Chem. Rev.* 236, 209–233.
- Clarke, M.J., Zhu, F., Frasca, D.R., 1999. Non-platinum chemotherapeutic metallopharmaceuticals. *Chem. Rev.* 99, 2511–2533.
- Cohen, S.M., Lippard, S.J., 2001. Cisplatin: from DNA damage to cancer chemotherapy. *Prog. Nucleic Acid Res. Mol. Biol.* 67, 93–130.
- Coluccia, M., Sava, G., Loseto, F., Nassi, A., Boccarelli, A., Giordano, D., Alessio, E., Mestroni, G., 1993. Antileukemic action of RuCl₂(DMSO)₄ isomers and prevention of brain involvement on P388 leukemia and on P388/DDP subline. *Eur. J. Cancer* 29A, 1873–1879.
- Farrell, N., 1996. Current status of structure-activity relationships of platinum anticancer drugs: activation of the *trans* geometry. In: Sigel, A., Sigel, H. (Eds.), *Metal Ions in Biological Systems*, vol. 32. Marcel Dekker, Inc., New York, pp. 603–639.
- Farrell, N., 2004. Polynuclear platinum drugs. In: Sigel, A., Sigel, H. (Eds.), *Metal Ions in Biological Systems*, vol. 42. Marcel Dekker, Inc., New York, Basel, pp. 251–296.
- Farrell, N., Kelland, L.R., Roberts, J.D., Van Beusichem, M., 1992. Activation of the *trans* geometry in platinum antitumor complexes: a survey of the cytotoxicity of *trans* complexes containing planar ligands in murine-L1210 and human tumor panels and studies on their mechanism of action. *Cancer Res.* 52, 5065–5072.
- Frasca, D., Ciampa, J., Emerson, J., Umans, R.S., Clarke, M., 1996. J. Met.-based Drugs 3, 197–209.
- Frasca, D.R., Gehrig, L.E., Clarke, M.J., 2001. Cellular effects of transferin coordinated to Cl(NH₃)₅RuCl₂ and *cis*-Cl₂(NH₃)₄RuCl. *J. Inorg. Biochem.* 83, 139–149.
- Fruhauf, S., Zeller, W.J., 1991. New platinum, titanium, and ruthenium complexes with different patterns of DNA damage in rat ovarian tumour cells. *Cancer Res.* 51, 2943–2948.
- Galanski, M., Arion, V.B., Jakupec, M.A., Keppler, B.K., 2003. Recent developments in the field of tumor-inhibiting metal complexes. *Curr. Pharm. Des.* 9, 2078–2089.
- Galeano, A., Berger, M.R., Keppler, B.K., 1992. Antitumor activity of some ruthenium derivatives in human colon cancer cell lines in vitro. *Arzneimittel—Forschung/Drug Research* 42, 821–824.
- Gallori, E., Vettori, C., Alessio, E., Vilchez, F.G., Vilaplana, R., Orioli, P., Casini, A., Messori, L., 2000. DNA as a possible target for antitumor ruthenium(III) complexes—a spectroscopic and molecular biology study of the interactions of two representative antineoplastic ruthenium(III) complexes with DNA. *Arch. Biochem. Biophys.* 376, 156–162.
- Gelasco, A., Lippard, S.J., 1999. Anticancer activity of cisplatin and related complexes. In: Clarke, M.J., Sadler, P.J. (Eds.), *Metallopharmaceuticals I. DNA Interactions*. Springer, Berlin, pp. 1–43.
- Giaccone, G., 2000. Clinical perspectives on platinum resistance. *Drugs* 59, 9–17.
- Gopal, Y.N.V., Jayaraju, D., Kondapi, A.K., 1999. Inhibition of topoisomerase II catalytic activity by two ruthenium compounds: a ligand-dependent mode of action. *Biochemistry* 38, 4382–4388.
- Gopal, Y.N.V., Kondapi, A.K., 2001. Topoisomerase II poisoning by indazole and imidazole complexes of ruthenium. *J. Biosci.* 26, 271–276.
- Gopal, Y.N.V., Konuru, N., Kondapi, A.K., 2002. Topoisomerase II antagonism and anticancer activity of coordinated derivatives of [RuCl₂(C₆H₆)(DmsO)]. *Arch. Biochem. Biophys.* 401, 53–62.
- Grguric-Sipka, S., Vilaplana, R., Perez, J., Fuertes, M., Alonso, C., Alvarez, Y., Sabo, T., Gonzalez-Vilchez, F., 2003. Synthesis, characterization, interaction with DNA and cytotoxicity of the new potential antitumour drug *cis*-K[Ru(eddp)Cl₂]. *J. Inorg. Biochem.* 97, 215–220.
- Grover, N., Welch, T.W., Fairley, T.A., Cory, M., Thorp, H.H., 1994. Covalent binding of aquaruthenium complexes to DNA. *Inorg. Chem.* 33, 3544–3548.
- Ho, Y.P., AuYeung, S.C.F., To, K.K.W., 2003. Platinum-based anticancer agents: innovative design strategies and biological perspectives. *Med. Res. Rev.* 23, 633–655.
- Hotze, A.C.G., van der Geer, E.P.L., Kooijman, H., Spek, A.L., Haasnoot, J.G., Reedijk, J., 2005. Characterization by NMR spectroscopy, X-ray analysis and cytotoxic activity of the ruthenium(II) compounds [RuL₃](PF₆)₂ (L = 2-phenylazopyridine or *o*-tolylazopyridine) and [RuL'₂L'']₂(PF₆)₂ (L' = 2-phenylazopyridine, 2,2'-bipyridine). *Eur. J. Inorg. Chem.*, 2648–2657.
- Jamieson, E.R., Lippard, S.J., 1999. Structure, recognition, and processing of cisplatin–DNA adducts. *Chem. Rev.* 99, 2467–2498.
- Johnson, N.P., Butour, J.-L., Villani, G., Wimmer, F.L., Defais, M., Pearson, V., Brabec, V., 1989. Metal antitumor compounds: the mechanism of action of platinum complexes. *Prog. Clin. Biochem. Med.* 10, 1–24.
- Kapitza, S., Jakupec, M.A., Uhl, M., Keppler, B.K., Marian, B., 2005a. The heterocyclic ruthenium(III) complex KP1019 (FFC14A) causes DNA damage and oxidative stress in colorectal tumor cells. *Cancer Lett.* 226, 115–121.

- Kapitzka, S., Pongratz, M., Jakupec, M.A., Heffeter, P., Berger, W., Lackinger, L., et al., 2005b. Heterocyclic complexes of ruthenium(III) induce apoptosis in colorectal carcinoma cells. *J. Cancer Res. Clin. Oncol.* 131, 101–110.
- Kartalou, M., Essigmann, J.M., 2001a. Mechanisms of resistance to cisplatin. *Mutat. Res.* 478, 23–43.
- Kartalou, M., Essigmann, J.M., 2001b. Recognition of cisplatin adducts by cellular proteins. *Mutat. Res.* 478, 1–21.
- Kasparkova, J., Marini, V., Najajreh, Y., Gibson, D., Brabec, V., 2003. DNA binding mode of the cis and trans geometries of new antitumor nonclassical platinum complexes containing piperidine, piperazine or 4-picoline ligand in cell-free media. Relations to their activity in cancer cell lines. *Biochemistry* 42, 6321–6332.
- Keppler, B.K., 1993. Metal Complexes in Cancer Chemotherapy. VCH Verlagsgesellschaft, VCH Publishers, Weinheim.
- Keppler, B.K., Lipponer, K.-G., Stenzel, B., Kratz, F., 1993. New tumor-inhibiting ruthenium complexes. In: Keppler, B. (Ed.), *Metal Complexes in Cancer Chemotherapy*. VCH Verlagsgesellschaft, VCH Publishers, Weinheim, pp. 187–220.
- Kratz, F., Hartmann, M., Keppler, B., Messori, L., 1994. The binding properties of two antitumor ruthenium(III) complexes to apotransferrin. *J. Biol. Chem.* 269, 2581–2588.
- Loseto, F., Alessio, E., Mestroni, G., Lacidogna, G., Nassi, A., Giordano, D., et al., 1991. Interaction of $\text{RuCl}_2(\text{dimethylsulphoxide})_4$ isomers with DNA. *Anticancer Res.* 11, 1549–1553.
- Malina, J., Novakova, O., Keppler, B.K., Alessio, E., Brabec, V., 2001. Biophysical analysis of natural, double-helical DNA modified by anticancer heterocyclic complexes of ruthenium(III) in cell-free media. *J. Biol. Inorg. Chem.* 6, 435–445.
- Mestroni, G., Alessio, E., Calligaris, M., Attia, W.M., Quadrioglio, F., Cauci, S., Sava, G., Zorzet, S., Pacor, S., Monti-Bragadin, C., Tamaro, M., Dolzani, L., 1989. Chemical, biological and antitumor properties of ruthenium(II) complexes with dimethylsulfoxide. *Prog. Clin. Biochem. Med.* 10, 71–87.
- Milkevitch, M., Shirley, B.W., Brewer, K.J., 1997a. Mixed-metal poly-metallic platinum complexes designed to interact with DNA. *Inorg. Chim. Acta* 264, 249–256.
- Milkevitch, M., Storrie, H., Brauns, E., Brewer, K.J., Shirley, B.W., 1997b. A new class of supramolecular, mixed-metal DNA-binding agents: The interaction of Ru-II/Pt-II and Os-II/Pt-II bimetallic complexes with DNA. *Inorg. Chem.* 36, 4534–4538.
- Morris, R.E., Aird, R.E., Murdoch, P.D., Chen, H.M., Cummings, J., Hughes, N.D., Parsons, S., Parkin, A., Boyd, G., Jodrell, D.I., Sadler, P.J., 2001. Inhibition of cancer cell growth by ruthenium(II) arene complexes. *J. Med. Chem.* 44, 3616–3621.
- Mura, P., Camalli, M., Messori, L., Piccoli, F., Zanello, P., Corsini, M., 2004. Synthesis, structural characterization, solution chemistry, and preliminary biological studies of the ruthenium(III) complexes $\text{TzH trans-RuCl}_4(\text{Tz})_2$ and $\text{TzH trans-RuCl}_4(\text{DMSO})(\text{Tz})$. (DMSO), the thiazole analogues of antitumor ICR and NAMI-A. *Inorg. Chem.* 43, 3863–3870.
- Natile, G., Coluccia, M., 2004. Antitumor active *trans*-platinum compounds. In: Sigel, A., Sigel, H. (Eds.), *Metal Ions in Biological Systems*, vol. 42. Marcel Dekker, Inc., New York, pp. 209–250.
- Neyhart, G.A., Cheng, C.C., Thorp, H.H., 1995. Kinetics and mechanism of the oxidation of sugars and nucleotides by oxoruthenium(IV): model studies for predicting cleavage patterns in polymeric DNA and RNA. *J. Am. Chem. Soc.* 117, 1463–1471.
- Novakova, O., Hofr, C., Brabec, V., 2000. Modification of natural, double-helical DNA by antitumor *cis*- and *trans*- $[\text{Cl}_2(\text{Me}_2\text{SO})_4\text{Ru}]$ in cell-free media. *Biochem. Pharmacol.* 60, 1761–1771.
- Novakova, O., Chen, H., Vrana, O., Rodger, A., Sadler, P.J., Brabec, V., 2003. DNA interactions of monofunctional organometallic ruthenium(II) antitumor complexes in cell-free media. *Biochemistry* 42, 11544–11554.
- Novakova, O., Kasparkova, J., Bursova, V., Hofr, C., Vojtiskova, M., Chen, H., Sadler, P.J., Brabec, V., 2005. Conformation of DNA modified by monofunctional Ru(II) arene complexes: recognition by DNA-binding proteins and repair. Relationship to cytotoxicity. *Chem. Biol.* 12, 121–129.
- Novakova, O., Kasparkova, J., Vrana, O., van Vliet, P.M., Reedijk, J., Brabec, V., 1995. Correlation between cytotoxicity and DNA binding of polypyridyl ruthenium complexes. *Biochemistry* 34, 12369–12378.
- Perez, J.-M., Fuertes, M.A., Alonso, C., Navarro-Ranninger, C., 2000. Current status of the development of *trans*-platinum antitumor drugs. *Crit. Rev. Oncol. Hematol.* 35, 109–120.
- Pluim, D., van Waardenburg, R.C.A.M., Beijnen, J.H., Schellens, J.H.M., 2004. Cytotoxicity of the organic ruthenium anticancer drug NAMI-A is correlated with DNA binding in four different human tumor cell lines. *Cancer Chemother. Pharmacol.* 54, 71–78.
- Pongratz, M., Schluga, P., Jakupec, M.A., Arion, V.B., Hartinger, C.G., Allmaier, G., et al., 2004. Transferrin binding and transferrin-mediated cellular uptake of the ruthenium coordination compound KP1019, studied by means of AAS, ESI-MS and CD spectroscopy 19. *J. Anal. Atom. Spectrom.* 19, 46–51.
- Rademaker-Lakhai, J.M., van den Bongard, D., Pluim, D., Beijnen, J.H., Schellens, J.H.M., 2004. A phase I and pharmacological study with imidazolium-*trans*-DMSO-imidazole-tetrachlororuthenate, a novel ruthenium anticancer agent. *Clin. Cancer Res.* 10, 3717–3727.
- Rosenberg, B., Van Camp, L., Krigas, T., 1965. Inhibition of division in *Escherichia coli* by electrolysis products from a platinum electrode. *Nature* 205, 698–699.
- Rosenberg, B., Van Camp, L., Trosko, J.E., Mansour, V.H., 1969. Platinum compounds: a new class of potent antitumor agents. *Nature* 222, 385–386.
- Sava, G., Alessio, E., Bergano, A., Mestroni, G., 1999. Sulfoxide ruthenium complexes: non toxic tools for the selective treatment of solid tumour metastases. In: Clarke, M.J., Sadler, P.J. (Eds.), *Topics in Biological Inorganic Chemistry. Metallopharmaceuticals*, vol. 1. Springer, Berlin, pp. 143–169.
- Sava, G., Bergamo, A., 2000. Ruthenium-based compounds and tumour growth control. *Int. J. Oncol.* 17, 353–365.
- Sava, G., Pacor, S., Bregant, F., Ceschia, V., Mestroni, G., 1990. Metal complexes of ruthenium: antineoplastic properties and perspectives. *Anti-cancer Drugs* 1, 99–108.
- Seelig, M.H., Berger, M.R., Keppler, B.K., 1992. Antineoplastic activity of three ruthenium derivatives against chemically induced colorectal carcinoma in rats. *J. Cancer Res. Clin. Oncol.* 118, 195–200.
- Torigoe, T., Izumi, H., Ishiguchi, H., Yoshida, Y., Tanabe, M., Yoshida, T., Igarashi, T., Niina, I., Wakasugi, T., Imaizumi, T., Momii, Y., Kuwano, M., Kohno, K., 2005. Cisplatin resistance and transcription factors. *Curr. Med. Chem.-Anti-cancer Agents* 5, 15–27.
- van der Schilden, K., Garcia, F., Kooijman, H., Spek, A.L., Haasnoot, J.G., Reedijk, J., 2004. A highly flexible dinuclear ruthenium(II)–platinum(II) complex: crystal structure and binding to 9-ethylguanine. *Angew. Chem. Int. Ed.* 43, 5668–5670.
- van Houten, B., Illenye, S., Qu, Y., Farrell, N., 1993. Homodinuclear (Pt,Pt) and heterodinuclear (Ru,Pt) metal compounds as DNA–protein cross-linking agents: potential suicide DNA lesions. *Biochemistry* 32, 11794–11801.
- van Vliet, P.M., Toekimin, S.M.S., Haasnoot, J.G., Reedijk, J., Novakova, O., Vrana, O., Brabec, V., 1995. *mer*- $[\text{Ru}(\text{terpy})\text{Cl}_3]$ (*terpy* = 2,2':6',2''-terpyridine) shows biological activity, forms inter-strand cross-links in DNA and binds two guanine derivatives in a *trans* configuration. *Inorg. Chim. Acta* 231, 57–65.
- Vrana, O., Brabec, V., Kleinwächter, V., 1986. Polarographic studies on the conformation of some platinum complexes: relations to antitumour activity. *Anti-cancer Drug Des.* 1, 95–109.
- Wang, F., Bella, J., Parkinson, J.A., Sadler, P.J., 2005. Competitive reactions of a ruthenium arene anticancer complex with histidine, cytochrome *c* and an oligonucleotide. *J. Biol. Inorg. Chem.* 10, 147–155.
- Wang, F., Chen, H., Parsons, S., Oswald, I.D.H., Davidson, J.E., Sadler, P.J., 2003. Kinetics of aquation and anation of Ruthenium(II) arene

- anticancer complexes, acidity and X-ray structures of aqua adducts. *Chem. Eur. J.* 9, 5810–5820.
- Weiss, R.B., Christian, M.C., 1993. New cisplatin analogs in development. A review. *Drugs* 46, 360–377.
- Wernyj, R.P., Morin, P.J., 2004. Molecular mechanisms of platinum resistance: still searching for the Achilles' heel. *Drug Resist. Update* 7, 227–232.
- Wong, E., Giandomenico, C.M., 1999. Current status of platinum-based antitumor drugs. *Chem. Rev.* 99, 2451–2466.
- Xu, H., Liang, Y., Zhang, P., Du, F., Zhou, B.-R., Wu, J., Liu, J.-H., Liu, Z.-G., Ji, L.-N., 2005. Biophysical studies of a ruthenium(II) polypyridyl complex binding to DNA and RNA prove that nucleic acid structure has significant effects on binding behaviors. *J. Biol. Inorg. Chem.* 10, 529–538.
- Zamble, D.B., Lippard, S.J., 1999. The response of cellular proteins to cisplatin-damaged DNA. In: Lippert, B. (Ed.), *Cisplatin. Chemistry and Biochemistry of a Leading Anticancer Drug*. VHCA/Wiley-VCH, Zürich, pp. 73–110.
- Zeller, W.J., Fruhauf, S., Chen, G., Keppler, B.K., Frei, E., Kaufmann, M., 1991. Chemoresistance in rat ovarian tumours. *Eur. J. Cancer* 27, 62–67.
- Zhang, C.X., Lippard, S.J., 2003. New metal complexes as potential therapeutics. *Curr. Opin. Chem. Biol.* 7, 481–489.

16.

Conformation, protein recognition and repair of DNA interstrand and intrastrand cross-links of Antitumor *trans*-[PtCl₂(NH₃)(thiazole)]

Victoria Marini, Petros Christofis, Olga Novakova, Jana Kasparkova, Nicholas Farrell¹ and Viktor Brabec*

Institute of Biophysics, Academy of Sciences of the Czech Republic, CZ-61265 Brno, Czech Republic and ¹Department of Chemistry, Virginia Commonwealth University, Richmond, VA 23284-2006, USA

Received July 26, 2005; Revised September 2, 2005; Accepted September 20, 2005

ABSTRACT

Replacement of one ammine in clinically ineffective *trans*-[PtCl₂(NH₃)₂] (transplatin) by a planar N-heterocycle, thiazole, results in significantly enhanced cytotoxicity. Unlike 'classical' cisplatin [*cis*-[PtCl₂(NH₃)₂]] or transplatin, modification of DNA by this prototypical cytotoxic transplatinum complex *trans*-[PtCl₂(NH₃)(thiazole)] (*trans*-PtTz) leads to monofunctional and bifunctional intra or interstrand adducts in roughly equal proportions. DNA fragments containing site-specific bifunctional DNA adducts of *trans*-PtTz were prepared. The structural distortions induced in DNA by these adducts and their consequences for high-mobility group protein recognition, DNA polymerization and nucleotide excision repair were assessed in cell-free media by biochemical methods. Whereas monofunctional adducts of *trans*-PtTz behave similar to the major intrastrand adduct of cisplatin [J. Kasparkova, O. Novakova, N. Farrell and V. Brabec (2003) *Biochemistry*, 42, 792–800], bifunctional cross-links behave distinctly differently. The results suggest that the multiple DNA lesions available to *trans*-planaramine complexes may all contribute substantially to their cytotoxicity so that the overall drug cytotoxicity could be the sum of the contributions of each of these adducts. However, acquisition of drug resistance could be a relatively rare event, since it would have to entail resistance to or tolerance of multiple, structurally dissimilar DNA lesions.

INTRODUCTION

The clinical inactivity of *trans*-diamminedichloroplatinum(II) (transplatin) (Figure 1A) is a paradigm for the structure–activity relationships of platinum drugs. A structurally diverse set of transplatin analogues exhibiting different spectra of cytotoxicity, including activity in tumor cells resistant to cisplatin [*cis*-diamminedichloroplatinum(II)] (Figure 1A), have been identified by replacement of one or both NH₃ ligands (1–3). There is a large body of experimental evidence that the success of platinum complexes in killing tumor cells results from the formation of covalent adducts on DNA (4). Hence, it is reasonable to hypothesize that the reasons for the enhanced pharmacological properties and activation of bifunctional mononuclear *trans*-platinum(II) compounds is that they bind to DNA in a manner fundamentally different from that of the clinically ineffective 'parent' transplatin.

Cytotoxic *trans*-platinum(II) complexes whose DNA-binding modes have been intensively investigated include complexes of the general structure *trans*-[PtCl₂(NH₃)(L)], where L = planar amine such as pyridine, thiazole (Figure 1A) or quinoline (1). To understand the mechanism of cytotoxicity, biochemical and biophysical methods as well as molecular modeling techniques were used to study the modifications of natural, high molecular mass DNA by *trans*-[PtCl₂(NH₃)(thiazole)] (*trans*-PtTz) (Figure 1A) or *trans*-[PtCl₂(NH₃)(quinoline)] (*trans*-PtQ) (5–8). The adducts of these compounds preferentially terminate *in vitro* RNA synthesis in transcription mapping experiments at guanine residues and at similar sites as the adducts of cisplatin (5). DNA modified by these analogues is recognized by cisplatin-specific antibodies but not by transplatin-specific antibodies, suggesting that these newer analogues behave in some aspects similar to cisplatin. Importantly, the planar ligand in all or in

*To whom correspondence should be addressed. Tel: +42 5 41517148; Fax: +42 5 41240499; Email: brabec@ibp.cz
Correspondence may also be addressed to Nicholas Farrell. Tel: +1 804 828 6320; Fax: +1 804 828 8599; Email: nfarrell@mail1.vcu.edu

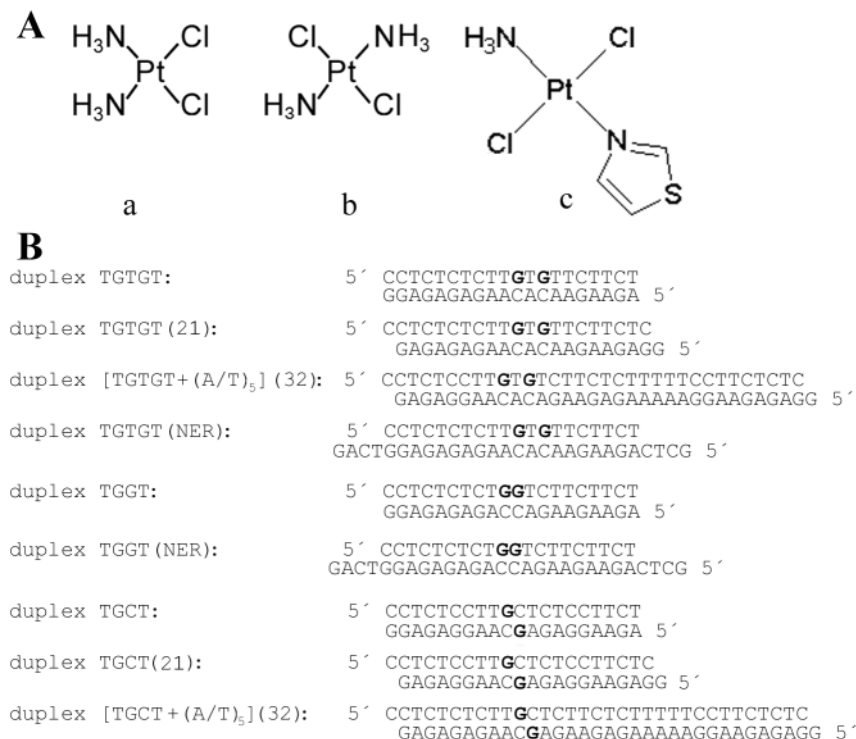


Figure 1. Structures of platinum compounds and sequences of the synthetic oligodeoxyribonucleotides with their abbreviations. (A) Structures: a, cisplatin; b, transplatin; and c, (*trans*-PtTz). (B) Sequences: the top and bottom strands of each pair in the figure are designated 'top' and 'bottom,' respectively, throughout. The boldface letters in the top and bottom strands of the duplexes indicate the platinated residues.

a significant fraction of covalent DNA adducts of these transplatin analogues is well positioned to interact with the duplex, presumably through stacking interactions.

Monofunctional DNA adducts formed by *trans*-PtTz and *trans*-PtQ are formed at a rate similar to that of transplatin (5). The rate of rearrangement to bifunctional adducts is relatively slow but similar to that observed for transplatin. In contrast to transplatin, however, the analogues with planar ligands form considerably more interstrand cross-links (CLs) (~30–40% after 48 h) with a much shorter half-time ($t_{1/2}$) ~5 h (5) [~12% interstrand CL is formed by transplatin after 48 h with $t_{1/2}$ > 11 h (9)]. Further, the interstrand CLs are formed between guanine residues at the 5'-GC/5'-GC sites—formally equivalent to cisplatin but different from transplatin, which forms these adducts between complementary guanine and cytosine residues (9). A significant fraction of the monofunctional adducts persist over time (30–40% after ~48 h) so that 20–40% of the total adducts are intrastrand, presumably mainly 1,3 CLs (5). Thus, no one specific adduct, i.e. monofunctional or bifunctional interstrand and intrastrand CLs, represents a major lesion. Formation of one or all of these adducts may be relevant to the cytotoxicity of *trans*-[PtCl₂(NH₃)(planar amine)], meriting a detailed study of their impact on DNA conformation and some 'downstream' intracellular processes, such as DNA damage recognition by specific proteins, DNA polymerization and repair, which all play a crucial role in the mechanism of antitumor activity of 'classical' cisplatin (4).

Site-specific adducts containing one defined lesion give more information on the structural details of 'global' DNA

binding. The results to date indicate that DNA conformational changes of *trans*-[PtCl₂(NH₃)(planar amine)] are relatively independent of the nature of the planar amine. To examine the consequences of specific adducts containing planar amines we have used *trans*-PtTz as a suitable representative as it is water-soluble and formally exhibits antitumor, albeit moderate, activity (1). Monofunctional DNA adducts of *trans*-PtTz, in contrast to monodentate [PtCl(dien)]Cl or [PtCl(NH₃)₃]Cl, inhibit DNA synthesis and create a local conformational distortion similar to that produced by the 1,2-GG intrastrand CL of cisplatin, which is considered the lesion most responsible for its anticancer activity (8). In addition, *trans*-PtTz monofunctional adducts are recognized by HMGB1 domain proteins and are removed by the nucleotide excision repair (NER) system similar to the 1,2-GG intrastrand CL of cisplatin.

This paper describes the analysis of short duplexes containing the single, site-specific interstrand and 1,3-intrastrand CLs of *trans*-PtTz to obtain a more complete picture on the DNA modifications produced by this compound. The conformational changes, subsequent consequences with respect to protein recognition, DNA polymerization and repair compared to cis and transplatin are highly dependent on the nature of the adduct. The interstrand CL of *trans*-PtTz affects DNA conformation and its recognition by high mobility group (HMG) domain proteins differently from the interstrand CLs formed by the parent transplatin, but similarly, although in a lesser extent, as the interstrand CL of cisplatin. In addition, the results indicate that in contrast to transplatin, *trans*-PtTz forms long-lived 1,3-intrastrand CLs that distort DNA conformation in double-helical DNA, but are weakly repaired.

MATERIALS AND METHODS

Chemicals

trans-PtTz was prepared according to the previously published methods (10). Cisplatin and transplatin were obtained from Sigma. The stock solutions of platinum compounds were prepared at the concentration of 5×10^{-4} M in 10 mM NaClO₄ and stored at 4°C in the dark. The synthetic oligodeoxyribonucleotides (Figures 1B, 5C and 6) were purchased from VBC-Genomics (Vienna, Austria) and were purified as described previously (11). Restriction endonucleases, Klenow fragment of *Escherichia coli* DNA polymerase I deficient in 3'→5' proofreading exonuclease activity (KF⁻), and T4 polynucleotide kinase were purchased from New England Biolabs (Beverly, MA). Reverse transcriptase of human immunodeficiency virus type 1 (RT HIV-1) was from Amersham Pharmacia Biotech, Nonidet N P-30 was from Fluka (Prague, Czech Republic). Acrylamide, bis(acrylamide), urea and NaCN were from Merck. Radioactive products were from Amersham Biosciences. ATP was from Roche Applied Science.

Platination of oligonucleotides

The duplexes containing single, intrastrand CL of cisplatin, transplatin or *trans*-PtTz in the top strand [the duplexes in Figure 1B that contained two guanine (G) residues in the top strand] were prepared as described previously (8,12,13). The interstrand cross-linked duplexes were also prepared as described previously (7,9,14).

Gel-mobility shift assay

The 5' end labeled 20 bp oligonucleotide duplexes with blunt ends containing the central sequences in the top strands TGCT, TGTGT and TGGT (these duplexes were identical to TGCT, TGTGT and TGGT duplexes shown in Figure 1B except that overhanging nucleotides at 3' ends were paired with their complementary nucleotides) either unplatinated (controls) or containing the central platinum CL were used and their reaction with HMG-domain proteins was performed and analyzed as described previously (15). The electrophoresis was performed for 50 min at 4°C, gels were dried and visualized by using the FUJIFILM bio-imaging analyzer and the radioactivities associated with bands were quantified with the AIDA image analyzer software. Competition experiments performed to determine apparent dissociation constants, $K_{D(app)}$, were performed as described previously (15). $K_{D(app)}$ values were estimated in the manner described in Ref. (15). Each $K_{D(app)}$ is the average of at least two measurements.

Nucleotide excision assay

The 148 bp substrates containing single, central intrastrand or interstrand CL were assembled from three oligonucleotide duplexes as described previously (16,17). Oligonucleotide excision reactions were performed in cell-free extracts (CFEs) prepared from the HeLa S3 and CHO AA8 cell lines as described previously (18). These extracts were kindly provided by J. T. Reardon and A. Sancar (University of North Carolina, Chapel Hill, NC). *In vitro* repair was measured with excision assay using these CFEs and 148 bp linear DNA substrates (see above) as described previously (18).

Inhibition of DNA polymerization

The 30mer or 23mer templates (Figure 5) containing a single 1,3-GTG intrastrand CL of *trans*-PtTz or 1,2-GG intrastrand CL of cisplatin were prepared in the same way as described above. The 17mer or 8mer DNA primers (the sequence of the 17mer primer is shown in Figure 6) were complementary to the 3' termini of the 23mer or 30mer templates, respectively. The DNA substrates (1.5×10^{-7} M) were formed by annealing templates and 5' end-labeled primers at a molar ratio of 3:1. All experiments using RT HIV-1 were performed at 37°C in a volume of 50 µl in a buffer containing 50 mM Tris-HCl (pH 8.0), 10 mM MgCl₂, 50 mM KCl, 3 mM DTT, 0.1% Nonidet N P-30, 100 µM dATP, 100 µM dCTP, 100 µM dGTP, and 100 µM TTP and 1.0 U of RT HIV-1. The experiments with KF⁻ were performed at 25°C using the same volume, 50 mM Tris-HCl (pH 7.4), 10 mM MgCl₂, 0.1 mM DTT, 50 µM BSA/ml; the nucleoside triphosphates were at a concentration of 25 µM and 0.5 U of KF⁻ was used. Reactions were terminated by the addition of EDTA, so that its resulting concentration was 20 mM, and heating at 100°C for 30 s. Products were resolved by denaturing 24% polyacrylamide (PAA)/8 M urea gel and then visualized and quantified by using the FUJIFILM bioimaging analyzer and AIDA image analyzer software. Other details were published previously (19,20).

RESULTS

Structural consequences of interstrand cross-linking

Unwinding and bending. The structural details responsible for bending and unwinding of cisplatin and transplatin-DNA interstrand adducts have been elucidated recently (21). Therefore, it was of interest to compare the bending and unwinding induced by a single, site-specific interstrand CL of *trans*-PtTz. Multimers of the oligonucleotide platinated at a single site may show strong anomalies in their electrophoretic mobilities as a consequence of coherent addition in-phase platinum-induced bends. The maximum anomalies are observed if the match between the sequence repeat and the helix screw is optimized (22). In addition, if the interplatinum distance in these multimers is systematically varied in polymers containing the adduct, the multimer that migrates most slowly gives the optimal phasing for cooperative bending, from which the degree of unwinding can be determined (23). Thus, electrophoretic migration of the multimers formed from the series of oligonucleotide duplexes of different lengths, which contain a single, site-specific platinum adduct can be evaluated in terms of a quantitative measure of the extent of planar curvature and unwinding (13,24–26).

Oligodeoxyribonucleotide duplexes TGCT (20–23) (20–23 bp long) were used for these studies. The sequences were identical or similar to that of the duplex TGCT (21) shown in Figure 1B; the sequence of the duplex TGCT (20) had one marginal C-G base pair deleted, whereas one or two additional TA base pairs were added to one or two ends in the duplexes TGCT (22) or TGCT (23), respectively. The ligation products of the unplatinated or CL-containing duplexes were analyzed on native PAA electrophoresis gels (Figure 2A). The DNA unwinding of the *trans*-PtTz interstrand adduct was

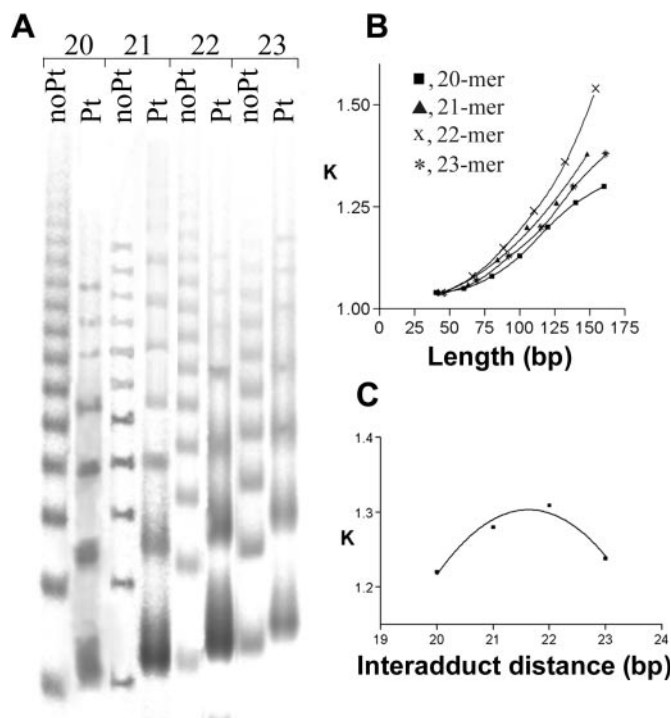


Figure 2. DNA bending. The mobility of the ligation products of 20–23 bp duplexes containing single, site-specific interstrand CL of *trans*-PtTz formed between guanine residues in the central sequence 5'-TGCT/5'-AGCA in an 8% PAA gel. (A) Phosphorimage of the ligation products. Lanes: NoPt, unplatinated duplexes; Pt, duplexes containing the CL. The sequence of the 21 bp duplex TGCT (21) is shown in the Figure 1B. The sequences of the 20mer, 22mer and 23mer duplexes are described in the text. (B) Plots showing the relative mobility K versus sequence length curves for the oligomers 20–23 bp long containing the CL. (C) Plot showing the relative mobility K versus interadduct distance in bp for the oligomers 20–23 bp long containing the CL with a total length of 126 bp. The experimental points represent the average of three independent electrophoresis experiments. The curves represent the best fit of these experimental points to the equation $K = ad^2 + bd + c$ (23).

found to be $20 \pm 2^\circ$, considerably higher than that induced by the interstrand CL of transplatin [12° ; (12)], but lower than that induced by the interstrand CL of cisplatin (76 – 80°). Moreover, the interstrand CL bends DNA by $\sim 22 \pm 2^\circ$ toward the minor groove [the direction of the bend was determined using the duplex [TGCT(A/T)₅] (32) (Figure 1B) (27)]. Thus, the bending is similar to those afforded by the interstrand CL of cisplatin or transplatin using the same experimental procedure [20 – 40° or 20° , respectively (21)]. Interestingly, in contrast to the cisplatin or transplatin interstrand CLs, the ligation of duplexes with *trans*-PtTz interstrand CLs did not result in the formation of circles, suggesting that the flexibility of the double helix is not increased (12,28).

Chemical probes of DNA conformation. The duplex TGCT (21) (Figure 1B) containing a single, site-specific interstrand CL of *trans*-PtTz was treated with several reagents that act as chemical probes for the existence of conformations other than canonical B-DNA (Figure S1 in Supplementary Data), as described previously (12). The interstrand CL induces in DNA a distortion extending over at least 4 bp and localized mainly at the base pairs containing the platinated G residues.

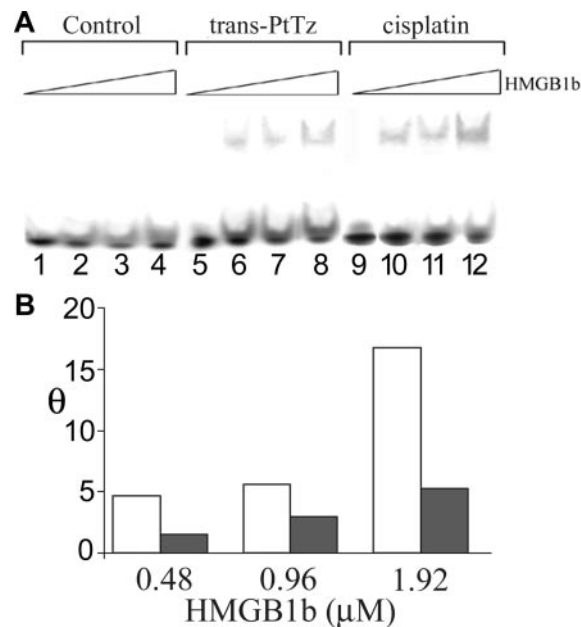


Figure 3. Recognition of interstrand CLs by HMGB1b protein. Gel-mobility shift assay analysis of the titration of the 20 bp duplexes containing the single, site-specific CLs of *trans*-PtTz or cisplatin with HMGB1b protein. (A) Phosphorimage: lanes 1–4, unplatinated TGCT (20) duplex; lanes 5–8, TGCT (20) duplex-containing interstrand CL of *trans*-PtTz; lanes 9–12, TGCT (20) duplex-containing interstrand CL of cisplatin. The duplexes were at the concentration of 20 nM. Lanes 1, 5, 9: no protein added; lanes 2, 6 and 10: 0.48 μ M HMGB1b added, respectively; lanes 3, 7 and 11: 0.96 μ M HMGB1b added, respectively; and lanes 4, 8 and 12: 1.92 μ M HMGB1b added, respectively. (B) Plot of θ values (ratio of protein-bound duplex to total duplex) obtained from gel-shift experiments. Open bars, interstrand CL of cisplatin and closed bars, interstrand CL of *trans*-PtTz.

Recognition by HMG domain proteins. An important feature of the mechanism of antitumor activity of several platinum drugs (depending on the cell type) is that their adducts are recognized by proteins containing HMG domains (3,29–31). For instance, the major 1,2-GG intrastrand CL of cisplatin and the monofunctional adducts of *trans*-PtTz are readily recognized by HMGB1 domains A and B (8,32) and the interstrand CL of cisplatin by the HMGB1 domain B (33). In contrast, the cisplatin 1,3-GNG intrastrand CL and DNA modified by transplatin or monodentate [PtCl(dien)]Cl or [PtCl(NH₃)₃]Cl, are not recognized by these cellular proteins (3,29,30). The interactions of the rat HMGB1 domain A (HMGB1a) and HMGB1 domain B (HMGB1b) with the 20 bp duplex TGCT (20) containing a single, site-specific interstrand CL of *trans*-PtTz were investigated using a gel-mobility shift assay and binding was detected by retardation of the migration of the radiolabeled 20 bp probes through the gel (Figure 3) (33,34). Consistent with previous reports (15), a shifted band upon incubation of the duplex containing 1,2-GG intrastrand CL of cisplatin with both HMGB1a and HMGB1b was observed (data not shown) indicating that both proteins recognize the duplex containing this adduct. The HMGB1a exhibited under the same experimental conditions no binding to the 20 bp duplex when unplatinated or containing the interstrand CL of either cisplatin [consistent with previous results (33)] or *trans*-PtTz (data not shown). The HMGB1b exhibited under the same experimental

conditions no binding to the unplatinated 20 bp duplex (Figure 3, lanes 1–4), but a shifted band upon incubation of the interstrand CLs of cisplatin (Figure 3A, lanes 9–12) or *trans*-PtTz (Figure 3A, lanes 5–8) was clearly observed indicating that the protein recognizes the duplex containing these interstrand CLs. Thus, HMGB1b, but not HMGB1a, protein exhibited affinity for the interstrand CL of *trans*-PtTz which was similar, although somewhat less pronounced, compared with that for the interstrand CL of cisplatin (Figure 3B).

Nucleotide excision repair. In mammalian cells, the NER pathway is an important mechanism for the removal of bulky, helix-distorting DNA adducts, such as those generated by various chemotherapeutics, including cisplatin (3,35,36). Efficient repair of 1,2-GG or 1,3-GTG intrastrand CL of cisplatin and no excision repair of interstrand CLs of cisplatin have been reported from various NER systems, including human and rodent excinucleases (3,37). The results in Figure 4A, lanes 4 and 8, demonstrating NER by the rodent excinuclease, are consistent with these reports. The major excision fragment contains 28 nt, and other primary excision

fragments are 23–27 nt in length. No excision products were, however, detected for the interstrand CL of *trans*-PtTz under identical conditions where the cisplatin 1,2- or 1,3-intrastrand CLs were readily removed by both rodent and human excinuclease (shown in Figure 4A, lane 12 for the CL treated with rodent excinuclease).

Structural consequences of intrastrand CL

Steric constraints prevent the formation of transplatin intrastrand CLs between adjacent base residues in double-helical DNA. The *trans* compounds can, however, cross-link two bases on the same strand separated by at least one intervening base, forming mostly 1,3-GNG intrastrand CLs (where N = A, C, G or T).

Stability of the 1,3-GNG intrastrand CLs. The 1,3-GNG intrastrand CL (N = any nucleotide) of transplatin is stable in single-stranded DNA under physiological conditions. Pairing of single-stranded DNA containing this 1,3-GNG intrastrand adduct with the complementary DNA sequences results in rearrangement into interstrand CLs (38). The stability of 1,3-GNG intrastrand CLs of *trans*-PtTz was investigated using 20mer oligodeoxyribonucleotides (the top strands of the duplexes CGCGC, TGCCT and TGTGT shown in Figure 5C) that were radioactively labeled at their 5' ends and platinated so that they contained single and central, site-specific 1,3-GCG or GTG intrastrand CLs, respectively. The single-stranded oligonucleotides containing this CL or the corresponding duplexes were incubated in 0.2 M NaClO₄ at 37°C. At various time intervals, aliquots were withdrawn and analyzed by gel electrophoresis under denaturing conditions. Only 2–5% of these intrastrand CLs were transformed into interstrand CLs after 24 h (Figure 5B). In contrast, 70% of the transplatin 1,3-intrastrand CLs in the duplex TGTGT were transformed into interstrand CLs after 24 h [Figure 5A and B and (39)]. Further, the 1,3-GNG intrastrand adduct of *trans*-PtTz in the single-stranded oligonucleotides was inert over a long period of time (>5 days) (data not shown).

Unwinding and bending. Bending and unwinding studies of the 1,3-intrastrand CL were performed in the oligodeoxyribonucleotide duplexes TGTGT (19–22) (19–22 bp long) (12,13). The sequences were identical or similar to that of the duplex TGTGT (21) shown in Figure 1B; the 19 and 20 bp duplexes had one or two marginal C-G pairs deleted, respectively, whereas one additional T-A pair was added to one end in the 22 bp duplex. The DNA bending toward the minor groove and unwinding owing to one 1,3-intrastrand adduct of *trans*-PtTz were measured at 40 ± 2 and $15 \pm 2^\circ$, respectively [the direction of the bend was determined using the duplex [TGTGT(A/T)₅] (32) (Figure 1B) as described previously (27)]. Moreover, the ligation of the duplexes containing 1,3-intrastrand CL of *trans*-PtTz did not result in the formation of circles, suggesting that these 1,3-intrastrand CLs did not increase the flexibility of the double helix (12,28).

Chemical probes of DNA conformation. The single, site-specific 1,3-GTG intrastrand CL in the duplex TGTGT (21) induces a distortion extending over at least 6 bp and is localized mainly at the base pair between the platinated G residues and the base pairs on its 5' side (Figure S2 in Supplementary Data).

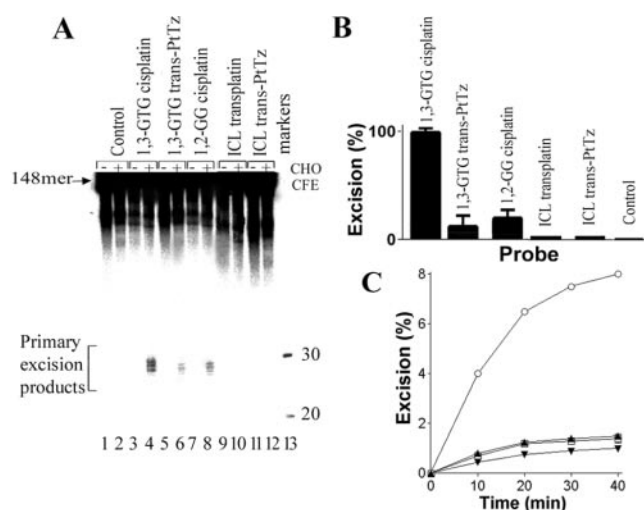


Figure 4. Excision of the intrastrand and interstrand CLs of platinum complexes by rodent excinuclease. (A) Phosphorimage. The substrates were incubated with CHO AA8 CFE and subsequently treated overnight with NaCN before analysis in 10% PAA/8 M urea denaturing gel. Lanes 1 and 2, control, unplatinated substrate; lanes 3 and 4, the substrate containing the 1,3-GTG intrastrand CL of cisplatin; lanes 5 and 6, the substrate containing the 1,3-GTG intrastrand CL of *trans*-PtTz; lanes 7 and 8, 1,2-GG intrastrand CL of cisplatin; lanes 9 and 10, the substrate containing the interstrand CL (ICL) of transplatin; lanes 11 and 12, the substrate containing the interstrand CL of *trans*-PtTz; lanes 1, 3, 5, 7, 9 and 11, no extract added; lanes 2, 4, 6, 8, 10 and 12, the substrates were incubated with CHO AA8 CFE for 40 min at 30°C. Lane 13, the 20 and 30 nt markers. (B) Quantitative analysis of removal of the adducts. The columns marked as 1,3-GTG cisplatin, 1,3-GTG *trans*-PtTz, 1,2-GG cisplatin, ICL cisplatin, ICL *trans*-PtTz and Control are for 1,3-GTG intrastrand CL of cisplatin, 1,3-GTG intrastrand CL of *trans*-PtTz, 1,2-GG intrastrand CL of cisplatin, the interstrand CL of transplatin, the interstrand CL of *trans*-PtTz and unplatinated substrate, respectively. The radioactivity associated with the fragments excised from the duplex containing the 1,3-GTG intrastrand CL of cisplatin was taken as 100% and corresponded to 8% excision. Data are the average of two independent experiments performed under the same conditions; bars indicate the range of excision. (C) Quantitative analysis of the kinetic experiment. Removal of 1,3-GTG intrastrand CL of cisplatin (open circles), 1,3-GTG intrastrand CL of *trans*-PtTz (inverted closed triangle), 1,2-GG intrastrand CL of cisplatin (closed triangles) and monofunctional adduct of *trans*-PtTz (open squares).

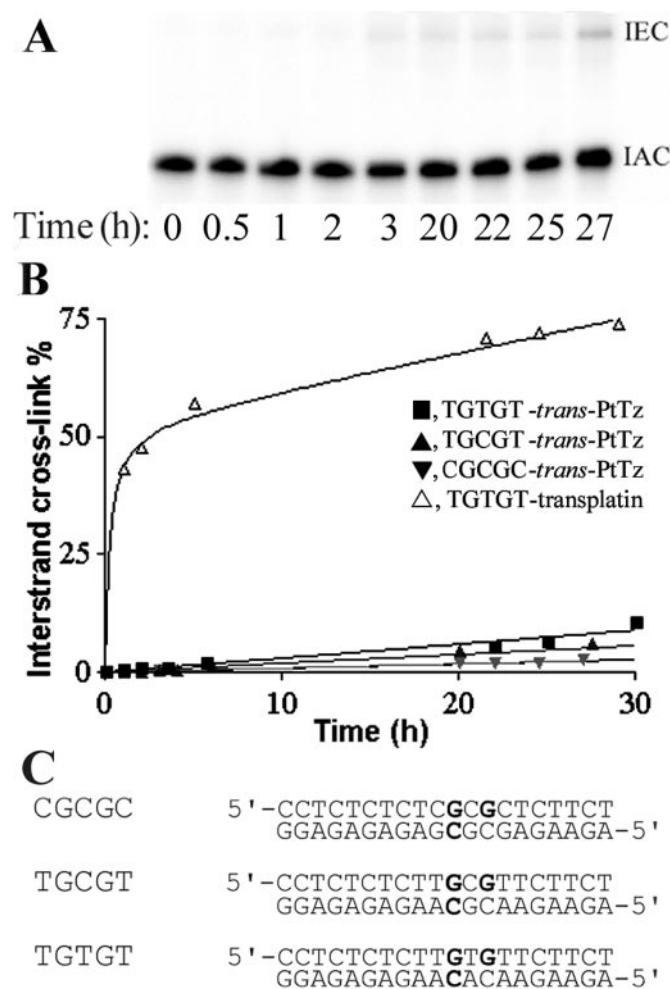


Figure 5. Rearrangement of the 1,3-intrastrand CLs formed by *trans*-PtTz and transplatin in the 20 bp duplexes into the interstrand CLs. The samples of the 20 μ M duplexes TGTGT, TGCCT and CGCGC containing the single, site-specific 1,3-intrastrand CL were incubated at 37°C in 0.2 M NaClO₄, 5 mM Tris-HCl buffer (pH 7.5) and 0.1 mM EDTA; at various time intervals, the aliquots were withdrawn and analyzed by electrophoresis in 12% PAA/8 M urea gel. (A) Phosphorimage of the gel of the duplex TGTGT modified by *trans*-PtTz radioactively labeled at the 5' end of its top strand. Incubation times in hours are indicated under each lane. Lane 0 refers to the 5' end labeled single-stranded top (platinated) strand. The upper bands corresponding to more slowly migrating species contain the interstrand cross-linked oligonucleotides (ICLs) whereas the bottom bands corresponding to more rapidly migrating species contain the intrastrand cross-linked oligonucleotides (IACs). (B) Plots of the percentages of interstrand CL versus time in TGTGT, TGCCT and CGCGC duplexes. These percentages were calculated from the ratio of the radioactivity associated with the interstrand cross-linked product to the total radioactivity loaded in each lane (multiplied by 100). Data for the plot demonstrating the rearrangement of the 1,3-intrastrand CL formed by transplatin in the duplex TGTGT were identical to those published previously (39). For other details, see the text. (C) The nucleotide sequences of the duplexes TGTGT, TGCCT and CGCGC.

Recognition by HMG domain proteins. Using the same experimental approach as for the *trans*-PtTz interstrand CL, neither HMGB1a nor HMGB1b was found to bind the 20 bp probe containing the intrastrand CL of *trans*-PtTz (data not shown).

Nucleotide excision repair. Importantly, excision repair substrates containing the site-specific *trans*-PtTz 1,3-GTG

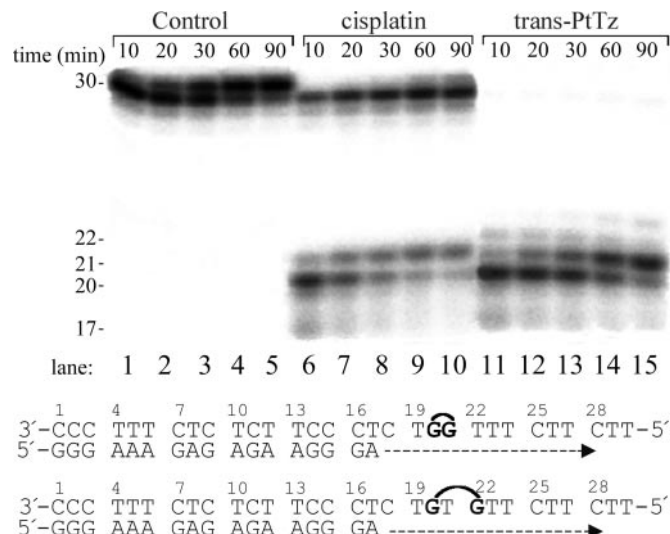


Figure 6. Primer extension activity of RT-HIV1. The experiments were conducted using the 17mer/30mer primer-template duplexes (their nucleotide sequences are shown at the bottom of this figure) for the times indicated. Lanes 1–5, undamaged template; lanes 6–10, the template containing 1,2-GG intrastrand CL of cisplatin; lanes 11–15, the template containing 1,3-GTG intrastrand CL of *trans*-PtTz. The strong pause sites opposite the platinated guanines were marked 20 and 21.

intrastrand CL were repaired by both human and rodent excinucleases, but with a markedly lower efficiency than the intrastrand CLs of cisplatin (shown in Figure 4A, lane 6, and in Figure 4B and C for the adduct repaired by rodent excinuclease).

Inhibition of DNA polymerization. DNA secondary structures have significant effects on processivity of a number of prokaryotic, eukaryotic and viral DNA polymerases. The character of DNA templates containing site-specific platinum adducts dictate whether prokaryotic and eukaryotic DNA polymerases are blocked or can traverse through the lesion. DNA polymerization using the templates site-specifically modified by *trans*-PtTz or cisplatin by RT HIV-1 was investigated to reveal the potential differences in conformational alterations imposed on DNA by these two adducts. We constructed the 17mer/30mer primer-template duplexes TGTGT and TGGT (Figure 6) unplatinated or containing either the 1,3-GTG intrastrand CL of *trans*-PtTz or the 1,2-GG intrastrand CL of cisplatin, respectively. The first 17 nt on the 3' terminus of the 30mer template strand were complementary to the nucleotides of the 17mer primer, and the 3' guanine involved in the 1,3-GTG CL of *trans*-PtTz or in 1,2-GG CL of cisplatin on the template strand was located at its 20th position from the 3' terminus (Figure 6). After annealing the 17 nt primer to the 3' terminus of the unplatinated or platinated template strand (positioning the 3' end of the primer three bases before the adduct in the template strand), we examined DNA polymerization through the unique CLs on the template by RT HIV-1 in the presence of all four deoxyribonucleoside 5'-triphosphates. The reaction was stopped at various time intervals, and the products analyzed using a sequencing gel (Figure 6). Polymerization using the template containing the CL of cisplatin proceeded rapidly up to the nucleotides at

the sites opposite the CL, such that the 20 and 21 nt products accumulated to a significant extent (shown in Figure 6, lanes 6–10). There was only a slight accumulation of larger DNA intermediates, whereas no intermediate products were seen with the 30mer control template as the full-length product was being formed (shown in Figure 6, lanes 1–5). The full-length products were also noticed with the 23mer template containing the CL of cisplatin, although in a smaller amount. The results are in agreement with previously published work (40) using T7 DNA polymerase and RT HIV-1 and confirm that the 1,2-GG intrastrand CL of cisplatin inhibits DNA synthesis, but translesion synthesis may occur. In contrast, under the same experimental conditions, DNA polymerization by RT HIV-1 on the *trans*-PtTz 1,3-intrastrand CL template proceeded up to the nucleotide at the site opposite the 3' G involved in the CL (Figure 6, lanes 11–15). There was almost no accumulation of shorter and larger DNA intermediates, and importantly, no full-length products accumulated. This result indicates that the 1,3-GTG intrastrand CLs of *trans*-PtTz impede elongation of DNA to a greater extent than the major adducts of cisplatin (Figure 6).

The effects of the 1,3-intrastrand CL of *trans*-PtTz on polymerization by KF[−] were also examined. This enzyme possesses template-dependent DNA polymerase activity but relatively better processivity and fidelity (41). In these studies, elongation of the 8mer/23mer primer–template duplexes was tested (data not shown). The *trans*-PtTz 1,3-intrastrand CL constitutes a fairly strong block to DNA synthesis catalyzed by both DNA polymerases. The high degree of structural and sequence conservation of the domains among eukaryotic, prokaryotic and viral polymerases (42), suggests that the results from studies of the RT HIV-1 and KF[−] should be also applicable to other DNA polymerases (43,44). Hence, the stronger inhibition of DNA polymerization by the

trans-PtTz 1,3-intrastrand CL reflects an important difference in biological processes of replication or DNA repair in comparison with the major adduct of cisplatin.

DISCUSSION

Transplatinum complexes with sterically hindered ligands [planar N-heterocycles; iminoethers (45), aliphatic amines (46) and aliphatic heterocycles, such as piperazine (39)] display significantly increased cytotoxicity over the 'parent' *trans*-[PtCl₂(NH₃)₂] compound. *trans*-PtTz is a representative example of the structural class of cytotoxic compounds of general formula *trans*-[PtCl₂(L)(L')] containing at least one planar amine. The planar ligand clearly has significant consequences for the DNA conformational changes induced by these molecules. It appears likely from the work published to date that all planar ligands will have similar effects. The cytotoxicity of transplatinum complexes containing planar ligands is characterized by values similar to cisplatin and the retention of activity in cisplatin-resistant cells. A distinct profile of cytotoxicity in the NCI tumor cell line panel is also observed (47). It is therefore of interest to consider how the DNA binding of the various adducts summarized in Table 1 may contribute to these biological properties.

Unlike 'classical' cisplatin or transplatin, modification of DNA by *trans*-PtTz leads to monofunctional and bifunctional intra and interstrand CLs in roughly equal proportions. The bending of ~34° toward the major groove and local unwinding of 12–13° of the monofunctional adduct are uncannily similar to those of the 1,2-intrastrand CL of cisplatin and as a consequence the lesion is susceptible to NER and recognized by HMG-family proteins (8). Thus, other downstream biological effects of the *trans*-PtTz monofunctional adduct are also likely to be similar to those induced by cisplatin.

Table 1. Summary and comparison of basic characteristics of DNA CLs of *trans*-PtTz(*t*-PtTz), transplatin and cisplatin^a

	1,3-Intrastrand CL of <i>t</i> PtTz	Interstrand CL of <i>t</i> PtTz	Monofunctional adduct of <i>t</i> PtTz	Interstrand CL of transplatin	Interstrand CL of cisplatin	1,2-Intrastrand CL of cisplatin
Frequency (%)	20–40 ^b	30–40 ^b	30–40 ^b	~12 ^c	~6 ^c	~90 ^d
Reactivity of chemical probes (bp)	6	4	2 ^e	4 ^f	ND	ND
DNA bending	40° toward minor groove	22° toward minor groove	34° toward major groove ^e	~20° toward minor groove ^{f,g}	40–45° toward minor groove ^h	32–34° toward major groove ⁱ
DNA unwinding	15°	20°	12° ^e	~12° ^{f,g}	76–79° ^h	13° ⁱ
HMGB1a recognition	≥1.5 μM	≥1.5 μM	38.5 nM ^e	ND ^j	≥1.5 μM	30.8 nM ^e
HMGB1b recognition	≥30 μM	13.40 μM	2.05 μM ^e	ND ^j	4.60 μM	1.85 μM
Translesion synthesis	No	ND	20% ^e	ND	ND	6% ^e
NER by eukaryotic excinuclease (% excision) ^k	1.0	No	1.4 ^e	no ^{l,m}	no ^m	1.5 ^e

ND, not determined.

^aIf not stated otherwise, the data are from this work. The 1,3-intrastrand CL of transplatin is not included because these adducts are unstable in double-helical DNA and readily isomerize to interstrand CLs (38,39).

^bData are from Ref. (5,7).

^cData are from Ref (9).

^dData are from Ref (52).

^eData are from Ref (8).

^fData are from Ref (12).

^gData are from Ref (53).

^hData are from Ref. (54,55).

ⁱData are from Ref (23).

^jData are only available for recognition by full-length rat HMGB1, which indicated no recognition (56).

^kData taken from Figure 4; the substrates were incubated with CHO AA8 CFE for 40 min at 30°C.

^lData are from Ref (19).

^mData are from Ref (19).

The steric effect of the planar ligand results in the formation of bifunctional interstrand CLs between adjacent guanines in a 5'-GC/5'-GC bp. The DNA bending and unwinding are quantitatively significantly smaller than those of the analogous cisplatin interstrand CL. Nevertheless, similar to that adduct but in contrast to that of transplatin, the *trans*-PtTz interstrand CL is a weak substrate for HMGB1b protein recognition and is not repaired in NER assays.

Transplatin does not form stable 1,2-intrastrand CLs in double-helical DNA (38) and this property has been related to its clinical inefficiency (48,49). Replacement of one ammine by a thiazole ligand results in a distinctively enhanced stability of the 1,3-GNG intrastrand CLs in short oligoexy-ribonucleotide duplexes (Figure 5). Despite the similarity in bending to that of the 1,2-GG intrastrand CL of cisplatin no recognition of the *trans*-PtTz 1,3-intrastrand CL by HMG-domain proteins was observed. A plausible explanation may be that the bending owing to the *trans*-PtTz 1,3-intrastrand CL is in the opposite direction than that of the 1,2-intrastrand CL of cisplatin, thus preventing DNA bending toward the major groove required for its accommodation in the complex with HMGB1 protein (8,32).

Several reports have demonstrated that NER is a major mechanism contributing to cisplatin resistance (18,37,50). The 1,3-intrastrand CL of *trans*-PtTz is not removed as readily by excision repair as the cisplatin intrastrand adducts (Figure 4). The repercussion of stronger inhibition of DNA polymerization by the 1,3-intrastrand CL of *trans*-PtTz in comparison with the major adduct of cisplatin (Figure 6) adds a new dimension to the impact of the activated *trans* geometry in platinum compounds on biological processes, possibly including replication or DNA repair. However, it is not surprising that the interstrand CL of *trans*-PtTz is not excised in the assays we have used. Excision repair factors, most notably XPF-ERCC1, are involved in the interstrand CL repair, but there are no published data describing cell extracts proficient in the interstrand CL removal when assayed in a way similar to that described in the present work.

The cytotoxicity profile of *trans*-PtTz may be reasonably attributed to the structural consequences of DNA damage and the variety of adducts or lack of dominance of one specific adduct may correlate with the unusual profile seen. Thus, while long-lived monofunctional adducts simulate the biological consequences of cisplatin, the bifunctional adducts will induce cellular effects unique from the clinical drug. HMG-domain proteins sensitize cells to cisplatin (32,51), possibly owing to shielding of cisplatin-DNA adducts from excision repair or recruitment of these proteins from their native transcriptional regulatory function (3,15,30,51). For the subset of *trans*-PtTz bifunctional adducts with weak or no HMG binding these hypothetical pathways will not operate. Thus, a certain proportion of adducts will circumvent the cellular control induced for cisplatin and indeed other DNA-damaging agents and such circumvention may be reflected as a different cytotoxicity profile.

The multiple DNA lesions available to *trans*-planaramine complexes may all contribute substantially to their cytotoxicity so that the overall drug cytotoxicity could be the sum of the contributions of each of these adducts. However, an intriguing scenario consistent with the cytotoxicity profile different from cisplatin may be that that acquisition of drug

resistance is a relatively rare event, since it would have to entail resistance to or tolerance of multiple, structurally dissimilar DNA lesions.

A long-term goal of our investigations is to place the cytotoxicity of metal-based compounds into the context of molecular pathways leading to tumor cell death. We believe that the significance of the results of the present work consists in improvement of the theoretical background needed for the design of new anticancer metal-based drugs.

SUPPLEMENTARY DATA

Supplementary Data are available at NAR Online.

ACKNOWLEDGEMENTS

The authors acknowledge that this work was also carried out within the Institutional Research Plan AVOZ50040507 and that their participation in the European Commission Cooperation in the Field of Scientific and Technical Research Chemistry Action D20 enabled them to exchange regularly the most recent ideas in the field of platinum anticancer drugs with several European colleagues. J.K. is the international research scholar of the Howard Hughes Medical Institute. We are grateful to Erin Ma from Virginia Commonwealth University for providing *trans*-PtTz compound. This research was supported by the Grant Agency of the Czech Republic (Grant 305/05/2030), the Grant Agency of the Academy of Sciences of the Czech Republic (Grants 5004101, 5004301 and 1QS500040581) and the Grant Agency of the Ministry of Health of the Czech Republic (NR8562-4/2005). The research of N.F. was also supported by the National Science Foundation. Funding to pay the Open Access publication charges for this article was provided by the Grant Agency of the Czech Republic.

Conflict of interest statement. None declared.

REFERENCES

- Farrell, N. (1996) Current status of structure-activity relationships of platinum anticancer drugs: activation of the *trans* geometry. In Sigel, A. and Sigel, H. (eds), *Metal Ions in Biological Systems*. Marcel Dekker, Inc., New York, Basel, Hong Kong, Vol. 32, pp. 603-639.
- Natile, G. and Coluccia, M. (1999) In, *trans*-Platinum compounds in cancer therapy: a largely unexplored strategy for identifying novel antitumor platinum drugs. In Clarke, M.J. and Sadler, P.J. (eds), *Metallopharmaceuticals*. Springer, Berlin, Vol. 1, pp. 73-98.
- Brabec, V. (2002) DNA modifications by antitumor platinum and ruthenium compounds: their recognition and repair. *Prog. Nucleic Acid Res. Mol. Biol.*, **71**, 1-68.
- Johnson, N.P., Butour, J.-L., Villani, G., Wimmer, F.L., Defais, M., Pierson, V. and Brabec, V. (1989) Metal antitumor compounds: the mechanism of action of platinum complexes. *Prog. Clin. Biochem. Med.*, **10**, 1-24.
- Zakovska, A., Novakova, O., Balcarova, Z., Bierbach, U., Farrell, N. and Brabec, V. (1998) DNA interactions of antitumor *trans*-[PtCl₂(NH₃)(quinoline)]. *Eur. J. Biochem.*, **254**, 547-557.
- Bierbach, U., Qu, Y., Hambley, T.W., Peroutka, J., Nguyen, H.L., Doedee, M. and Farrell, N. (1999) Synthesis, structure, biological activity and DNA binding of platinum(II) complexes of the type *trans*-[PtCl₂(NH₃)L] (L = planar nitrogen base). Effect of L and *cis/trans* isomerism on sequence specificity and unwinding properties observed in globally platinated DNA. *Inorg. Chem.*, **38**, 3535-3542.
- Brabec, V., Neplechova, K., Kasparkova, J. and Farrell, N. (2000) Steric control of DNA interstrand cross-link sites of trans platinum

- complexes: specificity can be dictated by planar nonleaving groups. *J. Biol. Inorg. Chem.*, **5**, 364–368.
8. Kasparkova, J., Novakova, O., Farrell, N. and Brabec, V. (2003) DNA binding by antitumor *trans*-[PtCl₂(NH₃)(thiazole)]. Protein recognition and nucleotide excision repair of monofunctional adducts. *Biochemistry*, **42**, 792–800.
 9. Brabec, V. and Leng, M. (1993) DNA interstrand cross-links of *trans*-diamminedichloroplatinum(II) are preferentially formed between guanine and complementary cytosine residues. *Proc. Natl Acad. Sci. USA*, **90**, 5345–5349.
 10. Van Beusichem, M. and Farrell, N. (1992) Activation of *trans* geometry in platinum antitumor complexes. Synthesis, characterization and biological activity of complexes with the planar ligands pyridine, *N*-methylimidazole, thiazole, and quinoline. Crystal and molecular structure of *trans*-dichlorobis(thiazole)platinum(II). *Inorg. Chem.*, **31**, 634–639.
 11. Brabec, V., Reedijk, J. and Leng, M. (1992) Sequence-dependent distortions induced in DNA by monofunctional platinum(II) binding. *Biochemistry*, **31**, 12397–12402.
 12. Brabec, V., Sip, M. and Leng, M. (1993) DNA conformational distortion produced by site-specific interstrand cross-link of *trans*-diamminedichloroplatinum(II). *Biochemistry*, **32**, 11676–11681.
 13. Kasparkova, J., Mellish, K.J., Qu, Y., Brabec, V. and Farrell, N. (1996) Site-specific d(GpG) intrastrand cross-links formed by dinuclear platinum complexes. Bending and NMR studies. *Biochemistry*, **35**, 16705–16713.
 14. Lemaire, M.A., Schwartz, A., Rahmouni, A.R. and Leng, M. (1991) Interstrand cross-links are preferentially formed at the d(GC) sites in the reaction between *cis*-diamminedichloroplatinum(II) and DNA. *Proc. Natl Acad. Sci. USA*, **88**, 1982–1985.
 15. He, Q., Ohndorf, U.-A. and Lippard, S.J. (2000) Intercalating residues determine the mode of HMG1 domains A and B binding to cisplatin-modified DNA. *Biochemistry*, **39**, 14426–14435.
 16. Matsunaga, T., Mu, D., Park, C.-H., Reardon, J.T. and Sancar, A. (1995) Human DNA repair excision nuclease. *J. Biol. Chem.*, **270**, 20862–20869.
 17. Novakova, O., Kasparkova, J., Bursova, V., Hofr, C., Vojtiskova, M., Chen, H., Sadler, P.J. and Brabec, V. (2005) Conformation of DNA modified by monofunctional Ru(II) arene complexes: recognition by DNA-binding proteins and repair. Relationship to cytotoxicity. *Chem. Biol.*, **12**, 121–129.
 18. Reardon, J.T., Vaisman, A., Chaney, S.G. and Sancar, A. (1999) Efficient nucleotide excision repair of cisplatin, oxaliplatin, and bis-aceto-ammine-dichloro-cyclohexylamine-platinum(IV) (JM216) platinum intrastrand DNA diadducts. *Cancer Res.*, **59**, 3968–3971.
 19. Novakova, O., Kasparkova, J., Malina, J., Natile, G. and Brabec, V. (2003) DNA-protein cross-linking by *trans*-[PtCl₂(E-iminoether)₂]. A concept for activation of the *trans* geometry in platinum antitumor complexes. *Nucleic Acids Res.*, **31**, 6450–6460.
 20. Kasparkova, J., Novakova, O., Marini, V., Najajreh, Y., Gibson, D., Perez, J.-M. and Brabec, V. (2003) Activation of *trans* geometry in bifunctional mononuclear platinum complexes by a piperidine ligand: Mechanistic studies on antitumor action. *J. Biol. Chem.*, **278**, 47516–47525.
 21. Brabec, V. (2000) Chemistry and structural biology of 1,2-interstrand adducts of cisplatin. In Kelland, L.R. and Farrell, N.P. (eds), *Platinum-Based Drugs in Cancer Therapy*. Humana Press Inc, Totowa/NJ, pp. 37–61.
 22. Rice, J.A., Crothers, D.M., Pinto, A.L. and Lippard, S.J. (1988) The major adduct of the antitumor drug *cis*-diamminedichloroplatinum(II) with DNA bends the duplex by 40° toward the major groove. *Proc. Natl Acad. Sci. USA*, **85**, 4158–4161.
 23. Bellon, S.F., Coleman, J.H. and Lippard, S.J. (1991) DNA unwinding produced by site-specific intrastrand cross-links of the antitumor drug *cis*-diamminedichloroplatinum(II). *Biochemistry*, **30**, 8026–8035.
 24. Koo, H.S., Wu, H.M. and Crothers, D.M. (1986) DNA bending at adenine-thymine tracts. *Nature*, **320**, 501–506.
 25. Koo, H.S. and Crothers, D.M. (1988) Calibration of DNA curvature and a unified description of sequence-directed bending. *Proc. Natl Acad. Sci. USA*, **85**, 1763–1767.
 26. Bellon, S.F. and Lippard, S.J. (1990) Bending studies of DNA site-specifically modified by cisplatin, *trans*-diamminedichloroplatinum(II) and *cis*-Pt(NH₃)₂(N3-cytosine)Cl⁺. *Biophys. Chem.*, **35**, 179–188.
 27. Kostrehunova, H. and Brabec, V. (2000) Conformational analysis of site-specific DNA cross-links of cisplatin–distamycin conjugates. *Biochemistry*, **39**, 12639–12649.
 28. Huang, H.F., Zhu, L.M., Reid, B.R., Drobny, G.P. and Hopkins, P.B. (1995) Solution structure of a cisplatin-induced DNA interstrand cross-link. *Science*, **270**, 1842–1845.
 29. Jamieson, E.R. and Lippard, S.J. (1999) Structure, recognition, and processing of cisplatin–DNA adducts. *Chem. Rev.*, **99**, 2467–2498.
 30. Kartalou, M. and Essigmann, J.M. (2001) Recognition of cisplatin adducts by cellular proteins. *Mutat. Res.*, **478**, 1–21.
 31. Wei, M., Burenkova, O. and Lippard, S.J. (2003) Cisplatin sensitivity in Hmgbl^{−/−} and Hmgbl^{+/+} mouse cells. *J. Biol. Chem.*, **278**, 1769–1773.
 32. Ohndorf, U.M., Rould, M.A., He, Q., Pabo, C.O. and Lippard, S.J. (1999) Basis for recognition of cisplatin-modified DNA by high-mobility-group proteins. *Nature*, **399**, 708–712.
 33. Kasparkova, J., Delalande, O., Stros, M., Elizondo-Riojas, M.A., Vojtiskova, M., Kozelka, J. and Brabec, V. (2003) Recognition of DNA interstrand cross-link of antitumor cisplatin by HMGB1 protein. *Biochemistry*, **42**, 1234–1244.
 34. Malina, J., Kasparkova, J., Natile, G. and Brabec, V. (2002) Recognition of major DNA adducts of enantiomeric cisplatin analogs by HMG box proteins and nucleotide excision repair of these adducts. *Chem. Biol.*, **9**, 629–638.
 35. Sancar, A. (1996) DNA excision repair. *Annu. Rev. Biochem.*, **65**, 43–81.
 36. Naegeli, H. (1997) Mechanisms of DNA Damage Recognition In Mammalian Cells. Springer, NY.
 37. Zamble, D.B., Mu, D., Reardon, J.T., Sancar, A. and Lippard, S.J. (1996) Repair of cisplatin–DNA adducts by the mammalian excision nuclease. *Biochemistry*, **35**, 10004–10013.
 38. Dalbies, R., Payet, D. and Leng, M. (1994) DNA double helix promotes a linkage isomerization reaction in *trans*-diamminedichloroplatinum(II)-modified DNA. *Proc. Natl Acad. Sci. USA*, **91**, 8147–8151.
 39. Kasparkova, J., Marini, V., Najajreh, Y., Gibson, D. and Brabec, V. (2003) DNA binding mode of the *cis* and *trans* geometries of new antitumor nonclassical platinum complexes containing piperidine, piperazine or 4-picoline ligand in cell-free media. Relations to their activity in cancer cell lines. *Biochemistry*, **42**, 6321–6332.
 40. Suo, Z., Lippard, S. and Johnson, K. (1999) Single d(GpG)/*cis*-diammineplatinum(II) adduct-induced inhibition of DNA polymerization. *Biochemistry*, **38**, 715–726.
 41. Johnson, K.A. (1993) Conformational coupling in DNA-polymerase fidelity. *Annu. Rev. Biochem.*, **62**, 685–713.
 42. Hubscher, U., Nasheuer, H.P. and Syvaaja, J.E. (2000) Eukaryotic DNA polymerases, a growing family. *Trends Biochem. Sci.*, **25**, 143–147.
 43. Steitz, T.A. (1999) DNA polymerases: structural diversity and common mechanisms. *J. Biol. Chem.*, **274**, 17395–17398.
 44. Lam, W.C., Thompson, E.H.Z., Potapova, O., Sun, X.J.C., Joyce, C.M. and Millar, D.P. (2002) 3′-5′ Exonuclease of Klenow fragment: role of amino acid residues within the single-stranded DNA binding region in exonucleolysis and duplex DNA melting. *Biochemistry*, **41**, 3943–3951.
 45. Natile, G. and Coluccia, M. (2004) Antitumor active *trans*-platinum compounds. In Sigel, A. and Sigel, H. (eds), *Metal Ions in Biological Systems*. Marcel Dekker Inc., Basel, NY, Vol. 42, pp. 209–250.
 46. Perez, J.-M., Montero, E.L., Quiroga, A.G., Fuentes, M.A., Alonso, C. and Navarro-Ranninger, C. (2001) Cellular uptake, DNA binding and apoptosis induction of cytotoxic *trans*-[PtCl₂(*N,N*-dimethylamine)(isopropylamine)] in A2780cisR ovarian tumor cells. *Metal-Based Drugs*, **8**, 29–37.
 47. Fojo, T., Farrell, N., Ortuzar, W., Tanimura, H., Weinstein, J. and Myers, T.G. (2005) Identification of non-cross-resistant platinum compounds with novel cytotoxicity profiles using the NCI anticancer drug screen and clustered image map visualizations. *Crit. Rev. Oncol. Hematol.*, **53**, 25–34.
 48. Dalbies, R., Boudvillain, M. and Leng, M. (1995) Linkage isomerization reaction of intrastrand cross-links in *trans*-diamminedichloroplatinum(II)-modified single-stranded oligonucleotides. *Nucleic Acids Res.*, **23**, 949–953.
 49. Leng, M., Schwartz, A. and Giraud-Panis, M.J. (2000) Transplatin-modified oligonucleotides as potential antitumor drugs. In Kelland, L.R. and Farrell, N.P. (eds), *Platinum-Based Drugs in Cancer Therapy*. Humana Press Inc., Totowa/NJ, pp. 63–85.
 50. Moggs, J.G., Szymkowski, D.E., Yamada, M., Karran, P. and Wood, R.D. (1997) Differential human nucleotide excision repair of paired and mispaired cisplatin–DNA adducts. *Nucleic Acids Res.*, **25**, 480–491.

51. Zamble, D.B. and Lippard, S.J. (1999) The response of cellular proteins to cisplatin-damaged DNA. In Lippert, B. (ed.), *Cisplatin. Chemistry and Biochemistry of A Leading Anticancer Drug*. VHCA, WILEY-VCH, Zürich, Weinheim, pp. 73–110.
52. Fichtinger-Schepman, A.M.J., Van der Veer, J.L., Den Hartog, J.H.J., Lohman, P.H.M. and Reedijk, J. (1985) Adducts of the antitumor drug *cis*-diamminedichloroplatinum(II) with DNA: formation, identification, and quantitation. *Biochemistry*, **24**, 707–713.
53. Paquet, F., Boudvillain, M., Lancelot, G. and Leng, M. (1999) NMR solution structure of a DNA dodecamer containing a transplatin interstrand GN7-CN3 cross-link. *Nucleic Acids Res.*, **27**, 4261–4268.
54. Malinge, J.M., Perez, C. and Leng, M. (1994) Base sequence-independent distortions induced by interstrand cross-links in *cis*-diamminedichloroplatinum(II)-modified DNA. *Nucleic Acids Res.*, **22**, 3834–3839.
55. Paquet, F., Perez, C., Leng, M., Lancelot, G. and Malinge, J.M. (1996) NMR solution structure of a DNA decamer containing an interstrand cross-link of the antitumor drug *cis*-diamminedichloroplatinum(II). *J. Biomol. Struct. Dyn.*, **14**, 67–77.
56. Kasparkova, J. and Brabec, V. (1995) Recognition of DNA interstrand cross-links of *cis*-diamminedichloroplatinum(II) and its trans isomer by DNA-binding proteins. *Biochemistry*, **34**, 12379–12387.

17.

Conformation of DNA Modified by Monofunctional Ru(II) Arene Complexes: Recognition by DNA Binding Proteins and Repair. Relationship to Cytotoxicity

Olga Novakova,¹ Jana Kasparkova,¹
Vendula Bursova,¹ Ctirad Hofr,¹ Marie Vojtiskova,¹
Haimei Chen,² Peter J. Sadler,^{2,*}
and Viktor Brabec^{1,*}

¹Institute of Biophysics
Academy of Sciences of the Czech Republic
Kralovopolska 135
CZ-61265 Brno
Czech Republic

²School of Chemistry
University of Edinburgh
West Mains Road
Edinburgh, EH9 3JJ
United Kingdom

Summary

We analyzed DNA duplexes modified at central guanine residues by monofunctional Ru(II) arene complexes $[(\eta^6\text{-arene})\text{Ru(II)(en)(Cl)}]^+$ (arene = tetrahydroanthracene or *p*-cymene, Ru-THA or Ru-CYM, respectively). These two complexes were chosen as representatives of two different classes of Ru(II) arene compounds for which initial studies revealed different binding modes: one that may involve DNA intercalation (tricyclic-ring Ru-THA) and the other (mono-ring Ru-CYM) that may not. Ru-THA is ~20 times more toxic to cancer cells than Ru-CYM. The adducts of Ru-THA and Ru-CYM have contrasting effects on the conformation, thermodynamic stability, and polymerization of DNA in vitro. In addition, the adducts of Ru-CYM are removed from DNA more efficiently than those of Ru-THA. Interestingly, the mammalian nucleotide excision repair system has low efficiency for excision of ruthenium adducts compared to cisplatin intrastrand crosslinks.

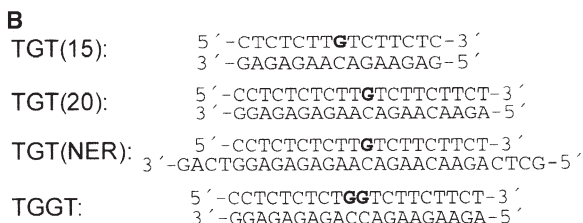
Introduction

There is much current interest in the potential of ruthenium complexes as new metal-based antitumor drugs [1, 2]. Although the pharmacological target for antitumor ruthenium compounds has not been unequivocally identified, several ruthenium(III) compounds have been found to inhibit DNA replication, exhibit mutagenic activity, induce the SOS repair mechanism, bind to nuclear DNA, and reduce RNA synthesis, which is consistent with DNA binding of these compounds in vivo [2]. Thus, DNA interactions of antitumor ruthenium agents are of potential importance. Organometallic ruthenium(II) arene complexes of the type $[(\eta^6\text{-arene})\text{Ru(II)(en)Cl}][\text{PF}_6]$ (en = ethylenediamine) constitute a relatively new group of anticancer compounds [3, 4]. These monodentate complexes appear to be novel anticancer agents with a mechanism of action different from those of the ruthenium(III) complexes $(\text{ImH})[\text{trans-Ru(III)Cl}_4\text{Im}(\text{Me}_2\text{SO})]$ (Im = imidazole, NAMI-A) and $(\text{IndH})[\text{trans-}$

$\text{RuCl}_4(\text{Ind})_2]$ (Ind = indazole, KP1019), which are currently in clinical trials [5]. The $(\eta^6\text{-arene})\text{Ru(II)} \pi$ bonds in the monofunctional $[(\eta^6\text{-arene})\text{Ru(II)(en)(Cl)}]^+$ complexes are inert toward hydrolysis, but the chloride ligand is readily lost, and the complex is transformed into the corresponding more reactive, aquated species [6]. It has also been shown that in cell-free media ethylenediamine Ru(II) arene compounds, in which arene = biphenyl, dihydroanthracene, tetrahydroanthracene, *p*-cymene, or benzene, bind preferentially to guanine residues in natural double-helical DNA. In addition, DNA binding of the complexes containing biphenyl, dihydroanthracene, or tetrahydroanthracene ligands can involve combined coordination to G N7 and noncovalent, hydrophobic interactions between the arene ligand and DNA, which may include arene intercalation and minor groove binding [7, 8]. In contrast, the single hydrocarbon rings in the *p*-cymene and benzene ruthenium complexes cannot interact with double-helical DNA by intercalation [8]. Interestingly, adducts of the complex containing the *p*-cymene ligand, which has methyl and isopropyl substituents, distort the conformation and thermally destabilize double-helical DNA distinctly more than the adducts of the tricyclic-ring Ru(II) arene compounds. It has been suggested that the different character of conformational alterations induced in DNA as a consequence of its global modification, and the resulting thermal destabilization, may affect differently further “downstream” effects of damaged DNA [8] and consequently may result in different biological effects of this new class of metal-based antitumor compounds.

To achieve a rational design of novel antitumor Ru(II) arene compounds capable of circumventing inherent or acquired resistance to metal-based drugs already used in the clinic, it is important to understand in detail the differences in DNA binding properties of these new ruthenium complexes and their possible relationship to cytotoxicities in different tumor cell lines. This may provide grounds for establishing new structure-pharmacological activity relationships for this class of metal-based complexes. In this work, we have considered the activity of two Ru(II) arene complexes from the $[(\eta^6\text{-arene})\text{Ru(II)(en)(Cl)}]^+$ family (arene = tetrahydroanthracene and *p*-cymene, Ru-THA and Ru-CYM, respectively, Figure 1A) in two tumor cell lines. These two complexes were chosen as representatives of two different classes of Ru(II) arene compounds for which initial studies of global modification of natural DNA revealed [8] different binding modes: one that may involve DNA intercalation (tricyclic-ring Ru-THA) and the other (mono-ring Ru-CYM) that cannot interact with double-helical DNA by intercalation. We compare the cytotoxicity data with those for DNA binding obtained previously [8], new data obtained in the present work relating to conformational distortions induced by single, site-specific monofunctional adducts of the Ru(II) arene complexes in short oligodeoxyribonucleotide duplexes, and the recognition of these DNA adducts by specific proteins and their repair, i.e., the most important factors that

*Correspondence: pjs01@staffmail.ed.ac.uk; brabec@ibp.cz



(A) Structures. (a) Ru-THA; (b) Ru-CYM.

(B) Sequences. The top and bottom strands of the pair of oligonucleotides are designated "top" and "bottom," respectively. The boldface letter in the top strand of the duplexes indicates the ruthenated residues.

modulate the antitumor effects of platinum antitumor drugs already used in the clinic.

Results

Chemical Probes of DNA Conformation

We demonstrated in our preceding paper [8] that Ru(II) arene compounds bind preferentially to guanine residues in natural double-helical DNA forming monofunctional adducts. In order to obtain information on how these adducts affect DNA conformation, the oligonucleotide duplexes containing a site-specific monofunctional adduct of Ru-THA or Ru-CYM (Figure 1A), $[(\eta^6\text{-tetrahydroanthracene})\text{Ru(II)(en)(Cl)}]^+$ and $[(\eta^6\text{-}p\text{-cymene})\text{Ru(II)(en)(Cl)}]^+$, respectively, at the G residue were further analyzed by chemical probes of DNA conformation. The ruthenated duplex TGT(20) (Figure 1B) was treated with several chemical agents that are used as tools for monitoring the existence of conformations other than canonical B DNA. These agents include KMnO_4 and diethyl pyrocarbonate (DEPC). They react preferentially with single-stranded DNA and distorted double-stranded DNA [9, 10]. We used for this analysis exactly the same methodology as described in detail in our recent papers in which we studied DNA adducts of various antitumor platinum drugs [9, 10], and, therefore, these experiments are described in more detail in the Supplemental Data (see the Supplemental Data available with this article online). The results demonstrated in Figure 2 indicate that the distortion induced by the nonintercalating Ru-CYM extended over at least 7 base pairs (bp), whereas the distortion induced by Ru-THA was less extensive.

Isothermal Titration Calorimetry

A calorimetric technique was employed to characterize the influence of the monofunctional adduct of Ru-THA

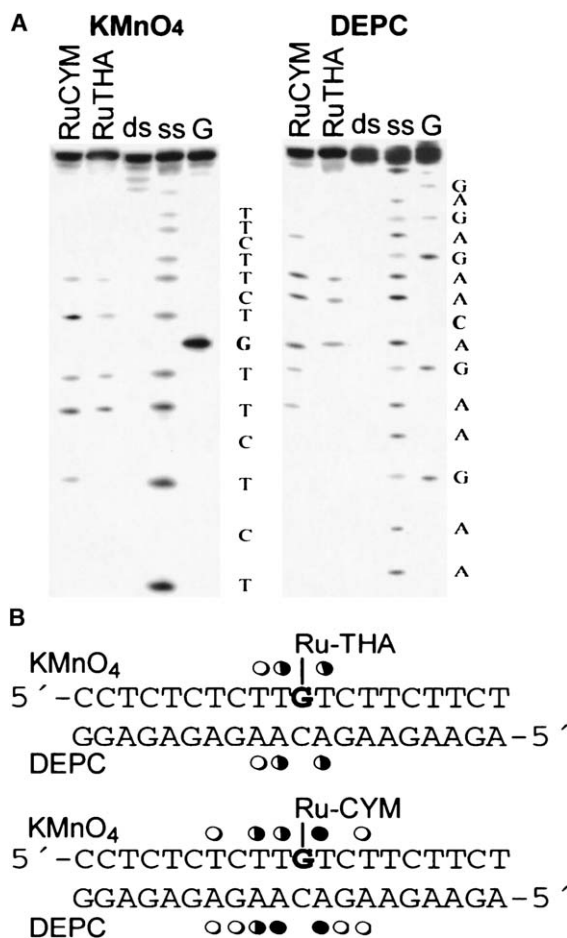


Figure 2. Chemical Probes of DNA Conformation

(A) Piperidine-induced specific strand cleavage at KMnO_4 -modified (lanes marked with KMnO_4) and DEPC-modified (lanes marked with DEPC) bases in the nonmodified TGT(20) duplex or that containing the single, monofunctional adduct at the central G in the top strand. The oligomer was 5'-end labeled at its top (KMnO_4) or bottom (DEPC) strand. Lanes: ss, the nonmodified single strand; ds, the nonmodified duplex; RuTHA, the duplex containing an adduct of Ru-THA; RuCYM, the duplex containing an adduct of Ru-CYM; G, a Maxam-Gilbert-specific reaction for the unplatinated duplex. The boldface letters in the sequences indicate the ruthenated G and complementary C residues.

(B) Summary of the reactivity of chemical probes of DNA conformation. Upper panel, adduct of Ru-THA; lower panel, adduct of Ru-CYM. Filled circle, strong reactivity; half-filled circle, medium reactivity; open circle, weak reactivity. The boldface letter in the top strand of the duplexes indicates the ruthenated G residue.

and Ru-CYM on the thermal stability and energetics of the site-specifically ruthenated 15 bp DNA duplex. Such thermodynamic data can reveal how the ruthenium adduct influences duplex stability, a property that has been shown to play a significant role in cellular processes such as recognition of DNA damage by DNA binding proteins and repair of this damage, i.e., the processes that may modulate potency of antitumor drugs, including metal-based cytostatics. Recently, differential scanning calorimetry (DSC) was employed to characterize the influence of different crosslinks of platinum

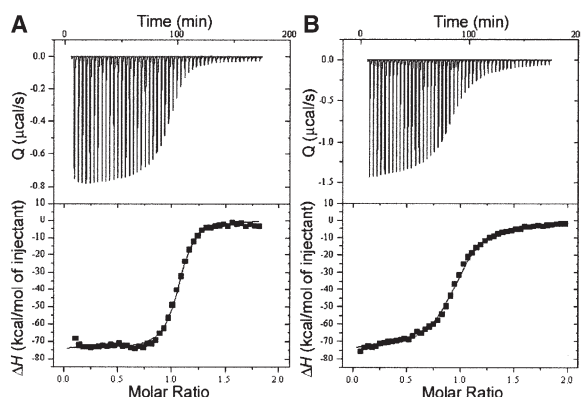


Figure 3. Isothermal Titration Calorimetry

(A and B) ITC binding isotherm for the association of the top strand of the 15 bp TGT duplex containing a single, monofunctional adduct of (A) Ru-THA or (B) Ru-CYM with the complementary (non-modified) strand (bottom strand of the duplex TGT(15)) at 25°C in 10 mM phosphate buffer (pH 7.0) containing 50 mM NaCl. The upper panels show total heat released upon injecting 5 μ l aliquots of the 50 μ M bottom strand into a 1.4 ml reaction cell containing the 5 μ M top strand. The lower panels show the resultant binding isotherm (full squares) obtained by integrating the peak areas of each injection. The continuous line represents the nonlinear least squares fit of the affinity (K), enthalpy (ΔH), and stoichiometry (n) to a single-site binding model. For other details, see the text.

antitumor drugs on the thermal stability and energetics of 15–20 bp DNA duplexes site-specifically modified by these drugs [11–13]. We decided to expand these studies to oligodeoxyribonucleotide duplexes containing unique monofunctional adducts of the Ru-THA or Ru-CYM complexes. DSC makes it possible to measure excess heat capacity versus temperature profiles for the thermally induced transitions of nonmodified DNA duplexes and those containing a unique adduct of the metal-based drug. Such thermograms are usually recorded with the heating rate of 60°C/hr, and after reaching the maximum temperature of 95°C, the samples are cooled at the same rate to the starting temperature of 25°C [11–13]. This implies that the duplexes containing the unique adduct are exposed to higher temperatures for a relatively long period of time. Therefore, we verified first the stability of the Ru(II) arene adducts at various temperatures and found that the adducts formed in the TGT(15) duplex by Ru-THA and Ru-CYM are stable for more than 2 hr only at temperatures lower than 50°C. Hence, it is apparent that DSC cannot be used to analyze the duplexes containing the adducts of these two Ru(II) arene complexes. A suitable alternative is isothermal titration calorimetry (ITC), which makes it possible to study the thermodynamic parameters of the duplex formation from its two complementary single strands over a range of temperatures including those at which the DNA adducts of Ru(II) arene compounds were stable for a long period of time [14].

Figure 3 shows ITC profiles of duplex formation from the nonmodified bottom strand of the duplex TGT(15) titrated into the complementary nonmodified top strand of the duplex TGT(15) or the same strand containing a single monofunctional adduct of Ru-THA or Ru-CYM at

25°C. It was verified that the melting temperature of the duplexes was significantly higher than this temperature and that the adducts of Ru-THA and Ru-CYM formed in the TGT(15) duplex or in its single-stranded top strand were stable for more than 24 hr. The ITC profiles were analyzed as described in the [Experimental Procedures](#) to obtain the results listed in [Table 1](#). Inspection of these thermodynamic parameters reveals that the exothermic formation of the single monofunctional adduct in the duplex TGT(15) by Ru-THA or Ru-CYM resulted in a large decrease of the change in the enthalpy of duplex formation by 4.4 and 7.4 kcal/mol, respectively. In other words, the monofunctional adduct of Ru-THA or Ru-CYM enthalpically destabilizes the duplex relative to its nonmodified counterpart. In addition, the formation of the monofunctional adducts by Ru-THA or Ru-CYM resulted in a substantial increase in the entropy of the duplex TGT(15) of 11.6 or 18.2 cal/K.mol ($T\Delta\Delta S = 3.6$ and 5.4 kcal/mol at 25°C), respectively. In other words, the monofunctional adduct of Ru-THA or Ru-CYM increases the entropy of the ruthenated duplexes and, in this way, entropically stabilizes the duplex. Thus, the 4.4 or 7.4 kcal/mol enthalpic destabilization of the TGT(15) duplex due to the monofunctional adduct of Ru-THA or Ru-CYM is partially, but not completely, compensated by the entropic stabilization of the duplex induced by these adducts of 3.5 or 5.4 kcal/mol at 25°C, respectively. The net result of these enthalpic and entropic effects is that the formation of the monofunctional adducts of Ru-THA and Ru-CYM with the duplex TGT(15) at 25°C induces a decrease in duplex thermodynamic stability ($\Delta\Delta G_{25}$) of 0.8 or 2.0 kcal/mol, respectively, with this destabilization being enthalpic in origin. In this respect, the monofunctional adduct of Ru-CYM was considerably more effective than that of Ru-THA.

Probing by DNA Polymerase

It has been demonstrated that various DNA secondary structures have significant effects on the processivity of a number of prokaryotic, eukaryotic, and viral DNA polymerases. Interestingly, with DNA templates containing site-specifically placed adducts of various platinum compounds, a number of prokaryotic and eukaryotic DNA polymerases were blocked but could also traverse through the adducts depending on their character and conformational alterations induced in DNA. Inhibition of prokaryotic DNA-dependent RNA polymerase by the adducts on DNA globally modified by Ru arene compounds, including Ru-THA and Ru-CYM, has already been demonstrated in *in vitro* transcription mapping experiments [8]. Interestingly, monofunctional adducts of cisplatin or transplatin and those of the monodentate compounds such as chlorodiethylenetriamineplatinum(II) chloride ([PtCl(dien)]Cl) or [PtCl(NH₃)₃]Cl terminate DNA synthesis by DNA polymerases *in vitro* markedly less efficiently than crosslinks of platinum complexes [15, 16]. It is, therefore, interesting to examine whether a DNA polymerase, which processes DNA substrates containing monofunctional adducts of Ru-THA or Ru-CYM, can reveal potential specific features of conformational alterations imposed on DNA by the monofunctional adducts of these two Ru(II) arene compounds.

Table 1. Calorimetrically Derived Thermodynamic Parameters for the Formation of the 15 bp Nonmodified Duplexes or Those Containing Single, Site-Specific Monofunctional Adducts of Ru-THA or Ru-CYM at 25°C

Duplex	ΔH^a (kcal/mol)	ΔS^a (cal/K.mol)	ΔG_{25}^a (kcal/mol)	K^b (M ⁻¹)	N^b
TGT(15)	-79.3	-228	-11.3	1.98×10^8	1.08
TGT(15)-Ru-THA	-74.9	-216	-10.5	3.8×10^7	1.06
TGT(15)-Ru-CYM	-71.9	-210	-9.3	6×10^6	0.94

The ΔH and ΔS values are averages derived from three independent experiments.

^a ΔH , ΔS , and ΔG_{25} denote, respectively, the enthalpy, entropy, and free energy (at 25°C) of duplex formation.

^b K and n denote, respectively, association constant and binding stoichiometry for strand association.

We constructed 8-mer/23-mer primer/template non-modified duplexes or those containing the monofunctional adduct of Ru-THA, Ru-CYM or [PtCl(dien)]Cl in the central TGT sequence (for sequences, see [Figure 4](#)). The first eight nucleotides on the 3' terminus of the 23-mer template strand were complementary to the nucleotides of the 8-mer primer, and the guanine involved in the monofunctional adduct of Ru-THA, Ru-CYM, or [PtCl(dien)]Cl on the template strand was located at the 13th position from the 3' terminus ([Figure 4](#)). After annealing the 8-mer primer to the 3' terminus of the non-modified or metallated template strand, positioning the 3' end of the primer five bases before the adduct in the template strand, we examined DNA polymerization through the single, monofunctional adducts of Ru-THA, Ru-CYM, or [PtCl(dien)]Cl by a Klenow fragment of DNA polymerase I (KF) in the presence of all four deoxyribonucleoside 5' triphosphates. The reaction was stopped at various time intervals, and the products were analyzed by using a sequencing 24% polyacrylamide (PAA)/8 M urea gel (shown for the monofunctional adducts of Ru-THA and Ru-CYM in [Figure 4](#)). Polymerization with the 23-mer template containing the adduct of

Ru-THA proceeded rapidly up to the nucleotide preceding and at the sites opposite the adduct, such that the 12 and 13 nucleotide products accumulated to a significant extent (shown in Figure 4, lanes 6–10). The larger DNA intermediates were not observed to a considerable extent, whereas no intermediate products were seen with the 23-mer control template or the template containing the monofunctional adduct of [PtCl(dien)]Cl as the full-length products were formed (shown in Figure 4 for control template, lanes 1–5). The full-length products were also noticed with the 23-mer template containing the adduct of Ru-THA (Figure 4, lanes 6–10). This result demonstrates that the monofunctional adduct of Ru-THA effectively inhibits DNA synthesis, but translesion synthesis may occur. Under the same experimental conditions, DNA polymerization by KF with the template containing the monofunctional adduct of Ru-CYM proceeded up to the nucleotide preceding the site opposite the ruthenated G involved in the adduct and to the following nucleotide residue (Figure 4, lanes 11–15). There was no accumulation of shorter intermediates, but larger DNA intermediates (corresponding to 14 and 15 nucleotide products) and the full-length products were noticed. The amount of the full-length products increased with reaction time, but with a somewhat lower rate compared to the polymerization with the template containing the adduct of Ru-THA.

Repair

Figure 5A illustrates an experiment that measures DNA repair synthesis by a repair-proficient HeLa cell-free extract (CFE) in pUC19 plasmid modified at $r_b = 0.05$ by Ru-THA or Ru-CYM, and for comparative purposes, also by cisplatin. Repair activity was monitored by measuring the amount of incorporated radiolabeled nucleotide. A similar amount of undamaged pBR322 of a slightly different size is included in the reactions to show the background incorporation into undamaged plasmid. This background incorporation was subtracted from that found for metallated pUC19 plasmid. Considerably different levels of damage-induced DNA repair synthesis were detected in the plasmid modified by Ru-THA, Ru-CYM, and cisplatin (**Figures 5A and 5B**). The level of the synthesis detected in the plasmid modified by Ru-THA was ~ 6 times lower than that in the plasmid modified by Ru-CYM.

DNA repair synthesis can be due to various DNA repair mechanisms. Bulky, helix-distorting DNA adducts, such as those generated by various chemotherapeutics, including cisplatin, are removed from DNA by nucleotide excision repair (NER), which is an important

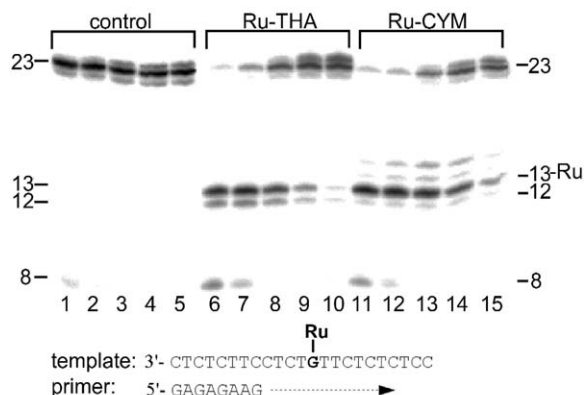


Figure 4. Primer Extension Activity of Klenow Fragment of DNA Polymerase I

Experiments were conducted by incubating 8-mer/23-mer primer/template duplex for various times (lanes 1–5), or the template containing a monofunctional adduct of Ru-THA (lanes 6–10) or of Ru-CYM (lanes 11–15). Timings were as follows: 1 min, lanes 1, 6, and 11; 3 min, lanes 2, 7, and 12; 15 min, lanes 3, 8, and 13; 30 min, lanes 4, 9, and 14; 60 min, lanes 5, 10, and 15. The pause sites opposite the ruthenated guanine and the preceding residues are marked 13 and 12, respectively (the site opposite the ruthenated residue is still marked "Ru"). The nucleotide sequences of the template and the primer are shown beneath the gels.

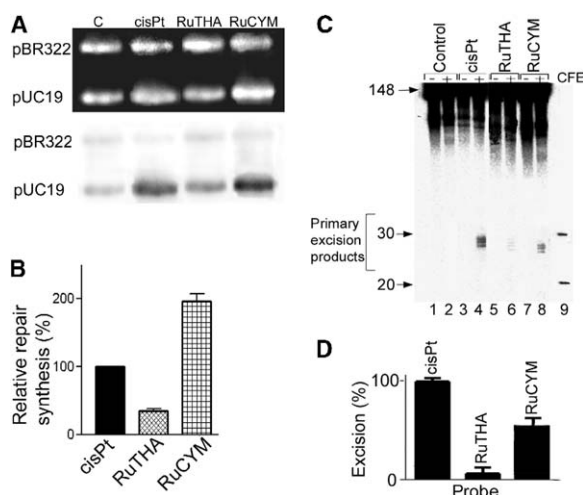


Figure 5. Repair DNA Synthesis and Nucleotide Excision Repair
(A and B) In vitro repair synthesis assay of the extract prepared from the repair-proficient HeLa cell line. Repair synthesis used as substrates nonmodified pBR322 plasmid and nonmodified pUC19 plasmid (lane C) or pUC19 plasmid modified at $r_b = 0.05$ by cisplatin, Ru-THA, or Ru-CYM (lanes cisPt, RuTHA, and RuCYM, respectively). (A) Results of a typical experiment. The top panel is a photograph of the EtBr-stained gel, and the bottom panel is the autoradiogram of the gel showing incorporation of [α - 32 P]dCMP. (B) Incorporation of dCMP into nonmodified, platinated, or ruthenated plasmids. For all quantifications representing mean values of three separate experiments, incorporation of radioactive material is corrected for the relative DNA content in each band. The radioactivity associated with the incorporation of [α - 32 P]dCMP into DNA modified by cisplatin was taken as 100%.
(C and D) Excision of the adducts of ruthenium complexes by rodent excinuclease. (C) The 148 bp substrates were incubated with CHO AA8 CFE and subsequently treated overnight with NaCN prior to analysis in 10% PAA/8 M urea denaturing gel; lanes: 1 and 2, control, nonmodified substrate; 3 and 4, the substrate containing the 1,2-GG intrastrand crosslink of cisplatin; 5 and 6, monofunctional adduct of Ru-THA; 7 and 8, the monofunctional adduct of Ru-CYM. Lanes 1, 3, 5, and 7, no extract added; lanes 2, 4, 6, and 8, the substrates were incubated with CHO AA8 CFE for 40 min at 30°C. Lane M, the 20- and 30-mer markers. (D) Quantitative analysis of removal of the adducts. The columns marked cisPt, RuTHA, and RuCYM represent 1,2-GG intrastrand crosslink of cisplatin, the monofunctional adduct of Ru-THA, and the monofunctional adduct of Ru-CYM, respectively. The radioactivity associated with the fragments excised from the duplex containing the 1,2-GG intrastrand CL of cisplatin was taken as 100%. Data are the average of two independent experiments performed under the same conditions.

component of the mechanism underlying the biological effects of these agents. Efficient removal of crosslinks formed in DNA by platinum antitumor compounds has already been reported for various NER systems, including human and rodent excinucleases [17–20]. The result presented in Figure 5C, lane 4 is consistent with these reports. The major excision fragment contains 28 nucleotides, and other primary excision fragments are 24–29 nucleotides in length [17–20]. In contrast, the monofunctional adducts of Ru-THA and Ru-CYM were also excised by both human and rodent excinucleases (shown for rodent excinuclease in Figures 5C and 5D), although with a noticeably lower efficiency than the major intrastrand crosslink of cisplatin; the adduct of Ru-

CYM was excised slightly more than that of Ru-THA. Consistent with this observation were the results of the gel mobility shift assay analysis (Supplemental Figure S1) employing replication protein A (RPA) (which belongs to the initial damage-sensing factors of eukaryotic excision nuclease initiating repair) and DNA probes containing the adducts of Ru-THA, Ru-CYM, or cisplatin. The analysis performed with the substrate containing the major intrastrand crosslink of cisplatin revealed considerably higher binding than that performed with the substrate containing the adduct of Ru-THA or Ru-CYM (Supplemental Figure S1). In addition, a lower binding of RPA to the substrate containing the adduct of Ru-THA than to the substrate with the adduct of Ru-CYM was observed (Supplemental Figure S1). Thus, these results (described in detail in the Supplemental Data) corroborate the findings in Figures 5C and 5D and demonstrate the low efficiency of the mammalian NER systems employed in the present work to excise Ru(II) arene adducts and especially that of Ru-THA.

Cytotoxicity

The cytotoxic activity of the Ru(II) arene compounds tested in the present work was evaluated as described previously [3, 4] and has been determined in two cancer cell lines, A2780 and HT29. The compounds were incubated for 24 hr with the tumor cell lines [3, 4]. IC₅₀ values (compound concentration that produces 50% of cell killing) of 0.4 and 10 μ M were obtained in A2780 cells, and values of 3 and >100 μ M were obtained in HT29 cells for Ru-THA and Ru-CYM, respectively (D.I. Jodrell and R. Aird, personal communication). Hence, the tricyclic-ring complex Ru-THA was considerably more potent than the Ru-CYM complex. Thus, the capability of the Ru(II) arene complex to intercalate DNA correlates with the noticeably enhanced activity of this class of Ru(II) arene compounds in several cancer cell lines.

Discussion

Our initial studies [8] suggested that Ru(II) arene compounds containing multi-ring biphenyl, dihydroanthracene, or tetrahydroanthracene ligands bind to DNA differently in comparison to the complexes containing single hydrocarbon rings, such as *p*-cymene or benzene. DNA binding of the multiring Ru(II) arene complexes involves not only coordination to G N7 together with C6O \cdots (en) H-bonding, but also noncovalent, hydrophobic interactions between the arene ligand and DNA, which may include arene intercalation and minor groove binding. In contrast, the Ru arene compounds containing single hydrocarbon rings cannot interact with double-helical DNA by intercalation. Therefore, we tried first to find out whether this different DNA binding mode correlates with the cytotoxicity of the Ru(II) arene compounds in different tumor cell lines. Interestingly, the results of the previous [3, 4] and present work (vide supra) support the view that the presence of an arene ligand in these classes of ruthenium complexes that is capable of noncovalent, hydrophobic interaction with DNA (presumably intercalation) considerably enhances the cytotoxicity in a number of tumor cell lines.

It has been demonstrated that the biological activity of several transition metal-based complexes is modulated by the “downstream” effects of damaged DNA, such as recognition of damaged DNA by specific proteins and/or repair [21, 22]. For instance, recognition of DNA adducts of several antitumor metal-based drugs and removal of these adducts from DNA is dependent on the character of the distortion and thermodynamic destabilization induced in DNA by these adducts [11, 23]. A more detailed analysis of conformational distortions induced in DNA by Ru-THA and Ru-CYM carried out in the present work revealed substantial differences in the character of these distortions. Their analysis by chemical probes of DNA conformation demonstrated (Figure 2) that the distortion induced by the nonintercalating Ru-CYM extended over at least 7 bp, whereas the distortion induced by Ru-THA was less extensive. Consistent with this observation were the results of the ITC analysis (Figure 3 and Table 1). The association constants, K , for the formation of duplexes containing adducts of Ru-THA or Ru-CYM were 5 or 33 times lower, respectively, than the K value for the formation of the control (nonmodified) duplex (Table 1). Hence, the adducts of both Ru-THA and Ru-CYM thermodynamically destabilized DNA, with this destabilization being enthalpic in origin. The adduct of Ru-CYM destabilized DNA significantly more than the adduct of Ru-THA, whose DNA binding mode, additionally, involves noncovalent, hydrophobic interactions between the arene ligand and DNA, such as arene intercalation. Various intercalators thermodynamically stabilize DNA since they lengthen and unwind DNA, increasing the phosphate spacing along the helix axis [24, 25]. Hence, it is reasonable to suggest that the higher thermodynamic stability of DNA containing the adducts of Ru-THA observed in the present work is associated with this hydrophobic interaction.

Consistent with the different character of the adducts of Ru-THA and Ru-CYM and with the different impact of these adducts on DNA conformation and stability are also their different effects on primer extension activity of KF (Figure 4). The results of the present work suggest that the monofunctional adducts of Ru-THA and Ru-CYM efficiently inhibit DNA polymerization and in different ways. These studies demonstrate that the monofunctional adducts of Ru-THA and Ru-CYM constitute a fairly strong block to DNA synthesis catalyzed by KF; however, this block is not absolute, allowing translesion DNA synthesis with a limited efficiency. Hence, DNA polymerization appears to be inhibited by Ru(II) arene adducts markedly more strongly than by the adducts of simple monofunctional platinum(II) compounds. This provides a new dimension to the design of Ru(II) arene compounds for affecting processes in tumor cells, possibly including replication or DNA repair.

It has been suggested [21, 22] that HMG domain proteins play a role in sensitizing cells to cisplatin. It has been shown [26] that HMG domain proteins recognize and bind to DNA crosslinks formed by cisplatin. The details of how the binding of HMG domain proteins to cisplatin-modified DNA sensitize tumor cells to cisplatin are still not completely resolved, but possibilities such as shielding cisplatin-DNA adducts from repair or that these proteins could be recruited from their native

transcriptional regulatory function have been suggested [21, 22] as clues for how these proteins are involved in the antitumor activity. In addition, an important structural motif recognized by HMG domain proteins on DNA modified by cisplatin is a directional bend of the helix axis toward the major groove [27]. No recognition of the DNA monofunctional adducts of Ru-THA or Ru-CYM by HMGB1 protein was observed in the present work (see the Supplemental Data). A plausible explanation of this observation may be that these adducts do not bend DNA, thus affording no structural motif recognized by HMG domain proteins. From these considerations, we could conclude that the mechanism of antitumor activity of Ru(II) arene compounds does not involve recognition of its DNA adducts by HMG domain proteins as a crucial step, in contrast to the proposals for cisplatin and its direct analogs [21, 22].

Another important feature of the mechanism underlying antitumor effects of DNA binding metal-based compounds is repair of their DNA adducts [21, 28]. A persistence of these DNA adducts may potentiate their antitumor effects in the cells sensitive to these compounds [21, 22, 29]. DNA repair synthesis was investigated in the present work by using the CFE from human tumor cells and DNA substrates randomly modified by the Ru(II) arene compounds (Figures 5A and 5B). Importantly, Ru-THA adducts induced a considerably lower level of repair synthesis than the adducts of Ru-CYM and also of cisplatin (Figure 5B), suggesting a less efficient removal from DNA and enhanced persistence of the adducts of more potent multi-ring and intercalating Ru(II) arene compounds in comparison with the adducts of less potent and nonintercalating Ru(II) arene compounds. Additionally, the level of DNA repair synthesis induced by the adducts of Ru-CYM was still markedly higher than that induced by cisplatin; this finding is consistent with the lower cytotoxicity of this ruthenium compound (*vide supra*).

There are several types of DNA repair, for instance base excision, NER, mismatch, and recombination repair. The assay based on the measurement of DNA repair synthesis may reflect the effectiveness of all of these repair mechanisms. Several reports have demonstrated [30–32] that NER is a major mechanism contributing to cisplatin resistance. The examination of excision of monofunctional adducts of Ru-THA and Ru-CYM has revealed that these adducts also can be removed from DNA by NER (Figures 5C and 5D), but considerably less efficiently than the adducts of cisplatin. This is in contrast to the results of DNA repair synthesis (Figures 5A and 5B) and implies a less significant role of NER in the mechanism underlying the antitumor effects of Ru(II) arene compounds than in the mechanism of cisplatin. In other words, the results of the present work indicate that the adducts of Ru(II) arene compounds are preferentially removed from DNA by repair mechanisms other than NER, which provides additional support for a mechanism of antitumor activity of Ru(II) arene compounds different from that of cisplatin. Nevertheless, the results of both repair assays employed in the present work (Figure 5) demonstrate clearly that the adducts of Ru-CYM, which distort and destabilize DNA more than the adducts of Ru-THA, are removed from

DNA more effectively, independent of the type of the repair mechanism.

Hence, the character and extent of DNA distortion induced in DNA by the adducts of Ru(II) arene complexes and resulting thermodynamic destabilization of DNA control the biological effects of this class of ruthenium complexes. The results of the present work afford further details, which allow for improving the structure-pharmacological relationship of Ru(II) arene compounds, and should provide a more rational basis for the design of new antitumor ruthenium drugs and chemotherapeutic strategies.

Significance

Organometallic ruthenium(II) arene complexes of the type $[(\eta^6\text{-arene})\text{Ru(II)(en)Cl}][\text{PF}_6]$ (en = ethylenediamine) constitute a new group of anticancer compounds. To achieve a rational design of novel antitumor Ru(II) arene compounds, it is important to understand the differences in DNA binding properties of these complexes and their possible relationship to cytotoxicities in different tumor cell lines. In this work, we studied the activity of two Ru(II) arene complexes from the $[(\eta^6\text{-arene})\text{Ru(II)(en)(Cl)}]^+$ family (arene = tetrahydroanthracene and p-cymene, Ru-THA, and Ru-CYM, respectively) in two tumor cell lines, conformational distortions induced by monofunctional adducts of these complexes, and their recognition by DNA binding proteins and repair, i.e., the most important factors that modulate the antitumor effects of related platinum drugs. These two ruthenium complexes were chosen as representatives of two different classes of Ru(II) arene compounds that modify DNA differently: one that may interact with DNA by intercalation (tricyclic-ring Ru-THA), and the other (mono-ring Ru-CYM) that cannot.

The presence of the arene ligand in this class of ruthenium complexes capable of noncovalent, hydrophobic interaction with DNA considerably enhances cytotoxicity in several tumor cell lines. An analysis of DNA duplexes modified by Ru-THA and Ru-CYM revealed substantial differences in the impact of their monofunctional adducts on the conformation and thermodynamic stability of DNA and DNA polymerization *in vitro*. In addition, the adducts of Ru-CYM are removed from DNA more efficiently than those of Ru-THA. Interestingly, the adducts of Ru(II) arene compounds are preferentially removed from DNA by mechanisms other than nucleotide excision repair. This provides additional support for a mechanism underlying antitumor activity of Ru(II) arene compounds different from that of cisplatin. Hence, the character of DNA distortion induced in DNA by the adducts of Ru(II) arene complexes and the resulting thermodynamic destabilization of DNA control the biological effects of this class of ruthenium complexes.

Experimental Procedures

Starting Materials

The complexes Ru-THA and Ru-CYM (Figure 1A) were prepared by the methods described in detail previously [3, 7]. Cisplatin, glyco-

[PtCl(dien)]Cl was kindly provided by G. Natile. The stock solutions of the ruthenium and platinum complexes at the concentration of 5×10^{-4} M in H₂O were prepared in the dark at 25°C. Plasmids pUC19 (2686 bp) and pBR322 (4363 bp) were isolated according to standard procedures. The synthetic oligodeoxyribonucleotides were purchased from VBC-Genomics (Vienna, Austria) and were purified as described previously [33]. Restriction endonucleases, T4 polynucleotide kinase, KF, and bovine serum albumin were purchased from New England Biolabs. A CFE was prepared from the HeLa S3 cell line as described [18]. This extract was kindly provided by J.T. Reardon and A. Sancar from the University of North Carolina. Acrylamide, agarose, bis(acrylamide), ethidium bromide (EtBr), urea, and NaCN were purchased from Merck KGaA. Creatine phosphokinase and creatine phosphate were purchased from ICN Biomedicals, Inc. The radioactive products were purchased from Amersham.

Metallation of Oligonucleotides

The single-stranded oligonucleotides (the top, pyrimidine-rich strands containing a single central G of the TGT(15), TGT(20), or TGT(NER) duplexes; Figure 1B) were reacted in stoichiometric amounts with either Ru-THA, Ru-CYM, or [PtCl(dien)]Cl. The ruthenated or platinated oligonucleotides were purified by ion-exchange fast protein liquid chromatography (FPLC). It was verified by ruthenium or platinum flameless atomic absorption spectrophotometry (FAAS) and by optical density measurements that the modified oligonucleotides contained one ruthenium or platinum atom. It was also verified by using DMS footprinting of ruthenium or platinum on DNA [34] that one molecule of ruthenium or platinum complex was coordinated to the N7 atom of the single G in the top strand of each duplex. FPLC purification and FAAS measurements were carried out on a Pharmacia Biotech FPLC System with a MonoQ HR 5/5 column and a Unicam 939 AA spectrometer equipped with a graphite furnace, respectively. The duplexes containing a single, central 1,2-GG intrastrand crosslink of cisplatin in the pyrimidine-rich top strand were prepared as described [12]. The nonmodified, ruthenated, or platinated duplexes used in the studies of recognition by RPA protein were purified by electrophoresis on native 15% PAA gels (mono:bis[acrylamide] ratio = 29:1).

Isothermal Titration Calorimetry

The standard isothermal titration calorimetry (ITC) buffer for these studies contained 50 mM NaCl with 10 mM phosphate buffer (Na₂HPO₄/NaH₂PO₄ [pH 7.0]). Sufficient quantities of ITC solutions were prepared to perform a set of titrations of the 50 μ M solution of the bottom strand of the duplex TGT(15) (for its sequence, see Figure 1B) into the 5 μ M solution of the top strand of nonmodified TGT(15) or that containing the single, site-specific monofunctional adduct of Ru-THA or Ru-CYM at 25°C. Molar extinction coefficients for the single-stranded oligonucleotides (related to the strands that were 15 nucleotides long) used in ITC experiments were determined by phosphate analysis [35]. The following extinction coefficients at 260 nm and 25°C were obtained: 108,000 and 128,000 M⁻¹·cm⁻¹ for the upper and bottom strands of the nonmodified TGT(15) duplex, respectively; 113,000 and 111,000 M⁻¹·cm⁻¹ for the upper strand of the TGT(15) containing the single monofunctional adduct of Ru-THA and Ru-CYM, respectively. Stock solutions of the strands for ITC studies were prepared in the ITC buffer and were exhaustively dialyzed against this buffer. It was verified that enthalpies of ITC injections of each individual oligomer into buffer, of buffer into buffer, and of excess oligomer into a solution of duplex were all the same as water into water injections, within error. From these data, it was concluded that effects of any solvent mismatching are negligible. Titrations were carried out on a VP-ITC instrument (MicroCal LLC, Northampton, MA). For each titration, the top strand of the nonmodified TGT(15) duplex or that containing the single, site-specific adduct of Ru-THA or RuCYM was loaded into the 1.4 ml sample cell, and the complementary oligomer (bottom strand of the duplex TGT(15)) was loaded into the 300 μ l injection syringe. The stirring rate of the injection syringe was 400 rpm, and samples were equilibrated thermally prior to a titration until the baseline had leveled off and the rms noise was less than 0.015 μ cal·s⁻¹. A typical titration consisted of 50 injections of 5 μ l each,

with 3 min between injections. Data from individual titrations were analyzed by using the Origin 5.0 software package (Origin, Northampton, MA) to extract the relevant thermodynamic parameters (the enthalpy change $[\Delta H]$, the entropy change $[\Delta S]$, the stoichiometry $[n]$, and the equilibrium constant $[K]$ for strand association).

Inhibition of DNA Polymerization

We investigated DNA polymerization using the templates site-specifically modified by Ru-THA or Ru-CYM by KF. The DNA polymerase I class of enzymes has served as the prototype for studies on structural and biochemical mechanisms of DNA replication [36, 37]. The 23-mer templates containing a single monofunctional adduct of Ru-THA or Ru-CYM were prepared in the same way as described above. The eight-mer DNA primer was complementary to the 3' terminus of the 23-mer template. The DNA substrates were formed by annealing templates and 5'-end-labeled primers at a molar ratio of 3:1. All experiments were performed at 25°C in a volume of 50 μ l in a buffer containing 50 mM Tris-HCl (pH 7.4), 10 mM MgCl₂, 50 μ g/ml BSA, 25 μ M dATP, 25 μ M dCTP, 25 μ M dGTP, 25 μ M TTP and 0.5 U KF. Reactions were terminated by the addition of EDTA so that its resulting concentration was 20 μ M and by heating at 100°C for 30 s. Products were resolved on a denaturing 24% PAA/8 M urea gel and then visualized and quantified by using the FUJIFILM bio-imaging analyzer and AIDA image analyzer software.

Repair Synthesis by Human Cell Extracts

Repair DNA synthesis of CFEs was assayed by using pUC19 and pBR322 plasmids. Each reaction of 50 μ l contained 250 ng non-modified pBR322 and 250 ng nonmodified or platinated pUC19; 2 mM ATP; 30 mM KCl; 0.5 mg/ml creatine phosphokinase (rabbit muscle); 20 mM of each dGMP, dCTP, and TTP; 8 mM dATP; 74 kBq [α -³²P]dAMP in the buffer composed of 40 mM HEPES-KOH (pH 7.5), 5 mM MgCl₂, 0.5 mM dithiothreitol, 22 mM creatine phosphate, 1.4 mg/ml bovine serum albumin, and 150 μ g CFE. Reactions were incubated for 3 hr at 25°C and terminated by adding EDTA to a final concentration of 20 mM, SDS to 0.6%, and proteinase K to 250 μ g/ml and then incubating for 30 min. The products were extracted with 1 volume 1:1 phenol:chloroform. The DNA was precipitated from the aqueous layer by the addition of 1/50 volume 5 M NaCl, 5 mg glycogen, and 2.5 volumes ethanol. After 20 min of incubation on dry ice and centrifugation at 12,000 \times g for 30 min at 4°C, the pellet was washed with 0.5 ml 70% ethanol and dried in a vacuum centrifuge. DNA was finally linearized before electrophoresis on a 1% agarose gel containing 0.3 mg/ml EtBr. The basic principles of this assay are shown schematically in [Supplemental Figure S2A](#).

Nucleotide Excision Assay

The 149 bp substrates containing a single monofunctional adduct of Ru-THA or Ru-CYM were assembled from three oligonucleotide duplexes. The central duplex was TGT(NER) duplex (shown in [Figure 1B](#)) to which two duplexes (arms) with random base pair sequences with overhangs partially overlapping those of the modified duplex were ligated (one to each side) by T4 DNA ligase. The top strand of the modified central duplexes were 5'-end labeled with ³²P before ligation. Substrates containing a single, central 1,2-GG intrastrand crosslink of cisplatin were prepared in a similar way to that described previously [38]. Full-length substrates (nonmodified, containing the monofunctional adduct of Ru-THA or Ru-CYM or the 1,2-intrastrand crosslink of cisplatin) were separated from unligated products on a denaturing 6% PAA gel, purified by electroelution, reannealed, and stored in annealing buffer (50 mM Tris-HCl [pH 7.9], 100 mM NaCl, 10 mM MgCl₂, and 1 mM dithiothreitol) at 20°C. In vitro repair of monofunctional adducts of Ru(II) arene complexes and of the 1,2-intrastrand crosslink of cisplatin was measured in an excision assay as described previously [38], with minor modifications. The reaction mixtures (25 μ l) contained 10 fmol radiolabeled DNA, 50 μ g CFE, 20 μ M dATP, 20 μ M dCTP, 20 μ M dGTP, and 20 μ M TTP in reaction buffer (23 mM HEPES [pH 7.9], 44 mM KCl, 4.8 mM MgCl₂, 0.16 mM EDTA, 0.52 mM dithiothreitol, 1.5 mM ATP, 5 μ g bovine serum albumin, and 2.5% glycerol) and were incubated at 30°C for 40 min. DNA was depro-

teinized and precipitated by ethanol. Reaction products were treated overnight with 0.4 M NaCN (pH 10–11) at 45°C and precipitated by ethanol prior to resolution on the gels. The excision products were separated on denaturing 10% PAA gels and visualized by using the PhosphorImager. The basic principles of this assay are shown schematically in [Supplemental Figure S2B](#).

Supplemental Data

A description of the experiments with chemical probes of DNA conformation, recognition by HMGB1 and RPA proteins, corresponding experimental procedures, and the basic principles of repair DNA synthesis and nucleotide excision repair assays are available at <http://www.chembiol.com/cgi/content/full/12/1/121/DC1/>.

Acknowledgments

This research was supported by the Grant Agency of the Czech Republic (Grants 305/02/1552), the Grant Agency of the Academy of Sciences of the Czech Republic (Grants B5004301), Wellcome Trust (Grant 073646/Z/03/Z), Edinburgh Technology Fund, and OncoSense Ltd. J.K. is the international research scholar of the Howard Hughes Medical Institute. We are grateful to Dr. Duncan Jodrell (University of Edinburgh) for providing cytotoxicity data and for stimulating discussions and comments on the manuscript. The authors acknowledge that their participation in the European Commission Cooperation in the Field of Scientific and Technical Research Chemistry Action D20 enabled them to exchange regularly the most recent ideas in the field of ruthenium anticancer drugs with several European colleagues.

Received: October 7, 2004

Revised: November 3, 2004

Accepted: November 5, 2004

Published: January 21, 2005

References

1. Keppler, B.K., Lipponer, K.-G., Stenzel, B., and Kratz, F. (1993). New tumor-inhibiting ruthenium complexes. In *Metal Complexes in Cancer Chemotherapy*, B. Keppler, ed. (Weinheim, NY: VCH Verlagsgesellschaft, VCH Publishers), pp. 187–220.
2. Clarke, M.J. (2003). Ruthenium metallopharmaceuticals. *Coord. Chem. Rev.* 236, 209–233.
3. Morris, R.E., Aird, R.E., Murdoch, P.D., Chen, H.M., Cummings, J., Hughes, N.D., Parsons, S., Parkin, A., Boyd, G., Jodrell, D.I., et al. (2001). Inhibition of cancer cell growth by ruthenium(II) arene complexes. *J. Med. Chem.* 44, 3616–3621.
4. Aird, R., Cummings, J., Ritchie, A., Muir, M., Morris, R., Chen, H., Sadler, P., and Jodrell, D. (2002). In vitro and in vivo activity and cross resistance profiles of novel ruthenium (II) organometallic arene complexes in human ovarian cancer. *Br. J. Cancer* 86, 1652–1657.
5. Sava, G., and Bergamo, A. (2000). Ruthenium-based compounds and tumour growth control (Review). *Int. J. Oncol.* 17, 353–365.
6. Wang, F., Chen, H., Parsons, S., Oswald, I.D.H., Davidson, J.E., and Sadler, P.J. (2003). Kinetics of aquation and anation of ruthenium(II) arene anticancer complexes, acidity and X-ray structures of aqua adducts. *Chem. Eur. J.* 9, 5810–5820.
7. Chen, H.M., Parkinson, J.A., Parsons, S., Coxall, R.A., Gould, R.O., and Sadler, P.J. (2002). Organometallic ruthenium(II) diamine anticancer complexes: arene-nucleobase stacking and stereospecific hydrogen-bonding in guanine adducts. *J. Am. Chem. Soc.* 124, 3064–3082.
8. Novakova, O., Chen, H., Vrana, O., Rodger, A., Sadler, P.J., and Brabec, V. (2003). DNA interactions of monofunctional organometallic ruthenium(II) antitumor complexes in cell-free media. *Biochemistry* 42, 11544–11554.
9. Nielsen, P.E. (1990). Chemical and photochemical probing of DNA complexes. *J. Mol. Recognit.* 3, 1–24.
10. Brabec, V., Sip, M., and Leng, M. (1993). DNA conformational

- distortion produced by site-specific interstrand cross-link of trans-diamminedichloroplatinum(II). *Biochemistry* 32, 11676–11681.
11. Pilch, D.S., Dunham, S.U., Jamieson, E.R., Lippard, S.J., and Breslauer, K.J. (2000). DNA sequence context modulates the impact of a cisplatin 1,2-d(GpG) intrastrand cross-link on the conformational and thermodynamic properties of duplex DNA. *J. Mol. Biol.* 296, 803–812.
12. Hofr, C., Farrell, N., and Brabec, V. (2001). Thermodynamic properties of duplex DNA containing a site-specific d(GpG) intrastrand crosslink formed by an antitumor dinuclear platinum complex. *Nucleic Acids Res.* 29, 2034–2040.
13. Malina, J., Hofr, C., Maresca, L., Natile, G., and Brabec, V. (2000). DNA interactions of antitumor cisplatin analogs containing enantiomeric amine ligands. *Biophys. J.* 78, 2008–2021.
14. Holbrook, J.A., Capp, M.W., Saecker, R.M., and Record, M.T. (1999). Enthalpy and heat capacity changes for formation of an oligomeric DNA duplex: interpretation in terms of coupled processes of formation and association of single-stranded helices. *Biochemistry* 38, 8409–8422.
15. Heiger-Bernays, W.J., Essigmann, J.M., and Lippard, S.J. (1990). Effect of the antitumor drug cis-diamminedichloroplatinum(II) and related platinum complexes on eukaryotic DNA replication. *Biochemistry* 29, 8461–8466.
16. Kasparkova, J., Novakova, O., Farrell, N., and Brabec, V. (2003). DNA binding by antitumor trans-[PtCl₂(NH₃)(thiazole)]. Protein recognition and nucleotide excision repair of monofunctional adducts. *Biochemistry* 42, 792–800.
17. Zamble, D.B., Mu, D., Reardon, J.T., Sancar, A., and Lippard, S.J. (1996). Repair of cisplatin-DNA adducts by the mammalian excision nuclease. *Biochemistry* 35, 10004–10013.
18. Reardon, J.T., Vaisman, A., Chaney, S.G., and Sancar, A. (1999). Efficient nucleotide excision repair of cisplatin, oxaliplatin, and bis-aceto-amine-dichloro-cyclohexylamine-platinum(IV) (JM216) platinum intrastrand DNA diadducts. *Cancer Res.* 59, 3968–3971.
19. Kasparkova, J., Novakova, O., Marini, V., Najajreh, Y., Gibson, D., Perez, J.-M., and Brabec, V. (2003). Activation of trans geometry in bifunctional mononuclear platinum complexes by a piperidine ligand: mechanistic studies on antitumor action. *J. Biol. Chem.* 278, 47516–47525.
20. Zehnulova, J., Kasparkova, J., Farrell, N., and Brabec, V. (2001). Conformation, recognition by high mobility group domain proteins, and nucleotide excision repair of DNA intrastrand cross-links of novel antitumor trinuclear platinum complex BBR3464. *J. Biol. Chem.* 276, 22191–22199.
21. Cohen, S.M., and Lippard, S.J. (2001). Cisplatin: from DNA damage to cancer chemotherapy. In *Progress in Nucleic Acid Research and Molecular Biology*, Volume 67, K Moldave, ed. (San Diego: Academic Press, Inc.), pp. 93–130.
22. Brabec, V. (2002). DNA modifications by antitumor platinum and ruthenium compounds: their recognition and repair. In *Progress in Nucleic Acid Research and Molecular Biology*, Volume 71, K Moldave, ed. (San Diego: Academic Press, Inc.), pp. 1–68.
23. Plum, G.E., Gelfand, C.A., and Breslauer, K.J. (1999). Physicochemical approaches to structural elucidation. Effects of 3,N₄-ethenodeoxycytidine on duplex stability and energetics. In *Exocyclic DNA Adducts in Mutagenesis and Carcinogenesis*, Publication No. 150, B. Singer, and H. Bartsch, eds. (Lyon: International Agency for Research on Cancer), pp. 169–177.
24. Maeda, Y., Nunomura, K., and Ohtsubo, E. (1990). Differential scanning calorimetric study of the effect of intercalators and other kinds of DNA-binding drugs on the stepwise melting of plasmid DNA. *J. Mol. Biol.* 215, 321–329.
25. Bjorndal, M.T., and Fygenson, D.K. (2002). DNA melting in the presence of fluorescent intercalating oxazole yellow dyes measured with a gel-based assay. *Biopolymers* 65, 40–44.
26. Jamieson, E.R., and Lippard, S.J. (1999). Structure, recognition, and processing of cisplatin-DNA adducts. *Chem. Rev.* 99, 2467–2498.
27. Ohndorf, U.M., Rould, M.A., He, Q., Pabo, C.O., and Lippard, S.J. (1999). Basis for recognition of cisplatin-modified DNA by high-mobility-group proteins. *Nature* 399, 708–712.
28. Brabec, V., and Kasparkova, J. (2002). Molecular aspects of resistance to antitumor platinum drugs. *Drug Resist. Updat.* 5, 147–161.
29. Kasparkova, J., Zehnulova, J., Farrell, N., and Brabec, V. (2002). DNA interstrand cross-links of the novel antitumor trinuclear platinum complex BBR3464. Conformation, recognition by high mobility group domain proteins, and nucleotide excision repair. *J. Biol. Chem.* 277, 48076–48086.
30. Furuta, T., Ueda, T., Aune, G., Sarasin, A., Kraemer, K.H., and Pommier, Y. (2002). Transcription-coupled nucleotide excision repair as a determinant of cisplatin sensitivity of human cells. *Cancer Res.* 62, 4899–4902.
31. Wang, D., Hara, R., Singh, G., Sancar, A., and Lippard, S.J. (2003). Nucleotide excision repair from site-specifically platinum-modified nucleosomes. *Biochemistry* 42, 6747–6753.
32. Selvakumaran, M., Pisarcik, D.A., Bao, R., Yeung, A.T., and Hamilton, T.C. (2003). Enhanced cisplatin cytotoxicity by disturbing the nucleotide excision repair pathway in ovarian cancer cell lines. *Cancer Res.* 63, 1311–1316.
33. Brabec, V., Reedijk, J., and Leng, M. (1992). Sequence-dependent distortions induced in DNA by monofunctional platinum(II) binding. *Biochemistry* 31, 12397–12402.
34. Brabec, V., and Leng, M. (1993). DNA interstrand cross-links of trans-diamminedichloroplatinum(II) are preferentially formed between guanine and complementary cytosine residues. *Proc. Natl. Acad. Sci. USA* 90, 5345–5349.
35. Murphy, J.H., and Trapane, T.L. (1996). Concentration and extinction coefficient determination for oligonucleotides and analogs using a general phosphate analysis. *Anal. Biochem.* 240, 273–282.
36. Lam, W.C., Van der Schans, E.J.C., Sowers, L.C., and Millar, D.P. (1999). Interaction of DNA polymerase I (Klenow fragment) with DNA substrates containing extrahelical bases: implications for proofreading of frameshift errors during DNA synthesis. *Biochemistry* 38, 2661–2668.
37. Patel, P.H., Suzuki, M., Adman, E., Shinkai, A., and Loeb, L.A. (2001). Prokaryotic DNA polymerase I: evolution, structure, and 'base flipping' mechanism for nucleotide selection. *J. Mol. Biol.* 308, 823–837.
38. Malina, J., Kasparkova, J., Natile, G., and Brabec, V. (2002). Recognition of major DNA adducts of enantiomeric cisplatin analogs by HMG box proteins and nucleotide excision repair of these adducts. *Chem. Biol.* 9, 629–638.

18.

Induced-fit recognition of DNA by organometallic complexes with dynamic stereogenic centers

Haimei Chen[†], John A. Parkinson[†], Olga Nováková[‡], Juraj Bella[†], Fuyi Wang[†], Alice Dawson[†], Robert Gould[†], Simon Parsons[†], Viktor Brabec^{§¶}, and Peter J. Sadler^{†¶}

[†]School of Chemistry, University of Edinburgh, West Mains Road, Edinburgh EH9 3JJ, United Kingdom; [‡]Department of Pure and Applied Chemistry, University of Strathclyde, Glasgow G1 1XQ, United Kingdom; and [§]Institute of Biophysics, Academy of Sciences of the Czech Republic, Kralovopolska 135, CZ-61265, Brno, Czech Republic

Edited by Jack Halpern, University of Chicago, Chicago, IL, and approved October 7, 2003 (received for review July 1, 2003)

Organometallic chemistry offers novel concepts in structural diversity and molecular recognition that can be used in drug design. Here, we consider DNA recognition by η^6 -arene Ru(II) anticancer complexes by an induced-fit mechanism. The stereochemistry of the dinuclear complex $[(\eta^6\text{-biphenyl})\text{RuCl}(\text{en}))_2\text{-(CH}_2\text{)}_6\text{]}^{2+}$ (**3**, en = ethylenediamine) was elucidated by studies of the half unit $[(\eta^6\text{-biphenyl})\text{RuCl}(\text{Et-en})]^+$ (**2**, where Et-en is Et(H)NCH₂CH₂NH₂). The structures of the separated $R_{\text{Ru}}^*R_{\text{N}}^*$ and $S_{\text{Ru}}^*R_{\text{N}}^*$ diastereomers of **2** were determined by x-ray crystallography; their slow interconversion in water ($t_{1/2} \approx 2$ h, 298 K, pH 6.2) was observed by NMR spectroscopy. For **2** and **3** the $R_{\text{Ru}}^*R_{\text{N}}^*$ configurations are more stable than $S_{\text{Ru}}^*R_{\text{N}}^*$ (73:27). X-ray and NMR studies showed that reactions of **2** and **3** with 9-ethylguanine gave rise selectively to $S_{\text{Ru}}^*R_{\text{N}}^*$ diastereomers. Dynamic chiral recognition of guanine can lead to high diastereoselectivity of DNA binding. The dinuclear complex **3** induced a large unwinding (31°) of plasmid DNA, twice that of mononuclear **2** (14°), and effectively inhibited DNA-directed RNA synthesis *in vitro*. This dinuclear complex gave rise to interstrand cross-links on a 213-bp plasmid fragment with efficiency similar to bifunctional cisplatin, and to 1,3-GG interstrand and 1,2-GG and 1,3-GTG intrastrand cross-links on site-specifically ruthenated 20-mers. Complex **3** blocked intercalation of ethidium considerably more than mononuclear **2**. The concept of induced-fit recognition of DNA by organometallic complexes containing dynamic stereogenic centers via dynamic epimerization, intercalation, and cross-linking may be useful in the design of anticancer drugs.

Organometallic chemistry can provide novel concepts in structural diversity and molecular recognition that can be applied to the design of pharmaceuticals (1). For example, Jaouen *et al.* (2) have designed antiestrogenic cyclopentadienyl complexes that recognize the estrogen receptor and have potential for treatment of breast cancer, and other workers have also carried out pioneering studies on the recognition of nucleobases, amino acids, and peptides by organometallic centers (1, 3–5). However, as far as we are aware, there are few investigations of specific interactions of organometallic arene complexes with natural DNA (6).

The biological chemistry of Ru(η^6 -arene) complexes is relatively unexplored, although there are many reports of their use as chiral catalysts (7–9) or as synthetic reagents for peptide synthesis (3). We have discovered the anticancer potential of the ethylenediamine (en) complexes $[(\eta^6\text{-arene})\text{RuCl}(\text{en})]^+$, which exhibit *in vitro* and *in vivo* activity, for example in a cisplatin-resistant A2780 xenograft model of human ovarian cancer (10, 11). The cytotoxicity appears to increase with increasing size of the η^6 -arene. A potential target is DNA. Complexes of the type of $[(\eta^6\text{-arene})\text{RuCl}(\text{en})]^+$ exhibit remarkably high selectivity for G compared with the other nucleobases in DNA. This is strongly related to the en NH₂ group that is attractive toward exocyclic carbonyl oxygens but repulsive toward exocyclic amino groups of nucleobases (12).

In addition, hydrophobic interactions between the arene ring and nucleobase (including arene-purine π - π stacking) have a significant influence on both the kinetics and thermodynamics of DNA binding (12, 13). DNA binding modes involving simultaneous intercalation and coordination can be proposed for this type of $[(\eta^6\text{-arene})\text{RuCl}(\text{en})]^+$ complex (14).

Here, we elaborate a multifunctional mode of DNA binding for organometallic complexes based on the linking of two $\{(\eta^6\text{-arene})\text{RuCl}(\text{diamine})\}$ units, with a flexible chain. This introduces stereogenic centers at Ru and N, giving potential for dynamic chiral DNA recognition since epimerization at these centers is expected to be facile (15–19). Such a recognition mechanism contrasts with “static” concepts, such as “shape-match” for selective DNA recognition by octahedral metallo-intercalators (20).

Experimental Procedures

Synthesis. The tetraamine ligand *N,N'*-bis(2-aminoethyl)-1,6-diaminohexane was synthesized stepwise as the tetrahydrochloride salt (Scheme 1), which is published as supporting information on the PNAS web site. This was reacted with $[(\eta^6\text{-Bip})\text{RuCl}_2]_2$ to form the dinuclear complex $[(\eta^6\text{-Bip})\text{RuCl}(\text{en}))_2\text{-(CH}_2\text{)}_6\text{]}^{2+}$ [BisRu(Bip), **3**], where Bip is biphenyl. The mononuclear complex $[(\eta^6\text{-Bip})\text{RuCl}(\text{Et-en})][\text{PF}_6]$ (**2**) was prepared by reaction of *N*-ethyl-en (Et-en) with $[(\eta^6\text{-Bip})\text{RuCl}_2]_2$. Slow diffusion of ether into a methanol solution of **2** produced crystals suitable for x-ray diffraction. Crystalline **2** consisted of a mixture of orange lumps of diastereomer **2A** ($R_{\text{Ru}}^*R_{\text{N}}^*$) and yellow flakes of diastereomer **2B** ($S_{\text{Ru}}^*R_{\text{N}}^*$), which were separated by hand. The 9-ethylguanine (9EtG) adducts $[(\eta^6\text{-Bip})\text{Ru}(N7\text{-}9\text{EtG})(\text{Et-en})]^{2+}$ (**4**) and $[(\eta^6\text{-Bip})\text{Ru}(N7\text{-}9\text{EtG})(\text{en}))_2\text{-(CH}_2\text{)}_6\text{]}^{4+}$ (**5**) were prepared by reactions of 9EtG with **2** or $[(\eta^6\text{-Bip})\text{Ru}(\text{H}_2\text{O})(\text{en}))_2\text{-(CH}_2\text{)}_6\text{]}^{4+}$ (**3ww**) in water (G/Ru = 1.2:1). Recrystallization of **4** (PF_6^- salt) from methanol gave yellow crystals suitable for x-ray diffraction. Full details of synthesis and characterization are in the *Supporting Text*, which is published as supporting information on the PNAS web site.

Kinetic Studies. Reactions of chloro or aqua complexes **1–3** (2.55 mM Ru, except 0.5 mM for **3**) with 9EtG in a 1:1 Ru/9EtG molar ratio were carried out in 10% D₂O/90% H₂O in NMR tubes. Aqua complexes were prepared by treatment of chloro com-

This paper was submitted directly (Track II) to the PNAS office.

Abbreviations: Bip, biphenyl; dien, diethylenetriamine; CT, calf thymus; en, ethylenediamine; 9EtG, 9-ethylguanine.

Data deposition: The x-ray crystal structures of complexes **2A**, **2B**, and **4** have been deposited in the Cambridge Structural Database, Cambridge Crystallographic Data Centre, Cambridge CB2 1EZ, United Kingdom, (CSD reference nos. 223919, 223918, and 223917, respectively).

[¶]To whom correspondence should be addressed. E-mail: brabec@ibp.cz or p.j.sadler@ed.ac.uk.

© 2003 by The National Academy of Sciences of the USA

plexes with a stoichiometric amount of AgNO₃. Interconversion of diastereomers **2A** and **2B** (0.5 mM Ru) was studied in D₂O in NMR tubes. When necessary, 180 mM NaCl was used to suppress hydrolysis. Interconversion rate constants (k_1 , **2A** → **2B**; k_{-1} , **2B** → **2A**) were obtained by fitting rate equations for first-order reversible reactions by using the program SCIENTIST (version 2.0, MicroMath, St. Louis).

DNA Modification. Calf thymus (CT) DNA and plasmid DNAs were incubated with metal complexes in 10 mM NaClO₄ at 310 K for 48 h in the dark, unless stated otherwise. The molar ratios of bound metal complex to nucleotide phosphate (r_b) were determined by flameless atomic absorption spectrophotometry. CD spectra of DNA modified by **3** were recorded at 298 K on a Jasco (Tokyo) J-720 spectropolarimeter, after samples had been incubated for 24 h at 310 K and then dialyzed for 2 days at 277 K in 10 mM NaClO₄.

DNA Transcription by RNA Polymerase *in Vitro*. Transcription of the (*Nde*I/*Hpa*I) restriction fragment of pSP73KB DNA with SP6 or T7 RNA polymerase and electrophoretic analysis of transcripts were performed according to the protocols recommended by Promega as described (21). Before aliquots containing the transcripts were loaded on the polyacrylamide gel, the radioactivity associated with these samples was adjusted so that equal amounts of radioactivity were loaded into each well. For comparative purposes, the intensity at each site was determined by calculating the peak area and the background was subtracted. The average relative intensities of each band from three independent experiments were compared.

Unwinding of Negatively Supercoiled DNA. Unwinding of closed circular supercoiled pSP73KB plasmid DNA was studied by an agarose gel mobility-shift assay (22). The mean unwinding angle $\Phi = 18 \sigma/r_b(c)$, where σ is the superhelical density, and $r_b(c)$ the value of r_b at which the supercoiled and nicked forms comigrate. Under the present experimental conditions, σ was calculated to be -0.063 based on cisplatin for which $\Phi = 13^\circ$. Experimental details are given in *Supporting Text*.

X-Ray Crystallography. Diffraction data for all compounds were collected with Mo-K α radiation, for **2A**, at 220 K on a Stoe (Darmstadt, Germany) Stadi-4 diffractometer, for **2B** and **4** at 150 K on a Bruker-AXS (Madison, WI) SMART APEX CCD diffractometer; both were equipped with Oxford Cryosystems (Long Hanborough, U.K.) low-temperature devices. Absorption corrections were carried out by using ψ -scans or the multiscan procedure SADABS (23). All structures were solved by direct methods and refined against F^2 by using all data [SHELXTL (24) for **2A** and **2B**, CRYSTALS (25) for **4**]. H atoms were placed in calculated positions, and non-H atoms were modeled with anisotropic displacement parameters. WEBLAB VIEWERPRO 4.0 was used for the graphics in Fig. 2.

NMR Spectroscopy. NMR data were acquired on Bruker DMX 500 (¹H = 500 MHz) and Avance 600 (¹H = 600 MHz) spectrometers. Standard pulse sequences were used for 2D heteronuclear single quantum coherence (HSQC), total correlation spectroscopy, COSY, double quantum filtered COSY, NOESY (mixing time up to 1,000 ms), and rotating-frame Overhauser effect spectroscopy (mixing time 150 ms). The water resonance was suppressed via the double pulsed-field-gradient spin-echo method (26). 2D [¹H,¹⁵N] HSQC NMR spectra were acquired for complexes **2-5** with ¹⁵N in natural abundance. Data processing was carried out by using XWIN-NMR (version 3.0, Bruker Biospin, Karlsruhe, Germany). ¹H NMR chemical shifts were internally referenced to (CD₂H)₂SO (2.50 ppm), (CD₂H)₂CO (2.06 ppm), sodium 3-(trimethylsilyl)-2,2,3,3-d₄-propionate (0

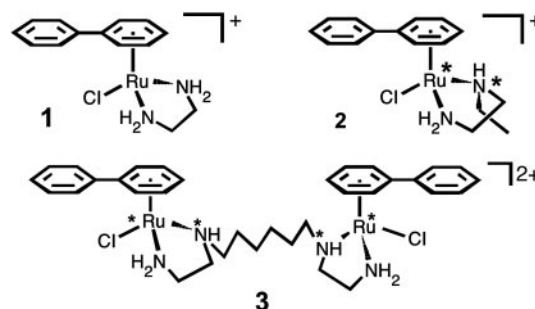


Fig. 1. Structures of mono- and bis-Ru(Bip) chloride complexes. * indicate stereogenic centers.

ppm), or dioxane (3.76 ppm), and ¹⁵N to 1 M ¹⁵NH₄Cl in 1.5 M HCl (external) at 0 ppm.

Molecular Modeling. Modeling was carried out by using SYBYL (version 6.3, Tripos Associates, St. Louis) by docking a model of {((η^6 -Bip)Ru(*N*7-G)(en))₂-(CH₂)₆}, based on the x-ray structure of **4**, onto B-form duplex DNA 5'-AATGTCTAA-3'/3'-TTACAGATT-5'.

Supporting Information. Full details for experimental procedures (materials, synthesis, acidity constants, DNA experiments, and kinetics), Tables 1–4 (crystallographic data, rate constants, half-lives, equilibrium constants), and Figs. 6–21 (¹H NMR, 2D COSY, heteronuclear single quantum coherence, NOESY, and rotating-frame Overhauser effect spectroscopy spectra for **2-5**; kinetics of 9EtG and CT DNA binding, cross-linking, ethidium fluorescence, modeling) are published as supporting information on the PNAS web site.

Results and Discussion

Stereogenic Preferences and Epimerization Rates. We synthesized the dinuclear complex [(η^6 -Bip)RuCl(en))₂-(CH₂)₆]²⁺ [BisRu(Bip), **3**] by linking two {(η^6 -Bip)RuCl(en)} units with a hexamethylene chain, which is long and flexible enough to allow each Ru unit to behave independently (Fig. 1). The strategy of linking two or three Pt centers has already been used successfully in drug design (27). Complex **3** contains four stereogenic centers (Ru, N, N, Ru), giving rise to 10 possible configurations (Fig. 13). Studies of the mononuclear analogue [(η^6 -Bip)RuCl(en))⁺ (**2**), which contains similar stereogenic Ru and N centers, allowed subsequent elucidation of the structure and dynamics of **3**.

Synthesis of **2** gave rise to two diastereomers **2A**(*R*_{Ru}^{*}*R*_N^{*}) and **2B**(*S*_{Ru}^{*}*R*_N^{*}) (28)^{||} in a 73.7:26.3 mol ratio, as revealed by x-ray crystallography (Figs. 2 and 6) and NMR studies (Figs. 8–11). The 2D [¹H,¹⁵N] heteronuclear single quantum coherence NMR spectra of **2** and **3** in DMSO-*d*₆ are almost identical (Fig. 8), suggesting that each Ru unit of **3** is present as either an *A*(*R*_{Ru}^{*}*R*_N^{*}) or *B*(*S*_{Ru}^{*}*R*_N^{*}) configuration and that each Ru unit has little influence on the other. Complex **3** can be treated as a diastereomeric mixture of *AA* (I), *AB* (II), and *BB* (III) (Figs. 3A, 12, and 13). The *AA*/*AB*/*BB* ratio was determined to be 67.7:24.0:8.3 by 2D total correlation spectroscopy NMR (Fig. 3B), consistent with that of 72.9:27.1 for *A*/*B* from 2D [¹H,¹⁵N] NMR (Fig. 8ii).

The displacement of Cl by H₂O appears to have negligible

^{||}The formal absolute configuration at Ru was determined by using the general priority order: Bip > Cl/O/N7 > N2 > N1 for diastereomers **2A**(Cl, H₂O), **2B**(Cl, H₂O), and **4**(*N*7-9EtG) (28). No CD signals were detected for **2A**, **2B**, or **4** in DMSO or water, consistent with each diastereomer being present as an enantiomeric pair in a 1:1 ratio as in the crystals.

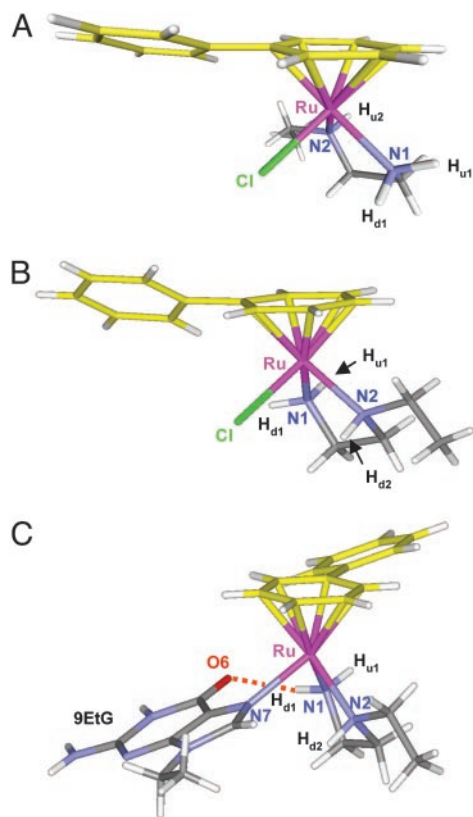


Fig. 2. Structures of $R_{Ru}R_N$ (**2A**) (A) and $S_{Ru}R_N$ (**2B**) (B) diastereomers of $[(\eta^6\text{-Bip})\text{RuCl}(\text{Et-en})]^+$, and $S_{Ru}R_N$ (**4**) diastereomer of $[(\eta^6\text{-Bip})\text{Ru}(\text{N7-9EtG})(\text{Et-en})]^{2+}$ (C) [H-bonds $\text{O6}\cdots\text{H-N1}$: $\text{O6}\cdots\text{N1}$ 2.840 (7) Å, $\angle\text{N1-H}\cdots\text{O6}$ 160.72°]. Their respective enantiomers **2A'** ($S_{Ru}S_N$), **2B'** ($R_{Ru}S_N$), and **4'** ($R_{Ru}S_N$) are present in the same unit cell. In text, labels **A** ($R_{Ru}^*R_N^*$) and **B** ($S_{Ru}^*R_N^*$) refer to the enantiomeric pairs **A** ($R_{Ru}R_N/S_{Ru}S_N$) and **B** ($S_{Ru}R_N/R_{Ru}S_N$). Crystallographic data are in Tables 1 and 2. Note that H on N2 points toward the coordinated arene in **A** ($R_{Ru}^*R_N^*$) but away in **B** ($S_{Ru}^*R_N^*$).

influence on the configurational abundance of **A** ($R_{Ru}^*R_N^*$) and **B** ($S_{Ru}^*R_N^*$) for the aqua complexes **2w** and **3ww** (for structures, see Fig. 7), as revealed by NMR, the ratio of 77:23 was found for **2Aw** ($R_{Ru}^*R_N^*$)/**2Bw** ($S_{Ru}^*R_N^*$). The ^1H NMR spectrum for the linker of **3ww** showed a similarly complicated pattern as for **3** (Cl,Cl) and indicated that the aqua Ru units adopt both **A** ($R_{Ru}^*R_N^*$) and **B** ($S_{Ru}^*R_N^*$) configurations, with type **A** predominating as for **3** (Cl,Cl). Under the present experimental conditions, **2Aw** and **2Bw** are largely protonated since the pK_a (H_2O) values are $7.57(\pm 0.01)$ and $7.35(\pm 0.01)$, respectively (Fig. 17).

The dynamic interconversion of diastereomers **2A** and **2B** was studied by ^1H NMR spectroscopy at 298 K. Separated **2A** (or **2B**) was observed to convert slowly into **2B** (or **2A**) on dissolution in D_2O (containing 180 mM NaCl to suppress hydrolysis) (Figs. 7 and 9), with the equilibrium ratio of $\text{2B}/\text{2A} = 28:72$ (Table 3). The rate constant was determined to be $k_{-1} 4.3 \times 10^{-3} \text{ min}^{-1}$ for $\text{2B}(\text{Cl}) \rightarrow \text{2A}(\text{Cl})$, 2.5 times faster than the reverse reaction ($k_1 1.7 \times 10^{-3} \text{ min}^{-1}$) at pH 6.2, half-life 117 min (Table 3). The inversion rate at N for $R/S(\text{N})$ -[PtCl₂(*R*-2-[2-methyl-2-aminopropyl]amino)-1-butanol] is reported to be of a similar order of magnitude (18). With no added NaCl, a stepwise conversion from **2A**(Cl) to **2A**(H_2O), to **2B**(H_2O), then to **2B**(Cl) was observed with a half-life of 150 min (Figs. 7i and 9iv). The equilibrium ratio was 18.5 **2A**(Cl):52.2 **2A**(H_2O):9.5 **2B**(Cl):19.8 **2B**(H_2O). The interconversion rate was slightly faster at pH 2.0 ($t_{1/2}$ 98 min), but much faster at pH 9.2 ($t_{1/2}$ 60 min, Table 3). No interconversion was observed in DMSO solution (Fig. 9i).

Each Ru unit of **3**(Cl or H_2O) can be envisioned to undergo a similar interconversion process in aqueous solution, giving rise to the same observed equilibrium ratio of 72 **A**:28 **B** as for **2**. Our studies suggest that for both **2** and **3** (Cl or H_2O) the **A** ($R_{Ru}^*R_N^*$) configurations are thermodynamically preferred, and that each Ru unit is in dynamic equilibrium between configurations **A** ($R_{Ru}^*R_N^*$) and **B** ($S_{Ru}^*R_N^*$).

Diastereoselectivity in Guanine N7 Recognition. Reaction of 9EtG with the diastereomeric mixture of **3** (**A/B** = 72.9:27.1) or **2** (**A/B** = 73.7:26.3) gave rise to the final products $[(\eta^6\text{-Bip})\text{Ru}(\text{N7-9EtG})(\text{en}))_2\text{-(CH}_2\text{)}_6]^{4+}$ (**5**) and $[(\eta^6\text{-Bip})\text{Ru}(\text{N7-9EtG})(\text{Et-en}))]^{2+}$ (**4**), respectively, with $\approx 90\%$ formation (Fig. 7). N7 coordination for **4**, **5**, and **3gw** [intermediate (9EtG-N7)Ru~Ru(H_2O)] was confirmed by pH titrations, giving associated pK_a values: $\text{pK}_a(\text{G N1H})$ 8.03 (**4**), 7.83 (**3gw**), 7.86 (**5**), compared with 9.66 (G N1H) and 2.4 (G N7) for free 9EtG (Figs. 7 and 14).

Analysis of the configurations of **5** was aided by the structural analysis of **4**. X-ray crystallography (Figs. 2C and 6iv) and NMR studies (Figs. 8 and 15) showed that **4** contains a single (95%) diastereomeric pair **B** ($S_{Ru}^*R_N^*$), with the N2 H_{d2} proton pointing down toward the G base. Complex **5** showed one set of en NH crosspeaks in the 2D [^1H , ^{15}N] heteronuclear sequential quantum correlation NMR spectrum (acetone- d_6), almost identical to that for **4** (Fig. 8), indicating that each Ru unit of **5** has the same configuration **B** ($S_{Ru}^*R_N^*$) as for **4**. This was confirmed by other 2D NMR data (Figs. 3C and 16).

The **B** ($S_{Ru}^*R_N^*$) configurations are therefore highly favored (95%) for the 9EtG adducts **4** and **5** (Figs. 7 and 8), whereas the **A** ($R_{Ru}^*R_N^*$) configurations are strongly destabilized by steric interactions between G and the en alkyl substituent. This finding is in contrast to their parent chloro complexes **2** or **3** and their aqua adducts, for which the **A** ($R_{Ru}^*R_N^*$) configuration is thermodynamically preferred (72%) and in which the en alkyl substituent points down toward Cl or H_2O . Displacement of Cl or H_2O by 9EtG forces the alkyl substituent to tilt up and to give the **B** configuration, which can be stabilized by stereospecific H bonding between en NH and G O6 (Fig. 2). Facile epimerization at Ru or N centers appears to allow dynamic switching between configurations, leading to high diastereoselectivity in the formation of G adducts.^{††} In a reported study (5), reaction of the diastereomeric mixture of $[(\eta^6\text{-C}_6\text{H}_6)\text{RuCl}(\text{L-ala})]$ with 9EtG did not change the abundance of $R_{Ru}S_C$ and $S_{Ru}S_C$ (65:35). In this case, the $\alpha\text{-C}$ center has a fixed configuration S_C and no epimerization potential; its methyl substituent is distant from the G base and has little influence on the reaction.

Structural and dynamic studies of interactions of 9EtG with **3** and **2** provided insights into the recognition of natural DNA by **3**. Substitution of an en NH proton in **1** by the alkyl group to give **2** or **3** (Fig. 1) had little effect on the kinetics of reaction of the chloro complexes with CT DNA (**1**, $t_{1/2}$ 10 min; **3**, $t_{1/2}$ 15 min), or on reactions of the aqua (**1w**, **2w**, **3ww**: $t_{1/2} \approx 35$ min) or chloro (**1**, **2**: $t_{1/2} \approx 85$ min) complexes with 9EtG (Table 4). All of these reactions were $>80\%$ complete, indicating that the alkyl substituent does not significantly hinder G binding when epimerization is facile.

Dinuclear BisRu(Bip) Distorts DNA. The dinuclear complex **3** binds rapidly to CT DNA (Fig. 18). The binding was stable with little loss of bound Ru after extensive dialysis in 0.01 M NaClO₄ or

^{††}NMR data for the 5' GMP adducts $[(\eta^6\text{-Bip})\text{Ru}(\text{N7-5'GMP})(\text{Et-en}))]^{2+}$ (H8: 8.73 and 8.82 ppm) and $[(\eta^6\text{-Bip})\text{Ru}(\text{N7-5'GMP})(\text{en}))_2\text{-(CH}_2\text{)}_6]^{4+}$ (H8: 8.72 and 8.83 ppm) are consistent with this interpretation. ^1H NMR peaks for the $S_{Ru}R_N$ -($\beta\text{-D}$) and $R_{Ru}S_N$ -($\beta\text{-D}$) diastereomers were present in a 1:1 mol ratio (10% D_2O , pH 7.2), suggesting that there may be no enantioselectivity between $S_{Ru}R_N$ and $R_{Ru}S_N$ for DNA binding.

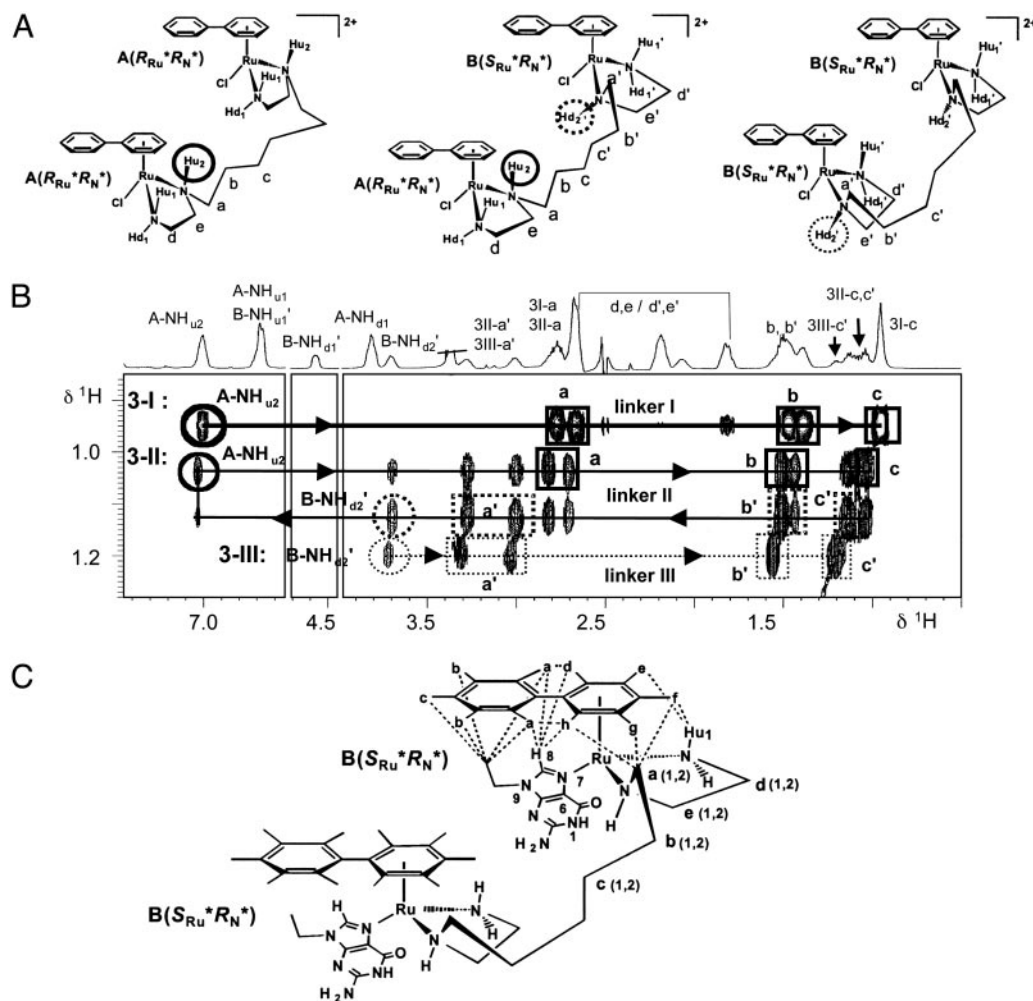


Fig. 3. Configurations of dinuclear complexes **3** and **5**. (A) Diastereomers AA (**3-I**, 68%), AB, (**3-II**, 24%) and BB (**3-III**, 8%) for **3**, with species distribution (%) based on 2D total correlation spectroscopy (TOCSY) cross-peak intensities. For full structures, see Fig. 13. (B) 2D TOCSY NMR spectrum of en NH and linker CH₂ region of **3** in DMSO-*d*₆, showing three spin-systems, with cross-peak connectivities of NH_{u2}→a→b→c for **3-I** (thick solid line), NH_{u2}→a→b→c→c'→b'→a'→NH_{d2'} for **3-II** (thin solid line), and NH_{d2'}→a'→b'→c' for **3-III** (dotted line). (C) Structure of 9EtG adduct **5** with rotating-frame Overhauser effects indicated by dotted lines. A single set of signals for **5** was detected by 2D NMR (Figs. 8iv and 16), suggesting the presence of **B**(*S*_{Ru}^{*}*R*_N^{*}) configuration for each Ru unit and *syn* conformation for the pendant phenyl ring with respect to 9EtG. Adduct **5** is mainly present as configuration BB (95%). Labels a-e and a'-e' represent a pair of (nonequivalent) protons on the same C.

1.0 M NaCl. An assay of DNA-directed RNA synthesis revealed that each Ru unit of **3** coordinates preferentially to G bases of DNA (Fig. 4). Complex **3** shows termination sequences somewhat different from cisplatin, although the intensity of the bands corresponding to major stop sites was similar (Fig. 4A). Furthermore, adducts of complex **3** inhibit RNA synthesis more effectively than those of mononuclear complexes **1** (14), **2** (Fig. 4A), and **2A** (data not shown). The pattern of stop sites for transplatin is different, and no termination is observed for monofunctional [Pt(dien)Cl]⁺ (dienPt, Fig. 4A), where dien is diethylenetriamine. The higher sequence preference of **3** for G can be attributed to interactions with en NH, being attractive toward exocyclic carbonyl oxygens but repulsive toward exocyclic amino groups of nucleobases (12). We can assume that binding of **3** to double-helical DNA involves dynamic chiral recognition in a similar manner to the reaction of **3** with 9EtG (Figs. 7iii and 3C), with preferential formation of the **B**(*S*_{Ru}^{*}*R*_N^{*}) configuration. This allows most of **3** (84%) to coordinate to DNA.

Conformational distortions of DNA induced by **3** are evident from CD spectra (Fig. 5A). Binding of **3** to CT DNA induced a

positive CD band centered ≈370–380 nm with increasing intensity as a function of *r*_b. This band may arise from coupling between the transition dipole moment of nucleobases and the bound metal complex, suggesting intercalation of the extended phenyl ring into DNA, or groove binding (29). This spectral change is similar to that observed for mononuclear **1** (14). Such induced CD bands are not observed for reaction of CT DNA with the analogs [(η⁶-*p*-cymene)RuCl(en)]⁺ and [(η⁶-benzene)RuCl(en)]⁺ where the *p*-cymene or benzene ring cannot insert into DNA base pairs.

The CD results correlate with those of plasmid DNA unwinding. A large unwinding angle of 31° per dinuclear complex was induced by binding of **3** to pSP73KB DNA (Fig. 5B), twice that for the mononuclear complexes **1** (14°) (14) and **2** (14°, Fig. 5C) and **2A** (data not shown). Previous studies (14) have shown that **1** induces an unwinding angle twice that of [(η⁶-*p*-cymene)RuCl(en)]⁺ (7°) because of the contribution from the Bip ring, possibly by intercalation. Compared with the DNA unwinding induced by the linkage isomers *cis*-[Pt(NH₃)₂(N3/N8-ethidium)Cl]²⁺ [15°/19° (22)], the dinuclear complex [*trans*-PtCl(NH₃)₂]₂-H₂N(CH₂)₆NH₂]²⁺ [10° (30)], trinuclear

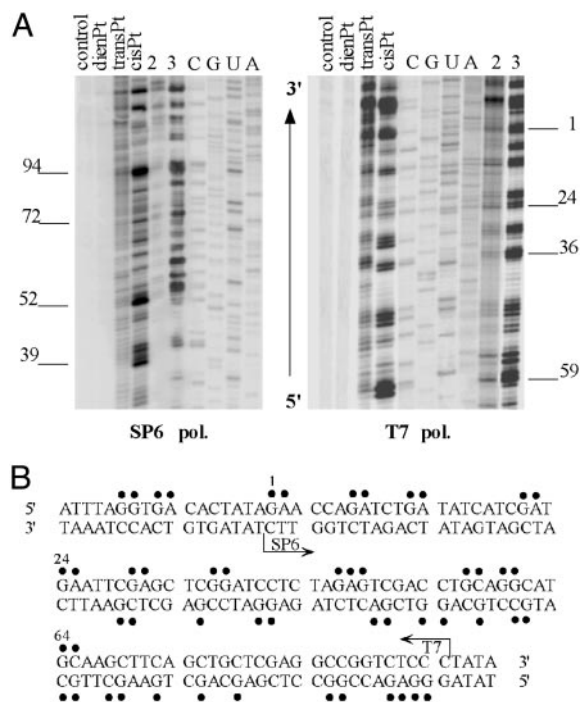


Fig. 4. Inhibition of RNA synthesis. (A) Autoradiograms of 6% polyacrylamide/8 M urea sequencing gels showing inhibition of RNA synthesis by SP6 (Left) or T7 RNA polymerases (Right) on the *NdeI/HpaI* fragment containing adducts of Ru and Pt complexes (r_b 0.01). Lanes are: unmodified template control; templates modified by dienPt, transPt, cisPt, 2 and 3; C, G, U and A (chain terminated marker RNAs). (B) Schematic diagram showing portion of sequence used to monitor inhibition of RNA synthesis by 3. Arrows indicate start of SP6 and T7 RNA polymerase, which used the bottom or upper strand of *NdeI/HpaI* fragment as templates. ● indicate major stop signals (from A) for 3. Numbers correspond to nucleotide numbering in the sequence map of pSP73KB plasmid.

BBR3464 [14° (31°)], and mononuclear transplatin (9°), the larger unwinding angle (31°) induced by **3** can be attributed to cross-linking of DNA and perturbation of DNA structure by the two pendant phenyl rings. Additionally, complex **3** blocked intercalation of ethidium (about two times) more effectively than mononuclear **2** (Fig. 20), and **2** is more effective than $[(\eta^6\text{-}p\text{-cymene})\text{RuCl}(\text{en})]^+$ (**14**) or $[\text{Pt}(\text{dien})\text{Cl}]^+$ (Fig. 20). These results suggest that both the linker chain and phenyl rings contribute to the interaction.

The Bip ligand possesses fluxionality through rotation around the arene-Ru bonds and propeller twisting of Bip (**13**). NMR studies on the 9EtG products **4** (Fig. 15) and **5** (Fig. 3C) show that in solution the guanine base is *syn* to the pendant phenyl ring, indicating potential hydrophobic interactions between Bip and nucleobase (**13**), which could stabilize intercalation into duplex DNA.

Further evidence for DNA cross-linking by **3** was obtained. The efficiency of interstrand cross-linking on a 213-bp *NdeI/EcoRI* fragment of pSP73 randomly modified by **3** ($\approx 5\%$ frequency) was similar to that for cisplatin (Fig. 5D), and a site-specifically ruthenated 20-mer formed a 1,3-GG (5' to 5') interstrand cross-link (20% frequency, Fig. 19). Studies of -TGGT- and -TGTGT- 20-mer duplexes showed that complex **3** is also able to form intrastrand 1,2-GG and 1,3-GTG cross-links. A model for possible 1,3 interstrand cross-linking by **3** on B-form duplex DNA (5'-AATGTCTAA-3'/3'-TTACAGATT-5') is shown in Fig. 21. Each Ru unit adopts the $B(S_{\text{Ru}}^*R_{\text{N}}^*)$ configuration, and the two Ru atoms are coordinated to N7 of G4 and G13 with en NH H-bonding to G O6. The pendant phenyl ring from each Bip is partially intercalated

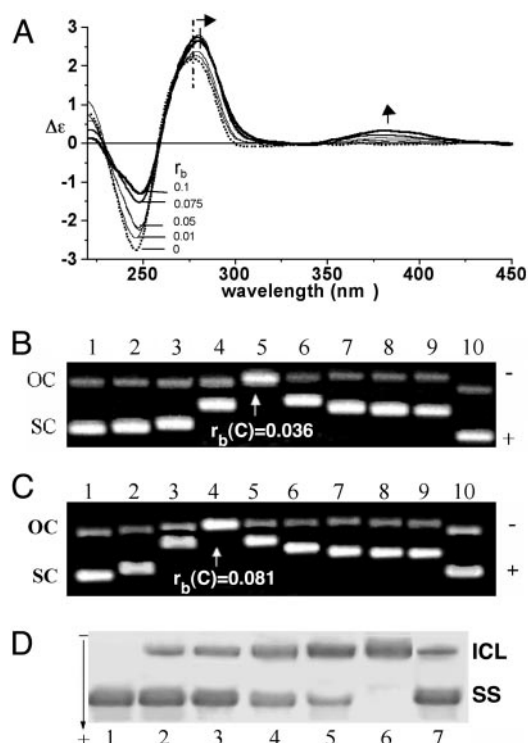


Fig. 5. (A) CD spectra of CT DNA modified by **3** (298 K, r_b 0–0.1, DNA 30 $\mu\text{g}\cdot\text{ml}^{-1}$). (B) Unwinding of supercoiled pSP73KB plasmid DNA by **3**. Plasmid DNA modified by **3** with r_b values of 0.004, 0.008, 0.017, 0.036, 0.05, 0.067, 0.076, and 0.084 corresponds to lanes 2–8. Lanes 1 and 10 show control, unmodified DNA ($r_b = 0$). The coalescence point (comigration of OC and SC) corresponds to $r_b(c)$ of 0.036 and unwinding angle Φ of $31 \pm 2^\circ$. (Upper) Nicked plasmid, open circular (OC); (Lower) closed negatively supercoiled plasmid (SC). (C) Unwinding of supercoiled pSP73KB plasmid DNA by **2**. Plasmid DNA modified by **2** with r_b values of 0.03, 0.06, 0.081, 0.10, 0.11, 0.13, 0.16, and 0.17 corresponds to lanes 2–8. Lanes 1 and 10 indicate control, unmodified DNA ($r_b = 0$). The coalescence point corresponds to $r_b(c)$ of 0.081 and unwinding angle Φ of $14 \pm 2^\circ$. (D) Formation of interstrand cross-links by dinuclear **3** and cisplatin in linear *NdeI/EcoRI* fragment of pSP73 plasmid (213 bp). Autoradiogram of native 1% agarose gel of 3' end-labeled DNA fragment. Interstrand cross-linked (ICL) DNA appears as the top bands migrating more slowly than single-stranded (SS) DNA in the bottom bands. Fragment modified by **3** with r_b of 0.015, 0.03, 0.05, 0.08, and 0.10 corresponds to lanes 2–6, and by cisplatin with r_b of 0.015 corresponds to lane 7. Lane 1 indicates nonmodified fragment (control).

into the DNA base pairs. Modeling therefore suggests that the multifunctional interactions with DNA proposed for **3** are compatible.

In contrast to octahedral metalointercalators such as Tris-(phenanthroline)Ru(II) derivatives (**20**, **32**), $[\text{Ru}(\text{phenanthroline})_2\text{Cl}_2]$ (**33**), and $[\text{Ru}(\text{bipyridine})_2\text{Cl}_2]$ (**34**), which are essentially inert to racemization, have rigid frameworks, and recognize DNA mainly by shape-match (**20**), the $\{(\eta^6\text{-arene})\text{Ru}(\text{II})\}$ complexes studied here have dynamic stereogenic centers and fluxional $\eta^6\text{-arene}$ ligands. Binding of these Ru-(arene) complexes to DNA can be accompanied by configurational changes that allow recognition by an induced fit mechanism. It should be possible to enhance DNA recognition by modification of the chelate en, the linker and the arene ring system. DNA is also flexible and can optimize its fit with Ru(arene) via unwinding, base-twisting, and bending (**35**). Distortions of DNA structure are recognized by downstream processing, including protein binding (**36**), and can play an important role in anticancer activity. Such considerations may aid the design of clinically more effective antitumor drugs, and thus

expand the potential of organometallic (η^6 -arene)Ru(II) complexes in medicine.

We thank European Community Cooperation in Science and Technology Action D20 and Dr. D. Jodrell and colleagues (Western General Hospital, Edinburgh) for stimulating discussions and Drs. E. Zhang and

P. Wang for advice on amine synthesis. We thank the Committee of Vice-Chancellors and Principals for an Overseas Research Scholarship Award (to H.C.), the Wellcome Trust, the Grant Agency of the Czech Republic (Grants 305/02/1552 and 305/01/0418) and the Grant Agency of the Academy of Science of the Czech Republic (Grant A5004101) for support.

1. Fish, R. H. & Jaouen, G. (2003) *Organometallics* **22**, 2166–2177.
2. Jaouen, G., Vessièrès, A. & Butler, I. S. (1993) *Acc. Chem. Res.* **26**, 361–369.
3. Severin, K., Bergs, R. & Beck, W. (1998) *Angew. Chem. Int. Ed.* **37**, 1634–1654.
4. Kuo, L. Y., Kanatzidis, M. G., Sabat, M., Tipton, A. L. & Marks, T. J. (1991) *J. Am. Chem. Soc.* **113**, 9027–9045.
5. Sheldrick, W. S. & Heeb, S. (1990) *Inorg. Chim. Acta* **168**, 93–100.
6. Gopal, Y. N. V., Jayaraju, D. & Kondapi, A. K. (1999) *Biochemistry* **38**, 4382–4388.
7. Consiglio, G. & Morandini, F. (1987) *Chem. Rev.* **87**, 761–778.
8. Faller, J. W., Patel, B. P., Albrizzio, M. A. & Curtis, M. (1999) *Organometallics* **18**, 3096–3104.
9. Davies, D. L., Fawcett, J., Garratt, S. A. & Russell, D. R. (2001) *Organometallics* **20**, 3029–3034.
10. Aird, R. E., Cummings, J., Ritchie, A. A., Muir, M., Morris, R. E., Chen, H., Sadler, P. J. & Jodrell, D. I. (2002) *Br. J. Cancer* **86**, 1652–1657.
11. Morris, R. E., Aird, R. E., del Socorro Murdoch, P., Chen, H., Cummings, J., Hughes, N. D., Parsons, S., Parkin, A., Boyd, G., Jodrell, D. I. & Sadler, P. J. (2001) *J. Med. Chem.* **44**, 3616–3621.
12. Chen, H., Parkinson, J. A., Morris, R. E. & Sadler, P. J. (2003) *J. Am. Chem. Soc.* **125**, 173–186.
13. Chen, H., Parkinson, J. A., Parsons, S., Coxall, R. A., Gould, R. O. & Sadler, P. J. (2002) *J. Am. Chem. Soc.* **124**, 3064–3082.
14. Novakova, O., Chen, H., Vrana, O., Rodger, A., Sadler, P. J. & Brabec, V. (2003) *Biochemistry* **42**, 11544–11554.
15. Brunner, H. (2001) *Eur. J. Inorg. Chem.* 905–912.
16. Faller, J. W., Parr, J. & Lavoie, A. R. (2003) *New J. Chem.* **27**, 899–901.
17. Buckingham, D. A., Marzilli, L. G. & Sargeson, A. M. (1969) *J. Am. Chem. Soc.* **91**, 5227–5232.
18. Saito, R., Goto, M., Hirose, J. & Kidani, Y. (1992) *Bull. Chem. Soc. Jpn.* **65**, 1428–1437.
19. Williams, K. M., Scarcia, T., Natile, G. & Marzilli, L. G. (2001) *Inorg. Chem.* **40**, 445–454.
20. Erkkila, K. E., Odom, D. T. & Barton, J. K. (1999) *Chem. Rev.* **99**, 2777–2795.
21. Brabec, V. & Leng, M. (1993) *Proc. Natl. Acad. Sci. USA* **90**, 5345–5349.
22. Keck, M. V. & Lippard, S. J. (1992) *J. Am. Chem. Soc.* **114**, 3386–3390.
23. Siemens Industrial Automation (1996) SADABS: *Area-Detector Absorption Correction* (Siemens Industrial Automation, Madison, WI).
24. Sheldrick, G. M. (2001) SHELXTL (Univ. of Göttingen, Göttingen, Germany).
25. Watkin, D. J., Prout, C. K., Carruthers, J. R., Betteridge, P. W. & Cooper, R. I. (2003) CRYSTALS (Chemical Crystallography Laboratory, Oxford, U.K.).
26. Hwang, T.-L. & Shaka, A. J. (1995) *J. Magn. Reson. Ser. A* **112**, 275–279.
27. Farrell, N., Qu, Y., Bierbach, U., Valsecchi, M. & Menta, E. (1999) in *Cisplatin: Chemistry and Biochemistry of a Leading Anticancer Drug*, ed. Lippert, B. (Wiley, Weinheim, Germany), pp. 479–496.
28. Stanley, K. & Baird, M. C. (1975) *J. Am. Chem. Soc.* **97**, 6598–6599.
29. Pasternack, R. F., Gibbs, E. J. & Villafranca, J. J. (1983) *Biochemistry* **22**, 2406–2414.
30. Farrell, N., Appleton, T. G., Qu, Y., Roberts, J. D., Soares Frontes, A. P., Skov, K. A., Wu, P. & Zou, Y. (1995) *Biochemistry* **34**, 15480–15486.
31. Brabec, V., Kašpárková, J., Vrána, O., Nováková, O., Cox, J. W., Qu, Y. & Farrell, N. (1999) *Biochemistry* **38**, 6781–6790.
32. Barton, J. K., Basile, L. A., Danishefsky, A. & Alexandrescu, A. (1984) *Proc. Natl. Acad. Sci. USA* **81**, 1961–1965.
33. Barton, J. K. & Lolis, E. (1985) *J. Am. Chem. Soc.* **107**, 708–709.
34. Grover, N., Gupta, N. & Thorp, H. H. (1992) *J. Am. Chem. Soc.* **114**, 3390–3393.
35. Bostock-Smith, C. E., Harris, S. A., Laughton, C. A. & Searle, M. S. (2001) *Nucleic Acids Res.* **29**, 693–702.
36. Zamble, D. & Lippard, S. J. (1999) in *Cisplatin: Chemistry and Biochemistry of a Leading Anticancer Drug*, ed. Lippert, B. (Wiley, Weinheim, Germany), pp. 73–110.

19.

DNA–protein cross-linking by *trans*-[PtCl₂(*E*-iminoether)₂]. A concept for activation of the *trans* geometry in platinum antitumor complexes

Olga Novakova, Jana Kasparkova, Jaroslav Malina, Giovanni Natile¹ and Viktor Brabec*

Institute of Biophysics, Academy of Sciences of the Czech Republic, CZ-61265 Brno, Czech Republic and

¹Department of Pharmaceutical Chemistry, University of Bari, I-70125 Bari, Italy

Received August 26, 2003; Revised and Accepted September 30, 2003

ABSTRACT

The structure–pharmacological activity relationships generally accepted for antitumor platinum compounds stressed the necessity for the *cis*-[PtX₂(amine)₂] structure while the *trans*-[PtX₂(amine)₂] structure was considered inactive. However, more recently, several *trans*-platinum complexes have been identified which are potently toxic, antitumor-active and demonstrate activity distinct from that of conventional cisplatin (*cis*-[PtCl₂(NH₃)₂]). We have shown in the previous report that the replacement of ammine ligands by iminoether in transplatin (*trans*-[PtCl₂(NH₃)₂]) results in a marked enhancement of its cytotoxicity so that it is more cytotoxic than its *cis* congener and exhibits significant antitumor activity, including activity in cisplatin-resistant tumor cells. In addition, we have also shown previously that this new *trans* compound (*trans*-[PtCl₂(*E*-iminoether)₂]) forms mainly monofunctional adducts at guanine residues on DNA, which is generally accepted to be the cellular target of platinum drugs. In order to shed light on the mechanism underlying the antitumor activity of *trans*-[PtCl₂(*E*-iminoether)₂] we examined oligodeoxyribonucleotide duplexes containing a single, site-specific, monofunctional adduct of this transplatin analog by the methods of molecular biophysics. The results indicate that major monofunctional adducts of *trans*-[PtCl₂(*E*-iminoether)₂] locally distort DNA, bend the DNA axis by 21° toward the minor groove, are not recognized by HMGB1 proteins and are readily removed from DNA by nucleotide excision repair (NER). In addition, the monofunctional adducts of *trans*-[PtCl₂(*E*-iminoether)₂] readily cross-link proteins, which markedly enhances the efficiency of this adduct to terminate DNA polymerization by DNA polymerases *in vitro* and to inhibit removal of this adduct from

DNA by NER. It is suggested that DNA–protein ternary cross-links produced by *trans*-[PtCl₂(*E*-iminoether)₂] could persist considerably longer than the non-cross-linked monofunctional adducts, which would potentiate toxicity of this antitumor platinum compound toward tumor cells sensitive to this drug. Thus, *trans*-[PtCl₂(*E*-iminoether)₂] represents a quite new class of platinum antitumor drugs in which activation of *trans* geometry is associated with an increased efficiency to form DNA–protein ternary cross-links thereby acting by a different mechanism from ‘classical’ cisplatin and its analogs.

INTRODUCTION

cis-diamminedichloroplatinum(II) (cisplatin) (Fig. 1) is an efficient anticancer drug for the treatment of testicular and other germ-cell tumors (1). Since the discovery of its antitumor activity, the search continues for an improved platinum antitumor agent. The search is motivated by the desire to improve platinum chemotherapy since clinical use of cisplatin and some of its direct analogs is associated with diminished activity against a number of cancers, the acquired resistance developed by many tumors and severe side effects. In this search the hypothesis that platinum drugs which bind to DNA in a fundamentally different manner to that of cisplatin will have altered pharmacological properties has been tested (2). This concept has already led to the synthesis of several new unconventional platinum antitumor compounds that violate the original structure–activity relationships (3–5). The clinical inactivity of *trans*-diamminedichloroplatinum(II) (transplatin) is considered a paradigm for the classical structure–activity relationships of platinum drugs (6), but to this end several new analogs of transplatin which exhibit a different spectrum of cytostatic activity including activity in tumor cells resistant to cisplatin have been identified (reviewed in 5,7,8). Examples of these antitumor *trans*-platinum complexes are the analogs of transplatin in which one ammine group is replaced by ligands such as thiazole,

*To whom correspondence should be addressed. Tel: +420 54 151 7148; Fax: +420 54 124 0499; Email: brabec@ibp.cz

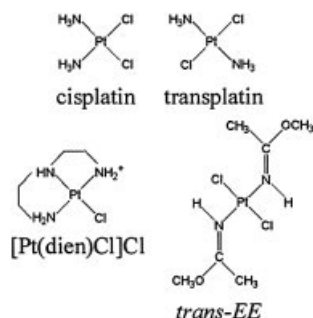


Figure 1. Structures of the platinum complexes.

piperidine, piperazine, 4-picoline and cyclohexylamine; the analogs with branched asymmetric aliphatic amines; and the analogs containing iminoether groups of general formula *trans*-[PtCl₂(E-iminoether)₂] (*trans-EE*, Fig. 1) (5,7–9).

trans-EE is not only more cytotoxic than its *cis* congener, but is also endowed with significant antitumor activity, including activity in cisplatin-resistant tumor cells (10–12). These results strongly imply a new mechanism of action for *trans-EE*. By analogy with the diamminedichloroplatinum(II) compounds, the inhibition of DNA synthesis by *trans-EE* (10,11) implies a role for DNA binding in the mechanism of action.

Bifunctional *trans-EE* preferentially forms stable monofunctional adducts at guanine residues in double-helical DNA (~90% of monofunctional adducts are formed after 48 h at 37°C in 10 mM NaClO₄) (13). The random modification of natural DNA in cell-free media results in non-denaturational alterations in the conformation of DNA (14), similar to the modification by cisplatin, but different from the modification by transplatin [which produces denaturational distortions in DNA (15)]. The most striking feature of the lesions of *trans-EE* is that they prematurely terminate RNA synthesis at similar sites and with a similar efficiency to major DNA adducts of cisplatin. This is a very intriguing finding since the prevalent lesions formed on DNA by *trans-EE* are monofunctional adducts at guanine residues and monofunctional DNA adducts of other platinum(II) complexes {such as those of [PtCl(NH₃)₃]Cl, chlorodiethylenetriamineplatinum(II) chloride ([PtCl(dien)]Cl), cisplatin and transplatin} do not terminate RNA synthesis (16,17). In addition, it is generally accepted that monofunctional DNA adducts of cisplatin are not relevant to its cytostatic effects.

Recently, a short duplex containing a single, monofunctional adduct of *trans-EE* at a central guanine residue has been analyzed by NMR spectroscopy (18). This analysis has yielded a model in which the bending induced by the monofunctional adduct of *trans-EE* was ~45° towards the minor groove.

Since other structural details of the monofunctional DNA adducts formed by this antitumor transplatin analog are not yet available, it remains uncertain how these lesions affect conformation of DNA and how these alterations are further processed in the cells. Therefore, in order to shed light on the mechanism underlying activity of *trans-EE*, we examined in detail in the present work short oligodeoxyribonucleotide duplexes containing a single, site-specific, monofunctional

adduct formed by this drug at a central guanine residue. We investigated how this adduct affects the local conformation of DNA (in particular bending and unwinding) and how this adduct is further processed by some cellular components in cell-free media.

MATERIALS AND METHODS

Chemicals

trans-EE (Fig. 1) and its mononitrato *trans*-[Pt(NO₃)Cl(E-iminoether)₂] analog was prepared by the methods described in detail previously (13,19). Cisplatin (Fig. 1A) was obtained from Sigma (Prague, Czech Republic). [PtCl(dien)]Cl was from Lachema a.s. (Brno, Czech Republic). The stock solutions of platinum compounds were prepared at concentrations of 5×10^{-4} M in 10 mM NaClO₄ and stored at 4°C in the dark. The synthetic oligodeoxyribonucleotides were synthesized and purified as described previously (20). Expression and purification of domains A (residues 1–84) and B (residues 85–180) of the HMGB1 proteins (HMGB1a and HMGB1b, respectively) (HMG = high-mobility-group) were carried out as described (21,22). T4 DNA ligase, the Klenow fragment from DNA polymerase I (exonuclease minus, mutated to remove the 3'→5' proofreading domain) (KF⁻), restriction endonuclease EcoRI and T4 polynucleotide kinase were purchased from New England Biolabs (Beverly, MA). Reverse transcriptase from human immunodeficiency virus type 1 (RT HIV-1) was from Calbiochem (San Diego, CA). Histone H1 and deoxyribonucleoside 5'-triphosphates were from Roche Diagnostics, GmbH (Mannheim, Germany). Acrylamide, bis(acrylamide), urea and NaCN were from Merck KgaA (Darmstadt, Germany). Dimethyl sulfate (DMS), KMnO₄, diethyl pyrocarbonate (DEPC), KBr and KHSO₅ were from Sigma (Prague, Czech Republic). Nonidet P-30 was from Fluka (Prague, Czech Republic). Radioactive products were from Amersham (Arlington Heights, IL). Proteinase K and ATP were from Boehringer (Mannheim, Germany).

Platinations of oligonucleotides

The single-stranded oligonucleotides (the top, pyrimidine-rich, strands containing a single central G of the 19–23 bp duplexes) were reacted in stoichiometric amounts with either [PtCl(dien)]Cl or the mononitrato analog of *trans-EE*. The platinated oligonucleotides were purified by ion-exchange fast protein liquid chromatography (FPLC). It was verified by platinum flameless atomic absorption spectrophotometry (FAAS) and by optical density measurements that the modified oligonucleotides contained one platinum atom. It was also verified using DMS footprinting of platinum on DNA (23) that one *trans-EE* or [PtCl(dien)]Cl molecule was coordinated to the N7 atom of the single G in the top strands of each duplex. FPLC purification and FAAS measurements were carried out on a Pharmacia Biotech FPLC System with MonoQ HR 5/5 column and a Unicam 939 AA spectrometer equipped with a graphite furnace, respectively. The duplexes containing single, central 1,2-GG intrastrand cross-links (CL) of cisplatin in the pyrimidine-rich top strand were prepared as described (20). The unmodified or platinated duplexes used in the studies of recognition by HMGB1 domain proteins were still purified by electrophoresis on native 15% polyacrylamide

(PAA) gel [mono:bis(acrylamide) ratio = 29:1]. Other details have been described previously (20,24).

Ligation and electrophoresis of oligonucleotides

Unplatinated 19–23mer single strands (bottom strands in Fig. S1A in Supplementary Material) were 5′-end-labeled with [γ - ^{32}P]ATP using T4 polynucleotide kinase. They were then annealed with their phosphorylated complementary strands (unplatinated or containing monofunctional adduct of *trans-EE* at the G residue). The duplexes were allowed to react with T4 DNA ligase. The resulting samples along with ligated unplatinated duplexes were subsequently examined on 8% native PAA [mono:bis(acrylamide) ratio = 29:1] electrophoresis gels. Other details of these experiments were as described in previous papers (25–27).

Chemical modifications

The modifications by KMnO_4 , DEPC and KBr/KHSO_5 were performed as described previously (24,28–30). The strands of the duplexes were 5'-end-labeled with $[\gamma\text{-}^{32}\text{P}]\text{ATP}$. In the case of the platinated oligonucleotides, the platinum complex was removed after reaction of the DNA with the probe by incubation with 0.2 M NaCN (pH 11) at 45°C for 10 h in the dark.

Gel-mobility-shift assay

The 5'-end labeled 20 bp oligonucleotide duplexes either unplatinated (controls) or containing the central platinum adduct in their top strands were used and their reaction with HMG-domain proteins was performed and analyzed as described previously (31).

Inhibition of DNA polymerization

We investigated in the present work DNA polymerization using the templates site-specifically modified by *trans-EE* or cisplatin by two DNA polymerases, which differ in processivity and fidelity. The DNA polymerase I class of enzymes has served as the prototype for studies on structural and biochemical mechanisms of DNA replication (32,33). In addition, as the most extensive genetic, biochemical and structural studies have been carried out on Klenow fragment of DNA polymerase I (including its exonuclease-deficient analog) this enzyme appears to be an ideal model system for investigating the molecular mechanisms associated with template-directed DNA synthesis (32,33). The other DNA polymerase used in these studies was RT HIV-1, showing a different mechanism underlying its catalytic activity and relatively low processivity and fidelity (34).

The 23-, 30- or 40mer templates (Figs 2 and 3) containing a single monofunctional adduct of *trans-EE* or [PtCl(dien)]Cl or 1,2-GG intrastrand CL of cisplatin were prepared in the same way as described above. Eight- or 17mer DNA primers whose sequences are also shown in Figures 2 and 3 were complementary to the 3' termini of the 23, 40 or 30mer templates, respectively. The DNA substrates were formed by annealing templates and 5'-end-labeled primers at a molar ratio of 3:1. All experiments using KF⁻ and RT HIV-1 were performed at 25°C in a volume of 50 µl in a buffer containing 50 mM Tris-HCl (pH 7.4), 10 mM MgCl₂, 0.1 mM dithiothreitol, 50 µg/ml BSA, 0.1% Nonidet P-30, 25 µM dATP, 25 µM dCTP, 25 µM dGTP, 25 µM TTP and 0.5 U KF⁻. The experiments with RT

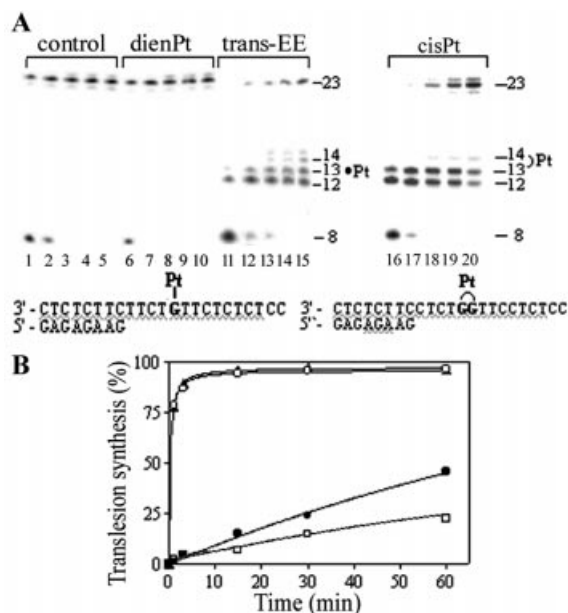


Figure 2. Primer extension activity of exonuclease-deficient Klenow fragment of DNA polymerase I (KF⁻). **(A)** Experiments were conducted using the 8mer/23mer primer/template duplex for various times using undamaged template (lanes 1–5), the template containing monofunctional adduct of [Pt(dien)Cl]Cl (lanes 6–10), monofunctional adduct of *trans-EE* (lanes 11–15) or 1,2-GG intrastrand CL of cisplatin (lanes 16–20). Timings were as follows: 1 min, lanes 1, 6, 11 and 16; 3 min, lanes 2, 7, 12 and 17; 15 min, lanes 3, 8, 13 and 18; 30 min, lanes 4, 9, 14 and 19; 60 min, lanes 5, 10, 15 and 20. The pause sites opposite the platinated guanines and flanking residues are marked 12, 13 and 14 (the sites opposite the platinated residues are still marked 'Pt'). The nucleotide sequences of the templates and the primer are shown beneath the gels. **(B)** The time dependence of the inhibition of DNA synthesis on undamaged (control) template (open circles), DNA containing monofunctional adduct of [Pt(dien)Cl]Cl (closed triangles), DNA containing monofunctional adduct of *trans-EE* (open squares) or DNA containing 1,2-GG intrastrand CL of cisplatin (closed circles). Data are means (\pm SE) from three different experiments with two independent template preparations.

HIV-1 were performed at 37°C using the same conditions except that the nucleoside triphosphates were at a concentration of 100 µM and 1.0 U of the enzyme was used. Reactions were terminated by the addition of EDTA so that its resulting concentration was 20 mM and by heating at 100°C for 30 s. Products were resolved by denaturing 24 or 15% PAA/8 M urea gel and then visualized and quantified by using the FUJIFILM bio-imaging analyzer and AIDA image analyzer software.

Nucleotide excision assay

The 148 bp substrates containing single, central, monofunctional adducts of *trans-EE*, [PtCl(dien)]Cl or 1,2-GG intra-strand CL of cisplatin were assembled from three oligonucleotide duplexes as described previously (35,36).

Oligonucleotide excision reactions were performed in cell-free extracts (CFEs) prepared from the HeLa S3 and Chinese hamster ovary (CHO) AA8 cell lines as described (37,38). *In vitro* repair was measured with excision assay using these CFEs and 148 bp linear DNA substrates in the same way as described previously (38). Reaction products were still treated overnight with 0.4 M NaCN, pH 10–11, at 45°C to remove

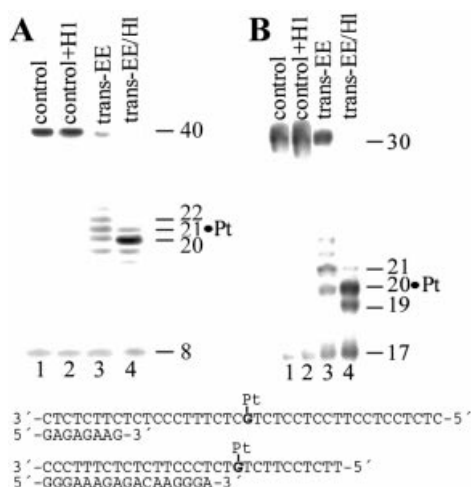


Figure 3. Primer extension activity of exonuclease-deficient Klenow fragment of DNA polymerase I (KF-) (A) and RT HIV-1 (B) using the 8mer/40mer and 17mer/30mer primer/template duplexes, respectively. The experiments were conducted for 30 min using undamaged templates (lanes 1), undamaged templates to which histone H1 was added at a molar ratio of 4:1 (lanes 2), the templates containing monofunctional adduct of *trans-EE* (lanes 3) and monofunctional adduct of *trans-EE* cross-linked to histone H1 (lanes 4). The pause sites opposite the platinated guanines and flanking residues are marked 19, 20, 21 and 22 (the sites opposite the platinated residue are still marked 'Pt'). The nucleotide sequences of the templates and the primers are shown beneath the gels.

platinum from excised fragments. The NaCN treatment was included to eliminate both the effect of the positively charged platinum complex bound to the excised fragments and the protein cross-linked to the excised fragments on their migration in the gel.

Mapping of incision sites was performed as described in the preceding reports (38). The major excision product (gel-purified) was further incubated for 10 min at 30°C with T4 DNA polymerase (0.25 U) in 10 µl of buffer composed of 50 mM Tris-HCl (pH 8.8), 15 mM (NH₄)₂SO₄, 7 mM MgCl₂, 0.1 mM EDTA, 50 mM β-mercaptoethanol and 20 µg BSA/ml, supplemented with 0.5 µg Smal-digested pBluescript DNA and visualized by autoradiography following resolution in 10% denaturing PAA gel. Similar analyses using radio-labeled, platinated 20mers (used in the nucleotide excision assays) were also used to identify the nucleotide(s) at which the exonuclease activity of T4 DNA polymerase is blocked 3' to the lesion. The location of the 5' incision site made by the excinuclease was determined by comparison with the length of excision products observed in the absence of T4 DNA polymerase digestion.

RESULTS

Bending, unwinding and chemical probes of DNA conformation

Important structural motifs induced in DNA by antitumor platinum compounds that play a significant role in the mechanism underlying their antitumor activity are the unwinding and bending of the helix axis (5,39). For DNA adducts of cisplatin, the structural details of the bending and unwinding have been elucidated (26,40,41). Given the recent

advances in our understanding of the structural basis of the bending and unwinding of DNA caused by cisplatin, it is of considerable interest to examine how the major monofunctional adduct of *trans-EE* affects these conformational properties of DNA. In this work we performed studies on the bending and unwinding afforded by a single, site-specific, monofunctional adduct formed by *trans-EE* at guanine residues using electrophoretic retardation as a quantitative measure of the extent of planar curvature (25,26).

Oligodeoxyribonucleotide duplexes (19–23 bp) (see Fig. S1A in Supplementary Material for their sequences) containing, in the top pyrimidine-rich strand, a central TGT sequence (42) were used for the bending and unwinding studies of the present work. The ligation products of these duplexes unplatinated or containing a single, site-specific, monofunctional adduct of *trans-EE* at the central guanine residue in the top strand were analyzed on native PAA electrophoresis gel (see Fig. S1B in Supplementary Material). Experimental details of these studies are given in our recent reports (23,27,43).

The *K* factor is defined as the ratio of calculated to actual length. The calculated length is based on a multimer's mobility, and is obtained from a calibration curve constructed from the mobilities of unplatinated multimers. The variation of the *K* factor versus sequence length obtained for multimers of the 19–23 bp duplexes and containing the monofunctional adduct of *trans-EE* is shown in Figure S1C (Supplementary Material). Maximum retardation was observed for the 21 bp duplex. This observation suggests that the natural 10.5 bp repeat of B-DNA was not markedly changed. The exact helical repeat of the duplex containing the adduct of *trans-EE*, and from it the unwinding angle, were calculated by interpolation with the use of the *K* versus interadduct distance curve as described in the previous papers for other platinum adducts (23,40). The maximum of these curves constructed for the duplexes modified by *trans-EE* with a total length of 130 bp (see Fig. S1D in Supplementary Material) was determined to be 21.10 ± 0.01 bp. Total sequence lengths other than 130 bp were examined and gave identical results. To convert the interadduct distance in base pairs corresponding to the curve maximum into a duplex unwinding angle in degrees, the value is compared with that of the helical repeat of B-DNA, which is 10.5 ± 0.05 bp (44). The difference between the helical repeat of B-DNA and the DNA-containing monofunctional adduct of *trans-EE*, therefore, is $[(21.10 \pm 0.01) - 2(10.5 \pm 0.05)] = 0.10 \pm 0.06$ bp. There are $360^\circ/10.5$ bp, so the DNA unwinding due to one monofunctional adduct of *trans-EE* is $3 \pm 2^\circ$.

The quantitation of the bend angle of the monofunctional adduct of *trans-EE* was performed in the way described previously (24,26,41,45), utilizing the empirical equation

$$K - 1 = (9.6 \times 10^{-5} L^2 - 0.47)(RC)^2 \quad 1$$

where *L* represents the length of a particular oligomer with relative mobility *K*, and RC the curvature relative to a DNA bending induced at the tract of six adenines (A₆ tract) (45). Application of 1 to the 120, 130 or 140 bp multimers of the 21 bp oligomers containing the single, monofunctional adduct of *trans-EE* (see Fig. S1C in Supplementary Material) leads to a mean curvature of 0.53, relative to an A₆ tract. The average

bend angle per helix turn can be calculated by multiplying the relative curvature by the absolute value of an A_6 tract bend [20° (26)]. The results indicate that the bend induced by the monofunctional adduct of *trans-EE* is $\sim 21^\circ$. That this bend was oriented towards the minor groove of DNA was verified in the same way as previously using the duplex [TGT+(A/T)₅](32) (see Fig. S1A in Supplementary Material for its sequence) (41,46).

Further studies of the present work were focused on analysis of the distortion induced by the monofunctional adducts of *trans-EE* by chemical probes of DNA conformation. The 20 bp duplex [the duplex TGT(20) in Fig. S1A in Supplementary Material] containing the single, site-specific adduct of *trans-EE* was treated with several chemical agents used as tools for monitoring the existence of conformations other than canonical B-DNA. These agents included $KMnO_4$, DEPC and bromine. They react preferentially with single-stranded DNA and distorted double-stranded DNA (24,47). We used for this analysis the same methodology described in detail in our recent papers dealing with DNA adducts of various antitumor platinum drugs (43,48). The results (see Fig. S2 in Supplementary Material) indicate that the adduct of *trans-EE* induces in DNA a distortion that extends over at least 2 bp and is localized mainly at the base pair containing the platinated G residue and the adjacent base pairs on the 5' side.

Recognition by the domains A and B of HMGB1

An important feature of the mechanism that underlies the antitumor activity of cisplatin and its direct analogs in a number of tumor cells is that the major adducts of these drugs (1,2-GG intrastrand CLs) are recognized by proteins containing HMG domains (5,39,49). Importantly, DNA modified by transplatin or monodentate platinum(II) compounds, such as [PtCl(dien)]Cl or [PtCl(NH₃)₃]Cl, is not recognized by these cellular proteins. Since the monofunctional adducts of *trans-EE* distort DNA in a different way to the monofunctional adducts of transplatin, [PtCl(dien)]Cl or [PtCl(NH₃)₃]Cl, we examined whether the monofunctional adducts of *trans-EE* enhance affinity of HMG-box proteins to DNA. The interactions of the rat HMGB1 domain A (HMGB1a) and HMGB1 domain B (HMGB1b) with DNA modified by *trans-EE* were investigated using gel-mobility-shift assay (31,50,51) (Fig. S3A and B in Supplementary Material). In these experiments, the 20 bp duplex (see Fig. S3C in Supplementary Material for its sequence) was modified so that it contained a single, site-specific, monofunctional adduct of *trans-EE*. The binding of HMGB1a and HMGB1b to these DNA probes was detected by retardation of the migration of the radiolabeled 20 bp probes through the gel (Fig. S3A and B in Supplementary Material) under identical conditions described in detail in our recent papers (42,52).

As indicated by the presence of a shifted band whose intensity increases with growing protein concentration, both HMGB1a and HMGB1b recognized the duplex containing the 1,2-GG intrastrand CL of cisplatin (Fig. S3A and B in Supplementary Material), consistent with earlier observations (49,53,54). These proteins exhibited, under the same experimental conditions, negligible binding to the 20 bp duplex unplatinated or containing the monofunctional adduct of *trans-EE* (see Fig. S3A and B in Supplementary Material).

These data indicate that HMGB1 proteins do not bind the probe containing the major adducts of *trans-EE*.

Probing *trans-EE* adducts by DNA polymerases

It has been demonstrated that various DNA secondary structures have significant effects on processivity of a number of prokaryotic, eukaryotic and viral DNA polymerases (55–57). Interestingly, with DNA templates containing site-specifically placed adducts of various platinum compounds, a number of prokaryotic and eukaryotic DNA polymerases were blocked but could also traverse through platinum adducts depending on their character and conformational alterations induced in DNA. Inhibition of prokaryotic DNA and RNA polymerases by the adducts on DNA globally modified by *trans-EE* has already been demonstrated in *in vitro* replication or transcription mapping experiments (10,14). Similarly, the inhibition of DNA synthesis in human tumor cells treated with *trans-EE* has been demonstrated and found to be greater than that with the *cis* isomer (11). Monofunctional adducts of cisplatin or transplatin and those of the monodentate compounds such as [PtCl(dien)]Cl or [PtCl(NH₃)₃]Cl terminate DNA synthesis by DNA polymerases *in vitro* markedly less efficiently than major 1,2-GG intrastrand CLs of cisplatin (55). It is, therefore, interesting to examine whether DNA polymerases, processing DNA substrates containing either the major monofunctional adduct of *trans-EE* or bifunctional 1,2-GG intrastrand CL of cisplatin, could reveal potential differences in conformational alterations imposed on DNA by these two adducts.

We constructed the 8mer/23mer primer/template duplexes unplatinated or containing the monofunctional adduct of *trans-EE* or [PtCl(dien)]Cl in the central TGT sequence or the 1,2-GG intrastrand CL of cisplatin in the central TGGT sequence (for their sequences, see Fig. 2A). The first eight nucleotides on the 3' terminus of the 23mer template strand were complementary to the nucleotides of the 8mer primer and the guanine involved in the monofunctional adduct of *trans-EE*, [PtCl(dien)]Cl or the 3' guanine in the 1,2-GG CL of cisplatin on the template strand were located at the 13th position from the 3' terminus (Fig. 2A). After annealing the 8 nt primer to the 3' terminus of the unplatinated or platinated template strand positioning the 3'-end of the primer five bases before the adduct in the template strand, we examined DNA polymerization through the single, monofunctional adduct of *trans-EE* or [PtCl(dien)]Cl and the 1,2-intrastrand CL of cisplatin by KF^- in the presence of all four deoxyribonucleoside 5'-triphosphates. The reaction was stopped at various time intervals, and the products were analyzed using a sequencing 24% PAA/8 M urea gel (Fig. 2A). Polymerization using the 23mer template containing the CL of cisplatin proceeded rapidly up to the nucleotide preceding and at the sites opposite the CL, such that the 12 and 13 nt products accumulated to a significant extent (shown in Fig. 2A, lanes 16–20). The larger DNA intermediates were not observed in a considerable extent, whereas no intermediate products were seen with the 23mer control template or the template containing the monofunctional adduct of [PtCl(dien)]Cl as the full-length products were formed (shown in Fig. 2A, lanes 1–10). The full-length products were also noticed with the 23mer template containing the CL of cisplatin, although in a significantly smaller amount (Fig. 2A, lanes 16–20). This result is in

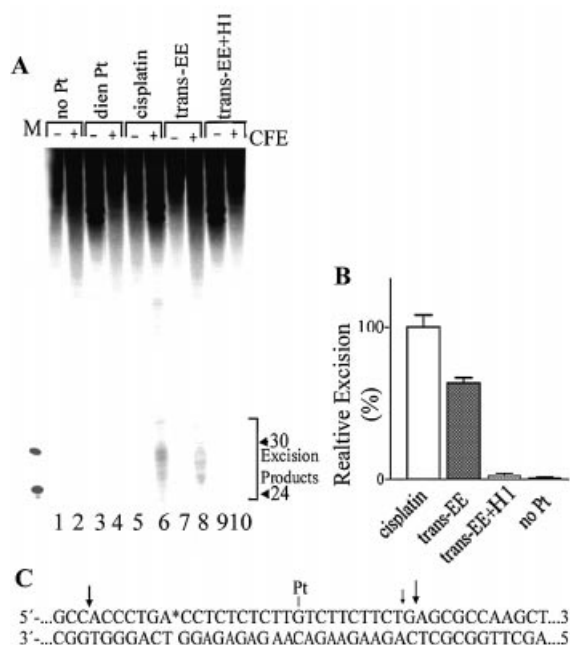


Figure 4. Excision of the adducts of platinum complexes by rodent excinuclease. (A) The 148 bp substrates were incubated with CHO AA8 CFE and subsequently treated overnight with NaCN prior to analysis in 10% PAA/8 M urea denaturing gel. Lanes 1 and 2, control, unplatinated substrate; lanes 3 and 4, the substrate containing the monofunctional adduct of [Pt(dien)Cl]Cl; lanes 5 and 6, 1,2-GG intrastrand CL of cisplatin; lanes 7 and 8, the monofunctional adduct of *trans-EE*; lanes 9 and 10, the monofunctional adduct of *trans-EE* cross-linked to histone H1. Lanes 1, 3, 5, 7 and 9, no extract added; lanes 2, 4, 6, 8 and 10, the substrates were incubated with CHO AA8 CFE for 40 min at 30°C. Lane M, the 20 and 30 nt markers. (B) Quantitative analysis of removal of the adducts. The columns marked cisplatin, *trans-EE*, *trans-EE*+H1 and noPt represent 1,2-GG intrastrand CL of cisplatin, monofunctional adduct of *trans-EE*, monofunctional adduct of *trans-EE* cross-linked to histone H1 and unplatinated substrate, respectively. The radioactivity associated with the fragments excised from the duplex containing the 1,2-GG intrastrand CL of cisplatin was taken as 100%. Data are the average of two independent experiments performed under the same conditions; bars indicate range of excision. (C) The central sequence of the 148 bp substrate. The site of the monofunctional adduct of *trans-EE* or [Pt(dien)Cl]Cl is marked 'Pt' and arrows indicate the major incision sites.

agreement with a previously published work (58) in which T7 DNA polymerase and RT HIV-1 were used and confirms that 1,2-GG intrastrand CL of cisplatin inhibits DNA synthesis (55), but translesion synthesis may occur. Under the same experimental conditions, DNA polymerization by KF⁻ using the template containing the monofunctional adduct of *trans-EE* proceeded up to the nucleotide preceding the site opposite the platinated G involved in the adduct and to the following nucleotide residue (Fig. 2A, lanes 11–15). There was almost no accumulation of shorter and larger DNA intermediates and, importantly, the full-length products were also noticed. The amount of the full-length products increased with reaction time, but with a noticeably lower rate compared to polymerization using the template containing the CL of cisplatin (Fig. 2B). This result suggests that the monofunctional adducts of *trans-EE* are even more efficient inhibitors of DNA polymerization than the major adducts of cisplatin.

In order to further support the latter conclusion, we have also examined the effects of the monofunctional adduct of

trans-EE on DNA polymerization by RT HIV-1. In these studies elongation of the 17mer/30mer primer/template duplexes was tested by rapidly mixing a solution of RT HIV-1 and DNA with a solution containing all four deoxyribonucleoside 5'-triphosphates. The 30mer template was non-modified or contained the monofunctional adduct of *trans-EE* located at the 20th position from the 3' terminus (for its sequence, see the bottom sequence in Fig. 3). The reaction was stopped at various times, and the products were analyzed using a sequencing 15% PAA/8 M urea gel. Polymerization using the *trans-EE* template proceeded rapidly up to the nucleotide at the site opposite the platinated and following residues, such that 20 and 21 nt intermediates accumulated to a significant extent (shown in Fig. 3B for the incubation time of 30 min). Nevertheless, the synthesis by the RT HIV-1 across the monofunctional adduct of *trans-EE* was still possible, as in the case of the polymerization by KF⁻. Hence, we confirmed also by using DNA polymerase showing a different mechanism underlying its catalytic activity than KF⁻ that the monofunctional adduct of *trans-EE* constitutes a fairly strong block to DNA synthesis catalyzed by KF⁻ and RT HIV-1 but not absolute, thus permitting translesion DNA synthesis with a limited efficiency. Since there is a high degree of structural and sequence conservation of the domains among eukaryotic, prokaryotic and viral polymerases (59) insights gleaned from studies of the KF⁻ and RT HIV-1 also should be applicable to other DNA polymerases (32,60,61). Hence, the observation that DNA polymerization is inhibited by *trans-EE* adducts more strongly than by the adducts of other simple monofunctional platinum(II) compounds and even by the major CL of cisplatin add a new dimension to the impact of the activation of the *trans* geometry in platinum compounds by iminoether ligands on processes in tumor cells, possibly including replication or DNA repair.

Nucleotide excision repair (NER)

NER is a pathway used by human cells for the removal of damaged nucleotides from DNA (62,63). In mammalian cells, this repair pathway is an important mechanism for the removal of bulky, helix-distorting DNA adducts, such as those generated by various chemotherapeutics including cisplatin (64). Efficient repair of 1,2-GG or 1,3-GNG intrastrand CL of cisplatin has been reported by various NER systems including human and rodent excinucleases (38,65–69). The result presented in Figure 4A, lane 6 is consistent with these reports. The major excision fragment contains 28 nt and other primary excision fragments are 24–29 nt in length (38,70). In contrast, consistent with previous reports (42,71,72), no excision fragments were noticed if the monofunctional adduct of [PtCl(dien)]Cl was used as a substrate for human and rodent excinucleases (shown in Fig. 4A, lane 4 for rodent excinuclease). Importantly, the monofunctional adduct of *trans-EE* was also repaired by both human and rodent excinucleases, although with a somewhat lower efficiency than the major intrastrand CLs of cisplatin [shown in Fig. 4A (lane 8) and B for the adduct removed by rodent excinuclease].

T4 DNA polymerase 3'→5' exonuclease activity was used to map the primary sites of incision in the same way as described in recent papers (73). The major 3' incision site is 10 nt (or at the 11th phosphodiester bond) 3' to the adduct (the minor 3' incision site is at the 10th phosphodiester bond) and

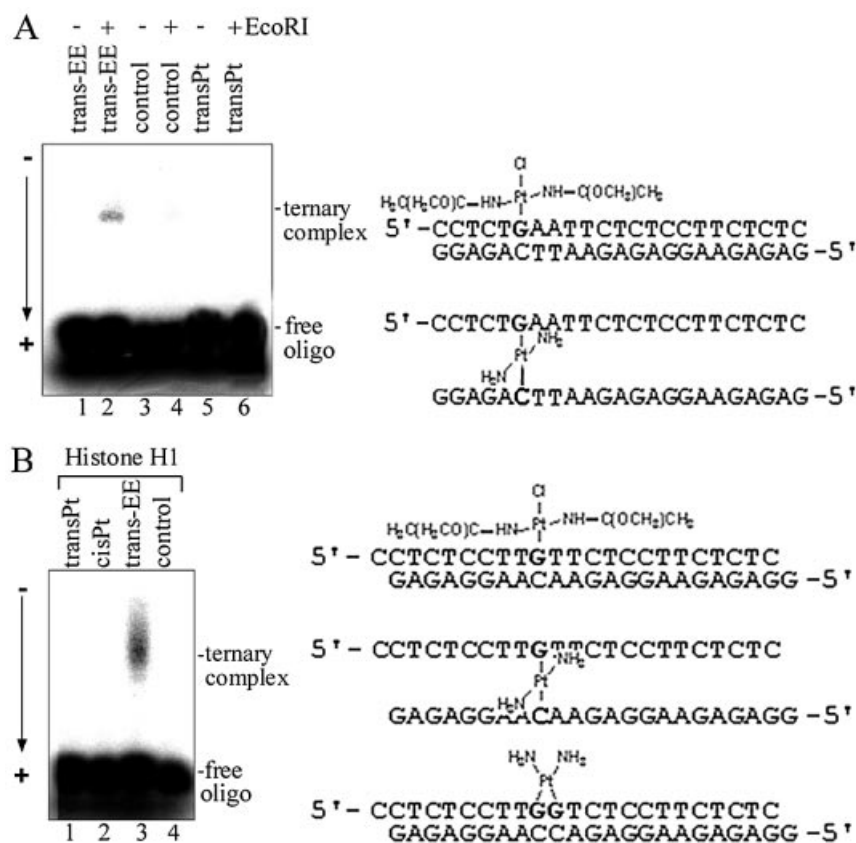


Figure 5. Ternary complex formation of unmodified and platinated oligodeoxyribonucleotide duplexes containing single, site-specific platinum adduct with EcoRI (A) or histone H1 (B) assessed by SDS-PAGE gel electrophoresis. (A) Lanes 1 and 2, the 23 bp duplex containing the monofunctional adduct of *trans-EE*; lanes 3 and 4, non-modified duplex; lanes 5 and 6, the duplex containing the interstrand CL of transplatin. Lanes 1, 3 and 5, no enzyme added; lanes 2, 4 and 6, EcoRI added. (B) Lane 1, the 22 bp duplex containing the interstrand CL of transplatin; lane 2, the duplex containing the 1,2-GG intrastrand CL of cisplatin; lane 3, the duplex containing the monofunctional adduct of *trans-EE*; lane 4, non-modified duplex. The nucleotide sequences of the duplexes with the platinum adducts are shown to the right of each panel.

the other major incision site at the 18th phosphodiester bond 5' to the adduct (Fig. 4C).

Ternary DNA-protein complex formation

The monofunctional DNA adducts of *trans-EE* were investigated for their ability to specifically cross-link proteins. The 1,2-GG intrastrand CL of cisplatin and the interstrand CL of transplatin formed between G and complementary C were used as controls. The 22 or 23 bp duplexes 5'-end-labeled at their top, pyrimidine-rich strands (the sequences of which are given in Fig. 5) were modified by *trans-EE* so that they contained a single, site-specific, monofunctional adduct at the G residue. Ternary DNA-protein cross-linking efficiency was assessed by gel mobility shift assays. The 23 bp duplex containing the monofunctional adduct of *trans-EE* was mixed with EcoRI restriction endonuclease, a sequence-specific DNA-binding protein. A fraction was detected by denaturing gel electrophoresis with significantly retarded mobility (Fig. 5A, lane 2) compared with that of the free probe. This fraction was eliminated after treatment with sodium cyanide or proteinase K converting it to that of the unmodified probe (not shown). These results suggest that the species is a protein-DNA CL tethered by platinum-guanine and platinum-protein covalent bonds. While the proteinase K

and NaCN experiments clearly indicate that protein is the species cross-linked to DNA, the amino acids participating in the cross-linking reaction have not been determined.

Representative, non-sequence-specific DNA-binding protein, the linker histone H1 (which is an abundant nuclear protein) also effectively cross-links the 22 bp duplex containing the monofunctional adduct of *trans-EE*, as monitored by standard gel shift assays (Fig. 5B, lane 3) and confirmed by the treatment with NaCN and proteinase K. No ternary complexes containing EcoRI or histone H1 were formed under the same experimental conditions between the duplexes containing the CL of cisplatin or transplatin [Fig. 5A (lane 6) and B (lanes 1 and 2)]. Thus, in all cases studied it is clear that formation of the ternary DNA-platinum-protein complex is efficient for the major monofunctional adducts of *trans-EE*.

The 40- or 30mer templates cross-linked to histone H1 by *trans-EE* were isolated from the gel, purified, hybridized with 8- or 17mer primers, respectively and used as substrates to investigate the translesion synthesis across the monofunctional adduct of *trans-EE*. As shown in lanes 4 of Figure 3, polymerization by KF⁻ or RT HIV-1 using the template cross-linked to histone H1 mainly proceeded to the sites close to the platinated G. However, in contrast to the polymerization using the same templates but containing the adduct of *trans-EE* not

cross-linked to a protein, no full-length products were noticed and the polymerization was terminated mainly at the platinated site. Similarly, no removal of the monofunctional adducts of *trans-EE* cross-linked to histone H1 from the 148 bp substrates containing single, central, monofunctional adduct of *trans-EE* by human or rodent excinuclease was observed under conditions when the same adduct not cross-linked to a protein was readily excised [shown for rodent excinuclease in Fig. 4A (lane 10) and B].

DISCUSSION

It is generally accepted that the key intracellular target for antitumor platinum drugs is DNA on which these compounds form various types of adducts (74). The adducts of conventional cisplatin distort DNA conformation, inhibit replication and transcription (but they are also bypassed by DNA or RNA polymerases), and trigger apoptosis or necrosis (75). In addition, cisplatin adducts are removed from DNA mainly by NER. They are, however, also recognized by a number of proteins, such as, for instance, HMG-domain proteins. The details of how the binding of HMG-domain proteins to cisplatin-modified DNA sensitizes tumor cells to cisplatin are still not completely resolved, but possibilities such as shielding cisplatin–DNA adducts from excision repair or that these proteins could be titrated away from their transcriptional regulatory function, have been suggested as clues for how they are involved in antitumor activity. Experimental support of these aspects of the mechanism underlying antitumor activity of cisplatin or resistance of some tumors to this drug has recently been thoroughly reviewed (5,75–78). On the other hand, it has also been demonstrated (79) that the ability of HMGB1 protein, and probably other cisplatin–DNA-binding proteins, to influence the efficacy of the drug may be dependent on tumor cell type.

Lack of activity of transplatin against tumors has been proposed to be associated with selective recognition of its DNA adducts by cellular repair systems resulting in their removal (80,81). Moreover, the monofunctional transplatin–DNA intermediates are much longer lived than their cisplatin analogs (81). The transplatin intermediates may react readily with sulfur-containing nucleophiles, such as glutathione or metallothioneins, preventing closure to the bifunctional cytotoxic lesion. This feature of the monofunctional adducts of transplatin and the fact that the free transplatin molecules can readily react with sulfur-containing nucleophiles (81,82) may be at least partly responsible for clinical inefficiency of transplatin (8,81,83–85). *trans-EE* forms on DNA stable monofunctional adducts preferentially at guanine residues (13). These lesions distort DNA, although differently from the adducts of cisplatin or transplatin (11,13,14,86). These adducts can inhibit DNA polymerization to a limited extent so that they can also be bypassed by DNA polymerases (Figs 2 and 3). In contrast to the adducts of cisplatin, the monofunctional adducts of *trans-EE* are not recognized by HMG-domain proteins. An important structural motif recognized by HMG-domain proteins on DNA containing the major 1,2-GG intrastrand CL of cisplatin is a stable, directional bend of the helix axis toward the major groove (87). As demonstrated in the present work the major monofunctional adduct of *trans-EE* also bends the helix axis of DNA (by 21°), but towards the

minor groove, and no recognition of these adducts by HMGB1 proteins was observed. Plausible explanation of this observation may be that the pre-bending due to the monofunctional adduct of *trans-EE* is too small and/or in an incorrect direction to be recognized by HMG-domain proteins. Thus, from these considerations we could conclude that the mechanism of antitumor activity of *trans-EE* does not involve recognition by HMG-domain proteins as a crucial step, in contrast to the proposals for cisplatin and its direct analogs in certain types of cells.

Several reports have demonstrated (38,66) that NER is a major mechanism contributing to cisplatin resistance. The examinations of excision of monofunctional adducts of *trans-EE* have revealed that these adducts can also be efficiently removed by NER (Fig. 4). Hence, by analogy to the mechanism proposed for antitumor effects of cisplatin, the monofunctional adducts of *trans-EE* should be shielded by damaged-DNA recognition proteins, such as those containing HMG-domains, to prevent their repair. However, we demonstrate in the present work that, in contrast to cisplatin CLs, the adducts of *trans-EE* are not recognized by HMG-domain proteins. Hence, it is reasonable to assume that the monofunctional adducts of *trans-EE* would be removed from DNA too early to trigger downstream processes leading to toxicity of *trans-EE* toward tumor cells sensitive to this drug, unless other factors than affinity of the HMG-domain proteins to the adducts protect them from being removed from DNA. In addition, lack of affinity of HMG-domain proteins for the adducts of *trans-EE* implies that these proteins will not be titrated away from their transcriptional regulatory function as they can be in certain types of cells in the presence of cisplatin CLs (88). Thus, a reasonable alternative for the mechanism underlying antitumor effects of *trans-EE* may also be that proteins other than HMG-domain proteins bind to DNA adducts of this drug and by other mechanisms.

The results of the present work demonstrate for the first time that the monofunctional adducts of *trans-EE* readily cross-link proteins (Fig. 5). Interestingly, earlier observations have demonstrated that cisplatin and transplatin also form DNA–protein ternary CLs (89–97). However, the monofunctional adducts of cisplatin formed in the first step of the reaction with DNA close to bifunctional CLs with a relatively fast rate so that these adducts do not persist for long enough to allow their extensive cross-linking to proteins to occur (82). Consistent with this conclusion is the relatively very low frequency of the DNA–protein ternary CLs produced in cells treated with cisplatin (<1%) (98). Transplatin forms more monofunctional adducts on DNA than cisplatin, and the rate of rearrangement of monofunctional to bifunctional adducts is considerably slower compared to cisplatin [24 h are required for ~50% rearrangement of monofunctional adducts of transplatin (81)], but still considerably faster than that of the monofunctional adducts of *trans-EE* (13). In addition, in contrast to *trans-EE*, free transplatin and its monofunctional DNA adducts readily react with sulfur-containing nucleophiles, such as glutathione or thiourea, which may translablize transplatin from DNA (81). On the other hand, free *trans-EE* and its DNA monofunctional adducts react with sulfur-containing nucleophiles, such as thiourea (13), glutathione or Zn-MT2 metallothionein (unpublished results) much less readily than free cisplatin, transplatin and their monofunctional DNA

adducts. Hence, the formation of the DNA–protein ternary CLs in cells treated with transplatin is much less likely than in the cells treated with *trans-EE*. Taken together, the capacity of the monofunctional DNA adducts of *trans-EE* to cross-link proteins supports the idea that the capability of *trans-EE* monofunctional DNA adducts to cross-link proteins represents an important feature of the mechanism underlying antitumor effects of this platinum compound.

The results of the present work demonstrate that cross-linking proteins to monofunctional DNA adducts of *trans-EE* markedly enhances the efficiency of this adduct to terminate DNA polymerization by DNA polymerases *in vitro* (Fig. 3) and to inhibit removal of this adduct from DNA by NER (Fig. 4). Hence, it is reasonable to suggest that DNA–protein ternary CLs produced by *trans-EE* could persist considerably longer than their non-cross-linked monofunctional adducts, potentiating the toxicity of *trans-EE* toward tumor cells sensitive to this drug. In other words, covalent cross-linking of DNA and proteins by *trans-EE* represents a potential novel mechanism through which this compound could exert its antitumor activity.

To date several strategies on ways to activate *trans* geometry in bifunctional platinum(II) compounds, including circumvention of resistance to cisplatin, have been proposed. One strategy consists of chemical modification of the ineffective transplatin which results in an increased efficiency to form in DNA interstrand CLs and/or in an increased stability of its 1,3-intrastrand CLs in double-helical DNA (99). Examples of such compounds are the analogs of transplatin in which at least one ammine ligand is replaced by a heterocyclic amine ligand [such as quinoline, thiazole or pyridine (7,100) or piperidine, piperazine or 4-picoline (99)]. Another strategy consists of a chemical modification of transplatin resulting in the capability of the new complex to form DNA adducts that mimic the structure of the adducts of cisplatin (42,101). For instance, antitumor *trans*-[PtCl₂(NH₃)(thiazole)] forms on DNA monofunctional adducts which mimic 1,2-intrastrand CLs of cisplatin including their recognition by HMG-domain proteins and NER (42). In addition, this *trans* compound also forms interstrand CLs which are similar to those formed in DNA by cisplatin (101).

Efforts to investigate the generality of the DNA–protein ternary CLs formed by *trans-EE* are under study in these laboratories and will be reported in due course. Given that cellular DNA is intimately associated with proteins, DNA–protein ternary CLs formed by *trans-EE* stresses the importance of this type of DNA damage for antitumor effects of the new platinum compound. Although formation of DNA–protein CLs seems to be limited to proteins that are able to bind to DNA, the potential *in vivo* CL formation with other DNA-binding proteins, including those directly related to neoplastically transformed cells, is not excluded. The capacity of *trans-EE* to cross-link the oncoproteins or other functional proteins with nuclear DNA *in vivo* would represent a potentially novel mechanism that might contribute to the antitumor efficacy of *trans-EE* by abrogating the functional integrity of these proteins.

In conclusion, *trans-EE* represents a quite new class of platinum antitumor drugs in which activation of the *trans* geometry is associated with an increased efficiency to form DNA–protein ternary CLs. In addition, our results provide

additional strong support for the hypothesis that platinum drugs which bind to DNA in a fundamentally different manner to that of cisplatin have altered pharmacological properties. Hence, *trans-EE* and its analogs may represent a novel class of platinum anticancer drugs acting by a different mechanism to cisplatin and its analogs.

SUPPLEMENTARY MATERIAL

Supplementary Material is available at NAR Online.

ACKNOWLEDGEMENTS

We thank J. T. Reardon and A. Sancar for HeLa and CHO cells. We also acknowledge participation in the EC COST Chemistry Actions D20 and D21, which enabled us to regularly exchange the most recent ideas in the field of platinum anticancer drugs with several European colleagues. This research was supported by the Grant Agency of the Czech Republic (grant no. 305/02/1552A), the Grant Agency of the Academy of Sciences of the Czech Republic (grant no. KJB5004301), the Wellcome Trust (to J.K. and V.B.) and by the Italian Ministry for Education, University and Research.

REFERENCES

- O'Dwyer, P.J., Stevenson, J.P. and Johnson, S.W. (1999) Clinical status of cisplatin, carboplatin and other platinum-based antitumor drugs. In Lippert, B. (ed.), *Cisplatin. Chemistry and Biochemistry of a Leading Anticancer Drug*. VCH, Wiley-VCH, Zürich, Weinheim, pp. 31–72.
- Farrell, N., Kelland, L.R., Roberts, J.D. and Van Beusichem, M. (1992) Activation of the *trans* geometry in platinum antitumor complexes: a survey of the cytotoxicity of *trans* complexes containing planar ligands in murine-L1210 and human tumor panels and studies on their mechanism of action. *Cancer Res.*, **52**, 5065–5072.
- Wong, E. and Giandomenico, C.M. (1999) Current status of platinum-based antitumor drugs. *Chem. Rev.*, **99**, 2451–2466.
- Judson, I. and Kelland, L.R. (2000) New developments and approaches in the platinum arena. *Drugs*, **59**, 29–36.
- Brabec, V. (2002) DNA modifications by antitumor platinum and ruthenium compounds: their recognition and repair. *Prog. Nucleic Acids Res. Mol. Biol.*, **71**, 1–68.
- Reedijk, J. (1996) Improved understanding in platinum antitumor chemistry. *Chem. Comm.*, 801–806.
- Farrell, N. (1996) Current status of structure-activity relationships of platinum anticancer drugs: Activation of the *trans* geometry. In Sigel, A. and Sigel, H. (eds), *Metal Ions in Biological Systems*. Marcel Dekker, Inc., New York, Basel, Hong Kong, Vol. 32, pp. 603–639.
- Perez, J.-M., Fuertes, M.A., Alonso, C. and Navarro-Ranninger, C. (2000) Current status of the development of *trans*-platinum antitumor drugs. *Crit. Rev. Oncol. Hematol.*, **35**, 109–120.
- Natile, G. and Coluccia, M. (1999) *trans*-Platinum compounds in cancer therapy: a largely unexplored strategy for identifying novel antitumor platinum drugs. In Clarke, M.J. and Sadler, P.J. (eds), *Metallopharmaceuticals*. Springer, Berlin, Germany, Vol. 1, pp. 73–98.
- Coluccia, M., Nassi, F., Loseto, F., Boccarelli, A., Marigió, M.A., Giordano, D., Intini, F.P., Caputo, P. and Natile, G. (1993) A *trans*-platinum complex showing higher antitumor activity than the *cis* congeners. *J. Med. Chem.*, **36**, 510–512.
- Coluccia, M., Boccarelli, A., Marigió, M.A., Cardellicchio, N., Caputo, P., Intini, F.P. and Natile, G. (1995) Platinum(II) complexes containing iminoethers: A *trans* platinum antitumor agent. *Chem. Biol. Interact.*, **98**, 251–266.
- Coluccia, M., Nassi, A., Boccarelli, A., Giordano, D., Cardellicchio, N., Intini, F.P., Natile, G., Barletta, A. and Paradiso, A. (1999) *In vitro* antitumor activity and cellular pharmacological properties of the platinum-iminoether complex *trans*-[PtCl₂{E–HN=C(OMe)Me}₂]. *Int. J. Oncol.*, **15**, 1039–1044.

13. Brabec, V., Vrana, O., Novakova, O., Kleinwachter, V., Intini, F.P., Coluccia, M. and Natile, G. (1996) DNA adducts of antitumor *trans*-[PtCl₂(E-imino ether)]₂. *Nucleic Acids Res.*, **24**, 336–341.
14. Zaludova, R., Zakovska, A., Kasparkova, J., Balcarova, Z., Vrana, O., Coluccia, M., Natile, G. and Brabec, V. (1997) DNA modifications by antitumor *trans*-[PtCl₂(E-iminoether)]₂. *Mol. Pharmacol.*, **52**, 354–361.
15. Brabec, V., Kleinwachter, V., Butour, J.L. and Johnson, N.P. (1990) Biophysical studies of the modification of DNA by antitumor platinum coordination complexes. *Biophys. Chem.*, **35**, 129–141.
16. Lemaire, M.A., Schwartz, A., Rahmouni, A.R. and Leng, M. (1991) Interstrand cross-links are preferentially formed at the d(GC) sites in the reaction between *cis*-diamminedichloroplatinum(II) and DNA. *Proc. Natl Acad. Sci. USA*, **88**, 1982–1985.
17. Brabec, V. and Leng, M. (1993) DNA interstrand cross-links of *trans*-diamminedichloroplatinum(II) are preferentially formed between guanine and complementary cytosine residues. *Proc. Natl Acad. Sci. USA*, **90**, 5345–5349.
18. Andersen, B., Margiotta, N., Coluccia, M., Natile, G. and Sletten, E. (2000) Antitumor *trans* platinum DNA adducts: NMR and HPLC study of the interaction between a *trans*-Pt iminoether complex and the deoxy decamer d(CCTCGCTCTC).d(GAGAGCGAGG). *Metal-Based Drugs*, **7**, 23–32.
19. Cini, R., Caputo, P.A., Intini, F.P. and Natile, G. (1995) Mechanistic and stereochemical investigation of iminoethers formed by alcoholysis of coordinated nitrils: X-ray crystal structure of *cis*- and *trans*-[bis(1-imino-1-methoxyethane) dichloroplatinum(II)]. *Inorg. Chem.*, **34**, 1130–1137.
20. Brabec, V., Reedijk, J. and Leng, M. (1992) Sequence-dependent distortions induced in DNA by monofunctional platinum(II) binding. *Biochemistry*, **31**, 12397–12402.
21. Stros, M. (1998) DNA bending by the chromosomal protein HMG1 and its high mobility group box domains. Effect of flanking sequences. *J. Biol. Chem.*, **273**, 10355–10361.
22. Stros, M. (2001) Two mutations of basic residues within the N-terminus of HMG-1 B domain with different effects on DNA supercoiling and binding to bent DNA. *Biochemistry*, **40**, 4769–4779.
23. Kasparkova, J., Mellish, K.J., Qu, Y., Brabec, V. and Farrell, N. (1996) Site-specific d(GpG) intrastrand cross-links formed by dinuclear platinum complexes. Bending and NMR studies. *Biochemistry*, **35**, 16705–16713.
24. Brabec, V., Sip, M. and Leng, M. (1993) DNA conformational distortion produced by site-specific interstrand cross-link of *trans*-diamminedichloroplatinum(II). *Biochemistry*, **32**, 11676–11681.
25. Koo, H.S., Wu, H.M. and Crothers, D.M. (1986) DNA bending at adenine-thymine tracts. *Nature*, **320**, 501–506.
26. Bellon, S.F. and Lippard, S.J. (1990) Bending studies of DNA site-specifically modified by cisplatin, *trans*-diamminedichloroplatinum(II) and *cis*-Pt(NH₃)₂(N₃-cytosine)Cl⁺. *Biophys. Chem.*, **35**, 179–188.
27. Kasparkova, J., Farrell, N. and Brabec, V. (2000) Sequence specificity, conformation and recognition by HMG1 protein of major DNA interstrand cross-links of antitumor dinuclear platinum complexes. *J. Biol. Chem.*, **275**, 15789–15798.
28. Bailly, C., Gentle, D., Hamy, F., Purcell, M. and Waring, M.J. (1994) Localized chemical reactivity in DNA associated with the sequence-specific bisintercalation of echinomycin. *Biochem. J.*, **300**, 165–173.
29. Ross, S.A. and Burrows, C.J. (1996) Cytosine-specific chemical probing of DNA using bromide and monoperoxysulfate. *Nucleic Acids Res.*, **24**, 5062–5063.
30. Bailly, C. and Waring, M.J. (1997) Diethylpyrocarbonate and osmium tetroxide as probes for drug-induced changes in DNA conformation *in vitro*. In Fox, K.R. (ed.), *Drug-DNA Interaction Protocols*. Humana Press Inc, Totowa, NJ, pp. 51–79.
31. He, Q., Ohndorf, U.-A. and Lippard, S.J. (2000) Intercalating residues determine the mode of HMG1 domains A and B binding to cisplatin-modified DNA. *Biochemistry*, **39**, 14426–14435.
32. Lam, W.C., VanderSchans, E.J.C., Sowers, L.C. and Millar, D.P. (1999) Interaction of DNA polymerase I (Klenow fragment) with DNA substrates containing extrahelical bases: Implications for proofreading of frameshift errors during DNA synthesis. *Biochemistry*, **38**, 2661–2668.
33. Patel, P.H., Suzuki, M., Adman, E., Shinkai, A. and Loeb, L.A. (2001) Prokaryotic DNA polymerase I: Evolution, structure and 'base flipping' mechanism for nucleotide selection. *J. Mol. Biol.*, **308**, 823–837.
34. Johnson, K.A. (1993) Conformational coupling in DNA-polymerase fidelity. *Annu. Rev. Biochem.*, **62**, 685–713.
35. Matsunaga, T., Mu, D., Park, C.-H., Reardon, J.T. and Sancar, A. (1995) Human DNA repair excision nuclease. *J. Biol. Chem.*, **270**, 20862–20869.
36. Buschta-Hedayat, N., Buterin, T., Hess, M.T., Missura, M. and Naegeli, H. (1999) Recognition of non-hybridizing base pairs during nucleotide excision repair of DNA. *Proc. Natl Acad. Sci. USA*, **96**, 6090–6095.
37. Manley, J.L., Fire, A., Cano, A., Sharp, P.A. and Gefter, M.L. (1980) DNA-dependent transcription of adenovirus genes in a soluble whole-cell extract. *Proc. Natl Acad. Sci. USA*, **77**, 3855–3859.
38. Reardon, J.T., Vaisman, A., Chaney, S.G. and Sancar, A. (1999) Efficient nucleotide excision repair of cisplatin, oxaliplatin and bis-aceto-amine-dichloro-cyclohexylamine-platinum(IV) (JM216) platinum intrastrand DNA diadducts. *Cancer Res.*, **59**, 3968–3971.
39. Jamieson, E.R. and Lippard, S.J. (1999) Structure, recognition and processing of cisplatin-DNA adducts. *Chem. Rev.*, **99**, 2467–2498.
40. Bellon, S.F., Coleman, J.H. and Lippard, S.J. (1991) DNA unwinding produced by site-specific intrastrand cross-links of the antitumor drug *cis*-diamminedichloroplatinum(II). *Biochemistry*, **30**, 8026–8035.
41. Huang, H.F., Zhu, L.M., Reid, B.R., Drobný, G.P. and Hopkins, P.B. (1995) Solution structure of a cisplatin-induced DNA interstrand cross-link. *Science*, **270**, 1842–1845.
42. Kasparkova, J., Novakova, O., Farrell, N. and Brabec, V. (2003) DNA binding by antitumor *trans*-[PtCl₂(NH₃)₂(thiazole)]₂. Protein recognition and nucleotide excision repair of monofunctional adducts. *Biochemistry*, **42**, 792–800.
43. Zehnulova, J., Kasparkova, J., Farrell, N. and Brabec, V. (2001) Conformation, recognition by high mobility group domain proteins and nucleotide excision repair of DNA intrastrand cross-links of novel antitumor trinuclear platinum complex BBR3464. *J. Biol. Chem.*, **276**, 22191–22199.
44. Rhodes, D. and Klug, A. (1980) Helical periodicity of DNA determined by enzyme digestion. *Nature*, **286**, 573–578.
45. Rice, J.A., Crothers, D.M., Pinto, A.L. and Lippard, S.J. (1988) The major adduct of the antitumor drug *cis*-diamminedichloroplatinum(II) with DNA bends the duplex by 40° toward the major groove. *Proc. Natl Acad. Sci. USA*, **85**, 4158–4161.
46. Kosthunova, H. and Brabec, V. (2000) Conformational analysis of site-specific DNA cross-links of cisplatin-distamycin conjugates. *Biochemistry*, **39**, 12639–12649.
47. Nielsen, P.E. (1990) Chemical and photochemical probing of DNA complexes. *J. Mol. Recognit.*, **3**, 1–24.
48. Malina, J., Hofr, C., Maresca, L., Natile, G. and Brabec, V. (2000) DNA interactions of antitumor cisplatin analogs containing enantiomeric amine ligands. *Biophys. J.*, **78**, 2008–2021.
49. Wei, M., Cohen, S.M., Silverman, A.P. and Lippard, S.J. (2001) Effects of spectator ligands on the specific recognition of intrastrand platinum-DNA cross-links by high mobility group box and TATA-binding proteins. *J. Biol. Chem.*, **276**, 38774–38780.
50. Ohndorf, U.M., Rould, M.A., He, Q., Pabo, C.O. and Lippard, S.J. (1999) Basis for recognition of cisplatin-modified DNA by high-mobility-group proteins. *Nature*, **399**, 708–712.
51. Cohen, S.M., Mikata, Y., He, Q. and Lippard, S.J. (2000) HMG-domain protein recognition of cisplatin 1,2-intrastrand d(GpG) cross-links in purine-rich sequence contexts. *Biochemistry*, **39**, 11771–11776.
52. Kasparkova, J., Zehnulova, J., Farrell, N. and Brabec, V. (2002) DNA interstrand cross-links of the novel antitumor trinuclear platinum complex BBR3464. Conformation, recognition by high mobility group domain proteins and nucleotide excision repair. *J. Biol. Chem.*, **277**, 48076–48086.
53. Stehlikova, K., Kosthunova, H., Kasparkova, J. and Brabec, V. (2002) DNA bending and unwinding due to the major 1,2-GG intrastrand cross-link formed by antitumor *cis*-diamminedichloroplatinum(II) are flanking-base independent. *Nucleic Acids Res.*, **30**, 2894–2898.
54. Kasparkova, J., Delalande, O., Stros, M., Elizondo-Riojas, M.A., Vojtiskova, M., Kozelka, J. and Brabec, V. (2003) Recognition of DNA interstrand cross-link of antitumor cisplatin by HMG1 protein. *Biochemistry*, **42**, 1234–1244.
55. Comess, K.M., Burstyn, J.N., Essigmann, J.M. and Lippard, S.J. (1992) Replication inhibition and translesion synthesis on templates containing site-specifically placed *cis*-diamminedichloroplatinum(II) DNA adducts. *Biochemistry*, **31**, 3975–3990.
56. Suo, Z. and Johnson, K. (1998) DNA secondary structure effects on DNA synthesis catalyzed by HIV-1 reverse transcriptase. *J. Biol. Chem.*, **273**, 27259–27267.

57. Vaisman, A., Warren, M.W. and Chaney, S.G. (2001) The effect of DNA structure on the catalytic efficiency and fidelity of human DNA polymerase beta on templates with platinum-DNA adducts. *J. Biol. Chem.*, **276**, 18999–19005.
58. Suo, Z., Lippard, S. and Johnson, K. (1999) Single d(GpG)/cis-diammineplatinum(II) adduct-induced inhibition of DNA polymerization. *Biochemistry*, **38**, 715–726.
59. Hubscher, U., Nasheuer, H.P. and Syvaaja, J.E. (2000) Eukaryotic DNA polymerases, a growing family. *Trends Biochem. Sci.*, **25**, 143–147.
60. Steitz, T.A. (1999) DNA polymerases: Structural diversity and common mechanisms. *J. Biol. Chem.*, **274**, 17395–17398.
61. Lone, S. and Romano, L.J. (2003) Mechanistic insights into replication across from bulky DNA adducts: A mutant polymerase I allows an N-acetyl-2-aminofluorene adduct to be accommodated during DNA synthesis. *Biochemistry*, **42**, 3826–3834.
62. Sancar, A. (1996) DNA excision repair. *Annu. Rev. Biochem.*, **65**, 43–81.
63. Wood, R.D. (1996) DNA repair in eukaryotes. *Annu. Rev. Biochem.*, **65**, 135–167.
64. Reardon, J.T. and Sancar, A. (1998) Molecular mechanism of nucleotide excision repair in mammalian cells. In Dizdaroglu, M. and Karakaya, A. (eds), *Advances in DNA Damage and Repair*. Plenum Publishing Corp., New York, NY, pp. 377–393.
65. Jones, S.L., Hickson, I.D., Harris, A.L. and Harnett, P.R. (1994) Repair of cisplatin-DNA adducts by protein extracts from human ovarian carcinoma. *Int. J. Cancer*, **59**, 388–393.
66. Zamble, D.B., Mu, D., Reardon, J.T., Sancar, A. and Lippard, S.J. (1996) Repair of cisplatin-DNA adducts by the mammalian excision nuclease. *Biochemistry*, **35**, 10004–10013.
67. Moggs, J.G., Szymkowski, D.E., Yamada, M., Karran, P. and Wood, R.D. (1997) Differential human nucleotide excision repair of paired and mispaired cisplatin-DNA adducts. *Nucleic Acids Res.*, **25**, 480–490.
68. Koberle, B., Masters, J.R.W., Hartley, J.A. and Wood, R.D. (1999) Defective repair of cisplatin-induced DNA damage caused by reduced XPA protein in testicular germ cell tumours. *Curr. Biol.*, **9**, 273–276.
69. Li, M.J. and Yang, L.Y. (1999) Use of novel plasmid constructs to demonstrate fludaurine triphosphate inhibition of nucleotide excision repair of a site-specific 1,2-d(GpG) intrastrand cisplatin adduct. *Int. J. Oncol.*, **15**, 1177–1183.
70. Huang, J.-C., Svoboda, D.L., Reardon, J.T. and Sancar, A. (1992) Human nucleotide excision nuclease removes thymine dimers from DNA by incising the 22nd phosphodiester bond 5' and the 6th phosphodiester bond 3' to the photodimer. *Proc. Natl Acad. Sci. USA*, **89**, 3664–3668.
71. Calsou, P., Frit, P. and Salles, B. (1992) Repair synthesis by human cell extracts in cisplatin-damaged DNA is preferentially determined by minor adducts. *Nucleic Acids Res.*, **20**, 6363–6368.
72. Buterin, T., Hess, M.T., Gunz, D., Geacintov, N.E., Mullenders, L.H. and Naegeli, H. (2002) Trapping of DNA nucleotide excision repair factors by non-repairable carcinogen adducts. *Cancer Res.*, **62**, 4229–4235.
73. Malina, J., Kasparkova, J., Natile, G. and Brabec, V. (2002) Recognition of major DNA adducts of enantiomeric cisplatin analogs by HMG box proteins and nucleotide excision repair of these adducts. *Chem. Biol.*, **9**, 629–638.
74. Johnson, N.P., Butour, J.-L., Villani, G., Wimmer, F.L., Defais, M., Pierson, V. and Brabec, V. (1989) Metal antitumor compounds: The mechanism of action of platinum complexes. *Prog. Clin. Biochem. Med.*, **10**, 1–24.
75. Fuertes, M.A., Alonso, C. and Perez, J.M. (2003) Biochemical modulation of cisplatin mechanisms of action: Enhancement of antitumor activity and circumvention of drug resistance. *Chem. Rev.*, **103**, 645–662.
76. Guo, Z.J. and Sadler, P.J. (1999) Metals in medicine. *Angew. Chem. Int. Ed.*, **38**, 1513–1531.
77. Jordan, P. and Carmo-Fonseca, M. (2000) Molecular mechanisms involved in cisplatin cytotoxicity. *Cell. Mol. Life Sci.*, **57**, 1229–1235.
78. Cohen, S.M. and Lippard, S.J. (2001) Cisplatin: From DNA damage to cancer chemotherapy. *Prog. Nucleic Acid Res. Mol. Biol.*, **67**, 93–130.
79. Wei, M., Burenkova, O. and Lippard, S.J. (2003) Cisplatin sensitivity in Hmgb1^(-/-) and Hmgb1^(+/+) mouse cells. *J. Biol. Chem.*, **278**, 1769–1773.
80. Ciccarelli, R.B., Solomon, M.J., Varshavsky, A. and Lippard, S.J. (1985) *In vivo* effects of cis- and trans-diamminedichloroplatinum(II) on SV 40 chromosomes: Differential repair, DNA-protein cross-linking and inhibition of replication. *Biochemistry*, **24**, 7533–7540.
81. Eastman, A. and Barry, M.A. (1987) Interaction of trans-diamminedichloroplatinum(II) with DNA: Formation of monofunctional adducts and their reaction with glutathione. *Biochemistry*, **26**, 3303–3307.
82. Bancroft, D.P., Lepre, C.A. and Lippard, S.J. (1990) Pt-195 NMR kinetic and mechanistic studies of cis-diamminedichloroplatinum and trans-diamminedichloroplatinum(II) binding to DNA. *J. Am. Chem. Soc.*, **112**, 6860–6871.
83. Lepre, C.A. and Lippard, S.J. (1990) Interaction of platinum antitumor compounds with DNA. In Eckstein, F. and Lilley, D.M.J. (eds), *Nucleic Acids and Molecular Biology*. Springer-Verlag, Berlin, Heidelberg, Germany, Vol. 4, pp. 9–38.
84. Kelland, L.R. (1993) New platinum antitumor complexes. *Crit. Rev. Oncol. Hematol.*, **15**, 191–219.
85. Leng, M., Schwartz, A. and Giraud-Panis, M.J. (2000) Transplatin-modified oligonucleotides as potential antitumor drugs. In Kelland, L.R. and Farrell, N.P. (eds), *Platinum-Based Drugs in Cancer Therapy*. Humana Press Inc, Totowa, NJ, pp. 63–85.
86. Zaludova, R., Natile, G. and Brabec, V. (1997) The effect of antitumor trans-[PtCl₂(E-iminoether)₂] on B→Z transition in DNA. *Anti-Cancer Drug Des.*, **12**, 295–309.
87. Zamble, D.B. and Lippard, S.J. (1999) The response of cellular proteins to cisplatin-damaged DNA. In Lippert, B. (ed.), *Cisplatin. Chemistry and Biochemistry of a Leading Anticancer Drug*. VCH, Wiley-VCH, Zürich, Weinheim, pp. 73–110.
88. Kartalou, M. and Essigmann, J.M. (2001) Recognition of cisplatin adducts by cellular proteins. *Mutation Res.*, **478**, 1–21.
89. Zwelling, L.A., Anderson, T. and Kohn, K.W. (1979) DNA-protein and DNA interstrand cross-linking by cis- and trans-platinum(II)diamminedichloride in L1210 mouse leukemia cells and relation to cytotoxicity. *Cancer Res.*, **39**, 365–369.
90. Banjar, Z.M., Hnilica, L.S., Briggs, R.C., Stein, J. and Stein, G. (1984) cis- and trans-Diamminedichloroplatinum(II)-mediated cross-linking of chromosomal non-histone proteins to DNA in HeLa cells. *Biochemistry*, **23**, 1921–1926.
91. Olinski, R., Wedrychowski, A., Schmidt, W.N., Briggs, R.C. and Hnilica, L.S. (1987) *In vivo* DNA-protein cross-linking by cis- and trans-diamminedichloroplatinum(II). *Cancer Res.*, **47**, 201–205.
92. Baudin, F., Romby, P., Romaniuk, P.J., Ehresmann, B. and Ehresmann, C. (1989) Crosslinking of transcription factor TFI_{II} to ribosomal 5S RNA from *X. laevis* by trans-diamminedichloroplatinum(II). *Nucleic Acids Res.*, **17**, 10035–10046.
93. Miller, C.A., Cohen, M.D. and Costa, M. (1991) Complexing of actin and other nuclear proteins to DNA by cis-diamminedichloroplatinum(II) and chromium compounds. *Carcinogenesis*, **12**, 269–276.
94. Olinski, R.B.R.C. (1991) DNA-protein cross-linking in L1210 cells and resistant to cis-diamminedichloroplatinum(II). *Mol. Biol. Rep.*, **15**, 81–86.
95. Comess, K.M. and Lippard, S.J. (1993) Molecular aspects of platinum-DNA interactions. In Neidle, S. and Waring, M. (eds), *Molecular Aspects of Anticancer Drug-DNA Interactions*. The MacMillan Press Ltd, Houndmills, UK, Vol. 1, pp. 134–168.
96. Wozniak, K. and Walter, Z. (2000) Induction of DNA-protein cross-links by platinum compounds. *Z. Naturforsch. C*, **55**, 731–736.
97. Chichiarelli, S., Coppari, S., Turano, C., Eufemi, M., Altieri, F. and Ferraro, A. (2002) Immunoprecipitation of DNA-protein complexes cross-linked by cis-diamminedichloroplatinum. *Anal. Biochem.*, **302**, 224–229.
98. Plooy, A.C.M., Van Dijk, M. and Lohman, P.H.M. (1984) Induction and repair of DNA cross-links in Chinese hamster ovary cells treated with various platinum coordination compounds in relation to platinum binding to DNA, cytotoxicity, mutagenicity and antitumor activity. *Cancer Res.*, **44**, 2043–2051.
99. Kasparkova, J., Marini, V., Najajreh, Y., Gibson, D. and Brabec, V. (2003) DNA binding mode of the cis and trans geometries of new antitumor non-classical platinum complexes containing piperidine, piperazine or 4-picoline ligand in cell-free media. Relations to their activity in cancer cell lines. *Biochemistry*, **42**, 6321–6332.
100. Zakovska, A., Novakova, O., Balcarova, Z., Bierbach, U., Farrell, N. and Brabec, V. (1998) DNA interactions of antitumor trans-[PtCl₂(NH₃)(quinoline)]. *Eur. J. Biochem.*, **254**, 547–557.
101. Brabec, V., Nepelchova, K., Kasparkova, J. and Farrell, N. (2000) Steric control of DNA interstrand cross-link sites of trans platinum complexes: specificity can be dictated by planar non-leaving groups. *J. Biol. Inorg. Chem.*, **5**, 364–368.

20.

Activation of Trans Geometry in Bifunctional Mononuclear Platinum Complexes by a Piperidine Ligand

MECHANISTIC STUDIES ON ANTITUMOR ACTION*^[S]

Received for publication, May 6, 2003, and in revised form, September 3, 2003
Published, JBC Papers in Press, September 10, 2003, DOI 10.1074/jbc.M304720200

Jana Kasparkova^{‡§¶}, Olga Novakova[‡], Victoria Marini[‡], Yousef Najajreh^{¶**}, Dan Gibson^{¶**},
Jose-Manuel Perez^{‡‡}, and Viktor Brabec[‡]

From the [‡]Institute of Biophysics, Academy of Sciences of the Czech Republic, CZ-61265 Brno, Czech Republic,
[¶]Department of Medicinal Chemistry and Natural Products, School of Pharmacy and the ^{**}David R. Bloom
Center for Pharmacy, The Hebrew University of Jerusalem, Jerusalem 91120, Israel, and ^{‡‡}Departamento
de Química Inorgánica, Facultad de Ciencias, Universidad Autónoma de Madrid, 28049 Madrid, Spain

A paradigm for the structure-pharmacological activity relationship of bifunctional platinum antitumor drugs is that the trans isomer of antitumor cisplatin (transplatin) is clinically ineffective. To this end, however, several new complexes of the trans structure have been identified that exhibit cytotoxicity in tumor cells that is even better than that of the analogous cis isomers. We reported recently (Kasparkova, J., Marini, V., Najajreh, Y., Gibson, D., and Brabec, V. (2003) *Biochemistry* 42, 6321–6332) that the replacement of one ammine ligand by the heterocyclic ligand, such as piperidine, piperazine, or 4-picoline in the molecule of transplatin resulted in a radical enhancement of its cytotoxicity. We examined oligodeoxyribonucleotide duplexes bearing a site-specific cross-link of the transplatin analogue containing the piperidine ligand by biochemical methods. The results indicate that in contrast to transplatin, *trans*-(PtCl₂(NH₃)(piperidine)) forms stable 1,3-intrastrand cross-links in double-helical DNA that distort DNA and are not readily removed from DNA by nucleotide excision repair system. Hence, the intrastrand cross-links of *trans*-(PtCl₂(NH₃)(piperidine)) could persist for a sufficiently long time, potentiating its toxicity toward tumor cells. *trans*-(PtCl₂(NH₃)(piperidine)) also forms in DNA minor interstrand cross-links that are similar to those of transplatin so that these adducts appear less likely candidates for genotoxic lesion responsible for antitumor effects of *trans*-(PtCl₂(NH₃)(piperidine)). Hence, the role of structurally unique intrastrand cross-links in the antitumor effects of transplatin analogues in which one ammine group is replaced by a heterocyclic ligand may predominate.

The more widespread clinical applicability of *cis*-diamminedichloroplatinum(II) (cisplatin)¹ (Fig. 1A) and its ana-

logue *cis*-diamminecyclobutanedicarboxylatoplatinum(II) is limited to a relatively narrow range of tumors (1–3); some tumors have natural resistance to these platinum drugs, whereas others develop resistance after the initial treatment. Cisplatin also has limited solubility in aqueous solution and is administered intravenously. There are also significant problems in terms of inducing severe side effects (especially kidney damage and vomiting/nausea). The drawbacks coupled with cisplatin and *cis*-diamminecyclobutanedicarboxylatoplatinum(II) toxicity have been the impetus for the development of improved platinum drugs.

The paradigm for structure-pharmacological activity relationship of platinum complexes is that the trans isomer of cisplatin (transplatin) (Fig. 1A) is clinically ineffective. To this end, however, several new complexes of the trans structure have been identified that exhibit an enhanced cytotoxicity in tumor cell lines, such that cytotoxicity is equivalent or even better than that of the analogous cis isomers and, indeed, cisplatin itself (for reviews, see Refs. 4–6). Examples of such new antitumor transplatinum compounds are (i) analogues containing planar amine ligand of general structure *trans*-(PtCl₂(NH₃)(L)), where L represents planar amine such as quinoline or thiazole; (ii) analogues containing iminoether groups of the general formula *trans*-(PtCl₂(*E*-iminoether)₂) (*trans-EE*); and (iii) analogues with asymmetric aliphatic ligands and *trans*-(PtCl₂(NH₃)(L)), where L represents cyclohexylamine.

We have recently reported (7–9) that the replacement of one ammine ligand by the heterocyclic ligand, such as piperidine (pip) (Fig. 1A), piperazine, or 4-picoline in the molecule of transplatin results in a radical enhancement of its activity in tumor cell lines both sensitive and resistant to cisplatin. For instance, the IC₅₀ (the concentration of the compound that afforded 50% cell killing) of *trans*-(PtCl₂(NH₃)(pip)) in the A2780 cell line was more than 40 times lower than that of transplatin. Since DNA is considered the major pharmacological target of antitumor platinum drugs (10), it appears important that due to this replacement, the analogues of transplatin alter the properties of DNA in a markedly different way than the parent compound. This is an intriguing finding, because the

* This work was supported by Grant Agency of the Czech Republic Grant 305/02/1552A, Grant Agency of the Academy of Sciences of the Czech Republic Grant B5004301, and the Wellcome Trust (to J. K. and V. B.). The costs of publication of this article were defrayed in part by the payment of page charges. This article must therefore be hereby marked "advertisement" in accordance with 18 U.S.C. Section 1734 solely to indicate this fact.

^[S] The on-line version of this article (available at <http://www.jbc.org>) contains four additional figures.

[§] International Scholar of Howard Hughes Medical Institute.

[¶] To whom correspondence should be addressed. Tel.: 420-541517174; Fax: 420-541240499; E-mail: jana@ibp.cz.

¹ The abbreviations used are: cisplatin, *cis*-diamminedichloroplatinum(II); transplatin, *trans*-diamminedichloroplatinum(II); pip, piperi-

dine; CL, cross-link; HMG, high mobility group; HMGB1a, HMGB1 domain A; HMGB1b, HMGB1 domain B; RPA, replication protein A; KF⁻, Klenow fragment of *E. coli* DNA polymerase I deficient in 3' → 5' proofreading exonuclease activity; RT HIV-1, reverse transcriptase from the human immunodeficiency virus type 1; PAA, polyacrylamide; CFE, cell-free extract; NER, nucleotide excision repair; CHO, Chinese hamster ovary.

same replacement in the molecule of antitumor cisplatin (Fig. 1A) results in a reduced activity of the drug in both sensitive and resistant cell lines (for instance, the IC_{50} measured in A2780 cell line was ~ 12 times higher than that of cisplatin (9)). Thus, the latter observation represents an additional example of activation of *trans* geometry in bifunctional mononuclear platinum(II) compounds, although the reasons for this activation have not been completely clarified.

Preliminary mechanistic studies using the analogues of transplatin containing piperidine, piperazine, or 4-picoline nonleaving ligand (9) suggest that one strategy how to activate *trans* geometry in antitumor bifunctional platinum(II) compounds may consist in a chemical modification of the ineffective transplatin, resulting in an increased stability of its intrastrand cross-links (CLs) in double-helical DNA and/or in an increased efficiency to form interstrand CLs. Hence, the latter suggestion is consistent with the concept of designing new platinum drugs (acting by a new mechanism and with activity complementary to drugs such as cisplatin) based on the observation that the replacement of the ammine ligand in transplatin can modulate their DNA binding mode and consequently their activity in cancer cell lines (11).

Initial data on calf thymus and plasmid DNA globally modified in cell-free media by analogues of transplatin in which one ammine ligand was replaced by piperidine, piperazine, or 4-picoline have been reported in our previous work (9). The results have demonstrated that these analogues form on DNA mainly intrastrand and interstrand CLs (for instance *trans*-($PtCl_2(NH_3)(pip)$) forms $\sim 26\%$ interstrand and $\sim 59\%$ intrastrand CLs if DNA is incubated with this compound for 48 h). These results are of fundamental importance, because the clinical ineffectivity of transplatin has been proposed to be associated with a low stability of its intrastrand CLs in double-helical DNA and in general with its reduced capability to form in double-helical DNA bifunctional adducts (12, 13). Because structural details of individual DNA adducts formed by these analogues of transplatin are not yet available, it remains uncertain how these CLs affect conformation of DNA and how these alterations are further processed in the cells. Therefore, in order to shed light on the mechanism that underlies activity of transplatin analogues containing a heterocyclic ligand we examine in the present work in detail short oligodeoxyribonucleotide duplexes containing single, site-specific intrastrand or interstrand CL of the transplatin analogue containing the nonplanar piperidine ligand (Fig. 1A). The piperidine analogue of transplatin was chosen as the representative of this class of new platinum compounds. This choice was made because the changes in the activity in cancer cell lines and some features of its DNA binding mode in a cell-free medium due to the replacement of one ammine ligand by the heterocyclic group in the parent compound were most pronounced (9). We investigated how the CLs affect the local conformation of DNA (in particular, bending and unwinding) and how these adducts are stable in double-helical DNA and further processed by some cellular components in cell-free media.

Antitumor activity of platinum compounds is also affected by the factors that do not operate directly at the level of DNA adducts. Among these factors are also those that affect the amount of platinum complex that can reach target DNA in cancer cells by changing the cell accumulation of the complexes. Therefore, we also compared the cellular uptake of transplatin and its analogue containing the piperidine ligand and determined the amount of platinum bound to DNA in the cells treated with these platinum compounds.

EXPERIMENTAL PROCEDURES

Chemicals—*trans*-($PtCl_2(NH_3)(pip)$), where pip represents piperidine (Fig. 1A), was prepared by the methods described in detail previously (8). Cisplatin and transplatin (Fig. 1A) were obtained from Sigma. The stock solutions of platinum compounds were prepared at the concentration of 5×10^{-4} M in 10 mM $NaClO_4$ and stored at 4 °C in the dark. The synthetic oligodeoxyribonucleotides (Fig. 1B) were synthesized and purified as described previously (14). Human recombinant replication protein A (RPA) was purified from *Escherichia coli* (15) and was a kind gift of John J. Turchi. Human XPA protein was prepared and purified as in our previous paper (16). Restriction endonucleases, Klenow fragment of *E. coli* DNA polymerase I deficient in 3' \rightarrow 5' proofreading exonuclease activity (KF^-) and T4 polynucleotide kinase were purchased from New England Biolabs (Beverly, MA). Reverse transcriptase from human immunodeficiency virus type 1 (RT HIV-1) was from Calbiochem. Nonidet P-30 was from Fluka (Prague, Czech Republic). Acrylamide, bis(acrylamide), urea, and NaCN were from Merck. Radioactive products were from Amersham Biosciences. Proteinase K, RNase A, and ATP were from Roche Applied Science.

Measurements of Platinum Accumulation in CH1cisR Cells and Determination of Platinum Binding to DNA in Culture Cells—All details of these experiments were recently published (17, 18).

Platinations of Oligonucleotides—The duplexes containing single, intrastrand CL of cisplatin, transplatin, or *trans*-($PtCl_2(NH_3)(pip)$) in the top strand (the duplexes in Fig. 1B that contained two guanine (G) residues in the top strand) were prepared as described (9, 19, 20). The interstrand cross-linked duplexes were also prepared and characterized in the same way as described previously (21, 22).

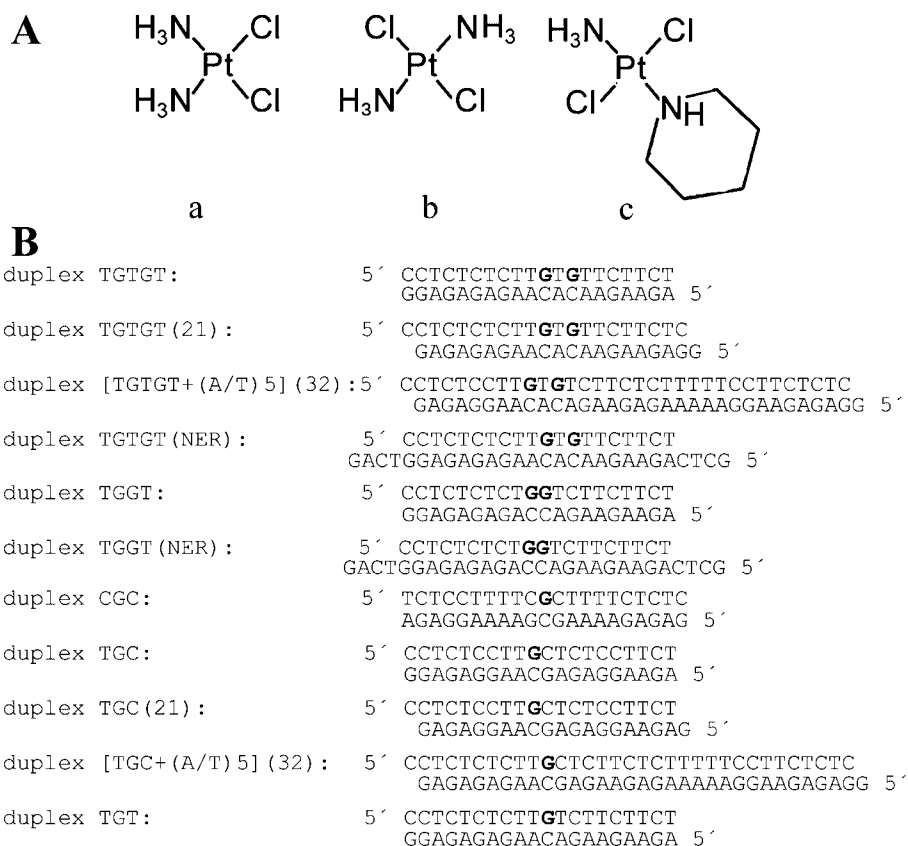
Hydroxyl Radical Footprinting of Interstrand CLs—Platinated (or unplatinated) oligodeoxyribonucleotide duplexes (their concentration was 6 nM) that had either the top or bottom strand ^{32}P -labeled at the 5'-end were dissolved in the medium of 50 mM NaCl, 10 mM Tris-HCl, pH 7.5. The cleavage of the phosphodiesteric bonds was performed by incubating the duplexes in 0.04 mM $Fe(NH_4)_2(SO_4)_2$, 0.08 mM EDTA, 0.03% H_2O_2 , and 2 mM sodium ascorbate for 5 min at 20 °C. The reaction was stopped by adding 15 mM thiourea, 3 mM EDTA, 0.3 M sodium acetate, and 0.3 mg tRNA/ml. After precipitation, the samples were loaded onto a 24% denaturing polyacrylamide (PAA)/8 M urea gel. Maxam-Gilbert sequencing reactions were run in parallel.

Inhibition of DNA Polymerization—The 23- or 30-mer templates (see Fig. 4) containing a single 1,3-GTG intrastrand CL of *trans*-($PtCl_2(NH_3)(pip)$) or 1,2-GG intrastrand CL of cisplatin were prepared in the same way as described (9, 19, 20). 8- or 13-mer DNA primers whose sequences are also shown in Fig. 4 were complementary to the 3' termini of the 23- or 30-mer templates, respectively. The DNA substrates were formed by annealing templates and 5'-end-labeled primers at a molar ratio of 3:1. All experiments using KF^- and RT HIV-1 were performed at 25 °C in a volume of 50 μ l in a buffer containing 50 mM Tris-HCl (pH 7.4), 10 mM $MgCl_2$, 0.1 mM dithiothreitol, 50 μ g/ml bovine serum albumin, 0.1% Nonidet P-30, 25 μ M dATP, 25 μ M dCTP, 25 μ M dGTP, and 25 μ M TTP and 0.5 unit of KF^- . The experiments with RT HIV-1 were performed at 37 °C using the same conditions, except that the nucleoside triphosphates were at a concentration of 100 μ M and 1.0 unit of RT HIV-1 was used. Reactions were terminated by the addition of EDTA, so that its resulting concentration was 20 mM, and heating at 100 °C for 30 s. Products were resolved by denaturing 24% PAA/8 M urea gel and then visualized and quantified by using the FUJIFILM bioimaging analyzer and AIDA image analyzer software.

Gel Mobility Shift Assay—Reactions with RPA and XPA. ^{32}P -Labeled DNA substrates (0.5 nM) and the amounts of RPA or XPA indicated were incubated at 20 °C in reactions of 20 μ l containing 25 mM HEPES-KOH (pH 8.3), 30 mM KCl, 4 mM $MgCl_2$, 1 mM EDTA, 0.9 mM dithiothreitol, 45 μ g/ml bovine serum albumin, and 10% glycerol. The reaction with XPA was still supplemented by unlabeled and unplatinated competitor duplex (20-bp, 70 nM). To assess binding at equilibrium, reactions were stopped after 30 min by cooling the samples to 0 °C. Following the addition of gel loading buffer (4 μ l) containing 100 mM Tris-HCl (pH 8.3), 10% glycerol, and 0.05% Orange G, the extent of binding was determined on 6% native PAA gel. The electrophoresis was performed for 50 min at 4 °C, gels were dried and visualized by using the FUJIFILM bio-imaging analyzer, and the radioactivities associated with bands were quantitated with the AIDA image analyzer software.

Nucleotide Excision Assay—The 148-bp substrates containing single, central intrastrand or interstrand CL were assembled from three oligonucleotide duplexes as described previously (23, 24).

Oligonucleotide excision reactions were performed in cell-free extracts (CFEs) prepared from the HeLa S3 and CHO AA8 cell lines as



described (25, 26). These extracts were kindly provided by J. T. Reardon and A. Sancar (University of North Carolina, Chapel Hill, NC). *In vitro* repair was measured with excision assay using these CFEs and 148-bp linear DNA substrates (see above) in the same way as described previously (26).

RESULTS

Cellular Platinum Complex Uptake—Platinum complexes of novel structure may have an altered pharmacology associated with drug uptake that may affect their cytotoxicity. Therefore, we examined first how the replacement of the ammine group in transplatin by piperidine ligand affects its accumulation in tumor cell lines.

Results in CH1cisR cells (this cancer cell line was among those used for testing activity of the novel transplatin analogues in which *trans*-(PtCl₂(NH₃)(pip)) exhibited a markedly enhanced activity in comparison with transplatin (9)) show that the replacement of the ammine group by the piperidine ligand considerably reduces the amount of platinum associated with the cells (Fig. 2A). Given that significantly less *trans*-(PtCl₂(NH₃)(pip)) appears to be accumulated in cells, the question arises as to how the piperidine ligand affects the binding of transplatin analogues to DNA in cells. Results in Fig. 2B demonstrate that *trans*-(PtCl₂(NH₃)(pip)) binds to DNA in CH1cisR cells treated with this transplatin analogue more slowly and to a lesser extent than the parent complex. This is in contrast to the data showing that transplatin and *trans*-(PtCl₂(NH₃)(pip)) bind to DNA in a cell-free medium with approximately the same rate (9). Hence, it is reasonable to suggest that the slower binding rate and the lesser binding level of *trans*-(PtCl₂(NH₃)(pip)) to DNA in culture cells is mainly a consequence of its lower intracellular concentration.

Fig. 2 shows that the markedly enhanced cytotoxicity of *trans*-(PtCl₂(NH₃)(pip)) in comparison with transplatin (9) is not due to either enhanced cellular accumulation or higher levels of DNA platination in the cells. Since the cytotoxicity

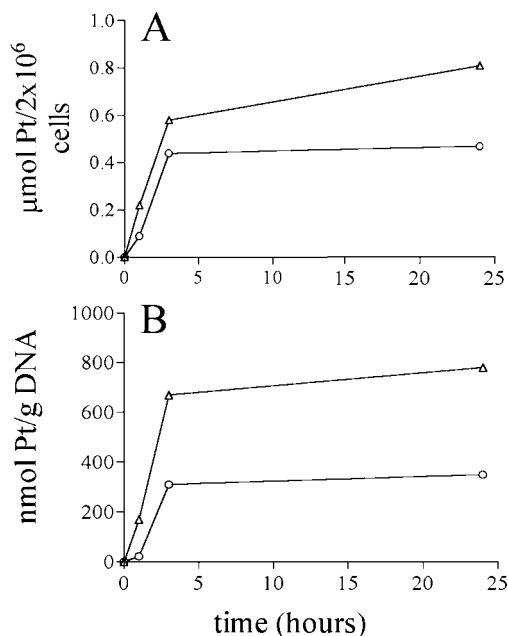


FIG. 2. CH1cisR cell uptake of platinum complexes and platinum accumulation on DNA isolated from CH1cisR cells treated with platinum complexes. A, uptake. Δ , transplatin; \circ , *trans*-(PtCl₂(NH₃)(pip)). B, accumulation. Δ , transplatin; \circ , *trans*-(PtCl₂(NH₃)(pip)). Each data point represents the mean \pm S.D. of four determinations from two independent experiments. The absence of error bars indicates that the size of the calculated error bar is smaller than the symbol. For other details, see "Results."

cannot be correlated with the levels of DNA modification, it is intuitively appealing to suggest that the enhanced cytotoxicity may be related to the nature of the adducts that are formed with the DNA and to the effects of the altered DNA properties on downstream cellular events.

Intrastrand Cross-links—Unlike cisplatin, due to steric reasons, transplatin and its analogues cannot form intrastrand CLs in double-helical DNA between adjacent base residues. The trans compounds can cross-link two bases on the same strand only if they are separated by at least one intervening base, forming mostly 1,3-GNG intrastrand CLs (where N represents adenine, cytosine, or thymine). These adducts formed by the antitumor analogues of transplatin, in which the ammine group was replaced by the heterocyclic ligand, are stable in double-helical DNA and represent major DNA adducts of this class of antitumor trans compounds. It was, therefore, of great interest to examine how single, site-specific 1,3-GTG intrastrand CL of *trans*-(PtCl₂(NH₃)(pip)) affects conformation of double-helical DNA and what are some subsequent “downstream” effects of this type of DNA damage, such as recognition by some damaged DNA-binding proteins and repair capacity for this lesion of eukaryotic nucleotide excision repair (NER) system.

Important structural motifs induced in DNA by antitumor platinum compounds that play a significant role in the mechanism underlying their antitumor activity are the bending and unwinding of the helix axis (27). For DNA intrastrand adducts of cisplatin and transplatin, the structural details responsible for bending and unwinding have been elucidated (28, 29). In this work we further performed studies on the bending and unwinding induced by single, site-specific intrastrand CL of *trans*-(PtCl₂(NH₃)(pip)) using electrophoretic retardation as a quantitative measure of the extent of planar curvature.

The oligodeoxyribonucleotide duplexes TGTGT(19–22) (19–22 bp long, whose sequences were identical or similar to that of the duplex TGTGT (21) shown in Fig. 1B; the 19- and 20-bp duplexes had one or two marginal C-G pairs deleted, respectively, whereas one additional T-A pair was added to one end in the 22-bp duplex) were used for the bending and unwinding studies of the present work. The ligation products of these unplatinated or CL containing duplexes were analyzed on native PAA electrophoresis gel. Experimental details of these studies are given in our recent reports (20, 30, 31). The DNA bending toward the minor groove and unwinding due to one 1,3-intrastrand adduct of *trans*-(PtCl₂(NH₃)(pip)) has been found 30 ± 2 and 8 ± 2°, respectively (the direction of the bend was determined using the duplex (TGTGT+(A/T)₅)(32) (Fig. 1B) in the same way as in our recent papers (21, 32, 33)). Moreover, the ligation of the 21- and 22-bp duplexes containing 1,3-intrastrand CL of *trans*-(PtCl₂(NH₃)(pip)) resulted in the formation of circles, suggesting that the 1,3-intrastrand CLs of this transplatin analogue increased the flexibility of the double helix (29, 34).

Further studies of the present work were focused on analysis of the distortion induced by the 1,3-intrastrand CL of *trans*-(PtCl₂(NH₃)(pip)) by chemical probes of DNA conformation. The duplex TGTGT (Fig. 1B) containing a single, site-specific adduct was treated with several chemical agents that are used as tools for monitoring the existence of conformations other than canonical B-DNA. These agents included KMnO₄, diethyl pyrocarbonate, and bromine. They react preferentially with single-stranded DNA and distorted double-stranded DNA (34, 35). We used for this analysis exactly the same methodology described in detail in our recent papers dealing with DNA adducts of various antitumor platinum drugs (21, 31, 34, 36, 37). Therefore, these experiments are only described in more detail in the Supporting material (see “Chemical Probes” and Fig. S2). The results schematically summarized in Fig. 3A indicate that 1,3-intrastrand CL of *trans*-(PtCl₂(NH₃)(pip)) induces in DNA the distortion that extends over at least 6 bp and

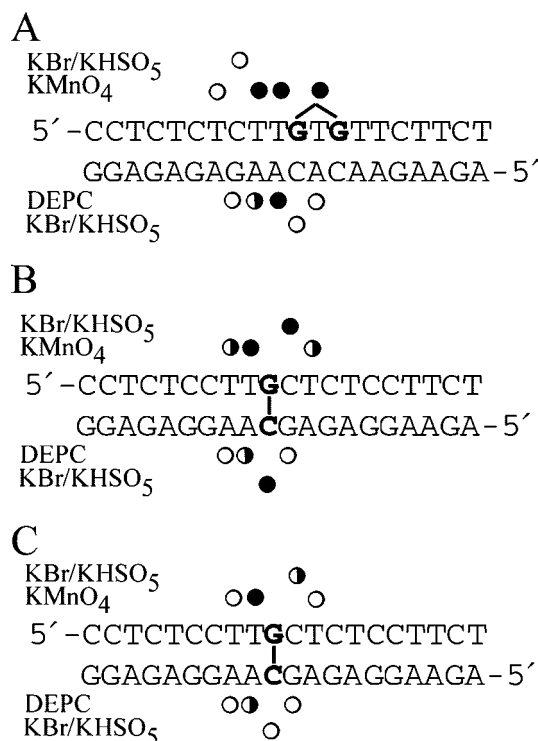


FIG. 3. Summary of the reactivity of chemical probes of DNA conformation. Piperidine-induced specific strand cleavage at KBr/KHSO₅, KMnO₄, and diethyl pyrocarbonate-modified bases in the duplexes TGTGT (21 bp) or TGT (20 bp) containing single, 1,3-GTG intrastrand CL of *trans*-(PtCl₂(NH₃)(pip)) (A), interstrand CL of *trans*-(PtCl₂(NH₃)(pip)) (B), or interstrand CL of transplatin (C). The oligomers were 5'-end-labeled at their top or bottom strands. Filled circle, strong reactivity; half-filled circle, medium reactivity; open circle, weak reactivity.

is localized mainly at the base pair between the platinated G residues and the base pairs on its 5' side.

It has been demonstrated that various DNA secondary structures have significant effects on processivity of a number of prokaryotic, eukaryotic, and viral DNA polymerases (38, 39). Interestingly, with DNA templates containing site-specifically placed adducts of various platinum compounds, a number of prokaryotic and eukaryotic DNA polymerases were blocked but could also traverse through platinum adducts, depending on their character and conformational alterations induced in DNA. It is therefore of great interest to examine whether DNA polymerases, processing DNA substrates containing either the 1,3-intrastrand CL of *trans*-(PtCl₂(NH₃)(pip)) or 1,2-GG intrastrand CL of cisplatin, could reveal potential differences in conformational alterations imposed on DNA by these two adducts. We investigated in the present work DNA polymerization using the templates site-specifically modified by *trans*-(PtCl₂(NH₃)(pip)) or cisplatin by two DNA polymerases, which differ in processivity and fidelity. In the first series of our experiments, we used Klenow fragment of DNA polymerase I as a model enzyme frequently used in the studies aimed at understanding the processes in which nucleic acid polymerases take part.

We constructed the 8-mer/23-mer primer-template duplexes TGTGT(KF) and TGGT(KF) (Fig. 4A) unplatinated or containing either 1,3-GTG intrastrand CL of *trans*-(PtCl₂(NH₃)(pip)) in the central TGTGT sequence or 1,2-GG intrastrand CL of cisplatin in the central TGGT sequence. The first 8 nucleotides on the 3' terminus of the 23-mer template strand were complementary to the nucleotides of the 8-mer primer, and the 3' guanine involved in the 1,3-GTG CL of *trans*-(PtCl₂(NH₃)(pip))

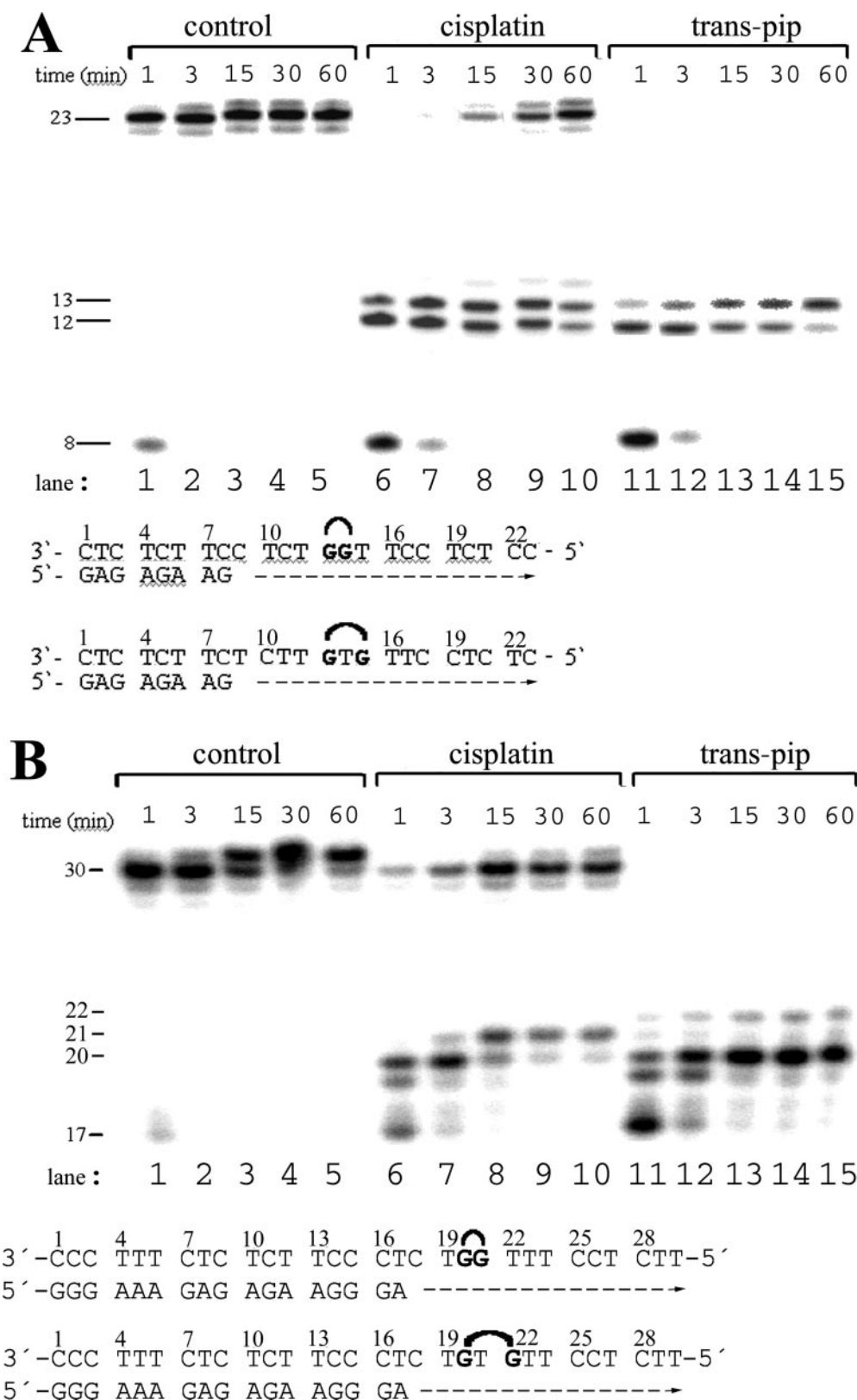


FIG. 4. Primer extension activity of exonuclease-deficient Klenow fragment of DNA polymerase I (A) and reverse transcriptase from the human immunodeficiency virus type 1 (B). The experiments were conducted using the 8-mer/23-mer (A) or 17-mer/30-mer primer-template (B) duplexes for the times indicated. Lanes 1–5, undamaged template; lanes 6–10, the template containing 1,2-GG intrastrand CL of cisplatin; lanes 11–15, the template containing 1,3-GTG intrastrand CL of *trans*-(PtCl₂(NH₃)₂(pip)). The strong pause sites opposite the platinated guanines were marked 12 and 13 in A or 20, 21, and 22 in B.

or in 1,2-GG CL of cisplatin on the template strand was located at its 13th position from the 3' terminus (Fig. 4A). After annealing the 8-nucleotide primer to the 3' terminus of the un-

platinated or platinated template strand (positioning the 3'-end of the primer five bases before the adduct in the template strand), we examined DNA polymerization through the single

1,3-CL of *trans*-(PtCl₂(NH₃)(pip)) or 1,2-intrastrand CL of cisplatin on the template by KF[−] in the presence of all four deoxyribonucleoside 5'-triphosphates. The reaction was stopped at various time intervals, and the products were analyzed using a sequencing gel (Fig. 4A). Polymerization using the template containing the CL of cisplatin proceeded rapidly up to the nucleotide preceding and at the sites opposite the CL, such that the 12- and 13-nucleotide products accumulated to a significant extent (shown in Fig. 4A, lanes 6–10). There was only a slight accumulation of larger DNA intermediates, whereas no intermediate products were seen with the 23-mer control template as the full-length product was being formed (shown in Fig. 4A, lanes 1–5). The full-length products were also noticed with the 23-mer template containing the CL of cisplatin, although in a smaller amount. This result is in an agreement with previously published work (40) in which T7 DNA polymerase and RT HIV-1 were used and confirms that 1,2-GG intrastrand CL of cisplatin inhibits DNA synthesis (38), but translesion synthesis may occur. In contrast, under the same experimental conditions, DNA polymerization by KF[−] using the template containing the 1,3-intrastrand CL of *trans*-(PtCl₂(NH₃)(pip)) proceeded up to the nucleotide preceding and at the site opposite the 3' G involved in the CL (Fig. 4A, lanes 11–15). There was almost no accumulation of shorter and larger DNA intermediates, and importantly, no full-length products accumulated. This result indicates that the character of the 1,3-GTG intrastrand CLs of *trans*-(PtCl₂(NH₃)(pip)) and alterations induced in DNA by this adduct are distinctly different from the features of the major adduct of cisplatin so that the adducts of *trans*-(PtCl₂(NH₃)(pip)) could potentially impede elongation of DNA to a higher extent than the major adducts of cisplatin (Fig. 4A).

We have also examined the effects of the 1,3-intrastrand CL of *trans*-(PtCl₂(NH₃)(pip)) on polymerization by RT HIV-1. This enzyme also possesses DNA template-dependent DNA polymerase activity but relatively low processivity and fidelity (41). In these studies, elongation of the 17-mer/30-mer primer-template duplexes was tested. As is demonstrated in Fig. 4B, we confirmed also by using this DNA polymerase showing a different mechanism underlying its catalytic activity than KF[−] that the 1,3-intrastrand CL of *trans*-(PtCl₂(NH₃)(pip)) constitutes a fairly strong block to DNA synthesis catalyzed by both DNA polymerases. Since there is a high degree of structural and sequence conservation of the domains among eukaryotic, prokaryotic, and viral polymerases (42), insights gleaned from studies of the KF[−] and RT HIV-1 should be also applicable to other DNA polymerases (43–45). Hence, the repercussion of stronger inhibition of DNA polymerization by the 1,3-intrastrand CL of *trans*-(PtCl₂(NH₃)(pip)) in comparison with the major adduct of cisplatin adds a new dimension to the impact of the activated trans geometry in platinum compounds on biological processes, possibly including replication or DNA repair.

An important feature of the mechanism that underlies the antitumor activity of cisplatin and its analogues is that the major adducts of these drugs (1,2-GG intrastrand CLs) are recognized by proteins containing HMG domains (27). Importantly, DNA modified by transplatin or monodentate platinum(II) compounds, such as chlorodiethylenetriamineplatinum(II) chloride or (PtCl(NH₃)₃)Cl, is not recognized by these cellular proteins. We examined whether also the replacement of the ammine group in transplatin by piperidine (resulting in the enhancement of cytotoxicity in tumor cell lines) also affects affinity of HMG-box proteins to the intrastrand adduct of this transplatin analogue. The interactions of the rat HMGB1 domain A (HMGB1a) and HMGB1 domain B (HMGB1b) with the 1,3-GTG intrastrand CLs of *trans*-(PtCl₂(NH₃)(pip)) were investigated using a gel mobility shift assay (46, 47). In these experiments (described in more detail in Supplemental Mate-

rial under "Recognition by HMGB1 proteins" (Fig. S4)), the 20-bp duplex TGTGT (Fig. 1B) was modified so that it contained a single, site-specific 1,3-intrastrand CL of *trans*-(PtCl₂(NH₃)(pip)). The binding of the HMGB1a and HMGB1b to these DNA probes was detected by retardation of the migration of the radiolabeled 20-bp probes through the gel (not shown) under identical conditions described in detail in our recent papers (21, 33).

Consistent with the previous reports (21, 46), a shifted band due to the incubation of the duplex containing 1,2-GG intrastrand CL of cisplatin with both HMGB1a and HMGB1b was observed, indicating that both proteins recognize the duplex containing the major adduct of cisplatin (Fig S4, lanes 5 and 6). These proteins exhibited under the same experimental conditions no binding to the 20-bp duplex unplatinated or containing the 1,3-intrastrand CL of *trans*-(PtCl₂(NH₃)(pip)) (Fig. S4, lanes 8 and 9). These data indicate that HMGB1 proteins do not bind the probe containing the 1,3-GTG intrastrand CL of *trans*-(PtCl₂(NH₃)(pip)).

NER is a pathway used by human cells for the removal of damaged nucleotides from DNA (48, 49). In mammalian cells, this repair pathway is an important mechanism for the removal of bulky, helix distorting DNA adducts, such as those generated by various chemotherapeutics including cisplatin (50). Efficient repair of 1,2-GG or 1,3-GNG intrastrand CL of cisplatin has been reported by various NER systems including human and rodent excinucleases (26, 51–55). The results presented in Fig. 5A, lanes 4 and 8, are consistent with these reports. The major excision fragment contains 28 nucleotides, and other primary excision fragments are 23–27 nucleotides in length (26, 56). Importantly, the 1,3-GTG intrastrand CL of *trans*-(PtCl₂(NH₃)(pip)) was also repaired by both human and rodent excinucleases, but with a markedly lower efficiency than the intrastrand CLs of cisplatin (shown in Fig. 5A, lane 6, and in Fig. 5B for the adduct repaired by rodent excinuclease).

The initial and rate-determining step of NER is the recognition of the damaged DNA (48, 57). This recognition process involves multiple protein components, and, for example, RPA and XPA belong to the initial damage-sensing factors of eukaryotic excision nuclease initiating repair (16, 58). These recognition proteins preferentially bind to damaged DNA so that binding of RPA and/or XPA to damaged DNA may be a sensitive indicator to predict whether mammalian NER could be effective in the removal of damaged nucleotides.

The binding of RPA is thought to proceed via the denaturation of the DNA substrate followed by high affinity binding to the single-stranded DNA (15, 16, 59). On the other hand, XPA binds most efficiently to rigidly bent DNA but not to single-stranded structures (16). To determine the effect of 1,3-intrastrand CL of *trans*-(PtCl₂(NH₃)(pip)) on RPA and XPA binding, the 20-bp TGTGT duplexes were prepared so that they contained a single, site-specific 1,3-GTG intrastrand CL of this compound. RPA or XPA binding to this duplex was assessed in a gel mobility shift assay. The duplex with blunt ends was purified so that it contained no contaminating single-stranded DNA, as was evident from analysis on native PAA gel (not shown). The 20-bp duplex TGGT containing single, site-specific 1,2-GG intrastrand CL of cisplatin was run as a positive control. The results of the gel mobility shift assay analysis (Fig. 6) demonstrated that increasing RPA or XPA concentrations resulted in the increasing amounts of these proteins bound to the 1,2-GG intrastrand CL of cisplatin, consistent with the previous observations (16). On the other hand, the same analysis performed with the substrate containing the single, site-specific 1,3-intrastrand CL of *trans*-(PtCl₂(NH₃)(pip)) revealed lower binding of RPA and no binding of XPA protein (Fig. 6).

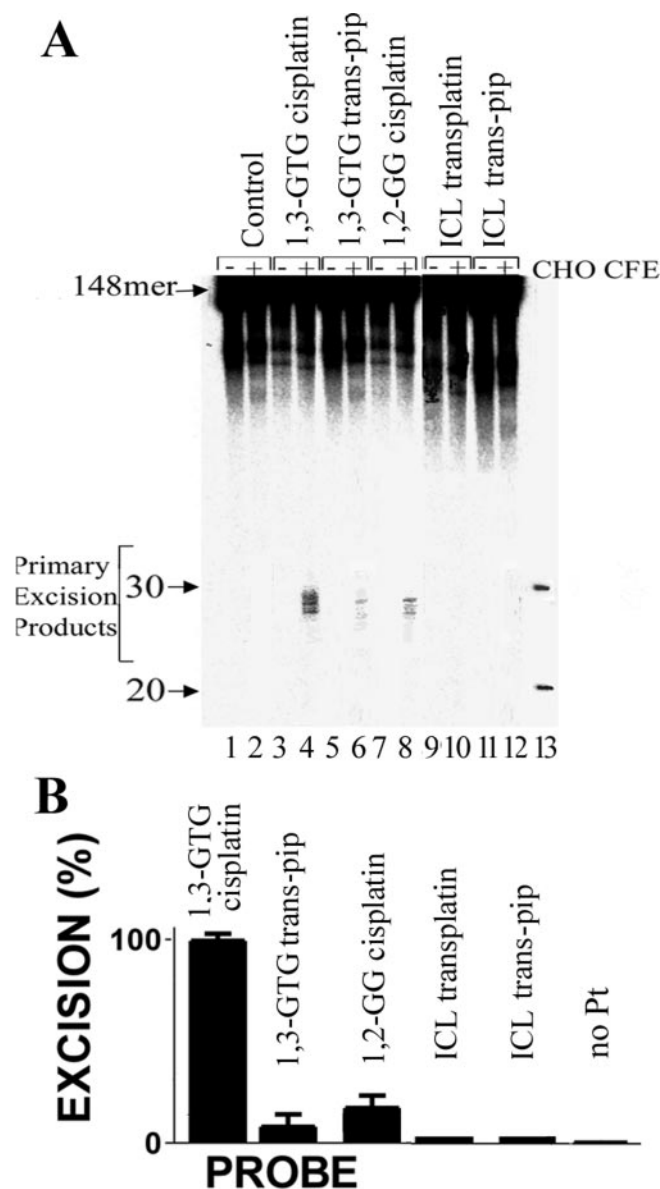


FIG. 5. Excision of the intrastrand and interstrand cross-links of platinum complexes by rodent excinuclease. A, the substrates were incubated with CHO AA8 CFE and subsequently treated overnight with NaCN prior to analysis in 10% PAA/8 M urea denaturing gel. Lanes 1 and 2, control, unplatinated substrate; lanes 3 and 4, the substrate containing the 1,3-GTG intrastrand CL of cisplatin; lanes 5 and 6, the substrate containing the 1,3-GTG intrastrand CL of *trans*-(PtCl₂(NH₃)(pip)); lanes 7 and 8, 1,2-GG intrastrand CL of cisplatin; lanes 9 and 10, the substrate containing the interstrand CL (ICL) of transplatin; lanes 11 and 12, the substrate containing the interstrand CL of *trans*-(PtCl₂(NH₃)(pip)); lanes 1, 3, 5, 7, 9, and 11, no extract added; lanes 2, 4, 6, 8, 10, and 12, the substrates were incubated with CHO AA8 CFE for 40 min at 30 °C. Lane 13, the 20- and 30-nucleotide markers. B, quantitative analysis of removal of the adducts. The columns marked as 1,3-cisplatin, 1,3-GTG transplatin, 1,2-GG cisplatin, ICL transplatin, ICL trans-pip, and noPt represent 1,3-GTG intrastrand CL of cisplatin, 1,3-GTG intrastrand CL of *trans*-(PtCl₂(NH₃)(pip)), 1,2-GG intrastrand CL of cisplatin, the interstrand CL of transplatin, the interstrand CL of *trans*-(PtCl₂(NH₃)(pip)), and unplatinated substrate, respectively. The radioactivity associated with the fragments excised from the duplex containing the 1,3-GTG intrastrand CL of cisplatin was taken as 100%. Data are the average of two independent experiments done under the same conditions; bars indicate range of excision.

These results are consistent with the view that the low efficiency of the mammalian NER system to remove the 1,3-intrastrand CLs of *trans*-(PtCl₂(NH₃)(pip)) is associated with inca-

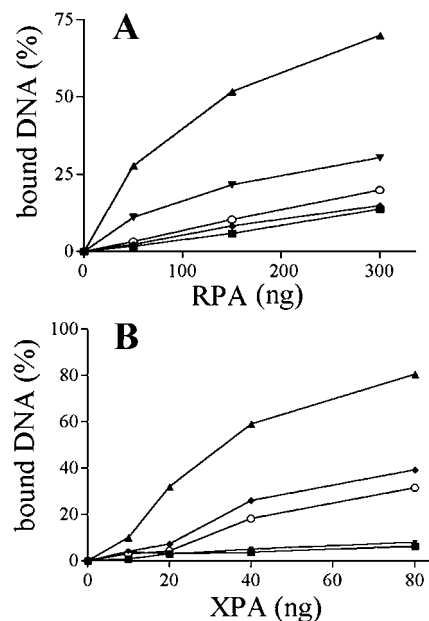


FIG. 6. Recognition of platinated duplexes by nucleotide excision repair proteins. Shown is quantitative evaluation of the recognition of platinated 21-bp DNA containing single, site-specific CLs of *trans*-(PtCl₂(NH₃)(pip)), cisplatin, and transplatin by RPA (A) and XPA (B) proteins. ■, control, unplatinated duplex; ▲, 1,2-GG intrastrand CL of cisplatin; ▼, 1,3-GTG intrastrand CL; ◆, interstrand CL of *trans*-(PtCl₂(NH₃)(pip)); ○, interstrand CL of transplatin.

pability of the NER system to recognize this type of platinum damage.

Interstrand Cross-linking—Frequent, although not major, adducts formed by bifunctional antitumor analogues of transplatin containing a heterocyclic ligand are interstrand CLs (9, 60). Interestingly, transplatin forms these CLs preferentially between G and complementary C residues (19), whereas quite surprisingly its analogues, such as *trans*-(PtCl₂(NH₃)(quinoline)) or *trans*-(PtCl₂(NH₃)(thiazole)) (i.e. the trans complexes containing a planar heterocyclic ligand) form these CLs between G residues in the 5'-GC/5'-GC sequences (22) (i.e. "cisplatin-like" interstrand CLs) (61). Therefore, it was of interest to unambiguously identify the residues involved in the interstrand CL formed by *trans*-(PtCl₂(NH₃)(pip)). Diamminedichloroplatinum(II) complexes react with DNA in a two-step process (62). Monofunctional adducts are formed preferentially at N-7 atoms of G residues. These lesions subsequently close to bifunctional CLs (intrastrand and/or interstrand). Considering this fact, we have designed synthetic oligodeoxynucleotide duplexes (duplexes CGC, TGC, and TGT in Fig. 1B). The pyrimidine-rich top strands of these duplexes contain a unique G residue at which the monofunctional adduct of transplatin or its piperidine analogue was formed. Thus, the choice of this nucleotide allowed for a cross-linking study under competitive conditions (i.e. interstrand CLs were in principle possible: in the CGC duplex, between the central G in the top strand and either complementary C or adjacent 5' or 3' Gs on the opposite strand; in the case of the TGC duplex, between the central G in the top strand and complementary C or adjacent 5' G in the bottom strand; in the case of the TGT duplex, between the central G in the top strand and complementary C. The top strands of the duplexes containing the monofunctional adduct of transplatin or *trans*-(PtCl₂(NH₃)(pip)) were hybridized with their complementary (bottom), 5'-end ³²P-labeled strands. The mixtures were incubated at 37 °C in 0.1 M NaClO₄, and the aliquots were withdrawn at various time intervals and subjected to gel electrophoresis under denaturing (strand-separat-

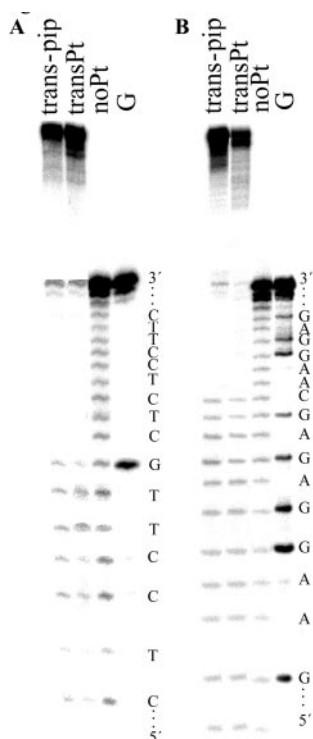


FIG. 7. **Hydroxyl radical footprinting of interstrand cross-links.** Shown is an autoradiogram of denaturing 24% PAA/8 M urea gel of the products of the reaction between hydroxyl radicals and the duplex TGC either unmodified or containing an interstrand CL of transplatin or *trans*-(PtCl₂(NH₃)(pip)). The top (A) or bottom (B) strand was 5'-end-labeled. *noPt* lane, unplatinated duplex; *transPt* lane, the duplex containing interstrand CL of transplatin; *trans-pip* lane, the duplex containing interstrand CL of *trans*-(PtCl₂(NH₃)(pip)); *G* lane, a Maxam-Gilbert-specific reaction for the unplatinated duplex. For other details, see "Results."

ing) conditions to separate and quantify the interstrand cross-linked duplexes. It was found (not shown) that the half-times of the interstrand cross-linking reactions of *trans*-(PtCl₂(NH₃)(pip)) in the duplexes CGC, TGC, and TGT were 13, 15, and 26 h, respectively, whereas these half-times found for the cross-linking by transplatin were 1.5 times higher.

The interstrand cross-linked samples obtained after 48 h were further analyzed by hydroxyl radical footprinting (63). From the observation that all fragments were detected corresponding to the cleavage by hydroxyl radicals from the 5'-end up to the interstrand CL and separated according to size on a PAA gel (shown for the duplex TGC in Fig. 7), the exact location of the bases involved in the interstrand CL was deduced (63). The interstrand adducts formed by transplatin or *trans*-(PtCl₂(NH₃)(pip)) in all duplexes were unambiguously identified as the interstrand adducts involving the central G site in the top strand and its complementary cytosine residue in the bottom strand. Thus, substitution of NH₃ by a nonplanar piperidine produces "transplatin-like" interstrand CLs (*i.e.* this replacement does not change the sites involved in the CL in contrast to the substitution by quinoline or thiazole ligand) (22).

For DNA interstrand adducts of cisplatin and transplatin, the structural details responsible for bending and unwinding have recently been elucidated (34, 64–66). We further performed studies on the bending and unwinding induced by single, site-specific interstrand CL of *trans*-(PtCl₂(NH₃)(pip)) using electrophoretic retardation as a quantitative measure of the extent of planar curvature in the same way as described in the present work for 1,3-intrastrand CL (see below).

The oligodeoxyribonucleotide duplexes TGCT(19–22) (19–22

bp long) were used for the bending and unwinding studies of the present work. The DNA unwinding due to one interstrand adduct of *trans*-(PtCl₂(NH₃)(pip)) has been found to be $20 \pm 4^\circ$. Moreover, the interstrand CL of *trans*-(PtCl₂(NH₃)(pip)) bends DNA by about $26\text{--}30^\circ$ toward the minor groove (the direction of the bend was determined using the duplex (TGC+(A/T)₅)(32) (Fig. 1B) in the same way as in our recent papers (32)). Thus, the bending and local unwinding induced by the interstrand CL of *trans*-(PtCl₂(NH₃)(pip)) are very similar to those afforded by the interstrand CL of transplatin using the same experimental procedure (34).

Further studies of the present work were focused on analysis of the distortion induced by the interstrand CL of *trans*-(PtCl₂(NH₃)(pip)) by chemical probes of DNA conformation also in the same way as described in the present work for 1,3-intrastrand CL (see above). The results described in more detail in the Supplemental Material (see "Chemical Probes" and Fig. S3) and summarized in Fig. 3, B and C, indicate that this adduct induces in DNA the distortion that extends over at least 5 bp and is localized mainly at the platinated base pairs. The distortion induced by the CL of *trans*-(PtCl₂(NH₃)(pip)) was stronger than that induced by the parent compound.

We also examined how the interstrand CL of *trans*-(PtCl₂(NH₃)(pip)) is recognized by DNA-binding proteins, such as HMGB1 domain and RPA and XPA proteins using the same experimental approach as demonstrated in the present work for 1,3-intrastrand CL of this transplatin analogue. The data indicate that HMGB1a, HMGB1b (Fig. S4, lanes 11 and 12), and RPA proteins (Fig. 6A) do not bind the probe containing the interstrand CL of *trans*-(PtCl₂(NH₃)(pip)). XPA exhibited affinity to the probe containing this lesion, but it was markedly lower than that to the probe containing the 1,2-GG intrastrand CL of cisplatin ($\sim 50\%$) (Fig. 6B).

Excision repair substrates containing a site-specific interstrand CL of *trans*-(PtCl₂(NH₃)(pip)) or transplatin were also prepared and analyzed using both human and rodent excinucleases. No excision products were detected under conditions when 1,2- or 1,3-intrastrand CLs were readily excised (shown in Fig. 5A, lanes 10 and 12 for the CLs treated with rodent excinuclease).

DISCUSSION

The results of the present work (Fig. 2) demonstrate that the replacement of one of the ammine group in transplatin results in the reduced cellular accumulation of this drug in comparison with the parent compound, which, however, does not correlate with its markedly enhanced activity in the cancer cell lines (9). It is therefore reasonable to expect that there are other biochemical factors dominating the mechanism of action of transplatin analogues containing a heterocyclic nonleaving ligand, such as piperidine in tumor cells. DNA is a major pharmacological target of platinum compounds (10). Hence, among these factors might be also those associated with the modulation of the platinum-DNA interaction, with subsequent effects on further "downstream" effects of damaged DNA, such as for instance repair capacity for the platinum-DNA lesions (11).

The results of the interstrand cross-linking assay (Fig. 7) and transcription mapping experiments (Fig. S1) are consistent with the view that the replacement of one NH₃ nonleaving group in transplatin by piperidine has not significantly altered base sequence selectivity of the parent platinum drug and the spectrum of its DNA adducts. On the other hand, the results of our recent work (9) suggest that the rate of the formation of the bifunctional adducts is considerably enhanced by this replacement.

It has been also demonstrated (67) that transplatin does not form in several nucleotide sequences of double-helical DNA

TABLE I

Summary and comparison of basic characteristics of DNA cross-links of *trans*-(PtCl₂(NH₃)(piperidine)) (*trans*-pip), transplatin, and cisplatin. If not stated otherwise, the data are from this work.

	1,3-Intrastrand CL of <i>trans</i> -pip	Interstrand CL of <i>trans</i> -pip	Interstrand CL of transplatin	1,2-Intrastrand CL of cisplatin
Frequency (%)	~60 ^a	26 ^a	~12 ^b	~90 ^c
Reactivity of chemical probes (bp)	6	5	4 ^d	5 ^e
DNA bending ^e	~30° toward minor groove	~26–30° toward minor groove	~20° toward minor groove ^{e,f}	~32–34° toward major groove ^g
DNA unwinding (degrees) ^e	~8	~20	~12 ^{e,f}	13 ^g
HMGB1 recognition	No	No	No ^h	Strong ⁱ
RPA recognition	Weak	No	No	Medium
XPA recognition	No	Weak	Weak	Medium
NER by eukaryotic excinuclease	Weak	No	No	Medium
Translesion DNA synthesis	No	ND ^j	ND	Medium

^a Data from Ref. 9.

^b Data from Ref. 19.

^c Data from Ref. 75.

^d Determined by gel electrophoresis.

^e Data from Ref. 34.

^f Data from Ref. 66.

^g Data from Ref. 29.

^h Data from Ref. 71.

ⁱ Data from Ref. 76.

^j ND, not determined.

stable intrastrand CLs, and this property of transplatin has been related to its clinical inefficiency (13, 68). We have demonstrated in our recent work (9) that the replacement of one ammine ligand in “classical” transplatin by piperidine, piperazine, or 4-picoline ligand results in a distinctively enhanced stability of the 1,3-GNG intrastrand CLs formed by these compounds in several sequence contexts in short oligodeoxynucleotide duplexes. This result correlates with the markedly enhanced activity of these transplatin analogues in tumor cell lines.

The characteristics of this most frequent 1,3-intrastrand CL of *trans*-(PtCl₂(NH₃)(pip)) are summarized and compared with the interstrand CLs of this compound and transplatin and 1,2-GG intrastrand CL of cisplatin in Table I. There are several reports (12, 28, 29, 69) describing properties of short oligodeoxynucleotide duplexes containing single, site-specific 1,3-intrastrand CLs of transplatin. These CLs were, however, formed in the sequence TGTGT in which these adducts are unstable in double-helical DNA and readily isomerize in interstrand CLs (9, 67). Thus, no reliable data on 1,3-intrastrand CLs of transplatin in double-helical DNA are available so that a comparison of the 1,3-intrastrand CLs of *trans*-(PtCl₂(NH₃)(pip)) and transplatin is impossible.

The bending experiments were carried out with the oligodeoxynucleotide duplexes containing the unique intrastrand CL of *trans*-(PtCl₂(NH₃)(pip)) in their central sequence. The phasing assay has revealed that the 1,3-GTG intrastrand CL results in a directional bending of helix axis (30° toward the minor groove) and a relatively small duplex unwinding (8°). In addition to these bending and unwinding effects, the 1,3-intrastrand CLs formed by *trans*-(PtCl₂(NH₃)(pip)) create rather extensive local conformational distortions revealed by the chemical probes extending over 6 bp (Fig. 3A).

It has been suggested (46, 70) that HMG domain proteins play a role in sensitizing cells to cisplatin. It has been shown that HMG domain proteins recognize and bind to DNA CLs formed by cisplatin between bases in neighboring base pairs (46, 70, 71). The molecular basis for this recognition is still not entirely understood, although several structural details of the 1:1 complex formed between HMG domain and the duplex containing 1,2-GG intrastrand CL of cisplatin were recently elucidated (46). The details of how the binding of HMG domain proteins to cisplatin-modified DNA sensitize tumor cells to cisplatin are also still not completely resolved, but possibilities

such as shielding cisplatin-DNA adducts from excision repair or that these proteins could be recruited from their native transcriptional regulatory function have been suggested (6, 70, 72, 73) as clues for how these proteins are involved in the antitumor activity.

An important structural motif recognized by HMG domain proteins on DNA containing the major 1,2-GG intrastrand CL of cisplatin is a stable, directional bend of the helix axis toward the major groove. As demonstrated in the present work (Table I) the 1,3-GTG intrastrand CL of *trans*-(PtCl₂(NH₃)(pip)) bends the helix axis almost as efficiently as the intrastrand CLs of cisplatin (29, 74). However, no recognition of DNA intrastrand CL of *trans*-(PtCl₂(NH₃)(pip)) by HMGB1 proteins was observed in the present work. A plausible explanation of this observation may be that the bending due to the 1,3-intrastrand CL of *trans*-(PtCl₂(NH₃)(pip)) is in the opposite direction from that due to the 1,2-intrastrand CL of cisplatin. Hence, it is possible that *trans*-(PtCl₂(NH₃)(pip)) in the 1,3-intrastrand CL prevents the DNA bending toward the major groove required for its accommodation in the complex with HMGB1 protein. Thus, from the results of the present work, it is clear that the DNA intrastrand CLs of antitumor *trans*-(PtCl₂(NH₃)(pip)) are not a substrate for recognition by HMG domain proteins (Fig. S4). From these considerations and from the fact that also interstrand CLs of *trans*-(PtCl₂(NH₃)(pip)) are not recognized by HMG domain proteins, we could conclude that the mechanism of antitumor activity of *trans*-(PtCl₂(NH₃)(pip)) does not involve recognition of its DNA adducts by HMG domain proteins as a crucial step, in contrast to the proposals for cisplatin and its direct analogues (70).

Several reports have demonstrated (26, 52, 53) that NER is a major mechanism contributing to cisplatin resistance. The examinations of excision repair of 1,3-intrastrand CL of *trans*-(PtCl₂(NH₃)(pip)) have revealed that these adducts cannot be removed so readily by excision repair as intrastrand adducts of antitumor cisplatin (Fig. 5). Hence, the intrastrand CLs of bifunctional *trans*-(PtCl₂(NH₃)(pip)) would not have to be shielded by damaged DNA recognition proteins, such as those containing HMG domains, as efficiently as 1,2-intrastrand CLs of cisplatin to prevent their repair. It is reasonable to suggest that intrastrand CLs of *trans*-(PtCl₂(NH₃)(pip)) could persist for a sufficiently long time even without being shielded by HMG box proteins, which would potentiate its toxicity toward tumor cells sensitive to this drug.

trans-(PtCl₂(NH₃)(pip)) also forms in DNA minor interstrand CLs. Their basic characteristics are also summarized in Table I and compared with those of transplatin. The properties of interstrand CLs of *trans*-(PtCl₂(NH₃)(pip)) and clinically ineffective transplatin investigated in the present work are very similar. The only more pronounced difference consists in a higher efficiency of *trans*-(PtCl₂(NH₃)(pip)) to form this type of the adducts. Despite this difference, the interstrand CLs remain minor adducts of *trans*-(PtCl₂(NH₃)(pip)). Hence, the interstrand CLs are probably less likely candidates for genotoxic lesion responsible for antitumor effects of this compound. Nonetheless, the cytotoxic effects of *trans*-(PtCl₂(NH₃)(pip)) may realistically be due to a cumulative effect of the structurally heterogeneous adducts produced by this drug, but the role of structurally unique intrastrand CLs in the antitumor effects of transplatin analogues in which one ammine group is replaced by a heterocyclic ligand may predominate.

Acknowledgments—We thank J. T. Reardon and A. Sancar for HeLa and CHO cell extracts and J. J. Turchi for replication protein A. We also acknowledge that the participation in the EC COST Chemistry Actions D20 and D21 enabled us to exchange regularly the most recent ideas in the field of platinum anticancer drugs with several European colleagues.

REFERENCES

- O'Dwyer, P. J., Stevenson, J. P., and Johnson, S. W. (1999) in *Cisplatin: Chemistry and Biochemistry of a Leading Anticancer Drug* (Lippert, B., ed) pp. 31–72, Verlag Helvetica Chimica Acta, Wiley-VCH, Zürich
- Highley, M. S., and Calvert, A. H. (2000) in *Platinum-based Drugs in Cancer Therapy* (Kelland, L. R., and Farrell, N. P., eds) pp. 171–194, Humana Press Inc., Totowa, NJ
- Lokich, J., and Anderson, N. (1998) *Ann. Oncol.* **9**, 13–21
- Farrell, N. (1996) in *Metal Ions in Biological Systems* (Sigel, A., and Sigel, H., eds) Vol. 32, pp. 603–639, Marcel Dekker, Inc., New York
- Perez, J.-M., Fuentes, M. A., Alonso, C., and Navarro-Ranninger, C. (2000) *Crit. Rev. Oncol. Hematol.* **35**, 109–120
- Brabec, V. (2002) in *Prog. Nucleic Acids Res. Mol. Biol.* **71**, 1–68
- Khazanov, E., Barenholz, Y., Gibson, D., and Najajreh, Y. (2002) *J. Med. Chem.* **45**, 5196–5204
- Najajreh, Y., Perez, J. M., Navarro-Ranninger, C., and Gibson, D. (2002) *J. Med. Chem.* **45**, 5189–5195
- Kasparkova, J., Marini, V., Najajreh, Y., Gibson, D., and Brabec, V. (2003) *Biochemistry* **42**, 6321–6332
- Johnson, N. P., Butour, J.-L., Villani, G., Wimmer, F. L., Defais, M., Pierson, V., and Brabec, V. (1989) *Prog. Clin. Biochem. Med.* **10**, 1–24
- Farrell, N., Kelland, L. R., Roberts, J. D., and Van Beusichem, M. (1992) *Cancer Res.* **52**, 5065–5072
- Boudvillain, M., Dalbies, R., Aussourd, C., and Leng, M. (1995) *Nucleic Acids Res.* **23**, 2381–2388
- Leng, M., Schwartz, A., and Giraud-Panis, M. J. (2000) in *Platinum-based Drugs in Cancer Therapy* (Kelland, L. R., and Farrell, N. P., eds) pp. 63–85, Humana Press Inc., Totowa, NJ
- Brabec, V., Reedijk, J., and Leng, M. (1992) *Biochemistry* **31**, 12397–12402
- Hermanson-Miller, I. L., and Turchi, J. J. (2002) *Biochemistry* **41**, 2402–2408
- Missura, M., Buterin, T., Hindges, R., Hubscher, U., Kasparkova, J., Brabec, V., and Naegeli, H. (2001) *EMBO J.* **20**, 3554–3564
- Alvarez-Valdes, A., Perez, J. M., Lopez-Solera, I., Lannegrand, R., Continente, J. M., Amo-Ochoa, P., Camazon, M. J., Solans, X., Font-Bardia, M., and Navarro-Ranninger, C. (2002) *J. Med. Chem.* **45**, 1835–1844
- Kasparkova, J., Novakova, O., Najajreh, Y., Gibson, D., Perez, J.-M., and Brabec, V. (2003) *Chem. Res. Toxicol.*, in press
- Brabec, V., and Leng, M. (1993) *Proc. Natl. Acad. Sci. U. S. A.* **90**, 5345–5349
- Kasparkova, J., Mellish, K. J., Qu, Y., Brabec, V., and Farrell, N. (1996) *Biochemistry* **35**, 16705–16713
- Kasparkova, J., Zehnulova, J., Farrell, N., and Brabec, V. (2002) *J. Biol. Chem.* **277**, 48076–48086
- Brabec, V., Neplechova, K., Kasparkova, J., and Farrell, N. (2000) *J. Biol. Inorg. Chem.* **5**, 364–368
- Matsunaga, T., Mu, D., Park, C.-H., Reardon, J. T., and Sancar, A. (1995) *J. Biol. Chem.* **270**, 20862–20869
- Buschta-Hedayat, N., Buterin, T., Hess, M. T., Missura, M., and Naegeli, H. (1999) *Proc. Natl. Acad. Sci. U. S. A.* **96**, 6090–6095
- Manley, J. L., Fire, A., Cano, A., Sharp, P. A., and Gefter, M. L. (1980) *Proc. Natl. Acad. Sci. U. S. A.* **77**, 3855–3859
- Reardon, J. T., Vaisman, A., Chaney, S. G., and Sancar, A. (1999) *Cancer Res.* **59**, 3968–3971
- Jamieson, E. R., and Lippard, S. J. (1999) *Chem. Rev.* **99**, 2467–2498
- Anin, M. F., and Leng, M. (1990) *Nucleic Acids Res.* **18**, 4395–4400
- Bellon, S. F., and Lippard, S. J. (1990) *Biophys. Chem.* **35**, 179–188
- Kasparkova, J., Farrell, N., and Brabec, V. (2000) *J. Biol. Chem.* **275**, 15789–15798
- Zehnulova, J., Kasparkova, J., Farrell, N., and Brabec, V. (2001) *J. Biol. Chem.* **276**, 22191–22199
- Loskotova, H., and Brabec, V. (1999) *Eur. J. Biochem.* **266**, 392–402
- Kasparkova, J., Novakova, O., Farrell, N., and Brabec, V. (2003) *Biochemistry* **42**, 792–800
- Brabec, V., Sip, M., and Leng, M. (1993) *Biochemistry* **32**, 11676–11681
- Nielsen, P. E. (1990) *J. Mol. Recogn.* **3**, 1–24
- Malina, J., Hofr, C., Maresca, L., Natlie, G., and Brabec, V. (2000) *Biophys. J.* **78**, 2008–2021
- Kostrhunova, H., and Brabec, V. (2000) *Biochemistry* **39**, 12639–12649
- Comess, K. M., Burstyn, J. N., Essigmann, J. M., and Lippard, S. J. (1992) *Biochemistry* **31**, 3975–3990
- Suo, Z., and Johnson, K. (1998) *J. Biol. Chem.* **273**, 27259–27267
- Suo, Z., Lippard, S., and Johnson, K. (1999) *Biochemistry* **38**, 715–726
- Johnson, K. A. (1993) *Annu. Rev. Biochem.* **62**, 685–713
- Hubscher, U., Nasheuer, H. P., and Syvaaja, J. E. (2000) *Trends Biochem. Sci.* **25**, 143–147
- Lam, W. C., VanderSchans, E. J. C., Sowers, L. C., and Millar, D. P. (1999) *Biochemistry* **38**, 2661–2668
- Steitz, T. A. (1999) *J. Biol. Chem.* **274**, 17395–17398
- Lone, S., and Romano, L. J. (2003) *Biochemistry* **42**, 3826–3834
- Ohndorf, U. M., Rould, M. A., He, Q., Pabo, C. O., and Lippard, S. J. (1999) *Nature* **399**, 708–712
- He, Q., Ohndorf, U.-A., and Lippard, S. J. (2000) *Biochemistry* **39**, 14426–14435
- Sancar, A. (1996) *Annu. Rev. Biochem.* **65**, 43–81
- Wood, R. D. (1996) *Annu. Rev. Biochem.* **65**, 135–167
- Reardon, J. T., and Sancar, A. (1998) in *Advances in DNA Damage and Repair* (Dizdaroğlu, M., and Karakaya, A., eds) pp. 377–393, Plenum Publishing Corp., New York
- Jones, S. L., Hickson, I. D., Harris, A. L., and Harnett, P. R. (1994) *Int. J. Cancer* **59**, 388–393
- Zamble, D. B., Mu, D., Reardon, J. T., Sancar, A., and Lippard, S. J. (1996) *Biochemistry* **35**, 10004–10013
- Moggs, J. G., Szymkowski, D. E., Yamada, M., Karran, P., and Wood, R. D. (1997) *Nucleic Acids Res.* **25**, 480–490
- Koberle, B., Masters, J. R. W., Hartley, J. A., and Wood, R. D. (1999) *Curr. Biol.* **9**, 273–276
- Li, M. J., and Yang, L. Y. (1999) *Int. J. Oncol.* **15**, 1177–1183
- Huang, J.-C., Svoboda, D. L., Reardon, J. T., and Sancar, A. (1992) *Proc. Natl. Acad. Sci. U. S. A.* **89**, 3664–3668
- Sancar, A. (1995) *J. Biol. Chem.* **270**, 15915–15918
- Wakasugi, M., and Sancar, A. (1999) *J. Biol. Chem.* **274**, 18759–18768
- Patrick, S. M., and Turchi, J. J. (1999) *J. Biol. Chem.* **274**, 14972–14978
- Zakovska, A., Novakova, O., Balcarova, Z., Bierbach, U., Farrell, N., and Brabec, V. (1998) *Eur. J. Biochem.* **254**, 547–557
- Lemaire, M. A., Schwartz, A., Rahmouni, A. R., and Leng, M. (1991) *Proc. Natl. Acad. Sci. U. S. A.* **88**, 1982–1985
- Bancroft, D. P., Lepre, C. A., and Lippard, S. J. (1990) *J. Am. Chem. Soc.* **112**, 6860–6871
- Leng, M., Locker, D., Giraud-Panis, M. J., Schwartz, A., Intini, F. P., Natlie, G., Pisano, C., Boccarelli, A., Giordano, D., and Coluccia, M. (2000) *Mol. Pharmacol.* **58**, 1525–1535
- Huang, H. F., Zhu, L. M., Reid, B. R., Drobný, G. P., and Hopkins, P. B. (1995) *Science* **270**, 1842–1845
- Coste, F., Malinge, J. M., Serre, L., Shepard, W., Roth, M., Leng, M., and Zelwer, C. (1999) *Nucleic Acids Res.* **27**, 1837–1846
- Paquet, F., Boudvillain, M., Lancelot, G., and Leng, M. (1999) *Nucleic Acids Res.* **27**, 4261–4268
- Dalbies, R., Payet, D., and Leng, M. (1994) *Proc. Natl. Acad. Sci. U. S. A.* **91**, 8147–8151
- Dalbies, R., Boudvillain, M., and Leng, M. (1995) *Nucleic Acids Res.* **23**, 949–953
- Bellon, S. F., Coleman, J. H., and Lippard, S. J. (1991) *Biochemistry* **30**, 8026–8035
- Zamble, D. B., and Lippard, S. J. (1999) in *Cisplatin: Chemistry and Biochemistry of a Leading Anticancer Drug* (Lippert, B., ed) pp. 73–110, Verlag Helvetica Chimica Acta, Wiley-VCH, Zürich
- Kasparkova, J., and Brabec, V. (1995) *Biochemistry* **34**, 12379–12387
- He, Q., Liang, C. H., and Lippard, S. J. (2000) *Proc. Natl. Acad. Sci. U. S. A.* **97**, 5768–5772
- Kartalou, M., and Essigmann, J. M. (2001) *Mutat. Res.* **478**, 1–21
- Rice, J. A., Crothers, D. M., Pinto, A. L., and Lippard, S. J. (1988) *Proc. Natl. Acad. Sci. U. S. A.* **85**, 4158–4161
- Eastman, A. (1987) *Pharmacol. Ther.* **34**, 155–166
- Dunham, S. U., and Lippard, S. J. (1997) *Biochemistry* **36**, 11428–11436

21.

DNA Interactions of Monofunctional Organometallic Ruthenium(II) Antitumor Complexes in Cell-free Media[†]

Olga Novakova,[‡] Haimei Chen,[§] Oldrich Vrana,[‡] Alison Rodger,^{||} Peter J. Sadler,^{*,§} and Viktor Brabec^{*,‡}

Institute of Biophysics, Academy of Sciences of the Czech Republic, Kralovopolska 135, CZ-61265 Brno, Czech Republic, School of Chemistry, University of Edinburgh, West Mains Road, Edinburgh EH9 3JJ, United Kingdom, and Department of Chemistry, University of Warwick, Coventry CV4 7AL, United Kingdom

Received May 30, 2003; Revised Manuscript Received August 5, 2003

ABSTRACT: Modifications of natural DNA in a cell-free medium by antitumor monodentate Ru(II) arene compounds of the general formula $[(\eta^6\text{-arene})\text{Ru}(\text{en})\text{Cl}]^+$ (arene = biphenyl, dihydroanthracene, tetrahydroanthracene, *p*-cymene, or benzene; en = ethylenediamine) were studied by atomic absorption, melting behavior, transcription mapping, circular and linear dichroism, plasmid unwinding, competitive ethidium displacement, and differential pulse polarography. The results indicate that these complexes bind preferentially to guanine residues in double-helical DNA. The data are consistent with DNA binding of the complexes containing biphenyl, dihydroanthracene, or tetrahydroanthracene ligands that involves combined coordination to G N7 and noncovalent, hydrophobic interactions between the arene ligand and DNA, which may include arene intercalation and minor groove binding. In contrast, the single hydrocarbon rings in the *p*-cymene and benzene ruthenium complexes cannot interact with double-helical DNA by intercalation. Interestingly, the adducts of the complex containing *p*-cymene ligand, which has methyl and isopropyl substituents, distort the conformation and thermally destabilize double-helical DNA distinctly more than the adducts of the three multiring ruthenium arene compounds. It has been suggested that the different character of conformational alterations induced in DNA, and the resulting thermal destabilization, may affect differently further “downstream” effects of damaged DNA and consequently may result in different biological effects of this new class of metal-based antitumor compounds. The results point to a unique profile of DNA binding for Ru(II) arene compounds, suggesting that a search for new anticancer compounds based on this class of complexes may also lead to an altered profile of biological activity in comparison with that of metal-based antitumor drugs already used in the clinic or currently on clinical trials.

Platinum coordination compounds are widely used as antitumor drugs. The first platinum antitumor drugs introduced in the clinic were *cis*-diamminedichloroplatinum(II)¹ (cisplatin) and its somewhat less toxic analogue carboplatin [*cis*-diammine-1,1-cyclobutanedicarboxylatoplatinum(II)]. Both compounds show the same spectrum of antitumor activity. The clinical efficacy of these anticancer drugs is diminished by intrinsic and acquired tumor resistance. Owing to these limitations, there is an intense effort to design new transition-metal-based compounds that are capable of overcoming problems associated with cisplatin and carboplatin chemotherapy while delivering the therapeutic effect.

Cisplatin and carboplatin target cellular DNA, forming covalent adducts (1). The most abundant adducts formed by cisplatin in linear DNA are 1,2-d(GpG) (~65%) or 1,2-d(ApG) (25%) intrastrand and 1,2-d(GG) (~6%) interstrand cross-links (2–4). In the years following the introduction of cisplatin, the design of new platinum antitumor drugs concentrated mainly on direct cisplatin analogues which adhered to the set of structure–activity relationships established as early as 1973 (5, 6). More recently, there have been efforts to design rationally unconventional platinum complexes that violate these original structure–activity relationships, such as polynuclear platinum complexes or analogues of the clinically ineffective *trans* isomer of cisplatin (*trans*-platin) (7–9). There have also been efforts directed at the

[†] Supported by the Grant Agency of the Czech Republic (Grant Nos. 305/02/1552, 305/01/0418), the Grant Agency of the Academy of Sciences of the Czech Republic (Grant No. A5004101), The Wellcome Trust (U.K.), the Committee of Vice-Chancellors and Vice-Principals (Overseas Research Scholarship to HC), and the Edinburgh Technology Fund. The authors acknowledge that this research is also a part of the European Cooperation in the field of Scientific and Technical Research network (COST projects D20/0003/00 and D20/0005/01).

* Corresponding authors. VB: telephone, 420-541517148; fax, 420-541240499; e-mail, brabec@ibp.cz. PJS: telephone, +44-131-6504729; fax, +44-131-6506452; e-mail, P.J.Sadler@ed.ac.uk.

[‡] Institute of Biophysics, Academy of Sciences of the Czech Republic.

[§] School of Chemistry, University of Edinburgh.

^{||} Department of Chemistry, University of Warwick.

¹ Abbreviations: BEN, benzene; BIP, biphenyl; CD, circular dichroism; cisplatin, *cis*-diamminedichloroplatinum(II); CT, calf thymus; CYM, *p*-cymene; DHA, dihydroanthracene; DPP, differential pulse polarography; en, ethylenediamine; EtBr, ethidium bromide; FAAS, flameless atomic absorption spectrophotometry; LD, linear dichroism; [Pt(dien)Cl]Cl, chlorodiethylenetriamineplatinum(II) chloride; dien = diethylenetriamine; poly(dG-dC), polymer of alternating dG and dC residues; poly(dA-dT), polymer of alternating dA and dT residues; r_b , the number of metal atoms bound per nucleotide residue; r_i , the molar ratio of free metal complex to nucleotide-phosphates at the onset of incubation with DNA.; THA, tetrahydroanthracene; t_m , DNA melting temperature; *trans*-platin, *trans*-diamminedichloroplatinum(II).

design of other transition-metal antitumor agents. Possible advantages in using transition-metal ions other than Pt(II) include the availability of additional coordination sites in octahedral complexes and the altered shape of the complex, alterations in ligand affinity and substitution kinetics, changes in oxidation state, and photodynamic approaches to therapy. In the design of these new drugs, ruthenium complexes have attracted much interest (10–12).

Organometallic ruthenium(II) arene complexes of the type $[(\eta^6\text{-arene})\text{Ru(II)(en)Cl}][\text{PF}_6]$ (en = ethylenediamine) constitute a relatively new group of anticancer compounds (13, 14). These are pseudo-octahedral “piano-stool” complexes with the arene ring occupying three coordination sites and two diamine nitrogens and the halide ligand occupying the remaining three sites. Importantly, the arene ligand is strongly bound and stabilizes ruthenium(II): the complexes do not readily undergo oxidation to ruthenium(III). Moreover, most of the compounds are ionic and have a reasonable aqueous solubility. These monodentate Ru(II) arene complexes have been considered novel anticancer agents with a mechanism of action different from that of the ruthenium(III) complex $[\text{ImH}][\text{trans-Ru(III)Cl}_4\text{Im}(\text{Me}_2\text{SO})]$ {Im = imidazole, NAMI-A}, which is currently on clinical trial (11, 15).

Broadening the chemotherapeutic arsenal depends on understanding existing agents with a view toward developing new modes of attack. Interestingly, a direct correlation between cytotoxicity and DNA binding has already been observed for several ruthenium compounds in cell cultures (16). Also consistent with DNA binding *in vivo*, a number of ruthenium compounds inhibit DNA replication, exhibit mutagenic activity, induce the SOS repair mechanism, bind to nuclear DNA, and reduce RNA synthesis (16). Similarly, several antitumor ruthenium compounds have also been shown (17–21) to bind to DNA and inhibit DNA replication *in vitro*, but the pharmacological target for ruthenium compounds and the mechanism underlying its biological effects are not known.

The $(\eta^6\text{-arene})\text{Ru(II)}$ bonds are inert toward hydrolysis, but the monofunctional complexes $[(\eta^6\text{-arene})\text{Ru(II)(en)(Cl)}]^+$ readily lose their chloride ligand and transform into the corresponding, more reactive, aquated species (22). It has also been shown (14) that the complex $[(\eta^6\text{-}p\text{-cymene})\text{Ru(II)(en)(Cl)}]^+$ binds to a short, single-stranded deoxyribo-oligonucleotide (14-mer), forming monofunctional adducts, and that the preferential sites of ruthenation in this oligomer are guanine residues. To address further fundamental questions about DNA binding modes of ruthenium(II) arene antitumor compounds, the experiments described in the present paper were carried out. More specifically, the interactions of polymeric B-DNAs with $[(\eta^6\text{-arene})\text{Ru(II)(en)(Cl)}]^+$ complexes [where arene = biphenyl (BIP), dihydroanthracene (DHA), tetrahydroanthracene (THA), *p*-cymene (CYM), or benzene (BEN)] in cell-free media were investigated by various biochemical and biophysical methods with the goal to contribute to understanding their biological effects and to help establish structure–pharmacological relationships for this class of ruthenium anticancer compounds.

MATERIALS AND METHODS

Starting Materials. $[(\eta^6\text{-arene})\text{Ru(II)(en)(Cl)}]\text{PF}_6$ complexes (Figure 1) were prepared as described previously (23).

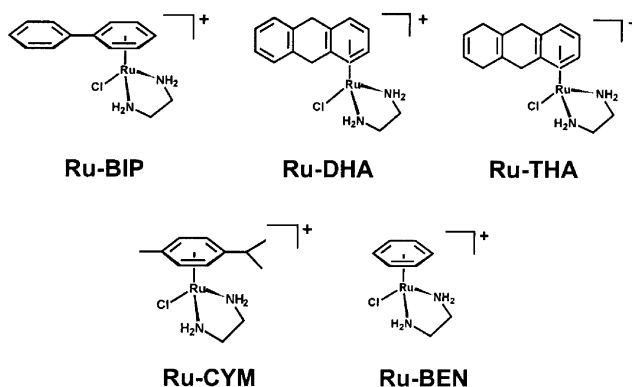


FIGURE 1: Structures of Ru(II) arene complexes used in this work.

Cisplatin, *trans*-diamminedichloroplatinum(II) (transplatin), and chlorodiethylenetriamineplatinum(II) chloride $\{[\text{Pt}(\text{dien})\text{Cl}_2]\text{Cl}\}$ were synthesized and characterized at Lachema (Brno, Czech Republic). The stock solutions of the ruthenium and platinum complexes (5×10^{-4} M in H_2O) were prepared in the dark at 25 °C and stored for at least 7 days before they were used. Aquation of these Ru(II) arene complexes is relatively rapid in water (22), and as for cisplatin, the aqua adducts are more reactive than the chloro complexes. Calf thymus (CT) DNA (42% G + C, mean molecular mass $\sim 2 \times 10^7$) was also prepared and characterized as described previously (24, 25). Poly(dG-dC) and poly(dA-dT) were obtained from Amersham Pharmacia-Biotech (Piscataway, NJ) and were used without further purification.

Plasmid pSP73KB [2455 bp (26)] was isolated according to standard procedures and banded twice in CsCl/EtBr equilibrium density gradients. Restriction endonucleases were purchased from New England Biolabs (Beverly, MA). Riboprobe Gemini System II for transcription mapping containing SP6 and T7 RNA polymerases was purchased from Promega (Madison, WI). Ethidium bromide (EtBr) and agarose were from Merck KgaA (Darmstadt, Germany). The radioactive products were from Amersham (Arlington Heights, IL).

Metalation Reactions. CT DNA and plasmid DNAs were incubated with ruthenium or platinum complex in 10 mM NaClO_4 (pH ~ 6) at 37 °C for 48 h in the dark, if not stated otherwise. The number of atoms of the metal bound per nucleotide residue (r_b values) was determined by flameless atomic absorption spectrophotometry (FAAS) (21).

DNA Transcription by RNA Polymerase *In Vitro*. Transcription of the (*Nde*I/*Hpa*I) restriction fragment of pSP73KB DNA with SP6 or T7 RNA polymerase and electrophoretic analysis of transcripts were performed according to the protocols recommended by Promega (Promega Protocols and Applications, 43–46 (1989/90)) and previously described in detail (26, 27).

Unwinding of Negatively Supercoiled DNA. Unwinding of closed circular supercoiled pSP73KB plasmid DNA was assayed by an agarose gel mobility shift assay (28). The unwinding angle, Φ , induced per metal–DNA adduct was calculated upon the determination of the r_b value at which the complete transformation of the supercoiled form to the relaxed form of the plasmid was attained. Samples of pSP73 plasmid were incubated with Ru(II) arene or cisplatin in 10 mM NaClO_4 at 37 °C in the dark for 48 h. All samples were precipitated by ethanol and redissolved in TAE buffer (0.04

M Tris-acetate + 1 mM EDTA, pH 7.0). An aliquot of the precipitated sample was subjected to electrophoresis on 1% agarose gels running at 25 °C in the dark with TAE buffer with a voltage set at 30 V. The gels were then stained with EtBr, followed by photography on Polaroid 667 film with transilluminator. The other aliquot was used for the determination of r_b values by FAAS.

Circular Dichroism (CD) and Linear Dichroism (LD). If not stated otherwise, CD and LD spectra of DNA modified by the ruthenium complexes were recorded at 25 °C in 10 mM NaClO₄ on JASCO J-720 and adapted J-715 spectropolarimeters.

Differential Pulse Polarography. Differential pulse polarographic (DPP) curves of DNA were measured after nonmodified DNA or DNA modified by either Ru(II) arene compound used in the present work was redissolved in a medium consisting of 0.3 M ammonium formate plus 0.05 M phosphate (Na₂HPO₄/NaH₂PO₄) buffer, pH 6.8. DPP curves were recorded with the aid of an EG&C PARC electrochemical analyzer, model 384B at 25 °C using the following apparatus settings: voltage scan rate of 2 mV/s, pulse amplitude of 5 mV, drop time of 1.0 s. The potentials are relative to the saturated calomel reference electrode (SCE).

Fluorescence Measurements. Fluorescence measurements in the presence of EtBr of CT DNA modified by ruthenium arene complexes were performed at an excitation wavelength of 546 nm, and the emitted fluorescence was analyzed at 590 nm. The fluorescence intensity was measured at 25 °C in 0.4 M NaCl to avoid secondary binding of EtBr to DNA (29, 30). The concentrations were 0.01 mg/mL for DNA and 0.04 mg/mL for EtBr, which corresponded to the saturation of all intercalation sites of EtBr in DNA (29, 30). These measurements were performed on a Shimadzu RF 40 spectrofluorophotometer using a 1 cm quartz cell.

DNA Melting. The melting curves of DNA were recorded by measuring the absorbance at 260 nm. The melting curves of unruthenated or ruthenated DNA were recorded after Tris-HCl/EDTA buffer and NaClO₄ were added so that the resulting media contained 0.01–0.2 M NaClO₄ with 1 mM Tris-HCl/0.1 mM EDTA, pH 7.4. The value of the melting temperature (t_m) was determined as the temperature corresponding to a maximum on the first-derivative profile of the melting curves. The t_m values were thus determined with an accuracy of ± 0.3 °C.

Other Methods. Absorption spectra were measured with Beckmann DU-7400 and Cary 1E spectrophotometers. FAAS measurements were carried out on a Unicam 939 AA spectrometer with a graphite furnace. For FAAS analysis, DNA was precipitated with ethanol and dissolved in 0.1 M HCl.

RESULTS

DNA Binding. Solutions of double-helical CT DNA at a concentration of 0.1 mg/mL were incubated with Ru(II) arene complexes at an r_i (molar ratio of free ruthenium complex to nucleotide phosphates at the onset of incubation with DNA) value of 0.1 in 10 mM NaClO₄ at 37 °C. At various time intervals, an aliquot of the reaction mixture was withdrawn, quickly cooled on an ice bath, and precipitated by ethanol, and the content of ruthenium in the supernatant

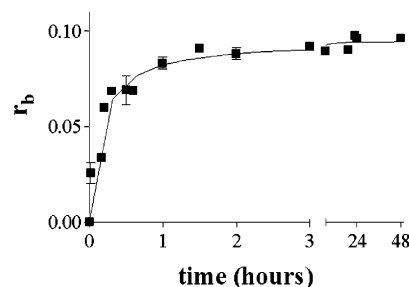


FIGURE 2: Kinetics of the binding of the Ru(II) arene compound Ru-BIP to calf thymus DNA. Medium: 10 mM NaClO₄ at 37 °C. The concentration of DNA was 0.1 mg/mL; $r_i = 0.1$. Data measured in triplicate varied on average $\pm 3\%$ from their mean.

of these samples was determined by FAAS. Figure 2 shows a plot of r_b (the number of atoms of metal bound per nucleotide residue) against the time of DNA incubation with Ru-BIP ($r_i = 0.1$). The amount of ruthenium bound per DNA nucleotide phosphate (r_b) increased with time. After ~ 3 h, approximately 90% of the molecules of the Ru-BIP present in the reaction mixture were bound to DNA. In these binding reactions, the time at which the binding reached 50% ($t_{50\%}$) was ~ 10 , 15, and 10 min and 3.5 h for the compounds Ru-BIP, Ru-DHA, Ru-THA, and Ru-CYM, respectively. The value of $t_{50\%}$ for the reaction of cisplatin with DNA under conditions identical to those specified in Figure 2 was ~ 2 h (31).

The binding of Ru(II) arene compounds to CT DNA was also quantified in two other ways. Aliquots of the reaction mixture withdrawn at various time intervals were quickly cooled on an ice bath and then exhaustively dialyzed against 10 mM NaClO₄ at 4 °C or filtered using Sephadex G50 to remove free (unbound) ruthenium compound. The content of ruthenium in these DNA samples was determined by FAAS. Results identical to those obtained using the assay based on DNA precipitation by ethanol were obtained.

In further experiments, CT DNA was also incubated with the Ru(II) arene complexes at $r_i = 0.2$ and essentially a similar rate of binding was observed as for the reaction at $r_i = 0.1$. When Ru complexes were added to a higher level ($r_i = 0.25$), the DNA precipitated immediately, probably due to electrostatic interactions between the positively charged Ru(II) arene complexes and DNA.

The binding experiments carried out in this work indicated that modification reactions resulted in the irreversible coordination of the Ru(II) arene complexes to polymeric double-helical DNA, which thus facilitated sample analysis. Hence, it was possible to prepare easily and precisely samples of DNA modified by the ruthenium complex at a preselected value of r_b . Thus, except where stated, samples of DNA modified by Ru(II) arene compounds and analyzed further by biophysical or biochemical methods were prepared in 10 mM NaClO₄ at 37 °C. After 24 h of the reaction of DNA with the complex, the samples were precipitated in ethanol and dissolved in the medium necessary for a particular analysis, and the r_b value in an aliquot of this sample was checked by FAAS. In this way, most of the analyses described in the present paper were performed in the absence of unbound (free) Ru(II) arene complex.

In Vitro Transcription of DNA Containing Ru(II) Arene Adducts. In vitro RNA synthesis by RNA polymerases on DNA templates containing several types of bifunctional

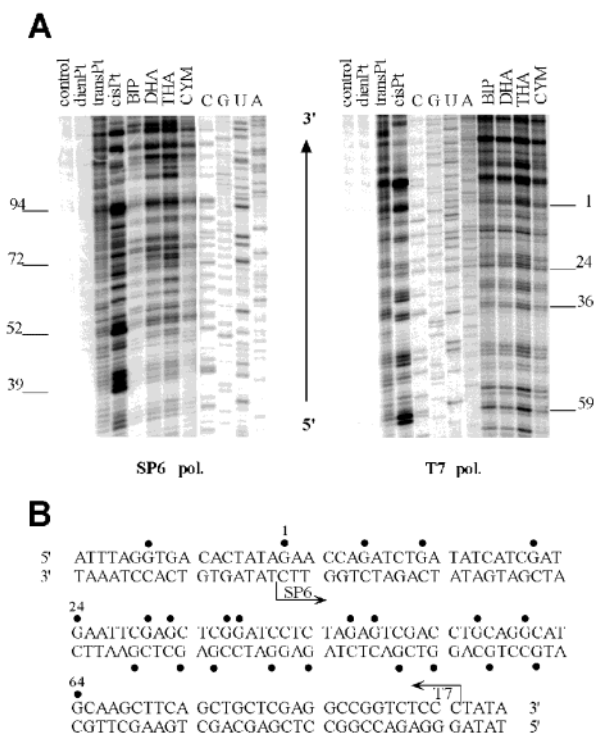


FIGURE 3: Inhibition of RNA synthesis by SP6 and T7 RNA polymerases on the *NdeI/HpaI* fragment of pSP73KB plasmid modified by Ru(II) arene and platinum complexes. (A) Autoradiograms of 6% polyacrylamide/8 M urea sequencing gels showing inhibition of RNA synthesis by SP6 (left) or T7 RNA polymerases (right) on the *NdeI/HpaI* fragment containing adducts of ruthenium or platinum complexes. Lanes: control, unmodified template; BIP, DHA, THA, CYM, cisPt, transPt, and dienPt, the template modified by Ru-BIP, Ru-DHA, Ru-THA, Ru-CYM, cisplatin, transplatin, or [Pt(dien)Cl]Cl at $r_b = 0.01$, respectively; A, U, G, and C, chain terminated marker RNAs. (B) Schematic diagram showing the portion of the sequence used to monitor inhibition of RNA synthesis by ruthenium and platinum complexes. The arrows indicate the start of the SP6 and T7 RNA polymerase, which used as template the bottom or upper strand of the *NdeI/HpaI* fragment of pSP73KB DNA, respectively. (●) major stop signals (from Figure 3A) for DNA modified by Ru-BIP. The numbers correspond to the nucleotide numbering in the sequence map of pSP73KB plasmid.

adducts of platinum complexes can be prematurely terminated at the level or in the proximity of adducts (26, 27). Importantly, monofunctional DNA adducts of several platinum complexes are unable to terminate RNA synthesis (26, 27, 32).

Cutting of pSP73KB DNA by *NdeI* and *HpaI* restriction endonucleases yielded a 212-bp fragment (26, 27) (a substantial part of its nucleotide sequence is shown in Figure 3B). This fragment contained SP6 or T7 RNA polymerase promoters [in both strands close to their 3'-ends (Figure 3B)]. The experiments were carried out using this linear DNA fragment modified by Ru(II) arene complexes, cisplatin, transplatin, or [Pt(dien)Cl]Cl at $r_b = 0.01$, for RNA synthesis by SP6 or T7 RNA polymerase (Figure 3A, lanes BIP, DHA, THA, CYM, cisDDP, transDDP, or dienPt, respectively). RNA synthesis on the fragment modified by the ruthenium and bifunctional platinum complexes yielded fragments of defined sizes, which indicates that RNA synthesis on these templates was prematurely terminated. The major stop sites produced by ruthenium compounds were identical for all four Ru(II) arene compounds Ru-BIP, Ru-DHA, Ru-THA, and Ru-CYM (Ru-BEN was not studied in this assay) and were

mainly at guanine residues. The corresponding bands on the autoradiogram were of similar intensity for the compounds Ru-BIP, Ru-DHA, and Ru-THA, whereas the bands produced by Ru-CYM were markedly less intense. For comparative purposes, the inhibition of RNA synthesis by DNA adducts of cisplatin, transplatin, and monofunctional [Pt(dien)Cl]Cl is also shown (Figure 3A, lanes cisPt, transPt, and dienPt) and demonstrates more termination for cisplatin but at the same termination sites as those for the Ru(II) arenes, different termination sites than those for transplatin, and no termination of RNA synthesis by monofunctional [Pt(dien)Cl]Cl. The sequence analysis reveals that the major bands resulting from termination of RNA synthesis by the adducts of cisplatin and Ru(II) arene compounds preferentially appear one or a half nucleotide preceding G sites and to a considerably less extent preceding A sites (in AGAG or AGGAG sequences). Taken together, Ru(II) arene compounds exhibit a base sequence selectivity similar to that of cisplatin. Nevertheless, the efficiency of the adducts of Ru(II) arene complexes to terminate RNA synthesis in vitro is in general reduced relative to that of cisplatin. Furthermore, the efficiency of the Ru-CYM complex was noticeably lower than that of the other three ruthenium compounds examined in this assay.

Circular and Linear Dichroism Spectroscopy. A sizable CD spectrum can be induced into the absorbance bands of a number of low-molecular-mass molecules upon their binding to double-helical DNA (33). Ideally, ligand absorbance bands that do not overlap with DNA bands (below 300 nm) are used to probe the interaction. The Ru(II) arene compounds investigated here are achiral (not optically active) when free in solution. Binding of the Ru(II) arene complexes to DNA was indicated by the induction of a sizable CD spectrum for the Ru(II)-arene absorption bands [e.g. Ru(II) to arene π^* charge-transfer transitions at 375 nm] in the presence of double-helical DNA.

CD spectra for CT DNA in the absence and in the presence of increasing amounts of Ru(II) arene compounds bound to DNA are compared in Figure 4 (panels A–D). Binding of the compounds Ru-BIP, Ru-DHA, and Ru-THA to CT DNA results in the appearance of a positive CD band centered around 370–380 nm, and its intensity increased with the level of DNA ruthenation. Interestingly, the induced CD signal of Ru-BIP was the largest, whereas the binding of Ru-CYM to double-helical DNA resulted in no induced CD band in this region (Figure 4D). The different intensities of the induced CD bands produced by the compounds Ru-BIP, Ru-DHA, and Ru-THA are, at least partly, due to the different extinction coefficients (ca. 380, 280, and 150 $M^{-1} cm^{-1}$, respectively) of the free compounds at the wavelengths corresponding to this CD band.

Upon binding of Ru(II) arene compounds to CT DNA, the approximately conservative CD spectrum normally found for B-DNA at wavelengths below 300 nm (Figure 4A–D) is also changed. As a function of r_b , there was a marked increase in the intensity of the positive band around 280 nm when DNA was modified by the compounds Ru-BIP, Ru-DHA, and Ru-THA, accompanied by a decrease in the intensity of the negative band at 245 nm (Figure 4A–C). This induced CD signal is due to changes in both the intrinsic DNA CD and the ligand-induced CD. On the other hand, when DNA was modified by Ru-CYM, no such increase

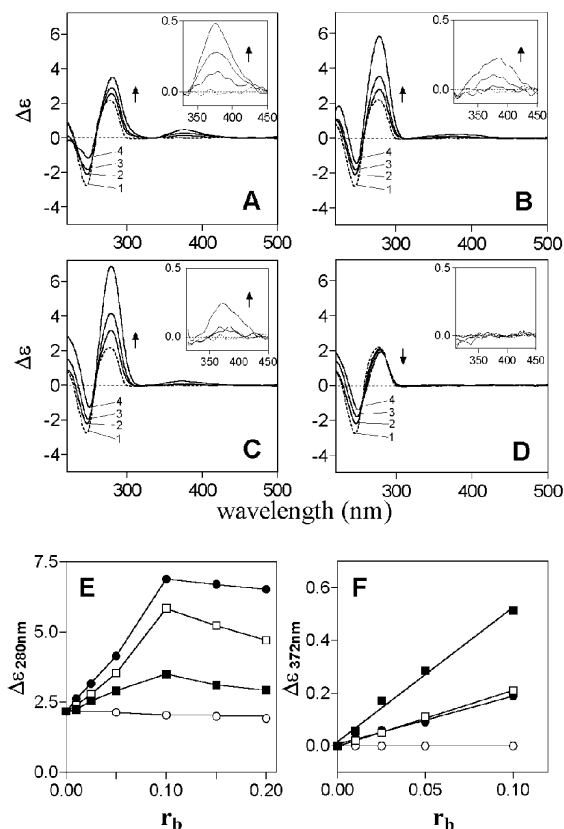


FIGURE 4: CD spectroscopy of calf thymus DNA modified by Ru(II) arene compounds. The spectra were recorded for DNA at the concentration 30 $\mu\text{g/mL}$ in 10 mM NaClO_4 . (A–D) CD spectra of DNA modified by Ru–BIP, Ru–DHA, Ru–THA, or Ru–CYM, respectively. Curves in parts A–C (from the bottom to the top at ~ 250 , ~ 275 , and 375 nm): 1 (---), control (nonmodified) DNA; 2, $r_b = 0.025$; 3, $r_b = 0.05$; 4, $r_b = 0.1$. Curves in part D (at ~ 250 nm, the order of appearance of the curves is the same as that given for Ru–BIP, Ru–DHA, and Ru–THA in parts A–C, whereas it is reversed at ~ 275 nm): 1 (---), control (nonmodified) DNA; 2, $r_b = 0.05$; 3, $r_b = 0.1$; 4, $r_b = 0.2$. Inset in parts A–D: a part of the CD spectrum (at 280–450 nm) recorded at a higher sensitivity of the CD instrument. (E) Dependence of the maximum ellipticity of the positive CD band at around 280 nm on r_b : (■) Ru–BIP; (□) Ru–DHA; (●) Ru–THA; (○) Ru–CYM. (F) Dependence of the maximum ellipticity of the positive CD band at around ~ 370 nm on r_b : (■) Ru–BIP; (□) Ru–DHA; (●) Ru–THA; (○) Ru–CYM. Data points measured in duplicate varied on average $\pm 1\%$ from their mean.

in the intensity of the positive band around 280 nm was seen, but instead there was a small decrease.

We also recorded CD spectra of CT DNA and the synthetic double-stranded polynucleotide complexes poly(dG–dC) and poly(dA–dT) in the presence of these four Ru complexes and also the benzene complex Ru(BEN) at $r_i = 0.2$. An induced CD band at 350–410 nm was observed not only for interaction of Ru–BIP, Ru–THA, and Ru–DHA with CT DNA but also for interaction with poly(dG–dC) (Figure 5A and B). For poly(dG–dC), as for CT DNA, no induced band in the near UV region was observed for Ru–CYM, or for Ru–BEN (Figure 5A and B). For poly(dA–dT), only the complexes with extended π systems, Ru–BIP, Ru–THA, and Ru–DHA, induced any spectral changes, and these were small and confined to the region 260–280 nm (Figure 5C). These small changes may be due to weak hydrophobic interactions between the arene and the DNA bases. Neither

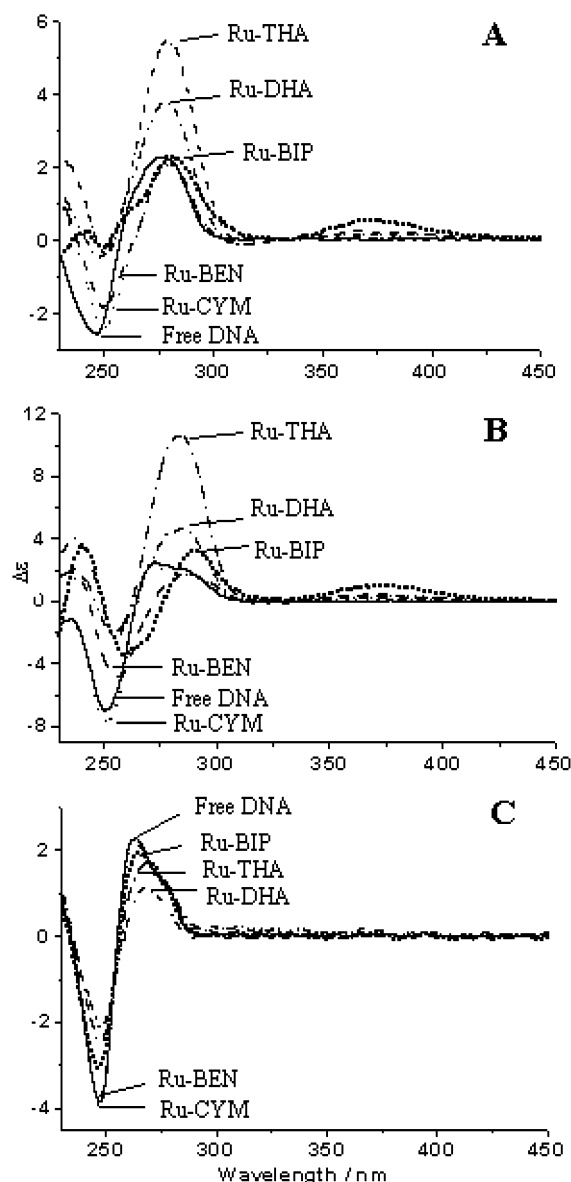


FIGURE 5: Comparisons of the effects of different arene ligands on the CD spectra of (A) CT DNA, (B) poly(dG–dC), and (C) poly(dA–dT) in 10 mM NaClO_4 in the presence of various Ru(arene) complexes at $r_i = 0.2$. The spectra were recorded at 25 $^{\circ}\text{C}$ after samples had been incubated for 24 h at 37 $^{\circ}\text{C}$.

Ru–CYM nor Ru–BEN induced any spectral changes in poly(dA–dT).

The flow linear dichroism data for CT DNA (Figure S1A) resemble those of poly(dG–dC) DNA (Figure S1B) and show that the binding of all Ru complexes causes bending of the DNA. The three complexes Ru–THA, Ru–DHA, and Ru–BIP cause a significant red shift (ca. 10 nm) of the main DNA band near 260 nm, whereas the two complexes Ru–BEN and Ru–CYM cause no shift. The wavelength shifts in the region of DNA absorption for Ru–THA, Ru–DHA, and Ru–BIP are consistent with intercalation of the arene ligands, but the bending precludes full intercalation which would rigidify the DNA and thus increase the LD. Ru–BEN and Ru–CYM complexes rigidify poly(dA–dT) DNA with no 260 nm band shift (Figure S1C); the other three complexes, Ru–DHA, Ru–THA, and Ru–BIP, cause significant bending while retaining sufficient orientation to produce an LD signal for these compounds. Ru–DHA

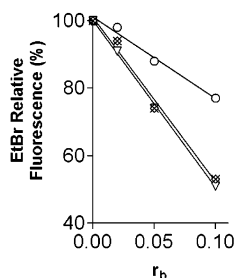


FIGURE 6: Dependences of the EtBr fluorescence on r_b for DNA modified by Ru(arene) complexes in 10 mM NaClO₄ at 37 °C for 24 h: (x) Ru-BIP; (◇) Ru-DHA; (▽) Ru-THA; (○) Ru-CYM. Data points measured in triplicate varied on average $\pm 2\%$ from their mean.

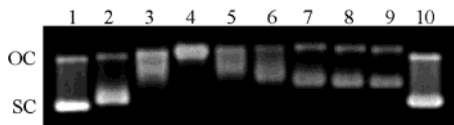


FIGURE 7: Unwinding of supercoiled pSP73KB plasmid DNA by the compound Ru-BIP. The plasmid was incubated with the ruthenium complex for 24 h at 37 °C. Lanes: 1 and 10, control, nonmodified DNA ($r_b = 0$); 2, $r_b = 0.03$; 3, $r_b = 0.06$; 4, $r_b = 0.08$; 5, $r_b = 0.10$; 6, $r_b = 0.11$; 7, $r_b = 0.13$; 8, $r_b = 0.16$; 9, $r_b = 0.17$. The top bands correspond to the form of nicked plasmid, and the bottom bands, to the closed, negatively supercoiled plasmid.

binding induces the most bending. The LD observed for the binding to poly(dA-dT) is consistent with a mode involving the aromatic ligands of Ru-DHA, Ru-THA, and Ru-BIP inserted into the minor groove, giving a positive signal for the transitions in the 260–280 nm ligand y-polarized region and probably a negative one for the 240–255 nm z-polarized region (according to the film LD assignments, Figure S2).

Characterization of DNA Adducts by EtBr Fluorescence. EtBr as a fluorescent probe can be used to distinguish intercalating and nonintercalating ligands (34). Binding of EtBr to DNA by intercalation is blocked in a stoichiometric manner by formation of a wide spectrum of DNA-binding ligands including intercalators. On the other hand, modification of DNA by monofunctional nonintercalative ligands, such as [Pt(dien)Cl]Cl, results in only a slight decrease of EtBr fluorescence intensity as compared with that for the complex of nonmodified DNA with EtBr. Competitive binding of other intercalators leads to a loss of fluorescence because of depletion of the DNA–EtBr complex (free EtBr is poorly fluorescent).

Double-helical DNA was modified by Ru arene compounds for 24 h. The levels of the modification corresponded to the values of r_b in the range between 0 and 0.1. Modification of DNA by Ru-BIP, Ru-DHA, and Ru-THA resulted in a marked decrease of EtBr fluorescence (Figure 6). In contrast, the decrease of the fluorescence intensity by the adducts of Ru-CYM was only very small and similar to that induced by the adducts of [PtCl(dien)]Cl (35).

DNA Unwinding. Electrophoresis in native agarose gels was used to determine the unwinding induced in negatively supercoiled pSP73KB plasmid DNA by monitoring the degree of supercoiling (28) (Figure 7). A compound that unwinds the DNA duplex reduces the number of supercoils in closed circular DNA, which in turn causes a decrease in the rate of migration through the agarose gel.

Figure 7 shows an electrophoresis gel from experiments in which variable amounts of Ru-BIP were bound to a

Table 1: Unwinding of Supercoiled pSP73KB DNA by Ru(II) Arene Complexes

compd	$r_b(c)$	unwinding angle ^a
Ru-BIP	0.08 ± 0.005	$14 \pm 1^\circ$
Ru-DHA	0.08 ± 0.005	$14 \pm 1^\circ$
Ru-THA	0.08 ± 0.005	$14 \pm 1^\circ$
Ru-CYM	0.16 ± 0.01	$7 \pm 0.5^\circ$

^a The unwinding angle was calculated as described in the text.

mixture of relaxed and negatively supercoiled pSP73KB DNA. The mean unwinding angle is given by $\Phi = 18\sigma/r_b(c)$, where σ is the superhelical density and $r_b(c)$ is the value of r_b at which the supercoiled and nicked forms comigrate (28). Under the present experimental conditions, σ was calculated to be -0.063 on the basis of data for cisplatin for which the value $\Phi = 13^\circ$ was used to determine $r_b(c)$ (28). The $r_b(c)$ values for all ruthenium arene compounds studied, along with the mean unwinding angles calculated in this way, are summarized in Table 1. The unwinding angles were $14 \pm 1^\circ$ per bound Ru-BIP, Ru-DHA, and Ru-THA, and $7 \pm 0.5^\circ$ for Ru-CYM.

DNA Melting. CT DNA was modified by Ru(II) arene compounds added at various r_b values (0–0.1) in 10 mM NaClO₄ at 37 °C for 24 h. The salt concentration was then further adjusted by addition of NaClO₄ to values in the range 0.01–0.1 M. The effect on t_m is dependent both on the amount of ruthenium bound and on the salt concentration. At low concentrations of NaClO₄ (0.01 M) an increase in t_m was observed for the three compounds Ru-BIP, Ru-DHA, and Ru-THA, and this became more pronounced with increasing r_b values (Figure 8A–C). With increasing ionic strength, the enhancement of t_m (Δt_m) due to the presence of the Ru compounds decreased, and at salt concentrations of 0.2 M, t_m decreased. In contrast, the melting behavior of DNA modified by Ru-CYM resulted in a similar decrease of t_m at all ionic strengths (Figure 8D).

Differential Pulse Polarography. This is a sensitive method for distinguishing between nondenaturational and denaturational conformational alterations in DNA induced by various physical or chemical agents (36). The analysis is based on the observation that intact double-helical DNA is polarographically inactive because its reduction sites are involved in hydrogen bonds and are unable to make contact with the working electrode in a manner suitable for electron transfer. Electroreduction of adenine or cytosine residues present in distorted but still double-stranded (nondenatured) regions of DNA is responsible for the appearance of the small DPP peak II (Figure 9A, curve 1). Base residues in these distorted regions become more accessible for electroreduction at the mercury electrode and can yield a small polarographic current. On the other hand, the appearance of a more negative peak III in DPP curves of DNA indicates the presence of single-stranded, denatured regions in the DNA molecule, in which hydrogen bonds between complementary bases have been broken (36). Differences in the adsorption properties of double-helical and denatured DNA at the mercury electrode have been suggested to give rise to the different reduction potentials observed for the two DNA conformations. Importantly, less than 1% of the denatured material in the presence of an excess of double-helical DNA can be determined by DPP (37).

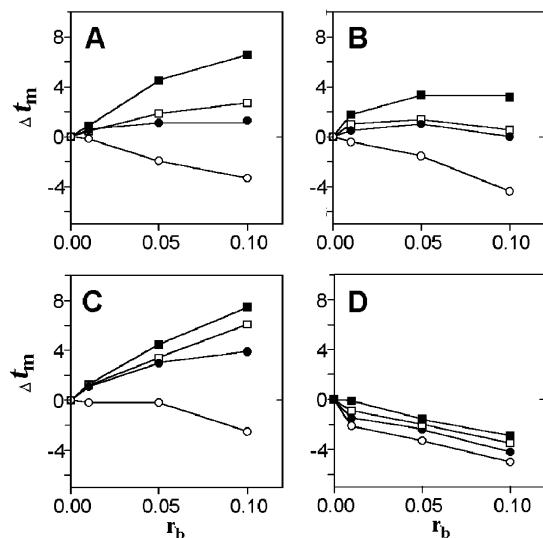


FIGURE 8: Plots showing the dependence of Δt_m values on r_b for calf thymus DNA modified by Ru(II) arene compounds: A, Ru-BIP; B, Ru-DHA; C, Ru-THA; D, Ru-CYM. The melting curves were measured in 0.01 M (■), 0.05 M (□), 0.1 M (●), or 0.2 M (○) NaClO₄ plus 1 mM Tris-HCl with 0.1 mM EDTA, pH 7.4. Δt_m is defined as the difference between the t_m values of ruthenated and nonmodified DNAs. Data measured in triplicate varied on average $\pm 2\%$ from their mean.

DPP has already been used to analyze DNA modified by various physical or chemical agents, including platinum and ruthenium compounds with different clinical efficacy (20, 38, 39). It has been found that DNA globally modified by antitumor cisplatin, its antitumor analogues, or *cis*- or *trans*-[RuCl₂(Me₂SO)₄] at r_b values up to 0.05 yields the more positive DPP peak II, indicating that these antitumor drugs induce nondenaturational conformational changes in DNA (38). In contrast, the more negative peak III is evident on DPP curves of DNA globally modified by clinically ineffective transplatin and other inactive platinum(II) complexes, indicating that the clinically ineffective platinum complexes induce denaturational conformational alterations in DNA (38, 39).

DPP analysis also sheds considerable light on the conformational basis for DNA binding of the Ru(II) arene compounds tested in this work. Modification of CT DNA by Ru-BIP, Ru-DHA and Ru-THA at r_b values of 0.0005–0.01 resulted in an increase in intensity of the DPP peak II with increasing levels of the modification (shown for Ru-DHA in Figure 9B). The more negative peak III was not detected even for the DPP curves recorded for DNA modified at the highest r_b value used in our experiments (0.01). As regards the DPP analysis of DNA modified by Ru-THA, peak II was markedly distorted by a current corresponding to the higher background electrolyte discharge, so that the measurement of the height of this peak II at r_b values of 0.001 and higher was impossible. On the other hand, it was clear even from these distorted DPP curves that no peak III was present even at $r_b = 0.01$. It could be argued that the absence of peak III on the DPP curves recorded for the samples of DNA modified by Ru-BIP, Ru-DHA and Ru-THA at relatively high r_b values (~ 0.02) could be due to an increase in the slope of the part of the DPP curve corresponding to the background electrolyte discharge (Figure 9B, curve 4). The fact that peak III was not buried under the background electrolyte discharge curve was verified using

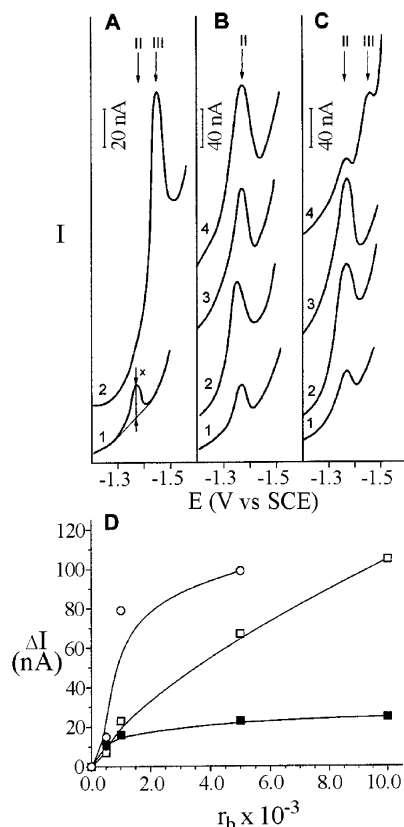


FIGURE 9: Differential pulse polarographic analysis of CT DNA modified by Ru(II) arene compounds. Double-helical DNA at a concentration of 0.32 mg/mL in 0.3 M ammonium formate with 0.01 M phosphate buffer, pH 6.8. (A) DPP curves of nonmodified DNA: 1, double-helical DNA; 2, thermally denatured DNA at the concentration of 0.030 mg/mL. (B and C) DPP curves of double-helical DNA modified by Ru-DHA (B) and Ru-CYM (C) at the following r_b values: 1, 0.0005; 2, 0.001; 3, 0.005; 4, 0.01. The arrows in parts A–C marked by II and III indicate the potentials E [against saturated calomel electrode (SCE)] at which native or denatured DNA samples yielded DPP peaks II or III, respectively (see the text). The procedure used to measure the height of the DPP peak (x) in the present work is shown in Figure 9A, curve 1. (D) Dependence of the relative height of the DPP peak II, ΔI , yielded by DNA modified by the ruthenium complexes on r_b : (■) Ru-BIP; (□) Ru-DHA; (○) Ru-CYM. The value of ΔI was calculated as the ratio of the peak height yielded by the modified DNA over the peak height yielded by the control (nonmodified) DNA.

the samples of DNA modified by Ru-BIP, Ru-DHA or Ru-THA at $r_b = 0.01$ to which 0.8% thermally denatured calf thymus DNA was added. For this sample, a small, more negative peak III on the DDP curve (recorded under conditions specified for curve 4 in Figure 9B) was clearly observed (not shown). Thus, the absence of peak III on the DPP curves of DNA modified by Ru-BIP, Ru-DHA, or Ru-THA suggests that these ruthenium complexes induce nondenaturational conformational distortions in DNA at relatively low levels of the global modification ($r_b \leq 0.01$), a behavior similar to that for the antitumor drug cisplatin and its antitumor analogues (38, 39). In contrast, a relative increase in the intensity of peak II due to the global modification by Ru-CYM was also seen, but only at lower levels of the DNA modification ($r_b \leq 0.005$) (Figure 9C). At higher levels of DNA modification by Ru-CYM, a well-developed more negative DPP peak III, characteristic of the formation of single-stranded segments in double-helical

DNA, was observed. This finding supports the view that the DNA binding mode of Ru–CYM is different from that of the BIP, DHA, and THA ruthenium arene compounds and that the modification by Ru–CYM may even lead to denaturational distortions of DNA.

DISCUSSION

Our studies of the binding of the Ru(II) arene ethylenediamine complexes Ru–BIP, Ru–DHA and Ru–THA to natural double-helical CT DNA show that the reactions are about an order of magnitude faster than that for cisplatin (Figure 2). However, the rate of binding is markedly dependent on the type of arene ligand: binding of Ru–CYM, a complex with a single arene ring and methyl and bulky isopropyl substituents, binds to CT DNA more slowly than cisplatin. The binding is almost quantitative in each case (>90% after 24 h), and the DNA–Ru adducts are stable, with little loss of bound Ru after extensive dialysis. Transcription mapping experiments (Figure 3) have shown that guanine residues are the preferential binding sites when polymeric DNA is modified with Ru(II) arene complexes in a random fashion.

The selectivity of these pseudo-octahedral Ru(II) arene ethylenediamine complexes for G bases was also found previously in our studies of model reactions of monomeric nucleosides and nucleotides (23, 40). Ru(II) in arene ethylenediamine complexes bind strongly to GN7, and C6O of G can then form a strong intramolecular H-bond with an NH of the coordinated ethylenediamine (23, 40). For adenine and cytosine unfavorable interactions between the amino groups on these bases and the amino groups of coordinated en have been demonstrated (23, 40). Binding to thymine N3 requires displacement of the N3H proton, which is not favorable at pH values in the physiological range and not accessible in double-helical DNA. Also, when the arene contains an extended π -electron system, as in biphenyl or the anthracene derivatives studied in this work, an additional stabilization of the interaction can arise from hydrophobic π – π stacking of the coordinated arene ring system with the purine ring (23, 40). Such hydrophobic π – π stacking is enhanced when one or both partners are electron-poor (41). Ru(II) binding to G N7 decreases the electron density on the purine but increases electron density on Ru(II) which, in turn, enhances π -back-bonding of Ru(II) to the η^6 -arene (42).

Slower reactions between CT DNA and Ru–CYM (Figure 1), or Ru–BEN, compared to Ru–BIP, Ru–DHA and Ru–THA are expected from our model studies of the kinetics of binding of these complexes to cyclic-3',5'-GMP (23). Reactions of Ru–BIP, Ru–DHA and Ru–THA with cGMP are greater than three times faster. This difference may arise from the ability of the extended π system of the arene ligand in the faster-reacting complexes to take part in hydrophobic π – π stacking interactions with the purine ring of G, as observed in model complexes. This is not possible for the monoarene complexes Ru–CYM or Ru–BEN, since the π -electron system of these ligands is fully involved in coordination to Ru(II). Hence, it is reasonable to suggest that hydrophobic interactions can contribute to the driving force for the binding of chloro Ru(II) arene complexes to double-helical DNA.

By analogy with the changes in the CD spectra and DPP behavior of DNA modified by cisplatin and antitumor-inactive transplatin or [Pt(dien)Cl]Cl, it is reasonable to suggest that the binding of Ru–BIP, Ru–DHA, and Ru–THA results in conformational alterations in double-helical DNA of nondenaturational character, as is the case for DNA modification by antitumor cisplatin (38). The CD and DPP results (Figures 4, 5, and 9) also suggest that the conformational changes induced in DNA by Ru–CYM and Ru–BEN are different from those induced by the other three ruthenium arene compounds and, in contrast, are of denaturational character, similar to the case of DNA modification by transplatin or monofunctional [Pt(dien)Cl]Cl complexes. The LD data (Figures S1 and S2) showed that Ru–CYM stiffened poly(dA–dT) DNA, while the other complexes bend it, and for Ru–BIP, Ru–DHA, and Ru–THA the main effect of binding to poly(dG–dC) and CT-DNA appears to be the induction of DNA bending, making it difficult to draw conclusions about the local orientations of the complexes on the DNA. The coordination of Ru–BIP, Ru–DHA, or Ru–THA to double-helical DNA also results in the appearance of a CD band centered around 370–380 nm (Figure 4A–C). The induced CD bands for achiral molecules bound to DNA arise either from coupling between the dipole transition moment of the nucleobases and the bound metal complex or from distortion of the geometry of the metal complex. Since binding of neither Ru–CYM (Figure 4D) nor Ru–BEN (Figure 5) to DNA gives rise to such a CD band in this region of the spectrum, and these complexes contain only a single ring, it seems likely that the metal-centered induced band is related either to intercalation of the extended arene ligands into DNA or to groove binding. The observation of such bands is well documented for other intercalating metal complexes (43, 44). For example, the binding of [Pt(terpyridine)(CH₃)]⁺ to DNA at $r_i = 0.1$ gives rise to positive CD bands at 315–340 nm, indicating possible intercalation of the terpyridine ligand (45). Similar CD bands were observed for binding of Ru(II) arene complexes to poly(dG–dC) as for CT DNA (Figure 5A,B), but not for poly(dA–dT) (Figure 5C). From model studies of mononucleotides (23, 40), only weak binding to A or T is expected, accounting for the differences in binding to poly(dA–dT). From the assignments made by film LD experiments, the effects on the LD spectrum of poly(dA–dT) DNA are consistent with a binding mode involving insertion of the extended π -systems of Ru–DHA, Ru–THA, and Ru–BIP into the minor groove, giving a positive signal for the transitions in the 260–280 nm ligand y-polarized region and probably a negative signal for the 240–255 nm z-polarized region.

The CD changes observed for double-helical DNA modified by the Ru(II) arene compounds also correlate with the results of DNA unwinding (Figure 7 and Table 1) and competitive EtBr displacement (Figure 6) experiments. The monofunctional adducts of Ru–BIP, Ru–DHA, or Ru–THA are considerably more efficient in DNA–EtBr fluorescence quenching and in DNA unwinding than those of Ru–CYM. One plausible explanation for this observation may be an associated large additional contribution to fluorescence quenching and unwinding from intercalation of the extended arene ligand of the compounds Ru–BIP, Ru–DHA, or Ru–THA into the duplex or from other types of

noncovalent interaction of these complexes with DNA upon their monofunctional binding. The large unwinding angles of 15 or 19° produced by the platinum compounds *cis*-[Pt(NH₃)₂(N3-ethidium)Cl]²⁺ and *cis*-[Pt(NH₃)₂(N8-ethidium)Cl]²⁺, respectively, which incorporate the well-known DNA intercalator ethidium and which can form only monofunctional adducts with DNA, have been explained in this way (28). Thus, the arene moiety in the monofunctional adducts of the compounds Ru-BIP, Ru-DHA, and Ru-THA could be geometrically well positioned to intercalate between the base pairs of the helix, so producing also the induced CD bands (Figure 5). Consistent with this conclusion is the observation that the adducts of the compound Ru-CYM, which (like Ru-BEN) produces no induced CD bands in the visible spectrum and quenches DNA-EtBr fluorescence only slightly, unwinds DNA only by 7° (Figure 7D, Table 1), a similar behavior to that of the monofunctional adducts of [Pt(dien)Cl]Cl [unwinding angle 6° (28)]. Thus, the results of unwinding experiments support the view that the arene ligand in Ru-BIP, Ru-DHA, and Ru-THA interacts substantially with the double helix upon coordination of the ruthenium complex. Hence, these results strengthen the case for combined intercalative and monofunctional binding modes which may be facilitated by the fluxionality of the arene ligand in these complexes (40). On the other hand, it seems reasonable to suggest that the *p*-cymene and benzene ligands in the compounds Ru-CYM do not interact with the double helix in a similar way, thus also supporting a different DNA binding mode for these compounds in comparison with the other three Ru(II) arene complexes studied in the present work.

The arene-purine hydrophobic interactions and/or arene-base stacking involved in the binding of the arene compounds to double-helical DNA may also affect its melting behavior. Previously, three factors have been invoked to account for the thermal stability of DNA modified by ruthenium and platinum complexes: stabilizing effects of the positive charge on the ruthenium and platinum moieties and of DNA interstrand cross-links, and a destabilizing effect of conformational distortions such as intrastrand cross-links induced in DNA by ruthenium and platinum coordination. At least two additional factors may be involved in DNA stabilization by intercalators: (i) favorable stacking interactions between the base residues and the intercalator, and (ii) the separation of negative backbone charges inherent to intercalation (due to elongation and unwinding of DNA), that is, changes in solvent structure and the counterion distribution around the phosphate groups which may help to overcome electrostatics unfavorable for the hybridization of the strands of the duplex (46, 47). The dependence of the transition melting temperature of DNA modified by nonintercalating platinum or ruthenium drugs on ionic strength can be explained by competing electrostatic effects as the salt concentration is varied (48). Under the incubation conditions, we expect all Ru(II) arene complexes to have produced monofunctional adducts so that the effect of interstrand cross-links need not be considered. Thus, the observed change in melting temperature will reflect the relative proportion and contribution of all limiting binding modes. Inherently, we predict that conformational distortions due to the formation of the adducts will destabilize the helix, as has been consistently observed in earlier studies with various ruthenium and platinum

compounds.

At low ionic strength (0.01 M), it is reasonable to conclude that the increases in t_m due to the modification of DNA by Ru-BIP, Ru-DHA, or Ru-THA (Figure 8A-C) are caused by the positive charges on ruthenium {(arene)Ru(en)}⁺ moieties and by the intercalation. An interesting and as yet unresolved question, therefore, is why the modification of DNA by these three Ru(II) arene compounds appears to result in smaller thermal stabilization or even destabilization if the melting curves are measured at high salt concentrations. It is possible that the smaller increase or decrease in t_m due to the modification by the compounds Ru-BIP, Ru-DHA, and Ru-THA and observed at high ionic strength is a consequence of conformational changes induced by the adducts of these Ru(II) arene compounds that then compensate more efficiently the "stabilizing" effects. At high salt concentration the stabilizing effects due to the modification of DNA by Ru-BIP, Ru-DHA, or Ru-THA are reduced, since the electrostatic effects of these compounds are apparently lowered with increasing concentration of Na⁺ counterions.

As pointed out above, the melting behavior of DNA modified by the compound Ru-CYM is different (cf. parts A-C and D of Figure 8). Modification by Ru-CYM already decreases t_m at low concentrations of Na⁺, indicating that the effects of the factors responsible for the thermal stabilization of DNA are noticeably reduced. As also mentioned above, two factors have been invoked to account for the increase of the thermal stability of DNA due to the modification by Ru(II) arene complexes: stabilizing effects of the positive charge on the ruthenium atom and those associated with intercalation of the arene ligand in these ruthenium compounds into the duplex. Hence, it seems reasonable to conclude that the effect of one or both these factors is markedly reduced so that the destabilization effect of conformational alterations induced by Ru-CYM predominates already at low salt concentrations. The results are consistent with the formation of a monofunctional adduct of Ru-CYM with DNA (coordination to G N7) and the absence of intercalation, as expected for this substituted single-ring arene ligand. Hence, the stabilization of DNA typical of intercalators (vide supra) would not be effective, for obvious reasons. In addition, the stabilizing effects of the positive charge on the ruthenium atom of the compound Ru-CYM might be considerably reduced due to a substantially different location of the ruthenium atom in the adduct of Ru-CYM relative to the DNA sugar-phosphate backbone. This location might be unfavorable from the viewpoint of the efficiency of the positive charge on the ruthenium atom to neutralize negative charges of DNA phosphate groups. The suggestion that the positive charge on the ruthenium atom in the adducts of Ru-CYM does not markedly contribute to the thermal stability of DNA is also consistent with the observation that the lowering of the melting temperature of DNA due to modification by Ru-CYM is almost independent of the Na⁺ concentration (Figure 8D). Thus, the solution behavior of the DNA adducts of Ru(II) arene complexes appears interesting and merits further study.

Circular dichroism and polarographic analyses of DNA modified by Ru(II) arene anticancer compounds (Figures 4, 5, and 9) demonstrate that the formation of the monofunctional adducts of these complexes distorts the DNA confor-

mation. The compounds Ru-BIP, Ru-DHA, or Ru-THA, which contain arene ligands with extended π -systems, induce nondenaturational alterations in DNA. On the other hand, the adducts of Ru-CYM, which contains a single arene ring but with methyl and bulky isopropyl substituents, distort DNA more severely, so that even denaturational changes may occur. The mechanisms underlying the biological effects of antitumor metal-based drugs may also involve further "downstream" effects of damaged DNA. These effects include processing of DNA adducts of these compounds by cellular components, for example, recognition of the adducts by specific proteins, and their repair (49, 50). This processing may also be affected by both the character of the conformational alterations induced in DNA and the resulting thermodynamic destabilization of this polynucleotide. For instance, minor 1,3-intrastrand cross-links of cisplatin, which probably do not contribute significantly to the antitumor effects of this drug, or the same adducts of its clinically ineffective trans isomer induce denaturational alterations in DNA (51). On the other hand, nondenaturational alterations occur in DNA as a consequence of the formation of the major 1,2-intrastrand cross-link of cisplatin (52). Interestingly, it has been shown that high-mobility-group (HMG)-domain proteins play an important role in the antitumor effect of cisplatin in several tumor cell lines (49, 50), and while the 1,2-intrastrand cross-link of cisplatin is recognized by these proteins (53), the 1,3-intrastrand cross-links of cisplatin or transplatin are not (50, 53). In addition, the 1,3-intrastrand cross-links of cisplatin are more readily removed from DNA than its major 1,2-intrastrand cross-links (54), and it has been shown (49, 55) that enhanced repair of the adducts of cisplatin contributes to enhanced resistance to this drug. Thus, an intriguing eventuality for future research is to correlate different DNA binding modes of Ru-CYM and Ru-BEN and the other three Ru(II) arene compounds tested in the present work with their cytotoxicity in tumor cell lines.

In summary, the present work demonstrates that the concept based on Ru(II) arene complexes represents an interesting possibility for studies aimed at improving knowledge of the mechanisms underlying the biological effects of ruthenium compounds. Whether this concept is applicable to the development of new anticancer drugs has still to be examined.

SUPPORTING INFORMATION AVAILABLE

Flow linear dichroism spectra of CT, poly(dG-dC), and poly(dA-dT) DNA after reaction with Ru(II) arene complexes (Figure S1), and determination of transition polarizations of dihydroanthracene (Figure S2). This material is available free of charge via the Internet at <http://pubs.acs.org>.

REFERENCES

1. Johnson, N. P., Butour, J.-L., Villani, G., Wimmer, F. L., Defais, M., Pierson, V., and Brabec, V. (1989) *Prog. Clin. Biochem. Med.* 10, 1–24.
2. Brabec, V. (2000) in *Platinum-Based Drugs in Cancer Therapy* (Kelland, L. R., and Farrell, N. P., Eds.) pp 37–61, Humana Press Inc., Totowa, NJ.
3. Fichtinger-Schepman, A. M. J., Van der Veer, J. L., Den Hartog, J. H. J., Lohman, P. H. M., and Reedijk, J. (1985) *Biochemistry* 24, 707–713.
4. Eastman, A. (1987) *Pharmacol. Ther.* 34, 155–166.
5. Cleare, M. J. (1974) *Coord. Chem. Rev.* 12, 349–405.
6. Cleare, M. J. (1977) *J. Clin. Hematol. Oncol.* 7, 1–25.
7. Farrell, N. (1996) in *Metal Ions in Biological Systems* (Sigel, A., and Sigel, H., Eds.) pp 603–639, Marcel Dekker, Inc., New York, Basel, Hong Kong.
8. Brabec, V., Kasparkova, J., Vrana, O., Novakova, O., Cox, J. W., Qu, Y., and Farrell, N. (1999) *Biochemistry* 38, 6781–6790.
9. Farrell, N. (2000) in *Platinum-Based Drugs in Cancer Therapy* (Kelland, L. R., and Farrell, N. P., Eds.) pp 321–338, Humana Press Inc., Totowa, NJ.
10. Keppler, B. K. (1993) *Metal Complexes in Cancer Chemotherapy*, VCH Verlagsgesellschaft, VCH Publishers, Weinheim, New York.
11. Sava, G., and Bergamo, A. (2000) *Int. J. Oncol.* 17, 353–365.
12. Clarke, M. J. (2003) *Coord. Chem. Rev.* 236, 209–233.
13. Aird, R., Cummings, J., Ritchie, A., Muir, M., Morris, R., Chen, H., Sadler, P., and Jodrell, D. (2002) *Br. J. Cancer* 86, 1652–1657.
14. Morris, R. E., Aird, R. E., Murdoch, P. D., Chen, H. M., Cummings, J., Hughes, N. D., Parsons, S., Parkin, A., Boyd, G., Jodrell, D. I., and Sadler, P. J. (2001) *J. Med. Chem.* 44, 3616–3621.
15. Sava, G., Alessio, E., Bergano, A., and Mestroni, G. (1999) in *Topics in Biological Inorganic Chemistry. Metallopharmaceuticals I* (Clarke, M. J., and Sadler, P. J., Eds.) pp 143–169, Springer, Berlin.
16. Clarke, M. J., Zhu, F., and Frasca, D. R. (1999) *Chem. Rev.* 99, 2511–2533.
17. Sava, G., Pacor, S., Coluccia, M., Mariggio, M., Cocchiello, M., Alessio, E., and Mestroni, G. (1994) *Drug Invest.* 8, 150–161.
18. Novakova, O., Kasparkova, J., Vrana, O., van Vliet, P. M., Reedijk, J., and Brabec, V. (1995) *Biochemistry* 34, 12369–12378.
19. Barca, A., Pani, B., Tamaro, M., and Russo, E. (1999) *Mutation Res.* 423, 171–181.
20. Novakova, O., Hofr, C., and Brabec, V. (2000) *Biochem. Pharmacol.* 60, 1761–1771.
21. Malina, J., Novakova, O., Keppler, B. K., Alessio, E., and Brabec, V. (2001) *J. Biol. Inorg. Chem.* 6, 435–445.
22. Wang, F., Chen, H., Parsons, S., Oswald, I. D. H., Davidson, J. E., and Sadler, P. J. (2003) *Chem. Eur. J.*, in press.
23. Chen, H. M., Parkinson, J. A., Morris, R. E., and Sadler, P. J. (2003) *J. Am. Chem. Soc.* 125, 173–186.
24. Brabec, V., and Palecek, E. (1970) *Biophysik* 6, 290–300.
25. Brabec, V., and Palecek, E. (1976) *Biophys. Chem.* 4, 76–92.
26. Lemaire, M. A., Schwartz, A., Rahmouni, A. R., and Leng, M. (1991) *Proc. Natl. Acad. Sci. U.S.A.* 88, 1982–1985.
27. Brabec, V., and Leng, M. (1993) *Proc. Natl. Acad. Sci. U.S.A.* 90, 5345–5349.
28. Keck, M. V., and Lippard, S. J. (1992) *J. Am. Chem. Soc.* 114, 3386–3390.
29. Butour, J. L., and Macquet, J. P. (1977) *Eur. J. Biochem.* 78, 455–463.
30. Butour, J. L., Alvinerie, P., Souchard, J. P., Colson, P., Houssier, C., and Johnson, N. P. (1991) *Eur. J. Biochem.* 202, 975–980.
31. Bancroft, D. P., Lepre, C. A., and Lippard, S. J. (1990) *J. Am. Chem. Soc.* 112, 6860–6871.
32. Brabec, V., Boudny, V., and Balcarova, Z. (1994) *Biochemistry* 33, 1316–1322.
33. Rodger, A., and Norden, B. (1997) *Circular Dichroism and Linear Dichroism*, Oxford University Press, Oxford, New York, Tokyo.
34. Jenkins, T. C. (1997) in *Drug-DNA Interaction Protocols* (Fox, K. R., Ed.) pp 195–218, Humana Press Inc., Totowa, NJ.
35. Marini, V., Kasparkova, J., Novakova, O., Scolaro, L. M., Romeo, R., and Brabec, V. (2002) *J. Biol. Inorg. Chem.* 7, 725–734.
36. Palecek, E. (1983) in *Topics in Bioelectrochemistry and Bioenergetics* (Milazzo, G., Ed.) pp 65–155, John Wiley and Sons, Ltd., New York.
37. Palecek, E. (1971) *Methods Enzymol.* 21, 3–24.
38. Brabec, V., Kleinwachter, V., Butour, J. L., and Johnson, N. P. (1990) *Biophys. Chem.* 35, 129–141.
39. Vrana, O., Kleinwachter, V., and Brabec, V. (1984) *Experientia* 40, 446–451.
40. Chen, H. M., Parkinson, J. A., Parsons, S., Coxall, R. A., Gould, R. O., and Sadler, P. J. (2002) *J. Am. Chem. Soc.* 124, 3064–3082.
41. Janiak, C. (2000) *J. Chem. Soc., Dalton Trans.*, 3885–3896.
42. Stebler-Röthlisberger, M., Hummel, W., Pittet, P.-A., Bürgi, H.-B., Ludi, A., and Merbach, A. E. (1988) *Inorg. Chem.* 27, 1358–1363.

43. Long, E. C., and Barton, J. K. (1990) *Acc. Chem. Res.* 23, 271–273.
44. Lyng, R., Rodger, A., and Norden, B. (1991) *Biopolymers* 31, 1709–1720.
45. Arena, G., Monsu Scolaro, L., Pasternack, R. F., and Romeo, R. (1995) *Inorg. Chem.* 34, 2994–3002.
46. Maeda, Y., Nunomura, K., and Ohtsubo, E. (1990) *J. Mol. Biol.* 215, 321–329.
47. Bjorndal, M. T., and Fygenon, D. K. (2002) *Biopolymers* 65, 40–44.
48. Zaludova, R., Kleinwachter, V., and Brabec, V. (1996) *Biophys. Chem.* 60, 135–142.
49. Cohen, S. M., and Lippard, S. J. (2001) in *Prog. Nucleic Acid Res. Mol. Biol.* (Moldave, K., Ed.) pp 93–130, Academic Press Inc., San Diego, CA.
50. Brabec, V. (2002) in *Prog. Nucleic Acid Res. Mol. Biol.* (Moldave, K., Ed.) pp 1–68, Academic Press Inc., San Diego, CA.
51. Anin, M. F., and Leng, M. (1990) *Nucleic Acids Res.* 18, 4395–4400.
52. Gelasco, A., and Lippard, S. J. (1999) in *Topics in Biological Inorganic Chemistry. Metallopharmaceuticals I* (Clarke, M. J., and Sadler, P. J., Eds.) pp 1–43, Springer, Berlin.
53. Jamieson, E. R., and Lippard, S. J. (1999) *Chem. Rev.* 99, 2467–2498.
54. Zamble, D. B., Mu, D., Reardon, J. T., Sancar, A., and Lippard, S. J. (1996) *Biochemistry* 35, 10004–10013.
55. Brabec, V., and Kasparkova, J. (2002) *Drug Resist. Updates* 5, 147–161.

BI034933U

22.

DNA Binding by Antitumor *trans*-[PtCl₂(NH₃)(thiazole)]. Protein Recognition and Nucleotide Excision Repair of Monofunctional Adducts[†]Jana Kasparikova,[‡] Olga Novakova,[‡] Nicholas Farrell,^{*,§} and Viktor Brabec^{*,‡}

Institute of Biophysics, Academy of Sciences of the Czech Republic, Kralovopolska 135, CZ-61265 Brno, Czech Republic, and Department of Chemistry, Virginia Commonwealth University, Richmond, Virginia 23284-2006

Received August 9, 2002; Revised Manuscript Received November 23, 2002

ABSTRACT: Antitumor effects of *cis*-diamminedichloroplatinum(II) (cisplatin) and the clinical inactivity of its *trans* isomer (transplatin) have been considered a paradigm for the classical structure–activity relationships of platinum drugs. However, several new analogues of transplatin which exhibit a different spectrum of cytostatic activity including activity in tumor cells resistant to cisplatin have been recently identified. Analogues containing the planar amine ligand of the general structure *trans*-[PtCl₂(NH₃)(L)], where L = planar amine, represent an example of such compounds. DNA is believed to be the major pharmacological target of platinum compounds. To contribute to the understanding of mechanisms underlying the activation of *trans* geometry in transplatin analogues containing planar amine ligands, various biochemical and biophysical methods were employed in previous studies to analyze the global modifications of natural DNA by *trans*-[PtCl₂(NH₃)(L)]. These initial studies have revealed some unique features of the DNA binding mode of this class of platinum drugs. As the monofunctional lesions represent a significant fraction of stable adducts formed in DNA by bifunctional antitumor *trans*-platinum compounds with planar ligands, we analyzed in the present work short DNA duplexes containing the single, site-specific monofunctional adduct of a representative of this class of platinum drugs, antitumor *trans*-[PtCl₂(NH₃)(thiazole)]. It has been shown that, in contrast to the adducts of monodentate chlorodiethylenetriamineplatinum(II) chloride or [PtCl(NH₃)₃]Cl, the monofunctional adduct of *trans*-[PtCl₂(NH₃)(thiazole)] inhibits DNA synthesis and creates a local conformational distortion similar to that produced in DNA by the major 1,2-GG intrastrand CL of cisplatin, which is considered the lesion most responsible for its anticancer activity. In addition, the monofunctional adducts of *trans*-[PtCl₂(NH₃)(thiazole)] are recognized by HMGB1 domain proteins and removed by the nucleotide excision repair system similarly as the 1,2-GG intrastrand CL of cisplatin. The results of the present work further support the view that the simple chemical modification of the structure of an inactive platinum compound alters its DNA binding mode into that of an active drug and that processing of the monofunctional DNA adducts of the *trans*-platinum analogues in tumor cells may be similar to that of the major bifunctional adducts of “classical” cisplatin.

There is a large body of experimental evidence that the success of platinum complexes in killing tumor cells results from their ability to form on DNA various types of covalent adducts (1–3). Hence, in the search for new platinum antitumor drugs the hypothesis that platinum compounds which bind to DNA in a manner fundamentally different from that of *cis*-diamminedichloroplatinum(II) (cisplatin)¹ will have altered pharmacological properties has been tested. This concept has already led to the synthesis of several new unconventional platinum antitumor compounds that violate the original structure–activity relationships; the advance to

the clinic of the novel trinuclear compound BBR3464 validates the hypothesis (4). The clinical inactivity of transplatin is considered a paradigm for the classical structure–activity relationships of platinum drugs, but to this end several new analogues of transplatin which exhibit a different spectrum of cytostatic activity including activity in tumor cells resistant to cisplatin have been identified (3, 5–7).

The antitumor *trans*-platinum(II) complexes whose DNA binding mode has been already intensively investigated also include analogues containing a planar amine ligand of the

[†] Supported by the Grant Agency of the Czech Republic (Grant 305/02/1552A), the Grant Agency of the Academy of Sciences of the Czech Republic (Grant A5004101), and the Internal Grant Agency of the Ministry of Health of the Czech Republic (Grant NL6058-3/2000). J.K. is an international research scholar of the Howard Hughes Medical Institute. The research of J.K. and V.B. was also supported in part by the Wellcome Trust (U.K.).

* Corresponding authors. V.B.: tel, 420-5-41517148; fax, 420-5-41240499; e-mail, brabec@ibp.cz. N.F.: tel, 1-804-828-6320; fax, 1-804-828-8599; e-mail, nfarrel@mail1.vcu.com.

[‡] Institute of Biophysics.

[§] Department of Chemistry, Virginia Commonwealth University.

¹ Abbreviations: bp, base pair; carboplatin, *cis*-diamminedichlorobutenedicarboxylatoplatinum(II); CFE, cell-free extract; cisplatin, *cis*-diamminedichloroplatinum(II); CL, cross-link; DEPC, diethyl pyrocarbonate; DMS, dimethyl sulfate; HMG, high-mobility group; HMGB1a, domain A of HMGB1 protein; HMGB1b, domain B of HMGB1 protein; FAAS, flameless atomic absorption spectrophotometry; FPLC, fast protein liquid chromatography; KF, Klenow fragment of *Escherichia coli* DNA polymerase I deficient in 3'→5' proofreading exonuclease activity; NER, nucleotide excision repair; PAA, polyacrylamide; [PtCl₂(dien)]Cl, chlorodiethylenetriamineplatinum(II) chloride; RP-HPLC, reversed-phase high-pressure liquid chromatography; *trans*-PtTz, *trans*-[PtCl₂(NH₃)(thiazole)].

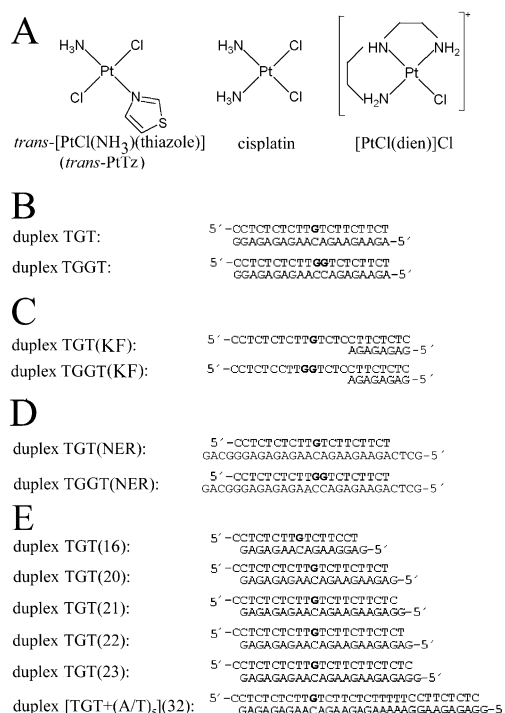


FIGURE 1: Structures of platinum complexes (A) and sequences of the synthetic oligodeoxyribonucleotides used in the present study with their abbreviations (B–E). The top and bottom strands of each pair are designated top and bottom, respectively, in the text. The bold letter in the top strands of all duplexes except TGGT and TGGT(NER) indicates the location of the monofunctional adduct of *trans*-PtTz. The bold letters in the top strands of the duplexes TGGT and TGGT(NER) indicate the location of the intrastrand CL after modification of the duplexes by cisplatin.

general structure *trans*-[PtCl₂(NH₃)(L)], where L = planar amine such as quinoline or thiazole (5), and *trans*-[PtCl₂L₂], where L = pyridine or thiazole, for example (8). To contribute to the understanding of mechanisms underlying the antitumor activity of these transplatin analogues, various biochemical and biophysical methods as well as molecular modeling techniques have been employed to study the modifications of natural, high molecular mass DNA by antitumor *trans*-[PtCl₂(NH₃)(thiazole)] (*trans*-PtTz) (Figure 1A) or *trans*-[PtCl₂(NH₃)(quinoline)] (9). These compounds bind monofunctionally to DNA with a rate similar to that of transplatin. The overall rate of the rearrangement to bifunctional adducts is also similar to that observed in the case of DNA modification by transplatin; i.e., it is relatively slow (10). In contrast to transplatin, however, the analogues containing the planar ligand form considerably more interstrand cross-links (CLs) (~30–40% after 48 h) with a much shorter half-time ($t_{1/2}$ = ~5 h) (9, 11) [~12% interstrand CL is formed by transplatin after 48 h with $t_{1/2}$ > 11 h (12)]. However, a significant fraction of the adducts formed by *trans*-[PtCl₂(NH₃)(quinoline)] or *trans*-PtTz remains monofunctional even after long reaction times (after 48 h ca. 30–40% adducts remain monofunctional) (9, 11).

Additional work has shown that *trans*-[PtCl₂(NH₃)(quinoline)] and *trans*-PtTz preferentially form DNA interstrand CLs between guanine residues at the 5'-GC/5'-GC sites (9). Thus, DNA interstrand cross-linking by these transplatin analogues is formally equivalent to that by antitumor cisplatin but different from clinically ineffective transplatin, which preferentially forms these adducts between complementary

guanine and cytosine residues (13). These results have shown for the first time that the simple chemical modification of structure of an inactive platinum compound alters its DNA binding mode into that of an active drug.

The adducts of the transplatin analogues containing the planar ligand terminate in vitro RNA synthesis in transcription mapping experiments preferentially at guanine residues and at similar sites as the adducts of cisplatin (9). Interestingly, DNA modified by the *trans*-platinum compounds containing the planar ligand is recognized by cisplatin-specific antibodies and not by transplatin-specific antibodies, which suggests that these transplatin analogues behave in some respects like cisplatin (9).

Importantly, the planar ligand in all or in a significant fraction of DNA adducts of these transplatin analogues, in which platinum is coordinated by base residues, is well positioned to interact with the duplex. Models for both monofunctional adducts and bifunctional interstrand CLs have proposed (9, 14) that the combination of monofunctional covalent binding and a stacking interaction between the planar ligand and the DNA bases can produce a kink in the duplex.

Further investigations, which are described in the present work, have focused on the analysis of short duplexes containing the single, site-specific monofunctional adduct of *trans*-PtTz. This compound exhibits antitumor activity (5) so that it is a suitable representative of antitumor *trans*-platinum compounds with planar ligands. It has been shown that the monofunctional adduct of *trans*-PtTz affects DNA conformation, its recognition by cellular proteins and repair distinctly different from the monofunctional adduct formed by chlorodiethylenetriamineplatinum(II) chloride ([PtCl(dien)]Cl) (Figure 1A) or [PtCl(NH₃)₃]Cl [the monodentate complexes (15)]. The monofunctional adduct of *trans*-PtTz creates a local conformational distortion very similar to that produced in DNA by the major 1,2-GG intrastrand CL of antitumor cisplatin. In addition, these monofunctional adducts are recognized by HMGB1 domain proteins (HMG = high mobility group) and removed by the nucleotide excision repair (NER) system similarly as the 1,2-GG intrastrand CL of antitumor cisplatin. As the monofunctional lesions represent a significant fraction of stable adducts formed in DNA by bifunctional antitumor *trans*-platinum compounds with planar ligands, the results of the present work may contribute to understanding the molecular mechanism that underlies antitumor activity of this class of platinum drugs.

MATERIALS AND METHODS

Chemicals. *trans*-PtTz (Figure 1A) was prepared by standard methods (16). Cisplatin (Figure 1A) was obtained from Sigma-Aldrich sro (Prague, Czech Republic). The stock solutions of platinum compounds were prepared at the concentration of 5×10^{-4} M in 10 mM NaClO₄ and stored at 4 °C in the dark. The synthetic oligodeoxyribonucleotides (Figure 1B–E) were synthesized and purified as described previously (17). Expression and purification of domains A (residues 1–84) and B (residues 85–180) of recombinant rat HMGB1 protein (HMGB1a and HMGB1b, respectively) were carried out as described (18, 19). T4 DNA ligase, T4 polynucleotide kinase, and the Klenow fragment of *Escherichia coli* DNA polymerase I deficient in 3'→5' proofreading

exonuclease activity (KF) were purchased from New England Biolabs (Beverly, MA). Acrylamide, bis(acrylamide), urea, and NaCN were from Merck KgaA (Darmstadt, Germany). Dimethyl sulfate (DMS), KMnO_4 , diethyl pyrocarbonate (DEPC), KBr, KHSO_5 , DNase I from bovine pancreas, nuclease P1 from *Penicillium citrinum*, and alkaline phosphatase from calf intestine were from Sigma-Aldrich sro (Prague, Czech Republic). $[\gamma\text{-}^{32}\text{P}]\text{ATP}$ was from Amersham (Arlington Heights, IL). ATP was from Boehringer (Mannheim, Germany). Deoxyribonucleoside 5'-triphosphates were purchased from Pharmacia.

Platinations of Oligonucleotides. The single-stranded oligonucleotides [the top strands of the duplexes in Figure 1B–E except duplexes TGGT, TGGT(KF), and TGGT(NER)] were reacted in stoichiometric amounts with the monoadduct derivative of *trans*-PtTz generated by allowing this complex to react with 0.9 molar equiv of AgNO_3 . The platinated oligonucleotides were repurified by ion-exchange fast protein liquid chromatography (FPLC). It was verified by platinum flameless atomic absorption spectrophotometry (FAAS) and by the measurements of the optical density that the modified oligonucleotides contained one platinum atom. It was also verified using DMS footprinting of platinum on DNA (12) that one *trans*-PtTz molecule was coordinated to a single G at the N7 position in the top strands of all duplexes. FPLC purification and FAAS measurements were carried out on a Pharmacia Biotech FPLC System with a MonoQ HR 5/5 column and a Unicam 939 AA spectrometer equipped with a graphite furnace, respectively. The duplexes TGGT, TGGT(KF), and TGGT(NER) (Figure 1B–D) containing the single, 1,2-GG intrastrand CL of cisplatin in the top strand were prepared as described (12). The unmodified or platinated duplexes used in the studies of recognition by HMGB1 domain proteins were still purified by electrophoresis on native 15% polyacrylamide (PAA) gel [monoacrylamide:bis(acrylamide) ratio = 29:1]. Other details have been described previously (12, 17, 20).

High-Pressure Liquid Chromatographic (HPLC) Analyses. These analyses were performed using a Hitachi Series 4 liquid chromatograph equipped with a LCI-100 computing integrator and a Waters μ Bondapak C18 column. The products were separated by reversed-phase HPLC (RP-HPLC). The products of the enzymatic digestion were analyzed using isocratic elution with 0.1 M ammonium acetate, pH 5.5, in 3.9% CH_3CN at a 1 mL/min flow rate. The following enzymatic digestion protocol was used to characterize the platinated deoxyribooligonucleotide duplexes. The samples (50 μg of the duplex) were incubated with 72 units of DNase I at 37 °C. After 4 h nuclease P1 (40 μg) was added, and the reaction was allowed to continue at 37 °C for 18 h. Finally, alkaline phosphatase (39 units) was added and the incubation continued for an additional 4 h at 37 °C. The digested samples containing constituent nucleosides were then heated for 2 min at 80 °C and centrifuged, and the supernatant was analyzed by RP-HPLC. In the experiments in which dissociation of thiazole from the monofunctional adduct of *trans*-PtTz was examined, the concentration of the duplex was 1 mM (related to the monomer content) and the concentration of thiazole and *trans*-PtTz was 0.1 mM. In these experiments, the products were separated using isocratic elution with 3.9% CH_3CN in

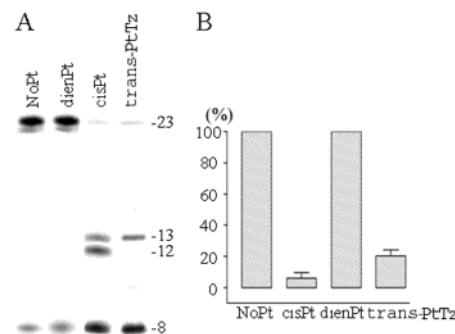


FIGURE 2: Primer extension activity of the exonuclease-deficient Klenow fragment of DNA polymerase I using the 8-mer/23-mer primer/template duplex. The experiments were conducted for 1 min using undamaged template (panel A, lane NoPt) or template containing the 1,2-GG intrastrand CL of cisplatin (panel A, lane cisPt), the monofunctional adduct of $[\text{PtCl}(\text{dien})]\text{Cl}$ (panel A, lane dienPt), or *trans*-PtTz (panel A, lane *trans*-PtTz). The graph (B) shows relative inhibition of DNA synthesis (%) on undamaged (control) template (NoPt) or on DNA containing the 1,2-GG intrastrand CL of cisplatin (cisPt), the monofunctional adduct of $[\text{PtCl}(\text{dien})]\text{Cl}$ (dienPt), or *trans*-PtTz (*trans*-PtTz). Data are the means (\pm standard error) from three different experiments with two independent template preparations.

water at a 1 mL/min flow rate. Other details are in the text below.

DNA Synthesis. The 23-mer templates (for sequences, see Figure 1C) containing a single monofunctional adduct of *trans*-PtTz or $[\text{PtCl}(\text{dien})]\text{Cl}$ or the 1,2-GG intrastrand CL of cisplatin were prepared in the same way as described in the paragraph Platinations of Oligonucleotides (vide supra). The 8-mer DNA primer whose sequence is also shown in the Figure 2A was complementary to the 3' termini of the 23-mer template. The DNA substrates were formed by annealing templates and 5'-end-labeled primers at a molar ratio of 3:1. All experiments using KF were performed at 25 °C in a volume of 50 μL in a buffer containing 50 mM Tris-HCl (pH 7.4), 10 mM MgCl_2 , 0.1 mM dithiothreitol, 50 $\mu\text{g}/\text{mL}$ BSA, 25 μM dATP, 25 μM dCTP, 25 μM dGTP, 25 μM TTP, and 0.5 unit (approximately 1 pmol) of KF. Reactions were terminated by the addition of EDTA so that its resulting concentration was 20 mM and heated at 100 °C for 30 s. Products were resolved by denaturing 24% PAA/8 M urea gel and then visualized and quantified by using a Molecular Dynamics PhosphorImager and ImageQuant software.

The relative inhibition of DNA synthesis on damaged templates was calculated as follows: % inhibition of DNA synthesis = $(1 - \text{Pt}/\text{NoPt}) \times 100$, where Pt = full-length DNA synthesis on the platinated template/total primer termini and NoPt = full-length DNA synthesis on the control, unplatinated template/total primer termini. This calculation was made for that concentration and incubation time for which replication was incomplete (i.e., not all molecules of the primer had been fully elongated) on both the control and platinated templates. Thus, the inhibition of DNA synthesis relative to synthesis on unplatinated DNA templates was determined for 1 min incubation.

Gel Mobility Shift Assay. The 5'-end-labeled 20 base pair (bp) oligonucleotide duplexes (TGT or TGGT shown in Figure 1B) either unplatinated (controls) or containing the central platinum adduct in their top strands were used, and

their reaction with HMG-domain proteins was performed and analyzed as described previously (21). Apparent dissociation constants, $K_{D(\text{app})}$, were estimated in the manner described in ref 21. Each $K_{D(\text{app})}$ is the average of at least two measurements.

Nucleotide Excision Assay. The 148 bp substrates containing the single, central monofunctional adduct of *trans*-PtTz, [PtCl(dien)]Cl, or the 1,2-GG intrastrand CL of cisplatin were assembled from three oligonucleotide duplexes as described previously (22, 23).

Oligonucleotide excision reactions were performed in cell-free extracts (CFEs) prepared from the HeLa S3 and CHO AA8 cell lines as described (24, 25). These extracts were kindly provided by J. T. Reardon and A. Sancar from the University of North Carolina (Chapel Hill, NC). In vitro repair was measured with excision assay using these CFEs and 148 bp linear DNA substrates (vide supra) in the same way as described previously (25).

Ligation, Electrophoresis of Oligonucleotides, and Chemical Modifications. Details of these experiments were as described in previously published papers (26–28).

RESULTS

Stability of the Adduct. We demonstrated previously (9, 11) that preferential G binding of *trans*-[PtCl₂(NH₃)-(quinoline)] or *trans*-PtTz results in monofunctional adducts and CLs. Quantitation of monofunctional adducts revealed that these adducts are equally or even more probable than interstrand or intrastrand CLs. Considering these facts, we have designed a series of synthetic oligodeoxyribonucleotide duplexes, TGT, whose sequences are shown in Figure 1B–E. The pyrimidine-rich top strands of these duplexes only contained one G residue in the central sequence TGT (printed in bold in the Figure 1B–E). These top strands were modified by *trans*-PtTz so that they contained its single monofunctional adduct at the G residue at the central sequence TGT. The platinated top strands were hybridized with their complementary strands. The samples of the platinated duplexes in which either the upper or bottom strand was only 5'-end-labeled with ³²P were reacted with DMS, which does not react with platinated G because the N7 position is no longer accessible (12). The adducts were removed by NaCN, and then the samples were treated with piperidine. In the unplatinated duplexes, the central G residue in the top strands or all G residues in the bottom strands were reactive with DMS (not shown). The single G residue in the top strands was no longer reactive in the platinated duplexes whereas reactivity of all G residues in the complementary bottom strands remained unchanged. This observation confirms that the single G residue in the upper strands remained platinated even after the duplex was formed whereas no G residue in the bottom strands of these duplexes became platinated. The stability of the central monofunctional adducts in the top strands of these duplexes was also confirmed by electrophoretic analysis in denaturing PAA gel (12, 28), demonstrating that no interstrand CL was formed (not shown).

The platinated site in the 20 bp duplex TGT (for the nucleotide sequence, see Figure 1B) modified by *trans*-PtTz in the way described above was also identified using enzymatic digestion analysis. The platinated or nonmodified

duplexes TGT were treated with DNase I, P1 nucleases, and finally alkaline phosphatase to yield corresponding deoxyribonucleosides. An RP-HPLC analysis of the products of this enzymatic digestion procedure revealed well-separated peaks A, C, G, and T, which corresponded to nonmodified deoxyriboadenosine, deoxyribocytidine, deoxyriboguanosine, and thymidine, respectively, assigned by co-injection with samples of pure deoxyribonucleosides (29). The area under peak G yielded by the platinated duplex was only reduced, and this reduction was exactly eight-ninths of that found for the nonmodified, control duplex (containing nine guanine residues) (not shown). The only reasonable explanation of this result is consistent with only one platinated guanine residue in the platinated duplex. We have found conditions for RP-HPLC analysis which allowed detecting quantitatively free thiazole in the presence of *trans*-PtTz also free (not bound to DNA) in the solution. The lower limit of this determination was 0.5% thiazole in the presence of *trans*-PtTz. The 20 bp duplex TGT (Figure 1B) containing the single monofunctional adduct at the central G residue in the top strand was dissolved in 0.01 and 1.0 M NaClO₄ or NaCl and incubated in the dark at 37 °C for 1 week. No peak in the RP-HPLC profile corresponding to free thiazole or *trans*-PtTz was observed, indicating that no thiazole spontaneously dissociated from the monofunctional adduct of *trans*-PtTz in any of the solutions tested and also confirming the stability of this monofunctional lesion.

DNA Synthesis. It is generally accepted that antitumor effects of platinum drugs, such as cisplatin, are associated with the capability of DNA adducts of these compounds to inhibit replication and/or transcription and induce programmed cell death (30). Inhibition of transcription of DNA globally modified by a transplatin analogue with a planar amine ligand in in vitro transcription mapping experiments has been already demonstrated (9). On the other hand, replication or transcription of the adducts of "classical" monofunctional platinum(II) compounds, such as [PtCl(dien)]-Cl or [PtCl(NH₃)₃]Cl, is not inhibited or is inhibited much less effectively than replication or transcription of platinum CLs (3). It is, therefore, of fundamental importance to know whether the monofunctional adducts of *trans*-PtTz can inhibit replication.

In the present work we constructed the 8-mer/23-mer primer/template duplexes TGT(KF) and TGGT(KF) (Figure 1C) unplatinated or containing either the monofunctional adduct of *trans*-PtTz or [PtCl(dien)]Cl at the G residue of the template strand in the central TGT sequence or the 1,2-GG intrastrand CL of cisplatin in the central TGGT sequence. The first eight nucleotides on the 3' terminus of the 23-mer template strand were complementary to the nucleotides of the 8-mer primer and single monodentately modified guanine, or two adjacent guanines cross-linked by cisplatin on the template strand were located at its 13th or 13th and 14th position, respectively, from the 3' terminus (Figure 1C). After annealing a eight nucleotide primer to the 3' terminus of the unplatinated or platinated template strand, positioning the 3'-end of the primer five bases before the adduct in the template strand, we examined DNA polymerization through the single monofunctional adduct or the 1,2-intrastrand CL on the template by KF in the presence of all four deoxyribonucleoside 5'-triphosphates. The reaction was stopped at 1 min, and the products were analyzed using a sequencing

gel (Figure 2A). Polymerization using the 23-mer template containing the CL of cisplatin proceeded rapidly up to the nucleotide preceding and at the sites opposite the CL, such that the 12 and 13 nucleotide products accumulated to a significant extent (shown in Figure 2A, lane cisPt). There was almost no accumulation of larger DNA intermediates, whereas no intermediate products were seen with the 23-mer control template as the full-length product was being formed (shown in Figure 2A, lane NoPt). The full-length products were also noticed with the 23-mer template containing the CL of cisplatin, but only in a relatively very low amount. This result is in agreement with previously published work (31) in which HIV-1 reverse transcriptase and T7 DNA polymerase were used and confirms that the 1,2-GG intrastrand CL of cisplatin strongly inhibits DNA synthesis (32). In contrast, under the same experimental conditions no products shorter than the full-length product were seen with the 23-mer template containing a single monofunctional adduct of [PtCl(dien)]Cl, and the full-length product was only formed (shown in Figure 2A, lane dienPt). This result confirms that monofunctional adducts of [PtCl(dien)]Cl inhibit DNA synthesis much less efficiently or negligibly in comparison with the 1,2-GG intrastrand CL of cisplatin.

DNA polymerization by KF was also examined under identical conditions as in the previous experiment using the template containing the monofunctional adducts of *trans*-PtTz. Polymerization using this 23-mer template proceeded up to the nucleotide opposite the platinated G (Figure 2A, lane *trans*-PtTz). There was almost no accumulation of shorter and larger DNA intermediates. A small amount of the full-length products accumulated also with the 23-mer template containing the monofunctional adduct of *trans*-PtTz. This result indicates that the monofunctional adducts of *trans*-PtTz are very efficient inhibitors of DNA synthesis in contrast to the monofunctional adducts of [PtCl(dien)]Cl, but similarly as major 1,2-intrastrand CLs of cisplatin (Figure 2B) (the inhibition of DNA synthesis after 1 min incubation due to the 1,2-GG intrastrand CL of cisplatin and the monofunctional adduct of *trans*-PtTz was 94% and 80%, respectively). Hence, from the viewpoint of inhibition of replication, the monofunctional adducts of *trans*-PtTz resemble the 1,2-GG intrastrand CLs of cisplatin (although some features are different) and not the adducts of the clinically ineffective monofunctional platinum(II) compounds.

Recognition by HMGB1 Proteins. DNA modified by the *trans*-platinum compounds containing the planar ligand is recognized by cisplatin-specific antibodies, which suggests that these transplatin analogues behave in some respects like cisplatin (9). An important feature of the mechanism that underlies the antitumor activity of cisplatin is that the major adducts of this platinum drug (1,2-GG intrastrand CLs) are recognized by proteins containing HMG domains (2, 3). Importantly, DNA modified by transplatin or monodentate platinum(II) compounds, such as [PtCl(dien)]Cl or [PtCl(NH₃)₃]Cl, is not recognized by these cellular proteins. It has been also shown (2, 3) that the binding of these proteins to DNA modified by cisplatin mediates antitumor effects of this platinum drug. Therefore, we tested in the present work whether the monofunctional adducts which are frequent lesions of *trans*-PtTz are also recognized by HMGB1 box proteins similarly as the 1,2-GG intrastrand CLs of cisplatin.

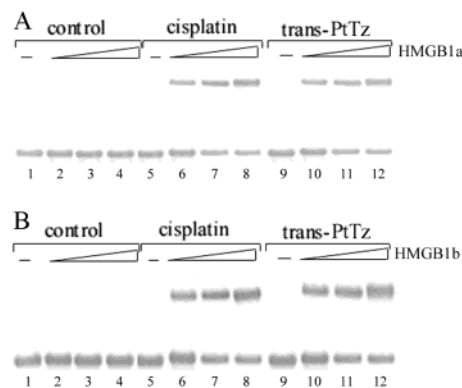


FIGURE 3: Analysis of the binding affinity of 20 bp DNA containing the single, site-specific monofunctional adduct of *trans*-PtTz or the 1,2-GG intrastrand CL of cisplatin to the HMGB1 domain A (A) and the HMGB1 domain B (B) proteins in a 6% PAA gel. The duplexes were at the concentration of 20 nM. Key: unplatinated duplex (lanes 1–4); the duplex containing the intrastrand CL of cisplatin (lanes 5–8); the duplex containing the monofunctional adduct of *trans*-PtTz (lanes 9–12). Lanes 1, 5, and 9: no protein added. Lanes 2, 6, and 10 in panels A and B: 19 nM HMGB1a and 109 nM HMGB1b added, respectively. Lanes 3, 7, and 11 in panels A and B: 38 nM HMGB1a and 273 nM HMGB1b added, respectively. Lanes 4, 8, and 12 in panels A and B: 72 nM HMGB1a and 546 nM HMGB1b added, respectively.

The interactions of the rat HMGB1 domain A (HMGB1a) and HMGB1 domain B (HMGB1b) with the monofunctional adduct of *trans*-PtTz were investigated. In these experiments, the 20 bp duplex TGT (Figure 1B) was modified so that it contained a single, site-specific monofunctional adduct of *trans*-PtTz at the G residue. For comparative purposes we also prepared the 20 bp duplex TGGT (Figure 1B), which was modified so that it contained a single, site-specific 1,2-GG intrastrand CL of cisplatin. The binding of the HMGB1a and HMGB1b to these DNA probes was detected by retardation of the migration of the radiolabeled 20 bp probes through the gel (21, 33, 34) (Figure 3).

HMGB1a and HMGB1b exhibited negligible binding to the nonmodified 20 bp duplexes. As indicated by the presence of a shifted band whose intensity increases with increasing protein concentration, both HMGB1a and HMGB1b recognize the duplex containing the monofunctional adduct of *trans*-PtTz (Figure 3). Since only a single-shifted band forms following incubation of the TGT duplex containing the monofunctional adduct of *trans*-PtTz with either HMGB1a or HMGB1b, detailed titration studies were possible (only the results of some typical analyses of these detailed titration studies are shown in Figure 3). Evaluations of these titration data afforded $K_{D(\text{app})}$ values reported in Table 1. These titration data indicate that HMGB1a binds the probe containing the monofunctional adduct of *trans*-PtTz with a relatively high affinity, which was similar to that of HMGB1a to the analogous probe but containing the 1,2-GG intrastrand CL of cisplatin.

The titration of the 20 bp duplex containing the monofunctional adduct of *trans*-PtTz with HMGB1b has revealed (Figure 3B) that this protein also binds to the monofunctional adduct of *trans*-PtTz with an affinity similar to that of the probe containing the 1,2-GG intrastrand CL of cisplatin. The affinity of HMGB1b to these platinum lesions was, however, considerably smaller (~50 times) than that of HMGB1a.

One Pt–Cl bond of *trans*-PtTz in its DNA monofunctional adduct remains available for coordination. Hence, a ternary

Table 1: Summary and Comparison of Basic Characteristics of the Monofunctional Adduct of *trans*-PtTz with the 1,2-GG Intrastrand CL of Cisplatin and the Monofunctional Adduct of [PtCl(dien)]Cl^a

	monofunctional adduct of <i>trans</i> -PtTz	1,2-GG intrastrand CL of cisplatin	monofunctional adduct of [PtCl(dien)]Cl
termination of DNA synthesis	yes	yes	no
DNA bending ^b	34°	32–34° ^c	no ^d
DNA unwinding ^b	12°	13° ^c	no ^d
K _{D(app)} (HMGB1a recognition)	38.5 nM	30.8 nM	no ^e
K _{D(app)} (HMGB1b recognition)	2.05 μM	1.85 μM	no ^e
NER by eukaryotic excinuclease	yes	yes	no

^a If not stated otherwise, the data are from this work. ^b Determined by gel electrophoresis. ^c Bellon and Lippard (27), Bellon et al. (69), and Stehlikova et al. (54). ^d Marrot and Leng (55) and Brabec et al. (17). ^e Donahue et al. (64) and Pil and Lippard (65).

DNA–Pt–protein complex could be formed if HMGB1a or HMGB1b is bound to the duplex containing the monofunctional adduct of *trans*-PtTz (Figure 3B). This eventuality was tested in the following way. The 20 bp duplex TGT (Figure 1B) containing the monofunctional adduct of *trans*-PtTz was incubated with HMGB1a or HMGB1b proteins in the same way as in the experiments shown in Figure 3 (for 1 h at 0 °C). The reactions were further incubated at 25 °C for 16 h, then divided in two, and analyzed by native PAA and 5%/10% SDS/PAA gel electrophoresis (not shown). Whereas analysis performed on native gels clearly revealed more slowly migrating bands due to formation of the complex between the platinated duplex and the protein (the results were the same as those shown in Figure 3), no such bands were noticed if the same samples were analyzed on SDS/PAA gel. This result indicates that HMGB1a and HMGB1b proteins were able to bind the 20 bp DNA duplex containing the monofunctional adducts of *trans*-PtTz but were unable to be cross-linked to this platinated DNA.

Nucleotide Excision Repair. NER is a pathway used by human cells for the removal of damaged nucleotides from DNA (35, 36). In mammalian cells, this repair pathway is an important mechanism for the removal of bulky, helix-distorting DNA adducts, such as those generated by various chemotherapeutics including cisplatin (37). Efficient repair of the 1,2-GG intrastrand CL of cisplatin has been reported by various NER systems including human and rodent excinucleases (25, 38–42). The result presented in Figure 4A, lane 8, is consistent with these reports. The major excision fragment contains 28 nucleotides, and other primary excision fragments are 23–27 nucleotides in length, although 22–31 nucleotide long fragments are also observed (43). This range of product sizes reflects variability at both the 3' and 5' incision sites (25, 44); smaller excision products are due to degradation of the primary excision products by exonucleases present in the extracts (25). Importantly, the monofunctional adduct of *trans*-PtTz was also repaired with a similar efficiency by both human and rodent excinucleases (shown in Figure 4A, lane 6, and in Figure 4B for the adduct repaired by rodent excinuclease). We have also examined whether the adduct of [PtCl(dien)]Cl is a substrate for mammalian excinucleases because it has been shown (45) that this monofunctional adduct is even a better substrate

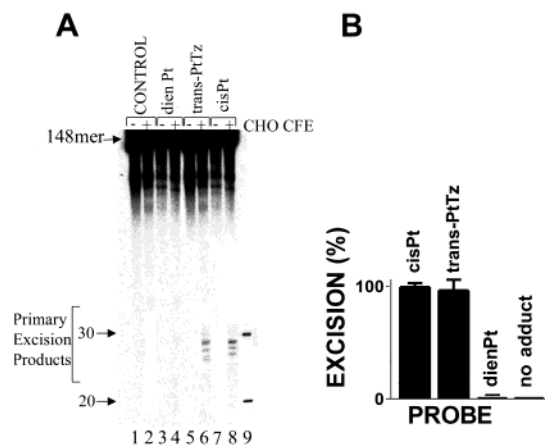


FIGURE 4: Excision of the monofunctional adduct of *trans*-PtTz or [PtCl(dien)]Cl and the 1,2-GG intrastrand CL of cisplatin by rodent excinuclease. (A) The substrates were incubated with CHO AA8 CFE for 40 min at 30 °C and subsequently treated overnight with NaCN prior to analysis in 10% PAA/8 M urea denaturing gel. Lanes: 1 and 2, control, unplatinated substrate; 3 and 4, the substrate containing the monofunctional adduct of [PtCl(dien)]Cl; 5 and 6, the substrate containing the monofunctional adduct of *trans*-PtTz; 7 and 8, the substrate containing the 1,2-GG intrastrand CL of cisplatin; 1, 3, 5, and 7, no extract added; 2, 4, 6, and 8, the substrates were incubated with CHO AA8 CFE for 40 min at 30 °C; all substrates were subsequently treated overnight with NaCN prior to analysis in 10% PAA/8 M urea denaturing gel. Lane 9: 20 and 30 nt markers. (B) Quantitative analysis of removal of the adducts. The columns marked cisPt, dienPt, and trans-PtTz are for the 1,2-d(GpG) intrastrand CL of cisplatin, the monofunctional adduct of [PtCl(dien)]Cl, and *trans*-PtTz, respectively. Data are the average of two independent experiments done under the same conditions; bars indicate range of excision.

than the 1,2-GG intrastrand CL of cisplatin for prokaryotic *E. coli* ABC excinuclease. Consistently with previous reports (46, 47) no excision fragments were noticed if the monofunctional adduct of [PtCl(dien)]Cl was used as a substrate for human and rodent excinucleases (shown in Figure 4A, lane 4, for rodent excinuclease).

Bending, Unwinding, and Chemical Probes of DNA Conformation. Important structural motifs that attract HMG-domain and NER proteins to 1,2-intrastrand CLs of cisplatin are the bending and unwinding of the helix axis (2, 3, 48, 49). For DNA adducts of cisplatin, the structural details responsible for bending and unwinding and subsequent protein recognition have recently been elucidated (33, 50). Given the recent advances in our understanding of the structural basis for the bending of DNA caused by cisplatin CLs, it is of considerable interest to examine how frequent monofunctional adducts of *trans*-PtTz affect conformational properties of DNA such as bending and unwinding. In this work we further performed studies on the bending and unwinding induced by a single, site-specific monofunctional adduct of *trans*-PtTz using electrophoretic retardation as a quantitative measure of the extent of planar curvature. Molecular modeling had previously indicated that such bending might be possible for the trans planar compounds (45).

The oligodeoxyribonucleotide duplexes TGT (16, 20–23) (16 and 20–23 bp long shown in Figure 1E) were used for the bending and unwinding studies of the present work. Experimental details of these studies are given in our recent reports (51–53) and are also described in detail in the

Supporting Information. The DNA unwinding due to one monofunctional adduct of *trans*-PtTz has been found to be $12 \pm 2^\circ$.

Moreover, the monofunctional adduct of *trans*-PtTz bends by about 34° DNA toward the major groove. The bending and local unwinding induced by the monofunctional adduct of *trans*-PtTz are very similar to those afforded by the 1,2-GG interstrand CL of cisplatin using the same experimental procedure [$32\text{--}34^\circ$ and 13° , respectively (27, 54)], but in a distinct contrast to the monofunctional adduct of [PtCl(dien)]Cl which does not bend DNA and unwinds it only negligibly (17, 55). Further studies of the present work were also focused on analysis of the distortion induced by the monofunctional adduct of *trans*-PtTz by chemical probes of DNA conformation using the duplex containing the single, site-specific adduct. The platinated duplex TGT (Figure 1B) was treated with several chemical agents that are used as tools for monitoring the existence of conformations other than canonical B-DNA. These agents include KMnO_4 , DEPC, and bromine. They react preferentially with single-stranded DNA and distorted double-stranded DNA (20, 56). We used for this analysis exactly the same methodology described in detail in our recent papers aimed at DNA adducts of various antitumor platinum drugs (53, 57) so that these experiments are only described in more detail in the Supporting Information. The results indicate that this adduct induces in DNA the distortion that extends over at least 2 bp and is localized mainly at the platinated base pair and that on its 5' side.

DISCUSSION

Binding of *trans*-PtTz to DNA in a monofunctional fashion represents a binding mode previously expected not to result in antitumor activity. This feature of the classical structure–pharmacological activity relationship of platinum(II) compounds was mainly based on the observation that clinically ineffective monofunctional compounds, such as [PtCl(dien)]Cl or [PtCl(NH₃)₃]Cl, do not inhibit replication and transcription. Chemical modification such as the presence of one planar ligand clearly modifies the structures of DNA adducts in such a way that new biological activity is seen. More recently, several platinum(II) compounds have been synthesized that form on DNA stable monofunctional adducts, inhibit replication (and/or transcription), and exhibit antitumor activity. For instance, monofunctional agents *cis*-[Pt(Am)Cl(NH₃)₂]⁺, in which Am is a derivative of pyridine, pyrimidine, purine, or aniline, demonstrate activity against murine and human tumor systems and block DNA replication (58). In addition, a novel monofunctional compound, *cis*-[PtCl(NH₃)₂(N7-ACV)]⁺ (59), which contains in the coordination sphere of cisplatin antiviral acyclovir (ACV), exhibits activity against various herpes viruses and has been also found as effective as cisplatin when equitoxic doses are administered in vivo to P388 leukemia-bearing mice. Also interestingly, the antitumor *trans*-[PtCl₂(*E*-iminoether)₂] complex, which preferentially forms stable monofunctional adducts at guanine residues in DNA (90%) (60), is also endowed with significant antitumor activity (61), and its DNA adducts inhibit replication and transcription (61, 62). In addition, the results of the present work indicate that the monofunctional adducts of antitumor *trans*-PtTz inhibit DNA synthesis in vitro (Figure 2). Thus, the cytotoxicity of some platinum(II) compounds in tumor cells may also arise from

the formation of monofunctional adducts that inhibit replication although the exact details of the mechanism that underlies these antitumor effects remain to be clarified.

The studies described in the present paper were carried out to understand the role of DNA monofunctional adducts of *trans*-PtTz in the antitumor effects of this drug as these adducts represent a significant fraction (30–40%) of all adducts formed by this drug on DNA. There is a large body of experimental evidence indicating that antitumor effects of cisplatin are mediated by cellular proteins that bind specifically to DNA CLs of cisplatin (2, 63) but not to its monofunctional adducts or to DNA adducts of clinically ineffective transplatin or [PtCl(dien)]Cl (64, 65). An example of the cellular proteins, whose interactions with the major adduct of cisplatin (1,2-intrastrand CL) have been studied in detail, is a class of HMG-domain proteins (2, 63). The results of the present work clearly demonstrate that HMGB1 proteins bind to the monofunctional adducts of *trans*-PtTz with the same affinity as to the 1,2-GG intrastrand CL of cisplatin (Figure 3). This observation is unique in the field of DNA interactions of antitumor platinum compounds because this is for the first time when it is shown that HMG-domain proteins bind to monofunctional adducts of platinum(II) compounds or that these proteins bind to the adducts of a *trans*-platinum compound.

The structural motif recognized by HMG-domain proteins on DNA modified by cisplatin is a rigid bend directed toward the major groove (33). It has been shown (17, 55, 66) that the monofunctional adducts of [PtCl(dien)]Cl, which are used as models of the initial (monofunctional) step of the binding of cisplatin or transplatin to DNA (67), do not bend DNA and the character of conformational distortions induced by these adducts is distinctly different from those induced by 1,2-intrastrand CLs of cisplatin (recognized by HMG-domain proteins with a high affinity). It was, therefore, somewhat surprising that the monofunctional adducts of *trans*-PtTz attract and bind to HMGB1 proteins.

A working hypothesis that has been further tested in the present work is that the monofunctional adducts of *trans*-PtTz in contrast to the adducts of [PtCl(dien)]Cl distort DNA conformation in a similar way as 1,2-intrastrand CLs of cisplatin. As summarized in Table 1, this hypothesis has strong experimental support. An intriguing observation is that the monofunctional adduct of *trans*-PtTz bends and unwinds DNA in the same way and extent as the 1,2-intrastrand CL of cisplatin. The reasons why this type of distortion, so far only observed in the case of the bifunctional CLs of platinum compounds, is also induced by the monofunctional platinum adducts may be due to the secondary perturbations of the planar ligand resulting in a bend mimicking the structural distortion produced by the 1,2-intrastrand CL of cisplatin (9). This conclusion is substantiated by the fact that the planar ligand in the *trans*-PtTz complex is *cis* to the binding site, affording a situation that allows the planar ligand to interact or stack with DNA (68). Details of the mechanisms underlying antitumor activity of cisplatin or resistance to this drug have been already proposed (3, 50). One hypothesis is based on the fact that a number of proteins that exhibit an enhanced affinity to DNA modified by cisplatin, such as transcription factors, have key roles in the cells. Cisplatin–DNA adducts may hijack these proteins away from their normal binding sites, thereby disrupting fundamental cellular processes. As

the monofunctional adducts of *trans*-PtTz attract the cellular proteins with a similar efficiency as the major adduct of cisplatin, it is reasonable to suggest that this hijacking mechanism of antitumor activity is also effective in the case of antitumor analogues of transplatin containing the planar ligand.

Adducts formed by cisplatin distort DNA conformation, inhibit replication and transcription, but are also bypassed by DNA or RNA polymerases (3, 70). Another hypothesis of the mechanism that underlies antitumor effects of cisplatin is associated with the observation that cisplatin intrastrand CLs are removed from DNA mainly by NER. They are, however, also recognized by a number of proteins (2, 3) which could block DNA adducts of cisplatin from damage recognition needed for repair. These adducts may thus persist, which would potentiate their cytotoxicity. Consistent with this hypothesis is the fact that the adducts of clinically ineffective transplatin are more efficiently repaired than those of cisplatin (71). Hence, this shielding mechanism might be also applicable for the mechanism of antitumor activity of *trans*-PtTz since the monofunctional adducts of this drug are removed by NER (Figure 4).

The observation that monofunctional adducts of *trans*-PtTz are removed by eukaryotic NER systems (Figure 4) deserves further discussion. The NER of monofunctional adducts of platinum compounds, such as those of [PtCl(dien)]Cl, has been already examined. Whereas the monofunctional adducts of [PtCl(dien)]Cl are removed by prokaryotic ABC excinuclease more efficiently than 1,2-intrastrand CLs of cisplatin (45), the opposite is observed, as shown in the present work, in the case of the NER by eukaryotic excinucleases (Figure 4). The monofunctional adduct of [PtCl(dien)]Cl is only excised negligibly whereas the 1,2-GG intrastrand CL of cisplatin is excised considerably more readily. This observation is consistent with the view that monofunctional lesions induced in DNA of eukaryotic cells treated with platinum compounds are tolerated by a mechanism much more effective in eukaryotic cells. However, the monofunctional adducts of *trans*-PtTz are removed from DNA by eukaryotic excinuclease considerably more efficiently than the adducts of [PtCl(dien)]Cl and it is particularly interesting that with almost identical efficiency as the 1,2-intrastrand CLs of cisplatin (Figure 4). Thus, it is necessary for a role of the monofunctional adducts of *trans*-PtTz in the mechanism of antitumor activity of this drug that the repair of these adducts is inhibited so that they will persist and inhibit replication (transcription) or trigger apoptosis. In the case of the major adducts of cisplatin, their repair is inhibited by shielding these CLs by cellular proteins, such as HMG-domain proteins. As the monofunctional adducts of *trans*-PtTz are also specifically recognized and bound to cellular proteins, such as HMG-domain proteins (Figure 3), they could be also protected from repair in the same way as 1,2-intrastrand CLs of cisplatin, which would potentiate antitumor effects of *trans*-PtTz.

The affinity of cellular proteins, such as HMG-domain proteins, to the monofunctional adducts of *trans*-PtTz (Figure 3) may have another consequences for their role in the mechanism of antitumor effects of this drug. The clinical ineffectivity of transplatin is also related to a relatively slow rate of the conversion of its monofunctional adducts into the interstrand CLs. It has been suggested that long-lived

monofunctional adducts of transplatin may be trapped by sulfur-containing compounds (for instance, by glutathione), which may be a process leading to the inhibition of the biological effects of transplatin (10, 72). The monofunctional adducts of *trans*-PtTz also persist, but in contrast to the adducts of transplatin they are shielded by cellular proteins, which may protect them also from trapping by sulfur-containing compounds. In addition, it has been shown (73, 74) that binding of HMG-domain proteins to the major 1,2-GG intrastrand CL of cisplatin markedly reduces translesion synthesis by DNA polymerases across this adduct, which also may potentiate its cytostatic effects in the tumors sensitive to this drug. As HMG-domain proteins also bind to the monofunctional adducts of *trans*-PtTz with a similar affinity as to 1,2-intrastrand CLs of cisplatin (Figure 3), it is possible to expect that translesion synthesis by DNA polymerases will be also reduced across the monofunctional adduct of *trans*-PtTz, which may also contribute to the importance of this adduct for its antitumor effects.

The cytotoxic effects of *trans*-PtTz may most likely be due to a cumulative effect of the structurally heterogeneous adducts (bifunctional intrastrand and interstrand adducts as well as the monofunctional adducts discussed in the present work) produced by this drug, but the role of monofunctional adducts in the antitumor effects of *trans*-PtTz could be significant. This work demonstrates that transplatin analogues containing a planar amine ligand are unique from a mechanistic point of view and, therefore, worthy of further studies. These studies should reveal all details of the mechanism underlying antitumor effects of this new class of platinum anticancer drugs that would allow reevaluating the structure—pharmacological relationships of platinum compounds needed for the search and design of new, more effective platinum anticancer drugs. In conclusion, the results of the present work further support the view that the simple chemical modification of the structure of an inactive platinum compound alters its DNA binding mode into that of an active drug and that processing of the monofunctional DNA adducts of these *trans*-platinum analogues in tumor cells may be similar to that of the major bifunctional adducts of classical cisplatin.

ACKNOWLEDGMENT

The authors acknowledge that their participation in the EC COST Chemistry Actions D20 and D21 enabled them to exchange regularly the most recent ideas in the field of platinum anticancer drugs with several European colleagues.

SUPPORTING INFORMATION AVAILABLE

Results describing in detail DNA bending, unwinding, and conformational distortion by chemical probes as a consequence of the formation of the monofunctional adduct of *trans*-PtTz. This material is available free of charge via the Internet at <http://pubs.acs.org>.

REFERENCES

1. Johnson, N. P., Butour, J.-L., Villani, G., Wimmer, F. L., Defais, M., Pierson, V., and Brabec, V. (1989) *Prog. Clin. Biochem. Med.* 10, 1–24.
2. Jamieson, E. R., and Lippard, S. J. (1999) *Chem. Rev.* 99, 2467–2498.

3. Brabec, V. (2002) in *Progress in Nucleic Acid Research and Molecular Biology* (Moldave, K., Ed.) pp 1–68, Academic Press, San Diego, CA.
4. Farrell, N. (2000) in *Platinum-based drugs in cancer therapy* (Kelland, L. R., and Farrell, N. P., Eds.) pp 321–338, Humana Press, Totowa, NJ.
5. Farrell, N. (1996) in *Metal ions in biological systems* (Sigel, A., and Sigel, H., Eds.) pp 603–639, Marcel Dekker, New York, Basel, and Hong Kong.
6. Natile, G., and Coluccia, M. (1999) in *Metallopharmaceuticals* (Clarke, M. J., and Sadler, P. J., Eds.) pp 73–98, Springer, Berlin.
7. Perez, J. M., Fuertes, M. A., Alonso, C., and Navarro-Ranninger, C. (2000) *Crit. Rev. Oncol. Hematol.* 35, 109–120.
8. Farrell, N., Kelland, L. R., Roberts, J. D., and Van Beusichem, M. (1992) *Cancer Res.* 52, 5065–5072.
9. Zakovska, A., Novakova, O., Balcarova, Z., Bierbach, U., Farrell, N., and Brabec, V. (1998) *Eur. J. Biochem.* 254, 547–557.
10. Eastman, A., and Barry, M. A. (1987) *Biochemistry* 26, 3303–3307.
11. Brabec, V., Nepelchova, K., Kasparkova, J., and Farrell, N. (2000) *J. Biol. Inorg. Chem.* 5, 364–368.
12. Brabec, V., and Leng, M. (1993) *Proc. Natl. Acad. Sci. U.S.A.* 90, 5345–5349.
13. Brabec, V. (2000) in *Platinum-based drugs in cancer therapy* (Kelland, L. R., and Farrell, N. P., Eds.) pp 37–61, Humana Press, Totowa, NJ.
14. Bierbach, U., Qu, Y., Hambley, T. W., Peroutka, J., Nguyen, H. L., Doedee, M., and Farrel, N. (1999) *Inorg. Chem.* 38, 3535–3542.
15. Brabec, V., Kleinwächter, V., Butour, J. L., and Johnson, N. P. (1990) *Biophys. Chem.* 35, 129–141.
16. Van Beusichem, M., and Farrell, N. (1992) *Inorg. Chem.* 31, 634–639.
17. Brabec, V., Reedijk, J., and Leng, M. (1992) *Biochemistry* 31, 12397–12402.
18. Stros, M. (1998) *J. Biol. Chem.* 273, 10355–10361.
19. Stros, M. (2001) *Biochemistry* 40, 4769–4779.
20. Brabec, V., Sip, M., and Leng, M. (1993) *Biochemistry* 32, 11676–11681.
21. He, Q., Ohndorf, U.-A., and Lippard, S. J. (2000) *Biochemistry* 39, 14426–14435.
22. Matsunaga, T., Mu, D., Park, C.-H., Reardon, J. T., and Sancar, A. (1995) *J. Biol. Chem.* 270, 20862–20869.
23. Buschta-Hedayat, N., Buterin, T., Hess, M. T., Missura, M., and Naegeli, H. (1999) *Proc. Natl. Acad. Sci. U.S.A.* 96, 6090–6095.
24. Manley, J. L., Fire, A., Cano, A., Sharp, P. A., and Gefter, M. L. (1980) *Proc. Natl. Acad. Sci. U.S.A.* 77, 3855–3859.
25. Reardon, J. T., Vaisman, A., Chaney, S. G., and Sancar, A. (1999) *Cancer Res.* 59, 3968–3971.
26. Koo, H. S., Wu, H. M., and Crothers, D. M. (1986) *Nature* 320, 501–506.
27. Bellon, S. F., and Lippard, S. J. (1990) *Biophys. Chem.* 35, 179–188.
28. Kasparkova, J., Novakova, O., Vrana, O., Farrell, N., and Brabec, V. (1999) *Biochemistry* 38, 10997–11005.
29. Balcarova, Z., Kasparkova, J., Zakovska, A., Novakova, O., Sivo, M. F., Natile, G., and Brabec, V. (1998) *Mol. Pharmacol.* 53, 846–855.
30. Jordan, P., and Carmo-Fonseca, M. (2000) *Cell. Mol. Life Sci.* 57, 1229–1235.
31. Suo, Z., Lippard, S., and Johnson, K. (1999) *Biochemistry* 38, 715–726.
32. Comess, K. M., Burstyn, J. N., Essigmann, J. M., and Lippard, S. J. (1992) *Biochemistry* 31, 3975–3990.
33. Ohndorf, U. M., Rould, M. A., He, Q., Pabo, C. O., and Lippard, S. J. (1999) *Nature* 399, 708–712.
34. Cohen, S. M., Mikata, Y., He, Q., and Lippard, S. J. (2000) *Biochemistry* 39, 11771–11776.
35. Sancar, A. (1996) *Annu. Rev. Biochem.* 65, 43–81.
36. Wood, R. D. (1996) *Annu. Rev. Biochem.* 65, 135–167.
37. Reardon, J. T., and Sancar, A. (1998) in *Advances in DNA damage and repair* (Dizdaroğlu, M., and Karakaya, A., Eds.) pp 377–393, Plenum Publishing Corp., New York.
38. Jones, S. L., Hickson, I. D., Harris, A. L., and Harnett, P. R. (1994) *Int. J. Cancer* 59, 388–393.
39. Zamble, D. B., Mu, D., Reardon, J. T., Sancar, A., and Lippard, S. J. (1996) *Biochemistry* 35, 10004–10013.
40. Moggs, J. G., Szymkowski, D. E., Yamada, M., Karran, P., and Wood, R. D. (1997) *Nucleic Acids Res.* 25, 480–490.
41. Koberle, B., Masters, J. R. W., Hartley, J. A., and Wood, R. D. (1999) *Curr. Biol.* 9, 273–276.
42. Li, M. J., and Yang, L. Y. (1999) *Int. J. Oncol.* 15, 1177–1183.
43. Malina, J., Kasparkova, J., Natile, G., and Brabec, V. (2002) *Chem. Biol.* 9, 629–638.
44. Huang, J.-C., Svoboda, D. L., Reardon, J. T., and Sancar, A. (1992) *Proc. Natl. Acad. Sci. U.S.A.* 89, 3664–3668.
45. Page, J. D., Husain, I., Sancar, A., and Chaney, S. G. (1990) *Biochemistry* 29, 1016–1024.
46. Calsou, P., Frit, P., and Salles, B. (1992) *Nucleic Acids Res.* 20, 6363–6368.
47. Buterin, T., Hess, M. T., Gunz, D., Geacintov, N. E., Mullenders, L. H., and Naegeli, H. (2002) *Cancer Res.* 62, 4229–4235.
48. Missura, M., Buterin, T., Hindges, R., Hubscher, U., Kasparkova, J., Brabec, V., and Naegeli, H. (2001) *EMBO J.* 20, 3554–3564.
49. Patrick, S. M., and Turchi, J. J. (2002) *J. Biol. Chem.* 277, 16096–16101.
50. Zamble, D. B., and Lippard, S. J. (1999) in *Cisplatin. Chemistry and biochemistry of a leading anticancer drug* (Lippert, B., Ed.) pp 73–110, VCH, Wiley–VCH, Zürich and Weinheim.
51. Kasparkova, J., Mellish, K. J., Qu, Y., Brabec, V., and Farrell, N. (1996) *Biochemistry* 35, 16705–16713.
52. Kasparkova, J., Farrell, N., and Brabec, V. (2000) *J. Biol. Chem.* 275, 15789–15798.
53. Zehnulova, J., Kasparkova, J., Farrell, N., and Brabec, V. (2001) *J. Biol. Chem.* 276, 22191–22199.
54. Stehlikova, K., Kostrhunova, H., Kasparkova, J., and Brabec, V. (2002) *Nucleic Acids Res.* 30, 2894–2898.
55. Marrot, L., and Leng, M. (1989) *Biochemistry* 28, 1454–1461.
56. Nielsen, P. E. (1990) *J. Mol. Recognit.* 3, 1–24.
57. Malina, J., Hofr, C., Maresca, L., Natile, G., and Brabec, V. (2000) *Biophys. J.* 78, 2008–2021.
58. Hollis, L. S., Sundquist, W. I., Burstyn, J. N., Heiger-Bernays, W. J., Bellon, S. F., Ahmed, K. J., Amundsen, A. R., Stern, E. W., and Lippard, S. J. (1991) *Cancer Res.* 51, 1866–1875.
59. Coluccia, M., Boccarelli, A., Cermelli, C., Portolani, M., and Natile, G. (1995) *Met.-Based Drugs* 2, 249–256.
60. Brabec, V., Vrana, O., Novakova, O., Kleinwachter, V., Intini, F. P., Coluccia, M., and Natile, G. (1996) *Nucleic Acids Res.* 24, 336–341.
61. Coluccia, M., Nassii, F., Loseto, F., Boccarelli, A., Marigió, M. A., Giordano, D., Intini, F. P., Caputo, P., and Natile, G. (1993) *J. Med. Chem.* 36, 510–512.
62. Zaludova, R., Zakovska, A., Kasparkova, J., Balcarova, Z., Vrana, O., Coluccia, M., Natile, G., and Brabec, V. (1997) *Mol. Pharmacol.* 52, 354–361.
63. Brabec, V., and Kasparkova, J. (2002) *Drug Resist. Updates* 5, 147–161.
64. Donahue, B. A., Augot, M., Bellon, S. F., Treiber, D. K., Toney, J. H., Lippard, S. J., and Essigmann, J. M. (1990) *Biochemistry* 29, 5872–5880.
65. Pil, P. M., and Lippard, S. J. (1992) *Science* 256, 234–237.
66. Brabec, V., Boudny, V., and Balcarova, Z. (1994) *Biochemistry* 33, 1316–1322.
67. Brabec, V., Vrána, O., Platonova, G. A., Kogan, E. M., and Sidorova, N. S. (1991) *Chem.-Biol. Interact.* 78, 1–12.
68. Keck, M. V., and Lippard, S. J. (1992) *J. Am. Chem. Soc.* 114, 3386–3390.
69. Bellon, S. F., Coleman, J. H., and Lippard, S. J. (1991) *Biochemistry* 30, 8026–8035.
70. Chaney, S. G., and Vaisman, A. (2000) in *Platinum-based drugs in cancer therapy* (Kelland, L. R., and Farrell, N. P., Eds.) pp 129–148, Humana Press, Totowa, NJ.
71. Ciccarelli, R. B., Solomon, M. J., Varshavsky, A., and Lippard, S. J. (1985) *Biochemistry* 24, 7533–7540.
72. Bancroft, D. P., Lepre, C. A., and Lippard, S. J. (1990) *J. Am. Chem. Soc.* 112, 6860–6871.
73. Hoffmann, J.-S., Locker, D., Villani, G., and Leng, M. (1997) *J. Mol. Biol.* 270, 539–543.
74. Vaisman, A., Lim, S. E., Patrick, S. M., Copeland, W. C., Hinkle, D. C., Turchi, J. J., and Chaney, S. G. (1999) *Biochemistry* 38, 11026–11039.

23.

Jaroslav Malina · Olga Novakova
Bernhard K. Keppler · Enzo Alessio · Viktor Brabec

Biophysical analysis of natural, double-helical DNA modified by anticancer heterocyclic complexes of ruthenium(III) in cell-free media

Received: 13 September 2000 / Accepted: 18 January 2001 / Published online: 28 March 2001

© SBIC 2001

Abstract Modifications of natural DNA by three anticancer heterocyclic ruthenium(III) compounds were studied by methods of molecular biophysics. These methods included DNA binding studies using atomic absorption spectrophotometry, inhibition of restriction endonucleases, mapping of DNA adducts by transcription assay, interstrand cross-linking employing gel electrophoresis under denaturing conditions, DNA unwinding studied by gel electrophoresis, circular dichroism analysis of the B→Z transition in DNA, and DNA melting curves measured by absorption spectrophotometry. The results indicate that the complexes $\text{HIm}[\text{trans-Cl}_4\text{Im}_2\text{Ru}^{\text{III}}]$, $\text{HInd}[\text{trans-Cl}_4\text{Ind}_2\text{Ru}^{\text{III}}]$, and $\text{Na}[\text{trans-Cl}_4\text{Im}(\text{Me}_2\text{SO})\text{Ru}^{\text{III}}]$ (Im and Ind stand for imidazole and indazole, respectively) coordinate irreversibly to DNA. Their DNA binding mode is, however, different from that of cisplatin. Interestingly, $\text{Na}[\text{trans-Cl}_4\text{Im}(\text{Me}_2\text{SO})\text{Ru}^{\text{III}}]$ binds to DNA considerably faster than the other two ruthenium compounds and cisplatin. In addition, when $\text{Na}[\text{trans-Cl}_4\text{Im}(\text{Me}_2\text{SO})\text{Ru}^{\text{III}}]$ binds to DNA it exhibits an enhanced base sequence specificity in comparison with the other two ruthenium complexes. $\text{Na}[\text{trans-Cl}_4\text{Im}(\text{Me}_2\text{SO})\text{Ru}^{\text{III}}]$ also forms bifunctional intrastand adducts on double-helical DNA which are capable of terminating RNA synthesis in vitro, while the

capability of the other two ruthenium compounds to form such adducts is markedly lower. This observation has been interpreted to mean that the bifunctional adducts of $\text{HInd}[\text{trans-Cl}_4\text{Ind}_2\text{Ru}^{\text{III}}]$ and $\text{Na}[\text{trans-Cl}_4\text{Im}_2\text{Ru}^{\text{III}}]$ formed on rigid double-helical DNA are sterically more crowded by their octahedral geometry than those of $\text{Na}[\text{trans-Cl}_4\text{Im}(\text{Me}_2\text{SO})\text{Ru}^{\text{III}}]$. In addition, the adducts of all three ruthenium compounds affect the conformation of DNA, $\text{Na}[\text{trans-Cl}_4\text{Im}(\text{Me}_2\text{SO})\text{Ru}^{\text{III}}]$ being most effective. It has been suggested that the altered DNA binding mode of ruthenium compounds in comparison with cisplatin might be an important factor responsible for the altered cytostatic activity of this class of ruthenium compounds in tumor cells.

Keywords DNA · Ruthenium · Cisplatin · Cross link · Anticancer drug

Abbreviations CT: calf thymus · EtBr: ethidium bromide · FAAS: flameless atomic absorption spectrophotometry · Im: imidazole · Ind: indazole

Introduction

cis-Diamminedichloroplatinum(II) (cisplatin) is one of the most widely utilized antitumor drugs in the world [1, 2]. It is highly effective in treating a number of cancers, mainly testicular and ovarian cancers, but its applicability is still limited to a relatively narrow range of tumors [3]. Some tumors have natural resistance to cisplatin, while others develop resistance after the initial treatment. Cisplatin also has limited solubility in aqueous solution and is administered intravenously, another inconvenience to outpatient treatment. These drawbacks, coupled with cisplatin toxicity, have been the impetus for the development of an improved metal-based drug. Therefore, the search continues for an improved metal-based antitumor agent, motivated by

J. Malina · O. Novakova · V. Brabec (✉)
Institute of Biophysics,
Academy of Sciences of the Czech Republic,
Kralovopolska 135, 61265 Brno, Czech Republic
E-mail: brabec@ibp.cz
Fax: +420-5-41240499

B.K. Keppler
Institute of Inorganic Chemistry, University of Vienna,
Währingerstrasse 42, 1090 Vienna, Austria

E. Alessio
Dipartimento di Scienze Chimiche, Università di Trieste,
Via L. Giorgieri 1, 34127 Trieste, Italy

the desire to design a less toxic compound that is non-cross-resistant with cisplatin and its direct analogues.

In the years following the introduction of cisplatin, the design of new platinum antitumor drugs concentrated mainly on direct cisplatin analogues, which adhered to the set of structure-activity relationships established already in 1973 [4, 5]. More recently, there have been efforts to rationally design unconventional platinum complexes that violate these original structure-activity relationships, such as transplatinum compounds and polynuclear platinum complexes [6, 7]. There have also been efforts directed at the design of other transition-metal antitumor agents. Possible advantages in using transition-metal ions other than platinum may involve additional coordination sites, alterations in ligand affinity and substitution kinetics, changes in oxidation state, and photodynamic approaches to therapy. In the design of these new drugs, ruthenium complexes have raised great interest [8, 9, 10, 11].

Heterocyclic complexes of Ru^{III} constitute a relatively new group of anticancer compounds [9, 11]. The general formula of this class of compounds is $\text{HB}[\text{trans-B}_2\text{Cl}_4\text{Ru}^{\text{III}}]$, where B stands for a heterocyclic base, such as imidazole (Im) or indazole (Ind) (Fig. 1). These complexes exhibit activity in various tumor models and are particularly effective against cisplatin-resistant colorectal tumors [9]. Later an analogue of these complexes was developed, namely $\text{Na}[\text{trans-Cl}_4\text{Im}(\text{Me}_2\text{SO})\text{Ru}^{\text{III}}]$ (Fig. 1), which exhibits encouraging antitumor and antimetastatic properties [11, 12, 13]. Thus, the spectrum of the antitumor effects of these ruthenium compounds differs significantly from that of cisplatin, while showing lower systemic toxicity than platinum(II) compounds [14].

Broadening the chemotherapeutical arsenal depends on understanding existing agents with a view toward developing new modes of attack. Interestingly, a direct correlation between cytotoxicity and DNA binding has been observed for $\text{HB}[\text{trans-B}_2\text{Cl}_4\text{Ru}^{\text{III}}]$ compounds in cell cultures [10, 15]. Also consistent with DNA binding in vivo, these ruthenium compounds inhibit DNA replication, exhibit mutagenic activity, induce the SOS repair mechanism, bind to nuclear DNA, and reduce RNA synthesis [10]. Similarly, $\text{Na}[\text{trans-Cl}_4\text{Im}(\text{Me}_2\text{SO})\text{Ru}^{\text{III}}]$ has been also shown [16, 17, 18] to bind DNA and inhibit DNA replication in vitro, but the pharmacological target for $\text{Na}[\text{trans-Cl}_4\text{Im}(\text{Me}_2\text{SO})\text{Ru}^{\text{III}}]$ and the mechanism underlying its biological effects are not known.

$\text{HB}[\text{trans-B}_2\text{Cl}_4\text{Ru}^{\text{III}}]$ and $\text{Na}[\text{trans-Cl}_4\text{Im}(\text{Me}_2\text{SO})\text{Ru}^{\text{III}}]$ are pseudooctahedral with four equatorial chloride ligands and the heterocyclic bases and Me_2SO as axial ligands. The complexes lose their chloride ligands and transform into the corresponding, more reactive, aquated species [9, 10, 19, 20]. In order to address further fundamental questions about DNA binding modes of ruthenium antitumor compounds containing the heterocyclic base as axial ligands, the

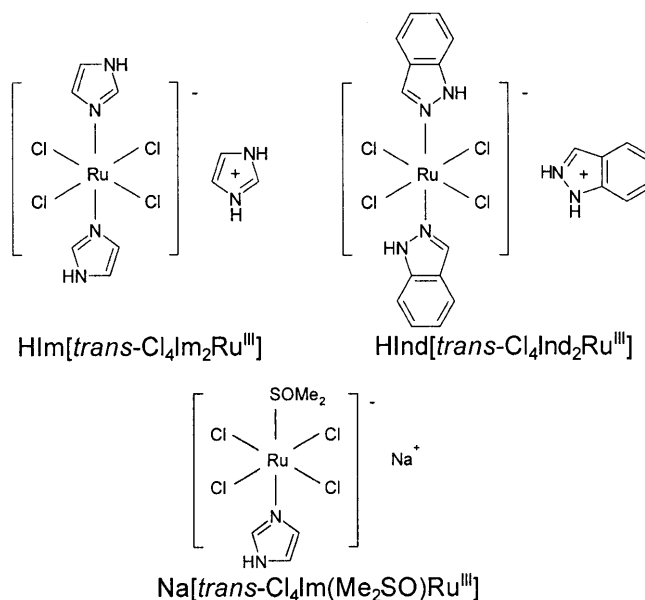


Fig. 1 Structures and abbreviations of the ruthenium compounds used in the present work

experiments described in the present paper were carried out. More specifically, the interactions of polymeric natural DNAs with $\text{HIm}[\text{trans-Cl}_4\text{Im}_2\text{Ru}^{\text{III}}]$, $\text{HInd}[\text{trans-Cl}_4\text{Ind}_2\text{Ru}^{\text{III}}]$, and $\text{Na}[\text{trans-Cl}_4\text{Im}(\text{Me}_2\text{SO})\text{Ru}^{\text{III}}]$ in cell-free media were investigated by various methods of molecular biophysics, with the goal to contribute to understanding their biological effects and to help establish the structure-pharmacological relationship of this class of ruthenium anticancer compounds.

Material and methods

Starting materials

$\text{HIm}[\text{trans-Cl}_4\text{Im}_2\text{Ru}^{\text{III}}]$, $\text{HInd}[\text{trans-Cl}_4\text{Ind}_2\text{Ru}^{\text{III}}]$, and $\text{Na}[\text{trans-Cl}_4\text{Im}(\text{Me}_2\text{SO})\text{Ru}^{\text{III}}]$ (Fig. 1) were synthesized, recrystallized, and characterized as previously reported [21, 22]. Cisplatin and *trans*-diamminedichloroplatinum(II) (*trans*platin) were from Sigma. The stock solutions of the ruthenium and platinum complexes ($5 \times 10^{-4} \text{ M}$ in 10 mM NaClO_4) were prepared in the dark at 25°C and only used after at least 5 days after dissolving the complex. Calf thymus (CT) DNA (42% G+C, mean molecular mass ca. 20,000 kD) was also prepared and characterized as described previously [23, 24]. Plasmids pSP73 [2464 base pairs (bp)] and pUC19 (2686 bp) were isolated according to standard procedures and banded twice in CsCl/ethidium bromide (EtBr) equilibrium density gradients. The synthetic double-helical alternating polydeoxyribonucleotide poly(dG-m⁵dC) was purchased from Boehringer-Mannheim Biochemica [all references in the text to poly(dG-m⁵dC) refer to duplex molecules and its concentrations are related to its phosphorus content]. Restriction endonucleases were purchased from New England Biolabs. The Klenow fragment of DNA polymerase I was from Boehringer-Mannheim Biochemica. The Riboprobe Gemini System II for transcription mapping containing T7 RNA polymerase was purchased from Promega. EtBr and agarose were from Merck. The radioactive products were from Amersham.

Metallation reactions

CT or plasmid DNAs were incubated with the ruthenium or platinum complex in 10 mM NaClO₄ at 37 °C in the dark, if not stated otherwise. After 48 h, the samples of plasmid DNA were precipitated by ethanol and redissolved in the medium required for subsequent biochemical or biophysical analysis, whereas the samples of CT DNA were exhaustively dialyzed against such a medium. An aliquot of these samples was used to determine the value of r_b (r_b is defined as the number of molecules of the ruthenium compound coordinated per nucleotide residue) by flameless atomic absorption spectrophotometry (FAAS).

The dependencies of the r_b values on time for the ruthenium complexes tested in the present work were also obtained in the following way. Solutions of CT DNA at the concentration of 0.32 mg/mL were incubated with the ruthenium complex at an r_i value of 0.01 or 0.1 (r_i is defined as the molar ratio of free ruthenium complex to nucleotide phosphates at the onset of incubation with DNA). At various time intervals, aliquots were withdrawn and reaction was stopped by adding 1/10 of volume of 1.5 M NaCl including quick cooling to -20 °C. DNA was then precipitated by ethanol. The amount of the free ruthenium complexes (not bound to DNA) in the supernatant was determined by FAAS. The results of these analyses were identical to those when we employed the method described in the preceding paragraph.

Assay based on restriction-enzyme cleavage of ruthenated plasmid DNA

pSP73 DNA was first linearized by the *SspI* or *EcoRI* endonucleases. After these cleavage reactions the restriction enzymes were removed by phenol/chloroform extraction. The linearized fragments were modified by the ruthenium complexes to various r_b values (vide supra). Subsequent digestions were performed after ethanol precipitation by incubating the unmodified or ruthenated primary digests of pSP73 DNA with *BamHI* or *EcoRI* (in the case of the primary cleavage by *SspI*) or by *SspI* (in the case of the primary cleavage by *EcoRI*). The amount of the enzyme used in the secondary digestions (performed in the media recommended and supplied by the manufacturer) was that necessary to cut 1 µg of linearized DNA in 1 h at 37 °C. The resulting DNA fragments were subjected to electrophoresis in agarose (1% gel) in TAE buffer (0.04 M Tris-acetate+1 mM EDTA, pH 7.0) at 25 °C with a potential drop of 0.8 V/cm. The gel was stained with EtBr and samples visualized and photographed under UV light. The intensities of the bands were quantified by means of a Molecular Dynamics Phosphor Imager (Storm 860 system with ImageQuant software). Importantly, pSP73 DNA only contains one cleavage site of *BamHI*, *EcoRI*, or *SspI* at the positions 45, 24, and 2014, respectively (these numbers correspond to the nucleotide numbering in the sequence map of pSP73 plasmid).

DNA transcription by RNA polymerase in vitro

Transcription of the (*NdeI/HpaI*) restriction fragment of pSP73 DNA with DNA-dependent T7 RNA polymerase and electrophoretic analysis of transcripts were performed according to the protocols recommended by Promega (Promega protocols and applications 43–46 (1989/90) and previously described in detail [25, 26]).

Interstrand cross-link assay

If not stated otherwise, HIm[*trans*-Cl₄Im₂Ru^{III}], HInd[*trans*-Cl₄Ind₂Ru^{III}], or Na[*trans*-Cl₄Im(Me₂SO)Ru^{III}] at varying concentrations were incubated with 2 µg of pSP73 DNA after it had been linearized by *EcoRI*. The ruthenated samples were precipi-

tated by ethanol and analyzed for DNA interstrand cross-links in the same way as described in several recent papers [26, 27]. The linear duplexes were first 3'-end labeled by means of the Klenow fragment of DNA polymerase I and [α -³²P]dATP. The samples were deproteinized by phenol, precipitated by ethanol, and the pellet was dissolved in 18 µL of 30 mM NaOH with 1 mM EDTA, 6.6% sucrose, and 0.04% bromophenol blue. The amount of interstrand cross-links was analyzed by electrophoresis under denaturing conditions on alkaline agarose gel (1%). After the electrophoresis was completed, the intensities of the bands corresponding to single strands of DNA and interstrand cross-linked duplex were quantified by means of a Molecular Dynamics Phosphor Imager (Storm 860 system with ImageQuant software). The frequency of interstrand cross-links, F (the number of interstrand cross-links per adduct), was calculated as $F = XL/4928 \times r_b$ (pSP73 plasmid contained 4928 nucleotide residues). XL is the number of interstrand cross-links per one molecule of the linearized DNA duplex, which was calculated assuming Poisson distribution of the interstrand cross-links as $XL = -\ln A$, where A is the fraction of molecules running as a band corresponding to the non-cross-linked DNA [27].

Unwinding of negatively supercoiled DNA

Unwinding of closed circular supercoiled pUC19 plasmid DNA was assayed by an agarose gel mobility shift assay [28]. The unwinding angle F induced per ruthenium-DNA adduct was calculated upon the determination of the r_b value at which the complete transformation of the supercoiled to relaxed form of the plasmid was attained. Samples of pUC19 plasmid were incubated with HIm[*trans*-Cl₄Im₂Ru^{III}], HInd[*trans*-Cl₄Ind₂Ru^{III}] or Na[*trans*-Cl₄Im(Me₂SO)Ru^{III}] for 48 h, precipitated by ethanol and redissolved in TAE buffer. An aliquot of the precipitated sample was subjected to electrophoresis on 1% agarose gels running at 25 °C in the dark with TAE buffer with a voltage set at 30 V. The gels were then stained with EtBr, followed by photography on Polaroid 667 film with transilluminator. The other aliquot was used for the determination of r_b values by FAAS.

DNA melting

The melting curves of CT DNAs were recorded by measuring the absorbance at 260 nm. If not stated otherwise, the melting curves were recorded in media containing various concentrations of NaClO₄ (the melting curves of unmodified or ruthenated DNA were recorded after they were transferred into media of pH 7.4 containing 0.01–0.2 M NaClO₄ and 1 mM Tris-HCl/0.1 mM EDTA). The value of the melting temperature (t_m) was determined as the temperature corresponding to a maximum on the first-derivation profile of the melting curves. The t_m values could be thus determined with an accuracy of ± 0.3 °C.

Other methods

Absorption spectra were measured with a Beckmann DU-7400 spectrophotometer. FAAS measurements were carried out on a Unicam 939 AA spectrometer with a graphite furnace. For FAAS analysis, DNA was precipitated with ethanol and dissolved in 0.1 M HCl. Circular dichroism (CD) spectra were recorded at 25 °C using a JASCO spectropolarimeter, model J720.

Results and discussion

DNA binding

Solutions of CT DNA at a concentration of 0.32 mg/mL were incubated with the ruthenium compounds at the r_i value of 0.1 in 10 mM NaClO₄ at 37 °C. At various time intervals an aliquot of the reaction mixture was withdrawn and assayed by FAAS for ruthenium not bound to DNA. The amount of ruthenium bound to DNA (r_b) was calculated by subtracting the amount of free (unbound) ruthenium from the total amount of ruthenium present in the reaction. No changes in the pH of the reaction mixture containing DNA and ruthenium compound were measured within 48 h after mixing DNA with the ruthenium complex. The amount of ruthenium coordinated to DNA increased with time and after approximately 24 h the complex was quantitatively bound (Fig. 2). The half-times ($t_{1/2}$) of these binding reactions were ~6, 10, and 1 h for HIm[*trans*-Cl₄Im₂Ru^{III}], HInd[*trans*-Cl₄Ind₂Ru^{III}], and Na[*trans*-Cl₄Im(Me₂SO)Ru^{III}], respectively. The binding of Na[*trans*-Cl₄Im(Me₂SO)Ru^{III}] is considerably faster than that of cisplatin under similar conditions, whereas the binding of the other two ruthenium compounds is noticeably slower than that of cisplatin. In a further experiment, CT DNA was incubated with the ruthenium compounds at $r_i=0.01$ and essentially the same rates of binding were observed as at $r_i=0.1$.

The binding studies described above were performed in the medium 10 mM NaClO₄, which is used as a standard medium if DNA interactions of antitumor platinum complexes are investigated in cell-free media. For comparative purposes, the binding to DNA of the three ruthenium compounds tested in the present work was also investigated in the buffer containing 10 mM Tris-HCl with 1 mM EDTA at pH 7.4 (TE buffer), i.e. in the medium used in some previous studies of DNA modifications by ruthenium complexes. The components of this buffer are potential ligands of transition metal complexes which compete with DNA for metal [29]. This fact can significantly affect the rate of the binding of ruthenium complexes to DNA. DNA binding of the ruthenium compounds measured after 24 h in TE buffer was decreased by ca. 30% in the case of the binding of HIm[*trans*-Cl₄Im₂Ru^{III}] or HInd[*trans*-Cl₄Ind₂Ru^{III}] and even by ca. 40% in the case of the binding of Na[*trans*-Cl₄Im(Me₂SO)Ru^{III}]. On the other hand, if DNA was first modified by all three ruthenium complexes in 10 mM NaClO₄ to the r_b value in the range 0.001–0.05, the level of the modification (r_b) remained unchanged even after transferring DNA modified by the ruthenium complex into the media in which their rate of DNA binding is noticeably decreased (vide supra). This observation was also consistent with the results of the following experiment. CT DNA modified by

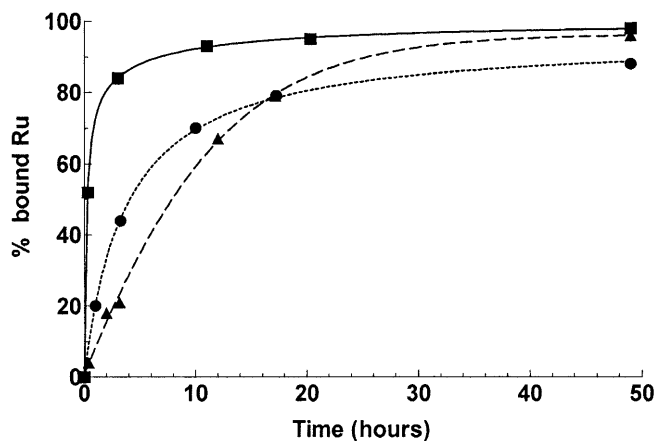


Fig. 2 Kinetics of the binding of HIm[*trans*-Cl₄Im₂Ru^{III}] (●), HInd[*trans*-Cl₄Ind₂Ru^{III}] (▲), and Na[*trans*-Cl₄Im(Me₂SO)Ru^{III}] (■) to CT DNA in the medium of 10 mM NaClO₄ at 37 °C, determined by FAAS. The concentration of DNA was 0.32 mg/mL and r_i was 0.1

the ruthenium complex in 10 mM NaClO₄ was precipitated by ethanol, redissolved in the medium of TE buffer (containing no ruthenium complex), further incubated at 37 °C for an additional 48 h, again precipitated by ethanol, and the content of ruthenium in these samples (r_b) determined by FAAS. No changes in r_b values were noticed.

The binding experiments of the present work indicate that modification reactions resulted in the irreversible coordination of the ruthenium complexes to polymeric double-helical DNA, which facilitates sample analysis. Hence, it is possible to prepare easily and precisely the samples of DNA modified by the ruthenium complexes at a preselected value of r_b . Importantly, it is also reasonable to assume that the levels of DNA modifications by the ruthenium complexes reached in 10 mM NaClO₄ remained unchanged after transferring the samples into the medium required for subsequent analyses by biophysical or biochemical methods. Thus, the samples of DNA modified by the ruthenium complexes and analyzed further by biophysical or biochemical methods were prepared in 10 mM NaClO₄ at 37 °C except where stated. After 48 h of the reaction of DNA with the complex the samples were precipitated in ethanol, dissolved in the medium necessary for a particular analysis, and the r_b value in an aliquot of this sample was checked by FAAS. In this way, the analyses described in the present paper were performed in the absence of unbound (free) ruthenium complex.

Inhibition of restriction endonucleases

A typical experiment demonstrating *Bam*HI digestion of linearized pSP73 DNA unmodified or containing the adducts of Na[*trans*-Cl₄Im(Me₂SO)Ru^{III}] is shown

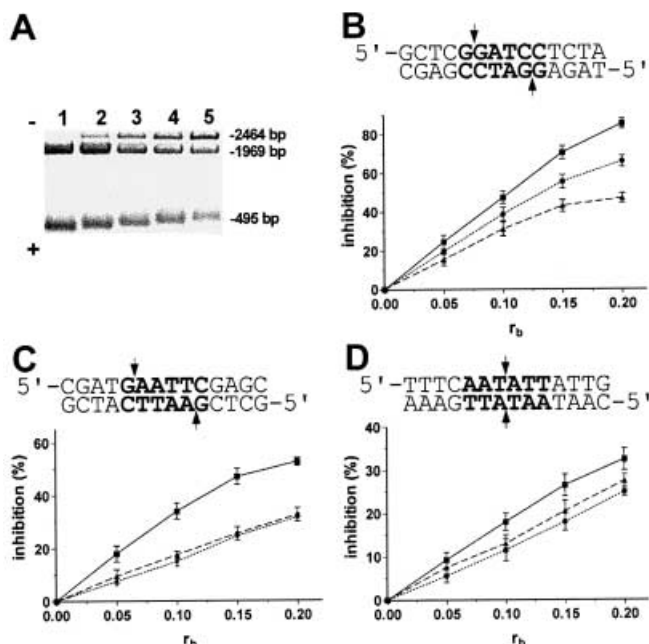


Fig. 3A–D Digestion with restriction endonucleases of linearized pSP73 DNA modified by ruthenium compounds. **A** Electrophoregram of an agarose gel following digestion with *Bam*HI of pSP73 DNA linearized by *Ssp*I and modified by Na[*trans*-Cl₄Im(Me₂SO)Ru^{III}]. Lane 1, $r_b=0$ (control); lane 2, $r_b=0.05$; lane 3, $r_b=0.1$; lane 4, $r_b=0.15$; lane 5, $r_b=0.2$. **B–D** Inhibition of digestion with *Bam*HI (**B**), *Eco*RI (**C**), or *Ssp*I (**D**) of pSP73 DNA linearized by *Ssp*I (**B**, **C**) or *Eco*RI (**D**) and modified by HIm[*trans*-Cl₄Im₂Ru^{III}] (●), HInd[*trans*-Cl₄Ind₂Ru^{III}] (▲), and Na[*trans*-Cl₄Im(Me₂SO)Ru^{III}] (■); the recognition sequences and cleavage sites are shown at the top of each panel

in Fig. 3A. With no modification or at very low levels of binding ($r_b < 0.001$) there is complete splicing, with all DNA migrating as bands corresponding to DNA fragments of 495 and 1969 bp. As the amount of Na[*trans*-Cl₄Im(Me₂SO)Ru^{III}] bound to DNA increases, the yield of these fragments gradually decreases. Densitometric evaluation of these results permitted us to quantify the inhibition of this cleavage (Fig. 3B).

The cleavage of the linearized pSP73 DNA also modified by the other two ruthenium complexes tested in the present work by *Bam*HI was analyzed in the same way (Fig. 3B). The results indicate that DNA adducts of both HIm[*trans*-Cl₄Im₂Ru^{III}] and HInd[*trans*-Cl₄Ind₂Ru^{III}] also inhibited cleavage by *Bam*HI, but less efficiently than those of Na[*trans*-Cl₄Im(Me₂SO)Ru^{III}].

In addition, the cleavage of the linearized pSP73 DNA modified by the three ruthenium compounds by two other restriction endonucleases was also analyzed. The cleavage by *Eco*RI and *Ssp*I was also inhibited by all three metal compounds. The efficiency of the endonucleases tested in the present work to digest DNA modified by the ruthenium compounds decreased in the order *Ssp*I > *Eco*RI > *Bam*HI. On the

other hand, similarly as in the case of the cleavage by *Bam*HI, the inhibition of cleavage by *Eco*RI and *Ssp*I due to the modification by Na[*trans*-Cl₄Im(Me₂SO)Ru^{III}] was clearly more pronounced than that due to the modification by HIm[*trans*-Cl₄Im₂Ru^{III}] and HInd[*trans*-Cl₄Ind₂Ru^{III}].

We verified that the inhibition of the digestion by restriction endonucleases was not caused by the metallation of the enzyme or a ruthenium-induced DNA-enzyme cross-link. All three restriction endonucleases cleave unmodified pSP73 DNA in the presence of additional DNA modified by the ruthenium complexes to $r_b=0.2$.

The recognition site of *Bam*HI, the capability of which to cleave ruthenated DNA is inhibited most effectively, contains two adjacent guanine residues and DNA is cleaved between these two guanines. In contrast, the recognition sequence of *Ssp*I, which digests ruthenated DNA most easily, contains no guanine residues. Thus, it seems reasonable to suggest that the preferential DNA binding sites of ruthenium compounds tested in the present work are guanine residues. Consistent with this conclusion, *Eco*RI, which contains in its recognition sequence only one guanine residue, exhibits a medium efficiency to digest ruthenated DNA. Hence, the results of the analysis based on inhibition of restriction endonucleases suggest that anticancer heterocyclic complexes of ruthenium(III) tested in the present work preferentially bind to guanine residues, with this preference being more pronounced for Na[*trans*-Cl₄Im(Me₂SO)Ru^{III}].

Transcription mapping of DNA adducts

In vitro RNA synthesis by RNA polymerases on DNA templates containing several types of bifunctional adducts of metal complexes can be prematurely terminated at the level or in the proximity of adducts [25, 26, 30, 31]. Importantly, monofunctional DNA adducts of several platinum complexes are unable to terminate RNA synthesis.

Cutting of pSP73 DNA [25, 26] by *Nde*I and *Hpa*I restriction endonucleases yielded a 221-bp fragment (a substantial part of its nucleotide sequence is shown in Fig. 4B). This fragment contained T7 RNA polymerase promoter [in the upper strand close to its 3'-end (Fig. 4B)]. The experiments were carried out using this linear DNA fragment, modified by HIm[*trans*-Cl₄Im₂Ru^{III}], HInd[*trans*-Cl₄Ind₂Ru^{III}], Na[*trans*-Cl₄Im(Me₂SO)Ru^{III}], cisplatin, or transplatin at $r_b=0.01$, for RNA synthesis by T7 RNA polymerase (Fig. 4A). RNA synthesis on the template modified by Na[*trans*-Cl₄Im(Me₂SO)Ru^{III}] or the platinum compounds yielded fragments of defined sizes (Fig. 4A), which indicates that RNA synthesis on these templates was prematurely terminated. The major stop sites produced by the ruthenium complex (Fig. 4A, lane Im/DMSO-Ru) were identical to some of those

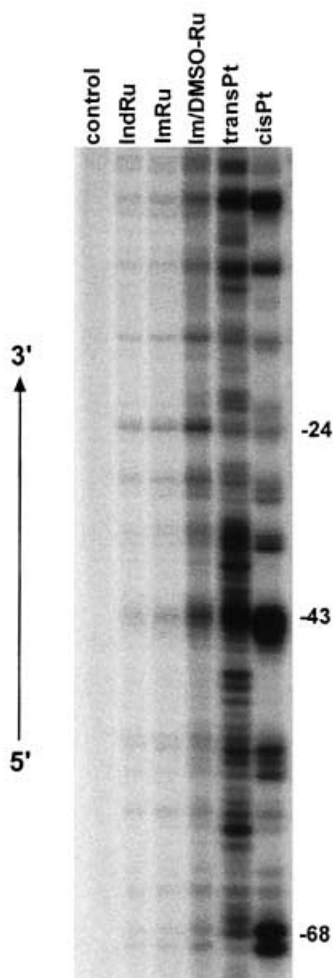
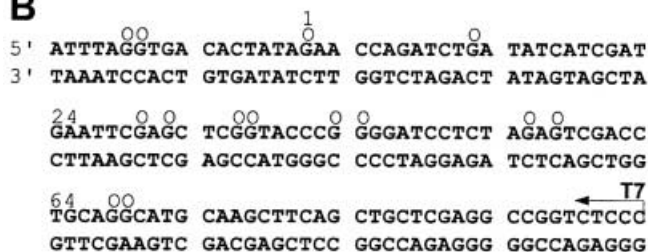
A**B**

Fig. 4A, B Inhibition of RNA synthesis by T7 RNA polymerase on the *NdeI/HpaI* fragment of pSP73 plasmid modified by ruthenium and platinum complexes. **A** Autoradiogram of 6% polyacrylamide/8M urea sequencing gel. Lanes: control, unmodified template; *IndRu*, *ImRu*, *Im/DMSO-Ru*, *transPt*, *cisPt*, the template modified by *HInd[trans-Cl₄Im₂Ru^{III}]*, *HIm[trans-Cl₄Im₂Ru^{III}]*, *Na[trans-Cl₄Im(Me₂SO)Ru^{III}]*, transplatin, or cisplatin at $r_b=0.01$, respectively. **B** Schematic diagram showing the portion of the nucleotide sequence of the template of the *NdeI/HpaI* fragment used to monitor inhibition of RNA synthesis by *Na[trans-Cl₄Im(Me₂SO)Ru^{III}]*. The arrow indicates the start of the T7 RNA polymerase. (o) Major stop signals (from Fig. 4A, lane *Im/DMSO-Ru*). The numbers correspond to the nucleotide numbering in the sequence map of the pSP73 plasmid

produced by cisplatin (Fig. 4A, lane *cisPt*), but different from those produced by clinically ineffective transplatin (Fig. 4A, lane *transPt*). The stop sites produced by *Na[trans-Cl₄Im(Me₂SO)Ru^{III}]* mainly appeared at guanines also contained in GG sequences (GG sequences are preferential DNA binding sites of cisplatin at which this antitumor drug forms intrastrand cross-links [32, 33]). Interestingly, the bands produced by *Na[trans-Cl₄Im(Me₂SO)Ru^{III}]* had a lower intensity than those yielded by cisplatin, which suggests that this ruthenium complex also produces adducts on DNA incapable of terminating RNA synthesis and that the amount of these DNA adducts (presumably monofunctional lesions) was considerably higher than that formed in the case of cisplatin. Taken together, the results of these mapping experiments are consistent with suggestion that *Na[trans-Cl₄Im(Me₂SO)Ru^{III}]* could also form on double-helical DNA some amount of bidentate adducts similar to the DNA cross-links formed by cisplatin.

DNA adducts of the other two ruthenium compounds tested in the present work produced only faint bands corresponding to stop sites (Fig. 4A, lanes *ImRu* and *IndRu*). This observation is consistent with capability of *HIm[trans-Cl₄Im₂Ru^{III}]* and *HInd[trans-Cl₄Im₂Ru^{III}]* to form on DNA a considerably lesser amount of adducts that would be similar to those formed by cisplatin in being capable of terminating RNA synthesis in vitro.

Interstrand cross-linking

The analysis based on inhibition of restriction endonucleases and transcription mapping experiments (Figs. 3 and 4) suggest that the anticancer heterocyclic complexes of ruthenium(III) tested in the present work could form bidentate adducts on polymeric DNA, but these studies could not distinguish whether these adducts were intrastrand or interstrand cross-links. Therefore, further experiments were carried out to compare the amounts of the interstrand cross-links formed by *HIm[trans-Cl₄Im₂Ru^{III}]*, *HInd[trans-Cl₄Im₂Ru^{III}]*, and *Na[trans-Cl₄Im(Me₂SO)Ru^{III}]* in linear DNA. We used in these experiments the pSP73 plasmid (2464 bp) which was modified by the ruthenium compounds after it had been linearized by *EcoRI* (*EcoRI* cuts only once within pSP73 plasmid). The samples were analyzed for the interstrand cross-links by agarose gel electrophoresis under denaturing conditions [26, 34].

An electrophoretic method for precise and quantitative determination of interstrand cross-linking by metal complexes in DNA was described previously [26, 27]. Upon electrophoresis under denaturing conditions, 3'-end-labeled strands of linearized pSP73 plasmid containing no interstrand cross-links migrate as a 2464-nucleotide single strand, whereas the interstrand cross-linked strands migrate more slowly as a

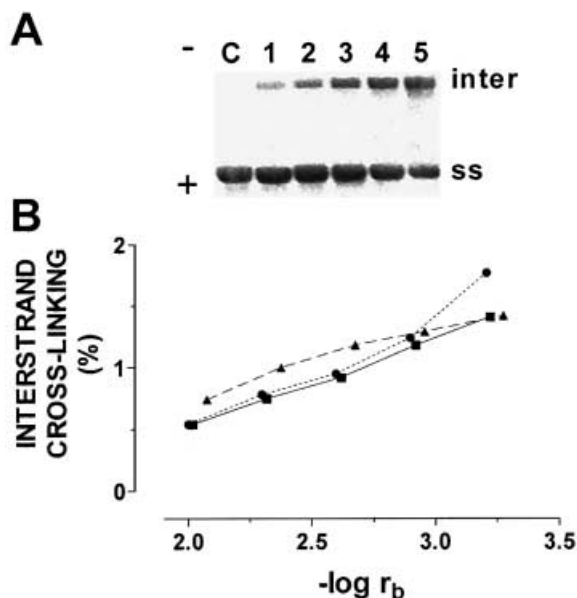


Fig. 5A, B The formation of interstrand cross-links by ruthenium complexes in pSP73 plasmid linearized by *Eco*RI. **A** Autoradiogram of a denaturing 1% agarose gel of linearized DNA which was 3'-end labeled; the interstrand cross-linked DNA appears as the top bands migrating on the gels more slowly than the single-stranded DNA (contained in the bottom bands); the plasmid linearized by *Eco*RI was incubated with $\text{Na}[\text{trans-Cl}_4\text{Im}(\text{Me}_2\text{SO})\text{Ru}^{\text{III}}]$ for 48 h at 37 °C; lane C, $r_b=0$ (control); lanes 1–5, $r_b=0.0006, 0.0012, 0.0024, 0.0048, 0.0096$, respectively. **B** Dependence on r_b of the percentage of interstrand cross-links per adduct [interstrand cross-linking (%)] formed by $\text{HIm}[\text{trans-Cl}_4\text{Im}_2\text{Ru}^{\text{III}}]$ (●), $\text{HInd}[\text{trans-Cl}_4\text{Ind}_2\text{Ru}^{\text{III}}]$ (▲), or $\text{Na}[\text{trans-Cl}_4\text{Im}(\text{Me}_2\text{SO})\text{Ru}^{\text{III}}]$ (■) in linearized DNA within 48 h. Data measured in triplicate varied on average by $\pm 3\%$ from their mean

higher molecular mass species. The bands corresponding to the more slowly migrating interstrand-cross-linked fragments were noticed if either ruthenium complex was used to modify DNA at a r_b value as low as 6×10^{-4} (shown in Fig. 5A for $\text{Na}[\text{trans-Cl}_4\text{Im}(\text{Me}_2\text{SO})\text{Ru}^{\text{III}}]$). The intensity of the more slowly migrating band increased with the growing level of the modification. The radioactivity associated with the individual bands in each lane was measured to obtain estimates of the fraction of non-cross-linked or cross-linked DNA under each condition. The frequency of interstrand cross-links (the amount of interstrand cross-links per one molecule of the ruthenium complex coordinated to DNA) was calculated using the Poisson distribution in combination with the r_b values and the fragment size [26, 27] (for details see the section Materials and methods).

As summarized in Fig. 5B, all three ruthenium compounds showed a relatively low and roughly identical interstrand cross-linking efficiency (at $r_b=0.001$ –1%, which is approximately six times less than cisplatin forms under identical conditions [26, 34]). Thus, these results indicate that the interstrand cross-links are only minor adducts in linear double-helical DNA

modified by anticancer heterocyclic ruthenium(III) complexes.

Unwinding

Electrophoresis in native agarose gel was used to quantify the unwinding induced in pUC19 plasmid by the ruthenium complexes by monitoring the degree of supercoiling (Fig. 6). A compound that unwinds a DNA duplex reduces the number of supercoils in closed, negatively supercoiled DNA so that the negative superhelical density of closed circular DNA decreases. This decrease upon binding of unwinding agents causes a decrease in the rate of migration through agarose gel, which makes it possible that the unwinding can be observed and quantified [28]. Figure 6 shows electrophoresis gels in which increasing amounts of $\text{HIm}[\text{trans-Cl}_4\text{Im}_2\text{Ru}^{\text{III}}]$, $\text{HInd}[\text{trans-Cl}_4\text{Ind}_2\text{Ru}^{\text{III}}]$, or $\text{Na}[\text{trans-Cl}_4\text{Im}(\text{Me}_2\text{SO})\text{Ru}^{\text{III}}]$ have been bound to a mixture of relaxed and negatively supercoiled pUC19 DNA. The unwinding angle is given by $F=18s/r_b(c)$, where s is the superhelical density and $r_b(c)$ is the value of r_b at which the supercoiled and relaxed forms comigrate [28]. Under the present experimental conditions, s was calculated to be -0.063 on the basis of the data of cisplatin for which the $r_b(c)$ was determined in this study and

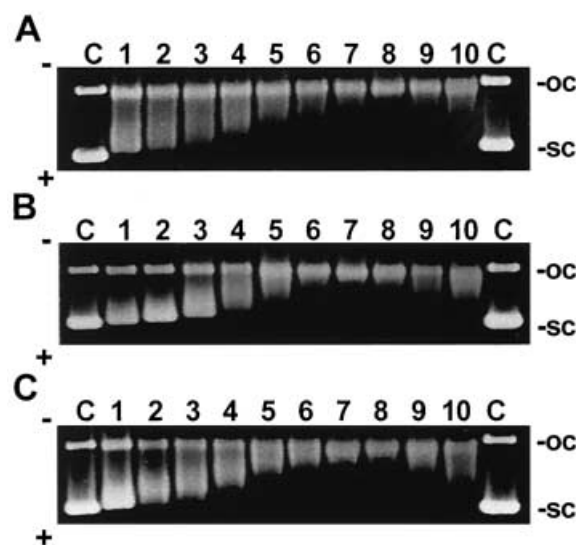


Fig. 6A–C Unwinding of negatively supercoiled pUC19 plasmid DNA by ruthenium complexes. The plasmid was incubated with $\text{HIm}[\text{trans-Cl}_4\text{Im}_2\text{Ru}^{\text{III}}]$ (A), $\text{HInd}[\text{trans-Cl}_4\text{Ind}_2\text{Ru}^{\text{III}}]$ (B), or $\text{Na}[\text{trans-Cl}_4\text{Im}(\text{Me}_2\text{SO})\text{Ru}^{\text{III}}]$ (C) for 48 h at 37 °C and precipitated by ethanol. **A** Lane C, control (unmodified DNA); lanes 1–10, $r_b=0.051, 0.062, 0.074, 0.086, 0.099, 0.112, 0.125, 0.135, 0.148, 0.165$, respectively. **B** Lane C, control (unmodified DNA); lanes 1–10, $r_b=0.070, 0.094, 0.118, 0.130, 0.141, 0.153, 0.165, 0.177, 0.203, 0.211$, respectively. **C** Lane C, control (unmodified DNA); lanes 1–10, $r_b=0.031, 0.042, 0.052, 0.060, 0.071, 0.082, 0.093, 0.103, 0.114, 0.127$, respectively. The top bands (oc) correspond to the form of nicked plasmid and the bottom bands (sc) to the closed, negatively supercoiled plasmid

Table 1 Unwinding of supercoiled pUC19 DNA by ruthenium complexes

Compound	$r_b(c)$	Unwinding angle ^a
HIm[<i>trans</i> -Cl ₄ Im ₂ Ru ^{III}]	0.135	8±2°
HInd[<i>trans</i> -Cl ₄ Ind ₂ Ru ^{III}]	0.165	7±2°
Na[<i>trans</i> -Cl ₄ Im(Me ₂ SO)Ru ^{III}]	0.103	11±2°

^aThe unwinding angle was calculated as described in the text

$F=13^\circ$ was assumed [28, 35]. Using this approach the DNA unwinding angle of 8±2°, 7±2°, or 11±2° was determined for HIm[*trans*-Cl₄Im₂Ru^{III}], HInd[*trans*-Cl₄Ind₂Ru^{III}], or Na[*trans*-Cl₄Im(Me₂SO)Ru^{III}], respectively (see also Table 1). Thus, the highest unwinding angle was found for Na[*trans*-Cl₄Im(Me₂SO)Ru^{III}], which was close to the unwinding angle observed if DNA was globally modified by cisplatin (13° [28]).

B→Z transition

The effect of various metal-based compounds, especially antitumor platinum drugs, on the salt-induced B→Z transition in poly(dG-dC) or poly(dG-m⁵dC) has already been described in several papers [36, 37, 38, 39]. For instance, cisplatin was found to facilitate the B→Z transition, but the resulting Z form was distorted and the transition cooperativity was considerably reduced [40, 41].

The effect of the binding of the three ruthenium compounds tested in the present work upon the B→Z transition in DNA was investigated in poly(dG-m⁵dC) during salt-induced transition from the right- to left-handed double helix. The transition was monitored by CD spectroscopy at a series of NaClO₄ concentrations between 0 and 1.0 M added to the medium containing 10 mM NaClO₄, 1 mM phosphate buffer (pH 7.4), and 0.1 mM EDTA. All of our experiments were done at r_b values of 0 or 0.1. The r_b value of 0.1 was chosen as a compromise between a low value which would have some relevance to the therapeutic effects of the ruthenium compounds and a larger value which would cause more pronounced changes in the spectra.

The CD spectra of unmodified poly(dG-m⁵dC) at various concentrations of NaClO₄ are shown in Fig. 7A. The figure shows the characteristic inversion in the CD spectrum on going from the right-handed B form to the left-handed Z form after addition of at least 1.0 M NaClO₄, and is used as the standard with which to compare the ruthenium-treated duplexes. The CD spectra at different NaClO₄ concentrations of poly(dG-m⁵dC) pretreated with either HIm[*trans*-Cl₄Im₂Ru^{III}], HInd[*trans*-Cl₄Ind₂Ru^{III}], or Na[*trans*-Cl₄Im(Me₂SO)Ru^{III}] in 10 mM NaClO₄ (i.e. the polymer was treated when it was in the B conformation) are shown in Fig. 7B–D, respectively.

A plot of the molar ellipticity at 293 nm as a function of the concentration of NaClO₄ added to 10 mM

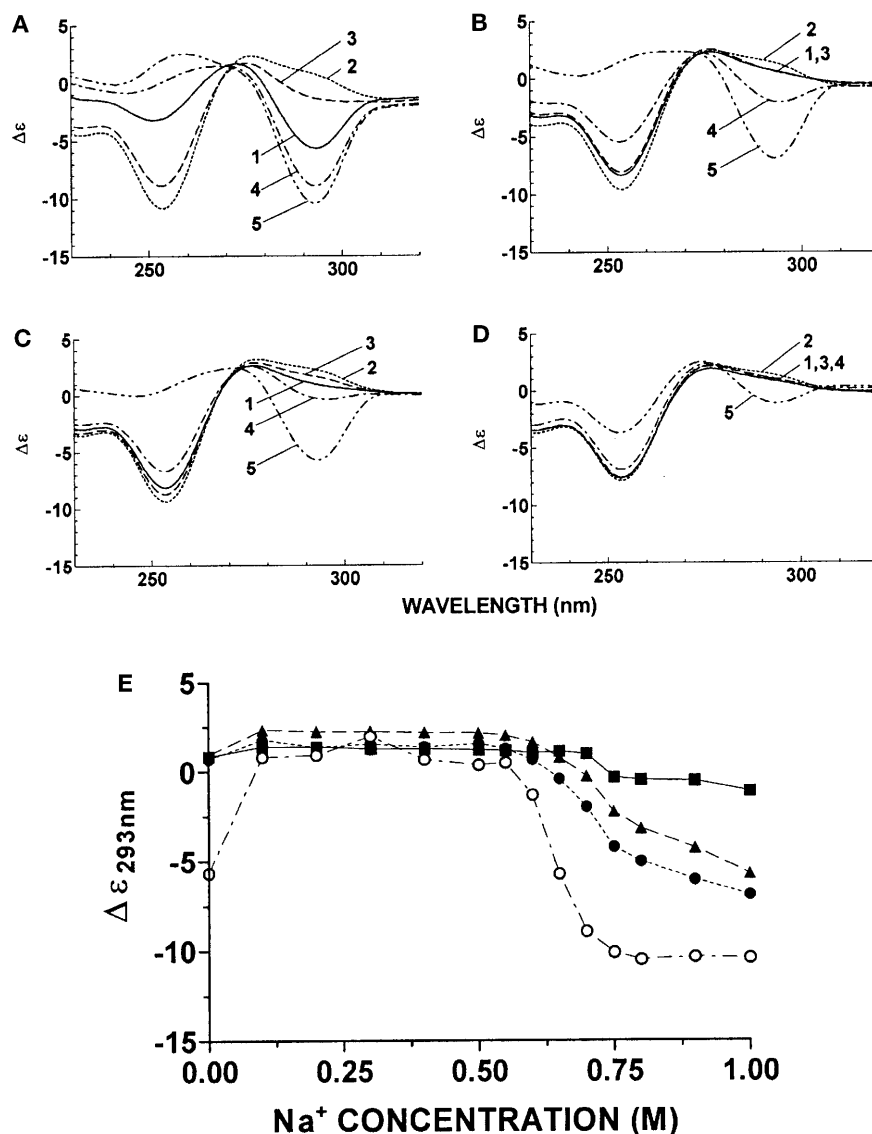
NaClO₄ with 0.1 mM EDTA plus 1 mM phosphate buffer, pH 7.4 (Fig. 7E), can be used to monitor the B→Z transition in poly(dG-m⁵dC) [38]. From an examination of these plots presented in Fig. 7E it is evident that the maximum variation in the ellipticity at 293 nm for the unmodified (control) polymer and the polymers treated with the ruthenium compound occurs over a more or less narrow range of salt concentration. Thus, the transitions appear to be cooperative. While the inversion of the positive CD band at 293 nm found for the control, unmodified DNA was clearly observed with the transition midpoint at 0.62 M NaClO₄, this inversion observed for the ruthenated polymers was considerably inhibited (Fig. 7). The ruthenium compounds tested in the present work affected the B→Z transition differently, Na[*trans*-Cl₄Im(Me₂SO)Ru^{III}] being significantly more effective than the other two complexes.

DNA melting

CT DNA was modified by HIm[*trans*-Cl₄Im₂Ru^{III}], HInd[*trans*-Cl₄Ind₂Ru^{III}], or Na[*trans*-Cl₄Im(Me₂SO)Ru^{III}] to various r_b values (0–0.1) in 10 mM NaClO₄ at 37 °C for 48 h. The salt concentration was then further adjusted by addition of NaClO₄ to values in the range 0.01–0.2 M. The effect on t_m is dependent both on the amount of ruthenium bound and the salt concentration. If the melting was measured at low concentrations of NaClO₄ (0.01 M), the binding of the ruthenium complexes to DNA resulted in a considerable increase of t_m (Fig. 8). This increase was most pronounced for the binding of Na[*trans*-Cl₄Im(Me₂SO)Ru^{III}] (+9 °C at $r_b=0.1$ at a concentration of 0.01 M NaClO₄) (Fig. 8C). At high salt concentrations (0.2 M) the modification of DNA by HIm[*trans*-Cl₄Im₂Ru^{III}] or HInd[*trans*-Cl₄Ind₂Ru^{III}] resulted in no change of t_m , while the modification by Na[*trans*-Cl₄Im(Me₂SO)Ru^{III}] resulted in a decrease of t_m which became more pronounced with increasing r_b values (Fig. 8C). This behavior is in marked contrast to cisplatin, where the modification of DNA results in a decrease of t_m if DNA melting is measured in salt concentrations from 0.01 to 0.2 M [42]. The heterocyclic ruthenium compounds represent an intermediate case, with an increase in t_m at low ionic strength and relatively little or more pronounced reduction of t_m at the higher salt values.

Previously, three factors have been invoked to account for the thermal stability of DNA modified by metal complexes: stabilizing effects of the positive charge on the metal moiety and of DNA interstrand cross-links, and a destabilizing effect of conformational distortions such as intrastrand cross-links induced in DNA by platinum coordination [42]. The dependence of the transition melting temperature on ionic strength was explained by competing electrostatic effects as the salt concentration was varied.

Fig. 7 CD spectroscopy of poly(dG-m⁵dC) unmodified (**A**) or treated with HIm[*trans*-Cl₄Im₂Ru^{III}] (**B**), HInd[*trans*-Cl₄Ind₂Ru^{III}] (**C**), or Na[*trans*-Cl₄Im(Me₂SO)Ru^{III}] (**D**) at $r_b=0.1$. The polymer was modified when it was in the B form (in 10 mM NaClO₄) and subsequently transferred into the media containing 10 mM NaClO₄ with 1 mM phosphate buffer (pH 7.5) plus 10 mM EDTA and various concentrations of NaClO₄. Curves in **A–D**: 1, no NaClO₄ added; 2, 0.2 M NaClO₄; 3, 0.6 M NaClO₄; 4, 0.7 M NaClO₄; 5, 1.0 M NaClO₄. **E** Plot of the molar ellipticity at 293 nm ($\Delta\epsilon_{293}$) as a function of Na⁺ concentration for poly(dG-m⁵dC) unmodified (○) or treated with HIm[*trans*-Cl₄Im₂Ru^{III}] (●), HInd[*trans*-Cl₄Ind₂Ru^{III}] (▲), or Na[*trans*-Cl₄Im(Me₂SO)Ru^{III}] (■) at $r_b=0.1$. Data points measured in duplicate varied on average $\pm 1\%$ from their mean. Other details are described in the text



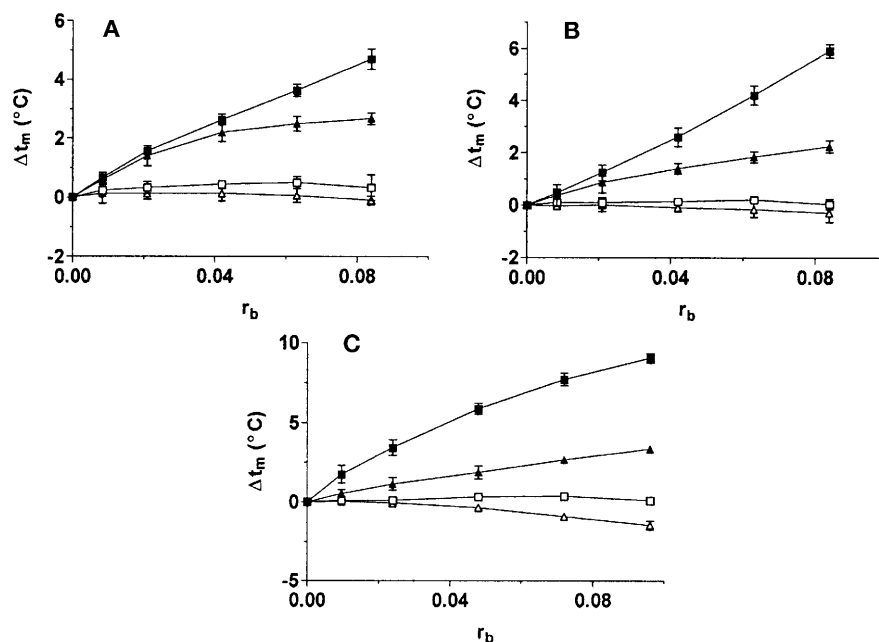
Under the incubation conditions, we expect all ruthenium compounds to have produced a range of adducts. The observed change in melting temperature will reflect the relative proportion and contribution of the two limiting binding modes. Inherently, we predict conformational distortions due to adduct formation to destabilize the helix, as has been consistently observed in studies with cisplatin or other antitumor platinum compounds. In contrast, interstrand cross-linking is predicted to stabilize the helix by preventing strand dissociation. At low ionic strength it is reasonable to conclude that the increases in t_m are caused by the small percentage of interstrand cross-links formed by both the ruthenium compounds and by positive charges on the ruthenium moieties. An interesting and as yet unresolved question, therefore, is why a high salt concentration appears to result in destabilization due to the binding of Na[*trans*-Cl₄Im(Me₂SO)Ru^{III}], even in the presence of small amount of interstrand cross-links. It is possible that the observed decrease in

t_m at high ionic strength is a consequence of conformational changes induced by the ruthenium adducts that then dominate over the combination of “stabilizing” effects. At high salt concentration the stabilizing effects are reduced since electrostatic effects of the ruthenium compounds are apparently lowered with increasing concentration of Na⁺ counter ions. Thus, the solution behavior of the DNA adducts of antitumor heterocyclic ruthenium(III) compounds appears significantly different to that of cisplatin and merits further study.

Conclusions

The results of the present work demonstrate that Na[*trans*-Cl₄Im(Me₂SO)Ru^{III}] binds DNA considerably faster than HIm[*trans*-Cl₄Im₂Ru^{III}] or HInd[*trans*-Cl₄Ind₂Ru^{III}] (Fig. 2). The faster binding of Na[*trans*-Cl₄Im(Me₂SO)Ru^{III}] is apparently due to a

Fig. 8 Plots of Δt_m values of CT DNA modified by HIm[*trans*-Cl₄Im₂Ru^{III}] (A), HInd[*trans*-Cl₄Ind₂Ru^{III}] (B), and Na[*trans*-Cl₄Im(Me₂SO)Ru^{III}] (C) on r_b measured in 0.01 M (■), 0.05 M (▲), 0.1 M (□), or 0.2 M (△) NaClO₄ plus 1 mM Tris-HCl with 0.1 mM EDTA, pH 7.4. Δt_m is defined as the difference between the t_m values of ruthenated and unmodified DNAs. Data measured in triplicate varied on average $\pm 2\%$ from their mean



higher rate of hydrolysis of this complex in aqueous media in comparison with the other two ruthenium compounds tested in the present work [9, 10, 19, 20]. The aqua species carries a higher positive charge which facilitates interaction with polyanionic DNA. An important finding of the present work also discussed below is that the binding of Na[*trans*-Cl₄Im(Me₂SO)Ru^{III}] results in its enhanced base sequence specificity.

Interestingly, Na[*trans*-Cl₄Im(Me₂SO)Ru^{III}] inhibits digestion of DNA by restriction endonucleases markedly more effectively than the other two ruthenium compounds at the same level of the modification (Fig. 3). This implies that the DNA binding mode of HIm[*trans*-Cl₄Im₂Ru^{III}] or HInd[*trans*-Cl₄Ind₂Ru^{III}] is different from that of Na[*trans*-Cl₄Im(Me₂SO)Ru^{III}]. In addition, these results are consistent with guanines being preferential binding sites of anticancer heterocyclic ruthenium compounds in double-helical DNA and that this base sequence specificity is most pronounced in the case of Na[*trans*-Cl₄Im(Me₂SO)Ru^{III}] binding. The results of the transcription mapping experiments (Fig. 4) support these conclusions and further suggest that, in contrast to HIm[*trans*-Cl₄Im₂Ru^{III}] or HInd[*trans*-Cl₄Ind₂Ru^{III}], Na[*trans*-Cl₄Im(Me₂SO)Ru^{III}] forms intrastrand cross-links although in a significantly smaller amount than cisplatin. We suggest that different properties of the DNA adducts of Na[*trans*-Cl₄Im(Me₂SO)Ru^{III}] on one hand and HIm[*trans*-Cl₄Im₂Ru^{III}] or HInd[*trans*-Cl₄Ind₂Ru^{III}] on the other hand are associated with the observation that the second chloride in Na[*trans*-Cl₄Im(Me₂SO)Ru^{III}] can be replaced by water markedly more easily and with a higher yield than in other two ruthenium compounds [9, 10, 19, 20]. The replacement of the second chloride in the molecules of the ruthenium compounds is a pre-

requisite for the formation of their bifunctional adducts. In addition, HIm[*trans*-Cl₄Im₂Ru^{III}] or HInd[*trans*-Cl₄Ind₂Ru^{III}] contain two bulky heterocyclic bases as axial ligands, in contrast to Na[*trans*-Cl₄Im(Me₂SO)Ru^{III}] in which the base is replaced by Me₂SO. Hence, the two bulky heterocyclic axial ligands in HIm[*trans*-Cl₄Im₂Ru^{III}] or HInd[*trans*-Cl₄Ind₂Ru^{III}] could present a larger steric hindrance to the formation of the bifunctional adducts in the rigid structure of double-helical DNA than when such adducts are formed by Na[*trans*-Cl₄Im(Me₂SO)Ru^{III}] in which one heterocyclic ligand is replaced by Me₂SO. We suggest that the lower efficiency of HIm[*trans*-Cl₄Im₂Ru^{III}] or HInd[*trans*-Cl₄Ind₂Ru^{III}] to form bifunctional adducts on double-helical DNA in comparison with Na[*trans*-Cl₄Im(Me₂SO)Ru^{III}] may be also associated with these steric constraints.

The present study also demonstrates that formation of the adducts by all three heterocyclic ruthenium compounds affects the conformation of DNA. This conclusion is supported by the results of DNA unwinding experiments (Fig. 6), analysis of the B→Z transition in ruthenated DNA and, in the case of DNA binding of Na[*trans*-Cl₄Im(Me₂SO)Ru^{III}], also by the reduction of t_m of the ruthenated DNA if its melting was investigated in the medium containing high concentration of the salt (Fig. 8C). Importantly, the adducts of Na[*trans*-Cl₄Im(Me₂SO)Ru^{III}] are considerably more effective in inducing conformational alterations in DNA than those of the other two ruthenium compounds. This observation is consistent with the idea and support the hypothesis that Na[*trans*-Cl₄Im(Me₂SO)Ru^{III}] can form in DNA noticeably more bifunctional adducts than the other two ruthenium compounds tested in the present work (vide supra). In addition, Na[*trans*-Cl₄Im(Me₂SO)Ru^{III}]

affects DNA more than the other two heterocyclic ruthenium(III) compounds tested, which might be relevant to the improved chemotherapeutic properties of the former agent.

Finally, the biochemical and biophysical analysis of DNA interactions with the heterocyclic ruthenium(III) anticancer drugs described in this report provides experimental support that the binding of these ruthenium complexes modifies DNA in a way which is different from the modification by cisplatin. As DNA is a possible pharmacological target of both platinum and ruthenium complexes [10, 18, 43], the latter view is also consistent with the hypothesis that the altered DNA binding mode of ruthenium compounds is an important factor responsible for their altered cytostatic activity in tumor cells (in comparison with cisplatin). Thus, "downstream" effects modulated by recognition by specific proteins, DNA-processing enzymes, and other cell components are not likely to be the same as the subset of cell components which recognize cisplatin adducts [44, 45, 46].

Acknowledgements This research was supported by the Grant Agency of the Czech Republic (grant nos. 305/99/0695, 204/97/P028), and the Internal Grant Agency of the Ministry of Health of the Czech Republic (grant nos. NL6058-3/2000 and NL6069-3/2000). J.M. is supported by a doctoral fellowship from the Faculty of Sciences, Masaryk University, Brno. This work was also a part of research performed within EU program COST D8, project no. D8/0017/97 and the Greek-Czech International Cooperation Program "KONTAKT".

References

- Rosenberg B (1999) In: Lippert B (ed) *Cisplatin. Chemistry and biochemistry of a leading anticancer drug*. Wiley-VCH, Zürich, pp 3–30
- O'Dwyer PJ, Stevenson JP, Johnson SW (1999) In: Lippert B (ed) *Cisplatin. Chemistry and biochemistry of a leading anticancer drug*. Wiley-VCH, Zürich, pp 31–72
- Wong E, Giandomenico CM (1999) *Chem Rev* 99:2451–2466
- Cleare MJ (1974) *Coord Chem Rev* 12:349–405
- Cleare MJ (1977) *J Clin Hematol Oncol* 7:1–25
- Farrell N (1996) In: Sigel A, Sigel H (eds) *Metal ions in biological systems*, vol 32. Dekker, New York, pp 603–639
- Farrell N. (2000) In: Kelland LR, Farrell NP (eds) *Platinum based drugs in cancer therapy*. Humana, Totowa, NJ, pp 321–338
- Clarke MJ (1993) In: Keppler BK (ed) *Metal complexes in cancer chemotherapy*. VCH, Weinheim, pp 129–156
- Keppler BK, Lipponer K-G, Stenzel B, Kratz F (1993) In: Keppler BK (ed) *Metal complexes in cancer chemotherapy*. VCH, Weinheim, pp 187–220
- Clarke MJ, Zhu F, Frasca DR (1999) *Chem Rev* 99:2511–2533
- Sava G, Bergamo A (2000) *Int J Oncol* 17:353–365
- Sava G, Clerici K, Capozzi I, Cocchietto M, Gagliardi R, Alessio E, Mestroni G, Perbellini A (1999) *Anti-Cancer Drugs* 10:129–138
- Cocchietto M, Salerno G, Alessio E, Mestroni G, Sava G (2000) *Anticancer Res* 20:197–202
- Keppler BK (1993) *Metal complexes in cancer chemotherapy*. VCH, Weinheim
- Frasca D, Ciampa J, Emerson J, Umans RS, Clarke M (1996) *J Met-Based Drugs* 3:197–209
- Sava G, Pacor S, Coluccia M, Mariggio M, Cocchietto M, Alessio E, Mestroni G (1994) *Drug Invest* 8:150–161
- Barca A, Pani B, Tamaro M, Russo E (1999) *Mutation Res* 423:171–181
- Gallori E, Vettori C, Alessio E, Vilchez FG, Vilaplana R, Orioli P, Casini A, Messori L (2000) *Arch Biochem Biophys* 376:156–162
- Ni Dhubghaill OM, Hagen WR, Keppler BK, Lipponer K-G, Sadler PJ (1994) *J Chem Soc Dalton Trans* 3305–3310
- Sava G, Alessio E, Bergano A, Mestroni G. (1999) In: Clarke MJ, Sadler PJ (eds) *Topics in biological inorganic chemistry*, vol 1. Springer, Berlin Heidelberg New York, pp 143–169
- Seelig MH, Berger MR, Keppler BK (1992) *J Cancer Res Clin Oncol* 118:195–200
- Alessio E, Balducci G, Lutman A, Mestroni G, Calligaris H, Attia WM (1993) *Inorg Chim Acta* 203:205–217
- Brabec V, Palecek E (1970) *Biophysik* 6:290–300
- Brabec V, Palecek E (1976) *Biophys Chem* 4:76–92
- Lemaire MA, Schwartz A, Rahmouni AR, Leng M (1991) *Proc Natl Acad Sci USA* 88:1982–1985
- Brabec V, Leng M (1993) *Proc Natl Acad Sci USA* 90:5345–5349
- Farrell N, Qu Y, Feng L, Van Houten B (1990) *Biochemistry* 29:9522–9531
- Keck MV, Lippard SJ (1992) *J Am Chem Soc* 114:3386–3390
- Prenzler PD, McFadyen WD (1997) *J Inorg Biochem* 68:279–282
- Zaludova R, Zakovska A, Kasparkova J, Balcarova Z, Kleinwachter V, Vrana O, Farrell N, Brabec V (1997) *Eur J Biochem* 246:508–517
- Kasparkova J, Novakova O, Vrana O, Farrell N, Brabec V (1999) *Biochemistry* 38:10997–11005
- Fichtinger-Schepman AMJ, Van der Veer JL, Den Hartog JHJ, Lohman PHM, Reedijk J (1985) *Biochemistry* 24:707–713
- Eastman A (1987) *Pharmacol Ther* 34:155–166
- Vrana O, Boudny V, Brabec V (1996) *Nucleic Acids Res* 24:3918–3925
- Bellon SF, Coleman JH, Lippard SJ (1991) *Biochemistry* 30:8026–8035
- Ushay HM, Santella RM, Caradonna JP, Grunberger D, Lippard SJ (1982) *Nucleic Acids Res* 10:3573–3588
- Perez-Martin JM, Requena JM, Craciunescu D, Lopez MC, Alonso C (1993) *J Biol Chem* 268:24774–24779
- Zaludova R, Natile G, Brabec V (1997) *Anti-Cancer Drug Des* 12:295–309
- McGregor TD, Balcarova Z, Qu Y, Tran MC, Zaludova R, Brabec V, Farrell N (1999) *J Inorg Biochem* 77:43–46
- Peticolas WL, Thomas GA (1985) In: Clementi E, Corongiu G, Sarma MH, Sarma RH (eds) *Structure and motion: membranes, nucleic acids and proteins*. Adenine, New York, pp 497–519
- Rahmouni A, Malinge JM, Schwartz A, Leng M (1985) *J Biomol Struct Dyn* 3:363–375
- Zaludova R, Kleinwachter V, Brabec V (1996) *Biophys Chem* 60:135–142
- Johnson NP, Butour J-L, Villani G, Wimmer FL, Defais M, Pierson V, Brabec V (1989) *Prog Clin Biochem Med* 10:1–24
- Zamble DB, Mu D, Reardon JT, Sancar A, Lippard SJ (1996) *Biochemistry* 35:10004–10013
- Jamieson ER, Lippard SJ (1999) *Chem Rev* 99:2467–2498
- Zamble DB, Lippard SJ (1999) In: Lippert B (ed) *Cisplatin. Chemistry and biochemistry of a leading anticancer drug*. Wiley-VCH, Zürich, pp 73–110

24.



Modification of Natural, Double-Helical DNA by Antitumor *cis*- and *trans*-[Cl₂(Me₂SO₄)₄Ru] in Cell-Free Media

Olga Nováková, Ctirad Hofr and Viktor Brabec*

INSTITUTE OF BIOPHYSICS, ACADEMY OF SCIENCES OF THE CZECH REPUBLIC, CZ-61265 BRNO, CZECH REPUBLIC

ABSTRACT. Modifications of natural DNA in cell-free media by the antitumor ruthenium compounds *cis*- and *trans*-[Cl₂(Me₂SO₄)₄Ru] were studied by various biochemical and biophysical methods. These methods included: binding studies by means of flameless atomic absorption spectrophotometry, mapping of DNA adducts by means of transcription assay, use of ethidium bromide as a fluorescent probe of DNA adducts of metal complexes, an interstrand cross-linking assay employing gel electrophoresis under denaturing conditions, measurements of DNA unwinding by gel electrophoresis, differential pulse polarographic analysis of DNA conformation, and analysis of liquid crystalline dispersions of DNA by circular dichroism. The results indicated that both ruthenium compounds irreversibly coordinated to DNA; the rate of binding of the *cis* isomer was considerably lower than that of the *trans* isomer. The DNA-binding mode of *trans*-[Cl₂(Me₂SO₄)₄Ru] included formation of bifunctional adducts such as intrastrand cross-links between neighboring purine residues and a small amount (~1%) of interstrand cross-links. *cis*-[Cl₂(Me₂SO₄)₄Ru] formed mainly monofunctional lesions on natural DNA. Both ruthenium isomers induced conformational alterations of non-denaturational character in DNA, the *trans* compound being more effective. In addition, DNA adducts of *trans*-[Cl₂(Me₂SO₄)₄Ru] were capable of inhibiting RNA synthesis by DNA-dependent RNA polymerases, while the adducts of the *cis* isomer were not. Thus, several features of the DNA-binding mode of *trans*-[Cl₂(Me₂SO₄)₄Ru] were similar to those of antitumor *cis*-diamminedichloroplatinum (II), which may be relevant to the biological effects of this antitumor ruthenium drug. On the other hand, the different DNA-binding mode of *cis*-[Cl₂(Me₂SO₄)₄Ru] was consistent with its less pronounced biological effects. *BIOCHEM PHARMACOL* 60;12:1761–1771, 2000. © 2000 Elsevier Science Inc.

KEY WORDS. DNA adducts; DNA conformation; transcription; antitumor; cross-link; liquid crystals

In recent years, metal-based antitumor drugs have played a relevant role in antineoplastic chemotherapy [1–4]. Cisplatin† in particular is regarded as one of the most effective anticancer drugs used in the clinic. In spite of the great efficacy of cisplatin against several human tumors, this drug displays limited activity against some of the most common tumors, such as colon and breast cancers [4, 5]. In addition, a variety of adverse effects and acquired resistance are observed in patients receiving cisplatin chemotherapy. The great success of cisplatin on the one hand and these limitations on the other have initiated efforts to develop new metal-based agents that will display improved therapeutic properties.

Broadening the spectrum of antitumor drugs depends on understanding existing agents, with a view toward developing new modes of attack. After the discovery of cisplatin, the new platinum antitumor drugs so far introduced in the clinic were *cis*-diammine-1,1-cyclobutanedicarboxylatoplatinum(II) (carboplatin) and (*trans*-*R,R*)1,2-diamminocyclohexanecarboxylatoplatinum(II) (oxaliplatin) [5–7]. Carboplatin and oxaliplatin differ from cisplatin only in the more inert leaving group. Hence, as these new compounds are direct structural analogues of cisplatin that exhibit reactivity qualitatively similar to that of cisplatin [8, 9], it is not surprising that they also induce similar biological consequences [5–7].

One approach in the search for new, metal-based anticancer agents that would exhibit antitumor activity markedly different from that of cisplatin and its direct analogues is to examine complexes that would contain another transition metal. Possible advantages in using transition metal ions other than platinum may involve additional coordination sites, alterations in ligand affinity and substitution kinetics, changes in oxidation state, and photodynamic approaches to therapy [3]. In the design of these new drugs, ruthenium complexes have raised great interest [1, 3, 10].

* Corresponding author: Dr. Viktor Brabec, Institute of Biophysics, Academy of Sciences of the Czech Republic, CZ-61265 Brno, Czech Republic. Tel. +420 5 415 17 148; FAX +420 5 412 11 293; E-mail: brabec@ibp.cz

† Abbreviations: cisplatin, *cis*-diamminedichloroplatinum(II); Me₂SO₄, dimethyl sulfoxide; [Cl(dien)Pt]Cl, chlorodiethylenetriamineplatinum(II) chloride; CT, calf thymus; EtBr, ethidium bromide; PEG, poly(ethyleneglycol); r_b, the number of molecules of the ruthenium compound bound per nucleotide residue; FAAS, flameless atomic absorption spectrophotometry; r_b, the molar ratio of free ruthenium complex to nucleotide phosphates at the onset of incubation with DNA; TE buffer, 10 mM Tris · HCl plus 1 mM EDTA, pH 7.2; and DPP, differential pulse polarography.

Received 21 February 2000; accepted 17 April 2000.

The antitumor activity of platinum and other metal-based drugs is frequently related to their binding to DNA [3, 11]. These drugs form adducts on DNA that block DNA and RNA synthesis and induce programmed cell death. Thus, intracellular interactions with these adducts are likely to be of importance in explaining their biological activity or at least some of its features. Dimethyl sulfoxide complexes of both Ru^{II} and Ru^{III} constitute a relatively new group of anticancer compounds [3, 12, 13]. For instance, these complexes exhibit antitumor activity comparable to cisplatin at equitoxic dosage in animal models of metastasizing tumors, but with less severe side effects and prolonged host survival times [12, 14, 15]. In addition, these ruthenium compounds inhibit DNA replication, exhibit mutagenic activity, and induce the SOS repair mechanisms, which is consistent with the DNA binding of these compounds *in vivo* [16, 17].

A small series of complexes whose parent compounds are *cis*- and *trans*-[Cl₂(Me₂SO₄)₄Ru] constitute one class of dimethyl sulfoxide Ru^{II} compounds. The examination of their effect on primary tumor and on metastasis development has revealed antimetastatic activities superior to the effects on primary tumor growth [12, 14, 18]. The initial studies were performed with *cis*-[Cl₂(Me₂SO₄)₄Ru] because of its similarity to cisplatin [19]. However, the comparisons between the antitumor effects of *cis*- and *trans*-[Cl₂(Me₂SO₄)₄Ru] revealed the superiority of the latter [15]. *cis*- and *trans*-[Cl₂(Me₂SO₄)₄Ru] contain two chlorides in the octahedral structure [14, 20]. In *cis*-[Cl₂(Me₂SO₄)₄Ru], the three Me₂SO₄ molecules are S-bound in a facial configuration and the fourth is O-bonded. In *trans*-[Cl₂(Me₂SO₄)₄Ru] all the Me₂SO₄s are S-bound. When dissolved in water, the *cis* isomer immediately undergoes loss of the O-bonded dimethyl sulfoxide ligand, whereas the *trans* compound rapidly loses two yielding *cis*-diaqua species. Both hydrolyzed isomers then undergo slow reversible chloride dissociation, forming cationic compounds. After this step, the *trans* compound contains three reactive groups, the *cis* isomer only two [14, 20]. In addition, the three remaining Me₂SO₄ ligands in the *cis* isomer represent a considerable steric hindrance, which makes the *cis*-aqua species relatively inert in contrast to the *trans* isomer. Importantly, this difference correlates with a higher potency of the *trans* isomer to act as the antitumor agent [21].

Both *cis*- and *trans*-[Cl₂(Me₂SO₄)₄Ru] bind to DNA in cell-free media [14, 21]. Whereas DNA modifications by platinum antitumor drugs have been studied systematically and described in detail [22], the modifications of high-molecular-mass natural DNA by *cis*- and *trans*-[Cl₂(Me₂SO₄)₄Ru] have been much less explored [3]. Some early studies based on the analysis of circular dichroism (CD) spectra of DNA suggested that coordination of the *cis* isomer to DNA does not significantly alter the conformation of B-DNA [14, 23]. The *trans* isomer binds to DNA more rapidly, with some changes in the CD spectra indicating conformational alterations [14]. Studies of the inter-

actions of both isomers with monomeric constituents of nucleic acids and very short single-stranded oligonucleotides (di- and tetranucleotides) have revealed that both isomers may have some preference for bifunctional binding to neighboring guanine residues at their N7 atoms, with the *trans* isomer being more effective [24–27]. This suggestion has been indirectly corroborated by the restriction enzyme analysis of plasmid DNA modified by these ruthenium compounds [21]. These studies showed that DNA modified by *trans*-[Cl₂(Me₂SO₄)₄Ru] was protected most effectively from cutting by *Bam*HI restriction endonuclease, which contains two neighboring guanine residues in its recognition sequence.

In order to address further fundamental questions about the DNA-binding modes of ruthenium antitumor compounds containing Me₂SO₄ ligands, the experiments described in the present paper were carried out. More specifically, the interactions of polymeric natural DNAs with *cis*- and *trans*-[Cl₂(Me₂SO₄)₄Ru] in cell-free media were investigated by various methods of molecular biophysics, the aim being to contribute to the understanding of the differences in the biological effects of these isomers.

MATERIALS AND METHODS

Starting Materials

cis- and *trans*-[Cl₂(Me₂SO₄)₄Ru] were synthesized, recrystallized, and characterized as previously reported [20]. Cisplatin and [Cl(dien)Pt]Cl were synthesized and characterized in Lachema. Stock solutions of the ruthenium and platinum complexes (5×10^{-4} M in 10 mM NaClO₄) were prepared in the dark at 25°. CT DNA (42% G + C, mean molecular mass *ca.* 20,000 kDa) was also prepared and characterized as described previously [28, 29]. CT DNA used for the formation of liquid crystalline dispersions was depolymerized by ultrasound, so that its average molecular mass was ~500 kDa (determined by agarose gel electrophoresis). Plasmids pSP73 (2464 bp) and pSP73KB (2455 bp [30]) were isolated according to standard procedures and banded twice in CsCl/EtBr equilibrium density gradients. Restriction endonucleases were purchased from New England Biolabs. Klenow fragment of DNA polymerase I was from Boehringer Mannheim Biochemica. Riboprobe Gemini System II for transcription mapping containing T7 and SP6 RNA polymerase was purchased from Promega. EtBr and agarose were from Merck KgaA. PEG (molecular mass 4600 kDa) was purchased from Sigma. The radioactive products were from Amersham.

Metallation Reactions

CT or plasmid DNAs were incubated with the ruthenium or platinum complex in 10 mM NaClO₄ at 37° in the dark if not stated otherwise. After 48 hr, the samples of plasmid DNA were precipitated by ethanol and redissolved in the medium required for subsequent biochemical or biophysical analysis, whereas the samples of CT DNA were exhaus-

tively dialyzed against such a medium. An aliquot of these samples was used to determine the r_b value by FAAS.

The dependencies of the r_b values on time for the ruthenium complexes tested in the present work were obtained in the following way. Solutions of CT DNA at the concentration of ca. 0.1 mg/mL were incubated with the ruthenium complex at an r_i value of 0.1. At the various time intervals, aliquots were withdrawn and the reaction was stopped by adding 1/10 of a volume of 1.5 M NaCl, including quick cooling to -20° . DNA was then precipitated by ethanol. The amount of the free ruthenium complexes (not bound to DNA) in supernatant was determined by FAAS. The amount of ruthenium bound to DNA (r_b) was calculated by subtracting the amount of ruthenium remaining in solution (determined by FAAS) from the total amount of ruthenium present in the reaction.

DNA Transcription by RNA Polymerase In Vitro

Transcription of the (*NdeI/HpaI*) restriction fragment of pSP73KB DNA with DNA-dependent T7 and SP6 RNA polymerases and electrophoretic analysis of the transcripts were performed according to the protocols recommended by Promega (Promega Protocols and Applications, 43–46 [1989/90]) and previously described in detail [30, 31].

Interstrand Cross-Link Assay

If not stated otherwise, *cis*- and *trans*-[Cl₂(Me₂SO₄)₄Ru] at varying concentrations were incubated with 2 μ g of pSP73 DNA either in negatively supercoiled form or after it had been linearized by *EcoRI*. The modified samples were precipitated by ethanol, and the circular DNA already modified by ruthenium complex was subsequently linearized by *EcoRI*. The linear duplexes were then analyzed for DNA interstrand cross-links in the same manner as described in several recent papers [31, 32]. The linear duplexes were first 3'-end labeled by means of Klenow fragment of DNA polymerase I and [α -³²P]dATP. The samples were deproteinized by phenol, precipitated by ethanol, and the pellet dissolved in 18 μ L of 30 mM NaOH with 1 mM EDTA, 6.6% sucrose, and 0.04% bromophenol blue. The amount of interstrand cross-links was analyzed by electrophoresis under denaturing conditions on alkaline agarose gel (1%). After the electrophoresis was completed, the intensities of the bands corresponding to single strands of DNA and interstrand cross-linked duplex were quantified by means of a Molecular Dynamics PhosphorImager (Storm 860 system with ImageQuant software). The frequency of interstrand cross-links, F (the number of interstrand cross-links per adduct), was calculated as $F =$

$\frac{XL}{4928 \cdot r_b}$ (pSP73 plasmid contained 4928 nucleotide residues). XL is the number of interstrand cross-links per one molecule of the linearized DNA duplex which was calculated assuming Poisson distribution of the interstrand cross-

links as $XL = -\ln A$, where A is the fraction of molecules running as a band corresponding to the non-cross-linked DNA [32].

Fluorescence Measurements

Fluorescence measurements of DNA modified by ruthenium complexes in the presence of EtBr were performed at an excitation wavelength of 546 nm, and the emitted fluorescence was analyzed at 590 nm. The fluorescence intensity was measured at 25° in 0.4 M NaCl to avoid secondary binding of EtBr to DNA [33, 34]. The concentrations were 0.01 mg/mL for DNA and 0.04 mg/mL for EtBr, which corresponded to the saturation of all intercalation sites of EtBr in DNA [33, 34]. These measurements were performed on a Shimadzu RF 40 spectrofluorophotometer using a 1-cm quartz cell.

Differential Pulse Polarography

DPP curves of DNA were measured after non-modified DNA or DNA modified by the ruthenium complex was redissolved in the medium of 0.3 M ammonium formate plus 0.05 M phosphate (Na₂HPO₄/NaH₂PO₄) buffer, pH 6.8 [35]. DPP curves were recorded with the aid of an EG&C PARC Electrochemical Analyzer, Model 384B at 25° using the following apparatus settings: voltage scan rate 2 mV/sec, pulse amplitude of 5 mV, drop time of 1.0 sec. The potentials are against the saturated calomel reference electrode.

Unwinding of Negatively Supercoiled DNA

Unwinding of closed circular supercoiled pSP73 plasmid DNA was assayed by an agarose gel mobility shift assay [36]. The unwinding angle Φ , induced per platinum–DNA adduct, was calculated upon the determination of the r_b value at which the complete transformation of the supercoiled to relaxed form of the plasmid was attained. Samples of pSP73 plasmid were incubated with *cis*- or *trans*-[Cl₂(Me₂SO₄)₄Ru] for 48 hr, precipitated by ethanol, and redissolved in TAE buffer (0.04 M Tris–acetate + 1 mM EDTA, pH 7.0). An aliquot of the precipitated sample was subjected to electrophoresis on 1% agarose gels running at 25° in the dark with TAE buffer with a voltage set at 30 V. The gels were then stained with EtBr, followed by photography on Polaroid 667 film with transilluminator. The other aliquot was used for the determination of r_b values by FAAS.

Liquid Crystalline Dispersions of DNA

Liquid crystalline dispersions of DNA modified by the metal complexes were formed by mixing DNA and PEG solutions as described earlier [37, 38]. Briefly, 1 mL of non-modified DNA or DNA modified by the metal complex dissolved in 0.01 M NaClO₄ at the concentration of

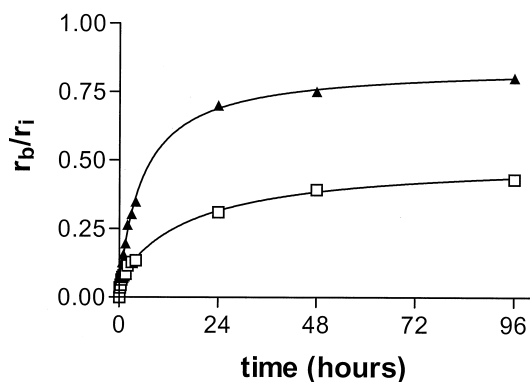


FIG. 1. Kinetics of the binding of *cis*- $[\text{Cl}_2(\text{Me}_2\text{SO}_4)_4\text{Ru}]$ (□) and *trans*- $[\text{Cl}_2(\text{Me}_2\text{SO}_4)_4\text{Ru}]$ (▲) to CT DNA. Medium: 10 mM NaClO_4 at 37° . The binding was determined by FAAS after precipitation by ethanol. The concentration of DNA was 0.1 mg/mL, $r_i = 0.1$. Data measured in triplicate varied on average $\pm 3\%$ from their mean. For other details, see the text.

0.06 mg/mL was mixed vigorously with 3 mL PEG at the concentration of 200 mg/mL (also dissolved in 0.3 M NaClO_4) for 1 hr.

Other Methods

Absorption spectra were measured with a Beckmann DU-8 spectrophotometer. FAAS measurements were carried out on a Unicam 939 AA spectrometer with a graphite furnace. For FAAS analysis, DNA was precipitated with ethanol and dissolved in 0.1 M HCl. CD spectra were recorded at 25° using a JASCO spectropolarimeter, Model J720.

RESULTS

DNA Binding

Solutions of double-helical CT DNA at a concentration of 0.1 mg/mL were incubated with *cis*- and *trans*- $[\text{Cl}_2(\text{Me}_2\text{SO}_4)_4\text{Ru}]$ at r_i values of 0.1 at 37° in three media: 10 mM NaClO_4 , TE buffer, or 1 mM phosphate buffer ($\text{NaH}_2\text{PO}_4/\text{Na}_2\text{HPO}_4$, pH 7.0). At various time intervals, an aliquot of the reaction mixture was withdrawn; the reaction was then terminated by adjusting NaCl concentration to 0.15 M followed by quick cooling to -20° and precipitating DNA by ethanol. The supernatant was assayed by FAAS for the amount of free ruthenium not bound to DNA. The amount of ruthenium bound to DNA, r_b , was calculated by subtracting the amount of ruthenium remaining in solution from the total amount of ruthenium present in the reaction. Figure 1 shows a plot of r_b against the time of DNA incubation with *cis*- or *trans*- $[\text{Cl}_2(\text{Me}_2\text{SO}_4)_4\text{Ru}]$ in 10 mM NaClO_4 . The amount of ruthenium coordinated to DNA increased with time. After 48 hr, the binding reached its maximum values, which corresponded to approximately 40 or 75% of the molecules of *cis*- or *trans*- $[\text{Cl}_2(\text{Me}_2\text{SO}_4)_4\text{Ru}]$, respectively, present in the reaction mixtures. Importantly, both ruthenium compounds reacted with DNA at a similar rate, with r_i values in the

range of 0.001–0.1. Thus, the rate of binding to natural polymeric DNA of both ruthenium compounds tested in the present work was lower than that of cisplatin [39]. These results also confirmed that DNA binding of the *cis*- $[\text{Cl}_2(\text{Me}_2\text{SO}_4)_4\text{Ru}]$ is considerably less effective than that of its *trans* isomer.

The binding studies described above were performed in the medium of 10 mM NaClO_4 , which is used as a standard medium if DNA interactions of antitumor platinum complexes are investigated in cell-free media. For comparative purposes, the binding of the two ruthenium compounds to DNA was also investigated in TE or phosphate buffers, i.e. in the media used in some previous studies of DNA modifications by ruthenium complexes. The components of these buffers are potential ligands of transition metal complexes that compete with DNA for metal [40]. This fact can significantly affect the rate of the binding of ruthenium complexes to DNA. DNA binding of *trans*- $[\text{Cl}_2(\text{Me}_2\text{SO}_4)_4\text{Ru}]$ measured after 24 hr in TE or phosphate buffers was decreased from 70% in 10 mM NaClO_4 to 20 or 50%, respectively. Similarly, DNA binding of the *cis* isomer under the same experimental conditions was decreased from 30% to 5 or 10%, respectively. Identical results were obtained when the binding of both isomers was measured in the media containing TE or phosphate buffers at ten times lower concentrations. On the other hand, if DNA was first modified by *cis*- or *trans*- $[\text{Cl}_2(\text{Me}_2\text{SO}_4)_4\text{Ru}]$ in 10 mM NaClO_4 to an r_b value in the range of 0.001–0.05, the level of the modification (r_b) remained unchanged even after DNA modified by ruthenium complex was transferred into the media in which their rate of DNA binding is noticeably decreased (*vide supra*). This observation was also consistent with the results of the following experiment. CT DNA modified by the ruthenium complex in 10 mM NaClO_4 was precipitated by ethanol, redissolved in the medium of TE or phosphate buffer (containing no ruthenium complex), further incubated at 37° for an additional 48 hr, again precipitated by ethanol, and the content of ruthenium in these samples (r_b) determined by FAAS. No changes in r_b values were noticed.

The binding experiments of the present work indicate that modification reactions resulted in the irreversible coordination of molecules of the ruthenium complexes to polymeric double-helical DNA. In addition, these results made it possible to prepare easily and precisely the samples of DNA modified by the ruthenium complexes at a preselected value of r_b . Importantly, it is also reasonable to assume that the levels of DNA modifications by the ruthenium complexes reached in 10 mM NaClO_4 remained unchanged after the sample of DNA modified by the ruthenium complex was transferred into the medium required for subsequent biophysical or biochemical analyses. Thus, the samples of DNA modified by the ruthenium complexes and analyzed further by biophysical or biochemical methods were prepared in 10 mM NaClO_4 at 37° . After 48 hr of the reaction of DNA with the complex, the samples were precipitated in ethanol, dissolved in the

medium necessary for a particular analysis, and the r_b value in an aliquot of this sample checked by FAAS. In this way, the analyses described in the present paper were performed in the absence of unbound (free) ruthenium complex.

Transcription Mapping of DNA Adducts

In vitro RNA synthesis by RNA polymerases on DNA templates containing several types of bifunctional adducts of metal complexes can be prematurely terminated at the level or in the proximity of adducts [30, 31, 41, 42]. Importantly, monofunctional DNA adducts of several platinum complexes are unable to terminate RNA synthesis.

Cutting of pSP73KB DNA [30, 31] by *NdeI* and *HpaI* restriction endonucleases yielded a 212-bp fragment (a substantial part of its nucleotide sequence is shown in Fig. 2B). This fragment contained convergent T7 and SP6 RNA polymerase promoters (in the upper and lower strands, respectively, close to its 3'-ends [Fig. 2B]). The experiments were carried out using this linear DNA fragment, modified by *cis*-[Cl₂(Me₂SO₄)₄Ru], its *trans* isomer, or cisplatin at $r_b = 0.01$, for RNA synthesis by T7 and SP6 RNA polymerases (Fig. 2A, lanes *cisRu*, *transRu*, or *cisPt*, respectively). RNA synthesis on the template modified by *trans*-[Cl₂(Me₂SO₄)₄Ru] or cisplatin yielded fragments of defined sizes (Fig. 2A, lanes *transRu* and *cisPt*), which indicates that RNA synthesis on these templates was prematurely terminated. The major stop sites produced by *trans*-[Cl₂(Me₂SO₄)₄Ru] were identical to those produced by cisplatin, i.e. mainly appearing at G sites and to a considerably lesser extent at A sites. These G and A sites were mostly contained in GG or AG sites, which are preferential DNA-binding sites of cisplatin. Interestingly, the bands produced by the *trans* ruthenium complex had a lower intensity than those yielded by cisplatin, which suggests that *trans*-[Cl₂(Me₂SO₄)₄Ru] also produces DNA adducts incapable of terminating RNA synthesis and that the amount of these DNA adducts (presumably monofunctional lesions) was considerably higher than that formed in the case of cisplatin. Taken together, the results of these mapping experiments suggest that *trans*-[Cl₂(Me₂SO₄)₄Ru] can also form, on double-helical DNA, an amount of bidentate adducts similar to DNA cross-links formed by cisplatin.

DNA adducts of *cis*-[Cl₂(Me₂SO₄)₄Ru] produced only faint bands corresponding to stop sites (Fig. 2A, lane *cisRu*). This observation is consistent with capability of *cis*-[Cl₂(Me₂SO₄)₄Ru] to form a considerably smaller amount of adducts on DNA that would be similar to those formed by *trans*-[Cl₂(Me₂SO₄)₄Ru] or cisplatin.

Characterization of DNA Adducts by EtBr Fluorescence

EtBr as a fluorescent probe has been used to characterize perturbations induced in DNA by adducts of several platinum compounds [33, 43–45]. Double-helical CT DNA was modified by cisplatin, monofunctional [Cl(dien)Pt]Cl, and

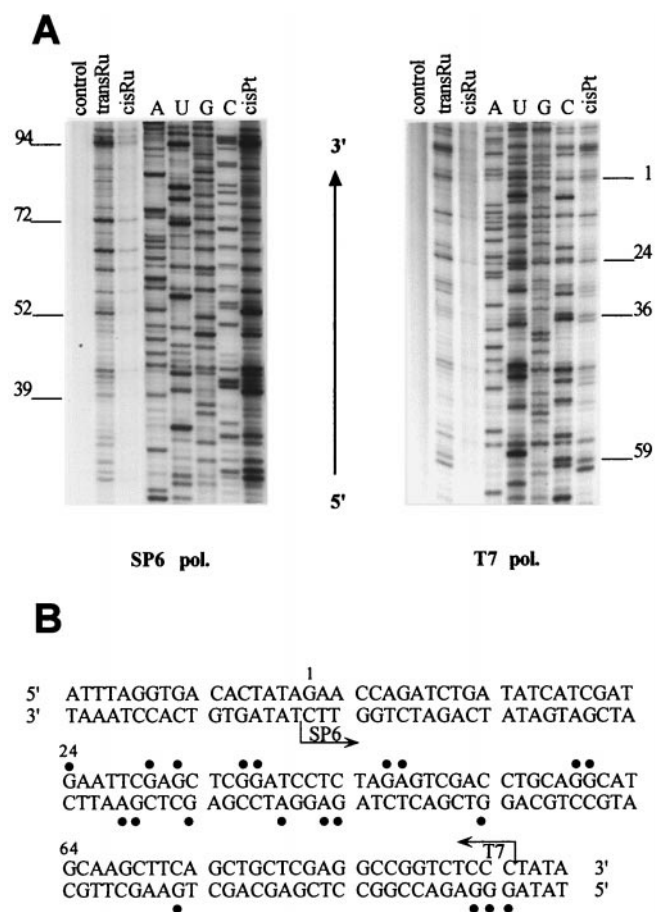


FIG. 2. Inhibition of RNA synthesis by SP6 (left) and T7 (right) RNA polymerases on the *NdeI/HpaI* fragment of pSP73KB plasmid modified by ruthenium and platinum complexes. (A) Autoradiograms of 6% polyacrylamide/8 M urea sequencing gels. Lanes: control, non-modified template; *cisPt*, *cisRu*, and *transRu*, the templates modified by cisplatin, *cis*-[Cl₂(Me₂SO₄)₄Ru], and *trans*-[Cl₂(Me₂SO₄)₄Ru] at $r_b = 0.01$, respectively. (B) Schematic diagram showing the portion of the nucleotide sequence of the template (upper) strand of the *NdeI/HpaI* fragment used to monitor inhibition of RNA synthesis by *trans*-[Cl₂(Me₂SO₄)₄Ru]. The arrows indicate the start of the T7 or SP6 RNA polymerases. (●), major stop signals (from Fig. 2A, lanes *transRu*). The numbers correspond to the nucleotide numbering in the sequence map of pSP73KB plasmid.

cis- or *trans*-[Cl₂(Me₂SO₄)₄Ru]. The levels of the modification corresponded to the values of r_b in the range of 0–0.1. Modification of DNA by all-metal complexes resulted in a decrease in EtBr fluorescence as compared with the control DNA–EtBr complex (Fig. 3). The decrease caused by the adducts of *trans*-[Cl₂(Me₂SO₄)₄Ru] complexes was similar to that induced by the DNA adducts of cisplatin at equivalent r_b albeit somewhat smaller. On the other hand, modification of DNA by *cis*-[Cl₂(Me₂SO₄)₄Ru] resulted in a pronouncedly smaller decrease in EtBr fluorescence as compared with that due to the modification by *trans*-[Cl₂(Me₂SO₄)₄Ru] or cisplatin, but one that was still larger than that due to the modification by monofunctional [Cl(dien)Pt]Cl.

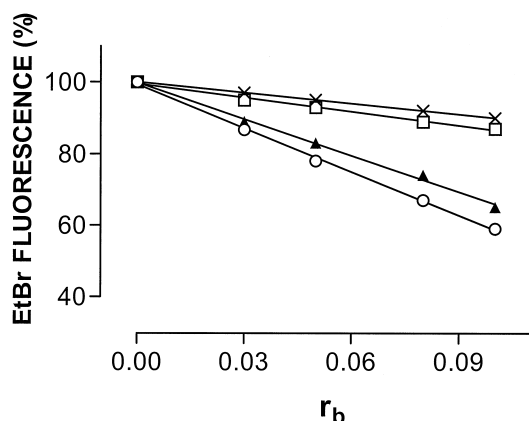


FIG. 3. Dependencies of ethidium bromide fluorescence on r_b for CT DNA modified by various metal complexes in 10 mM NaClO₄ at 37° for 48 hr. [Cl(dien)Pt]Cl (x), cisplatin (○), *cis*-[Cl₂(Me₂SO₄)₄Ru] (□), and *trans*-[Cl₂(Me₂SO₄)₄Ru] (▲). Data measured in triplicate varied on average $\pm 2\%$ from their mean.

Interstrand Cross-linking

Transcription mapping experiments and EtBr fluorescence analysis (Figs. 2 and 3) were consistent with the capability of ruthenium complexes to form on polymeric DNA bidentate adducts, but these studies could not distinguish whether these adducts were intrastrand or interstrand cross-links. Therefore, further experiments were carried out to compare the amounts of the interstrand cross-links formed by *cis*- or *trans*-[Cl₂(Me₂SO₄)₄Ru] in negatively supercoiled or linear DNA. In these experiments, we used pSP73 plasmid (2464 bp, native supercoil density $\sigma = -0.063$), which was modified by *cis*- or *trans*-[Cl₂(Me₂SO₄)₄Ru] complexes in two ways. One series of samples was prepared by modifying the plasmid only after it had been linearized by *Eco*RI (*Eco*RI cuts only once within pSP73 plasmid). The samples of the other series were prepared by a modification of the supercoiled plasmid by ruthenium complexes, and only after the modification reaction was completed was the plasmid linearized by *Eco*RI. Thus, we prepared two types of linear DNA molecules of the same length and nucleotide sequence modified by ruthenium complexes, which could be differently affected by this drug if different DNA topology were to play a role during the modification reaction. The two samples were analyzed for interstrand cross-links by agarose gel electrophoresis under denaturing conditions in an attempt to reveal these differences. It was also verified by FAAS whether the amount of ruthenium complexes coordinated to the base residues in DNA was independent of DNA topology during the modification reaction over a broad range of r_i values (0.001–0.1) and at any reaction time.

An electrophoretic method for precise and quantitative determination of interstrand cross-linking by metal complexes in DNA has been described previously [31, 32]. Upon electrophoresis under denaturing conditions, 3'-end labeled strands of linearized pSP73 plasmid containing no

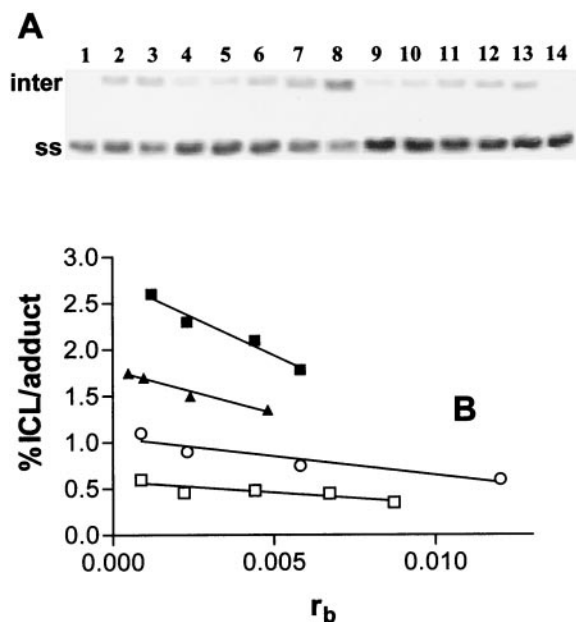


FIG. 4. The formation of interstrand cross-links by ruthenium complexes in negatively supercoiled and linearized pSP73 plasmid. (A) Autoradiogram of a denaturing 1% agarose gel of linearized DNA which was 3'-end labeled; the interstrand cross-linked DNA appears as the top bands migrating on the gels more slowly than the single-stranded (ss) DNA (contained in the bottom bands). The plasmid linearized by *Eco*RI was incubated with cisplatin (lanes 2 and 3), *trans*-[Cl₂(Me₂SO₄)₄Ru] (lanes 4–8), or *cis*-[Cl₂(Me₂SO₄)₄Ru] (lanes 9–13) for 48 hr at 37°; r_b values: 0 (control, non-modified DNA), lanes 1 and 14; 0.0005, lane 2; 0.001, lane 3; 0.0048, lane 4; 0.00096, lane 5; 0.0024, lane 6; 0.0048, lane 7; 0.0096, lane 8; 0.00087, lane 9; 0.0022, lane 10; 0.0044, lane 11; 0.0067, lane 12; 0.0087, lane 13. (B) Dependence on r_b of the percentage of interstrand cross-links (ICL) per adduct (interstrand cross-linking [%]) formed by *cis*-[Cl₂(Me₂SO₄)₄Ru] (▲, □) or *trans*-[Cl₂(Me₂SO₄)₄Ru] (■, ○) in supercoiled (closed symbols) or linearized (open symbols) DNA within 48 hr. Data measured in triplicate varied on average $\pm 3\%$ from their mean.

interstrand cross-links migrate as a 2464-nucleotide single strand, whereas the interstrand cross-linked strands migrate more slowly as a higher-molecular-mass species. The bands corresponding to more slowly migrating interstrand cross-linked fragments were observed if the *trans*-[Cl₂(Me₂SO₄)₄Ru] complex was used to modify DNA in both linearized and supercoiled forms at r_b as low as 5×10^{-3} (Fig. 4A). The intensity of the more slowly migrating band increased with the growing level of the modification. The radioactivity associated with the individual bands in each lane was measured to obtain estimates of the fraction of non-cross-linked or cross-linked DNA under each condition. The frequency of interstrand cross-links (the amount of interstrand cross-links per one molecule of *trans*-[Cl₂(Me₂SO₄)₄Ru] complex coordinated to DNA) was calculated using the Poisson distribution in combination with the r_b values and the fragment size [32] (for more details, see Materials and Methods).

As summarized in Fig. 4B, *trans*-[Cl₂(Me₂SO₄)₄Ru]

showed a relatively low interstrand cross-linking efficiency in both linear and negatively supercoiled DNA, i.e. approximately 6 times less than formed by cisplatin under identical conditions [31, 46]. Importantly, *cis*-[Cl₂(Me₂SO₄)₄Ru] forms an even smaller amount of interstrand cross-links (roughly half), which is consistent with a tendency of the *cis* isomer to preferentially form on double-helical DNA monofunctional adducts. These results indicate that the interstrand cross-links are only highly minor adducts in double-helical DNA modified by [Cl₂(Me₂SO₄)₄Ru] complexes.

Differential Pulse Polarography

DPP analysis readily and with great sensitivity distinguishes between non-denaturational and denaturational conformational alterations induced in DNA by various physical or chemical agents [47, 48]. This analysis is based on the observation that intact double-helical DNA is polarographically inactive, because its reduction sites are involved in hydrogen bonds and are unable to make contact with the working electrode in a manner suitable for electron transfer. Electroreduction of adenine or cytosine residues present in distorted but still double-stranded (non-denatured) regions of DNA is responsible for the appearance of the small DPP peak II (Fig. 5A, curve 1). Base residues in these distorted regions become more accessible for electroreduction at the mercury electrode and can yield a small polarographic current. On the other hand, the appearance of a more negative peak III on DPP curves of DNA indicates the presence of single-stranded, denatured regions in the DNA molecule, in which hydrogen bonds between complementary bases have been broken [47, 48]. Differences in the adsorption properties of double-helical and denatured DNA at the mercury electrode have been suggested to give rise to the different reduction potentials that are observed for the two DNA conformations. Importantly, less than 1% denatured material in the excess of double-helical DNA can be determined by DPP [49].

DPP has already been used to analyze DNA modified by various physical or chemical agents, including platinum compounds with different clinical efficacy [50, 51]. It has been found that DNA globally modified by antitumor cisplatin or its analogues at r_b values up to 0.05 yields the DPP peak II, indicating that these antitumor drugs induce non-denaturational conformational changes in DNA [32, 35]. In contrast, the more negative DPP peak III is observed on DPP curves of DNA globally modified by clinically ineffective transplatin and other inactive platinum(II) complexes, indicating that the clinically ineffective platinum complexes induce denaturational conformational alterations in DNA [50, 51].

DPP analysis also sheds considerable light on the conformational basis for DNA binding of *cis*- or *trans*-[Cl₂(Me₂SO₄)₄Ru]. The modification of CT DNA by these ruthenium complexes at r_b of 0.005–0.02 resulted in an increase in DPP peak II with a growing level of modifica-

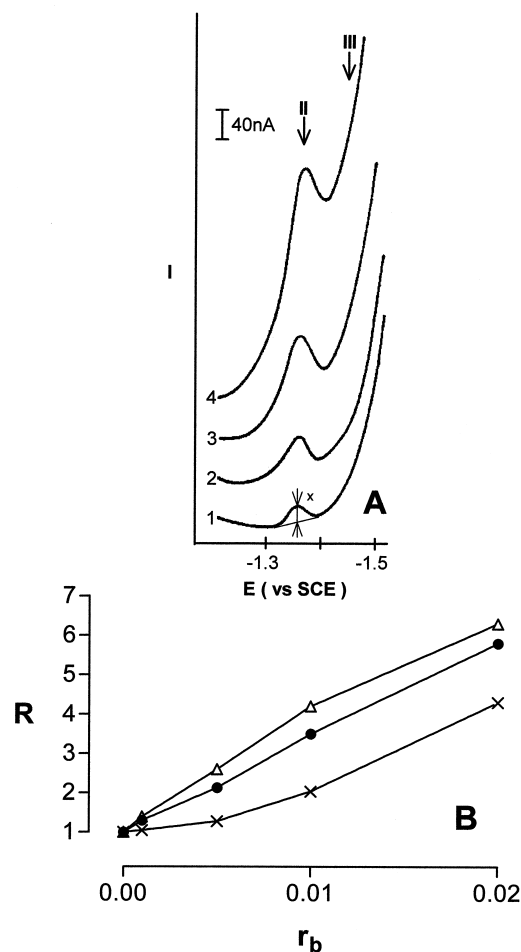


FIG. 5. Differential pulse polarographic analysis of CT DNA modified by ruthenium complexes. DNA at a concentration of 0.4 mg/mL in 0.3 M ammonium formate with 0.01 M phosphate buffer, pH 6.8. (A) DPP curves; DNA modified by *trans*-[Cl₂(Me₂SO₄)₄Ru]; r_b values: 0 (control, non-modified DNA), curve 1; 0.005, curve 2; 0.01, curve 3; and 0.02, curve 4. The arrows in Fig. 5A marked by II and III indicate potentials E (against saturated calomel electrode [SCE]) at which native or denatured DNA samples yielded DPP peaks II or III, respectively (see the text). The way in which the height of the DPP peak (x) was measured in the present work is shown in Fig. 5A, curve 1. (B) Dependence of the relative height of DPP peak II, R , yielded by DNA modified by the ruthenium complexes on r_b : (x—x), *cis*-[Cl₂(Me₂SO₄)₄Ru]; (●—●), *trans*-[Cl₂(Me₂SO₄)₄Ru]; and (△—△), cisplatin. The value of R was calculated as the ratio of the peak height yielded by the modified DNA over the peak height yielded by the control (non-modified) DNA.

tion (shown for the *trans* isomer in Fig. 5A). The more negative peak III was not detected even on the DPP curves recorded for DNA modified at the highest r_b value used in our experiments (0.02). It could be argued that the absence of peak III on the DPP curves recorded for the samples of DNA modified at relatively high r_b values (~ 0.02) could be due to an increase in the slope of the part of the DPP curve corresponding to the background electrolyte discharge (Fig. 5A, curve 4). The observation that peak III was not buried under the background electrolyte discharge curve was



FIG. 6. Unwinding of negatively supercoiled pSP73 plasmid DNA by ruthenium complexes. The plasmid was incubated with *trans*-[Cl₂(Me₂SO₄)₄Ru] for 48 hr at 37° and precipitated by ethanol. r_b values: 0 (control, non-modified DNA), lanes 1 and 15; 0.06, lane 2; 0.07, lane 3; 0.08, lane 4; 0.09, lane 5; 0.1, lane 6; 0.11, lane 7; 0.12, lane 8; 0.13, lane 9; 0.14, lane 10; 0.15, lane 11; 0.16, lane 12; 0.2, lane 13; and 0.26, lane 14. The top bands (oc) correspond to the form of nicked plasmid and the bottom bands (sc) to the closed, negatively supercoiled plasmid.

verified using the sample of DNA modified by *cis*- or *trans*-[Cl₂(Me₂SO₄)₄Ru] at $r_b = 0.02$ to which 0.8% thermally denatured CT DNA was added. This sample yielded a small, more negative peak III on the DDP curve (recorded under conditions specified for curve 4 in Fig. 5A) (not shown). Thus, the absence of the peak III on the DPP curves of DNA modified by *cis*- or *trans*-[Cl₂(Me₂SO₄)₄Ru] suggests that these ruthenium complexes, as with antitumor cisplatin and other antitumor analogues of this drug, induce non-denaturational conformational distortions in DNA at relatively low levels of the global modification ($r_b \leq 0.02$). The DNA-binding mode of *cis*- or *trans*-[Cl₂(Me₂SO₄)₄Ru] is also in profound contrast to the modification of DNA by clinically ineffective transplatin [50, 51]. In addition, the relative increase in peak II due to the global modification by *cis*-[Cl₂(Me₂SO₄)₄Ru] was considerably smaller at the same level of DNA modification (r_b) (Fig. 5B) than the increase in peak II due to the modification by *trans*-[Cl₂(Me₂SO₄)₄Ru]. This finding supports the view that non-denaturational distortions of DNA due to the global binding of *trans*-[Cl₂(Me₂SO₄)₄Ru] are more extensive than those due to the binding of *cis*-[Cl₂(Me₂SO₄)₄Ru].

Unwinding

Electrophoresis in native agarose gel was used to quantify the unwinding induced in pSP73 plasmid by the ruthenium complexes by monitoring the degree of supercoiling (Fig. 6). A compound that unwinds DNA duplex reduces the number of supercoils in closed, negatively supercoiled DNA so that the negative superhelical density of closed circular DNA decreases. This decrease upon binding of unwinding agents causes a decrease in the rate of migration through agarose gel, which makes it possible for the unwinding to be observed and quantified [36]. Figure 6 shows an electrophoresis gel in which increasing amounts of *trans*-[Cl₂(Me₂SO₄)₄Ru] were bound to a mixture of relaxed and negatively supercoiled pSP73 DNA. Interestingly, *trans*-[Cl₂(Me₂SO₄)₄Ru] accelerated the mobility of the relaxed form in a similar fashion to cisplatin, whose bifunctional binding to DNA shortens and condenses the DNA helix [52, 53]. In contrast, *cis*-[Cl₂(Me₂SO₄)₄Ru] affected the mobility of the relaxed form markedly less (not shown), implying that its binding results in shortening or conden-

sation of DNA to a very small extent. The unwinding angle is given by $\Phi = 18 \sigma / r_b(c)$, where σ is the superhelical density and $r_b(c)$ is the value of r_b at which the supercoiled and relaxed forms co-migrate [36]. Under the present experimental conditions, σ was calculated to be -0.063 on the basis of the data for cisplatin, for which the $r_b(c)$ was determined in this study and $\Phi = 13^\circ$ was assumed. Using this approach, the DNA unwinding angle of $7 \pm 1^\circ$ was determined for *trans*-[Cl₂(Me₂SO₄)₄Ru]. On the contrary, the co-migration of the relaxed and negatively supercoiled DNAs was not observed even at such a high level of modification by *cis*-[Cl₂(Me₂SO₄)₄Ru] as is that corresponding to the r_b value of 0.25, indicating a negligible efficiency of the *cis* isomer to unwind DNA.

Liquid Crystals

The cholesteric liquid crystalline dispersions of DNA, which can simulate the principal properties of DNA molecules within cells, such as their spatial ordering in condensed and packed state, have been used as model systems *in vivo* [38, 54]. This model system was used in the present work to provide information on the possible consequences of the binding of *cis*- or *trans*-[Cl₂(Me₂SO₄)₄Ru] on the formation and stability of the condensed DNA. In the presence of PEG water-containing salt solutions, linear double-stranded DNA is condensed, forming helically twisted liquid crystalline dispersions of DNA molecules (the left-handed helicoidal structure of cholesteric phase from the right-handed DNA molecules). The peculiar properties of this phase caused by anisotropic orientations can be analyzed by measuring CD spectra. The occurrence of the cholesteric liquid crystalline form of DNA is accompanied by the origin of the intense negative CD band at ca. 275 nm (Fig. 7) [55–57]. The decrease in the amplitude of this band in the CD spectra of liquid crystalline dispersions of DNA modified by antitumor platinum complexes is associated with the disappearance of the helical twist of the liquid crystalline microphase due to alterations of DNA secondary structure, such as disturbances in the stacking interactions of bases [37, 55, 58]. Interestingly, clinically ineffective platinum complexes, such as *trans* isomer of cisplatin or monofunctional platinum(II) compounds, only negligibly or weakly affected the CD spectra of liquid crystalline dispersions of DNA. Thus, the CD spectra of liquid crystalline microphases of DNA modified by platinum compounds are very sensitive to the status of the antitumor activity of platinum compounds and have been suggested [37] for preliminary testing of the antitumor activity of novel metal-based drugs.

We recorded CD spectra of the liquid crystalline dispersions of sonicated CT DNA modified by *cis*- or *trans*-[Cl₂(Me₂SO₄)₄Ru] at a wide range of r_b values in the presence of PEG (shown for the *trans* isomer in Fig. 7A), and the data were compared with those obtained for DNA modified by cisplatin and monofunctional [Cl(dien)Pt]Cl. In the CD spectrum of the liquid crystalline dispersions of

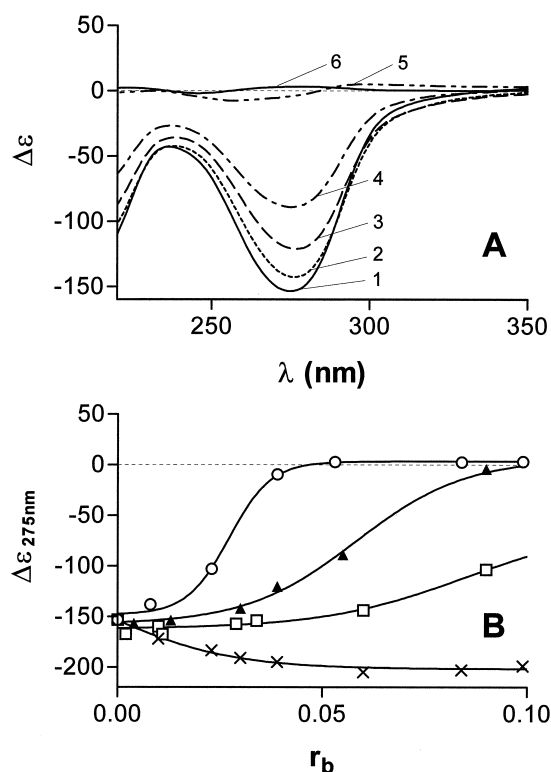


FIG. 7. (A) Circular dichroism spectra of liquid crystalline dispersions formed from non-modified CT DNA and CT DNA modified by *trans*-[Cl₂(Me₂SO₄)₄Ru] in the presence of 150 mg of PEG/mL. *r_b* values: 0 (control, non-modified DNA), curve 1; 0.03, curve 2; 0.039, curve 3; 0.055, curve 4; 0.098, curve 5; and 0.12, curve 6. (B) The dependence on *r_b* of the relative amplitude of the negative circular dichroism band at ~275 nm, $\Delta\epsilon_{275\text{nm}}$, of liquid crystalline dispersions formed from CT DNA modified by [Cl(dien)Pt]Cl (x), cisplatin (○), *cis*-[Cl₂(Me₂SO₄)₄Ru] (□), and *trans*-[Cl₂(Me₂SO₄)₄Ru] (▲) in the presence of 150 mg PEG/mL. For other details, see the text.

the control, non-modified DNA, an intense negative band at around 275 nm was observed. The amplitude of this band decreased as a consequence of the increasing amount of *cis*- or *trans*-[Cl₂(Me₂SO₄)₄Ru] bound to DNA (Fig. 7B). At the level of binding of *trans*-[Cl₂(Me₂SO₄)₄Ru] corresponding to *r_b* ≥ 0.1, the negative band disappeared. It is also evident from Fig. 7B that *cis*-[Cl₂(Me₂SO₄)₄Ru] was markedly less efficient in decreasing the amplitude of the negative CD band at 275 nm than its *trans* isomer.

The results shown in Fig. 7B also indicate that *cis*-[Cl₂(Me₂SO₄)₄Ru] only disturbs DNA liquid crystals weakly, but more than monofunctional [Cl(dien)Pt]Cl. On the other hand, although *trans*-[Cl₂(Me₂SO₄)₄Ru] disturbs these crystals markedly more than its *cis* isomer, its efficiency is in this respect lower than that of cisplatin. Hence, these results are consistent with the view that disturbance of the secondary structure of DNA by *trans*-[Cl₂(Me₂SO₄)₄Ru] has some features similar to those induced by cisplatin, which might be relevant to the antitumor activity observed for this ruthenium compound earlier. On the other hand, *cis*-[Cl₂(Me₂SO₄)₄Ru] could be rather grouped with clinically less effective or ineffective metal-

based compounds that alter conformation of DNA in a way only resulting in a negligible or weak disturbance of its liquid crystalline dispersions.

DISCUSSION

The present work demonstrates that antitumor *cis*- and *trans*-[Cl₂(Me₂SO₄)₄Ru] irreversibly coordinate to the residues in high-molecular-mass DNA. The rate of DNA binding of *cis*-[Cl₂(Me₂SO₄)₄Ru] is considerably lower than that of the *trans* isomer. The lower reactivity of the *cis* isomer is very likely associated with the presence of three bulky Me₂SO₄ ligands after this compound is dissolved in water, in contrast to only two Me₂SO₄ groups remaining in the dissolved molecules of the *trans*-isomer. Importantly, the reactivity of these metal-based compounds toward DNA is strongly affected by potential ligands of ruthenium complexes that may be present in the reaction medium, for instance as components of the reaction buffers.

Some details about the nature of the adducts formed by *cis*- and *trans*-[Cl₂(Me₂SO₄)₄Ru] on natural, double-helical DNA have emerged from the present work, such as transcription mapping of these adducts, the analysis of DNA by the EtBr fluorescent probe, and the DNA interstrand cross-linking assay. The results of these investigations are consistent with the view that *trans*-[Cl₂(Me₂SO₄)₄Ru], like antitumor cisplatin, forms a significant amount of intrastand cross-links in DNA between neighboring purine residues, but their amount was considerably smaller than that formed by the platinum drug. Interestingly, *trans*-[Cl₂(Me₂SO₄)₄Ru] can also form DNA interstrand cross-links, a previously unobserved phenomenon, although their amount is very low (~1%). *cis*-[Cl₂(Me₂SO₄)₄Ru] preferentially forms on DNA monofunctional lesions.

One of the important features of the DNA-binding mode of metal-based antitumor drugs relevant to their biological effects is the conformational alteration induced by the formation of the adduct. The assays based on differential pulse polarographic analysis, gel electrophoresis of negatively supercoiled and nicked plasmids, and the formation of liquid crystalline dispersions of DNA revealed that both ruthenium complexes are capable of inducing local conformational alterations of a non-denaturational character. The extent of these alterations induced by the *trans* isomer was noticeably higher than that induced by the *cis* isomer. Thus, the global character of conformational changes induced in DNA by the two ruthenium isomers is similar to that induced by antitumor cisplatin and different from distortions induced in DNA by clinically ineffective transplatin or monofunctional platinum complexes such as [Cl(dien)Pt]Cl or [Cl(NH₃)₃Pt]Cl.

The results of these studies also demonstrate that bifunctional DNA adducts of *trans*-[Cl₂(Me₂SO₄)₄Ru] inhibit RNA synthesis and specifically block RNA polymerases at the sites of the modified guanine and, to a lesser extent, adenine residues. Importantly, DNA adducts of therapeutically less effective *cis*-[Cl₂(Me₂SO₄)₄Ru] are unable to

inhibit RNA synthesis, very likely because this ruthenium compound binds DNA in a monodentate fashion, a binding mode expected to result in antitumor activity only in rare cases.

Taken together, several features of the DNA-binding mode of *trans*-[Cl₂(Me₂SO₄)₄Ru] described in the present work are similar to those of antitumor cisplatin, which may be relevant to the biological effects of this antitumor ruthenium drug. DNA binding of *cis*-[Cl₂(Me₂SO₄)₄Ru] mainly results in the formation of monofunctional adducts, and the extent of conformational distortions induced in DNA is considerably smaller in comparison with distortions induced by its *trans* isomer. This observation is consistent with the less pronounced biological effects of *cis*-[Cl₂(Me₂SO₄)₄Ru] in comparison with its *trans* isomer. Whatever the detailed mechanism, however, the ruthenium compounds are interesting from a mechanistic point of view and, therefore worthy of additional testing. Further studies should reveal the extent to which ruthenium complexes hold promise as clinically useful antitumor compounds.

This work was supported by the Grant Agency of the Czech Republic (Grant nos. 305/99/0695 and 204/97/P028). V.B. was supported in part by an International Research Scholar's award from the Howard Hughes Medical Institute. This research was also a part of the European Cooperation in the field of Scientific and Technical Research network (project COST D8/0017/97).

References

1. Keppler BK, Metal complexes as anticancer agents. The future role of inorganic chemistry in cancer therapy. *New J Chem* **14**: 389–403, 1990.
2. Kopf-Maier P, Complexes of metals other than platinum as antitumor agents. *Eur J Clin Pharmacol* **47**: 1–16, 1994.
3. Clarke MJ, Zhu F and Frasca DR, Non-platinum chemotherapeutic metallopharmaceuticals. *Chem Rev* **99**: 2511–2533, 1999.
4. Wong E and Giandomenico CM, Current status of platinum-based antitumor drugs. *Chem Rev* **99**: 2451–2466, 1999.
5. O'Dwyer PJ, Stevenson JP and Johnson SW, Clinical status of cisplatin, carboplatin, and other platinum-based antitumor drugs. In: *Cisplatin. Chemistry and Biochemistry of a Leading Anticancer Drug* (Ed. Lippert B), pp. 31–72. VCH, Wiley-VCH, Zürich, Weinheim, 1999.
6. Lokich J and Anderson N, Carboplatin versus cisplatin in solid tumors: An analysis of the literature. *Ann Oncol* **9**: 13–21, 1998.
7. Raymond E, Chaney SG, Taamma A and Cvitkovic E, Oxaliplatin: A review of preclinical and clinical studies. *Ann Oncol* **9**: 1053–1071, 1998.
8. Blommaert FA, van Dijk-Knijnenburg HC, Dijt FJ, den Engelse L, Baan RA, Berends F and Fichtinger-Schepman AMJ, Formation of DNA adducts by the anticancer drug carboplatin: Different nucleotide sequence preferences *in vitro* and in cells. *Biochemistry* **34**: 8474–8480, 1995.
9. Woynarowski JM, Chapman WG, Napier C, Herzig MC and Juniewicz P, Sequence- and region-specificity of oxaliplatin adducts in naked and cellular DNA. *Mol Pharmacol* **54**: 770–777, 1998.
10. Sava G, Clerici K, Capozzi I, Cocchietto M, Gagliardi R, Alessio E, Mestroni G and Perbellini A, Reduction of lung metastasis by ImH[*trans*-RuCl₂(DMSO)Im]: Mechanism of the selective action investigated on mouse tumors. *Anticancer Drugs* **10**: 129–138, 1999.
11. Johnson NP, Butour JL, Villani G, Wimmer FL, Defais M, Pierson V and Brabec V, Metal antitumor compounds: The mechanism of action of platinum complexes. *Prog Clin Biochem Med* **10**: 1–24, 1989.
12. Sava G, Pacor S, Bregant F, Ceschia V and Mestroni G, Metal complexes of ruthenium: Antineoplastic properties and perspectives. *Anticancer Drugs* **1**: 99–108, 1990.
13. Mestroni G, Alessio E, Sava G, Pacor S, Coluccia M and Boccarelli A, Water-soluble ruthenium(III)–dimethyl sulfoxide complexes: Chemical behaviour and pharmaceutical properties. *Metal-Based Drugs* **1**: 41–63, 1994.
14. Mestroni G, Alessio E, Calligaris M, Attia WM, Quadrifoglio F, Cauci S, Sava G, Zorzet S, Pacor S, Monti-Bragadin C, Tamaro M and Dolzani L, Chemical, biological and antitumor properties of ruthenium(II) complexes with dimethylsulfoxide. *Prog Clin Biochem Med* **10**: 71–87, 1989.
15. Sava G, Pacor S, Zorzet S, Alessio E and Mestroni G, Antitumor properties of dimethylsulfoxide ruthenium(II) complexes in the Lewis lung carcinoma system. *Pharmacol Res* **21**: 617–628, 1989.
16. Monti-Bragadin C, Tamaro M and Banfi E, Mutagenic activity of platinum and ruthenium complexes. *Chem Biol Interact* **11**: 469–472, 1975.
17. Monti-Bragadin C, Ramani L, Samer L, Mestroni G and Zassinovich G, Effect of *cis*-dichlorodiammineplatinum(II) and related transition metal complexes on *Escherichia coli*. *Antimicrob Agents Chemother* **7**: 825–827, 1975.
18. Coluccia M, Sava G, Loseto F, Nassi A, Boccarelli A, Giordano D, Alessio E and Mestroni G, Anti-leukemic action of RuCl₂(DMSO)₄ isomers and prevention of brain involvement on P388 leukemia and on P388/DDP subline. *Eur J Cancer* **29A**: 1873–1879, 1993.
19. Sava G, Zorzet S, Giraldi T, Mestroni G and Zassinovich G, Antineoplastic activity and toxicity of an organometallic complex of ruthenium(II) in comparison with *cis*-DDP in mice bearing solid malignant neoplasms. *Eur J Cancer Clin Oncol* **20**: 841–847, 1984.
20. Alessio E, Mestroni G, Nardin G, Attia WM, Calligaris M, Sava G and Zorzet S, *cis*- and *trans*-Dihalotetrakis (dimethyl sulfoxide) ruthenium(II) complexes (RuX₂(DMSO)₄; X = Cl, Br): Synthesis, structure, and antitumor activity. *Inorg Chem* **27**: 4099–4106, 1988.
21. Loseto F, Alessio E, Mestroni G, Lacidogna G, Nassi A, Giordano D and Coluccia M, Interaction of RuCl₂(dimethylsulphoxide)₄ isomers with DNA. *Anticancer Res* **11**: 1549–1553, 1991.
22. Jamieson ER and Lippard SJ, Structure, recognition, and processing of cisplatin–DNA adducts. *Chem Rev* **99**: 2467–2498, 1999.
23. Cauci S, Alessio E, Mestroni G and Quadrifoglio F, Reaction of *cis*-RuII(DMSO)₄Cl₂ with DNA and with some of its bases in aqueous solution. *Inorg Chim Acta - Bioinorg Chem* **137**: 19–24, 1987.
24. Alessio E, Xu Y, Cauci S, Mestroni G, Quadrifoglio F, Viglino P and Marzilli LG, Novel diastereomers with opposite chirality at ruthenium formed by N7, a-PO₄ chelation of 5'-dGMP to the antimetastatic agent *trans*-RuCl₂(DMSO)₄: NMR and CD evidence. *J Am Chem Soc* **111**: 7068–7071, 1989.
25. Cauci S, Viglino P, Esposito G and Quadrifoglio F, Reaction of the octahedral antitumor complex *trans*-RuCl₂(DMSO)₄ with 2'-deoxyguanosine. *J Inorg Biochem* **43**: 739–751, 1991.
26. Esposito G, Cauci S, Fogolari F, Alessio E, Scocchi M, Quadrifoglio F and Viglino P, NMR structural characterization of the reaction product between d(GpG) and the

- octahedral antitumor complex *trans*-RuCl₂(DMSO)₄. *Biochemistry* **31**: 7094–7103, 1992.
27. Anagnostopoulou A, Moldrheim E, Katsaros N and Sletten E, Interaction of *cis*- and *trans*-RuCl₂(DMSO)₄ with the nucleotides GpA, d(GpA), ApG, d(ApG) and d(CCTGGTCC): High-field NMR characterization of the reaction products. *J Biol Inorg Chem* **4**: 199–208, 1999.
28. Brabec V and Paleček E, The influence of salts and pH on polarographic currents produced by denatured DNA. *Biophysik* **6**: 290–300, 1970.
29. Brabec V and Paleček E, Interaction of nucleic acids with electrically charged surfaces. II. Conformational changes in double-helical polynucleotides. *Biophys Chem* **4**: 76–92, 1976.
30. Lemaire MA, Schwartz A, Rahmouni AR and Leng M, Interstrand cross-links are preferentially formed at the d(GC) sites in the reaction between *cis*-diamminedichloroplatinum(II) and DNA. *Proc Natl Acad Sci USA* **88**: 1982–1985, 1991.
31. Brabec V and Leng M, DNA interstrand cross-links of *trans*-diamminedichloroplatinum(II) are preferentially formed between guanine and complementary cytosine residues. *Proc Natl Acad Sci USA* **90**: 5345–5349, 1993.
32. Farrell N, Qu Y, Feng L and Van Houten B, Comparison of chemical reactivity, cytotoxicity, interstrand cross-linking and DNA sequence specificity of bis(platinum) complexes containing monodentate or bidentate coordination spheres with their monomeric analogues. *Biochemistry* **29**: 9522–9531, 1990.
33. Butour JL and Macquet JP, Differentiation of DNA–platinum complexes by fluorescence. The use of an intercalating dye as a probe. *Eur J Biochem* **78**: 455–463, 1977.
34. Butour JL, Alvinerie P, Souhard JP, Colson P, Houssier C and Johnson NP, Effect of the amine nonleaving group on the structure and stability of DNA complexes with *cis*-[Pt(R-NH₂)₂(NO₃)₂]. *Eur J Biochem* **202**: 975–980, 1991.
35. Brabec V, Reedijk J and Leng M, Sequence-dependent distortions induced in DNA by monofunctional platinum(II) binding. *Biochemistry* **31**: 12397–12402, 1992.
36. Keck MV and Lippard SJ, Unwinding of supercoiled DNA by platinum ethidium and related complexes. *J Am Chem Soc* **114**: 3386–3390, 1992.
37. Akimenko N, Cheltsov P, Balcarová Z, Kleinwächter V and Yevdokimov Y, A study of interactions of platinum(II) compounds with DNA by means of CD spectra of solutions and liquid crystalline microphases of DNA. *Gen Physiol Biophys* **4**: 597–608, 1985.
38. Yevdokimov YM, Skuridin SG and Salyanov VI, The liquid crystalline phases of double-stranded nucleic acids *in vitro* and *in vivo*. *Liquid Cryst* **3**: 1443–1459, 1988.
39. Bancroft DP, Lepre CA and Lippard SJ, Pt-195 NMR kinetic and mechanistic studies of *cis*-diamminedichloroplatinum and *trans*-diamminedichloroplatinum(II) binding to DNA. *J Am Chem Soc* **112**: 6860–6871, 1990.
40. Prenzler PD and McFadyen WD, Reactions of cisplatin and the *cis*-diamminediaqua platinum(II) cation with Tris and Hepes. *J Inorg Biochem* **68**: 279–282, 1997.
41. Žaludová R, Žáková A, Kašpárková J, Balcarová Z, Kleinwächter V, Vrána O, Farrell N and Brabec V, DNA interactions of bifunctional dinuclear platinum(II) antitumor agents. *Eur J Biochem* **246**: 508–517, 1997.
42. Kašpárková J, Nováková O, Vrána O, Farrell N and Brabec V, Effect of geometric isomerism in dinuclear platinum antitumor complexes on DNA interstrand cross-linking. *Biochemistry* **38**: 10997–11005, 1999.
43. Žaludová R, Žáková A, Kašpárková J, Balcarová Z, Vrána O, Coluccia M, Natile G and Brabec V, DNA modifications by antitumor *trans*-[PtCl₂(E-iminoether)₂]. *Mol Pharmacol* **52**: 354–361, 1997.
44. Žáková A, Nováková O, Balcarová Z, Bierbach U, Farrell N and Brabec V, DNA interactions of antitumor *trans*-[PtCl₂(NH₃)(quinoline)]. *Eur J Biochem* **254**: 547–557, 1998.
45. Brabec V, Kasparkova J, Vrana O, Novakova O, Cox JW, Qu Y and Farrell N, DNA modifications by a novel bifunctional trinuclear platinum Phase I anticancer agent. *Biochemistry* **38**: 6781–6790, 1999.
46. Vrána O, Boudný V and Brabec V, Superhelical torsion controls DNA interstrand cross-linking by antitumor *cis*-diamminedichloroplatinum(II). *Nucleic Acids Res* **24**: 3918–3925, 1996.
47. Paleček E, Modern polarographic (voltammetric) techniques in biochemistry and molecular biology. Part II. Analysis of macromolecules. In: *Topics in Bioelectrochemistry and Bioenergetics* (Ed. Milazzo G), Vol. 5, pp. 65–155. J Wiley, New York, 1983.
48. Brabec V, Vetterl V and Vrána O, Electroanalysis of biomacromolecules. In: *Bioelectrochemistry: Principles and Practice* (Eds. Brabec V and Milazzo G), Vol. 3, pp. 287–359. Birkhäuser Verlag, Basel, 1996.
49. Vrána O and Brabec V, Electrochemical analysis of antitumor platinum drugs and their complexes with DNA. *Bioelectrochem Bioenerg* **19**: 145–160, 1988.
50. Vrána O, Brabec V and Kleinwächter V, Polarographic studies on the conformation of some platinum complexes: Relations to anti-tumour activity. *Anticancer Drug Des* **1**: 95–109, 1986.
51. Brabec V, Kleinwächter V, Butour JL and Johnson NP, Biophysical studies of the modification of DNA by antitumor platinum coordination complexes. *Biophys Chem* **35**: 129–141, 1990.
52. Cohen GL, Bauer WR, Barton JK and Lippard SJ, Binding of *cis*- and *trans*-dichlorodiammineplatinum(II) to DNA: Evidence for unwinding and shortening of the double helix. *Science* **203**: 1014–1016, 1979.
53. Scovell WM and Collart F, Unwinding of supercoiled DNA by *cis*- and *trans*-diamminedichloroplatinum(II): Influence of the torsional strain on DNA unwinding. *Nucleic Acids Res* **13**: 2881–2895, 1985.
54. Livolant F, Levelut AM and Benoit JP, The highly concentrated liquid-crystalline phase of DNA is columnar hexagonal. *Nature* **339**: 724–726, 1989.
55. Akimenko N, Kleinwächter V and Yevdokimov Y, Liquid crystalline microphases of DNA molecules complexed with compounds of platinum(II). *FEBS Lett* **156**: 58–62, 1983.
56. Belyakov VA, Orlov VP, Semenov SV, Skuridin SG and Yevdokimov YM, Comparison of calculated and observed CD spectra of liquid crystalline dispersions formed from double-stranded DNA and from DNA complexed with coloured compounds. *Liquid Cryst* **20**: 777–784, 1996.
57. Livolant F and Maestre M, Circular dichroism microscopy of compact forms of DNA and chromatin *in vivo* and *in vitro*: Cholesteric liquid-crystalline phases of DNA and single dinoflagellate nuclei. *Biochemistry* **27**: 3056–3068, 1988.
58. Yevdokimov YM, Skuridin SG, Salyanov VI, Damaschun G, Damaschun H, Misselwitz R and Kleinwächter V, Effect of platinum (II) chemotherapeutic agents on properties of DNA liquid crystals. *Biophys Chem* **35**: 143–153, 1990.

25.

Correlation between Cytotoxicity and DNA Binding of Polypyridyl Ruthenium Complexes[†]

Olga Nováková,[‡] Jana Kašpárková,[‡] Oldřich Vrána,[‡] Paul M. van Vliet,[§] Jan Reedijk,[§] and Viktor Brabec^{*,‡}

Institute of Biophysics, Academy of Sciences of the Czech Republic, Královopolská 135, 612 65 Brno, Czech Republic, and Leiden Institute of Chemistry, Gorlaeus Laboratories, Leiden University, P.O. Box 9502, 2300 RA Leiden, The Netherlands

Received March 17, 1995; Revised Manuscript Received July 6, 1995[®]

ABSTRACT: The cytotoxicity of chloropolypyridyl ruthenium complexes of structural formulas [Ru(terpy)-(bpy)Cl]Cl, *cis*-[Ru(bpy)₂Cl₂], and *mer*-[Ru(terpy)Cl₃] (terpy = 2,2':6'2''-terpyridine, bpy = 2,2'-bipyridyl) has been studied in murine and human tumor cell lines. The results show that *mer*-[Ru(terpy)Cl₃] exhibits a remarkably higher cytotoxicity than the other complexes. Moreover, investigations of antitumor activity in a standard tumor screen have revealed the highest efficiency for *mer*-[Ru(terpy)Cl₃]. In a cell-free medium, the ruthenium complexes coordinate to DNA preferentially at guanine residues. The resulting adducts can terminate DNA synthesis by thermostable Vent_r DNA polymerase. The reactivity of the complexes to DNA, their efficiency to unwind closed, negatively supercoiled DNA, and a sequence preference of their DNA adducts (studied by means of replication mapping) do not show a correlation with biological activity. On the other hand, the cytotoxic *mer*-[Ru(terpy)Cl₃] exhibits a significant DNA interstrand cross-linking, in contrast to the inactive complexes which exhibit no such efficacy. The results point to a potential new class of metal-based antitumor compounds acting by a mechanism involving DNA interstrand cross-linking.

Complexes of transition elements of the platinum group hold a promise in the design of new anticancer agents [for general reviews, see Clarke (1993), Frühauf and Zeller (1991), Heim (1993), Köpf-Maier (1994), Loehrer and Einhorn (1984), and Reedijk (1992)]. *cis*-Diamminedichloroplatinum(II) (cisplatin)¹ and *cis*-diammine(cyclobutane-1,1-dicarboxylato)platinum(II) (carboplatin) are the first antitumor drugs of this type which are currently in clinical use. At present, a research effort is directed to the synthesis of other platinum complexes which could help to overcome clinical problems associated with the relatively limited activity of cisplatin and carboplatin against the broad spectrum of human malignancies, acquired resistance, and side effects.

In attempts to find a new, metal-based anticancer drug with activity complementary to cisplatin, the complexes containing a ruthenium center, mostly in its lower oxidation

states, have also been prepared and tested for antitumor activity [for reviews, see Clarke (1993), Keppler (1989), and Mestroni et al. (1994)]. Several ruthenium compounds with nitrogen ligands not only have been shown to exhibit good activity in screening studies, but many also preferentially localize in tumor tissue. The significant structural differences between ruthenium and most platinum-based antitumor drugs give a promise that ruthenium-based drugs could be suitable alternatives to cisplatin and carboplatin. Antitumor ruthenium compounds usually possess octahedral, six-coordinated geometry as opposed to the square-planar arrangement of the ligands of cisplatin or carboplatin. In addition, the two additional coordination sites for ruthenium as opposed to the platinum(II) center in cisplatin or carboplatin may allow for new modes of binding to intracellular targets and, with some ligands, provide for chirality in the complexes and in their interactions with the target structure.

In the last decade, particular attention has been paid to the ruthenium complexes of polypyridyl ligands. Some of these complexes exist as chiral molecules capable of enantioselective recognition of DNA. Thus, DNA binding and cleavage properties of various polypyridyl ruthenium compounds have been intensively investigated since they have been proposed as possibly useful probes of DNA conformation (Barton, 1986; Erikson et al., 1994; Grover et al., 1992; Satyanarayana et al., 1993) or DNA cleavage agents (Grover et al., 1994; Gupta et al., 1992, 1993; Neyhart et al., 1993). The analogues of these ruthenium complexes containing, besides polypyridyl ligands, aqua or chloro groups have been also synthesized and were found to bind DNA covalently in cell-free media (Barton & Lolis, 1985; Grover et al., 1992, 1994). The aqua or chloro ligands in these complexes represent leaving ligands in contrast to the kinetically more stable pyridyl groups (Grover et al., 1994; Moyer & Meyer, 1981). In spite of the fact that these polypyridyl ruthenium complexes coordinate to DNA and that several ruthenium

[†] Supported in part by the Internal Grant Agency of the Academy of Sciences of the Czech Republic, the Grant Agency of the Czech Republic (Grant No. 203/93/0052), and the Internal Grant Agency of the Ministry of Health of the Czech Republic (Grant No. 1893-3). This joint research is also a part of the European Cooperation in the field of Scientific and Technical Research (COST) network (COST Projects D1/0002/92 and D1/0001/95).

[‡] Academy of Sciences of the Czech Republic.

[§] Leiden University.

[®] Abstract published in *Advance ACS Abstracts*, September 1, 1995.

¹ Abbreviations: bp, base pair; bpy, 2,2'-bipyridyl; carboplatin, *cis*-diammine(cyclobutane-1,1-dicarboxylato)platinum(II); cisplatin, *cis*-diamminedichloroplatinum(II); DPP, differential pulse polarography; EtBr, ethidium bromide; FAAS, flameless atomic absorption spectroscopy; ID₅₀, the concentration of the drug required to inhibit cell growth by 50%; *r*_b, the ratio of metal atoms fixed per nucleotide; *r*_b(c), the value of *r*_b at which the supercoiled and relaxed forms of DNA comigrate; *r*_i, the molar ratio of free metal complex to nucleotide phosphates at the onset of incubation; *t*_{1/2}, half-time; T/C, the ratio of the mean survival times of treated over nontreated tumor-bearing mice; *T*_m, melting temperature; terpy, 2,2':6',2''-terpyridine; XCL, cross-linked fraction of DNA; XL/A, number of interstrand cross-links per adduct.

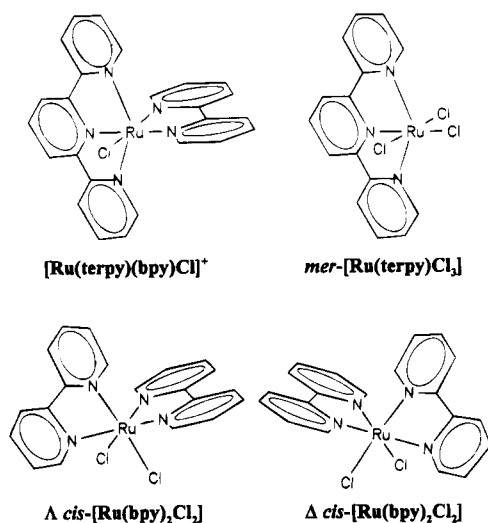


FIGURE 1: Schematic structures of ruthenium complexes used in this study. In the case of *cis*-[Ru(bpy)₂Cl₂], a racemic mixture or the complex enriched by the Δ -enantiomer was used (see the text).

complexes of different types exhibit antitumor activity, the biological effects of polypyridyl ruthenium complexes and the underlying biochemical mechanisms have not yet been investigated.

In this work, we describe cytotoxicity in murine and human tumor cell lines of the three chloropolypyridyl ruthenium complexes (Figure 1), which differ in the number of leaving ligands. The results of these investigations are compared with DNA binding in a cell-free medium. We find a clear correlation between the cytotoxicity of the polypyridyl ruthenium complexes and their DNA interstrand cross-linking capability.

MATERIALS AND METHODS

Chemicals. [Ru(terpy)(bpy)Cl]Cl, *cis*-[Ru(bpy)₂Cl₂], and *mer*-[Ru(terpy)Cl₃] (Figure 1) (terpy = 2,2':6',2''-terpyridine, bpy = 2,2'-bipyridyl) were synthesized as described in the literature (Adcock et al., 1984; Sullivan et al., 1978; Takeuchi et al., 1984). Their stock solutions (5×10^{-4} M) were made in double-distilled water, kept in the dark, and used after 48 h of equilibration at 37 °C. *cis*-[Ru(bpy)₂Cl₂] enriched by the Δ -isomer was prepared by the procedure based on a preferential binding of Δ -isomers of polypyridyl chlororuthenium complexes to B-DNA (Barton & Lolis, 1985; Grover et al., 1992). An initial cycle of this procedure involved mixing calf thymus double helical DNA at the concentration of 0.32 mg/mL with racemic *cis*-[Ru(bpy)₂Cl₂] at $r_i = 0.1$ in the medium of 10 mM NaClO₄ at 37 °C in the dark (r_i is defined as the molar ratio of free metal complex to nucleotide phosphates at the onset of incubation). After 2 h, the mixture was ultrafiltered in 10 mL of cells from Amicon with an 8000 molecular mass cutoff membrane, and the resulting solution was concentrated by vacuum distillation. In the next cycle, double helical DNA was added to this filtrate so that its concentration was 0.32 mg/mL and r_i was 0.1. This mixture was again incubated and filtered as in the preceding step. The preferential binding of Δ -isomer was quantified by measuring circular dichroism spectra using a JASCO spectropolarimeter, Model J-720. The enrichment of the *cis*-[Ru(bpy)₂Cl₂] sample by the Δ -isomer was calculated using the molar ellipticity yielded by the filtrates at 280 nm and their comparison with the published molar ellipticity of the

Δ -isomer at the same wavelength (Arce Sagüés et al., 1980). These cycles were repeated until the value of molar ellipticity of the filtrate at 280 nm no longer changed. The sample designated in the following text as *cis*-[Ru(bpy)₂Cl₂] enriched by the Δ -enantiomer contained ca. 75% Δ -isomer and ca. 25% Λ -isomer.

Fischer's and Dulbecco's modified Eagle's (DME) media, bovine insulin, penicillin, Streptomycin, and *Micrococcus lysodeikticus* DNA were from Sigma. Bovine fetal calf serum was purchased from Sebak (Germany). Calf thymus DNA was isolated and characterized as previously described (Brabec & Paleček, 1976). Plasmid pSP73 (2464 base pairs) was either purchased from Promega or prepared by transformation of the plasmid into Sure competent cells (*Escherichia coli* strain) from Stratagene, amplification of a clone, and purification using a Plasmid maxi kit from Qiagen (Germany). The prepared supercoiled DNA was identified by electrophoresis on a 1% agarose gel running with Promega plasmid pSP73. The sample of the plasmid prepared in this laboratory contained a 90% negatively supercoiled form. The CircumVent Thermal Cycle Dideoxy DNA Sequencing Kit with Vent_R(exo⁻) or Vent_R(exo⁺) DNA polymerases, the Klenow fragment of DNA polymerase I, and restriction endonucleases were purchased from BioLabs. T4 polynucleotide kinase was from Boehringer. A primer 5'-GATTAGGTGACACTATA-3' was from BioVendor (Brno, Czech Republic). All radioactive products were from Amersham.

Physical and Physicochemical Methods. Absorption spectra were collected on a Beckman DU-8B UV/VIS spectrophotometer. Flameless atomic absorption spectroscopy (FAAS) measurements were carried out on a Unicam 939 AA spectrometer with a graphite furnace. Differential pulse polarographic (DPP) analysis was performed with the aid of an EG&G PARC Polarographic Analyzer, Model 384B, equipped with an EG&G Static mercury drop electrode, Model 303A; platinum wire and saturated calomel electrode (SCE) were used as counter and reference electrodes, respectively. DPP analysis was performed at the following apparatus settings: drop time, 1.0 s; scan rate, 2 mV/s; and pulse amplitude, -50 mV.

In Vitro Cytotoxicity Assays. Wild-type L1210 murine leukemia and human cervix carcinoma HeLa cells were cultured as suspensions in Fischer's or DME's medium, respectively, supplemented with 10% bovine fetal calf serum from Sebak (Germany), 10 μ g of bovine insulin/mL, 100 units of penicillin/mL, and 100 μ g of streptomycin/mL at 37 °C. For testing purposes, cells in the logarithmic growth phase were diluted to 1×10^5 cells/mL, and 4.5 mL of cell suspension was aliquoted to Müller's tissue culture tubes. Test compound, dissolved in 1 mM phosphate buffer, pH 7.0, was then added to the appropriate tubes (0.5 mL/tube) to attain the final concentration, and cells were maintained under growth conditions. After the time allowed for ruthenium complex exposure at 37 °C in the dark, the concentrations of L1210 or HeLa cells were determined by using a Coulter counter or were first harvested with trypsinization and counted using Bürker chambers, respectively.

Cellular Ruthenium Complex Uptake. Experiments were performed with logarithmic growth phase L1210 cells from a culture maintained and treated with ruthenium complexes as described above. Ruthenium complexes were tested at a concentration of 3×10^{-5} M, and the time allowed for the treatment of the cells was 11 h. Unassociated ruthenium

complex was separated from the cell sample by repetitive centrifugation and resuspension of the sample in 0.15 M NaCl with 10 mM phosphate buffer, pH 7.0 (three times). The washed cell pellet was resuspended in 0.4 mL of 0.1% Triton X-100 and was sonicated for 30 s with a Dynatech sonicator set at 100 W. Ruthenium associated with the cell pellet was measured with FAAS.

In Vivo Efficacy Studies. Female (BALB/c \times C₅₇BL/6)-F₁ mice weighing 20–23 g were obtained from the Institute of Biophysics, Brno, and housed in an environment having controlled humidity, temperature, and photoperiods. The animals had food and water available *ad libitum*, the wood chip bedding was changed daily, and they were randomized before treatment. The transplantable LS/BL ascitic tumor, widely disseminating lymphosarcoma of C₅₇BL mice, was maintained by successive intraperitoneal (ip) isologous transplants of 10⁶ cells at 7-day intervals in (BALB/c \times C₅₇BL)-F₁ mice. For testing purposes, 10⁶ tumor cells were inoculated ip (day 0) and mice were administered five doses of test compound dissolved in 0.5 mL of 5 mM phosphate buffer, pH 7.0 ip, on days 1, 3, 5, 7, and 9. Mice in the control group were administered only pure buffer in the same schedule. Animals (10 mice in each group) were observed daily for signs of toxicity, and deaths and the day of death were recorded for each animal that died during the 40-day observation period. The efficacy of each dose of compound tested was evaluated by calculating the percent increased life span, which was determined by dividing the mean survival time of treated mice (using the day of death of only those animals that died during the 40-day period) by the mean survival time of nontreated tumor-bearing control animals (% T/C). Compounds exhibiting a % T/C of >140 are considered to have significant antitumor activity (Farrell et al., 1990a).

Modification of DNA by Ruthenium Complexes. If not stated otherwise, mammalian, bacterial, or plasmid DNAs were modified in 10 mM sodium perchlorate with 1 mM phosphate buffer, pH 7.0, for 24 h at 37 °C in the dark. The ratio of metal atoms fixed per nucleotide residue (r_b) was determined by DPP. The paper containing the details of this assay will be published elsewhere (Nováková et al., unpublished experiments) so that we describe in this paper only its main principles. DNA was mixed with the ruthenium complex in 10 mM NaClO₄ with 1 mM phosphate buffer, pH 7.0, so that the resulting DNA concentration was 0.3 mg/mL. At the time of this reaction chosen for the r_b measurement, the aliquot of 18 μ L was withdrawn. Then 2 μ L of 3 M sodium acetate was added to this aliquot, and DNA in this sample was precipitated by addition of 40 μ L of ethanol and subsequent incubation at –20 °C. After centrifugation, 3 μ L of the supernatant was added to 3.0 mL of 0.9 M ammonium formate with 0.15 M NaH₂PO₄, pH 5.4 (DPP buffer), and subjected to DPP analysis at 25 °C. This analysis is based on the observation that various ruthenium complexes, including those tested in this work, yield in this medium a DDP peak at around –1.35 V vs SCE. This DPP peak corresponds to the catalytic hydrogen current, and its height is linearly increased with the growing concentration of the ruthenium complex in the range of 5×10^{-10} to 1×10^{-8} M. The lower limit of the analytical determination of Ru complexes using this DDP activity is 10^{-9} M. In addition, if a reaction mixture containing free ruthenium and ruthenium–DNA complex is precipitated by

ethanol, free ruthenium (not that bound to DNA) only yields the DPP catalytic hydrogen peak at around –1.35 V. Thus, the DPP analysis described above gives the amount of unreacted ruthenium. The amount of ruthenium bound to DNA (and from it the value of r_b) can be calculated by subtracting the unreacted amount from the amount of ruthenium present at the onset of the reaction. Importantly, the precipitation of DNA or ruthenium–DNA complex immediately stops the reaction of ruthenium with DNA and does not cause dissociation of ruthenium which had already been bound. Thus, this polarographic assay is also suitable for easy determination of the kinetics of DNA–ruthenium complexation. It was verified that this DPP assay gives r_b values identical with those obtained by FAAS.

Unwinding of Negatively Supercoiled DNA. Unwinding of closed circular supercoiled pSP73 plasmid DNA was assayed by an agarose gel mobility shift assay (Keck & Lippard, 1992). The unwinding angle Φ , induced per ruthenium–DNA adduct, was calculated upon the determination of the r_b value at which the complete transformation of the supercoiled to relaxed form of the plasmid was attained. Samples of pSP73 plasmid were incubated for 24 h at 37 °C in the dark. All samples were precipitated by ethanol and redissolved in the TBE buffer (Tris-borate/EDTA). An aliquot of the precipitated sample was subjected to electrophoresis on 1% agarose gels running at 25 °C in the dark with TBE buffer with a voltage set at 30 V. The gels were then stained with ethidium bromide (EtBr) and were followed by on Polaroid 667 film with a transilluminator. The other aliquot was used for the determination of r_b values by DPP.

Interstrand Cross-Link Assay. DNA interstrand cross-linking by the ruthenium complexes was determined by two methods. One procedure employed calf thymus DNA, and the cross-linking was measured by the EtBr fluorescence technique (Brent, 1984; Morgan & Pulleyblank, 1974). Control or Ru-modified DNAs at the concentration of 0.1 mg/mL were dialyzed against 10 mM NaClO₄ with 1 mM phosphate buffer, pH 7.0. This solution (0.2 mL) was added to 3.0 mL of EtBr (0.5 μ g/mL) in 20 mM K₂HPO₄ with 0.4 mM EDTA, pH 11.8. The samples were incubated at 90 °C for 10 min and then rapidly cooled on an ice bath. The fluorescence was measured at 25 °C before and after this heating/cooling step (excitation and emission wavelengths were 525 and 580 nm, respectively). The cross-linked fraction of DNA (XCL) was calculated using the equation $XCL = (F_{Ru} - F_C)/(1 - F_C)$, where F_C and F_{Ru} are values of the fluorescence of control and ruthenium-modified DNAs, respectively, measured after the heating/cooling step divided by the fluorescence before this step.

Plasmid DNA was used in a further series of experiments. The ruthenium complexes at varying concentrations were incubated with 2 μ g of closed circular pSP73 DNA or with this DNA linearized by *Eco*RI restriction enzyme in 10 mM NaClO₄ with 1 mM phosphate buffer, pH 7.0, for 24 h at 37 °C in the dark. The r_b values were determined by the DPP assay. Then the samples were precipitated by ethanol, and closed circular DNA already modified by the ruthenium complexes was subsequently linearized by *Eco*RI. The linear duplexes were 3'-end labeled by means of the Klenow fragment of DNA polymerase I and [α -³²P]dATP. The samples were deproteinized by phenol and precipitated by ethanol, and the pellet was dissolved in 18 μ L of 10 mM

NaOH with 1 mM EDTA, 6.6% sucrose, and 0.04% bromophenol blue. The amount of cross-links was analyzed by electrophoresis under denaturing conditions on alkaline agarose gel (1%). After electrophoresis was complete, the bands corresponding to the single strands of DNA and interstrand cross-linked duplex were cut off, and their radioactivity was quantified on a LKB Wallac 1410 Betaspectrometer (Finland).

Sequence Specificity of Ruthenium–DNA Adducts. Mapping of DNA lesions induced by the ruthenium complexes in the pSP73 plasmid DNA was conducted in a way similar to that used for mapping of DNA adducts of cisplatin and its four platinum analogues (Murray et al., 1992a,b). The Circum Vent Thermal Cycle Dideoxy DNA Sequencing Kit with Vent_R(exo[−]) or (exo⁺) DNA polymerases was used along with the protocol for thermal cycle DNA sequencing with 5′-end-labeled primer recommended by the manufacturer with small modifications. Two picomoles of 5′-end-labeled primer oligonucleotide 5′-GATTTAGGTGACAC-TATA-3′ (complementary to the SP6 promoter nucleotide sequence in the template strand of pSP73) was added to 100 ng of double-stranded template DNA (pSP73 plasmid linearized by the *Hpa*I restriction endonuclease). This DNA was modified by the ruthenium complexes or cisplatin at $r_b = 0.05$ or 0.01, respectively [eventual traces of free (unbound) metal complexes were removed from the template DNA by precipitation by ethanol]. These solutions containing control or modified DNA were further mixed with 1.5 μ L of the sequencing buffer composed of 100 mM KCl, 100 mM (NH₄)₂SO₄, 200 mM Tris-HCl, pH 8.8, and 50 mM MgSO₄, 1 μ L of 3% Triton X-100, 2 units of Vent_R(exo⁺) DNA polymerase, and distilled water to a total volume of 16 μ L. A total of 3.2 μ L of this reaction mixture was immediately added to 3 μ L of the solution containing 100 μ M dATP, dCTP, dGTP, and dTTP and overlaid with 50 μ L of mineral oil. In the same experiment, dideoxy double-stranded DNA sequencing was performed using the same unmodified plasmid and primer and Vent_R(exo[−]) instead of (exo⁺) DNA polymerase as DNA sequence standards. Linear amplification by thermal cycling was carried out at 95 °C for 30 s (time at the temperature), 47 °C for 30 s, and 72 °C for 30 s for 25 cycles in a Techne PHC-2 DNA Thermal Cycler. The reaction was terminated by the addition of 4 μ L of stop/loading dye solution containing deionized formamide with 0.3% xylene cyanol, 0.3% bromophenol blue, and 0.37% EDTA (pH 7.0) to each tube, beneath the mineral oil. The total of 2 μ L of the reaction mixture was loaded onto a 6% polyacrylamide/8 M urea DNA sequencing gel.

RESULTS

Cytotoxicity and Antitumor Activity Studies. *In vitro* cytotoxicity of all ruthenium complexes in tissue cultures was examined first in a murine L1210 tumor cell line (Figure 2A). The results show that *mer*-[Ru(terpy)Cl₃] exhibits markedly higher cytotoxicity than racemic *cis*-[Ru(bpy)₂Cl₂] or [Ru(terpy)(bpy)Cl]Cl. This higher cytotoxicity of *mer*-[Ru(terpy)Cl₃] was observed in the range of the final concentrations of the ruthenium complexes of 1×10^{-6} to 2×10^{-5} M. To confirm that this observation applies to human tumors, the compounds were also assayed for cytotoxicity in a human cervix carcinoma HeLa cell line (Figure 2B). There is a similarity in the behavior pattern of the complexes

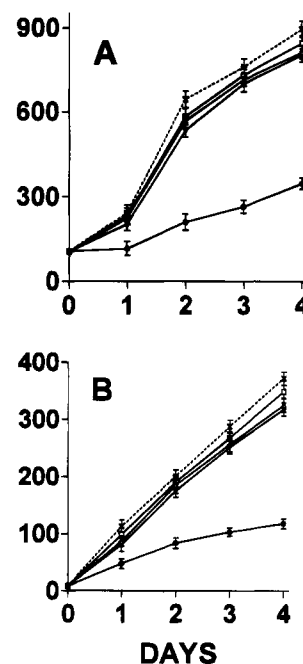


FIGURE 2: *In vitro* cytotoxicity of ruthenium complexes in murine L1210 leukemia (A) and human cervix carcinoma HeLa cells (B). The cells were treated with the complexes at their final concentration of 1×10^{-5} M: (x—x), control; (□—□), [Ru(terpy)(bpy)Cl]Cl; (Δ—Δ), racemic *cis*-[Ru(bpy)₂Cl₂]; (▽—▽), *cis*-[Ru(bpy)₂Cl₂] enriched by the Δ-enantiomer (75% Δ-isomer + 25% Λ-isomer); (●—●), *mer*-[Ru(terpy)Cl₃].

toward this clinically relevant human cell line and the murine L1210 leukemia results. The cytotoxicity of the ruthenium complexes tested in this work can also be compared by means of the ID₅₀ values, i.e. the concentrations of the drug required to inhibit cell growth by 50%. This value could be determined only for *mer*-[Ru(terpy)Cl₃]. For instance, after 72 h of ruthenium exposure, ID₅₀ in L1210 and HeLa cells was 8 and 7 μ M, respectively. Unfortunately, the ID₅₀ values for racemic *cis*-[Ru(bpy)₂Cl₂] or [Ru(terpy)(bpy)Cl]Cl were impossible to determine because of the limited solubility of these compounds. Nevertheless, 50% inhibition of the cell growth by the treatment with racemic *cis*-[Ru(bpy)₂Cl₂] or this complex enriched by its Δ-enantiomer and [Ru(terpy)(bpy)Cl]Cl for 72 h was not attained if their concentrations were even 70 times higher than the value of ID₅₀ of *mer*-[Ru(terpy)Cl₃]. Interestingly, intracellular ruthenium uptake was determined in L1210 cells and was found to be almost identical for racemic *cis*-[Ru(bpy)₂Cl₂] and *mer*-[Ru(terpy)Cl₃] and about 7 times higher for [Ru(terpy)(bpy)Cl]Cl (Table 1).

The antitumor activity of polypyridyl ruthenium complexes has been initially studied on murine lymphosarcoma LS/BL (Table 2). The objective was to ascertain which ruthenium complexes examined in this work show *in vivo* activity in standard murine screen. The present preliminary studies indicate that the complex *mer*-[Ru(terpy)Cl₃], which showed a pronounced *in vitro* cytotoxicity (Figure 2), also exhibits significant antitumor activity. On the other hand, the activities of [Ru(terpy)(bpy)Cl]Cl, racemic *cis*-[Ru(bpy)₂Cl₂], or this complex enriched by its Δ-enantiomer, which all exhibited only a slight *in vitro* cytotoxicity, were very small under identical conditions. A larger series of murine and human tumors and regimes of administration are being extensively tested and will be the subject of a more

Table 1: L1210 Cell Uptake of Polypyridyl Ruthenium Complexes^a

compound ^b	pmol of Ru (10 ⁶ cells) ⁻¹ μM ⁻¹ c
[Ru(terpy)(bpy)Cl]Cl	0.58 ± 0.07
racemic <i>cis</i> -[Ru(bpy) ₂ Cl ₂]	0.08 ± 0.01
<i>cis</i> -[Ru(bpy) ₂ Cl ₂] enriched by its Δ-isomer ^d	0.08 ± 0.01
<i>mer</i> -[Ru(terpy)Cl ₃]	0.08 ± 0.02

^a The period of the treatment was 11 h; for other details, see Material and Methods. ^b The Ru complexes were at the concentration of 3×10^{-5} M. ^c The values represent mean ± SEM of six determinations from two independent experiments. ^d 75% Δ-isomer plus 25% Λ-enantiomer.

Table 2: Summary of Antitumor Activity of Polypyridyl Ruthenium Complexes in LS/BL Tumor Cells^a

compound	dose, mg/kg ^b	% T/C
[Ru(terpy)(bpy)Cl]Cl	5 × 5	108
	10 × 5	110
	15 × 5	110
racemic <i>cis</i> -[Ru(bpy) ₂ Cl ₂]	5 × 5	104
	10 × 5	101
	15 × 5	106
<i>cis</i> -[Ru(bpy) ₂ Cl ₂] enriched by its Δ-isomer ^c	5 × 5	107
	10 × 5	102
	15 × 5	103
<i>mer</i> -[Ru(terpy)Cl ₃]	5 × 5	134
	10 × 5	157
	15 × 5	142

^a Tests conducted as described in Materials and Methods. ^b The appropriate dose was administered on day 1, 1 day after tumor inoculation. The second, third, fourth, and fifth doses were administered on days 3, 5, 7, and 9, respectively. ^c 75% Δ-isomer plus 25% Λ-enantiomer.

detailed paper confirming the antitumor activity of *mer*-[Ru(terpy)Cl₃].

cis-[Ru(bpy)₂Cl₂] complex is chiral (its racemic mixture contains equal amounts of Δ- and Λ-enantiomers). We have also tested a hypothesis that cellular uptake of these enantiomers could be different. A mixture of the two isomers of *cis*-[Ru(bpy)₂Cl₂] was prepared which was enriched by the Δ-enantiomer (75% Δ-enantiomer + 25% Λ-enantiomer). Importantly, the amounts of ruthenium found in L1210 cells treated with the racemic complex or the complex enriched by the Δ-isomer under conditions specified in the legend to Table 1 were identical. The cytotoxicity (Figure 2) and antitumor activity (Table 2) of the racemic or enriched *cis*-[Ru(bpy)₂Cl₂] were almost identical. These results are consistent with the view that, in the experiments described in this work, there was no substantial difference in the intracellular ruthenium uptake and cytotoxicity for individual enantiomers of *cis*-[Ru(bpy)₂Cl₂].

DNA Binding. Given the cytotoxicity results, it is of particular interest to elucidate the similarities and differences in the behavior of the polypyridyl chlororuthenium complexes toward isolated DNA in solution and to relate these properties to their biological effects. The DNA binding, unwinding, and interstrand cross-linking were examined by a combination of techniques of molecular biophysics including polarography and gel electrophoresis.

In order to demonstrate that the ruthenium complexes tested in this work coordinate to DNA, we used procedures slightly modified in comparison with those already applied to prove coordination to DNA of other polypyridyl ruthenium

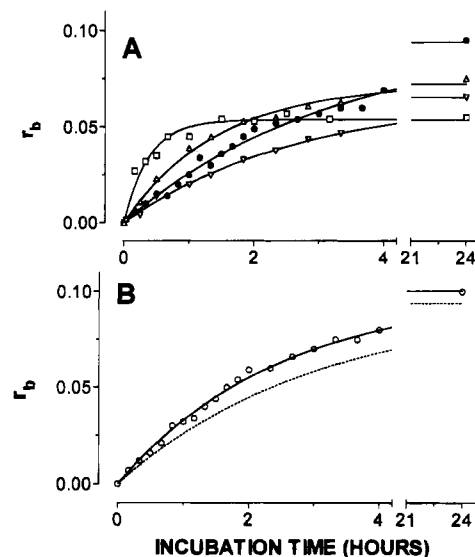


FIGURE 3: Formation of DNA adducts by ruthenium complexes as a function of incubation time. (A) Reaction of calf thymus DNA with [Ru(terpy)(bpy)Cl]Cl (□), racemic *cis*-[Ru(bpy)₂Cl₂] (Δ), *cis*-[Ru(bpy)₂Cl₂] enriched by the Δ-enantiomer (75% Δ-isomer + 25% Λ-isomer) (▽), or *mer*-[Ru(terpy)Cl₃] (●). (B) Reaction of *Micrococcus lysodeikticus* DNA with *mer*-[Ru(terpy)Cl₃] (○); for comparative purposes, the dashed line shows the dependence for calf thymus DNA with *mer*-[Ru(terpy)Cl₃] taken from panel A. See Materials and Methods for details.

complexes (Lolis & Barton, 1985; Grover et al., 1992). Solutions of calf thymus DNA at the concentration of 0.3 mg/mL were incubated with the ruthenium complex for various time intervals at r_i values of 0.1. Following incubation, ethanol was added to precipitate the DNA, with unbound ruthenium remaining in solution. An aliquot of this supernatant was added to the DPP buffer and assayed by DPP. The amount of ruthenium bound to DNA (r_b) was calculated by subtracting the amount of ruthenium remaining in solution (determined by DPP) from the total amount of ruthenium present in the reaction. Figure 3A shows a plot of r_b vs time upon incubation of DNA with *cis*-[Ru(bpy)₂Cl₂], [Ru(terpy)(bpy)Cl]Cl, and *mer*-[Ru(terpy)Cl₃] at 37 °C. Ruthenium associated with the precipitated DNA (i.e. which did not remain in the solution after precipitation of DNA) was already detected at short incubation times (several minutes), thus indicating its coordination to DNA. The amount of ruthenium bound to DNA increased with time and reached maximum after ca. 24 h. The maximum binding of *mer*-[Ru(terpy)Cl₃] corresponded to the binding of almost all molecules present in the reaction mixture. In contrast, the maximum modification by racemic *cis*-[Ru(bpy)₂Cl₂] or [Ru(terpy)(bpy)Cl]Cl was less extensive (75 or 55%, respectively) (Figure 3A). If r_i was decreased to 0.01 (at the concentration of DNA of 1 mg/mL), the fraction of *cis*-[Ru(bpy)₂Cl₂] or [Ru(terpy)(bpy)Cl]Cl molecules, which remained unbound after 24 h, was found to be the same. Half-times ($t_{1/2}$) for the binding reactions can be estimated from Figure 3. The $t_{1/2}$ values of 16, 59, 111, and 129 min were found for DNA binding of [Ru(terpy)(bpy)Cl]Cl, racemic *cis*-[Ru(bpy)₂Cl₂], *cis*-[Ru(bpy)₂Cl₂] enriched by the Δ-enantiomer, and *mer*-[Ru(terpy)Cl₃], respectively in 10 mM NaClO₄ with 1 mM phosphate buffer, pH 7.0, at 37 °C. Thus, our results on the binding of the ruthenium complexes to DNA are consistent with the earlier work on other aqua or chloropolypyridyl ruthenium complexes (Barton & Lolis,

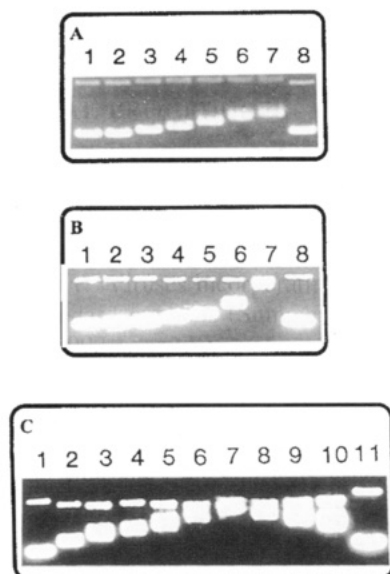


FIGURE 4: Unwinding of supercoiled pSP73 plasmid DNA by ruthenium complexes. See also Table 3. In each panel, the top bands correspond to the form of nicked plasmid and the bottom bands to closed, negatively supercoiled plasmid. In panel A, the plasmid was incubated with $[\text{Ru}(\text{terpy})(\text{bpy})\text{Cl}]\text{Cl}$ with r_b values of 0 (control), 0.03, 0.06, 0.08, 0.11, 0.14, 0.17, and 0 (lanes 1–8, respectively). In panel B, $\text{cis-}[\text{Ru}(\text{bpy})_2\text{Cl}_2]$ was studied in the same way with r_b values of 0 (control), 0.004, 0.008, 0.023, 0.038, 0.053, 0.075, and 0 (lanes 1–8, respectively). In panel C, DNA was incubated with $\text{mer-}[\text{Ru}(\text{terpy})\text{Cl}_3]$ with r_b values of 0 (control), 0.09, 0.11, 0.13, 0.15, 0.17, 0.18, 0.19, 0.20, 0.21, and 0 (lanes 1–11, respectively).

1985; Grover et al., 1992, 1994) and with our preliminary work describing coordination of $\text{mer-}[\text{Ru}(\text{terpy})\text{Cl}_3]$ to DNA with the aid of spectrophotometric assay (van Vliet et al., 1995).

The metal complexes were also reacted with *M. lysodeikticus* DNA, which contains more guanine + cytosine (G + C) than calf thymus DNA (72 and 42%, respectively). The initial rate of the binding of the ruthenium complexes to DNA increased as a consequence of the higher G + C content in DNA (shown for $\text{mer-}[\text{Ru}(\text{terpy})\text{Cl}_3]$ at $r_i = 0.1$ in Figure 3B).

The DNA binding experiments were also conducted with the ruthenium complexes from their stock solutions which were supplemented with NaCl to reach its concentration of 0.5 M and subsequently incubated for 48 h at 37 °C in the dark. The reaction of these ruthenium complexes with DNA was allowed to proceed in 0.5 M NaCl with 1 mM phosphate buffer, pH 7.0, at 37 °C for 48 h and assayed by DPP. In this case, all ruthenium remained in solution after precipitation of DNA, indicating no coordination of ruthenium to DNA. This result suggests the importance of hydrolysis of the polypyridyl chlororuthenium complexes, involving exchange of their chloride ligands, for binding to DNA.

Unwinding Induced in DNA by Ru Binding. Agarose gel electrophoresis was used to determine the unwinding induced in pSP73 plasmid by $\text{cis-}[\text{Ru}(\text{bpy})_2\text{Cl}_2]$, $[\text{Ru}(\text{terpy})(\text{bpy})\text{Cl}]\text{Cl}$, or $\text{mer-}[\text{Ru}(\text{terpy})\text{Cl}_3]$ by monitoring the degree of supercoiling (Keck & Lippard, 1992) (Figure 4). A compound that unwinds the DNA duplex reduces the number of supercoils so that the superhelical density of closed circular DNA decreases. This decrease upon binding of unwinding agents causes a decrease in the rate of migration through agarose gel, which makes it possible that the unwinding can

Table 3: Unwinding of Supercoiled pSP73 DNA by Ruthenium Complexes

compound	$r_b(c)$	unwinding angle (deg) ^a
$[\text{Ru}(\text{terpy})(\text{bpy})\text{Cl}]\text{Cl}$	$\gg 0.17^b$	$\ll 7$
$\text{cis-}[\text{Ru}(\text{bpy})_2\text{Cl}_2]$	0.075	15
$\text{mer-}[\text{Ru}(\text{terpy})\text{Cl}_3]$	0.18	6

^a The unwinding angle was calculated as described in the text. ^b The comigration of supercoiled and relaxed DNA did not occur even at an r_b value as high as 0.17. At higher levels of the modification by this complex, DNA precipitated.

be observed and quantified. Figure 4 shows electrophoresis gels in which increasing amounts of the ruthenium complexes have been bound to be relaxed and supercoiled pSP73 DNA. The complexes $\text{cis-}[\text{Ru}(\text{bpy})_2\text{Cl}_2]$ and $[\text{Ru}(\text{terpy})(\text{bpy})\text{Cl}]\text{Cl}$ did not apparently alter the mobility of the relaxed form, implying that their binding does not result in shortening or condensation of DNA. This result is consistent with the formation of monofunctional DNA adducts of $\text{cis-}[\text{Ru}(\text{bpy})_2\text{Cl}_2]$ and $[\text{Ru}(\text{terpy})(\text{bpy})\text{Cl}]\text{Cl}$. In contrast, $\text{mer-}[\text{Ru}(\text{terpy})\text{Cl}_3]$ accelerated the mobility of the relaxed form in a manner similar to that of cisplatin, whose bifunctional binding to DNA shortens and condenses the DNA helix (Cohen et al., 1979; Scovell & Collart, 1985). The unwinding angle is given by $\Phi = 18\sigma/r_b(c)$ where σ is the superhelical density and $r_b(c)$ is the value of r_b at which the supercoiled and relaxed forms comigrate. Under the present experimental conditions, σ was calculated to be -0.063 on the basis of the data of cisplatin for which the $r_b(c)$ was determined in this study and $\Phi = 13^\circ$ was assumed (Bellon et al., 1991; Keck & Lippard, 1992). The unwinding angle was also determined under the same experimental conditions for $\text{cis-}[\text{Ru}(\text{bpy})_2\text{Cl}_2]$ enriched by the Δ -isomer (not shown). The value of the angle obtained was the same as it was for the racemic complex. This result suggests that there was no marked difference in the effectivity of the individual isomers of $\text{cis-}[\text{Ru}(\text{bpy})_2\text{Cl}_2]$ in unwinding DNA duplex. Unwinding angles for the ruthenium complexes tested in this work are listed in Table 3 with unwinding ability in the order $\text{cis-}[\text{Ru}(\text{bpy})_2\text{Cl}_2] > \text{mer-}[\text{Ru}(\text{terpy})\text{Cl}_3] > [\text{Ru}(\text{terpy})(\text{bpy})\text{Cl}]\text{Cl}$.

Interstrand Cross-Linking. The interstrand cross-linking was assayed by two independent procedures. The EtBr technique is based on the observation that the fluorescence of this compound is markedly enhanced if it is intercalated in double-stranded DNA. A little intercalation occurs in denatured DNA. In addition, if DNA contains covalent interstrand adduct, it renatures in a markedly higher extent than DNA without such lesions. Thus, the enhanced EtBr fluorescence yielded by the samples of DNA modified by ruthenium in comparison with the control (unmodified) DNA, after they were denatured and subsequently treated with the intercalator, can be used to quantify DNA interstrand cross-links (Brent, 1984; Morgan & Pulleyblank, 1974). A very small enhancement of the EtBr fluorescence was only noticed in the case of calf thymus DNA modified by $\text{cis-}[\text{Ru}(\text{bpy})_2\text{Cl}_2]$ (racemic complex or the complex enriched by the Δ -enantiomer) or $[\text{Ru}(\text{terpy})(\text{bpy})\text{Cl}]\text{Cl}$ at $r_b = 0.005$ – 0.02 . This enhancement gave the amount of interstrand cross-linked DNA, calculated as described in Materials and Methods, less than 2%. On the other hand, this enhancement observed in the case of calf thymus DNA modified by $\text{mer-}[\text{Ru}(\text{terpy})\text{Cl}_3]$ gave the amount of interstrand cross-linked

DNA as 16 or 34% at r_b of 0.005 or 0.01, respectively. These initial studies indicated that *mer*-[Ru(terpy)Cl₃] was markedly more efficient in DNA interstrand cross-linking than [Ru(terpy)(bpy)Cl]Cl or both isomers of *cis*-[Ru(bpy)₂Cl₂].

A more precise method for determination of DNA interstrand cross-linking by the polypyridyl ruthenium complexes exploited the linearized pSP73 DNA as described previously (Brabec & Leng, 1993; Lemaire et al., 1991). In one series of experiments, plasmid DNA was modified by varying concentrations of the ruthenium complexes after it had been linearized by *Eco*RI restriction endonuclease. In the other series, plasmid DNA was modified in the closed, negatively supercoiled form, and only after it had been modified by the metal complex was it linearized by *Eco*RI. Upon electrophoresis under denaturing conditions, noninterstrand cross-linked 3'-end-labeled strands of linearized pSP73 plasmid migrate as a 2464-base single strand, whereas the interstrand cross-linked strands migrate more slowly as a higher molecular mass species.

No bands corresponding to the fragments migrating more slowly than the 2464-base single strand were observed if superhelical or linearized pSP74 DNAs were modified in a broad range of r_b values up to 0.1 by the complexes [Ru(terpy)(bpy)Cl]Cl or *cis*-[Ru(bpy)₂Cl₂] (racemic or the complex enriched by the Δ -enantiomer) (shown for racemic *cis*-[Ru(bpy)₂Cl₂] in Figure 5A). This result confirmed that [Ru(terpy)(bpy)Cl]Cl and the isomers of *cis*-[Ru(bpy)₂Cl₂] exhibited, under the conditions used, no DNA interstrand cross-linking efficiency. On the other hand, the bands corresponding to the more slowly migrating interstrand cross-linked fragments were noticed if DNA was modified by *mer*-[Ru(terpy)Cl₃] at as low an r_b value as 5×10^{-4} (Figures 5B,C). The intensity of this band increased with the growing level of the modification. Quantitation of the cross-links per adduct formed was carried out in essentially the same manner as previously described (Farrell et al., 1990b). The radioactivity associated with each band was measured to obtain estimates of the fraction of non-cross-linked or cross-linked DNA under each condition. The frequency of interstrand cross-links was calculated using the Poisson distribution from the fraction of non-cross-linked DNA in combination with the r_b values and the fragment size. As summarized in Figure 5D, *mer*-[Ru(terpy)Cl₃] showed a much higher frequency of interstrand cross-links in superhelical DNA in comparison with their formation in the linearized form. In addition, while the number of interstrand cross-links formed in the linearized DNA per one ruthenium adduct was independent of r_b , the frequency of the interstrand cross-links formed in superhelical DNA increased with a decreasing level of the modification.

Sequence Preference of DNA–Ruthenium Adducts. This procedure involved the extension by Vent_R(exo⁺) DNA polymerase (which exhibits extreme thermostability) at the 3'-end of the 5'-end radioactively labeled primer up to the metal adduct on the template strand of pSP73 plasmid. Using thermal cycling, this process was repeated many times in order to amplify the signal. The products of this linear amplification were then examined on DNA sequencing gels, and the sequence specificity of ruthenium adduct formation was determined to the exact base pair.

Vent_R(exo⁺) DNA polymerase has active 3' → 5' exonuclease similar to that of several other native DNA polymerases. Vent_R(exo[−]) DNA polymerase is genetically engineered from Vent_R(exo⁺) DNA polymerase, retaining the

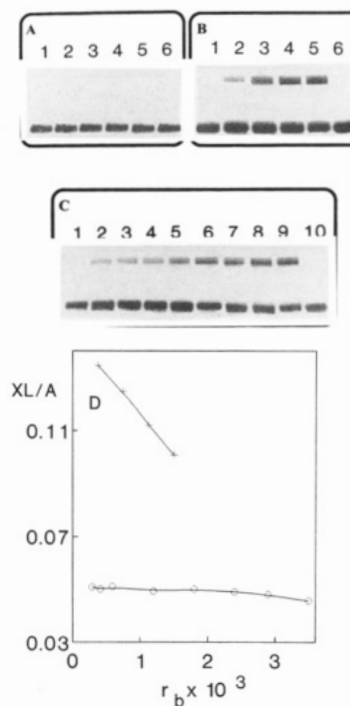


FIGURE 5: Interstrand cross-linked formation induced by ruthenium complexes in linearized or closed negatively supercoiled pSP73 plasmid (2464 bp). (A–C) Autoradiograms of a denaturing 1% agarose gel of DNA which was 3'-end labeled. The interstrand cross-linked DNA appears as the top bands migrating more slowly on the gel than the single-stranded DNA (contained in the bottom bands). (A) Linearized plasmid was incubated with *cis*-[Ru(bpy)₂Cl₂] with r_b values of 0 (control), 0.002, 0.005, 0.012, 0.023, and 0 (lanes 1–6, respectively). (B) Closed negatively supercoiled DNA was incubated with *mer*-[Ru(terpy)Cl₃] with r_b values of 0 (control), 0.00034, 0.00075, 0.00125, 0.0015, and 0 (lanes 1–6, respectively); after the modification, the closed DNA was linearized by the *Eco*RI restriction enzyme. (C) Linearized DNA was incubated with *mer*-[Ru(terpy)Cl₃] with r_b values of 0 (control), 0.00029, 0.00041, 0.00059, 0.0012, 0.0018, 0.0024, 0.0029, 0.0035, and 0 (lanes 1–10, respectively). (D) Dependence on r_b of the number of interstrand cross-links per adduct (XL/A) in the pSP73 plasmid modified by *mer*-[Ru(terpy)Cl₃]. DNA was either modified in closed negatively supercoiled form (and linearized by the restriction enzyme after the modification) (+), or already in linearized form (linearization of plasmid DNA was performed before its modification) (O). The ratio of interstrand cross-links to total ruthenium bound was calculated as described previously (Zou et al., 1993). XL/A was then calculated by dividing this ratio by the number of adducts per DNA molecule.

polymerase activity but having no 3' → 5' exonuclease activity. The absence of exonuclease activity makes it suitable for the finest DNA sequencing so that we used Vent_R(exo[−]) DNA polymerase for dideoxy sequencing of control-unmodified DNA. On the other hand, it has been shown (Comess et al., 1992) that, for mapping studies to detect the location of metal–DNA adducts in a heterogeneous population, DNA polymerases, which have active 3' → 5' exonuclease, are suitable. It is so because these enzymes permit only a very weak translesion synthesis in contrast to their counterparts, which have no associated 3' → 5' exonuclease activity. Therefore, we used Vent_R(exo⁺) DNA polymerase for mapping of ruthenium–DNA adducts.

In vitro DNA synthesis on double-stranded templates containing the adducts of *cis*-[Ru(bpy)₂Cl₂], *mer*-[Ru(terpy)Cl₃], or [Ru(terpy)(bpy)Cl]Cl generated a population of DNA fragments indicating that these adducts terminate duplex synthesis (Figure 6A, lanes Ru1–3). Results identical to

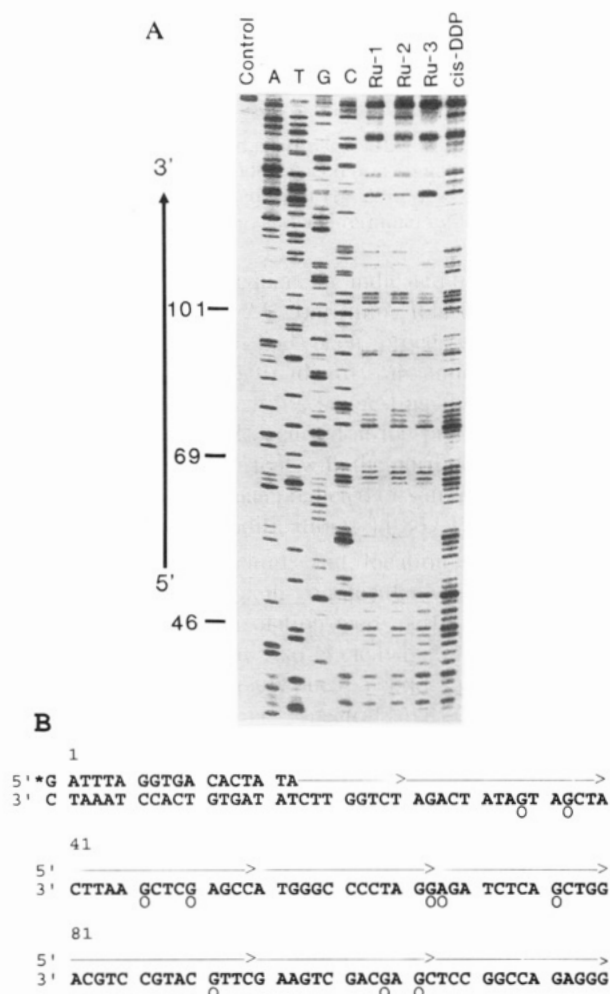


FIGURE 6: (A) Autoradiogram of 6% polyacrylamide/8 M urea sequencing gel showing inhibition of DNA synthesis by *VentR* DNA polymerase on the pSP73 plasmid DNA linearized by *HpaI* restriction enzyme and subsequently modified by metal complexes. The gel contained the linear amplification products of DNA treated with the three ruthenium analogues and cisplatin. Lanes: control, unmodified template; Ru-1, DNA modified by $[\text{Ru}(\text{terpy})(\text{bpy})\text{Cl}]\text{Cl}$ at $r_b = 0.05$; Ru-2, DNA modified by $\text{cis-}[\text{Ru}(\text{bpy})_2\text{Cl}_2]$ at $r_b = 0.05$; Ru-3, DNA modified by $\text{mer-}[\text{Ru}(\text{terpy})\text{Cl}_3]$ at $r_b = 0.05$; cis-DDP, DNA modified by cisplatin at $r_b = 0.01$; and A, T, G, and C, chain-terminated marker DNAs (note that these dideoxy sequencing lanes give the sequence complementary to the template strand). The numbers correspond to the nucleotide sequence numbering of panel B. (B) Schematic diagram showing a portion of the sequence used to monitor inhibition of DNA synthesis on the template containing adducts of the ruthenium complexes or cisplatin. The star indicates the 5'-end labeling of the primer. The arrow indicates the start site of the DNA polymerase and the direction of the synthesis. \circ represents stop signals from panel A, lane Ru-1. Nucleotides 1 and 18 correspond respectively to nucleotides 2548 and 1 on the pSP73 nucleotide sequence map.

those shown for the racemic $\text{cis-}[\text{Ru}(\text{bpy})_2\text{Cl}_2]$ (Figure 6A, lane Ru-2) were obtained if the DNA synthesis was performed on the template modified by this ruthenium complex enriched by its Δ -isomer (not shown). If the same synthesis was performed with *VentR*(*exo*⁻) DNA polymerase, the sequence dependence of the termination was considerably less regular (not shown). Sequence analysis of the termination sites produced by all ruthenium complexes suggests a sequence preference for isolated dG sites in double helical DNA (Figure 6B). This result is consistent with the observation that these complexes were bound with a higher initial rate to DNA, which had a higher content of G + C

(Figure 3B). The sequence dependence of the inhibition is not identical to that found for cisplatin (Figure 6A, lane cis-DDP), indicating a sequence preference of DNA adducts of the ruthenium complexes somewhat different from that exhibited by antitumor cisplatin. Interestingly, the ruthenium complexes form less adducts effective in inhibiting DNA polymerase at d(GG) or oligo(dG) sites. In addition, at the same level of modification, the bands produced by the ruthenium complexes were considerably weaker. This result suggests that the ruthenium complexes tested in this work also form more types of DNA adducts and that some of these adducts are unable to inhibit DNA synthesis by *VentR*(*exo*⁺) DNA polymerase.

DISCUSSION

The purpose of this study was to examine cytotoxicity of several polypyridyl ruthenium complexes (Figure 1) and to compare this biological activity with their DNA binding. The results presented here show that $\text{mer-}[\text{Ru}(\text{terpy})\text{Cl}_3]$ exhibits a significant cytotoxicity in both murine and human tumor cell lines and antitumor activity in a standard tumor screen. In contrast, $[\text{Ru}(\text{terpy})(\text{bpy})\text{Cl}]\text{Cl}$ or both isomers of $\text{cis-}[\text{Ru}(\text{bpy})_2\text{Cl}_2]$, i.e. the complexes with only one or two leaving chloride ligands, respectively, show markedly lower cytotoxic activities in the same tumor models.

A possible pathway of discrimination between $\text{mer-}[\text{Ru}(\text{terpy})\text{Cl}_3]$ and inactive $\text{cis-}[\text{Ru}(\text{bpy})_2\text{Cl}_2]$ or $[\text{Ru}(\text{terpy})(\text{bpy})\text{Cl}]\text{Cl}$ is intracellular ruthenium uptake. However, the accumulation of the ruthenium complexes in the cells (Table 1) exhibited no apparent correlation with their cytotoxicity. This observation supports the view that a different cytotoxicity found for the ruthenium complexes tested in this work was not only due to a different extent of exposure of an intracellular target structure to these compounds.

Antitumor agents derived from the coordination complexes of the transition metals with nitrogen ligands and anionic leaving groups are assumed to have a nuclear DNA as the target site (Clarke, 1989; Johnson et al., 1989). It implies a role for DNA binding in the mechanism of cytotoxic action of the ruthenium complexes investigated in this work. In a cell-free system, the polypyridyl chlororuthenium complexes coordinate to DNA. $\text{mer-}[\text{Ru}(\text{terpy})\text{Cl}_3]$ exhibited a slightly higher affinity to DNA at longer reaction times than the inactive complexes (Figure 3A) (after 24 h, $\text{mer-}[\text{Ru}(\text{terpy})\text{Cl}_3]$ was bound 1.3 or 1.8 times more than $\text{cis-}[\text{Ru}(\text{bpy})_2\text{Cl}_2]$ or $[\text{Ru}(\text{terpy})(\text{bpy})\text{Cl}]\text{Cl}$, respectively). It could be argued that, at the same intracellular concentrations of the ruthenium complexes, a higher cytotoxicity of $\text{mer-}[\text{Ru}(\text{terpy})\text{Cl}_3]$ was due to a higher extent of the modification of DNA. However, on the basis of the ID_{50} values (see Results), $\text{mer-}[\text{Ru}(\text{terpy})\text{Cl}_3]$ was found to be many times more cytotoxic than $\text{cis-}[\text{Ru}(\text{bpy})_2\text{Cl}_2]$ (both racemic or enriched by the Δ -enantiomer) or $[\text{Ru}(\text{terpy})(\text{bpy})\text{Cl}]\text{Cl}$. Thus, the slightly different DNA binding of the ruthenium complexes (Figure 3A) can hardly explain their markedly distinct cytotoxicity in murine and human tumor cells observed in this work (Figure 3).

The binding to DNA occurs preferentially at isolated guanine residues (Figures 3B and 6) and results in conformational alterations in DNA as represented by unwinding of superhelical DNA (Figure 4). These results also indicate differences in the DNA adducts formed by the ruthenium

complexes but do not show a correlation with cytotoxicity exhibited by these compounds in the tumor models used in this work.

On the other hand, the results of this work show that the cytotoxic complex *mer*-[Ru(terpy)Cl₃] exhibits a significant DNA interstrand cross-linking in contrast to the inactive ruthenium complexes which exhibit no such efficiency (Figure 5). Thus, an important feature for biological activity of polypyridyl ruthenium complexes is DNA interstrand cross-linking.

It is for obvious reasons why the formally monofunctional [Ru(terpy)(bpy)Cl]Cl does not form on DNA the bifunctional interstrand cross-link. On the other hand, no DNA interstrand cross-linking capability of bifunctional *cis*-[Ru(bpy)₂Cl₂] reported in this work deserves a deeper discussion. Recently, thermal denaturation studies on DNA modified by a group of mono- and diaqua polypyridyl complexes of ruthenium including racemic *cis*-[Ru(bpy)₂(H₂O)₂]²⁺ (Grover et al., 1994) were described. These recent investigations yielded the result that *cis*-[Ru(bpy)₂(H₂O)₂]²⁺ increased the melting temperature of DNA (*T_m*) by 6.1 °C at *r_b* = 0.024. This observation was interpreted to mean that the bifunctional complex *cis*-[Ru(bpy)₂(H₂O)₂]²⁺ formed DNA interstrand cross-links responsible for the increase of *T_m* (Grover et al., 1994). Since the nature of the DNA adducts of *cis*-[Ru(bpy)₂(H₂O)₂]²⁺ and its dichloro counterpart has been proposed to be the same (Grover et al., 1992), it implies that *cis*-[Ru(bpy)₂Cl₂] should also be an effective DNA interstrand cross-linking agent. On the other hand, the conclusion on interstrand cross-linking by *cis*-[Ru(bpy)₂(H₂O)₂]²⁺ has only been based on the *T_m* measurements, and no additional, more direct evidence has been presented (Grover et al., 1994). It is well-established that the increase of *T_m* due to the binding of a cationic compound to DNA does not necessarily imply DNA interstrand cross-linking [see Kleinwächter et al., (1969) and Waring (1965)]. Also importantly, there is no further published result except that based on the *T_m* measurements suggesting that *cis*-[Ru(bpy)₂(H₂O)₂]²⁺ or *cis*-[Ru(bpy)₂Cl₂] forms in reaction with DNA or its monomeric constituents some type of disubstituted products. On the contrary, the single crystal X-ray analysis and ¹H nuclear magnetic resonance spectroscopy revealed that both *cis*-[Ru(bpy)₂(H₂O)₂]²⁺ and *cis*-[Ru(bpy)₂Cl₂] with an excess of 9-ethylguanine or 9-methylhypoxanthine (1:10 mixture) gave only monosubstituted products in a chloride-free medium (van Vliet et al., 1994). A similar analysis of the products of the reaction of *mer*-[Ru(terpy)Cl₃] with these bases only in stoichiometric amounts revealed two bases coordinated at the N7 site in a *trans* configuration (van Vliet et al., 1995).

Therefore, we reevaluated the DNA interstrand cross-linking capability of *cis*-[Ru(bpy)₂Cl₂] with the aid of two independent methods routinely used for sensitive and quantitative determination of DNA interstrand cross-links. In accordance with the results on the ruthenium adducts of monomeric nucleic acid bases (van Vliet et al., 1994, 1995), we find in this work that *mer*-[Ru(terpy)Cl₃] cross-linked the complementary strands in double helical DNA while both isomers of *cis*-[Ru(bpy)₂Cl₂] formed other types of adducts (Figure 5).

DNA interstrand cross-links formed by several cytotoxic or antitumor agents have been proposed to be relevant to their biological activity (Larminat et al., 1993; Lee & Gibson,

1993; Masuda et al., 1988; Zwelling et al., 1979). These bidentate adducts could inhibit DNA and/or RNA synthesis (Brabec et al., 1993; Lemaire et al., 1991) or can produce in DNA a specific lesion which could be an important structural motif in recognition of damaged DNA by some specific, DNA binding proteins. *mer*-[Ru(terpy)Cl₃] forms in linear DNA ca. 5% interstrand cross-links. This amount is almost identical with that formed under similar conditions by antitumor cisplatin (Brabec & Leng, 1993). Interestingly, *mer*-[Ru(terpy)Cl₃] forms markedly more interstrand cross-links in a closed, supercoiled DNA than in linear DNA (Figure 5). This observation might be associated with the fact that formation of the interstrand cross-link in double helical DNA by *mer*-[Ru(terpy)Cl₃] requires a distortion in this biomacromolecule. Distortions have already been described in DNA duplexes containing unique interstrand lesions of cisplatin or its *trans* isomer (Brabec et al., 1993; Malinge et al., 1994). The occurrence of such distortions in DNA may be assisted by the effect of negative supercoiling. The excess energy possessed by a negatively supercoiled molecule can be used to help provide the energy needed to distort double helical DNA. The enhanced interstrand cross-linking efficiency of *mer*-[Ru(terpy)Cl₃] in supercoiled DNA might be of particular importance for understanding some aspects of molecular mechanisms of cytotoxic activity of ruthenium complexes in cells. Most DNA present in the cells exists in the negative supercoiled state complexed with specific DNA binding proteins (Kornberg & Klug, 1981; McGhee & Felsenfeld, 1981; Morse & Cantor, 1985).

In summary, polypyridyl ruthenium complexes which exhibit cytotoxic effects in tumor cells may be designed. The results presented here further support the working hypothesis that ruthenium complexes may also exhibit their biological effects via their capability to form DNA interstrand cross-links. Further investigation of the mechanism of action of these species is warranted to define their clinical potential and to contribute to a rational approach for developing a new antitumor metal-based drug with antitumor properties complementary to those exhibited by the drugs already used in clinic.

REFERENCES

- Adcock, P. A., Keene, F. R., Smythe, R. S., & Snow, M. R. (1984) *Inorg. Chem.* 23, 2336.
- Arce Sagüés, J. A., Gillard, R. D., Smalley, D. H., & Williams, P. A. (1980) *Inorg. Chim. Acta* 43, 211.
- Barton, J. K. (1986) *Science* 233, 727.
- Barton, J. K., & Lolis, E. (1985) *J. Am. Chem. Soc.* 107, 708.
- Bellon, S. F., Coleman, J. H., & Lippard, S. J. (1991) *Biochemistry* 30, 8026.
- Brabec, V., & Paleček, E. (1976) *Biophys. Chem.* 4, 79.
- Brabec, V., & Leng, M. (1993) *Proc. Natl. Acad. Sci. U.S.A.* 90, 5345.
- Brabec, V., Sip, M., & Leng, M. (1993) *Biochemistry* 32, 11676.
- Brent, T. P. (1984) *Cancer Res.* 44, 1887.
- Clarke, M. J. (1989) in *Progress in Clinical Biochemistry and Medicine*, Vol. 10, p 25, Springer, Berlin.
- Clarke, M. J. (1993) in *Metal Complexes in Cancer Chemotherapy* (Keppler, B. K., Ed.) p 129, VCH Verlagsgesellschaft, Weinheim, and VCH Publishers, New York.
- Cohen, G. L.; Bauer, W. R., Barton, J. K., & Lippard, S. J. (1979) *Science* 203, 1014.
- Comess, K. M., Burstyn, J. N., Essigmann, J. M., & Lippard, S. J. (1992) *Biochemistry* 31, 3975.

- Erikson, M., Leijon, M., Hiort, C., Norden, B., & Graslund, A. (1994) *Biochemistry* 33, 5031.
- Farrell, N., Qu, Z., & Hacker, M. P. (1990a) *J. Med. Chem.* 33, 2179.
- Farrell, N., Qu, Z., & Van Houten, B. (1990b) *Biochemistry* 29, 9522.
- Frühauf, S., & Zeller, W. J. (1991) *Cancer Res.* 51, 2943.
- Grover, N., & Thorp, H. H. (1991) *J. Am. Chem. Soc.* 113, 7030.
- Grover, N., Gupta, N., & Thorp, H. H. (1992) *J. Am. Chem. Soc.* 114, 3390.
- Grover, N., Welch, T. W., Fairley, T. A., Cory, M., & Thorp, H. H. (1994) *Inorg. Chem.* 33, 3544.
- Gupta, M., Grover, N., Neyhart, G. A., Singh, P., Liang, W., & Thorp, H. H. (1992) *Angew. Chem., Int. Ed. Engl.* 31, 1048.
- Gupta, M., Grover, N., Neyhart, G. A., Singh, P., & Thorp, H. H. (1993) *Inorg. Chem.* 32, 310.
- Heim, M. E. (1993) in *Metal Complexes in Cancer Chemotherapy* (Keppler, B. K., Ed.) p 9, VCH Verlagsgesellschaft, Weinheim, and VCH Publishers, New York.
- Johnson, N. P., Butour, J. L., Villani, G., Wimmer, F. L., Defais, M., Pierson, V., & Brabec, V. (1989) in *Progress in Clinical Biochemistry and Medicine*, Vol. 10, p 1, Springer, Berlin.
- Keck, M. V., & Lippard, S. J. (1992) *J. Am. Chem. Soc.* 114, 3386.
- Keppler, B. K. (1989) in *Progress in Clinical Biochemistry and Medicine*, Vol. 10, p 41, Springer, Berlin.
- Kleinwächter, V., Balcarová, Z., & Boháček, J. (1969) *Biochim. Biophys. Acta* 174, 188.
- Köpf-Maier, P. (1994) *Eur. J. Clin. Pharmacol.* 47, 1.
- Kornberg, R. D., & Klug, A. (1981) *Sci. Am.* 244, 52.
- Larminat, F., Zhen, W., & Bohr, V. A. (1993) *Biol. Chem.* 268, 2649.
- Lee, C.-S., & Gibson, N. W. (1993) *Biochemistry* 32, 9108.
- Lemaire, M. A., Schwartz, A., Rahmouni, A. R., & Leng, M. (1991) *Proc. Natl. Acad. Sci. U.S.A.* 88, 1982.
- Loehrer, P. J., & Einhorn, L. H. (1984) *Ann. Intern. Med.* 100, 704.
- Malinge, J.-M., Pérez, C., & Leng, M. (1994) *Nucleic Acids Res.* 22, 3834.
- Matsuda, K., Nakamura, T., Shimomura, T., Shibata, T., Terano, H., & Kohsaka, M. (1988) *J. Antibiot.* 41, 1497.
- McGhee, J. D., & Felsenfeld, G. (1980) *Annu. Rev. Biochem.* 49, 1115.
- Mestroni, G., Alessio, E., Sava, G., Pacor, S., Coluccia, M., & Boccarelli, A. (1994) *Met.-Based Drugs* 1, 41.
- Morgan, A. R., & Pulleyblank, D. E. (1974) *Biochem. Biophys. Res. Commun.* 61, 396.
- Morse, R. H., & Cantor, C. C. (1985) *Proc. Natl. Acad. Sci. U.S.A.* 82, 4653.
- Moyer, B. A., & Meyer, T. J. (1981) *Inorg. Chem.* 20, 436.
- Murray, V., Motyka, H., England, P. R., Wickham, G., Lee, H. H., Denny, W. A., & McFadyen, W. D. (1992a) *J. Biol. Chem.* 267, 18805.
- Murray, V., Motyka, H., England, P. R., Wickham, G., Lee, H. H., Denny, W. A., & McFadyen, W. D. (1992b) *Biochemistry* 31, 11812.
- Neyhart, G. A., Grover, N., Smith, S. R., Kalsbeck, W. A., Fairley, T. A., Cory, M., & Thorp, H. H. (1993) *J. Am. Chem. Soc.* 115, 4423.
- Reedijk, J. (1992) *Inorg. Chim. Acta* 198-200, 873.
- Satyanarayana, S., Dabrowiak, J. C., & Chaires, J. B. (1993) *Biochemistry* 32, 2573.
- Scovell, W. M., & Collart, F. (1985) *Nucleic Acids Res.* 13, 2881.
- Sullivan, B. P., Salmon, D. J., & Meyer, T. J. (1978) *Inorg. Chem.* 17, 3334.
- Takeuchi, K. J., Thompson, M. S., Pipes, D. W., & Meyer, T. J. (1984) *Inorg. Chem.* 23, 1845.
- van Vliet, P. M., Haasnoot, J. G., & Reedijk, J. (1994) *Inorg. Chem.* 33, 1934.
- van Vliet, P. M., Toekimin, S. M. S., Haasnoot, J. G., Reedijk, J., Nováková, O., Vrána, O., & Brabec, V. (1995) *Inorg. Chim. Acta* 231, 57.
- Waring, M. J. (1965) *J. Mol. Biol.* 13, 269.
- Zou, Y. B., Van Houten, B., & Farrell, N. (1993) *Biochemistry* 32, 9632.
- Zwelling, L. A., & Anderson, T., & Kohn, K. W. (1979) *Cancer Res.* 39, 365.

BI950605L